European Commission

JRC CONFERENCE AND WORKSHOP REPORTS

ESARDA 39th Annual Meeting

2017 Symposium
16-18 May 2017
Meliá Düsseldorf
Düsseldorf, Germany

Filippo Sevini
Andrea De Luca
Elena Stringa

2017

ESARDA Symposium 2017 | 39th Annual Meeting | 15-18 May 2017, Jülich/Düsseldorf (DE)

Institute of Energy and Climate Research
IEK-6 | Nuclear Waste Management and Reactor Safety

Joint Research Centre

EUR 28795 EN

Contact information
Name: Filippo Sevini
Address: DG Joint Research Centre, Directorate G - Nuclear Safety and Security, Department G.II - Nuclear Security and Safeguards, Unit G.II.7 – Nuclear Security, T.P. 800, Via E Fermi 2749, 21027 Ispra, Italy
Email: filippo.sevini@ec.europa.eu
Tel.: +39 0332 78 6793

JRC Science Hub
https://ec.europa.eu/jrc

JRC107151

EUR 28795 EN

PDF ISBN 978-92-79-73861-6 ISSN 1831-9424 doi:10.2760/631364

Luxembourg: Publications Office of the European Union, 2017

How to cite this report: Author(s), *Title*, EUR, doi

Contents

Plenary Speeches

01 Implementation of Safeguards

02 Non-destructive Analysis – Gamma Measurements

03 International Collaboration

06 Geological Repositories

07 Non-destructive Analysis: Neutron I

08 Arms Control and Nuclear Disarmament Verification II

09 Destructive Analysis I

10 Spent Fuel Verification and Spent Fuel Transfer

11 Training and Knowledge Management

12 Destructive Analysis II

13 Non-destructive Analysis: Tomography

14 Evaluation

15 Containment & Surveillance

16 Non-destructive Analysis: Neutron II

17 Nuclear Security

18 Process Monitoring

19 Statistical Methodologies

Poster Session

Plenary Speeches

Welcome and Opening

Irmgard Niemeyer, president of ESARDA

Distinguished Guests, Ladies and Gentlemen, dear colleagues and friends,

Good morning and welcome.

My name is Irmgard Niemeyer, and in my capacity as the current president of the European Safeguards Research and Development Association (ESARDA), and also as a local, it is my great pleasure to welcome you to the 39th Annual Meeting of ESARDA here in Düsseldorf.

Since the first ESARDA Annual Meeting in 1979, this year's meeting is the fifth Annual Meeting being held in Germany. The other meetings took place in Karlsruhe in 1981 and 1988, Aachen in 1995 and Dresden in 2000.

ESARDA existed already for a while – 10 years to be precise - before the first Annual Meeting was held. Created in 1969, our association slowly but surely heads towards its 50th anniversary.

Those of you who may be in a similar phase of their own lives or may have passed it already, possibly have realised that this can be the time for increased reflection. Reflections about the many routines and habits in your life, about long-established patterns of thought, structures and controlled procedures, including question like "Did I really imagine my life this way?". At the same time, you may realise that it takes you much longer than ten or twenty years ago to make yourself familiar with new approaches, topics or technologies.

Is this, to some extent, also true for ESARDA? Does it apply to ESARDA at all?

Let's spend a few minutes on the current state of ESARDA.

ESARDA is a network of organisations including national regulatory authorities, nuclear facilities operators, nuclear industry, research centres, and universities, aiming to bring together the international nuclear safeguards community. Its main goals are research collaboration, exchange of information and joint implementation of research and development programmes. ESARDA is currently formed by 32 Parties from the European Union (EU), 7 non-EU Associated Members as well as 10 Individual Members, bound by the ESARDA Agreement. In recent years, usually one to three new organisations have joined

ESARDA per year, with an increase of Associated Members from the US in the last couple of years.

If you look at the list of participants of this year's Symposium, you will understand the variety of countries and professional groups involved in ESARDA (Figure 1).

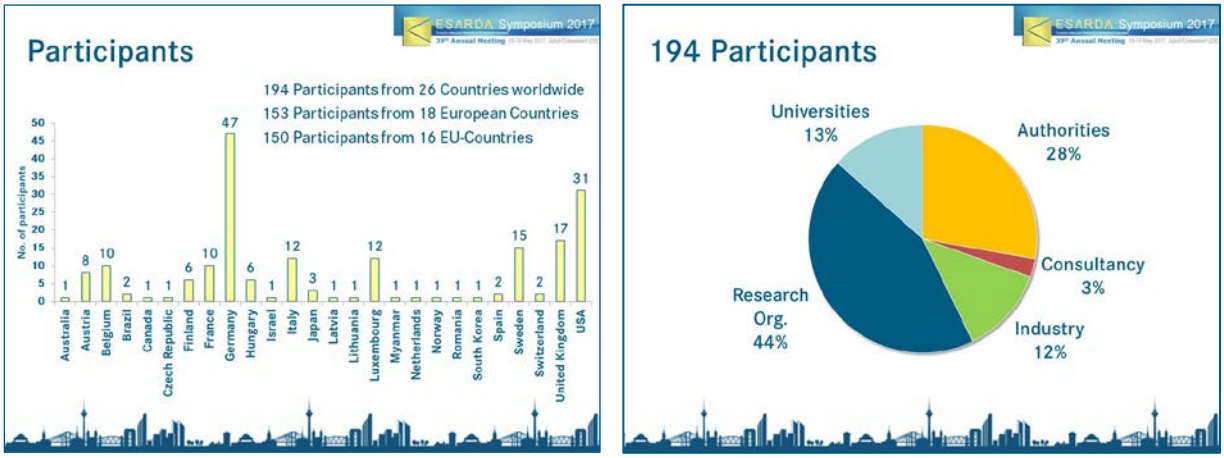

Figure 1: Participants per country (left) and professional groups (right).

The Symposium has attracted 194 participants from 26 countries worldwide. While Germany, as the host country, forms the largest group of participants, the second largest group of attendees comes from the US. Nearly 80% of the participants belong to institutions in Europe, and the European Union is represented by 150 participants from 16 out of the 28 countries.

In terms of professional groups, most of the participants work at research organisations (44%) or authorities (28%). Universities (13%) and industry (12%) provide one-eighth of the participants each.

The geographical and professional distributions of the Symposium participants may not be representative for ESARDA in general; however, it at least illustrates the interest in this particular ESARDA activity. For future symposia, we may consider how to increase the number of European Union countries, and possibly also whether we would like to see a higher percentage of universities and nuclear industry, including operators.

Lastly, I also wanted to mention the number of female participants at the Symposium. Whereas more and more women have got involved in safeguards-related activities in the past years, the share of women among the attendees – only a quarter - is still not satisfying.

The main activities of ESARDA were already in place when I got involved 15 years ago:

1. Annual Meetings and Symposia, providing an opportunity for collaboration and information exchange.
2. Dedicated working group (WG) activities, with eight WGs being the "backbone" of ESARDA.
3. The one-week ESARDA Course on nuclear safeguards and non-proliferation, which complements nuclear engineering studies by including nuclear safeguards in the academic curriculum.
4. Technical publications, in particular the ESARDA Bulletin including peer-reviewed articles.

Those activities come along with particular well-functioning schedules, processes and procedures. Can we assume these schedules, processes and procedures to be proven practices or do we need to review them in light of the current and future challenges for research collaboration, exchange of information and joint implementation of R&D programmes?

Overall, while ESARDA is a vital network with many active members today, it might be worth considering some kind of preventive measures in terms of "anti-aging".

In addition, strategies for supporting safeguards implementation and promoting safeguards-related research and development require a substantial rethinking in certain intervals if they are to remain relevant.

It is also important to take into account that ESARDA doesn't act in isolation. This is all the more true in a world which is changing ever faster and is becoming increasingly complex.

Therefore, after the activities and recommendations of the ESARDA Reflection Groups in 2000 and 2010, the Executive Board agreed it its meeting of January 23-24, 2017, that the time has come to reassess ESARDA's future strategic direction in light of current and future non-proliferation and safeguards challenges. Thus, a new Reflection Group will be established with the objectives to review the strategy planning process within ESARDA and to draw a roadmap by 2019 (which marks ESARDA's 50th anniversary), possibly for the next three to five years, subject to the adoption of the terms of references.

The Reflection Group will be kicked off by the panel discussion on "Reflecting on ESARDA's future strategic direction" on Thursday, and I cordially invite you to attend this event. The

panel is aimed at learning about strategic planning and strategy plans of other organisations and at exchanging views on strategic partnerships and cooperation.

Each of the parties, members and other partners of ESARDA has its own challenges, as we will hear from some of our today's keynote speaker.

I invite you all to take part in this process. A questionnaire will be developed by the Reflection Group in order to get as many opinions and proposals for ESARDA's future strategic direction from you as possible.

Ladies and Gentlemen, the year 2017 marks the 20th anniversary of the 'Model Protocol Additional to the Agreement(s) between State(s) and the International Atomic Energy Agency for the Application of Safeguards', as laid down in INFCIRC/540(Corrected) – a good reason to reflect on its achievements, lessons learned, and future prospects.

In this line, we would like to invite you to attend the roundtable discussion on "20 years of the Additional Protocol" tonight, together with the IAEA, Euratom and Member States, and share your views on and experiences in the implementation of the Additional Protocol (AP).

Finally, I want to encourage you to take advantage of your time here, attend the technical sessions and interact with your colleagues. For continuing your discussion after the programme, the Old Town's 300 pubs, bars, restaurants, and cafés also named the "The Longest Bar in the World, will definitely provide a place for all of you.

Ladies and Gentlemen, while ESARDA may be only a tiny piece in the global system, I am confident that we can prove successful European collaboration, successful international cooperation, and the ability of providing sound scientific factual findings.

With this, I would like to open the 39th ESARDA Annual Meeting, the Symposium on Nuclear Safeguards and Non-proliferation. I wish you a fruitful meeting and a very pleasant stay in the city of Düsseldorf.

Thank you all for attending the Symposium and thank you for the attention.

Irmgard Niemeyer, ESARDA President

Phase-out and Safeguards in Germany

Keynote

Ursula Borak
Deputy Director General
Ministry for Economic Affairs and Energy

Dear Ms Niemeyer and Mr Sevini,
good morning to the fellow keynote speakers this morning,
Ladies and Gentlemen,
thank you for the invitation to this plenary.

1. Introduction

Safeguards measures are most relevant for the German government. The prevention of the abuse of nuclear material for non-civil uses is crucial for us.
We have always supported verification measures.

And we appreciate every opportunity for an exchange of views and information with the IAEA, Euratom and all the other national and international experts in the field of safeguards.

My first key message is: the political decision in Germany to phase out nuclear energy for electricity production does by no means have the effect that we are no more interested in the field of safeguards. Just the opposite is the case!

2. Energiewende

The major topic in Energy politics in Germany is, of course, the Energy Transition or *Energiewende*.

Just a few figures of the energy mix at the current phase of the Energy Transition:
The share of renewables in power generation has reached 30 %.
Whereas nuclear energy contributes about 13 %.

With regards to power consumption, the share of renewables has reached over 32 %, already.
Compared to 2010 almost a doubling.

The aim for the share of renewables for the year 2025 is over 40 %.

The biggest challenge for the “Energiewende” stems from the delayed grid expansion. This is especially relevant for the north-south corridor from the wind power regions in the north to the industrial centers in the south.

But despite growing demand on the grids, grid quality in Germany remains very high, and is thereby contributing to the security of supply:

The supply failures were limited to only
12 minutes per customer in 2015.
In comparison, the failures in the US were over 100 minutes and in France and the UK 50 minutes.
Nevertheless, we have to further advance grid integration and expansion.

3. Phase-out of nuclear energy

But certainly, for this conference another aspect of energy policy in our country might be more relevant:

As I mentioned in the beginning:
The Energy Transition includes the **phase-out of nuclear energy for electricity production**.
In Germany, this decision is based on a solid and stable political consensus in our society.

Since 1962, a total of 37 nuclear power plants have been built in Germany and put into commercial operation. Today, eight commercial reactors are still operating.

In less than six years – at the end of 2022 at the latest – the last nuclear power plant in Germany will be shut down.

As a result of this decision, the amount of radioactive waste requiring final storage is now limited and easier to calculate than before.

At the same time, the amount of time during which income can be generated from the operations is limited, too.
And more limited as before is the time in which provisions can be made for the disposal of the waste.

4. Foundation under public law

In line with the polluter-pays principle and the respective legal requirements, it is the operators of nuclear power plants that must pay for the decommissioning and dismantling, as well as for the management of the nuclear waste, including the cost of final storage.

As a consequence of the phase-out, an equally solid and broad consensus was needed for the adjustment of the financing of the disposal of the waste.

Therefore, the Federal Government in 2015 set up an independent commission of experts, with members and stakeholders from all parts of society: the *Commission to Review the Financing for the Nuclear Phase-Out,* or as the German abbreviation sounds: *KFK*.

The task of the commission was, to assess how the financing for decommissioning and dismantling of nuclear power plants and for nuclear waste disposal can be organised most efficiently, given the new situation.
The companies responsible should still be financially capable of meeting their obligations, including in the long term.

The final report was unanimously adopted by the commission in April 2016 and presented to the Federal Government. It sets out a proposal on how this can be achieved in a way that is acceptable to policy-makers across party lines, and to society at large.

The proposal was:

1. The responsibility for interim and final storage is to lie with the government,
2. the financial burden is to be borne by the companies. The companies are to provide the necessary liquidity by paying into a fund established under public law. This means: In future, operational as well as financial responsibility are combined in the hands of the government.

My second key message is: The work of the commission paved the way for a solid, broadly accepted political roadmap.

On the basis of this recommendation of the independent commission an act was drafted by the Federal Government.

The German parliament in December 2016 voted with a broad majority for the "Act reorganizing responsibility for nuclear waste management".

Under the new regulations, on the one hand, the operators will continue to bear the full responsibility for the decommissioning and dismantling of the nuclear power plants, as well as for the packaging of the waste.
On the other hand, the Federal Republic will assume responsibility for the management and financing of interim and final storage. - The management of final storage has been the state's responsibility, already.

The funds for the interim and final storage will be provided by the operators of nuclear power plants. For this purpose, they will be obliged to transfer a total of about 17 billion to a public fund. This amount is due on July 1.
The amount corresponds to the total amount of provisions built by the energy companies in order to finance the management of the nuclear waste.

In addition, the operators will have the opportunity to pay a voluntary risk surcharge, amounting to a total of 6 billion euros. Paying this surcharge, they will not be obliged to provide additional capital to the fund in case of a capital shortage in the future.

As a sum, somewhat over 24 billion euros could be the overall volume of the fund.

The fund collecting the payments of the operators will be set up as a foundation under public law.
It will invest the funds provided by the operators and reimburse the costs incurred by the Federal Republic in connection with the interim and final storage of nuclear waste.

For the management of interim storage, the Federal government has taken the first steps to establish a new state-owned company.

It will take over the operators' various interim storage sites as of 1 January 2019 (for high active nuclear waste), and as of 1 January 2020 (for low and medium active nuclear waste).

My third key message is:
In the next 10 years, the sheer number of waste packages that have to be verified, will increase considerably.

This is not only relevant for Germany, of course, but in many countries of the EU. More than 50 of the operated nuclear power plants will be shut down till 2025.

5. German Joint Safeguards Programme with the IAEA

Therefore, efficient methods and techniques for safeguarding will be essential.

As you know, in Germany the Federal Ministry for Economic Affairs and Energy is funding the German Joint Safeguards Programme with the IAEA. Forschungszentrum Jülich is the scientific coordinator.

And as an aside:
Next autumn – around the time of the IAEA's General Conference in September - our *"Joint Programme on the Technical Development and further improvement of IAEA Safeguards"* will be active 40 years.

I am optimistic that the various member state support programmes, including the German, can deliver adequate tools and expertise to support verification and safeguarding for the intermediate dry storage facilities in the coming years.

The German Safeguards Support Programme will continue to deliver expertise and research funding on a reliable basis.

6. Conclusion

In the first section, this afternoon already, probably some of the "Challenges for Safeguards in Germany" will be discussed in more detail.

Until Thursday, there are as much as 18 sections with different topics on the agenda.
For all of these, I wish fruitful discussions and success to ESARDA for this symposium.

Thank you for your attention.

IAEA SAFEGUARDS: INCREASING CHALLENGES, NEW OPPORTUNITIES

ESARDA Symposium – 16 MAY 2017

Tero Varjoranta, Deputy Director General and Head of the Safeguards Department, IAEA

Over the past two weeks in Vienna, the parties to the Non-Proliferation Treaty met in Preparatory Committee in advance of the 2020 NPT Review Conference. It was an opportunity to remind everyone that the verification assurance provided by IAEA safeguards is the foundation of the non-proliferation pillar of the NPT. And that the credibility of the IAEA's safeguards conclusions is, by extension, vital to international peace and security.

Today, across the world, IAEA safeguards are being implemented in 181 States. We are safeguarding nearly 1,290 nuclear facilities and locations - containing nuclear material sufficient to make over 204,000 nuclear explosive devices. This is over ten times more than the actual number of nuclear weapons in the world today. It is a truly global effort, conducted 24/7 that will need to continue for the foreseeable future.

I believe the IAEA's safeguards work is something of which we can be proud. But we cannot afford to be complacent. The nuclear landscape is constantly changing: throwing up new challenges as it does so. More nuclear facilities and nuclear material are coming under safeguards all the time, the complexity of the facilities that we are safeguarding is increasing, and in an ever more globalized world, there is more nuclear cooperation and trade than ever before. In addition, we are seeing more transfers of spent fuel and decommissioning of nuclear plants. These trends look set to continue.

Money is another challenge. Funding for IAEA safeguards has not kept pace with demand, and in the present economic climate, it is unlikely to do so anytime soon. Like any business, the Department of Safeguards has to provide value for money to our customers – in this case, our Member States. Similarly, we have to be results

driven – we need to produce credible safeguards conclusions for each and every State in which we apply safeguards. And the key word here is “credible”, because if our safeguards conclusions lack credibility they will reassure no-one and – in time – could lead to an unravelling of the non-proliferation regime itself.

In light of this and given that our workload is driven by the need to fulfil our *legal* obligations, the answer can only lie in improving our productivity.

There are three main ways in which we are doing this:

- First, through streamlining our processes. We are constantly seeking ways to do things more effectively and efficiently inside the Department, including through the pursuit of a lean management agenda, which I have introduced.
- Second, through improving cooperation with States in daily safeguards implementation. There are a number of areas where better cooperation from States would make our job of implementing safeguards easier and more efficient.
- Third, through the use of modern technology.

The Safeguards Department regularly monitors and assesses developments in its operating environment, including in the area of technology. As part of that effort, in February this year we organized an Emerging Technologies Workshop, to increase our awareness of, and prepare for, new technologies. During the course of this workshop a number of new challenges were identified that we will need to address.

- New types of nuclear reactor are advancing and diversifying – some of which will present new challenges for safeguards: for example, transportable reactors.
- The development of laser technologies may also pose challenges.
- Accelerator-driven systems could enable the misuse of subcritical reactors.
- Some non-nuclear technologies may increase proliferation risks (e.g. additive manufacturing/3D printing)

On the other hand, the workshop also highlighted a number of opportunities for safeguards in terms of newly emerging technologies which could serve our purpose.

- Data collection, integration, processing and analysis are constantly being improved, with artificial intelligence and machine learning offering the means to automate and reduce repetitive tasks.
- Data visualization tools enable safeguards analysts to focus on better understanding, analyzing and presenting data.
- The transparency and security features of shared ledger technology show potential for safeguards application (e.g. nuclear material accounting).

Investing in new technologies can bring significant improvements in efficiencies – whether it is new IT software that can collect safeguards–relevant information faster; or the greater use of remote data transmission, thereby relieving inspectors of the task of collecting such data themselves; or installing instruments in our laboratories that can analyze nuclear samples with greater precision than ever before.

Investment decisions obviously need to be made years in advance and this requires proper planning. That is why we are currently updating the Department's Long-Term Research and Development (R&D) Plan. But as well as our longer term planning in relation to investments in new technologies we need to be agile – to be responsive to changing international circumstances, some of which may be unexpected. Let me take the example of the JCPOA – the Iran nuclear deal – where the Agency was required to ensure that Iran's enrichment of uranium in UF6 does not go above 3.67% U–235. This required us to procure and speedily deploy a new piece of technology from the US – the On-Line Enrichment Monitor (OLEM). This technology is now installed in Natanz and verifying one of Iran's key nuclear commitments under the deal.

In the context of R&D and investment in new technologies, the IAEA is heavily dependent on support from our Member States, as it does not have its own R&D capability. These Member State Support Programmes - as they are known – provide

significant “extrabudgetary” contributions to the effective and efficient implementation of safeguards. For example, they provide funds for the modernization of our IT system and to improvements in our nuclear material sampling capability. These are not “nice to have” add-ons: they are an intrinsic part of our effective operations. We are now in the process of establishing a new review mechanism involving MSSPs in assessing projects from the ‘Development and Implementation Support (D&IS) Programme for Nuclear Verification’ to ensure that we can improve our interface with the support programmes. *[David Peranteau will be making a presentation on MSSPs later in the symposium]*

As I look to the future, I emphasize once again that our overarching objective must be to sustain the credibility of safeguards conclusions. To achieve that goal we in the Department of Safeguards will need to continue to rely on the support of our Member States, particularly in the area of R&D and emerging technologies. We will need to plan carefully for the future and to exercise agility in response to changing circumstances.

In this way we can ensure that the IAEA – and safeguards in particular – will continue to make a vital contribution to international security in the interest of all humanity.

ESARDA 2017 Plenary talk

Paul Meylemans, DG Energy, Euratom Safeguards Directorate

Mrs President, dear colleagues and friends,

It is a great pleasure for me to be with you today as representative of Euratom Safeguards, the Commission's service for safeguards in the European Union.

Let me first convey to you the best wishes of the Euratom Safeguards Director, Mr Stephan Lechner, who cannot not be with us this morning but who will be with us later today to attend the round-table discussion in the evening.

[Introduction]

Ladies and Gentlemen,

This meeting of the ESARDA Community takes place at a very particular moment: This year, we have celebrated 60 years of the Euratom Treaty!

This Treaty has been the basis for fostering nuclear energy and research in the European Union and beyond! It has made sure that there was no diversion of nuclear materials, for now sixty years. It has made sure that the EU today is the most controlled area in the world, in what concerns Safeguards.

This Euratom Treaty has served us very well for sixty years: It is now for us to adapt our current rules for safeguards to new challenges and to learn from the experiences of the past. We must make sure that we continue to provide the European citizen and the international community with the highest level possible of nuclear safety, security and safeguards.

Many of my colleagues and I, have devoted a large part of our professional career to Euratom safeguards and, knowing that we were doing something indispensable and useful, we have done so with pride!

In our complex world of today, comprehensive undertakings such as safeguards are, usually, not undertaken by one institution or one service alone: In order to succeed you need to cooperate with partners and you need to liaise with interlocutors all across the globe.

At Euratom, we are very aware that we cannot succeed all by ourselves: We need the exchange and discussion with our partners to succeed: We need the continuous exchange with our Member States, with the IAEA, with the third countries, with the Joint Research Centre, the European Commission's in house scientific service, with the global R&D community, the INMM, and, last but by no means least, with you: ESARDA.

This is why, in this contribution, I would like to firstly look at the evolution of the wider Euratom safeguards context, at the related challenges for the future, and then at the cooperation with our partners including the IAEA and ESARDA.

[Evolution of political context for Euratom safeguards]

The nuclear safeguards landscape is constantly evolving, both in terms of political context as well as of technological development, presenting both challenges and opportunities.

In spite of a wider context marked, on one hand, by increasing amounts of nuclear material and, on the other, by shrinking resources, we invest into the improvement of Safeguards in Europe on a constant basis. Nonetheless, we make every effort to fulfill our mandate as well as ever.

Since 2007, the Commission's Staff Working Document "Implementing Euratom Treaty Safeguards", abbreviated as IETS, has provided the practical orientation for our daily work.

Almost a decade later and in view of considerable changes in our political context, it seems about time to revisit this guidance document, in order to see how and to what extent it still reflects current as well as new challenges for Safeguards in the EU of today.

The political opportunity for doing so could not be better as we are currently framing the European Energy Union in a number of fields of energy policy so as to prepare ourselves for the future.

Our main aim in the IETS review process will be to identify and implement all possible means and measures for improving the quality and reliability of our verification results and conclusions, while facing all current Safeguards challenges. We identify these challenges and we analyse the options by which we can address them.

It goes without saying that in this review of the IETS document, we shall take the Member States comments on board. Following our preliminary internal study and analysis in the coming months, we shall be in a position to engage in further dialogue with Member States and stakeholders in the appropriate fora.

This is how we intend to go ahead in adapting the Euratom safeguards to continue to deliver on our Euratom Treaty mandate – on the basis of an unchanged Treaty but under constantly changing circumstances.

[Challenges for the future]

Adapting to change does not only mean adapting to a change of the wider political circumstances. For us, it also means focusing on our internal demographics and trying to assure continuity and keeping up our specialized knowledge in view of a strong evolution of our personnel: In other words: In some years time, we will have to deliver on our mandate with what I would dare to call "a new generation of nuclear inspectors". And, as you would expect, we are already about to select the officials for this highly responsible set of tasks.

A number of fascinating professional challenges await this new generation of officials: They will be involved into a wide variety of tasks many of which are either new or unprecedented in type and scale of the operation to be undertaken:

- the defueling of German reactors being phased out of service with the eventual transfers of all spent fuel into CASTOR containers;
- the expansion of Remote Data Transmission in order to save resources invested in our costly on-site verifications;
- addressing the new challenges arising from the construction of new types of facilities, such as reactors of new design or else the first underground geological repositories and related encapsulation plants for spent fuel.

[Cooperation with our partners]

Cooperation with the IAEA

We are closely cooperating **with the IAEA** as regards safeguards within EU borders, and we fully support the IAEA in the process of implementing their State Level Concept.

The IAEA is rightly attempting to demonstrate that every State is treated on an equal footing, taking into account State-specific factors. We are very pleased to

note that the IAEA increasingly recognizes the opportunities that cooperation with EURATOM can offer.

In terms of practical cooperation with the IAEA, we have established, inter alia, a prioritised list of Facility Attachments that need to be drafted and we implement a similar campaign with respect to the Commission Decisions on Particular Safeguards Provisions that need to be updated.

We have also advanced on further practical joint actions with the IAEA, such as:

- Joint Use of Equipment;

- Remote Data Transmission; and

- Joint training of inspectors,

just to name some of the most important ones.

Together with the Commission's Joint Research Centre, we hold meetings with the IAEA to further improve the coordination in the field of safeguards equipment and we attempt to improve the processes of developing new safeguards equipment. Here also the Member States Support Programmes to the IAEA play a crucial role for the entire safeguards community, including Euratom.

In concluding, I think it is only fair to say that, in spite of our diverging mandates, we have made good progress in our cooperation with the IAEA and that is how it should be.

Cooperation with the JRC

It is, of course, not only important to cooperate with other international players but certainly at least as important to also cooperate with your partners inside your own institution. In this context, we have been very pleased to cooperate with the Commission's Joint Research Centre, or in today`s politically correct language, with the Commission's "in-house science and knowledge management service" and in line with our cooperation agreement.

The JRC has strongly supported us with a view to the on-site laboratories but has also provided us with significant technology support. For the future, we would very much like to further expand our cooperation with the JRC in the fields of "commercial off the shelf" as well as data analysis.

Cooperation with ESARDA

We have to prove that our resources are well spent and could not be spent any better.

This will require that in doing our job we use the most advanced equipment available which is based on the latest technology available. And this is where you, the Safeguards R&D community, come into play.

The EU R&D has to anticipate and address the future needs of international safeguards. This is done by extrapolating and expanding on the evolution of safeguards from a material and technology-based control system to one that has a lot more information to acquire and process. This will require substantial investment in R&D and novel technologies.

The integration of innovative technologies in modern Euratom approaches has multiple aims, namely the creation of improved tools for more effective and efficient inspections, reduction of inspectors' dose uptakes and important financial savings.

Amongst the innovative technologies for safeguards, I would wish to highlight:

- Tomographic and radiographic imaging techniques
- Unattended monitoring systems with Remote Data Transmission
- Next Generation Surveillance Systems (NGSS)
- Electronic Seals
- Nuclear forensic methods.

In this regard, the various thematic working groups of ESARDA:

- are providing substantial input and expertise in R&D domains that are crucial for safeguards;

- are paving the way for new solutions and cutting-edge technologies;

- are enriching the toolbox available to Euratom for the fulfilment of its objectives.

Along with the Joint Research Centre, ESARDA is a key partner for the Commission who helps to broaden our R&D horizon.

All of your ESARDA members: Operators, national regulators, the academic and commercial sector, they all are called upon to contribute from their own perspective and with their specific knowledge and abilities to the provision of new solutions addressing modern safeguards challenges.

Euratom is pleased to benefit from its presence at the ESARDA board and from its participation in all ESARDA working groups, witnessing the development of new concepts and techniques that will shape tomorrow's safeguards.

We are very glad to see ESARDA expanding, attracting new membership, extending their outreach to universities and to the younger generation and also opening up channels with the IAEA.

As we have underlined on the occasion of previous ESARDA Conferences: “We need ingenuity, innovation and technological advancement. For that, we strongly count on the contribution of ESARDA.”

Next year we shall be celebrating the 40th ESARDA Annual Symposium. We shall be very privileged and happy to host that event in Luxembourg and you can already earmark 15-17 May 2018 as a date for this event.

In this spirit, let me thank you very much, more generally, for the past years of fruitful cooperation and, much more specifically, let me thank you very much for your attention for the past minutes in listening to this speech!

Development and updating of State-level safeguards approaches: Experience and lessons learned

Therese Renis, Van Zyl de Villiers, Zbigniew Radecki, Edgar W Vela Espinoza

Department of Safeguards, International Atomic Energy Agency
Vienna International Centre, P O Box 100,
A-1400 Vienna, Austria

Abstract:

In order to maintain effective and efficient safeguards over time, the IAEA continues to address new challenges, taking into account experience gained from previous safeguards implementation and taking advantage of new techniques and technologies. In recent years the IAEA has continued to enhance the effectiveness and efficiency of safeguards by making greater use of its ability to consider a State's nuclear and nuclear-related activities and capabilities as a whole, within the scope of the State's safeguards agreement. In doing so, more systematic consideration has been given to, and better use made of, State-specific factors in updating and developing State-level safeguards approaches (SLAs) for all States with safeguards agreements, beginning with the updating of SLAs for States under integrated safeguards. By the end of April 2017, the IAEA has updated SLAs for 53 States (and Taiwan, China) with comprehensive safeguards agreements and additional protocols in force, for which the broader conclusion[1] had been drawn, and for twelve other States. This process has been carried out in close consultation with the States, particularly on the implementation of in-field measures. In order to ensure that SLAs are developed in a consistent and non-discriminatory manner the IAEA uses uniform processes and well-defined procedures to guide the development and implementation of the SLAs. Based on the experience gained, there has been further development and documentation of internal procedures, guidance and tools, and adjustments to the training programme. This paper provides an overview of the IAEA's experience to date in the updating of SLAs and the further development of internal guidance and procedures based on lessons learned.

Keywords: State-level safeguards approach; acquisition path analysis; State-specific factors.

1. Introduction

International nuclear safeguards are implemented by the International Atomic Energy Agency (IAEA) on the basis of safeguards agreements between the State or States concerned and the IAEA.[2] For many years after 1972 when the IAEA first started implementing safeguards pursuant to comprehensive safeguards agreements (CSAs), safeguards activities were primarily focused on nuclear material and facilities declared by States to provide assurances that there was no diversion of declared nuclear material from peaceful nuclear activities.

In the early 1990s, the IAEA embarked on a series of efforts to strengthen the effectiveness and efficiency of safeguards to provide for IAEA verification of the correctness and completeness of the declarations of States with CSAs, so that there is credible assurance of the non-diversion of nuclear material from declared activities and of the absence of undeclared nuclear material and activities in the State. For States with a CSA and an additional protocol (AP) to that agreement in force, when the IAEA has carried out sufficient activities and conducted comprehensive State evaluation based on all safeguards relevant information available about the State's nuclear and nuclear-related activities and has found no indications of diversion of declared nuclear material and no undeclared nuclear material or activities in a State, the IAEA can draw the broader conclusion that all nuclear material in a State remained in peaceful activities. Beginning in 2001, the IAEA has developed State-level safeguards approaches (SLAs) for those States, then referred to as 'integrated safeguards' approaches for States, based on an 'optimized' combination of measures available under the CSA and AP for the State.

Those early approaches were, for the most part, based on facility-specific 'model' integrated safeguards approaches.

The term 'State-level concept' was first introduced in the Safeguards Implementation Report (SIR) to the IAEA Board of Governors for 2004 to describe safeguards implementation that is based on SLAs developed using safeguards objectives common to all States with CSAs and taking State-specific factors into account. As the SIR for 2004 noted, the State-level concept was being implemented for States with integrated safeguards and would be extended to all other States with CSAs.

In recent years, the IAEA has given more systematic consideration to, and made better use of, State-specific factors when updating and developing SLAs. For States with CSAs in force with the IAEA, it does so by analysing all technically plausible paths by which a State could pursue the acquisition of nuclear material for the development of a nuclear weapon or other nuclear explosive device; this process is known as 'acquisition path analysis' (APA). The IAEA then establishes and prioritises technical objectives and identifies safeguards measures for addressing those technical objectives. These are all done in consideration of State-specific factors. An SLA is developed in close consultation with State and regional authorities, particularly with regard to the means of implementing in-field verification activities.

Using this process, since 2014 SLAs have been updated for 53 States (and Taiwan, China) that were under 'integrated safeguards' and new SLAs are being progressively developed for other States with safeguards agreements in force. SLAs have been developed for twelve other States as of the end of April 2017. During the process of updating and developing the SLAs, experience gained has been used to refine the associated processes, procedures and tools to ensure consistency and non-discrimination in safeguards implementation. This paper elaborates on that experience and how it has been used to improve the processes and guidance.

2. Process of developing State-level safeguards approaches

An SLA is a customized approach to implementing safeguards for an individual State. It consists of technical objectives as well as applicable safeguards measures to achieve those objectives.

SLAs are developed by State evaluation groups (SEGs) that have been established for each State. SEGs consist of staff members with the appropriate expertise to evaluate all safeguards relevant information, typically safeguards inspectors and safeguards analysts. The SEGs conduct acquisition path analysis and develop SLAs for States with a CSA using internal guidance documents. They also use collaborative analysis techniques and tools.

The process of developing an SLA begins with the consolidation of all safeguards relevant information about the State available to the IAEA. Using that information, the SEG identifies the technically possible paths by which the State could acquire nuclear material suitable for a nuclear weapon or other nuclear explosive device. This is followed by a detailed analysis of the strategies that could be used by the State and the time needed to accomplish each step of the possible acquisition paths. Once those steps have been analysed, an overall assessment is made of the approximate amount of time that it might take to accomplish each possible path, specifically to determine which paths would be technically plausible within five years. [1]

Technical objectives are then established to fulfil the generic safeguards objectives for the State. Technical objectives are established for the detection of each step in the technically plausible acquisition paths. The technical objectives are prioritized based on the assessment of acquisition path steps to determine where to most effectively apply IAEA safeguards resources for the State. Next, safeguards measures are identified for each technical objective. Identifying more than one safeguards measure, if possible, provides flexibility and options thereby allowing safeguards implementation to be less predictable. The frequency and intensity of the safeguards activities are determined based on the priority of the technical objectives and in consideration of State-specific factors and key assessments made during acquisition path analysis.

In conducting acquisition path analysis and developing SLAs, more systematic consideration has been given to and better use made of State-specific factors. Those State-specific factors are:

i. The type of safeguards agreement in force for the State and the nature of the safeguards conclusion drawn by the IAEA;
ii. The nuclear fuel cycle and related technical capabilities of the State;
iii. The technical capabilities of the State or regional system of accounting for and control of nuclear material (SSAC/RSAC);
iv. The ability of the IAEA to implement certain safeguards measures in the State;
v. The nature and scope of cooperation between the State and the IAEA in the implementation of safeguards; and
vi. The IAEA's experience in implementing safeguards in the State.

State-specific factors (i) and (ii) are used during acquisition path analysis and all factors are used at various stages of developing SLAs.

Senior inspectors and Section Heads guide the work of the SEGs and review their progress. In order to ensure consistency in the processes and non-discrimination in the results, all SLAs undergo review by an internal committee and are subject to final approval for implementation by the Deputy Director General, Head of the Department of Safeguards.

During the updating of the SLAs, Operations Divisions consult with State and regional authorities, particularly with regard to possible modifications to in-field verification measures and the practical means for implementing them. In cases when there were no proposed changes to in-field measures, States are informed of this.

3. Experience and lessons learned

The Department has systematically recorded feedback from the SEGs on their insights and experience in updating and developing SLAs. The following outlines that experience and the lessons learned to date.

Overall, the process of updating SLAs has been carried out using a structured and analytical approach to ensure the effectiveness of safeguards for the State. Through the process of conducting more in-depth acquisition path analysis, SEG members gained a greater understanding of the nuclear programme and nuclear-related capabilities of the States for which they are responsible. In many cases, they needed to supplement their knowledge of the State's nuclear fuel cycle-related capabilities, including historical capabilities and current research and development activities. They did this by searching through safeguards information archives and previous versions of State evaluation reports, by conducting targeted searches for a wider range of information about a State's industrial infrastructure and by conducting specific in-field activities.

SEGs recognized that - in addition to State evaluation reports (SERs), SLAs and annual implementation plans as key internal documents - lower level information, results of analyses and key assessments had to be documented. This has led to more high quality and structured documentation to support the SLAs. This also contributes to the capture and management of related knowledge that will facilitate future analyses and support future country officers and SEG members in understanding the safeguards relevant information about a State.

Many SEGs identified the challenges in managing large amounts of safeguards relevant information and the need to organize it well. Different ways of storing the data were explored, from organizing it by facility and fuel cycle stage in a Wiki format to condensing it into a more meaningful and 'digestible' format. It was recognized that additional tools may be needed to facilitate the organization of and efficient access to the information.

The SEGs appreciated the opportunity to apply critical thinking. In-depth discussions in the SEGs created a unified and soundly based common understanding of the safeguards relevant information about the State. The analytical processes have also led to more informed, knowledgeable country officers and inspectors who more fully understand the objectives of their safeguards activities.

In approaching the task of updating an SLA, many SEGs sought the advice of country officers and senior inspectors who had already undertaken such an exercise for other States. They also called upon experts in selected nuclear fuel cycle technologies to assist in their assessments. In some cases, SEGs working on SLAs for States with a similar level of nuclear activities worked together, particularly when tackling some challenging aspects of the analysis. The sharing of experiences and good practices among SEGs, senior inspectors and drafters of related guidance documents led to streamlining and greater consistency of the processes.

Although acquisition path analysis has been a key aspect of the State evaluation process, experience has shown that a much more detailed and structured analysis was needed for developing an SLA. Conducting the initial in-depth acquisition path analysis, particularly for States with significant nuclear activities has often been a lengthy process. The APA guidance document has been updated based on early experience, and supplemental templates and examples were developed which have facilitated the analyses. However, there is a need for the development of software tools to assist in conducting APA and documenting the results. APAs will need to be updated periodically, as triggered by time or new information. However it is expected that with the initial good documentation of the analyses, the updating will require much less time and will be done as part of the periodic State evaluation process.

In addition, many SEGs identified the need for further assistance in assessing the capabilities of the State and the time required for the State to complete an acquisition path step, particularly with regard to development of new nuclear fuel cycle capabilities.

In describing and assessing the scenarios for diversion of declared nuclear material and the misuse of facilities, SEGs developed a clearer insight into specific safeguards activities that should be conducted in the field, particularly with respect to visual observation and design information verification.

Because of the articulation and prioritization of technical objectives, headquarters activities (such as collection and analysis of open source information) were better targeted at areas of priority for a particular State. This focus has also led to more effective safeguards approaches, shifting activities to where they were most needed to address priority technical objectives, while avoiding conducting more activities than needed to address lower priority objectives.

When determining the frequency and intensity of safeguards activities in the field, many SEGs were hesitant to make significant changes based on APA assessments. SEGs tended to make conservative assessments that did not substantially deviate from current safeguards practices. Nevertheless, the SEGs came to better understand why each activity is performed and how it connects to the technical objectives. As experience is gained, additional guidance will be needed on setting verification goals based on the prioritization of technical objectives and the time required to complete any acquisition path.

For States with a sizable nuclear fuel cycle, the updating of an SLA is being done in phases. Additional safeguards ‘sub-approaches’ addressing aspects of a State’s nuclear fuel cycle will need to be updated over the next few years to reflect the objectives and verification goals set at the State level.

4. Development of internal processes, procedures and tools

Throughout the process of updating and developing SLAs, SEGs were asked to give feedback in order for the Department to develop and refine its processes, procedures and tools, as needed. The following summarizes some of the key areas of improvement.

4.1 Update guidance documents for conducting acquisition path analysis and developing an SLA for a State with a CSA

The Department conducted an intensive series of individual meetings with SEGs to gather practical feedback based on their experience while conducting APAs and developing SLAs. Such feedback contributed to a better understanding of areas in the existing guidance documents that needed further elaboration to be more helpful. Revision of the guidance has provided clarification and streamlining of the processes. Some of the key areas of improvement include: clarification of terminology, how to document key assessments, examples of the use of State-specific factors and better guidance on

establishing and prioritizing technical objectives. The updating included the development of more figures, templates and example cases to facilitate this understanding. Complementing the updated guidance documents, fully developed APA and SLA examples for fictitious States with different levels of nuclear development are being developed.

4.2 Internal processes for review and approval of APAs and SLAs

A well-structured yet flexible process for review and approval of APAs and SLAs has been documented. In particular, the notion of a 'peer review' of draft APA results has been adopted. Moreover, additional clarification on the available assistance and expert advice within the Department, streamlined requirements for the documentation of APA results and conditions for revising and updating APAs and SLAs have been provided. The process for the review and clearance of SLAs, including within a Division, by a departmental committee and by the Head of the Department have been documented. All these are being used in practice and incorporated into updated APA and SLA guidance documents. Further refinement and clarification will be provided as more experience is gained.

4.3 Means for SEGs to exchange experience and tips

The following practices have been adopted to share experience. SEGs for States with similar nuclear fuel cycles have been sharing experience with each other through seminars, meetings and informal exchanges. Some staff members that participate in several SEGs are bringing the experience gained to other SEGs. Senior inspectors and country officers are also sharing experience and advising SEGs.

At the departmental level, lessons learned are distributed in the form of minutes following the departmental review committee meetings and incorporated, whenever deemed appropriate, into the revised guidance documents. In addition, the establishment of an internal website to share these lessons is under consideration.

4.4 Software tools for developing, documenting and visualizing APAs and SLAs

APA involves technical assessments of a State's nuclear fuel cycle related capabilities; software can help to record, analyse, report and visualize information in variety of formats to support those assessments. Prototypes of the APA methodologies and software have been developed by three Member State support programmes. Elements of those technical methodologies are being considered for introduction into software that is being developed in-house.

As part of the Modernization of Safeguards Information Technology (MOSAIC) project, software is also under development to use the elements of SLAs to support and integrate the safeguards processes for the planning, implementation and evaluation of safeguards verification activities.

4.5 Document guidelines for SLA-related consultations with State (and regional) authorities

The IAEA must protect sensitive information and methods to maintain the independence of its conclusions. While the consultation process facilitates the exchange of information with the State (and regional) authorities on the implementation of in-field safeguards activities, it has to be conducted in a way that ensures that sensitive information is not disclosed.

Guidance documentation was developed to ensure consistency in aspects of SLA-related consultations. The guidance clarifies the scope and subject of consultations, what information can be shared and discussed and what should be discussed with the State cautiously in order not to reveal information that might undermine safeguards effectiveness. It also addresses the means of official communications during consultations.

The guidance recognizes the need for the IAEA and State (and regional) authorities to have a clear understanding of how in-field verification activities will be conducted. Therefore consultations may include the joint development of detailed implementation procedures.

4.6 Use of analytical techniques during the process of APA and developing SLAs.

The departmental training programme, for many years, has included dedicated training on a variety of analytical techniques that contribute to conducting APA and developing SLAs. There is an internal reference manual on structured analytical techniques and the use of these techniques has been elaborated in the updated APA and SLA guidance documents. Facilitators in the use of analytical techniques have been trained and, upon the request of SEGs, are available to assist in the use of the techniques when analysing acquisition paths and developing an SLA.

5. Summary

The IAEA Department of Safeguards completed the updating of SLAs for 53 States (and for Taiwan, China) under integrated safeguards by the end of 2016 and SLAs had been developed for twelve other States by the end of April 2017.

Experience gained in conducting acquisition path analysis and developing SLAs has been used to update and elaborate the guidance documents and to streamline and improve internal processes and procedures accordingly. This has led to increased consistency, uniformity and objectivity of the SLAs.

While there have not been significant changes to safeguards approaches or significant cost savings, the process has led to the implementation of modified approaches to conducting some in-field activities. Through the process of conducting in-depth acquisition path analysis, SEG members have gained greater understanding of the nuclear programme and nuclear-related capabilities of the States for which they are responsible. Because of the need to document the analyses and key assessments that led to the SLAs, there is more high quality and structured documentation to support those approaches and to contribute to the capture and management of related knowledge that will facilitate future analyses and support future country officers and SEG members in understanding the safeguards relevant information about a State. The analytical processes have also led to more informed, knowledgeable country officers and inspectors who more fully understand the objectives of their safeguards activities.

Because of the articulation and prioritization of technical objectives, headquarters activities, such as collection and analysis of open source information, are more targeted at areas of priority for a particular State. This focus has also led to greater effectiveness of safeguards approaches and optimization with regard to shifting activities where most needed to address priority technical objectives and while avoiding conducting more activities than needed to address other objectives. In some cases, SLAs put more emphasis on some technical objectives while reducing activities for lower priority technical objectives.

The IAEA will continue to progressively develop SLAs for other States, in close cooperation with State and regional authorities. In order to do so, it will continue to develop and update the guidance relevant to States with item-specific or voluntary offer safeguards agreements. SLAs will continue to be updated periodically, or as necessary based on new information. State-specific annual implementation plans will be developed based on the SLAs.

The guidance and software needed to conduct these processes in an efficient and consistent manner will continue to be enhanced. While the development of some software tools has begun, further development is needed to record and assist in documenting the APA, record the technical objectives of the SLA, assist in developing and recording plans for safeguards activities in an annual implementation plan for each State based on the SLA, and tracking the implementation of activities that will provide the basis for the evaluation of safeguards effectiveness based on achievement of technical objectives.

Guidance is also being developed on the assessment of a State’s ability to conduct acquisition path steps, particularly with regard to development of new nuclear fuel cycle capabilities.

The IAEA continues to further enhance the effectiveness and efficiency of safeguards implementation by making better use of its ability to consider the State’s nuclear and nuclear-related activities and capabilities as a whole in developing a customized State-level safeguards approach for each State,

within the scope of the State's safeguards agreement. In doing so, the emphasis continues to be on the attainment of safeguards objectives, with consideration of all safeguards relevant information and of State-specific factors. This allows the IAEA to concentrate its efforts on areas of greater safeguards significance and implement safeguards in a manner that is more responsive to changing circumstances. As the processes, guidance documents and tools evolve, SLAs will continue to be updated accordingly.

As requested by the Safeguards resolution from the General Conference of the IAEA during its sixtieth session in September 2016 [2], the Director General will report to the Board of Governors about lessons learned and experience gained in SLAs for States under integrated safeguards after SLAs have been updated and are being implemented for all such States.

[1] *That all nuclear material remained in peaceful nuclear activities.*
[2] *Some agreements include two or more States parties and/or third parties, such as their regional safeguards organizations.*

References

[1] Renis T, Yudin Y, Hori M; *Conducting Acquisition Path Analysis for Developing a State-level Safeguards Approach*; Proceedings of the INMM 2014 Annual Meeting
[2] GC(60)/RES/13, *Strengthening the effectiveness and improving the efficiency of Agency* Safeguards; GC(60)/RES/DEC (2016). *Resolutions and other Decisions of the General Conference; IAEA*

Session 01

Implementation of Safeguards

Safeguards in Germany – Challenges and Perspectives

K. van Bevern[1], M. Hahn[2], A. Jussofie[3]

[1]VGB PowerTech e.V., Deilbachtal 173, 45257 Essen, Germany
[2]PreussenElektra Gemeinschaftskernkraftwerk Grohnde, 31860 Emmerthal, Germany
[3]Gesellschaft für Nuklear-Service mbH, Frohnhauser Str. 67, 45127 Essen, Germany

Abstract:
Germany's current situation of nuclear power supply and spent fuel management derives from the decision that is now embodied in the German legislation: 13th Amendment of the Atomic Energy Act in response to Japan's Fukushima disaster in 2011. It included Germany's decision to phase out nuclear energy by the end of 2022 at the latest. It is foreseen that all spent fuel assemblies will have been loaded into casks and transferred to spent fuel storage facilities (SFSF) by the end of 2027. The defueling of NPP generates an extra workload for operators and the inspectorates of IAEA and EURATOM especially due to the temporary increase of cask loadings per year. To tackle this challenge different approaches and techniques had been developed and are now in use e.g. "cask sealing by operators" in the absence of EURATOM and IAEA inspectors, but under surveillance and by using an EOSS-seal interface, verification by means of "Digital Cherenkov Viewing Device" and developing a "Safeguards-approach for a newly developed quiver for damaged fuel rods". Moreover, the implementation of remote data transmission (RDT) in all SFSF is in progress after successful completion of the pilot project for RDT-implementation at Ahaus. Furthermore, two pilot projects for RDT are running in reactors.
A new challenge is based on the last revision of the Atomic Energy Act at the end of 2016, which leads to a reorganization of nuclear waste management in Germany. The responsibility of all interim storage facilities for low, medium and high radioactive waste will be transferred from NPP-operators to the state. With the future separation of responsibilities for interims storages between State and NPP-operators new questions like "How to manage Safeguards-sites, where the SFSF-related MBA close to the reactor will not belong to the NPP-operator but to another (state-owned) company" have to be answered.
The presentation will show an overview of challenges in the last years and give future perspectives.

Keywords: Germany, RDT, SFSF, EOSS, Digital Cherenkov Viewing Device

1. Current Situation in Germany

Germany's current situation of nuclear power supply and spent fuel management derives from the nuclear energy phase out decision settled through German legislation in form of 13th amendment of the Atomic Energy Act in 2011. Germany's decision to phase out nuclear energy until end of 2022 led to an enforced shut-down of eight from a total of 17 nuclear power plants. This shift in German´s energy policy is a challenge for Safeguards. The defueling of nuclear power plants generates an extra workload for the operators and the two inspectorates of IAEA and Euratom due to the temporary increase of cask loadings per year.

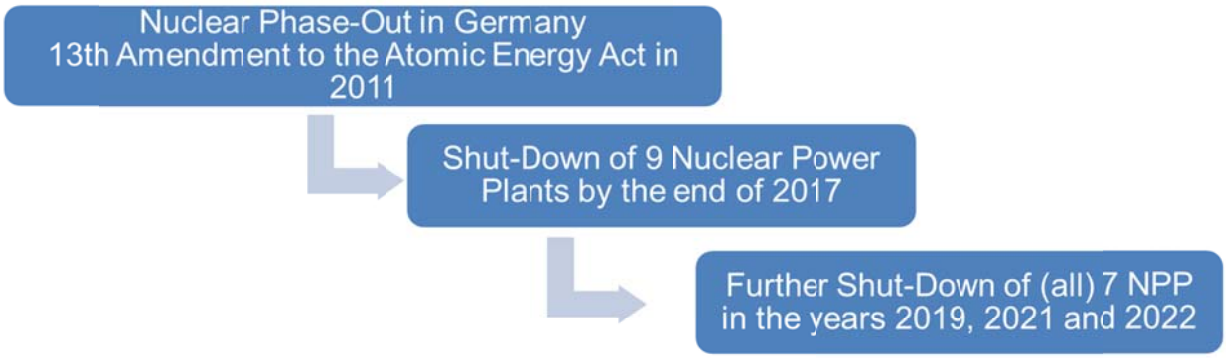

Figure 1: Nuclear Phase-Out in Germany

In order to tackle this challenge, an approach is the cask sealing by the operator in the absence of Euratom and IAEA. An EOSS seal interface was developed to guide the operator through the sealing procedure and confirm its successful termination as a saveable message. According to the act of site selection, the operation of the repository might start in 2055 and cease in 2095. Therefore, an extension of the dry interim storage period that is currently limited to 40 years will become necessary. This timeline emphasizes the importance of dry interim storage for Spent Fuel Management and the need for long-term reliable unattended Safeguards measures in order to maintain continuity of knowledge. Remote transmission of Safeguards-data from the dry storage facilities in Germany to Euratom and IAEA can be regarded as a reasonable step towards this goal.

2. Use and Application of New Techniques and Procedures

Approaches to tackle the challenging situation in Germany are mainly based on four different measures. Apart from the NPP specific information, which is given to Euratom by the operator, VGB as an association for the German nuclear power plant operators regularly hands in the planning for the future cask loading campaigns to Euratom. The planning is provided on a half year basis and contains the loading campaigns for all German NPPs in total with a time horizon of approx. 3 years. These planning data shall support Euratom with their preparation on inspection planning, especially during the current situation of high number of cask loading campaigns per year. Accordingly, the number of cask loading planned for 2017 is higher than 100 cask loadings.

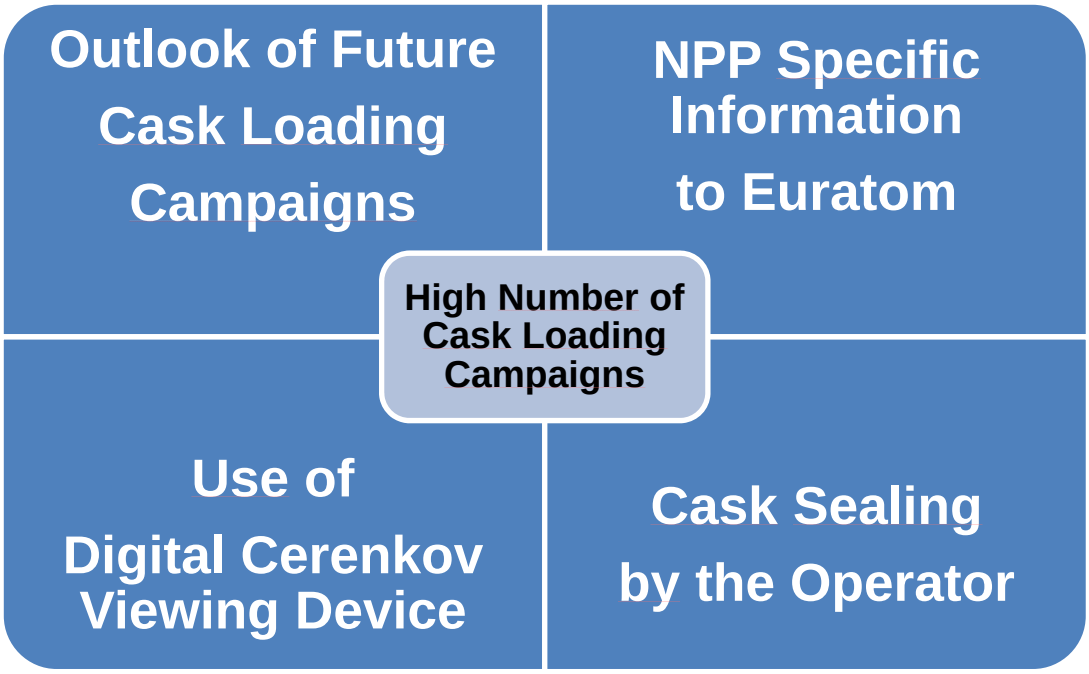

Figure 2: Approaches to tackle high number of cask loading campaigns

Sealing by the operator

Sealing by the operator is another opportunity to reduce operators´ and inspectors´ effort during long lasting loading campaigns. Sealing of casks by the operators in the absence of Euratom and IAEA inspectors requires the acknowledgment of successful sealing execution as a printable and saveable message by EOSS Enhanced Seal Interface (ESI) connected to the electronic EOSS-seal linked to the surveillance camera.

In June 2014 a pilot trial at NPP Unterweser was executed and sealing by the operator using the new developed ESI was tested. Before the first cask had been loaded operators employees were familiarized with the sealing process and trained by Euratom in the correct setting of seals and the use of ESI. After successful training the first cask sealing was done by the operator in the presence of Euratom Inspector. From this point of time operators were well prepared for the following sealing processes in the absence of Euratom.

The figure 3 shows a part of the equipment, which is used during the sealing procedure and transport: EOSS, ESI, cables and a device -developed by the operator - to store EOSS safely at the cask during the transport to the SFSF.

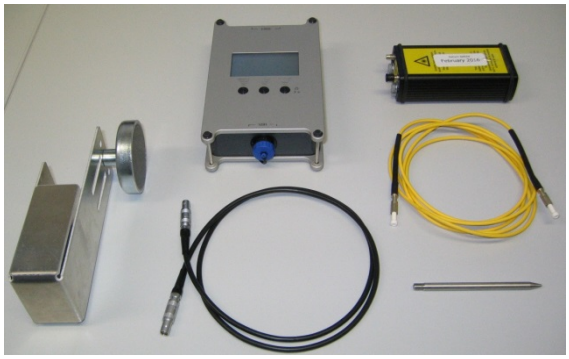

Figure 3: Sealing Equipment - Source: NPP Unterweser, PreussenElektra

Cask sealing is carried out by the operators in the reactor but its verification and seal replacement is done by Euratom/IAEA in the SFSF. It is important that the verification of the seals is done if a row of cask inside the SFSF has been filled completely. If there is a big time-delay of verification, it is possible that due to placements of subsequent casks the possibility for verification is no longer given.

Digital Cerenkov Viewing Device (DCVD)

DCVD first application had been taken place at NPP Biblis and Unterweser. Results of these first applications showed that through the use of DCVD inspections can be planned and measurements executed time-flexible and (far) before a cask loading campaign starts. This fact made the new technique attractive for its application in the field. Especially for those NPP who faces long loading campaigns consisting of more than five casks within a loading campaign. In case of shorter campaigns the use of DCVD is not efficient due to the high installation and verification time. This applies in particular NPP which are still in operation.

Euratoms´ requirement for usage of this verification method includes that there is no shifting of spent fuel in the pool between DCVD-measuring and the beginning of the cask loading campaign. After the successful appliance of DCVD at NPP Biblis and Unterweser further German operators are willing to or have already applied this technique.

Digital Cerenkov Viewing Device (DCVD) and cask-sealing by the operator

The following conclusions can be drawn from the simultaneous application of the two new techniques and methods:

Application of DCVD and cask-sealing by the operator run smoothly. However, due to the fact that DCVD-measurements of the whole spent fuel pool last up to 5 days in a week, the measurement time per day is bound to the maximum working hours of the NPP employees e.g. platform driver.

Furthermore, the operators observed that cooperation with Euratom and IAEA is result-oriented and efficient. The work is most efficient if both, inspectors as well as technicians of the team of IAEA and Euratom are experienced and well trained.

The usage of DCVD in combination with cask-sealing by the operator leads to the benefit that the presence of both - inspectors of IAEA and Euratom - during the loading campaign is not necessary any longer. But verification of the cask in the SFSF is required, at the latest when a row in the SFSF is filled and the next casks are placed in front of the complete row. Consequently, a verification or an exchange of seals is not any longer possible or leads to a higher radiation exposure of the inspectors involved.

Defueling the spent fuel pool

As already described, the aim of the operators of NPP in decommissioning is to get the reactor and the spent fuel pool free from spent fuel as soon as possible. The parallel application of both, DCVD and cask-sealing by the operators, guaranteed time flexibility for the long-term cask loading campaigns with minor communication effort for both, the inspectorates and the operators.

Another challenge is to handle the broad range of fuel rods, which exist for example in the form of irradiated or non-irradiated fuel, test rods, broken rods, single pellets or smaller pieces. In cooperation with the German nuclear power plant operators GNS developed a technical solution in order to be able to store such fuel in CASTOR® casks: a quiver for damaged fuel rods.

Through the VGB-Working Group “Safeguards” both German power plant operators and GNS involved Euratom at an early phase in the quiver development. This enabled Euratom to give their opinion and come forward with their ideas on how a quiver could be verified and to develop a Safeguards concept. The cold trial run of the quiver was done in April 2017. The first hot dispatch of a PWR-quiver is planned for the second half of 2018. At the moment different verification methods (DCVD and tomography) are being tested in the field by IAEA and Euratom.

3. Remote Data Transmission

Remote Data Transmission (RDT) at SFSF

According to the new Site Selection Act from July 2013, the final decision for a repository site has to be made in the end of 2031. Based on this milestone initial operation of the repository may be expected in the 2050ies due to the process of licensing and the construction phase. This timeline emphasizes the importance of dry interim storage for SF management and the need for long-term reliable unattended Safeguards measures in order to maintain continuity of knowledge.
Remote transmission of Safeguards data from SFSF in Germany to Euratom and IAEA can be regarded as a reasonable step towards this goal since RDT in dry SFSF promises a fast response to the functional loss of permanently installed Safeguards equipment consisting of seals proving the integrity of spent fuel stored in casks and cameras for optical surveillance of cask and consequently spent fuel cask movements. RDT contributes to continuity of knowledge, since failures of the SF-equipment are not currently returned to Euratom and IAEA.

For the German operators, it is important that RDT has no impact on plant operation and that the transmission of operating data and the monitoring of personnel and storage operation are excluded. The easiest way to achieve this is a communication line that is completely isolated from the operators’ own data network. Furthermore it is essential for the operator to differentiate between state of health data (SoH) for monitoring of surveillance equipment and functional states of electronic seals on one hand and image data on the other hand. Images of the material balance area may affect the physical protection of the storage or economic interests. Efficiency gains under IS substantially depend on the condition that no re-verification of the nuclear inventory will be required. Therefore, remote transmission of SoH during the period between inspection notification and inspection execution is also in the operators` interest. Compared to SoH, the transmission of sensitive image data needs higher security requirements for the RDT system in order to counteract the growing threat of targeted attacks to spy and manipulate data. The image transmission with a delay of 24 h is important for the operators enabling the operators to be on the same level of information as Euratom and IAEA. On the other hand a delay of 24 h represents no impairment in the routine image transmission for Euratom.

In preparation of the RDT-implementation in all German interim dry SFSF, a full-functional solution was established by performing a field test in 2012/2013 as a task of the German support programme to the IAEA. The RDT system provided a complete and reliable data transmission applicable under daily use conditions. Interruptions of the RDT-operation for several days remained without consequences due to the local storage capacity of the RDT system and its subsequent automatic synchronization. From the operators‘ point of view, it is essential that the technical solution for RDT meets the German security requirements for sensitive data. Through the application of security technologies certified by the Federal Office for Information Security, the operators‘ main concern of a risk of an unauthorized access to safeguards data was taken into account.

During the early phase of RDT implementation Federal Ministry for the Environment, Nature Conservation, Building and Nuclear Safety approved RDT implementation in all German dry SFSF on the federal level. In the next step the Federal Ministry of Economics and Energy (BMWi) instructed the Federal state authorities to support the implementation of RDT in German interim dry SFSF officially by a letter on 28 May 2014 and also informed the German operators on the upcoming RDT implementation in their dry SFSFs in the mid of June 2014. The first RDT that has then been in operation was limited to the transmission of EOSS data from the research reactor FRM II in Munich, where no camera is installed, to Euratom/IAEA. Due to the deliveries of HEU, the uranium usually exceeds the significant amount of 25 kg so that a monthly inspection of nuclear material has been mandatory. Upon the RDT-implementation, the number of inspections was halved thus enabling a significant reduction of man-days on-site.
The RDT system of the interim storage facility “Zwischenlager Nord” (ZLN) in Rubenow was already installed in the mid of September 2014. Currently, RDT implementation phase is still going on. Up to

date RDT-Implementation in eight SFSF is finalized. It is expected that further the RDT implementation of all German dry SFSFs will be finished in 2017 or 2018 at the latest.

Date of Implementation	SFSF
09/2012-01-2013	Ahaus
10/2014	Zwischenlager Nord
03/2015	Biblis
06/2015	Krümmel
10-11/2015	Emsland
10-11/2015	Gundremmingen
planned in 2017	Brunsbüttel
planned in 2017	Philippsburg
01/2016	Neckarwestheim
04/2016	Gorleben
planned in 2017	Brokdorf
planned in 2017	Grafenrheinfeld
planned in 2017	Grohnde
planned in 2017	Isar
planned in 2017	Unterweser

Table 1: Overview of RDT-Implementation in Germany SFSF

RDT at Nuclear Power Plants

In contrast to the interim dry SFSF, Safeguards by Design with regard to RDT has not been taken into account in the case of NPPs in Germany. Therefore the situation for RDT implementation in German reactors is much more difficult compared to dry SFSF, especially because of the higher protection requirements to data and IT-systems in NPPs. Besides that, the availability of an isolated communication line is not usual in a reactor compartment as it is the case in the SFSF. Last but not least there is no long term perspective for RDT from reactors, since the shut-down of the last German reactor is expected in 2022 at the latest.

Due to the fact that EURATOM aimed at performing a pilot field trial for RDT from a German reactor, the German operators offered two NPPs to carry out pilot projects. As first pilot plant NPP Neckarwestheim II was selected as a NPP in operation, as second pilot plant NPP Kruemmel was chosen as a NPP that is currently being shut down.

For Remote Data Connection the system already installed in the SFSF are used:

NPP (Containment) → SFSF → Euratom → IAEA

RDT was already implemented at NPP Neckarwestheim in July 2016. The data connection to Euratom Headquarter showed no problems so far. In September 2016, the RDT implementation started at NPP Kruemmel, but the installation of the camera system has been planned for the end of April 2017.

In both cases, RDT at SFSF and NPPs the language of the contract between Euratom and the operator is still an issue, because from the operators' point of view the contract has to be written in the language of the respective member state.

4. Challenges and Perspective

In Germany, new nuclear acts have or will be entered into force. The act on the transfer of disposal tasks together with the act on the reorganization of responsibility in nuclear waste management, regulate the future financing and responsibility of decommissioning, waste management and final disposal in Germany. All SFSF at the NPP sites including the two central storages located at Gorleben and Ahaus will be transferred from the operator to a state owned company at the latest on 1st January 2019.

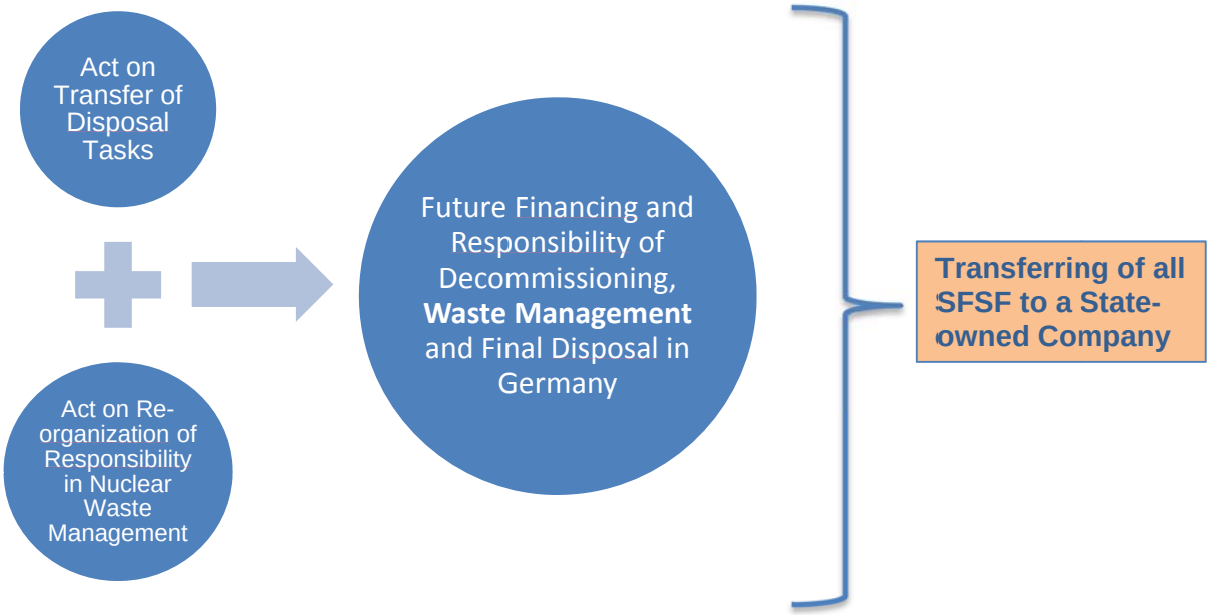

Figure 4: Overview - Re-organization of Responsibility in Nuclear Waste Management

In the first step, the state owned company that has been founded on 1st March 2017, is going to be staffed and is expected to take over the operational management of the storages at Ahaus and Gorleben as of 1st August 2017. The SFSF at the NPP-sites will follow on 1st January 2019. In this context, regulatory issues have to be solved. With regard to Safeguards, the upcoming actions are not limited to those taken to execute the formal transfer of ownership from one operator to the other but also call for a good cooperation between the two owners and with the inspectorates as well. Some of the main questions are shown in figure 5.

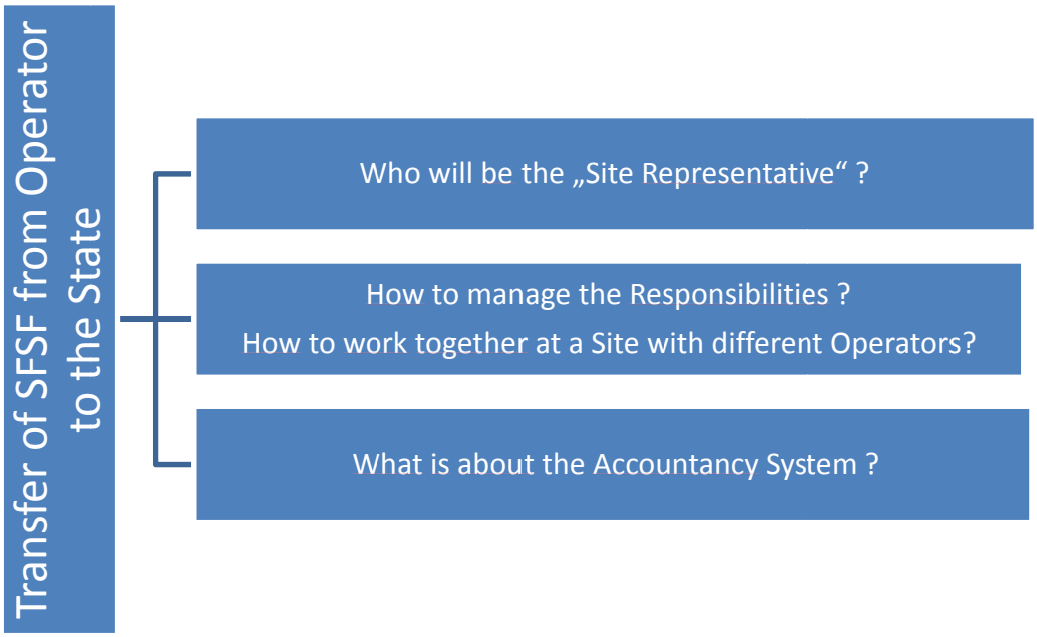

Figure 5: Main questions – Transfer SFSF to a different operator

According to the current state of knowledge, Euratom calls for the appointment of a single site representative, although there will be two owners for each NPP-site from 2019 - the respective utility and the state-owned company as the new operator of the dry interim storages.
Sites e.g. research centre Juelich, where a transfer of ownership of some facilities has already taken place from the research centre Juelich to Juelicher Entsorgungsgesellschaft für Nuklearanlagen (JEN) could possibly provide guidance to the operators and the state-owned company. Challenges that will ultimately have to be overcome in the next future will include the development of a process chain with coordinated interfaces between the utility and the state-owned company.

French system for accountancy and control

François LANAVE

Institute for Radioprotection and Nuclear Safety (IRSN)
Non-Proliferation and Nuclear Material Accountancy Department
Nuclear Material Accountancy Unit
B.P. 17 – 92262 Fontenay-aux-roses Cedex France

E-mail: francois.lanave@irsn.fr

Abstract

IRSN is the French Technical Support Organization in nuclear and radiation risks. Among its numerous activities, it carries out the centralized accountancy of nuclear materials as part of the French obligations towards international non-proliferation agreements. The purpose of this paper is to demonstrate how a centralized accountancy, within the context of a national regulatory framework, is a strong contributor for safeguards.

Any operator who wishes to carry out activities involving nuclear material should obtain authorization from the competent authority before it begins operation. The authorization regime requires:

- *an accounting at the facility level;*
- *the communication to the centralized accountancy of a daily report for any inventory change;*
- *a monthly verification conducted with the centralized accountancy.*

Specific areas for accounting purposes have to be defined. They are mainly safeguarded "accountancy zones". The centralized accountancy processes every working day the accounting records sent by all the facilities in the country. These records have to be sent by a secure transfer system not later than one day before the transaction (e.g. receipt, shipment, enrichment, blending operation, category change, transfer to waste). They include a lot of information such as the accountancy zone in which the activity occurred, type of nuclear material, characteristics and quantities, etc. By crossing information, the system verifies the validity of the data and their consistency (e. g. matching of the data between shipper and receiver, availability in stocks, international obligations, enrichment). The data are if necessary, corrected by the operators and lead for each accountancy zone to monthly accounting reports. The centralized accountancy enables the knowledge in real-time of all the stocks of nuclear materials and their localization in the country. The monthly verification of the accounting books between every single accountancy zone in the facilities and the centralized accountancy allows the required accuracy.

This procedure together with an enhanced computer control enables to ensure the fulfillment of domestic and international obligations.

Key Words: Nuclear material accountancy and control, safeguards, international obligations

1. Introduction

IRSN – the French Institute for radiological protection and nuclear safety - is the French Technical Support Organization in nuclear and radiation risks. It provides technical support to all the government authorities involved in the safety and security of nuclear facilities, nuclear material, transportation and protection of the population. Among these many activities, IRSN carries out the centralized accountancy of nuclear materials as part of the French obligations towards international non-proliferation agreements.

The purpose of this paper is to illustrate and demonstrate:

- How the accountancy of nuclear materials, within both the context of a national structured regulatory framework and the context of international obligations, operates on a daily basis at local and centralized levels;
- How the Centralized Accountancy Unit as constituent part of the Non-Proliferation Department, acts in an integrated approach to achieve the objective of compliance with the international safeguards agreements.

2. The French national legislative and regulatory framework

2.1 Historical context

In the second half of the twentieth century France developed a nuclear program of great magnitude. For a long time, a public state institution known as the CEA has been the sole owner of the nuclear materials present on French soil. The transition to the industrial stage has led to the multiplication of private stakeholders in the civil nuclear fuel cycle. This has resulted in the need to create in the early eighties a national legislative and regulatory framework especially for nuclear materials., which is a part of the French Code of Defense which deals with the protection of nuclear material, nuclear facilities and the transportation of nuclear material against malicious acts.

In parallel, France developed a defense program and is a nuclear weapon state.

2.2 Administrative organization

This legislative and regulatory framework has an integrated approach including physical monitoring and accountancy measures designed to track with accuracy the quantities of nuclear material present at facilities and its location, together with physical protection measures. It also establishes a centralized accountancy of all nuclear material used for civil purposes in France which is managed by IRSN.

2.3 The different regimes set out in the French regulation

A graded approach is applied for the licensing of operators according to the nature and quantity of the nuclear material. Different requirements are set in order to cover the wide range of operators. For this reason, three regimes have been defined by the French regulations (see Table I) in regards with the physical follow-up and accountancy.

TABLE I: The different regimes

	Exemption	Declaration	License
Plutonium	<1 g	Between 1 and 3 g	> 3 g
Uranium 233	<1 g	Between 1 and 3 g	> 3 g
Uranium ≥ 20%	<1 g	Between 1 and 15 g of ^{235}U	> 15 g ^{235}U
Uranium < 20%	<1 g	Between 1 and 250 g of ^{235}U	> 250 g ^{235}U
Natural Uranium	<1 kg	Between 1 and 500 kg	> 500 kg
Depleted uranium	<1 kg	Between 1 and 500 kg	> 500 kg
Thorium	<1 kg	Between 1 and 500 kg	> 500 kg
Deuterium	<1 kg	>1 kg	
Tritium	<0.01 g	Between 0.01 and 2 g	> 2 g
Lithium (^{6}Li)	<1 g	Between 1 g and 1 kg	> 1 kg ^{6}Li

The above mentioned criteria are consistent with the stringency of measures to be taken based on the quantities of the nuclear materials in the context of a graded approach.

2.4 Requirements concerning the accounting

2.4.1 License

For the issuance and maintaining of a license, any operator shall demonstrate the following:

- Accurate knowledge of any variation such as shipment, receipt, conversion, processing, blending operation, irradiation, etc … with full description of the type, characteristics and quantity of each nuclear material;
- Accurate knowledge for each nuclear material of the particular obligation code as well as, for safeguarded zones, of the key measurement point, measurement code and material container code;
- Daily recording of the identified variation in the accounting ledger.

The following conditions should be met:

- The recorded variations shall be communicated on a daily basis to the centralized accountancy;
- At any time on request, a book inventory including all the possessed materials can be produced;
- Systematically at the end of each month a complete accounting closure shall be produced;
- Verification shall be carried out on a monthly basis of the local accounting balance in comparison with the existing balance of the centralized accountancy in order to identify any discrepancy;
- When a discrepancy is identified, it shall be communicated within twelve working days in a report called Reconciliation Report to the centralized accountancy and the operator has the obligation to resolve the issue in a timely manner.

The above mentioned requirements target six categories of nuclear material: Plutonium, Uranium (depleted, natural or divided into three enrichment ranges), Thorium, Lithium enriched in ^{6}Li, Deuterium, and Tritium.

Besides these accounting requirements, the French legislation set forth organizational requirements. The licensee has to appoint a “special representative” who formalizes and assigns responsibilities and missions and shape the staffing structure for both physical follow-up and accountancy with the following features:

- Staff in charge of accounting or physical protection system cannot handle nuclear material;
- Staff in charge of physical follow-up cannot perform tasks related to accounting or to physical protection;
- Physical follow-up, physical protection and accounting systems do not share any equipment or procedure.

2.4.2 Declaration

Small-holders of nuclear materials are submitted to less stringent obligations:

- The operator has to record any inventory changes (type, characteristics and quantity) on nuclear material in his accounting ledger;
- Potential mistakes in the accountancy must be corrected in light of a physical inventory taking;
- An annual report with variations and book inventory as of 31 December has to be transmitted to the centralized accountancy;
- The separation of duties between physical follow-up and accounting is not required.

3. The French international obligations towards safeguards agreements

3.1 Signed agreements

France has made commitments to several major agreements with IAEA, Euratom, and other bilateral agreements with countries such as USA, Australia, Canada, Japan in favour of a non- proliferation regime and a safeguarded system. France is thus mainly a party of:

- the Non-Proliferation-Treaty;
- INFIRC/207 (advance notification to the Agency of exports and imports);
- a “voluntary offer” concluded with the trilateral agreement INFIRC/290;
- the additional protocol (trilateral agreement) INFIRC/290/add.1;
- the Commission Regulation 302/2005.

On the basis of these agreements, France has committed to fulfilling many requirements such as, among others, collecting, analyzing, producing and providing various accounting data and reports.

3.2 Administrative organization

The Euratom Technical Committee (CTE), placed directly under the authority of the Prime Minister services, is in charge of the implementation of international controls on nuclear materials, equipment and technologies on French territory in relationship with IAEA and the European Commission. The CTE benefits from the technical support from IRSN’s Non-Proliferation and Accounting Department for all aspects such as escorting international inspections, assisting the operators, checking, analyzing data and producing reports, assessing documentation. A unit of this department is specifically dedicated to the national Centralized Accountancy and the collecting of international data.

4. The operations of the French centralized accountancy

4.1 The breakdown in accountancy zone and physical monitoring zone

An “accountancy zone” is a part of an installation subject to license that may contain nuclear materials and in which any operation affecting the book inventory is registered. An accountancy zone may contain one or more physical monitoring zones.

A “physical monitoring zone” is a part of an installation subject to inspection of arrivals and departures of nuclear materials.

As part of the issuance of the license, the operator has to define the most relevant breakdown of the facility in one or several accounting zones. The accounting breakdown in France is in many cases reduced to a smaller area compared to the MBA (Material Balance Area) established for international safeguards. The purpose is to make control easier and to reduce the size of the area to which an unauthorized removal or loss can be imputed. They are mainly safeguarded zones.

4.2 The flows and crossing of information

The efficiency of the accounting system is mainly based on:

- A daily information flow between facilities and the centralized accountancy;
- An ongoing verification of the transmitted data and of their consistency.

All the French authorized facilities daily transmit their variation reports to the centralized accountancy through a VPN (Virtual Private Network) connection. These variations data are recorded on the same day in the accountancy at facility level- also called local accountancy- where the transaction occurred. Transactions include receipt, shipment, enrichment, blending operation, category change, transfer to waste, etc... They include a lot of information such as accounting zones, type of nuclear material, characteristics, irradiation status, quantities, etc.

The variations mainly reflect operations among licensed facilities but, to a lesser extent, between licensed and small-holders entities.

The data are checked in order to verify any inconsistency (non- matching data between shippers and receivers, material stock smaller than quantity to be cleared, anomaly in enrichment, non-conservation of mass etc…) or prohibited transactions (unauthorized change in particular obligation, incorrect rebatching etc…). After possible corrections, the postings are made both at facility level and at centralized accountancy level.

The stock lines are affected by the daily variations according to the combination of these five parameters: Element category / Isotopic composition / Irradiation / Safeguards obligation / Material form.

Following closure of each monthly accounting, the centralized accountancy sends for each accounting area a monthly report to facilities in regards with:

- The variations;
- The book inventory.

A reconciliation of the national data with those of the local accountancy has to be carried out by the assigned persons at facility level. A signed report identifying any possible discrepancy and its justification has to be sent back within twelve calendar days to the centralized accountancy. This report is binding.

The flows of information with the small-holders take place annually. Each facility has to transmit a report that includes a book inventory closing on December 31 together with the annual variation records. The official deadline for transmission of the report is January 31.

Afterwards a thorough analysis of small-holders variation data is conducted by the centralized accountancy. It includes cross-checks between:

- Small-holders;
- Small-holders and licensed facilities (in conjunction with daily declarations).

Any possible inconsistency has to be investigated and resolved by the operator and a new revised version of the report has to be sent. Furthermore, in case the report shows that one or more of the thresholds are exceeded, the competent authority may decide to adapt the legal regime to be applied.

4.3 The data collecting and processing for Euratom

In addition to this data processing work for national purposes within the French centralized accountancy structure, the Accountancy Unit carries out a data collecting and first level control work dedicated for Euratom purposes. As a matter of fact, the Accountancy Units is in charge to collect Euratom accountancy reports (Inventory Change Reports, Physical Inventory Listings, and Material Balance Reports) from French operators every month.

Table II and III show guidance on the annual volume of respectively national and Euratom data processed.

TABLE II: Annual volume of processed national data in 2016 by the Accountancy Unit

Accounting areas	Lines of records	Variation records	Annual declarations (Small-holders)
405	209 122	77 264	458

TABLE III : Annual volume of processed Euratom data in 2016 by the Accountancy Unit

ZBM	ICR	PIL	MBR
171	244 891	309 859	9 874

5. The contribution of the centralized accountancy for international safeguards

The efficiency of both the safeguards system depends greatly upon the accuracy and reliability of the accountancy in every facility. The French system is characterized by a double level of control to increase its efficiency:

- An organizational and human separation between physical follow-up and accountancy at facility level;
- An ongoing cross-checking of accounting data between the local and the centralized level.

The system implies more constraints at facility level and requires human and material resources at central level. In return, a good reliability of the accounting is strengthened through this permanent auditing.

The French regulation also stipulates that the transport of nuclear material is done by authorized carriers. The latter are required to declare each shipment to IRSN based on information of physical follow-up, independently of the accounting declaration of the shipper and the receiver. In the end, IRSN has therefore the accounting declaration not only of the shipper but also of the receiver and the carrier. These declarations are systematically cross examined to detect any irregularities. It allows

consolidating at all times the relevance of data stored in the accounts based on separate databases. This organizational and operating system was primarily implemented for national security purposes, however safeguards concerns have been integrated. As a matter of fact, some of the computer controls focus more specifically on safeguards aspects (particular obligation code, reference(s) of authorization(s) in case of change, import/export notification, etc …).

The Accountancy Unit relies on these national accounting data, crossed-checked with other sources, to produce following reports for international purposes:

- imports/Exports of nuclear materials;
- passage of material under Safeguards to non-Safeguards and vice-versa;
- swaps;
- production of mines;
- transparency regarding stocks of plutonium and highly enriched uranium.

In addition, the verification of the completeness and correctness of the Euratom reports, benefits from the upstream work and cross-checked possibilities within the national centralized accountancy.

Of course, the providing of accounting data and reports is only one part of the task required to meet the international commitments. The Non-Proliferation Department plays a leading part to live up to following expectations:

- supplying of additional extensive information on activities carried out in cooperation with non-nuclear weapon states (irrespective of wether nuclear materials are involved or not);
- support and technical assistance to the authorities, operators and industrialists;
- accompanying a number of international inspections following-up of complementary access required by the Agency.

REFERENCES

[1] Arrêté du 9 juin 2011 fixant les conditions de mise en oeuvre du suivi physique et de la comptabilité des matières nucléaires dont la détention relève d'une autorisation.

[2] Arrêté du 31 mai 2011 relatif aux mesures de suivi physique, de comptabilité et de protection physique applicables aux matières nucléaires faisant l'objet d'une déclaration ainsi qu'à la forme et aux modalités de déclaration

[3] Manuel de codification comptable des matières nucléaires

http://www.irsn.fr/fr/expertise/rapports_expertise/surete/pages/manuel-codification-comptable-matieres-nucleaires.aspx#.V8bZY6NOJaQ

Digital Declaration Site Map Submissions for Additional Protocol Article 2.a.(iii)

Joshua Rutkowski[1], Antero Keskinen[2], Jacqueline Idinger[2], Irmgard Niemeyer[1], Alain Rialhe[2] and Arnold Rezniczek[3]

[1] Forschungszentrum Jülich GmbH, IEK-6: Nuclear Waste Management and Reactor Safety
[2] International Atomic Energy Agency, Department of Safeguards
[3] UBA Unternehmensberatung GmbH

Abstract:

States with additional protocols [1] *to comprehensive safeguards agreements in force are required under Article 2.a.(iii) to submit to the IAEA a map for each site. As the current guidelines* [2] *do not specify a special format for the map submission, they are typically delivered in a variety of formats. Using modern geographic information systems (GIS) to assist with the site map creation and annual updates, a joint Member State Support Programme (MSSP) task on Digital Declaration Site Maps (DDSM) is investigating how the submission procedures could be improved in line with new Information Technology (IT) infrastructure and software developments at the IAEA. Specifically, this includes the Protocol Reporter 3 (PR3) and the Geospatial Exploitation System (GES) software. This paper provides an overview of some of the activities under the MSSP task, including the typical submission process beginning with the creation of an operator's site map through the submission process cycle for the annual updates using Protocol Reporter or the Commission's Additional Protocol Editor (CAPE) software. To demonstrate how site maps are created by operators and how these new procedures might benefit operators, State or regional authorities (SRA) and the IAEA, this paper will document some of the common challenges in converting site maps from paper maps to digital GIS data formats. It will also address the preparation of site entries and declarations using the Protocol Reporter software for the submission to the IAEA.*

Keywords: Digital Declaration Site Map, Geographical Information System (GIS), IAEA, Model Additional Protocol, Protocol Reporter

1. Introduction

Using existing geographic information technology to support State declaration activities demonstrates new ways that the Department of Safeguards can utilize current information technology infrastructure to support the mission of the IAEA Department of Safeguards. Four IAEA Member States participate in a support programme task which investigates the potential for using Geographic Information Systems (GIS) for the declaration site maps related to the Model Protocol Additional to Safeguards Agreements (INFCIRC/540) (hereafter referred as Additional Protocol or AP) section 2.a.(iii). To date, Germany has contributed by drafting of the initial framework document titled *Framework Document on Digital Delivery of Spatial Data to the IAEA as a part of the Declaration Activities of the Member States* and updating subsequent versions to provide comprehensive standards, specifications and guidance for the use of the participating States. In 2015 and 2016, the IAEA enhanced the submission protocols and guidelines for digital declaration site map submission by creating a draft specification document which was tested and evaluated by selected site operators in the participating States. This paper highlights some of these activities by examining the existing Additional Protocol requirements and associated guidelines [2], explaining the objectives, status and expected benefits of this task, describing a typical workflow procedure for converting existing site maps to the newly proposed standardized data templates and finally by examining some of the challenges associated with adopting the standards and specifications designed under this task.

Geographic Information Systems is the general term used to describe the "complex computer systems for storing, manipulating, and displaying geospatial data" [3] and is used in many industries. Examples of GIS used in nuclear fuel cycle related industries include: mapping and surveying for mining operations, asset management for power plants, power line utility planning and monitoring, planning

and monitoring for shipment and material transportations. Cartographic products (maps) are a common output from a GIS. Since the Additional Protocol 2.a.(iii) relies on a declaration site map for each site within a State, a GIS is commonly used as part of the preparation for declaration submission. While static map products (paper or pdf files) are still common, the underlying spatial and attribute information used to create the maps are usually stored in a GIS. Benefits of using GIS have been realized by operators since the GIS is able to act as a central data store, increase clear communication due to inherent geographic attributes and permit spatial and temporal data tracking and analysis. The aim of the this paper is not to advocate for the use of GIS in any given site but the authors wanted to note the importance that GIS already plays in planning, implementing, managing and monitoring industrial sites worldwide. Since many site operators have already implemented GIS in their operative processes, the IAEA would clearly benefit from using common GIS datasets in their mission to verify States' annual AP declarations. Sharing and using one common site map would improve the efficiently and overall verification process at the IAEA. Simplified and standardized processes for individual sites result in more consistency across different sites within a State.

2. Safeguards Additional Protocol and State declarations

The Additional Protocol was approved in May 1997 by the IAEA Board of Governors. The Additional Protocol is a legal document that supplements States' IAEA safeguards agreements and grants the IAEA complementary legal authority to verify State's safeguards reporting obligations. The information to be provided to the IAEA by States under the AP is identified in Article 2. The section on 2.a.(iii) provides specific guidance of the Model Protocol as follows:

Article 2.a.(iii)

"..... shall provide the Agency with a declaration containing:

> *(iii) A general description of each building on each site, including its use and, if not apparent from that description, its contents. The description shall include a map of the site."*

Currently (as of October 2016), Additional Protocols are in force with 129 States and EURATOM, and another 17 States have signed an Additional Protocol but have yet to bring it into force.

The initial Additional Protocol reporting guidelines of the IAEA were published in August 1997 and the revised version of the guidelines, based on cumulative experience of States and the IAEA, was published in May 2004. The guidelines provide a standard format for the preparation of AP declarations by States pursuant to Article 2 and 3 of the AP. The guidelines have generally been effective in providing specificity of what information is required, the appropriate level of detail and a standardized, consistent reporting format for submission. These guidelines are not mandatory but rather intended as advice for States on preparing declarations. The text of the Additional Protocol remains the only legally binding document. The IAEA plans to update the guidelines in the near future.

The section 7 in the guidelines document provides specific guidance of a declaration site map as follows:

"A current diagram or map of the site showing the exact boundary of the site, the location of all buildings and other structures, railways, roads, rivers, etc., is to be attached to the Article 2.a.(iii) declaration for each site. The scale and geographical orientation to the North of the map or diagram should be indicated. If possible, geographical coordinates for at least one reference location in the map or diagram should be provided. The availability of coordinates will facilitate the identification by the Agency of buildings on maps and satellite images."

The guidelines have been supplemented with the Protocol Reporter software developed by the IAEA for States to prepare their AP declarations in electronic format. Presently, States use different versions of the Protocol Reporter software: Protocol Reporter 1 (PR1.0.0), Protocol Reporter 2 (PR2.0) and Protocol Reporter 3 (PR3). A few States still provide AP declarations in hardcopies. In addition, a derivation of the Protocol Reporter, the European Commission's Additional Protocol Editor (CAPE) software, which is adapted to the specific requirements of EURATOM members, is being used by EURATOM and by several EURATOM States. Some EURATOM States are using PR2.0 and PR1.0.0

for the preparation of AP declarations, also for the part they send as non-side letter States to EURATOM, which has to be converted by EURATOM into CAPE for processing and use and thereon forwarded in CAPE format to the IAEA.

The IAEA typically receives AP declarations in electronic format but also sometimes in hardcopies. If States use PR1.0.0 or PR2.0 for the preparation of AP declarations, .txt or .xml files are received which can be directly loaded into the IAEA's Additional Protocol System (APS). However, even when the IAEA receives electronic declarations prepared in PR1.0.0 or PR2.0, the attachments to declarations (including maps) cannot be linked to the respective declarations. This separation of AP declarations from attached documents and maps causes problems in subsequent data storage and retrieval.

In 2013, the IAEA partnered with the United States' Department of Energy (DOE) to update the Protocol Reporter software. The new version, Protocol Reporter 3 (PR3), provides for the first time a capability to include attachments (documents or maps) in the AP submission packages which are sent to the IAEA. An attachment can be linked to a single entry of a declaration, to a declaration, or to the whole AP submission in PR3 regardless of the format of the attachment. This includes maps generated with GIS or CAD software and maps in pdf format. The roll-out of PR3 to States began in September 2016. The first quarterly declarations in PR3 format were received at the IAEA in October 2016 and the first annual updates in December 2016. Newcomer States to the AP and, increasingly, States which face compatibility problems of PR 2 and PR 1 with newer operating systems, have already requested the PR3 software for the preparation of their AP declarations.

Although the use of the PR3 software for the preparation of AP declarations is not mandatory for States, the compatibility problems of previous versions with currently used operating systems and the incentives to profit of the advantages of PR3 will most likely push forward the roll-out of the software. The regular use and the acceptance of the PR3 by States will reveal the necessity for further updates or improvements.

3. Overview of this Member State Support Programme task

The German Member State Support Programme has a longstanding relationship with the IAEA dating back to 1978. The joint development of methods and techniques by various research groups within Germany have contributed to the mission of the IAEA Department of Safeguards and continues a strong partnership with the Department. As recently presented at the 2016 INMM annual meeting, the German support programme offers certain field tests in commercial sites within Germany [4]. Such opportunities to interact with site operators for research purposes broaden the understanding of specific research tasks by using real examples to illustrate promising research. In this line, the IAEA issued a call for a MSSP regarding the submission of digital declaration site maps for the Additional Protocol 2.a.(iii).

As mentioned in the introduction, GIS offers advantages for site operators, States and the IAEA. Static maps (paper or pdf files) are basic representations of geographic information and unfortunately do not offer the full potential to exploit the underlying datasets used to create the map. These static maps can only be used as a reference and cannot be used to directly access and further use their original data content. For instance, the transportation networks (roads, railways, etc.) in paper or pdf map might contain simple labels indicating the name of certain roads but the underlying data layers usually contain much more information such as road construction type, date of construction, accurate length and width, etc. In other words, various attribute information linked to each geometry feature on the static map cannot be queried or analyzed and therefore remains inaccessible to the map reader. Similarly, building attribute information is often extensive but cannot be accessed in these types of maps. On the other hand, a GIS offers the user to access all attribute information associated with each feature on the map. Such access lends itself to assist in clearer communication about the location and function of entities represented on the map, assures spatial accuracy of features' geometries and enables integration of current and historical datasets due to the geographic context. Thus, other datasets may be added to the GIS for seamless user interrogation.

Beginning of 2012, the University of Bonn's Center for Remote Sensing of Land Surfaces drafted a preliminary framework document describing the efforts required to submit the site maps in a digital GIS

format which complies with the current guidelines from the IAEA. In addition, the University created several site maps in a GIS for nuclear sites within Germany using satellite imagery as the primary source for digitization of building and ancillary structures on the sites. Since German site operators are obliged to submit similar information to EURATOM, this was also considered in part of the task. This work laid the foundation for creating a support programme task proposal since it demonstrated the utility of submitting specific information, namely information required under 2.a (iii) of the Additional Protocol, using digital, geographically attributed information.

In 2013, the IAEA issued a call to participate in a support programme task proposal on this subject. The task was aligned with the Development and Implementation Support (D&IS) Programme with a specific emphasis on key objective 2 “Enhance geospatial data storage, management, dissemination” [5] and aimed to contribute to the goals of the IAEA Long-term R&D plan 2012-2023 section 9.1 “Develop updated software tools for use by SRAs in creating and submitting accountancy reports and additional protocol declarations, supporting the further integration of State declared information within the electronic State file” [6]. The digital declaration site map task was accepted by four IAEA member states: Canada, Finland, Germany and Japan. This paper will focus solely on the activities of the German Support Programme participation in this task. The task contains three phases of which phase 1 surveyed site operators in Germany to understand which technologies are currently in practice for creating and updating declaration site maps at the site. This information was supplied to the IAEA and will not be reported here. In phase 2, the IAEA created a data specification document and standard data schema for the use of States. The document is intended to provide adequate guidance on the creation of digital site maps by giving the necessary background information, published guidelines and detailed specifications of the data model used in this task and compatible with IAEA’s Geospatial Exploitation System (GES). In addition, the participating States’ operators were asked to provide feedback on the document and share comments on the design and further editing of the Framework document. Phase 3 of the task aims at understanding how site operators may change their existing procedures to accommodate new methods for preparing and submitting site maps. The lessons learned from this phase contribute to the latter part of this paper for data conversion processes and common challenges faced. The third phase is on-going and the IAEA continues to work closely with the selected site operators, SRAs and the task managers in the respective States.

These phases can only be realized due to the implementation of the Integrated Safeguards Environment (ISE) in the Department of Safeguards’ information technology (IT) infrastructure. This isolated, secure computing environment that hosts Safeguards applications, data, and services creates a platform for implementing the results from this task. ISE was implemented to facilitate a Department-wide, improved collaboration environment, while securely hosting, processing and delivering relevant safeguards data, information and applications in a timely manner to those who need it in Headquarters, Regional Offices (Toronto and Tokyo) and in the field.

The Department of Safeguards has set on objective to have a modernised Information Technology (IT) system in place in 2018 that will allow it to perform safeguards implementation processes more efficiently, effectively, and securely [7]. The Modernization of Safeguards Information Technology (MOSAIC) programme was initiated in 2015 and the programme comprises over 20 projects, each of which is developing applications and software to take Safeguards IT capabilities into the future, enable major upgrade to safeguards implementation and allow the Department to be more productive in all areas of safeguards where collecting, processing or evaluating safeguards-related information, or establishing findings.

Since 2001, the current Additional Protocol System (APS) has assured the secure storage and handling of information that the IAEA has obtained from States in the context of the AP as well as information pertaining to planning and performing Complementary Access (CA) activities. The APS has been used by IAEA analysts, inspectors and managers who are responsible for State evaluation. The aim of the APS project under the MOSAIC programme is to reengineer the parts of the APS to ensure completeness and correctness of the State-supplied AP information by providing enhanced tools for the initial data review and processing as well as analysis of AP declarations. One of the expected benefits is to enable processing of State declarations submitted using the PR3 software. The project also investigates the ways of and enables connecting the AP declarations and declaration entries to other databases in other applications such as to building objects in the GES.

Another MOSAIC initiative, the State Declarations Portal (SDP) project will create a web-based portal for the use of States and the IAEA to support secure, bidirectional information exchange and reporting

between States (SRAs) and the IAEA. The new system will streamline the submission of safeguards declaration by States, make the process more efficient and reduce the overall time needed for the IAEA to process them [8]. The portal provides a platform for more direct transfer of information between the IAEA and SRAs. Secure authentication and authorization controls will ensure proper handling of sensitive State information. Declarations submitted through the portal will be automatically transferred to the ISE network. The SDP will complement the current means of communicating State declarations between the SRAs and the IAEA, such as email, postal and fax submissions. The SDP is expected to be available to States in 2017.

The Geospatial Exploitation System (GES) was designed to provide a full enterprise-wide Geographic Information System (GIS) which is used to support the analysis of satellite imagery, geospatial data and associated assets for staff within the Department of Safeguards [9]. The GES was the first analytical application specifically developed and successfully deployed into the IAEA's ISE network in December 2011. The GES demonstrates the integration of commercial off-the-shelf (COTS) software with customized imagery analysis, mapping and analytical tools for the development of desktop applications that support processing, analysis, visualization, and dissemination of imagery, geospatial data, and derived products securely to authorized users. In order to enable the sharing of these data and products, the GES uses service-oriented architecture (SOA) to share and consume valuable information from disparate applications and sources from across the Department. As an example, the GES uses facility information from the Safeguards Master Data (SGMD) to identify the facilities on a site. The GES provides capabilities for evaluating temporal changes in the nuclear site's infrastructure based on imagery analysis, AP declaration data and SGMD that are used by the IAEA geospatial analysts to generate geospatial products referred as 'site plans'.

As part of the MOSAIC programme, the Geospatial Exploitation System 2 (GES 2) project will create a web-based GIS portal that replaces the current GES system deployed since 2011. The GES 2 is expected to be operational in mid-2017 and to be used mainly by the satellite imagery and geospatial analysts. The GES 2 will evolve, including through the adaptation of its data model architecture and performance, and improvement of the tools, to exploit imagery, geospatial data, and other safeguards-relevant information such as State reports and AP declarations. Conversely, other applications within ISE may benefit from imagery, geospatial data (e.g. site plan
s), and analytic products generated and published in GES that will further interoperability among different software applications within a collaborative environment. The Geobased Data Integration (GDI) project will provide geospatial data (e.g. from GES 2) to support the needs of inspectors, country officers, and SEG (State Evaluation Group) members in their activities related to the implementation of safeguards in assigned States.

4. Description of typical data conversions

This section reviews a common workflow involving the conversion of site map information from conventional static maps or Computer Aid Software (CAD) data format into GIS formats. In general, the process usually undergoes several steps using one or more software packages. To begin, the map or set of maps for the site must be scanned as raster datasets. Afterwards, the data processor must extract the features on the map, e.g. road networks, building footprints, etc. Extracting such information is either done through heads-up digitizing or using automated software extraction software. The features are extracted and stored in vector format. This process ought to also include referencing the files to a geographic coordinate system either before the data is converted to vector or afterwards.

Many sites began operation before modern GIS or CAD software packages existed. Based on the survey information gained during phase 1 of this task, some site operators have retained paper maps as their primary source for map generation. Such a case typically exists when there was no later need to update the technology for map generation. More common though, is a steady progression by site operators to update their map data and associated workflows according to current cartographic technology, primarily to GIS or CAD. Site operators oftentimes use maps and their underlying data for other purposes besides submitting declarations to the IAEA or EURATOM.

Maps, and their underlying data, usually contain the utility infrastructure of the site, including gas pipes, power lines, material flow patterns, transportation networks, etc. CAD files are common in many

industries including nuclear industry. More recently, the use of GIS for site management has been trending in the industrial settings and the integration of geographic coordinates for CAD is becoming more commonplace. Many of the major CAD software packages now contain GIS plugins to facilitate conversion and maintenance of geographic information [10] in a GIS format. However, CAD data oftentimes does not contain all of the necessary attribute information required to generate datasets desired under this task. In addition, not all CAD datasets contain geographic coordinates and oftentimes require updates in order to be projected in a geographic coordinate plane.

Although GIS is the IAEA preferred file format, it is possible to convert most CAD drawing files, which contain geospatial information, to a format compatible with the GES. The conversion workflow from CAD to GIS, however, typically requires several steps including quality control of the output. The process and results also depend on how (software, methods, standards, data quality requirements etc.) the CAD data was initially generated. Thus, CAD should be a solution for the digital data submission only if CAD software is already being used by a site operator or State and there are existing CAD datasets available. Thus, if there is neither pre-existing CAD software nor CAD data yet in use, GIS should be considered as the optimal solution for digital declaration site map submission to the IAEA. In addition to the support for IAEA digital site declarations, GIS technology has acknowledged benefits and it is routinely being used to support nuclear operators in their asset management for civil infrastructure, capital planning and site management [11].

In many cases, site operators use GIS or CAD for preparing their declaration site maps but submit the maps to the IAEA in a static picture format (e.g. pdf) that does not allow IAEA to access the underlying data but use the map as a reference only. For instance, attribute information stored in a GIS database and associated with each feature on the map cannot be analysed unless they are visible on the map. Depending on the data format (CAD or GIS) currently used in the site, operators need to either apply conversion workflow from CAD to GIS (see above) or apply IAEA standards and specifications for the preparation of their existing GIS data (see below).

The *Framework Document on Digital Delivery of Spatial Data to the IAEA as a part of the Declaration Activities of the Member States* supports States that are participating or planning to participate in this pilot project on the submission of digital declaration site maps (DDSM) to the IAEA. The document provides detailed guidance, specifications and standards for the preparation of DDSM data with appropriate data structure and content. As part of the document, the IAEA provides data templates in a geodatabase and shapefile formats that should be used by States to populate the geospatial declaration site map data with all relevant features and their attributes. This will ensure that the data is compatible with the IAEA's infrastructure, namely GES. These empty template data files contain standard data structure for all classes of possible geographic features (e.g. roads) and AP information table on a declaration site map. Numeric coded domain values (e.g. 1 or 2) or corresponding descriptions (e.g. single lane road or multiple lane road) should be used for each geographic feature to describe the characteristics of data, e.g. the type of a road. Additionally, the document provides detailed instructions on how to prepare the data appropriately, an example of a complete digital declaration site map based on the data templates, a sample dataset in both geodatabase and shapefile formats, and instructions on how to provide an appropriate metadata to describe the content, quality, condition, origin, processing and other characteristics of the data.

A common scenario encountered in this task and anticipated in future data conversion scenarios is when a site operator had paper copies of the site maps submitted to the IAEA. The ultimate goal of this process is to contain all the existing map information (feature geometries and attribute information) and the descriptive tables from 2.a.iii declarations in a GIS file format. As mentioned previously in this paper, such a file format permits clearer communication and eases the verification activities by providing a more precise site map which can be more easily interrogated by Department of Safeguards. The desired file format specifications are given in detail to site operators participating in this task. Each of the features specified in the Framework document were derived from the current AP guidelines document. Therefore, the existing guidelines are still honored with the new format but are formatted for better exploitation.

According to the AP guidelines [1] [2], the following categories of data should be part of a digital declaration site map submission: site boundary, buildings and structures, transportation and rivers. Additionally, fences and walls, utilities (supply lines) and water features are requested to be voluntarily

provided. Each of these categories is further distinguished within the category. For example, the site boundary category may distinguish between site boundary, facility boundary, location outside facility (LOF) boundary or other important distinctions which clarify ownership or responsibility within a site. In addition to these categories, a table describing building related information, specified in the AP guidelines document is also included in the dataset. The initial declaration contains information about each building on a site but subsequent annual declarations only need to mention changes to existing building, whether the changes related to building function or location. This means that subsequent declarations will possibly have a different number of records than the initial declaration. The new PR3 software will help to keep track of changes in site declarations in the way that each annual update should represent a consolidated update of a site, meaning that always the full picture of a site has to be reported in each annual update when using PR3 software. Such changes can also be easily tracked in a GIS since tabular and spatial changes may be detected during analysis. Detailed instructions on how to prepare the data is provided in the Framework document. Once the site map is properly formatted in GIS compatible software, it needs to be edited in order to conform to the IAEA specifications. Under this task, several site operators provided feedback to the IAEA on this matter. Each site faced unique situations that are categorized and discussed in the next section of this paper.

5. Common challenges observed during task activities

The previous section detailed a typical workflow required to convert paper, electronic or CAD site maps into a GIS format as observed by several site operators under this task. In a broader view, certain challenges exist if an IAEA Member State adopted the new data format for their annual AP declaration site map submissions. This section will examine some of the issues. A Canadian case study was presented at the 2016 INMM annual meeting [12] and noted some issues including three broad challenges for implementing a new digital declaration site map submission process:

1) The need to harmonize data between each location within a country
2) Data model differences between CAD and GIS
3) Need for State or regional authority responsible for the implementation of Safeguards to review and analyse the data using a GIS software and analysis

Additionally, some more challenges are as follows, in no particular ranking of significance.

5.1 Data conversion

Legacy data stored in different formats present a challenge to users faced with using such data. CAD data is often used by civil engineers for construction and maintenance work within sites. While CAD datasets contain a coordinate system, they are often are not referenced to a common geographic datum and therefore must be transformed to a well-known datum. Each dataset may contain unique parameters which prevent an automated transformation process. Additionally, the CAD storage uses layers with minimal attribute information compared to a GIS attribute database. The process of linking attributes may be painstaking. This conversion process is not uncommon in the CAD and GIS industry but does require foresight and planning. As part of this task and the Framework document, standards and guidelines for converting CAD to GIS data were created since several of the participating site operators in States are using CAD to store their site information.

5.2 Knowledge management of site map design and submission process

This topic is not special to the site map requirements for the Additional Protocol but rather extends to most parts of the submission process. Training and retaining knowledgeable staff on safeguards requirements is ongoing for most sites. Adding an additional sophisticated tool to the process may sound daunting but the recent advances of GIS technology for decentralized IT infrastructure (cloud computing and portal technology) mean that users may, depending on the implementation of the GIS, use web browsers to add, manipulate and publish site maps. This means that datasets are no longer required to be stored in a local file system or one central server. Such an environment can also force data conformity through data integrity and standard checks upon data upload. The “garbage in-garbage out” idea may be avoided here with some thoughtful pre-planning.

5.3 GIS software compatibility

Licensed software, such as ArcGIS or AutoCAD, use proprietary data files but some of these files such as the ESRI file geodatabase are compatible with other software programs with limited functionality. The Open Geospatial Consortium (OGC) is an international industry consortium of over 521 companies, government agencies and universities participating in a consensus process to develop publicly available interface standards" [13]. These standards make it possible to share geospatial data in common formats. The use of web platforms for GIS technology means that the server software running the website pages become much less important to the users as long as their requirements are met.

5.4 AP software compatibility with GIS data

During the submission process, a State may use a different version of the Protocol Reporter software or submit their declarations in CAPE, MS Excel or in paper format. As mentioned earlier in this paper, the PR3 software provides the capability to include attachments in various formats (e.g. GIS) in the AP submission packages. Likewise, future versions of the CAPE software should consider GIS datasets for the submission. The current version of the APS at the IAEA is lacking the capability to link the AP data declaration entries (in case of 2.a.(iii) declaration equivalent to buildings) to data in other applications (e.g. building geometries in GES). Therefore, geospatial analysts must link each AP building entry manually to its corresponding building geometry in GIS. Connections between the APS and GES databases should be created to avoid duplicate data creation in these two systems.

5.5 Different data schemas and standards used by the IAEA and States

States may have used more detailed data schemas, different methodology and standards for creating their data than what is needed for the purpose of IAEA verification activities. Converting data into IAEA standards may take additional efforts. For example, a site where the standard for storing road data features as small segments is not preferred by the IAEA.

5.6 Secure data transfer from States to IAEA

The importance of a secure data transfer method for AP data submission and different security standards and encryption methods have been acknowledged as challenges during the task. Protocol Report software does not include transfer of the AP data but only the preparation of a submission package in a standard data format (.xml file). Provision method of the data depends on a State; some States used encrypted emails or similar secure methods whereas other States may submit their declarations in a paper format. In the future, States may adopt the future State Declarations Portal for their method of secure data transfer and communication to/from the IAEA.

6. Conclusion

This paper provides an overview of the activities under the Digital Declaration Site Maps (DDSM) MSSP task, including the typical submission process beginning with the creation of an operator's site map through the submission process cycle for the annual updates using Protocol Reporter 3 software. The expected benefits of the task highlighted in this paper as well as the latest development of the Department of Safeguards' information technology (IT) will permit the task to move forward. Furthermore, the concept of the Safeguards Additional Protocol Article 2.a.(iii), its related guidelines document, different software used by the IAEA, States and EURATOM and the development of the Protocol Reporter 3 software were introduced. The MSSP task history, current events and future activities were presented. The typical data conversion processes from existing static maps, from CAD to GIS format and the limitations of the static maps and CAD for the purpose of the task were broadly explained. The content of IAEA's Framework document was briefly presented to provide understanding of the standards, specifications and guidance for the implementation of the task by States. Finally, some of the common challenges faced in this task and expected to be faced in the future were discussed.

7. Acknowledgements

This work was supported by the Federal Ministry for Economic Affairs and Energy, Germany, through the German Safeguards Support Programme to the IAEA under task B.29/D1983.

References

[1] International Atomic Energy Agency. INFCIRC/540 (Corrected). *Model Protocol Additional to the Agreemens(s) between State(s) and the International Atomic Energy Agency for the Application of Safeguards*. 1997 September.

[2] International Atomic Energy Agency, Services Series 11: *Guidelines and Format for Preparation and Submission of Declarations Pursuant to Articles 2 and 3 of the Model Protocol Additional to Safeguards Agreements*, D.o. Safeguards, Editor. 2004, International Atomic Energy Agency: Vienna.

[3] Westra, E., *Python geospatial development*. 2016: Packt Publishing Ltd.

[4] Niemeyer, I., et al. *Join Programme on the Technical Development and Further Improvement of IAEA Safeguards - The German MSSP*. in *Institute of Nuclear Material Management Annual Meeting*. 2016. Atlanta, Georgia, USA: INMM.

[5] International Atomic Energy Agency, *STR-377: Development and Implementation Support Programme for Nuclear Verification 2015-2015*. 2013, International Atomic Energy Agency: Vienna.

[6] International Atomic Energy Agency, *STR-375: Department of Safeguards Long-Term R&D Plan, 2012-2023*. 2012, International Atomic Energy Agency: Vienna.

[7] Agency, I.A.E., *MOSAIC, The Modernization of Safeguards Information Technology: Completing the picture*, I.A.E. Agency, Editor. 2016: Vienna.

[8] Li, J. *New Web-Based System Streamlines Safeguards Information Exchange With IAEA*. 2017 Thursday 13 April 2017 15:45 CEST [cited 2017 28 April 2017]; Available from: https://www.iaea.org/newscenter/news/new-web-based-system-streamlines-safeguards-information-exchange-with-iaea.

[9] Rutkowski, J., et al., *The Implementation and Use of the Geospatial Exploitation System within the IAEA's Department of Safeguards.* Journal of Nuclear Materials Management, 2016. XLIV(2): p. 39-44.

[10] See http://www.esri.com/software/arcgis/arcgis-for-autocad or https://www.bentley.com/en/products/product-line/asset-performance/bentley-map

[11] Smith, G. *Exploiting Spatial Data for Site Declarations*. in *IAEA-CN-220 Book of Abstracts, Presentations and Papers*. 2014. Vienna: International Atomic Energy Agency.

[12] Qureshi, F., et al. *Digital Declaration Site Maps for Additional Protocol Update - Collaborative Pilot Project undertaken by the CNSC, IAEA and Bruce Power*. in *Institute of Nuclear Materials Management Annual Meeting*. 2016. Atlanta, Georgia, USA.

[13] Open Geospatial Consortium. *About OGC*. 2016 [cited 2016 Jan 18]; Available from: http://www.opengeospatial.org/ogc.

Euratom On Site Laboratories Refurbishments and Developments

Lily Duinslaeger[a], Karin Casteleyn[a], Claudia-Iustina Andor[a], Razvan Buda[a], Ramon Carlos Marquez[a], Lorelei Commin[a], Francesco D'Amati[a], Lorenza Emblico[a], Timothy Enright[a], Marc Hild[a], Joan Horta Domenech[a], Arnaud Le Terrier[a], Klaus Luetzenkirchen[a], Sebastien Mialle[a], Sylvain Morel[a], Artur Muehleisen[a], Adrian Nicholl[a], Christophe Nourry[a], David Poublan[a], Miguel Ramos Pascual[a], Gert Rasmussen[a], Ana Maria Sanchez Hernandez[a], Francesco Sarli[a], Stephen Street[a], Gert Suurkuusk[a], Gabriel Toma[a], Magdalena Toma[a], Octavian Sorin Valu[a], Pieter Van Belle[a], Denis Wojnowski[a], Evelyn Zuleger[a] Ferenc Lipcsei[b], Peter Schwalbach[b], Sotiris Synetos[b]

[a]European Commission, Joint Research Centre, Directorate for Nuclear Safety and Security, P.O. Box 2340, D-76125 Karlsruhe, Germany
[b]European Commission, Directorate General Energy, Directorate Euratom Safeguards, L-2920 Luxembourg

Abstract:

The two Euratom On Site Laboratories located at the reprocessing plants in Sellafield, UK (the OSL) and La Hague, France (the LSS) have been operational for more than 15 years. Both On Site Laboratories, operated by DG JRC on behalf of DG ENER, are instrumental in providing independent assurance to the European Commission that nuclear material is not diverted from its declared use.
Over the years, the laboratories have been in constant evolution, some equipment became outdated and in need of refurbishment or replacement. Renewals in the laboratories are foreseen to continue over the coming years. The larger projects entailed replacement of a thermal ionization mass spectrometer, including decommissioning of its connected glove boxes and installation of a new glove box; renewal of the complete Hybrid K-edge analysis system, including installation of an independent gamma station and refurbishment of two glove boxes. Such tasks include the design, manufacture, purchase, installation and testing of the required equipment both at JRC-Karlsruhe and on site, as well as fulfilling elaborate procedures to obtain the operator's permission prior to any non-routine work being allowed to take place.
Over the years, a series of innovative equipment was developed at JRC-Karlsruhe, all tailored to the specific needs of the On Site Laboratories and taking into account the operational boundary conditions of industrial nuclear facilities. Examples are an infra-red based heater for alpha spectrometry with enhanced safety features, a hotplate based on a flexible low power heating element, a semi-automatic chemical separation unit, etc. The replacement of certain equipment parts (e.g. LEMO connections on glove boxes) also required ingenious solutions.

Keywords: Safeguards; refurbishment; equipment; On Site Laboratories

1. Introduction

In the European Union, irradiated fuel from nuclear power reactors is reprocessed at La Hague in France and Sellafield in the United Kingdom. The four reprocessing plants in these two sites are the largest nuclear facilities within the EU, processing hundreds of tons of nuclear material in a year. Under the Euratom Treaty, celebrating its 60th anniversary this year, the European Commission has the duty to assure that nuclear material is only used for declared purposes. The Directorate General for Energy (DG ENER), acting for the Commission, assures itself that the terms of Article 77 of Chapter VII of the Treaty have been complied with. In contrast to the Non-Proliferation Treaty, the

Euratom Treaty requires to safeguard all civil nuclear material in all EU member states – including the nuclear weapons states.

The considerable amount of fissile material separated per year (including several tonnes of Pu) calls for a stringent system of safeguards measures. The aim of safeguards is to deter diversion of nuclear material from peaceful use by maximising the chance of early detection. At a broader level, it provides assurance to the public that the European nuclear industry, the EU member states and the European Union honour their legal duties under the Euratom Treaty and their commitments to the Non-Proliferation Treaty.

A thorough analysis of the options to perform nuclear material accountancy and safeguard nuclear material at these reprocessing plants concluded – in the early 1990s – that sampling of material from the process streams would be required. Transport of the samples to a central Euratom laboratory should be avoided for reasons of cost effectiveness, timeliness and risk reduction [1]. Therefore, laboratories were established on the sites of Sellafield and La Hague that opened in 1999 and 2000, respectively.

The major advantages of On Site Laboratories are: inspectors receive sample results quickly (timeliness), in case of doubt re-verifications can be done with little delay, measures to make sure samples are authentic are simpler to implement, efficiency and cost effectiveness, waste reduction and reduced transport needs.

2. The Euratom Safeguards On Site Laboratories [2]

In October 1999, DG ENER, the JRC, and the plant operator started up the first “On-Site Laboratory” (OSL) at the site of the reprocessing plants in Sellafield to cover principally the activities of the newly constructed THORP plant together with several additional samples from the older Magnox plant [3] and with a capacity to add samples from the fuel fabrication plants in the UK (Sellafield MOX Plant, then under construction, and the LEU plant at Springfields). In June 2000, the second On Site Laboratory, the “Laboratoire-Sur-Site” (LSS) began operations at the reprocessing site in La Hague [4].

The official start of operations took place after a process of conception, planning, design, development, and construction which lasted about one decade. Analysts of JRC-Karlsruhe have since been operating both On Site Laboratories on behalf of Euratom Safeguards. Both On Site Laboratories were integrated into existing or new operator laboratories. The On Site Laboratories are run under the operator's site licence and can use supporting services. They have to follow all the site safety, operating, and security rules. Staff of the On Site Laboratories must be trained and certified under the existing site regulations and must comply with the same rules as the operator's staff.

Analysts of JRC-Karlsruhe are present on-site, ensuring a continuous flow of samples and results. The laboratories receive samples from all the plants on the respective sites, with dissolved spent fuel, plutonium products – including mixed oxide fuel – and inventory samples being the most important types of material from accountancy viewpoint. Since the start of the On Site Laboratories almost 15000 samples were received. The obtained analytical data are used by DG ENER for direct comparison with the operator’s declarations and allow evaluating the material flows and balance in a timely manner.

2.1. Methodology

As the nominal output of Pu can reach the order of a few tonnes per year for the big reprocessing plants, safeguards inspectors need high accuracy to have a chance to detect diversions of a few kg, which are significant. The sample measurement methods were thus selected using the criteria of highest possible measurement accuracy (less than 0.1 % uncertainty 1s relative) and a minimum of resource consumption. Most of the samples are analysed by radiometric methods: K-Edge Densitometry (KED) for plutonium or uranium concentration, X-Ray Fluorescence (XRF) for the uranium/plutonium ratio, and High Resolution Gamma Spectrometry (HGRS) for the analysis of individual uranium and plutonium isotopes. The combination of KED with XRF is called Hybrid K-edge (HKED).

The radiometric X-ray techniques must be calibrated against an absolute standard. Isotope Dilution Mass Spectrometry (IDMS) was chosen as the primary technique which also serves for quality control of the radiometric methods due to its superior accuracy. IDMS is more labour intensive and is therefore typically carried out only on a subset of about 10 % of the samples and allows measuring both the uranium and plutonium concentrations and the respective isotopic compositions. Thermal Ionisation Mass Spectrometry (TIMS) is used for analysis of individual uranium and plutonium isotopes.

Quality assurance measures – both internal and external quality control – are of particular importance for accountancy measurements at facilities with a large throughput of nuclear material. The work at the On Site Laboratories is performed according to quality management principles and follows the requirements of an ISO 17025 accredited laboratory. Analytical methods and procedures are whenever possible being improved and the laboratories are benchmarked through regular participation to inter-laboratory comparison exercises, such as EQRAIN (organised by CETAMA, France) and REIMEP (organised by JRC-Geel, Belgium). The On Site Laboratories aim to conform to the latest international standards and achieve this at daily operation.

2.2. Laboratory infrastructure and analytical capacity

The On Site Laboratories were designed with sufficient capacity, both in terms of instruments and staff, to analyse a certain number of samples. This number relates to the reprocessing capacity of the plants, to nuclear material accountancy regulations, the safeguards verification requirements, the material parameters to be measured, and the capacity of the different analytical methods. The analytical facilities are operated for about 45 weeks a year by typically 2-4 analysts a week. During operation, a minimum of two analysts must be present in the On Site Laboratories according to safety-at-work rules.

The type of samples the On Site Laboratories would receive was also identified during the conception phase. The newer reprocessing plants, such as UP3 and UP2-800 at La Hague and THORP at Sellafield, have different sample taking regimes than the older Magnox plant. The sample types foreseen to be analysed were decisive for layout and infrastructure of the individual laboratories.

2.2.1. The OSL laboratory at Sellafield

The OSL Sellafield receives samples both from the front-end but mainly from the back-end of the reprocessing cycle. The radioactivity levels are such that samples can be manipulated in the laboratory's glove boxes. The sample types are diverse and most of them require labour-intensive sample preparation steps. The OSL is located in a building which is part of Sellafield's Analytical Services. It comprises two 'active' laboratories, one 'cold' laboratory and an office space. All work with radioactive substances is performed in the two 'active' laboratories in glove boxes. There are 10 glove boxes of which the key boxes are:

- The "non-destructive analysis" glove box, where initial processing, analysis and sample preparation operations are carried out on product materials. Nearly all samples are analysed in this box. The glove box contains an analytical balance, a microwave oven (for dissolutions), a densitometer and the equipment to perform radiometric analytical measurements (HKED, XRF, HRGS).
- A glove box dedicated to prepare reference materials for mass spectrometry and for quantitative dilution of samples. The box is equipped with a bag-less transport system to transfer material to the chemical separation boxes that are also equipped with this system.
- Each laboratory houses a chain of glove boxes for mass spectrometry. The chain consists of a box used for chemical separation of uranium and plutonium from fission products and other actinides and for alpha spectrometry, and the glove boxes for preparing the mass spectrometer's sample holder. The mass spectrometer is connected to the sample preparation box so that the prepared aliquots can be introduced directly into the mass spectrometer.

Samples taken at the front-end of the reprocessing plants – at the Head End Accountancy Tanks -, so called 'Input samples', are spiked in the Sellafield Thorp High Active hot cells. Only fractions sufficiently diluted to radiation levels acceptable for processing in a glove box are sent over to the OSL for chemical separation and mass spectrometry.

2.2.2. The LSS laboratory at La Hague

The majority of the samples received in the LSS La Hague are highly active input liquor samples. The LSS is located in an annex building to the UP3 plant. It houses three active laboratories and an office.

- The “product laboratory” is equipped with a glove box for preparation of uranyl-nitrate samples for K-edge and mass spectrometry measurement, and to prepare mass spectrometry reference solutions. The laboratory further hosts a suite of five boxes partly equipped with master-slave manipulators, and is dedicated to the measurement of isotopic compositions of PuO_2 product samples. Samples are received directly into the box by pneumatic transfer. The suite is connected to a gamma detector, and houses a hotplate and balance for dissolution and dilution of samples prior to TIMS measurement.
- The “hot cell facilities”: The very high beta-gamma activities of input solutions and some product samples require the use of well-shielded hot cells equipped with master-slave manipulators. Because of the large number of input samples from different origin, and to avoid cross contamination, the hot cell suite consists of three interconnected hot cells which are all equipped with HKED spectrometers, balances and density measurement devices. The hot cells are connected to the plant’s pneumatic transfer for automated sample receipt and to a liquid waste tank for the disposal of measured sample material. A small glove box is available for storage and treatment of reference materials.
- The “IDMS laboratory” consists of a suite of four glove boxes. The chain consists of a box for reception of diluted samples from all other LSS facilities by pneumatic transfer, a box used for chemical separation of uranium and plutonium and for alpha spectrometry, a box for the assembly of the mass spectrometer's sample holder, and a box that allows introducing the sample holder into the mass spectrometer.

3. Methodology changes in the early years

The Euratom On Site Laboratories have been operated successfully since their start-up. Naturally, there were a number of unexpected difficulties to which the laboratories had to adapt. Whenever necessary, methods and procedures were changed in order to improve quality of results and/or overall efficiency.

3.1. Reference Materials

When the On Site Laboratories were installed it was planned to obtain certified reference materials from JRC-Geel, Belgium. Working spikes would be prepared and calibrated in JRC-Karlsruhe and sent over to the On Site Laboratories ready for use. Long delays in the delivery of reference materials, difficulties in organising nuclear transports and the fact that solutions with higher plutonium concentrations are to some extent unstable forced the On Site Laboratories to produce and certify their own calibration reference solutions and working spikes. The Large-Sized Dried spikes produced at JRC-Geel, IRMM-1027, serve as reference basis for these measurements. Hence, the quality and reliability of these reference materials determine the accuracy to which the laboratories can operate.

3.2. Analytical method changes

3.2.1. Separation chemistry in the OSL Sellafield

A fundamental step of the sample preparation for alpha spectrometry and mass spectrometry analyses is the separation of uranium and plutonium fractions from fission products and minor actinides in the various sample types. A fully automatic system, developed by JRC-Karlsruhe, based on a Zymark robot, was originally installed in both On Site laboratories. The separation method implemented in the OSL Sellafield was based on the PUREX process, a liquid-liquid extraction method. By the time the LSS La Hague was constructed a robotised method using chromatographic separation on resin (UTEVA®: Eichrom) had been developed [5]. The main advantage of the chromatographic separation method is a better recovery of U and Pu, meaning a smaller quantity of sample is needed, and no ozone depleting reagents are used.
When the lifetime of the robot installed in the OSL came to an end, the OSL abandoned the PUREX process in favour of the UTEVA® chromatography.

3.2.2. Additional pre-separation chemistry in the LSS La Hague

IDMS plays a key role in the On Site Laboratories as part of the quality control system. Strict limitations apply to the radiation level of samples allowed to be treated in glove boxes. An improvement which highly contributed to the quality of the IDMS technique involved the pre-separation of fission products from the input sample in the LSS hot-cell enclosures. This allowed transfer of solutions containing higher quantities of Pu and U allowing comfortable chemical separation of the two elements and simple mass spectrometry measurements on each fraction [6].

4. Refurbishment projects

After the On Site Laboratories had been running without interruption for some 10 years, it became apparent that some refurbishments and renewals were due in order to keep the laboratories functional, and to guarantee that the instrumentation remains up to the latest standard allowing high quality measurements. A major project started in 2010 with the replacement of a thermal ionisation mass spectrometer in the OSL Sellafield. Currently, a modernisation of the hybrid K-edge measurement system is ongoing in both On Site laboratories, and further upgrades of mass spectrometers are planned for 2017-2018.

Refurbishments in the On Site Laboratories tend to be rather complex. As a result of the multilateral nature of the On Site Laboratories projects (DG ENER, JRC-Karlsruhe, site operator, and in the case of refurbishments often also a contractor having to work on the site to install new equipment), clear agreements and contracts have to be established. DG ENER is the owner of the laboratories and provides the necessary budgets for operations, routine maintenance, and refurbishments. The On Site Laboratories are working under the respective Site Licences of the site operator and have to meet the requirements defined in these licences. They furthermore must comply with site specific safety rules, and follow site and building procedures. The site operators have specific procedures to be followed before any non-routine work is allowed to take place, and permission is needed before any new equipment may be installed. As a result, a huge amount of paperwork is to be completed and to be reviewed and accepted by the site operator. In most cases, the site operator is involved in the execution of the work, as they are responsible for the provision and operation of the infrastructure. It is challenging to set up a sound time schedule and align the activities of all the stakeholders. Small refurbishments, such as the installation of a small piece of new equipment, or a like for like replacement, are usually handled directly between the On Site Laboratories analysts and the relevant site operator's staff. For big projects, it is necessary to set up a dedicated contract to engage a site operator projects team.

4.1. IT Hardware replacement project

The first substantial refurbishment project done in the On Site Laboratories was the replacement of the IT hardware. The On Site Laboratories Laboratory Information Management System (LIMS) was developed in the nineties in the JRC-Karlsruhe, and consisted of a combination of software modules running under the OS/2 WARP operating system. The original computer network was put in place during installation of the On Site Laboratories and had been running for almost ten years. Modernisation had been blocked until the OS2 version of Windows XP became available, allowing an economic solution for the upgrade. The LIMS software packages were migrated from OS/2 WARP to a Web based Microsoft XP using emulation software (Virtual PC). All new hardware was prepared and tested in JRC-Karlsruhe and thereafter sent to the On Site Laboratories for installation. In the OSL Sellafield, the computer renewals also required an upgrading of the computer cables by the site operator.

4.2. Hybrid K-edge related projects

Improvements, developments, upgrades and renewals of the Hybrid K-edge system have been a continuous process since the early years of On Site Laboratories. Improvements were done to increase the efficiency of the laboratory and inevitably some broken equipment had to be replaced. Measures were taken to put a fall-back option in place to keep the OSL Sellafield operational in case of a fatal failure of the "non-destructive analysis" box. In the last couple of years preparations started for a complete modernisation of the Hybrid K-edge systems.

4.2.1. Installation of an independent gamma station (OSL Sellafield)

Gamma spectrometry combined with Multiple Group Analysis (MGA) spectrum evaluation is a non-destructive means of measuring the $^{238}Pu/^{239}Pu$, $^{240}Pu/^{239}Pu$ and $^{241}Pu/^{239}Pu$ isotopic ratios present in a sample and is the only practical means to quantify the americium/plutonium ratio via the $^{241}Am/^{241}Pu$ nuclide ratio. Owing to the exceptionally low γ-activity of ^{242}Pu, the $^{242}Pu/^{239}Pu$ ratio cannot be measured, but the ratio can nonetheless be estimated using isotope correlation data [7, 8].

Sample throughput in the OSL Sellafield is limited by the "non-destructive analysis" glove box, where nearly all product samples are analysed. Originally, also the gamma measurements took place in this glove box. However, gamma measurements could only be carried out when the x-ray generator of the Hybrid K-edge/XRF was switched off. In addition, the γ -spectrometer arrangement in that glove box offered no means for optimisation of detector count rates, leading to exceptionally long counting times for MOX samples and to prohibitively long counting times for oxalate mother solutions. For a gamma measurement there is actually no need to remove the sample from its protective packaging, and, provided that the samples are adequately double bagged, the samples can be measured outside the confinement of a glove box. To improve the sample throughput, to prevent an unnecessary shutdown of the X-ray generator and to allow all samples, including low-activity oxalate mother solutions, to be measured to better accuracy and with a reduced measurement time, it was decided to equip the OSL Sellafield with an external gamma station similar to the external gamma stations developed and in use at the JRC-Karlsruhe.

The external gamma station was manufactured in JRC-Karlsruhe. It consists of a high purity germanium detector, connected to a shielded sample cavity. The station is mounted on a trolley. Pending samples are stored in a lockable shielded safe. The external gamma station is connected to the data-taking electronics traditionally used for the glove box based gamma measurements. The gamma measurements, evaluation of the spectra and reporting of measurements to the LIMS are therefore under control of the Alpha Workstation.

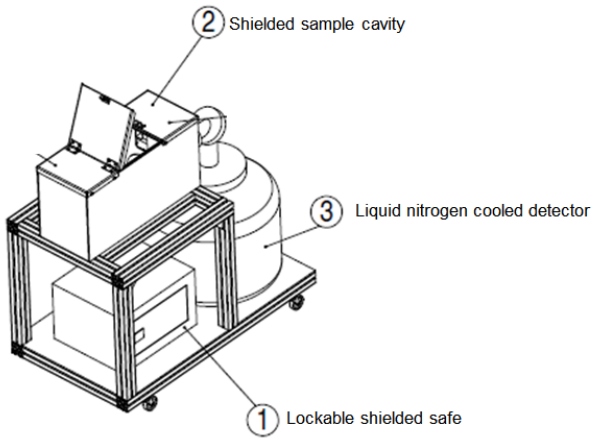

Figure 1. Drawing of the independent gamma station.

The use of the external gamma station in the OSL Sellafield represents a considerable improvement for the non-destructive analysis routine work in terms of sample throughput and quality of measurement and in terms of work organisation and flexibility. The station enables the whole sample to be viewed rather than a highly collimated portion of it; the gamma detector receives a noticeably higher amount of gamma rays, offers better count rate control and leads to quicker and more precise analysis. Also, the use of the external gamma station drastically improves the flexibility of the analysts work planning as gamma measurement can be performed in parallel to sample measurements involving K-edge/XRF.

4.2.2. Refurbishment of two glove boxes (OSL Sellafield)

In the OSL Sellafield nearly all product samples are prepared in the "non-destructive analysis" glove box and measured by the equipment inside or connected to the glove box using radiometric techniques. The high radiation of the samples as well as the acids used for sample preparation has caused and may continue to cause degradation of the glove box. The glove box will continue to be used with improvements and equipment repairs as needed. However, an alternative analysis route, based on chemistry/mass spectrometry, has been installed as a fall-back option in case of a major disruption in the "non-destructive analysis" glove box. This fall-back option was the subject of an "OSL glove box refurbishment project" involving DG ENER, the plant operator and the OSL, and consisted of the refurbishment of two glove boxes:

- Conversion of a uranium glove box which was used previously for preparation and initial analysis of pure uranium samples. The glove box was re-categorised as a uranium/plutonium box for performing second-step dilutions on sample aliquots to a concentration which is suitable for separation chemistry, and for preparation of reference solutions needed for the calibration of the OSL instrumentation.
- Conversion of the existing uranium/plutonium dilution glove box into a "dissolution-spiking" box. The glove box was refurbished to take over initial processing and sample preparation operations on all product samples: weighing, dissolution, dilution and spiking. No radiometric techniques are foreseen to be performed in this glove box.

All design was made in JRC-Karlsruhe and submitted to the plant operator for approval. Manufacturing of the new equipment and materials needed was mostly done in the JRC-Karlsruhe workshops, and thereafter sent over to the OSL Sellafield for installation by the OSL analysts. One of the most challenging tasks was to design all materials such that they could be introduced in the glove box via the existing posting ports, e.g. a new glove box floor. Some of the innovative design is described further in this paper.

4.2.3. Modernisation of the Hybrid K-edge densitometry system

The Hybrid K-edge / X-ray Fluorescence Densitometer instrumentation is used by Euratom and by the IAEA for Nuclear Material Accountancy Measurements [9]. It is the instrument of choice for Safeguards measurements at Nuclear Fuel Reprocessing Plants such as Sellafield, La Hague and Rokkasho. The instrument has been developed at JRC-Karlsruhe, some 30 years ago and continues to play an important role in Nuclear Safeguards measurements.

Although most of the instrument’s original OpenVMS-based software is still very capable, the instrument's hardware is getting very old. The Alpha workstation computers, which run the software, and the spectroscopy electronic modules, which measure the K-edge and XRF spectra, are no longer made and must be replaced by modern equivalents. However, a ready to use combination of all modules replacing the whole interface cannot be purchased on the market. An innovative solution needed to be worked out in JRC-Karlsruhe. A further improvement of hardware tackled at the same time is the replacement of the traditional liquid nitrogen-cooled HRGS detectors by electrically cooled detectors.

4.2.3.1. Installation of emulated Open VMS software

The Virtual Alpha emulator is a software application installed on a PC with Microsoft Windows® 7 OS (Host system) which emulates the functions of an Alpha workstation with OpenVMS operating system (Guest system). The guest system is saved as a virtual hard drive. This virtual hard drive is an image of a real hard drive of the VMS system running on an Alpha workstation. The emulator software enables the Open VMS and all the VMS software installed in the virtual hard drive to run on modern and most advanced PC architecture (x86 and the latest Intel Processors) with Windows® OS although designed for the Alpha workstation architecture. Hence this allows continuing to use VMS specific software (i.e. Canberra k-edge software, Neutron Counting software etc.) on modern hardware.

The system was first set up and tested in JRC-Karlsruhe in collaboration with an external contractor (Migration Specialties Europe, Tarthorst, Netherlands). Meanwhile most of the Alpha workstations in the On Site Laboratories have been replaced.

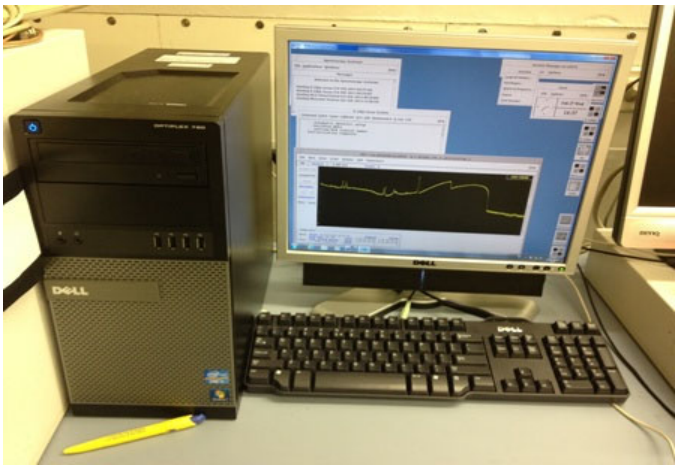

Figure 2. Virtual Alpha emulator installed on PC.

4.2.3.2. Replacement of NIM electronic modules by Lynx

The traditional Nuclear Instrumentation Modules (NIM) are no longer manufactured and the repair of broken NIM units is no longer guaranteed. The Lynx hardware produced by Canberra is a good alternative to traditional NIM. A software driver to allow Lynx to run with the Hybrid K-edge/XRF's OpenVMS operating system has been developed and tested in JRC-Karlsruhe, so the Hybrid K-edge/XRF software is now capable of using modern Lynx spectroscopy hardware. The Lynx hardware outperforms the traditional NIM hardware except for digital peak stabilization. The HKED system uses two peaks (22.1 and 88.04 keV), originating from a ^{109}Cd-source located close to the detector, as reference peaks for the digital stabilisation of the electronics. Properly peak-stabilized spectra are a crucial requirement for reliable Hybrid K-edge/XRF spectrum evaluation, and it is essential that this problem is remedied before the Lynx hardware can be used to replace the aging NIM electronics. An algorithm to improve upon the deficient Lynx peak stabilization has been developed at JRC-Karlsruhe. The computational approach performs better than the Lynx peak stabilization and even performs better than NIM-based peak stabilization. Tests on the post-processing algorithm have been completed, and the algorithm now has to be integrated into the OpenVMS-based Hybrid K-edge/XRF software. An additional advantage is that the new algorithm will be able to cope better with weaker ^{109}Cd radio-active sources.

4.2.3.3. Replacement of the X-ray generators (LSS La Hague)

The LSS has 4 Hybrid K-edge densitometry systems each equipped with a high voltage generator of 160 kV and 15 mA and X-ray tube control unit. The generators have exhibited increased breakdowns and reduced reliability. It is furthermore becoming more and more difficult to repair the instruments as spare parts are lacking. Merion – Canberra have indicated that future repairs cannot be guaranteed. New HV generators (GE Titan Isovolt) capable to deliver 160 kV and up to 15 mA and compatible with the existing X-ray tubes (Comet MIR 160/12) were ordered and will be installed in the near future. The replacement will ensure reliable operation for many years to come.

4.2.3.4. Installation of electrically cooled detectors

Replacement of the traditional liquid nitrogen-cooled detectors by electrically cooled detectors eliminates the need for liquid nitrogen, which has the following advantages:

- Independence from the availability of liquid nitrogen in the controlled areas of the operator site
- Elimination of the risks of working with liquid nitrogen (frostbite, asphyxiation)
- Use of an environment-friendly alternative to liquid nitrogen
- Significant savings in running costs (labour, liquid nitrogen)

In the OSL Sellafield three detectors with their associated 25L Dewars will be replaced by three Cryo-pulse® CP-5 U-style Ge detectors. The Canberra Cryo-Pulse® 5 Plus is an electrically powered cryostat for use with HPGe radiation detectors. It utilizes a pulse tube cooler, a highly reliable

technology originally used in military and space applications, which has proven its value for germanium detectors in the original Cryo-Pulse 5. As stated by the producer, like its predecessor, the Cryo-Pulse 5 Plus consists of a cold-head-assembly, to which the detector is attached, and an external power controller. The basic external design and interface of the cold-head have been preserved to maximize interchangeability between the previous and the new version. However, the cold-head internals and the controller have been completely redesigned and new features have been added to improve the performance and reliability and to better answer customers' requirements. In order to deal with the restricted space under the "non-destructive analysis" glove box and in the external gamma station, the CP5 have been custom built to offer a sideways-viewing detector head. The cryostats will be placed on metal support frames, manufactured in the JRC-Karlsruhe, so that the units can be positioned in the exact required location. The cryostats have been tested in the JRC-Karlsruhe prior to shipment to the OSL. They are ready for installation as soon as the administrative procedure to obtain permission from the site operator will be finalised.

A similar replacement action is foreseen for the seven HPGe detectors at the LSS La Hague since two of the detectors cannot be repaired anymore. As space restrictions are not an issue, the LSS opted for the hybrid detector cooling system, a combination of an electrically cooled detector with a liquid nitrogen cryostat, the Canberra Cryo-cycle II. Cooling is guaranteed by the liquid nitrogen in case of power outages. The cryostat can do without extra nitrogen for at least 6 months. A substantial reduction of liquid nitrogen consumption is to be expected.

Figure 3. Cryo-pulse® CP-5 U-style Ge detectors (left) for the OSL and Cryo-cycle II Ge detectors (right) for the LSS.

4.2.4. Replacement of K-edge cooling

In both On Site Laboratories, the refrigeration chillers which serve to cool down the X-ray tubes have been replaced when they became unrepairable. In the LSS La Hague a preliminary infrastructure study was performed by the JRC-Karlsruhe, the work itself was outsourced to a contractor. In the OSL Sellafield, the exchange of the refrigeration chiller was handled by the site operator's project team.

4.2.5. Replacement of Anton Paar densitometers

The instrumentation currently in use is the Anton Paar DMA 48 in conjunction with an external measuring cell DMA 401. Both the DMA 48 and the DMA 401 are equipped with a borosilicate glass U-tube. The resolution of the instrument is 0.00001 g/cm^3 and the accuracy can be as low as 0.00005 g/cm^3. The internal measuring tube is not used. The external measuring cell requires some modification before installation in the hot cells in the LSS and a glove box in the OSL. To maintain the temperature at 25 °C (in the LSS) or 20 °C (in the OSL) a water circulation is available.

The DMA 48 and the DMA 401 are no longer available on the market. JRC-Karlsruhe has successfully used the spare internal measuring cells to manufacture external measuring cells. Now, there are no cells available anymore. The densitometers currently available on the market are integrated within a desktop model. A modification of these models for use in a nuclear environment is not possible since too many important components are not resistant to radiation. Anton Paar offers a new external measuring cell with a hollow U- tube made of Hastelloy C-276 (DMA HPM) to be used in conjunction

with the mPDS5 evaluation unit. JRC-Karlsruhe is modifying and testing this instrument for future use in the On Site Laboratories.

4.3. Mass spectrometry refurbishment projects

Mass spectrometry serves a twofold purpose at the On Site Laboratories. Thermal Ionisation Mass Spectrometry is used to measure the uranium and plutonium isotopic compositions. Isotope Dilution Mass Spectrometry is employed to determine uranium and plutonium mass fractions using a well-characterized reference material, for example, "Large-Sized Dried Spikes" (LSD) [10, 11]. The latter results are also used to characterise the calibration solutions for the HKED densitometers.

4.3.1. Decommissioning of an old TIMS MAT261 mass spectrometer and installation of a Triton

In 2009, a project was set up to replace a broken down MAT261 mass spectrometer in the OSL Sellafield, and replace it with a Triton (Thermo Fisher Scientific GmbH) instrument. It was the first major refurbishment project in the OSL, involving four parties (DG ENER, JRC-Karlsruhe, Sellafield Ltd. and Thermo Fischer). A dedicated contract was signed between DG ENER and the site operator for their Projects' team to bring the project forward and perform the necessary infrastructure works. The purchase of the Triton was handled by JRC-Karlsruhe on behalf of DG ENER. Additional equipment such as a dedicated glove box was developed and manufactured in the JRC-Karlsruhe.

The following work phases were identified on site:

- Disconnection of two glove boxes from the mass spectrometry chain and their decommissioning
- Decommissioning of the broken MAT 261 mass spectrometer
- Preparation of the laboratory infrastructure to accommodate the Triton specifications
- Installation of the new mass spectrometer
- Installation of a new glove box and connection to the separation chemistry box and the new mass spectrometer
- Commissioning and validation

With the installation of the Triton the OSL acquired a state-of-the-art instrument for mass spectrometry. The number of samples that can be loaded on one magazine is significantly higher than for the MAT261, and the instrument can run in independent mode, allowing overnight measurements. Hence, due to the Triton the OSL managed to increase the efficiency of the laboratory with delivery of high quality results.

Figure 4. Triton connected to glove box (left) installed in the OSL and photo of the inauguration (right).

4.3.2. Upgrade of the Filament Degassing Unit (OSL Sellafield)

The Filament Degassing Unit (FDD) is needed to degas filaments before they can be used as sample holders for mass spectrometry. The FDD installed in the OSL Sellafield was a 30 years old instrument with limited capacity. Shortly after the installation of the Triton, the Filament Degassing Unit was refurbished:

- Upgrade of the electronics
- Replacement of the filament rack, the new rack containing 30 positions

Since the upgrade, the Filament Degassing Unit is more reliable, with the main advantage that 30 filaments can be baked at once, saving valuable time for the mass spectrometry analyst.

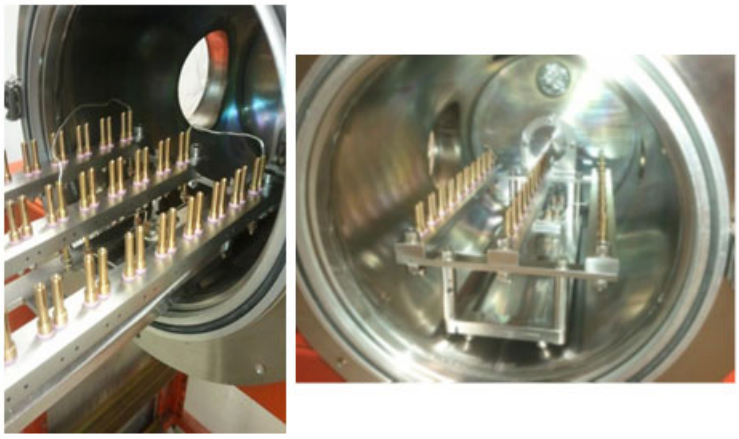

Figure 5. Filament rack containing 30 positions.

The FDD unit in the LSS La Hague has become dysfunctional and can only work on one side, thus degassing only half of its capacity. It will be replaced by a new instrument in the near future.

4.3.3. Upgrade of three TIMS MAT26x mass spectrometers

The JRC has three TIMS MAT261 mass spectrometers operational, one in the JRC-Karlsruhe, one in the LSS La Hague and one in the OSL Sellafield. Due to their different age (from 18 to 35 years old), the hardware/software components and the operation of the instruments is somewhat different. For the oldest instrument, located in the JRC-Karlsruhe, electronic modules are becoming sparse and it has become difficult to purchase original spare parts. Despite its age, the instrument remains important for training new analysts before they are allowed to work in the On Site Laboratories. Therefore it was decided to upgrade the three mass spectrometers. The company Spectromat provides commercial options for refurbishment of MAT26x instruments, such as the provision of modern electronics for operation and data acquisition, and some hardware components. The installation of Spectromat software is required for communication with the new electronic modules. Due to the different ages of the three mass spectrometers, the upgrades will be individually different, from new software only for the OSL instrument, to some hardware plus software upgrade for the LSS instrument and of a complete exchange of electronics, some hardware and software in JRC-Karlsruhe.

The approach will allow the three instruments to remain in operation over the coming 10+ years at a cost which is far lower than the purchase cost of new instruments. Moreover, all three mass spectrometers will be running with exactly the same software, which simplifies the work of the analysts.

5. Innovating developments

Over the years, the On Site Laboratories faced specific problems which required creative solutions. Also in the frame work of the extended refurbishment projects, some ideas were worked out and led to many innovative developments that could be relevant for other laboratories.

5.1. Modifications to the densitometers located in hot cells (LSS La Hague)

To introduce a liquid in the glass U-tube of the external measuring cell of the Anton Paar density meter the cell is equipped with a screwed on metal tube with an external diameter of 1.6 mm. It is however extremely difficult to mount a new tube or new flexible tubing. Although very resistant, the flexible tubing occasionally needs to be replaced. Also, the Teflon tips connected to the metal tube making contact with the glass cell break off after a certain time. The output side of the glass cell is connected

to a 3-way valve via a similar system. A breakdown of this tube connection system usually meant a long downtime for the density meter as only a very experienced analyst was able to perform the repair. Since no useable alternative was available on the market, JRC-Karlsruhe has developed a new flexible tubing connection system for the glass cell, and quick-snap connections in stainless steel for the 3-way valve.

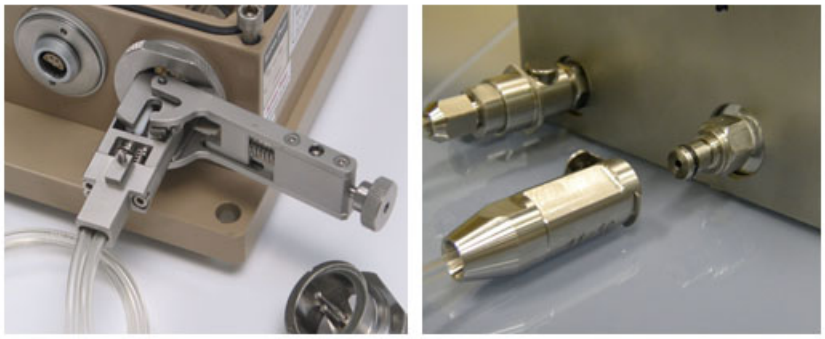

Figure 6. Flexible tubing connection for use with manipulators (left) and small stainless steel quick snap connections (right).

5.2. Infrared heater for preparation of alpha planchets

Alpha spectrometry measurements are required for all Pu fractions to be measured by mass spectrometry in order to de-convolute any possible isobaric interference from ^{238}U with ^{238}Pu. The system originally installed in the On Site Laboratories for the preparation of alpha measurement planchets (metal sample holders), was prone to frequent breakdowns of its heating element. The system was also limited to a maximum planchet temperature of 180 °C, and planchets had to be prepared one at a time. JRC-Karlsruhe developed and manufactured a stand-alone heating unit containing a 100 W infra-red element. The unit is foreseen with safety features to prevent the inadvertent contact of the heating platform with glove box gloves or other combustible material. It also incorporates a timer which locks the unit until sufficient cooling time has elapsed before the analyst can access the heating platform. The new unit delivers a planchet temperature of approximately 290 °C which in turn prepares better quality planchets. As a result almost no alpha planchets need repetition. Moreover, it is possible to prepare 4 planchets simultaneously, therefore reducing the overall preparation time.

Figure 7. Infrared heater for preparation of alpha planchets.

5.3. Semi-automated separation unit

A fully automated Zymark robot was originally installed in the On Site Laboratories for chemical processing of the samples. Chemical separation is required to remove decay and fission products and provide separated U and Pu fractions for mass spectrometry. After ten years of use the robots came to the end of their lifetime and repeated breakdowns led to long downtimes, while it became increasingly difficult to obtain spare parts after the commercially available device was withdrawn from the market.

While routine operations continued performing manual separations, a new solution was needed to replace the outdated robots. The device had to be safe to operate in a glove box, and be compact enough to allow posting it into the existing boxes via the posting ports. A semi-automated separation device for chromatographic separation on resin (UTEVA®: Eichrom) has been developed by the JRC-Karlsruhe in collaboration with the IAEA under the framework of the EC support programme to the IAEA [12]. The JRC-Karlsruhe planned and built the unit while the IAEA developed the controlling software based on an early version of JRC-Karlsruhe. The main features of the semi-automated separation unit are its modular construction for simple replacement of components, minimum need for operator intervention, its light structure built using materials resistant to acid environment and its remote control function via a LabView based software. The benefits of the semi-automated separation unit are a reduction of the radiation dose rates in the vicinity of the operators and an increase of the sample throughput. The device is expected to be installed in the LSS La Hague in the near future.

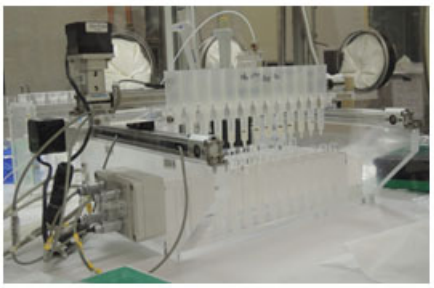

Figure 8. Semi-automated separation unit.

5.4. Foil heater, a hotplate based on a flexible low power heating element

A hotplate, fit-for-purpose of dissolving spiked samples or powders/pellets in a glove box has been designed, manufactured and tested at JRC-Karlsruhe. Heat is provided with a flexible heating element that can be purchased from several manufacturers (Minco, Termya, and Synomas). The element is made of wires insulated in a polyimide film (Kapton®). The operational range to dissolve samples is between 16 V and 20 V: within this operational range the power dissipated per unit of the hotplate surface varies from 0.26 W/cm^2 to 0.32 W/cm^2. Even lower voltages are suitable for spike-dissolutions. The heating element is enclosed in an outer casing made of polycarbonate with UL94 V-0 certification. The outer temperature on the surface of the outer casing reaches no more than 60 °C. Heat output and external-surface temperature of the foil heater enclosure are therefore acceptable for use inside a glove box. An outlet in the casing is connected to the ventilation system to remove acid fumes. The hotplate has inserts allowing secure placement of spike vials or various sizes of Erlenmeyer flasks. Several heating devices can be connected in series. The case(s) containing the flexible heating system and the temperature sensor are located in the glove box, while the power supply and the temperature control unit are located outside the glove box. The cabling is connected via feed-through "LEMO" connectors.

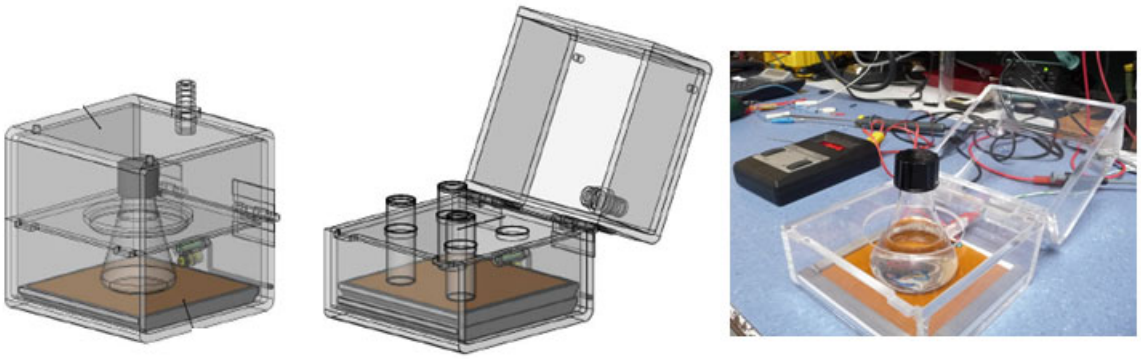

Figure 9. Foil heater for use with Erlenmeyer (left) or spike vials (middle) and prototype (right).

5.5. Mounting of additional lead shielding to glove boxes

The glove boxes installed in the OSL Sellafield are Perspex type boxes. The glove box window panels and ceiling consist of 12 mm Perspex, and the bottom plate is made of stainless steel. The glove boxes are supported on a steel frame. During installation, those glove boxes that would be used for the more active samples were foreseen with additional 2 cm thick lead glass window panels. In the framework of the OSL refurbishment, additional shielding has been mounted to some glove boxes to protect the operators from the increased radiation.

5.5.1. Additional shielding surrounding an existing Perspex type glove box

The steel frame work on which the Perspex glove box is resting, had no features foreseen to add heavy additional shielding. A design was made to clamp a second support frame to the existing glove box support frame. The arrangement did not require welding or drilling. The shielding comprised of half-thickness leaded-panels (in front of the Perspex side-windows) and painted lead shielding fitted to the forth side where a bagless transport system was in place.

5.5.2. Additional shielding underneath an existing glove box

Additional lead shielding was installed underneath two OSL Sellafield glove boxes. Lead sheets with a thickness of 2-3 mm (and sheathed with a 2 mm layer of aluminium) were inserted under the glove box, thereby increasing the shielding efficiency of the glove box's floor and protecting the lower half of the operator's body from radiation uptake. The installation of the extra shielding required neither particular intervention nor modification of the infrastructure. The lead sheets slide in between the existing glove box frame and existing lead window frame so that they are positioned under the glove box but on the top of the glove box stand. The lead sheets are secured in place with steel clips and an additional support bar. The overall weight, estimated of 55 kg, is well within the tolerance limit of the glove box stand.

5.6. Replacement of a glove box's flooring

In the framework of the refurbishment of a glove box in the OSL Sellafield it was decided to replace the glove box flooring. Several pieces of equipment were removed during the cleanout of the box, leaving the original plastic floor in an un-even and un-complete way. Not only would this have posed some restrictions in the possible layout of the refurbished box, but also the risk of accidental spillages would have been considerable.

5.6.1. Removal of the old flooring

The plastic floor sheet which covered 75% of the glove box floor had to be removed to allow the fitting of a new floor. JRC-Karlsruhe selected and trialled a powered cutting tool (Multimaster) for the cutting-up of the plastic floor sheet. Also some silicon sealing had to be removed, taking care not to damage any of the materials that form part of the glove box containment, such as the Perspex panels or the rubber sealant between Perspex and metal frame. An aluminium adjustable spacer was designed and attached to the cutting tool which allowed controlling the depth of the cut with high precision. Tests were performed and videoed in the JRC-Karlsruhe workshop and submitted to the plant operator to prove the safety of the tool. Training was given to the analysts in the use of the Multimaster in a mock-up glove box in JRC-Karlsruhe prior to performing the work on site.

5.6.2. Installation of new polycarbonate glove box flooring

The design of the new glove box floor was quite challenging:

- All materials needed had to be introduced into the glove box via the existing posting ports. Glove boxes in the OSL Sellafield have 8 inch ports, with one 16 inch port in the roof of the box.
- Only non-combustible or fire retardant and heat resistant materials are allowed to be used throughout the facility. The plant operator insisted on the use of a UL94 V-0 certified material, which is difficult to obtain in Europe in small quantities.

- The design must allow regular inspection of the area underneath the floor for spillages, as well as the possibility to clean up such spills

The new glove box floor is made from polycarbonate rods that slot together to form a frame, then levelled and covered by polycarbonate tiles. The polycarbonate used is Makrolon GP Clear 099 with the required UL94 V-0 certification. Once in place, the middle tiles are removable with the aid of a rubber plunger. A trial assembly was carried out in the JRC-Karlsruhe workshop prior to the flooring being delivered to site.

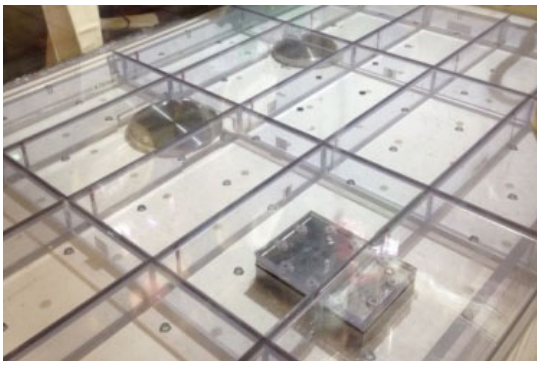

Figure 10. New polycarbonate glove box floor.

5.7. Replacement of feed-through LEMO connectors

The feed-through LEMO connectors originally fitted to the glove box panels in the On Site Laboratories were showing signs of corrosion and were going green in colour due to the material of manufacture and the glove box environment. JRC-Karlsruhe has developed two ways of addressing the problem.

5.7.1. Installation of additional LEMO connectors via a glove or posting port

In JRC-Karlsruhe, additional LEMO feed-through connectors are installed via a glove or posting port. An un-used port is closed off by a port cap containing the necessary feed-through connectors. The system is also used for throughput of reagents tubing.

Figure 11. Posting port with LEMO feed-through connectors.

In the LSS La Hague, additional feed-through connectors will also be installed via a posting port. However, the choice fell on titanium connectors from Souriau (formally Jupiter) in line with the plant operator practices.

5.7.2. Exchange of feed-through LEMO connectors (OSL)

In the OSL Sellafield feed-through LEMO connectors were replaced at the occasion of the refurbishment of two glove boxes. LEMO connectors which are no longer needed have been covered by stainless steel caps. All other LEMO connectors were replaced by stainless steel bulkhead LEMO plug/socket connectors. In the first glove box the contamination levels were so low, that, apart from wearing gloves and respirator protection, no additional measures were required. The contamination level in the second glove box called for a more stringent method to be developed. A set of specifically designed tools were developed to be used as safeguards during the exchanging procedure. The entire procedure is being patented by JRC-Karlsruhe and can therefore not be described in detail for the time being. The advantages of the developed method are that only the area immediately surrounding the feed-through connector had to be cleaned to "contamination free" levels, which facilitates the contamination monitoring, and all the steps of the process are protected via engineered safeguards which guarantees that no contamination can be released from the glove box during the exchange procedure.

6. Conclusions

The Euratom On Site Laboratories have been operated successfully for more than 15 years. Based on the operational experience, processes have continually been optimised and procedures streamlined. After the first ten years, optimisation alone was no longer sufficient to keep the laboratories operational in the long term. Therefore, laboratory refurbishment had to be looked at with an open mind for future needs. Renewals in the On Site Laboratories mostly involve specialised and fit for purpose equipment that cannot be purchased on the market without adaptations, or cannot be purchased at all. The analysts working in the On Site Laboratories have always been dedicated to come up with creative, purpose built, problem oriented solutions. The JRC-Karlsruhe in house design team and workshop have proved to be of utmost importance to support the On Site Laboratories. This cooperation resulted in a whole series of innovative developments, which may be useful for other laboratories in the nuclear and/or other fields. Also, the site operators play an important role in any refurbishment project. The refurbishment programs are still ongoing, and are foreseen to continue over the coming years. The On Site Laboratories are well placed to continue to deliver high quality results to DG ENER.

7. Acknowledgements

The authors would like to acknowledge the JRC-Karlsruhe design office and workshops for their invaluable contribution to all the innovations and refurbishments described. The authors also express their gratitude to the site operators of La Hague and Sellafield for their support.

8 Legal matters

8.1. Privacy regulations and protection of personal data

The author agrees that ESARDA may print her name/contact data/photograph/article in the ESARDA Bulletin/Symposium proceedings or any other ESARDA publications and when necessary for any other purposes connected with ESARDA activities.

8.2. Copyright

The author agrees that submission of an article automatically authorises ESARDA to publish the work/article in whole or in part in all ESARDA publications – the bulletin, meeting proceedings, and on the website.

The author declares that their work/article is original and not a violation or infringement of any existing copyright.

9. References

[1] IAEA Report of the LASCAR Forum; *Large Scale Reprocessing Plant Safeguards*; STI/PUB/922, Vienna, Austria, 1992.

[2] K. Casteleyn, L. Duinslaeger, P. Amador Celdran, P. Arboré, P. Chare, E. Dahms, O. Drinnhausen, H. Eberle, T. Enright, A. Guiot, M. Hild, J. Horta Domenech, A. Le Terrier, K. Lützenkirchen, S. Millet, S. Morel, M. Munoz Nieto Sandoval, A. Nicholl, S. Nucifora, H. Ottmar, D. Poublan, G. Rasmussen, F. Sarli, J. Schönfeld, H. Schorlé, P. Schwalbach, S. Street, P. van Belle, E. Zuleger; *The Euratom Safeguards On-Site Laboratories at the Reprocessing Plants of La Hague and Sellafield*; JRC Reference Report; 2011;
https://ec.europa.eu/jrc/en/publication/reference-reports/euratom-safeguards-site-laboratories-reprocessing-plants-la-hague-and-sellafield.

[3] U. Blohm-Hieber, F. MacLean, P. Chare, W. Kloeckner, K. Mayer, H.G. Schneider, and H. Ottmar; *"OSL" – Inauguration of the first EURATOM On-Site Laboratory*; Proceedings of the 22nd ESARDA Annual Meeting, Dresden, Germany; 2000.

[4] U. Blohm-Hieber, P. Chare, W. Kloeckner, P. Daures, H. Ottmar, P. Richir, G. Décobert, and X. Rincel; *"LSS" – Inauguration of the EURATOM "Laboratoire-sur-site"*; Proceedings of the 23rd ESARDA Annual Meeting, Bruges, Belgium; 2001.

[5] P. Richir, B. Brandalise, C. Apostolidis, R. Molinet, and K. Mayer; *Development of a robotized separation method for U-Pu samples using UTEVA resin*; Proceedings of the International Workshop on the Application of Extraction Chromatography in Radionuclide Measurement, Geel, Belgium; 1998.

[6] P. Richir, A. Guiot, A. Le Terrier, J. Horta, P. van Belle, and P. Daures; *Simple, robust and rapid method to separate the U-Pu fraction from an input solution in a hotcell facility prior to its transfer into a glove-box*; Proceedings of the 25th ESARDA Annual Meeting, Stockholm, Sweden; 2003.

[7] R. Gunninck. W.D. Ruther; *MGA: A Gamma-ray Spectrum Analysis Code for Determining Plutonium Isotopic Abundances, Vol.1 (Methods and Algorithms)*; Report UCRL-LR-103220, Vol.1, April 3; 1990.

[8] R. Gunninck. W.D. Ruther; *MGA: A Gamma-ray Spectrum Analysis Code for Determining Plutonium Isotopic Abundances, Vol.2 (A Guide to Using MGA)*; Report UCRL-LR-103220, Vol.2, September 1; 1990.

[9] K. J. Moody, D. A. Shaughnessy, K. Casteleyn, H. Ottmar, K. Lützenkirchen, M. Wallenius, T. Wiss; *Analytical Chemistry of Plutonium*. In *The Chemistry of the Actinide and Transactinide Elements*, L. R. Morss, N. M. Edelstein, J. Fuger, Eds.; Springer: Dordrecht, Vol. 6, pp 3889-4004; 2010.

[10] J. Berger, N. Doubek, G. Jammet, D. Donohue, G. Bagliano, K. Mayer, A. Verbruggen, C. Ingelbrecht, F. Hendricks, A. Alonso, P. De Bièvre, and H. J. Ahrenz; *Development and Experience with 235U and 239Pu Solid Spikes for IDMS of Spent Fuel Solutions*; Proceedings of the 17th ESARDA Annual Meeting, Aachen, Germany; 1995.

[11] E. Zuleger, K. Casteleyn, L. Duinslaeger, K. Mayer, P. Richir, and P. van Belle; *Accuracy and Precision achieved in Thermal Ionisation Mass Spectrometry of Uranium and Plutonium in a Safeguards Analytical Laboratory under Routine Conditions*; Proceedings of the 45th INMM Annual Meeting, Orlando, USA; 2004.

[12] R. Buda, S. De Vry Balsley, L. Emblico, A. Schachinger, E. Zuleger; *Semi-Automatic Separation Unit for Actinides at JRC-ITU and IAEA*; Proceedings of the 37th ESARDA Annual Meeting, Manchester, UK; 2015.

The ENEA Contribution to the Implementation of the National Nuclear Safeguards

Alessandro Dodaro, Giorgio Giorgiantoni, Nadia Cherubini, Giuseppe A. Marzo
ENEA, C. R. Casaccia, Roma, Italy

Abstract:

ENEA, The Italian Agency for New Technologies, Energy, and Sustainable Economic Development, the second R&D Institute in Italy, through its experts of the nuclear Division is one of the main consultant - since 2004 - of the Ministry of Economic Development (Mise) for the obligations stated in the Additional Protocol, since the government signed the NPT (Non Proliferation Treaty) that was ratified in 2003. Furthermore, in the periodic action plans that are submitted every three years to the Ministry, a great part of the economic resources allocated by MiSE are finalized to R&D activities. By means of this agreement, new instruments, new proposals, new information events and recently a mobile laboratory have been implemented to reach a prompt reaction in case of detection of suspicious materials during the various phases of the international and national trade that might result in illicit trafficking of nuclear material. In this framework ENEA is also member of ESARDA and follows all the main international events that are regarding R&D for the implementation of the safeguards. The final implementation of measures and practices under the safeguards regimes is a wide spectrum of disciplines, in which what is really important is the knowledge and the experience of the experts of our Division. Our Agency is by law committed in many activities that are involving the nuclear industry, also through its participated firm NUCLECO and the continuous effort to improve and diffuse procedures and tradition are a solid asset in the Italian scenario.

Keywords: Implementation, Nuclear Safeguards, Additional Protocol, Characterization of suspicious radioactive materials, Mobile laboratory, Analytical Instrumentation

1. Introduction

From IAEA definition: "*Safeguards are a set of technical measures applied by the IAEA on nuclear material and activities, through which the Agency seeks to independently verify that nuclear facilities are not misused and nuclear material not diverted from peaceful uses. States accept these measures through the conclusion of safeguards agreements*

IAEA safeguards are an essential component of the international security system. The Treaty on the Non-Proliferation of Nuclear Weapons (NPT) is the centrepiece of global efforts to prevent the further spread of nuclear weapons. Under the Treaty's Article 3, each Non-Nuclear Weapon State is required to conclude a safeguards agreement with the IAEA ".

The Additional Protocol to the NPT extends the control actions to materials and activities which are not specifically nuclear but that may directly or indirectly be used in the nuclear field. Furthermore the collection of information on these materials and activities is widened, includes also the verification and

inspections on use, possible presence of undeclared materials, adoption of new control systems and a better coordination among the public institutions….

Article 3, paragraph 2, of the Italian Law 332/2003 identifies ENEA, the Italian Agency for Energy, the Environment and the Sustainable Economic Development, as one of the Agancies to which MISE (the Italian Ministry of the Economic Development) can entrust the execution of studies and analysis and other specific activities related to the AP (Additional Protocol).

2. Methods

2.1 The Integrated Service

The ENEA Board of Directors, with a resolution of 4 June 1986 Doc. ENEA, (86) n. 33/CA Rev.1 approved the establishment of an «Integrated Service» for the management of low and medium radioactive wastes generated by external operators and defined that such a Service were undertaken partly directly by ENEA and partly entrusted to NUCLECO. The relations between the parties, to apply such a resolution are regulated through a specific Convention, whose first implementation goes back to the 15th June 1989.

The legal framework in which the Agency acts and supervises the authorized operators which are in the business, includes two main legislative decrees: the D.Lgs. 230/95, the general Italian act on the nuclear activities and mainly D.Lgs. 52/2007 [1].

- D.Lgs. 52/2007 Transposition and implementation of the Directive 2003/122/CE EURATOM on the control of the HASS (High Activity Sealed radioactive Sources) and orphan sources.
- Art. 2 paragraph 1 letter m). «Integrated Service» technical operative tool able to take charge of all the phases of the management cycle of the disused source.
- Art. 12 The ENEA Agency with no further charges to the government funding, is required to organize and manage training courses for the personnel who are operating in those installations in which orphan sources are likely to be found (i.e. customs, metal industries, the great scrap metal repositories, the intermodal shipping nodes) to achieve adequate knowledge and competence in the field. In such a context, the Agency makes available through internet characteristics, pictures, and features of radioactive sources collected in posters and other means of immediate consultation to minimize the danger of illicit trafficking of suspicious radioactive materials (see “de minimis” trading)
- Art. 17 paragraph 3, The Integrated Service guarantees all the phases of the management cycle of the disused sources like the preparation for shipment, the transport, eventually the conditioning and the temporary storage. All the plants and operators which undertake collection activities and eventual temporary storage of disused sources are allowed to join the Service. (They must be in possession of the relevant authorizations issued by the Ministry of Economic Development as regulated by the 230/95 act).

Under this act of the Italian parliament issued in May 2007, ENEA is responsible for providing an Integrated Service able to manage the collection and the storage of low and medium activity radioactive materials, including disused radioactive sources.

It can be imagined that the international legislative outline is in rapid evolution through a deeper harmonization among the European Union, encouraged by means of the IAEA guidelines. Italy is following this process, since all the legislative acts of the government and parliament are in compliant with the recommendations of the Agency and the EURATOM directives.

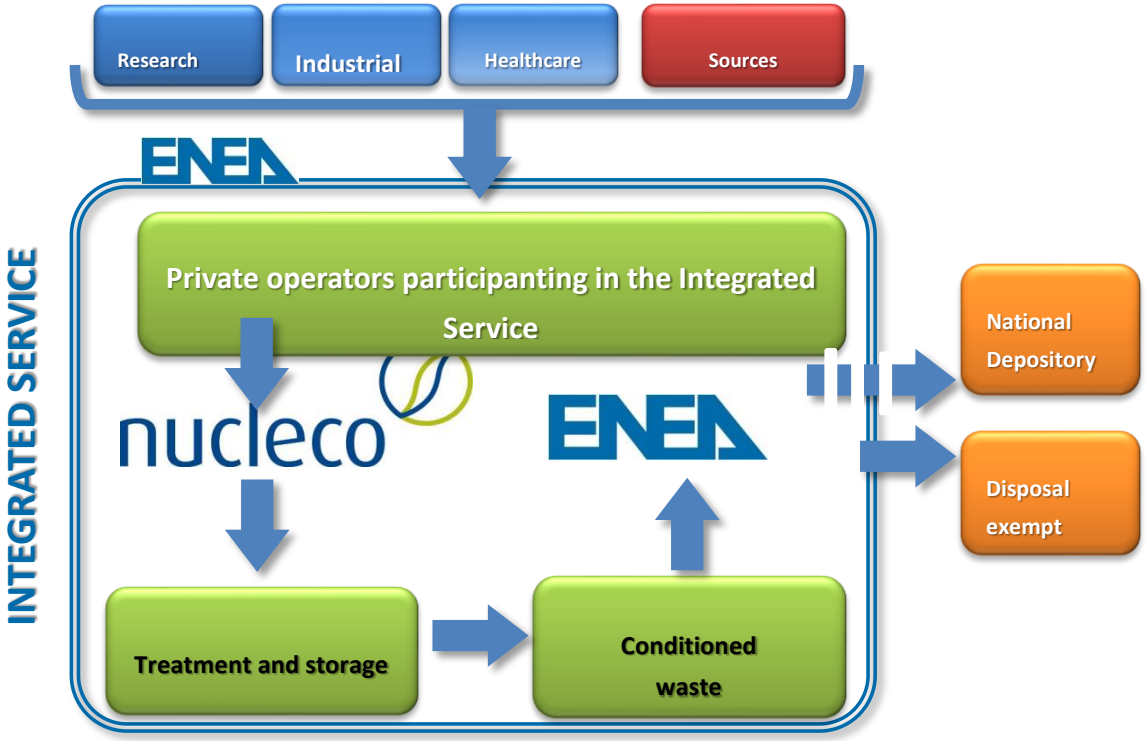

Fig. 1 Scheme of the integrated Service

In this area, ENEA makes consultation to the Italian Prefectures for the preparation of schemes, intervention plans and procedures in case of recovery of orphan sources or suspicious presence of sources in the territory of the province (art. 14 Dlgs. 52/2007).

If procedures and responsibilities were not clear, we could reach the stage in which serious accidents due to thefts, misuse,or illicit detention or abandoning could be unfortunately recorded. IAEA records in the last decades at least ten significant accidents worldwide in which orphan sources were involved due to poor quality of supervision and management.

ENEA is also the manager of the integrated service, at the end of the characterization phase, these radioactive materials including the sources, are hosted in the temporary NUCLECO repository where the liquid and solid wastes are treated, conditioned, and kept in custody, before their shipment to our final/temporary repository.

In this processes, the contractual obligations with our participated firm NUCLECO, prescribe the fulfilment of IAEA-EURATOM Directives, as far as all the accountancy records and material balance files are carefully kept and available in case of inspection.

Whenever these inspection are undertaken, experts and the personnel in general are recommended and have a cooperative and transparent behavior. In all circumstances Agency issues letters that everything complies with the clauses of the international treaties.

We have to point out that this continuous discussions between the experts of the Regulator body, R&D institutions, and operators has given a beneficial thrust to the updating of the so called “nuclear right” that implies the correct transposition of the European Directives and IAEA recommendations into the national law, because even in this field a strong rate of legal disputes is found and at the same time the necessity to update the background of lawyers and men of law.

2.2 Convention ENEA-MISE

Italy through the act n. 332 October 1st 2003 [1] ratified the Additional Protocol to the Non Proliferation Treaty which actually includes 188 countries and it commits the NWS (Nuclear Weapon States) not to provide nuclear weapons or nuclear explosive devices to the NNWS (Non Nuclear Weapon States), these must not to acquire nuclear weapons, accepting safeguards on all nuclear material. All the States parties agree in an export controls regime to facilitate the technology exchange and to pursue negotiations on nuclear disarmament [2].

The Additional Protocol to the NPT extends the control actions to materials and activities which are not specifically nuclear, but that may direct or indirect be used in the nuclear field. Furthermore the collection of information on these materials and activities is widened, also the verification and inspections on use, eventual presence of undeclared materials, adoption of new control systems and a better coordination.among the public institutions.

MISE and ENEA agreed that the most appropriate instrument to undertake the activities in this scenario was a so-called “Convention” that was signed for the first time on October 6th 2004, to be renewed on three years basis provided the approval of an agreed technical program [3]. The Convention went in detail and was essentially focused at first on the fulfilment of the clauses of the Additional Protocol. In fact the articles of the AP were carefully studied and were grouped for homogeneous areas; a data bank on the potentially interested sites was developed and the Agency played a dual role: body subjected to determined obligations and active part of coordination and support between the identified actors for the presentations of the declarations as per art. 2 of the treaty. There was also a fruitful interface with the international Authorities like EURATOM to implement the new regime of the safeguards. This phase was critical in the Italian scenario since the actuation decrees in the act 332 were initially outstanding and ENEA then was the actor that implemented in an essential way the operative modes for the presentation of the declarations that are required in art. 2, also with more intense cooperation with IAEA. The organization of the inspections of IAEA-EURATOM experts to the interested sites was also organized. The signature of the Convention led to the strengthening of the involvement of the Institute in the consultancy in the national Committees that are evaluating the export applications of the firms as far as the international commerce is concerned, to prevent the diversion of the technologies, the dual use, suitable to divert technologies for military purposes. In this scenario the membership of ENEA to ESARDA has to be mentioned. Top management understood the benefit of being part of an international organization specially dealing with the aspects of the strengthening of the safeguards, facilitating and enabling the circulation of the scientific information, widening interests and improving technological capability.

In this framework, the nuclear Division was asked to give evaluations and comments in the case of adoption of new commercial directives, advising for the approval or modification of the European Directives, since the rapid technological evolution needs continuous revision and updating to the national norms.

Ours is a research institute, then the aspect of R&D was always kept in the highest consideration. Being one of the few national institution highly specialized in the nuclear field, new inspection techniques and in general new technologies dedicated to improve the safeguard systems were investigated, new instrumentation has been procured for the detection of fissile materials.

In these last three years art. 2.a.x raised importance; it foresees the realization of the general plan regarding the activities related to the fuel cycle including the research activities approved by the Government for the following decade. Such a circumstance gives the possibility for a detailed investigation on studies on the fuel cycle that don’t foresee the use of nuclear material and that are required to be submitted to the Agency in the most detailed way.

ENEA is committed in the identification and screening of those institutions that are undertaking activities following in the articles. 2.a.i, 2.a.x and 2.b.i, through meetings, interviews and cooperation. This is especially the field of interaction with the Universities and the other research institutions of the national scenario.

Using publicly available data ENEA implemented the list of the national subjects who deal with goods or services whose production is of potential interest of the Additional Protocol. In particular, the investigation identified those subjects which are performing activities following in the Annex I and are producing components and systems suitable to be used in the nuclear sector and listed in Annex II.

Our Division then advises Ministry about the new technological developments and acts which are developed in the international institutions and committees and that are often under revision and modification, to make a comparison with the Annex II of the AP.

In this framework, the activity of training, organization of meetings and events in which European institutions representatives, industry managers and state bodies like customs and Ministry of Economic development might exchange experiences and information were organized with the scope of non proliferation purposes and knowledge of technologies and norms(see also ESARDA events in Rome).

It was commonly understood and not fully recognized previously, how qualified in technology and systems were the national companies that were involved in the international trading scenario and how much sensitive were the task to advise Ministry having the final scope not to create hurdles to the national capacity in the international trading of advanced components.

This of course, i.e. the participation to important events or active working groups had the purpose to make the diffusion of the results and make a more effective action not limited to the narrow bounds of the national landscape.

Another field that drew the attention of our management in the last three years in our Division was the increasing of our lab instrumentation set, gamma spectrometers, alpha and Raman, (every instrument was experimentally validated even through computer models), electronic dosimeters were procured and finally these instruments were acquired with the specific scope to be installed on a mobile vehicle which could cover the needing of a prompt action in the national territory.

In this area, a mobile laboratory was procured. Further to ENEA specifications, it was handed over in February 2016.

ENEA Agency has assigned (D.Lgs. 52/2007) the task of giving specific analytical service for qualitative and quantitative analysis of unidentified and suspicious materials.
The characterization of the nuclear material is performed by the staff of the of Nuclear Materials Characterization Laboratory of ENEA directly involved, by its own means and their own instrumentation, on the site with the mobile laboratory.

Fig.1: The ENEA Mobile Laboratory

If necessary, the sample can be transported, after a first radiological characterization, to the Nuclear Materials Characterization Laboratory operated at ENEA Casaccia Research Center for the execution of additional measurements not achievable using portable or transportable measurement techniques.

The mobile laboratory was specially designed to undertake “in situ” analysis on the wide spectrum of possible cases of intervention and the multiplicity of types with which components and suspicious radiological materials may arise, especially in case of loss of traceability and in the event of improper storage at intermodal shipment points (ports, airports or railway stations), waste controls or environmental samples containing fissile or radioactive material.

The presence of "suspect" material alerts the various actors in emergency management: the discovery of a "suspicious" material requires the coordinated action of more bodies and organizations to carry out complex tasks like:

- urgent intervention to limit risks to the population and the environment;
- identification and evaluation of the radioactive material;
- on site remediation and safe management of the material to be identified;
- investigative activity, where the substance has been the subject of theft.

The Agency ENEA is involved for the radiological characterization of the material to be identified. The objective of the radiological characterization is the identification and quantification of emitters radionuclides in nuclear material in order to make a proper management of material to be controlled.

The material to be identified is initially characterized in situ, using portable and/or transportable instrumentation. The operations performed during the first phase of finding and sample identification can be summarized as follows:

a) verify the integrity and visual examination of the sample;

b) acquisition of photographic images of the sample;

c) measure the size and weight of the sample;

d) measurement of beta / gamma and neutron contact dose rate;

e) measurement of surface contamination by "smear test".

The next phase consists in the real radiological characterization of the material to be identified that can be articulated as follows:

f) identification of the radioisotopes present in the sample;

g) evaluation of the activity of the sample and, possibly, the specific activity (with the relative measurement uncertainties);

h) assessment of the physical state of the sample and its size in order to identify the type of container suitable for transport in accordance with national and international regulations.

The instrumentation used for the purposes mentioned above is of a portable type or transportable.

It is essentially a version of a utility vehicle of common commercial production and is equipped for the characterization on site of radioactive materials. In the rear part a mobile platform is installed to have an easy handling of the ISOCS (In Situ Object Counting System).

The instrumentation which is fitted inside the mobile laboratory was acquired in the previous years of the Convention, and it is essentially based on the following equipment:

Radiochemical fumehood. This device is installed in the technical volume of the van and allows to safely manage small samples guaranteeing the operator and environmental protection from eventual risks of contamination.

ISOCS. (In Situ Object Counting System). The In Situ Object Counting System (ISOCS) developed by Canberra, Inc. is the portable, in-situ gamma spectroscopy system, to identify radioactive isotopes and to qualitatively determine the amount of radioactive material in the considered sample.

Portable Instrumentation

Inspector 1000. It is a portable system that uses a neutron probe and a gammaradiation detector.

LP 123P Berthold Plutonium Monitor. Portable system, designed to achieve the maximum efficiency in the detection of fission neutrons. It assesses also quantitatively the presence of Plutonium.

NT 200. It is used to evaluate an eventual surface contamination. It is a portable analyzer for on filter "smear test" measurements and in air contamination.

SSNC, Small Samples Neutron Counter. Transportable system for gamma contaminated materials based on passive neutron techniques.

The special authorization for the transport of radioactive materials (ADR) which the Radiochemical Mobile Laboratory is going to obtain will allow a radiological complete characterization of the "suspect" sample carried out in the Nuclear Materials Characterization Laboratory of ENEA Casaccia Research Center if the in situ characterization is incomplete.

Furthermore the ADR authorization will allow to use on site a newly designed Non Destructive Assay equipment [4] developed at the Nuclear Materials Characterization Laboratory that, by means of a neutron generator coupled with neutron and gamma measurement systems, allows the identification of dirty bombs or buried materials containing fissile radioisotopes.

2.3 Future

For the next years, ENEA will carry on the activities which started in the previous periods of validity of the Convention; the investigation and the detailed description of the activities of R&D on the fuel cycle without the use of nuclear materials and that are not directly authorized and funded by the state and the sites where these activities are developed will be revised.

The task of identifying those institutions that are committed in various ways and that are issuing publications and studies in this area will be continuously considered.

The complete list of the firms that are involved in the activities of the Annex I and are producing systems and components suitable in the nuclear sector will be subjected to a maintainance phase and will stand a geolocalization process.

The renovation will have three main aspects: a) control of the company name, b) typology of the activity and of the production, c) insertion of new firms or cancellation of those firms out of business.

As far as Annex II is concerned the ENEA activity will pursue two objectives: a) keep the record of the updates of the Trigger List (Nuclear Suppliers Group), to control and follow up eventual modifications, b) implementation of the interface between the geolocalization system of the firms and the list including the classification and the sensitive components listed in Annex II.

Another sector in which ENEA is a focal point in the country is the training activity and the preparation to dedicated events which will be tuned on the following aspects:

- International regulation developments, following up the technological evolution on the control instruments, exploring also further fields like the Intangible Technology.
- Dissemination of the control methodologies discussed internationally. This may result in great help for the national industrial operators. The presence of ENEA in these institutions can be encouraged and should be advisable.
- Coordination between operators and institutions. This was experimented when the ESARDA meeting Export control WG was held in Rome.
- Technical evolution of processes, materials and components that are resulting in a better efficiency of the nuclear works.

Since 2004, ENEA was entrusted by MiSE both for tetween the of the country's capacity in the field of the nuclear safeguards. ENEA is the Agency that in Italy has peculiar capacity and knowledge in the

nuclear field, starting from the beginning of the implementation of this technology in the Italian scenario. The body ENEA is a research institute and the action of our Division is focused on the radiation survey, in particular in the field of the nuclear safeguards. For instance an instrument prototype utilizing neutronic interrogation technique was made able to detect small quantities of fissile material inside shielded containers.

The R&D activity, on the basis of the international trends will be based on two main guidelines:

- Improvement of the actual technology to increase its efficiency and make it more sensitive to the detection of small quantities of fissile material and possibly portable.
- Exploration of other physical principles that are at the basis of revelation technologies, like the muonic interrogation.

Therefore R&D activity will be directed to the study of measurement techniques that will allow the quantification of the mass of fissile and fertile materials in suspected samples. For these last low limits of revelation will be pursued to allow the use of non destructive analysis techniques. Imaging techniques will be improved.

The Institute will work to design and prototype a new characterization system for SF from research reactors, in particular a transportable measurement system based on gamma spettrometry able to assess “in situ” the fuel burn up degree, the relevant isotope composition and the concentration of of fissile and fertile material in the fuel.

The work in the safeguards is for its nature international, then the institute intends to participate and to be part of the main institutions and points of discussion and bring its contribution to the studies that the international community encourage and support.

The Convention includes the submittal of a three years based action program which can start after Ministry’s approval and is specified year by year.

3. Conclusions

The safeguards as it is stated in the introduction, in which the definition has been given, is an environment of wide consistency, it involves before all the soundness of laws, regulations, clear responsibilities of the managers, qualification of the staff who must be efficiently trained and updated and should be efficiently organized in institutions transmitting knowledge and tradition.

The participation to the task forces of the supranational or European Organizations like IAEA and EURATOM gives a chance to give a contribution at first in the technical issues to be finalized in the political scenario to the final level of EC. It is not an improvised chain, but a heritage that should be encouraged with time.

We can also conclude that the treaties and agreements in this matter between the various countries that have signed them showed their effectiveness, we can mention the Verification Agreement between the IAEA and EURATOM of 1973 in which the States are accepting the inspection regime, with all the controls on the accountancy and storage of the materials used in the nuclear activities to prevent the diversion of their use.

The Additional Protocol to the Non Proliferation Treaty, ratified in Italy by Law 332/2003, aims to the strengthening of control actions of facilities and nuclear materials, enforces controls both on technologies and components that, even if basically for conventional use, could be used for nuclear weapons manufacturing, and on the exports to other Countries.

The good feedback of these measures is that the number of the states that signed the Additional Protocol raised from 37 at mid 2004 to 153 at mid 2014. The inspections with clarifications requests

declined from 350 to 20 nowdays, this is a synthom that these legal and political tools are worldwide robust and sound, means that operators and complying with the stringent clauses of inspection and report for accountancy of nuclear material and also that staff is more educated, trained, and more opened to cooperation.

The instrumentations and tools that ENEA is procuring through many years of implementation of the agreements with MiSE (Ministry of Economic Development) will enhance the response readiness in case in which suspect materials are detected in the normal circulation of the goods, and raw materials, potentially in all the intermodal transportation points. We find that the Institute feels constantly involved in this effort of improvement of experience and knowledge, and this is recognized by the credibility gained in all the country.

4. References

[1] L. 31 ottobre 2003, n. 332 (G.U. 22 novembre 2003 n. 276).
[2] 15th Edition of ESARDA Course, Nuclear Safeguards and Non Proliferation.
[3] MISE Convenzione per lo svolgimento degli adempimenti previsti nel PA fra ENEA e MISE.

[4] N. Cherubini, A. Dodaro, G. Gandolfo, L. Lepore, G. A. Marzo, E. Piccinelli, R. Remetti, “Field Prototype of the ENEA Neutron Active Interrogation Device for the Detection of Dirty Bombs” Challenges 2016, 7, 17; doi:10.3390/challe7020017.

Session 02

Non-destructive Analysis – Gamma Measurements

Using FRAM to determine enrichment of shielded uranium by portable electrically cooled HPGe detectors

J. Zsigrai[1], A. Frigerio[1], J. Bagi[1], A. Mühleisen[1], A. Berlizov[2]

[1]European Commission, Joint Research Centre, Directorate G, Karlsruhe, Germany
[2]International Atomic Energy Agency, Vienna, Austria

Abstract:

The capability of the FRAM software to accurately determine the enrichment of shielded uranium by portable electrically cooled HPGe detectors was studied. This can have applications in the future, e.g., for the verification of aged uranium-bearing products, scrap, and waste materials, especially during short-notice random or unannounced inspections, when detector cooling with liquid nitrogen is not feasible. More than 7000 high-resolution gamma spectra of certified reference materials were taken by the ORTEC "Detective" detector under well-defined measurement conditions. Up to 16 mm of steel was used for shielding. The ^{235}U enrichment of the reference materials varied from 0.31% to 4.46%. The settings of an existing FRAM parameter set were optimized and all the collected spectra were analysed using the default and the optimized parameter sets. The results obtained with these parameter sets are compared in this paper.

Keywords: FRAM, gamma-ray spectrometry, shielded uranium, electrically cooled detector

1. Introduction

The purpose of this work was to study and possibly improve the capability of the FRAM software to determine the enrichment of shielded uranium by portable electrically cooled HPGe detectors. This task was carried out at the JRC Karlsruhe site, within the support programme to the International Atomic Energy Agency (IAEA). In particular, new customized FRAM parameter sets were developed and can be used to get more accurate results for ^{235}U enrichment than with the default parameter sets.

An advantage of electrically cooled high-resolution gamma spectrometers (ECGS) for in-field use by safeguards inspectors is that they do not require liquid nitrogen for cooling. This makes them suitable for short notice random or unannounced inspections for the verification of aged uranium-bearing products, scrap, and waste materials.

FRAM is software that calculates uranium and plutonium isotopic composition from the gamma spectra of these materials [1], [2]. It has been developed at Los Alamos National Laboratory (USA) and it has been commercialized by ORTEC and Canberra. The version used in this study was 5.1 [3].

The so called parameter sets determine what FRAM exactly does. They define the type of material (U, Pu, MOX) and the type of detector. They also contain information about the isotopes and gamma peaks to be analyzed, peak fitting parameters, energy calibration, relative efficiency constraints, etc. FRAM contains a number of default parameter sets built into the software, which cover a large number of typical measurement configurations. However, users can also prepare modified or new parameter sets to suit their specific measurement configuration. In this work we focused on parameters sets for uranium. An analogous study with plutonium parameter sets is in progress.

More than 7000 high-resolution gamma spectra of various certified reference materials were taken by the ORTEC "Detective" detector under well-defined measurement conditions with different steel shielding. These spectra were used to develop a parameter set suitable for determining the isotopic

composition of shielded uranium. Using this parameter set, the difference between the ^{235}U enrichment determined by FRAM and the certified value (FRAM's bias) can be reduced to below 2%.

2. Method and equipment

The ORTEC Detective electrically cooled spectrometer was used to record the gamma spectra. It has a high-purity germanium (HPGe) crystal of 50 mm diameter and 30 mm depth (length). Its warranted resolution is ≤ 2.0 keV at 1332 keV and ≤1.0 keV at 122 keV, while its efficiency relative to a standard 2x2 inch NaI is 10%. The conversion gain of its amplifier is set in the factory so that it can take spectra up to 3 MeV. The electronics settings cannot be changed by the user.

Spectra of all 5 items from the certified reference material set EC NRM-171 (also known as the "CBNM uranium set") [4] were recorded in 8 different geometries (5x8=40 configurations):

- At 2 cm from the detector, with 0 mm Fe shielding
- At 5 cm from the detector, with 0, 2, 4, 8, and 16 mm Fe shielding
- At 10 cm from the detector, with 0 mm Fe shielding
- At 15 cm from the detector, with 0 mm Fe shielding

For each configuration 192 spectra were recorded with 5 minute real time (16 hours total measurement time), i.e., 40x192 = 7680 spectra were recorded. Each item of the reference material set contained 200 g of UO_2 in container with 2 mm Al window. The certified ^{235}U enrichments are shown in Table 1.

Table 1. Certified ^{235}U enrichment of the reference samples [4]

Sample name	Certified enrichment ± Uncertainty (2s) [mass %]
CBNM U031	0.3166 ± 0.0002
CBNM U071	0.7119 ± 0.0005
CBNM U194	1.9420 ± 0.0014
CBNM U295	2.9492 ± 0.0021
CBNM U446	4.4623 ± 0.0032

To investigate the effect of counting statistics on the results of FRAM the 5-minute spectra were added up to make spectra with various real times which are multiples of 5 minutes. A script was written in the Python 3.5 programming language for adding the spectra. To automatically analyse the large number of spectra an Excel macro was used, which interacts with the command-line mode of FRAM v5.1 and puts the results into an Excel sheet.

To measure the performance of FRAM and different parameter sets, two quantities were used: the average relative bias and the mean absolute value of the relative deviation (MARD) of the ^{235}U results. These two quantities were calculated for each configuration (defined by enrichment, distance and shield thickness) as

$$Average\ relative\ bias = \frac{\sum_{i=1}^{n} \frac{x_i - x_{Ref}}{x_{Ref}}}{n}, \qquad MARD = \frac{\sum_{i=1}^{n} \frac{|x_i - x_{Ref}|}{x_{Ref}}}{n},$$

where n is the number of spectra analysed (e.g. n=192 for the 5-minute spectra), x_i is the ^{235}U enrichment calculated by FRAM and x_{Ref} is the certified reference value for the ^{235}U enrichment. The average relative bias can be either positive or negative. It describes the expected accuracy of many (n) measurements. The MARD is always positive and it describes expected accuracy of a single measurement.

To see how the results from FRAM can be improved all spectra were first analysed using a "default" parameter set for the Detective supplied by ORTEC on the installation CD of FRAM 5.1. This is not one of the built-in parameter sets of FRAM, though it was made by the FRAM developers [5]. After each modification of the parameter set, the entire set of spectra was reanalysed and the average relative bias and the MARD recalculated for each configuration.

3. Results

3.1. Results with the "default" parameter set

To take a snapshot of the performance of FRAM using the default Detective parameter set [5], the 5-minute and the 80-minute spectra were analysed. The average relative bias and the MARD for these analyses are shown in Figure 1. The spectra were taken at a 5 cm source-to-detector distance. This distance was an acceptable guess for having a compromise between sufficient count rate and coincidence summing effects.

For the configuration with the depleted uranium sample, CBNM U031, and 16 mm Fe shielding the average bias is much higher (more negative than -14 %) than for the other configurations and is outside of the scale of the graphs. This large bias is probably due to two reasons. First, the heavy shielding extremely reduces the already low number of counts in the peaks of ^{235}U. E.g. the number of counts in the 186 keV peak with 16 mm shielding is about 8 times lower than with no shielding while the 143 keV peak is not even visible for the 5 minute spectra with 16 mm shielding. Even for 80 minutes measurement time the number of counts for the ^{235}U peaks stays low with 16 mm shielding. Second, the Compton scattering in the heavy shielding greatly increases the background below the ^{235}U peaks. Therefore, the ^{235}U peaks in the spectra of heavily shielded depleted uranium are very difficult to fit.

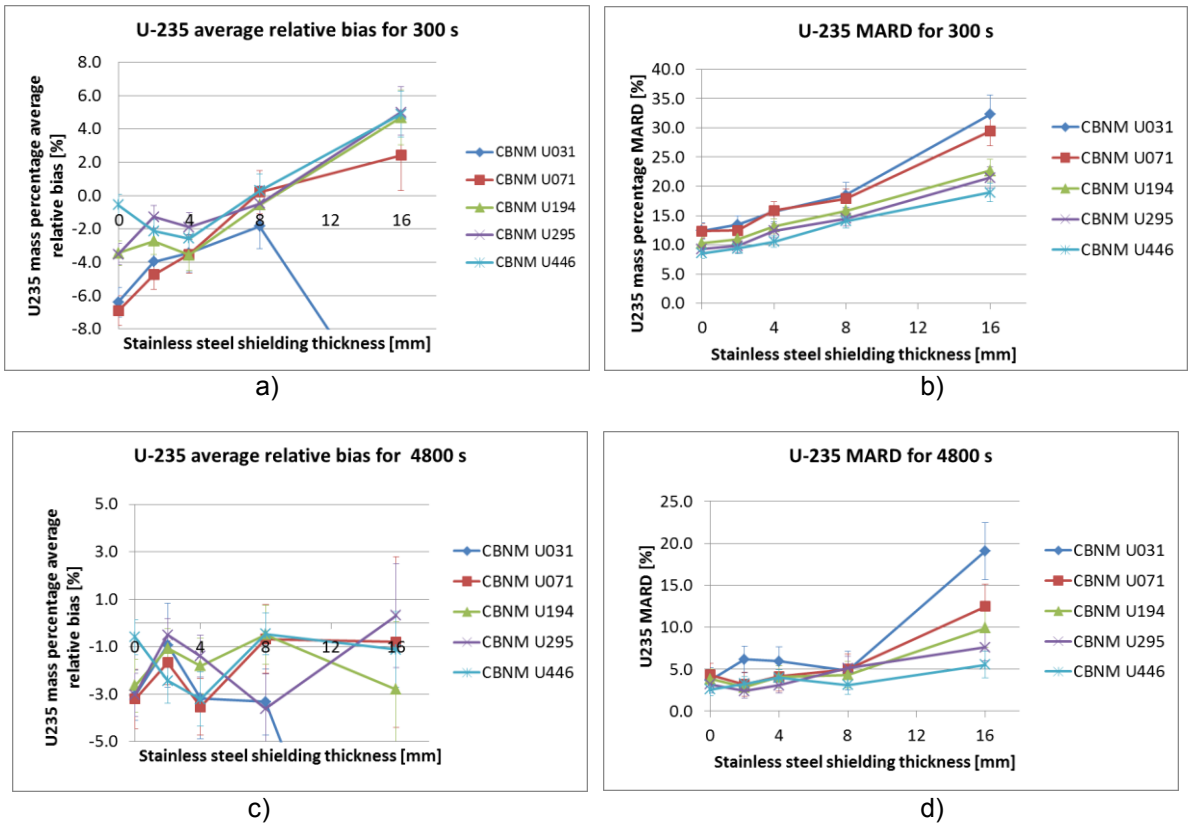

Figure 1. "Default" Detective parameter set: Average relative bias and MARD as a function of Fe shielding thickness for measurements at 5 cm from the detector: a) and b) for 5-minute spectra; c) and d) for 80-minute spectra. The error bars for the average bias are the corresponding MARDs divided by the square root of the number of measurements, while the error bars for the MARD are the corresponding average uncertainties reported by FRAM divided by the square root of the number of measurements.

3.2. Evolution of the parameter set

The parameter set was modified step-by-step, changing only one type of parameter at a time, to see the influence of each parameter on the bias and MARD. For Figure 2 the average biases for the various configurations were averaged over all samples and plotted for each step during the evolution of the parameter set and for each shield thickness. The outlier corresponding to the configuration for depleted uranium, CBNM U031, with 16 mm shielding was not included in this average.

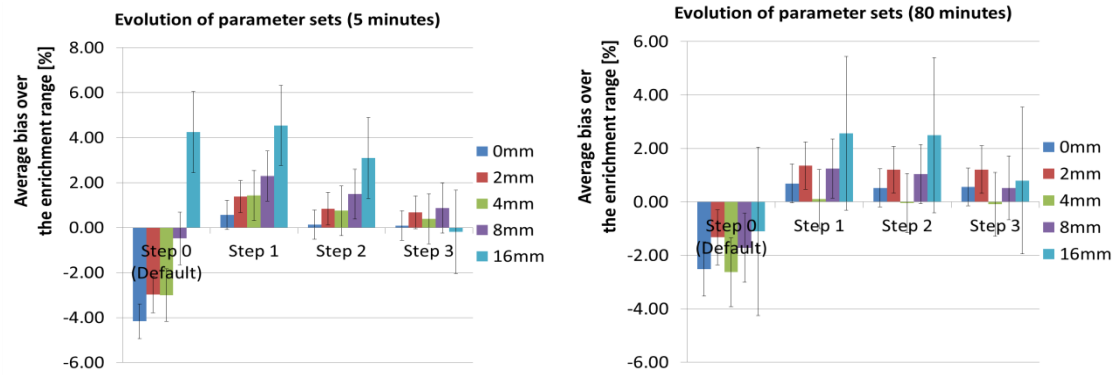

Figure 2. Steps in improving the parameter set: The average (over different enrichments) of average biases as a function of shield thickness is shown for each step for different Fe shield thicknesses. Error bars are the corresponding average MARDs divided by the square root of the number of spectra. a) for the 5-minute spectra, b) for the 80-minute spectra.

After a few trial-and-errors, the correct steps in modifying the parameter set were the following:

1. Turning off the coincidence summing correction. This dramatically improves the average bias of the results obtained from the measurements at 5 cm source-to-detector distance. This means that at this distance the coincidence summing effects are relatively small and FRAM overestimates the correction due to coincidence summing.
2. Fine-tuning the peak fitting parameters (energy calibration and peak-shape parameters), to improve the accuracy of the peak areas determined by FRAM. This has a minor impact on the results
3. Modifying the boundaries and types of absorber materials, to account for the effects of shielding. This involved removing Cd and adding Al as absorber (0-50 mm), and modifying the boundary values for effective Fe thickness (0-50 mm). This step has a major impact for the spectra taken with heavy shielding.

3.3. Results with the "optimal" parameter set

The optimal parameter set is Step 3 in Figure 2. The detailed results for the average relative bias and MARD obtained using this parameter set are shown in Figure 3. Just as for the default parameter set, the average bias for the configuration with the depleted uranium sample, CBNM U031, and 16 mm Fe shielding is outside of the scale of the graphs (it is more negative than -14 %).

The improvement of the average relative bias is evident by comparing Figure 3 to Figure 1. However, the modifications of the parameter set have hardly any impact on the MARD. This is because the MARD is mainly determined by the counting statistics, and is not much influenced by the bias.

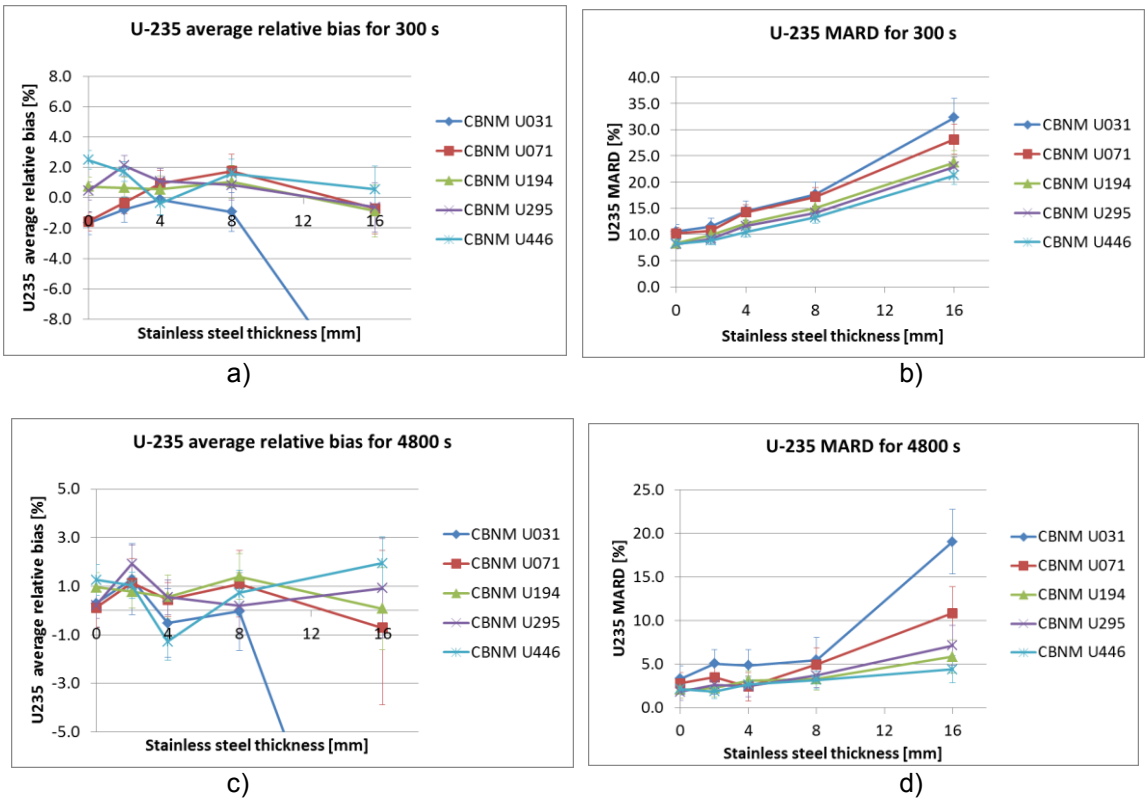

Figure 3. "Optimal" parameter set: Average relative bias and MARD as a function of Fe shielding thickness for measurements at 5 cm from the detector. a) and b) for 5-minute spectra; c) and d) for 80-minute spectra. Error bars are as in Figure 1.

3.4. Influence of sample-to-detector distance

As mentioned above, turning off the coincidence summing correction in the parameter set improves the results obtained from the spectra recorded at 5 cm source-to-detector distance. To further investigate the performance of the coincidence summing correction algorithm of FRAM, the spectra taken at different distances from the detector with no shielding were analysed by the default and the modified parameter set, as shown in Figure 4.

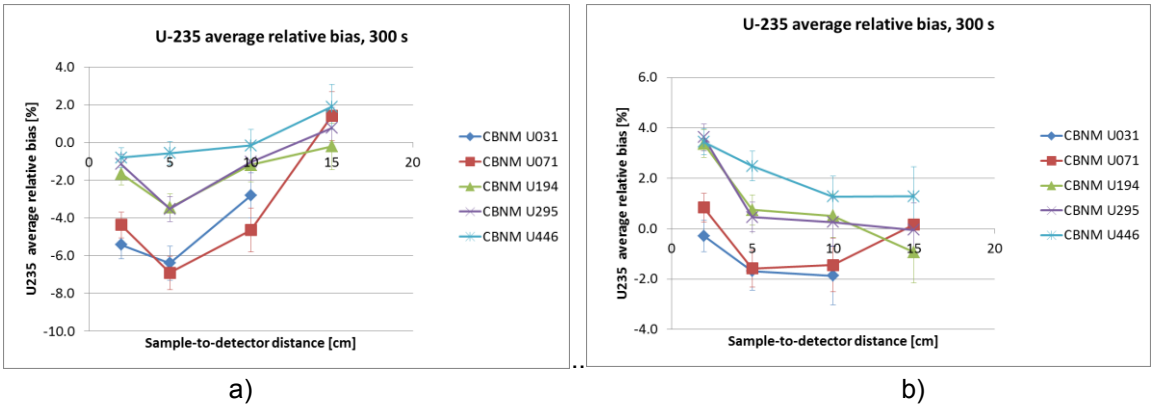

Figure 4. Average relative bias for unshielded samples as a function of source-to-detector distance with 5-minute measurement time. a) With default parameter set. b) With the modified parameter set, "Step 3". Error bars are as in Figure 1.

It can be seen in Figure 4 that the newly developed parameter set provides better results for most configurations. However, at 2 cm from the detector the effects of coincidence summing seem to be significant, and the correction algorithm would probably have to be turned on.

3.5. Influence of counting statistics

As observed by comparing Figure 1 and Figure 3, the MARD does not improve much by modifying the parameter set. This is because the MARD is mainly determined by the counting statistics, and the improvements in the relative bias are much smaller than the MARD. To investigate the influence of the counting statistics and measurement time on the MARD, an indicator has to be constructed which describes the statistical quality of the spectra. In this work we used a number constructed as the reciprocal value of the combined relative uncertainties of the 186 keV peak of ^{235}U and of the 1001 keV peak of ^{238}U:

$$Statistics\ indicator = \frac{1}{\sqrt{\left(\frac{\Delta S_{186}}{S_{186}}\right)^2 + \left(\frac{\Delta S_{1001}}{S_{1001}}\right)^2}},$$

where S_{186}, ΔS_{186}, S_{1001} and ΔS_{1001} denote the peak area and its absolute uncertainty of the 186 keV and 1001 keV peaks, respectively.

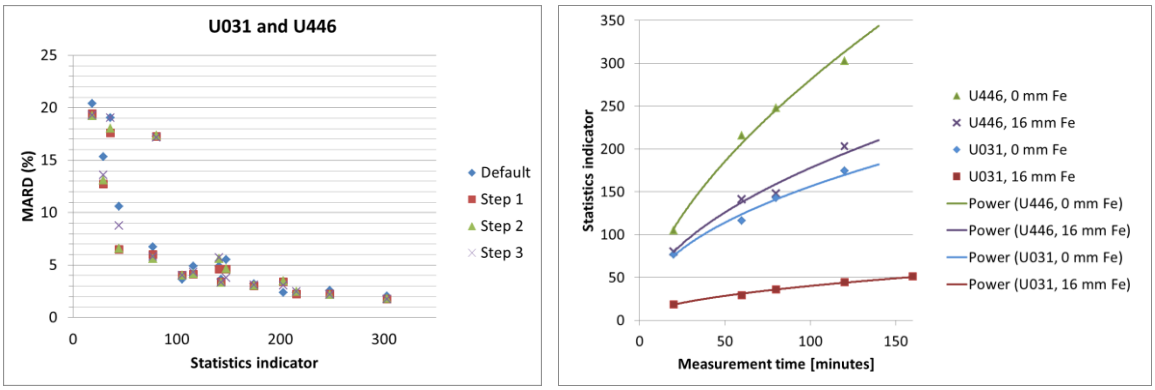

a) b)

Figure 5. a) Dependence of the MARD on the statistics indicator for the samples U031 and U446 measured at 5 cm with 0 mm and 16 mm of Fe shielding, for different parameter sets. b) Dependence of statistics indicator on the measurement time, for the sample U031 and U446 measured at 5 cm with 0 mm and 16 mm Fe shielding.

It can be seen from Figure 5a) that the MARD becomes smaller than 2 % if the statistics indicator is higher than about 200, almost independently of the sample (enrichment), shield thickness and parameter set used for obtaining the MARD. Furthermore, Figure 5b) shows that the statistics indicator does not go above 200 for most of the 5-minute and 80-minute spectra evaluated in this paper. That means that the statistics of most of the spectra used in this work is not enough for getting better precision (MARD) of the ^{235}U result calculated from a single spectrum, regardless of the improvements of the parameter set. Nevertheless, the analysis of the large number of spectra shows that the accuracy (bias) of the results is reduced by using the improved parameter set.

4. Conclusion

A new FRAM parameter set has been developed for analysing shielded LEU spectra taken with the ORTEC Detective. The performance of the default and the newly developed set was evaluated in detail for the ^{235}U enrichment range from 0.31% to 4.46 % and for Fe shield thicknesses up to 16 mm. It was shown that the new parameter set performs better, especially for heavily shielded samples. This parameter set can be equally used for shielded or unshielded samples. The parameter set will be made available to the IAEA within EC support programme.

References

[1] T. E. Sampson and T. A. Kelley, “PC/FRAM: A code for the non-destructive measurement of the isotopic composition of actinides for safeguards applications, LA-UR-96-3543,” 1996.

[2] T. E. Sampson, T. A. Kelley, and D. T. Vo, “Application Guide to Gamma-Ray Isotopic Analysis Using the FRAM Software, LA-14018,” 2003.

[3] D. T. Vo, “Operation and Performance of FRAM Version 5.1 Proceeding of the 52nd Annual Meeting of The Institute of Nuclear Materials Management, Palm Desert, CA, USA, July 17-21, 2011, LA-UR-11-03016,” 2011.

[4] “EC Certified Nuclear Reference Material 171, Certificate of Analysis, Commission of the European Communities, Joint Research Centre, Central Bureau for Nuclear Measurements, Geel,” 1985.

[5] T. E. Sampson, G. W. Buttler, D. T. Vo, T. Wenz, and S. C. Myers, “The use of FRAM with a portable, HPGe-based nuclide identifier to measure isotopic composition of plutonium and uranium, LANL report.”

Measurement of Uranium Enrichment Standards Using High Resolution Gamma Spectrometry with High Precision and Accuracy

Ramkumar Venkataraman and Stephen Croft

Oak Ridge National Laboratory, Oak Ridge, TN 37831, USA

Abstract:

The purpose of this work was to produce a quality data set of gamma-ray spectra that can be shared, thus facilitating independent analyses. This work is part of a larger research effort to quantify uncertainties for nuclear material measurements. Established gamma-ray isotopic analysis codes MGAU (Multi-Group Analysis for Uranium) and FRAM (Fixed Energy, Response Function Analysis with Multiple Efficiencies) use nuclear data including half-lives and gamma-ray absolute emission probabilities, along with measured peak intensities to determine enrichment or isotopic abundance) the isotopic composition of nuclear material. The propagated uncertainty in the measured enrichment is a combination of measurement uncertainties as well as the nuclear data uncertainties. In principle, by performing a careful measurement campaign, minimizing the measurement uncertainty component, it would be possible to determine the limiting uncertainty in the enrichment due only to nuclear data, and possibly identify the need for improvement. High-quality gamma-ray spectra of uranium enrichment standards were collected using a High-Purity Germanium spectrometry system. The Certified Reference Materials (CRM) 969 and CRM 146 uranium standards were measured, spanning a range of enrichments from. 0.3206 at. % to 93.233 at %. A Region of Interest (ROI)-based approach was used to analyze gamma-ray peaks from ^{235}U. The analysis was carried out using data from four different gamma ray peaks from ^{235}U, including the 185.715 keV peak. Correction factors were determined and applied for the attenuation through the wall, and the non-infinite thickness of the U_3O_8 layer in the CRM sources. A thorough evaluation of various sources of uncertainties was performed, and uncertainties quantified. The count rates from key gamma-ray peaks from ^{235}U were plotted as a function of uranium enrichment (atom %), based on the enrichment meter principle convention. Future analysis will focus on determining specific or atomic emission ratios between nuclides, which is aimed at improving relative nuclear data for internally calibrated isotopic codes.

Keywords: Uranium Enrichment Gamma Spectrometry Uncertainty Quantification

1. Introduction

Isotopic codes such as MGAU [1] and FRAM [2] use nuclear data such as the half-lives and gamma-ray absolute emission probabilities along with measured peak intensities to determine isotopic ratios (enrichment or isotopic abundance) as a measure of the isotopic composition of nuclear material.

$$\frac{N^i}{N^k} = \frac{C(E_j^i)}{C(E_l^k)} \times \frac{T_{1/2}^i}{T_{1/2}^k} \times \frac{BR_l^k}{BR_j^i} \times \frac{RE(E_l)}{RE(E_j)} \quad (1)$$

In Eqn. (1), N^i and N^k are the number of atoms of isotopes i and k, $C(E^i_j)$ and $C(E^i_k)$ are the net peak area or peak intensities, respectively, at gamma-ray energies E_j and E_l, $B(R^i_j)$ and $B(R^k_l)$ are the absolute emission probabilities (gamma-ray yields), and RE(Ej) and RE(El) are the relative efficiencies of the detector at energies E_j and E_l, respectively. The propagated uncertainty in the measured enrichment is a combination of measurement uncertainties as well as nuclear data uncertainties. Item-specific uncertainty estimates are difficult to make, and the reported uncertainties are usually limited to

precision. Furthermore, these codes currently use “adjusted” gamma-ray yields to obtain consistent analysis results, thus making the first principle uncertainty quantification impossible. If the accuracy of the nuclear data can be improved, one would not have to “adjust” the gamma-ray yields. By performing a careful measurement campaign, minimizing or eliminating the various sources of measurement uncertainties, it would be possible to determine the limiting uncertainty in the enrichment due to nuclear data.

High-quality gamma-ray spectra of uranium enrichment standards were collected using a High-Purity Germanium (HPGe) spectrometry system. The Certified Reference Materials (CRM) 969 [3] and CRM 146 [4] uranium enrichment standards were measured . The CRM 969 consists of a set of five standards with enrichments ranging from 0.32 at. % ^{235}U to 4.52 at. % ^{235}U. CRM 146 consists of a set of three uranium standards with enrichments ranging from 20.31 at. % ^{235}U to 93.23 at. % ^{235}U.

The spectra were collected by following good measurement practices, including: (i) using an HPGe detector of the Broad Energy Ge (BEGe) model with an energy resolution of 600 eV or better at 122 keV, (ii) stable electronics, (iii) graded shielding around the sides and the back of the HPGe detector, (iv) a reproducible source-to-detector geometry, (v) source placed far enough away from the detector to minimize the dependence on geometry and to avoid true coincidence summing effects, (vi) avoid count rate related losses due to random summing and pile-up, (vii) frequent background measurements, and (viii) acquire spectra in smaller time intervals and sum the counts, rather than acquire a single spectrum over a lengthy period of time. For each standard, 48 consecutive one-hour counting trials were conducted. This was done to monitor the stability of the counting system, and also to monitor any fluctuations in the background conditions.

The spectra were analyzed using the Peak Easy software package [5] provided by Los Alamos National Laboratory. In the results reported here, a Region of Interest (ROI)-based approach was used to analyze gamma-ray peaks from 235U. The count rates were plotted as a function of uranium enrichment in atomic %. The data was fit using the Deming statistical analysis code [6], taking into account the uncertainties in both the x and y coordinates. Various uncertainty components were considered, and bounding values for uncertainties were assigned. Review of the data in this way is a powerful overall quality check because a direct proportionality is expected between the full energy peak intensity and atomic %. The spectra and the analysis results will be shared with the International Atomic Energy Agency (IAEA) to facilitate independent analysis. Future spectral analysis will be aimed at improving relative nuclear data for internally calibrated isotopic codes.

2. Experimental Set-up and Measurement Procedure

The certified ^{235}U/U fractions for CRM 969 and CRM 146 standards are given in Table 1 and Table 2, respectively. The uncertainties in the certified values of ^{235}U fractions are quoted at the 2σ level of confidence. A photograph of the calibration standards are shown in Figure 1.

Material ID	031	071	194	295	446
Atom Percent (2σ uncert.)	0.3206 ±0.0002	0.7209 ±0.0005	1.9664 ±0.0014	2.9857 ±0.0021	4.5168 ±0.0032
Mass Percent (2σ uncert.)	0.3166 ±0.0002	0.7119 ±0.0005	1.9420 ±0.0014	2.9492 ±0.0021	4.4623 ±0.0032

Table 1. CRM 969 - Certified ^{235}U/U fractions

Source ID	NBL 0021	NBL 0022	NBL 0023
Atom Percent (2σ uncert.)	20.311 ±0.02	52.800 ±0.042	93.233 ±0.0053
Mass Percent (2σ uncert.)	20.107 ±0.02	52.488 ±0.042	93.1703 ±0.0052

Table 2. CRM 146 - Certified ^{235}U/U fractions

Figure 1. U Enrichment Standard Sources (supplied by NBL)

The measurement system consisted of a Canberra Model BE3825 Broad Energy Germanium detector (Ge crystal of 3800 mm^2 area and 25 mm thick), a Canberra Model Inspector 2000 Digital Signal Processor, and a personal computer for data acquisition. The detector was mounted on an ISOCS (In Situ Object Counting System) [6] cart and shielded on the sides and at the back with 2 in. thick lead. A Sn-Cu liner was configured on the inner surface of the lead shield ("graded shielding") to block the secondary the lead x rays. Figure 2 shows the top view of the shielded detector.

Figure 2. Top view of the BEGE detector showing the graded shielding

The conversion gain of the analog-to-digital converter (ADC) was set at 16,192 channels. The gain was adjusted such that the slope of the linear energy calibration fit was 0.075 keV/channel, a commonly used and recommended value for performing isotopic analyses using MGAU and FRAM in low-energy mode. Prior to measuring uranium sources, the stability of the digital signal processor (DSP) was studied using ^{57}Co and ^{137}Cs measurements. Forty-eight (48) counting trials were performed, each trial lasting for 1 h. The digital gain stabilizer in the IN2K DSP does not have the zero stabilization capability. During the first set of 48 counting trials with ^{57}Co and ^{137}Cs, the gain stabilization was turned off and the spectra were acquired. The average variations in the energy corresponding to the centroid channels and the standard deviations were: (121.982 ±0.007) keV and (661.442 ±0.041) keV. This is equivalent of less than one channel drift). The variations in the Full Width at Half Maximum (FWHM) were: (0.588 ±0.005) keV at 122 keV, (1.271 ±0.008) keV at 662 keV. The gain stabilization was turned on and a second set of 48 one hour counting trials were performed. The results were: (122.026 ±0.007) keV and (661.546 ±0.036) keV. It was decided to turn gain stabilization off for the uranium measurements since the system stability was practically the same. The gain drift was negligible.

A fixture was used to locate the uranium standards reproducibly, on-axis with respect to the detector, and at a distance of 63 cm from the front face of the detector. Source-detector distance was maintained the same for all standards for convenience, as well as to simplify interpretation of the results.

Good measurement practices were followed in setting up and acquiring the spectra. These are listed below.

(i) By locating the sample "far" away from the detector, several sources of systematic uncertainties were minimized. These include;

a. Minimization of uncertainty due to sample positioning.
b. Minimization of the high count rate related effects such as those due to pulse pile-up, and random summing. The dead time was approximately 3% for the highest enrichment standard, and it was lesser for lower enrichments.
c. Avoiding the bias due to loss or gain of counts because of true coincidence summing between gamma rays from ^{235}U decay.

(ii) Each standard was counted for a long period of time (48 h) to ensure good counting precision in the key gamma-ray peaks from ^{235}U. The counting period was divided into 48 one-hour trials (rather than one long 48 h count) so that the stability of the gamma spectrometry system could be monitored, and also so that any fluctuations in the ambient background could be flagged. The net peak areas from the 48 trials (at a given gamma energy) were summed, and the statistical uncertainties were propagated.

(iii) Background measurements were performed at the beginning and end of the campaign, and they were interspersed between standard measurements.

3. Discussion of uncertainty components and correction factors

The following uncertainty components were estimated.
- Uncertainty due to sample positioning
- Uncertainty due to counting statistics
- Uncertainty in system dead time correction
- Correction for non-infinite thickness and its uncertainty
- Correction factor for container wall attenuation
- Uncertainty in mass attenuation coefficient values due to isotopic enrichment

These are discussed in the sections below.

3.1. Uncertainty due to sample positioning

The source-to-detector distance was maintained at 63 cm using a custom fixture. An indentation in the fixture helped in holding the sample such that the bottom of the cylindrical sample was on-axis with respect to the detector. An uncertainty of ±0.1 cm (or ±0.32% on the rate) was estimated for the reproducibility of the source position. This was based on the tolerance of the indentation in the source holder where the bottom of the NBL can rested.

If a single spectrum was analyzed to determine quantitative results, the uncertainties in sample positioning would cause a systematic bias. In the present analysis where results from various trials using various standard sources are pooled and are assumed to be from the same population, the positioning uncertainty of ±0.32% ought to be considered as a random uncertainty.

3.2 Uncertainty due to counting statistics

The uncertainty range due to counting statistics obtained for the highly enriched uranium (HEU) and low-enriched uranium (LEU) standards are given in Table 3 below. For the HEU standards, the lower and upper bounds for precision correspond to an enrichment (atomic %) of 20.311 at. % and 93.233 at. %, respectively. For the LEU standards, the lower and upper bounds correspond to 0.3206 at. % and 4.5168 at. %, respectively.

Gamma Energy (keV)	Counting Statistics (HEU standards)	Counting Statistics (LEU standards)
140.76+143.76	0.036% - 0.080%	0.204% - 1.494%
163.356	0.048% - 0.106%	0.264% - 1.802%
182.62+185.715	0.011% - 0.024%	0.053% - 0.301%
205.316	0.035% - 0.078%	0.190% - 1.292%

Table 3. Uncertainty due to counting statistics

3.3 Uncertainty in system dead time correction

The gamma spectra were acquired by setting the DSP in the Live Time Correction (LTC) mode, which extends the live time to compensate for the loss of counts due to system dead time. However, there is an inherent uncertainty in how the dead time is determined for the DSP, which in turn would result in an uncertainty in the correction that is applied.

Canberra's IN2K DSP uses a filter with a trapezoidal shape. The trapezoidal pulse shape is made up of two parameters, the rise time (RT) and the flat-top (FT). The dead time τ is calculated as follows.

$$\tau = 2 * RT + FT \quad (2)$$

For the current measurement campaign, the rise time and the flat-top were set to RT = 5.6 μs and FT = 0.8 μs, respectively. Therefore the system dead time τ will be 12 μs. An uncertainty of ±5% was assigned to the system dead time parameter based on the information provided by the manufacturer (σ_τ=0.6 μs).

Assuming a paralyzable dead time model for the system, the count rate recorded by the multichannel analyzer (MCA) can be written as follows.

$$R_m = R_0 / e^{R_0 \tau} \quad (3)$$

In Eqn. (3), R_0 is the true count rate, R_m is the measured or recorded count rate and τ is the dead time parameter whose value is dictated by the shaping times used in pulse processing. At low count rates, the exponential term in the denominator of Eqn. (3) can be approximated as $(1+R_0.\tau)$. Our objective is to determine the true count rate R_0, knowing the recorded count rate R_m, and the dead time parameter τ. Using the approximation for the exponential and re-arranging terms, Eqn. (3) can be re-written as follows.

$$R_0 = \frac{R_m}{1 - R_m \tau} \quad (4)$$

The uncertainty in the true count rate due to the uncertainty in dead time can then be calculated.

$$\sigma_{R0} = \frac{R_m^2}{(1 - R_m \tau)^2} * \sigma_\tau \quad (5)$$

The true count rate from Eqn. (4) and the uncertainty in the true count rate from Eqn. (5) were determined for the three HEU standards. The results are given in Table 4.

Enrichment (at%)	Measured Count Rate (R_m) cps	Corrected count rate (R_0) cps	Uncertainty in R_0 due to dead time σ_{R0} cps	Relative. Uncertainty (σ_{R0}/R_0)
20.311	600	604.3	0.21	0.03%
52.800	1500	1527.5	1.35	0.09%
93.233	2300	2365.3	3.17	0.13%

Table 4. Uncertainty in system dead time correction

The relative uncertainty in the dead time correction factor is likely systematic, trending with the count rate. It is negligible for LEU in this work, and it somewhat scales with enrichment for HEU.

3.4 Correction for non-infinite thickness and its uncertainty

For relating the enrichment of ^{235}U to the measured net peak count rate from one of the gamma lines of ^{235}U, the sample being measured must be infinitely thick to the gamma rays at the given energy. The transmission T_S of gamma rays through the sample can be calculated or measured. For infinitely thick samples, T_S will be zero. Therefore, the factor $1/(1-T_S)$ is a measure of the correction that must be applied to the full energy peak count rates in order to correct for the non-infinite thickness of the

sample. In this work, the correction factor and the uncertainty were calculated using equations 6,7, and 8.

$$T_S = \exp\left[-\left(\frac{\mu}{\rho}\right)_S \cdot \overline{\rho t}\right] \quad (6)$$

$$CF_{non-Inf} = 1/(1 - T_S) \quad (7)$$

$$\sigma_{CF_{non-Inf}} = \frac{1}{(1-T_S)^2} \cdot \left(\frac{\mu}{\rho}\right)_S \cdot T_S \cdot \sigma_{\rho t} \quad (8)$$

The mass attenuation coefficients (MACs) (total – coherent scattering) for the sample material, U_3O_8, at the four gamma energies (143.76, 163.356, 185.715, and 205.315 keV) were obtained from the National Institute of Standards and Technology (NIST) XCOM database [7]. The parameter ρt in Eqn. (6) is the mass density in units of $g \cdot cm^{-2}$. The uncertainty in the mass density values of the LEU standards are given in the NBL CRM standards. These were propagated to yield the uncertainty in the correction factor $1/(1-T_s)$.

The non-infinite thickness correction factors are tabulated in Tables 5 for the 185.715 keV gamma ray energy for all the LEU and HEU standards. The uncertainties in the correction factors are given in the CRM certificates for the LEU standards only. The correction factors and their uncertainties for other (143.76, 163.356 and 205.315 keV) gamma energies from ^{235}U have been calculated and tabulated in an extended report of the work by the authors [8].

NBL Standard	Mass thickness ρt ($g \cdot cm^{-2}$)	Uncertainty in ρt ($g \cdot cm^{-2}$)	μ/ρ (cm^2/g) Tot-Coh 185.715 keV	Correction for non-infinite thickness (185.715 keV)	Uncertainty in non-inf thickness correction (185.715 keV)
031-078	5.22	0.3	1.2584	1.001442	0.000545
071-078	5.22	0.3	1.2584	1.001442	0.000545
194-078	5.22	0.3	1.2583	1.001445	0.000546
295-078	5.22	0.3	1.2583	1.001450	0.000548
446-078	5.22	0.3	1.2583	1.001457	0.000550
NBL0021	5.98	unavailable	1.2579	1.000541	-
NBL0022	5.98	unavailable	1.2572	1.000540	-
NBL0023	5.98	unavailable	1.2583	1.000540	-

Table 5. Correction for non-infinite thickness and its uncertainty

From the results presented in Table 5, it is seen that for the LEU standards, the correction for non-infinite thickness overlaps with unity at the 2σ level of its uncertainty. The mass density uncertainties for the HEU set are not provided in the CRM certificates. So the uncertainty in the correction factor could not be propagated for HEU standards.

3.5 Container wall attenuation: Correction factor and its uncertainty

The thickness of the bottom aluminum wall of the NBL standards is given in the certificates for the CRM 969 and CRM 146 standards, along with their uncertainties. The uncertainties in the wall thickness are random uncertainties since they are the standard deviation of the thickness values measured at various points on the surface of the bottom wall. The uncertainty in the correction factor for attenuation through the container wall was estimated using the uncertainty in the wall thickness. The correction factor due to gamma-ray attenuation through the container wall and its uncertainty are calculated using Equations (9) and (10).

$$CF_{wall} = 1/T_{wall} = e^{\left\{\frac{\mu}{\rho}\right\}.\rho t} \quad (9)$$

In Eqn. (9), T is the transmission factor, μ/ρ is the mass attenuation coefficient for aluminum, ρ is the density of aluminum, and t is the wall thickness.

$$\sigma_{CFwall} = \left(\frac{\mu}{\rho}\right) * \rho * CF_{wall} * \sigma_t \quad (10)$$

σ_{CFwall} and σ_t are the uncertainties in the transmission factor and the aluminum wall thickness, respectively.

The correction factor due to attenuation through the wall thickness and the uncertainty in the correction factor are given in Table 6 for the 185.715 keV gamma ray energy from ^{235}U.

NBL Standard	Al Wall Thickness (mm)	Uncertainty in Al wall thickness (1σ) (mm)	CF_{wall} (185.715 keV)	σ_{CFwall} (185.715 keV)
031-078	1.996	0.010	1.06796	0.00035
071-078	1.996	0.010	1.06796	0.00035
194-078	1.996	0.007	1.06796	0.00025
295-078	1.997	0.005	1.06799	0.00018
446-078	1.996	0.006	1.06796	0.00021
NBL0021	1.994	0.0052	1.06789	0.00018
NBL0022	1.994	0.0052	1.06789	0.00018
NBL0023	1.994	0.0052	1.06789	0.00018

Table 6. Wall attenuation correction and its uncertainty

3.6 Variation in mass attenuation coefficient values of U_3O_8 for different U enrichments

When the MAC values for uranium oxide (or other compounds) are obtained from the national database (e.g., NIST XCOM), it must be recognized that these are for the natural oxide, and not necessarily for the actual oxide that may have a different isotopic enrichment. The differences between the MAC for the natural U_3O_8 compound versus the MAC values for U_3O_8 with different ^{235}U enrichments were calculated for ^{235}U gamma energies. Results are given for the185.715 keV gamma.

NBL Standard	Enrichment (atom%)	MAC for U_3O_8 cm^2/g	Diff. in MAC values w.r.t. nat. U_3O_8
031-078	0.3206	1.258294	0.00%
071-078	0.7209	1.258285	0.00%
194-078	1.9664	1.258258	0.00%
295-078	2.9857	1.258236	0.00%
446-078	4.5168	1.258203	-0.01%
NBL0021	20.311	1.257855	-0.03%
NBL0022	52.800	1.257137	-0.09%
NBL0023	93.233	1.256219	-0.16%

Table 7. Influence of enrichment on MAC of U_3O_8

The influence of enrichment on MAC does not introduce an uncertainty in any attenuation factor calculation because the appropriate mass density of U_3O_8 is used with the corresponding MAC.

4. Analysis results and discussions

An ROI approach was adopted because of its simplicity and its amenability for propagating the uncertainties in a clear and technically defensible way. The objective of the ROI analysis was to verify whether the count rates from the ^{235}U gamma-ray peaks varied linearly with respect to the enrichment (atom %) The Peak Easy software supplied by Los Alamos National Laboratory was used to extract the ^{235}U net peak areas from the spectra that were collected. Figure 3 shows an example spectrum with the ROI that includes the 182.6 keV and 185.715 keV peaks from ^{235}U.

The 182.6-keV gamma ray from ^{235}U has an abundance of 0.39%, much smaller compared to the abundance of the 185.715-keV gamma ray (57.0%). However, at enrichments of 20% and higher, the intensity of the 182.6-keV peak is non-negligible. The ROI was therefore defined to include the

182.6-keV peak to avoid biases that may be induced while attempting to estimate the continuum counts to the left of the 185.715-keV peak. Including the 182.6-keV peak would yield more consistent results while studying the trends in the data from standards of different enrichments. Data from other ^{235}U gamma-ray peaks at energies of (140.76 + 143.76) keV, 163.356 keV, and 205.316 keV were also analyzed and the uncertainties propagated [8]. The analysis results from multiple gamma-ray peaks would help identify sources of biases that may selectively impact one of the energies and those that may impact all energies.

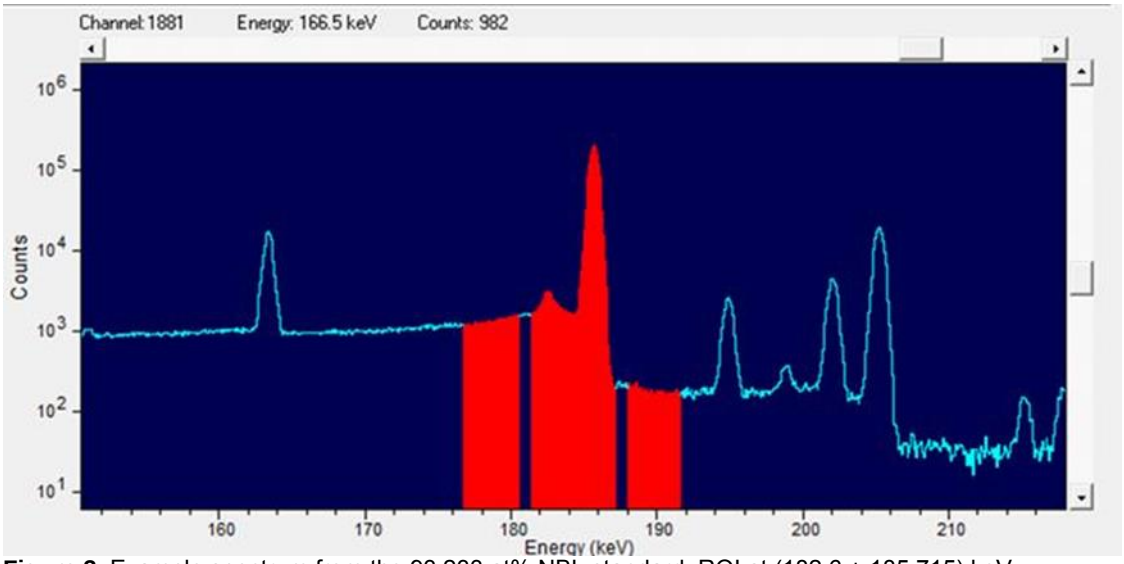

Figure 3. Example spectrum from the 93.233 at% NBL standard; ROI at (182.6 + 185.715) keV

The same ROI settings were used to analyze the spectra from all 48 trials for all the enrichment standards. The net peak area (counts) and its uncertainty (counts) were determined. The continuum under the peak was estimated using a linear model. . The peaked background contribution to the (182.62 + 185.715) keV ROI was subtracted (Eqn. 11) and the uncertainties propagated.

The same ROI settings were used to analyze the spectra from all 48 trials for all the enrichment standards. The net peak area (counts) and its uncertainty (counts) were determined using the following equations.

$$S = G - B - I \tag{11}$$

In Eqn. (11), S is the net peak area signal from the sample, G is the gross area in the peak ROI, B is the continuum counts under the peak ROI, and I is the peaked interference due to gamma rays present in the background. The continuum B was determined using a linear model, as given in Eqn. (12) below.

$$B = \frac{N}{2}\left[\frac{B_1}{n_1} + \frac{B_2}{n_2}\right] \tag{12}$$

In Eqn. (11), B_1 and B_2 are the summed counts in the continuum ROIs to the left and the right of the peak ROI, n_1 and n_2 are the number of channels in the continuum ROIs to the left and right of the peak ROI, and N is the number of channels in the peak ROI.

The propagated uncertainty in the continuum counts under the peak is calculated as follows.

$$\sigma_B = \sqrt{\left(\frac{N}{2n_1}\right)^2 \sigma_{B_1}^2 + \left(\frac{N}{2n_2}\right)^2 \sigma_{B_2}^2} \tag{13}$$

Since the counts B_1 and B_2, as well as the gross count G, are expected to reasonably obey Poisson statistics, variance is equal to the mean. Therefore the uncertainty in the net peak area is written as follows.

$$\sigma_S = \sqrt{G + \left(\frac{N}{2n_1}\right)^2 B_1 + \left(\frac{N}{2n_2}\right)^2 B_2 + \sigma_I^2} \qquad (14)$$

The contribution from background interference, I, was estimated using the same ROI settings used for the true signal. The uncertainty, σ_I, in the ambient background net peak ROI was propagated using the uncertainties in the gross and continuum counts in the background ROI

The peak count rates from the ROIs of interest were corrected for the non-infinite thickness of the measured samples and the attenuation through the bottom wall of the container. The uncertainties due to counting statistics were propagated along with the uncertainties in the correction factors, and the uncertainty in sample positioning. The corrected count rates were plotted as a function of enrichment (atom%).

The net peak area, the gross peak area, and the continuum counts at the 182.62 + 185.715-keV ROI were plotted as a function of ^{235}U enrichment (in atom %). The plots are shown in Figures 4, 5, and 6. The Deming curve fit program was used to fit a linear function through the data points. Uncertainties in both x and y axes (the corrected count rate and atomic %) were taken into consideration while performing the curve fit. The results of the curve fit are shown in Table 8.

The ratio of absolute value of residuals to measurement uncertainty for the 182.6 + 185.7-keV data are plotted in Figures 7, 8, and 9 for net peak count rate, gross count rate, and the continuum count rate at the 182.6 + 185.7 keV ROI. The y axis is thus a deviation in terms of the number of sigma values (nσ).

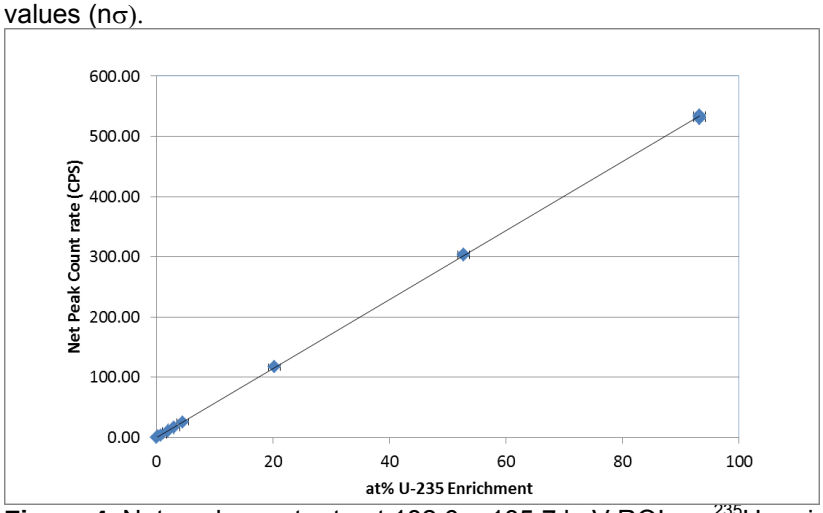

Figure 4. Net peak count rate at 182.6 + 185.7 keV ROI vs. ^{235}U enrichment

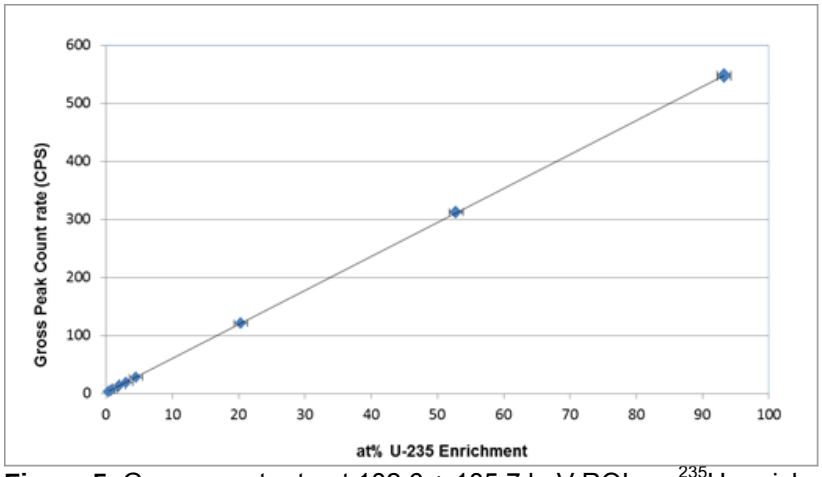

Figure 5. Gross count rate at 182.6 + 185.7 keV ROI vs. ^{235}U enrichment

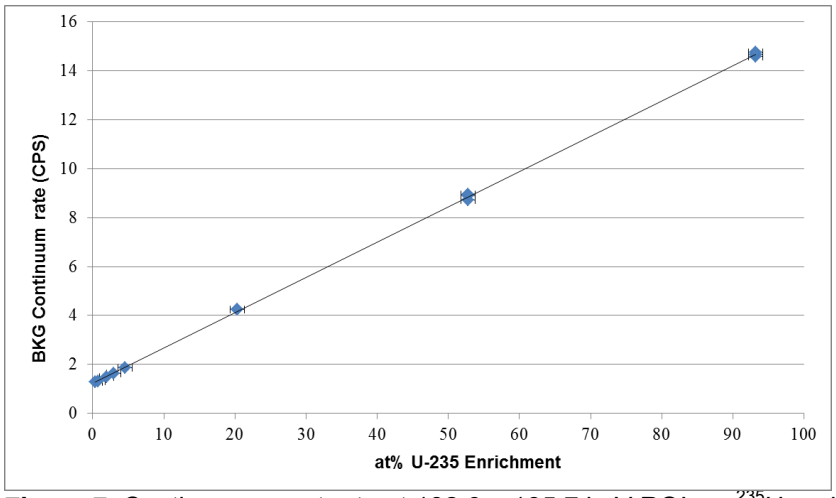

Figure 7. Continuum count rate at 182.6 + 185.7 keV ROI vs. ^{235}U enrichment

Data	Parameter a	Parameter b	Covariance	Reduced χ^2
Net peak area	0	5.729 ± 0.007	-	1.65
Gross peak area	1.212 ±0.014	5.875 ± 0.009	-5.078E-05	1.82
Continuum counts	1.211 ± 0.009	0.145 ± 0.0008	-2.696E-06	11.41

Table 8. Deming curve fit results for the count rates at 182.6 + 185.7 keV ROI

From the data presented in the plots (Figures 4,5, and 6) and Table 8, it is evident that the gross, continuum background, and net peak counts show a linear relationship with respect to uranium enrichment. This is to be expected because in the ROI-based analysis, the net count is derived from the gross and continuum background counts.

A two-parameter linear fit (Y intercept and slope) was performed for the gross and continuum count rate data. If a sample with a ^{235}U fraction of zero was measured, the gross count rate in the ^{235}U peak ROIs would be non-zero because of counts due to down-scattering of gamma rays emitted by ^{238}U and other isotopes present in the sample. The environmental background was subtracted since those gamma rays did not originate in the sample. The continuum background does not go down to zero at when the ^{235}U enrichment goes to zero. This is to be expected since the down-scattered photons emitted by other isotopes of uranium (namely ^{238}U) will contribute to the counts in the continuum at the (182.6 + 185.7)-keV peak ROI.

For the net peak count rate and gross peak count rate, the reduced χ^2 value is very reasonable, signifying that the observed deviation among the data points is consistent with the estimated uncertainties in the count rates. However, for the continuum count rate, the reduced χ^2 is high indicating that the deviation in the data are much higher than the propagated uncertainties. Possibly there are sources of uncertainties that have not been accounted for in the continuum count rate.

The plots showing the ratio of absolute value of the residuals to the propagated uncertainty σ are given below in Figures 7,8, and 9.

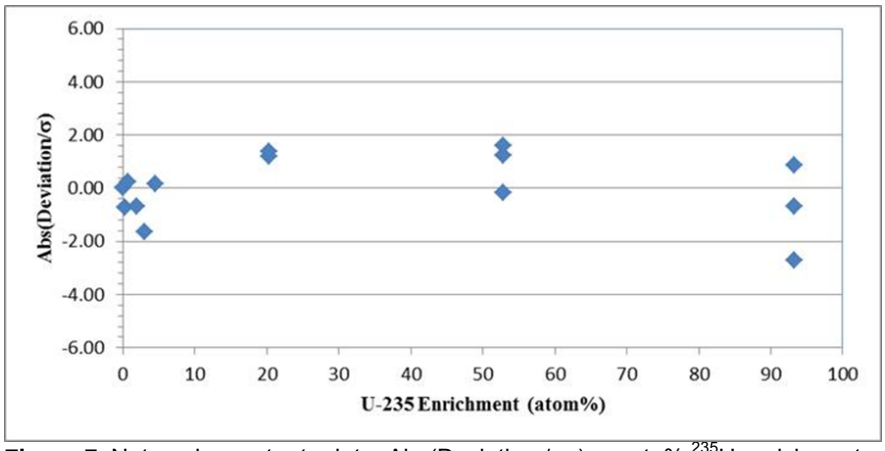

Figure 7. Net peak count rate data: Abs(Deviation / σ) vs. at. % ^{235}U enrichment

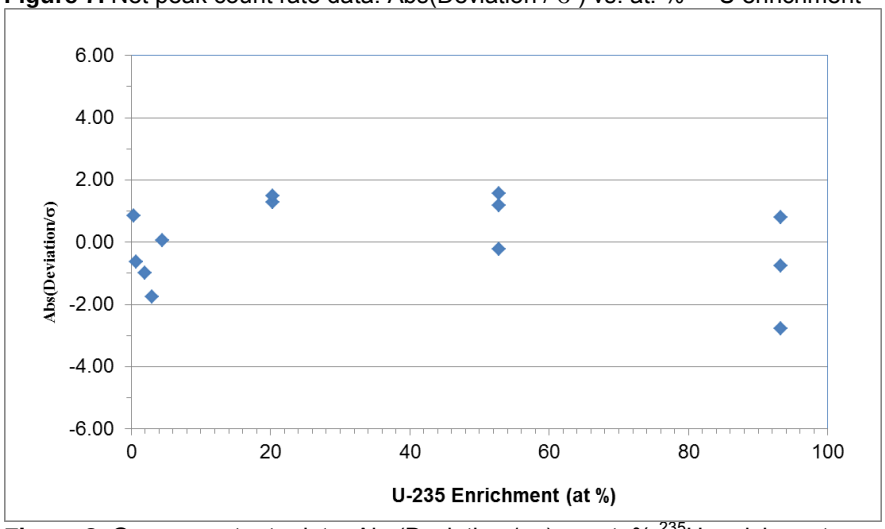

Figure 8. Gross count rate data: Abs(Deviation / σ) vs. at. % ^{235}U enrichment

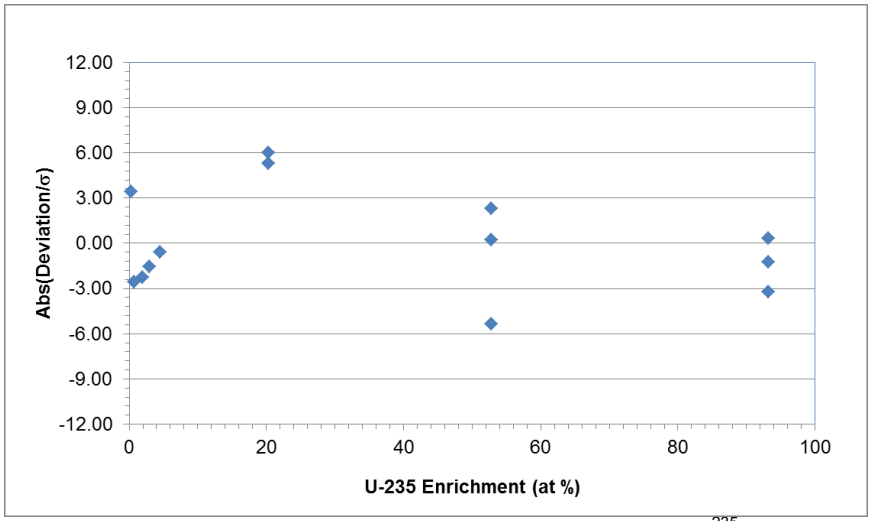

Figure 9. Continuum count rate data: Abs(Deviation / σ) vs. at. % ^{235}U enrichment

The nσ values for the net peak count rate and gross count rate data are within ±3σ. In an ideal scenario, reduced χ^2 equals 1, and the data points will scatter normally about n = 0. As mentioned earlier, for the continuum count data, the nσ values show a higher scatter, and the reduced χ^2 value is 11.41, much higher than unity than what was observed for the net peak and gross count rate data. The likely reason for this is an underestimation of uncertainty or unknown sources of uncertainties that were not considered.

In this paper, the results for the 185.715 keV gamma ray have been presented. The reader is referred to the ORNL report [8] that contains the analysis and results for data from the 143.76, 163.356, and 205.315 keV gamma rays.

5. Conclusions and Future work

The current analysis was performed based on an ROI approach and for four prominent gamma lines emitted by ^{235}U, namely143.76, 163.356, 185.715, and 205.315 keV. Future analysis will focus on determining specific or atomic emission ratios between nuclides, which is aimed at improving relative nuclear data for internally calibrated isotopic codes. The spectra and a summary of the work will be provided to the IAEA for its own evaluation and will also be made available to the international community e.g., International Working Group on Gamma-ray Spectrometry Techniques. The data set may be used in training classes gamma-ray spectroscopy and measurement uncertainty.

6. Acknowledgement

The authors thank the US Department of Energy, National Nuclear Security Administration, Office of Defense Nuclear Nonproliferation Research and Development, NA-22, for supporting this work under project “Uncertainty Quantification.” The authors acknowledge the contributions made by Dr. Adam Shepard to this project while he was a staff member at ORNL.

7. References

1. R. Gunnink, W. D. Ruhter, P. Miller, J. Goerten, M. Swinhoe, H. Wagner, J. Verplancke, M. Bickel, and S. Abousahl, *MGAU: A New Analysis Code for Measuring U-235 Enrichments in Arbitrary Samples*, IAEA-SM-333/88, Prepared for submittal to the IAEA Symposium on International Safeguards, Vienna, Austria, March 1994.

2. Sampson, T.E., Kelley, T.A. *The Los Alamos PC/FRAM Code for the Nondestructive Analysis of the Isotopic Composition of Plutonium and other Actinides*, LA-UR 96-1220, Los Alamos National Laboratory, May 1996.

3. *Standard Reference Material 969,Uranium Isotopic Standard Reference Material for Gamma Spectrometry Measurements*, National Bureau of Standards Certificate, June 27, 1985, Gaithersburg, Md. (Issued in cooperation with the Commission of the European Communities, Central Bureau for Nuclear Measurements, Geel, Belgium, and US Department of Energy New Brunswick Laboratory, Argonne, Illinois).

4. *Uranium Isotopic Standard for Gamma Spectrometry Measurements*, New Brunswick Laboratory Certified Reference Material CRM146, Certificate of Analysis, July 30, 1999.

5. Bill Harker, *Deming Curve Fitting Program for Windows, Version 2.00*, January 6, 2012.

6. Rooney, B., Garner, S., Felsher, P., Karpius, P., 2015, PeakEasy 4.82 [Computer Program], Los Alamos National Laboratory, Release LA-CC-13-040, https://PeakEasy.lanl.gov.

7. Canberra Industries Inc., *In Situ Gamma Spectroscopy with ISOCS, an In Situ Object Counting System*, 2008.

8. R. Venkataraman and S.Croft, *Measurement of Uranium Enrichment Standards Using High Resolution Gamma Spectrometry with High Precision and Accuracy*, ORNL/TM-2016/659, Oak Ridge National Laboratory, November 2016.

Characterization of a 500 mm^3 CdZnTe Detector for U and Pu Isotopic Composition Determination Tasks in Safeguards

I. Meleshenkovskii[1,3], A. Borella[1], K. Van der Meer[1], M. Bruggeman[2], N. Pauly[3], P.E. Labeau[3], P. Schillebeeckx[4]

[1]yaroslav.meleshenkovskii@sckcen.be; SCK•CEN; Nuclear Science and Technology Group; B-2400 Mol, Belgium, Tel. +32 14 33 80 41

[2]Belgian Nuclear Research Centre, SCK•CEN, Low-level Radioactivity Measurements Unit, B-2400 Mol, Belgium

[3]Université libre de Bruxelles, Service de Métrologie Nucléaire (CP/165/84)

[4]European Commission Joint Research Center, Retieseweg 111, B-2440 Geel, Belgium

Abstract:

High-purity Germanium (HpGe) detectors have traditionally been the detectors of choice for quantitative gamma-ray spectroscopy in safeguards applications. They benefit from the best resolution achievable nowadays yielding in the possibility to distinguish closely positioned peaks in complex spectra such as those of Pu or mixed materials. Their response has been very well characterized and a variety of existing software algorithms is available for isotopic composition determination tasks of U and Pu materials in safeguards applications. However, HpGe detectors require cooling either via the means of liquid nitrogen or thermoelectric cooling making the equipment heavy, bulky and thus inconvenient to use for hand held devices for nuclear inspectors, limited space locations or unattended nuclear installations.

CdZnTe (CZT) room temperature semiconductor detectors have been proposed as a viable alternative. These detectors exhibit usually an asymmetrical peak shape and worse resolution in comparison to HpGe detectors; therefore, their application to isotopic composition determination tasks in safeguards is not straightforward. CZT detectors have now been optimized in their design yielding resolution of 1.5% at 661 keV for a 10 mm x 10 mm x 5 mm device. Such detectors are also used in the framework of the Inter-Comparison Exercise on U and Pu Isotopic Measurements with Medium Resolution Gamma-Ray Spectrometers organized by the IAEA in cooperation with the ESARDA NDA Working Group and the International Working Group on Gamma-Spectrometry Techniques (IWG-GST).

The response function of these CZT detectors differs in important ways from that of HpGe detectors, requiring changes to the analytical software used for isotopic composition tasks in safeguards. This study will characterize the response of one of the latest generation of CZT detectors – the 500 mm3 hemispheric type at energies ranging from 59 keV to 1332 keV using analytical peak response models. It will present issues of CZT spectra gamma-ray analysis, including tailing on the low energy side of the peaks arising from incomplete charge collection efficiency, energy dependence of the peak shape and strategy to tackle them using mathematical detector response models. Finally, it will quantitatively compare two mathematical models that describe the peak shape of CZT detectors in terms of how well they describe the peak shape and the optimal energy range of application for each.

Keywords: CZT; CZT peak shape; tailing effect; isotopic composition; safeguards

1. Introduction

Due to continuous improvements in their design and related instrumentation room temperature, semiconductor detectors as CZT are finding numerous applications in the fields of radiation detection in industry, science and medicine[1,2,3]. CZT detectors offer several attractive features for quantitative gamma ray spectroscopy. They are characterized by a wide energy band gap allowing room temperature operation of these detectors[2]. Their high atomic number yields a high intrinsic efficiency

of gamma absorption (and thus a reduced size of the detector[2]). Finally, the spectral resolution of these detectors is significantly better in comparison with other room temperature semiconductor or scintillation devices, as shown in figure 1.

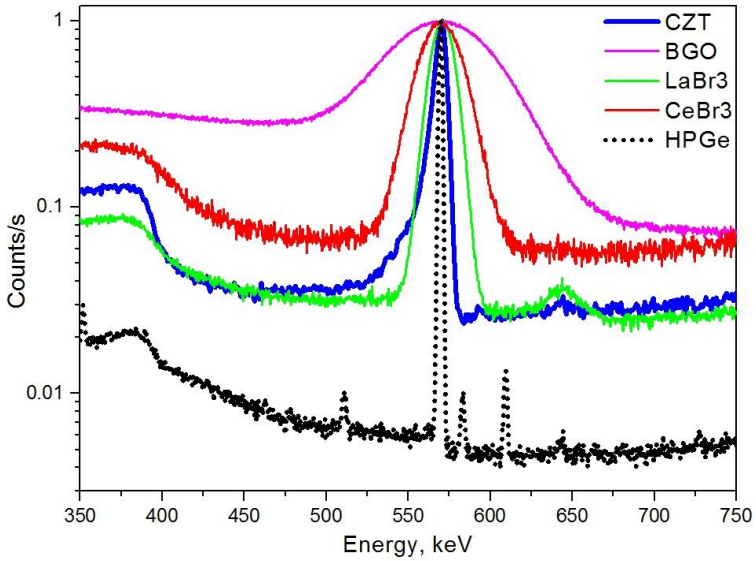

Figure 1: Comparison of detector resolution for different detectors with ^{207}Bi source.

Nuclear safeguards is one of the applications for these detectors because these detectors present a viable alternative to HpGe detectors used for quantitative gamma ray spectroscopy of uranium samples, plutonium samples and spent fuel assemblies[4,5].

Measurements of isotopic composition of U and Pu bearing samples in safeguards applications are usually based on non-destructive gamma assay methods. HpGe detectors have traditionally been used for these tasks accompanied by highly developed spectra analysis algorithms for isotopic composition determination tasks that are implemented in such commercially available codes as FRAM[6], MGA[7] and MGAU[8].

However, the necessity of cooling makes the equipment heavy, bulky and thus inconvenient to use for hand-held devices or in limited space locations, underwater applications and unattended nuclear installations which require small but efficient room-temperature detectors with good energy resolution[9]. CZT detectors, although being available nowadays in a wide range of types and sizes, are however limited in their practical application for U and Pu isotopic composition determination tasks due to the following issues. Indeed, these detectors exhibit a peak asymmetry due to incomplete charge collection processes and a high degree of peak overlapping in complex spectra, such as that of plutonium. Moreover, the existing isotopic composition determination algorithms were optimized for HpGe detectors.

The various algorithms developed to quantitatively unfold the information carried by the peaks in unknown spectra[10,11] are different in methodology. However, the conventional unfolding technique for the peaks in spectra is based on the correspondingly accurate knowledge of the peak shape and its dependence on energy. Several approaches have already been proposed for both small-size and large-size CZT detectors. Assessment of small size CZT detector characterization is available in review articles[12-15].

As for medium- to large-size CZT detectors various peak shape mathematical models have been proposed, differing in the number of parameters used to parameterize peaks and the way the tailing component is treated[16-19]. In this work we devote more attention to the study of possible peak shape mathematical models to be implemented in software for isotopic composition determination tasks specifically suited for CZT detectors.

The primary purpose of this paper is to quantitatively compare the performance of selected mathematical peak shape models in a wide range of energies from 59 keV to 1332 keV applied to a 500 mm^3 CZT detector response, and to determine the effective range of their application.

The current manuscript is organized as follows. Section 2 gives a short description of the point sources, instrumentation, measurement setup and data acquisition software used to obtain and process the data. Section 3 describes the analytical functions used for background and peak shape modelling as well as the fitting method implemented in a specially written for this purpose Matlab code. Section 4 presents the results of the study and Section 5 concludes the paper.

2. Equipment, software and data acquisition

Source. We used well-characterized point sources to determine the response of a 500 mm^3 CZT detector. The available point sources and their energies are listed in Table 1.

Source type	Energy, keV
^{241}Am	59
^{109}Cd	88
^{57}Co	122
^{139}Ce	165
^{113}Sn	391
^{85}Sr	514
^{137}Cs	661
^{54}Mn	834
^{65}Zn	1115
^{60}Co	1173
^{22}Na	1274
^{60}Co	1332

Table 1: List of point sources and their energies.

Instrumentation. The measurements were performed on a hemispheric CZT detector with 10 mm x 10 mm size and 5 mm thickness, fabricated by RITEC (Riga, Latvia)[20]. The detector was coupled with a digital GBS Elektronik Multi Channel Analyzer (MCA), model 527. The high-voltage bias applied to the detector was 1400 V. The preamp signals were processed by MCA using trapezoidal shaping with 1.2 μs constant and 4096 channels spectrum size. The coarse gain setting was 10 and fine gain setting was 1.5, the trigger filter was (+1,0,-2,0,+1) and the flat top parameter was 1 μs.

Software. The MCA-527 was controlled from a Dell Z00478 Optiplex 740HT desktop computer. The spectra were acquired using the WinSpec data collection software[21].

Measurement setup. The distance between the point source sample and the detector surface was 30.1 ±0.2 mm.

3. Analytical functions

3.1. Step-like contribution to background

According to Helmer and Lee[23] the background under the region of a peak is formed by the following main components:

(1) the pulses related to radiation from other sources (i.e., construction materials, cosmic radiation);

(2) the scattered pulses from higher energy gamma-rays of the source being measured;

(3) the pulses from the desired gamma-ray which due to loss of significant amount of energy in sensitive volume fall below the full absorption peak in the spectral distribution.

The first two contributions can be approximated by a low order polynomial, whereas the third contribution should be approximated by a step-like function. As discussed in the literature[23], if an ideal case is assumed when a detector has an infinitely narrow resolution and no tailing, the step-like increase in the counts probably results from events in which part of the gamma-ray energy escapes from the sensitive volume of the detector. This results in a step-function pulse distribution which cuts off at the peak maximum. However, in a real detector the resolution has a finite shape determined by the Gaussian distribution arising from the statistical fluctuation of the charge carriers and the division of absorbed energy between ionization and heating of the crystal lattice (Fano factor)[24]. Besides, incomplete charge collection due to the different lifetimes and mobilities of electrons and holes yields tailing on the low-energy side of the peak, what even more complicates the resulting peak shape[2]. Given these particularities of real detectors, the step-like function should be also broadened in order to reflect the physical aspects of the mentioned processes of a given detector.

A number of functions have been suggested in the literature to represent the step-like background. Helmer and Lee[23] have investigated the performance and summarized results for the major step-like functions used in quantitative gamma-ray spectroscopy.

In our study we have used a complimentary error corrected step-like function to model the background under the peak. We modify this function in such a way that not only the constant representing the background level on the high-energy side of the peak but also the constant representing former on the low energy side of the peak are both fitting parameters:

$$BKG(i) = \left(\left(\frac{1}{2} * erfc\left[\frac{(x - x_0)}{\sqrt{2} * \sigma}\right]\right) * step\_height\right) + offset$$

Where *step_height* is the parameter that represents the height of the background level on the low-energy side of the peak and *offset* is the parameter that represents the background level on the high-energy side of the peak.

In our implementation we add the background function to the analytical peak shape model as a component and fit together with the Gaussian and Tailing components.

3.2. Analytical peak shape models

Accurate modelling of the detector response is a challenging task due to complex nature of the physical and statistical phenomena involved. Besides, a peak shape can be very sensitive to such experimental parameters as count rate (quality of spectra), degree of collimation and scattering. Due to these particularities, it is desirable to determine an approximate functional representation of the peak shape directly from the measured data.

Thus, all mathematical representations of the peak shape include a central Gaussian part to account for fluctuations of the charge carriers and Fano factor. The differences between different mathematical peak shape models suggested in the literature[17,18,19,23] arise from the functional form of the tailing component to account for the distortion of the central Gaussian part. The functional forms investigated in this paper can be categorized into three groups. The first group contains only the Gaussian. The second group contains the Gaussian and one tailing component and the third one contains the Gaussian and two tailing components.

Although it is expected that a simple Gaussian can be applied for the mathematical representation of the complex peak shape of a CZT detector only at low energies where the incomplete charge collection effects do not yet cause serious asymmetry, it was included in the study only to contrast with more realistic approximations.

The second group of functions, consisting of a basic Gaussian shape with one tailing component to account for peak asymmetry caused by incomplete charge collection processes, includes contributions from several authors[19,25]. In both cases the tailing is represented by an exponential multiplied by a complementary error corrected function.

Thus, the sIGAle[19] peak shape model is represented in the following form with *model(i)* being the net counts in channel *i*, σ the Gaussian half width, *x* the channel number or independent variable, x_0 the peak centroid at maximum height, *T(i)* the tailing component at channel *i*, p_1 the relative tail height parameter and p_2 the tail slope parameter:

$$model(i) = y_0 * exp[-(x_i - x_0)^2/2\sigma^2] + T(i) + BKG(i)$$

$$T(i) = p_1 * y_0 * e^{\frac{x-x_0}{p_2*\sigma}} * erfc\left[\frac{x - x_0}{\sqrt{2} * \sigma} + \frac{1}{\sqrt{2} * p_2}\right]$$

Due to considerations described in section 4.1 there are seven fitting parameters in our implementation of the sIGAle[19] peak shape model: Gaussian peak height (y_0), Gaussian half width (σ), centroid position (x_0), relative tail height (p_1), tail slope (p_2), background height at the low energy side of the peak (*step_height*) and background height at the high-energy side of the peak (*offset*).

An alternative approach to single tailed peak shape models is the two-component tailing function used in the FRAM[6] code, with *x* being the channel number or independent variable, x_0 the peak centroid at maximum height, *T(i)* tailing components at channel *i*, *A* the short tailing height parameter, *B* the short tailing slope parameter, *C* the short tailing height parameter, *D* the short tailing slope parameter and δ terminating both tails at the gamma-ray energy limiting the contribution of both tails only on the low energy side of the peak (i.e. the Heaviside function):

$$T(i) = \left[A * exp\left(B * (x - x_0)\right) + C * exp\left(D * (x - x_0)\right)\right] * \left[1 - exp(-0.4 * \alpha * (x - x_0)^2)\right] * \delta$$

This third group approach separates the low energy tailing into two components – one tailing component represents a faster decaying contribution due to trapping and recombination (long-term tail) and the second component represents the low-energy step caused by photoelectron escape from the active region of the detector (short term tail).

In our implementation, the FRAM[6] peak shape model has nine fitting parameters – Gaussian peak height (y_0), Gaussian width parameter (α), centroid position (x_0), short-term tail height (*A*), short-term tail slope parameter (*B*), long-term tail height parameter (*C*), long-term tail slope parameter (*D*), background height at the low energy side of the peak (*step_height*) and background height at the high-energy side of the peak (*offset*).

3.3. Fitting method

Each of the functions described above was fitted to the point source peaks in a wide range of energies (see table 1 for details). For this purpose, the corresponding Matlab-based code was developed from scratch; it performs a non-linear least-squares fitting routine to minimize the reduced chi-square (corrected to the number of degrees of freedom being the number of free parameters used in each of the peak shape models):

$$\chi^2{}_R = \frac{1}{n}\sum_{roi\_l}^{roi\_r}\left[\frac{exp_i - model_i}{\sigma_i}\right]^2$$

$$n = roi_r - roi_l + 1 - NPAR$$

Where *roi_l*, *roi_r* specify the fitting interval (region of interest); *NPAR* is the number of degrees of freedom (number of fitting parameters); $model_i$ is the analytic approximation at channel *i*, exp_i is the counts at channel *i* and σ_i is the variance.

Identical regions were used for all fits of a particular full-energy peak in order to compare the various peak shape models directly. The optimization solver used in the fitting routine was a geometric (derivative-free) Nelder-simplex method.

4. Results and discussion

4.1. Quality of fitting

The χ^2_R values obtained for the functions investigated in this paper are shown in table 2. From the table it is clear that the best fit is achieved with a single-component tailing sIGAle[19] function within the whole range of energies. The more complex FRAM[6] function with two-component tailing, although giving fits that are quite acceptable, is less appreciable.

Source type	Energy, keV	Goodness of fit (χ^2 reduced)		
		FRAM[6] model	sIGAle[19] model	Gaussian only
^{241}Am	59	1.5	1.2	5.8
^{109}Cd	88	2.6	1.0	29.2
^{57}Co	122	4.0	2.0	45.7
^{139}Ce	165	3.1	1.2	-
^{113}Sn	391	3.9	1.5	-
^{85}Sr	514	3.1	2.7	-
^{137}Cs	661	3.2	3.0	-
^{54}Mn	834	10.1	8.5	-
^{65}Zn	1115	6.8	4.6	-
^{60}Co	1173	4.4	4.3	-
^{22}Na	1274	3.4	2.5	-
^{60}Co	1332	4.3	4.2	-

Table 2: Comparison of χ^2_R for different peak shape models.

The less attractive performance of the FRAM[6] model is due to the functional form of the equation describing the tailing components – as shown in section 3.2. The FRAM[6] equation for the tailing components terminates both tails at the gamma-ray energy, thus limiting their contribution strongly to the low energy side of the peak. However, as described in literature the charge collection efficiency is interaction-position dependent[2] and restriction noted above cannot adequately approximate the complex nature of an energy-dependent peak shape of a CZT detector.

To contrast these results a simple Gaussian fit to the data in the range of energies from 59 keV to 122 keV is included in the results in table 2. It is apparent that the underestimate of the data points dramatically increases with energy.

4.2. Components analysis

In order to analyze the performance of the two functions investigated in this paper, we have calculated the individual contributions of the peak components (Gaussian, tail(s)) normalized to the total net peak area. The total net peak area value was numerically calculated by integrating the background subtracted peak shape model functions with fitted parameters at given energies. As shown in figures 2 and 3 the Gaussian area for both functions decreases with energy. However, the behaviour of the tailing components is different. For the FRAM[6] function, the relative areas of both tails are significantly smaller than the Gaussian area. This behaviour is due to termination of both tails at the gamma-ray energy. Such a performance is acceptable in the cases where the physical origin of the events leading to asymmetry (such as incomplete charge collection) is relatively small compared to the other events (such as the fluctuation of the number of the charge carriers created in the sensitive volume of the detector). However, in case of a CZT detector it cannot adequately approximate the complex behaviour of an energy-dependent peak shape with significant asymmetry which was indicated by the values of χ^2_R.

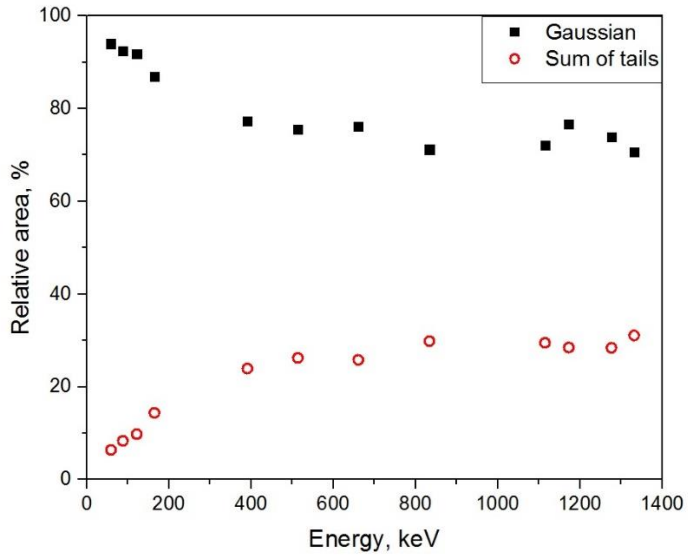

Figure 2: Relative contributions to the net peak area in FRAM[6] peak shape model.

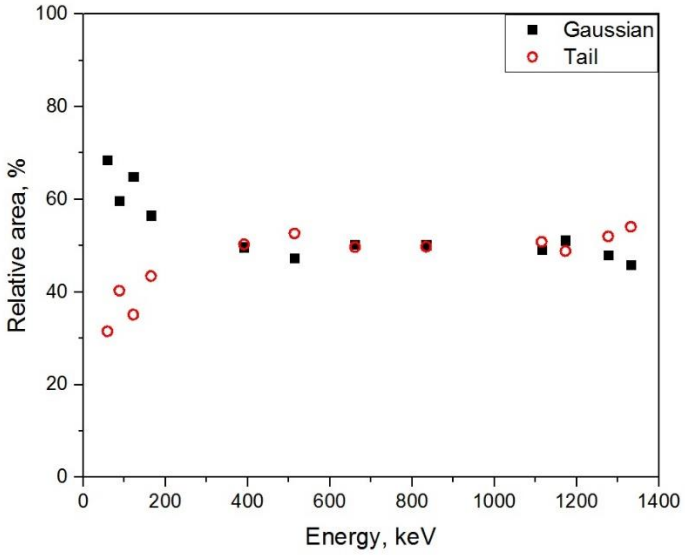

Figure 3: Relative contributions to the net peak area in sIGAle[19] peak shape model.

In contrast, the sIGAle[19] tailing function is not restricted to the low-energy side of the peak and its area can be significant relative to the Gaussian area, as indicated in figure 3. In case of a CZT detector with a large amount of tailing such a contribution may be realistic. Indeed, for a CZT detector the peak asymmetry is dependent on the charge collection efficiency which is a function of the incident photon interaction depth in the detector. For large volume CZT detectors, as considered in this study, for high-energy photons interacting in deeper regions of the detector, the distortion of the peak due to incomplete charge collection can be quite severe. Its contribution is thus comparable to the Gaussian part of the peak.

4.3. Parameters

The fitted parameters and corresponding uncertainties as a function of energy are shown in tables 3, 4 and 5. The width parameter increases with the energy for both peak shape models as shown in table 3. The width of the Gaussian fitted with no tailing components to the data is clearly larger than that for the fits with tailing components.

Source type	Energy, keV	Gaussian width		
		FRAM[6] model	sIGAle[19] model	Gaussian only
^{241}Am	59	6.22	6.08	6.43
^{109}Cd	88	6.04	5.82	6.45
^{57}Co	122	6.72	6.43	7.26
^{139}Ce	165	6.96	6.62	-
^{113}Sn	391	9.03	8.49	-
^{85}Sr	514	10.27	9.76	-
^{137}Cs	661	12.09	11.59	-
^{54}Mn	834	14.49	13.87	-
^{65}Zn	1115	17.88	17.21	-
^{60}Co	1173	17.51	16.73	-
^{22}Na	1274	19.6	18.91	-
^{60}Co	1332	20.01	19.03	-

Table 3: Gaussian peak width comparison.

The inverse tailing slopes for both tailing components of the FRAM[6] function decrease with energy as shown in table 4 along with the corresponding uncertainties. For the sIGAle[19] function the inverse tailing slope given by 1/(p2*sigma) decreases with energy, as shown in table 4 with the corresponding uncertainties.

Source type	Energy, keV	FRAM[6] model parameters					
		Short tail slope (B)	Short tail slope (B) uncertainty	Long tail slope (D)	Long tail slope (D) uncertainty	Gaussian width	Gaussian width uncertainty
^{241}Am	59	1.58	0.29	0.33	0.09	6.22	0.11
^{109}Cd	88	1.31	0.28	0.35	0.07	6.04	0.26
^{57}Co	122	0.30	0.54	0.27	0.03	6.72	0.12
^{139}Ce	165	0.40	0.05	0.24	0.04	6.96	0.25
^{113}Sn	391	0.18	0.13	0.11	0.01	9.03	0.35
^{85}Sr	514	0.15	0.03	0.11	0.02	10.27	0.55
^{137}Cs	661	0.10	0.04	0.10	0.02	12.09	0.47
^{54}Mn	834	0.11	0.01	0.05	<0.01	14.49	0.22
^{65}Zn	1115	0.11	0.01	0.05	0.01	17.88	2.03
^{60}Co	1173	0.06	0.01	0.06	<0.01	17.51	0.34
^{22}Na	1274	0.05	0.01	0.05	<0.01	19.60	0.43
^{60}Co	1332	0.05	<0.01	0.04	<0.01	20.01	0.35

Table 4: FRAM[6] peak shape model parameters and uncertainties.

Source type	Energy, keV	sIGAle[19] model parameters			
		Tail slope (p_2)	Tail slope (p_2) uncertainty	Gaussian width	Gaussian width uncertainty
^{241}Am	59	0.69	0.04	6.08	0.10
^{109}Cd	88	0.80	0.07	5.82	0.27
^{57}Co	122	1.04	0.06	6.43	0.29
^{139}Ce	165	1.32	0.05	6.62	0.25
^{113}Sn	391	2.15	0.09	8.49	0.38
^{85}Sr	514	2.19	0.08	9.76	0.36
^{137}Cs	661	2.35	0.11	11.59	0.23
^{54}Mn	834	2.91	0.14	13.87	0.38
^{65}Zn	1115	3.18	0.09	17.21	0.36
^{60}Co	1173	2.75	0.08	16.73	0.28
^{22}Na	1274	3.18	0.12	18.91	0.55
^{60}Co	1332	3.07	0.10	19.03	0.34

Table 5: sIGAle[19] peak shape model parameters.

The absolute values of peak component areas as well as the total net peak area uncertainties for both peak shape models investigated in this paper are shown in table 6. The results indicate that for both peak shape models the net peak areas do not significantly differ, however the contribution of the peak components to the total net peak area is significantly different between the two peak shape models. Thus, for all energies the Gaussian areas of the single-component tailing sIGAle[19] peak shape model are significantly smaller in comparison to those of the two-component tailing FRAM[6] peak shape model. Indeed, because the tailing component of the sIGAle[19] peak shape models is not terminated at the gamma-ray energy its area is significant to the Gaussian area and is larger for all energies in comparison with the FRAM[6] peak shape model where both tails are terminated at the gamma-ray energy. The net peak area uncertainties are larger for the more complicated two-component tailing FRAM[6] peak shape model due to its additional parameters. The net peak areas calculated using channel-by-channel summation technique indicate that both peak shape models estimate the net peak areas quite accurately.

Source type	Energy, keV	Net peak area calculation mode									
		FRAM[6] peak shape model				sIGAle[19] peak shape model				Channel-by-channel summation	
		Net peak area, counts	Net peak area σ, %	Gaussian relative area, %	Σ tails relative area, %	Net peak area, counts	Net peak area σ, %	Gaussian relative area, %	Tail relative area, %	Net peak area, counts	Net peak area σ, %
^{241}Am	59	93573	2.69	93	7	92135	1.16	68	22	91015	0.37
^{109}Cd	88	100803	3.96	92	8	99519	1.57	59	41	100037	0.35
^{57}Co	122	108387	2.98	91	9	107676	1.71	64	36	110477	0.34
^{139}Ce	165	104871	3.95	86	14	104277	1.26	56	44	107441	0.35
^{113}Sn	391	100502	4.71	77	23	99297	1.30	49	51	102382	0.41
^{85}Sr	514	148864	5.46	75	25	149650	1.02	47	53	155048	0.35
^{137}Cs	661	91098	5.56	76	24	92191	0.88	50	50	95670	0.46
^{54}Mn	834	423511	2.83	71	29	423098	1.26	50	50	448043	0.23
^{65}Zn	1115	194558	7.04	72	28	203497	0.61	49	51	216495	0.37
^{60}Co	1173	111729	3.11	76	24	114130	0.51	51	49	119375	0.65
^{22}Na	1274	54031	2.54	73	27	58504	0.85	47	53	61252	0.72
^{60}Co	1332	95843	3.10	70	30	98140	0.54	45	55	100514	0.53

Table 6: FRAM[6] & sIGAle[19] peak shape models net peak areas & uncertainties.

5. Conclusions

The performance of the two mathematical peak shape models was investigated in application to the response of a 500 mm^3 hemispheric CZT detector in a range of energies from 59 to 1332 keV. The investigated peak shape models have different functional representation of the tailing component to account for the peak asymmetry.

The results of this study indicate that there is no significant improvement in the quality of fit with a complex two-component tailing function. However, one tailing component is definitely necessary as shown in comparison with a single Gaussian fit. It is also apparent that a tailing component that does not terminate at the gamma-ray energy is preferable for a CZT detector due to a more realistic representation of the processes causing the asymmetry. The net peak areas for both peak shape models do not significantly differ, while the behaviour of the peak components is significantly different. The net peak area uncertainties are larger for a more complicated two-component tailing FRAM[6] peak shape model due to its additional parameters.

The results of this study will be further used in a uranium and plutonium isotopic composition determination algorithm that specifically suits the particularities of medium resolution spectra obtained on CZT detectors.

6. Legal matters

6.1. Privacy regulations and protection of personal data

In order to comply with the European Directive 95/46/EC as approved by the European Parliament and the Council of Ministers on the 24th October 1995 relating to the protection of individuals with respect to the processing of data of personal nature and on the free circulation of such data, it is necessary that you provide us with written consent. Feel free to use the example below as a template:

"I agree that ESARDA may print my name/contact data/photograph/article in the ESARDA Bulletin/Symposium proceedings or any other ESARDA publications and when necessary for any other purposes connected with ESARDA activities."

6.2. Copyright

The author agrees that submission of an article automatically authorises ESARDA to publish the work/article in whole or in part in all ESARDA publications – the bulletin, meeting proceedings, and on the website.

The author declares that their work/article is original and not a violation or infringement of any existing copyright.

7. References

[1] R. Arlt, V. Ivanov, K. Parnham, “Advantages and Use of CdZnTe Detectors in Safeguards Measurements”, presented at MPA&C Conference, Obninsk, Russia, May 2000; to be published in the conference proceedings in November, 2001;

[2] T. Takahashi and S. Watanabe, “Recent Progress in CdTe and CdZnTe Detectors”, IEEE Transactions on Nuclear Science, Page(s): 950 - 959 (Volume: 48, Issue: 4, Aug 2001);

[3] Y. Ramachers et al., “Energy resolution improvement in room-temperature CZT detectors”, Journal of Instrumentation, Volume 2, December 2007;

[4] V. Ivanov, P. Dorogov “Further development of hemispheric CZT detectors for safaguards applications”, Proceedings of the 21st ESARDA Annual Symposium, Sevilla, Spain, 4-6 May 1999;

[5] Wayne D. Ruhter “Application of CZT detectors in nuclear materials safeguards”, Proc. SPIE 3446, Hard X-Ray and Gamma-Ray Detector Physics and Applications, 204 (July 1, 1998); doi:10.1117/12.312892; http://dx.doi.org/10.1117/12.312892 ;

[6] T. E. Sampson, G. W. Nelson, and T. A. Kelley, “FRAM: A Versatile Code for Analyzing the Isotopic Composition of Plutonium from Gamma-Ray Pulse Height Spectra,” Los Alamos National Laboratory report LA-11720-MS (December 1989);

[7] R. Gunnink, “MGA: A Gamma-Ray Spectrum Analysis Code for Determining Plutonium Isotopic Abundances”, Report UCRL-LR-103220, Vol. 1 (ISPO No. 317, Task No. A.161), Lawrence Livermore National Laboratory, Livermore, CA, USA April 3,1990;

[8] R. Gunnink, W. D. Ruhter, P. Miller, J. Goerten, M. Swinhoe, H. Wagner, V. Verplancke, M. Bickel, S. Abousahl, “MGA-U: a new analysis code for measuring U-235 enrichments in arbitrary samples”, Proceedings of the IAEA Symposium on International Safeguards, Vienna, Austria, 1994;

[9] K. H. Czock, R. Arlt “Use of CZT detectors to analyze gamma emission of safeguards samples in the field”, Nuclear Instruments and Methods in Physics Research Section A, Volume 458, Issue 1-2, p. 175-182, 2001;

[10] J. C. Fleissner, GRPAUT, “GRPAUT: A Program for Pu Isotopic Analysis”, User's Guide, Mound Facility report MLM-2799/ISPO-128, (1981);

[11] T. E. Sampson, “Plutonium isotopic composition by gamma-ray spectroscopy”, Technical Report, Los Alamos Scientific Lab., NM (USA), 1980;

[12] R. Gunnink, R. Arlt, “Methods for evaluating and analyzing CdTe and CdZnTe spectra”, Nuclear Instruments & Methods in Physics research, vol. A458, pp.196-205, 2001;

[13] E. Vittone, F. Fizzoti, A. lo Giudice, P. Posello, C. Manfredotti, Nucl. Instr. And Meth. A 428 (1999) 81;

[14] M. G. Scannavini et al., Nucl. Instr. And Meth. A 353 (1994) 80;

[15] M. N. Nambooridi, A. D. Lavietes, J. H. McQuaid, “Gamma-ray peak shape from cadmium zinc telluride detectors”, Lawrence Livemore National Laboratory Report, UCRL-125271, 1996;

[16] P. Mortreau, R. Berndt, “Characterization of cadmium zinc telluride detector spectra – application to the analysis of spent fuel spectra”, Nuclear Instruments & Methods in Physics research, vol. A458, pp.183-188, 2001;

[17] R. Gunnink, R. Arlt, “Methods for evaluating and analyzing CdTe and CdZnTe spectra”, Nuclear Instruments & Methods in Physics research, vol. A458, pp.196-205, 2001;

[18] Y. X. Dardenne, T. F. Wang, A. D. Lavietes, G. J. Mauger, W. D. Ruhter, S. A. Kreek, Nucl. Instr. And Meth. A 422 (1999) 159;

[19] I. Espagnon, A. C. Simon, F. Lamadie, C. Mahe, “sIGAle, a new code for automatically determining radionuclide activities using CdZnTe spectrometry”, Page(s): 1159 – 1165, IEEE Transactions on Nuclear Science (Volume: 58, Issue: 3), June 2011;

[20] V. Ivanov, P. Dorogov, R. Arlt, “Development of large volume hemispheric CdZnTe detectors for use in safeguards applications”, ESARDA European Research and Development Association, Proceedings of Nineteenth Annual Symposium on Safeguards and Nuclear Material Management, Le Corum, Montpellier, France 13-15 May, 1997, p.447;

[21] M. Aparo, J. Arenas Corrasco, R. Arlt, V. Bytchkov, K. Esmailpour, O. Heionen, A. Hiermann, “Development and implementation of compact gamma spectrameters for spent fuel measurements”, Proceedings of the 21st ESARDA Annual Meeting, Sevilla, Spain, 4-6 May, 1999;

[22] I. Meleshenkovskii et al., “Instrumentation effects on U and Pu CBNM standards spectra quality measured on a 500 mm3 CdZnTe and a 2x2 inch LaBr3 detectors”, in preparation for the proceedings of the ANIMMA 2017 conference, June 2017, Liege, Belgium;

[23] R. G Helmer, M. A. Lee, “Analytical functions for fitting peaks from Ge semiconductor detectors”, Idaho National Engineering Laboratory, EG & G Idaho, Inc., Idaho Falls, Idaho 83415, USA, 1980;

[24] L. A. Mcnelles, J. L. Campbell, “Analytic approximations to peak shapes produced by Ge(Li) and Si(Li) spectrometers”, Department of Physics, University of Guelph, Guelph, Ontario, Canada, 1975;

[25] Marie-Christine Lepy, “Presentation of the COLEGRAM software”, Laboratoire National Henri Becquerel, LNHB 04/26, 2004;

Determination of Plutonium Mass and Isotopic Composition in ^{238}Pu-α-Li Neutron Source

Arturs Rozite, Hamid Tagziria and Santino Frison

European Commission, Joint Research Centre
Nuclear Safety and Security Directorate
Via E. Fermi 2749, TP 800
21027 Ispra (VA), Italy
E-mail: arturs.rozite@ec.europa.eu

Abstract:

Nuclear materials accountancy is an important instrument of a control over non-proliferation regime and implementation of passive non-destructive assay (NDA) methods by nuclear safeguards at the inspection of nuclear facilities is a common practice.
In this article a characterization of a neutron source having unknown plutonium mass and isotopic composition using classical methods of passive NDA is described. From gamma-ray energy spectrum of the source and neutron measurements it was confirmed that this is a ^{238}Pu-α-Li neutron source. Mass of plutonium-238 was measured using calorimetry. Mass-ratios of ^{238}Pu to ^{239}Pu, ^{241}Pu and ^{241}Am were determined by high-resolution gamma-ray spectrometry, a three duplets method for the analysis of ^{238}Pu-α-Li neutron sources on radio-isotopic composition is suggested.

Keywords: ^{238}Pu-α-Li source, gamma-ray spectrometry, calorimetry

1. Introduction

In the beginning of 2016 we have been asked for the characterisation of an orphan neutron source of unknown isotopic composition and mass. Source had markings: MRC-Pu8Li-17 and 10 μCi. In the result of the search for the information in the internet it became clear that MRC stands for Monsanto Research Corporation and Pu8Li possibly means ^{238}Pu-α-Li source.
Monsanto Research Corporation was responsible for the production of plutonium-238 primary for radioisotope thermoelectric generators since 1960th [1].
Plutonium-238 was produced in different chemical forms (metal, plutonium-zirconium alloy and in the form of dioxide) and average values of 80.2% and 91.6% of plutonium-238 enrichment have been reported for standard and high assay plutonium dioxide microspheres [2] which are most suitable for the alpha-n source fabrication.
For the confirmation of source type and for its radiological characterisation standard passive NDA methods have been applied, including neutron coincidence counting, high-resolution gamma-ray spectrometry and calorimetry.

2. Materials and methods

Neutron coincidence measurements were primary focused on the determination of source type and were made with JCC-31 high-level neutron coincidence counter; rates of singles and doubles were acquired with JSR-12 coincidence analyzer with a shift register.
Gamma-ray energy spectra were acquired with coaxial and planar high-purity germanium (HPGe) detectors and these measurements were done for the confirmation of source type and for the determination of its radio-isotopic composition.
Calorimetric measurements were made by means of small samples calorimeter (ANTECH, model 601C) using heat flow differences in twin (empty and loaded) measurement cells and were aimed on the determination of plutonium mass. Prior heat-flow measurement from the sample an electric-sample

calibration in range from 1 mW to 200 mW was made. Calorimeter was well characterized before by means of plutonium-gallium reference standards [3].

3. Experimental results

3.1. Determination of source type

Neutron measurements were made with JCC-31 counter having measured detection efficiency of 16.8% and die away time of 41.2 μs. From neutron measurements *(Table 1)* one may conclude that this is an alpha-n source, since rate of singles is much higher than doubles rate, and may observe that rate of doubles is not negligible, so an alpha-emitter is characterized by a certain fission rate.

Table 1 – Results of neutron measurements

Source ID	Measurement time, s	Singles rate, s^{-1}	Doubles rate, s^{-1}
Background	7200	4.5 ±0.8	0.09 ±0.04
MRC-Pu8Li-17	7200	164165 ±5.1	54.4 ±22.0

From the broad energy range spectrum *(Figure 1)* measured with a coaxial HPGe detector it is evident that this is a ^{238}Pu-α-Li source as long as there are intense ^{238}Pu spectral lines, as well as 478 keV peak with characteristic Doppler broadening produced by photons emitted from the source in the result of de-excitation of ^{7}Li nucleus. Excited state of ^{7}Li nucleus is formed in the result of ^{7}Li(α, α')^{7}Li* (0.48) nuclear reaction which is concurrent to ^{7}Li(α, n)^{10}B nuclear reaction.
^{208}Tl lines are observed in the tail of the spectrum due to the presence in the source of ^{232}U which is a decay product of ^{236}Pu.

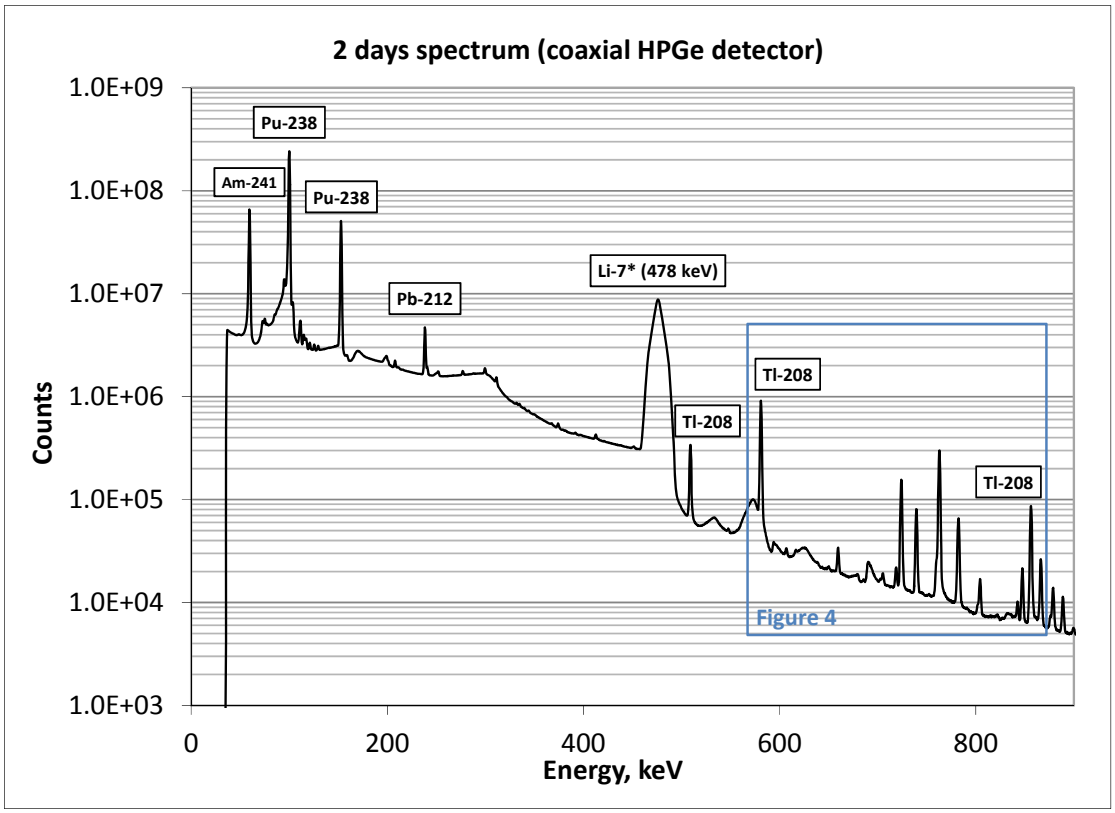

Figure 1 – Spectrum of source measured with coaxial HPGe detector

3.2. Determination of plutonium isotopic composition

Mass-ratios of ^{238}Pu to ^{239}Pu, ^{241}Pu and ^{241}Am were determined using high-resolution gamma-ray spectrometry. No signal from ^{240}Pu and ^{242}Pu was measured. Two different HPGe detectors (planar and coaxial) have been used: planar detector (Ø500×13mm) to get optimal energy resolution in 125 keV energy region of interest (ROI) and coaxial detector (with nominal relative detection efficiency of 12%) to cover broad energy range from 40 keV to 1 MeV.
Measurement with planar detector was made with an amplifier gain of 75 eV/channel, so spectrum *(Figure 2)* can be processed with Multi-Group Analysis (MGA) software code [4].

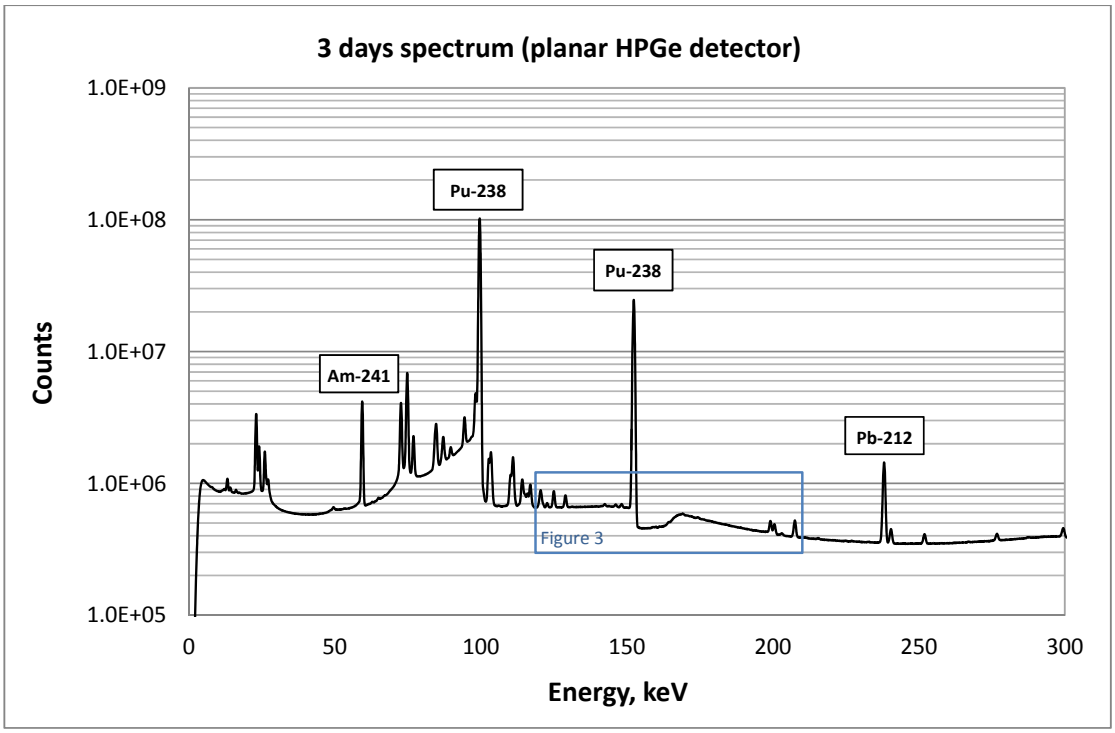

Figure 2 – Spectrum of source measured with planar HPGe detector

In the result of processing of the spectrum measured with planar HPGe detector with the MGA code an error message was generated by the program:

"ABORT: 239, 240 or 241Pu result was negative".

Manual analysis on isotopic composition was made. Analysis shows that in the spectrum of the planar detector a 100 keV ROI has a dominant ^{238}Pu line and 208 keV ROI is influenced by a Compton continuum induced by 478 keV photons, so in the result

a) multiplets of spectral lines in 100 keV ROI can't be resolved,
b) 160 keV spectral line of ^{240}Pu is suppressed by a Compton continuum,
c) in principle 125 keV ROI is suitable for the determination of plutonium isotopic composition.

For the manual determination of plutonium isotopic composition three duplets have been used. Two duplets (125/129 keV and 148/152 keV) from the 125 keV ROI *(Figure 3)* to obtain mass ratios of ^{241}Am/^{239}Pu and ^{241}Pu/^{238}Pu isotopes and third duplet (662/742 keV) from the spectrum measured with coaxial HPGe detector which allows to obtain ^{241}Am/^{238}Pu mass-ratio *(Figure 4)*.

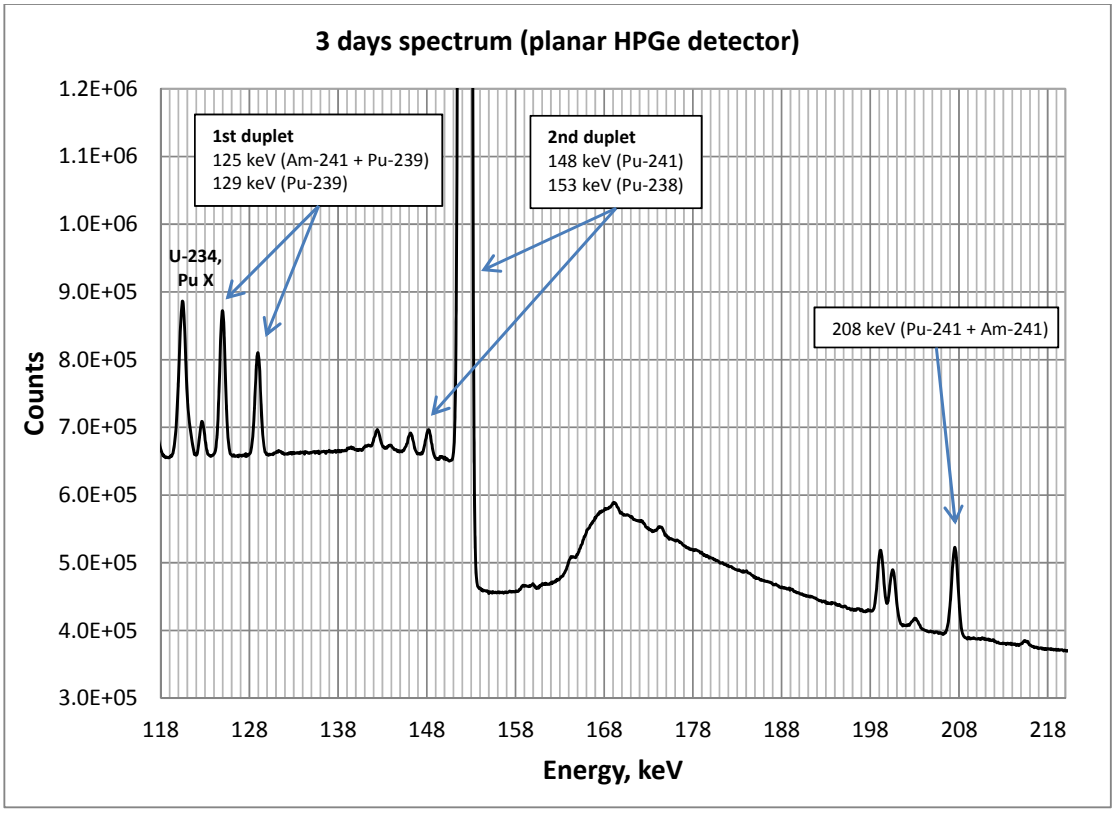

Figure 3 – Region of interest of the spectrum of source measured with planar HPGe detector

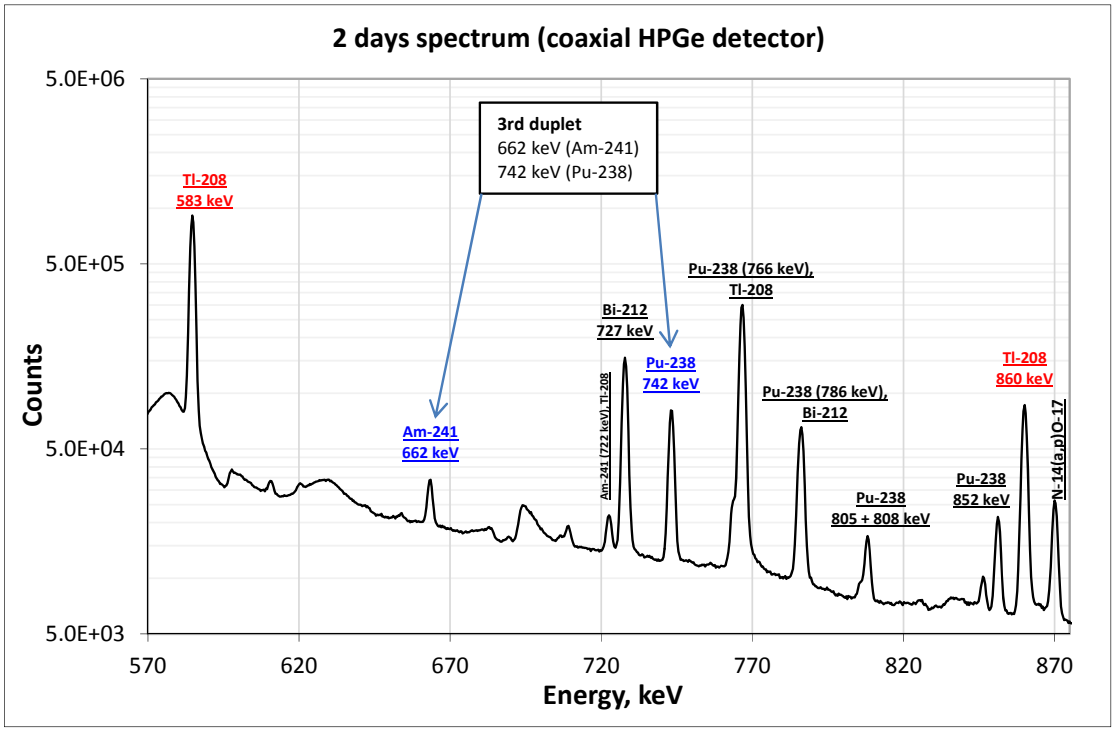

Figure 4 – Region of interest of the spectrum of source measured with coaxial HPGe detector

Since corresponding spectral lines of the third duplet are rather separated in energy (by 80 keV), a correction for the detection efficiency was made. Linear correction factor for the detection efficiency was calculated based on the measured intensities of 511, 583 and 860 keV spectral lines of ^{208}Tl normalized to corresponding branching ratios *(Table 2, Figure 5)*. Correction factor calculated from the ratio of relative detection efficiencies at 662 keV and 742 keV is equal to the 1.126.

Table 2 – Determination of relative detection efficiency based on the ^{208}Tl spectral lines

Isotope	Energy, keV	Net count rate, cps	Branching ratio, photons/disintegration	Normalized net count rate	Relative detection efficiency
^{208}Tl	511	9.32	0.226	41.23893805	1
^{208}Tl	583	27.97	0.845	33.10059172	0.802654
^{208}Tl	860	2.95	0.1242	23.75201288	0.575961

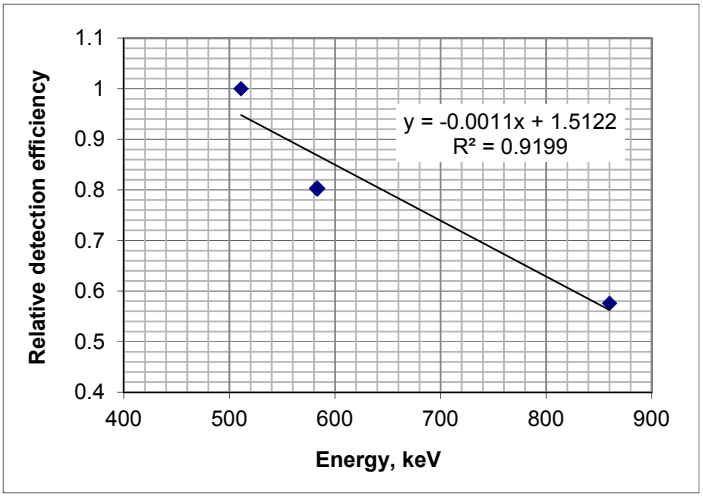

Figure 5 – Relative detection efficiency in energy range from 511 to 860 keV calculated from the intensities of ^{208}Tl spectral lines (linear fit)

To get mass-ratios of radionuclides, first, a measured net count rate in full-energy absorption peaks was normalized to specific activities of radionuclides at given energies and then ratios of the obtained values *(Table 3, last column)* have been calculated for the three duplets *(Table 4, second column)*.
For the third duplet linear correction for the detector detection efficiency was made based on the intensities of 511, 583 and 860 keV spectral lines of ^{208}Tl and corresponding branching ratios.
Emission probabilities used in calculations (branching ratios, specific activities) have been taken from the following reference works [5, 6].

Table 3 – Measured mass fractions of radionuclides for a given geometry and detection efficiency

Isotope	Energy, keV	Net count rate, s^{-1}	Uncertainty, s^{-1}	Activity, $s^{-1}g^{-1}$	Measured mass fraction, g
Planar detector					
^{241}Am	125.26	9.786	0.045	5.16E+06	1.90E-06
^{239}Pu	129.29	6.955	0.041	1.44E+05	4.83E-05
^{241}Pu	148.57	1.786	0.037	7.15E+06	2.50E-07
^{238}Pu	152.68	1153.1	0.09	6.05E+06	1.91E-04
Coaxial detector					
^{241}Am	662.42	0.505	0.007	4.61E+05	1.10E-06
^{238}Pu	742.82	2.485	0.007	3.28E+04	7.58E-05

Table 4 – Measured mass ratios of radionuclides

Isotopes	Mass ratio	Relative uncertainty, %	Notes
$^{239}Pu/^{241}Am$	25.42	1.05	1st duplet
$^{238}Pu/^{241}Pu$	764	2.08	2nd duplet
$^{238}Pu/^{241}Am$	77.59	1.67	3rd duplet with detection efficiency correction
$^{238}Pu/^{239}Pu$	3.05	2.72	3rd/1st duplet
$^{241}Am/^{241}Pu$	9.85	3.75	2nd/3rd duplet

3.3. Determination of plutonium mass

Heat flow from the source was measured by calorimetry.
Based on the measured $^{238}Pu/^{241}Am$ and $^{239}Pu/^{241}Am$ mass-ratios and corresponding values of specific power for these radionuclides (567.57 mW/g for ^{238}Pu, 114.2 mW/g for ^{241}Am and 1.93 mW/g for ^{239}Pu) it is calculated that only 0.26% of the total heat flow is produced by ^{241}Am and only 0.11% by ^{239}Pu.
Prior heat flow measurements from the source a calorimeter was calibrated using electrical samples in the range from 1 to 200 mW *(Table 5, Figure 6)*. Duration of each calibration measurement and interval between them was 180 minutes. For the calibration an average value of measured voltage for the last 5 minutes was used.

Table 5 – Results of calorimeter calibration

Run	Applied power, mW	Measured voltage, mV	Measurement time, min
		Last 5 minutes average	
1	1	0.13011	180
2	4	0.488556	180
3	7	0.847408	180
4	10	1.203614	180
5	40	4.789346	180
6	70	8.375567	180
7	100	11.94437	180
8	200	23.83546	180

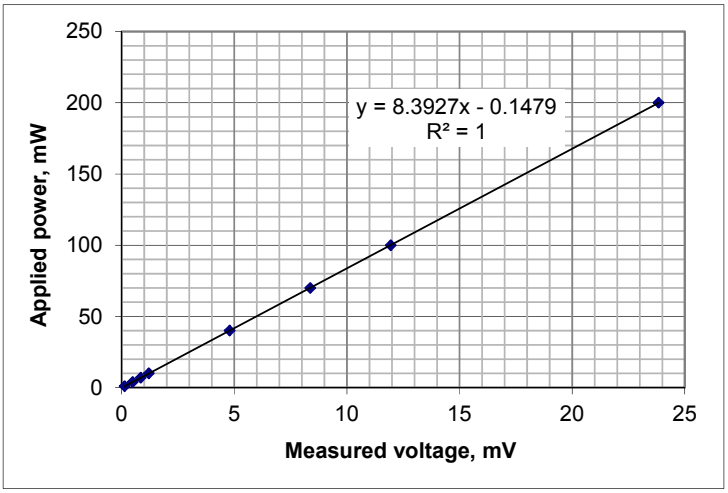

Figure 6 – Electrical calibration of small-samples calorimeter

Measurement of heat flow from source was made *(Figure 7)*. Measured value is 370.9 mW what corresponds to 0.65 g of plutonium-238.

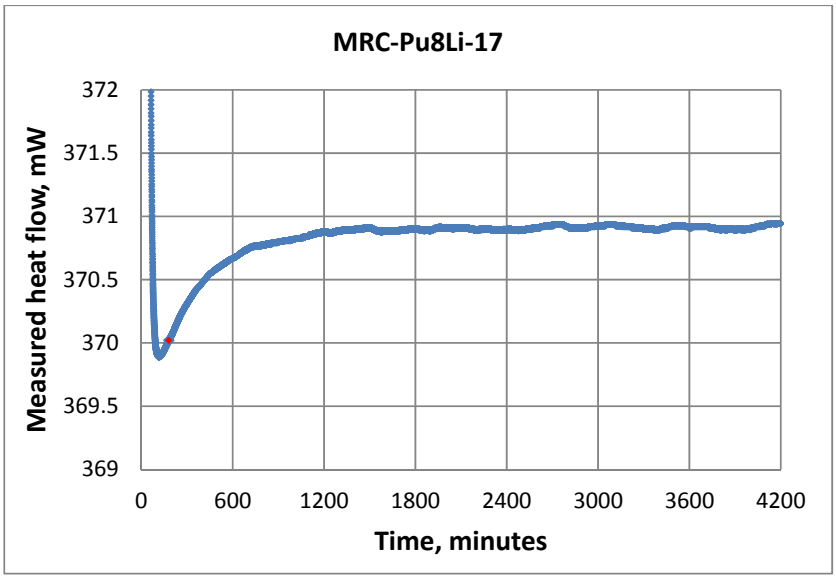

Figure 7 – Long term calorimetry measurement of the heat flow from the ^{238}Pu-α-Li source

4. Measurement errors

4.1. Gamma-ray spectrometry

Net peak areas have been calculated according to the equation 1:

$$N_{NET} = N_{GROSS} - \frac{k_P}{2}\left(\frac{N_{B1}}{k_{B1}} + \frac{N_{B2}}{k_{B2}}\right) \qquad (1)$$

N_{NET} = net peak area
N_{GROSS} – gross area of peak region
N_{B1} – gross area of 1st background region
N_{B2} – gross area of 2nd background region
k_p – number of channels in the peak
k_{B1}, k_{B2} – number of channels in the background regions
$k_{B1} = k_{B2} = 4$

In all calculations first background region corresponds to the 4 channel region before the peak (3 channels prior the peak plus first peak channel) and second background region corresponds to the 4 channel region after the peak (last peak channel plus three following channels).

Peak area uncertainties *(U)* have been calculated according to the equation 2:

$$U = \sqrt{N_{GROSS} + \left(\frac{k_p}{k_{B1}+k_{B2}}\right)^2 \times (N_{B1} + N_{B2})} \qquad (2)$$

Mass-ratio uncertainties have been determined purely as a sum of relative uncertainties of the count-rate in corresponding duplet peaks.

4.2. Calorimetry

Error of calorimetry measurements is illustrated by long-term measurement with a source *(Figure 7)*. Deviation of measured heat flow value after 180 minutes (red point = 370 mW) from the average measured value of 370.9 mW calculated for the time interval from 1500 to 4200 minutes is 0.25%.

5. Summary of experimental results

Summary of measured masses of radionuclides is given in *Table 6.*
^{241}Pu decays by α-decay to ^{241}Am with half-life 14.35 years. Age of plutonium was determined by gamma-ray spectrometry using mass-ratio of ^{241}Am ^{241}Pu to and assuming absence of ^{241}Am in plutonium at the date of plutonium production (chemical separation).
^{238}Pu decays by α-decay to ^{234}U with a half-life of 87.7 years. Mass of ^{234}U was determined based on measured mass of ^{238}Pu, age of source and half-live of ^{238}Pu.

Table 6 – Masses of radionuclides in MRC-Pu8Li-17 source

Radionuclide	Mass, g	Uncertainty, %	Method
^{238}Pu	0.652	± 0.25	Calorimetry
^{239}Pu	0.214	± 2.72	HRGS (^{238}Pu/^{239}Pu mass ratio)
^{240}Pu	-	-	
^{241}Pu	0.000853	± 2.08	HRGS (^{238}Pu/^{241}Pu mass ratio)
^{242}Pu	-	-	
^{241}Am	0.008403	± 1.67	HRGS (^{238}Pu/^{241}Am mass ratio)
^{234}U	0.315	± 1.90	^{238}Pu half-life, age of source* (^{241}Am/^{241}Pu mass ratio)
Pu mass, g	**0.867**		
Total mass, g	**1.190**	*Age of plutonium = 50.1 ±0.8 years	

6. Conclusion

In this article a characterization of a neutron source of unknown plutonium mass and isotopic composition using classical methods of passive NDA is described. From gamma-ray energy spectrum of the source and neutron measurements it was confirmed that this is a ^{238}Pu-α-Li neutron source. Mass-ratios of ^{238}Pu to ^{239}Pu, ^{241}Pu and ^{241}Am have been determined by gamma-ray spectrometry using method of three duplets: two duplets form the spectrum measured with planar HPGe detector (125/129 keV and 148/152 keV) and third duplet from the spectrum measured with coaxial HPGe detector (662/742 keV).
Mass of plutonium-238 was measured using calorimetry and masses of ^{239}Pu, ^{241}Pu and ^{241}Am were calculated relative to the mass of ^{238}Pu based on the results obtained with gamma-ray spectrometry.

7. References

[1] GARY H. RINEHART; *DESIGN CHARACTERISTICS AND FABRICATION OF RADIOISOTOPE HEAT SOURCES FOR SPACE MISSIONS;* Progress in Nuclear Energy, Vol. 39, No 3–4; 2001; pp. 305–319
[2] S.G. Abrahamson, D. G. Carfagno and B. R. Kokenge; *PLUTONIUM-238 ISOTOPIC FUEL FORM DATA SHEETS*; AEC Research and Development REPORT; 1968
[3] H. Tagziria, J. Bagi, B. Pedersen, P. Schillebeeckx; *Absolute determination of small samples of Pu and Am by calorimetry.* Nuclear Instruments and Methods in Physics Research A 691; 2012; pp. 90–96
[4] R. Gunnink, W. D. Ruther; *MGA: A Gamma-Ray Spectrum Analysis Code for Determining Plutonium Isotopic Abundances. A Guide to Using MGA;* UCRL-LR-103220, Vol. 2; 1990
[5] R. Gunnink, J. E. Evans and A. L. Prindle; *A REEVALUATION OF THE GAMMA-RAY ENERGES AND ABSOLUTE BRANCHING INTENSITIES OF* ^{237}U, $^{238, 239, 240, 241}$Pu AND ^{241}Am; UCRL-52139; 1976
[6] T. E. Sampson; *Plutonium Isotopic Composition by Gamma-ray Spectrometry: A Review;* LA-10750-MS; 1986

Comparative Testing of the MCA-527 and MCA-166 Mini Multi Channel Analysers

T. Köble[1], M.Risse[1], O. Schumann[1], M. Jöster[1], M. Heinrichs[2], M. Dürr[2], S. Ossowski[1]

[1]Fraunhofer Institut Naturwissenschaftlich-Technische Trendanalysen (INT)
Appelsgarten 2, D-53864 Euskirchen, Germany

[2]Forschungszentrum Jülich, Institute of Energy and Climate Research – Nuclear Waste Management and Nuclear Safety (IEK-6), 52425 Jülich, Germany

E-mail: theo.koeble@int.fraunhofer.de

Abstract:

This paper presents a comparative study of the two multichannel analysers MCA-166 and its successor the MCA-527 from GBS electronic with the focus of the operation at high counting rates. The MCA-166 is widely used by the IAEA and Euratom for safeguards inspections in the field. The performed tests included the influence of peak shaping parameters, count rate and temperature on the operation of the two multichannel analysers.

Keywords: Gamma measurement, Multichannel analyzer, comparative study

1. Introduction

In recent years the pulse height analysis of signals from all kinds of gamma detectors has largely shifted from analogue to digital electronics. Digital multichannel analysers promise better stability due to less analogue components with varying tolerances, lower dead time, and increased throughput because of digital signal processing and thus improved performance. The MCA-527 from GBS Elektronik is such a digital multichannel analyser and the successor of the widely deployed and successful MCA-166. In addition to a completely new and modern architecture, it features many minor improvements.

Under the German support program to the IAEA, Fraunhofer INT has conducted comparative performance tests with these two multichannel analysers in order to access the differences and similarities. These include the stability of gamma peak parameters as function of input count rate, time, and ambient temperature. Special attention was put to the performance under high count rate conditions. At Forschungszentrum Jülich, supplementary comparative testing was performed on LN-cooled HPGe detectors, these results will be presented elsewhere. Further tests included the performance of the multichannel scaling and multispectrum scaling modes and the non-linearity of the two MCAs. In a last test series, the influence of electromagnetic radiation on the operation of the MCA-527 and the effect on the recorded spectrum was examined. Performance test of these MCAs have been performed before [1,2], but these measurements were aimed especially for a comparative testing of both MCAs and especially under high count rate conditions.

2. Description of performed measurements

For the measurement at the Fraunhofer INT, the equipment was provided by the IAEA. This included one MCA-166 and one MCA-527, NaI and LaBr scintillation detectors, two different CZT semiconductor detectors, two laptops with the WinSpec software, as well as necessary accessories like a serial to USB converter. For the tests, radioactive sources of ^{60}Co (up to 380 MBq), ^{137}Cs (up to 1 GBq), ^{133}Ba (1 MBq) and ^{152}Eu (1 MBq) were available at Fraunhofer INT. With the two strong sources of ^{60}Co and ^{137}Cs count rates in the range of 10,000 to 200,000 cps were achievable. This allowed investigating the effect of different count rates on the performance of both MCAs and comparing the observations.

The performed tests included the influence of the count rates and peak shape parameters on the peak resolution, the influence of count rate, temperature, and time on the peak channel stability, measurements of the integral and differential nonlinearity, and the performance of the multichannel and multispectral scaling depending on the input count rate. Additionally, the battery performance at different environmental temperatures, the stability of the high voltage supply and the timing accuracy were compared. For the MCA-527 the possible effects of electromagnetic interferences on MCA operations were evaluated.

For the measurement of temperature effects, a small environmental chamber with forced air circulation was used. It allows changing the temperature according to a predetermined profile with fixed ramps and holding times. Both MCAs were placed inside the chamber at the same time to optimally utilize the measurement time. The temperature within the climate environmental chamber and at the surfaces of the MCAs was recorded by PT 100 sensors every 5 seconds. During these tests, only the MCAs were subjected to the varying temperatures, the source and detectors were placed outside the chamber and signals were routed to the MCAs by feedthroughs.

The electromagnetic influence tests were carried out in a TEM waveguide with fields of 10 V/m in the frequency range from 80 MHz to 1 GHz, with 3 V/m from 1.4 GHz to 2 GHz and with 1 V/m from 2 GHz to 2.7 GHz. Several distinct frequencies used for wireless communication were tested with 30 V/m. The MCA-527 was placed in the waveguide, along with the LaBr detector and all cabling. In order to avoid data transmission disturbances caused by malfunction due to RF, the connection to the laptop was via USB-to-fiber-optics-converters. During these tests, a small ^{60}Co source was used, in order to have the MCA to record a real spectrum with sufficient count rate in the order of 1000 cps. The WinSpec software was used in automatic measurement mode to record one spectrum every 10 seconds. While the frequency was ramped in the waveguide, this spectrum was observed by the operator and a possible deviation from the intended operation would have been recorded by him. These tests were performed in two orientations, with the E-Field in parallel and perpendicular to the cable harness, respectively.

During the course of these tests, more than 45,000 spectrum files have been recorded. In order to handle this large amount of data, a set of python scripts have been written and used to semi-automatically extract the relevant information. Both MCAs performed very well without any outage during the complete measurement campaign.

Comparative tests of the MCA-166 and the MCA-527 were performed with a High Purity Ge-Detector (Canberra Detector GL 0515R) at Forschungszentrum Jülich using a Ra-226 and a Am-241 source. For the MCA-527 digital pulse processing settings (Shaping Time, Flat Top, Trigger Filter, Base Line Restorer, Coarse/Fine Gain) were evaluated to find the optimal combination with respect to resolution and peak stability in the 0-300 keV energy window. These optimal settings were used to compare the performance with the MCA-166 for different count rates ranging from below 5,000 to a maximum count rate of approximately 125,000 cps. For each count rate 20 spectra with 300s live time were acquired. The peaks selected for evaluation where the gamma peak at 59 keV for Am-241 and 186 keV for Ra-226.

2.1 The two multichannel analysers MCA-166 and MCA-527

Figure 1: The two multichannel analysers under test, to the left, the analogue MCA-166, to the right the digital successor MCA-527. Both devices have roughly the same size.

The two multichannel analysers are both compact, battery powered devices, which integrate in addition to the multichannel analyser, a preamplifier power supply, a high voltage modules and the main amplifier. Together with a detector and a laptop, they form a complete detection system. The MCA-166 is now obsolete, because some of its electronic components are no longer available. Thus GBS Elektronik developed the MCA-527 as its successor, with similar features and some improvements.

	MCA-166	**MCA-527**
Technology	Analog	Digital, 14 bit ADC, 10 MSps
Channels	Max. 4k	Max. 16k
Main Amplifier	Gaussian shaping amplifier	Corse Amp. With 5 gains
Pulse Shaping	Shaping Time 1 and 2 µs Pile up rejection	Shaping Time 0.1 .. 25 µs Flat Top Time 0 .. 5 µs
Battery	Li-Ion, 32 Wh	Li-Ion, 10-25 h
Size	155 mm x 95 mm x 45 mm	164 mm x 111 mm x 45 mm
Weight	700 g	820 g
Environment	0°C … +50°C	-20°C … + 60°C
Temp. class	TK 100 (ADC), TK500 (Amp)	TK50
Interface	RS-232 (USB)	Ethernet, USB, RS-232

Table 1: Comparison of technical features the MCA-166 and the MCA-527. Information taken from the manual [3,4].

3. Results of the tests

In the following, we will present some exemplary results from the whole measurement campaign. These are data from the influence of the count rate and the peak shaping parameters on the recorded peak width and peak position for one combination of MCA and detector, the outcome of peak parameter dependence on the temperature and the results of the electromagnetic influence tests.

3.1. Influence of count rate and peak shaping parameters on peak parameters

One major difference between the MCA-166 and the MCA-527 is the implementation of the peak shape parameters. The MCA-166 only has two settings for the shaping time, 1 µs and 2 µs, respectively and in addition one can enable or disable the pile up rejection. This leaves exactly four different combinations for the peak shaping parameters, which were all used in these tests. The MCA527 on the other hand offers to set the shaping time and the flat-top time of its digital input filter. The shaping time is adjustable from 0.1 µs to 25 µs in 0.1 µs steps, the flat top time from 0 µs to 5 µs in 0.1 µs steps. Here, we used the parameters as supplied by the IAEA as a starting point and from these adjusted either the shaping time or the flat top time, but not both at the same time.

For each parameter set, the distance from the source to the detector was adjusted, so that a specific count rate was recorded. Five to seven different count rates were measured and the spectra recorded for 120 s. For each spectrum, the peaks of the used isotope were fit (662 keV for ^{137}Cs, 1173 keV and 1332 keV for ^{60}Co) with a gaussian and the peak position, area and FWHM were extracted. Figure 2

shows these data for one particular data set, the measurement of ^{60}Co with the LaBr detector and the MCA-527.

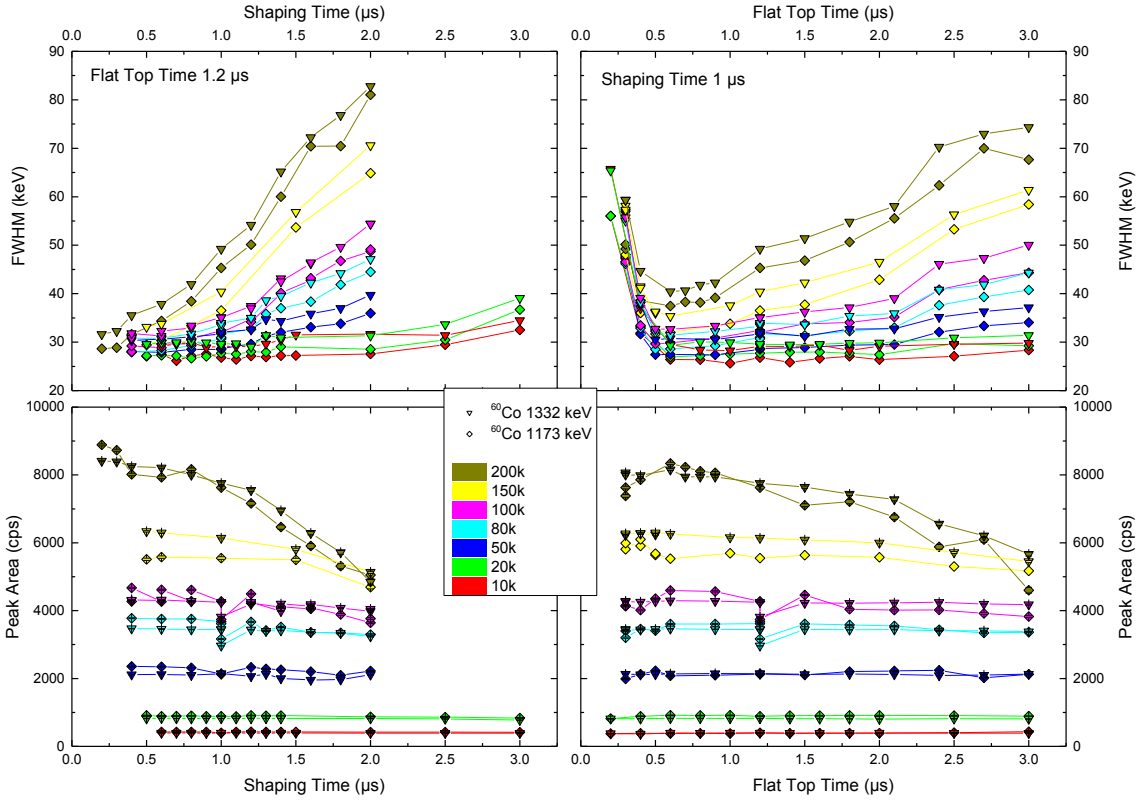

Figure 2: Influence of peak shape parameters on the peak area and width for different count rates for the MCA-527 and a LaBr detector. The supplied values for shaping and flat top time were 1.0 µs and 1.2 µs, respectively. A 380 MBq ^{60}Co source was used for these tests.

An increase in the shaping time leads to an increase in the peak width and a decrease in the peak area. The peak broadening is severe for count rate above 100 kcps. For lower than the nominal shaping time, the peak shape is still well defined. For the flat top time, the picture is different. While the peak area shows a similar behaviour as function of the flat top time compared to the shaping time dependence, the peak width shows a clear minimum as function of the flat top time. The best flat top time for this system is about 0.7 µs, while the value supplied by the IAEA was 1.2 µs. The effect in the peak broadening is only pronounced for count rates above 100 kcps.

3.2. Influence of ambient temperature on peak width and peak position

To determine the influence of the ambient temperature on the performance of the MCAs, tests with an environmental chamber were carried out. Both MCAs were subjected to the temperature program at the same time, but with different detectors, in order to save measurement time. One such temperature ramp could be finished per day. As explained in the experimental section, only the MCAs were subjected to temperature changes, the source and the detectors were placed outside the environmental chamber in the air-conditioned laboratory. The resulting spectra were automatically fitted and the peak position, peak with and peak area were extracted.

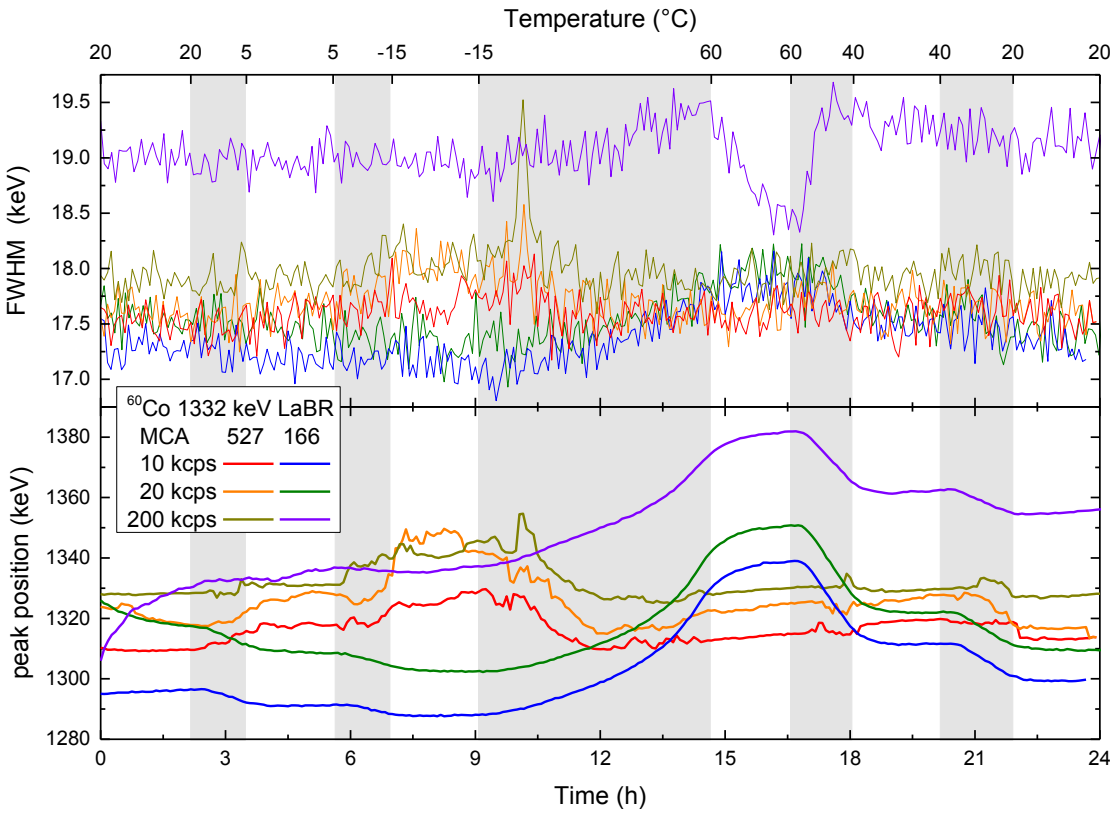

Figure 3: Peak position (lower panel) and peak width (upper panel) for three different count rates and both MCAs as the function of time and temperature. During the experiment time of 24 h, the temperature is first decreased from 20°C to -15°C, then heated to 60°C and finally decreased back to 20°C. The white vertical bands indicate times, for which the temperature was held constant, the grey band indicate temperature changes with a ramp of 15 K/h. The temperatures at the band boundaries are given at the upper scale.

Figure 3 shows the results of these tests for the LaBr detector. The data for the MCA-166 show a strong peak shift and peak broadening for the high count rate, the curves for 200 kcps is shifted up. The same is evident for the MCA-527, but to a much lesser extent and these effects are in line with the observations from e.g. the test described in section 3.1.

Additionally both MCA show a temperature dependency of the peak parameters. Most prominent feature is the increase in peak position for the MCA-166 at a temperature of 60°C. When increasing the temperature from -15°C to 60°C, also a slight increase of the peak width is visible. The high count rate data shows a large decrease of the peak width, while the MCA-166 is held at 60°C. The MCA-527 shows less pronounced features. But also here, a slight increase in peak position is identifiable the lowest temperature, and upon heating from -15°C a spike in the peak width is observable. One clear difference is the fact that the variations for the MCA-166 are a smooth function of temperature and time, while the smaller variations for the MCA-527 are somewhat noisier. This might indicate a varying component value (e.g. temperature dependencies of resistors or of capacitors), while the MCA-527 might use its internal temperature sensor to mitigate these effects by the firmware. In this case, BGS electronic might improve the behaviour at -15°C with a firmware upgrade.

On the other hand, these effects show no increase or decrease in strength with different count rates, with the exception of the peak with decrease at elevated temperature. So, while both MCAs show some effect on the peak parameters with ambient temperature, this is not strongly correlated to the count rate.

3.3. Results of the electromagnetic influence tests

The MCA-527 together with the LaBr detector was tested as an entire system for RF immunity according CE EMC standards. Is has been assumed that the single devices passed these tests individually as CE conform products. No visible changes in the spectrum have been observed by the test site operator during the RF exposure. As this was the defined failure criterion within these tests, no failure or anomaly was observed.

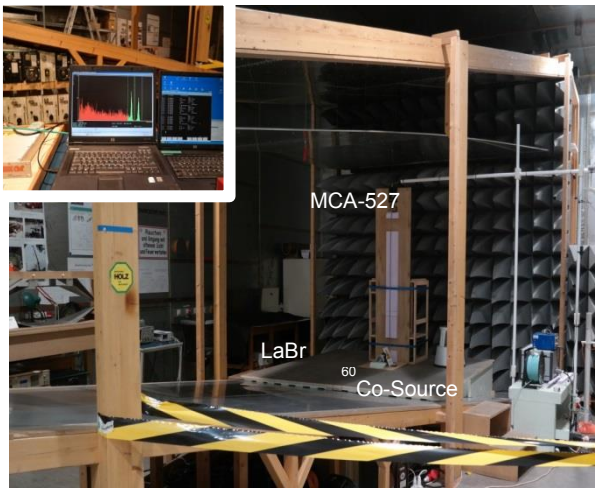

Figure 4: Setup for the electromagnetic influence tests. The MCA-527 and the LaBr detector are located inside the TEM waveguide. A ^{60}Co source is placed next to the detector. Upper insert: The recorded spectrum is shown to the site operator.

In retrospect, it was possible to examine the recorded spectra in more detail. Fits of the peak width and peak position showed virtually no effect. But combining all spectra for one frequency ramp in a waterfall diagram revealed finally three minor changes in the recorded spectra, as seen in figure 5. The set of spectra could not be linked afterwards to the recordings of the RF system, so an assignment of a frequency to these changes is not credibly possible. The changes were observed during the measurements in the 80 MHz to 1 GHz frequency band and for the distinct communication frequencies. No changes in the spectra were observed for the measurements in the 1.4 GHz to 2 GHz and the 2 GHz to 2.7 GHz bands. The exact frequency, where these changes happened and deeper investigation of the impact on a longer measurement or the possible cause could not be determined during this project.

3.4. Results of the comparative testing with HPGe detector

For each count rate and the average of 5 spectra was calculated and the FWHM in the ROI centered on the 59 keV (Am-241) and the 186 keV (Ra-226) peak was determined. Additionally, the peak stability is assessed by the variability of the centroid peak channel over the five measurements, which is calculated from the standard deviation of the centroid peak channel in each respective ROI. In Figure 5 the FWHM values (in [keV]) for both MCAs are plotted for both ROIs. The x-axis presents the five different count rate regimes. The values from the Ra-226 186.1keV peak resulted in higher FWHM values with larger error bars, which is a result of the low counting statistics for the gamma-line from the 300 s live time with a branching ratio of this gamma peak of only 3.28 %.

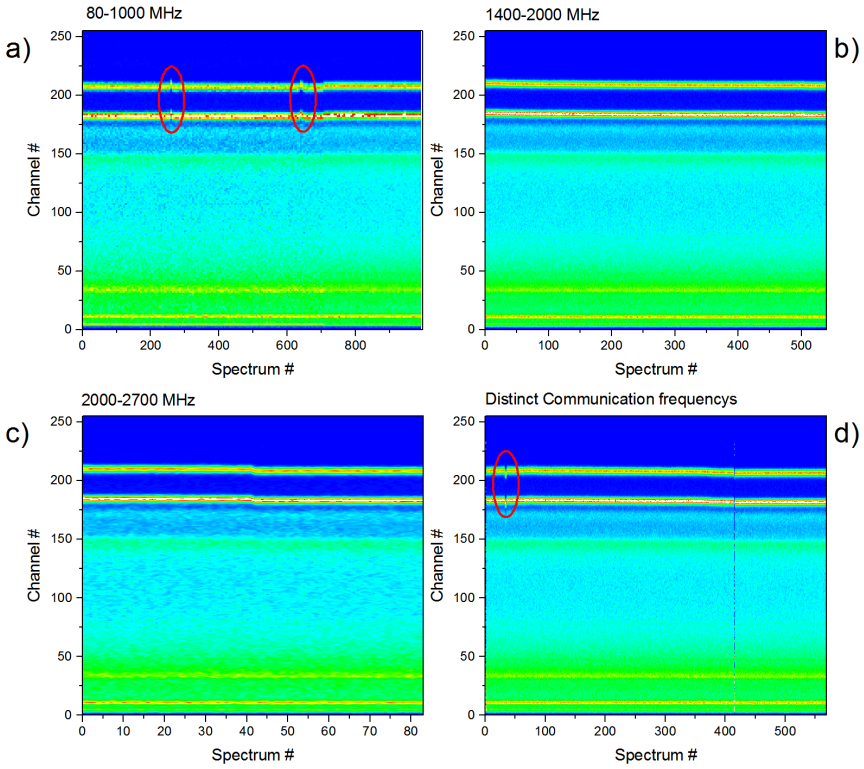

Figure 5: Waterfall diagrams of the recorded spectra during the electromagnetic influence tests. The x-axis shows the spectrum number since the start of the frequency sweep. The y-axis shows the channel number. The two ^{60}Co lines of 1173 keV and 1332 keV are located in the proximity of channel 200. The four graphs show the frequency sweeps from a) 80 MHz to 1 GHz, b) 1.4 GHz to 2 GHz, c) 2 GHz to 2.7 GHz and d) the distinct communication frequencies. Marked are the observed minor changes in the runs a) and d).

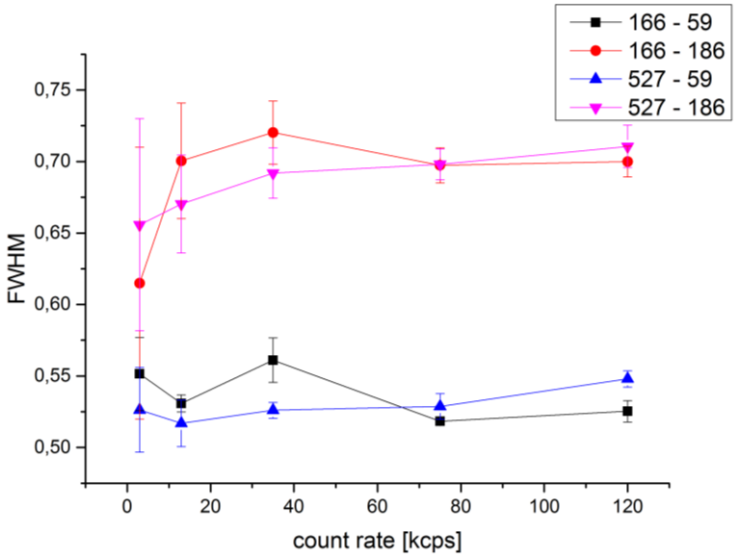

Figure 6: Comparison of resolution (FWHM in [keV] between MCA-166 and MCA-527 for two different gamma peaks at 59 keV and 186 keV.

As a conclusion of this comparison, the MCA-527 is at least as good as the MCA-166 in terms of resolution because the FWHM values for each line only differ by max. 0.04. What indicates an improvement of the MCA-527 is the lower variability of values and the slow, continuous slope of the lines. In the User Manual of the MCA-527 [3]**Fehler! Verweisquelle konnte nicht gefunden werden.** a resolution for typical 500 mm^2 planar HPGe detector (count rate ≤10.000cps) of ≤510eV at 1 µs shaping time (Am-241 source at 59keV) and ≤460eV at 2 µs shaping time (Am-241 source at 59keV) is listed. Figure 6 shows values between 520eV and 550eV. A possible reason may be the different detector used and the influence of the laboratory environment during the measurement. It is noteworthy, that the MCA-527 has a lower dead time which allows for a higher effective throughput (see Table 2), and therefore, in this respect outperforms the MCA-166.

	< 5 kcps	5-20 kcps	20-50 kcps	50-100 kcps	> 100 kcps
MCA-166	0.6 %	2.4 %	7.28 %	9.99 %	15.93 %
MCA-527	0.5 %	1.6 %	3.7 %	5.04 %	7.3 %

Table 2: Comparison of the dead time for acquisition of gamma spectra with the HPGe detector.

4. Conclusions

The presented results of this paper show a small part of the obtained results for the comparative study of the two multichannel analysers. Both MCAs showed a good performance during these tests and there was no indication that the MCA-527 would perform worse than its predecessor.

5. Acknowledgements

This work was supported under task C.40 / A1791 by the "Joint Programme on the Technical Development and Further Improvement of IAEA Safeguards between the Federal Republic of Germany and the IAEA".

6. References

[1] Berndt, R., Mortreau P.; *Performance test of the Multi-Channel Analyzer MCA-527 for Nuclear Safeguards Applications;* JRC Ispra, 2013

[2] Berndt, R., Brutscher, J., Mortreau P.; Neutron Counting and Gamma Spectrometry with MCA-527*;* JRC Ispra, 2014

[3] GBS Electronik; MCA-166 User's Manual Version 3.0; 2007 and MCA-527 User's Manual; 2012

Session 03

International Collaboration

Evolving Member State Support to the IAEA Department of Safeguards

David Peranteau and Akane Takano

Department of Safeguards
International Atomic Energy Agency
Vienna International Centre, PO Box 100
1400 Vienna, Austria

Abstract:

The International Atomic Energy Agency's (IAEA) nuclear verification mission relies on cutting edge capabilities across multiple scientific and technical domains. For forty years, these capabilities have been modernized and sharpened through a unique set of partnerships with Member States. These partnerships, known as Member State Support Programmes to IAEA Safeguards (MSSPs), have yielded a significant proportion of the methodologies and equipment that the IAEA currently deploys in 182 States around the world for its verification activities. With a steadily increasing workload and ongoing budget constraints in years to come, the Department of Safeguards must continue to become more agile and productive. Streamlined processes, smart use of technology, and strengthened partnerships form the core of the Department's strategy moving forward. As the challenges and opportunities for IAEA verification have evolved over four decades, so too has the nature of needed support. This paper makes use of IAEA plans, task statistics, trend data, case studies and analysis in an effort to tell that story and to offer insights into what the changing face of IAEA cooperation with MSSPs means for the future of these vital partnerships.

Keywords: partnerships; development; capabilities; statistics; MSSPs

1. Introduction

Member State Support Programmes to IAEA Safeguards (MSSPs) were first established in 1976. They came about for two main reasons: (1) A decision by the Board that any development needs would best be met through Member State assistance rather than having the IAEA develop its own in-house R&D capability; and (2) the recognition by the IAEA that certain safeguards needs could only be met through the continuous development of new equipment and techniques.[1] Today, 20 Member States and the European Commission have established MSSPs, which pursue tasks across the full range of the Department's multi-disciplinary technical work. This includes not only the development of instruments and techniques, but also facility and nuclear material access for training, nuclear material and environmental sample analysis through the Network of Analytical Laboratories (NWAL), expert consulting, quality control and much more.

Aspects of the MSSP system have remained largely unchanged for many years. For example, the primary task lifecycle, the conduct of Annual Review Meetings, and the publication of biennial planning documents are all long-standing practices. The nature of and mechanisms for support to the Department of Safeguards, however, are continuously evolving. This paper focuses on some prominent changes from recent years, with data and examples to illustrate key trends.

The main trends that will be reviewed include: (1) a reduction in custom equipment development towards commercial-off-the-shelf options and late-stage customization; (2) an increase in the number and diversity of training activities and analytical services support tasks; (3) an increase in in-house development, evaluation and direct user engagement related to Departmental information technology (IT) needs and the inspector tool-kit; and (4) the use of 'umbrella' tasks for activities that require more agility, collaboration or are inherently unsuited to extensive, up-front planning. In conclusion, the paper will highlight the need to maintain balance between supporting agile responses to emerging

challenges and opportunities and the structured, systematic pursuit of objectives that emerge from the Department's strategic planning process.

2. Review of Key Trends

2.1 Minimizing Custom Equipment Development

The Department of Safeguards must ensure that the inspectorate is equipped with effective, reliable, affordable, and user-friendly tools for in-field verification. Given the range of verification activities for which the Department is responsible, the number of potentially applicable technologies, both existing and under development, is vast. Such technologies must, however, be assessed within the context of demanding Departmental requirements for robustness and sustainability, as well as clear operational needs. Moreover, any unchecked proliferation of available tools poses a considerable risk to Departmental effectiveness and efficiency. Not only does it become harder to cope with increased maintenance and training burdens for each tool, but it makes inconsistent approaches to measurement situations more likely. As a result, the goal is to maintain an optimized and regularly reviewed 'pool' of proven, user-friendly equipment to address both routine and non-standard verification needs for meeting safeguards technical objectives and drawing safeguards conclusions.

At the same time, it is incumbent upon the Department of Safeguards to maintain awareness of new innovations that offer significant improvements to current practices and 'best available' measurement techniques to remain capable in a world of increasing responsibility and static resources. In rare but significant cases, the Department may be compelled to steer the development of technical solutions where none are commercially available. Past examples of this include the Next Generation Surveillance System (NGSS), the Digital Cerenkov Viewing Device (DCVD), the On-line Enrichment Monitor (OLEM) and the Next Generation Autonomous Data Acquisition Module (NGAM). In other cases, MSSPs support customisation of existing commercial equipment for safeguards activities, such as the HM-5 hand held assay probe, which was originally developed for nuclear security applications. A less successful case was the Universal Nondestructive Assay Data Acquisition Platform, in which a large investment of MSSP resources did not ultimately result in a deployed solution, prompting proposals to reform each stage of large development projects and including regular business case re-evaluation.

Since their inception, Member State Support Programmes have played a vital role in R&D and equipment development for the Department of Safeguards- including leading roles in each of the aforementioned examples. Given the unique nature of its mission, the Department of Safeguards is likely to rely on periodic requests for bespoke tools. A successor to the NGSS is likely to be a forthcoming example, requiring many years for full specification of requirements, proto-typing, testing, procurement and deployment.

Given the high cost, long timeframes and inherent risk associated with developing custom equipment, however, these activities are pursued only when commercial alternatives are unavailable. In recent years, the IAEA has accordingly requested fewer new equipment development tasks of MSSPs. This decrease, however, has been accompanied by crucial and practical MSSP support in equipment-related areas, such as the provision of advanced measurement expertise (e.g. through Cost-Free Experts and Junior Professional Officers), consulting, maintenance, vulnerability assessments and customisation of features, documentation, software, and firmware. Most of this work is achieved through a few long-lived support tasks with involved MSSPs, under which periodic new requests for work are issued as needed. As a result (as illustrated in Figure 1), there has been a decrease in the overall number of MSSP tasks related to equipment development.

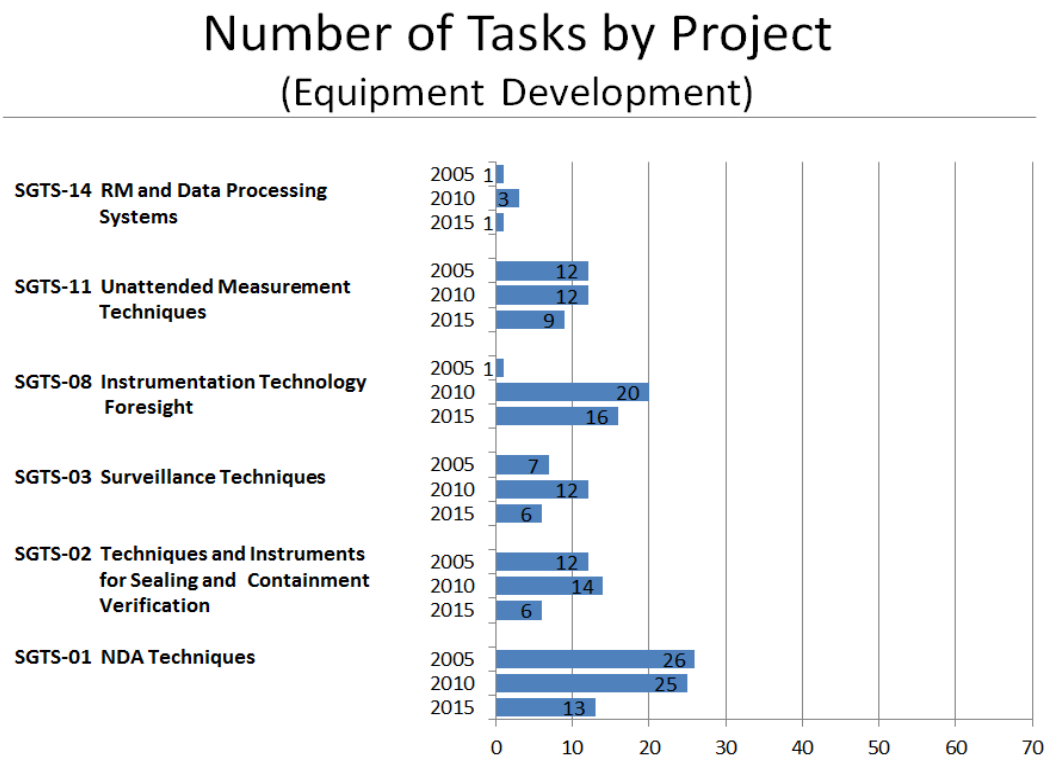

Figure 1: Total numbers of MSSP tasks within SGTS, grouped by Project area from the Development and Implementation Support Programme, 2016-2017. [2]

It is important not to overstate the scope of this trend. The Department is, for example, currently poised to derive benefits from bespoke equipment developed with considerable MSSP support over many years. The use of the Combined Procedure for Uranium Concentration and Enrichment Assay (COMPUCEA) for in-field analysis of uranium samples, the use of gamma emission tomography for spent fuel verification, and the potential offered by custom systems for unattended verification of UF_6 cylinders in enrichment facilities are notable cases. For each, the path forward will depend on operational demand and experience.

The Department will continue to rely on Member State Support Programmes to provide technical advice, scan and evaluate new innovations with potential to augment its capabilities and to assist on occasion with the transfer of technologies that have attained a certain level of maturity. Full, long-running development activities, however, are likely to remain exceptional.

2.2. A Focus on Training and Analytical Services

The nature and goals of Member State Support Programmes are well suited to helping the Department with training and analytical services tasks. Both are areas of continuous need for IAEA Safeguards that rely on the availability of specialist facilities, expertise and materials to ensure that inspector and laboratory analysis capabilities, respectively, are kept up-to-date. It is therefore not surprising that activities in these areas have been growing steadily in number, diversity and importance over the past decade. Indeed, both training and analytical services have active tasks with 18 of the 21 current Member State Support Programmes, a greater fraction than that enjoyed by any other area of Departmental work with MSSPs. As underlined in an internal programme evaluation report, “Support from Member States has been essential to the safeguards training programme, particularly to host courses involving practical works on nuclear facilities and material. Without this cooperation, safeguards training activities would suffer seriously.” [3]

Figure 2 illustrates some of this growth in terms of the number of associated tasks with Member State Support Programmes since 2005.

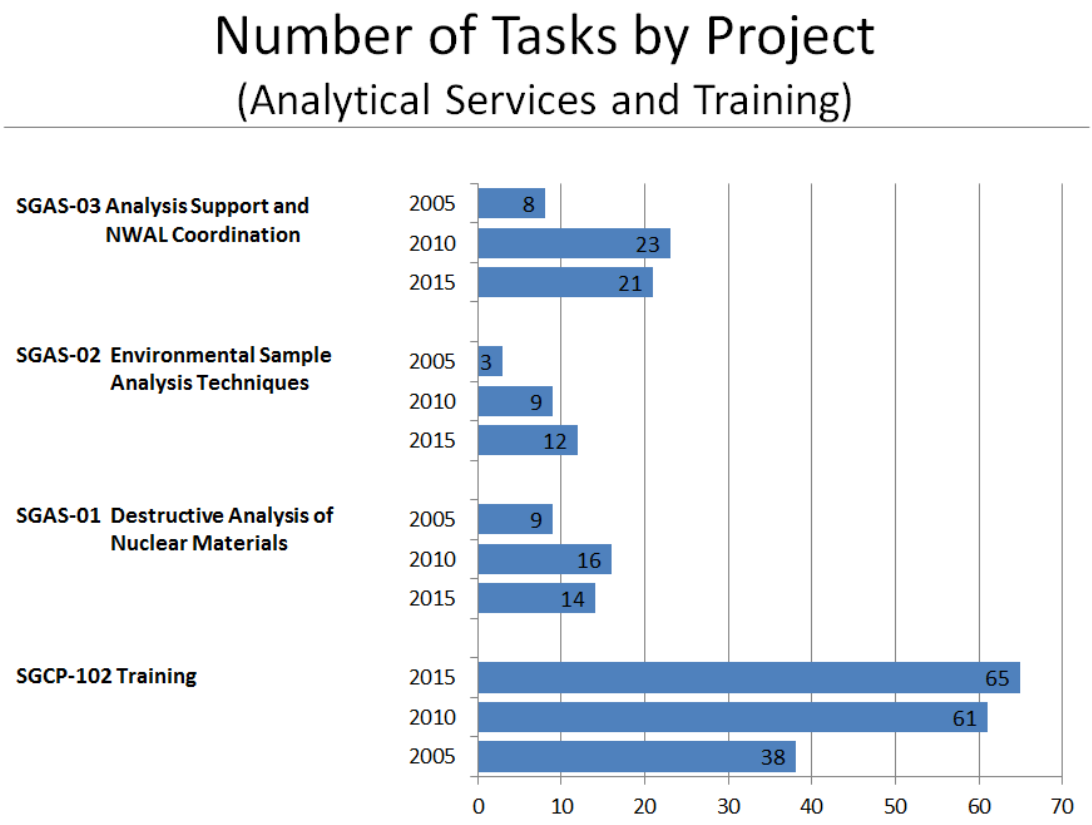

Figure 2: Total numbers of MSSP tasks under Analytical Service Projects and the Training project from the Development and Implementation Support Programme, 2016-2017.

2.2.1 Training

Since 2011, about 15 new or significantly reviewed training courses triggered new tasks with MSSP support to complete the Departmental Training Programme. Table 1 displays the new tasks that have been initiated to support this coursework with multiple MSSPs.

Task ID	Title	Year Requested	Status
ROK B 1907	Development of Virtual Training for Bulk Handling Facilities	2011	Active
JPN B 1897	Training on Reprocessing Activities at a Commercial, Engineering or...(JE-43	2011	Active
UK B 1903	Advanced Training on NFC Facilities to Assist State Evaluation (C1(w))	2011	Active
UK B 1940	Developing Analytical Skills for Safeguards (C1(x))	2012	Stand-by
JPN B 1926	DCVD Training for Spent Fuel Verification	2012	Completed
CAN B 1930	DCVD Training for Spent Fuel Verification	2012	Active
SWE B 1933	DCVD Training for Spent Fuel Verification	2012	Active
FIN B 1949	Specialized Training and Visits to Nuclear Facilities	2012	Stand-by
UK B 1936	Specialized Training and Visits to Nuclear Facilities (C1(y))	2012	Active
USA B 2256	Training Course on Plutonium Diversion Detection Scenario	2013	Active
UK B 1990	Design Information Verification at Bulk Handling Facilities Training Course	2013	Active
UK B 1991	Training on the Nuclear Fuel Cycle, Indicators and Proliferation Pathways	2013	Active
EC B 2019	Training on Application of iRAP Software for Unattended and Remote...	2014	Active
CAN B 2103	Radiation Safety Training	2014	Stand-by
USA B 2093	Radiation Safety Training (B.112)	2014	Active
USA B 2154	Support for Safeguards Leadership Development (B.115)	2015	Active
JPN B 2155	Training for Inspectors for the JNC-1 Site Facilities (JE-50)	2015	Active
ROK B 2217	Pyroprocessing Course at an Engineering Scale Demonstration Facility	2015	Active
USA B 2202	Hot Cell and Glove Box Verification Training (B.116)	2016	Active
JNT B 2237 JPN	DCVD Training for Spent Fuel Verification	2016	Active

Table 1: New MSSP tasks since 2011 related to the development of new courses or significant changes in existing courses for the Department of Safeguards. Note: table does not include tasks related to CFEs, JPOs or SSAC-related work.

As the table illustrates, new training often accompanies the release of new equipment or software (e.g. the Digital Cerenkov Viewing Device (DCVD) and the Integrated Review and Analysis Software (iRAP)) or is initiated to take advantage of unique opportunities (e.g. making use of Georgian hot cells for USA B 2202) or to meet training needs for safeguarding new technologies (e.g. at the Pyro-processing Integrated inactive Demonstration Facility (PRIDE) for ROK B 2217). Another point was to ensure the alignment of all courses with the implementation of the State-level Concept and the development of more robust techniques supporting collaborative analysis and the use of tools (Collaborative Analysis Platform).

At the same time, the need for offerings of long-established training courses has also increased, driven by increasing turn-over in the inspectorate. Training a new inspector is a multi-year endeavour, requiring many months of dedicated coursework even after the half-year Introductory Course for Agency Safeguards (ICAS). This impacts initial training like for the Comprehensive Inspection Exercise at the end of ICAS, or the non-destructive assay training. These courses have strict limits on class sizes given the need to ensure proper access to equipment, material, facilities and qualified trainers; an increasing flow of newly recruited inspectors requires more courses. This also impacts advanced training, which must be organized more frequently to maintain the same level of competencies. These circumstances compel the IAEA to periodically request multiple offerings of the same course in a given year to accommodate operational needs, which can be challenging for MSSPs to accommodate.

2.2.2 Analytical Services

For the IAEA's nuclear verification mission, Destructive Analysis (DA) of nuclear material and the analysis of environmental samples via the NWAL are core capabilities underlying credible safeguards conclusions. Analytical results must be accurate, timely, and reliable. The Department has initiated and grown a significant number of new partnerships with MSSPs in recent years to fulfil this mandate.

Figure 2 shows a significant increase in numbers of these analytical service tasks with MSSPs, but this is only part of the story. With analytical services in particular, a single task often represents a large and continuous commitment of MSSP resources to, for example, qualify an NWAL laboratory and support a certain number of sample analyses each year. The Department has also been working with MSSP counterparts to develop new sampling and measurement techniques to cope with challenges in the field and in the laboratory.

Recent priorities being supported by Member State Support Programmes include, inter alia:

- Development of the ABACC Cristallini method for reducing UF_6 sample sizes to cope with potential changes in shipment regulations;
- Improving analysis capabilities at the Joint On-Site analytical Laboratory in Rokkasho, Japan;
- Improving identification and isolation methods for individual uranium and plutonium particles from environmental swipe samples;
- Developing new particle production techniques for quality control purposes;
- Expansion of the NWAL, particularly for particle analysis of environmental samples and quality assurance support; and
- Production of new reference materials.

For MSSPs, support to analytical services is often among their highest priorities, making full use of technically advanced infrastructure with tangible results that support safeguards conclusions.

2.3. A Focus on the User: MSSP Support for In-house and Non-Traditional Development Activities

2.3.1 The Modernisation of Safeguards IT (MOSAIC) programme

In the context of software development, the use of agile development methodologies has been one way that large organizations, from governments to companies to NGOs, have successfully enhanced their capabilities in a fast, cost-effective manner that focuses on business needs. Agile development methodology involves an intense focus on users and user feedback to guide work. This necessitates the rapid production and demonstration of deliverables that can then be evaluated by users and adjusted to suit business needs.

Within the Department of Safeguards, the primary users of software and new technology are inspectors, technicians, analysts, managers and other technical staff. In an agile framework, making use of close and continuous proximity to these users is crucial to understanding and meeting their evolving needs. This is an important reason that the Department of Safeguards opted for an in-house approach to the Modernisation of Safeguards IT (MOSAIC) programme, which began in 2015 and now comprises over 20 individual projects.

MOSAIC has found success with a combination of PRINCE2 project management techniques and a particular agile methodology, the SCRUM agile framework. (For details on the goals, approach, achievements and plans of MOSAIC, see the IAEA publication *MOSAIC- The Modernization of Safeguards Information Technology: Completing the picture*. [4])

MOSAIC is an in-house programme that has worked with Member State Support Programmes to obtain financial support and provide key stakeholders with timely information on progress and plans. The in-house development approach, supported by external contributions, offers considerable advantages (particularly in the IT space) in terms of user interaction, safeguards information security, cost, sustainability, inter-operability and quality to alternatives that involve financing of off-site development from commercial vendors.

2.3.2 Technology Foresight

Agile project management, with its focus on iterative development, has applications that extend beyond software. The Technology Foresight effort within the Department is a prime example. As with the MOSAIC programme, the effort is characterized by a relentless focus on users (inspectors in this case), as well as rapid deployment and evaluation cycles to shape deliverables around user needs and feedback. Rather than focusing on over-the-horizon technology that may emerge someday, Technology Foresight looks to what has already emerged in other fields, working to understand whether Departmental users can derive significant benefit from modest expenditures and customization.

Examples of current projects include:

- The Instrument Records Integrator for Safeguards (IRIS), which makes use of time correlated indoor positioning data to organize the many different types of data collected on inspections;
- Gamma imaging, for identification of gamma sources during inspection activities;
- Exploration of robotics to support repetitive in-field activities; and
- A modular photogrammetric platform to provide inspectors with the capability to obtain different types of information from optical images, such as 2D and 3D object dimensions, thermal IR radiation, geo-location, etc.

For these and other Technology Foresight activities, MSSPs can contribute to identification, recommendation and support of technology providers from their respective Member States.

A new approach to technology transfer from the recent past offers an additional mechanism for MSSPs to support practical, low-cost solutions for non-unique safeguards equipment needs. In 2016, as part of the Technology Foresight effort, the Department launched a public, incentive-based ‘technology challenge’. In this case, the goal was to explore whether an image stacking algorithm could improve the quality of images obtained from the improved Cerenkov viewing device (ICVD), which is used extensively by inspectors to verify spent fuel assemblies stored underwater.

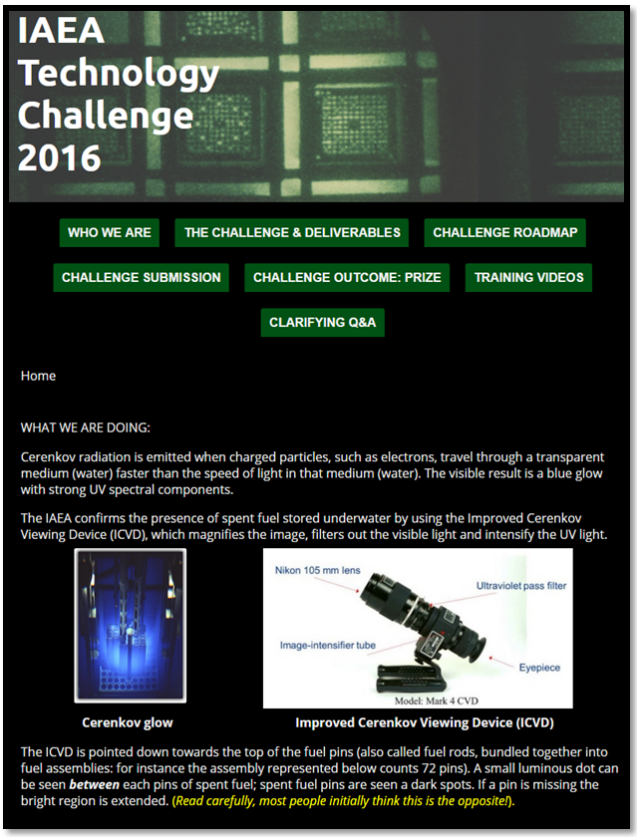

Figure 3: The social media announcement of the ICVD challenge from Technology Foresight, which garnered more than two million views and ten final submissions.

The results, as demonstrated in Figure 4, are striking. Grainy images, such as those on the left, can increase the uncertainty and time required for spent fuel verification. Real-time image clean-up would help inspectors cope with an ever-increasing amount of aging spent fuel around the world, which becomes harder to verify as Cerenkov emissions dim. SGTS is currently working to deploy a solution incorporating the winning algorithm for regular in-field use.

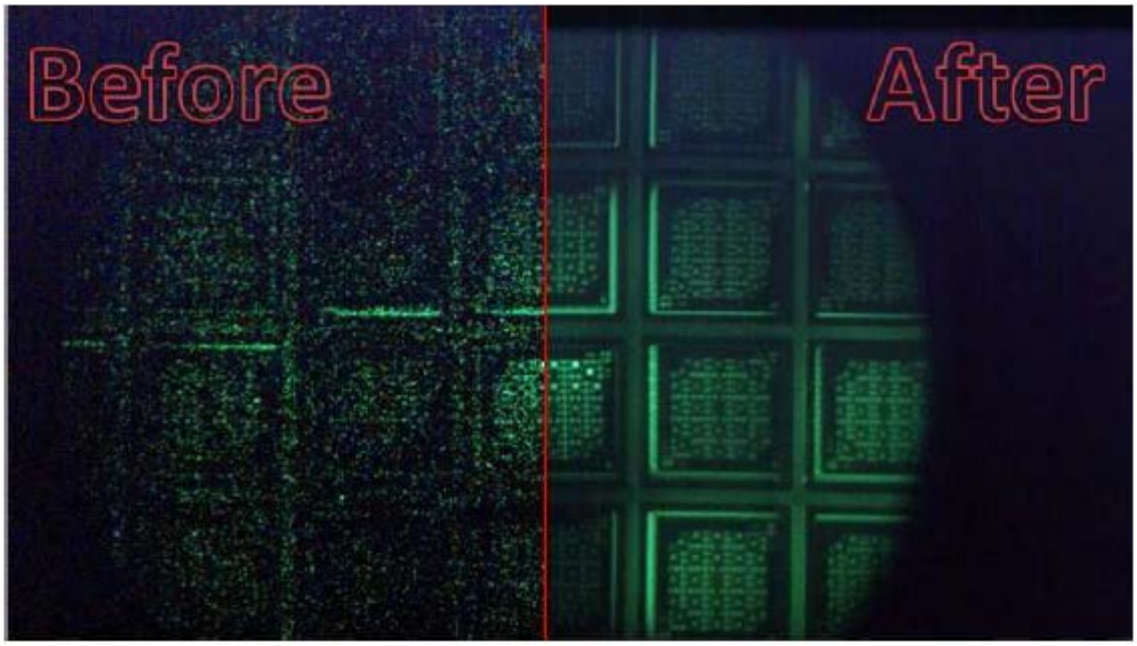

Figure 4: Example of original ICVD images (left) and improved results after processing (right).

In the future, MSSPs may be invited to support incentive-based challenges of this nature through the contribution of an award (12 000 EUR in the case of the ICVD challenge) or the support and identification of participants. The next technology challenge, already being developed, will focus on robotics.

2.4. 'Umbrella' Tasks

While the use of 'umbrella' tasks with MSSPs in the Department of Safeguards is not new, the uses to which such tasks are being put has changed in the past few years. At first, umbrella tasks were intended as a framework to conduct broad activities with multiple sub-components over a long period of time. Examples of this from the 1990s include support for information review and evaluation, development of integrated safeguards, improving the security of the safeguards network and communication infrastructure, and support work for remote monitoring and unattended surveillance systems.

Recent umbrella tasks have focused on identifying areas of support for which specific needs are evolving rapidly enough to make the initiation of detailed new task proposals and work plans impractical. The Technology Foresight work described above is perhaps the primary example of this. Other examples include a productive umbrella task with the European Commission Support Programme for the development and refinement of new containment techniques and an effort to work with multiple MSSPs to solicit expert guidance on estimating the timelines for hypothetical development by a State of undeclared fuel cycle capabilities for acquisition path analysis.

In each case, rather than specifying a full and detailed scope of work for each respective task with MSSPs up front, initial work focuses on establishing partnerships for a set of overarching and mutually agreed objectives. Subsequent individual work scopes are then established in close coordination with each MSSP based on its interests and available resources, and formalized via individual additional requests.

This approach can be seen in other current tasks that do not formally include the name 'umbrella' in their task titles. Examples include an effort to develop E-Learning content to support States in preparation of their declarations to the IAEA, and an initiative to establish a repository of well-characterized non-nuclear materials (metals at this stage) for the testing and evaluation of commercial tools for complementary access. Nevertheless, clear expectations remain a basic communication principle for Department-MSSP interactions to ensure prudent management practices for these productive partnerships.

3. Conclusion: Leveraging MSSPs for Agility and Strategy Execution

As the pace of technological change accelerates, the Department of Safeguards faces new challenges and opportunities every year. Success requires both flexibility and strategy. Flexibility with respect to approaches, tools, and arrangements is essential for navigating change. Strategy, which involves systematic efforts to identify what matters and where gaps exist, planning for attainable future states, and following-through on objectives, is essential for coherent communication and decision-making.

The partnerships that the Department of Safeguards has built with Member State Support Programmes are a vital mechanism to address both needs. Success relies on good communication, ensuring that the context, objectives and timeframes for requests are well understood.

To this end, the Department of Safeguards employs a thorough strategic planning process. The purpose of this process is to promote longer-term thinking within the Department, to sustain existing capabilities, prepare for the future, to ensure that short-term initiatives fit into longer-term goals, to support prioritization and resource allocation decisions, and to enable better communication with Member States.

The Department's strategic planning process and its history of interactions with MSSPs provide a firm basis for confidence that new task proposals from the Department of Safeguards are genuine priorities that form part of a coherent planning process rather than ad-hoc or fleeting desires. There is a difference, however, between knowing where you want to go and knowing exactly how best to get there. Unexpected obstacles and short-cuts can arise. Course corrections should be common and smooth.

The Department will continue to rely on MSSPs for advice, road-mapping and provision of the necessary human, financial and technological resources to meet its development and implementation support needs. Increasingly, however, the Department is calling upon MSSPs to help the Department obtain and make smart use of in-house resources, to work with the Department to identify solutions to complex, evolving problems, and to be flexible in identifying and taking advantage of opportunities that arise.

4. Acknowledgements

The authors would like to acknowledge the generous support of the Member States with active Support Programmes for their remarkable contributions to IAEA Safeguards. In alphabetical order: Argentina, Australia, Belgium, Brazil, Canada, People's Republic of China, Czech Republic, European Commission, Finland, France, Germany, Hungary, Japan, the Netherlands, Republic of Korea, Republic of South Africa, Russian Federation, Spain, Sweden, United Kingdom, United States of America.

The authors would also like to acknowledge the many Project Managers and Task Officers within the Department of Safeguards whose daily contributions and active collaboration with MSSPs have strengthened the work of the Department in countless ways.

5. References

1. Kurihara, H; *Role of support programmes in safeguards: A review of R&D activities and future trends*; *IAEA Bulletin*; 1/1998. IAEA; Vienna, Austria; pp. 13-14. Available at: https://www.iaea.org/sites/default/files/30103451317.pdf

2. International Atomic Energy Agency' *STR-382: Development and Implementation Support Programme for Nuclear Verification 2016-2017*; IAEA; Vienna, Austria; 2016. Available at: https://www.iaea.org/sites/default/files/16/05/development_and_implementation_support_programme_for_nuclear_verificatio.pdf

3. Internal International Atomic Energy Agency report.

4. International Atomic Energy Agency; *MOSAIC The Modernization of Safeguards Information Technology: Completing the picture*; IAEA; Vienna, Austria; 2017. Available at: https://www.iaea.org/sites/default/files/17/01/mosaic.pdf

Enhanced Cooperation among the IAEA, EC, VATESI and Ignalina NPP Operator as a Way to Effective and Efficient Verification of Spent Fuel Transfers at Ignalina NPP

Kostyantyn Gushchyn, Igor Tsvetkov, Graham Morris, Jose Araujo, Simone Rocchi

International Atomic Energy Agency (IAEA)

Petra Klump, Vitalija Segzdaite

European Commission (EC)

Sergei Monakhov

Ignalina Nuclear Power Plant (INPP)

Laima Narbute

State Nuclear Power Inspectorate (VATESI)

Abstract:

Spent fuel (SF) transfers from two shut-down reactors to interim dry storage facilities at the Ignalina nuclear power plant (NPP) and decommissioning of the reactors are currently the major nuclear activities in Lithuania. In preparation for safeguards verification of these transfers, which normally requires substantial resources both from the IAEA and the EC, cooperation between both State Nuclear Power Safety Inspectorate (VATESI) and the Ignalina NPP operator during 2014-2016 was organized in such a way as to optimise human and financial resources, share responsibilities for the installation of different safeguards equipment and to develop specific safeguards approach for SF verification during transfer campaign.

As a result of such cooperation all safeguards technical systems (containment and surveillance, non-destructive assay, etc.) were successfully installed at a new dry storage facility, upgraded at both reactor unit SF ponds, and tested during recent "cold" and "hot" tests.

Ignalina NPP is equipped with two RBMK-1500 on-load, water-cooled, graphite-moderated reactors. Experience gained by the IAEA in safeguarding this type of reactor has been used to develop, in cooperation with the EC, VATESI and the facility operator, an innovative safeguards approach. This new safeguards approach is designed to reduce the inspectors' presence and maintain continuity of knowledge on nuclear material during the transfer process. This approach makes full use of available technical devices, including Next Generation Surveillance System (NGSS) overhead and underwater cameras, neutron detectors and electronic seals (EOSS). Most of the data from technical devices is remotely transmitted to the IAEA and EC Headquarters, supporting scheduled and random safeguards inspections at Ignalina NPP facilities.

Full cooperation and support obtained by the IAEA and the EC from the Ignalina NPP operator (including early provision of information through an authorised mailbox system, and sealing of SF casks) will enhance the efficiency and effectiveness of safeguards implementation at the Ignalina NPP.

Keywords: spent fuel transfers; dry storage facility; safeguards approach; verification; cooperation

1. Introduction

The Ignalina Nuclear Power Plant (INPP, WLTA) in Lithuania consists of two RBMK-1500 on-load, water-cooled, graphite-moderated reactor units. Unit 1 was permanently shut down on 31 December 2004, and Unit 2 – five years later, on 31 December 2009. The plant is now in the process of decommissioning and one of the main activities going on there is removal of all spent nuclear fuel stored at both reactor units and its transfer to the dry storage facilities [1]. The process of spent fuel (SF) transfers started in 1999 when INPP was still in operation and when the open air dry spent fuel storage (WLTD) was commissioned. WLTD reached the full capacity in 2010, and after that the transfer campaign was suspended until the time when a new dry spent fuel storage (WLTE) was constructed. Special project called B-1 funded by European Bank of Reconstruction and Development (EBRD) was established for that purpose, and it took more than ten years to complete it. Finally, in October 2016 the new dry storage (WLTE) started receiving spent fuel from INPP.

It is planned to transfer all SF in Dry Storage Casks (DSCs) from WLTA to WLTE in about five years. Verifying SF transfers under the approach used before (during transfers to WLTD) would require weekly inspector presence over this five-year-period.

As a result of enhanced cooperation among all parties participating in the process (INPP operator, Lithuanian State Authority (VATESI), the EC and the IAEA) innovative safeguards approach using full support from INPP operator was developed. The approach is based on the verification/inspection activities as well as on the combination of containment, surveillance (C/S) and non-destructive assay (NDA) measures which allow maintaining continuity of knowledge (CoK) about SF during the whole loading and transfer process. The objective of this approach is to optimise inspection efforts, use available techniques and cooperation with the State/Regional authorities/operator to the extent possible, maintaining safeguards effectiveness and improving the efficiency of safeguards verifications for the spent fuel (SF) transfers.

2. Spent fuel loading and transfer processes

Each reactor unit at INPP includes a SF pond, adjacent to the reactor complex and a hot cell. At each pond there are SF compartments used for storing discharged ‘uncut’ SF assemblies (SFAs) and SF compartments used for storing ‘cut’ SF. The hot cell is used to cut SFAs into two half-assemblies (FBs) and then place them into a metallic basket (32M basket). After loading the cut SFAs into the 32M baskets (which can only occur in the hot cell), the full basket is moved from the hot cell to the SF pond. Before placement in SF pond FBs in the baskets are verified for gross defect and the baskets are placed under seals. After about 10 years of cooling, the SF basket is loaded into a DSC and then transferred to a SF dry storage (SFDS) facility for interim storage. Re-verification is not needed as long as the CoK is maintained for previously verified SF items.

The loading/transfer process to be used for WLTE is different from the one used for WLTD. The difference lies in the different DSC capacity and the loading sequence. For WLTD only one 32M basket was loaded into one DSC, but for the new DSC (CONSTOR RBMK-1500/M2, Figure 1) multiple 32M baskets are involved in the loading of one DSC and some partially emptied baskets could remain in SF pond after the loading is complete. This makes the loading process more complicated and time consuming.

The loading and transfer processes have the following sequence:

- A 32M basket is loaded into the central cavity of the DSC.
- Individual FBs are then lifted from this basket and placed into the outer ring of the DSC.
- When the loading of the outer ring is complete, the partially basket is removed from the central cavity and relocated to a storage position in the SF pond. Depending on the number of FBs taken from the first basket, further baskets may be needed – outer ring loading may involve one or multiple 32M baskets.
- After the ring basket is filled, a full 32M basket is loaded into the central cavity, thereby making the DSC fully loaded.

- The loaded DSC is lowered through a hatch in the SF ponds area and placed onto a special rail car.
- The DSC on the rail car is transported from the reactor unit (WLTA) to ISFSF (WLTE).
- At WLTE the transport lid is removed from the DSC and the outer lids are welded together. Protective lids are then positioned and bolted securely.
- When the lids installation process is completed, the DSC is transferred to its storage position and placed under seals.
- Next, an empty DSC is placed onto the rail car and transported to the loading pit in one of the SF ponds at WLTA, in preparation for the next SF cask loading and transfer.

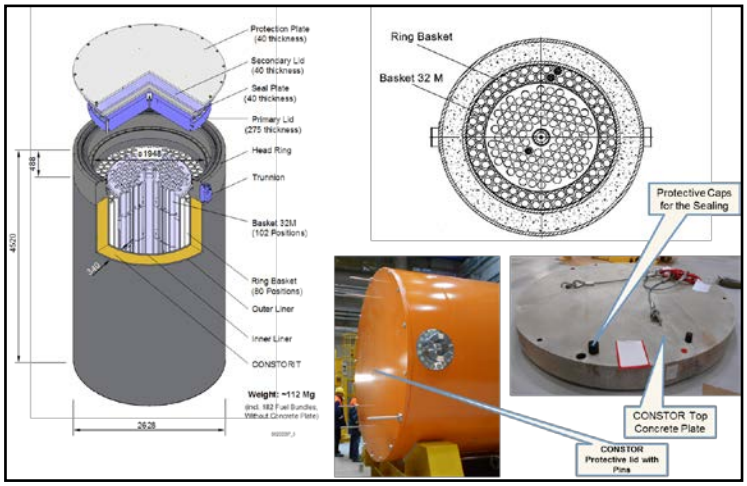

Figure 1: RBMK-1500/M2 Dry Storage Cask (DSC)

3. Safeguards approach, measures and devices

3.1. Containment, surveillance and NDA

At each of the two WLTA SF ponds, the DSC loading process is monitored by a Next Generation Surveillance System (NGSS) which include overhead cameras and underwater (UW) cameras at a DSC loading pit. In addition to being under surveillance, the previously verified SF is stored in 32M baskets under seals.

Baskets scheduled for loading need to be pre-positioned and the correspondent seals to be detached either by the operator (with prior notification) or by the inspector(s). All baskets not scheduled to be used in the current loading campaign should remain under seal. The pre-positioned baskets are queued in the same sequence as required for DSC loadings; any other relocation of SF is done only during inspector presence. The CoK on all baskets is maintained via surveillance, the data of which is remotely transmitted to IAEA and EC Headquarters for safeguards review and evaluation.

The UW surveillance cameras installed in the loading pit (see Figure 2) allow for monitoring of the DSC loading and item counting of loaded SF half-assemblies. The reactor Exit Hatch is also covered by the existing surveillance system. Essentially, under these conditions, no undetected movements of SF can take place in and out of the loading pit.

A sealable bar located in the SF pond separates the hot cell from the loading pit. No baskets from the hot cell can be added to the existing SF basket population with this sealable bar in place. Additionally, exit routes from the hot cell are monitored by a hot cell monitoring system (HCMS) equipped with neutron and gamma detectors. Re-verification of SF that has been previously verified is not required, as long as CoK on that fuel is maintained during the loading and transfer process. Containment and isolation of the SFAs involved in the loading process is the key to maintaining this CoK during DSC loading. SFAs in the partially emptied baskets left after loading will be later verified and sealed by the inspectors.

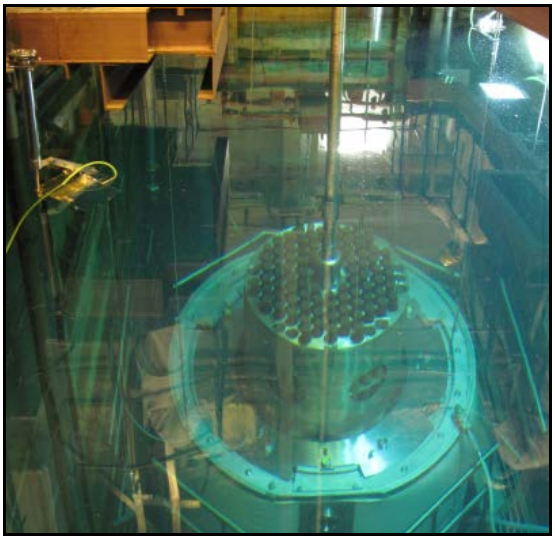

Figure 2: DSC loading pit with underwater cameras

Safeguards equipment for the actual DSC transfer process from WLTA to WLTE includes a NGSS camera in each of the SF transfer corridors (where DSC is placed on the rail car) and a NGSS camera and a Mobile Unit Neutron Detector (MUND) installed on the SF transfer rail car. These measures (surveillance and NDA monitoring) provide CoK on the DSC content during transfer. Since the MUND and NGSS camera installed on the rail car are battery powered, in order to keep them operating and in order to transfer collected data to the IAEA and the EC Headquarters, a special docking station has been installed at WLTE. Every time the rail car arrives at WLTE, it is connected to the docking station to charge the batteries and transfer the data.

At WLTE, unloading of the DSC from the rail car, welding of the outer lids, moving of the cask to the storage hall and re-loading the DSC in the hot cell (if and when the necessity arises) is monitored by the NGSS surveillance system and the Spent Fuel Monitoring System (SFMS) covering all possible SF routes. Both systems are equipped with remote data transfer (RDT) capabilities.

At the final position in the storage hall each DSC is sealed by fibre optic seal (COBRA) and each group of DSCs (up to six) is sealed with electronic seal (EOSS, see Figure 3). All EOSS seals have RDT capabilities.

Figure 3: DSCs sealed with COBRA seals and EOSS group seal

3.2. Inspection activities during SF transfers

Inspection activities during SF transfer campaign include scheduled inspections (with the frequency depending on the number of transfers planned) at both WLTA and WLTE and random interim inspections (RII). RIIs can also include unannounced inspections (UI).

The scheduled inspection activities will include the following:

- Review of operator DSC loading records;
- Verification of the contents of any unsealed SF baskets and attachment of seals;
- Collection of operator detached seals (in case of seal contamination the verification can be performed at the facility);
- Detachment of the seals to release any baskets to be loaded;
- Verification of the content of the SF baskets to be loaded by item counting and gross defect;
- Confirmation of the basket identification number;
- Verification of the sealing arrangement applied by the operator (WLTE);
- Item counting and tag check of newly arrived DSCs;
- Placement of newly arrived DSCs under group sealing.

The review of surveillance and NDA data is normally performed at the Headquarters. In addition to scheduled inspections, at least one UI in a calendar year will be conducted during SF transfer campaign with the main purpose to assure the absence of undeclared production or processing of nuclear material by visual observation, using radiation devices and taking of environmental samples. RIIs could also be conducted if needed with the activities the same as during scheduled inspections.

3.3. Provision of information and assistance by the INPP operator

In order for the IAEA and the EC to implement inspections for SF transfer and cover all verification needs, the Lithuanian State Authority (VATESI) and the facility operator shall provide both inspectorates with the detailed advanced information and periodic updates, as follows:

- Annual SF transfer plan;
- Monthly SF transfer plan as an update of the annual plan;
- DSC loading and transfer-related activities at each stage of the transfer process for each DSC including date and time;
- The number of SFAs and the basket identification number for any basket in the hot cell;
- The basket identification number, location, nuclear material weights and the date and time of discharge (for the baskets discharged from the hot cell);
- The date, time and number of any seal detached by the operator;
- General Ledger updates;
- DSC loading and transfer records (including basket loading sequence, identification numbers, loading maps of DSC central cavity and ring basket, amounts of nuclear material involved, the date and time of loading and the date and time of transfer);
- Location maps (including SF pond maps before and after DSC loading and WLTE storage map after each DSC receipt).

All relevant information (including updates) is provided by the operator to both inspectorates through authorized mailbox system installed and operating at INPP. The updates are normally provided on a weekly basis or as soon as the necessity in such update occurs. During the inspection activities inspectors can ask for any other additional documents/declarations required for successful fulfilment of their duties.

In addition to provision of necessary information and as a result of close cooperation among inspectorates, the INPP operator and VATESI, it was agreed that certain assistance will be provided by the operator. It will allow reducing the inspectors' presence and efforts during SF transfers, but at the same time enhance the efficiency and effectiveness of safeguards verifications. The agreed activities to be conducted by the operator at the SF ponds and at the dry SF storage are the following:

- Detachment of the seals at SF ponds to release 32M baskets to be loaded in DSCs. Such detachment will be done with prior notification to both inspectorates through authorized mail box system. After detachment, the full information including seal number, position, date and time of detachment will also be sent to the IAEA and the EC;
- Support in implementation of NDA devices (i.e. IRAT) for re-verification of SF bundles loaded in DSC (if ICVD verification is not possible);
- Attachment of COBRA seals at the dry storage after all lids are installed on the newly arrived DSC and later attachment of a group seal when this DSC is placed in the storage hall. During the next inspection those seal attachments will be checked by an inspector.
- Connection of the rail car to the docking station at WLTE to charge the batteries and transmit NDA and surveillance data. Normally this activity is performed every time the rail car arrives at WLTE. If the rail car is not used for a long period of time, it was agreed that the connection will be performed on a weekly basis.

4. Results of multilateral cooperation

The safeguards approach described above is a result of close multilateral cooperation among two inspectorates (IAEA and EC), facility operator and State authority (VATESI) during 2014-2016. A number of meetings and video conferences, as well as technical visits to INPP were conducted and it took great deal of discussions involving a lot of people in order to develop such a unique approach. The safeguards equipment purchase and delivery were shared between the IAEA and the EC, and its installation at WLTE and upgrade at WLTA were performed by the IAEA technicians with essential assistance provided by the facility operator and its sub-contractors. The IAEA and the EC also provided support in development of new accountancy software to be used at WLTE. VATESI also participated in all activities and provided useful support and assistance when it was necessary to facilitate the processes.

The developed approach is being tested now while the “hot” tests are in progress at INPP. Since such approach on loadings and transfers are done for the first time, both inspectorates as well as the operator are learning and gaining necessary experience. As a result of the experience gained and lessons learnt the Partnership approach for SF verification during transfers will be developed and used by the IAEA and the EC.

5. Conclusion

The safeguards approach born as a result of effective cooperation among all participating parties utilises a scheme of monthly inspections that provides for verification of all SF involved in the loading process, in combination with random inspections and remote transmission of data from safeguards devices to the IAEA and the EC Headquarters in Vienna and Luxembourg and relies upon the extensive support provided by the facility operator. It allows dramatically reduce the inspectors’ presence during loading and transfer operations, but at the same time enhances the effectiveness and efficiency of verification activities. By gaining additional experience during routine verification of SF transfers the designed approach will be further improved and optimized if necessary.

6. Acknowledgements

The authors would like to acknowledge great contribution done by the IAEA technicians, namely: Messrs J. Ely (former staff), R. Simlinger, R. Zweier, L. Re Falo, Y. Yellin, S. McNulty, C. Luca and T. Moskalev who performed all installation/upgrade activities at both reactor units and at the new dry SF storage in allocated period of time and with very high quality.

7. Legal matters

7.1. Privacy regulations and protection of personal data

"We agree that ESARDA may print our names/contacts data/photograph/article in the ESARDA Bulletin/Symposium proceedings or any other ESARDA publications and when necessary for any other purposes connected with ESARDA activities."

7.2. Copyright

The authors agree that submission of an article automatically authorises ESARDA to publish the work/article in whole or in part in all ESARDA publications – the bulletin, meeting proceedings, and on the website.

The authors declare that their work/article is original and not a violation or infringement of any existing copyright.

8. References

[1] Lithuanian National Report on Implementation of Council Directive 2011/70/EURATOM of 19 July 2011 Establishing a Community Framework for the Responsible and Safe Management of Spent Fuel and Radioactive Waste, Vilnius, 2015

Swedish information sharing in the Incident and Trafficking Database (ITDB) and international cooperation to combat illicit trafficking

Erika Sundén[1], Elisabeth Koblet[1], Lars van Dassen[2], Viviana Sandberg[2]

1. Section for Nuclear Non-proliferation and Security
2. Office for International Relations
Swedish Radiation Safety Authority
Solna Strandväg 96, SE-171 16 Stockholm, Sweden
E-mail: erika.sunden@ssm.se

Abstract:

Nuclear and radioactive material out of regulatory control is a worldwide issue that not only affects nuclear power states. Overarching authority and cooperation between states are needed in order to regain control over these sources and share information about them. Several governmental control measures are needed, such as an international and national legal framework, border controls and emergency preparedness plans. This paper starts with an overview of the Swedish system for control of radioactive sources and the systems in place for regaining control over sources previously out of regulatory control.

The Incident and Trafficking Database (ITDB) at the International Atomic Energy Agency (IAEA) is used for sharing information about incidents in which nuclear or other radioactive sources are, or were, out of regulatory control. The paper contains a subsequent description of the work carried out by the Section for Nuclear Non-proliferation and Security at the Swedish Radiation Safety Authority (SSM) to collect and share information using this tool. Over the past three years, SSM has stepped up its efforts in collecting information about incidents in Sweden, and work has been ongoing to expand the information sharing network within SSM and with other relevant authorities in Sweden.

Through its Office for International Relations, SSM is also highly involved in projects aimed at combating illicit trafficking abroad. Since 1999, many projects have been conducted in Central and Eastern Europe with the objective of strengthening the institutional capacity of the states' regulatory authorities by means of international conferences, workshops, training courses and field exercises. The paper concludes with an overview of this work.

Keywords: ITDB information sharing; International cooperation; Illicit trafficking

1. Introduction

Nuclear material and other radioactive sources out of sufficient control can be harmful to humans, animals and the environment. There are many initiatives being taken around the world to minimize the potentially harmful effects of such sources, from financial and outreach initiatives to collect unregistered and unwanted sources, to projects aimed at stopping malicious use of the sources and illegal trade in the same. Information sharing and training are also important aspects of the area, where sharing information about sources that have gone missing to a community that might be affected, or educating and training people who might be alerted to recover a source, can be essential for the safety of the individuals.

This paper will present the situation in Sweden today in terms of regaining control over nuclear and other radioactive materials out of regulatory control as well as other initiatives taken by Sweden in an international setting to further this cause.

In section 2, some of the more important parts of the international framework concerning nuclear and other radioactive material are presented, followed by presentations on border control in Sweden. Sweden shares a land border with Finland and Norway, and is connected to Denmark by the Øresund Bridge. Sweden has several ports for importing and exporting goods, the largest one being the Skandia port in Gothenburg where about 50% of all cross-border container traffic passes [1]. Arlanda Airport, close to Stockholm, is the largest hub for goods arriving by plane. Thus Sweden is a country that shares borders with European Union (EU) member states and third countries (outside of the EU).

This is followed by a presentation describing the Swedish emergency preparedness and response systems. Here, the major focus of emergency planning in this area is on accidents at nuclear facilities, in particular the nuclear power plants. Sweden is a state with a substantial proportion of the nuclear fuel cycle involving ten nuclear power reactors in operation, one fuel fabrication facility, one research and waste facility and a central interim storage facility for spent fuel. However, radioactive sources and nuclear material are also used in various research activities, industries and healthcare facilities. The next section, section 5, briefly presents the national legal framework for registering and controlling nuclear material and other radioactive sources, and the following section describes the endpoint for many radioactive sources outside regulatory control: the metal recycling industry.

When it has been discovered that nuclear or other radioactive material is, or was, out of regulatory control, it is defined as an incident that falls under the scope of the Incident and Trafficking Database (ITDB). The Database is a forum for international cooperation for the purpose of collecting information. The ITDB is managed by the IAEA. The following section, section 7, gives an introduction to the ITDB and describes incidents reported by Sweden and efforts to expand the national network for reporting of incidents.

In the area of nuclear and other radioactive material outside regulatory control, Sweden–through SSM's Office for International Relations–has participated actively in the international community by sponsoring and participating in many projects with the goal of regaining control. Here the emphasis is on countries formerly belonging to the USSR. The last chapter of this paper gives an introduction to this work, with some recent examples of projects.

2. International legal framework, binding resolutions and recommendations

The international framework for nuclear security is made up of a number of both binding and non-binding documents. There is a pronounced difference between the field of security as opposed to the nuclear safeguards field, where the legally binding system is broader and more detailed. Nuclear security is governed more on state level through international recommendations, conventions and codes of conduct. This section briefly presents some of the more important documents addressing the security of nuclear material and other radioactive sources related to the topic of this paper.

UN Security Council Resolution 1540 [2] is a binding resolution for all members of the UN and establishes inter alia that all states should take and enforce measures to establish domestic controls to prevent the proliferation of nuclear, chemical and biological weapons by, among other things, developing and maintaining appropriate and effective border controls and law enforcement efforts to detect, deter, prevent and combat illicit trafficking of such items. All states must also establish laws and regulations to control export, transit, trans-shipment and re-export of such items. In an investigation from 2008 [3] on the possibility of strengthening Swedish export control and non-proliferation work with reference to Resolution 1540, the investigator came to the conclusion that Sweden did not have a complete national legal framework to ensure compliance with all parts of Resolution 1540.

The Convention on the Physical Protection of Nuclear Material (CPPNM) [4] is a binding convention that entered into force in 1987. An addition that entered into force in May 2016 broadens the convention to also require states to establish, implement and maintain a national regime for physical protection and control, which includes maintaining the capability to swiftly identify and recover material out of regulatory control.

In the Council Regulation (Euratom) on shipments of radioactive substances between Member States [5], Article 3 states that controls of shipments for the purpose of radiation protection should be

performed as part of control procedures applied in a non-discriminatory manner throughout the territory of the Member State.

In addition to the binding agreements, there are several non-binding recommendations, for example in the IAEA Nuclear Security Series, which are aimed at giving guidance to states in the field of security of nuclear and radioactive material. This series includes the Code of Conduct on the Safety and Security of Radioactive Sources [6] and Response to Events Involving the Inadvertent Movement or Illicit Trafficking of Radioactive Materials [7].

3. Border controls of nuclear material and other radioactive sources

Swedish Customs is responsible for monitoring and checking international traffic across the Swedish border to ensure compliance with import and export regulations. No regular measurements to detect radioactivity are performed by Swedish Customs, with the exception of containers leaving Sweden for the USA, which is a requirement under the US Container Security Initiative, CSI [1].

Due to the Swedish interpretation of the EU's internal market regulations, Swedish Customs does not have a mandate to perform checks within the EU without having special indications that the cargo contains radioactive sources or nuclear material. More systematic checks would presuppose a change to national legislation [8]. However, if a vehicle is selected for control at the Skandia port in Gothenburg for some reason other than checking for radioactive sources, the vehicle is automatically scanned for radioactivity due to it passing the CSI portal on its way to the area of control. In this manner approximately 700 entities (containers and other vehicles) are scanned for radioactivity each year on a semi-random basis. Around ten alarms are triggered each year, though to date, only one alarm was due to an undeclared shipment of radioactive material. Due to the high sensitivity of portal monitors, naturally occurring radioactive material (NORM) can sometimes trigger an alarm although no action is necessary.

Swedish Customs also does not perform systematic checks of goods from countries outside the EU ('third countries') due to a lack of resources. In 2011 the Swedish Government assigned SSM together with Swedish Customs to review the capacity for detecting shipments of radioactive sources and nuclear materials across Swedish borders, from both the internal and external markets. In the final report it was suggested by SSM that the capacity of customs controls should be increased by installing eight portal monitors at the Skandia port in Gothenburg and six monitors at Arlanda Airport. The checks that occur due to searches for other reasons are deemed insufficient to ensure satisfactory control of incoming goods. The report is still under consideration by the Swedish Government.

In SSM's risk and vulnerability study of 2016 [9], it is stated that due to the lack of radiation controls at Swedish borders, Sweden runs the risk of becoming the gateway into the EU with respect to radioactive or other nuclear materials, which can injure public health and also damage the reputation of Sweden in an international setting.

Together with other authorities that oversee aspects of transportation, SSM does carry out unannounced inspections of vehicles. These inspections, coordinated by the Swedish Civil Contingencies Agency (MSB), are performed together with public authorities such as the Police, Swedish Customs, Coast Guard, Swedish Work Environment Authority, Swedish Transport Agency, county administrative boards and SSM. The inspections can be performed at any location, but the focus is mainly on the harbours of Stockholm and Gothenburg. Around 12 such inspections are carried out annually, with each authority present checking issues that fall under their responsibility. Radiation measurements are mainly performed from outside the vehicles using a GR-110 Gamma-Ray Scintillometer radiation detector. Some vehicles are opened and inspected internally. To date, no undeclared sources of radiation have been found during these inspections. Any nuclear material or other radioactive sources identified as being out of regulatory control must be reported to the ITDB, as will be further explained in section 7.

4. Emergency preparedness and response to events concerning nuclear or other radioactive material out of regulatory control

The nuclear and radiological emergency preparedness system in Sweden is governed by a graded approach, where the emergency preparedness categories, as defined by IAEA Safety Standard GSR Part 7 [10], are partly used as a basis for the determination. All nuclear power plants are placed in the highest emergency preparedness category, and the national emergency response plan for management of a nuclear accident [11] mainly focuses on accidents at these facilities, although the plan states that it also covers accidents at other nuclear facilities. The response plan describes the legal bases, authorities involved in the response to a nuclear accident, and the responsibilities of these authorities. The plan does not address the possibility of internal or external sabotage and is not based on a threat/hazard assessment, as was pointed out in the follow-up Integrated Regulatory Review Service (IRRS) Mission [12] conducted in Sweden in 2016.

A similar national plan for responding to accidents involving nuclear or other radioactive material outside the nuclear facilities, or for other types of incidents (possibly involving malicious intent), does not exist in the same way as the national response plan for accidents at nuclear power plants. In the event of such an incident the emergency response follows a set of general principles, i.e. the principles of responsibility, parity and proximity [13]. The principle of responsibility means that the entity (authority, county, etc.) that is responsible for an activity under normal conditions also should have the responsibility in an emergency. The county administrative board is responsible for planning and leading regional emergency preparedness work in the case of an accident at a nuclear facility which could warrant protective actions for the public. The board also decides on measures to be taken to protect the public, provide information and alert the public, and is responsible for managing decontamination activities. In the case of other radiological incidents the municipality has the corresponding responsibilities. The Government is responsible for crisis management on a national level, where the mandate is primarily strategic issues. For coordination on a national level, the Swedish Civil Contingencies Agency (MSB) is responsible, and supervises preparedness for off-site rescue services response to radioactive releases.

The role of SSM is regulated in Sections 15 to 17 of the Ordinance [14] with instructions for SSM. SSM is responsible for coordination of necessary emergency preparedness measures for preventing, identifying and detecting nuclear and radiological incidents. In the context of such an incident, SSM must (among other things) advise on radiation protection and decontamination, maintain and lead a national organisation for expert response, provide technical advice to other public authorities, and maintain the capability to perform radiation monitoring and sampling. If a criminal act is suspected, the Police, under the coordination of the National Operations Department, assumes a larger role and is responsible for investigating the crime, collecting information, restoring order and keeping the barriers necessary for securing evidence as well as for protecting the public.

SSM performs a risk and vulnerability study [9] every other year (prior to 2016, each year) in order to assess the preparedness of SSM within its areas of responsibilities. The risk analysis is partly based on a number of identified scenarios, covering both intentional actions and accidents. They are divided into three main categories: nuclear reactors, radioactive substances, and nuclear explosive devices and weapons. The category of radioactive substances contains the scenarios most relevant to the topic of this paper, e.g. theft, smuggling or illegal transfers of nuclear or other radioactive sources, and different types of accidents involving radioactive materials. The consequences of such incidents are typically limited to a smaller geographical area compared to a serious accident at a nuclear facility, but can have life-threatening effects on individuals. In the case of a dirty bomb, i.e. a conventional explosive device mixed with radioactive material, there is a risk that the radioactivity will remain undetected until the effect of radiation damage is detected on individuals. The risk and vulnerability study also points out complex areas of responsibilities in the event of an incident involving radioactive sources outside a facility, and underlines shortcomings in the radiation protection legislation governing e.g. police and rescue personnel response to an incident involving a radioactive source. Exercises in this area are needed to ensure swift and correct response. As already mentioned in the previous section, the study also underlines the fact that border controls in Sweden are very limited when it comes to detecting radioactivity.

5. Controlling nuclear material and other radioactive sources in Sweden

All nuclear material in Sweden is registered and subjected to international safeguards. SSM keeps a national registry for nuclear material. In addition, Swedish nuclear facilities report material balances and other information to the European Commission in accordance with Commission Regulation (Euratom) 302/2005 on the application of Euratom Safeguards [15]. Sealed radioactive sources with activity levels above those stated in the Council Directive on Basic Safety Standards [16] require an individual licence and are registered in a national registry. There are some exceptions, such as fire alarms and telescopic sights. Other unsealed sources fall under a more general licensing procedure where the individual source is not registered in a national registry. The handling and licensing procedures for nuclear and other radioactive sources are regulated by the Radiation Protection Act [17], Radiation Protection Ordinance [18], Act on Nuclear Activities [19], Ordinance on Nuclear Activities [20], and by regulations [21] issued by SSM.

All licensed holders of radioactive sources are required to keep an in-house registry of their sources, maintain adequate physical protection of the sources, and have an emergency plan for incidents. The licensee must also report all incidents to SSM. Incidents might involve accidental mishandling of a source or discovering that a source has been lost. Information that should be reported is usually specified by the terms of the licence. Details received by SSM through these incident reports are entered as part of the reporting made by SSM to the ITDB.

6. Metal recycling facilities and orphan sources

As already stated, most incoming goods are not subject to checks for radioactivity at the Swedish border. However, the metal recycling industry has realised the value of conducting their own measurements of both imported and domestic material before melting it or reselling scrap metal. This is to avoid running the risk of accidentally melting radioactive sources together with other metals, which can lead to contamination of the final product and, in a worst case scenario, the entire plant. For this reason, many of the largest companies in this industry have invested in portal monitors and pass all incoming and most outgoing goods through these portals. Portal monitors and other forms of controls for radioactivity are not regulated by SSM, implying that SSM cannot require the companies to report incidents where their detectors triggered alarms. However, since many items that trigger alarms in the portals are subject to regulations deriving from the Radiation Protection Act [17], SSM has included conditions for the portal monitors in licences for other equipment that the companies have, such as XRF detectors (X-ray fluorescent detectors). The conditions for example require the companies to safely handle and store the discovered radioactive materials and to report such incidents to SSM. There are around a dozen or so private firms in Sweden that have one or more portal monitors subject to licence conditions requiring incident reporting to SSM if any radioactive material is detected by the portals.

In the Ordinance [14] with instructions for SSM it is stated that SSM is responsible for regaining and maintaining control over orphan sources. Earmarked funding is provided to SSM each year from the Swedish Government, through the Swedish Environmental Protection Agency, for this purpose. Anyone who finds an orphan source or radioactive waste of any kind can contact SSM and apply for help to get the source taken care of. If SSM cannot find the original owner of the source, SSM commissions a company licensed to handle radioactive sources to collect the source and store it safely [22]. This mode of operation is often used by the metal recycling industry when radioactive sources are found among scrap metal loads, but a number of private individuals also apply each year for help to take care of unwanted radioactive material. This is another source of information used when reporting to the ITDB, as will be explained in the next section.

7. Incident and Trafficking Database (ITDB)

In 1995 the Board of Governors at the IAEA requested the Director General to develop a reliable database of information on incidents of illicit trafficking in order to assist Member States and to better inform the public [23]. In August 1995, the Illicit Trafficking Database was operational and the IAEA began accumulating information. In 2012 the name of the database was changed in order to better

reflect the scope of the database. The database is intended to cover illicit trafficking events, but also has a broader scope in that it encompasses all nuclear and other radioactive material out of regulatory control [24]. The new name was decided to be “Incident and Trafficking Database: Incidents of nuclear and other radioactive material out of regulatory control”.

The scope of the information in the ITDB is specified in the Terms of Reference as follows:
“The ITDB covers incidents involving unauthorized acquisition, provision, possession, use, transfer or disposal of nuclear and other radioactive materials, whether intentionally or unintentionally, with or without crossing international borders. It also covers unsuccessful or thwarted acts of the above type, the loss of materials and the discovery of uncontrolled materials.”

The IAEA states a number of purposes of the database: to assist states with the timely exchange of authoritative information on incidents within the scope of the ITDB; to maintain and analyse reported information with a view to identifying common threats, trends and patterns; to assist states in determining what actions may need to be taken or to help formulate policy towards combating illicit trafficking; and to support the Agency’s nuclear security activities. When appropriate, the information reported to the ITDB can also be used to provide media with reliable information concerning a region or a particular incident.

It is voluntary for states to join the ITDB programme. The member states of the ITDB are not identical to those that have signed the NPT [25] or to those that are member states of the IAEA. By April 2017, 134 states have signed up to join the programme, and nearly 3,000 incidents have been reported to the database since its inception in 1995. Of these incidents, 259 have been reported as Group I incidents, meaning that an incident is confirmed as, or likely to be, an act of trafficking or malicious use, or an instance of scam/fraud, or an attempt thereof. 807 incidents have been categorized in Group II, where it has not been deemed possible to determine whether the incident is related to trafficking or to malicious use. This group includes a number of incidents involving theft and missing material. A number of very old incidents are not placed in any group due to insufficient information, but the vast majority are Group III incidents involving a confirmed or likely absence of trafficking or malicious use. Note: This method of structuring the incidents into groups has evolved over time, as have the definitions of incidents, implying that one must be careful when using the entire database to view statistics and to draw conclusions.

7.1. Incidents reported by Sweden to the ITDB

Sweden has been a member of the ITDB programme almost since the very beginning, joining on 12 December 1995. The Point of Contact (PoC) for reporting to the ITDB is presently located in the Section for Nuclear Non-Proliferation and Security at SSM. Fortunately, during the lifespan of the ITDB programme, no incidents of trafficking or malicious use of nuclear or radioactive material have been discovered taking place in Sweden. However, Sweden has not been actively reporting all incidents falling under the scope of the ITDB throughout this time period.

Over the past three years, SSM has stepped up its efforts in collecting and sharing information about incidents falling under the scope of the ITDB. The majority of incidents discovered and reported fall under the incident description ‘unauthorized disposal’, which means that nuclear or other radioactive materials have been disposed of at facilities where these materials are not accepted. The second most common type of incident is ‘undeclared or unauthorized storage’ where, typically, a business or university is in possession of undeclared nuclear material, often historical material or materials used for non-nuclear research. Figure 1 is a graph displaying the number of reported incidents over time (up until April 2017), where the year on the x-axis reflects the incident date, not the reporting date. There is typically a time lag of a few months between an incident occurring and the incident being reported. The data is to be interpreted as reflecting an increase in reporting frequency and not as an increase in the actual number of incidents occurring. However, with greater international trade in scrap metals and a growing number of waste facilities installing portal monitors for detecting radiation, the number of detected incidents in the category ‘unauthorized disposal’ may be increasing over time.

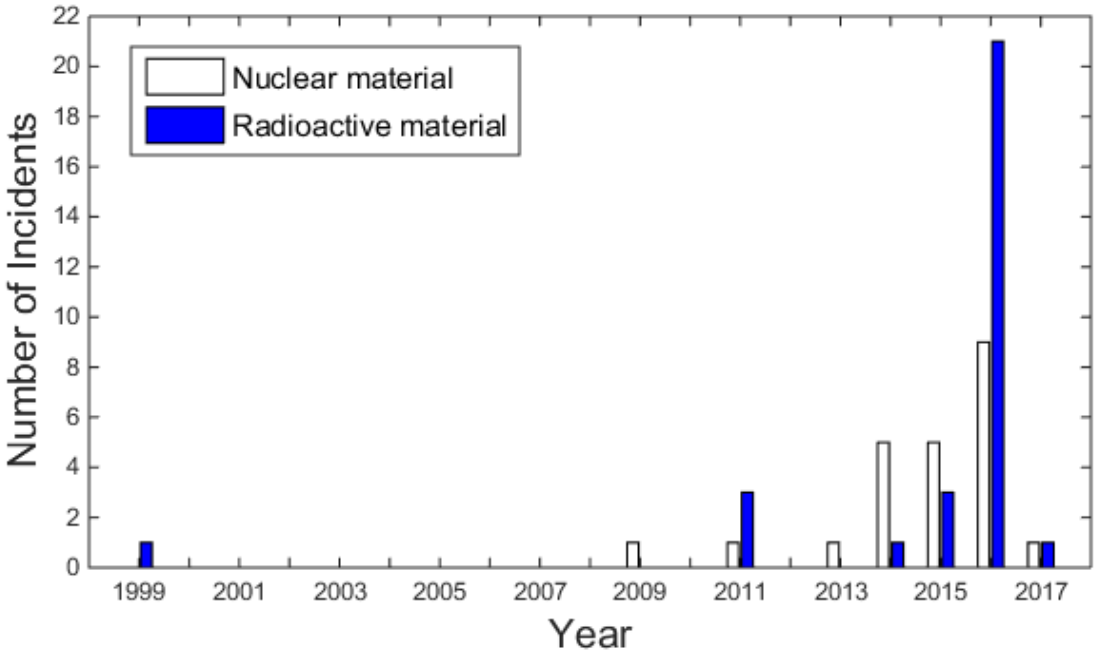

Figure 1: Number of incidents reported to the ITDB between 1999 and April 2017. The year on the x-axis reflects the date when the incident occurred, not the reporting date.

Around half of the incidents reported involved nuclear material, often uranium or thorium salts. Radium 226 is also a commonly occurring isotope in the reported incidents. Figure 2 shows a breakdown of the type of incident and material involved in the incidents reported between 1999 and April 2017. One incident can encompass several types of radiation sources and/or types of nuclear material.

There is a connection between some incidents reported to ITDB and ‘accidental gain’ and ‘loss’ of nuclear material reported under safeguards. Nuclear material that is found as unregistered under safeguards automatically comprises an incident to be reported to the ITDB, typically under the types ‘unauthorized storage’ or ‘possession’, or, if found at any type of waste treatment facility, under ‘unauthorized disposal’. To date, the reason behind failing to report the material under safeguards has been either a lack of knowledge of the regulations or being unaware of the type of material. For this reason all these incidents have been Group III incidents, i.e. neither related to trafficking nor to malicious use.

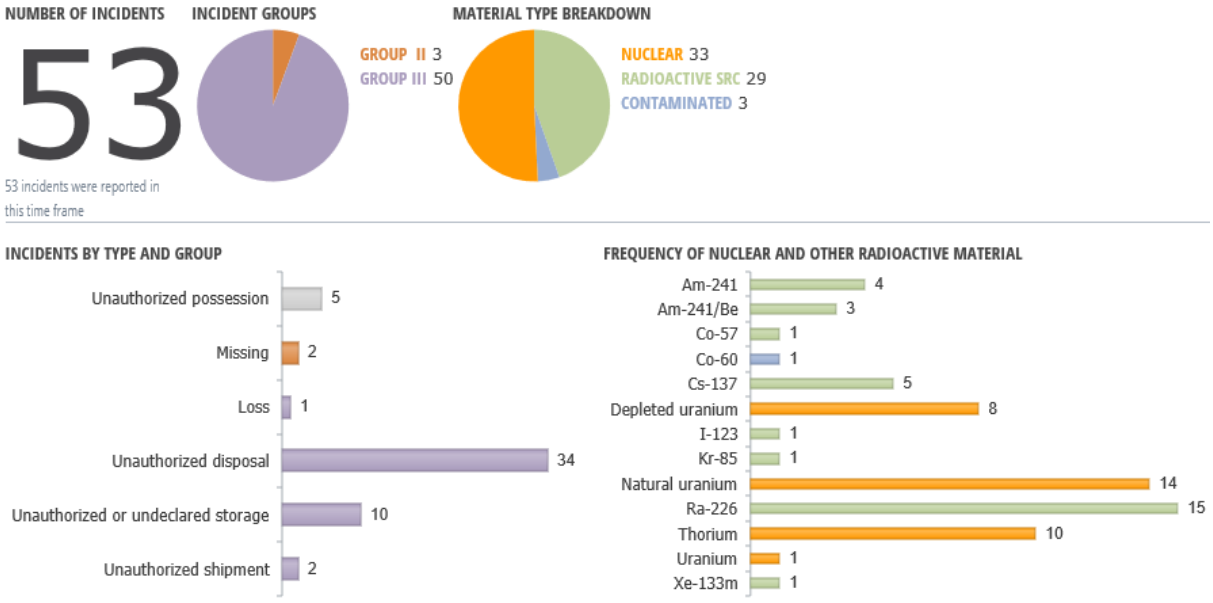

Figure 2: Breakdown of types of incidents reported by Sweden and the nuclear and radioactive source involved, from 1999 to April 2017. One incident can encompass several radiation sources and/or types of nuclear material. Screenshot from the ITDB dashboard on 19 April 2017.

7.2. Network for ITDB reporting

SSM is the competent authority on issues related to radiation. Therefore, most incidents falling within the scope of the ITDB are dealt with by one of the 16 sections belonging to SSM's departments. The challenge is to make the approximately 200 people working in these sections aware of when an incident they are processing should be communicated to the PoC for ITDB reporting. To increase awareness of the ITDB within SSM and to communicate the obligation each member state has to report incidents to the ITDB, the ITDB reporting group has started to initiate meetings with each section to communicate about and explain the purpose of the ITDB, and to discuss the types of incidents that a specific section might encounter in their daily work. Implementation of this in-house cooperation has mainly taken place with the Section for Transport and Waste and the Section for Nuclear Non-Proliferation and Security. Work on establishing a way to share information is currently ongoing with the Section for Medical Exposures and Section for Occupational Practices and Work Activities. A collaboration project with the national INES coordinator has also been established; here, reported information is shared between the two coordinators. The plan is to gradually expand this network throughout SSM.

Because some types of incidents might not come to the attention of SSM, at least not immediately, there is a need to expand the network to encompass other national authorities. In the case of theft (and attempt thereof), cooperation with the Police is needed, and in the case of scam/fraud in which no nuclear or other radioactive material was actually present, it might first and foremost come to the attention of Swedish Security Services. Some established groups are already in place with representatives attending from relevant authorities, e.g. within the area of export control, that could also potentially be used to establish a network for questions related to ITDB and reporting of incidents. SSM presently shares information from the ITDB with several Swedish authorities.

8. International cooperation to combat illicit trafficking

The collapse of the USSR between 1991 and 1992 initiated international cooperation between Sweden and a number of the new states that once were republics of the Soviet Union [26]. Over nearly 25 years now, several hundred projects have been implemented by SSM (*Strålsäkerhetsmyndigheten*, the Swedish Radiation Safety Authority) and its predecessors, the Swedish Radiation Protection Authority, SSI (*Statens strålskyddsinstitut*) and the Swedish Nuclear

Power Inspectorate, SKI (*Statens kärnkraftinspektion*) to ensure that radioactive and nuclear material and facilities are kept safe and secure.

In the early days of the new states' independence following the USSR's demise, the primary goal for the international community was to ensure control over nuclear weapons and to channel former Soviet military activities in the nuclear field into new structures of ownership and responsibility in the successor states. The United States was then heavily involved in funding and organizing the transportation of weapons-grade nuclear material from the former satellite states in the USSR to Russia, which is the state that succeeded the USSR as a nuclear weapons state under the NPT. In more recent times, the focus has shifted towards increasing the safety and security of civilian uses of nuclear material and other radioactive sources and facilities, where much work remains to be done.

The current Swedish commitments stem from the political objectives stated in the Nuclear Security Summits held from 2010, in addition to the objectives of the G-7 and its Declarations from Kananaskis in 2002 and Deauville in 2011. A legal basis is set through the UN Security Council Resolution 1540 [2] which requires all states to take measures to secure materials and facilities that could be used to manufacture weapons of mass destruction (see also section 2). Sweden carries out projects in cooperation with recipient states, often together with other partners, primarily in Norway, Finland, the United States, United Kingdom, Germany, Italy and Poland. Figure 3 shows the main locations where projects were implemented in 2015.

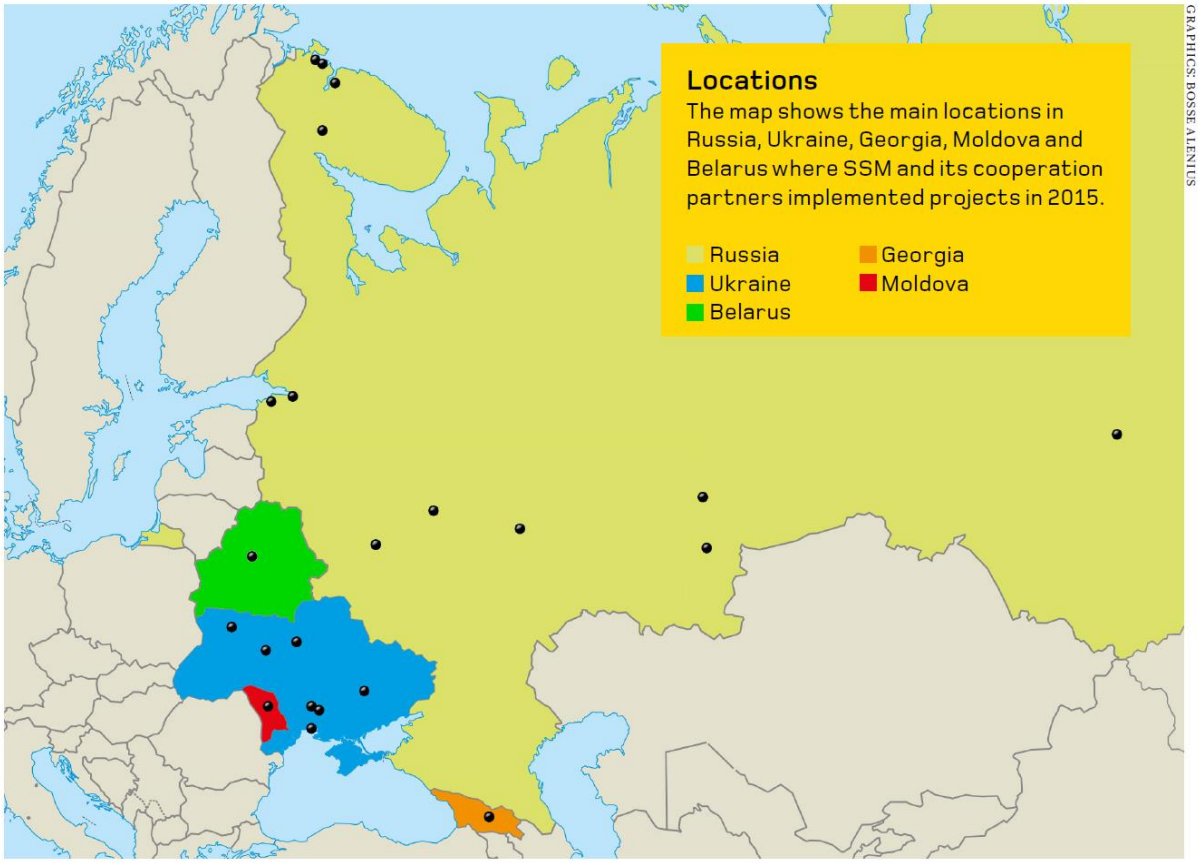

Figure 3: The main locations in Russia, Ukraine, Georgia, Moldova and Belarus where SSM, together with cooperation partners, implemented projects in 2015. From "Nuclear Security, Safety and Non-Proliferation: Sweden's International Cooperation in 2015" [26].

8.1. Projects related to combating illicit trafficking

Bilateral cooperation has gradually expanded between Sweden and Black Sea region states in the areas of nuclear security and non-proliferation, as well as in emergency preparedness work. The focus is on activities aimed at strengthening the institutional capacity of the states' regulatory authorities.

Problems in this region due to political instability, weak governance and corruption, in combination with poverty and weak rule of law, give scope for organized crime to increase. Since a number of nuclear facilities and large quantities of radioactive material are located in this region, the risk of illegal activities, including illegal trade and trafficking in nuclear or other radioactive materials, is increased.

Statistics from the ITDB[1] show that out of a total of 57 reported Group I incidents worldwide (related to trafficking or malicious use, or attempts thereof) since 2010, 32 of them were reported by either Ukraine, Moldova or Georgia. This is further motivation for working towards regaining control over nuclear and radioactive sources, as well as strengthening institutions and increasing border control to combat illegal trade in such materials.

Some of the projects in the Black Sea region that SSM participates in or has completed are presented in the following sections. As this is only a small selection of projects, the authors refer the reader to the webpage of SSM[2] for further information about other completed or ongoing projects.

8.1.1. Ukraine

Ukraine is a country with a vast number of radioactive sources, where around 25,000 sources are still in use and around half a million are disused. SSM has sponsored a project on modernizing the Ukrainian state registry of ionizing radiation sources by improving the technical infrastructure and the system's functionality to comply with new regulations. An outreach campaign on recovering orphan radioactive sources under institutional supervision was carried out in 2016, where SSM, in cooperation with the State Regulatory Inspectorate of Ukraine (SNRIU), set up a website to promote nuclear and radiological safety. Amnesty legislation with the purpose of encouraging enterprises, organisations and the general public to turn in orphan radioactive sources to Ukrainian authorities was passed in October 2016 and was promoted by the public website.

All disused radioactive sources in Ukraine are to be moved to the newly built central repository, VEKTOR, located in the Chernobyl exclusion zone. Many disused radioactive sources are presently stored in well-type storages with little documentation on the type and activity of the sources. SSM completed a project in 2016 with the Ukrainian national waste management operator on a feasibility study that resulted in recommendations on how to best move the sources from the wells to the new storage facility. A follow-up project will be carried out in 2017 involving a detailed design for removal of sources from a representative well-type storage located at the Kiev RADON site.

8.1.2. Republic of Moldova

A longstanding project in Moldova is to regain control over nuclear and other radioactive material out of regulatory control. In these efforts, SSM has delivered technical and financial support to the National Agency for Regulation of Nuclear and Radiological Activities in Moldova (NARNRA). During the period 2014-2016, 329 radioactive sources, including five cases containing nuclear materials, were discovered by NARNRA and transported to the State Radioactive Waste Repository for safe storage. Information on the identified sources has been submitted to the ITDB. A parallel pilot project on tracking of radioactive sources through social media has been implemented by the James Martin Center for Non-proliferation Studies in Monterey, California.

In September 2015, at the request of NARNRA, SSM supported organization of an international response exercise in Moldova on combating illicit trafficking of nuclear and radioactive materials. The exercise was conducted at the Giurgiulesti International Free Port, on the border between Moldova and Romania. The main purpose of the exercise was to test the effectiveness of existing response procedures for illicit trafficking incidents and the procedures' compatibility with those of EU border states. Participants included regulators, customs officials, border guards, police officers and intelligence organizations, as well as observers from international organizations.

[1] Search parameters of the ITDB from 2010-01-01 to 2017-04-20, Group I incidents.
[2] http://www.stralsakerhetsmyndigheten.se/In-English/Facts-about-us/International-work/

8.1.3. Georgia

With support from SSM, Georgia has recently established a comprehensive legal and regulatory framework for the management of radioactive waste. The Law on Radioactive Waste has been adopted by the Parliament of Georgia and a new, independent Agency of Nuclear and Radiation Safety (ANRS) has been established under the supervision of the Ministry of Environment and Natural Resources Protection of Georgia. The work and experience gained in collaboration with Swedish experts in 2016 facilitated elaboration of the National Waste Management Strategy and Action Plan, which were adopted by the Georgian Government in December 2016.

In September 2016, SSM supported several exercises on responses to the seizure of radiological materials at the Sarpi checkpoint located on the Georgian-Turkish border, as well as at the Batumi airport and Batumi seaport. More than 40 members of emergency teams and experts from Sweden, USA, Ukraine, Moldova and Romania participated in the exercises. The outcome of the evaluation demonstrated the relevant status and systems in place to detect, prevent and respond to the cases of smuggling attempts of nuclear and radioactive materials.

9. Summary and conclusions

Nuclear and other radioactive sources out of regulatory control can lead to unwanted and dangerous radioactive exposure of people, animals and the environment, either due to accidents, or in a worst case scenario, due to malicious use. The chain of individuals or entities running the risk of possible exposure to radiation can be quite long, from customs officials and transport companies to the end users or recycling facilities. Depending on the type of situation, several governmental and local institutions might be involved, having different areas of responsibilities. Coordination and sharing of relevant information become key elements for success.

This paper has given a brief overview of the Swedish system designed to maintain control over nuclear and other radioactive material, as well as the system in place to regain control over sources when they have been lost. Some shortcomings have been pointed out, such as the (according to many professionals) insufficient checks for radioactivity carried out on incoming goods across the Swedish border.

An additional effort made by SSM over the past three years is sharing information through the Incident and Trafficking Database (ITDB) about incidents when nuclear or other radioactive material is, or was, out of regulatory control. Expanding the national network to spread information is an ongoing and very important part of this work.

Last but not least, the paper presents some of the work being performed through SSM's Office for International Relations in the international arena to combat illicit trafficking in nuclear and radioactive material out of regulatory control. The Black Sea region is a part of the world that is heavily affected by trafficking in these types of materials. Thus, it is an important and a strategic region to support in these countries' own government efforts to combat these activities and regain control over such materials.

10. Acknowledgements

The authors gratefully acknowledge all those who have reviewed the content and contributed by providing information for this paper, in particular our colleagues at SSM from the Section for Emergency Preparedness and Response, Section for Transport and Waste, Section for Nuclear Non-proliferation and Security, and the Office for International Relations.

11. Legal matters

11.1. Privacy regulations and protection of personal data

The authors agree to allow ESARDA to print our names/contact data/photographs/article in the ESARDA Bulletin/Symposium proceedings, or any other ESARDA publications and, when necessary, for any other purposes connected with ESARDA activities.

11.2. Copyright

The authors agree that submission of an article automatically authorises ESARDA to publish the work/article in whole or in part in all ESARDA publications – the bulletin, meeting proceedings, and on the website.

The authors declare that their work/article is original and is not a violation or infringement of any existing copyright.

12. References

[1] *Slutrapport för regeringsuppdraget att se över samhällets förmåga att kontrollera radioaktiva ämnen vid Sveriges gräns*; Swedish Customs, STY 2011-405, M2011/2028/ke, 15 February 2012.

[2] United Nations Security Council Resolution 1540; S/RES/1540 (2004), 28 April 2004.

[3] Axelsson G, *Utredning om stärkt svensk exportkontroll och icke-spridningsarbete samt svenskt genomförande av FN:s säkerhetsråds resolution 1540 (2004)*; PM, UF2008/16048/NIS, 30 December 2008.

[4] INFCIRC/274, Convention on the Physical Protection of Nuclear Material; IAEA, Vienna, 1979.

[5] Council Regulation (Euratom) No. 1493/93 on shipments of radioactive substances between Member States; Official Journal L 148, 19 June 1993.

[6] Code of Conduct on the Safety and Security of Radioactive Sources; IAEA, Vienna, 2004.

[7] Response to Events Involving the Inadvertent Movement or Illicit Trafficking of Radioactive Materials; IAEA TECDOC-1313, Vienna, 2002.

[8] Amendment to the Act *Lag (1996:701) om Tullverkets befogenheter vid Sveriges gräns mot ett annat land inom Europeiska Unionen*; SFS 1996:701, 13 June 1996.

[9] *Strålsäkerhetsmyndighetens risk- och sårbarhetsanalys 2016*; SSM2016-4371-1, 2016.

[10] IAEA Safety Standard, Preparedness and response for a nuclear or radiological emergency; GSR Part 7, IAEA, Vienna, 2015.

[11] *Nationell beredskapsplan för hantering av en kärnteknisk olycka*; MSB, 2015.

[12] Integrated Regulatory Review Service (IRRS) follow-up mission to Sweden; IAEA-NS-2016/05, 2016.

[13] Sweden's seventh national report under the Convention on Nuclear Safety; Ministry of the Environment and Energy, Ds 2016:30, 2016.

[14] Ordinance with instructions for the Swedish Radiation Safety Authority (2008:452); 2008.

[15] Commission Regulation (Euratom) No 302/2005 of 8 February 2005 on the application of Euratom Safeguards; 8 February 2005.

[16] Council Directive 2013/59/EURATOM of 5 December 2013 laying down basic safety standards for protection against the dangers arising from exposure to ionising radiation; Appendix VII, Table B, 5 December 2013.

[17] Radiation Protection Act (*Strålskyddslagen (1988:220))*; 19 May 1988.

[18] Radiation Protection Ordinance (*Strålskyddsförordningen (1988:293))*; 19 May 1988.

[19] Act on Nuclear Activities (*Lag (1984:3) om kärnteknisk verksamhet)*; 12 January 1984.

[20] Ordinance on Nuclear Activities (*Förordning (1984:14) om kärnteknisk verksamhet)*; 12 January 1984.

[21] http://www.stralsakerhetsmyndigheten.se/In-English/Enactments/Regulations; SSM, 27 April 2017.

[22] *Handläggning av STÄDA-ärenden*; STYR2016-2, SSM, 31 March 2016.

[23] ITDB Terms of Reference; rev. 2016.07, IAEA, 2016.

[24] ITDB 2016 Fact Sheet; IAEA, 2016.

[25] Treaty on the Non-Proliferation of Nuclear Weapons (NPT); 1 July 1973.

[26] Nuclear Security, Safety and Non-Proliferation: Sweden's International Cooperation in 2015; SSM, 2016.

Current Safeguards Research and Development Efforts at National Nuclear Security Administration (NNSA)

Christopher Ramos[1] and Chris Pickett[2]

[1]National Nuclear Security Administration, Defense Nuclear Nonproliferation Washington DC; [2]Oak Ridge National Laboratory, Oak Ridge, TN
E-mail: christopher.ramos@nnsa.doe.gov; chris.pickett@nnsa.doe.gov

Abstract:

The National Nuclear Security Administration's (NNSA) Defense Nuclear Nonproliferation (DNN) Office of Proliferation Detection funds research and development (R&D) that improves the efficiency and effectiveness of current safeguards and efforts to strengthen existing safeguards measures to detect material diversion In declared facilities. DNN R&D develops advanced tools and methods to provide for comprehensive monitoring, detection and analysis of civilian nuclear fuel cycle programs. Sponsored research provides confidence that special nuclear material (SNM) is not being diverted or misused for the proliferation of nuclear weapons. A safeguards-specific goal is to develop and demonstrate new technologies and capabilities to cooperatively quantify and track SNM throughout a nuclear fuel cycle and detect any illicit diversion of these materials. These goals align with that of the International Atomic Energy Agency's Long Term Strategy for 2012-2023 to improve "technical capabilities by making use of scientific and technological innovation, and to enhance its readiness to safeguard new nuclear technology and support new verification missions." [1]

DNN supports research and development of technologies and methodologies that can significantly improve or enhance nondestructive assay methods, the tools needed to provide effective containment and surveillance, process and environmental monitoring, and destructive analyses. This paper will provide an overview of select R&D efforts; some that are currently underway and others that have recently transitioned to sponsors for deployment and implementation.

Keywords: safeguards, monitoring, detection, material, technology

1. Introduction

The National Nuclear Security Administration's Office of Defense Nuclear Nonproliferation Research and Development's (DNN R&D) mission is to advance U.S. capabilities to detect weapons development activities, including material production & movement and nuclear explosions globally.. The mission space of DNN R&D is applied research. A core DNN R&D research objective is the advancement of safeguards technologies. DNN R&D Safeguards focuses on developing and demonstrating new technologies and capabilities that: 1) Improve the efficiency and effectiveness of current safeguards and 2) Strengthen existing safeguard measures to ensure timely detection of material diversion and undeclared material production. .

DNN R&D Safeguards is required to develop and demonstrate new technologies and capabilities that provide comprehensive monitoring, detection, and analysis of civilian fuel cycle activities to ensure that SNM is not being diverted or misused for nuclear weapons programs. To meet this requirement Safeguards R&D strives to develop, through proof of principle, the next generation of technologies that can provide accurate and timely nuclear material accountancy. Our ultimate vision is to provide technologies and tools that can continuously and unobtrusively monitor, all SNM production and movements while providing instantaneous accountancy at safeguarded facilities. This paper will discuss some of the DNN R&D Safeguards projects that are nearing completion.

2. Current DNN R&D Safeguards Projects

The projects highlighted here represent current R&D efforts that are mid development cycle and will be available for transition to mission partners soon. The vignettes presented are summaries derived from the work of the principle investigators at the US National Laboratories.

2.1 Current R&D for Improving DA methods for Nuclear Fuel Cycle Materials

Field portable instrumentation that provides in-field sample collection and analysis of SNM at safeguarded facilities continues to be of high interest to the Safeguards community. DNN Safeguards R&D invests in new technologies and methods that can provide more efficient and safe sampling UF_6 and improve isotopic determination of UF_6 samples. The technologies described below focus on enhancing efficiency, reducing risk, reducing cost, and providing more timely information to the Safeguards community.

2.1.1. Development of Solid Materials for UF_6 Sampling

Uranium hexafluoride (UF_6) samples must be taken for enrichment verification as part of the comprehensive safeguards agreements at gaseous enrichment facilities. Sampling of these gases can be performed at cylinders or from process lines. In an effort to increase efficiency and freedom of operation at a UF_6 facility, a method based on the Argentine-Brazilian Agency for Accounting and Control of Nuclear Materials Cristallini technique (ABACC-Cristallini) is currently under development by Argonne National Laboratory through the DNN Safeguards R&D portfolio.

The ABACC- Cristallini Method allows UF_6 samples to be captured and stored as an inert salt, which mitigates hazards associated with transportation and handling. This project is developing a field-portable, hand-carried system to utilize the ABACC-Cristallini method for sampling UF_6 cylinders and storing the material as uranyl fluoride. This system is expected to reduce the weight of sampling materials and equipment carried by an inspector and reduce the necessary sampling time. The handheld operation for Uranium Sampling (HORUS) can be used to collect measurements at existing facilities using inspector-controlled technology. [2]

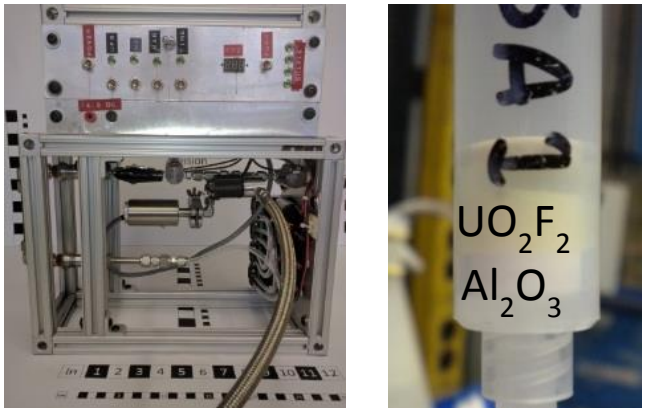

Figure 1. Left, image of the laboratory engineering prototype of HORUS. Right, image of uranyl band capture chamber.

HORUS uses an onboard power system and vacuum to actively pull the sample into a removable trap. A pressure transducer is used to read vacuum and UF_6 source pressure, and a timing circuit controls the mass of collected material. The HORUS system has been successfully tested with tungsten hexafluoride and uranium hexafluoride (DU). These tests demonstrated repeatability and good recovery for sampling. The initial tests have been successful and the lab device will undergo some additional refinements and systems engineering work to meet the requirements for safety and portability. The HORUS device has the potential to change the way inspection agencies are able to collect samples at uranium enrichment plants. The UF_6 samples will be able to be easily transported, the HORUS device can be brought to a site during inspections or left at the facility in secure storage until needed. The amount of sample and sampling time can greatly be

reduced from the time and amounts required by traditional methods. The device prototype will be completed and readied for testing at Pacific Northwest National Laboratory by the end of FY17. [3]

2.1.2. Fieldable Atomic Beam Laser Spectrometer for Isotopic Analysis

Los Alamos National Laboratory is developing a fieldable prototype device for the isotopic determination of uranium samples. The device can measure isotopic composition with high sensitivity, resolution, and speed. The method is based on generating a highly collimated atomic beam by heating the sample to 2500°C in rough vacuum, and measuring laser absorption through it. The use of an ultra-narrow linewidth diode laser allows the isotopic splitting of atomic absorption lines to be easily resolved. All of the system components are compact and rugged, and will be integrated into a vibration-immune prototype having a size under 2 ft^3, and requiring < 1500W of electrical power.

The system will be capable of determining the isotopic compositions of uranium/plutonium in the field with high precision and speed, in an easy-to-use system that requires no sample preparation steps, and no need for the transportation of chemical reagents. Samples are loaded directly in the system, and the instrument could be used in support of environmental sampling and inventory verification.

The immediate detection and characterization of isotopic signatures in the field aids in reassessing the course of an inspection if for example, the presence of undeclared nuclear materials are detected. When used as a method for on-site inventory verifications during routine inspections, better precision and sensitivity than currently used NDA measurements is expected, thus, the number of item verifications could be reduced while still meeting the required detection probability. [4]

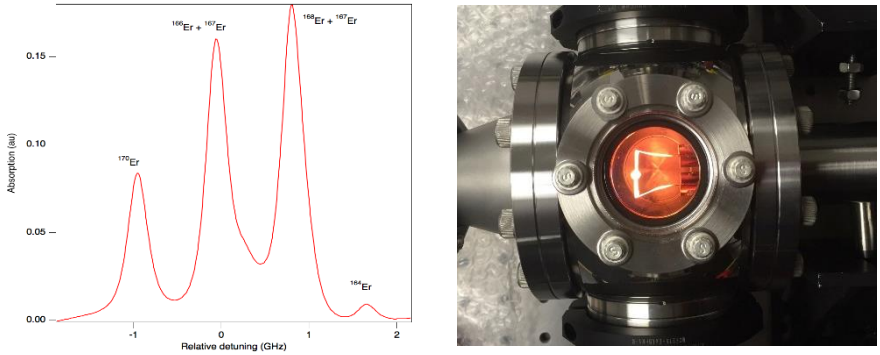

Figure 2. Left, Erbium spectrum showing several isotopes of Erbium. Right, heating element and nozzle of the micro-oven for atomic beam generation.

Using an atomic beam system allows for measurement of absorption lines virtually free from Doppler and collision broadening effects. The atomic beam width and laser beam width can be matched to ensure all the sample atoms travel through the interrogation volume. The result of this is a continuous signal that is nearly background free depending on the choice of the analyte.

This year the device will undergo analysis of highly enriched uranium, uranium oxide, and finalization of design for a fieldable prototype. This advantages of this technology over traditional mass spectrometry will allow for the immediate in-field isotopic analysis of SNM, and reassessment of the course of an ongoing inspection becomes a new possibility.

2.2 New Non-Destructive Analysis (NDA) Methods for SNM

The IAEA uses more than 100 different NDA systems to verify, check and monitor nuclear materials without changing their physical or chemical properties. NDA instruments range in size and complexity from small portable units used by safeguards inspectors during on-site verification activities to large in situ NDA systems designed for continuous unattended in-plant use.[5] Highly accurate, nondestructive assay methods represent major investment area for DNN Safeguards R&D. These investments are made with the intent of increasing current capabilities available to inspection agencies, enhancing function and portability, and supporting unattended process monitoring.

2.2.1. Commercially Viable Magnetic Micro-calorimeter γ-Detectors with Ultra-high Energy Resolution

Cryogenic gamma γ-detectors operated at temperatures below 0.1 K have been developed for the last decade because they offer ten times higher energy resolution than conventional high-purity Ge detectors, well below 100 eV FWHM at 100 keV. The reduction in errors from line overlap and background counts increases the accuracy of non-destructive isotope analysis (NDA) in nuclear safeguards applications. The high energy resolution trade-off is small detector volume and low count rates, providing the impetus for the development of γ-detector arrays. This work adapts metallic magnetic calorimeters (MMCs) based on Er-doped Au as γ-detectors for ultra-high resolution NDA. MMCs are paramagnetic sensors in which the absorption of a γ-ray produces a change in magnetization that can be read out with a superconducting quantum interference device (SQUID) preamplifier. Since MMCs have fewer noise sources and thus higher energy resolution than transition edge sensors (TESs), or larger pixel volume for the same energy resolution. They are also more linear than TESs and better suited for scaling to large detector arrays. Finally, MMC signals decay with a single thermal time constant. This should allow the use of novel pulse processing algorithms to increase their count rates by an order of magnitude, provided that the SQUID readout noise is sufficiently low.

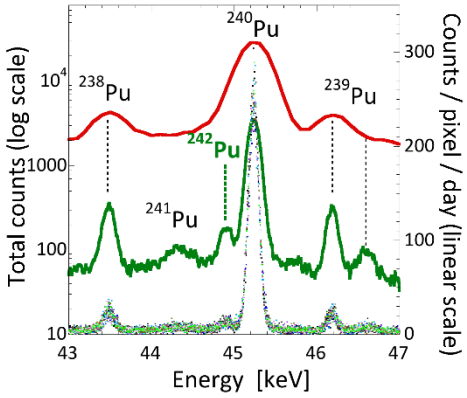

Figure 3. γ-spectrum of a mixed isotope of Pu sample. The MMCs can separate the ^{242}Pu line at 45.244 keV (green line). Note that the HPGe detector cannot separate these features (red line).

This technology has been applied to a number of case studies. With the MMCs one can conduct a total assay of Pu and directly detect ^{242}Pu (Figure 3) with accuracy of <1% ^{242}Pu being achievable. The MMCs can reduce the error in measurement of ^{242}Pu providing an independent measure of the initial enrichment in spent fuel, providing a check on operator declarations of initial enrichment of fuel rods. High resolution spectra provided by the MMCs can assist in the detection of undeclared uranium mining activities. In the absence of mining uranium will be in secular equilibrium with its decay products. Mining will alter the isotope ratios. Short lived isotopes (^{226}Ra/^{235}U) can then be used to characterize non-disturbed ore, tails, or products. Ge detectors suffer from line overlap for ^{266}Ra (186.21 keV) and the ^{235}U (185.71 keV) γ-lines. The high resolution MMC γ-detectors solves the line overlap issue and can aid in determining age estimations. The high resolution of the MMC γ-detectors can also be applied to resolving overlapping bands in the XKα region of uranium where lines from ^{235}U, ^{238}U, ^{231}Th, and ^{234}Th interfere in HPGe detectors. The higher resolution of the MMC γ-detectors will provide better accuracy of this measurement. Concerns about the fissile isotope, ^{233}U, from the thorium fuel cycle has led to the desire to more accurately measure the energies and branching ratios of ^{233}U. The MMC γ-detectors are uniquely capable to aid in these determinations. Improvements to the pixel design and addition of a liquid-cryogen-free dilution refrigerator high resolution operation at 10 mK will make MMC operation accessible to non-experts. Ultra-high energy resolution of MMCs will increase accuracy of NDA when HPGe detectors are limited by line overlap. [6]

2.2.2. List Mode Response Matrix for Advanced Correlated Neutron Analysis for Nuclear Safeguards

Partial defect detection presents a technical challenge for nuclear safeguards. Within the current safeguards technology toolkit and installed base of neutron non-destructive assay (NDA) systems, there is no existing

^{3}He-based detection capability to verify fuel pin loading patterns and partial defects in fresh fuel assemblies for nuclear safeguards applications. While current neutron collar detectors used for fresh fuel assay measurements employ twenty-four or more individual neutron detectors, only a single pulse train is analyzed from the combined detector array to derive two neutron counting rates from which safeguards conclusions must be drawn. Enhancing the capability of these NDA systems by extracting spatial information has not previously been explored, but it could prove crucial to detect fuel pin diversion.

To address the need for partial defect detection, a new correlated neutron analysis method, the "List Mode Response Matrix", is under development for implementation in a prototype ^{3}He-based List Mode Collar (LMCL). This system is designed to acquire and analyze pulse trains from the detector array to enable the verification of spatial information about the assay item for safeguards inspections. This spatial analysis has not previously been implemented in neutron collar detectors. Furthermore, spatial information will be combined with pattern recognition algorithms to detect changes in fresh fuel assemblies such as missing pins or pin replacement. The purpose of this research is to explore whether partial defect detection can be achieved using neutron NDA systems that have already been authorized for safeguards inspection use. One practical goal is to demonstrate that upgrading existing systems with new software and hardware is more cost-effective than system replacement, and show that this approach will maintain NDA system reliability and ease of use for safeguards inspections. The end goal of this research is to help nuclear safeguards inspectors to draw stronger conclusions about nuclear material diversion and partial defect scenarios. [7]

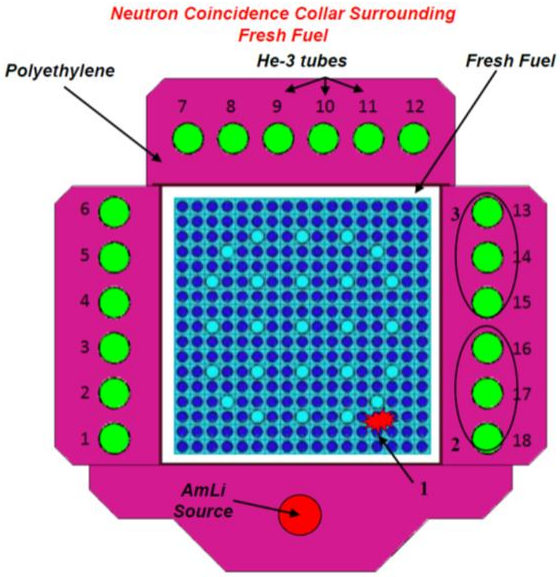

Figure 4: An Illustration of a standard neutron coincidence collar detector of the design fielded by the International Atomic Energy Agency (IAEA).

2.3 Containment and Surveillance/ Unattended Process Monitoring

Containment and surveillance (C&S) and process monitoring are important measures that compliment material accountancy and aid in the timely detection of diversion of SNM. These devices may include passive and active tags and seals, camera systems, and unattended process monitoring devices and systems like the online enrichment monitoring device (OLEM). Expanded deployment of unattended and remote monitoring systems has become an increasingly important element of IAEA efforts to maintain and increase safeguards effectiveness while reducing overall costs. [8] Ideally these systems are self-contained, have low power requirements, are easily maintained, and are unobtrusive to plant operations. DNN Safeguards R&D has recently invested in the following C&S/process monitoring devices to more efficiently monitor SNM activities and improve continuity of knowledge.

2.3.1. Whole Container Seal (WCS) for Sealing Existing Items and Equipment

Many safeguard sealing applications rely on loop type seals that can be inserted through a secure hasp type orifice associated with the item or object requiring protection. However there are many cases when adequate hasps do not exist or the containment of the item or device is inadequate for effective sealing. For these cases, a team from Oak Ridge National Laboratory has developed a versatile, inexpensive option for sealing things that were not initially designed for effective sealing. The Whole Container Seal is an actively monitored flexible conductive seal capable of enclosing monitored items of various shapes and sizes. It provides active monitoring that verifies the integrity of an entire object using commercially available components.

Breaches are indicated by changes in sensitive, four-point resistance measurements performed on the material at a plurality of measurement points. Multiple resistance measurements are performed over the entire enclosures in a short period of time to build up a signature of the conductive shield. Changes in the resistance signature indicate a breach. The sealing method can also support a variety of sensors that can be utilized to monitor the environmental conditions, detect movement and transport, or detect changes in physical attributes. [9]

Figure 5: Prototype whole container seal for encapsulating existing items or equipment in a tamper indicating shell made of novel material.

2.3.2. Viability of Acoustic Techniques for Density and Mass Flow in Enrichment Plants

The primary purpose of this research is to study the feasibility of acoustic signatures and sensors that support the accurate, noninvasive and unattended measurement of UF_6 gas density and mass flow rate in scenarios representative of uranium enrichment plants under safeguards by the International Atomic Energy Agency (IAEA). Non-invasive, unattended mass flow measurement at gaseous centrifuge enrichment plants would enable independent mass balance accounting. Current COTS acoustic techniques are capable of measuring mass flow down to 1 to 2 atmosphere pressures (760-1520 Torr). Header pipes at gaseous centrifuge enrichment plants typically operate in the range of 10-40 Torr. This technique has demonstrated sensitivity of acoustic signal to density at representative gas pressures.

For this safeguards application, acoustic measurements are two orders of magnitude more difficult: due to a very weak acoustic signal that passes through the gas. The acoustic signal that passes through the pipe wall is much stronger and provides clean reflections that can be used to gate the signal as it passes through the gas (see Figure 6).

This approach, coupled with a device like the On-line Enrichment Monitor (OLEM), may eliminate reliance on the use of in-line pressure sensor to determine the mass balance at gaseous centrifuge enrichment plants under international safeguards. This could be implemented in the current OLEM system and would eliminate the need to obtain host supplied data from a host owned pressure sensor. [10]

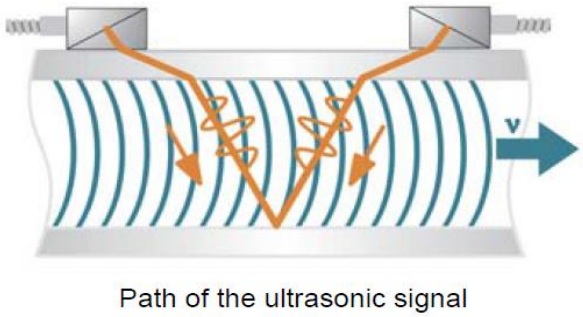

Figure 6. Path of the ultrasonic pulse through pipe walls and gaseous media to determine mass flow of UF_6.

3. Concluding Summary

The DNN mission focuses on utilizing world class resources to provide advanced technologies and methodologies that can achieve measureable impacts to the efficiency and effectiveness of domestic and international safeguards.

Figure 7: Facility Safeguards Vision: Unobtrusive Surveillance with Instantaneous Accountability.

The above is a depiction that represents the types of Safeguards systems envisioned for future facility Safeguards. This figure illustrates a facility where all SNM materials and personnel are continuously tracked and monitored. All materials are contained (kept in either monitored storage arrays or in containment that prevents direct access by personnel) and unattended real-time process monitoring is accomplished as the materials are processed and move through the facility.

Future safeguards approaches need to modernize by implementing new tools and technologies that provide timely detection of material diversion, maintain continuity of knowledge, and provide indications of facility misuse; while minimizing operational impacts and enhancing security, safety, and overall process efficiency.

The objective of current DNN Safeguards R&D is to provide support for this vision in these functional areas.

- Nuclear Material Measurements
- Unattended Monitoring of Material Inventories and Processes
- Containment and Surveillance
- Destructive Analysis Methods and Environmental Sampling
- Design Information Verification

The projects mentioned in this paper showcase some of the current R&D efforts that are being undertaken to support the full spectrum of needs associated with global safeguards.

4. Acknowledgements

The authors acknowledge the dedicated efforts by scientific and engineering staff at Argonne National Laboratory, Lawrence Livermore National Laboratory, Los Alamos National Laboratory, Oak Ridge National Laboratory, and Pacific Northwest National Laboratory for their collective R&D efforts in developing state-of-the-art technologies mentioned in this report. These efforts also involve collaborations with the other U. S. Government institutions, universities and private corporations. The technology development reported herein is supported by the Defense Nuclear Nonproliferation R&D in the U.S. Department of Energy/National Nuclear Security Administration (DOE/NNSA).

5. Legal matters

5.1 Privacy regulations and protection of personal data

I agree that ESARDA may print my name/contact data/photograph/article in the ESARDA Bulletin/Symposium proceedings or any other ESARDA publications and when necessary for any other purposes connected with ESARDA activities.

5.2 Copyright

The author agrees that submission of an article automatically authorizes ESARDA to publish the work/article in whole or in part in all ESARDA publications – the bulletin, meeting proceedings, and on the website. The author declares that their work/article is original and not a violation or infringement of any existing copyright.

6. References

[1] International Atomic Energy Agency, Department of Safeguards, Long-Term R&D Plan, 2012-2023, January 2013.

[2] Smith N. A., Hebden A. S., Savina J. A.: 2017, *Development of Solid Materials for UF_6 Sampling*, presented to Nuclear Security Applications Research and Development Program Review Meeting, Las Vegas, NV, April 2017.

[3] Smith N. A., Hebden A. S., Savina J. A.: 2017, *Development of Solid Materials for UF_6 Sampling*, presented to Nuclear Security Applications Research and Development Program Review Meeting, Las Vegas, NV, April 2017.

[4] Castro A., Savukov I., Xu N.: 2017, *Spectroscopic Methods for Ultra-low Isotopic Analysis of Proliferant Material,* presented to Nuclear Security Applications Research and Development Program Review Meeting, Las Vegas, NV, April 2017.

[5] Safeguards Techniques and Equipment: 2011 Edition; International Nuclear Verification Series No. 1 Rev 2; International Atomic Energy Agency; Vienna; 2011.

[6] Friedrich S., Kim G., Boyd S., Hummatov R., Cantor R., Hall A., Enns, C.: 2017, *Magnetic Micro Calorimeter with Ultra-high Energy Resolution,* presented to Nuclear Security Applications Research and Development Program Review Meeting, Las Vegas, NV, April 2017.

[7] Worral L., Nicholson, A.D., Britton C.L., Croft S., Davman K., Ericson N., McElroy R.D., Simone A., Stewart S.L.: 2017, *List Mode Response Matrix for Advanced Correlated Neutron Analysis for Nuclear Safeguards,* presented to Nuclear Security Applications Research and Development Program Review Meeting, Las Vegas, NV, April 2017.

[8] Safeguards Techniques and Equipment: 2011 Edition; International Nuclear Verification Series No. 1 Rev 2; International Atomic Energy Agency; Vienna; 2011.

[9] Stewart S., Younkin J.R., Roberts II C.K., Fountain C.L., Britton Jr. C.L., Warmack R.J.B., Krementz D., Jones J., Jones B., Smartt H.: 2017, *Whole Container Seal – Advanced Tools for Continuity of Knowledge,* presented to Nuclear Security Applications Research and Development Program Review Meeting, Las Vegas, NV, April 2017.

[10] Warren G., Ramuhalli P., Denslow K., Morris G., Jones M., Longoni G., Moran T., Smith E., Roy S.; 2017, *Viability of Acoustic Techniques for Density and Mass Flow in Enrichment Plants*, presented to Nuclear Security Applications Research and Development Program Review Meeting, Las Vegas, NV, April 2017.

Early Experience in Implementation of the Modified Small Quantities Protocol under the US-IAEA Caribbean Territories Safeguards Agreement (INFCIRC/366)

David H. Hanks
Hilary M. Lane

U.S. Nuclear Regulatory Commission
Washington, DC USA

Abstract:

Pursuant to Additional Protocol I to the Treaty of Tlatelolco, individual Safeguards Agreements were produced for France, the Netherlands, United Kingdom of Great Britain and Northern Ireland (UK) (signed but not ratified) and United States of America (U.S.) with the International Atomic Energy Agency (IAEA). Because there are minimal or no nuclear material or activities in the affected territories of these States, these agreements include a small quantities protocol (SQP) that holds in abeyance a majority of the IAEA reporting and access requirements. *The Agreement between the U.S. and the IAEA for the Application of Safeguards in Connection with the Treaty for the Prohibition of Nuclear Weapons in Latin America* (US-IAEA Caribbean Territories Safeguards Agreement) entered into force on April 6, 1989, along with its SQP to the agreement. In 2005, the IAEA identified proliferation concerns associated with holding most of the requirements in abeyance through an SQP, and has since urged States with an original SQP to adopt the modified model SQP. To ensure consistent reporting and access under the new requirements of the modified SQP, the Nuclear Regulatory Commission (NRC) has initiated rulemaking to modify Title 10 of the *Code of Federal Regulations* (10 CFR) Part 75 “Safeguards on Nuclear Material-Implementation of US-IAEA Agreement.” Additionally, the NRC has developed a robust outreach plan with the affected licensees in Puerto Rico and the U.S. Virgin Islands in order to ensure effective and timely implementation, once the modified SQP enters into force. This paper will address the basis for adopting the modified SQP, new requirements of the modified SQP, along with outreach and implementation efforts, to date, with affected NRC licensees in the U.S. Caribbean Territories.

Keywords: SQP; IAEA; Tlatelolco; NRC

Introduction

On April 6, 1989, *The Agreement between the* United States of America (U.S.) and the International Atomic Energy Agency (IAEA) *for the Application of Safeguards in Connection with the Treaty for the Prohibition of Nuclear Weapons in Latin America* (US-IAEA Caribbean Territories Safeguards Agreement) entered into force, along with its original small quantities protocol (SQP). This non-nuclear weapons State (NNWS) style comprehensive safeguards agreement (CSA) was documented in IAEA Information Circular 366 (INFCIRC/366), pursuant to treaty obligations of the U.S. under Additional Protocol I to the Treaty for the Prohibition of Nuclear Weapons in Latin America and the Caribbean (the Tlatelolco Treaty). The U.S. agreed to accept International Atomic Energy Agency (IAEA) safeguards in U.S. territories in the zone of application of the Tlatelolco Treaty — the Commonwealth of Puerto Rico, the Virgin Islands of the United States, Navassa Island, Serranilla Bank, Baja Nuevo Bank (Petrel Island), and the U.S. Naval Station at Guantanamo Bay. In 2005, the IAEA identified proliferation concerns associated with holding most of the requirements in abeyance through an SQP, and has since urged States with an original SQP to adopt the amended model SQP.

The US-IAEA Caribbean Territories Safeguard Agreement, unlike the US-IAEA Safeguards Agreement (INFCIRC/288), is not a Voluntary Offer Agreement and does not have a national security exclusion currently exercised by the five nuclear weapons States (NWS); China, France, Russia,

United Kingdom and United States. The modified SQP (ModSQP) only applies to articles in Part II of the US-IAEA Caribbean Territories Agreement. All paragraphs in Part I of the Agreement are in effect for the territories in the zone of application of the Tlatelolco Treaty.

The US Nuclear Regulatory Commission (NRC) revised part 75 of title 10 of the *Code of Federal Regulations* (10 CFR), "Part 75—Safeguards on Nuclear Material—Implementation of Safeguards Agreements between the United States and the International Atomic Energy Agency," in order to meet the U.S. Government obligations under the Agreement. These revised regulations apply to any NRC applicant, licensee, certificate holder, or possessor of nuclear material (any source or special nuclear material) outside facilities in the U.S. Caribbean Territories to accommodate additional obligations created as a result of the ModSQP. The revised regulations ensure the U.S. provides timely, correct and complete reports and declarations to the IAEA, and respond to IAEA requests. IAEA access under an ad hoc or special inspection to the physical location of nuclear material outside facilities (NMOF) is provided for in the revision.

Nuclear Material Reporting

A number of changes were made to U.S. regulations related to implementation of IAEA safeguards under the ModSQP which removed abeyance of several of the Articles of INFCIRC/366; 31-37, 39, 47, 48, 58, 60, 66, 67, 69, 71-75, 81, 83-89, 93 and 94 (slight variation from model). Regulation changes to 10 CFR Part 75 explain terms of reference describing possessors of NMOF as holders of nuclear material that is not in a facility, and is customarily used in amounts of one effective kilogram or less. Physical location of each possessor of NMOF (para. 47 of INFCIRC/366) is described as a specific geographical point or area, where either nuclear material subject to the US-IAEA Caribbean Territories Safeguards Agreement resides or activity subject to this agreement occurs.

Currently, possessors of NMOF are scattered throughout Puerto Rico and hold very small amounts of nuclear material, well below the thresholds defined to maintain an SQP, as outlined in Article 35. In order to improve efficiency, the U.S. declarations and reports originating from these Possessors of NMOF are considered one location outside facility (LOF) material balance area (MBA). Quantities of nuclear material transferred into/out of the MBA are regarded as imports/exports and reported on an annual basis to the IAEA. The annual physical inventory within the MBA is a composite of all nuclear material present at key measurement points assigned to each Possessor of NMOF.

Initial inventory taking of nuclear material held by Possessors of NMOF was based on domestic reporting requirements of licensees to the NRC under either a specific license or general license for use of nuclear material. A physical inventory is verified by the NRC to confirm the presence of nuclear material and ensure the initial inventory declared to the IAEA was correct and complete. The initial declaration constitutes the majority of the work required under the modified SQP. Subsequent reporting to the IAEA is required when there is a loss or suspected loss of material; an inability to detect unauthorized removal and when there are transfers of material into and out of MBA. A report may be generated when at the request of the IAEA to clarify a previous report.

Subsidiary Arrangements (SA) between the U.S. and IAEA establish how IAEA safeguards will be implemented in the U.S. Caribbean Territories, including codes for reporting nuclear material chemical and physical form, container, and irradiated status that are used when reporting the MBA inventory and import/exports. Under the ModSQP, the obligation to have a SA as described in paragraph 37 of INFCIRC/366 is not held in abeyance. Reporting codes outlined in the SA are captured under a MBA specific cache in the U.S. national database for tracking nuclear material, the Nuclear Material Management and Safeguards System (NMMSS). Although a Facility Attachment (FA) is not required for LOF MBAs, NMMSS programming errors are minimized by using agreed upon KMPs and strata codes for nuclear material in the MBA.

Outreach to the Possessors of NMOF included instructions on how to maintain on-site records regarding all the nuclear material in their physical inventory, which is reported to the NRC via the NMMSS database. These records will be accessible for review by the NRC and IAEA inspectors as needed. Shipping records to States outside the U.S. Caribbean Territories and logs of movements of nuclear material within the U.S. Caribbean Territories will be maintained by the Possessors of NMOF and provided to NMMSS for annual reporting to the IAEA. Shipments and receipts between U.S.

territories and one of the 50 United States covered by the US-IAEA Safeguards Agreement (INFCIRC/288) are considered foreign shipments/receipts.

Communications

Formal communications associated with implementation of IAEA safeguards in the U.S. and its territories is routed through the U.S. Mission to International Organizations in Vienna (UNVIE). Having a single point for information flow minimizes inaccuracies and ensures a timely response when needed. UNVIE conveys communications to the appropriate U.S. Department or Agency in the U.S. Government for information purposes or resolution of an issue. This pathway of formal communication applies to all US-IAEA Agreements related to IAEA safeguards.

However, a Possessor of NMOF may request that information of particular sensitivity that it customarily holds in confidence not be transmitted physically to the IAEA. A Possessor of NMOF who makes this request shall, at the time the information is submitted, identify the pertinent document or part thereof and make a full statement of the reasons supporting the request. The NRC takes into account the obligation of the IAEA to take every precaution to protect commercial and industrial secrets and other confidential information coming to its knowledge in the implementation of the safeguards agreements.

Several committees work together to form the majority of the U.S State System of Accounting and Control of nuclear material. Responsibilities of these committees, chairs and their members are briefly described as:

- The Department of State (DOS) Chairs the Subcommittee on International Safeguards and Monitoring (SISM)[1] of the interagency IAEA Steering Committee, and, through the United States Mission to International Organizations in Vienna, serves as the official communications link between the IAEA and the U.S. Government (USG).
- The Nuclear Regulatory Commission is responsible for activities related to safeguards and Additional Protocol (AP) implementation that take place at NRC licensed locations, except at Department of Energy (DOE) and Department of Defense (DOD) locations. NRC chairs the interagency Sub-group on IAEA Safeguards in the United States (SISUS).[2]
- The Department of Defense (DOD) is responsible for activities related to safeguards or AP implementation at DOD owned, operated or leased locations.
- The Department of Energy (DOE) is responsible for activities related to safeguards and AP implementation at DOE owned, operated or leased locations. The DOE chairs the interagency Subgroup on Safeguards Technical Support (SSTS)[3].
- The Department of Commerce (DOC) is responsible for AP implementation activities that take place at locations outside the responsibility of DOE, DOD and NRC. Within the USG, DOC compiles the information required under Articles 3(b), 3(c), and 3(d) of the Additional Protocol as provided from a range of sources

Working level communications for specific technical issues usually takes place through a designated point of contact. Addressing licensee reporting issues and facilitating IAEA inspections at licensed NMOF physical locations in the U.S. Caribbean Territories is the responsibility of the NRC.

[1] SISM is a standing group of U.S. government officials tasked with developing and coordinating U.S. policy on all aspects of the IAEA's safeguards and monitoring programs.
[2] SISUS tasks include coordinating and monitoring activities of the relevant U.S. Agencies with regard to implementation of (1) the U.S.-IAEA safeguards agreement (INFCIRC/288), the Reporting Protocol, and the Additional Protocol thereto; (2) The U.S.-IAEA Caribbean Territories Safeguards Agreement (INFCIRC/366) and the Small Quantities Protocol thereto; (3) other U.S. commitments for reporting of nuclear exports and related safeguards information to the IAEA (e.g. INFCIRC/207 and the voluntary reporting scheme), and (4) additional U.S. undertakings as may be appropriate.
[3] SSTS is the U.S. government interagency committee responsible for oversight, direction, and coordination of the United States Support Program (USSP).

Terms and Conditions of the Modified SQP

The U.S. Caribbean Territories eligibility for maintaining the INFIRC/366 ModSQP will no longer be in effect when the U.S. takes a decision to authorize construction of a facility, or exceed the limits stated in Article 35 of the US-IAEA Caribbean Territories Safeguard Agreement:

1) One kilogram in total of special fissionable material, which may consist of one or more of the following:
   (i) Plutonium;
   (ii) Uranium with an enrichment of 0.2 (20%) and above, taken account of by multiplying its weight by its enrichment; and
   (iii) Uranium with an enrichment below 0.2 (20%) and above that of natural uranium, taken account of by multiplying its weight by five times the square of its enrichment;
2) Ten metric tons in total of natural uranium and depleted uranium with an enrichment above 0.005 (0.5%);
3) Twenty metric tons of depleted uranium with an enrichment of 0.005 (0.5%) or below; and
4) Twenty metric tons of thorium.

As a consequence, the safeguards procedures in Part II INFCIRC/366 that were previously held in abeyance cease to be held in abeyance. If this were to occur an exchange of letters between the U.S. and the IAEA would acknowledge that the ModSQP was rescinded and no longer operational, and the full terms of the Agreement would apply

Additionally, the U.S. may request exemptions from or termination of IAEA safeguards. Exemptions may be requested for nuclear material that is either less than one effective kilogram or used for non-nuclear purposes (such as counterweights in a crane, or shielding in a container).

Articles 33 - 36 describe what may be exempted or terminated from safeguards. Article 34 of the U.S.-IAEA Caribbean Territories Safeguards Agreement states the following material may be exempted from safeguards:

- Special fissionable material used in gram quantities or less as a sensing component in instruments;
- Nuclear material when it is used in non-nuclear activities, but is considered recoverable (in contrast to material deemed practically irrecoverable); and
- Plutonium with an isotopic concentration of Pu-238 exceeding 80%

Termination of safeguards as described in Article 33 of the U.S.-IAEA Caribbean Territories Safeguards Agreement set forth in Article 11: “Safeguards shall terminate on nuclear material upon determination by the Agency that the material has been consumed, or has been diluted in such a way that it is no longer usable for any nuclear activity relevant from the point of view of safeguards, or has become practically irrecoverable.” Safeguards may also be terminated on material used in non-nuclear activities, “such as in the production of alloys or ceramics”[4] and on material transferred out of the Territories.

Outreach to U.S. NRC Licensees

Based on a detailed review of current licensing documents, the NRC developed a robust outreach plan with our licensees in Puerto Rico and the U.S. Virgin Islands, the only known U.S. Caribbean Territories to possess nuclear material.

[4] Article 33 also references Article 13 of the U.S.-IAEA Caribbean Territories Safeguards Agreement only addresses use in non-*nuclear* activities, such as the production of alloys or ceramics. This Article is identical to Article 13 of the VOA. Not included in either the U.S.-IAEA Caribbean Territories Safeguards Agreement or the VOA is the article discussing termination of safeguards used in non-*peaceful* activities (Article 14 of INFCIRC/153). This article states that if material is withdrawn from safeguards it will only be used in a peaceful nuclear activity and that it will not be used for the production of nuclear weapons or other nuclear explosive devices.

The first outreach trip in 2016 included NRC staff responsible for safeguards implementation in the U.S., and regional NRC inspectors who had inspection oversight of the U.S. Caribbean Territories. After documenting the quantities and types of nuclear material present during the site visit, staff provided guidance on the upcoming reporting and IAEA inspection access requirements. NRC staff also provided the IAEA Service Series 22 (Safeguards Implementation Guide for States with Small Quantities Protocols). Staff found it especially helpful to provide the Service Series in English and Spanish (the native language used in Puerto Rico). Of vital importance when presenting this new information was that licensees in the U.S. Caribbean Territories had little knowledge of IAEA international safeguards. To account for this, the NRC created a high-level summary guide (in English and Spanish), to explain the concept of the modified SQP and the requirements that must be met by NRC licensees. This guide was also shared with the IAEA.

Based on the results of the first outreach visit, there are currently nine NRC licensees (all possessing only source material) that must comply with the new requirements of the modified SQP. Currently, there are no NRC licensees in the U.S. Caribbean Territories possessing special nuclear material. The identified source material consists of depleted uranium used for medical and industrial radiography shielding and small laboratory-scale samples (such as uranyl acetate and uranyl nitrate). The laboratory-scale samples were typically not in use by the licensee, and pending future disposal.

NRC staff conducted a second outreach visit in 2017 to provide more in-depth instruction on how to fill out domestic nuclear material accountancy forms, which are already used by licensees in the U.S. Special instructions were provided to licensees that frequently ship and receive nuclear material, and will need to fill out an Inventory Change Report from time-to-time. All accountancy forms will be submitted by licensees to the U.S. system of accounting for reconciliation by NMMSS.

Conclusion

The Agreement between the U.S. and the IAEA for the Application of Safeguards in Connection with the Treaty for the Prohibition of Nuclear Weapons in Latin America entered into force on April 6, 1989. Pursuant to Additional Protocol I to the Treaty of Tlatelolco and the Safeguards Agreement signed by the U.S. with the IAEA a modified small quantities protocol was adopted due to minimal or no nuclear material or activities occurring in the affected U. S. Territories. The MSQP holds in abeyance a majority of the IAEA reporting and access requirements. To ensure consistent reporting and access under the requirements of the MSQP, the Nuclear Regulatory Commission (NRC) has initiated rulemaking to modify Title 10 of the *Code of Federal Regulations* (10 CFR) Part 75 “Safeguards on Nuclear Material-Implementation of US-IAEA Agreement.” Additionally, the NRC has developed a robust outreach plan with the affected licensees in Puerto Rico and the U.S. Virgin Islands in order to ensure effective and timely implementation, once the modified SQP enters into force.

Session 04

Geoscientific Methods

Site Monitoring with Synthetic Aperture Radar Satellite Imagery

Morton J. Canty[1] and Allan A. Nielsen[2]

1. Institute for Energy and Climate Research, IEK-6,
Jülich Research Center, D-52425 Jülich, Germany

2. DTU Compute, Department of Applied Mathematics and Computer Science,
Technical University of Denmark, DK-2800 Kgs. Lyngby, Denmark

Abstract:

Based on a statistical test for the equality of polarimetric matrices following the complex Wishart distribution and a factorization of the test statistic, change analysis in a time series of multi-look polarimetric SAR data in variance-covariance or polarimetric matrix representation is carried out. The test statistic and its factorization detect if and when change(s) occur. This paper provides a short explanation of the method, describes available software, and gives examples of potential applications for site monitoring.

Keywords: multi-temporal SAR imagery, polarimetry, change detection, site monitoring

1. Introduction

Space-borne synthetic aperture radar (SAR) sensors with spatial resolutions of the order of 5-20 meters, revisit times of the order of weeks and complete independence from solar illumination and cloud cover offer an attractive potential source of information remote for site-monitoring. Additionally, many of these platforms collect polarimetric data, increasing their capability to discriminate surface features. Satellite platforms with these capabilities include the Japanese ALOS-2, the Canadian Radarsat-2, the Italian COSMO-Skymed, the German TerraSAR-X, and the European Sentinel-1.

A characteristic task in site monitoring under some civil, military or environmental control regime involves the automatic registration of significant changes which might involve unreported or clandestine activity or environmentally significant events. In [1] change detection in a time series of polarimetric SAR data is described involving a so-called *omnibus test statistic* (and its factorization) for the equality of polarimetric matrices following the complex Wishart distribution. The procedure is capable of determining, on a per-pixel basis, if and when a change at any prescribed significance level has occurred in a time series of SAR images. Single polarization (intensity data), dual polarization (for example vertically polarized emission, vertical and horizontal reception) and full quad polarization (all four combinations of vertical and horizontal emission/reception) can be analyzed.

Since the omnibus method can detect not only if changes occur but also, within the temporal resolution of an image sequence, when they occur, long time series of frequent acquisitions over relevant sites are of especial interest. One convenient source of such data is the Google Earth Engine (GEE) [2] which ingests Sentinel-1a and Sentinel-1b data as soon as they are made available by the European Space Agency (ESA) and provides a very convenient application programming interface (API) for accessing and processing the data.

In the Section 2 below we provide a brief, qualitative description of the omnibus method. In Section 3 the available software tools are outlined and in Section 4 some examples involving Sentinel-1 data are presented. The paper concludes in Section 5 with an outlook to future developments and possibilities.

2. The omnibus method

The term “multi-look” in SAR imagery refers to the number of independent observations of a surface pixel area that have been averaged in order to reduce the effect of *speckle*, a noise-like consequence of the coherent nature of the radar signal emitted from the sensor. The observed signals are multivariate complex Gaussian distributed and their variance-covariance representations, when multiplied by the number of looks, are correspondingly complex Wishart distributed. This distribution is the multivariate complex analogue of the well-known chi-square distribution for the variance of Gaussian-distributed scalar observations.

The complex Wishart distribution is completely determined by a singe parameter $\sum$, the covariance matrix. Given two observations of the same area at different times, one can set up a so-called *hypothesis test* in order to decide whether or not a change has occurred between the two acquisitions. The *null hypothesis* is that $\sum_1 = \sum_2$, i.e., the two observations were sampled from the same distribution and no change has occurred, and the *alternative hypothesis* is $\sum_1 \neq \sum_2$, in other words, there was a change. Since the distributions are known, a *likelihood ratio test* can be formulated which allows one to decide to a desired degree of significance whether or not to reject the null hypothesis. Acceptance or rejection is based on the so-called p-value, which in turn may be derived from the (approximately known) distribution of the likelihood ratio test statistic. In the case of $k > 2$ observations this procedure can be generalized to test a null hypothesis that all of the k pixels are characterized by the same $\sum$, against the alternative that at least one of the $\sum_i$, $I = 1...k$, are different, i.e., that at least one change has taken place. Furthermore the omnibus test procedure can be factored into a sequence of tests involving hypotheses of the form:

$\sum_1 = \sum_2$ against $\sum_1 \neq \sum_2$
$\sum_1 = \sum_2 = \sum_3$ against $\sum_1 = \sum_2 \neq \sum_3$
and so forth. The tests are statistically independent under the null hypothesis. In the event of rejection of the null hypothesis at some point in the test sequence, the procedure is restarted from that point, so that multiple changes within the time series can be identified.

3. Software

The authors provide access to Matlab [2] and Python [3] code which is suitable for the analysis of multi-temporal polarimetric SAR imagery with the sequential omnibus algorithm. Data from any of the aforementioned platforms can be processed. For users with access to the Google Earth Engine [4] a web-based application is also available [5] with which long time series of Sentinel-1 images can be accessed from a browser. The data can either be downloaded for processing off-line with the Matlab or Python code, or evaluated directly on the Google servers. In the latter case the algorithm is programmed with the Earth Engine Python API.

3. Examples

The following examples are based exclusively on Sentinel-1 images obtained from the GEE database. The data, acquired in instrument Interferometric Wide Swath (IW) mode, are S1 Ground Range Detected (GRD) scenes, processed using the Sentinel-1 Toolbox [6] to generate a calibrated, ortho-corrected product. This processing includes thermal noise removal, radiometric calibration, and terrain correction using Shuttle Radar Topography Mission 30 m (SRTM 30) data. The change detection analyses were performed on-line with the GEE Python API on time series of 5-look, dual polarimetry diagonal only (VV, VH) images with a spatial resolution of 20m. The GEE software described in [5] allows the user to search anywhere on the globe for time series of Sentinel-1 SAR images, clipping the data to the time period and spatial region of interest, the desired viewing angle (relative orbit number, ascending or descending node) and polarization (dual or single).

Figures 1 and 2 show a change frequency map derived from a 24-image time series over the NATO air base at Geilenkirchen, Germany. The frequent movements of aircraft (in this case often AWACS training machines) to and from their parking positions are clearly evident.

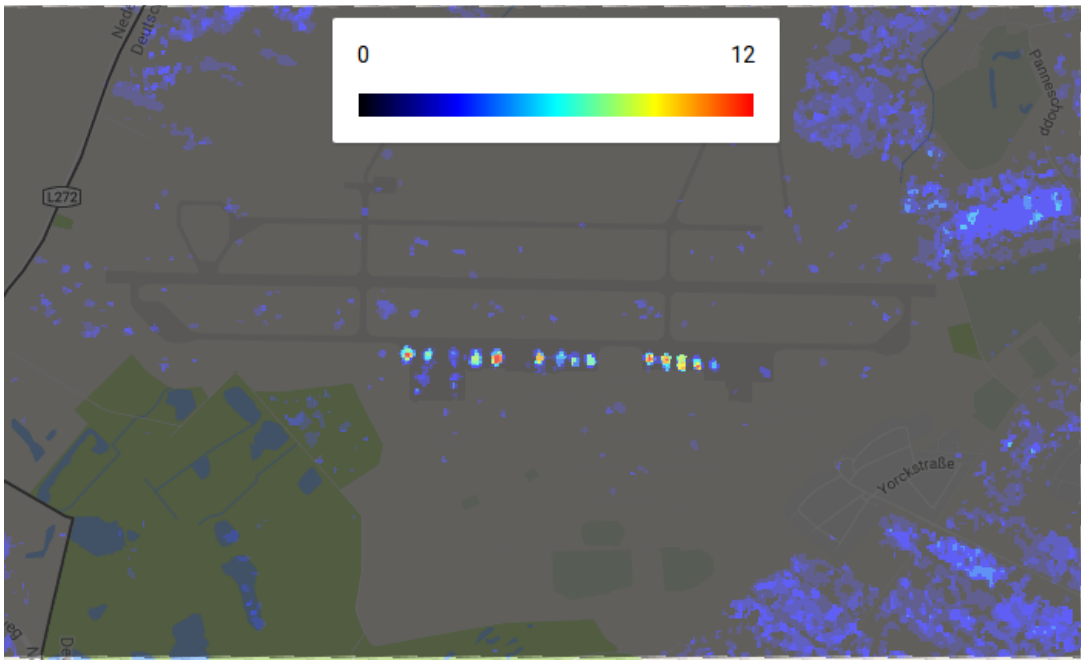

Figure 1. Change frequency map over the NATO Airbase at Geilenkirchen, Germany. The data were derived from a time series of 24 Sentinel-1 acquisitions, beginning Feb. 3, 2016, ending Oct. 10, 2016. The map is overlain onto a Google Maps background.

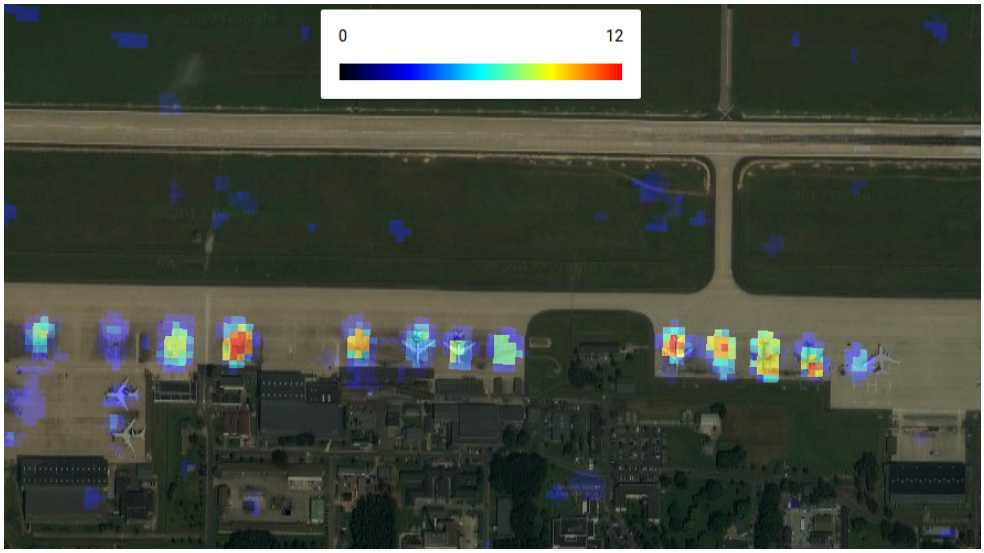

Figure 2. Frequency map as in Figure 1, now overlain onto a Google Earth background.

Figure 3 shows an example of flood monitoring, tracing the dangerous filling of the Oroville, California reservoir in late 2016, early 2017, which threatened to burst the retaining dam.

Figures 4 and 5 show two seaports on the Libyan coast, Tripolis and Benghazi, respectively. In the former one sees considerable shipping activity, whereas in the latter none at all.

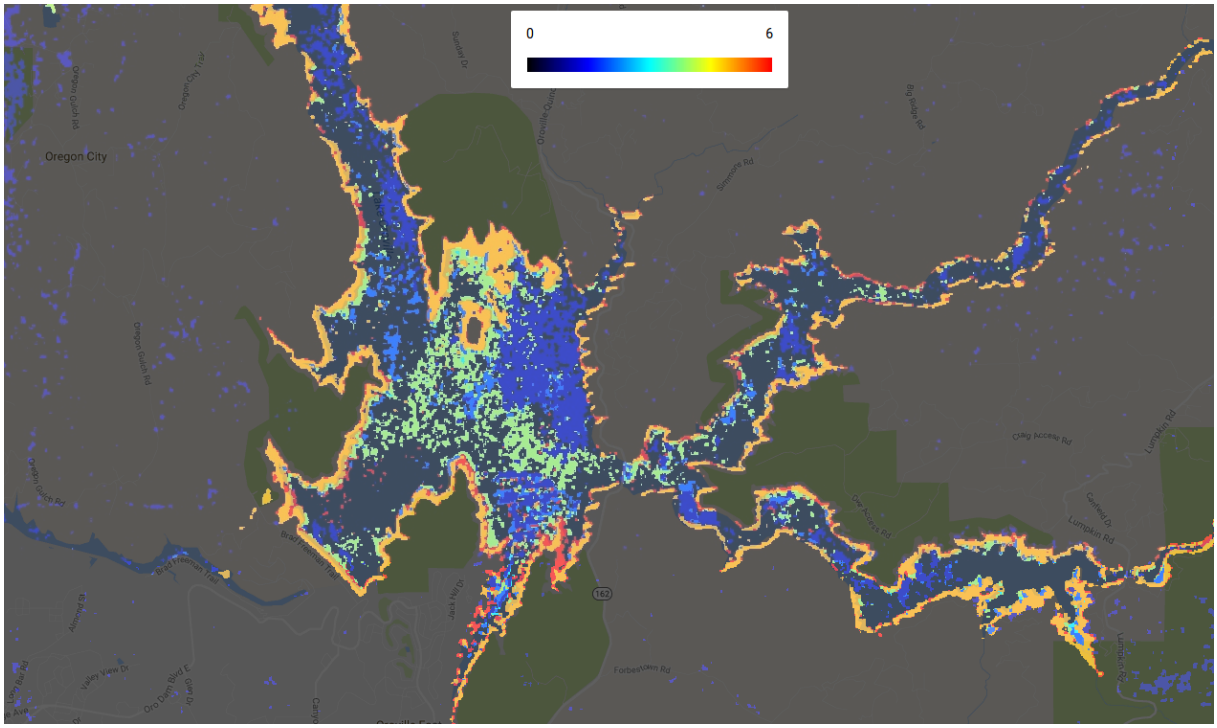

Figure 3. Change map showing the time of the first significant change in the Oroville, California reservoir over a time sequence of seven Sentinel-1 images beginning March 14, 2016 and ending Jan. 26, 2017: blue indicates change in the first, red in the last (sixth) interval.

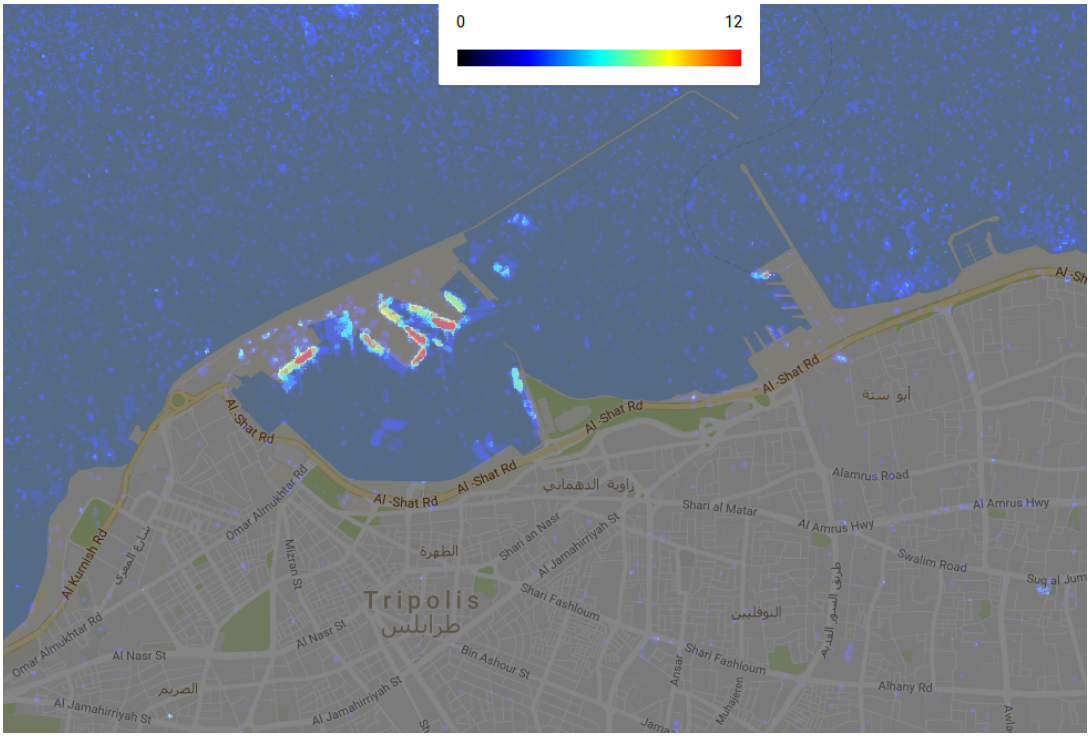

Figure 4. Change frequency map of the port of Tripolis, Libya. Time series of 28 images beginning Feb. 2, 2016 and ending Nov. 30, 2016.

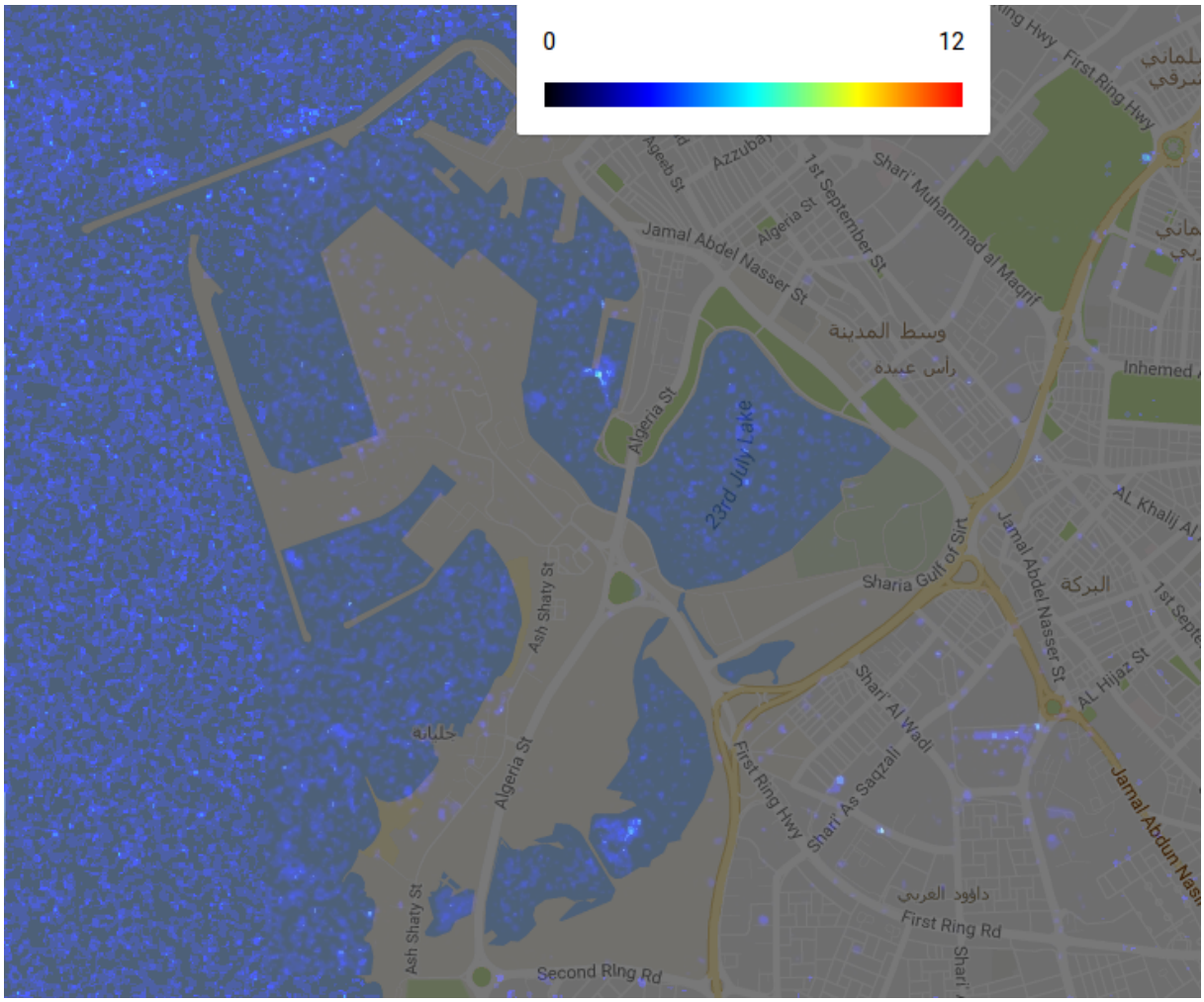

Figure 5. Change frequency map for the port of Benghazi for the same time period as Figure 4.

4. Conclusion

While the GEE platform has obvious advantages for historical or on-going site monitoring, there are currently some disadvantages: First, the complex off-diagonal elements of the polarimetric matrix are not available, implying some loss in discrimination. Second, the stored pixel values in the GEE database are clamped to the first and 99th percentile to preserve the dynamic range against anomalous outliers, and quantized to 16 bits. The resulting saturation of the brightest pixels tends to be concentrated in built-up areas or to be associated with other man-made objects, further reducing sensitivity. Finally, the ground resolution of 20m restricts the applicability of site monitoring to detection of correspondingly large changes. The examples chosen reflect this restriction in particular.

Nevertheless, we have demonstrated, making use a sound, statistically-based algorithm, that change detection for site monitoring with archived SAR data is both feasible and convenient.

References

[1] K. Conradsen, A. A. Nielsen, and H. Skriver, Determining the points of change in time series of polarimetric SAR data, *IEEE Transactions on Geoscience and Remote Sensing*, vol. 54, no. 5, pp. 3007--3024, May 2016, http://www.imm.dtu.dk/pubdb/p.php?6825.

[2] http://www.imm.dtu.dk/~alan/software.html

[3] http://mortcanty.github.io/SARDocker/

[4] Google Earth Engine Team, Google Earth Engine: A planetary-scale geo-spatial analysis platform, https://earthengine.google.com

[5] https://github.com/mortcanty/earthengine

[6] https://sentinel.esa.int/web/sentinel/toolboxes/sentinel-1

High Resolution 3D Earth Observation Data Analysis for Safeguards Activities

Pablo d'Angelo[a], Cristian Rossi[a], Joshua Rutkowski[b], Michael Eineder[a],

[a] German Aerospace Research Center, Remote Sensing Technology Institute
[b] Forschungszentrum Jülich

Abstract:

This paper provides an overview of the investigations performed at DLR with respect to the application of high resolution SAR and optical data for 3D analysis in the context of Safeguards. TerraSAR data acquisition was performed, and various ways to visualize and analyze stacks of radar images were evaluated. Interferometric coherence map interpretation allows the detection of traffic on dirt roads. The applicability of lower resolution, but freely available Sentinel-1 data was evaluated. For optical data, spaceborne video is becoming available. SkySat data is evaluated for geometric accuracy and it use for extraction of digital elevation models. Furthermore, digital elevation models were generated from 12 stereo datasets over Yongbyon and used for analysis tasks such as building height estimation. Height accuracy and completeness strongly depend on the stereo convergence, and off-nadir angles of the imagery.

Keywords*:* Remote Sensing; Radar; Optical; Safeguards

1. Introduction

The primary remote sensing datasets used for safeguards purposes are optical satellite images with a resolution from 0.5 to 1 m. Most information is obtained by visual analysis of the scenes by expert image analysts. However, optical data depends on good weather conditions and is typically acquired only in the late morning. Synthetic aperture radar (SAR) data is a complementary data source, as it provides weather independent datasets, but its unintuitive depiction of complex industrial facilities hampers visual interpretation of the data.

During a multi-year study, DLR has acquired extensive stacks of very high resolution TerraSAR-X high-resolution spotlight images over the Forschungszentrum Jülich as an example site with complex, industrial structure and adjacent mining areas. [1] The goal of the study was to better understand SAR imagery and to develop methodologies for exploitation of SAR imagery in context of safeguards relevant applications, focussing on applications such as visual interpretation, determination of 3D information such as building heights or volume change in mines and waste dumps. Additionally generation of digital surface models (DSM) were evaluated [2]. New work in this paper includes the evaluation of freely available, lower resolution Sentinel-1 SAR data, and evaluation of optical spaceborne video from the SkySat satellites, as well as a study on the impacts of various stereo image acquisition parameters on the DSM quality and interpretability.

2. SAR

Synthetic Aperture Radar (SAR) is a powerful instrument in the monitoring of structures, displacements and topography due to its intrinsic ability to be independent of solar illumination and local weather. Many applications have been exploited in our previous studies [1, 2]. They can be grouped in single-image and multi-image applications.

Single-image applications involve low-level operations such as the exploration of the SAR amplitude to inspect content of the acquisition (e.g. the number of buildings) or high-level operations such as the

measure of the building heights (e.g. from shadowing [2]). Image resolution is a fundamental parameter for these applications. For inspection at the building level, it is obvious that the higher resolution the better. For this reason, X-band imagery at the sub-meter resolution from missions like the TerraSAR-X [3] or the Cosmo-SkyMed one should be preferred over free medium-resolution (~10m) imagery from Sentinel-1. A comparison between a single TerraSAR-X High-Resolution Spotlight amplitude image over Berlin (Germany) and a mean of all the available Sentinel-1 amplitudes is shown in Figure 1. From this figure it can be appreciated how the quantity of information is much higher for the single high-res data.

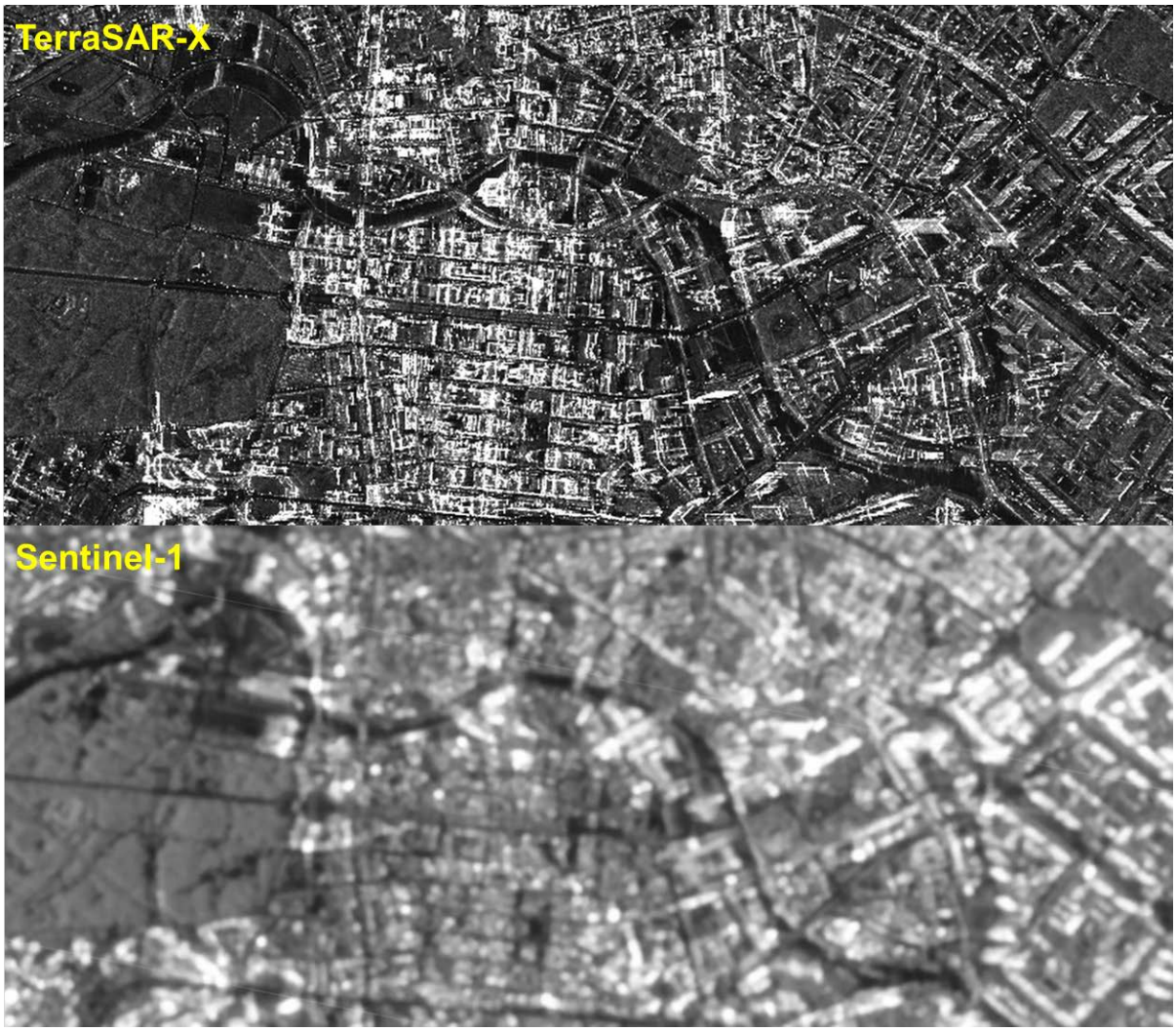

Figure 1: Comparison between a single sub-meter resolution TerraSAR-X image and an average of all the available decameter resolution Sentinel-1 images over Berlin, Germany.

Multiple-image image applications can be further categorized in two branches: interferometric and tomographic applications. These applications can be seen in the temporal domain, e.g. to characterize changes of any kind, such as topographical changes, land cover changes and displacements.

Interferometric applications require two images. By properly combining the complex images, products such as the interferometric coherence, the differential phase and eventually (in case of bistatic configuration) the digital elevation model can be derived with specialized software. The interferometric coherence can be seen as an instrument to detect temporal changes between the two images. An example in in Figure 2, where a network of dirt used roads can be recognized in black color [2].

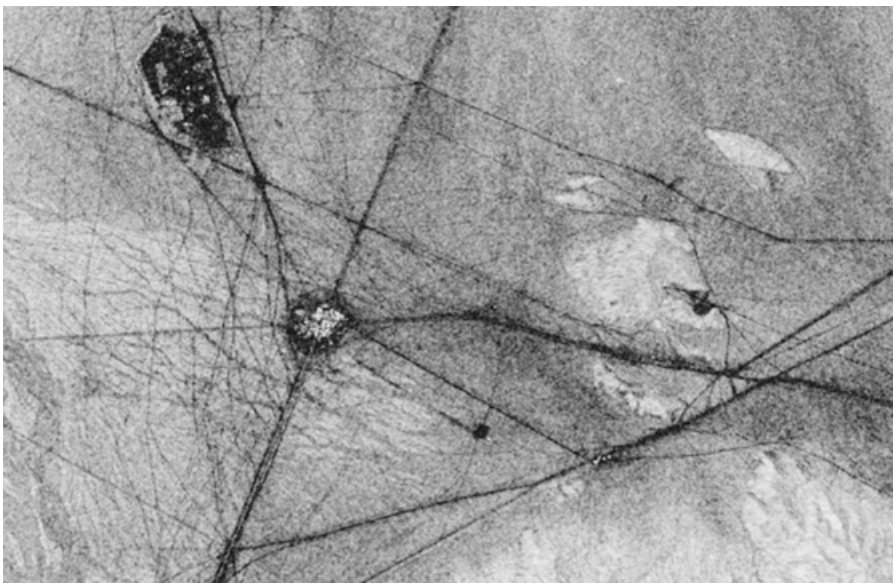

Figure 2. Interferometric coherence (11 days) over Fort Irwin (USA).

The differential phase shows instead the terrain deformations (e.g. deformations, fault slips, subsidence and etc.) occurred within the temporal frame of the two images. Typical examples are the detection of displacements from pre and post-earthquakes scenarios and subsidence generated by mining activities (e.g. the detection of illegal mining).

Digital elevation models (DEMs) at medium-high resolution (~10m) can be generated with TanDEM-X data, currently the only SAR interferometer in space [3, 4, 5]. While single DEMs can be of interest for a direct measurement of the elevation of the area of interest, multiple-DEMs show a very direct measure of topographical changes and can be used for instance in measuring the volume of excavations or material accumulations [2].

When a stack of images is acquired over a specific area under test, then advanced techniques like the Persistent Scatterer Interferometric (PSI) technique can be exploited to derive very precise (mm-level) displacement values for selected point on ground. An exemplary result of deformation map generated with PSI is shown in Figure 3. These maps are powerful tools for the evaluation of local subsidence or local uplift and nowadays are standard products of SAR service providers and research centres like DLR.

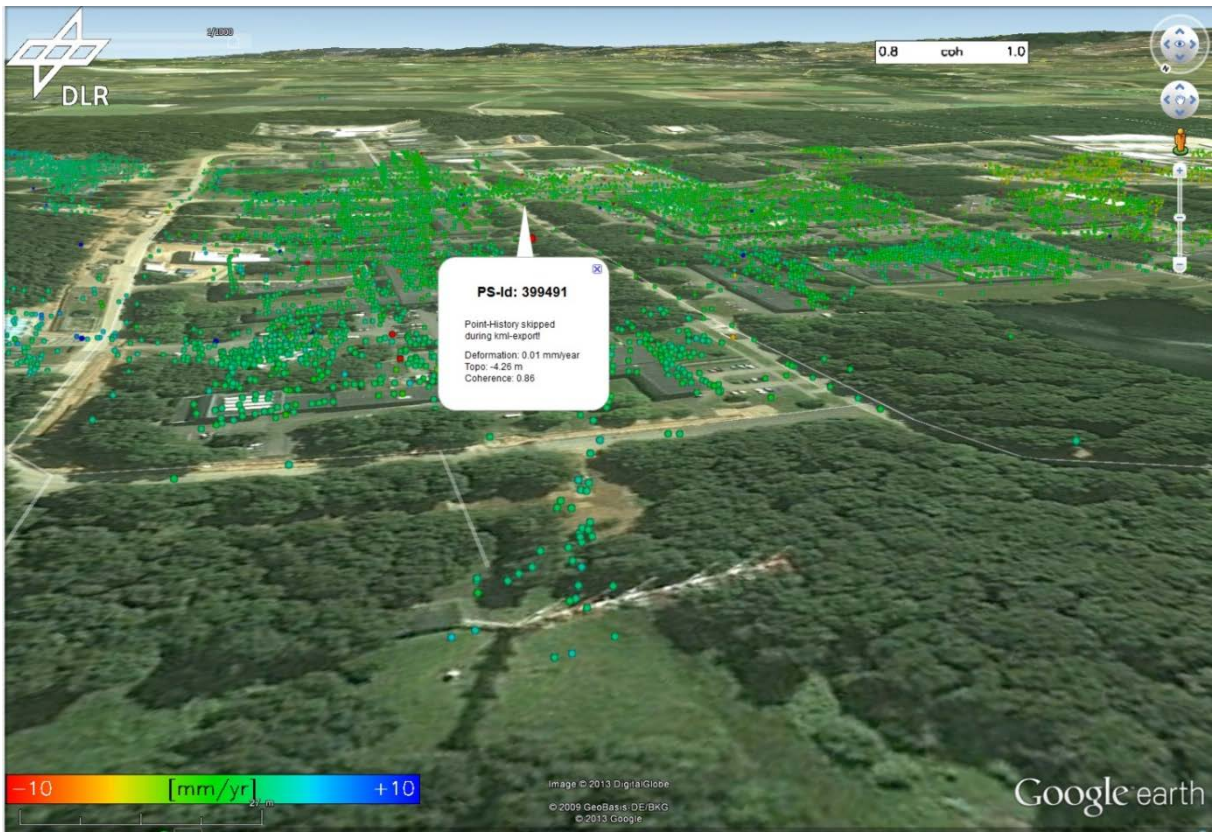

Figure 3: PSI deformation map over FZ Jülich using the descending HRS TerraSAR-X stack.

All these techniques have been exploited through the different phases of the collaboration between DLR and IAEA, providing to the IAEA the knowledge about the potential of SAR data for safeguards activities and set of routines finalized to the exploitation of SAR imagery in this context.

3. Optical images

In addition to radar imagery, optical images are widely employed for monitoring of safeguards relevant sides. Most safeguards relevant information can be derived with visual interpretation by image analysts. Additionally, advanced image matching techniques, together with sub-meter resolution stereo imagery can provide high resolution digital surface models (DSM) that resolve details of industrial buildings and provide a good base for monitoring of changes to buildings or excavation, dumping and mining activities.

In addition to satellites acquiring static images, a few systems for spaceborne videos exist, most notably the SkySat Satellites [6].

3.1. Spaceborne Video

The SkySat satellites of Skybox Imaging are a very interesting platform, as they provide new data with a resolution of 1 m or better, and can acquire both mapping products and Full HD video sequences of up to 90 seconds in length. The space segment is simplified as much as possible, and tasks usually executed on board of the satellites are performed by the ground station software. This reduces complexity of the space segment and allows construction of smaller and less expensive satellites and possibly the creation of large constellations with high revisit capabilities.

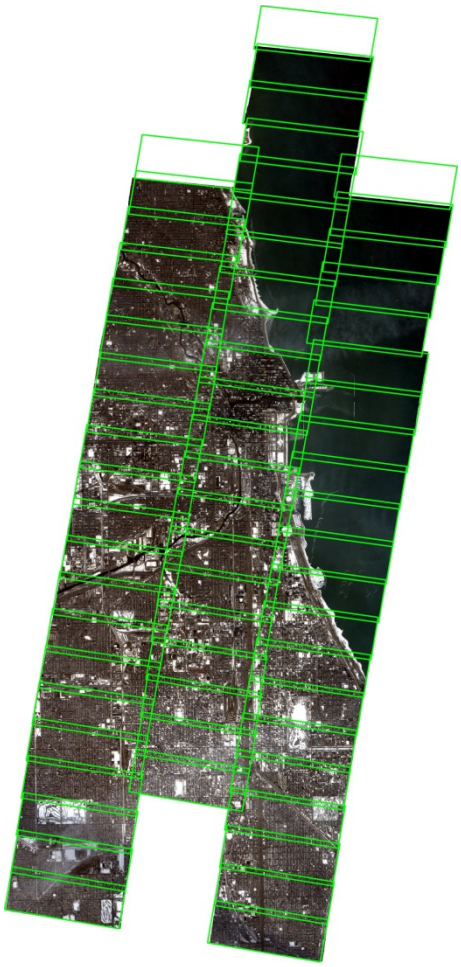

a) SkySat images

b) SkySat pansharpend image

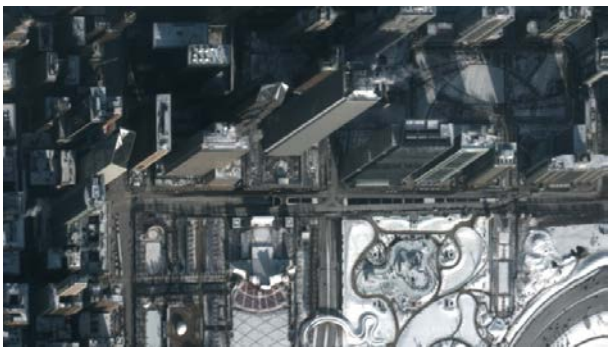

c) Worldview-3 multispectral image

d) NAIP reference image

Figure 4: Skysat Chicago acquisition and comparison to WorldView-3 and reference imagery used for evaluation of geolocation performance.

Most optical satellites use a single line of detectors in push-broom mode, which captures image rows with a high frequency. A two dimensional image is thus generated as the satellite rotates, and the imaged line scans across the earth's surface. To archive high image quality, a stable satellite platform is required, increasing cost of the satellites. In contrast, the SkySat satellites use conventional 2D frame sensors, similar to the ones used in ordinary digital cameras, and capture a full 2D image at a time, avoiding the requirement for a highly stable platform. To compensate for the lower image quality of each single image, multiple images with high overlap are captured and merged on the ground, resulting in a final image with lower noise and slightly improved image resolution. The use of frame sensors also enables capturing of short video sequences as the satellite passes over a region of interest.

3.2. SkySat Image evaluation

Both the SkyBox still image and the video products were evaluated. The still image product resembles classical VHR (very high resolution) satellite imagery, with a swath width of 8km and a resolution of 90 cm at nadir, with panchromatic image and 4 channel multi-spectral image covering the blue, green, red and near infrared bands. Image coverage, resolution and quality are thus roughly comparable to data from the IKONOS satellite. When “Still Imagery” SkySat products are used, the user receives a set of individual image frames. These will need to be oriented, orthorectified and merged into a mosaic covering the whole area. Figure 4 shows the individual image footprints of a SkySat-2 acquisition covering Chicago. As the satellite uses lower quality attitude determination systems compared to the much larger push-broom satellites, absolute accuracy of direct georeferencing is in the order of 100m.

To archive a good absolute georeferenced accuracy, a bundle block adjustment using many GCPs (ground control points) needs to be performed [7], at least when using typical COTS software, which does not understand the specific camera system used on board of the SkySat satellites. An absolute accuracy of 5 m was archived when using 51 GCP for orientation of the Chicago scene, cf. Figure 4. A WorldView-3 scene acquired 23 days before the SkySat-2 scene required only 2 GCPs for high quality orthorectification. It is thus advisable to directly order orthorectified SkySat products, even if this later leads to slightly increased co-registration errors when comparing acquisitions from different satellites and acquisition times.

Video sequences of the Yongbyon site and various other sites were available. Skysat can provide panchromatic video frames with a size of 2560x1080 pixels with 30 frames per second for a maximum time of 90 seconds.

The videos of the Yongbyon site showed little activity, so its main value are images taken from different viewing angles, which can be used for generation of DEMs (digital elevation models), and derivation of 3D information of the scene. If everything works as planned, 13 second generation SkySat satellites will be in orbit by the end of 2017, providing revisit rates of up to 3 times per day, which might improve the value of video for surveillance applications. During this work, the videos where used for DSM generation only.

3.3. DSM Generation

The algorithms used for DSM generation were described in the prior work [2]. Good results in industrial areas can be archived with stereo pairs with a convergence angle between 15 to 25 degrees, otherwise too many occlusions would occur. This will result in incomplete height measurements in dense building areas. For best quality, tri-stereo acquisitions with a relative convergence angle of around 15 degrees are recommended [8]. The scenes should be acquired in the same satellite pass, otherwise temporal and illumination changes can lead to incomplete DSMs.

In practise, these constraints can often not be fulfilled, leading to DSMs with many occluded areas, no-data zones and an increased amount of outliers. From generic site monitoring, mono acquisitions with larger time differences are usually available, as stereo dataset incur extra costs. Several DSM generation experiments with using images acquired at site monitoring at different dates mostly yielded height models of insufficient quality. For dense matching it is thus usually required to use images acquired on the same date, or at least temporally very close images.

To provide image analysts with a better understanding of the DSM quality to be expected with varying stereo configurations, 12 stereo pairs over the Yongbyon site were processed and the resulting DSMs were compared. Data processing was performed using the tools available to IAEA. Figure 5 shows the datasets used in this comparison.

Date	Sensor
2006-02-23	Ikonos Stereo
2009-09-22	WV-1 Stereo
2011-01-07	Ikonos Stereo
2011-05-02	Ikonos Stereo
2012-01-26	WV-2 Stereo
2012-10-11/17	GE-1 across track
2013-04-24	Pleiades Stereo
2013-06-14	Pleiades Stereo
2013-06-19	WV-1 Stereo
2013-07-29	Pleiades Stereo
2013-11-01	GE-1 Stereo
2014-08-07	SkySat-1 Video

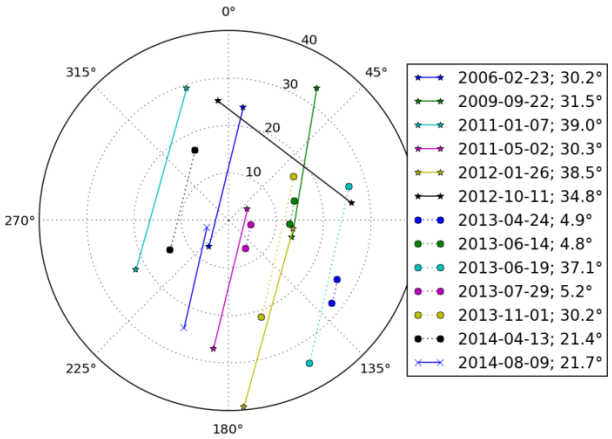

Figure 5: Stereo datasets over Yongbyon. The skyplot on the right shows the satellites azimuth and elevation angles of each stereo pair. The legend also includes the stereo convergence angles.

The Worldview-1 Stereo pair from 2009-09-22 was processed first, and the resulting Ortho image and DSM were used as reference for the remaining stereo pairs. The images of each pair were acquired on the same orbit, except for the GeoEye-1 images from 11th and 17th of October 2012. For the SkySat-1 video, using the first and last frame only resulted in noisy height values. Instead, the frames were temporally subsampled to 1 second, and all possible pairs with a temporal distance of 15 seconds or more were matched. The resulting 120 DSMs were merged using a pixel-wise median.

Results for all datasets are shown in Figure 6. It can be noticed that stereo pairs with a larger convergence angle are less complete due to an increased amount of occlusions. A good example for this is the 2012-01-26 scene, which has a 38° stereo convergence angle, and the second image was acquired almost 40° off nadir. The large convergence angle hinders dense image matching, and the large of nadir angle additionally leads to large occlusions on the northern side of buildings. The same effect is visible in the 2013-04-24, 2013-06-19 and 2013-11-01 scenes.

It is interesting to note that all images acquired by Ikonos, GeoEye and WorldView satellites had large stereo convergence angles, with a minimum angle of 30°, whereas the Pleiades acquisition were all captured with extremely small convergence angles of less than 6°. There is no technical reason for this, except that the default tasking of DigitalGlobe seems to favour convergence angles > 30°. This leads to high elevation accuracy in flat areas without steep objects, but complicates dense image matching, and leads to larger voids in the produced DSMs. In contrast the Pleiades angle is extremely small, as a result, dense image matching can easily find correspondences for almost all pixels, leading to a high completeness. The height accuracy suffers from this low angle, thus the shaded DSMs look quite noisy.

The largest no-data areas are present the DSM generated from images acquired on different days. The time difference of 6 days for the 2012-10-11/17 scenes still allowed successful matching of the buildings but resulted in voids in ground areas that changed between the image acquisitions, for example, the construction site, shadow areas and some vegetated areas. However it still contains useful information for manual or semi-automatic interpretation, for example the building heights can still be measured. While such data is not useable for most applications, which usually require gapless data, it is still useful for careful evaluated by image analysts. For example, building heights can still be determined.

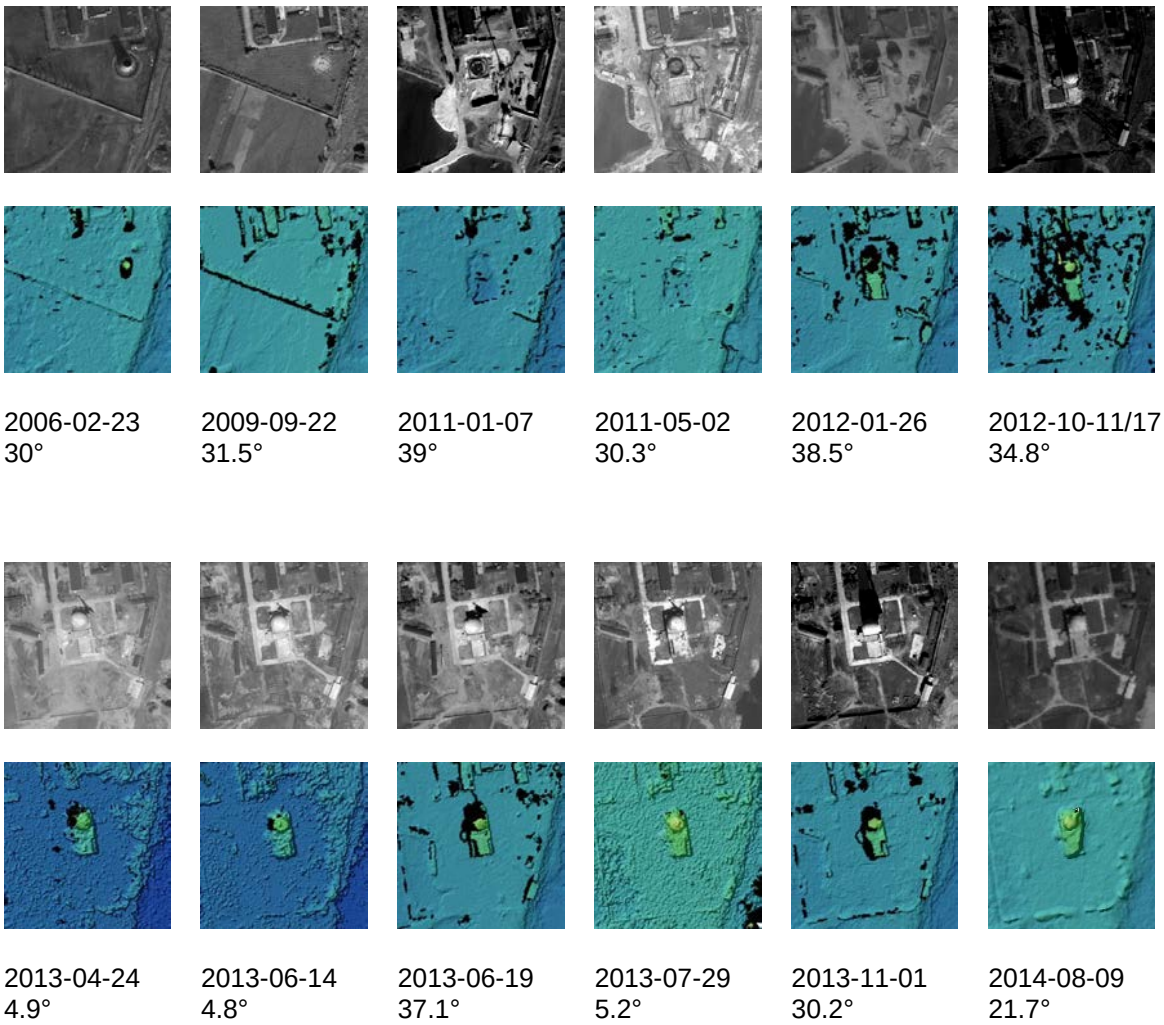

Figure 6. Images and DSMs of the light-water reactor at Yongbyon, from different stereo pairs. For each DSM, the acquisition date and the stereo convergence angle are given. No height could be determined for areas marked in black.

4. Summary and conclusion

The study has shown that valuable information can be derived from SAR images, although some techniques are not readily applicable without large stacks of data, such as persistent scatterer analysis. This large amount of data is often not available, as acquisition of stacks needs to be performed over a long time period, and results in large data costs.

Therefore techniques that require only one or at most two SAR images are most relevant in a practical scenario. High resolution SAR imagery is important, observation of industrial complexes with free, but lower resolution Sentinel-1 showed only limited success.

Evaluation of the SkySat satellites showed that video acquisitions need to be performed at the right time, often only limited or no action is visible in the short acquisitions. For still imagery, it is preferable to order ortho-rectified imagery, as properly ortho-rectifying the SkySat still imagery product is a challenge with RPC based COTS software. The raw video product has been successfully used for generation of digital elevation models.

An evalution of 12 stereo acquisitions over Yongbyon showed that stereo convergence angle is the most important factor for DSMs of industrial areas. The standard DigitalGlobe stereo convergence angle of 30° or more leads to large occlusions and increased mismatches when applying automatic dense image matching. The resulting DSMs still contain valuable height information about buildings,

but need to be interpreted carefully, increasing image analysis effort. Effort which would not be required when using smaller stereo convergence angles of 15 to 20 degrees. On the other hand, very small stereo convergence angles as seen in the Pleiades products used in this study lead to increased height noise. Thus it is important to specify the desired stereo convergence angle range when tasking stereo observations of complex, built-up areas.

5. Acknowledgements

This paper was prepared as an account of work sponsored by the Government of the Federal Republic of Germany within the Joint Programme on the Technical Development and Further Improvement of IAEA Safeguards between the Federal Republic of Germany and the IAEA under GER SP Task JNT D1657. We thank Skybox Imaging and European Space Imaging for providing imagery used during this study.

6. References

[1] d'Angelo, P., Rossi, C., Minet, C., Eineder M., Flory, M., Niemeyer, I.; *High Resolution 3D Earth Observation Data Analysis for Safeguards Activities*; Proc: Symposium on International Safeguards, Vienna, 20-24 Oct. 2014

[2] Minet, C., Eineder M., Rezniczek A., Niemeyer I.; *High Resolution Radar Satellite Imagery Analysis for Safeguards Applications*; ESARDA BULLETIN, No. 46 (2011).

[3] Krieger G., et al.; *TanDEM-X: a satellite formation for high-resolution SAR interferometry*, IEEE TGRS; 2007.

[4] Rossi C., Gernhardt S.; *Urban DEM generation, analysis and enhancements using TanDEM-X*; ISPRS Journal of Photogrammetry and Remote Sensing 85; 2013; pp. 120-131.

[5] Rabus, B., Eineder M., Roth A., Bamler R.; *The shuttle radar topography mission- a new class of digital elevation models acquired by spaceborne radar*; Photogramm. Rem. Sens., vol. 57; 2003; pp. 241-262.

[6] Murthy, K., et al.; *SkySat-1: very high-resolution imagery from a small satellite*; In: Proc. SPIE 9241, Sensors, Systems, and Next-generation Satellites XVIII; Amsterdam, October 7, 2014

[7] d'Angelo, P., Máttyus, G., Reinartz, P.; *Skybox image and video product evaluation;* International Journal of Image and Data Fusion, vol. 6 (1); 2016; pp. 3-18

[8] Carl, S., Bärisch, S., Lang, F., d'Angelo, P., Arefi, H., Reinartz, P.; *Operational Generation of High Resolution Digital Surface Models from Commercial Tri-Stereo Satellite Data;* Photogrammetric Week 2013, pp. 261-269.

Seismic Monitoring of Final Repositories: The Contribution from Analytical Theory

Jürgen Altmann

Experimentelle Physik III, Technische Universität Dortmund,
44221 Dortmund, Germany

Abstract:

The potential of seismic sensing for detecting undeclared activities in/near an underground repository had been studied 2010-2015, focusing on a salt dome, first with measurements, then with three-dimensional numerical modelling using a complex underground structure. The modelling allowed frequency-dependent attenuation but had limited time and space resolution due to the large model volume: typical mesh size was limited to about 20 m, with the required low-pass filtering signal frequencies were below a few hundred Hz. The results showed that the changes of the seismic-wave amplitude on transmission through media boundaries were relatively modest, not very relevant for detection. Thus the underground is conceived as a homogeneous medium without any boundaries. Here the seismic excitation from a force pulse or an explosion can be described by analytic formulae, with the source time function as input, and arbitrarily high signal frequencies can be used, better corresponding to the excitation by real mining activities. This has been done for explosions first. The analytically derived amplitudes fit very well to the numerical ones; at distances beyond 50 to 100 m the far-field term dominates by far. With signals limited to a few hundred hertz, in salt and other consolidated sediments the numerically gained amplitudes start to fall below the analytic ones at around 1 km, probably because the latter do not include attenuation. It seems that the analytic treatment by a homogeneous medium can give useful results for the estimation of signal strengths at relevant distances in various media, such as salt, clay or granite, by using appropriate values of the seismic parameters (density, P- and S-wave velocity). Such amplitudes can be compared with the seismic background noise at potential sensor sites, allowing a first estimate of the capabilities of a monitoring system. Beside extension to force-pulse excitation, for more realistic results for higher frequencies at longer ranges frequency-dependent attenuation needs to be included.

Keywords: final repository, seismic monitoring, seismology

1. Introduction

Without reprocessing spent nuclear fuel contains plutonium, thus such material should remain under IAEA safeguards even after emplacement in an underground final repository. This presents a new challenge for monitoring; geophysical techniques and methods have been proposed for this task. During operation, the creation of undeclared cavities needs to be detected, and those parts of the mine already filled with refuse have to be kept under surveillance for undeclared re-opening. After the emplacement phase, when drifts and shafts will have been closed, and the above-ground parts of the final repository will have been cleared for other uses, the IAEA needs the capability of long-term monitoring for covert access to the mine.

One potential technique is seismic sensing. Mining and other underground operations produce vibration directly as well as via acoustic noise. Seismic excitation propagates through the ambient medium and can thus be used to detect activities at a distance. The main question with seismic monitoring is whether signals from undeclared activities can be separated from signals from other sources and from background noise. In the operational phase of the repository most noise stems from the normal activity (mining, transport, filling, etc.), and sensors can be deployed at many sites in the mine. After closure, no sensors and cables can remain in the mine; in this phase sensors need to be

located at some distance, but still underground in order to reduce seismic background, produced by traffic, industry, agriculture and weather at the surface.

The German Support Programme to the IAEA has since decades taken an interest in seismic monitoring for final-repository safeguards. In order to gain information on the capabilities, a project had been carried out 2010-2012, measuring the properties of seismic signals from mining activities [1, 2]. This had been followed by a project where seismic propagation was modelled numerically [3, 4]. Both projects had focused on the Gorleben salt dome that for decades had been the only possible repository site in Germany.[1] Exploration there, done since 1979 with seismic surveys, drill holes and since 1986 with an exploratory mine, has provided much information on the salt dome. The mine gave the opportunity to deploy seismic and acoustic sensors at various positions underground and at the surface and to measure various mining machines and vehicles. However, underground positions outside of the mine or even outside of the salt dome, as they would be used for seismic monitoring, could not be covered. The actual strengths and other properties of the signals from mining activities at such positions could in principle be determined from measurements, but these would require expensive drilling. The modelling project served as a prior step.

The measurements and their evaluations produced many results, among others about seismic amplitudes and their distance dependences. The modelling gave information about amplitudes and distance dependences as well. While the relative decrease with distance was roughly similar, there remained open questions about the absolute amplitudes. In the model, the source strengths had to be specified in terms of a force or, in case of an explosion, of a seismic moment. These values were not available, there had been no possibility to measure them in the measurement project. Thus, nominal values of 1 Newton (N) or of 1 Newton-metre (Nm) had been used. It was expected that once estimates of the real source strengths would become available, due to linearity in an elastic medium (outside of the fracture and non-linear zone close to the source) the model amplitudes could be scaled. One approach to such estimates is to use the total energy in the seismic waves and to compare it to the energy of the sources that are available for the case of explosions as well as for blows by a pick hammer. This approach is described here for explosions.

2. Some results of the measurements and the modelling

From the measurements [1,2] it turned out that explosions (ignited in 5-m long drill holes to extend a tunnel by this length) produced by far the strongest amplitudes, with seismic velocity around 10^{-1} m/s at 100 m distance in the 4.5-kHz bandwidth recorded. The next-strong source, a grader with its compactor plates vibrating, was at about $1.6 \cdot 10^{-4}$ m/s at such range, all other sources were between $7 \cdot 10^{-5}$ and $4 \cdot 10^{-7}$ m/s. In particular the pick hammer, the blows of which were to be used in the modelling, had about $5 \cdot 10^{-6}$ m/s. Another important result was that the amplitudes varied by a factor 1/3 to 3 for similar conditions. Thus for the question of detectability (amplitude sufficiently above background noise) order-of-magnitude estimates are advisable, more precise determination would not make much sense.

Because of the complicated structure of the salt dome and its surroundings, numerical modelling in three dimensions had been done [3,4], with the spectral-finite-element code called SpecFEM3D [6,7,8]. The model extended for 5.5 km * 1.0 km * 3.6 km, it was gained by sweeping a simplified two-dimensional section (Figure 1) through the third dimension. With the computing resources available (the LiDO computer cluster of TU Dortmund, of which 340 cores could be used for maximally 48 h for one run) typical mesh size was limited to about 20 m, resulting in about 2.5 million mesh elements. Time resolution was limited steps of 0.02 ms. With the required low-pass filtering the signal frequencies were limited to a few 100 Hz, one order of magnitude lower than the bandwidth of the measurements (4.5 kHz). As source time functions for a force pulse a quasi-Dirac function, modelled by a Gaussian function with so-called half duration (referring to a similar triangle function, see Figure 2b) h_{tr} = 5 or 10 ms was used. To model repeated pulses from a pick hammer, 100 pulses with 23 ms temporal spacing were superposed. An explosion was modelled by a quasi-Heaviside function for the seismic moment, approximated by a shifted error function (the integral of a Gaussian function) with the same “half duration” (Figure 2a). As mentioned, nominal source values for the (maximum) force had

[1] With the German Site Selection Act (Standortauswahlgesetz) of 2013 the site and geological medium is open again.

been F_0 = 1 N, for the (final) moment M_0 = 1 Nm. With these parameters, seismic velocity at 100 m had been around $4 \cdot 10^{-9}$ m/s for a force pulse and $1 \cdot 10^{-13}$ m/s for an explosion. As Table 1 shows, there are about twelve orders of magnitude between the explosion values, and about three between those of (repeated) force pulses. Such ratios were not understood and were flagged as topics for further research in 2015 (Figs. 10, 12 in [3] where comparison at several 100 m distance and a half duration of h_{tr} = 5 ms gave different ratios).

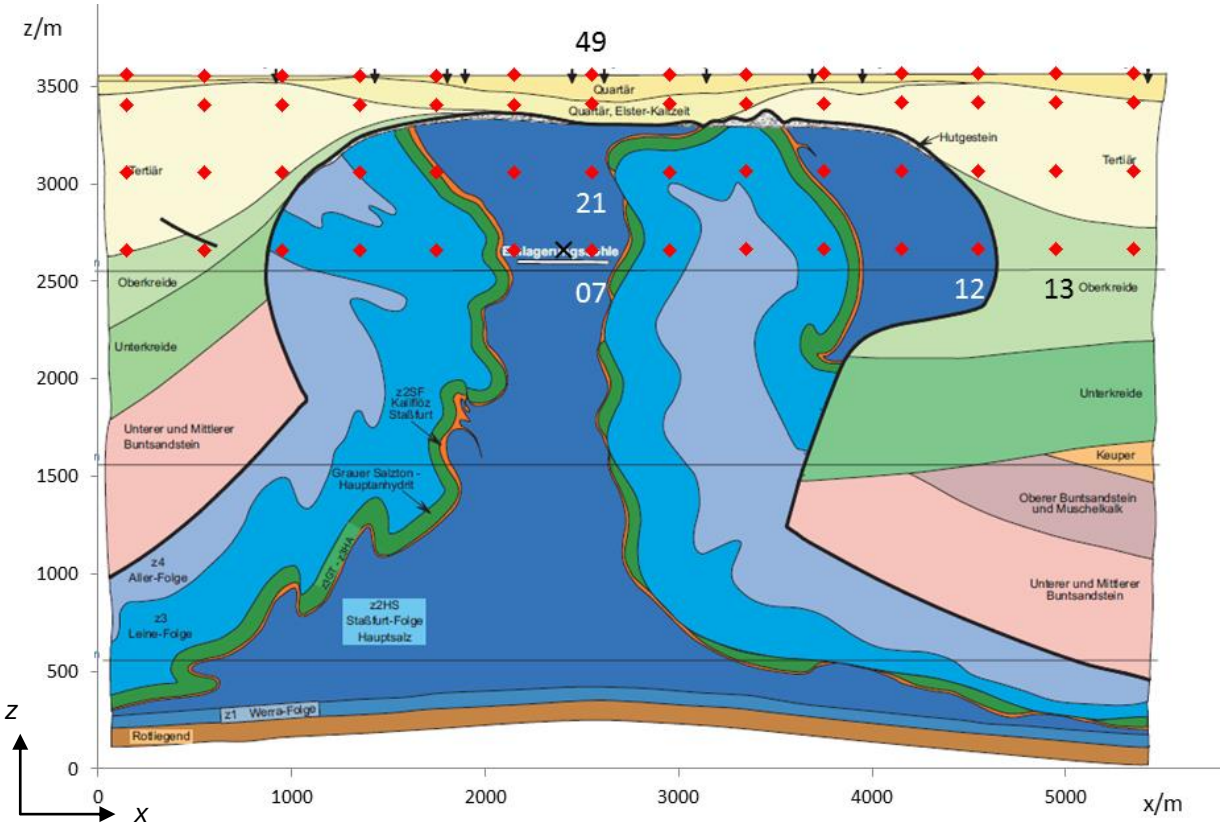

Figure 1: Simplified geological cross section in NW-SE direction through the Gorleben salt dome. A possible repository level at about 930 m depth is indicated. The *x* and *z* axes of the chosen co-ordinate system are shown, the *y* axis points into the section plane (with extension 1.0 km in the model). The section measures 5.52 km in the *x* and 3.57 km in the *z* direction, respectively. *x* is roughly south-east. In the model runs discussed here the source was put at 900 m depth (**X**). Red dots denote the sensor Positions 1 to 56 that lie in the centre plane at *y* = -500 m. (Based on Figure 36 in [5])

v_{PP} / (m/s)	Measurements	Model	Ratio
Explosion M_0 = 1 Nm, h_{tr} = 10 ms	$1 \cdot 10^{-1}$	$1 \cdot 10^{-13}$	$1 \cdot 10^{12}$
Force pulse F_0 = 1 N, h_{tr} = 10 ms	$5 \cdot 10^{-6}$	$1 \cdot 10^{-9}$	$5 \cdot 10^{3}$

Table 1: Comparison of the measured and model seismic peak-to-peak velocity at 100 m distance from the source for an explosion and a force pulse, approximate values. Model, explosion: spherical expansion at the source; given is the radial velocity component – only compressional (P) waves should be produced, propagating spherically symmetrically. Model, force pulse: force vertically downward, vertical velocity component at 100 m horizontal distance (there only shear (S) waves should occur). Model parameters as in Table 2.

Medium	ρ /(kg/m^3)	v_P /(m/s)	v_S /(m/s)	Q_κ	Q_μ
Main salt (z4HS)	2,200	4,400	2,600	9,999	125

Table 2: Seismic properties of the model; the first three are the ones of the central medium in the measurements. Given are the density ρ, the P-wave velocity v_P, the S-wave velocity v_S, the bulk quality Q_κ and the shear quality Q_μ. In order to have only shear attenuation, the Q_κ values were set to fictitious 9,999.

3. Analytical expressions for a homogeneous medium

3.1 General aspects

In case of a homogeneous, infinite elastic medium excited at one point by a force of arbitrary time course the displacement can be described by an analytic equation. The same holds for a complicated system of force couples as they are needed to describe an earthquake or an explosion. Seismic velocity, the quantity measured with geophones or seismometers, is just the time derivative of the displacement. The analytic formulae have the advantage that it arbitrary time courses can be input, in particular those with fast change or, in other words, those containing high frequencies. This is different from the case of a discrete model where the spatial and the temporal resolution is limited by the available computing power. However, the numerical program for the discrete model includes frequency-dependent attenuation that is not included in the straightforward analytical expressions.

How relevant is analytical theory in the present case? A salt dome as well as any other medium foreseen for a final repository will be approximately homogeneous in a certain volume around a repository. As long as the seismic waves originating from within have not yet hit a boundary to another medium, they should behave as in an infinite medium, provided attenuation is sufficiently low. In seismology the attenuation often increases linearly with frequency ν, described by $\exp(-\pi\ \nu\ r/(c\ Q))$ where r is the distance and c the propagation velocity. In salt with a quality value of $Q \approx 125$ as used in the model, frequencies of several 100 Hz have a range of several 100 m, at 100 Hz the range is nearly 2 km. Up to such a range the neglect of attenuation in the analytical equations should not produce marked deviations.

A final potential problem is the existence of media boundaries in real underground structures. Preferentially monitoring sensors should be placed outside of the repository medium so that at least one boundary will have to be crossed if excitation is inside the inner medium. At such boundaries, depending on the differences in densities and wave speeds and on the incidence angle, waves are partially reflected and partially transmitted, with conversion from P to S type and vice versa. Test computations for two boundaries of the salt dome showed that the transmitted amplitude did not change by more than a factor 1.5 (Section 5.4 in [3]), markedly less than the variation by a factor 1/3 to 3 that had been observed in the measured signals. Thus media boundaries have some effect, but for an order-of-magnitude estimation of signal amplitude for detectability they have no real importance.

3.2 Single force

For a force acting in the j co-ordinate direction at the origin with the time course $F_j(t)$ the displacement vector $\boldsymbol{u}_i$ (i=1, 2, 3 for the x, y, z co-ordinate) at an arbitrary point $\boldsymbol{x}$ with distance r from the origin at time t is given by [9]

$$u_i(\mathbf{x},t) = \frac{1}{4\pi\rho}\left(3\gamma_i\gamma_j-\delta_{ij}\right)\frac{1}{r^3}\int_{r/\alpha}^{r/\beta}\tau F_j(t-\tau)d\tau + \frac{1}{4\pi\rho\alpha^2}\gamma_i\gamma_j\frac{1}{r}F_j\left(t-\frac{r}{\alpha}\right) - \frac{1}{4\pi\rho\beta^2}(\gamma_i\gamma_j-\delta_{ij})\frac{1}{r}F_j\left(t-\frac{r}{\beta}\right) \quad (1)$$

with: ρ: density of the medium; α: speed of compressional (P) wave; β speed of translational (S) wave, δ_{ij} the Kronecker symbol, $\mathbf{x}=(x_1,x_2,x_3)$, $\gamma_i = x_i / r$ the directional cosines of the co-ordinates; the summation convention holds.
The first term is the near field, due to the integral it decays in proportion to r^{-2}. The second term is the far field of the P wave, the third the far field of the S wave; both far fields decrease with r^{-1}. The displacement is proportional to the time course of the force, delayed by the respective propagation time. Thus the velocity is proportional to the time derivative of the force.
For a point on the 1 (x) axis, if the force is in j = 1 direction, the displacement in i =1 direction becomes

$$u_1(\mathbf{x},t) = \frac{2}{4\pi\rho}\frac{1}{r^3}\int_{r/\alpha}^{r/\beta}\tau F_1(t-\tau)\,\mathrm{d}\tau + \frac{1}{4\pi\rho\alpha^2}\frac{1}{r}F_1\left(t-\frac{r}{\alpha}\right), \quad (2)$$

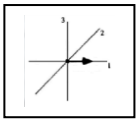

in 1 direction in the far field only a P wave propagates. If the force acts in the 3 direction (z, usually vertical), the displacement on the 1 axis is only vertical, in 3 direction. Along the 1 axis in the far field only an S wave propagates:

$$u_3(\mathbf{x},t) = \frac{-1}{4\pi\rho}\frac{1}{r^3}\int_{r/\alpha}^{r/\beta}\tau F_3(t-\tau)d\tau + \frac{1}{4\pi\rho\beta^2}\frac{1}{r}F_3\left(t-\frac{r}{\beta}\right). \quad (3)$$

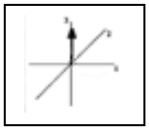

3.3 Force couples for earthquake or explosion

A system of force couples is described by a seismic-moment tensor $M_{jk}(t)$.[2] In this case the displacement at x is given by [10]

$$u_i(\mathbf{x},t) = \frac{1}{4\pi\rho}\left(15\gamma_i\gamma_j\gamma_k - 3\gamma_i\delta_{jk} - 3\gamma_j\delta_{ik} - 3\gamma_k\delta_{ij}\right)\frac{1}{r^4}\int_{r/\alpha}^{r/\beta}\tau M_{jk}(t-\tau)d\tau$$

$$+\frac{1}{4\pi\rho\alpha^2}\left(6\gamma_i\gamma_j\gamma_k - \gamma_i\delta_{jk} - \gamma_j\delta_{ik} - \gamma_k\delta_{ij}\right)\frac{1}{r^2}M_{jk}\left(t-\frac{r}{\alpha}\right) - \frac{1}{4\pi\rho\beta^2}\left(6\gamma_i\gamma_j\gamma_k - \gamma_i\delta_{jk} - \gamma_j\delta_{ik} - 2\gamma_k\delta_{ij}\right)\frac{1}{r^2}M_{jk}\left(t-\frac{r}{\beta}\right)$$

$$+\frac{1}{4\pi\rho\alpha^3}\gamma_i\gamma_j\gamma_k\frac{1}{r}\dot{M}_{jk}\left(t-\frac{r}{\alpha}\right) - \frac{1}{4\pi\rho\beta^3}(\gamma_i\gamma_j-\delta_{ij})\gamma_k\frac{1}{r}\dot{M}_{jk}\left(t-\frac{r}{\beta}\right). \quad (4)$$

The first term, the near field, decreases with to r^{-3}. The next two, the intermediate fields of P and S waves, respectively, decrease with to r^{-2}. The final two terms are the far fields of P and S waves, respectively, decreasing with to r^{-1}; their time course is proportional to the time derivative of the moment. Whereas earthquakes have complicated components M_{jk} of the moment, in case of a spherically symmetric explosion the off-diagonal elements are zero and the diagonal ones are equal: $M(t)$. In this case only spherical P waves are produced, without loss of generality the 1 component in 1 direction becomes

$$u_1(\mathbf{x},t) = \frac{1}{4\pi\rho\alpha^2}\frac{1}{r^2}M\left(t-\frac{r}{\alpha}\right) + \frac{1}{4\pi\rho\alpha^3}\frac{1}{r}\dot{M}\left(t-\frac{r}{\alpha}\right). \quad (5)$$

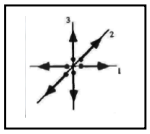

As an example Figure 2a shows the moment time function as it is used in the SpecFEM3D program: modelling a step function by a shifted error function. Its time derivative – proportional to the far-field displacement – is a Gaussian function (Figure 2 b). In the program the width parameter of this signal h is defined by the half duration of a similar triangle function.[3] The velocity is proportional to the second derivative (Figure 2 c).

As examples Figure 3 shows the displacement and velocity signals resulting from the moment “step” of Figure 2a at two different distances, 10 m and 100 m. The displacement intermediate field is proportional to the “step”, but its amplitude decreases with distance in proportion to r^{-2}. The far field is proportional to the derivative, decreasing only with r^{-1}, thus dominating the sum of both already at 100 m. The velocity is given by forming another derivative.

[2] The moment is the usual product of force times lever, but concentrated in one point by shrinking the lever length to zero while keeping the product constant.

[3] The Gaussian is described by a width parameter $h = h_{tr} / 1.628$, the standard deviation is $\sigma = h_{tr} / (1.628\ \sqrt{2})$.

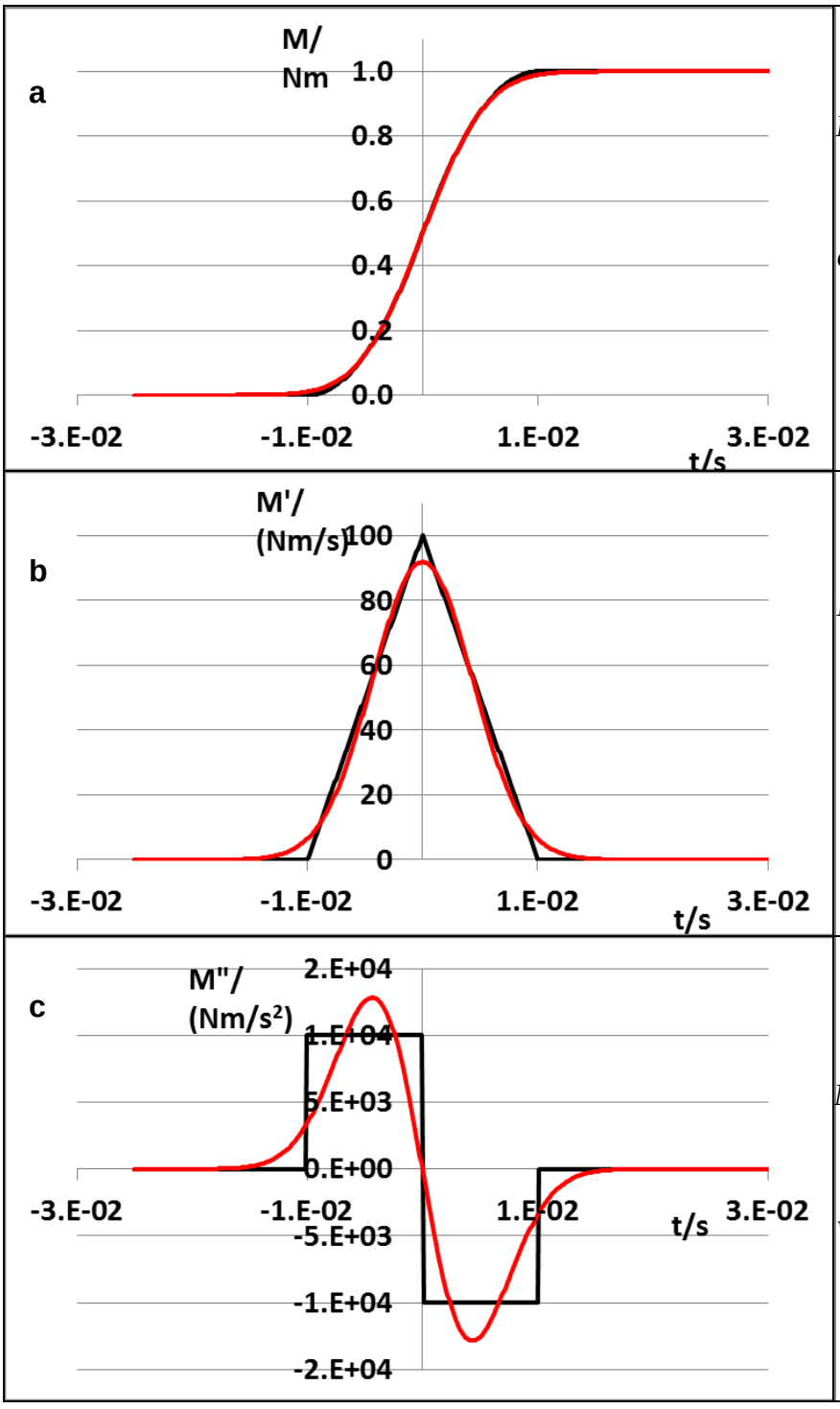

Moment

$$M(t) = \frac{M_0}{2}(1 + \mathrm{erf}(\frac{t}{h}))$$

with

$$erf(t) = \frac{2}{\sqrt{\pi}} \int_0^t \exp(-\tau^2) d\tau$$

First derivative

$$\dot{M}(t) = M_0 \frac{1}{\sqrt{\pi} h} \exp(-(\frac{t}{h})^2)$$

proportional to displacement

$$u_{far}(t)$$

Second derivative

$$\ddot{M}(t) = M_0 \frac{-2t}{\sqrt{\pi} h^3} \exp(-(\frac{t}{h})^2)$$

proportional to velocity

$$v_{far}(t) = \dot{u}_{far}(t)$$

Figure 2: Time course of seismic moment for an explosion (a) and its first (b) and second (c) derivatives. The far-field displacement is proportional to the first derivative, the far-field velocity to the second. The black triangle function of half duration h_{tr} in b simulates the Gaussian. The black curves in a and c are its integral and derivative, respectively. Parameters: M_0 = 1 Nm, h_{tr} = 0.01 s, thus h = 0.00614 s.

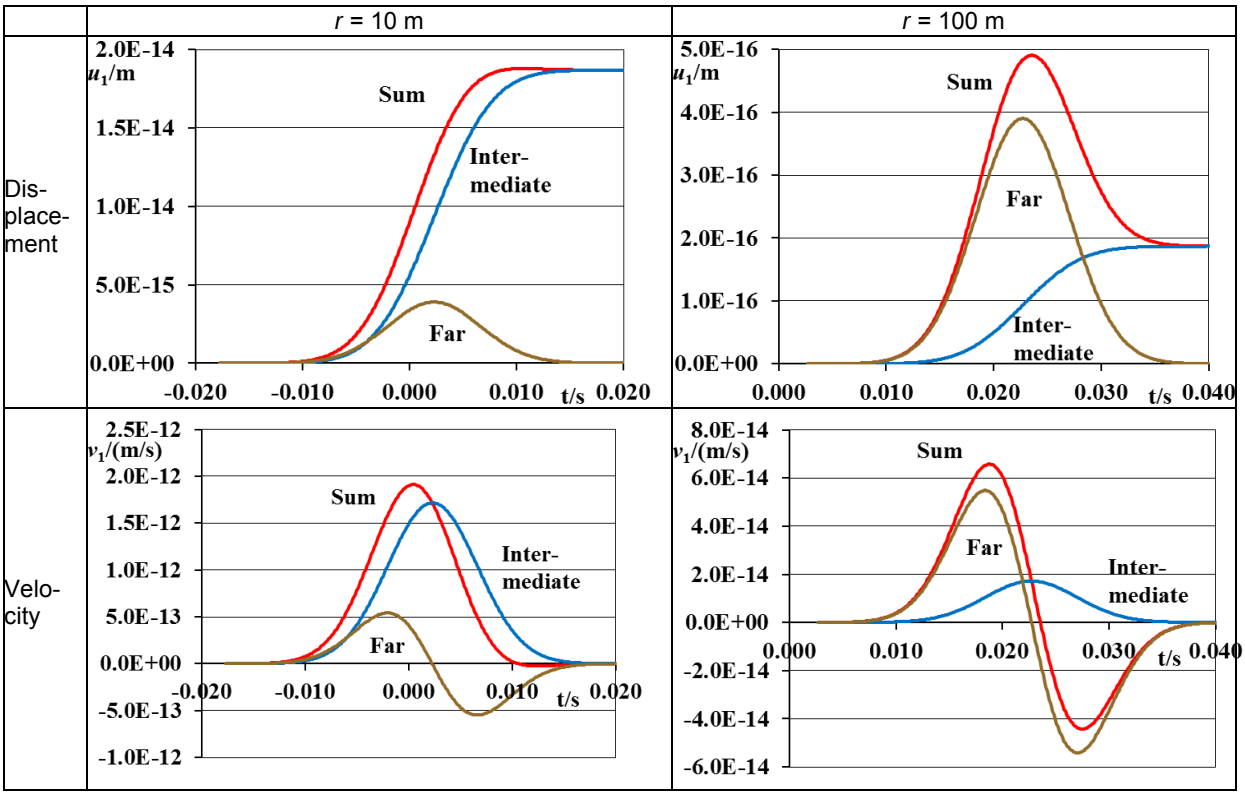

Figure 3: Displacement (top) and velocity (bottom) in 1 direction resulting from the seismic moment of Figure 2 at two points on the 1 axis, at 10 m (left) and at 100 m (right) according to Equation (5). Blue: intermediate, brown: far field, red: sum of both.

Figure 4 gives the peak-to-peak value of the far-field velocity and the one of the sum versus distance; obviously with the parameters chosen the intermediate field can be neglected already below 100 m. In addition several values from the numerical model are shown. Up to about 1 km there is no significant difference from the analytical curve. The decrease at larger distances is probably caused by the frequency-dependent attenuation of the model that was not included in the analytical signal. It is noteworthy that the transmission through the medium boundary from Main Salt to Upper Cretaceous (at about 2200 m, close to Sensor 12 in Figure 1) does not lead to a significant amplitude loss.

4. Comparison with measurements for explosions via an energy approach

Whereas with a moment-step of M_0 = 1 Nm and a half duration of h_{tr} = 10 ms in the analytical theory as well as in the numerical model the peak-to-peak velocity at 100 m is around 10^{-13} m/s, with real blasts values around 10^{-1} m/s had been measured (Figure 10 in [3]), 12 orders of magnitude higher.[4]
In a plane seismic wave the densities of kinetic and potential energy are given by [11]

$$\frac{E_{kin}}{V} = \frac{1}{2}\rho \dot{u}^2, \qquad \frac{E_{pot}}{V} = \frac{1}{2}\tau_{ij} e_{ij}\,, \qquad (6)$$

(V volume, ρ mass density, u displacement, τ_{ij} stress tensor, e_{ij} strain tensor, summation convention), and both are equal. Thus the total energy density at distance r at time t is

$$\frac{E_{tot}}{V}(r,t) = 2\frac{E_{kin}}{V}(r,t) = \rho v^2(r,t)\,. \quad (7)\ (v\text{: velocity}).$$

At a distance where the far field dominates, using the second derivative of the moment function in Figure 2 c, the velocity becomes

$$v_{far}(r,t) = \frac{1}{4\pi\rho\alpha^3}\frac{1}{r}\ddot{M}\left(t-\frac{r}{\alpha}\right) = \frac{1}{4\pi\rho\alpha^3}\frac{1}{r}M_0\frac{-2(t-\frac{r}{\alpha})}{\sqrt{\pi}h^3}\exp[-(\frac{t-\frac{r}{\alpha}}{h})^2]\,, \quad (8)$$

[4] With h_{tr} = 5 ms in the model the ratio had been $6\cdot10^{10}$ [3, Section 5.2].

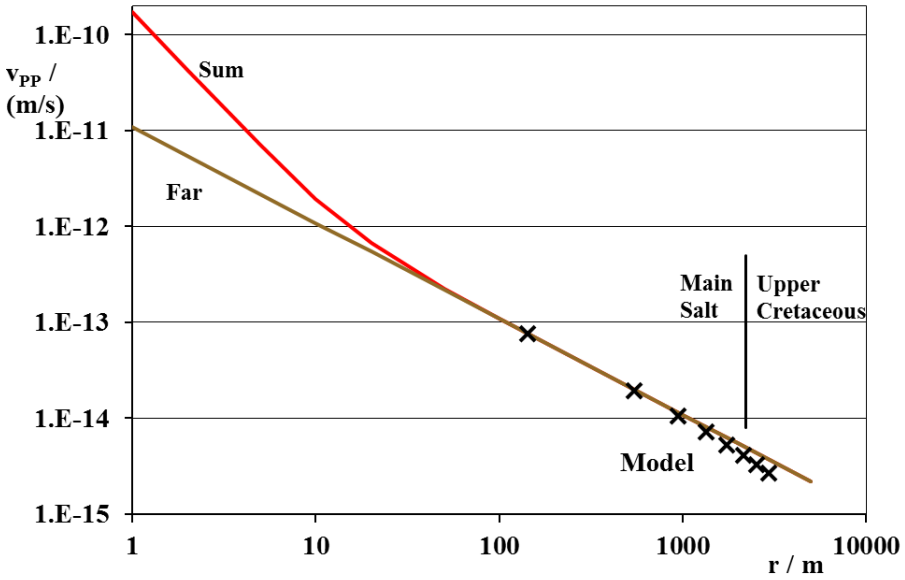

Figure 4: Peak-to-peak value of far-field velocity and of the sum signal (1 component) versus distance along the 1 (*x*) direction for the moment time course of Figure 2 and the Main-Salt parameters of Table 2. In addition the values from the numerical model at the Sensors 7 to 14 (see Figure 1) are given. The boundary between Main Salt and Upper Cretaceous is somewhat right of Sensor 12.

thus the total energy density is

$$\frac{E_{tot}}{V}(r,t) = 2\frac{E_{kin}}{V}(r,t) = \rho v^2(r,t) = \frac{\rho}{16\pi^2\rho^2\alpha^6}\frac{1}{r^2}M_0{}^2\frac{4(t-\frac{r}{\alpha})^2}{\pi h^6}\exp[-2(t-\frac{r}{\alpha})^2]$$
$$= \frac{M_0{}^2}{4\pi^3\rho^2\alpha^6h^6}\frac{1}{r^2}(t-\frac{r}{\alpha})^2\exp[-2(t-\frac{r}{\alpha})^2]\ . \quad (9)$$

The total seismic-wave energy in the full volume at a time *t* is given by the volume integral of the energy density. Due to the spherical symmetry with an explosion, this is

$$E_{tot}(t) = \int_V \frac{E_{tot}}{V}(r,t)dV = 4\pi\int_0^\infty r^2\frac{E_{tot}}{V}(r,t)dr\ , \quad (10)$$

the integral resulting in

$$E_{tot} = \frac{2M_0{}^2}{\pi^2\rho\alpha^5h^6}\left[\frac{\sqrt{\pi}h^3}{8\sqrt{2}}\mathrm{erf}(\frac{\sqrt{2}}{h}\tau) - \frac{\tau h^2}{4}\exp[-2(\frac{\tau}{h})^2]\right]_0^\infty, \quad (11)$$

thus

$$E_{tot} = \frac{M_0{}^2}{4\sqrt{2}\pi^{3/2}\rho\alpha^5h^3}\ . \quad (12)$$

Putting in the values M_0 = 1.0 Nm, h_{tr} = 0.01 s, h = 6.14 ms, ρ = 2.20 Mg/m^3, α = 4.40 km/s (see table 2), the total wave energy becomes $E_{tot} = 3.776\cdot10^{-17}$ J. In the numerical program there is the option of summing the total energy over the volume, this resulted in $E_{tot} = 3.77\cdot10^{-17}$ J if attenuation is switched off, in excellent agreement.

In a typical single blast shot, around 20 kg of explosive is consumed (possibly simultaneously in several boreholes). Thus I assume an energy yield of *Y* = 20 kg TNT equivalent = $8.4\cdot10^7$ J. In different media 1.5 to 17% of the yield goes into the seismic wave, in salt about 10% [12].[5] Thus the

[5] The rest goes into fracturing of rock and heat.

seismic energy from one shot should be E_{tot} = 10^6 .. 10^7 J – 23 orders of magnitude above the theoretical values. Can one bridge this discrepancy by adapting the parameters M_0 and h_{tr}?

Let us first look at the half duration of the source time function. The detonation velocity of the used explosive (Andex) is v_{Deton} = 3.0 km/s. Ignited at one end, propagation through the hole of length l = 5 m takes the time t_{Deton} = l/v_{Deton} = 1.67 ms, that is a half duration of 0.83 ms in case of a triangle function, smaller by 1/12.0 than the model value of 10 ms, thus h = 0.51 ms for the error-function model. Since h enters Equation 12 by the third power, this explains a factor 1750, leaving $5.7 \cdot 10^{19}$ of the 10^{23} discrepancy.

How about the second parameter M_0? Increasing it from 1 Nm to $(5.7 \cdot 10^{19})^{1/2}$ Nm = $7.6 \cdot 10^9$ Nm would close the gap. Is an M_0 value around $8 \cdot 10^9$ Nm reasonable? Figure 5 shows empirical values of the seismic moment for a large set of explosions in salt, from small chemical to large nuclear [13]. For Y = 20 kg TNT equivalent the trend line gives a seismic moment of M_0 = $2 \cdot 10^9$ Nm, in the correct order of magnitude; the missing factor 4 can easily be explained by the scatter in the data of Figure 5, the rough estimates of the yield itself, of the portion of the yield going into seismic-wave energy, and of the duration and time course of the blast.

Figure 6 compares the analytical far-field data gained from Equation (5) with h_{tr} = 0.83 ms and M_0 = $8 \cdot 10^9$ Nm with the ones from the measurements. They agree at 100 m distance. Beyond that the power-law trend line of the measurement data decreases with distance according to an exponent -2.2, not -1 as in Equation (5). This stronger decrease may be caused by the stronger attenuation at higher frequencies.

Thus for explosions the earlier discrepancy has been explained: to fit to the measured seismic-velocity values, the theoretical ones from a moment of 1 Nm and a triangle half duration of 0.01 s have to be increased by a factor around 10^{12}. Correspondingly the total energy – that is proportional to velocity squared – is higher by a factor 10^{23}.

It is hoped that a similar total-energy analysis for a force pulse will resolve the discrepancy there. With the parameters used (h_{tr} = 5 ms, F_0 = 1 N) the theoretical peak-to-peak seismic velocities had been lower by a factor 1/700 than the ones measured with a pick hammer. Since for a single force P- and S-waves are excited and the respective amplitudes are no longer spherically symmetric, the derivation of the total-energy expression will be somewhat more complicated than with an explosion.

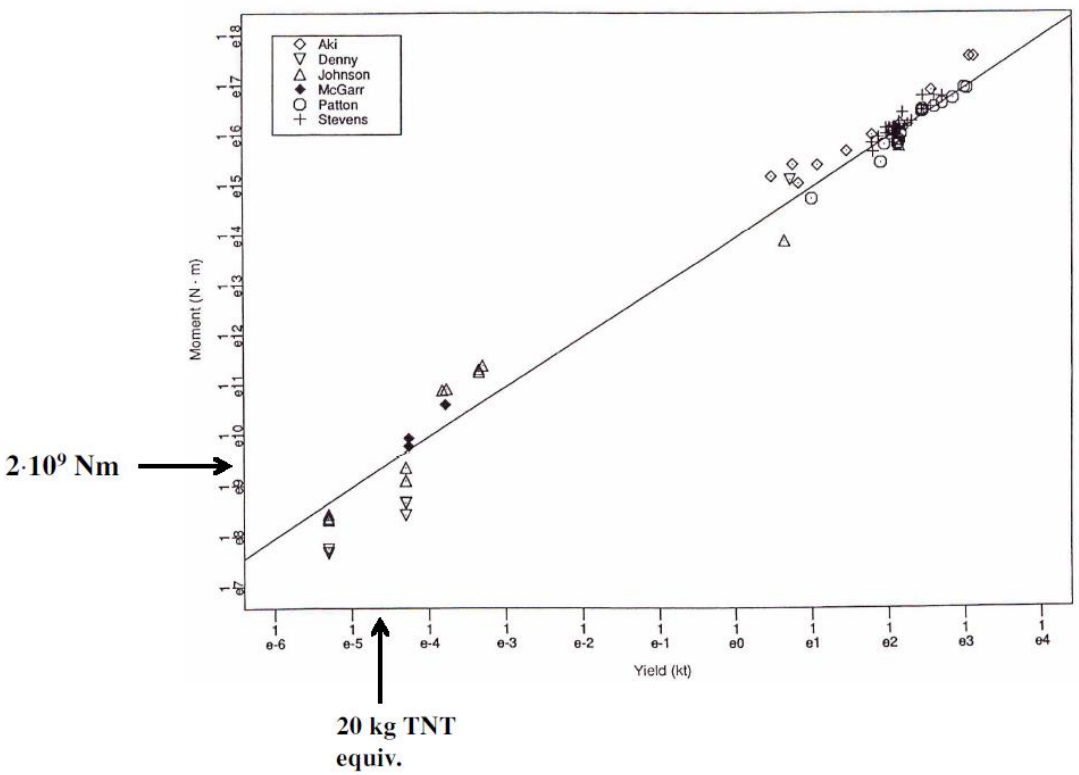

Figure 5: Empirical relationship between energy yield and seismic moment for chemical and nuclear explosions in salt (Figure 8 in [12]), with indications at 20 kg TNT equivalent and $2 \cdot 10^9$ Nm. The abscissa numbers go from 1E-6 to 1E4 kt TNT, the ordinate ones from 1E7 to 1E18 Nm.

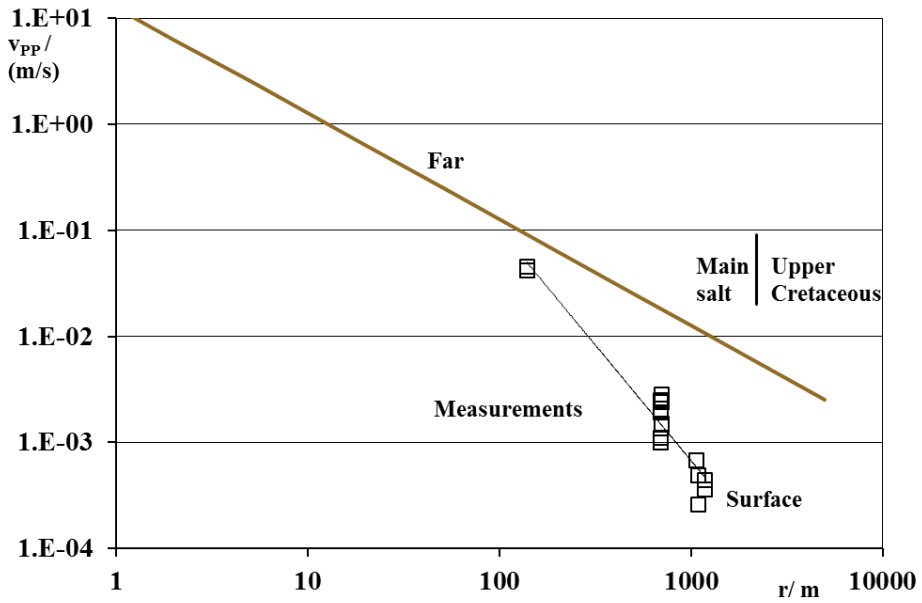

Figure 6: Peak-to-peak value of seismic velocity from analytical theory (from Equation (5) with h_{tr} = 0.83 ms, M_0 = $8 \cdot 10^9$ Nm and salt parameters of Table 2, far field only) and of the measurements. The power-law trend line of the latter hits the theoretical curve at 100 m. The decrease with distance with a stronger exponent than -1 may be a consequence of frequency-dependent attenuation that is not contained in the analytical equation. This holds in particular for sensors at the surface where the wave had to pass through about 300 m of loose sediment with a much lower Q value.

5. Ratio between signal strength from force versus explosion

To compare the signal strength from a single force with that from an explosion, model runs had been done with the source at the central position of Figure 1. The force direction had been horizontal in *x* direction. Thus for propagation in *x* direction both types of source produce mainly P waves (with horizontal movement of the medium). The *x* components of seismic velocity at the Sensors 7 to 14 (Figure 1) had been very similar. However, the peak-to-peak amplitudes of the explosion with moment M_0 = 1 Nm had been lower by a factor 1/4,400 than those of the force pulse of F_0 = 1 N (using the same half duration h_{tr} = 10 ms). This was flagged as a problem requiring further investigations [3, Section 5.4].
Using the analytical formulae this ratio can be explained now. For an explosion, the far-field displacement term for the 1 component of Equation (5) is

$$u_1(\mathbf{x},t) = \frac{1}{4\pi\rho\alpha^3}\frac{1}{r}\dot{M}\left(t-\frac{r}{\alpha}\right), \qquad (13)$$

while the 1 component of a single force in 1 direction of Equation (2) is

$$u_1(\mathbf{x},t) = \frac{1}{4\pi\rho\alpha^2}\frac{1}{r}F_1\left(t-\frac{r}{\alpha}\right). \qquad (14)$$

Since the force time function in the SpecFEM3D software is an area-normalised Gaussian function, expressed in Newton it is numerically equal to the time derivative of the error-function expression for the seismic moment, expressed in Nm/s:

$$\frac{F_1(\tau)}{\mathrm{N}} = \frac{\dot{M}(\tau)}{\mathrm{Nm/s}} \quad . \qquad (15)$$

Thus the difference between blast and force pulse is an additional factor (m/s) / α. Since α = 4,400 m/s this nicely explains the discrepancy found.[6]

5. Conclusion and outlook

Analytical theory can give important contributions to the problem of estimating the seismic-signal strength at various locations around a seismic source. This source can either exert a force in some direction or excite the ground in a spherically symmetric way as with an explosion. Strictly speaking the formulae hold only in a homogeneous medium. But the transmission through a boundary to a different underground medium often does not change the seismic-wave amplitude markedly. In the measurements much stronger variation of the strengths, e.g. by a factor 1/3 to 3, had been found. Thus for the probability of detection by an amplitude criterion smaller variations due to transmission do not really change the picture. As a consequence it is to be expected that for different media than salt, for example clay or granite, relatively good estimates of the signal strength versus distance can be gained from the analytical equations if the seismic properties of the respective medium are put into them. The time courses and peak/final values of force or seismic moment have to be known for this, they will depend on the medium.
One effect is not included in these equations, namely the seismic attenuation. In many cases the attenuation coefficient in the exponential amplitude decrease with distance is proportional to frequency, attenuation can be described by a quality factor (see Section 3.1). This means that higher frequencies in a seismic wave are attenuated preferentially; at a certain distance, they may have effectively vanished. This attenuation can be included by considering the spectra of the signals. Thus, knowledge of the quality factor of a medium is very relevant for estimating the detection ranges for certain excitation sources.
Consideration of the theoretical expression for the total seismic-wave energy allowed deriving an estimate for the final seismic moment and the duration of the moment step of explosions which had not been accessible directly during the measurements. The value range found fits to earlier literature data, providing confidence that it is about correct (within an order of magnitude). This solves one of the questions that came up in the evaluation of the model calculations.
Another earlier problem could also be solved: the ratio between the seismic amplitudes in the P waves from a force pulse on the one hand and from an explosion on the other. The explanation follows

[6] This is the ratio of the displacements, but the same ratio holds for the velocities (the time derivatives).

directly from the power of the P-wave velocity in the respective equations (and the way the force pulse and the moment step are defined in the seismic modelling program).
Two main tasks remain to be done:

- Deriving the source strength of a force pulse from the total seismic-wave energy similarly to the procedure used for an explosion. Possibly this can be compared with estimates from a mechanical model of e.g. a pick hammer.
- Including frequency-dependent attenuation in the analytical calculation.

More in-depth research may be interesting, such as the influence of broken-up and mixed layers or the difference from a spherical explosion of a cylindrical blast-hole geometry. But it may well be that for order-of magnitude estimates such investigations are not required.
In conclusion, analytical theory provides a tool to gain estimates of signal strengths at various potential monitoring locations around a planned final repository. It can become an important method in designing a safeguards monitoring system and can reduce the amount of confirmatory measurements at a potential site.

References

[1] Altmann, J., Kühnicke, H.; *Acoustic and Seismic Measurements for the Detection of Undeclared Activities at Geological Repositories – Results from the Gorleben Exploratory Mine*, JOPAG/11.13-PRG-404; Joint Programme on the Technical Development and Further Improvement of IAEA Safeguards between the Government of the Federal Republic of Germany and the International Atomic Energy Agency, Nov. 2013.

[2] Altmann, J.; *Seismic Monitoring of an Underground Repository in Salt – Results of the Measurements at the Gorleben Exploratory Mine*; *ESARDA Bulletin* no. 50, 61-78, Dec. 2013.

[3] Altmann, J.; *Modelling Seismic-Signal Propagation at a Salt Dome for Safeguards Monitoring*; *ESARDA Bulletin* no. 52, 60-79, June 2015.

[4] Altmann, J.; *Modelling of Seismic-Wave Propagation at a Salt Dome*; JOPAG/12.15-PRG-422; Joint Programme on the Technical Development and Further Improvement of IAEA Safeguards between the Government of the Federal Republic of Germany and the International Atomic Energy Agency, Dec. 2015.

[5] O. Bornemann et al.; *Standortbeschreibung Gorleben Teil 3 – Ergebnisse der über- und untertägigen Erkundung des Salinars*; Geologisches Jahrbuch C73; Hannover/Stuttgart: BGR/Schweizerbart, 2008 (English version via http://www.bgr.bund.de/DE/Themen/ Endlagerung/Aktuelles/2011_04_20_aktuelles_gorleben_engl_Part1bis3.html (29 April 2015)).

[6] Komatitsch, D., Vilotte, J.P.; *The spectral-element method: an efficient tool to simulate the seismic response of two-dimensional and three-dimensional geological structures*; *Bull. Seismol. Soc. Am.* 88 (2), 368-392, 1998.

[7] Komatitsch. D., Tromp, J.; *Introduction to the spectral-element method for three-dimensional seismic wave propagation*; *Geophys. J. Int.*, 139, 806-822, 1999.

[8] Computational Infrastructure for Geodynamics (CIG), Princeton University (USA), CNRS and University of Marseille (France), ETH Zürich (Switzerland); *SPECFEM 3D Cartesian User Manual*, Version 2.1; Sept. 30, 2013, via https://geodynamics.org/cig/software/specfem3d (20 Jan. 2014).

[9] Aki, K., Richards, P.G., *Quantitative Seismology – Theory and Methods, Vol. I*, San Francisco CA: Freeman, 1980, p. 78.

[10] Aki/Richards (note 9), p. 79.

[11] Aki/Richards (note 9), p. 125 ff.

[12] Larson, D.B., *Explosive energy coupling in geologic materials*, *International Journal of Rock Mechanics and Mining Sciences & Geomechanics Abstracts,* 19 (4), 157-166, 1982.

[13] Denny, L.R., Johnson, L.R., *The Explosion Seismic Source Function: Models and Scaling Laws Reviewed*, pp.1-24 in Taylor, S.R., Patton, H.J., Richards, P.G. (eds.), Explosion Source Phenomenology, Washington DC: American Geophysical Union, 1991.

Applicability of the directional radar technology for safeguards monitoring nuclear repositories in geological formations

Christian Holst, Dr. Dirk Orlowsky, Sven Uchtmann

DMT GmbH & Co. KG
Essen, Germany

Abstract:

The long term safety assessment of a nuclear repository implies the investigation of different scenarios of the repository and their influence to the safety. A feasibility study in the framework of the German Support Programme investigates the applicability of the 3D radar method for the monitoring of a geological repository. The aim of technical solution is the detection and localisation of clandestine underground mining activities. The radar system should form a kind of protective shield around a repository to detect and localise possible activities in an early stage and in a sufficient distance.

Repetitive surveys out of boreholes or drifts are conducted with disadvantages concerning safeguards requirements as high maintenance and positioning inaccuracies. In this study a static radar system is selected to omit these disadvantages. A monitoring system consisting of an array of static radar probes could probably be realized as a highly accurate, durable and low-maintenance automatic early warning system.

The detectability of different possible clandestine mining activities is investigated by simulations of radar wave propagation. The simulations involve the influence of baseline conditions to the data. By the use of real data examples the sensitivity of different radar antennas are analysed. Based on the real data an example for a possible monitoring system in a salt mine is given. Discussed are the requirements on a geophysical underground safeguards monitoring system as well as possibilities and limitations of radar for the monitoring task at various sites.

Keywords: safeguards; monitoring; directional radar; repository; salt dome

1. Introduction

Geophysical methods are suited for the monitoring of the environment of a geological repository. In this presentation, the usability of ground-penetrating radar (GPR) is examined as a possible method.
The objective is to use radar to detect and localize undeclared underground activities in and around a geological nuclear repository. To this end, the idea is to use a radar monitoring system setting up a "shield" of electromagnetic waves around a nuclear repository enabling an early detection of activities in a sufficient distance to the stored material.

The motivation of an unauthorized access could be theft, sabotage or illegal transfers. Access types for those activities could be drillings, cavern leaching, hydraulic fracturing, explosives or heading techniques which could occur from all sides of the repository.
Mining activities like cavern leaching and hydraulic fracturing are directly related to drillings. In advance of heading also exploration drillings could be expected. For the impact of the barrier system by explosives an access route is needed, e.g. by a borehole. It is most likely that a drilling would precede every access type.

Within geotechnical engineering radar is mainly used in form of repetitive linear measurements. For safeguarding, repetitive surveys out of boreholes or drifts are conducted with disadvantages as high maintenance and positioning inaccuracies. In this study a static radar system is selected to omit these disadvantages. Directive radar antennas provide the direction of activities. A monitoring system consisting of an array of directed static radar probes could probably be realized as a highly accurate,

durable and low-maintenance automatic early warning system. The applicability of the radar method is restricted to locations with low conductive conditions like in dry rock salt and in some crystalline formations.

2. Modelling of unauthorized activities

The influence of geology and mining activities on the data of a stationary radar antenna is investigated by 2D finite difference simulations [1]. As a basis for the first simulations a section of the Gorleben salt dome is used. An area of 250 m x 200 m of the north western flank of the salt dome is selected for the modelling work. The model of the section of the Gorleben salt dome is shown in FIG 1a. The electromagnetic parameter of the model layers are chosen as mean values from different references. As a compromise of resolution and range a measuring frequency of 50 MHz was chosen for the simulations. According to the wavelength of this frequency in rock salt, a discretization distance of 0.125 m in both directions and a time increment of 0.2 ns were selected. The maximum travel time of the modelling work is 1,600 ns. To prevent reflections at the borders of the model, absorbing boundary conditions are used. The simulations are carried out with a idealized point source of the type “Küpper” which consists of two half cycles. The position of the point source in the model is (0 m/816.5 m).

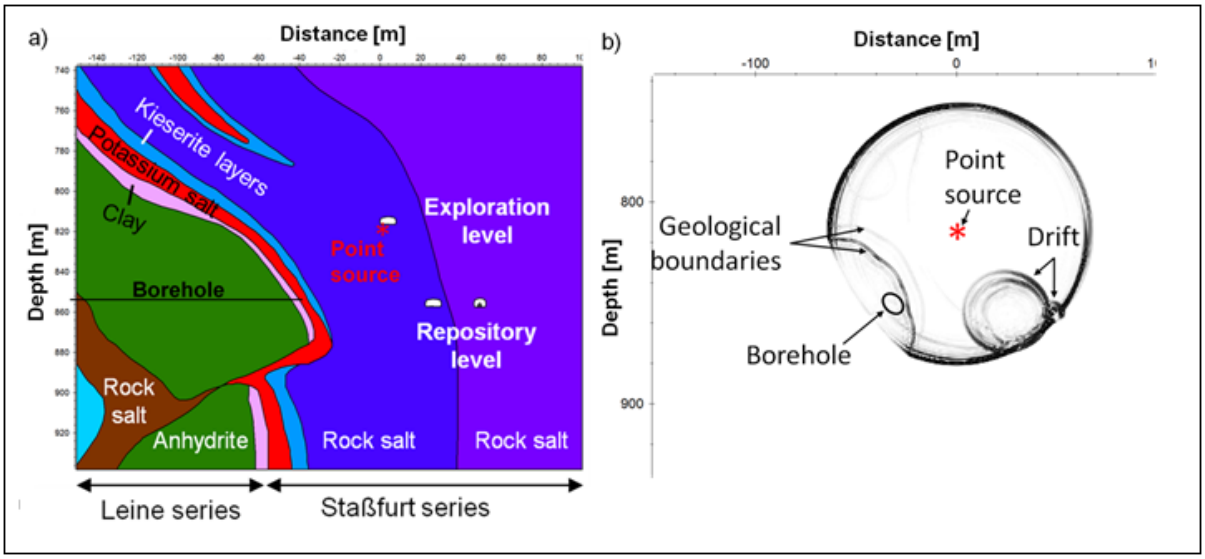

Figure 1: 2D finite difference simulations. a) Model of a section of the Gorleben salt dome used for the simulations. A horizontal borehole with diameter of 0.125 m approaches the potassium salt in a depth of about 856 m. b) Simulated wave field of the model in a) at a travel time of 536 ns.

The electromagnetic wave is transmitted at the source point and is spread in all directions. After certain travel times reflections at the geologic boundaries and at the drifts occur. Figure 1b shows the modelled wave field at a travel time of 536 ns.

With the following simulations an access attempt in the form of a thin conductive borehole to the repository is examined. Examined is a static case in the past-closure phase, in which a repository cask was brought into the storage gallery and all open galleries in the model were filled with crushed salt. The borehole with a diameter of 0.125 m approaches the repository area from the left at a depth of approximately 854 m.

The first data trace in Figure 2a shows the respective baseline data without any borehole. In the following data records the access attempt gradually reaches the geological layer boundaries of clay (b), potassium salt (c), kieserite layers (d) and the Staßfurt rock salt (e). In part, the simulated data show low-amplitude changes at a travel time of approximately 900 ns.

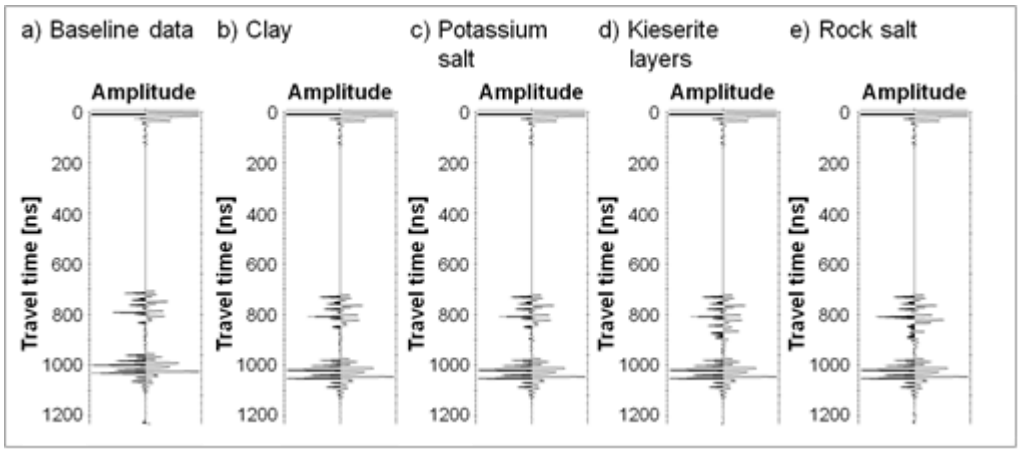

Figure 2: Simulated data regarding the progress of an access attempt in the form of a thin borehole.

The calculation of the difference of the data with regard to the baseline record makes the changes clearly visible (Figure 3). When the borehole reaches clay (b), no data changes are registered compared to the baseline data (a). After reaching potassium salt (c) a low-amplitude signal shows at a travel time of about 900 ns. Starting with the kieserite layers (d) the change of the data traces becomes more and more visible.

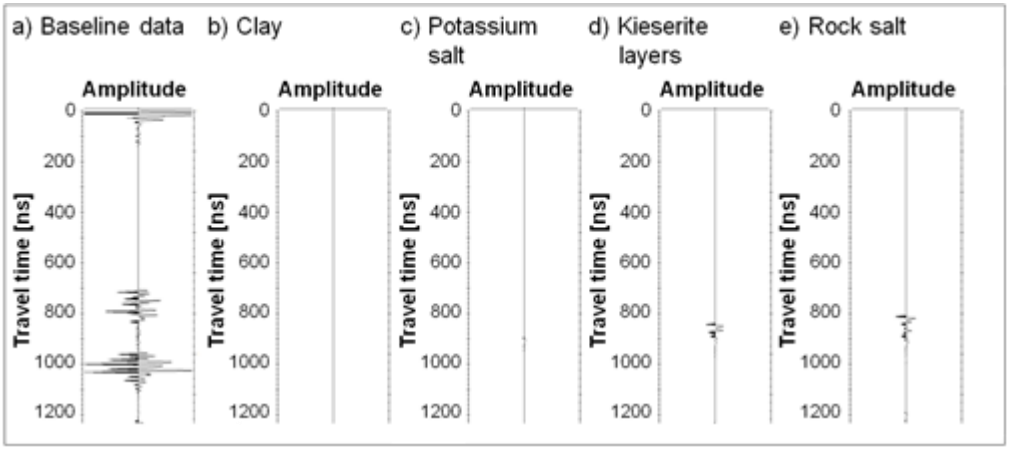

Figure 3: Simulated data regarding the progress of an access attempt in the form of a thin borehole, difference between measured data and baseline data. Changes of the measured data caused by the borehole become visible.

Due to the high electric conductivity of clay, severe reflection and absorption occurs at the boundary layer salt to clay. For this reason, with the radar system it is impossible to obtain information from the area within and behind a thick clay layer. This shows that a geological layer boundary may have a possible shielding effect on the radar waves. After passing through the shielding layer, the access attempt can be located with radar.

The positioning of stationary antennas is very exact, whereby also the geological noise occurring is identical at different measuring times. By subtracting the measuring data, the geological noise can be eliminated completely, whereas uncorrelated data would become visible. This means a higher sensitivity of stationary antennas for the detection of unauthorized activities.

3. Sensitivity analysis

The sensitivity area of an antenna is defined as the volume, in which a very weak signal is at least barely be distinguishable from the noise. The boundaries of this sensitivity are equivalent to the range of the radar. The range of an antenna is based on the system properties and the site parameters and can be estimated applying the radar equation. This equation summarizes the losses regarding the

travelling radar signals, allowing for a more accurate assessment of the depth of penetration to be expected for a diffractor [2]:

$$P_r = P_t \frac{G^2 \lambda_c^2 \sigma}{(4\pi)^3 r^4} e^{-4\alpha r} \qquad \text{(I)}$$

With

- P_r received signal power in W,
- P_t transmitted signal power in W,
- G antenna gain of the combined transmitting-receiving antenna relative to a sphere dipole,
- λ_c wavelength of the centre frequency in rock in m,
- σ effective reflecting area (radar cross section) in m²,
- α attenuation factor in 1/m,
- r distance of the reflector in m.

In this study, a sensitivity analysis of a borehole radar is performed based on a real data example. The data was recorded at a cavern storage site in rock salt by a direction-sensitive borehole radar. The data record in Figure 4 shows a section of the measurement result in depths of approximately 750 m to 950 m. The length of the radargram of approximately 11,000 ns in dry rock salt corresponds to a distance of approximately 700 m from the borehole. Numerous reflections were recorded on the profile which can be correlated to geological layer boundaries and technical structures like boreholes and caverns.

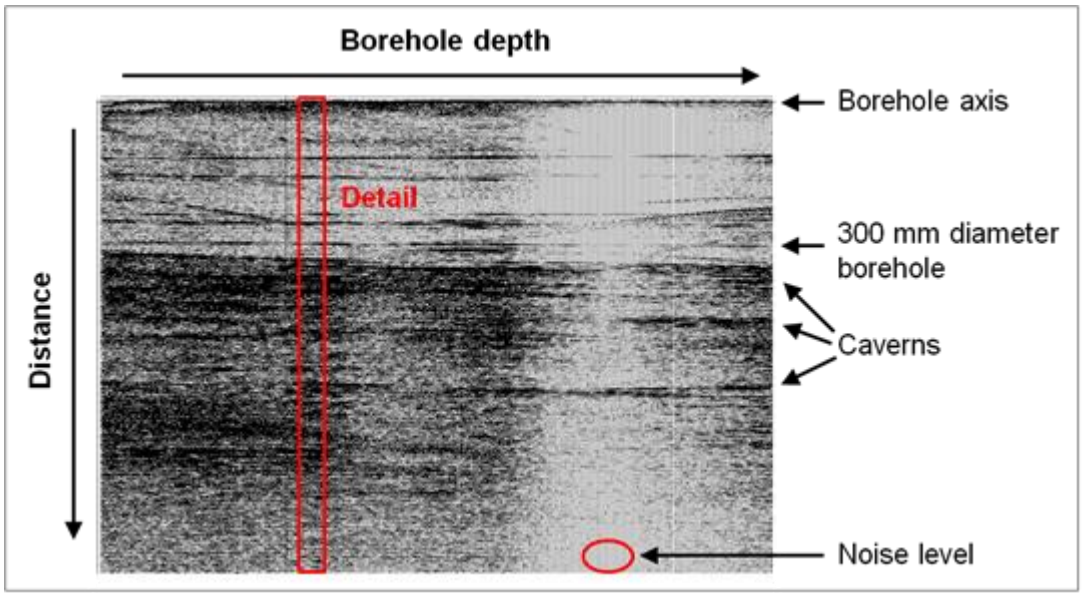

Figure 4: Real data example of a borehole measurement.

The sensitivity of the radar system is estimated by the detection limit, up to which a known borehole can be located, before its signal is superposed by noise. Therefore, the amplitude of the reflection of the borehole and the magnitude of the noise level are determined. The investigated borehole has a diameter of 300 mm and a distance of approximately 210 m to the profile (Figure 5). For the measurement a transmitter (dipole) with a transmitting power of 6 kW was used. The reflection of the investigated borehole was registered with a reflected power of 10 nW.

The noise level is determined in a section with high attenuation at a large distance to the borehole (Figure 4). In this example the noise level amounts to approx. 200 pW. This value applies to a signal in the direction of maximum radiation. A radar signal in this main direction of the ray can be detected, if its amplitude is above this level.

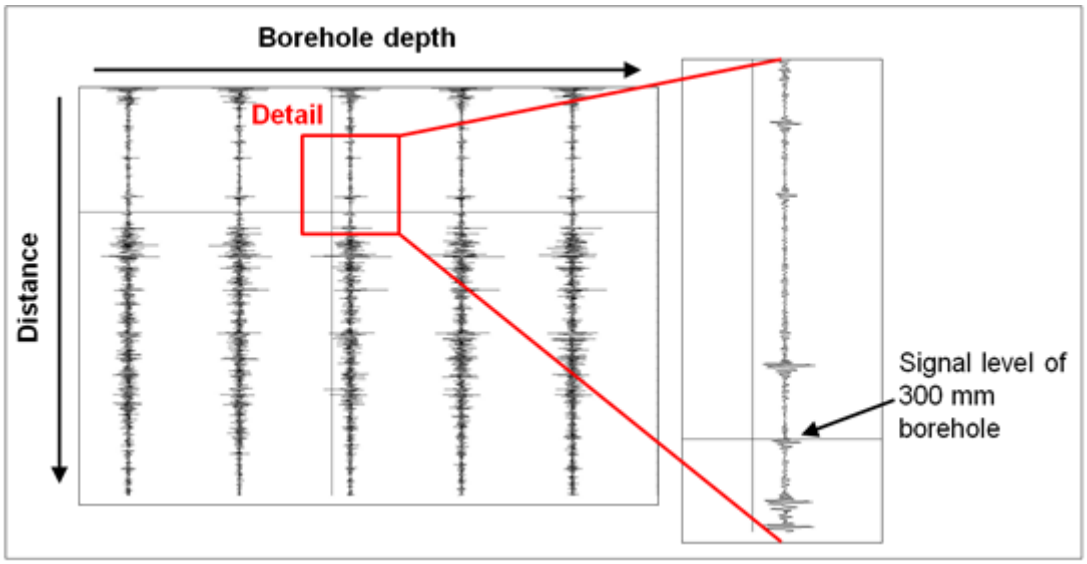

Figure 5: Selection of a reflection in form of a borehole.

A criterion for the directivity of an antenna is the opening angle, also referred to as peak width at half-height. The opening angle δ is defined as the range within the radiation field, in which the power density does not fall below -3 dB which corresponds to a factor of approximately 0.5 of the maximum amplitude. That means, in this range signals can definitely be detected when the amplitude exceeds twice the determined noise level. Hence, the following considerations assume a noise level of 400 pW.

The opening angle of a dipole signal corresponds to 360°. By using a planar reflector, the directivity can be increased while the opening angle decreases. The directivity of a planar reflector (3 m x 3 m) achieves an antenna gain of approximately 2 dB (Figure 6). The opening angle decreases to approximately 72°.

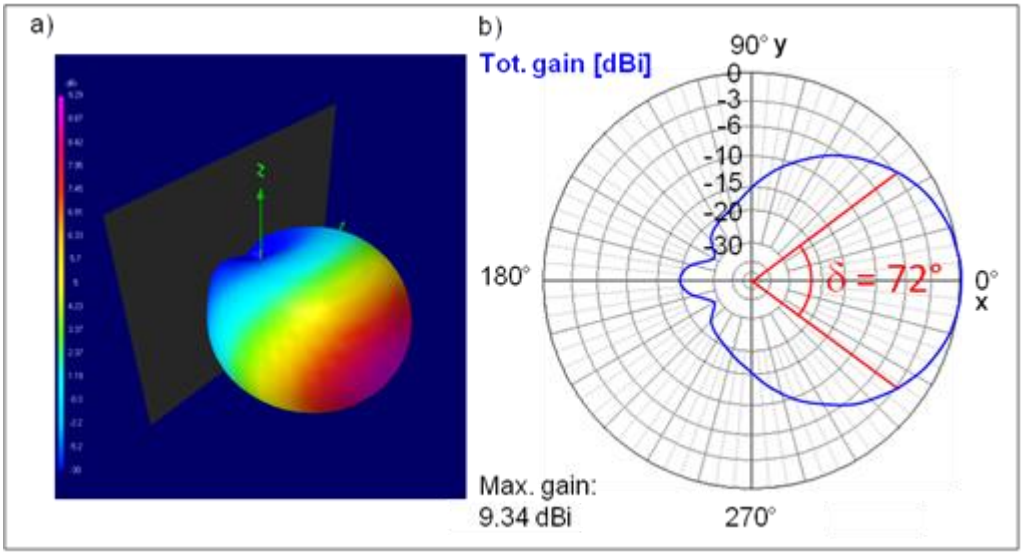

Figure 6: Radiation pattern of a dipole in front of a planar reflector (3 m x 3 m), a) 3D presentation, b) in xy-plane.

According to the aforementioned explanations, a signal level must exceed 400 pW to detect it with the radar system. Applying the radar equation (I) results in the diagram in Figure 7. The parameters specified in the equation are the wavelength of the centre frequency of the radar antenna used, the signal power, the antenna gain, the attenuation within the medium, the distance of the borehole and the effective reflecting area of the investigated reflection.

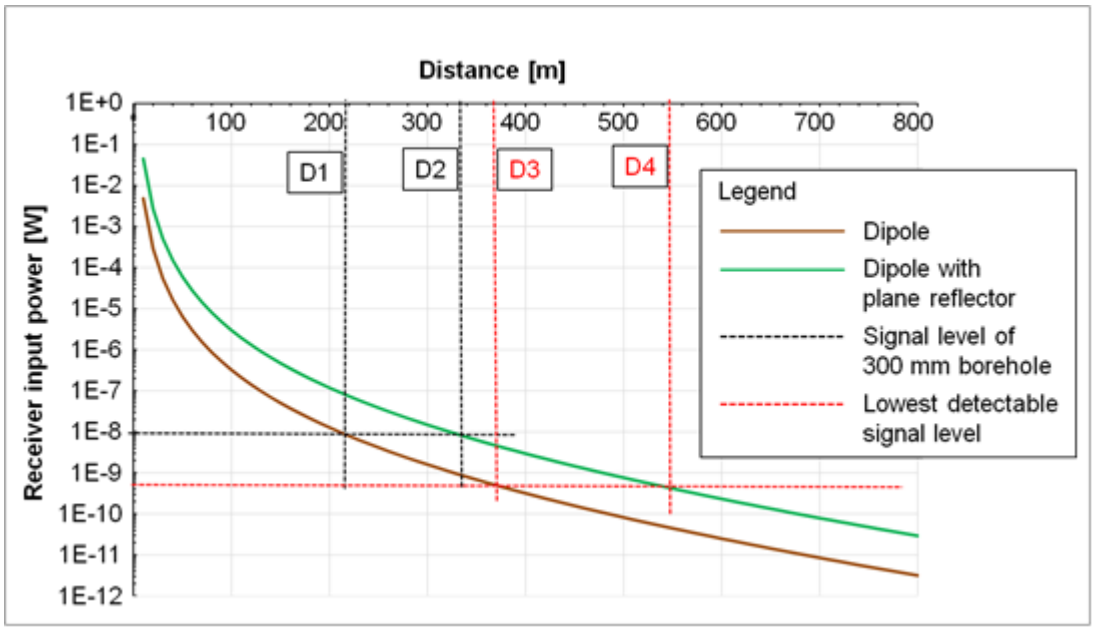

Figure 7: Range estimation based on sensitivity analysis.

Resulting from the calculations, the diagram in Figure 7 shows the drop of the power level as a function of the distance to the borehole. The brown curve illustrates the power level of a simple dipole antenna. D1 is the point at which the borehole was detected at a distance of approximately 210 m. The black horizontal line corresponds to the signal level generated by the reflection of this borehole (10 nW). The red horizontal line shows the lowest power level, in which the signal of the borehole is still just above the noise level of 400 pW. Thus, the intersection of the red line and the power level of the dipole mark the maximum depth D3, at which the borehole can be still detected. Accordingly, the detection limit of a standard dipole is approximately 370 m.

Owing to the higher directivity, a directional antenna is expected to have a larger range. For the comparison, a directional antenna consisting of a dipole with a planar reflector of 3 m x 3 m (see also Figure 6) was selected. This antenna shows a decrease of the power level according to the green curve in Figure 7. In comparison to the dipole signal (brown), the power level of the directed antenna is higher over the whole depth. Thus, with the respective antenna, a higher maximum range is to be expected. The range is marked by the intersection of the noise level (red) with the power level of the directed antenna (green) and corresponds to a value of approximately 550 m (D4).

By the combination of these results with the radiation field of the directional antenna (Figure 6) it is possible to determine the sensitivity of an individual radar antenna (Figure 8). The sensitivity volume is defined via the opening angle. The opening angle is defined as the range within the radiation field, in which the power density does not fall short of 3 dB (approximately half amplitude). This area is defined in the presentation of the directivity in Figure 8 a by orange, red and purple areas. The sensitive volume can be extracted from the three-dimensional radiation field. In this work, the sensitivity volume is approximated by a cone-shaped volume (Figure 8b). At the tip of the cone, the antenna is positioned. The radiating cone shows the sensitivity range and thus also the range area of the radar antenna.

The sensitivity cone can now be used to develop a radar “protective shield” consisting of several antennas. The result of the aforementioned calculations is a maximum range of a dipole antenna of approximately 370 m and range of a directional antenna of approximately 550 m. Since the environment of the repository can be disturbed by mine workings and geological layer boundaries, which may decrease the range, a lower value of 450 m was selected for the detection limit.

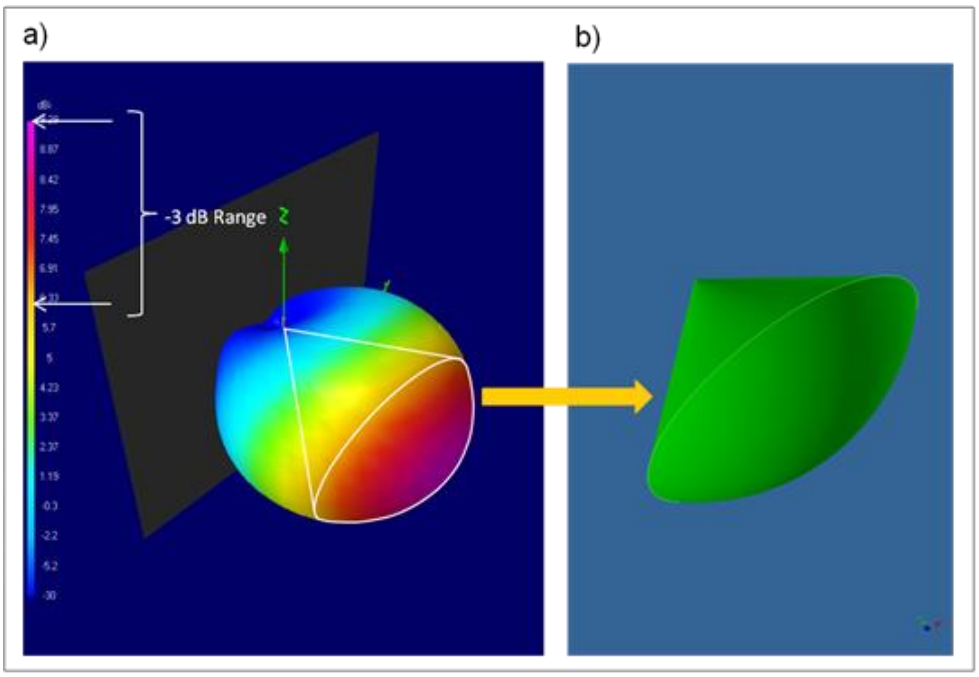

Figure 8: Range estimation based on sensitivity analysis.

The example of a radar “protective shield” is shown in Figures 9. In the example several single antennas of the monitoring system are positioned around a plane repository of 900 m x 300 m (yellow). The detection volume of the horizontal monitoring area is shown in grey and the vertical monitoring area in green. The tips of the sensitivity cones each present the sensor positions. This is an idealized view, since usually transmitter and receiver of a sensor are separated from one another also spatially. For a better overview, two different cross sectional views of the possible layouts are presented in the figures.

The sensitivity of a radar monitoring system is the product of the sensitivities of all single radar antennas. A warning system in form of a “protective shield” can be implemented by a special sensors arrangement. To ensure a complete coverage all around the repository, the sensitivity should not show any gaps in the surfaces.

In the example the horizontal area of the layout was fully covered using 10 directional antennas (grey in Figures 29 and 30). To cover the edges of the repository, in every repository corner, two antennas were positioned with different orientations. The horizontal shield was completed on the long sides of the repository by one more antenna on each side.

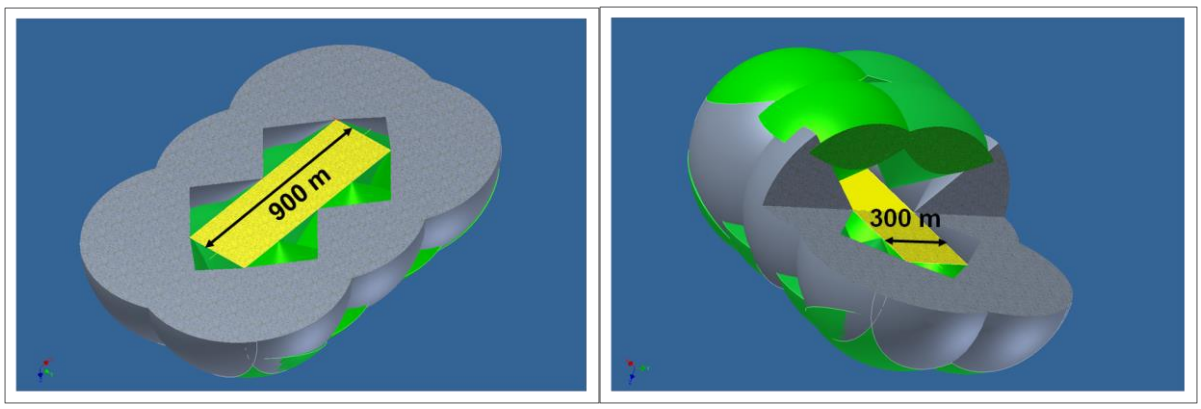

Figure 9: Left: Horizontal section through the layout. Right: Layout of a three-quarter section. Yellow: repository, grey/green: protective shield estimation based on sensitivity analysis.

The example shows that theoretically a repository with the dimensions 900 m x 300 m located in dry rock salt can be safeguarded by a monitoring system consisting of 26 antennas. At other sites, such as in solid crystalline rock, lower ranges are expected. With a lower range, the number of individual sensors must be increased accordingly. In the example presented, half the range would require approximately twice as many detectors to enable a complete coverage of the repository. However, the amount of detectors is depending on the repository concept and may be even higher.

5. Conclusions

Simulation calculations of various unauthorized activities show that under favourable conditions even very minor activities at a large distance to the radar antenna can be detected. However, the range is affected severely by the mass conductivity of the rock or the filling of the pores as well as by the conductivity or magnetizability of fractures. The respective range should be determined in advance by test measurements at various locations of a site. In addition, certain geological layer boundaries may have a shielding effect so that areas behind them can either be monitored to a limited degree or not at all.

At suitable sites, radar has a high potential as a monitoring technique. The use of stationary antennas facilitates zero maintenance and a clear positioning. The use of directional antennas allows the localization of underground activities; moreover, the influence of known events from the inside of the mine is reduced.

6. References

[1] Sandmeier, K.-J.; *ReflexW Version 7.2, Windows 9x/NT/2000/XP/7 – Program for the processing of seismic, acoustic or electromagnetic reflection, refraction and transmission data* ; Karlsruhe: Sandmeier scientific software; 2014.

[2] Militzer, H. and Weber, F.; *Angewandte Geophysik;* Vienna: Springer-Verlag; 1985

Session 05

Arms Control and Nuclear Disarmament

Verification I

The challenges of nuclear disarmament verification: defining a Group of Scientific Experts for disarmament verification[i]

Andreas Persbo and Noel Stott
Verification Research, Training and Information Centre (VERTIC)

Abstract:

Crucial to the process of multi-lateral nuclear disarmament are three key principles: transparency; irreversibility and verifiability. Without these, nuclear disarmament cannot be credibly assured or provide the trust and confidence needed by all States in their quest for a world without nuclear weapons. This has been repeatedly emphasised in many international forums including, most recently, in the final report of the 2016 United Nations General Assembly's Open-ended Working Group Taking Forward Multilateral Nuclear Disarmament Negotiations and in Resolution 71/67 adopted on 14 December 2016 by UNGA. Currently, not many agreed verification solutions exist. However, there are valuable previous and ongoing initiatives in this field and lessons that can be learnt from other processes in order to tackle the complex technical, legal and political issues surrounding multilateral verification.

This paper will explore the benefits of creating a multilateral Group of Scientific Experts on Nuclear Disarmament Verification as a means to increase the international knowledge-base of verification options as reflected in the outcomes of two recently held workshops with European and African stakeholders. It will also examine how such a Group could address the challenges moving forward including strategies for sustainable and inclusive verification capacity building and how to address unforeseen technological advancements.

Keywords: Disarmament; Verification; Nuclear; Scientific Experts

1. Introduction

The importance of verification has repeatedly been emphasised in many international forums including recently in Resolution 71/67 adopted on 14 December 2016 by the United Nations General Assembly (UNGA). The resolution, with 175 states voting in favour and none against, mandates the UN Secretary-General to establish a group of governmental experts (GGE) to consider the role of verification in advancing nuclear disarmament.

Effective nuclear disarmament verification is an essential precondition for achieving 'a world without nuclear weapons'. Without verification and the two fundamental principles of transparency and irreversibility, nuclear disarmament activities may not credibly provide the trust and confidence needed by all states in a world where all nuclear weapons have been abolished. While verification is not an end in itself, further development of the multilateral nuclear disarmament verification capabilities will be required for the achievement and maintenance of a world without nuclear weapons. Resolution 71/67 expresses the General Assembly's conviction that 'identifying and developing practical and effective measures of nuclear disarmament verification and monitoring' will 'foster confidence and facilitate efforts to achieve and maintain a world without nuclear weapons.' International co-operation in addressing the underlying scientific and technical questions on nuclear disarmament verification measures is of great importance.

While past and on-going initiatives in this field have carried out valuable research and explored useful approaches, this work needs to be not only be captured and preserved but sustained, better co-ordinated and continuously renewed as technology advances. Thus, the creation of a multilateral Group of Scientific Experts on Nuclear Disarmament Verification (GSE-NDV) could, in the long-term, assist in the development of a truly shared and trusted understanding of the technical, procedural and policy challenges of nuclear disarmament verification (especially between nuclear and non-nuclear weapon armed states and between the nuclear armed states themselves). It could also generate sustained dialogue between scientific and technical experts, diplomats and policy-makers within and between the nuclear- and non-nuclear weapon states. A GSE-NDV could also consolidate efforts in

the field to date, identify and co-ordinate research needs and initiate ways and means to undertake such research within limited budgets and organisational capacity.

2. Background to the GSE-CTBT

The establishment of groups of qualified experts in the form of a Group of Governmental Experts (GGE) or a Group of Scientific Experts (GSE) is a relatively common approach within the United Nations system as well as in other intergovernmental organisations such as the European Union. These groups are often mandated to undertake in-depth studies on a particular topic and to make recommendations to the body that created them. Importantly, they are not mandated to negotiate, for example, a treaty or convention.

There are many examples of such bodies in the arms control, non-proliferation and disarmament fields as well as in other areas of international concern. Examples include the GGE tasked with making recommendations on possible aspects that could contribute to a treaty banning the production of fissile material for nuclear weapons or other nuclear explosive devices. Another example is the GGE on lethal autonomous weapons systems.

The Intergovernmental Panel on Climate Change (IPCC), established by the United Nations Environment Programme (UNEP) and the World Meteorological Organization (WMO) is perhaps the most well-known expert group with a long-term mandate in a non-arms control field. The IPCC's mission is to provide a clear scientific view on the current state of knowledge on climate change and its potential environmental and socio-economic impacts.

A regional example is the European Commission's GSE that focussed on ways to counter potential biological and chemical terrorism. It undertook an assessment of knowledge and capacity regarding bio-defence and looked into future research requirements.

In the context of disarmament verification, a prime example is the Ad Hoc Group of Scientific Experts to Consider International Co-Operative Measures to Detect and Identify Seismic Events, commonly referred to as the 'Group of Scientific Experts' (GSE-CTBT).

While a comprehensive ban on nuclear testing had been a foreign policy objective for many governments since the mid-1950s, US-Soviet relations were coloured by the Cold War. There were also scientific and political disagreements over the verifiability of a proposed treaty prohibiting nuclear testing. To achieve at least partial progress on the issue, Sweden proposed the establishment of a group to study the technical aspects of verification. This GSE was established under the auspices of the Conference on Disarmament (CD).

This GSE comprised mostly of seismologists, was active for 20 years, from 1976 until 1996. The group was tasked to 'specify the characteristics of an international monitoring system' using seismological monitoring. It reported directly to the CD and produced several substantive reports throughout its lifetime. Four senior political officers from the United Nations (UN) supported the Group as secretaries over the years that it met.

This GSE helped to keep the notion of a comprehensive test ban alive despite being established at a time when there was little or no political appetite for such a treaty. During the cold war, it was the only ongoing multilateral dialogue on disarmament issues and while progress was slow, the work to design a global verification system allowed for the sharing of knowledge on how a seismic verification system could, in principle, be achieved.

It is a key example of how expert groups can be used to provide capabilities that facilitate agreement on difficult technical issues for the monitoring or verification of compliance with a treaty.[ii]

Its research agenda and the scientific progress that came out of it were unconnected to political negotiations. Its agenda was broad enough to enable continuous work through two decades, ultimately leading to the creation of a shared understanding of verification options. The GSE-CTBT also shows that scientists from across the political divide, working side-by-side over many years, can significantly assist diplomatic processes and ensure that later agreements can be implemented.[iii]

3. Key considerations when applying the concept to NDV

A key question is whether this concept can be exported to the institutional realities of 2017.

Presently, political conditions are challenging. Deep divisions between major nuclear powers, especially the United States (US) and Russia; uncertainty about the Trump Administration's future nuclear posture and its apparent disdain for arms control and disarmament; rising tensions on the Korean Peninsula; lack of progress in the context of the NPT review process and no progress toward entry-into-force of the Comprehensive Nuclear-Test-Ban Treaty (CTBT), to list but a few.

Moreover, views on approaches to nuclear disarmament vary. However, all states remain committed to the long-term goal of irreversible disarmament. The unanimous support for Resolution 71/67 on nuclear disarmament verification demonstrates this commitment.

Clearly, the research scope for multilateral disarmament verification would have to be much broader than was the case for the GSE-CTBT as the 'objects of verification' includes many different types of materials, processes, equipment and facilities, some of which are highly sensitive. Defining a scope and set of research tasks would be more complex and would require that no political assumptions on what disarmament activities states should or will take are made.

However, as was undoubtedly shown by the GSE-CTBT, it is possible to conduct preparatory scientific and technical analysis before political negotiations or indeed without a commitment to commence such negotiations, in other words, in world not conducive to global disarmament.

A GSE mandated to explore nuclear disarmament verification measures (like the GSE-CTBT) would need to be linked to a multilateral body such as the Conference on Disarmament or the UNGA in order to provide a formal framework allowing states, to not only commit experts to participate in meetings, but also to make considerable investments in research and outreach activities and for its efforts to be sustained, consistent, and focused.[iv]

Such a group would need to take into account previous and current initiatives on verification, such as the UK-Norway Initiative and its successor – the Quad Nuclear Verification Partnership – as well as the International Partnership for Nuclear Disarmament Verification (IPNDV), which is due to enter phase two of its programme of work in 2018. Other older processes would also need to be examined for applicability – including, for example, the Black Sea Experiments of the late 1980s and the Trilateral Initiative which was launched in 1996 by the US, Russia and the International Atomic Energy Agency (IAEA).

With this in mind, and to possibly feed into the GGE's deliberations in 2018 and 2019, VERTIC has designed a series of four regional consultations: in Africa, Asia, Europe and Latin America to be hosted in 2017. Importantly, VERTIC aimed not to prejudge or pre-empt any recommendation that may be made by the GGE established by UNGA/RES/71/67.

4. VERTIC Workshops

VERTIC has so far hosted two of the four workshops – one in Vienna for European states and organisations and one in South Africa for Africans – both in April 2017. The workshops were structured in such a way that participants could discuss whether a multilateral GSE-NDV would be able to:

a. consolidate efforts in the field to date;
b. identify and co-ordinate research needs and initiate ways and means to undertake such research within limited budgets and organisational capacity; and
c. generate sustained dialogue between scientific and technical experts, diplomats and policy-makers within and between the nuclear-armed and non-nuclear-armed states.

The two-day consultations involved 33 researchers, diplomats and policy makers, drawn from eleven countries and 16 organisations on the two continents. Half of the participants were drawn from governments. All individuals took part in their personal capacity although they were also able to articulate what they thought their government's or organisation's view might be. Each participant contributed subject to the Chatham House rule.

Each workshop was guided by a set of discussion papers designed to stimulate debate and produce practical suggestions. Discussion papers focussed on:

1. 'The Importance of Verification and Transparency for Nuclear Disarmament'—which examined why nuclear disarmament verification is an issue of concern for both non-armed weapon states and nuclear armed states and the important role of the scientific community in arms control, disarmament and non-proliferation activities;
2. 'The Role of the Group of Scientific Experts in the Negotiation of the Comprehensive Test Ban Treaty' — this paper examined what, if any, lessons can be learned from this experience and what role this group played in preparing the foundation for political progress until CTBT negotiations started;
3. 'An Overview of Past and Present Networks and Groupings Devoted to Nuclear Disarmament Verification' — this paper focused on current and past initiatives of direct relevance to nuclear disarmament verification. They included the United Kingdom-Norway Initiative (UKNi) – now with the addition of the USA and Sweden and renamed the Quad Nuclear Verification Partnership; the International Partnership for Nuclear Disarmament Verification (IPNDV), the US-UK Technical Cooperation Programme, and the so-called 'Trilateral Initiative'; as well as other initiatives such as those of ESARDA and the German Disarmament Verification Network;
4. 'What Role Could European/African States and Scientists Play in Nuclear Disarmament Verification?'—these food-for-thought papers, one produced for each meeting, served as a basis for discussion on how such a GGE-NDV could contribute to regional security and how involvement by the relevant bodies, such as the European Union and the African Union (AU), could move the debate forward; and
5. A final paper which provided a select list and description of GGEs and GSEs from other arms control, disarmament and non-proliferation initiatives and other fields.

VERTIC will hold two further workshops in the latter half of 2017, one for South American and one for Asian stakeholders. It will deliver its final report during the UN First Committee in October or November 2017.

5. Interim conclusions

The purpose of these workshops was neither to reach consensus nor to draw definitive conclusions regarding the feasibility or desirability of a GSE-NDV. Nevertheless, participants in both Vienna and Pretoria concurred that:

1. Nuclear disarmament verification is probably one thing that all states can agree or commit themselves to — although they may disagree on exactly what it means and on the measures needed to achieve it;

2. Many lessons could be derived from the GSE-CTBT. Above all, it demonstrated that it is possible and useful to conduct preparatory scientific and technical analysis and develop capabilities that could facilitate agreement on difficult technical issues for the monitoring or verification of compliance with a treaty;

3. The establishment of a GSE-NDV as an apolitical body would constitute an important means to conduct joint research into verification technologies and data-analysis methodologies, while the political environment is not conducive and while political processes are maturing;

4. One would, however, need to define 'nuclear disarmament verification'. In particular what stage of the disarmament process it refers to - such as dismantlement, material disposition or accounting.

5. A GSE-NDV's mandate should be set by the United Nations General Assembly (UNGA), as this would give ownership to all stakeholders, irrespective of geographical location or legal status under the 1968 Treaty on the Non-Proliferation of Nuclear Weapons (NPT). It would also give the group credibility and legitimacy. Finally, it could potentially provide a source of long-term funding (possibly supplemented by a mechanism such as a Voluntary Trust Fund).

6. A GSE-NDV's scope of work, even if broad and open-ended, would have to have clear scientific and technical parameters;

7. Further to that, a GSE-NDV's scope of work could be derived from UNGA/RES/71/67. In particular, participants highlighted the third operative paragraph, which calls for all States to work together to 'identify and develop practical and effective disarmament verification measures' through developing 'tools, solutions and methods and capacity-building.' Participants also noted the fourth operative paragraph, that calls for the 'development and strengthening of practical and effective nuclear disarmament verification measures.'

8. Scientists and technical experts should form the core of a GSE-NDV. However, provision should be made for policy-makers and legal experts to interact with it periodically;

9. Scientific and technical experts forming a GSE-NDV should be drawn from both nuclear- and non-nuclear armed states;

10. An important aspect of the work of a GSE-NDV should involve medium to long-term capacity-building processes and programmes on verification techniques and mechanisms;

11. States would need room to interpret the mandate to suit their foreign policy goals - NPT member states should be able to justify their work under Article VI. Non-NPT states should be able to justify their participation by their UN membership.

12. The mandate should also be broad enough to accommodate the policy positions of both 'immediate abolitionists' and 'step-by-step advocates'.

13. The GSE-NDV would need to strike a balance between what is politically desirable to achieve and what is practically feasible given the national security constraints of the work;

14. The GSE should aim to overcome issues relating to duplication, overlap and 'reinventing the wheel,' but should not necessarily be the sole vessel of international co-operation on disarmament verification.

15. In that sense, a GSE-NDV would need to develop a mandate and working methodology that a) takes into account existing initiatives; b) makes use of their work in this area; and c) benefits from the technical expertise in these groupings.

16. Following on from the GGE's work in 2018 and 2019, such a GSE-NDV could feasibly commence its work in the early 2020s and with a mandated but open agenda.

6. Conclusion

The complete elimination of nuclear weapons everywhere is in the long-term security interest of all states. However, both government representatives and various non-governmental experts point out that obstacles to nuclear disarmament include both the lack of favourable political and security conditions, and the challenges associated with verifying the dismantlement of nuclear weapons.

As part of efforts to implement Resolution 71/67, it may be prudent therefore for states to co-operate in establishing a group of scientific experts that would address technical challenges to, and advance the development of solutions for, nuclear disarmament verification in the longer term. The inspiration is the example of the group of scientific experts (GSE) that was created in 1976 to study monitoring and verification approaches for a nuclear test ban.[v]

The creation a multilateral Group of Scientific Experts on Nuclear Disarmament Verification, to complement existing initiatives and partnerships can only increase the international knowledge-base of verification options, enable all states to actively collaborate in developing practical methods that could contribute to the verification of irreversible dismantlement of nuclear weapons and provide a platform for long-term sustainability, capacity-building and consolidation.

It was scientists that brought nuclear weapons into being and it will be scientists and technical experts who will have as much a role in their abolition as they had in their creation.

---

[i] This paper is an edited version of 'Defining a Group of Scientific Experts for Disarmament Verification', *VERTIC Brief* 27, May 2017.

[ii] W.H. Dunlop, 'The role of Group of Scientific Experts in facilitating better international relations, particularly in arms control', Report: Lawrence Livermore National Laboratory, 2012. <https://e-reports-ext.llnl.gov/pdf/629112.pdf>

[iii] Arian L. Pregenzer, 'Enhancing Regional Security Agreements Through Cooperative Monitoring', Report: Sandia National Laboratories, May 1995. <http://www.iaea.org/inis/collection/NCLCollectionStore/_Public/26/074/26074525.pdf>

[iv] See: Ola Dahlman, 'How Can Science Support a Process Towards a World Free of Nuclear Weapons?', *Science & Global Security*, 21: 95–105, 2013.

[v] See "1993-1995: Prelude and Formal Negotiations," Preparatory Commission for the Comprehensive Nuclear Test Ban Treaty, https://www.ctbto.org/the-treaty/1993-1996-treaty-negotiations/1993-95-prelude-and-formal-negotiations/.

International Engagement in Arms Control Verification Using a Systems Approach

M. Dreicer[1], I. Niemeyer[2], G. Stein[3]

[1]Lawrence Livermore National Laboratory, Livermore, USA
[2] Forschungszentrum Jülich, Jülich, Germany
[3] Consultant, Bonn, Germany

Abstract:

A series of exercises and targeted meetings held by the European Safeguards Research and Development Association (ESARDA) Verification Technologies and Methodologies Working Group and the Institute of Nuclear Materials Management (INMM) Nonproliferation and Arms Control Technical Division have provided valuable insight into how a systems approach could help identify non-proliferation and arms control verification requirements. International experts from nuclear weapons states and non-nuclear weapons states, with a wide-range of expertise in nuclear safeguards, arms control verification, radiation detection, political science, and defense studies, participated in the discussions. It demonstrated that it is possible to design a transparent state-level systems framework to define verification objectives, processes, and timescales for an effective verification regime based on the strategic goals of a treaty, while taking into account restrictions from different security environments. It was also an effective mechanisms for international and technical engagement on these complicated issues. Possible future research activities could include: (1) increased efforts to link the material and weapons sectors of the nuclear weapons complex; (2) further attention on how to satisfy the competing needs for effective verification and protection of national security; (3) greater consideration on how to define the treaty-controlled items so that declarations can be verified effectively; (4) continued testing of a systems approach to analyze the pros and cons of possible verification regimes to conduct a form of sensitivity analysis and provide feedback and a better understanding of confidence levels that could be achieved; and (5) possible ideas of how to engage in substantive dialogue in a broad international environment, such as the on-going International Partnership for Disarmament Verification (IPNDV), while taking into account the range of weapons and verification experience and the need to uphold NPT Article VI.

Keywords: verification, arms control, systems approach

1. Introduction

Establishing a method to systematically identify verification options for nuclear weapons control agreements could significantly contribute to future development of an effectively verifiable treaty [1]. The presentation of a nation's nuclear defense complex would help define potential cheating pathways and facilitate the development of requirements for declarations/data exchanges and an inspection regime needed for verification. The increased transparency could foster confidence and improve communication between potential stakeholders.

The application of a systems approach, such as the International Atomic Energy Agency's State Level Concept (SLC) [2] to arms control agreements could help build a framework or verification architecture to be used to structure analysis. A series of technical meetings were organized in 2014 and 2015 to investigate the utility of a systems framework in the nuclear arms control context. International experts

from nuclear weapons states and non-nuclear weapons states, with a wide-range of expertise in, *inter alia*, nuclear safeguards, arms control verification, radiation detection, political science, and defence studies, participated in exercises and discussions to test the feasibility and identify knowledge gaps. To make the effort less abstract, two fictitious countries and a hypothetical treaty were devised for two exercises. An effort was made to represent some real-world complexity, without making it too difficult, so relatively simple physical models of national nuclear weapons enterprises were created. By formulating a scenario that incorporated more than the technical aspects of verification, it was possible to look at the state-as-a-whole and consider the additional factors that influence national security decision-making.

Unrealistically, two constraints were NOT applied during the exercises: (1) the declaration of security-sensitive information was allowed because a country could make the decision that it was in its interest to declassify information or share it under conditions deemed advantageous; and (2) the verification requirements focused only on the country to be verified without consideration of the acceptability of the same requirements being imposed on the verifier.

2. Workshops and Exercises

The initial exercise set out to analyze potential diversion (cheating) pathways and potential treaty verification measures that could be applied in a nuclear weapons state. It was hosted by the European Safeguards Research and Development Association (ESARDA) Verification Technologies and Methodologies Working Group Meeting at the Joint Research Centre, Ispra, Italy, in autumn of 2014 [3].

The model bilateral treaty between the two nuclear weapons states limited the total number of warheads deployed and stockpiled. During this exercise, the meeting participants considered the existence of undeclared warheads above the initially declared total of 1,970 for the fictitious state. It maintained six types of nuclear warheads that were deployed across three types of delivery platforms, and any warheads deployed above the maximum of 500 would constitute a form of cheating.

The nuclear weapons enterprise comprised a complete nuclear fuel cycle and weaponization facilities, which included a stockpile of military fissile material; warhead components production facilities; warhead production, maintenance, and dismantlement facilities; different types of storage depots; military bases; and delivery vehicles. A simple physical model of the enterprise was considered and potential cheating pathways debated. The group quickly learned that national security concerns and the country's defense posture greatly influenced the type of cheating and likelihood of cheating along particular pathways, so a second short exercise was held by the Institute of Nuclear Materials Management (INMM) at Lawrence Livermore National Laboratory during the summer of 2015 [4]. At this meeting, a simpler scenario was developed for the two fictitious neighbouring countries and the exercise was structured so that national security objectives would be taken into account, while considering the verification regime each country would require. A formal exercise framework (Figure 1) was suggested to focus the participants on national objectives and priorities.

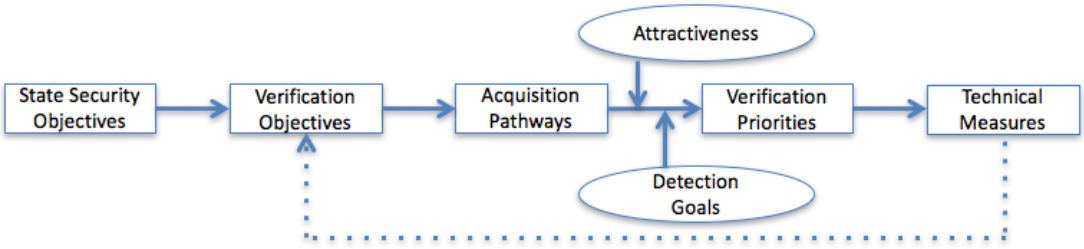

Figure 1. Framework used to explore the usefulness of a systems approach to development of a treaty verification regime.

For this exercise, the model treaty limited the total nuclear forces at existing levels for a period of 10 years, including strategic and tactical and deployed and non-deployed. Each type of delivery system and the deployed and total number of warheads (including deployed and non-deployed) were capped, and the development, testing, and deployment of new types of warheads and delivery systems was prohibited.

The neighboring countries were configured to represent different levels of development, capabilities, and populations. The larger power with a population of 200 million, was designed as a moderately advanced industrialized state with regional military and economic dominance with ambitions for broader global influence. It had a sophisticated nuclear weapons enterprise consisting of civilian and military nuclear fuel cycles and a total of 322 nuclear warheads. The smaller ascending power (population of 100 million) was newly industrialized with a modest conventional force, recently developed its nuclear capability and relied on a primitive nuclear deterrent. Its nuclear enterprise consisted of both civilian and military nuclear fuel cycles, and has possession of a total of 110 warheads.

The final discussion, held at the 8th INMM–ESARDA Joint Workshop at Jackson Hole, Wyoming, in October 2015 [5], was not directed towards any specific scenario, but instead focused more on application of systems engineering approaches and the complications that protection of sensitive national security information introduces into the process.

3. Key insights

The use of exercises, with fictitious states and model treaties, effectively focused the discussion on the application of a systems approach beyond International Atomic Energy Agency (IAEA) safeguards. It was interesting to invite both safeguards and arms control experts, some with expertise in international relations or political science, with the intent to challenge them to adapt their usual focus and methods to a different domain. Another unusual aspect of these meetings was the range of viewpoints that nuclear weapons state and non-nuclear weapons state experts brought to the development of a nuclear arms control verification regime. Overall, it was demonstrated that it is possible (albeit complicated) to design a state-level systems framework to define verification objectives, processes, and timescales for an effective verification regime based on the strategic goals of a treaty, while considering restrictions from different security environments. More work is needed but the authors believe that it is an effective mechanism for international and technical engagement on these complicated issues.

During the first exercise, most the participants came with vast experience in international safeguards and the group dove into acquisition pathway analysis with attempts to define attractive pathways and timeliness goals. As the effort bogged down, it was clear that the SLC would need to be modified to fit into this different context. Within the safeguards context, the goal is to prevent and detect the diversion of specifically defined nuclear materials. At the state-level, safeguards are applied in non-nuclear weapons states. The Nuclear Weapons States that implement a Voluntary Offer, apply safeguards in only volunteered facilities in the complex. In an arms control context, depending on the definition of the treaty accountable items, the cheating pathways would be found across the whole military and civilian complex. To conduct an integrated assessment, it will be necessary to link the material and weapons sectors of a nation's nuclear weapons complex. When planning for the verification of items, such as weapons or weapons components, the State's security and defense objectives will come into play.

Defining clear metrics to evaluate pathway "attractiveness" and "timeliness of detection" for possible cheating must also be modified for an arms control context. The metrics used by the IAEA will provide a good basis for further work. New or revised metrics would likely be dependent on the objectives of the treaty and the security situation of the countries involved. For example, the technical difficulty of cheating might not be the issue for an existing functioning facility but whether "stealth" or "denial and deception" could be implemented would be a key factor. When considering whether maintenance and operational costs are an obstacle to cheating using a particular pathway, it would be important to consider if those costs were already included in the national budget. If so, the cost would not likely have a great influence on the level of attractiveness to exploit the pathway.

The participants considered that the detection goals for diversion or production of significant quantities of treaty accountable items would be greatly influenced by the perceived stability in a region. Increased transparency but lower confidence verification of exact numbers might be acceptable between countries

with a trusted stable relationship. However, if each state has only a low number of weapons, accurate verification of numbers and locations might be a very strong requirement for treaty ratification.

An effort was made during the second exercise to simulate an environment where the security of the State was an integral part of the scenario. By better defining two states, and splitting the participants into two groups, each side could go through the process outlined in Figure 1 and determine its own national security and verification objectives. With this additional information, the analysis of the different cheating pathways could be considered in the context of strategic and/or defense advantage.

For example, if deterrence were the objective, having an undeclared (and undetected) cache of undeclared weapons would not provide much benefit. However, if the objective was to gain a strategic advantage for a certain area of a disputed border, it would be important to detect and cheating with respect to the number and locations of weapons.

The imbalance between the two-hypothetical nuclear capable states during the exercise illustrated how the security objectives would drive the focus of a verification regime. The more capable state was interested in maintaining its advantage and therefore required that no new capability could be achieved in the smaller state without detection. So, the pathway analysis focused on the material and weapons production sectors of the complex. The less capable state was less concerned about improvements in the neighbor's already powerful nuclear weapons capability than it was about the numbers and location of weapons near its borders.

Ultimately, finding the balance between the degree of intrusiveness and allowable transparency must be achieved to provide confidence in treaty compliance. A nation's national security requirements and the protection of sensitive information and facilities will constrain the final verification regime. Protection of nuclear weapons knowledge (including materials, facilities and processes) are crucial to national security and are governed by the Nuclear Non-proliferation Treaty (NPT) if nuclear and non-nuclear weapons states are involved. All these factors will influence the requirements for verification technology and acceptable uncertainty in the data that can be collected. Using an iterative process, verification measures could be developed to provide sufficient confidence in compliance in a way that would couple existing technical capabilities with operational and security requirements. It could also help point the way for future technology R&D programs.

Greater details on the scenarios and results of the technical discussions can be found in an upcoming book [6].

4. Future Research

Continued research can be done to advance implementation of an acquisition pathway analysis methodology in nuclear weapons states. Increased efforts to link the material and weapons sectors of the nuclear weapons complex are needed. More consideration should be given on how to define the treaty-controlled items. Specifically, further work to refine metrics for pathway attractiveness, detection probabilities and detection goals will depend on the items to be verified, related pathways and the security objectives of a state.

Continued testing of a systems approach to analyze the pros and cons of possible verification regimes should be carried out. This approach can also be used to conduct sensitivity analysis and provide feedback to better understand high priority pathways and how various confidence levels could be achieved. These results could impact the design of future declarations and provide more objective methods for evaluating effective verification.

A clear benefit from the series of ESARDA/INMM expert meetings was the development of a cadre of national technical experts that is becoming more familiar with these issues. Based on the positive experience of working across a diverse community, substantive dialogue in an international environment, such as the on-going International Partnership for Disarmament Verification (IPNDV), should be encouraged. A structured framework to guide complicated and sensitive discussion could facilitate engagement across a broad range of weapons and verification expertise and support Article VI of the NPT.

5. Acknowledgements

The authors would like to thank ESARDA and INMM for hosting the technical meetings and all those who participated and shared their expertise and idea. The authors would like to acknowledge Cliff Chen (Lawrence Livermore National Laboratory) and Keir Allen (Atomic Weapons Establishment) for their significant contributions to this effort.

6. Disclaimer

The views in this chapter do not represent the views of any governments, institutions or professional organizations. This work performed under the auspices of U.S. Department of Energy by Lawrence Livermore National Laboratory under contract DE-AC52-07NA27344. LLNL-CONF-731157

7. References

[1] Dreicer M, Stein G; Applicability of Nonproliferation Tools and Concepts to Future Arms Control; ESARDA Bulletin No. 49:95-99; 2013.

[2] Cooley J; The State-level Approach to International Safeguards; Institute of Nuclear Materials Management Conference Proceedings; 2009.

[3] Allen K, Dreicer M, Chen CD, Niemeyer I, Listner C, Stein G; Systems approach to arms control verification; ESARDA Bulletin No. 53:83-91; 2015.

[4] Chen CD, Dreicer M, Proznitz P, Benz J, Duckworth L; Systems Concept for Arms Control Verification; https://cgsr.llnl.gov/content/assets/docs/arms_control_verification_report.pdf; 2015.

[5] INMM/ESARDA Working Group 2 Report – Arms Control, Jackson Hole Wyoming; http://www.inmm.org/AM/Template.cfm?Section=8th_INMM_ESARDA_Workshop&Template=/CM/ContentDisplay.cfm&ContentID=6633; 2015.

{6} Niemeyer I, Dreicer M, Stein G, eds.; Nuclear Non-proliferation and Arms Control Verification. Innovative Systems Concepts; Springer (in publication) 2017.

Military Dimensions of Nuclear Disarmament Verification

Michel Richard

Independent Expert/Associate Researcher FRS
ARMIR Global Security Network
(micheljrichard@orange.fr)

Abstract:

Military dimensions associated with nuclear arms control, disarmament and non-proliferation verification of a state's commitments are key for any significant and solid progress to be made. Verification of compliance and assurances of the absence of cheating are very sensitive issues, in particular with respect to the military capabilities that form the foundation of strategic and political posture at a national, regional and global level. This article sets the scene through a brief historical review of the influence that verification has on the credibility of arms control measures, the effectiveness of nuclear non-proliferation efforts and the importance of the nuclear disarmament process. In the framework of nuclear disarmament verification the main features of the military nuclear system are the doctrines, research & development, production, deployment and elimination of nuclear weapons, and the verification measures associated with disarmament commitments. Finally, a brief description of the complexity of regional, multinational and international instruments is provided. Using a systems concept to establish a verification mechanism,, taking into account the specificity and the issues impacting individual states, could overcome the global complexity and national antagonisms and provide the confidence needed to enhance world global security.

Keywords: nuclear_disarmament, verification, military_dimensions, national_security,

1. Introduction[1]

Since the United States dropped the atomic bomb on Japan to end World War II, the possibility of use and the deterrence of use of nuclear weapons have been at the heart of military strategic doctrine. This is true for countries that possess nuclear weapons or rely on an ally's nuclear umbrella, those that do not currently possess nuclear weapons but may consider doing so in the future, and those that wish for global elimination.

In the fifties and sixties, the rapid growth of the United States (US) and the Soviet Union (USSR) nuclear arsenals, was followed by United Kingdom (UK), France, and China as they achieved nuclear status. This formed the club of five NPT nuclear weapon states. Later India (1974 and 1998) and Pakistan (1998), non-NPT parties, conducted nuclear weapons tests, more recently joined by North Korea's (2006, 2009, 2013, 2016) tests which withdrew from the NPT (2003). The threat of continued nuclear proliferation in Iraq, Libya, Iran and the increasing pressure for reduction and dismantlement of nuclear capacities, remain very sensitive issues and major factors in the political and strategic standing of states.

Nonetheless, significant progress has been made since the Cuban missile crisis (1962) and especially since the end of the Cold War in the early nineties. More than seventy years after Hiroshima and Nagasaki and 25 after the end of the Cold War, the world's nuclear arsenals are still estimated to total more than 15,300 warheads, nearly 93% of which are in the hands of the US and Russia.[2] This still remains a major concern but a real improvement compared to the 70,300 weapons active in 1986[3].

In the aftermath of the disintegration of the USSR, the end of the Cold War and the new strategic context, which began with the perspective of a more peaceful world, brought new hopes and gave a new momentum to the nuclear disarmament process. Alas, at the turn of the century, the resumption of antagonism between the western bloc, young Russia, and emerging China plus regional disputes (i.e. India and Pakistan) have soon slowed down the pace of nuclear disarmament process.

Nuclear weapons remain a major component of the security posture and backbone of military political and alliance strategy for those who wish to possess them. This includes the countries that rely on the umbrella of US deterrence. Some states see nuclear weapons as a global strategic stability factor and others view them as a regional power vector. If strategic, regional and national conditions are met, progress on nuclear disarmament would be an important enhancement of global and regional security. This progress is not possible without the confidence that security it not undermined. The key challenge is to set the right balance between efficiency of disarmament instrument's verification systems and the legitimate rights of states to protect sensitive national security information. Transparency and effective verification will be essential to build confidence between states or group of states and allow progress towards that goal. Confidence building measures, such as:

- verifiable declarations,
- voluntary actions,
- changes in state doctrines,
- irreversible destruction of equipment,
- facilities or testing sites,
- disposition of fissile material stocks no longer needed for defense purpose, and
- removal of nuclear warheads, with ad hoc visits

could all efficiently contribute to the establishment of a climate conducive to progress, as stated by UNSCR 1887 Preamble, unanimously adopted by heads of state.[4]

Over the last thirty years, a renewed nuclear landscape has emerged in uncertain strategic environment, with new actors and new threats and a higher risk of nuclear use. Global Strategic Stability is more and more elusive and fragile.[5] Any progress expected in nuclear disarmament should proceed stepwise carefully taking into account the strategy, policy, doctrines, regional or international context, culture, military capacity, compliance with existing instruments, and nuclear capacities, both military and civilian, of the states involved. This does not mean that ultimately, everything should or could be verified but the whole system should be considered.

If these conditions are met, nuclear disarmament will proceed steadily, slowly and stepwise. Unfortunately, these conditions are not met currently and there is little hope they will be in foreseeable future, as relations with Russia are worsening. China continues to build up its military nuclear capacities and to manifest tendencies to regional hegemony. Tensions between India and Pakistan did not subside. In the Middle East, the nuclear deal with Iran (Joint Comprehensive Plan of Action) and its verification protocol bring some hope of removing the risk of a nuclear capable Iran (temporarily?). But tensions are still very high and Israel does not appear to be ready to make any move to drop its nuclear guard.

This pessimistic picture of the international context prevents progress in nuclear disarmament and related verification. Progress will only occur if policy-makers feel it's in their country's national interest. It will only happen when political and security conditions enable it to happen[6]. Transparent, verifiable and irreversible nuclear disarmament complemented with credible disarmament measures in all other fields, such as conventional forces, missile defense and space and backed up by a fair and efficient verification regime taking into account all aspects of state's security, complemented by confidence building measures, is the key to movement towards disarmament.

Today the landscape is a mix of hope and pessimism. On one hand, no new progress advancing international instruments has been seen. We are still waiting for some major steps towards a future global nuclear disarmament, such as entry-into-force of the Comprehensive Nuclear Test Ban Treaty (CTBT) and the continuation of negotiations for a Fissile Material Cut-off Treaty (FMCT). The Conference on Disarmament (CD) in Geneva, the multinational fora for disarmament negotiations, has produced no major progress for almost two decades. The fact that some nuclear powers keep modernizing their strategic forces and some continue to increase their nuclear arsenal (India[7], Pakistan[8], China?[9]) shows more is still needed to achieve the common goal of a global nuclear

disarmament. CTBT cannot enter-into-force until major nuclear players as USA, China, India, Pakistan Iran, Israel and North Korea (DPRK) ratify the treaty[10]. Although important work was conducted in 2014-2015, negotiations for a treaty banning the production of fissile materials for nuclear weapon (FMCT or cut-off treaty) have not yet re-started at the CD.

On the other hand, there has been significant progress in recent years. France and UK announced reductions of their nuclear arsenals and put forward transparency measures[11]. France closed the South Pacific test site and begun dismantling its nuclear weapons fissile material production facilities. New START, the Treaty between the US and Russian on *Measures for the Further Reduction and Limitation of Strategic Offensive Arms* has entered into force. No further reduction of fissile material available for nuclear weapons has been announced, after the significant reductions undertaken by US and Russia.

2. Setting the Scene

The linkage between nuclear disarmament verification and strategic postures, nuclear deterrence doctrines and military capabilities is evolving so the strategic context becomes more elusive and complex. Since the end of World War II we have seen that military dimensions, verification processes, improvement in the security context and confidence between states are closely interlinked and can only proceed together.

***Growth of nuclear arsenals*[12]**: In the aftermath of the Second World War, the direct confrontation of both Western and Communist blocs triggered and fueled considerable growth in the US and former Soviet Union's nuclear arsenals. This was seen during Cuba missile crisis which brought the world to the edge of a nuclear war. During this period, United Kingdom, France and China acquired nuclear status and began to develop their own nuclear military capabilities, albeit much smaller than those of the US and USSR. After several setbacks (e.g. Vietnam, Suez, etc.) these states chose not be completely dependent on the two superpowers. The possession of nuclear weapons gave them the political and strategic stature needed, in particular to become members of the UN Security Council.

At the same time, several other states, some very close to the nuclear threshold, concluded that their security would be better without nuclear weapons and renounced them.[13] Others renounced possession of nuclear weapons and campaigned for nuclear disarmament while choosing to be sheltered under the nuclear umbrella of one or other of the superpowers (e.g. NATO members, Japan, Korea under the American umbrella, members of the Warsaw Pact under the Soviet Union). This complicates the military dimensions of nuclear arms reduction talks.

- ***Fissile Materials & Technology control*:** Very soon after the end of World War II, the US became aware of the risk the diffusion of nuclear material and the uncontrolled spread of nuclear technology. As the USSR developed their nuclear capability, they gradually came to share this view. The fear of the huge destructive power of nuclear weapons raised the vital need to block their dissemination. This required the control of the spread of sensitive materials and technologies without hindering peaceful applications of nuclear energy. This "fearful dilemma" inspired the speech of President Eisenhower "*Atoms for Peace*" (December 1953)[14] and gave birth to the International Atomic Energy Agency (IAEA)[15]. The treaty establishing the European Atomic Energy Community (EAEC, 1957), known as "EURATOM treaty." require, *inter alia,* the application of nuclear safeguards to all members of EU whatever their nuclear status[16] (contrary to IAEA safeguards which were applied only to non-nuclear weapons states, unless volunteered by a nuclear weapons state)

- ***De-escalation*:** After the Cuban missile crisis (1962), the world, and in particular the two superpowers became concerned with the risk of a a global nuclear war being triggered by a local crisis. US and USSR began talks on mutual reduction of their arsenals and limiting nuclear testing in the atmosphere. The first agreement was a treaty banning all nuclear weapons test detonations in the atmosphere, outer space, and underwater environments, allowing continued underground testing (PTBT, 1963 see, section 4). Abolition of underground testing was addressed by the CTBT 30 years later. By then, the establishment of a verification system of controls and mutual inspections for underground explosions had been negotiated between the USSR and Western countries. The competing requirements of security and confidentiality were already clear when considering the means to detect and evaluate suspicious events.

- ***Proliferation awareness*:** After the accession of UK, France and China to nuclear status, it appeared that other countries were seeking to acquire nuclear weapons increasing the risk of regional nuclear conflict. "*There are indications because of new inventions, that 10, 15, or 20 nations could have a nuclear capacity, including Red China, by the end of the Presidential office in 1964. This is extremely serious. I think the fate not only of our own civilization, but I think the fate of world and the future of the human race is involved in preventing a nuclear war.*"[17] Discussions in Conference on Disarmament, established under UN auspices in Geneva to prevent the proliferation of nuclear weapons, resulted in the adoption of the Treaty of the Non-proliferation of Nuclear Weapons (NPT, 1970). This is the cornerstone of nuclear disarmament and nonproliferation and intended to close the door to the "nuclear club" while allowing the peaceful uses of nuclear energy. Only the five members having already detonated a nuclear weapon would have the legal right to possess them (US, USSR (later Russia), UK, France and China). Any other nation that tested a nuclear weapon after entry into force of the NPT has been accepted as a Nuclear Weapons State.

- ***Post-NPT era (1970-1990)***: During the Cold War, the main concerns were that the arms race between the US and USSR increased nuclear arsenals, improved nuclear weapons (yield, penetration, hardening of nuclear warheads, development of multiple independently targetable reentry vehicle (MIRV), decoys, maneuverable warhead, stealth warhead) and improved the ability to deliver the weapons (precision, range, discretion of strategic bombers, Intercontinental Ballistic Missile (ICBM), Submarine-Launched Ballistic Missile (SLBM) and Anti-Ballistic Missile (ABM) systems). The risk of mutual annihilation was so high that the two super powers concluded agreements for limitation of and reduction of strategic arms (SALTs and START treaties, respectively - see section 4). The number of nuclear weapons in the world had peaked at approximately 70,300 in 1986 but began to decline significantly, in particular after the end of the Cold War. The number decreased to an estimated 15,350 by early-2016. An overwhelming portion of the reduction happened in the 1990s as show in Fig. 1. Since then, the pace of reduction has slowed significantly[18].

  In the two decades between the entry into force of the NPT and the collapse of the USSR, some important events regarding disarmament and non-proliferation occurred. In 1972 SALT I entered into force[19]. In 1974, with a nuclear test, India demonstrated its possession of nuclear weapons. In response, the Nuclear Suppliers Group (NSG) was created to limit the export of nuclear equipment, materials or technology. The 70'S and 80's saw the strengthening of the non-proliferation regime.

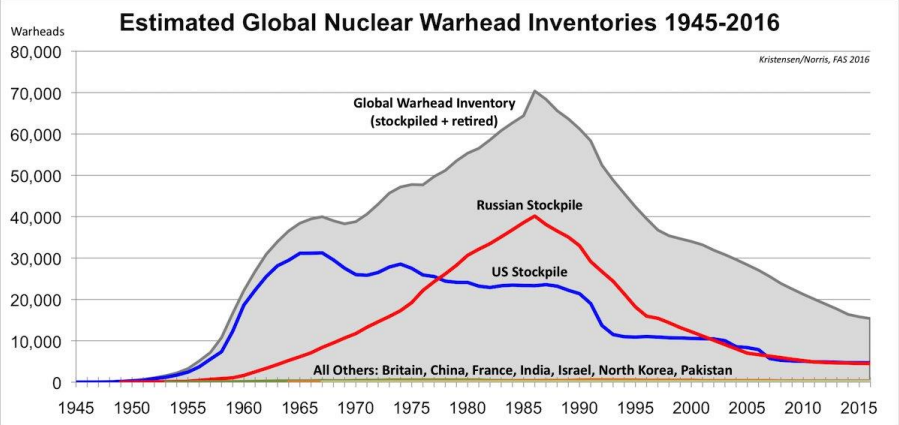

Fig.1 The number of nuclear weapons in the world has declined significantly since the Cold War (credit FAS/CSIS) [20]

- ***Post-cold war era (1990-2010)***: Progress during the first years following the collapse of USSR stalled during the late 1990's and the international context worsened. Some positive progresses were recorded but they were counterbalanced at the same time by negative steps as serious nuclear crisis just started, inter alia:
  - Important progress in nuclear disarmament with START II (1992) and several agreements between USA and Russia.

- Start of the discussion for an FMCT (1992)
- Adoption of the CTBT (1996)
- Indian and Pakistan test nuclear weapons (1998)
- Proliferation crisis with the discovery of nuclear weapons program of North Korea, Iraq, Libya and Iran
- Adoption of the IAEA Additional Protocol which from the disclosure of Iraq clandestine nuclear weapons program
- Iran non-proliferation crisis (2002) and disclosure of its nuclear weapons program
- Reinforcement of export control: NSG issues the double-use items list and strengthened if after the unveiling of A.Q. Khan Proliferation's network (2004).
- North Korea nuclear tests (2006, 2009, 2013, 2016 (2 tests)

- ***Current context***: since the 2000's there has not been much progress on nuclear disarmament agreements. The only significant advance was the conclusion of the New START treaty which entered into force in February 2011. It replaced the expired START and included a modified inspection and verification regime. In 2002, the Moscow Treaty (SORT) was agreed but it did not provide for any verification measures. It was terminated[21] when New START entered-into-force in 2011. New START limits the number of deployed strategic nuclear warheads to 1,550, and the number of deployed and non-deployed inter-continental ballistic missile (ICBM) launchers, submarine-launched ballistic missile (SLBM) launchers, and heavy bombers equipped for nuclear armaments to 800. The CTBT has not yet entered-into-force because a requisite number of required countries have not yet ratified. However the International Monitoring System (IMS), built to verify the treaty, is over 80% completed and operational.

  Possible negotiations to ban fissile material production for nuclear weapon (Fissile Material Cut-off treaty) were attempted several times but quickly extinguished in the blocked Conference on Disarmament. Treaty text proposals of have been tabled, in particular by France, but to-date the Conference did not moved forward.[22] Nevertheless, important work, undertaken in the framework of the Governmental Group of Experts (GGE: 2014-2015, see section 4),[23] prepares the ground for future negotiations of a cut-off treaty.

  A key accomplishment was the Joint Comprehensive Plan of Action (JCPOA), agreed between Iran and the P5+1 (China, France, Germany, Russia, the UK, and the US) and the European Union, in July 2015.[24]. This ended the crisis triggered by the discovery of an Iranian nuclear weapons program in 2002 and the inability of the IAEA to inspect Iranian suspected facilities.

  IAEA is committed to making a contribution to nuclear disarmament. The IAEA Department of Safeguards Strategic Plan commits to: "Contribute to nuclear arms control and disarmament, by responding to requests for verification and other technical assistance associated with related agreements and arrangements" and by preparing to play an active role in the verification of a Fissile Material Cut-off Treaty when and if it enters into force.

3. Military dimensions of nuclear disarmament

The military dimension in the nuclear disarmament negotiation process involves all features of the military nuclear complex: doctrines, research & development, production capacity, military nuclear fuel cycle, fissile materials and equipment, testing facilities and sites, means of delivery, nuclear strategic and non-strategic forces, conventional forces, and deployment of nuclear weapons. It must also take into account the existing nuclear disarmament commitments and the associated verification regimes, which are a very complex pattern of commitments.[25]

Existing Commitments: A state's membership in regional and/or international agreements influences its military stance with respect to nuclear disarmament verification. It adds a regional, multinational and international complexity that must be addressed.

Nuclear weapons control agreements can be organized into four interlinked categories. These non comprehensive reviews of regional, multinational and international agreements, that relate to nuclear weapons, include those in-force, expected to enter-in-force soon, and pending negotiation.

- **Treaties limiting nuclear weapons testing**: Historically nuclear weapon testing treaties were the first to be negotiated. The CTBT (1996) was preceded by several treaties limiting

nuclear testing capacity. Partial Test Ban Treaty between USA, USSR and UK (PTBT, 1963) allowed only underground testing. Treaty on the Limitation of Underground Nuclear Weapon Tests, between USA and USSR also known as the Threshold Test Ban Treaty (TTBT, 1974) capped the yield to 150kt. The Comprehensive Test Ban Treaty (CTBT, 1996) which forbids all nuclear weapon test explosion is not yet into force as the ratification of several annex II countries required for entry into force are still missing.[26] The CTBT is equipped with a very comprehensive and efficient monitoring and verification system which is almost completed.

- **Treaties preventing the proliferation of nuclear weapons.** The keystone of the nonproliferation regime is the Non Proliferation Treaty (NPT, 1970) which limits the number of countries which have legally the right to possess nuclear weapon to the five countries which carried out a nuclear weapon test before the 1st January 1967. Countries which tested nuclear weapons after this date as India Pakistan and the Democratic People Republic of Korea (DPRK) could not accede to the NPT without renoucing their nuclear weapons. Israel is presumed to have nuclear weapons but never officially acknowledge it. Some other countries host foreign nuclear weapons and some other had in the past nuclear weapons but have renounced to them. Figure 2 presented a comprehensive overview of countries status regarding nuclear weapons.

  In coherence with the NPT countries of a same region gathered to ban nuclear weapon through ***Nuclear-Weapon-Free Zone Treaties*** and negotiated ***Security Assurances*** to prevent the use of nuclear weapons against them[27]. For the implementation of article IV of the NPT regarding peaceful uses of nuclear technology Export Control regimes (e.g. Zangger Committee, NSG (Dual use items 1992),Wassenaar) have been set by concerned group of nuclear countries

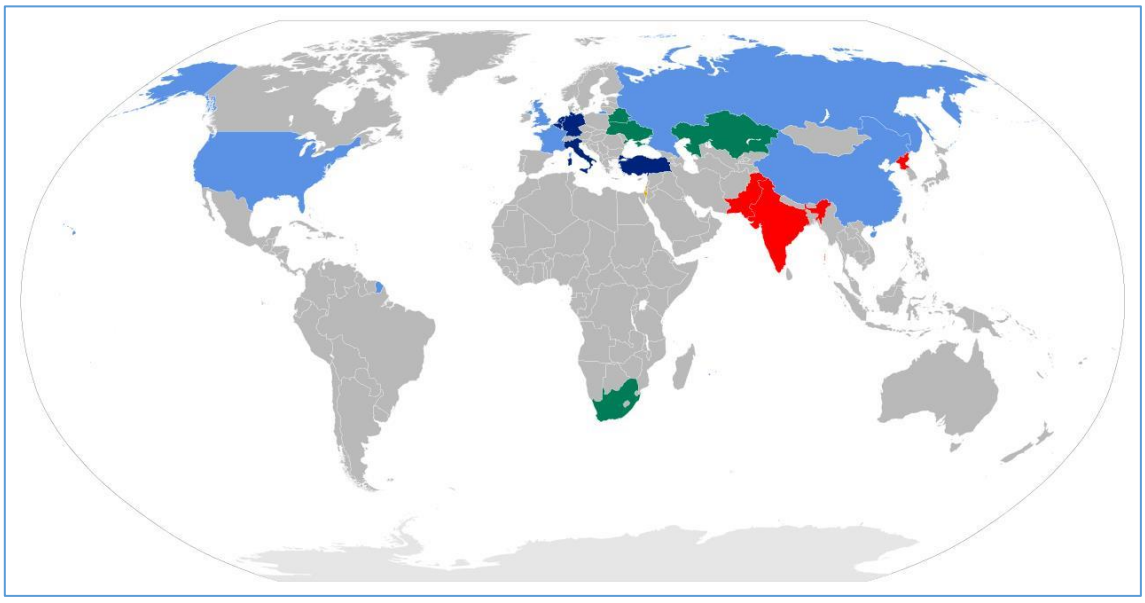

Map of nuclear-armed states of the world.

- NPT-designated nuclear weapon states (China, France, Russia, United Kingdom, United States)
- Other states with nuclear weapons (India, North Korea, Pakistan)
- Other states presumed to have nuclear weapons (Israel)
- NATO nuclear weapons sharing states (Belgium, Germany, Italy, Netherlands, Turkey)
- States formerly possessing nuclear weapons (Belarus, Kazakhstan, South Africa, Ukraine)

Fig. 2 List of states with nuclear weapons (From Wikipedia, the free encyclopedia: https://en.wikipedia.org/wiki/List_of_states_with_nuclear_weapons)

In accordance with Article VI of the NPT, any instrument, whether a treaty, a convention or an agreement contributing to the ultimate goal of nuclear disarmament should be "in principle" universal, non-discriminatory, multilateral, internationally and effectively verifiable. Such an instrument would have considerable impact on the international and regional strategic context. A verification protocol, along with transparency and confidence building measures, will be a key element. It must maintain a delicate balance of upholding Article I of the NPT to prevent proliferation of confidential data and technologies to non-nuclear weapon states (inter alia the limitation of

access to knowledge, know-how and technologies through managed access) and allowing for the necessary transparency provide assurances of compliance and confidence in the implementation of the instrument to all parties.

- **Treaties reducing strategic forces and nuclear weapons arsenals**[28,29]: Strategic offensive arms agreements between, USA and USSR (and then Russia) provide a great deal of negotiation and implementation experiences on mutual verification systems, technologies, inspections, managed access, and data exchange which may be useful for any future disarmament agreement negotiations Agreements related to strategic weapons systems are:
  - SALT I (Strategic Arms Limitation Talks, 1969),
  - SALT II (1972) START I (Strategic Arms Reduction Treaty 1991),
  - START II (1992 not entered-into-force), START III Framework (1997), SORT (Strategic Offensive Reductions Treaty or Moscow Treaty, 2002),
  - New START between the United States and Russia (2011).
  - Nonstrategic Nuclear Arms Control: Intermediate-Range Nuclear Forces (INF Treaty; 1987).

Treaties to control production of fissile material for nuclear weapons: Since the end of the cold war, important efforts to reduce available fissile material stocks for use in nuclear weapons have been completed through voluntary measures. Most of nuclear countries have declared a moratorium on production and some have irreversibly dismantled their production facilities. As of January 2015, the global stockpile of highly enriched uranium (HEU) is estimated to be about 1370 ± 125 tons. The global stockpile of separated plutonium is about 500 tons (270 in civilian custody). Most of this material (>93%) is hold by USA and Russia[30] (Fig 3). Fissile material disposition instruments includes (inter alia):

- Fissile materials declared no longer needed for defense purpose[31]
- 2000 Plutonium Management and Disposition Agreement and update
- Fissile Material Cut-off Treaty (FMCT negotiation not started yet. Nevertheless, some work has been done in the framework of the Group of Governmental Experts (GGE[32])

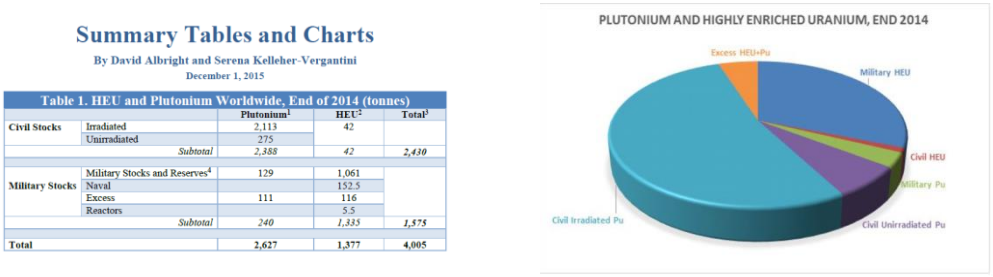

Summary Tables and Charts

By David Albright and Serena Kelleher-Vergantini

December 1, 2015

Table 1. HEU and Plutonium Worldwide, End of 2014 (tonnes)

		Plutonium[1]	HEU[2]	Total[3]
Civil Stocks	Irradiated	2,113	42	
	Unirradiated	275		
	Subtotal	*2,388*	*42*	*2,430*
Military Stocks	Military Stocks and Reserves[4]	129	1,061	
	Naval		152.5	
	Excess	111	116	
	Reactors		5.5	
	Subtotal	*240*	*1,333*	*1,575*
Total		2,627	1,377	4,005

Fig 3: Plutonium and Highly Enriched Uranium Inventories, 2015
(Credit: Institute for Science and international Security (ISIS))[33]

4. A brief review of the components of the military dimension:

- **Doctrines, posture and deterrence**: a nuclear country's policy on the use of nuclear weapons and conventional forces is very important. It indicates the role that weapons play in maintaining the status and the global image of a state[34] and reflects the state's perception of the role that nuclear weapons play in ensuring national security and defense capacity, in the context of its international policy. Most of the nuclear countries publish their nuclear doctrine. The North Atlantic Treaty Organization (NATO), an alliance relying on the nuclear capacity of three of its members, has also published its doctrine. It covers a large array of complex positions from "no first use" of China) to the deterrence (France, India) and the preemptive strike against a major conventional attack or a non-conventional aggression (chemical, bio, cyber, etc.). Nuclear and military doctrines are major elements to take into account when considering disarmament verification.

- **Military nuclear fuel cycle**: the extend (i.e. from mine to weapon) and the development (i.e. advanced enrichment methods) of the military nuclear fuel cycle determines the capacity of a state to resume or cover clandestine activities.
- **Fissile materials**: production and/or acquisition of weapon grade fissile materials (highly enriched uranium or plutonium) are a mandatory step in nuclear weapon development process. Putting an end to this stage of weapons manufacturing is the keystone of nuclear arms control and ultimately elimination. It would encompass the control of fissile materials production for nuclear weapons: enrichment, reprocessing, and other processes. A future cut-off treaty, equipped with an efficient verification process, would be the tool to master that stage. Absent a treaty, another way to manage the stocks of fissile material, would be to irreversibly place the disposition of fissile material no longer needed for defense purposes (fissile materials in excess of defines needs) under safeguards.

- **Testing:** testing is the ultimate stage in the nuclear weapons research and development process before militarization, therefore prohibiting nuclear testing is important when moving towards nuclear disarmament. Except for DPRK, all NPT and non-NPT nuclear weapon states have declared or applied a *de facto* moratorium of testing. In the continuity of previous nuclear testing agreements (Partial Nuclear Test Ban Treaty, Threshold Test Ban Treaty) a CTBT banning any nuclear testing has been adopted and is pending ratification of the US, China, India, Pakistan, Iran and Israel. It includes a monitoring and verification system (IMS & OSI). Definite closure of nuclear test sites and associated facilities are also important signals that countries are moving towards nuclear disarmament. To-date, only France and the UK have completed this step.

- **Nuclear weapons arsenals**: transparency of nuclear arsenal composition is also a key element of progress towards nuclear disarmament. The arsenals of the US and Russia have been declared and considerably downsized within the implementation of bilateral arms control reduction treaties (see section 4). France and the UK have also completed significant downsizing and declared the size and the composition of their arsenals. Published evaluations of India[35], Pakistan[36] and China[37][38] indicate they are increasing their arsenal.

- **Nuclear strategic and non-strategic forces/Means of delivery versus conventional forces:** the size, composition and technological advance of strategic, non-strategic (tactical or theater nuclear weapons) and conventional forces, means of delivery, ground and submarine missiles and cruise missiles, military satellites, radar networks, etc. will influence the disarmament process. Some less advanced countries may maintain a small nuclear capability (i.e . Pakistan vs India or in the past NATO vs USSR) for national security purposes.

- **Former verification experiences**: Previous nuclear weapon dismantlement verification exercises provide a great deal of experience in verification processs, development and implementation of *ad hoc* technologies, military aspects, confidentiality issues, managed access, confidence building measures and mutual verification. Some former experiences are:
    - Early days field test 34 (1967)
    - Threshold Test Ban Treaty US-USSR mutual verification (1974)
    - Black Sea US-USSR joint experiment (1989)
    - DoE studies (1996-1997)
    - Trilateral initiative (US-Russia, IAEA 1996-2002)
    - Bilateral arm reduction treaties between USA and Russia START (1991) and New START (2010)
    - UK-Norway initiative
    - Other experiences as INF treaty (Intermediate-Range and Shorter-Range Missiles, 1987) or Conventional Armed Forces in Europe treaty (CFE 1972) has also to be taken into account…

The role of the IAEA in the verification process: The IAEA is the multinational organization that carries out verification of compliance assessment for NPT commitments Nuclear Weapons Free Zone agreements and other related agreements, through a complex and efficient system of safeguards. Based on its statutes, the IAEA had not invested in the disarmament verification until

proliferation crises (listed below) and nuclear weapons fissile material disposition initiatives drove the Agency to focus on these issues:

- DPRK (North Korea ; agreed framework)
- Iraq (IAEA): Action Team then INVO
- Iran – P5 +1 Joint Comprehensive Plan of Action JCPOA),
- Libya and A. Q. Khan nuclear black market network

Since the United Nations Security Council entrusted the Director General of the IAEA verification of the nuclear part of the disarmament of Iraq, the position of the Agency evolved. . Building on the skills acquired on these issues and the implementation of the Additional Protocol, the IAEA is positioned to play an important role in the verification of future disarmament agreements such as the verification of a cut-off treaty[39]. The Agency is staffed by international civil servants representing the Member State from both NPT Nuclear and Non-nuclear Weapons States. This introduces both proliferation and security concerns with designing a verification regime run by the IAEA. It has not been universally agreed that the IAEA has the resources or mandate to continue to support the world community in this way but it is likely to play a pivotal role

5. Conclusion/ future prospects

Reduction or elimination of nuclear weapons is not likely to occur in a foreseeable future. The international, regional and national security context is deteriorating and confidence is lacking. So there is no incentive for countries possessing nuclear weapons to disarm. After a long period comprising of a mix of fruitful dialog and chaotic confrontations resulting in a large decrease of arsenals, strategic forces and fissile material stocks, the relationship between the US and Russia is getting more and more difficult. Russia does not appear to be interested in the results achieved during 1990-2010 and is modernizing its strategic forces. An increasingly aggressive strategy to rebuild its lost empire is being implemented. US-China relations are also deteriorating, as China continues to develop its nuclear arsenal and rapidly modernizing its strategic forces to support its expansionist policies. Antagonism between India and Pakistan continues at a high level. Both countries continue to produce fissile materials for weapons, increasing the number of nuclear warhead and improving their means of delivery. The security situation in the South Asia remains very tense as India, Pakistan, USA, China and Russia confront instable alliances and antagonism.

In the last decades, the UK and France[40] have made very important and unprecedented efforts towards nuclear disarmament by downsizing their arsenal and decommissioning and closing critical facilities as nuclear test sites, plutonium production reactors, reprocessing and enrichment facilities. Even though negotiations with Iran on the verification of its nuclear complex's verification resulted in the conclusion of the Joint Comprehensive Plan of Action to monitor the absence of cover nuclear program, the current situation in the Middle East does not provide an incentive for Israel to lower its nuclear posture.

There is still a perception that maintaining or developing nuclear weapons arsenals is needed to support national security.[41] Any voluntary downsizing of countries nuclear posture in the legal framework must be balanced by the assurance that its national security interests will not be jeopardized but strengthened. Nevertheless, one should be reasonably optimistic. The road to a world without nuclear weapons will be long, tortuous, with setbacks, but unavoidable. One of the great challenges to overcome will be to achieve the needed transparency, verifiability and irreversibility of disarmament measures. A systematic approach that creates a climate of confidence, while taking into account the security interests and military dimension of all stakeholders, will greatly ease the process. Achieving such confidence on a national-level followed by a regional level (European, Middle East, South Asia and Eastern Asia) to ultimately on the international level is pivotal.

6. References

1 For a discussion on how to advance in nuclear disarmament, see Marc Finaud " Cooperative Security: A new paradigm for a world without nuclear weapons?" Cadmus, November 2013.

2 http://fas.org/issues/nuclear-weapons/status-world-nuclear-forces/

3 Robert S. Norris and Hans M. Kristensen, "Global nuclear weapons inventories, 1945–2010", Bulletin of the Atomic Scientists, vol. 66, no. 4, 2010, pp. 77–83.

4 "*Resolving to seek a safer world for all and to create the conditions for a world without nuclear weapons, in accordance with the goals of the Treaty on the Non-Proliferation of Nuclear Weapons (NPT), in a way that promotes international stability, and based on the principle of undiminished security for all*". UNSCR 1887, 24 September 2009)

5 For a comprehensive discussion on the future of doctrines and deterrence, see the monograph "Nuclear Deterrence in the 21st century, Lessons from the Cold War for a New Era of Strategic Piracy" by Ms. Therese Delpech edited by Rand Corporation (http://www.rand.org, 2012) and the Fondation pour la Recherche Strategique (http://www.frstrategie.org/, 2013) published by Odile Jacob for the French version

6 See Remarks at the Global Zero Conference, Paris F**e**bruary 2nd 2010, Pierre Sellal Secretary General of the French Ministry of Foreign Affairs.

7 http://thebulletin.org/2015/september/indian-nuclear-forces-20158728

8 http://fas.org/wp-content/uploads/2015/10/Nov-Dec-Pakistan-FINAL.pdf

9 Hans M. Kristensen and Robert S. Norris, "Chinese Nuclear Forces 2015," Bulletin of Atomic Scientists, 01 July 2015

10 For any information on CTBT see the CTBTO Preparatory Commission web site: https://www.ctbto.org/

11 Discours sur la dissuasion nucléaire - Déplacement auprès des forces aériennes stratégiques. Istres http://www.elysee.fr/declarations/article/discours-sur-la-dissuasion-nucleaire-deplacement-aupres-des-forces-aeriennes-strategiques-istres-3/

12 See section 5

13 Sweden, Switzerland Brazil, South Africa and many other countries started to develop a nuclear weapons programs in the sixties. Most ended by the time NPT started and some others much later. See Institute for Science and International Security (ISIS): Nuclear Weapons Programs Worldwide: An Historical Overview (http://isis-online.org/nuclear-weapons-programs)

14 United States of America President Eisenhower (1953): "Atom for Peace" speech to the United Nations General Assembly on the 8th December 1953

15 Birth of the International Atomic Energy Agency (IAEA) see https://www.iaea.org/about/history.

16 Eur-lex.europa.eu › EUROPA › EU law and publications › EUR-Lex

17 Third Nixon-Kennedy Presidential Debate, October 13, 1960 from JFK on Nuclear Weapons and Non-Proliferation, Proliferation Analysis, Carnegie Endowment for International Peace, November 17, 2003

18 Chart and comment from FAS Status of World Nuclear Forces By Hans M. Kristensen and Robert S. Norris http://fas.org/issues/nuclear-weapons/status-world-nuclear-forces/

19 U.S.-Russian Nuclear Arms Control Agreements at a Glance. https://www.armscontrol.org/factsheets/ US RussiaNuclearAgreementsMarch2010, David Kimball

20 Reproduction with the kind permission of FAS: .Status of World Nuclear Forces, by Hans M. Kristensen and Robert S. Norris, Federation of American Scientist (FAS)

21 New START replaced the Treaty of Moscow (SORT), which ended in December 2012. It is a follow-up to the START I treaty, which expired in December 2009. START II treaty never entered into force and the negotiations of START III treaty were never concluded.

22 Draft Fissile Material Cut-off Treaty, http://www.delegfrance-cd-geneve.org/Projet-francais-de-Traite (April 10, 2015) and CD /2020 (13 April 2015)

23 UNGA in its resolution 67/53 (2012) requested the Secretary General to establish a Group of Governmental Experts. The Group was mandated to make recommendations on possible aspects that could contribute to, but not negotiate, a treaty banning the production of fissile material for nuclear weapons or other nuclear explosive devices,1 on the basis of document CD/1299 and the mandate contained therein. The GGE met over four two-week sessions in Geneva during 2014-2015 (CD /2023,24June 2015)

24 The five permanent members of the United Nations Security Council—China, France, Russia, United Kingdom, United States—plus Germany) and the European Union.

25 For a comprehensive review of non proliferation and disarmament instruments see the "NPT Briefing Book (2015 Edition and previous ones) edited by King College and Center for Nonproliferation Studies (CNS) at http://www.kcl.ac.uk/sspp/departments/warstudies/research/groups/csss/pubs/NPT-Briefing-Book-2015/New-sections-April-2015/NPT-BB-2015-Final-April.pdf

26 There are eight Annex 2 States that have yet to ratify the Treaty - China, Egypt, Iran, Israel, and the United States of America, which have signed the Treaty, and North Korea, India, and Pakistan, which have not signed.
27 http://www.reachingcriticalwill.org/resources/fact-sheets/critical-issues/5442-negative-security-assurances and [29]
28 Ibid [18]
29 Ibid [24] Section O: Bilateral Measures – Russia-United States
30 For the actual status of fissile material disposition see "Global Fissile Material Report 2015" International Panel on Fissile Materials (IPFM).
31 Verified and irreversible elimination of weapon usable nuclear material is one of the essential elements of the nuclear disarmament effort. The Action Plan adopted at the 2010 Nuclear Non-Proliferation Treaty (NPT) Review Conference calls on nuclear-weapon states "to declare fissile material designated as no longer required for military purposes, and to place this material under safeguards to ensure that it remains permanently outside military programmes" 2010 NPT Action Plan, action 16.
32 Ibid 22
33 Reproduction with the kind permission of D. Albright, Director of ISIS.
34 For a discussion on doctrines and their roles vis-a vis nuclear disbarment see the Foreword by Academician Alexander A. Dynkin at the Conference “Contemporary Nuclear Doctrines” Institute of World Economy and International Relations/Russian Academy of Sciences and Nuclear Threat Initiative. Moscow 2010 and ibid 9 chapter 3.
35 Indian nuclear forces, 2015/Hans M. Kristensen and Robert S. Norris/ Bulletin of the Atomic Scientists, 2015, Vol. 71(5) 77–83
36 Pakistani nuclear forces, 2015/ Hans M. Kristensen and Robert S. Norris/Bulletin of the Atomic Scientists, 0(0) 1–8
37 Chinese nuclear forces, 2016/ Hans M. Kristensen and Robert S. Norris/Nuclear Note Book/ 3 July 2016
38 China's Strategic Forces in the 21st Century: The PLA's Changing Nuclear Doctrine and Force Posture/ Dan Blumenthal and Michael Mazza/NonProliferation Policy Education Center/April 06, 2011
39 See IAEA Department of Safeguards Long-Term Strategic Plan (2012 -2023) "*Contribute to nuclear arms control and disarmament, by responding to requests for verification and other technical assistance*". https://www.iaea.org/safeguards/symposium/2014/.
40 http://www.diplomatie.gouv.fr/en/french-foreign-policy/disarmament-and-non-proliferation/fr...
41 Ibid [9] Rand issue pages 36 and 38 "*Ninth, short of pretending that lions and sheep should be able to lie together before contemplating nuclear disarmament, the political conditions for a secure nonnuclear—or at least less nuclear—world are considerable. Serious political efforts should therefore accompany nuclear weapon reductions*".

We shouldn't focus on confirming the characteristics of nuclear materials when looking to verify nuclear weapons

Keir Allen

King's College, London

Abstract:

Since the early 1990s, when it was thought that negotiations for START III might take place, there has been an interest in verifying nuclear warheads and nuclear weapons directly, rather than verifying the delivery systems that had been the focus of earlier agreements. In the decades since, the technical arms control community has expended much effort in developing systems that might help to positively confirm that an item declared to be a nuclear warhead truly is one. But focusing on verifying the correctness of a declaration in this way conflates the scientific objective of uncovering the truth with a strategic objective of nuclear arms control: to maintain stable relations between treaty partners. This paper argues that the approach taken in focusing on correctness contributes marginally to ensuring overall numbers are reduced whilst threatening to complicate and delay future negotiations.

Keywords: Arms control; verification; systems; strategy

1. Introduction

Since the early 1990s, when it was thought that negotiations for START III might take place, there has been an interest in verifying nuclear warheads directly, rather than verifying the delivery systems that had been the focus of previous iterations of the strategic arms reduction treaties.

In handing over the requirement to verify warhead stockpiles and warhead destruction to the technical community, a lot of technical effort has been directed at the perceived problem of verifying that items declared to be warheads truly are warheads. But the approach taken by the technical community does not align well with the strategic aims of arms control and could be an inadvertent complication to the establishment verification mechanisms for future arms control agreements.

This paper will review the use of positive confirmation and the technologies developed to achieve it. It will then discuss the strategic impetus behind the development and evolution of nuclear weapons arsenals and will argue that the assumptions underpinning the positive contribution approach to warhead verification may not be suitable when directed at weapons stockpiles that evolved under the influence of competitive and expensive deterrence relationships. Finally it will outline how more systematic approaches to nuclear stockpile verification could maintain stability whilst progress is made towards lower numbers of weapons. Because of this, a systematic approach could provide a better means for identifying strategic technical verification requirements.

2. Positive confirmation

For treaties involving the verification of nuclear warheads, suggested solutions often include the need to verify that an item declared to be a warhead truly is one. This seems to make sense: If a state is submitting nuclear weapons for monitoring under an agreement, then the other parties may wish to ensure that the state really does submit its nuclear arsenal and not something else. If the other party cannot confirm that that the items are nuclear weapons, then the concern may arise that the state is secretly withholding weapons in order to gain a later advantage.

The act of verifying that a nuclear weapon truly is one is complicated by states' national security priorities and nonproliferation obligations: nuclear weapons possessing states are extremely cautious about sharing any weapon design information either amongst themselves or with others. It is further complicated by the fact that a nuclear weapon is the product of advanced design and engineering and so there is no one design solution to which all weapons conform. Positive confirmation is complex because nuclear weapons characteristics vary and states are unwilling (and unable) to discuss the characteristics of their particular systems beyond.

The technical solutions often proposed for overcoming these challenges broadly fall into one of two types of system: Attribute confirmation systems and template matching systems.

2.1. Attribute systems

Attribute confirmation systems are typically designed based on the assumption that certain design characteristics of a weapons system would be disclosed by a state entering into an arms control agreement. Such characteristics may include the type of fissile material contained in the weapons, the isotopic 'grade' of the material, and perhaps other details [1]. Attribute systems perform an analysis of the declared item based on detectable characteristic signatures to ensure that the item correctly meets expectations of what a nuclear weapon is.

2.1. Template systems

Template matching systems seek to confirm that one object matches another object declared to be of the same type. One object is chosen as the reference object and provides the template. Often the template is provided by radiation produced by the fissile material that is assumed to be in the weapon system, though this need not necessarily be the case. All other systems of the same type are expected to conform to the reference object and are subject to comparison with it [2]. Only systems of the same type should correctly match the template. Radiation detection statistics, changes in object configuration or changes in the measurement environment may all effect the results of the comparison.

Either type of system, without further consideration, could facilitate the disclosure of sensitive information. In order to prevent this from happening the systems are commonly conceived of operating in conjunction with an information barrier. An information barrier acts as a filter, allowing only the agreed information about the item to be assessed.

The reliance of both types of system on the assumption (and declaration) of the presence of fissile material with particular characteristics could create complications for the use of such systems in future. States might be very reluctant to provide even general declaration that covers design characteristics of their stockpiles because the secrecy over weapon design details extends to stockpile characteristics. The next sections explore why this might be the case.

3. Deterrence and stockpile evolution

The nuclear weapon stockpiles of the nuclear weapons possessing state have evolved in response to developments in the arsenals of other nuclear weapons possessing states, with each trying to ensure they can deter at least the state they each perceive to be their most significant threat.

Deterrence is a political tool: To deter requires an aggressive adversary to believe that the possessor state has the means to retaliate to an extent that the costs of aggression would outweigh any gains made by being aggressive. The important factor in a deterrent relationship is credibility: each side must believe the other is capable of retaliation. Each of the nuclear weapon possessing states has established their own credibility via nuclear weapons tests and delivery vehicle development programs.

A stable relationship of mutual deterrence requires the parties to continue to believe each possesses a credible stockpile that is invulnerable to a first strike. At least in part, the overall size of the stockpile may well contribute to credibility and invulnerability. Certainly parity in overall stockpile size has been an important aspect of the relationship between the US and Russia. Other states may also determine their own requirements for overall stockpile size at least in part by assessing the size of adversaries' capabilities. Nevertheless, not mean that items professed to be weapons necessarily are.

In a deterrent relationship there are potential benefits to be gained from inflating a capability, for instance, by maintaining an appearance of strength even if it is only a facade. If deterrence fails, the target of an attack suffers equally whether they retaliate with nuclear weapons or not. A cost effective means of deterring is therefore attractive. If the appearance of strength is enough to deter an aggressor then the facade fulfils its purpose and is more cost effective than investing in real systems.

Since the Greeks used a wooden horse to defeat Troy, subterfuge and deception have been used for strategic advantage. During the early nuclear age, the Soviet Union used deception to inflate the apparent size of its strategic bomber fleet [3] Later, Soviet leader, Khrushchev also encouraged the perception of Soviet superiority in numbers of intercontinental ballistic missile systems by boasting that Soviet factories "were turning out missiles like sausages"[4]. He explained his reasons for doing so, saying "the number of missiles we had wasn't important… The important thing was that Americans believed in our power" [4]. Deception by capability inflation has therefore been present in nuclear dynamics and the concept of strategic deception could be extended to stockpiles of nuclear weapons. States might have taken a decision to inflate the size of their nuclear weapons stockpiles in order to maintain the perception of strength in a cost effective manner. Objects that did not in reality meet the design criteria of the items they were professed to be, could nonetheless help create the appearance of strength so long as they looked similar enough to fully developed systems.

3.1. Strategic stability and arms control

To date, nuclear weapons arms control agreements have been designed to maintain stability even as numbers of deployed strategic systems have been reduced. This has been achieved by focusing on the completeness of states' declarations rather than the correctness, i.e. the focus has been on ensuring the agreed limit of weapons is not exceeded, not that items that fall within the limit truly are nuclear weapons. A focus on completeness makes sense since the worst case scenario for which each state needs to plan for its own deterrence purposes is the scenario in which all items within their adversaries' stockpile truly are nuclear weapons.

This description is a simplified model of the dynamic nuclear relationship between states, but is sufficient for the purposes of this paper. Arms control agreements and their associated verification methods should maintain the stability of the relationship between adversaries whilst that relationship remains one based upon deterrence. Anything that revealed that a state was less strong that it professed to be could be destabilizing.

4. Positive confirmation and instability

A potential challenge to the inclusion of positive confirmation measurements in future nuclear weapons treaties is that they could undermine stability. By positively testing the design details of individual systems, overall stockpile characteristics could be revealed which could undermine the credibility of the state's stockpile or make the option of a preemptive strike more attractive to an aggressor.

For instance, one could imagine a state having inflated its stockpile with deceptive non-weapons objects in order to look strong. Deceptive objects might contain no fissile material of the assumed or expected grade. The use of attribute measurements systems designed to test for the presence of such attributes would therefore reveal the fact that the state maintains some number of fake objects. Positive measurement in this case could therfore undermine the overall credibility of that states' stockpile, or make it appear more vulnerable to first strike. The stability of the relationship between the state and its adversary could be adversely effected. Where the perception of parity is important in the relationship, this dynamic would be effected negatively.

Clearly the situation described would be unacceptable to a state negatively affected by the proposal to disclose any such design information and so any proposal to use positive confirmation measurements would no doubt be vetoed.

Furthermore, though such a revelation may not prove disconcertingly destabilizing, the state may consider any such admission to be humiliating and so may find any such verification methods unacceptable for this reason.

Similarly, the use of template based confirmation systems could require states to first declare distinctions between stockpile items that had previously been deployed under a single identity or designation. Such a distinction could again reveal stockpile characteristics that could undermine the stability of the relationship between adversaries. Additionally, if a template measurement is proposed in order to increase confidence in the nuclear nature of a declared weapon, then the positive presence of some nuclear attributes must first be confirmed before a template is generated. This is because a template on its own will be generated whether those attributes are present or not. In such a situation, the same conditions would be present as when attribute confirmation systems are proposed.

A state could choose not to make any such declarations about its stockpile, but each time a result did not meet the expectations of the other side the relationship between the states involved could suffer and deteriorate.

The use of either attribute or template systems to positively confirm items as nuclear weapons could therefore prove to be destabilizing and unacceptable to states whilst they still rely on nuclear weapons for deterrence purposes.

Of course, it might be the case that all nuclear weapon states have been transparent throughout the evolution of their stockpiles and have only ever deployed genuine weapons. In this case, there should be fewer concerns about revealing stockpile characteristics and the theoretical challenge outlined above will be insignificant. But if it is acknowledged that positive confirmation approaches could tend towards being destabilizing, then it might be better to develop other means of verifying future nuclear arms control agreements.

5. A strategic-stability focused, systems assessment approach

Positive confirmation approaches to nuclear arms control verification potentially face a significant challenge to being accepted in future nuclear arms control negotiations because they could destabilize relationships by revealing characteristics of states' overall stockpiles that could undermine their

deterrent effects whilst they were still relied upon to deter. However, such measurements may not be necessary and other means of verifying nuclear arms control agreements whilst maintaining stability can be extrapolated from the past.

In order to systematically reduce stockpiles a valuable approach is to continue along the lines laid out by previous nuclear arms control agreements, where completeness of a declaration is prioritized over correctness. Under such arrangements items declared to be nuclear weapons (or fissile components of nuclear weapons) could be treated as such and placed under controls or monitoring tailored to a specific agreement; until such time as the agreement ends or states no longer require nuclear weapons. The approach engenders stability because it maintains the ambiguity regarding stockpile and design characteristics that contribute to the maintenance of credibility whilst allowing states to be prepared against the worst case scenario.

By default, all items declared to be nuclear weapons are treated as nuclear weapons. Over time the absence of any undeclared stockpiles that could meaningfully effect the stability of the deterrent relationship between adversaries would be assured, and so this approach would provide the transparency and predictability necessary for states to incrementally reduce overall stockpile sizes.

The reality of the configuration of each individual system is of less importance. Eventually all stockpiles reduce in size whilst aggressors are deterred from using force by the possibility that the others stockpile consists solely of nuclear weapons.

This approach certainly has logistical challenges, but the challenges would all exist whether the ‘correctness’ of a declaration was tested or not – since completeness will need to be assured no matter what. At the same time, a focus on completeness would reduce the perceived acuteness of challenges such as initiating objects declared weapons into a verification process since any item declared would count towards the agreed limit. Nonetheless it may be technically easier to verify that an item declared not to be a warhead is not one, than trying to prove the a warhead is a warhead

6. Conclusion

There is a popular desire to confirm that items declared to be nuclear weapons contain fissile materials with certain characteristics. However, such an approach could reveal more about overall weapons stockpiles than proponents of the method would advocate. Such revelations could destabilize relationships based upon nuclear deterrence and thus could well be voted if proposed during future nuclear arms control discussions. At the same time, such methods are neither sufficient nor necessary for controlling any fissile materials contained within nuclear weapons stockpiles and thus contribute marginally to verifying that overall stockpiles of weapons are reduced. Instead, the technical nuclear arms control community should move beyond a focus on the nuclear part of nuclear weapons verification and consider strategically and systematically what it is verification systems will need to achieve in future. One day, it will be important to verify that all fissile material that was once used in nuclear weapons is placed under monitored conditions. But verifying military stockpiles of fissile material is not the same as using fissile material as a proxy for verifying nuclear weapons.

7. References

[1] LANGNER D, *et al*; *'Attribute Verification Systems With Information Barriers For Classified Forms Of Plutonium In The Trilateral Initiative*'; IAEA-SM-367/17/02; http://www-pub.iaea.org/MTCD/publications/PDF/ss-2001/PDF%20files/Session%20

17/Paper%2017-02.pdf; accessed 2nd May 2017

[2] Merkle P *et al*; *Next Generation Trusted Radiation Identification System*; https://www.nti.org/media/pdfs/SNL-1_FINAL_INMM_2010_Next_Generation_Trusted_Radiation_System.pdf?_=1438113016; accessed 2nd May 2017

[3] Krepon M; *The Bomber Gap*; Arms Control Wonk; http://www.armscontrolwonk.com/archive/403428/the-bomber-gap/ April 30th 2012 (accessed 12th April 2017)

[4] Khrushchev S; *Nikita Khrushchev and the Creation of a Superpower*; University Park, PA; Pennsylvania University Press; p.315; quoted in: Thielmann G; *The Missile Gap Myth and its Progeny;*, Arms Control Today, May 3rd, 2011

Verification of Nuclear Warhead Dismantlement: Joining Dots

Craig Everton, Malcolm Coxhead

Australian Safeguards and Non-Proliferation Office
RG Casey Bldg, John McEwen Crescent, Barton, ACT 0221, Australia

Abstract:

The sensitivity around nuclear weapons and weapons materials means that measurement by inspectors providing strong confirmation that a declared item is in fact a nuclear explosive device may be impossibly intrusive. Analysis of this challenge is one focus for the International Partnership on Nuclear Disarmament Verification (IPNDV) which is now in its second year of substantive work to outline the objectives, methods and technology for verifying future steps toward nuclear disarmament.

A consequence of this problem is that an effective regime to verify the dismantlement of nuclear warheads cannot rely only on inspectors monitoring a dismantlement procedure. Verification of a future treaty commitment to dismantle warheads as a step toward nuclear disarmament will need to build assurance of compliance by tying together a series of observations, both within and beyond the dismantlement process, many of which could be quite disparate and disconnected. It may be that only by monitoring multiple steps towards nuclear disarmament, potentially over many years, will it be possible for a verification regime to offer fully adequate assurance.

Keywords: nuclear; weapons; disarmament; verification

1. Introduction

The verification of the dismantlement of a nuclear warhead under any international system comprises two seemingly intractable challenges: the inspector must have high confidence that the inspected item is in fact a nuclear warhead; and, the host (i.e. the holder of the nuclear warhead) must have high confidence that the inspector has not accidentally or deliberately acquired some knowledge of the classified attributes of the warhead – a **confidence-secrecy trade-off**. The challenge to achieving this trade-off is to develop measurement technologies (combinations of hardware and software) that can measure or confirm key attributes of warheads, and can be authenticated and certified to ensure that there are no accidental or deliberate backdoors through which classified information can leak[1] or through which the information can be tampered with. And as has been recognised for a long time in other disarmament initiatives, national technical means (NTM) also has a role, in bridging the technical and political[2].

A future disarmament verification inspectorate should approach the task with a mindset of “trust but verify”; the maxim that the IAEA applies to its verification mission. What this means is that the interactions between the inspectorate and inspected states should be respectful and non-adversarial while still maintaining credible verification mechanisms to preserve international confidence in the compliance of states. With this in mind, the working hypothesis for the verification system would need to be that attempts to spoof or tamper with the inspection process, while unlikely, cannot be discounted absolutely, so a risk-based system would be put in place to test against this working hypothesis. This will no doubt go the other way as well. Potential inspected states would apply a working hypothesis that attempts by an inspector to discover classified information cannot be ruled out absolutely either; so the measurement system would need to minimise this risk as well.

So, what level of confidence is sufficient for both sides of this confidence-secrecy trade-off? This has both a technical element and an element of political judgement. The technical element comes down to what verification technologies can confirm attributes of a warhead (such as nuclear material isotopics, density, mass), how these can be used without revealing classified details of the attributes, and then what statistical level of confidence can be assigned to the measurement.

The political element is the judgement of the level of confidence (for the inspectorate and host) sufficient to persuade decision makers to sign up to commitments. History has shown that arms control treaties can sometimes be contentious in national legislatures, where concerns about cheating or shortcomings (justified or not) can lead to a failure to ratify agreements. There is a lot at stake therefore in designing a verification regime that engenders as much confidence as possible in its effectiveness and robustness.

There may be a need for different approaches to apply to different countries to take into account different risk profiles and circumstances. And no detection system or technical solution will be perfect, so the process of verifying the dismantlement of warheads cannot rest on one technology or a single inspection process alone. This paper will consider what is needed for the inspections, verification technology/approaches, and political judgement to fit together – i.e. joining the dots.

2. History and background

The challenges with disarmament verification have been recognised for a very long time, for example going right back to the Charter of the League of Nations following World War 1. The negotiating parties to the Charter decided that the Commission in charge of advising on States' adherence to the Charter's commitments to hold armaments to a minimum, should not have inspection powers. The view at that time was that inspections would not be consistent with the assumption of mutual good faith on which the League was founded, and that it was not practical to design inspections to discover undeclared research into new explosive. The view was that any large-scale preparations for war could not be concealed from national intelligence services[3]. Moving forward some seventy years, to earlier work on nuclear warhead disarmament verification, a report commissioned by the US Department of Defense in 1993 in relation to US-Russia disarmament work, *Verification of Dismantlement of Nuclear Warheads and Controls on Nuclear Materials*[4], summarised the situation as: "In any conceivable dismantlement/disarmament/cut-off regime, verification will of necessity be less than perfect. Therefore, a decision as to whether a particular informal agreement, or formal treaty is in the United States national interest must rely on difficult political/strategic judgments, as well as technical ones, as to its risks and benefits". The report went on to make recommendations that an effective monitoring system be developed that integrates both cooperative verification procedures between the parties and national technical means.

The summation of the challenge outlined in that 1993 report still holds true today, but since that time some "real life" experience in disarmament verification has been built, and good progress has been made in some promising technologies and techniques. Some examples of disarmament experience include:

- **South Africa disarmament**: IAEA verification in 1993 that all nuclear material inventory from South Africa's terminated and dismantled weapons program had been accounted for[5].
- **Ukraine, Kazakhstan, Belarus disarmament**: The repatriation and dismantlement to Russia in the 1990s of nuclear weapons stationed in former Soviet states of Ukraine, Kazakhstan and Belarus[6].
- **START I and START II**: Under these treaties, the USA and Russia limited the number of deployed nuclear weapon delivery systems and the number of warheads per system, verified under very detailed arrangements[7] for confirming the number of warheads systems are armed with.
- **US-Russia HEU purchase agreement**: Under this agreement concluded in 1993, Russia down-blended 500 metric tonnes of HEU over several years for use in US commercial nuclear power generation. This agreement included transparency measures allowing for US monitoring[8].
- **Fissile Material Transparency Technology Demonstration**: A Los Alamos National Laboratories demonstration to Russian officials in August 2000 of a technology for monitoring nuclear materials removed from military programs. The demonstration measured six attributes, plutonium isotopics, plutonium mass, absence of oxide, presence of plutonium, symmetry of plutonium package, and, age of plutonium, using information barriers displaying a simple yes/no for each attribute[8].

- **Trilateral Initiative**: A joint project between the US, Russia and the IAEA from 1996-2001 that investigated the technical, legal and financial issues associated with IAEA verification of nuclear disarmament[9], focussing particularly on approaches that would permit the IAEA to conduct inspections without coming into conflict with Article I of the Non-Proliferation Treaty (NPT)[10].
- **UK-Norway Initiative:** A first of a kind initiative between a nuclear-weapon State and non-nuclear-weapon State, which began in 2007, exploring issues related to nuclear disarmament such as information barriers and managed access[11].

As well as building experience in disarmament verification approaches, there have also been some promising developments in technologies and techniques.

3. Disarmament verification technologies and approaches

3.1 Templates vs attributes

There are two quite fundamentally different measurement approaches that have been explored for verifying nuclear warhead dismantlement without revealing sensitive, classified information. The **attribute** approach, as the name suggests, directly measures attributes of the device to assess whether it appears to be a warhead, but with the measurement results obscured to only reveal to the inspector that each attribute is within a range, or less than or more than a threshold. Essentially, the attribute approach measures some "soft" minimum standard agreed between the host and inspectorate as providing enough information to give sufficient confidence that the item measured is a warhead. **Template** measurements, on the other hand, assess whether two items are the same by confirming there are no differences in attributes, within measurement tolerances. In the template approach, one item is a pre-confirmed warhead template, and the other a warhead candidate. In both of these measurement approaches the warhead being measured is obscured, for example in a sealed container, to prevent the inspector from viewing the device. This provides an **information barrier** to prevent the inspecting party from learning details of the classified attributes through the measurement process[12].

The attribute approach verifies intrinsic characteristics of nuclear warheads, such as: ratios of plutonium isotopes ^{240}Pu to ^{239}Pu; plutonium mass; and, symmetry of the plutonium. These can be measured either using passive measurement techniques (e.g. measuring characteristic gamma spectra of plutonium or uranium using high purity germanium detectors), or active measurement techniques (e.g. x-ray or neutron transmission measurements, or neutron activation analysis). Active techniques can also be used to verify attributes associated with components of warheads such as the presence of explosives[13], or to confirm that the plutonium is not in the form of plutonium oxide[14]. The specific attributes measured are classified, so the system must be designed such that the inspector does not see the measurements directly. The parties instead must agree on unclassified threshold values that are displayed to the inspector, e.g. *plutonium mass* $>$ 2kg; and ^{240}Pu / ^{239}Pu ratio $>$ 0.1. Attribute measurements also require a way to authenticate the measurement system using a standard that isn't itself classified.

The template approach does not measure attributes, but rather compares the physical signature (e.g. radiation from the transmission of neutrons or x-rays) of an inspected item against a known standard. This approach can be thought of as measuring attribute deltas between two presumed identical items, rather than measuring the attributes themselves. For the template approach to work there needs to be multiple warheads of the same type, and of course the inspector must have high confidence that the item used as the template warhead is in fact a real warhead.

3.2 Promising developments in template approaches

One type of template approach proposed recently[15] by researchers at the MIT Laboratory for Nuclear Security and Policy would radiograph a candidate warhead using transmission nuclear resonance fluorescence to resolve geometric and isotopic attributes, in combination with a scattering foil for the transmitted x-rays that serves as an encryption key. The high-energy x-ray beam used to probe the warhead would resolve classified details if the measurement were recorded. However, before the radiograph is

recorded, and therefore seen by the inspector, the x-rays scatter off an encryption foil obscuring the information contained. The host manufactures and supplies the encryption foil and then in coordination with the inspector selects a warhead from which the template measurement would be taken. The remaining candidate warheads would then be measured against this template measurement.

A variation on this technique that has been developed recently by a team of researchers at Princeton University and Microsoft Research, is something known as a zero-knowledge proof protocol[16]. Zero-knowledge proofs were invented in the 1980s and are used in cryptographic applications such as data mining where privacy must be preserved[17]. Under this technique, a radiographic image of each candidate warhead is compared against the template warhead. The detector system or array of detectors used to construct the image would be pre-loaded with what is essentially a “negative” image (conceptually similar to the negatives of photographs) of the template warhead. The measurement of a candidate warhead using the pre-loaded detector system would therefore produce a saturated image that contains no information whatsoever, provided the candidate is identical to the template. The image would only contain information of the measured warhead if some attribute of the candidate did not match the template, in which case there would be information leakage on an attribute of the warhead. The risk of this is also a disincentive to trying to cheat the measurement.

This approach has been developed further by the authors to use superheated emulsion bubble detectors[18], rather than electronic detector systems, for taking a neutron radiographic profile of the inspected item. The “image” taken by an array of emulsion detectors, would be a count per detector of the number of transmission neutrons detected represented by the number of bubbles in each detector – each detector representing a pixel in the image array. Using a measurement technique that essentially involves counting bubbles, means the system is far less prone to electronic tampering by an inspector to try and reveal classified attributes.

3.3 Continuity of knowledge, chain of custody

Continuity of knowledge is a well-established concept in verification activities where the inspectorate must maintain confidence that an item has not been tampered with, disassembled, moved or swapped after it has been verified. When applied in the implementation of IAEA safeguards it refers to a combination of containment (e.g. using tamper-indicating seals) and surveillance (e.g. remote monitoring of an area using event-triggered cameras) applied to verified nuclear material. The process of maintaining continuity of knowledge while bringing a verified item under containment and/or surveillance would be more challenging than most IAEA safeguards scenarios, given the inspector cannot would have tightly constrained access to the item. However, once the item is in its containment vessel or box, the standard containment and surveillance technologies could in principle still be used.

3.4 Initialisation problem, authentication and validation

The difference, strengths and weaknesses between the attribute approach and template approach are being examined carefully in academic circles (see for example, the review article by Yan and Glaser[19]), The template approaches is generally considered to be most appropriate in a scenario where numerous warheads of the same type are measured; with the attribute approach more appropriate for warheads not of the same type but similar features. The template approach is generally considered to be the more robust against cheating, but is likely to be more technically challenging to implement. For example, a template-based measurement might require very careful physical alignment whereas an attribute measurement would likely be less constrained.

One issue both approaches must contend with, though to different degrees, is the “**initialisation problem**”: how can the inspector be sure that the warhead template, or set of warhead attributes are in fact characteristic of the candidate warheads that are to be verified? As noted above, the working hypothesis the inspectorate should apply is that spoofing of measurements cannot be ruled out absolutely, so the initialisation problem needs to be addressed in any measurement system.

There are some approaches that can be taken to increase the confidence of the inspector that the template is legitimate. To be confident that a template warhead is in fact a warhead, the inspector could randomly select a few warheads from the full population. To spoof this by adding some fake or incomplete warheads to the population, would require the gamble by the inspected party that the inspector would not choose a fake warhead; a likelihood that could be designed to be very small. Alternatively, the host could in principle spoof this with a full population of entirely fake warheads, but this is where the notion of context and use of NTM become invaluable (discussed further below). To be confident that no "backdoors" or modifications have been made to equipment used in the inspection, techniques such as "blind buying", random selection and purchasing off-the-shelf hardware can be used. This principle was incorporated in design of the next generation attribute measurement system (NG-AMS) by Los Alamos National Laboratories[20].

3.5 Situational context

A potentially important concept to build confidence about the initialisation problem, is context – which could be formalised as a specified confidence-building measure in the treaty instrument, or could arise through the inspectorate building situational awareness of the environment over time. An accumulation of situational observations or proximate facts on the ground could build situational context collateral. This situational context collateral combined with the measurements themselves could be used to increase confidence.

For example, the approach described above of randomly selecting warheads from a full population would be enhanced by the situational context of knowing that the warhead was chosen while present in a fleet of missiles. If the inspectors could not witness the removal of a warhead from a randomly selected missile, then some sort of tagging system could be used instead on the selected missile/warhead combination. The argument would be that a nuclear deterrent relies on the presence of real warheads in missiles, so a properly designed process of randomly selecting one or more template warheads known to have been present on a missile is very likely to be a real warhead. Another example is scrutinising a credible record of custody of the chosen template warheads.

Baseline declarations of a nuclear weapons program and its history would also provide situational context which would help with verification of disarmament actions. Information of the full lifecycle of an individual type of nuclear weapon and on the ways in which it was deployed would provide collateral support for the assertion that an item is a nuclear warhead, as well as for checking that all (or a designated fraction) of warheads of a certain type are being verifiably dismantled. The history of production of fissile material by a state may also be useful information. In this regard, the NTI publication, "Cultivating Confidence"[21] has proposed that: "all states with nuclear weapons could be investing in extensive research into the history of their nuclear programs and developing information to support initial declarations of nuclear materials production; warhead production, deployment, retirement, and disposition; nuclear materials production capabilities; and delivery systems inventories."

This sort of technique was used in the IAEA's verification of the dismantlement of South Africa's nuclear weapons program in 1993[5]. Considerable effort by the inspection team was put into determining the mutual consistency of the inventory of nuclear installations and material, including reviewing historical operating records, to ensure the completeness of material being verified. The declared inventory was evaluated from production, import and usage records, and then compared against a calculation of the isotopic balance. This comparison did at first indicate a discrepancy in the quantity of high enriched uranium produced. This was resolved by what the inspectors described as an exhaustive examination of the performance of one of the enrichment plants, using thousands of operating records to model the plant on a daily basis from the beginning of its operation to estimate the total quantity of HEU produced from first principles.

Another piece of context that could build confidence is the relationship between the numbers and types of dismantled warheads and the fissile material removed. While this material remains in sensitive forms it could not easily be quantified by inspectors. However, direct measurement would be possible for nuclear material once brought under safeguards. Examining the quantitative relationship between a number of dismantled warheads and the quantity of nuclear material resulting may raise sensitivities for an inspected state, but could offer useful additional assurance if an approach that respects these sensitivities can be found. For example, different measurement approaches that complement one another could be considered.

Situational context can build as the inspection and inspected party work together on developing the verification approaches, involving access to locations holding inspected items, and building experience over time through inspections. This has been the case with the work between the US and Russia on verification under the original and new START treaties. Another aspect of context is the use of NTM, as this also builds situational awareness of the environment from where the warheads have been withdrawn. Incorporating NTM into a multi-lateral verification regime would present challenges, particularly in promoting a level playing field. The Open Skies Treaty which allows Parties to overfly other each other's territory and take images in specified optical, infra-red and radar is a potentially useful model for supporting a multilateral disarmament verification treaty, especially for states that don't have access to satellite imagery[22]. The examples of challenge inspections under the Comprehensive Nuclear-Test-Ban Treaty (CTBT) and the Chemical Weapons Convention (CWC) could also provide a starting point for considering how NTM could be incorporated. These are examples of where NTM may be incorporated into multilateral verification, but differ from the case of multilateral disarmament verification in that they deal with specific non-compliance concerns, rather than supporting routine verification.

And finally, there is the situational context of why a state is subjecting itself willingly to disarmament verification and its transparency and cooperation with the inspectorate. Using again the example of South Africa, the circumstances that led to it subjecting its dismantled warheads to verification were considered plausible, the South African Government had a policy of transparency, and the South African authorities were cooperative. Trying to quantify such factors when drawing conclusions is fraught, but these are contextual factors that can support confidence nonetheless. A paper by von Baeckmann, Dillon and Perricos (IAEA inspectors involved in the South African disarmament verification) summed it up as: "These general conclusions [about the correctness and completeness of the declared nuclear inventory] had strong technical bases and were significantly supported by the transparency and openness of the South African authorities with respect to access to information and locations, in particular the stated and demonstrated willingness of the authorities to facilitate access to any location that the IAEA may identify."[5]

4. How can the dots be joined?

The various kinds of observations and information that can help build confidence in declarations and actions of States subjecting warhead dismantlement to verification are potentially disparate. Some would require the access that only inspectors can gain. Others may draw on open source information, or information from NTM. A substantial challenge for the design of disarmament verification will be to craft mechanisms through which stakeholder states are presented with a picture that joins the dots and provides adequate confidence, and/or with information that enables them to themselves join the dots. And the circumstance could vary widely from one state to another, given differences in: warhead design and incorporation in delivery systems; accessibility of sites holding warheads; numbers of warheads and locations; security and safety protocols for providing access; completeness of historical production records; etc. Any disarmament verification arrangements will likely need to incorporate acceptance that adaptability will be required for the different circumstances. Developing an inspection protocol in detail would be a very big task, but that should not stop efforts to map out the general principles and basic framework, which is one of the tasks of the IPNDV.

5. International Partnership on Nuclear Disarmament Verification (IPNDV)[23]

Analysis of the range of challenges that face nuclear warhead disarmament verification is the focus of the International Partnership on Nuclear Disarmament Verification (IPNDV). IPNDV is a public-private partnership between the US Department of State and the Nuclear Threat Initiative (NTI) that began work in 2015. It comprises representatives from around 25 countries, including all five NPT nuclear weapons states, and is broken up into three working groups:

- Working Group 1: Monitoring and verification objectives – co-chairs, The Netherlands, Italy
- Working Group 2: On-site inspections (OSI) – co-chairs, Australia, Poland
- Working Group 3: Technical challenges and solutions – co-chairs, Sweden, USA

	Description	Key questions and assessments
Working Group 1	Assess potential monitoring and verification objectives, methods and activities for key phases of the nuclear weapons lifecycle: deployment and storage of warheads; disassembly and dismantlement process: and, disposition of nuclear materials arising from dismantlement.	• Key terms and definitions • Framework for analysing monitoring and verification activities • Monitoring and verification objectives for key aspects of the warhead dismantlement process, including information needed to meet objectives • Evaluation criteria for assessing monitoring and verification regimes, including potential trade-offs • Skills, areas of expertise and resources needed to support future work
Working Group 2	Explore the lessons learned from various on-site inspection regimes and identify fundamental OSI principles common to those regimes, assess the applicability and utility of these principles to potential future nuclear arms control agreements, and identify potential new inspection activities and techniques that could effectively verify compliance with future agreements.	• Roles and objectives of OSI in verifying nuclear disarmament undertakings, including identifying parts of the lifecycle where OSI will be of value; • Lessons learned from existing regimes related to conventional and nonconventional weapons and their non-proliferation, wherever OSI is used as a verification mechanism. • Ways in which verification objectives can be achieved notwithstanding limitations related to safety, security, national interests and non-proliferation, including through the application of managed access. • Desirable knowledge and skills for inspectors, escorts, and support staff at locations where inspection and/or monitoring activities occur, as well as considerations relevant to the capability and composition of inspection teams.
Working Group 3	Develop solutions for key technical challenges related to nuclear disarmament verification, particularly issues with warhead authentication, chain of custody, and data and equipment authentication.	• Confirming the presence or absence of nuclear warheads and relevant nuclear materials without revealing proliferation sensitive information • Effective methods and procedures for establishing and maintaining chain of custody for items at different stages in lifecycle • Strategies and tools for software and hardware certification and authentication.

Table 1: IPNDV Working Groups

Drawing on the considerable expertise across many States (both nuclear-weapon States and non-nuclear-weapon States) in areas such as on-site inspections, technology development, disarmament verification, treaty evaluation processes and criteria, etc, the IPNDV is advancing understanding of this complex, multi-disciplinary challenge. In the area of on-site inspections, IPNDV includes specialists with experience in inspections under the IAEA, OPCW, CTBT and bilateral disarmament agreements such as the START treaties. Drawing on the theme of this paper, once the present work of the IPNDV is complete, an aspect of the disarmament verification that would be worthwhile examining would be the “joining the dots” challenge.

6. Closing remarks

A point of discussion that arose in an IPNDV Working Group 2 meeting was “what does confidence look like?” for nuclear disarmament. It was observed that there are already a few examples of nuclear disarmament: South Africa’s complete disarmament of its nuclear arsenal in the early 1990s; Kazakhstan, Belarus, and Ukraine’s repatriation of nuclear warheads to Russia in the early 1990s; USA and Russian disarmament of delivery systems under the START treaty (Strategic Arms Reduction Treaty). The

international community has confidence that these countries fully disarmed, and that the USA and Russia have made large reductions in warheads and delivery systems under START 1 and 2. And this confidence was reached in completely different ways with different approaches to verification. Some were multilateral verification approaches (the IAEA's verification of South Africa's disarmament), some were unilateral (Russia's retrieval of warheads from Ukraine and Kazakhstan), and some where bilateral (US and Russian START arrangements). And it is to be hoped that a time will come when DPRK disarms, which will build more international experience in disarmament verification.

The circumstances in each of these cases is obviously quite different to the considerable challenge of a multi-lateral verification regime, particularly in the situation where the number of remaining warheads is approaching zero, but nonetheless this does reinforce that there are many different pathways to building confidence in the disarmament space, that it is possible to adapt verification arrangements to the circumstances, and that confidence builds over time with the understanding of the situational context.

In the meantime, maintaining efforts in developing technologies, approaches, techniques, evaluation methods, etc, such as being spearheaded by the IPNDV partnership is very important, so that when the geo-political circumstances present an opportunity for further disarmament (partial or full) in one, some or many States, the body of expertise and experience in this field can provide verification solutions.

This was neatly summed up by the Nobel Prize winning economist, Milton Friedman, although for a different purpose, but quite apt for the challenge of disarmament verification:

> "There is enormous inertia—a tyranny of the status quo—in private and especially governmental arrangements. Only a crisis—actual or perceived— produces real change. When that crisis occurs, the actions that are taken depend on the ideas that are lying around. That, I believe, is our basic function: to develop alternatives to existing policies, to keep them alive and available until the politically impossible becomes politically inevitable."[24]

End Notes

[1] For example, a highly mono-energetic high energy x-ray beam could be used to selectively excite the nuclear resonance of only one isotope in a measured warhead. However, if the beam has a broader energy distribution (such as a bremsstrahlung x-ray source) then resonances of other isotopes could be also excited revealing information about the isotopic composition of the item (see discussion in reference 15)

[2] The 1991 START 1 treaty (*Treaty Between the United States of America and the Union of Socialist Soviet Republics on Further Reduction and Limitation of Strategic Offensive Arms*) states in Article XI: "For the purpose of ensuring verification of compliance with the provisions of this Treaty, each Party shall use national technical means of verification at its disposal in a manner consistent with generally recognized principles of international law". The 2010 START II treaty has a similar provision on the parties using national technical means consistent with generally recognized principles of international law in Article X.

[3] Discussion on Article VIII of the Charter of the League of Nations: Butler G, *A Handbook to the League of Nations*; Longmans Green and Co; 1919.

[4] Drell S, et al.; *Verification of Dismantlement of Nuclear Warheads and Controls on Nuclear Materials*; JASON, MITRE Corporation, McLean, VA; Technical Report JSR-92-331; 1993.

[5] For a detailed discussion of how the IAEA verified the dismantlement of South Africa's nuclear weapons program see: von Baeckmann A, Dillon G, Perricos D; *Nuclear Verification in South Africa*; IAEA Bulletin 1/1995.

[6] Allison G; *What Happened to the Soviet Superpower's Nuclear Arsenal? Clues for the Nuclear Security Summit*; Harvard Kennedy School, Belfer Center for Science and International Affairs; March 2012.

[7] The Annex on Inspection Activities to the Protocol to the START II treaty runs to 91 pages.

[8] *Technology R&D for Arms Control*; US Department of Energy, National Nuclear Security Administration publication, Arms Control and Nonproliferation Technologies; Spring 2001

[9] Shea T; *IAEA Verification of Weapon-Origin Fissile Material in the Russian Federation and the United States: The Trilateral Initiative*; IAEA-SM-367/9/01; presented at the 2001 IAEA Safeguards Symposium.

[10] Article 1 of the NPT prohibits nuclear-weapon States, *inter alia*, from assisting, encouraging or inducing any non-nuclear-weapon State in acquiring nuclear weapons or other nuclear explosive devices. The prevailing interpretation of Article 1 of the NPT is that revealing classified details about nuclear weapon design, even during a disarmament verification activity, would violate Article 1 obligations.
[11] http://ukni.info/
[12] Using a simplistic example, consider a scenario where one had to verify the weight and size of a classified ball, without knowing the actual weight and size. Using the attribute approach the verification system could measure the weight using spring scales and the diameter using callipers. These measurements would then be presented to the inspector as something like: x kg < *weight* < y kg; and, *diameter* > z cm. Using the template approach the weight could be measured using balance scales (rather than spring scales) with the pre-confirmed template ball and candidate ball on either end, both obscured within identical boxes. Such a measurement would confirm to the inspector that both balls are identical in mass (within a narrow tolerance) without revealing the actual mass. For the size measurement, say both balls are fed through a cascade of many progressively finer sieves. If both balls have the same diameter within the tolerances of the sieve cascade then they will both come to rest between the same pair of adjacent sieves. If the inspector then confirms that both balls are caught by the same sieve pair, the inspector could be confident that the sizes are the same (within tolerances), without needing to know the actual hole sizes in the sieve pair or knowing where the sieve pair lies in the full cascade. In both examples great care would obviously need to be taken in designing the systems so that they could not easily be spoofed by the host.
[13] All explosive compounds contain nitrogen, typically 20-40% by weight. The gammas emitted from neutron activation on nitrogen is a much higher energy (10.83MeV) than that from neutron activation on almost any other element and from the gammas from the decays of uranium and plutonium. This makes neutron activation analysis a very powerful technique to verify the presence of explosives.
[14] The measurement looks for the characteristic gamma energy from the activation of oxygen by neutron capture. This sort of measurement is a surrogate for verifying that the plutonium is in metallic form; the argument being that if the plutonium is not oxide then it's likely to be metal. The direct determination that the plutonium is in metallic form is not considered technically feasible (reference 8).
[15] Kempt R.S; *Physical Cryptographic Verification of Nuclear Warheads*; Proceedings of the National Academy of Sciences of the United States of America (PNAS); Vol. 113, No. 31; August 2016.
[16] Glaser A, Barak B, Goldston R J; *A Zero-Knowledge Protocol for Nuclear Warhead Verification*; Nature; Vol 510; June 2014
[17] Chazelle, B; *The Security of Knowing Nothing*; Nature; Vol. 446; 2007.
[18] Philippe S, Goldston R J, Glaser A, d'Errico F; *A Physical Zero-Knowledge Object-Comparison System for Nuclear Warhead Verification*; Nature Communications; DOI: 10.1038/ncomms12890; September 2016
[19] Yan J, Glaser A; *Nuclear Warhead Verification: A Review of Attribute and Template Systems*; Science & Global Security; Vol. 23; 2015
[20] Shergur J; *An Overview of the Design of a Next Generation Attribution Measurement System*; 46th Annual INMM Meeting, 10–14 July 2005, Phoenix AZ
[21] Hinderstein C; *Cultivating Confidence Verification, Monitoring, and Enforcement for a World Free of Nuclear Weapons*; a publication of the Nuclear Threat Initiative; Washington, DC; 2010.
[22] See for example discussions in references 4 and 21.
[23] www.nti.org/about/projects/international-partnership-nuclear-disarmament-verification/
[24] Preface to the 1982 edition of: Friedman M; *Capitalism and Freedom*; The University of Chicago Press.

Session 06

Geological Repositories

Elements of a Swedish Safeguards Policy for the Spent Fuel Disposal System

G. af Ekenstam, L. Hildingsson, R. Fagerholm, C. Andersson

Section for Nuclear Non-proliferation and Security,
Swedish Radiation Safety Authority
Solna Strandväg 96, SE-171 16 Stockholm, Sweden

Abstract:

This paper presents an outline of the Swedish encapsulation and deposition processes, possible national measures in support of international safeguards, and possible national measures implemented for domestic purposes. All these measures are only in support of nuclear material accountancy and are not in any way aimed at other scenarios that would be in violation of Swedish law, e.g., theft, falsification, sabotage, etc. Only the operational phase of the geological repository is considered in this paper.

The IAEA has developed safeguards approaches under integrated safeguards for encapsulation plants and geological repositories. The approaches are very generic for these two facility types and cannot be used for devising detailed safeguards approaches. In this context, a compatibility evaluation of the generic IAEA approaches vis-à-vis the Swedish system has been conducted. This evaluation also takes into account the conclusion drawn under the Additional Protocol, i.e., the confirmed State-wide absence of undeclared nuclear activities.

Two elements of the Swedish system that will need careful consideration are: (1) the high throughput encapsulation process–which may limit the time available for safeguards measurements; and (2) the unavailability of the copper canisters for measurement and evaluation of C/S once they have been loaded into transport casks. While also taking into consideration that ongoing daily operations over a period of several decades is expected at both facilities, there is apparent justification to develop very robust techniques for unattended verification and monitoring involving remote data transition capabilities.

For the Swedish concept, it appears imperative that the transport casks containing the canisters are covered by robust C/S measures from the time of canister loading at the encapsulation plant up to the time of entering the underground areas of the geological repository. It is considered undesirable to have routine inspection activities (including C/S activities) conducted underground.

Lastly, due to safety requirements, the operator is expected to perform comprehensive measurements on all individual fuel elements. These measurement results, in addition to equipment, may also be used by the IAEA and Euratom. Consequently, authentication and sharing issues may need to be addressed.

Keywords: Final disposal; spent nuclear fuel; safeguards.

1. Introduction

Spent nuclear fuel from Swedish reactors must be managed and disposed of in a safe manner, including safeguards. The Swedish concept for handling spent nuclear fuel has been developed by the Swedish Nuclear Fuel and Waste Management Company (SKB) [1]. In brief, the concept is based on

encapsulating the spent fuel in copper canisters and depositing them in granite bedrock about 500 m below ground. In 2011 SKB formally submitted an application for an encapsulation plant and a final repository.

Spent fuel from Swedish reactors is shipped to Clab, an interim storage facility located in Oskarshamn. Here, the spent fuel is placed in storage pools in the bedrock about 30 m underground. Clab has been in operation since 1985 and is used to store spent fuel from all the nuclear power plants in Sweden [2]. Today there are about 32,000 spent fuel assemblies, at Clab corresponding to 6,300 tonnes of uranium and 59 tonnes of plutonium. The spent fuel stored at Clab consists primarily of BWR and PWR fuel with a few additions of older experimental fuel and spent fuel debris [3]. The flow of spent nuclear fuel in Sweden is illustrated schematically by Figure 1. A proposed encapsulation plant and a geological repository are also included in the figure.

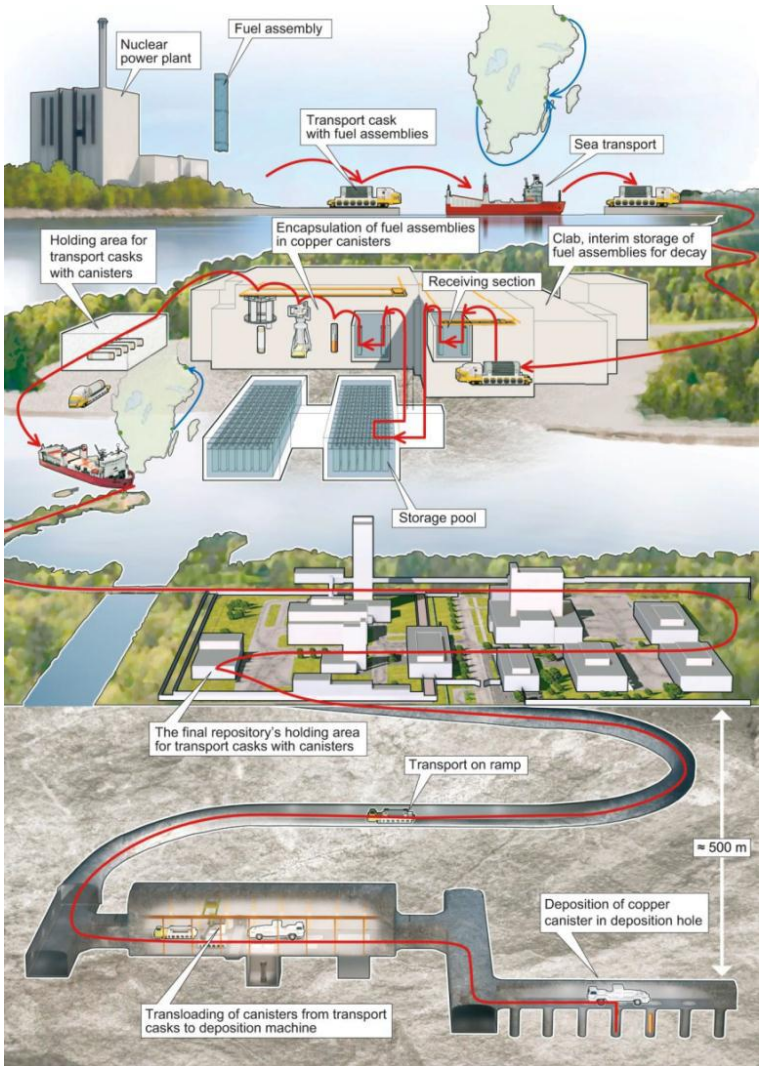

Figure 1. Schematic illustration of the flow of spent fuel in Sweden, from nuclear power plants to final deposition. Source: SKB.

2. The encapsulation plant

SKB has applied for permission to build the encapsulation plant, which is to be co-located with the existing facility, Clab the interim storage as an extension above ground. Thus there will be no need for transports between interim storage and the encapsulation plant. The combined facility will be named ‘Clink’ [4]. Cooling times of the spent fuel that will be encapsulated will typically be 40 years, but it may vary from 10 to 60 years. Burn-up will range from a few GWH/tU up to 60 GWh/tU..

Fuel to be encapsulated will be moved to a measuring position. Here, the operator will verify important parameters of the fuel, such as thermal residual power and burn-up. After the operator's verification, the fuel will be moved to a transfer canister, which will be moved to the handling cell where the assemblies will be dried and placed in a copper canister. In a series of steps, a copper lid will be put on and stir welded to the copper canister. The weld will be quality checked by the operator and the surface of the canister will be polished and decontaminated. Lastly, the canister will be placed in a transport cask and temporarily stored at the facility before being shipped to the geological repository site.

Each copper canister will have an insert of cast iron with positions for 12 BWR fuel or four PWR fuel assemblies. Fuel will be encapsulated during campaigns arranged separately for BWR and PWR fuel. It is envisaged that 150 canisters will be treated per year. During routine operation, this means loading one canister per workday, corresponding to a flow of 12 BWR assemblies, or four PWR assemblies, per day.

3. The geological repository

The plan is to build the geological repository at Forsmark, about 360 km north of the encapsulation plant. The repository will be close to, though separated from, the Forsmark NPP and the final storage facility for low and intermediate level radioactive waste, SFR, located there.

The geological repository will consist of a surface area and an underground deposition part, about 500 m below ground. The surface area will encompass a terminal and buildings for elevators, ventilation and backfill materials. There will be a transport ramp for vehicles connecting the above ground area with the underground repository; this will include the vehicle for transporting the transport casks containing the copper canisters. Copper canisters from the transport vehicle will be reloaded to a deposition machine in the underground Central Area. Transport tunnels will lead from the Central Area to the deposition tunnels, each having about 30 drilled vertical holes for one copper canister each. When all positions in a deposition tunnel have been filled, the tunnel will be backfilled and sealed with a concrete plug. A schematic illustration of the geological repository site is shown in Figure 2.

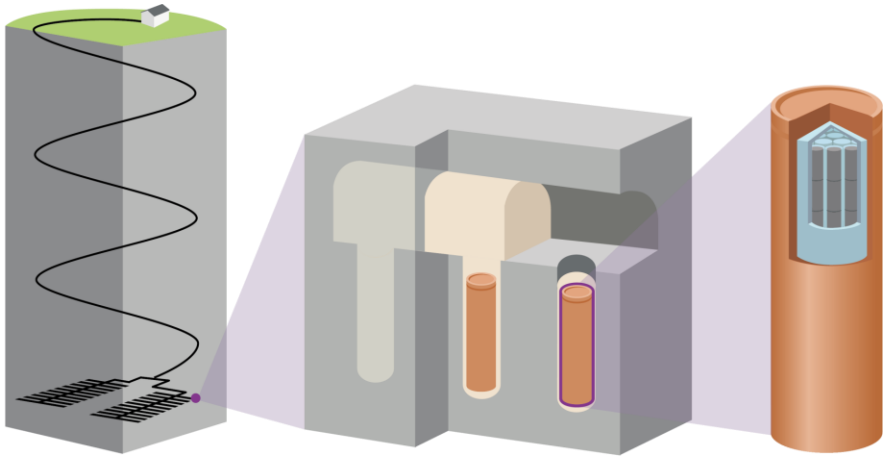

Figure 2. A schematic illustration of the geological repository's proposed layout.

Deposition tunnels will be excavated in a rock excavation zone, separated from the deposition and backfilling zone by a protection zone (with no blasting) and a separation wall. Excavation, deposition and backfilling can thus take place simultaneously, although physically separated. When the deposition tunnels have been backfilled, the separation wall will be moved, and the next step of excavation, deposition and backfilling can begin. One such step will take at least one year.

A specially designed ship will deliver transport casks containing filled copper canisters from the encapsulation plant to the geological repository. The transport casks will be temporarily stored at

surface level in a terminal building before being transported by a ramp vehicle underground to the Central Area. The copper canisters will then be transferred from the transport cask into a radiation shield of the deposition vehicle. The deposition vehicle will bring the copper canister from the Central Area to its final deposition position. Lastly, the ramp vehicle will return to the surface with the empty transport cask. The facility will deposit 150 canisters per year during normal operation. This means an average of one transport cask with copper canisters will be transported each day from the surface terminal building to the subsurface Central Area and deposited.

If approved, construction of the encapsulation plant can start in 2022 at the earliest and the plant would be in operation in 2030 at the earliest. Excavation works for the geological repository can start in 2020 at the earliest, with the first spent nuclear fuel being received starting in 2030. Both facilities will be in operation for about 45 years. After this period of operations, the surface buildings will be removed and the repository sealed [5].

4. Legal requirements and national policy

One basic national legal requirement is that operators of nuclear facilities are responsible for ensuring that all the necessary measures are taken for safe management and disposal of spent nuclear fuel. This includes fulfilling all obligations as prescribed by Sweden's agreements aimed at preventing the proliferation of nuclear weapons [6].

According to national regulations [6], SKB must ensure that sufficient nuclear material accountancy information and knowledge are in place and available on the part of the spent fuel prior to its deposition. This can be carried out by verifying that the documentation accompanying the nuclear material is complete and correct, and in the event of uncertainty, performing the necessary measurements or analyses. SKB is also required to have a system in place guaranteeing that necessary and correct information about the nuclear material is documented and retained following the material's disposal.

As a consequence of Sweden's international obligations, all requirements must be met as effectively and efficiently as possible. This should involve the inclusion of design features that further facilitate the implementation of international safeguards. In order to achieve this, early discussions between the parties involved will be necessary. Therefore, early provision of the required documentation is of importance for fostering efficient and cost-effective safeguards.

One of the main legal requirements is the operators maintaining records on locations to where all their spent fuel has been transported. As the licensees have assigned management and disposal of spent fuel to the Swedish Nuclear Fuel and Waste Management Company, SKB, the responsibility rests with SKB. Insofar as a geological repository is concerned, the main national policy in Sweden with regard to nuclear material accountancy is to provide assurance domestically and internationally that all deposited nuclear fuel is as declared. Information on the item identification and quantities of nuclear material must be correct. This should be assured by using a specially designed "paper trail" (e.g., source and operating documents) verification procedure covering the entire fuel history. SKB should be able to provide sufficient information for this verification. SKB also intends to conduct its own measurements of the spent fuel for safety purposes.

5. Compatibility with IAEA safeguards models

The IAEA model integrated safeguards approach for an encapsulation plant [6] assumes that the encapsulation plant is a separate facility and that the spent fuel will be transferred from an interim storage facility in a transportation cask to an assembly handling cell of the encapsulation facility. The Swedish encapsulation plant will, however, be co-located with the spent fuel interim storage facility and form a combined facility. The encapsulation part of the facility will not have an area for receiving and storing spent fuel transport casks. The spent fuel from the NPPs will be stored in the interim storage area and stored in pools for several years before being moved internally to the encapsulation plant.

The IAEA model integrated safeguards approach for a geological repository [7] assumes a separate facility similar to the Swedish concept. However, there are a few differences. The IAEA model assumes that the copper canister can be identified upon receipt at the geological repository and that canister identification can be performed when a canister is transferred between the above ground area and the geological repository at the entrance of the repository. In the Swedish model, however, the copper canisters will be shielded by a transport cask until they reach the underground central area.

The model assumes that a redundant C/S system is to be applied to the disposal canister during transport from the encapsulation plant to the repository. During temporary canister storage above ground, dual C/S systems should be applied. In this context, we want to stress the importance of having robust C/S systems on the transport cask, i.e., systems that can be fully operated by facility employees while also providing credible assurance for the international community.

6. Safeguards considerations

6.1. General

On the basis of, inter alia, IAEA GOV/2002/8 [7], IAEA Model Integrated Safeguards Approaches for Spent Fuel Encapsulation Plants [8] and Geological Repositories [9] and the IAEA Safeguards Glossary (2001) [10], it is our understanding that the basic international verification requirements are:

- Yearly verification for “gross defects” (yes/no test whether or not all declared fissile material is missing) with “low detection probability” (20%) for spent fuel elements which are available for measurement and which are “difficult to dismantle”;

- Verification for “partial defects” (at least a yes/no test whether or not 50% of the declared fissile material is missing) for each spent fuel element which is being placed in a copper canister and for yearly verification of spent fuel elements which are available for measurement and which are not “difficult to dismantle”;

- Maintaining “dual C/S” or an equivalent system for spent fuel elements which are not available for measurement.

There is no completely clear definition of the concept “difficult to dismantle”. Rod exchange has been performed earlier on both BWR and PWR fuel in the ponds of Swedish nuclear power plants. However, with the absence of the required equipment for dismantlement at the Clab and Clink sites, it is reasonable to assume that all fuel that will be deposited can be classified as “difficult to dismantle”.

With the above requirements and assumption, it is expected that the nuclear material at Clink will be verified with low detection probability for gross defects on an annual basis. Spent fuel will be verified for partial defects immediately prior to encapsulation.

Thereafter a robust C/S system should be applied to the transport cask. This C/S should be evaluated upon entry into the underground area at SFK.

The activities under the Additional Protocol are not fully credited for the two IAEA approaches mentioned above. The confirmed state-wide absence of undeclared activities should render unnecessary certain proposed monitoring and verification activities. In this context, we would refer to an excerpt from the Minutes of the Experts’ Group on Safeguards for Final Disposal of Spent Fuel in Geological Repositories [11] and also the statement from DG to the IAEA Board of Governors in February 2002 [12].

“The important difference is that under Integrated Safeguards, geophysical methods may not be needed to detect excavations or excavation activities. For this purpose, geophysical tools could be replaced with Complementary Access and information analysis. Ground Penetrating Radar (GPR) may still be required for DIV purposes (i.e. detection of undeclared tunnels, rooms and boreholes, such as any permanent underground equipment and installations).” [11]

"The measures of the Model Additional Protocol were never intended to be simply superimposed as a new 'layer' of activity on top of safeguards as implemented under INFCIRC/153 (Corrected) and earlier strengthening measures. Given the additional assurances provided under an additional protocol, the need to avoid undue burden on States and facility operators, and the need for maximum efficiency in the light of the prevailing resource constraints, the new measures were to be 'integrated' with existing ones." [12]

Periodic DIVs and CAs under and above ground will provide sufficient assurance of the integrity of the site declarations and the absence of undeclared activities for both areas. The implementation of AP measures in the State will add more information on the nuclear capabilities.

As mentioned earlier, the last verification opportunities for the individual fuel elements exist at the encapsulation plant. The operator is expected to perform comprehensive measurements on all individual fuel elements for safety purposes. The optimal position for the operator's performance of these measurements is as early as possible in the material flow into the encapsulation process. This enables the operator to more easily reject assemblies that for safety or other reasons do not fit into the planned canister.

The IAEA and the European Commission, on the other hand, presumably prefer to have the verification measurement performed immediately prior to the canister lid being put on and welding being started. This verification is expected to be performed according to established IAEA criteria and practice, namely, a verification for "partial defects" for the spent fuel element.

Routine inspection activities underground at the final repository are not foreseen; underground activities will be limited to DIV only. Also, see the following recommendation from SAGOR:

"The recommended safeguards approach is to use item accounting supported by a reliable and comprehensive C/S system above-ground to verify, inter alia, the flow of full casks and overpacks. DIV is recommended as the primary safeguards measure underground. DIV would include geophysical methods."[13]

6.2 Measurements and possible use of operators' results

It is not desirable to have two completely different pieces of measurement equipment and perhaps also two different measurement positions for the required final verification of the spent fuel. This takes up space and will take more time. Also, it must be kept in mind that up to 12 assemblies will be encapsulated on a daily basis. It should be investigated to what extent the operators' measurement results and equipment can be shared with the IAEA and Euratom. It has to be assured that the operator's measurement results in principle are sufficient for the IAEA and Euratom. Therefore, the authentication issues must also be addressed to provide the international safeguards with the required opportunities for drawing independent conclusions.

Considering the fact that daily operations are expected to take place over the course of several decades, there appears to be a need to develop unattended verification techniques by means of remote data transition capabilities. The measurement position needs to be arranged at Clink in coordination with the IAEA and EU.

After measurement at the Clink site, proper C/S measures must be applied to assure Continuity of Knowledge (CoK) from the final measurements until the closure of the copper canister. If needed, as a backup to the C/S measures, a simple unattended quality control immediately prior to the assemblies being placed in the copper canister may also be considered. Such verification could involve reading the fuel identification number, measuring the weight of the assembly, and using a gross gamma detector. After the spent fuel has been placed in the copper canister, additional C/S measures have to be applied until the canister is placed in its final position in the geological repository.

If a method is developed and approved, verification of the copper canister may also be conducted at the encapsulation plant. However, for practical reasons, there are limitations to conducting similar

verification on the transport cask or on the copper canister underground at the final repository during normal operations. In exceptional cases, such verification underground could be performed in order to resolve anomalies.

6.3 Continuity of Knowledge

In the Swedish concept, it seems imperative that the transport casks containing the canisters are covered by robust C/S measures from canister loading at the encapsulation plant to entering the underground part of the geological repository.

The operational activities are expected to be run continuously for approximately 40-50 years with daily production of one copper canister and shipments on at least a bi-weekly basis, a sealing system that can be attached, also that the same seal can be detached by the operator, would be cost-efficient and enhance an efficient use of resources.

The inner walls of the underground tunnels and shafts define the primary containment of the geological repository. During construction and operation of the repository, there will be an access ramp, ventilation shaft, etc. These should be covered by C/S methods that are able to detect movements of spent fuel down to the deposition location and to detect any removal of nuclear material from the underground part. It is important to verify that a canister enters the underground part of the repository. This enables us to treat the underground part of the geological repository as a black box and there is thus no need for C/S and verification methods underground.

Also, as already discussed earlier, it is not considered desirable to have routine inspections of nuclear material accountancy activities, or verification of seals, etc. performed underground.

In the case of anomalies, a unique identifier for each copper canister resolution may contribute to its resolution, but not for routine use. Gamma and neutron measurements on the transport container may also be considered as a measure to resolve inconsistencies.

Verification of empty transport containers leaving the underground area is to be performed, e.g., weighing, gamma and neutron measurement.

6.4. Design Information Verification

The integrity of the geological repository can be verified during DIV, which may be conducted periodically. The main objectives are to confirm the following: that the excavations are performed as declared, there are no other undeclared nuclear activities, and that there are no clandestine removal routes or excavations. In this context, Complementary Access both above and below ground, information from satellite imagery and other open sources' information provide assurance for confirming the absence of clandestine activities at the area of the site. Hence, there is no need to continuously monitor the excavation by using geo-seismic monitoring.

7. Conclusions

The conclusions drawn under the Additional Protocol are not properly credited for in the IAEA approaches mentioned above. The confirmed state-wide absence of undeclared activities should render unnecessary certain monitoring and verification activities that have been proposed. Therefore, in this context, some of the facility-specific considerations in the IAEA model may not apply.

The last verification opportunities for individual fuel elements and also for routine verification of the canisters will exist at the encapsulation plant. The final spent fuel verification prior to canister welding at the encapsulation plant is expected to be performed according to established IAEA criteria and practice.

The maximum time available for verification will depend on the material flow. In the Swedish system, up to 12 assemblies will be encapsulated in one day, so the measurement times will probably be in the

order of minutes. Considering the fact that daily operations over the course of several decades are expected, there is a need to develop unattended verification techniques by means of remote data transition capabilities.

Due to safety requirements the operator is expected to perform comprehensive measurements on all individual fuel elements. It should be investigated if these measurement results can be shared with the IAEA. Therefore, authentication and sharing issues have to be addressed.

Inspections for DIV purposes are essential to confirm that the repository is constructed as declared and to confirm the absence of any undeclared activities. It is considered undesirable to have other routine and verification activities, including C/S, performed underground.

In the Swedish concept, it seems imperative that the transport casks containing the canisters are covered by robust C/S measures from the time of canister loading at the encapsulation plant up to the time of entering the underground part of the geological repository. It is considered undesirable to have routine inspection activities (including C/S activities) performed underground.

8. Acknowledgements

The authors gratefully acknowledge all those who have reviewed the content and contributed by providing information for this paper, in particular our colleagues at SSM and the SKB company.

9. Legal matters

9.1 Privacy regulations and protection of personal data

The authors agree to allow ESARDA to print our names/contact data/photographs/article in the ESARDA Bulletin/Symposium proceedings, or any other ESARDA publications and, when necessary, for any other purposes connected with ESARDA activities.

9.2 Copyright

The authors agree that submission of an article automatically authorises ESARDA to publish the work/article in whole or in part in all ESARDA publications – the bulletin, meeting proceedings, and on the website.

The authors declare that their work/article is original and is not a violation or infringement of any existing copyright.

10. References

[1] The NPPs at Forsmark, Oskarshamn, Ringhals and Barsebäck (the latter undergoing decommissioning).

[2] As of March 2017.

[3] This is fuel from the closed, experimental Ågesta reactor and some German fuel obtained in a swap with Swedish fuel that was intended to be reprocessed. The fuel debris consists of parts of spent fuel rods from the Studsvik Hot Cell laboratory. This is debris from examination of the fuel or leaking fuel rods that have been cut in smaller parts. The fuel debris is stored in closed containers.

[4] An acronym for the Swedish term *Clab och inkapslingsanläggning.*

[5] SKB TR-16-15: RD&D Programme 2016. Programme for research, development and demonstration of methods for the management and disposal of nuclear waste, September 2016.

[6] Swedish Act on Nuclear Activities (1984:3), Chapter 3, Section 10.

[7] IAEA Model Integrated Safeguards, IAEA GOV/2002/8.

[8] Model Integrated Safeguards Approach for a Spent Fuel Encapsulation Plant, SG-PR-1305 Version, 2010-10-06

[9] Model Integrated Safeguards Approach for a Geological Repository, SG-PR-1306 Version, 2010-10-06.

[10] IAEA Safeguards Glossary 2001, Edition International Nuclear Verification Series No. 3.

[11] Excerpt from Minutes from the Fourth Meeting of the Experts' Group on Safeguards for Final Disposal of Spent Fuel in Geological Repositories, Gimli, Manitoba, Canada, 24-26 July 2001.

[12] Report by DG to the IAEA BoG, February 2002.

[13] SAGOR report 1, September 1998, STR-312, Volume 1, Chapter 3, 2nd para.

GOSSER - Geological Safeguards and Security R&D Project in Finland - How STUK prepares itself for the Final Disposal in Finland

Olli Okko, Mikael Moring, Tapani Honkamaa, Elina Martikka, Marko Hämäläinen

Radiation and Nuclear Safety Authority
STUK, Finland

Abstract:

The licensed construction of the disposal facility in Finland begun in autumn 2016 as the foundation works for the encapsulation plant and the excavations of the access tunnels to the canister shaft and canister storages in the geological repository were initiated. The disposal of spent nuclear fuel is scheduled to start in Finland in mid 2020's after the operational licence is granted. To ascertain that necessary technical safeguards tools are available at that time, STUK, the Radiation and Nuclear Safety Authority of Finland has set up a national R&D project GOSSER (Geological Disposal Safeguards and Security R&D). GOSSER's main objective is the finalisation of the national Finnish concept for safeguarding the final disposal of the spent nuclear fuel. This concept and related R&D efforts are coordinated with the Finnish facilities, European Commission and the IAEA. Activities in GOSSER include so far: 1) Participation in R&D of robust, reliable, and accurate methods to verify spent nuclear fuel prior to final disposal. The work has been done in cooperation with Helsinki Institute of Physics, the IAEA and other international partners. 2) Participation in the Safeguards-by-Design process of the Finnish encapsulation plant and final repository and, when necessary, development of safeguards methodologies for attaining knowledge of the verified nuclear material and to maintain it for future generations.

Keywords: Spent Nuclear Fuel; Safeguards; IAEA; Geological Disposal; Final Disposal; Safeguards-by-Design

1. Introduction

In November 2015 the Finnish Government granted the licence to construct the disposal facility consisting of the encapsulation plant (EP) and the geological repository (GR). The operator (Posiva), Finnish State Regulatory Authority (STUK), IAEA and the European Commission are cooperating on developing safeguards measures and on designing the necessary safeguards infrastructure for these facilities. The spent fuel disposed of will not be accessible for verification using traditional safeguards measures. The international and national safeguards measures have to create confidence that no nuclear material is diverted before, during or after the disposal process and that no undeclared nuclear activities take place at the disposal facilities. Moreover, the operational phase of the facilities will last over a century, thus the safeguards-related technological infrastructure should be flexible and upgradable. Safeguards by design (SbD) e.g. planning the safeguards measures and designing the necessary safeguards infrastructure during the design phase of the facilities has many benefits. Cost-efficiency is assured by including safeguards equipment such as cameras, radiation detectors, cables and conduits, into the facility design.

A plan for the operators safeguards activities during the construction and operation of the disposal facility was included by the operator in the application for the construction licence. This included the main steps in nuclear material accountancy and control during the facility development and preliminary plans for the control and accountancy during spent fuel transfers through the encapsulation and disposal process. The plan was approved by STUK during the licensing process and an assessment was included in the STUK Statement [1]. However, in order to ascertain that necessary technical

safeguards tools are available at the time needed, STUK launched the national R&D project GOSSER (Geological Disposal Safeguards and Security R&D). The main objective of GOSSER is the finalisation of the national Finnish concept for safeguarding the final disposal of the spent nuclear fuel. This concept and related R&D efforts are coordinated with the Finnish operators, the European Commission and the IAEA.

The key task of GOSSER (named LOVE) is to develop a robust, reliable, and accurate method to verify spent nuclear fuel prior to final disposal. The IAEA requires that spent fuel is verified at a partial defect level before transfer to “difficult to access” locations; however, there is no current method available that can reliably detect a diversion of less than 50% of the pins in a fuel element. The Finnish Support Programme to the IAEA Safeguards has researched the applicability of Passive Gamma Emission Tomography (PGET), and it will be the main candidate for further investigation. Combined with other methods, like gamma spectrometry and neutron measurements, it can be used to verify the correctness and completeness of the declared fuel at pin level. Another task of GOSSER (named JOY) is to evaluate and, when necessary, develop safeguards methodologies for attaining knowledge of the verified nuclear material and to maintain it for future generations. This task may require different techniques from traditional C/S, including geophysics and novel technologies, as well as methods from societal verification and long term data management. GOSSER will recognise the interfaces between safeguards, security and safety [2]. Security and safeguards both share a common objective: spent nuclear fuel is secured from unlawful actions.

2. Verification of spent fuel prior to disposal

STUK has a regular NDA verification programme. The goal of this programme is to verify that information provided by the operator is correct and complete, maintain and develop NDA expertise, prepare for final disposal and support IAEA safeguards conclusions. STUK performs 1 – 2 measurement campaigns annually at each Finnish NPP site Olkiluoto and Loviisa. The traditionally used verification tools are SFAT, eFORK and GBUV [3]. Since early 2017 year also the PGET device is used for verification as well as testing.

The Finnish Support Programme to the IAEA Safeguards has studied the applicability of Passive Gamma Emission Tomography (PGET) [4]. Under the GOSSER project, a research group was established in 2015 to study and develop the PGET method further. The Finnish Funding Agency for Innovation (TEKES) provides funding for the Finland Distinguished Professor Programme (FiDiPro) at the Helsinki Institute of Physics (HIP) for the years 2015 – 2018. STUK has a guiding role in the work and also actively participates in method development. The aim is to develop a combination of robust, reliable, and accurate methods to verify spent nuclear fuel prior to final disposal, down to detecting diversion of single fuel pins. Because the IAEA and GOSSER project share the same main goal, to develop functional apparatus for partial defect level spent fuel verification, the LOVE project can provide in-kind support to the work conducted under IAEA MSSP tasks. This will include, for instance, arranging test campaigns with the NPPs.

The latest tests with the prototype have shown the applicability of the method. Combined with other methods, like gamma spectroscopy and neutron measurements, it can provide precise and accurate verification results. The first campaigns with the upgraded PGET took place in February 2017 in Loviisa and in April in Olkiluoto. The campaigns went very well. The deployment of the system was easy and the PGET demonstrated its ability to reconstruct and analyse images of various fuel types with relatively short acquisition times (about 5 min). Missing pins were detected with good confidence. Although the technology has been developed and demonstrated, some research is still needed to support system development.

3. Safeguards-by-Design process

In addition to the NDA measurements several other safeguards practices and measures are to be developed and implemented with the facility design, construction and commissioning. An equipment infrastructure to be installed in the Olkiluoto encapsulation plant is already developed in cooperation between the stakeholders, IAEA, European Commission, STUK and the operator [5]. However, the design of the facility is still being optimised by the operator. Continuous communication between the

stakeholders is essential, to assure that the operator maintains safeguardability of the facility and that the inspectorates are able to modify their equipment infrastructure according to changes in plant design. A similar process is foreseen to be conducted for geological repository during the initial planning and construction phase. Geological investigations and construction of the geological repository will continue in parallel through its operational period. Due to unforeseen elements in the geology and rock mechanics, the repository layout at Olkiluoto cannot be rigidly planned in advance, so any safeguards measures in the repository needs to have enough flexibility to adapt to design changes.

The operator presented its plan to control the integrity of the fuel canisters and to demonstrate and to document their safe transfer to the emplacement hole with their construction licence application. This plan was approved by STUK in 2015 with the remark that the operator has to facilitate safeguards measures by STUK, the EC and the IAEA in further plans and development. Currently, the material accountancy for fuel canisters are a part of the negotiations of the Facility Attachment. In the disposal process, the Continuity-of-Knowledge and supporting Containment and Surveillance measures will be essential; whereas the annual DIV/PIV cannot be carried out in a traditional manner. The Safeguards-by-Design concept will cover also these aspects.

STUK has direct access to the repository; and, in cooperation with safety, also de facto full time institutional presence at the active final disposal facility site. In the national concept development this asset will be utilised. STUK follows the daily research and work plans, and the continuous monitoring of the site. STUK has also contacts to other authorities in Finland that are e.g. licensing construction activities and therefore can report about any undeclared safeguards-relevant activities. However, international inspectorates lacks these capabilities and in order to detect undeclared activities, they are more or less obliged to employ technological solutions, which STUK has less need for that. However, STUK must be aware of the capabilities and properties of these techniques. In it’s project STUK does not need to perform its own research. It is sufficient to follow what other institutions are developing in Finland and abroad for the safety assessment and security precautions and to demonstrate this to the inspectorates. However, this work also needs resourcing.

4. Summary

The GOSSER project was launched because safeguards for spent fuel disposal is a new challenge and new concepts need to be developed and implemented already during the early design and construction of the final disposal facility licensed in 2015. The time span of the overall disposal project is more than100 years so process optimisation has high pay off opportunities. As the disposal facility is of a new kind to be safeguarded, the methods developed and applied in Finland have to gain international acceptance.

The disposal of spent fuel requires that safety, information security and other security arrangements and the safeguards required to prevent the proliferation of nuclear weapons are properly implemented. This requires the reconciliation of all areas resulting in the implementation of 3S in an appropriate manner. This, in turn, requires action from the operators producing, encapsulating or disposing of spent nuclear fuel as well as from the national authorities.

The novelty of the disposal concept calls for adequate research and provides the reasoning for establishment of GOSSER R&D project. If GOSSER is not successful, in the worst case there is a risk that the credibility of the disposal concept is questioned and; moreover, the future generations may not have adequate information to satisfy themselves that the spent fuel is fully and reliably disposed of in the repository. As the European Commission and the International Atomic Energy Agency (IAEA) have strong roles in the safeguarding of nuclear materials, their objectives are considered within this project. However, the main objective of GOSSER is the finalisation of the Finnish concept for safeguarding the disposal of the spent nuclear fuel by 2018.

8. References

[1] STUK, *STUK's statement and safety assessment on the construction of the Olkiluoto encapsulation plant and disposal facility for spent nuclear fuel.* STUK-B 196, November 2015.

[2] Honkamaa, T., Martikka, E., Moring, M., Hack, T., Okko, O. & Hämäläinen, M. *GOSSER - Geological Disposal Safeguards and Security R&D Project in Finland - How We Prepare Ourselves for 2023 When Final Disposal Starts in Finland.* INMM 57th Annual Meeting July 24 – 28, 2016, Atlanta, Georgia, USA.

[3] Honkamaa T. & Hämäläinen M. *How STUK verifies Spent Nuclear Fuel and Why?* in Proceedings. ESARDA 25. Annual Meeting. Symposium on Safeguards and Nuclear Materials Management, Stockholm, 2003.

[4] Honkamaa, T., Levai, F., Turunen, A., Berndt, R., Vaccaro S. & Schwalbach, P. *A Prototype for passive gamma emission tomography (PGET),*in IAEA Symposium on International Safeguards, 20 – 24 October 2014, Book of Abstracts, IAEA CN-220-189, p. 257.

[5] Ingegneri M., Baird K., Park W.-S., Coyne J. M., Enkhjin L., Chew L. S., Plenteda R., Sprinkle J., Yudin Y., Ciuculescu C., Koutsoyannopoulos C., Murtezi M., Schwalbach P., Vaccaro S., Pekkarinen J., Thomas M, Zein A., Honkamaa T., Hämäläinen M., Martikka E., Moring M., Okko O. *Safeguards by Design at the Encapsulation Plant in Finland.* IAEA Symposium on International Safeguards, 20 – 24 October 2014, Book of Abstracts, IAEA CN-220-023, p. 207.

Ultrasonic Identification Methods of Copper Canisters for Final Geological Repository

C. Clementi[1], F. Littmann[2], L. Capineri[2], C. Andersson[3], U. Ronneteg[4]

[1] Dept. Information Engineering – University of Florence, Florence, Italy
[2] European Commission, Joint Research Centre, Nuclear Security Unit, Ispra, Italy
[3] Swedish Radiation Safety Authority,
[4] Swedish Nuclear Fuel and Waste Management Co

Abstract:

The Swedish system for taking care of the spent nuclear fuel include long term geological disposal of the fuel encapsulated into copper canisters. *For such Safeguards applications, it is of upmost importance to be able to trace canisters once closed in order to keep the Continuity of Knowledge from the Encapsulation Plant to the Geological Repository. One possibility is to use a tagging of the canister. This work introduces an innovative system for tagging copper canisters based on the ultrasonic reading of cavities machined on copper lids. For corrosion reasons it is better to not engrave any code on the external parts of copper canisters. According to the copper lid geometry, the proposed solution envisages the machining from the inside of several inclined Flat Bottom Holes or chamfers around the circumference of the lid, while still keeping the required thickness of the copper for safety reasons. They represent a unique identification code for each canister, easily readable by an ultrasonic immersion probe on a 360° scan. A laboratory prototype for the identification system has been manufactured and successfully tested.*
The copper lid is reproduced on a scaled version and a series of chamfers 50° inclined are drilled around the bottom of the lid. The reading system hosted a probe placed 14° inclined according to the Snell's law. The received ultrasonic signal represents the binary code realized by the chamfers.
The paper will describe the optimization studies made on the transducers, the angle and width of chamfers, the binary identification codes, preliminary design and testing of a reading system.

Keywords: ultrasound; identification; copper canister, geological repository.

1. Introduction

The spent fuel coming from operations of Swedish nuclear power plants will be stored in deep geological repositories inserted into copper canisters. The Swedish Nuclear Fuel and Waste Management Company's (SKB) developed the method for final disposal of fuel in copper canisters surrounded by bentonite clay about 500 metres underground in Swedish bedrock. This solution will keep the fuel isolated from human beings and the environment for many years.

The new SKB's method for final disposal of fuel comprises a number of facilities that together provide a safe chain (Figure 1). The fuel coming from Swedish reactors is stored for one year minimum in the spent fuel ponds at the reactors before it is shipped to the interim storage facility. There the fuel is placed in storage baskets which are stored in ponds. Later storage canisters with spent fuel will be lifted from the pools and moved to the encapsulation plant where the fuel is inserted in copper canisters with iron inserts. After encapsulation, the canisters are transported to the final repository and then located in the deposition hole. About 6000 copper canisters will be deposited, with an average of one canister per day.

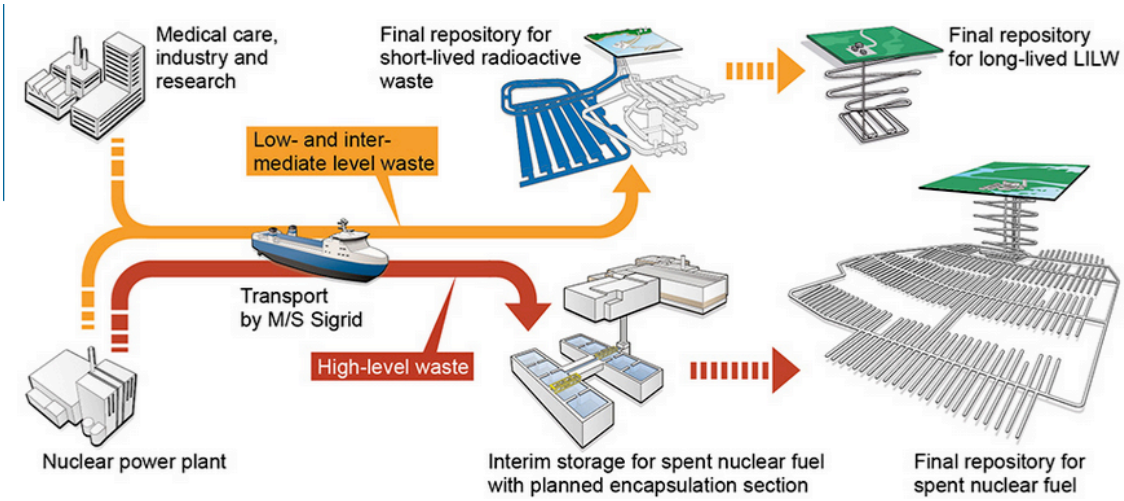

Figure 1: The Swedish system

Repositories present several new challenges for international Safeguards. One of them is maintaining the Continuity of Knowledge (CoK) from the encapsulation plant to the final repository.
The International Atomic Energy Agency and EURATOM safeguards approaches propose to use canisters identification during transport and deposition from the encapsulation plant to the final repository. SKB has to date not presented any method for labelling the copper canisters. An engraving or marking of the canister may impede the long term safety and integrity of the canister since it may reduce the corrosion barrier [1]. Therefore alternative solutions should be developed. Next paragraphs illustrate a possible identification method based on ultrasounds developed by the SILab, Seals and Identification Laboratory, of the Joint Research Centre of the European Commission in Ispra (VA). The first part of the research deals with studies oriented to identify the best positioning of holes or chamfers to be read by a specific transducer. Afterwards a series of simulations and experimental tests have been implemented on copper samples and slices of the copper canister (copper flanges) with the aim to demonstrate the possibility of identification of canisters by ultrasounds. In the end, the identification method is validated on a small scaled copper lid with chamfers investigated by an ultrasonic reading system prototype.

2. The identification method

Since many years, SILab develops ultrasonic identification techniques on bolt seals with artificial cavities made on stainless steel washers, giving a fingerprint from the reflection of unique patterns. In the case of copper canisters, the geometry and dimension of the lid are much bigger than seals, therefore an adaption of the ultrasonic method is required. In particular, the solution proposed in this paper deals with the identification of copper canisters by the ultrasonic investigation of a series of Flat Bottom Holes (FBHs) or chamfers milled on the inner surface of the lid where the copper thickness is higher than 50 mm, as shown in Figure 2. Because of corrosion reasons, in fact, the minimum copper thickness must be not less than 50 mm and the machining of holes or chamfers must not affect the integrity and the stability of canisters.

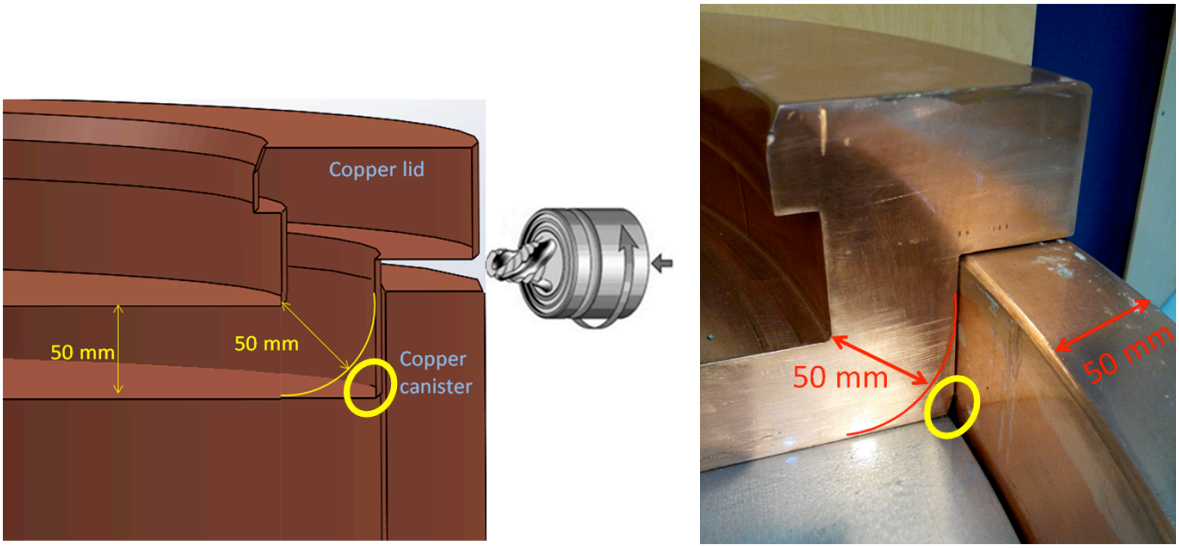

Figure 2: Area (circled in yellow) where the thickness of the lid is higher than 50 mm

The study of the best dimension and position of holes is realized by 3D simulations and experimental measurements carried out on copper samples. The first idea was to drill configurations of FBHs with different positions and dimensions on the bottom surface of copper lids as shown in Figure 2, on the left. The ultrasonic reading of these cavities was designed to be accomplished by a single probe located on the top of the lid, rotating 360° along with the lid circumference. Before machining FBHs in copper flanges, ultrasonic tests were carried out on cylindrical copper samples with different FBHs. The analysis of results revealed the possibility to acquire echoes, however, depending on the inspection frequency, the attenuation of ultrasound in copper could affect measurements negatively and then a different configuration of holes was studied [2]. In order to decrease the distance between cavities and probe, FBHs are replaced by inclined flat holes or chamfers arranged as illustrated in Figure 3, on the right.

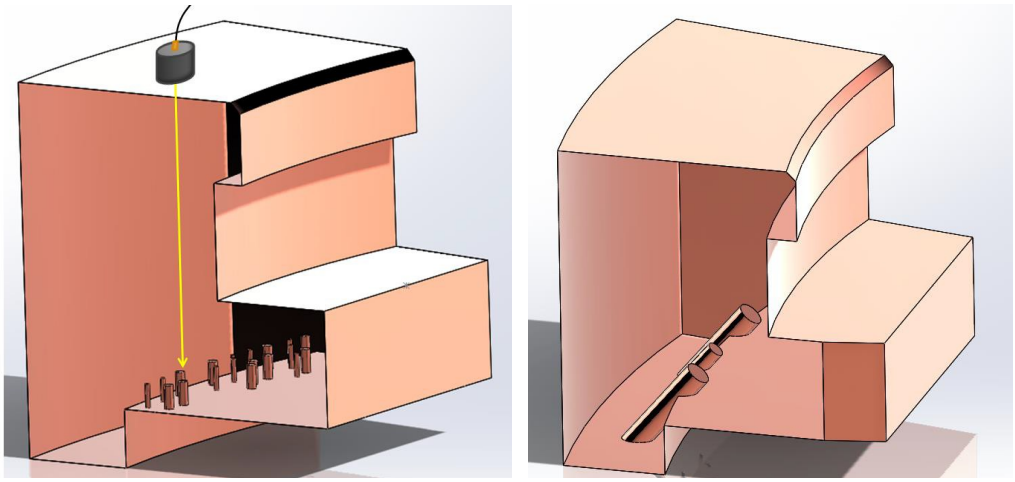

Figure 3: Two possible types of identification cavities: FBHs (left), inclined flat holes (right)

This new disposition of holes involves the repositioning of the transducer as shown in Figure 4. In fact the probe must be inclined according to the Snell's Law in order to guarantee the perpendicularity between the ultrasonic beam and reflectors. Considering the velocities of sound in water (V1=1500 m/s) and in copper (V2=4651 m/s), the probe angle should be around 14° assuming that the inclination of the chamfer is 50°.

$$\sin(\alpha 1)/V1=\sin(\alpha 2)/V2 \rightarrow \alpha 1=\sin^{-1}(1500/4651)\cdot\sin(50)=14.3° \quad (1)$$

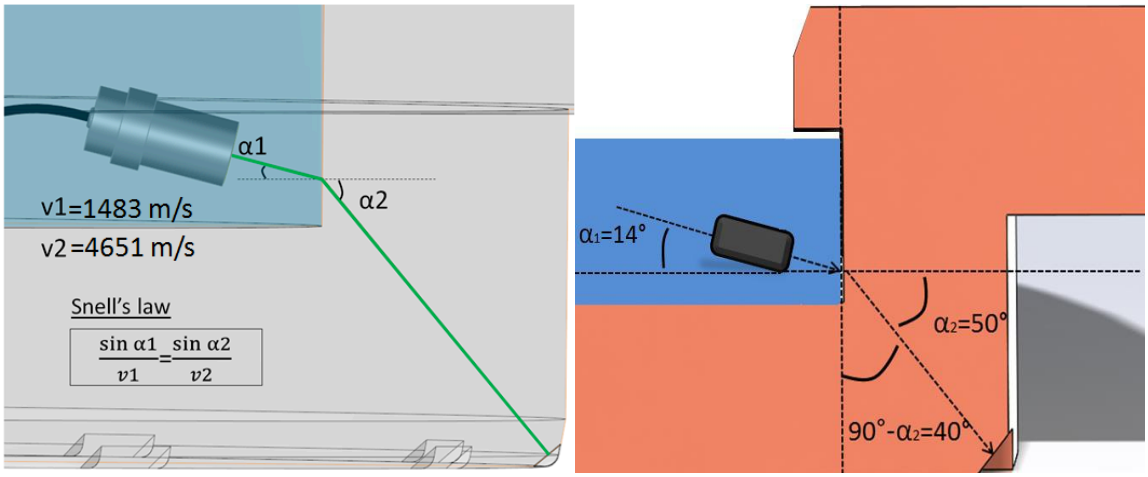

Figure 4: Position of the transducer according to the Snell's law

Depending on the configuration of chamfers around the lid circumference, different ultrasonic amplitude responses will be received by the transducer. Therefore, each canister can be identified by a unique code of chamfers readable by ultrasounds.

The implementation of this identification method will contribute to keep the CoK of copper canisters with nuclear spent fuel. However identification might not be sufficient to prevent attempts of falsification or duplication of canisters then another approach is necessary to ensure the originality of each container. For this purpose, authors developed an authentication method based on ultrasounds but the content will be not discussed in this paper.

3. Simulations and experimental tests

Several experimental tests were carried out on copper flanges with the aim to verify the possibility of detection of flat bottom holes 50° inclined [3]. The inclination of holes has been chosen at 50° by authors for tests but it could be changed in case of necessity. The following Figure 5 shows the set-up of measurement for the investigation of an inclined hole (on the left) and the corresponding A-scan signal (on the right).

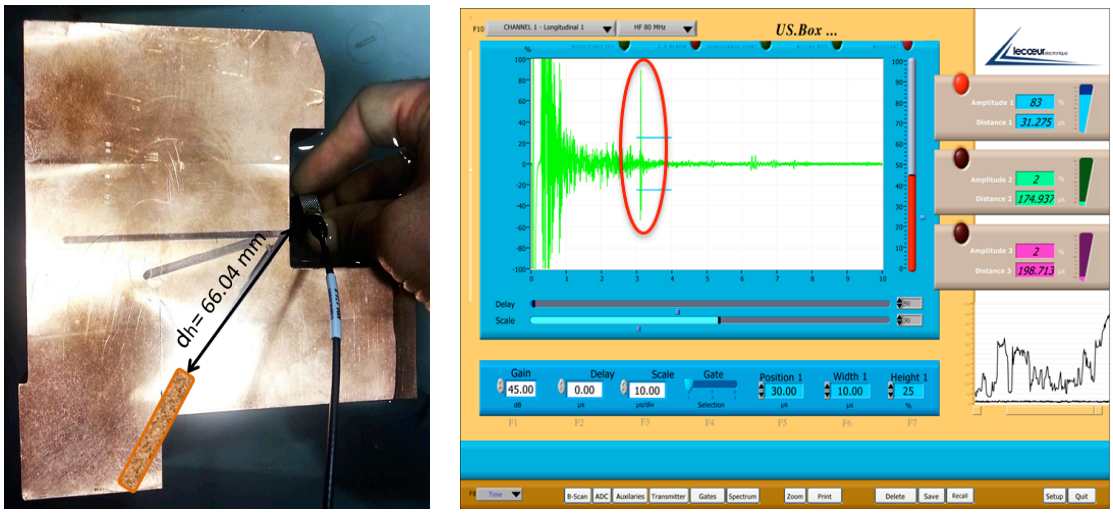

Figure 5: Set-up of the ultrasonic investigation and corresponding A-scan acquisition

Considering that the Time of Flight (TOF) of the echo received is 31.3 μs, the corresponding measured distance is 65.88 mm, value in accordance with the geometrical distance d_h.

As shown from the analysis of measurements, ultrasonic echoes reflected by inclined holes can be detected with a good signal to noise ratio,

Before validating the method on a laboratory prototype, simulations on the CIVA software were implemented to study the best dimensions and positions of chamfers to be machined on the copper lid circumference. The CIVA Ultrasonic Testing (UT) module is specific for ultrasonic NDT and offers two different types of evaluations: the beam computation and the inspection simulation, both useful for our purpose. The set-up simulated (Figure 6) is a 2D profile of the copper lid with a 50° inclined chamfer.

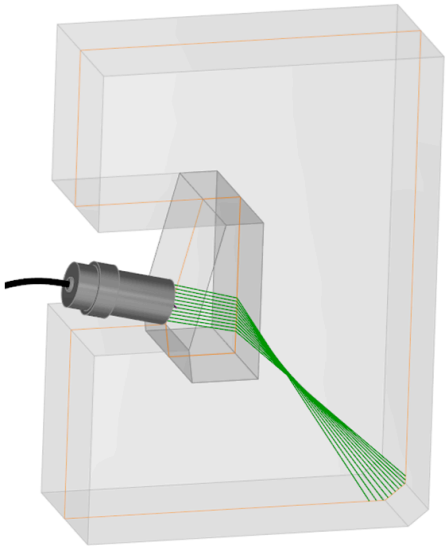

Figure 6: Simulated set-up

The setting of transducer parameters and position is made in accordance with the testing piece geometry. Before simulating the ultrasonic response of the chamfer, the beam computation is realized to appreciate how ultrasounds propagate in the test piece. As illustrated in Figure 7 the probe is not exactly focused in correspondence of the chamfer but the focal spot is located at a depth of about 25 mm from the impact point. However the beam divergence angle is approximately 7° and the focal spot diameter at the chamfer depth is 13.2 mm. As a result, if the chamfer width is too small compared to the focal spot diameter, the echo reflected back will be not revealed by the probe.

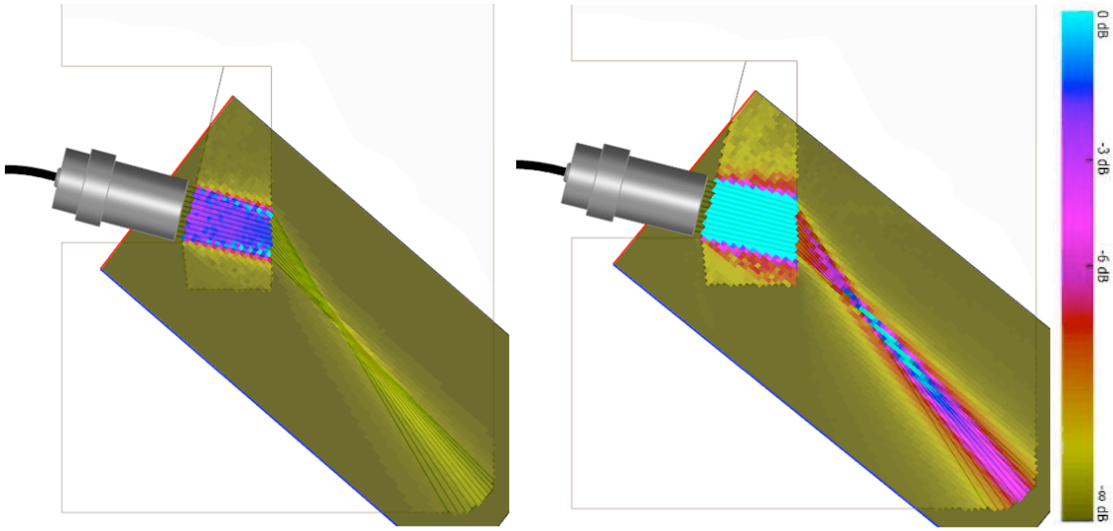

Figure 7: Beam computations for the first simulation set-up. On the left the default beam with 0dB of dynamic, on the right the post processed beam with 15dB of dynamic. Sky blue stands for the highest intensity, yellow for the lowest.

The simulation of the interactions between ultrasonic field and chamfers is implemented by the inspection simulation module. The aim of this study is identifying the best chamfers dimensions in order to do not engrave too much copper. Figure 8 illustrates four chamfers with different widths: 5, 10, 15 and 20 mm respectively. The yellow arc represents the minimum copper thickness of 50 mm to be always kept. As shown, the dimensions of all the chamfers agree with the thickness requirements but smaller they are better it is from the canister integrity point of view.

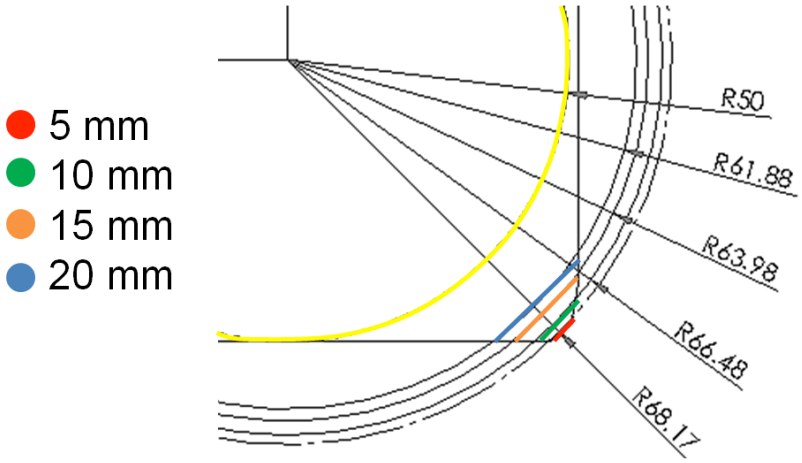

Figure 8: Study of best chamfer dimensions

The results of simulations pointed out the chance to receive good ultrasonic echoes from each one of the chamfers. However the larger the chamfer is, the better signal quality is received. By consequence, a good compromise could be a chamfer around 10 mm wide.

4. Validation on a laboratory prototype

Following the ultrasonic tests on copper samples and CIVA simulations, an identification reading system prototype has been developed. In particular, the validation of the identification method is carried out on a scaled version (¼) of the copper lid where a barcode of cavities and chamfers is realized (Figure 9). The scale is reduced but the geometry of the ultrasonic reading zone is scale 1 compared to the real one meter diameter copper lid.

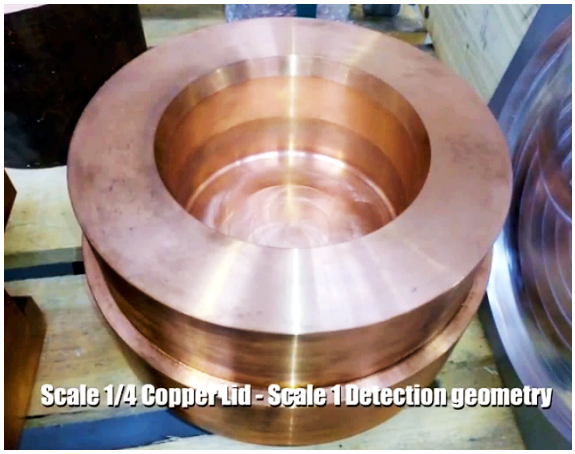

Figure 9: Picture of the small scaled copper lid (¼)

The chamfers, 50° inclined and 12 mm wide, are arranged around the small lid circumference 22.5° angle spaced (Figure 10). The binary code is created by an alternation of chamfers and cavities, which reflect the ultrasonic beam in different ways. The transducer, rotating around the circumference of the lid, will receive an echo in correspondence of chamfers only.

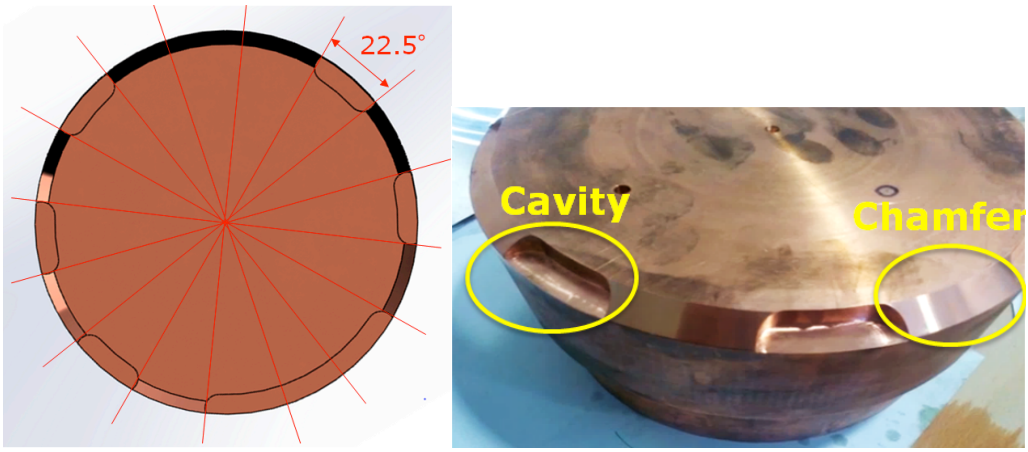

Figure 10: Chamfers arranged around the circumference of the prototype lid

The reading system prototype that hosts the probe is realized by a modified version of reading head used for seals verification (Figure 11). The transducer is installed 14° inclined in order to receive the signal reflected by chamfers according to the Snell's law. The ultrasonic reading of chamfers is realized by an immersion testing and then a bit of water is poured inside the lid. The signal acquired by a 360° rotation of the transducer represents the code realized by chamfers and cavities. As shown in Figure 10, on the right, the ultrasonic amplitude response reproduces a binary code depending on the chamfers position around the lid.

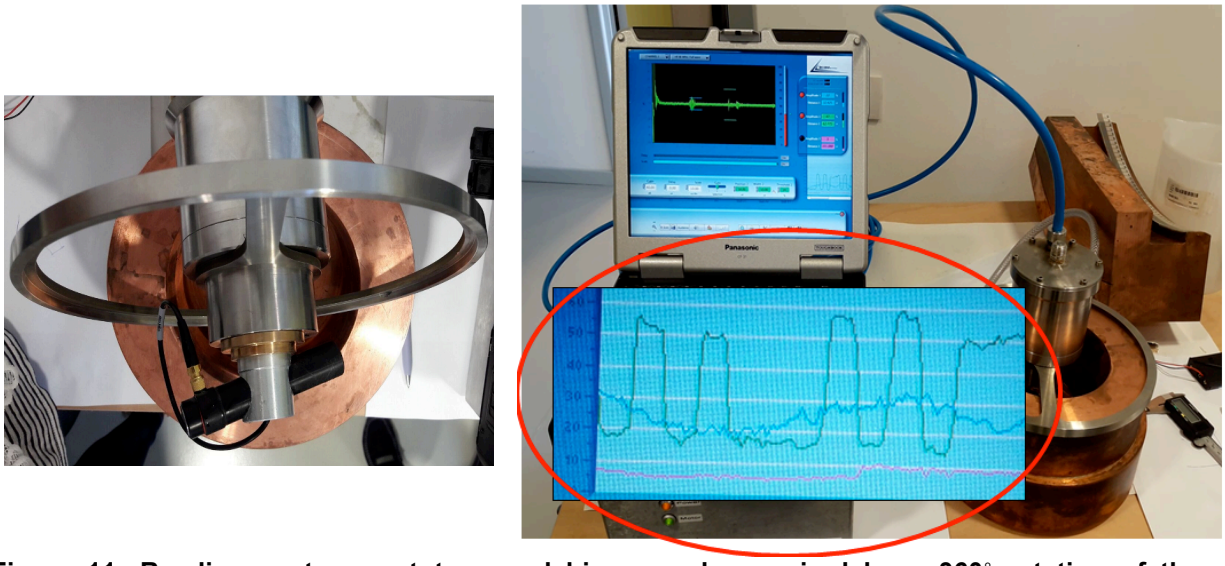

Figure 11: Reading system prototype and binary code acquired by a 360° rotation of the transducer around the small scaled copper lid

Afterwards the result of the experimental testing is compared to a CIVA simulation, reproducing the same set-up of measurement (Figure 12). The simulated echo is clearly evident in both A-scan and B-scan modes and the simulated amplitude ultrasonic response agrees with the experiments. As a result, we can state that the identification method is validated on this small scaled copper lid, which means that each future copper canister could have a different binary code made of chamfers.

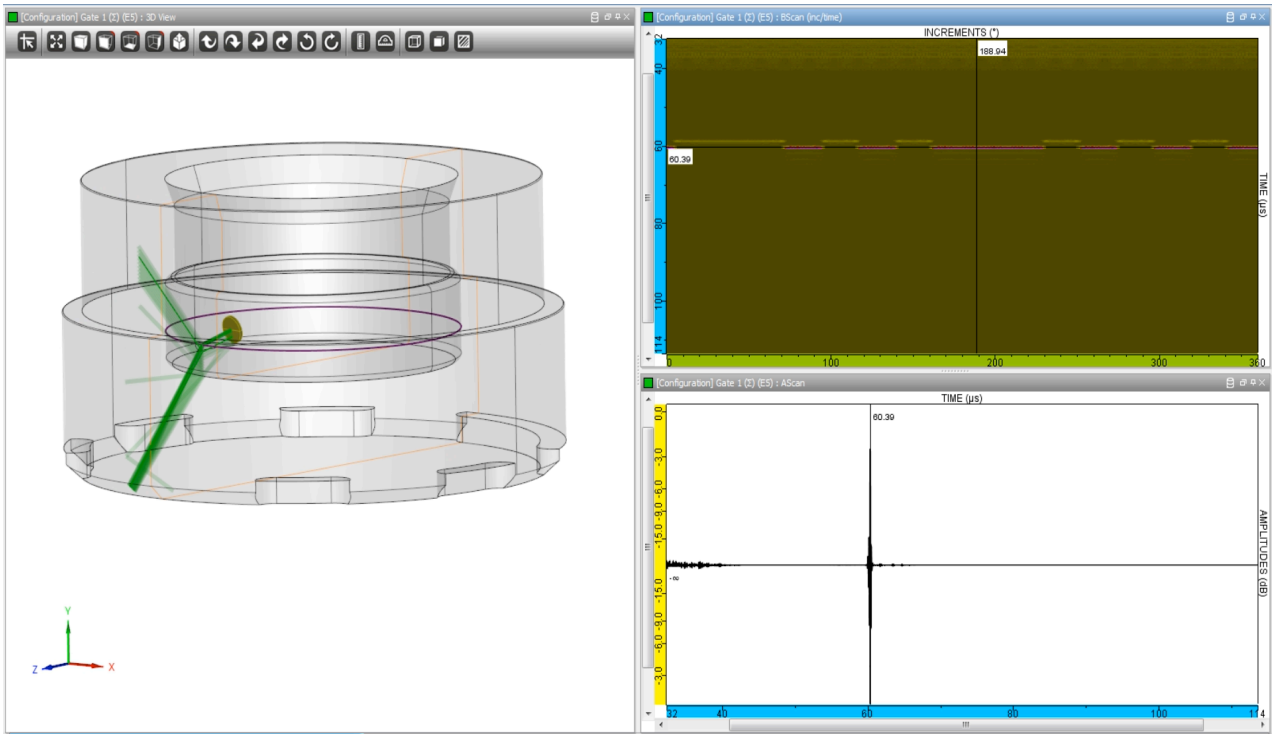

Figure 12: CIVA simulation of the ultrasonic investigation of the small scaled copper lid with chamfers and cavities

As a result from simulations and measurements on scaled copper lid, we can state that the identification method proposed is validated. This positive result paves the way for a future identification of all copper canisters which will be easy, cheap and reliable. When manufacturing the lid, it will be enough to mill or turn a few additional chamfers to deliver on each lid a different binary code, This code could be read at the Encapsulation Plant when the canisters is welded and then on arrival in the Geological Repository.

5. References

[1] Hildingsson L., Andersson C., *Safeguards aspects Regarding a Geological Repository in Sweden*; Swedish Radiation Safety Authority; Stockholm, Sweden.

[2] Capineri L., *Seal fingerprint acquisition device*, Final Technical Report Task 1, Contract JRC/IPR/2015/E.8/0051/NC, February 2016.

[3] Clementi C., Calzolai M., Capineri L., Littmann F., *Ultrasonic identification of copper canisters to be used for long term geological repository*, IEEE International Ultrasonics Symposium 2016, DOI: 10.1109/ULTSYM.2016.7728561, Tours, France, September 2016.

Management of Damaged Spent Fuel

A. Jussofie[1], M. Kaplik[1], A. Bannani[1], W. Cebula[1], K. van Bevern[2], W. Geißler[3]

[1]Gesellschaft für Nuklear-Service mbH, Frohnhauser Str. 67, 45127 Essen, Germany
[2]VGB PowerTech e. V., Deilbachtal 173, 45257 Essen, Germany
[3]RWE Power AG, Kraftwerk Biblis, 68647 Biblis, Germany

Abstract:

During the operation of German nuclear power plants there are damaged fuel rods (DFR) that had been removed from spent fuel assemblies due to their special condition. DFR can consist of various types, such as leak-tight e. g. deformed fuel rods and leaking fuel rods, from pin hole defects and hairline cracks up to exposed nuclear fuel, e.g. fragments, loose pellets or broken fuel rods and fuel rods in capsules or cartridges. These DFR can not be readily packed into the CASTOR® V-casks deployed for dry interim storage of spent fuel. Therefore, the DFR have to be supplied via a separate path to interim storage in order to achieve the defueled state of shut-down reactors.
This concerns both DFR from boiling and pressurized water reactors (BWR, PWR). A special quiver has been developed by GNS as a technical solution to accommodate DFR in CASTOR® V casks for interim dry storage. After gas-tight sealing by welding, the quiver can be stored in CASTOR® V-casks like spent fuel assemblies. The DFR with uranium or MOX fuel can be combined as desired within the quiver. Likewise, loading configurations with DFR from PWR and BWR are possible. The outer dimensions of the quiver are similar to those of fuel assemblies. Its major components include an inner basket with storing positions for the DFR and an outer base body in order to protect the inner basket especially from external mechanical stresses.
This paper will describe the major components of the quiver, the loading procedure and the further processing that lead to a permanently gas-proof packaging of DFR suitable to be loaded into CASTOR® V-casks. The focus is led on the continuity of knowledge during loading and processing of the quiver. Furthermore, the paper will present the first quiver loading with the aim of achieving a defueled reactor block A of Biblis NPP ahead of time. The quiver system has obtained its transport license.

Keywords: damaged spent fuel; quiver; dry interim storage; continuity of knowledge; Germany

1. Introduction

According to the Atomic Energy Act, nuclear power plants (NPP) in Germany will be operated until 2022 at the latest. At the end about 10.000 Mg heavy metal, representing about 13.000 spent fuel assemblies (SFA) from pressurized water reactors (PWR) and about 17.000 SFA from boiling water reactors (BWR), will have accumulated for dry interim storage in about 1.000 big-sized casks of the CASTOR® V type. The technical design of CASTOR® V-casks must fulfil the following four protection goals:

- Safe enclosure of the radioactive substances
- Safe removal of the decay heat
- Avoidance of unnecessary radiation exposure by shielding of gamma and neutron radiation
- Maintaining the sub-criticality

Designed for transport and storage, CASTOR® V casks have to guarantee these safety requirements not only under normal operating conditions but also under extreme mechanic and thermal accident conditions during storage and transport. Therefore, casks of the CASTOR® V type are suitable to transfer spent fuel assemblies from the NPP to the dry interim storage and to accommodate spent fuel

assemblies safely for several decades. The storage license of the 12 existing on site dry spent fuel storage facilities near the reactor has been granted for 40 years.

During the operation of German NPPs, damages of the cladding of single fuel rods may occur. These damaged fuel rods (DFR) cannot be used for a further cycle in a reactor. They have to be removed from the fuel assemblies and are stored in the spent fuel pools of the reactors. Depending on the extent of the damage, DFR can consist of various types, such as leak-tight e. g. deformed fuel rods and leaking fuel rods. Due to their special conditions, these DFR can not be readily packed into the CASTOR® V-casks. The fuel and the water that may be released by leaking fuel rods into the internal of the cask during the long period of storage may lead to a situation that the protection goals cannot be met any more.

The German phase-out policy has triggered a strong demand for a disposal option for DFRs because this is essential to achieve the defueled state of shut-down reactors as quickly as possible. Therefore the objective was to develop a technical solution that can be realized with CASTOR® V-casks and covers the individual needs of the German NPP operators. These include in particular the

- Disposal option of a broad range of fuel rods such as
  - Irradiated or unirradiated nuclear fuel in the form of fuel rods or fuel rod sections
  - Leak-tight and dry fuel rods with potential damages, e.g. reduced cladding thickness or deformed fuel rods,
  - Leaking fuel rods, with minor pin hole defects and hairline cracks up to exposed nuclear fuel, e.g. fragments, loose pellets, broken fuel rods or debris (cf. Fig. 1),
  - Fuel rods in capsules or cartridges,
  - Test rods from irradiation experiments
  - Fuel in capsules or cartridges

- Disposal of DFR by means of the already approved and licensed transport and storage casks of CASTOR® V/19 and CASTOR® V/52 type (96er-type)

As a technical solution, a quiver for damaged fuel rods suitable to be loaded into CASTOR® V-casks has been developed thus enabling to include the damaged fuel rods in the ordinary disposal route for SFAs. This paper presents the major components of the quiver, the loading procedure and the further processing under the aspect of the continuity of knowledge. Furthermore, the paper shows the first quiver loading with the aim of achieving a defueled reactor block A of Biblis NPP ahead of time.

2. Design of the Quiver for DFR

The design of the quiver for DFR is based on the requirement that the quiver has to fit into the standard fuel basket of CASTOR® V-casks. This requires a quiver with similar dimensions to those of a fuel assembly and an excellent mechanical robustness suitable to cope with mechanical loads during accident conditions of transport. Therefore the quiver for DFR consists of a forged monolithic base body in order to make the quiver resistant against mechanical loads. The base body is equipped with a head and a foot piece whereby the appearance of the quiver becomes more similar to that of a fuel assembly. The function of the basket inside the base body is to be loadable with a broad range of fuel rods, to enclose them safely and to hold them at a clearly defined distance. Differences in the diameter of the tubes have been defined according to the geometry and number of individual fuel rods that have to be disposed of. In particular, the tubes with the larger diameter allow to include deformed fuel rods. With respect to the achievement of the protections goals, the leaktightness of the quiver is crucial. For this purpose the quiver is equipped with a lid that can be bolted and welded as well. As a result the residual water and fuel inside the quiver is prevented from being released into the internal of the cask. Welding the lid has the advantage that the monitoring of the leaktightness can be omitted. Bolting the lid enables the filling of the quiver with further fuel rods. Regarding the aspect of Safeguards, it is to be noted that the inventory of the quiver is more resistant to manipulation than a fuel assembly as soon as the quiver has been welded, since it is more difficult to break open a welding seam than to screw off the head of fuel assemblies. From the view of the operator, the quiver should be regarded as an item as is the case for SFAs.

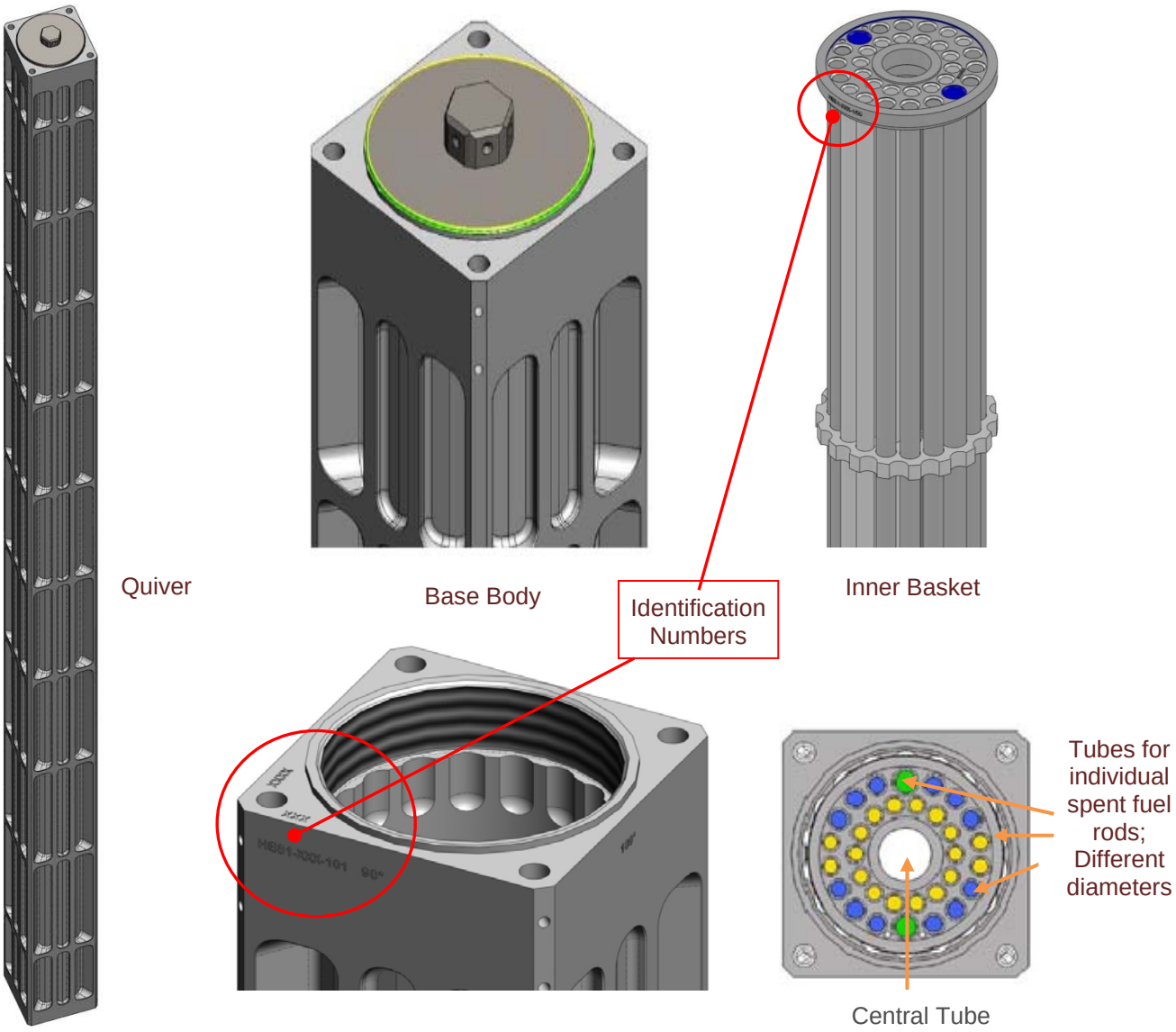

Fig. 1: Design of the quiver for damaged fuel rods

.

3. Handling of the Quiver for DFR

The handling of the quiver takes place on two levels, the spent fuel pool, where the quiver is loaded with individual fuel rods, and the reactor floor, where the further handling process of the quiver takes place (Fig. 2). The quiver has to be shielded when being transferred between the two levels and passing through the handling steps on the reactor floor in order to reduce the dose rate and to avoid unnecessary radiation exposure of the staff. At the beginning of the loading process, the quiver is placed into a primary shielding basket, which is in the loading station in the spent fuel pool. After completion of the loading, the shielding basket is closed by means of a head shielding and transferred from the spent fuel pool to the secondary shielding block of the dry handling station. Here the quiver passes through three processing steps: dewatering, drying and welding. After dewatering by means of a dewatering lance through the head shielding, a gas box is mounted on top of the secondary shielding block for the two further steps. The vacuum drying is necessary in order to limit the residual water in the quiver. Therefore, a substantial evaporation of water from the leaking fuel rods has to be ensured. For this purpose the quiver for DFR possesses a central tube that allows the water vapour to

escape from the leaking fuel rods to the exhaust system of the building. Then the quiver is filled with inert gas and closed with a lid that is bolted and then welded.

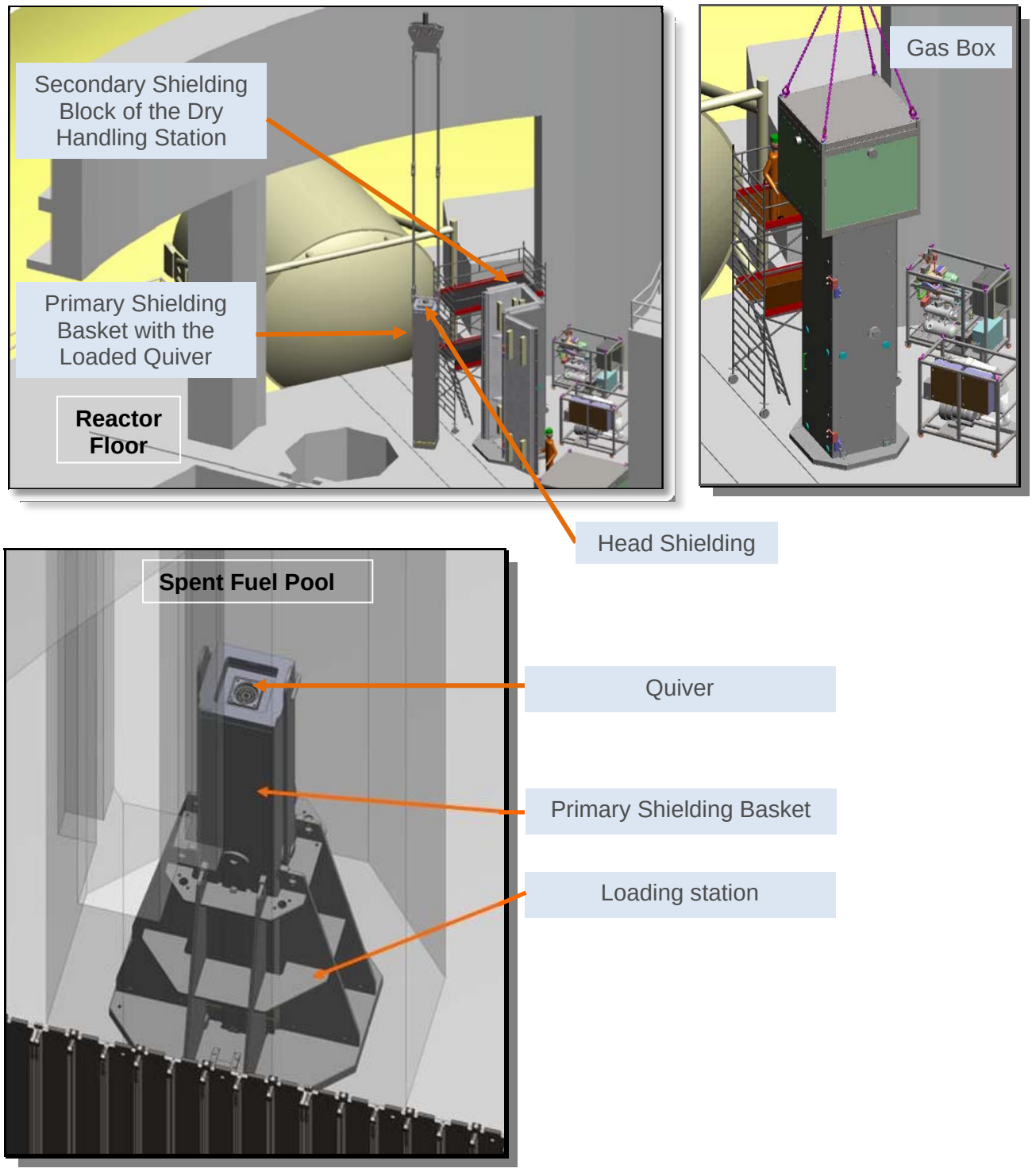

Fig. 2: Handling equipment for the quiver for damaged fuel rods on two levels

Afterwards the handled quiver inside the primary shielding basket is returned to the loading station, taken out of the shielding basket and placed in the fuel assembly storage rack, where it is stored until loading into a CASTOR® V-cask.

Regarding the Safeguards-aspect, it is to be noted that all process steps in the gas box are remotely handled and carried out under video surveillance. After welding the unloading of the quiver is no longer possible with simple means. Therefore, the inventory of welded quivers is also safely enclosed in terms of continuity of knowledge; from the operator's point of view the welded quiver can be regarded as an item to be verified by means of its unique identification number.

3.1 Traceability of the Quiver for DFR during the Handling Process

Base bodies, head pieces, internal baskets and the bolt-on and weldable lids are equipped with a unique identification number. The identity numbers are positioned in a way that they are clearly visible from above and from the side. Due to the side positioning of the identification number at the base body, a clear traceability of the loaded quiver is ensured throughout the entire handling process in the NPP.

4. Experience from the first Loading of the Quiver for DFR

The first hot loading of three quivers was executed in the NPP Biblis reactor block A in July 2016. The three quivers were loaded together with the latest three fuel assemblies into a CASTOR® V- cask. With the transport of this cask in November 2016 from reactor block A to reactor block B, the defueled status of block A was achieved. In block B the CASTOR® V- cask was unloaded. The quivers had not been filled completely and had only been bolted (not welded) so that further damaged fuel rods were added. Since the quivers then contained their intended inventory, they were ready for verification by the two inspectorates.

Fig. 3: Site of the nuclear power plant Biblis

The verification approach that was chosen by the inspectorates was the Digital Cherenkov Viewing Device (DCVD) method. The applicability of this method to quivers for individual fuel rods was tested for the first time on 5th April 2017. The application of the DCVD-method to a quiver turned out to be more difficult compared to a fuel assembly because the measurement of the Cherenkov radiation was limited to the water inside the central tube of the quiver. Altogether, the results were evaluated as satisfactory by the two inspectorates on-site: It could be clearly proven that fuel is inside the quiver. Furthermore, individual fuel rods were clearly visible. However, it remains to be seen whether results obtained with the DCVD method will correspond to the information value EURATOM and IAEA expect.

Session 07

Non-destructive Analysis: Neutron I

Advanced Neutron Detection Technology Rodeo

Anthony Belian[1], Arden Dougan[1], Anagha Iyengar[2], David Chichester[3], Shaun Clark[4], Stephen Croft[2], Dan Decman[5], William Geist[6], Paul Hausladen[2], Jianwei Hu[2], Robert McElroy[2], Howard Menlove[6], Jason Newby[2], Sara Pozzi[4], Manoj Prasad[5], Jeff Sanders[3], Tony Shin[4], Scott Thompson[3], and Jerome Verbeke[5]

[1]US Department of Energy / NNSA; [2]Oak Ridge National Laboratory; [3]Idaho National Laboratory; [4]University of Michigan; [5]Lawrence Livermore National Laboratory; [6]Los Alamos National Laboratory

Abstract:

The U.S. Department of Energy's Office of Nonproliferation and Arms Control sponsored different groups to design and simulate an instrument to measure fresh low enriched uranium fuel assemblies. The goal is to be less sensitive to the presence of burnable poisons relative to the current instrument in use – the Uranium Neutron Collar for LWR fuel (UNCL). Each group's chosen sensor is Commercial Off the Shelf but has been under development in recent years. The candidate technologies are: pulse shape discrimination plastic scintillators, corrugated boron straw detectors, high pressure helium-4 scintillators, boron-10 neutron plate detectors, stilbene scintillators, and liquid scintillators. Each group was provided a set of fresh fuel definitions in MCNP to calculate their detector's performance. In addition, they were judged on other criteria such as size, portability, safety, robustness, and cost. This paper will discuss the details of each design and its performance relative to the standard UNCL in use today.

Keywords: fast neutron, fresh fuel assay, burnable poisons, UNCL, MCNP simulation

1. Introduction

The objective of the Advanced Neutron Detection Technology Rodeo, henceforth simply referred to as the Rodeo, was to explore newly developed neutron detection materials to understand if they provide a benefit over existing technology in the area of nondestructive assay (NDA) of fresh fuel. The current methodology in use by the International Atomic Energy Agency (IAEA) for quantifying fresh fuel assemblies is active coincidence counting utilizing the Uranium Neutron Collar for Light water reactor fuel (UNCL) [1]. The UNCL is a thermal neutron detector based on Helium-3 (^{3}He) gas proportional counters embedded in polyethylene. The UNCL consists of 18 ^{3}He tubes at 4 atmospheres which amounts to ~6 liters of ^{3}He gas. Three neutron detection slabs surround a central cavity that will contain a fuel assembly during the measurement. The fourth side of the cavity is a polyethylene slab with a cavity to accommodate a removable americium-lithium (AmLi) neutron interrogation source. In addition to a measurement of the ambient background that gets subtracted from every measurement, the typical assay sequence consists of two measurements with a fuel assembly in place: a passive measurement without the AmLi source present to measure the neutron count rates from the spontaneous fission of ^{238}U, and an active measurement with the AmLi source in place to measure the count rates from the induced fission of ^{235}U plus the spontaneous fission of ^{238}U. The difference between the active and passive count rates is proportional to the ^{235}U linear density (g/cm). The use of a shift-register to analyze the neutron pulse stream from all the ^{3}He tubes allows for the determination of the real coincidence rate – the number of time-correlated neutrons that emanate from the fuel assembly per unit time. The only measureable source of time correlated neutrons in such a system is fission, thus the net coincidence rate (Doubles rate) is a function of the induced fission rate which is, in-turn, related to the ^{235}U linear density in the fuel.

The UNCL, shown in Figure 1, has two operational modes – thermal and fast. In the Thermal Mode, neutrons that are moderated in the polyethylene body of the UNCL are free to interact with the fuel assembly. Since ^{235}U has a much higher fission cross section for thermal neutrons relative to epi-thermal or fast neutrons, as seen in Figure 2, the count rates are dominated by fission induced by thermal neutrons. In the Fast Mode, the user places sheets of Cadmium (Cd) around the central cavity. The effect is that most of the neutrons that are below ~0.5 eV in energy are not able to pass into the fuel cavity and so the fuel assembly is interrogated with predominantly epi-thermal and fast neutrons. Due to the reduced interrogation neutron population and the lower ^{235}U fission cross section for higher-energy neutrons, the induced fission rate is reduced in the Fast Mode compared to the Thermal Mode. However, the count rate is dominated by uncorrelated neutrons from the AmLi source, therefore, to achieve the same Doubles precision the inspector is required to measure longer in the Fast Mode relative to the Thermal Mode. In practice, a Thermal Mode assay total measurement time is around 15 minutes whereas a Fast Mode assay will require a few hours or more to reach the same measurement precision. There are two commercially available designs for the UNCL – Type I and Type II. For the Type I UNCL (Figure 1) the fuel cavity size is adjustable by moving the two side slabs. In the configuration shown in Figure 1 PWR fuel is depicted, but can be changed to measure smaller fuel assembly types like BWR and VVER440. The Type II models have fixed geometries so can only accommodate either PWR or BWR/VVER440 fuel depending on which configuration is purchased. The Type II models have higher efficiency because of the addition of two ^{3}He tubes in the PWR case and closer coupling of the fuel to the detectors in the BWR case.

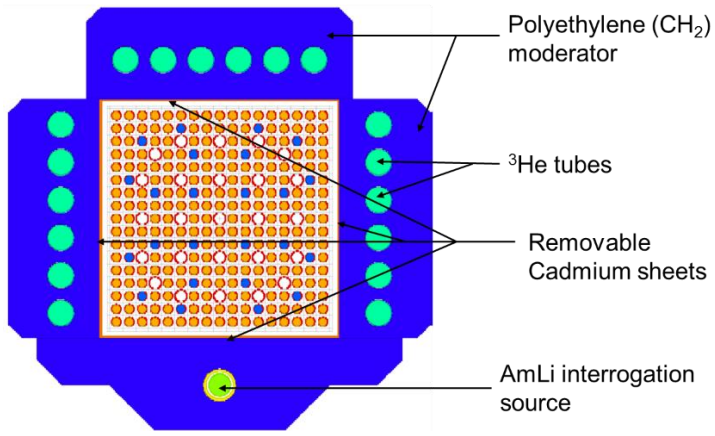

Figure 1: Cut-away view of the UNCL with a 17x17 PWR fuel assembly.

Some modern fuel designs with higher ^{235}U enrichments (> ~2.5%) require the addition of a neutron poison in order to keep the assembly reactivity below acceptable limits. The typical poison utilized is Gadolinium (Gd). The blue fuel pins in Figure 1 represent poisoned fuel. As the fuel assembly is "burned" in the reactor the Gd inventory is continuously reduced because of its very high thermal neutron cross section as seen in Figure 2 in green. This is roughly two orders of magnitude larger than the ^{235}U fission cross section (Figure 2 in red). The presence of the burnable poisons negatively impacts the assay of fresh fuel by removing neutrons that could otherwise induce fission or be detected. Thus, two fuel assemblies with the same ^{235}U loading but one containing burnable poison pins will return different count rates and would therefore be interpreted as having two different ^{235}U inventories. One of the approaches to reduce the influence of burnable poisons on the measured count rates is interrogating the fuel with neutrons that are minimally affected by the presence of the Gd – fast neutrons. There are many poisoned fuel designs that range in the concentration of Gd per pin but also in the number of poisoned pins in an assembly, anywhere from 4 to 24.

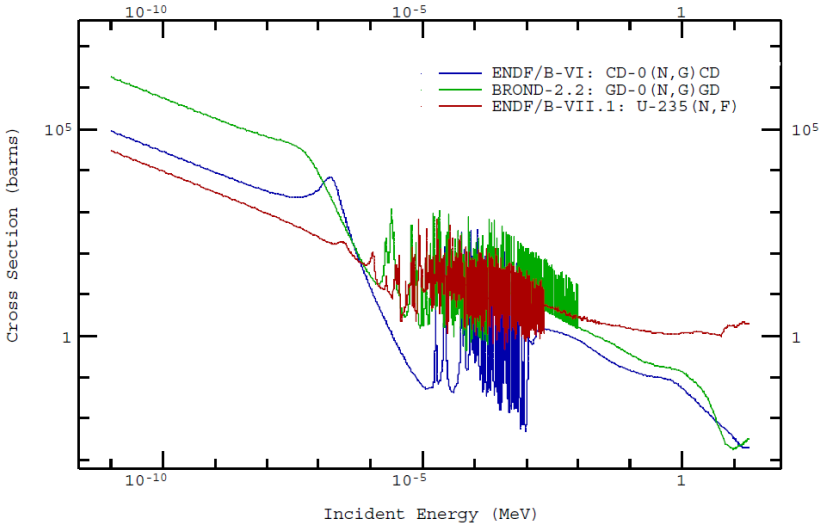

Figure 2: Neutron cross sections for Gadolinium capture, Cadmium capture, and ^{235}U fission.

By placing the Cadmium sheets, as indicated in Figure 1, and due to the existence of the large capture resonance for Cadmium at ~0.2 eV, as seen in Figure 2 in blue, most neutrons with energies < 0.5 eV are effectively prevented from passing through and interacting with the fuel. In this way the effect of the neutron poison is reduced but not entirely mitigated since Gd isotopes have many large resonances at energies above the Cadmium cut off. Creating a separate calibration for poisoned fuel is not an option since the Gd concentration per pin as well as the number and positions of poisoned pins in an assembly vary widely throughout the industry. The effect is a reduction in the Doubles rates that range from a few percent (Fast Mode, 4 poisoned pins with 6% Gd) to upwards of 35% (Thermal Mode, 24 poisoned pins with 10% Gd) for poisoned fuel compared to unpoisoned fuel with the same ^{235}U loading.

The current method most often utilized for assay of poisoned fuel is to use a multiplicative correction to the measured Doubles rate to compensate for the reduction due to burnable poisons. This correction factor requires knowledge of the concentration (in %) of Gd per fuel pin and the number of poison pins in the assembly. Since poisoned pins are identical in appearance to unpoisoned pins there is no way for the inspector to differentiate by visual inspection and must rely on the operator's declaration. The assay result is then no longer fully independent. The inspector could opt to perform the assay in the Fast Mode configuration but time constraints usually dictate that this is rarely done. In addition, there is still an effect of the poison even in the Fast Mode, and although it is smaller in magnitude it still needs to be corrected using the operator's declared information. There is a technique that utilizes the ratio of the Doubles rates from both a Fast Mode and Thermal Mode measurement [1] of a poisoned fuel assembly that can verify the operator's declaration of burnable poisons or directly estimate the multiplicative correction to the Doubles rate – this is, of course, typically not done because of time constraints.

Given these limitations of the current technology, the Rodeo sought to investigate detector technologies that could improve on the UNCL performance for poisoned fuel. The physics of the technique limits where improvements can be realized, such as control of the interrogating neutron flux and/or improved measurement time in the Fast Mode. Examination of the neutron cross sections plotted in Figure 2 shows that the Gd capture probability falls off rapidly at energies above the resonance region but the ^{235}U fission cross section is roughly constant. Therefore, a significant reduction in the sensitivity to burnable poisons can be realized if the moderation of neutrons in the area of the fuel is minimized. Improvements in neutron detection efficiency and/or coupling of unmoderated or slightly moderated interrogation source neutrons to the fuel can lower the measurement time in Fast Mode. Improvements to the precision of the Doubles rate such as being insensitive to neutrons from the AmLi interrogation source and/or being able to shorten the

coincidence gate width, which reduces the accidental coincidence rate, will also lower the needed count time in Fast Mode.

1.1. Rodeo Methodology

One of the challenges when evaluating disparate technologies is devising a testing plan that is fair and unbiased to all participants. For this Rodeo it was decided that the testing and comparison of the technologies would be done via Monte Carlo simulation of fresh fuel assemblies. Furthermore, that the fuel assembly definitions and models would be developed by someone not participating in the Rodeo.

The basic ground rules of the Rodeo were: each group design a UNCL-like instrument with their detector material with roughly the same form-factor and concept of use; the Monte Carlo simulation tool would be MCNP [2]; the interrogation source simulated was a 50,000 n/s AmLi source with a given (Obninsk) energy spectrum [3]; other neutron interrogation sources were allowed but a full set of simulations were required with the AmLi; the simulation of the detector response was done in both Fast and Thermal Mode.

Each group were given several sets of Pressurized Water Reactor (PWR) fuel assembly definitions to evaluate their detector model.

1. A set of 17x17 assemblies with 264 fuel pins and 25 guide tubes with ^{235}U linear densities (LD) of 15, 20, 25, 35, 45, 55, 60, and 65 g/cm. These were used to generate calibrations (Doubles rate vs. ^{235}U g/cm) in both the Fast and Thermal Mode.
    a. Fuel dimensions:
        i. Assembly width = 21.4 cm
        ii. Fuel pin pitch = 1.278 cm
        iii. Pellet density = 10.41 g/cm^3
        iv. Pellet diameter = 0.8255 cm
        v. Zircalloy cladding
2. A set of unpoisoned 14x14, 15x15, 16x16, and 17x17 fuel assemblies with various differences in fuel parameters such as: fuel pin pitch, numbers and locations of guide tubes, cladding thickness, fuel pellet diameter and density, and overall enrichment.
3. A set of 17x17 fuel assemblies with partial defects – where some normal Low Enriched Uranium (LEU) fuel pins have been substituted with Depleted Uranium (DU) fuel pins. The number of substituted pins simulated were: 8, 16, 24, 32, and 40
4. A set of 17x17 fuel assemblies containing burnable poisons in the form of Gd-oxide. Concentrations of Gd per pin were 6%, 8%, and 10% and the number of poisoned pins per assembly were 4, 8, 12, 16, 20, and 24.

The groups were asked to use the calibration assemblies (set #1 above) to determine coefficients for both Fast and Thermal Mode calibrations. These calibrations would then be used to calculate the “assayed” linear density of the fuel assemblies in sets 2, 3, and 4. The assayed linear densities for the fuel would then be compared to the known linear densities to calculate the mass difference, or mass defect. This comparison would highlight the sensitivity of the modeled detector to the given perturbation. It is these mass defects that will be compared across all of the different detector materials.

An estimate of the counting statistics on net count rates was also requested by simulating both passive and active assays. The passive assay counting statistics were determined assuming a 300 second measurement while the active statistics were calculated at 600 and 1800 seconds. These were done using the 55 g/cm 17x17 calibration assembly.

Finally, in order to have a baseline to compare the various detector designs to, the standard ^{3}He based UNCL was also simulated using the same sets of PWR fuel assemblies. The following teams and a short description of the materials tested are shown in Table 1. Each of these materials on its own is interesting enough to report on, however, that is not the purpose of this paper. Therefore, only

introductory information on each detector will be given and the reader is encouraged to find more in-depth information in the references provided in Table 1.

Group	Detector material
ORNL1	EJ-299 – Pulse Shape Discrimination (PSD) plastic is a bulk scintillator that has excellent discrimination properties between gamma rays and neutrons; fast-neutron detection mechanism via proton-recoil and scintillation coupled to photomultiplier tubes; crosstalk correction based on particle velocity [4][5]
ORNL2	Boron-coated straws – ^{10}B-lined cylindrical proportional counters that are cost effective, simple to make, and offer higher efficiency per tube compared to ^{3}He; low gamma ray sensitivity; thermal neutron detection, no detector-to-detector crosstalk [6][7][8]
LANL	Boron parallel-plates – ^{10}B lined plate layout with high detection efficiency per unit surface area; polyethylene sheets between plate detectors allow for neutron energy information; thermal neutron detection, no detector-to-detector crosstalk [9][10][11]
INL	^{4}He scintillators – high pressure ^{4}He has a high intrinsic fast neutron efficiency; low gamma sensitivity; low sensitivity to AmLi neutrons; least moderating design of those tested; fast-neutron detection mechanism via ^{4}He-recoil and scintillation coupled to photomultiplier tubes or SiPMs [12][13][14]
LLNL	Stilbene scintillators – solid organic scintillators with high sensitivity to fast neutrons; excellent neutron and gamma ray Pulse Shape Discrimination; can operate at low PSD threshold (~60 keVee); innovative model for correcting crosstalk [15][16][17]
UM	EJ309 – liquid scintillator; high flash point; non-toxic; excellent PSD properties, can operate at low PSD threshold (~50 keVee) [18][19][20]

Table 1. Summary of the groups and the detector materials simulated.

As seen in Table 1 there are a mix of thermal neutron detectors and fast neutron detectors. There are advantages and disadvantages of each type. For example, thermal neutron detectors typically have a higher intrinsic efficiency, are insensitive to gamma radiation from fresh fuel, and do not suffer from crosstalk since the neutron is absorbed as a result of the detection process. However, the process of thermalizing the neutrons for detection leaves the technique vulnerable to biases from burnable poisons. Additionally, thermal neutron detectors are also sensitive to neutrons from the interrogating AmLi neutron source which greatly impacts the precision of the measured Doubles rate. Fast neutron detectors are typically threshold detectors that are largely, but not completely, insensitive to the lower average neutron energy of AmLi. Due to the fact that neutrons from events of interest (fission) are born fast there is no need for moderation which greatly reduces the sensitivity to burnable poisons. The time window needed to observe truly coincident neutrons is orders of magnitude shorter for fast detectors relative to thermal detectors so that accidental coincidences are rare at the count rates observed with this type of measurement and improves Doubles rate precision and assay time. However, because the fast detection mechanism is neutron scattering there is some crosstalk between detector cells that must be corrected for. Finally, since most fast neutron detectors are bulk scintillators they are sensitive to gamma ray radiation and require either shielding and/or a robust method for discriminating between gammas and neutrons.

Because of the volume of data generated in the Rodeo project and the perceived need in the area of poisoned fresh fuel assay this report will focus only on the results in the Fast Mode. All of the simulated detectors performed at least as well as, and certainly a few of them better than, the standard UNCL in the Thermal Mode. However, in terms of performance, the standard UNCL is perfectly adequate in the Thermal Mode and exceeds the published international safeguards targets for accuracy and precision [21], therefore no performance enhancement need is envisioned at this time in Thermal Mode.

2. Detector materials

2.1. Pulse Shape Discrimination (PSD) plastic (EJ-299)

Recently, Oak Ridge National Laboratory (ORNL) evaluated a set of segmented detectors constructed from commercially available PSD plastic for the purpose of fast-neutron coincidence counting. These detectors were originally built to instrument the focal plane of a fast-neutron imager, but the position and time resolution permitted by segmented detectors enabled separation of fission coincidences from inter-detector scattering using the kinematics of neutron scattering. A photo of one of the PSD plastic cells is shown in Fig 3.

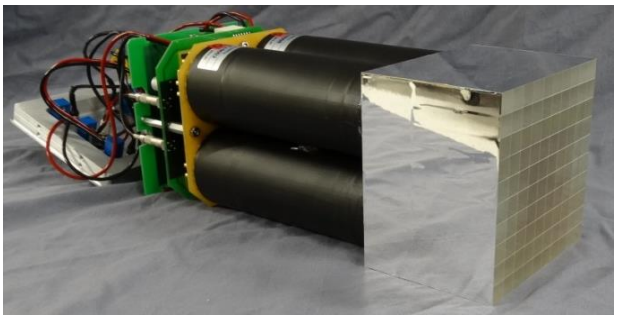

Figure 3. Photograph of a segmented PSD plastic detector module with 4 PMTs.

For the purposes of this simulation study, the philosophy of the notional design for the PSD plastic collar was to echo the present design of the UNCL while using detectors that were representative of the present ORNL segmented PSD plastic detectors. In this way, the study was intended to primarily provide information regarding the safeguards utility of fast proton-recoil scintillator, segmented detectors, and the ability to identify and compensate for inter-detector scattering. For instance, no significant effort was spent adjusting the geometry or constituents of the moderator to modify the interrogating neutron flux or spectrum. As a result, the instrument was modeled as a four-sided system similar to the UNCL with three sides of detectors and one side consisting of a moderated AmLi source identical to that used in the UNCL. In the Fast Mode, the fuel was surrounded by a 1 mm layer of cadmium extending 340 mm along the length of the fuel. Vertically centered about the cadmium liner were 12 PSD plastic volumes, each 12 × 12 cm on a face with a depth of 5 cm arranged in a 2 × 2 array on each of three sides. In each corner, a block of plastic was used as passive shielding to limit multiple scattering of neutrons between adjacent sides. A cross-sectional view of the (right) PSD-plastic collar and the (left) UNCL are shown in Figure 4. Additional inactive volumes, such as light guides, light readout [photomultiplier tubes or silicon photomultipliers (PMTs or SiPMs)], detector housings, and electronics were not included in the simulation.

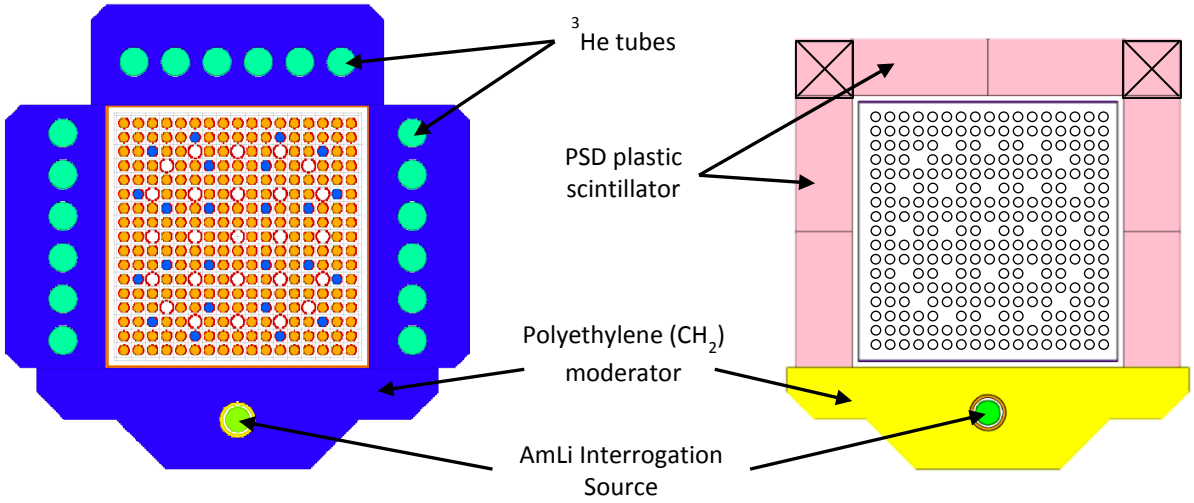

Figure 4. Comparison of the standard UNCL to the collar design with PSD Plastic modules.

Simulations were performed using Monte Carlo N-Particle (MCNP) 6.1.1b coupled with a locally authored detector response and coincidence analysis that used the MCNP6 "ptrac" stream. In the simulations, the Lawrence Livermore National Laboratory fission model was specified using the FMULT card via (e.g.) FMULT 92235 METHOD=5. Further details of this methodology can be found in [22].

2.2. Corrugated Boron Straw Detectors

The second ORNL entry consisted of a thermal neutron detector in the form of ^{10}B-lined cylindrical proportional counters (PCs) from Proportional Technologies Inc. (PTI). These are among the oldest and most highly developed neutron detection technologies, as described by Rossi and Staub back in 1949. However, when ^{3}He gas became widely available, ^{3}He-filled PCs quickly became the dominant approach to neutron detection because they were cost-effective, simple to make, and offered higher efficiency per tube. Recently the demand for ^{3}He has challenged the supply, costs have risen sharply, and there is a concern over the long-term supply. This has refocused attention on boron-lined PC approaches to providing general purpose safeguards solutions to neutron counting needs. Several important points can be made about this technology. First, gas-filled PCs are inherently reliable and stable. These characteristics are especially important in nuclear safeguards applications. Second, they can be operated with high gamma-to-neutron discrimination, comparable to or better that ^{3}He, which most credible alternatives cannot match. This is evidenced by the use of commercial detectors in reactor applications. Third the neutron capture process may be confidently simulated using standard transport code options. This is important because in NDA safeguards there is usually the need to extend existing calibrations and to calculate correction factors using computational methods. Multiple scattering, cross talk, and complicated pulse shape analysis do not need to be considered. In contrast to ^{3}He-gas-filled PCs, ^{10}B-lined counters have a continuous energy deposition spectrum, and the threshold needed to discriminate gamma-rays results in lost efficiency. A compromise between the boron layer thickness and detection threshold must be struck. Deposit thicknesses are normally limited to about 2 μm, and traditionally, this limited achievable detection efficiency. Recently, however, several changes in thinking and practice have taken place so that the measurement penalty is not as great as it was once assumed to be. Advances in coating technology and manufacturing capability mean that large, robust areas of boron carbide can now be laid down in an automated and reproducible way.

To overcome some of the disadvantages of the older ^{10}B counters noted above, boron-coated straws (BCSs) have recently been developed. As the name implies, using a small diameter straw with internal structure (corrugation), the boron concentration per unit volume of the moderator has been increased considerably. An additional and crucial benefit is that the boron is distributed throughout the moderator

more uniformly so that thermal neutrons can be absorbed at the point of thermalization, which reduces the system die-away time. For coincidence counting applications both efficiency and die-away time are important in governing system performance, and so a BCS design does not have to match a standard ^{3}He-based design on efficiency if it has a shorter die-away time. The realization that commercially available BCS detectors, the straw aspects of which are proven in the high energy physics community for image reconstruction, has provided viable and scalable ^{3}He-free solutions for a wide range of safeguards and other applications.

The basic design (round tube) and three advanced BCS designs are shown in Figure 5: six-point star (a-right), pie-6 (b), and pie-12 (c). The purpose of these advanced designs was to increase the internal wall areas for B_4C coating in order to increase overall neutron detection efficiency, while maintaining the same coating thickness. As a result, the total coating area has been increased by a factor of 1.4, 2.0, and 3.0 for the six-point star, pie-6, and pie-12 designs, respectively, compared with that of the basic design.

(a) **(b)** **(c)**

Figure 5. The basic straw design (round) and three advanced straw designs: the basic straw design (a-left) and the advanced six-point star (a-right); pie-6 (b); and pie-12 (c).

The model of the UNCL using the BCS detectors was optimized in terms of both efficiency and tailoring the neutron spectrum from the interrogation source. Figure 6 shows the optimized version of the BCS collar, referred to as the “BCS plus collar,” which is bigger than the base model and incorporates several novel design features. The width, length, and height of this model are 52, 49, and 50 cm, respectively, compared with the 43, 43, and 52 cm of UNCL. The number of straws was increased from the 1,076 of the base model to 1,802 to increase the overall neutron detection efficiency. This BCS plus collar has been optimized to reduce the sensitivity to the Gd rods in the fuel. The cadmium liners of the base model were replaced with gadolinium liners around the cavity in the plus model. A half cylindrical shell with top and bottom of stainless steel is added and placed behind the AmLi source to reflect the neutrons back to the interrogation target—the fuel assembly. Borated polyethylene was used for the source block to reduce the number of source neutrons traveling through those regions and then being detected by the straws. The coating thickness of the B_4C in the straws was 1.5 μm. In the analysis of both the base collar and the plus collar, it was assumed that the total B_4C coating area was doubled using the advanced straw designs, although only round straws are shown in corresponding figures.

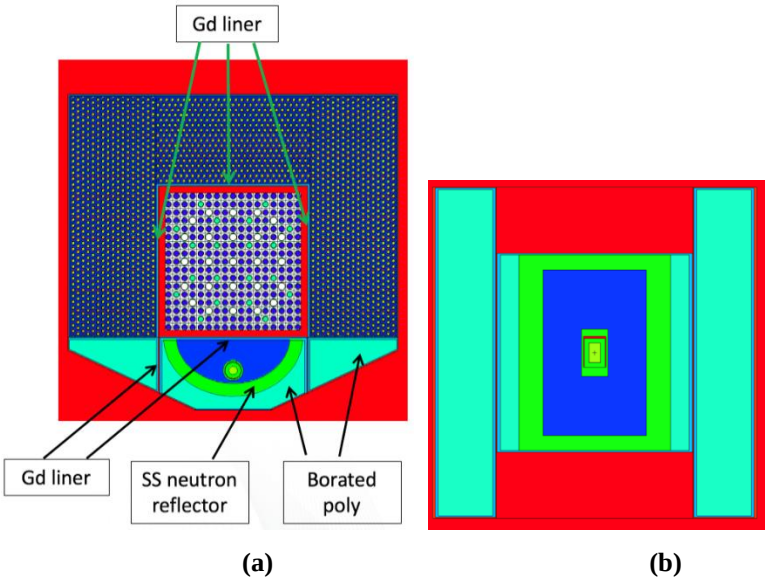

Figure 6. BCS plus collar: the XY cross-sectional view of the BCS plus collar (a); the XZ cross-sectional view of the plus collar with the Y plane cutting through the AmLi source (b).

2.3. ^{4}He Scintillator

Idaho National Laboratory (INL) submitted a UNCL design based on high-pressure ^{4}He scintillators. As a scintillator, ^{4}He is a fairly good one, with scintillation light emitted in the vacuum ultraviolet (VUV) region at a wavelength around 80 nm, requiring the use of a wavelength shifter in order to be detected in a meaningful way. Photon production is on the order of 18,000 VUV photons produced per MeV deposited by neutrons. The detectors simulated in this study utilize wavelength shifting paint on the interior of a 60-cm long detection cylinder, with silicon photomultipliers (SiPMs) placed axially along the cylinder to detect the light emitted from the scintillation events. For the present study, detection of a neutron event was based on the amount of energy transmitted from an incident neutron to the ^{4}He gas, so the method of light collection was not of primary concern, but may be important for further implementation or for other applications, particularly in high radiation dose situations. The ^{4}He elastic scattering cross section has a peak at around 1 MeV for neutrons, which makes it ideally suited for active interrogation applications. Figure 7 presents the scattering cross section of ^{4}He, AmLi neutron emission energy, and ^{235}U fission neutron emission energy.

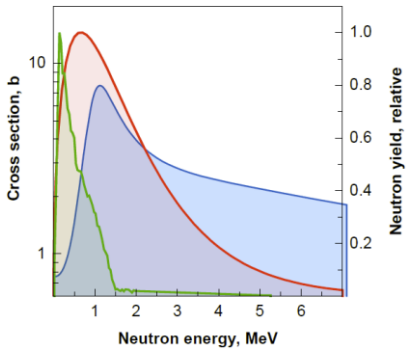

Figure 7. Elastic cross section for ^{4}He (blue, left axis), AmLi neutron emission (green, right axis) and U-235 fission neutron emission (red, right axis).

Monte Carlo models of ^{4}He scintillator detectors including inelastic scatter, light transmission and detection in PMTs or SiPMs have been developed and published using GEANT4 and MCNP-PoliMi

models. In order to have a benchmarked simulation basis upon which to compare results to other detectors being investigated under the current study, a model was developed in MCNP6.1b to simulate the ^{4}He detector response based on the energy transferred to ^{4}He gas from incident neutrons. The development and decay of excimer states was not modelled, nor was wavelength shifting or light collection. The model utilized pulse height and energy deposition tallies with the *ptrac coinc* option to provide information on coincident events both within a single detector, and between multiple detectors. This model was compared to simulated and experimentally measured detector responses published for ^{4}He detectors of different pressures and lengths, shown in Figure 8. Excellent agreement is observed between the developed MCNP model, the detector response from both GEANT4/MCNP-Pollimi simulations and experimental measurements.

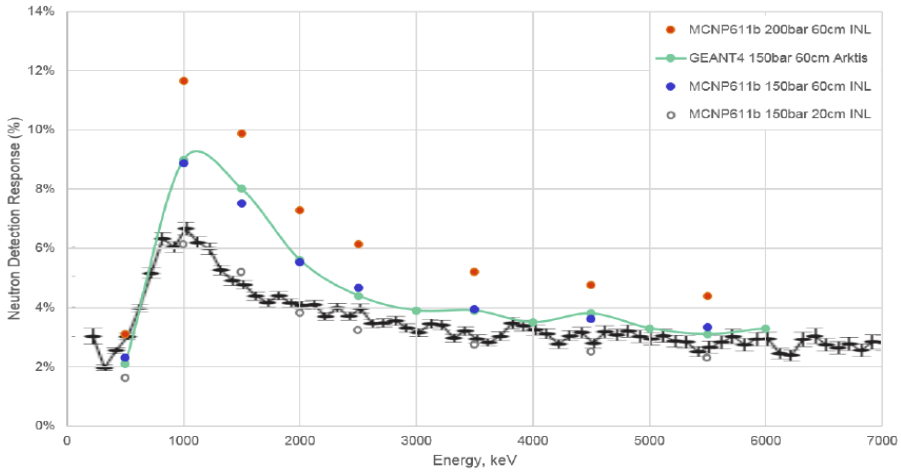

Figure 8. Single detector modelling and experimental comparison. Experimental data for 20cm, 150bar tubes shown in black [13]; GEANT4 data from [14]

For the present effort, commercially available Arktis Radiation Detectors Ltd. model S670 detectors were simulated. These detectors are 60 cm in active length and 4.4 cm in active diameter, with up to 200 bar ^{4}He fill gas. The tubes are comprised of three 20-cm sections, each with 8 SiPMs. Output from each section is analyzed utilizing a time-over-threshold (TOT) algorithm using integrated electronics, and a TTL output is provided from each tube. Figure 9 shows a cutaway view of the Arktis detectors.

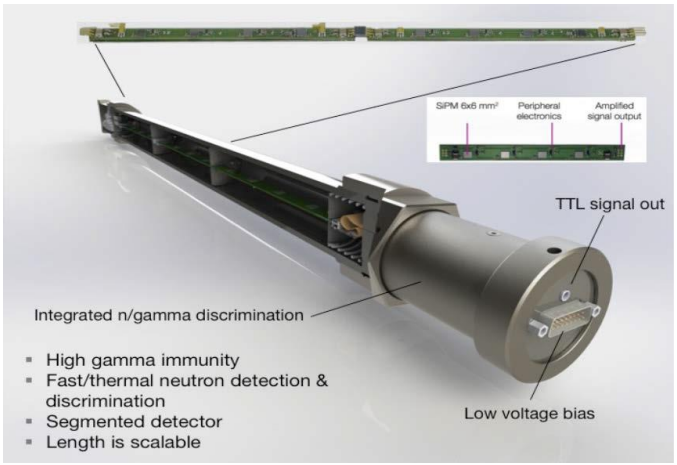

Figure 9. Cutaway view of the Arktis Radiation Detectors S670 tube [courtesy of Arktis Radiation Detectors, Ltd.]

One of the primary challenges of using fast neutron scintillation detectors for coincident or multiplicity measurements is scatter between detectors, possibly leading to false coincident neutron events. For

the developed detector model, events where an incident neutron was scattered and detected in multiple neighboring detectors were recorded in the *ptrac coinc* output and subtracted from the total coincident rate. As each detected event contains spatial and energy information, more sophisticated treatment of scattering events was investigated, but offered limited improvement for the present application. A plan view of the 31 detector model used in this study is shown in Figure10.

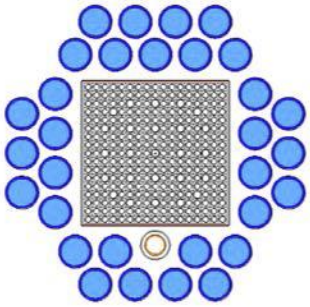

Figure 10. Plan view of the ^{4}He models with double rows of tubes completely surrounding FA, 60 cm in length.

2.3. Boron Plate Detectors

Los Alamos National Laboratory (LANL) utilized a COTS technology based on sealed-cell boron-coated plate detectors developed by Precision Data Technology (PDT). The newer version of the plate design that this work is based on utilizes a new boron coating material mixture and procedure that results in large increases (~ 50%) in the detection efficiency per unit of surface area. This proprietary method provides a 3-D surface area increase over the prior PDT coating method, and the boron surface area is considerably larger than the metal surface that supports it. A photograph of one of the slab units and a cutaway drawing showing the internal structure is shown in Figure 11.

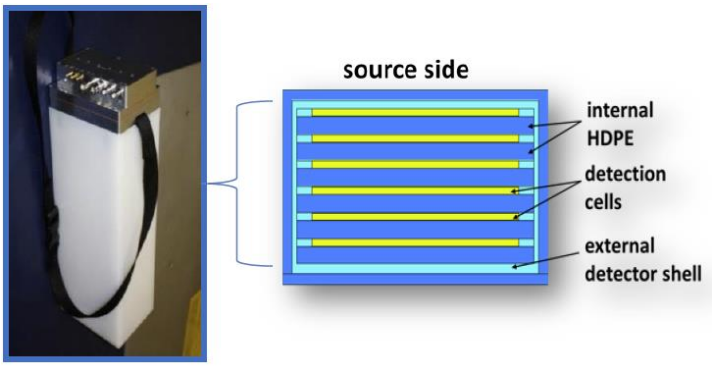

Figure 11. The PDT parallel plate detector pod with 6 internal ^{10}B lined cells.

The first UNCL design consisted of 4 PDT pods arranged to create detectors on three sides. The fourth side is a polyethylene slab with a hole for the AmLi source. This design creates a form factor which closely resembles the ^{3}He based UNCL system. To optimize the detector, there are several characteristics which were studied. These are the polyethylene thickness between the cells, the polyethylene thickness between the sample cavity and the first cell, the Cd layer thickness, and the AmLi source position.

All of the optimization runs were done with a 17x17 fuel assembly with a mass loading of 45 g/cm – one of the fuel assemblies that was provided by NNSA/NA-241 for creation of the calibration curve.

Both the Fast and Thermal modes in active and passive configuration were modeled. To find the best design, the error of the doubles rate was minimized for the Fast Mode configuration. Some of the detector characteristics were fixed during the optimization runs. This includes the sample cavity which was fixed at 23.4 cm by 23.4 cm. Each individual ^{10}B cell thickness is 0.6 cm with a 0.1 cm thick wall and a 2.1 μm thick boron layer. The total height of the UNCL is 51 cm that is approximately the same as the current UNCL. The electronics and cable connections are mounted at the top of the pod and are included in the 51 cm height.

MCNP version 6.1.1b was used for the Monte Carlo modeling. In active mode, AmLi neutrons were started with the Obninsk source spectrum definition provided by NNSA/NA-241. The coincidence count rate per source particle was obtained using a F8 capture tally. Multiplying this tally by the AmLi source strength resulted in the singles and doubles count rates. In an effort to make the MCNP model as close to reality as possible, the corrugation of the cells, shown in Figure 12, was incorporated into the model. The corrugated design allows for better charge collection and also makes the individual cell more ridged. All modeling includes dead spaces where the edges of the individual pods meet.

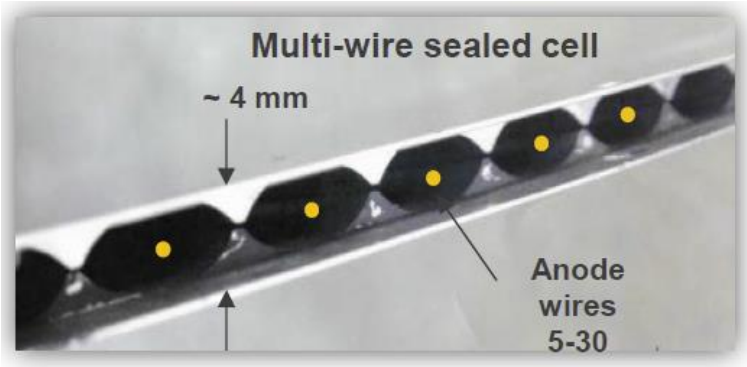

Figure 12. Diagram of the corregated geometry.

To achieve a better coupling between the AmLi source and the fuel assembly for Fast Mode operation, a notch was added to the slab that holds the AmLi source. This notch also would allow for a WWER fuel assembly to fit into the sample cavity as shown in Figure 13.

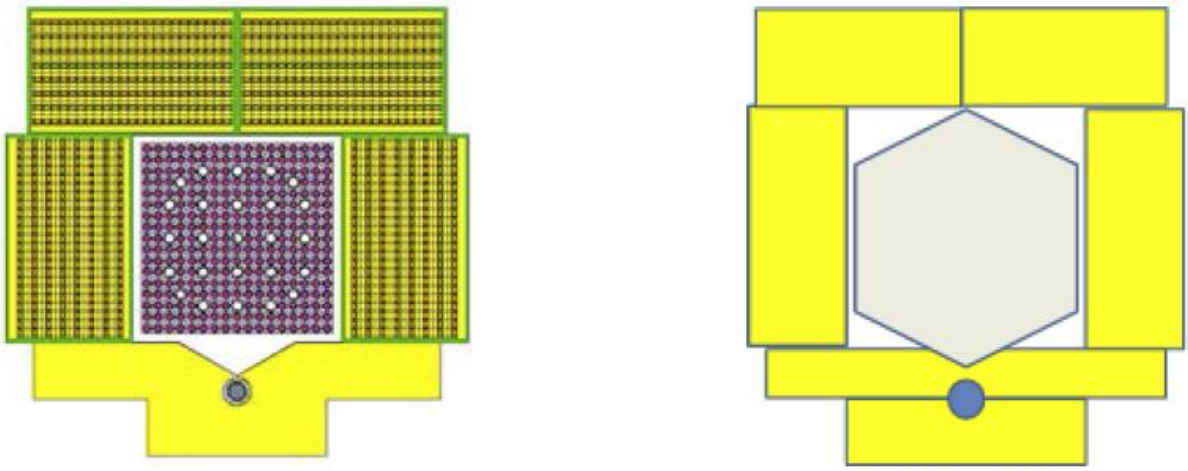

Figure 13. On the left is an MCNP model of the boron plate UNCL design with the corregated cell design shownig the 4 pods, AmLi slab, and fresh fuel assembly. On the right is a drawing representing how a WWER fuel assembly would fit into the boron plate UNCL design.

2.3. Stilbene

Lawrence Livermore National Laboratory (LLNL) designed their UNCL counter using stilbene scintillator crystals that are commercially available from Inrad Optics. The company uses a rapid, safe growth technique that was developed at LLNL which allows for large (4" x 2") crystals at lower cost than previously available. Like the other scintillators in this study stilbene is a fast neutron detector that relies on neutron scattering to produce energetic charged recoil ions that generate scintillation light. It has a fast response time on the order of a nano-seconds which allows for the resolution of individual fission chains (bursts) and permits a detailed analysis of the underlying neutron multiplication, as well as a much shorter coincidence gate for counting neutrons and their correlations with very few Accidentals. This leads to a precise and rapid assay in significantly lower measurement times. Since a fast 1 MeV neutron travels at 1.5 cm/ns, with nano-second time resolution it is possible to resolve the spatial distribution of SNM (special nuclear material) at centimeter scales using neutron and gamma correlations. While this is not a requirement for the Rodeo it is an important capability of fast neutron counting that can potentially be used to great advantage.

With scintillator based detection what is actually being measured is the scintillator light output spectrum. From this light output spectrum one can unfold the neutron energy spectrum of the neutrons being detected. Finally, stilbene is an optimal scintillator detector because it has the highest organic scintillation efficiency with much higher light yield than plastics or liquids. It has an excellent PSD (pulse shape discrimination) which allows for excellent gamma rejection which in turn implies high neutron detection efficiency. This high efficiency and short coincidence gating is critical to it being competitive with ^{3}He based neutron detectors.

The prototype stilbene neutron collar design described here uses 30 of these 4"x2" crystals that can fit into the form factor of standard ^{3}He based collar, as shown in Figure 14. The LLNL group used the Hansen-Richter quench function [23] to generate the stilbene light output spectrum by post-processing their custom LLNL MCNPX27e simulations of the neutron collar.

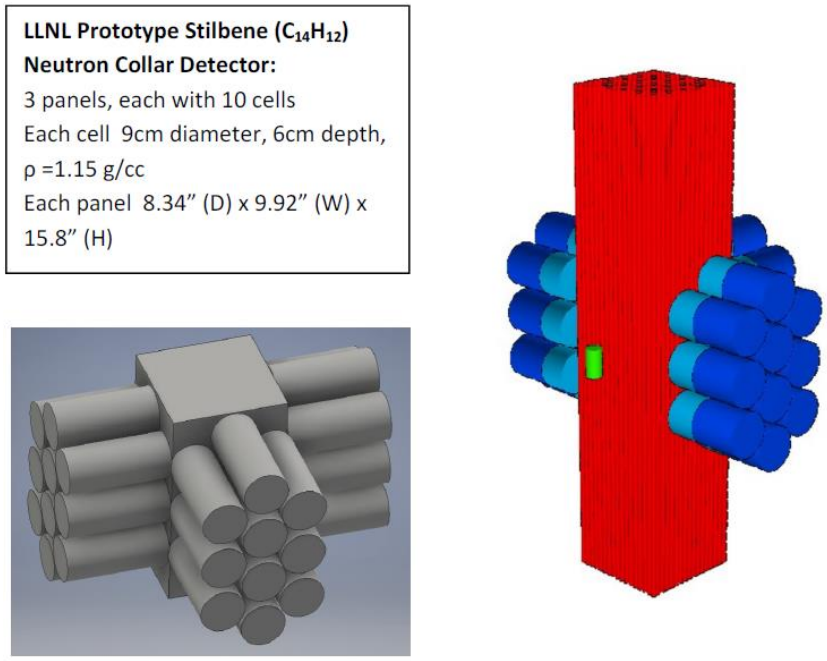

Figure 14. LLNL prototype stilbene neutron collar with 30 stilbene cells and a form factor similar to commercially available ^{3}He based UNCL. Also shown is a MCNP model of the stilbene collar with a fuel assembly and an AmLi interrogating neutron source (shown without the poly bank in which it is embedded).

Simulations with the custom MCNPX27e code use the LLNL fission library by setting *fism=5* in the 6th entry of the *PHYS:N* card. This setting samples a full measured distribution for the number of fission neutrons emitted in a fission event. The timestamps recorded by the custom LLNL MCNPX27e are in double precision, in contrast to the default MCNP PTRAC which uses single precision. This double precision is especially important when simulating fast neutron detector counting with sub nano-second time resolution to avoid false correlations.

The LLNL analysis methodology uses an inverse modeling approach to estimate and correct for multiple scatter neutron crosstalk. A detailed MCNPX27e model of the stilbene collar is used to generate a library of scintillator light output spectrum for a set of random point or extended source of mono-energetic neutrons with energies ranging from 1 to 10 MeV. A measured scintillator light output spectrum from a general unknown object is then fitted with the library of responses to simultaneously determine the neutron energy spectrum and the crosstalk correction.

2.4. Liquid Scintillator EJ309

The University of Michigan designed the UNCL with EJ309 (3”Ø x 3”) liquid scintillators which are scatter-based fast neutron detectors that directly detect the unmoderated fast fission neutrons. The primary mechanism for neutron detection in organic scintillators is through neutrons undergoing elastic scattering on protons within the active volume of the detector; the recoil protons generate scintillation light that is collected and read through a photomultiplier tube (PMT), or more recently through silicon photomultipliers (SiPM). These scintillators have relatively fast response times with waveforms on the order of tens of nanoseconds and coincident timing resolution of less than two nanoseconds at full-width half maximum. The EJ309 system is also able to count pairs of neutrons in much shorter time gates relative to thermal neutron detector systems as there is no need for moderation of the emitted fast neutrons; this allows for much lower rates of accidental correlations relative to true correlations. The fast response and shorter time gates of an EJ309 system results in the ability to assay the fuel assembly (to a degree of uncertainty) in shorter acquisition times relative to the traditional ^{3}He based systems. Figure 15 shows a typical waveform in an EJ309 and the timing resolution between pairs of EJ309 modules obtained experimentally from coincident measurement of ^{22}Na annihilation photons.

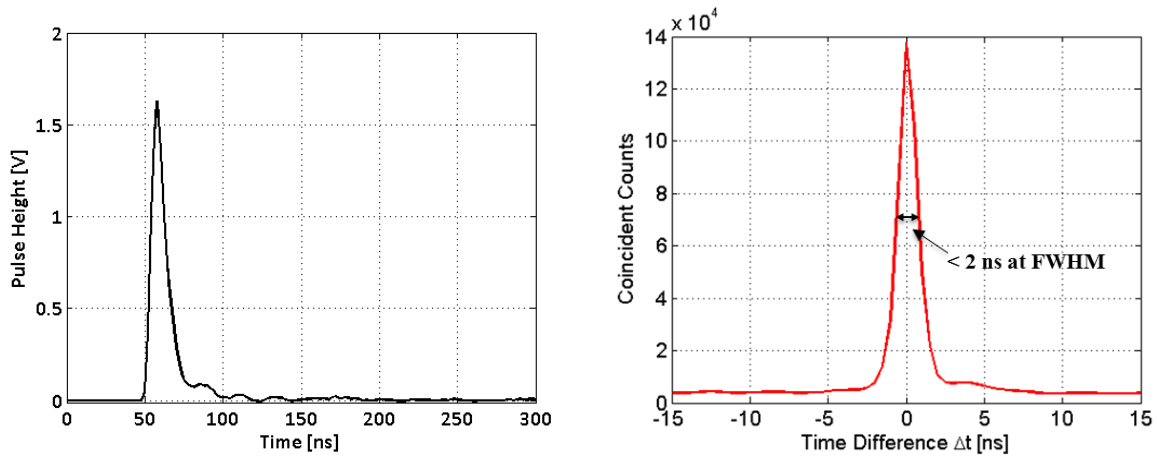

Figure 15. A typical pulse in an EJ309 (left) and the timing resolution between pairs of EJ309 measured with a ^{22}Na source (right).

The EJ309 system also exhibits additional capabilities that are not feasible in traditional ^{3}He based systems mainly due to the absence of moderating material. Without moderating material between the fuel assembly and the detectors, additional information characteristic to the impinging neutron can be retained. One measured quantity is the energy deposited within each detector cell (proportional to the collected light in the PMT and/or SiPM); this allows for neutron spectrum unfolding capabilities. Additionally, spatial and/or angular distributions of the fission neutrons can also be extracted which can potentially provide characteristic signatures pertinent to the assembly.

EJ309 cells are sensitive to both fast neutrons (> ~0.5 MeV at 50 keVee light threshold) and gamma rays. The two types of particles are distinguished from one another through pulse shape discrimination (PSD) techniques. Neutron pulses will exhibit a slower decay in the tail-region of the waveform relative to photon pulses of the same pulse height. The ratio of the charge in the tail-region to the total charge of the waveform provides a suitable discrimination parameter which allows for particle identification. The chance for particle misclassification increases for pulses of lower pulse heights; the detection threshold was set such that the gamma-ray misclassification rate (gamma rays that are classified as neutrons) was lower than 10^{-6} per detection. Figure 16 shows two distinct regions that correspond to neutron and gamma ray pulses.

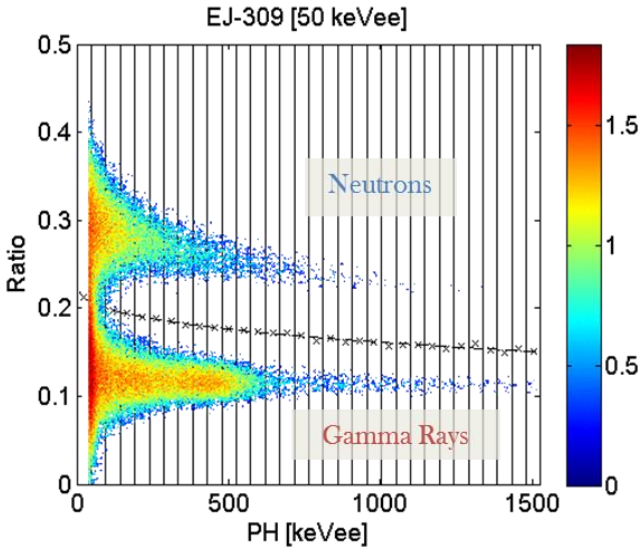

Figure 16. Scatter plot of the charge-ratio versus the pulse height showing two distinct regions for neutrons and gamma rays from a ^{252}Cf source; the black line is the optimized discrimination line for particle identification.

The prototype system design is comprised of an array of 23 EJ309 detectors arranged in to fit in the form factor of the standard ^{3}He based UNCL. MCNPX^{TM} v2.7e with the -PoliMi extension [24] was used to simulate fission events and its subsequent events. The MPPost detector response emulator code [25] was used to extract neutron multiplicity counting distribution, which was used to obtain the neutron doubles count rate (second-order factorial moment). The time gate was set to correlated neutrons within a 200 nanosecond window. Figure 17 shows the simulated model geometry of the prototype EJ309 system.

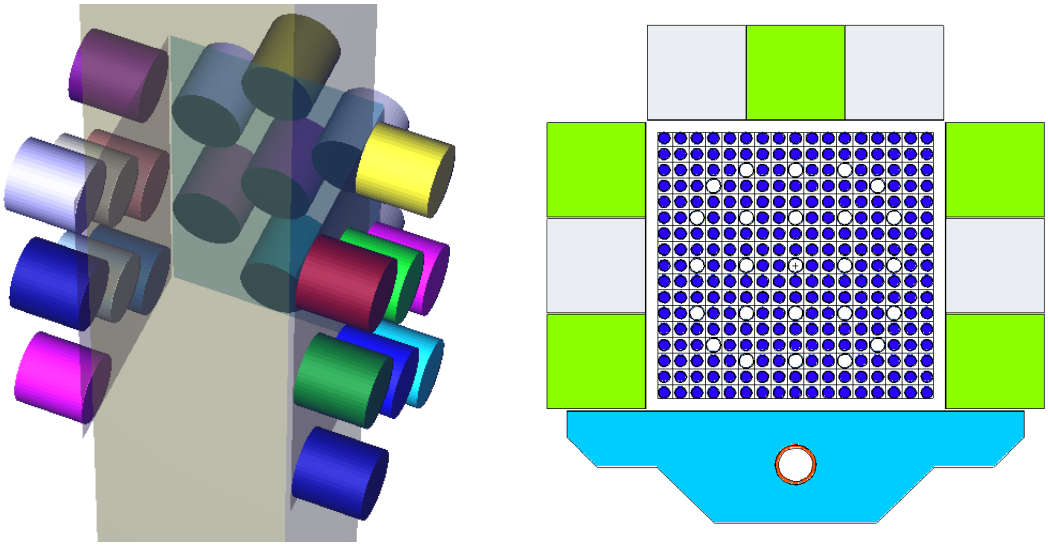

Figure 17. The simulated model geometry for the prototype EJ309 system consisting of 23 EJ309 detectors.

3. Results and Comparisons

In the sections that follow the simulation results will be presented for all the detector materials in this study. For comparison, the simulation results for the current standard Type I UNCL with ^{3}He tubes are also included. It should be noted that the Doubles rate from the active simulations is the quantity of interest for this Rodeo. In simulation space, the active Doubles is equivalent to the coincidence rate of interest, the Net Doubles rate. In an actual measurement, the Net Doubles is normally obtained by subtracting the passive Doubles from the active Doubles. This makes the simulation study more convenient in that it is not necessary to run passive simulations to obtain the net Doubles rate. Thus, going forward, the Doubles rate refers to the Net Doubles rate which is the quantity used to determine the LD of ^{235}U in the fuel assembly in a real world measurement.

3.1. Fast Mode Calibration

To achieve the Fast Mode most groups utilized either a 1.0 or 0.5 mm thick Cadmium liner around the fuel cavity to effectively prevent neutrons with energies < 0.5 eV from interacting with the fuel. The ORNL – ^{10}B Straws group used liners made of Gadolinium. Table 2 presents the simulated Singles (S) and Doubles (D) rates as a function of the linear density of ^{235}U in the calibration fuel assemblies provided.

	UNCL			ORNL - PSD plastic			ORNL - ^{10}B straws			LANL - ^{10}B Plates		
LD ^{235}U (g/cm)	S (1/s)	D (1/s)	σD (1/s)	S (1/s)	D (1/s)	σD (1/s)	S (1/s)	D (1/s)	σD (1/s)	S (1/s)	D (1/s)	σD (1/s)
15	821	5.6	0.06	196	7.7	0.12	918	6.1	0.16	1946	17.0	0.53
20	834	7.5	0.06	215	10.2	0.14	926	7.8	0.17	1964	21.5	0.53
25	846	9.3	0.07	234	12.3	0.15	933	9.4	0.17	1982	26.0	0.54
35	867	11.8	0.08	268	16.2	0.17	948	12.2	0.18	2014	34.2	0.55
45	887	14.5	0.09	299	19.2	0.19	959	15.0	0.18	2042	41.8	0.57
55	903	16.7	0.10	329	23.2	0.21	973	17.6	0.19	2068	49.3	0.58
60	911	18.0	0.10	342	24.2	0.21	978	18.8	0.19	2082	53.1	0.58
65	918	18.7	0.10	354	25.9	0.22	983	20.0	0.19	2094	56.7	0.59
	INL - ^{4}He			LLNL - Stilbene			UM - EJ309					
LD ^{235}U (g/cm)	S (1/s)	D (1/s)	σD (1/s)	S (1/s)	D (1/s)	σD (1/s)	S (1/s)	D (1/s)	σD (1/s)			
15	843	15.3	0.09	150	7.6	0.06	257	11.4	0.15			
20	856	16.0	0.09	163	9.2	0.07	279	14.0	0.17			
25	870	17.0	0.10	176	11.2	0.08	299	16.9	0.18			
35	897	19.2	0.10	198	14.1	0.09	336	21.5	0.21			
45	921	21.1	0.11	220	16.7	0.10	371	24.9	0.22			
55	945	22.6	0.11	238	19.5	0.10	402	28.2	0.24			
60	956	23.3	0.11	248	21.4	0.11	415	30.9	0.25			
65	965	24.1	0.12	256	22.2	0.11	430	32.9	0.26			

Table 2. Fast calibration data for all technologies based on a 50,000 n/s AmLi interrogation source.

The error in the Doubles rate are determined assuming an 1800 second assay and a shift-register analysis of the pulse stream from the detector. The methodology for the Doubles uncertainty is described in [26] and is dependent on the Singles and Doubles rates and the Gate Width. All calibrations are shown in Figure 18 on a lin-log scale. The error bars are too small to see in the plot.

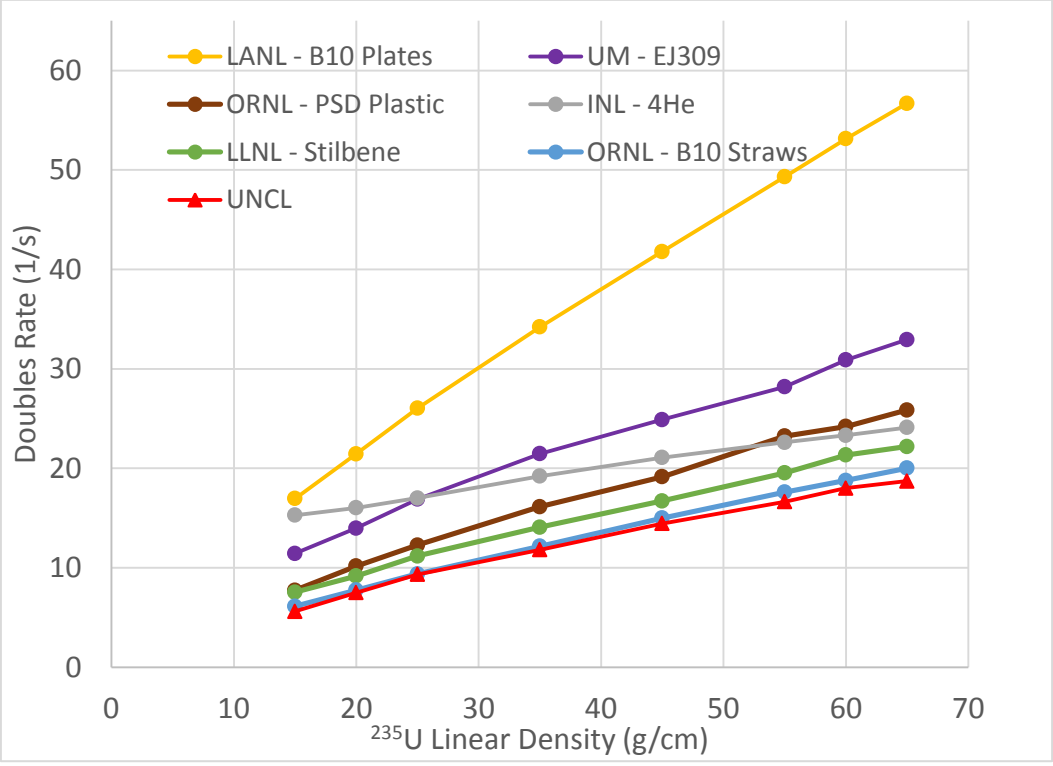

Figure 18. Plot of the Fast Mode calibrations for all the technologies.

The rates shown are calculated assuming a 5.0×10^4 n/s interrogation source. The different technologies provide a range of detector responses over the calibration LD range. Most of the detector calibrations can be fit with the typical fit of the form: $D = \frac{a*m}{1+b*m}$, where *a* and *b* are fitting constants and *m* is the ^{235}U linear density. The exception is the INL – ^{4}He detector that obtains a better fit with a linear or second order polynomial. The likely reason the ^{4}He detector material has a flatter response relative to the other materials is that there is no hydrogen associated with the detector material itself. In the case of the UNCL and the ^{10}B Straws or Plates, there is polyethylene that provides moderation to increase the detection efficiency. For EJ309, Stilbene, and PSD Plastic these detector materials are hydrocarbons which will also moderate the neutrons very well. Even though there are cadmium or gadolinium curtains between the detectors and the fuel, a good fraction of epi-thermal neutrons are able to interact with the fuel and thus, boost the fission rate as the linear density increases. However, for the ^{4}He material, since it is not as good as hydrogen at moderation, the neutron spectrum interrogating the fuel is much faster and so the multiplication in the fuel is relatively lower at the higher ^{235}U linear densities compared to the other detector types.

3.2. Fast Mode Unpoisoned In-tact Fuel

In order to test the calibrations determined from the fittings above the groups were tasked with simulating a variety of unpoisoned fuel found in the nuclear fuel industry. The fuel ranged from 14x14 up to 17x17 and have different design characteristics than the fuel used for calibration. The significant parameters of each fuel assembly are given in Table 3 and examples of two of the modeled fuel designs are shown in Figure 19. The results for each detector technology are shown in Tables 4 and 5. The data in the tables show the analyzed linear densities for each technology that were derived from their specific Fast Mode calibrations in addition to the difference between the actual LD and the analyzed LD (mass defect) as well its 3σ total uncertainty for comparison. The total uncertainty assumes an 1800 second active measurement and an assumed 2% systematic uncertainty.

Width (cm)	Pin Pitch (cm)	# Fuel Pins	Clad OD (cm)	Clad thickness (cm)	Pellet ρ (g/cm^3)	Pellet OD (cm)	Enrich. (%)	^{235}U LD (g/cm)	Fuel Design
19.70	1.437	179	1.016	0.0617	10.42	0.875	3.80	37.6	14x14A
20.60	1.499	176	1.118	0.0660	10.44	0.968	3.13	37.3	14x14B
19.70	1.437	179	1.016	0.0617	10.42	0.875	2.00	19.8	14x14C
21.40	1.452	204	1.072	0.0620	10.64	0.929	4.50	58.4	15x15A
21.50	1.459	205	1.075	0.0725	10.45	0.911	5.00	61.5	15x15B
21.70	1.472	208	1.090	0.0635	10.52	0.940	4.55	60.9	15x15C
19.70	1.252	235	0.914	0.0572	10.42	0.784	4.50	46.9	16x16A
20.70	1.317	184	0.950	0.0572	10.42	0.819	4.50	40.1	
20.70	1.317	52	0.950	0.0572	10.42	0.819	4.00	10.1	
20.70	1.317	236	0.950	0.0572	10.42	0.819	4.39	50.2	16x16B
20.70	1.317	136	0.950	0.0572	10.42	0.819	2.92	19.2	
20.70	1.317	100	0.950	0.0572	10.42	0.819	2.42	11.7	
20.70	1.317	236	0.950	0.0572	10.42	0.819	2.71	30.9	16x16C
22.96	1.459	236	1.075	0.0725	10.50	0.911	4.50	64.1	16x16D
21.40	1.278	264	0.950	0.0570	10.52	0.819	3.20	41.3	17x17A
21.40	1.278	264	0.950	0.0570	10.64	0.819	4.20	54.8	17x17B

Table 3. Details of the fuel designs for the in-tact unpoisoned fuel used to test the calibration. The design names are only of significance for this study.

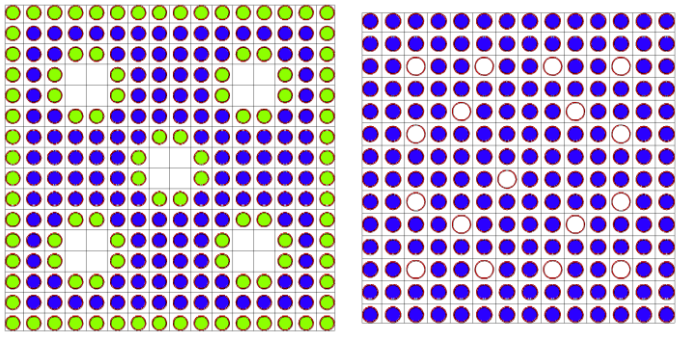

Figure 19. MCNP model representations of un-poisoned in-tact fuel: 16x16C (left) and 14x14A (right). The different color pins in the fuel indicate different enrichment.

		UNCL			ORNL - ^{10}B Straws		
Fuel Design	Declared LD ^{235}U (g/cm)	Analyzed LD 235U (g/cm)	LD mass defect (%)	1800 sec Total Uncert (%) 3σ	Analyzed LD 235U (g/cm)	LD mass defect (%)	1800 sec Total Uncert (%) 3σ
14x14A	37.6	35.0	-6.9%	9.2%	35.1	-6.7%	8.5%
14x14B	37.3	36.0	-3.5%	9.0%	36.0	-3.6%	8.3%
14x14C	19.8	17.9	-9.4%	12.1%	19.1	-3.5%	10.8%
15x15A	58.4	58.7	0.6%	8.5%	58.1	-0.5%	7.6%
15x15B	61.5	59.4	-3.5%	8.5%	61.7	0.2%	7.6%
15x15C	60.9	61.8	1.4%	8.5%	61.5	0.9%	7.6%
16x16A	46.9	44.4	-5.3%	8.6%	44.9	-4.3%	8.0%
16x16B	50.2	49.0	-2.4%	8.5%	48.3	-3.7%	7.8%
16x16C	31.0	29.4	-4.9%	9.6%	29.5	-4.7%	8.9%
16x16D	64.1	66.6	4.0%	8.6%	65.1	1.6%	7.6%
17x17A	41.3	41.7	1.0%	8.6%	40.4	-2.0%	8.0%
17x17B	54.8	52.6	-4.0%	8.4%	53.8	-1.9%	7.6%

		LANL - ^{10}B Plates		
Fuel Design	Declared LD ^{235}U (g/cm)	Analyzed LD 235U (g/cm)	LD mass defect (%)	1800 sec Total Uncert (%) 3σ
14x14A	37.6	34.5	-8.3%	9.0%
14x14B	37.3	35.4	-5.1%	8.7%
14x14C	19.8	18.4	-7.1%	11.5%
15x15A	58.4	57.9	-0.8%	8.2%
15x15B	61.5	60.9	-1.0%	8.3%
15x15C	60.9	61.6	1.1%	8.3%
16x16A	46.9	44.0	-6.3%	8.5%
16x16B	50.2	47.7	-5.0%	8.3%
16x16C	31.0	28.9	-6.6%	9.2%
16x16D	64.1	65.4	2.0%	8.2%
17x17A	41.3	40.2	-2.7%	8.4%
17x17B	54.8	53.9	-1.7%	8.2%

Table 4. Results for the in-tact unpoisoned fuel virtual assay for the thermal neutron detector materials.

		INL - ^{4}He			LLNL - Stilbene		
Fuel Design	Declared LD ^{235}U (g/cm)	Analyzed LD 235U (g/cm)	LD mass defect (%)	1800 sec Total Uncert (%) 3σ	Analyzed LD 235U (g/cm)	LD mass defect (%)	1800 sec Total Uncert (%) 3σ
14x14A	37.6	40.3	7.3%	8.4%	37.7	0.3%	7.5%
14x14B	37.3	33.0	-11.5%	8.8%	36.2	-2.9%	7.6%
14x14C	19.8	22.6	14.4%	9.8%	21.1	6.6%	9.4%
15x15A	58.4	55.5	-5.0%	7.4%	59.5	2.0%	7.4%
15x15B	61.5	58.3	-5.3%	7.4%	64.0	3.9%	7.8%
15x15C	60.9	53.8	-11.7%	7.5%	63.0	3.5%	7.7%
16x16A	46.9	48.3	3.0%	7.8%	47.3	0.8%	7.1%
16x16B	50.2	43.9	-12.5%	8.1%	51.0	1.7%	7.1%
16x16C	31.0	33.5	8.2%	8.8%	31.4	1.6%	8.1%
16x16D	64.1	59.0	-7.9%	7.5%	63.8	-0.5%	7.8%
17x17A	41.3	43.0	4.2%	8.2%	39.7	-3.8%	7.4%
17x17B	54.8	53.1	-3.2%	7.5%	54.3	-1.0%	7.2%

		UM - EJ309			ORNL - PSD plastic		
Fuel Design	Declared LD ^{235}U (g/cm)	Analyzed LD 235U (g/cm)	LD mass defect (%)	1800 sec Total Uncert (%) 3σ	Analyzed LD 235U (g/cm)	LD mass defect (%)	1800 sec Total Uncert (%) 3σ
14x14A	37.6	37.5	-0.3%	7.9%	41.1	9.4%	6.7%
14x14B	37.3	36.4	-2.6%	8.0%	38.3	2.7%	6.7%
14x14C	19.8	20.4	3.3%	10.2%	22.3	12.6%	7.1%
15x15A	58.4	60.0	2.8%	8.3%	60.4	3.5%	6.8%
15x15B	61.5	63.1	2.6%	8.6%	63.2	2.7%	6.9%
15x15C	60.9	58.2	-4.5%	8.1%	59.8	-1.8%	6.8%
16x16A	46.9	45.3	-3.3%	7.6%	51.7	10.3%	6.7%
16x16B	50.2	49.2	-1.9%	7.6%	53.7	7.0%	6.7%
16x16C	31.0	30.2	-2.5%	8.7%	32.7	5.6%	6.8%
16x16D	64.1	62.6	-2.3%	8.6%	62.8	-1.9%	6.8%
17x17A	41.3	40.0	-3.2%	7.8%	42.0	1.6%	6.7%
17x17B	54.8	50.2	-8.5%	7.6%	54.1	-1.3%	6.7%

Table 5. Results for the in-tact unpoisoned fuel virtual assay for the fast neutron detector materials.

It is well known that there are differences in fast neutron scattering and multiplication in fuel assemblies with differences in the total Heavy Metal (HM) loading, i.e. the total Uranium LD. For example, if the calibration of an instrument is done with all 17x17 fuel assemblies, as was done in this project, there can be significant systematic biases when assaying fuel with much lower HM loading. For the Rodeo, the calibration fuel assemblies have a Uranium LD of 1297 g/cm. Table 6 shows the Uranium LDs of the 12 unpoisoned in-tact fuel assemblies and demonstrates that there are instances where the HM loading is quite different. This is typically remedied in a normal UNCL assay with a correction to the measured Doubles rate based on the total Uranium loading, as shown in the last column of Table 6 for the standard UNCL. This makes it somewhat difficult to draw conclusions about how accurate each modeled detector would be since the HM correction is highly dependent on the neutron energy spectrum that is interrogating the fuel. However, in general, most of the unpoisoned in-

tact fuel assayed within 3σ total uncertainty for the given detector material. The ORNL PSD Plastic detector had four results where the difference in ^{235}U LD was larger than 3σ. These assemblies: 14x14A, 14x14C, 16x16A, and 16x16B all have the largest HM differences from the calibration fuel and thus, would need the largest correction factors in practice. The INL 4He Scintillator also had difficulties with four fuel assemblies (14x14B, 15x15C, 16x16B, and 16x16D) but they were generally not the assemblies with the largest HM differences relative to the calibration assemblies.

Another result of interest from the data in Tables 4 & 5 is the magnitude of the total uncertainties when comparing the detectors that rely on thermal neutron detection (UNCL, ^{10}B Straws, and ^{10}B Plates) and those that detect fast neutrons (PSD Plastic, ^{4}He Scintillator, Stilbene, and EJ309). In general, but not categorically, the fast neutron detectors have a lower overall uncertainty because of the very short coincidence gate that can be used with these fast detectors. The advantage being that it minimizes the number of accidental coincidences and improves the Doubles measurement precision. In the case of the ORNL ^{10}B Straws, they were able to approach the counting statistics of the fast neutron detectors by reducing both the Pre-Delay and coincidence gate width in addition to designing their interrogation source slab so as to minimize the number of thermalized source neutrons that reach the detector active areas directly. This was achieved by adding borated polyethylene on the wings of the source slab as seen in Figure 6a. Finally, Figure 20 shows the assayed assembly results (LD of ^{235}U) for all detectors and all unpoisoned in-tact fuel assemblies along with the actual declared LD values for comparison. The error bars shown are 3σ and show the generally acceptable results with a few exceptions.

Fuel Design	U LD g/cm	% diff to Calibration	UNCL HM correction factor
14x14A	989	-24%	1.12
14x14B	1192	-8%	1.04
14x14C	989	-24%	1.12
15x15A	1297	0%	1.00
15x15B	1231	-5%	1.03
15x15C	1339	3%	0.98
16x16A	1042	-20%	1.10
16x16B	1143	-12%	1.06
16X16C	1143	-12%	1.06
16x16D	1424	10%	0.95
17x17A	1290	-1%	1.00
17x17B	1305	1%	1.00
17x17 calibration	1297		1.00

Table 6. The in-tact unpoisoned fuel designs' total Uranium LDs and comparison to the 17x17 calibration assembly. Correction factors for each fuel design as determined for the UNCL.

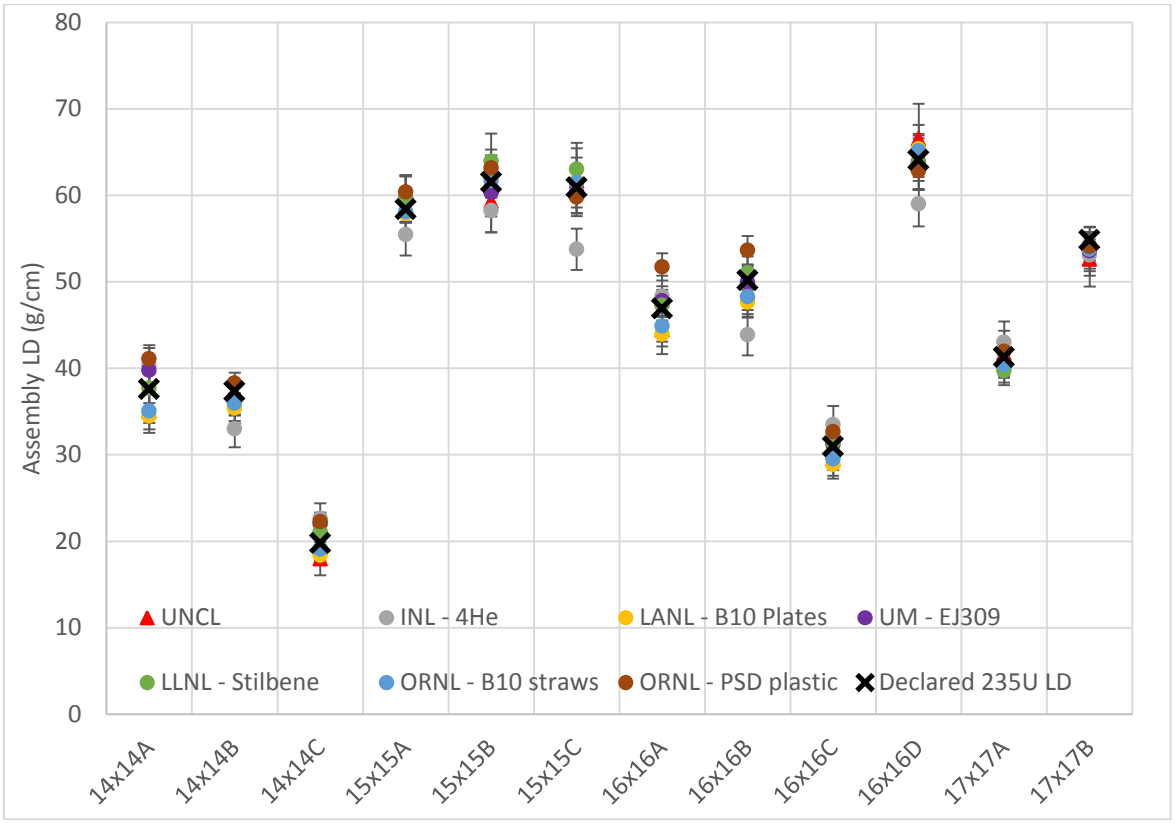

Figure 20. Comparison of assayed and declared ^{235}U linear densities of the in-tact unpoisoned fuel assemblies.

3.3. Fast Mode Partial Defect

The UNCL has been the workhorse instrument in international safeguards for detecting missing pins in fresh fuel assemblies for decades. For the Rodeo, teams were asked to determine the sensitivity of detecting substituted fuel pins for their detector material by using provided fuel definitions with different numbers of LEU pins substituted with DU pins as shown in Figure 21.

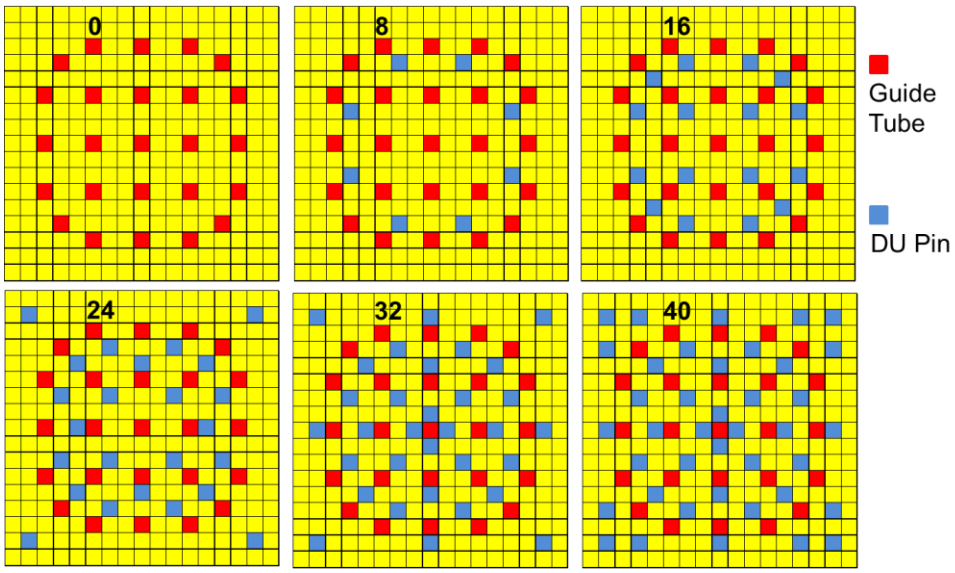

Figure 21. Fuel assembly patterns for partial defect sensitivity estimation.

The case with 0-pin substitutions has a ^{235}U LD of 51.9 g/cm which corresponds to a 17x17 fuel assembly populated uniformly with 4% enriched LEU fuel pins. The partial defect (PD) cases under evaluation are for substitutions of 8, 16, 24, 32, and 40 pins containing DU, these substitutions correspond to mass defects of 2.9%, 5.8%, 8.7%, 11.6%, and 14.5% respectively. The results for each detector are evaluated relative to the analyzed mass of the 0-pin substitution case to remove any systematic bias and to ensure the mass defect is always negative. The results, the analyzed mass defect and 3σ uncertainty for an 1800 second active assay, for each technology are shown in Table 7.

	UNCL		INL - ^{4}He		LLNL - Stilbene	
# of replaced pins	LD mass defect (%)	3σ 1800 sec (%)	LD mass defect (%)	3σ 1800 sec (%)	LD mass defect (%)	3σ 1800 sec (%)
0	0.0%	9.3%	0.0%	7.7%	0.0%	7.1%
8	-1.7%	9.3%	-2.6%	7.7%	-2.1%	7.1%
16	-4.5%	9.3%	-6.1%	7.9%	-5.6%	7.1%
24	-7.4%	9.4%	-9.1%	8.0%	-8.7%	7.1%
32	-11.3%	9.4%	-8.9%	8.0%	-12.8%	7.1%
40	-13.6%	9.4%	-13.1%	8.1%	-15.9%	7.2%

ORNL - ^{10}B Straws		LANL - ^{10}B plates		ORNL - PSD Plastic		UM - EJ309	
LD mass defect (%)	3σ 1800 sec (%)	LD mass defect (%)	3σ 1800 sec (%)	LD mass defect (%)	3σ 1800 sec (%)	LD mass defect (%)	3σ 1800 sec (%)
0.0%	7.7%	0.0%	7.8%	0.0%	6.9%	0.0%	7.6%
-4.3%	7.7%	-3.0%	7.8%	-4.5%	6.9%	-3.1%	7.6%
-6.9%	7.7%	-6.4%	7.9%	-4.5%	6.9%	-6.1%	7.6%
-9.9%	7.8%	-9.3%	7.9%	-8.3%	6.9%	-9.2%	7.6%
-12.3%	7.8%	-12.7%	8.0%	-12.8%	6.9%	-12.3%	7.6%
-16.4%	7.9%	-15.3%	8.1%	-15.6%	6.9%	-14.7%	7.6%

Table 7. Analyzed mass defects for the partial defect cases and their uncertainties.

The slope of the linear fit forced through the origin when plotting the LD mass defect (%) vs. the number of substituted pins gives the % defect per pin and can be used to determine the number of pins that would need to be diverted before rising above the 3σ level. For each technology investigated the sensitivity to partial defects is shown in Table 8.

Detector	Diverted Pin Sensitivity (# of pins)	Analyzed Mass Defect (%)	1800s 3σ Uncertainty (%)
UNCL	29	9.6%	9.4%
INL - ^{4}He	25	8.1%	7.9%
LLNL - Stilbene	19	7.3%	7.1%
UM - EJ309	18	7.0%	7.0%
ORNL - ^{10}B Straws	19	7.7%	7.7%
LANL - ^{10}B Plates	21	8.5%	8.2%
ORNL - PSD Plastic	19	7.2%	6.9%

Table 8. The partial defect sensitivies of each design based on the assay uncertainty.

There is clear improvement in the PD sensitivity over the standard UNCL with any of the new detection technologies. While these results along with those from the un-poisoned in-tact fuel are encouraging and provide confidence that improvement to the standard UNCL can be achieved with these new materials, the more pressing challenge is to make significant improvement in the assay of poisoned fuel.

3.4. Fast Mode Poisoned Fuel

The problem of accurate and independent assay of fuel containing burnable poisons is quickly becoming a major issue in international safeguards as evidenced by resource investments by inspectorates to solve this problem [27][28]. Especially as commercial fuel designers are using higher concentrations of these burnable poisons. For the Rodeo examination of this capability, the teams were asked to simulate fuel poisoned with Gadolinium (Gd). There are, of course, other poisons in use but Gd is the most widely used today. Similar to what was done with the PD testing, six different fuel designs were provided as shown in Figure 22.

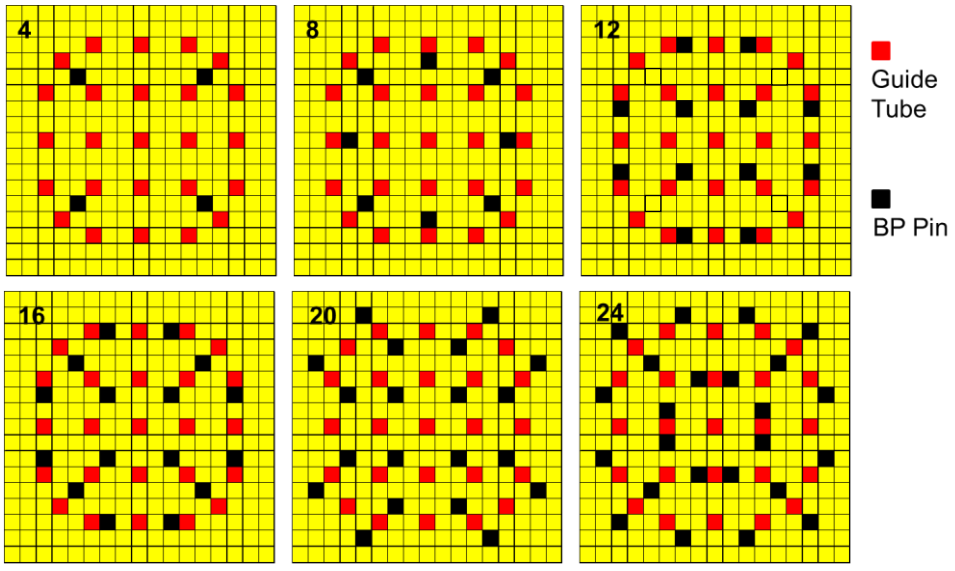

Figure 22. Fuel assembly patterns for testing of burnable poisons.

As can be seen, the numbers of poisoned pins simulated were 4, 8, 12, 16, 20, and 24 and the concentration of Gd was varied at three different levels: 6%, 8%, and 10%. Each group simulated the Fast Mode by placing a thermal neutron absorber around the cavity of the detector. Most groups chose to use Cadmium curtains as is used in the standard UNCL in practice. One group (ORNL - ^{10}B Straws) chose to use Gadolinium as the curtain material as it has a higher thermal neutron absorption cross section (see Figure 2) but also removes epi-thermal neutrons at the exact energies where the poison in the fuel is most reactive, thus, further lowering the sensitivity to the poison. The mass defects for the set of poisoned fuel assemblies for each technology is shown in Table 9. While the general trend is for the mass defect to rise with increasing Gd it is not true in all cases for all detectors. It is seen within the data that there are examples where added poisoned pins results in a decrease of the mass defect; such as for the UNCL with 6% Gd going from 12 poisoned pins to 16. The mass defect actually gets smaller, going from 4.6% to 4.2%. This is likely due to the pattern of pins having a larger effect than the number of pins, further emphasizing the fact that a single general absolute calibration for poisoned fuel is not possible.

		Mass Defects (%)						
Gd Content (%)	# of Poisoned pins	UNCL	INL - ^{4}He	LANL - ^{10}B Plates	LLNL - Stilbene	UM - EJ309	ORNL - ^{10}B Straws	ORNL - PSD Plastic
6	4	-1.9%	-8.1%	-1.9%	-1.7%	-4.7%	-1.5%	1.0%
	8	-2.9%	-8.3%	-3.6%	-4.7%	-5.0%	-2.9%	-2.1%
	12	-4.6%	-10.3%	-5.5%	-4.4%	-2.9%	-3.4%	-3.0%
	16	-4.2%	-6.4%	-6.3%	-5.3%	-3.6%	-3.5%	-2.9%
	20	-7.8%	-6.4%	-6.6%	-7.0%	-8.9%	-4.5%	-4.7%
	24	-8.2%	-9.9%	-8.0%	-4.0%	-8.5%	-5.0%	-4.8%
8	4	-1.7%	-7.8%	-2.3%	-2.5%	-5.0%	-1.2%	-1.0%
	8	-3.1%	-8.9%	-4.8%	-5.2%	-5.4%	-3.8%	-2.0%
	12	-5.2%	-11.2%	-6.3%	-5.2%	-5.4%	-3.7%	-7.1%
	16	-4.9%	-7.7%	-6.7%	-5.9%	-6.6%	-3.4%	-5.4%
	20	-10.5%	-6.8%	-8.0%	-7.9%	-9.8%	-4.6%	-7.9%
	24	-10.1%	-8.5%	-9.7%	-4.0%	-10.4%	-5.7%	-9.0%
10	4	-2.4%	-8.6%	-2.8%	-2.3%	-5.8%	-1.1%	1.5%
	8	-4.4%	-10.2%	-5.2%	-5.1%	-6.6%	-2.9%	-5.3%
	12	-6.1%	-10.1%	-6.9%	-6.6%	-6.9%	-4.9%	-4.0%
	16	-6.6%	-7.7%	-7.6%	-7.9%	-7.1%	-5.2%	-5.4%
	20	-10.9%	-9.3%	-9.2%	-8.4%	-12.3%	-6.8%	-5.3%
	24	-11.9%	-6.2%	-11.5%	-7.9%	-11.7%	-6.3%	-8.0%

Table 9. Mass defects due to burnable poisons.

The data in Table 9 shows the percentage of mass that is unaccounted for without correcting for the presence of the burnable poisons and that it can be large even in the Fast Mode. Though there are some obvious improvements relative to the UNCL especially at the higher poison loadings for the LLNL – Stilbene detector, the ORNL – ^{10}B Straws, and the ORNL – PSD Plastic. A plot of all the data displayed in Table 9 is show in Figure 23. The smaller the mass defect for a given fuel design the less sensitive the detector design is to the presence of the burnable poison.

For general comparison, the same mass defects for all technologies in the Thermal Mode range from ~10% - 55% for these same fuel assembly definitions, obviously quite a bit larger. There was, however, one notable exception in the Thermal Mode and that was for the INL – 4He detector which

had mass defects in the 5% - 25% range. This further demonstrates the importance of moderation on the sensitivity to burnable poisons.

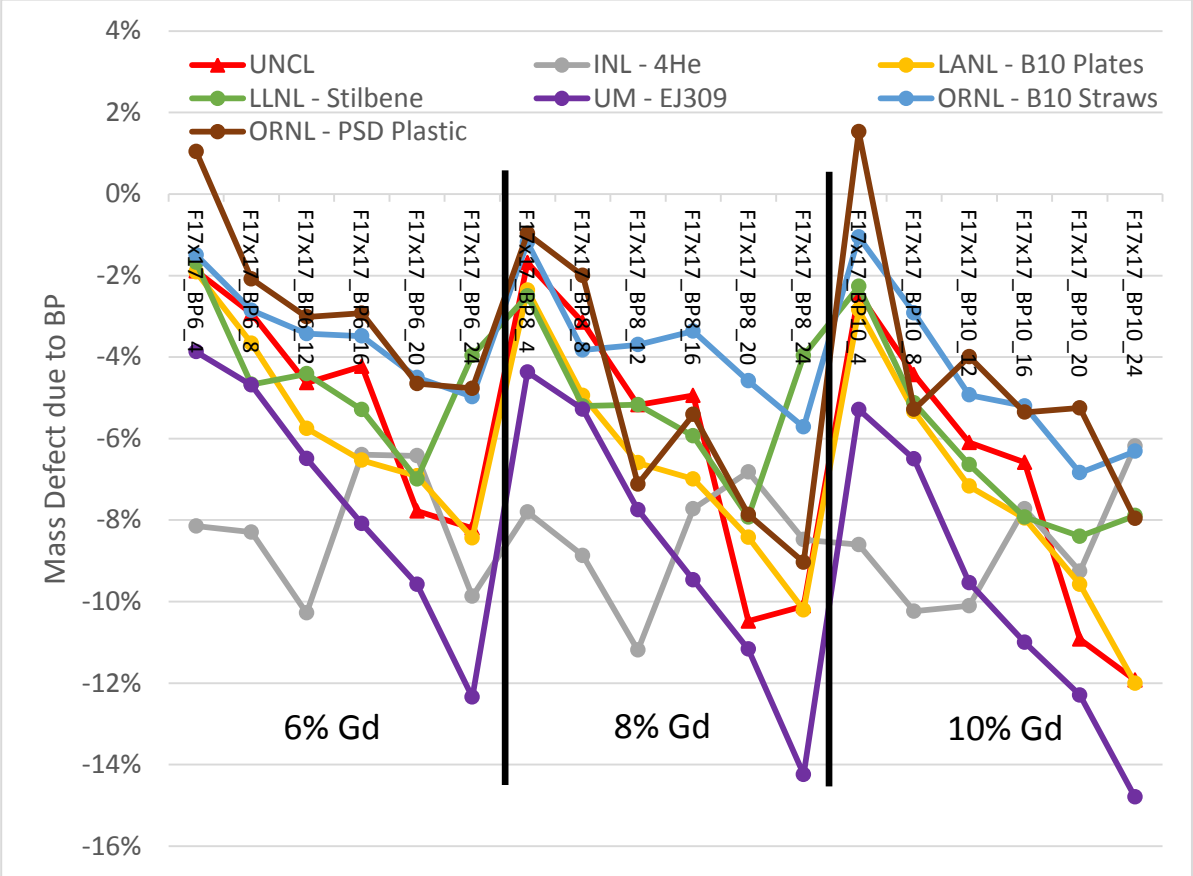

Figure 23. Burnable poison impacts of the mass defects in Fast Mode.

Another way to look at the sensitivity of the detector design to burnable poisons is to determine if the assayed mass is within three standard deviations of the declared value. That will demonstrate if the measurement is sensitive to a mis-declaration of the fuel assembly as being unpoisoned. That is, without correcting for the burnable poison content, would the assay result pass the 3σ test? Table 10 shows the results of that analysis for the 18 poisoned fuel assembly designs. In the “Random Error” column only the Doubles error and the calibration constant uncertainties are propagated into the mass uncertainty. In the “Random + 2% Systematic” column a 2% systematic error is also folded into the mass uncertainty. While it is clearly not known what the actual systematic uncertainty for a UNCL based on each detector material would be, this at least gives an idea of the impact. The data in Table 10 shows that with only the counting and calibration uncertainties, there is clear improvement for several of the technologies relative to the UNCL, however with the addition of a 2% systematic uncertainty the alternate only a couple of the technologies maintain some slight advantage over the UNCL.

	# of Poisoned FAs w/ Mass Defects > 3σ	
Detector	Random Error	Random + 2% Systematic
UNCL	6	4
INL - ^{4}He	0	0
ORNL - PSD Plastic	13	4
UM - EJ309	16	6
LLNL - Stilbene	15	4
ORNL - ^{10}B Straws	6	0
LANL - ^{10}B Plates	13	5

Table 10. Sensitivity of each detector technology to mis-declared poisoned fuel.

3.5. Net Doubles Uncertainty

The last test for these technologies was the statistical uncertainty for a full assay, passive and active, with count times of 300 and 600 seconds respectively. The results are sensitive to the detection efficiency, as evidenced by the magnitude of the Net Doubles, as well as the interference of Accidental coincidences that impact the precision of the Doubles rate. The Net Doubles and uncertainties from a passive and active assay of the 55 g/cm calibration fuel assembly are shown in Table 11 for both the Fast and Thermal modes. For a given mode the technologies are ordered by the relative Doubles uncertainty from lowest to highest after the UNCL to show which detectors have the best precision. In general the fast neutron detector types typically have the better result though not always the highest efficiency as is seen in the Net Doubles column.

	Fast Mode		
Detector	Net Doubles (1/s)	σD (1/s)	σD (%)
UNCL	16.7	0.5	2.9%
INL - ^{4}He	22.6	0.2	0.9%
ORNL - PSD Plastic	23.2	0.3	1.4%
UM - EJ309	28.3	0.4	1.2%
LLNL - Stilbene	19.5	0.3	1.6%
LANL - ^{10}B Plates	49.3	1.2	2.4%
ORNL - ^{10}B Straws	17.6	0.5	2.6%

	Thermal Mode		
Detector	Net Doubles (1/s)	σD (1/s)	σD (%)
UNCL	225	1.5	0.65%
ORNL - PSD Plastic	220	0.7	0.3%
LLNL - Stilbene	149	0.6	0.4%
ORNL - ^{10}B Straws	236	1.3	0.5%
LANL - ^{10}B Plates	426	2.4	0.6%
INL - ^{4}He	35.3	0.2	0.7%
UM - EJ309	287	3.1	1.1%

Table 11. The Net Doubles and uncertainties based on 300 second passive and 600 second active measurements.

Of interest in the context of the Net Doubles precision is the total measurement time required for a Fast Mode assay to achieve the same precision as the standard UNCL achieves in a 15 minute Thermal Mode assay (5 minutes passive and 10 minutes active). Assuming an active assay that is always twice the duration as a passive assay, the total measurement time to reach the 0.65% Net Doubles uncertainty of the UNCL Thermal Mode assay for all detector technologies is shown in Table 12.

	Fast Mode				
Detector	Net Doubles (1/s)	σD (1/s)	σD (%)	Total Time (hours) to reach UNCL Thermal Mode precision of 0.65%	Optimized Active:Passive Count Times
UNCL	16.7	0.109	0.65%	4.48	4 : 1
INL - ^{4}He	22.6	0.148	0.65%	0.46	4 : 1
ORNL - PSD Plastic	23.2	0.151	0.65%	1.10	2 : 1
UM - EJ309	28.3	0.185	0.65%	1.29	1.4 : 1
LLNL - Stilbene	19.5	0.127	0.65%	1.45	1.3 : 1
ORNL - ^{10}B Straws	17.6	0.115	0.65%	1.93	2 : 1
LANL - ^{10}B Plates	49.3	0.322	0.65%	3.21	4 : 1

Table 12. Needed total assay times in Fast Mode to reach the Net Doubles precision attained by the UNCL in a 15 minute Thermal Mode assay.

In the Rodeo, the Passive and Active count times for determining the Net Doubles precision were set to 300 s and 600 s respectively. While these are the typical count times used in the field, this 2:1 ratio may not always be optimal. The last column in Table 11 illustrates how the ideal ratio between the Active and Passive count times can be different for each technology.

3.6. Cost and Size

Lastly the groups were asked to estimate the cost, dimensions, and weight of a potential fieldable instrument. Those estimates are provided in Table 13 and illustrate the competitiveness of the technologies to the current UNCL. It is anticipated that the cost of the Stilbene crystals will continue to come down in price as the market expands.

Detector Material	Outside Dimensions (cm)	Weight (kg)	Cost ($k)
UNCL	42 x 42 x 51	38	$150
ORNL - ^{10}B Straws	52 x 49 x 50	70	$120
INL - ^{4}He	50 x 50 x 70	200	$100
LLNL - Stilbene	66 x 53 x 40	78	$305
LANL - ^{10}B Plates	50 x 56 x 51	72	$70
ORNL - PSD Plastic	68 x 54 x 40	48	$150
UM - EJ309	80 x 60 x 40	78	$145

Table 13. Estimated cost and physical attributes of instruments and data acquisition electronics based on the detector materials considered in the Rodeo.

4. Conclusions

The Advanced Neutron Detection Technology Rodeo explored many of the new and newly commercially available technology in the context of an important challenging problem for international safeguards in the assay of fresh nuclear fuel containing burnable poisons. Teams that have been researching these materials were asked to create a Monte Carlo model of a UNCL-like instrument that could potentially replace the standard UNCL in both form and function. In order to compare the different technologies in a fair test, identical sets of fuel assembly definitions were provided to each team and they were asked to simulate their instrument response in MCNP. As a way to compare to the current industry standard for these types of measurements, a non-participating researcher performed the same set of calculations with a model of the standard UNCL.

The ORNL ^{10}B Straws group explored and exploited the idea of spectrum tailoring to boost the performance of their design. The use of Gadolinium to achieve a Fast Mode interrogation flux with depressions at the resonance energies where the poison in the fuel is most sensitive helps minimize the sensitivity to its presence. In addition, the borated polyethylene on the wings of the AmLi source slab reduces the contribution of the source neutrons to the Accidental coincident rate thereby improving the Doubles precision. These improvements could be implemented in other instrument designs.

While the previous sections have shown that improvements over the standard UNCL can be seen with various detector technologies there was no single technology that demonstrated a consistent and substantial improvement. Though it is clear that the fast detection technologies offer promise towards improvement on Fast Mode assay of fresh fuel, the information gathered for this Rodeo effort fell short of providing a clear path forward with any single material. Further investigation and development of these fast neutron detector technologies is needed – keeping in mind the need for simplicity of implementation and data analysis. The reduction in the required count time to achieve Thermal Mode counting statistics in the Fast Mode is very encouraging.

One of the constraints placed on the participants of the Rodeo was that each technology's data analysis was required to produce information that could be used to conduct an assay the way they are currently conducted, i.e. the use of a Net Doubles rate to determine the ^{235}U linear density. This would allow a technology to be used by international safeguards inspectorates without much deviation from what is currently done. In practice, the methods used by the fast neutron technologies to determine a Doubles rate would necessarily be different from the neutron capture based technologies. In MCNP-space, the determination of the coincidence rate for the thermal neutron capture based technologies is more straightforward relative to the fast neutron scattering technologies. In these Rodeo results it is assumed that the interpretation of the MCNP based responses of the fast neutron detectors has provided accurate Doubles rates that have been corrected for cross-talk and have solid experimental benchmarks. Furthermore, what is also encouraging is the knowledge that some of these technologies reach into physics that are not possible with the standard UNCL. Thus, one can imagine that there are clever and, as of yet, unrealized ways to look at fresh fuel assay with burnable poisons that may be able to realize the goal of timely, accurate, and independent assay of such fuel.

The logical next steps for this area of investigation would be to focus more effort towards spectrum tailoring to minimize, to the extent possible, the sensitivity to burnable poisons; primarily focusing on the fast neutron detector materials as they provide the best counting statistics when measuring in the Fast Mode. In addition, development of data reduction techniques that are robust, can be automated, and do not require frequent recalibration is essential.

5. References

[1] Menlove H.O. et al.; *Neutron Collar Calibration and Evaluation for Assay of LWR Fuel Assemblies Containing Burnable Neutron Absorbers*; LA-11965-MS (ISPO-323); Los Alamos National Laboratory; 1990

[2] Goorley J.T. et al.; *Initial MCNP6 Release Overview - MCNP6 version 1.0*; LA-UR-13-22934; Los Alamos National Laboratory; 2013

[3] Croft S.; Favalli A.; Swinhoe M.T.; Rael C.D.; "State of the Art Monte Carlo Modeling of Active Collar Measurements and Comparison with Experiment," LA-UR-11-03760, *Proc. 52nd Annual INMM Meeting*, 2011

[4] Zaitseva N.; Rupert B.L.; Pawelczak I.; Glenn A.; Martinez H.P.; Carman L.; Faust M.; Cherepy N.; Payne S.; *Plastic Scintillators with Efficient Neutron/Gamma Pulse Shape Discrimination*; *Nucl. Inst. Meth. Phys. Res. A;* vol 668; 2012; p 88-93

[5] Hausladen P.A.; McElroy R.D.; Newby J.; *Active-Well Counting Using New 'PSD Plastic' Detectors*; ORNL/TM-2015/651; Oak Ridge National Laboratory; 2015

[6] Rossi B.B.; Staub H.H.; *Ionization chambers and counters: Experimental techniques*; McGraw-Hill Book Company, Inc.; 1949

[7] Bell Z.W.; Buckner M.A.; Smith D.B.; *A ^{10}B-based Solid State Thermal Neutron Detector*; *Proc. 37th Annual INMM Meeting*; Naples; Florida; USA; July 28 – August 1; 1996; p 414-419

[8] Lacy J.L.; Athanasiades A.; Martin C.S.; Sun L.; Vazquez-Flores G.L.; *The Evolution of Neutron Straw Detector Applications in Homeland Security*; *IEEE Transactions on Nuclear Science*; vol 60; 2013; p 1140-1146

[9] Henzlova D. et al.; *Integrated Test and Evaluation of 3He Replacement Technologies for Safeguards and Nonproliferation Applications – boron-based HLNB counter field trial*; LA-UR-15-27844 ver. 3; Los Alamos National Laboratory; 2015

[10] Henzlova D.; Menlove H.O.; *Integrated Test and Evaluation of 3He Replacement Technologies for Safeguards and Nonproliferation Applications – boron-based HLNC-B counter build*; LA-UR-13-27499; Los Alamos National Laboratory; 2013

[11] Menlove H.O.; Henzlova D.; *Improvements in Boron Plate Coating Technology for Higher Efficiency Neutron Detection and Coincidence Counting Error Reduction*; LA-UR-16-26496; Los Alamos National Laboratory Report; 2016

[12] Kelley R.; Enqvist A.; Jordan K.; *Pulse Shape Discrimination in Helium-4 Scintillation Detectors*; *Nucl. Inst. Meth. Phys. Res. A*; vol 830; 2016; p 44-52

[13] Kelley R.P.; Rolison L.M.; Lewis J.M.; Murer D.; Massey T.N.; Enqvist A.; Jordan K.A.; *Neutron response function characterization of 4He scintillation detectors*; *Nucl. Inst. Meth. Phys. Res. A*; vol 793; 2015; p 101–107

[14] Chandra R.; Davatz G.; Friederich H.; Gendotti U.; Murer D.; *Fast Neutron Detection with Pressurized 4He Scintillation Detectors;" J. Instr.;* vol 7; 2012

[15] Prasad M.; Shumaker D.; Snyderman N.; Verbeke J.; Wong J.; *Prototype Stilbene Neutron Collar*; LLNL-TR-707598; Lawrence Livermore National Laboratory; 2016

[16] Verbeke J. M.; *Customized MCNPX to Generate "List-Mode" 3He Neutron Captures and Scintillator Counts*; LLNL-TM-671194; Lawrence Livermore National Laboratory; 2015

[17] Hansen W.; Richter D.; *Determination of light output function and angle dependent correction for a stilbene crystal scintillation neutron spectrometer*; *Nucl. Inst. Meth. Phys. Res. A*; vol 476; 2002; p 195-199

[18] Di Fulvio A.; Shin T.H.; Jordan T.; Sosa C.; Ruch M.L.; Clarke S.D.; Chichester D.L.; Pozzi S.A.; *Fast Neutron Multiplicity Counter for the Assay of Plutonium Metal Plates*; *Nucl. Inst. Meth. Phys. Res. A*; vol. 855; pgs. 92-101; 2017

[19] Shin T.H.; Di Fulvio A.; Jordan T.; Chichester D.L.; Clarke S.D.; Pozzi S.A.; *Fast Neutron Multiplicity Counter Based on Stilbene and EJ-309 Scintillators for Nuclear Non-Destructive Assay; Proc. 57th Annual INMM Meeting*; Atlanta; 2016

[20] Polack J.K.; Flaska M.; Enqvist A.; Sosa C.S.; Lawrence C.C.; Pozzi S.A.; *An Algorithm for Charge-Integration; Pulse-Shape Discrimination and Estimation of Neutron/Photon Misclassification in Organic Scintillators*; *Nucl. Inst. Meth. Phys. Res. A*; vol. 795; 2015; p 253-267

[21] *International Target Values 2010 for Measurement Uncertainties in Safeguarding Nuclear Materials*; IAEA STR-368; Vienna; Austria; 2010

[22] Hausladen P.; Newby J.; McElroy R.; *Simulations of a PSD Plastic Neutron Collar For Assaying Fresh Fuel*; ORNL/TM-2016/680; Oak Ridge National Laboratory; 2016

[23] Hansen W.; Richter D.; *Determination of Light Output Function and Angle Dependent Correction for a Stilbene Crystal Scintillation Neutron Spectrometer*;" *Nucl. Inst. Meth. Phys. Res. A*; vol 476; 2002; p 195 - 199

[24] Pozzi S.A.; Clarke S.D.; Walsh W.; Miller E.C.; Dolan J.L.; Flaska M.; Wieger B.M.; Enqvist A.; Padovani E.; Mattingly J. K.; Chichester D.; Peerani P.; *MCNPX-PoliMi for Nuclear Nonproliferation Applications*; *Nucl. Inst. Meth. Phys. Res. A*; vol. 694; 2012; p 119-125

[25] Miller E.C.; Clarke S.D.; Flaska M.; Pozzi S.A.; Padovani E.; *MCNPX-PoliMi Post-Processing Algorithm for Detector Response Simulations*; *Jour. Nucl. Mat. Mgmt.*; vol. 40-2; 2012; p 34-41

[26] Reilly; D.; Ensslin; N.; Smith; H.; Kreiner; S.; *Passive Nondestructive Assay of Nuclear Materials*; United States Nuclear Regulatory Commission; LA-UR-90-732; NUREG/CR-5550; 1991; p 477

[27] Lee T.H.; Tomanin A.; Beaumont J.; *Liquid Scintillator-Based Fast Neutron Coincidence Counter for Fresh Nuclear Fuel Measurements*; American Nuclear Society; Advances in Nuclear Nonproliferation Technology and Policy Conference; Santa Fe; 2016

[28] Evans L.G.; Swinhoe M.T.; Menlove H.O.; Schwalbach P.; DeBaere P.; Browne M.C.; *A New Fast Neutron Collar for Safeguards Inspection Measurements of Fresh Low Enriched Uranium Fuel Assemblies Containing Burnable Poison Rods*; *Nucl. Inst. Meth. Phys. Res. A*; vol 729; 2013; p 740 – 746

LA-UR-17-23356

The Optimization and Calibration of the AWCC Using 252Cf Interrogation and the Comparison with an AmLi Neutron Source

H. O. Menlove, C. D. Rael, and J. B. Marlow
Los Alamos National Laboratory, Group NEN-1

Abstract

The Active Well Coincidence Counter (AWCC) has been used for national and international nuclear materials accountancy and safeguards inspections for more than 3 decades to measure the ^{235}U mass in bulk uranium samples. The AWCC uses active neutron interrogation with an Americium-Lithium (AmLi) neutron source. The AmLi neutrons induce fission reactions in the sample, and the resulting fission reaction neutrons are measured using ^{3}He detectors in a well-type geometry. The purpose of this paper is to provide information on the modifications to the AWCC for the use of ^{252}Cf interrogation sources instead of AmLi sources. The AmLi neutron sources that have been used for the AWCC and other active neutron interrogation instruments are no longer commercially available, and alternative neutron sources are needed. The ^{252}Cf sources provide the benefit that the interrogation source emits multiple neutrons per spontaneous fission that are time-correlated with the induced fission (IF) reactions in the sample. This increases the doubles signal and reduces the statistical uncertainty. This time correlated induced fission (TCIF) method makes use of the ^{252}Cf sources that are readily commercially available with the advantage of lower cost, and a radioactive level in the tens of micro-curie range compared with the AmLi neutron source in the curie range. This paper details the AWCC detector modifications for using ^{252}Cf in lieu of AmLi, including detector parameters such as dead-time, die-away time, efficiency, and calibration coefficients. Also, included in the paper is a direct measured comparison of ^{252}Cf with a standard AmLi source for a range of uranium samples to illustrate the improvement in the statistical uncertainty.

***Key Words**: neutron interrogation, active well coincidence counter, uranium assay*

1. Introduction

The Active Well Coincidence Counter (AWCC) [1] has been used for national and international nuclear material accountancy and safeguards inspections for more than 35 years to measure the ^{235}U mass in bulk uranium samples [2]. Modifications to the AWCC have also been used for the verification of fresh research reactor fuel [3]. The AWCC uses active neutron interrogation with an Americium-Lithium (AmLi) neutron source. The neutrons that are emitted randomly in time induce fission reactions in the sample, and the resulting fission reactions are measured using ^{3}He detectors in a well-type geometry. The purpose of this paper is to detail the modifications to the AWCC for the use of ^{252}Cf interrogation sources instead of AmLi sources. The AmLi neutron sources that have been used for the AWCC and other active neutron interrogation instruments are no longer readily available commercially, and alternative neutron sources are needed. The ^{252}Cf sources provide the benefit that the interrogation source emits multiple neutrons per spontaneous fission that are time-correlated with the induced fission (IF) neutrons in the sample. This increases the doubles signal and reduces the statistical uncertainty. The time correlated induced fission (TCIF) method [4] makes use of the ^{252}Cf sources that are readily commercially available with the advantage of lower cost, and a radioactive level in the tens of micro-curie range compared with the AmLi neutron source in the curie range. However, the relatively short half-life of the ^{252}Cf source (2.64

years) requires source replacement after about ten years and which will lessen the cost advantage. Prior AWCC systems used two AmLi sources of ~ 1.1 Ci each to provide a neutron yield of ~ 4.5×10^4 n/s each; whereas, a 10 µCi ^{252}Cf source yields 4.4×10^4 n/s. For the measurements presented in this paper, the ^{252}Cf source strength was ~ 400µCi (on 10/1/2015), so the source will have an adequate neutron yield for AWCC applications for more than 15 years. Three AWCCs have been fabricated by commercial vendors for the future use at the China Safeguards Center of Excellence for Nuclear Security (COE) [5].

This paper provides the AWCC detector modifications for using ^{252}Cf in lieu of AmLi including detector parameters such as dead-time, die-away time, efficiency, and calibration coefficients. Also, included in the paper is a direct measured comparison with the standard AmLi source (MRC-95) to compare the statistical precision of the two methods.

2. Time correlated interrogation concept

In the TCIF method, the sample is interrogated with neutrons from the ^{252}Cf source; however, the measured doubles rates are enhanced because the IF neutrons are also time correlated with the ^{252}Cf spontaneous fission (SF) interrogation source. Thus, the trigger events that initiate the coincidence gates can originate from either the SF and/or the IF neutrons. This higher effective average □is the basis of the improved precision for the TCIF method. The measured multiplicity rates (doubles and triples) increase rapidly with the effective □□(average neutrons per fission in the time gate). The average □ of the ^{252}Cf source is 3.76 and the induced fission □ for ^{235}U is 2.44, so the combined effective □ is higher than for random neutron interrogation; however, only a fraction of the time correlated neutrons are measured. This higher effective □significantly increases the multiplicity counting rates and improves the statistical precision.

There are three probabilities that come into play in the TCIF method:

1. The probability of a ^{252}Cf SF neutron inducing a fission reaction, primarily related to the physical coupling between the ^{252}Cf and the sample
2. The probability of counting at least one of the IF neutrons in the detector
3. The probability of counting at least one of the ^{252}Cf background neutrons in the detector.

The first coupling probability is a function of the separation distance between the ^{252}Cf source and the sample, the high density polyethylene (HDPE) moderator, the sample size and fissile mass, and any potential absorbers of the thermal neutrons in the sample such as ^{238}U. The probability for a least one ^{252}Cf source neutron causing an IF we can define as P_{IF}. It is a variable that can be determined from physical standards or MCNP calculations.

The second probability for measuring at least one of the IF neutrons depends on the detector efficiency for neutrons born at the sample location. For the modified AWCC used in these experiments, the measured efficiency was 38.2% for the sample position. Thus, each of the IF neutrons have a 38.2% chance of being detected, so the combined probability for the 2.44 neutrons that at least one of the neutrons is detected is equal to [6]

$$P_d = 1 - (1 - e)^{2.44} = 1 - (1 - 0.382)^{2.44} = 0.691,$$

where e is the detection efficiency.

The third probability, of measuring the ^{252}Cf neutrons is a function of the coupling of ^{252}Cf source relative to the detectors. Because this is measured without a sample, we call it the background efficiency. For the modified AWCC, the efficiency for the ^{252}Cf source in the bottom HDPE end plug was 26.3% and □is

3.76. Thus, the probability of measuring at least one neutron from a single spontaneous fission event would be

$P_{cf} = 1- (1- e)^{3.76} = 1- (1- 0.263)^{3.76} = 0.683.$

Note that the ^{252}Cf spontaneous fission emits an average of 3.76 neutrons, and when more than one of these SF neutrons cause an IF, the correlated measured doubles increase significantly regardless of the other two probabilities (items 2 and 3 above).

The three probabilities all combine in determining the doubles rate boost from the TCIF method. For the AWCC, the limiting factor in the combined probabilities is the coupling probability because the relatively small sample only reacts with a minor fraction of the ^{252}Cf spontaneous neutrons because of the small sample size.

The TCIF method has a longer die-away time than for the random neutron AmLi source interrogation. This longer die-away time is a combination of the detector specific die-away (~ 70 µs for the AWCC) and the die-away time (~ 80 µs) of the thermal-neutrons that cause the IF reactions. Thus, to have our gate interval include both SF and correlated IF, we need to open the gate to more than 100 µs. However, the statistical error is a function of the accidental counts (A) pileup, and a longer gate will make the A related error larger. An analysis of the data indicated that a gate length of 128 µs was near optimum.

3. Background Subtraction

There are neutron backgrounds that need to be subtracted from the active neutron measurement as follows:

1. Neutrons from the ^{252}Cf source (doubles and singles) (for no ^{235}U)
2. Neutrons from the room background (negligible for doubles but not singles)
3. Passive neutrons from the uranium sample (negligible)

Only the first of these backgrounds is significant for the high yield ^{252}Cf sources that are used in the COE AWCCs.

During the initial design of the AWCC [1], ^{252}Cf was discounted because of concerns about the doubles background from the ^{252}Cf source. The TCIF benefit in increasing the IF doubles above the SF background was not identified at the time.

The ^{252}Cf interrogation source background is impacted by the sample inside the detector because of neutron scattering from the sample and fast neutron fission in the ^{238}U. Thus, a dummy sample that contains no fissile mass was used for the background measurement. The background from fast-neutron fission in the ^{238}U component of the sample was determined by extrapolating the doubles response curve to zero fissile mass. The ^{252}Cf background was measured overnight so that its statistical error was negligible. For the present sample range (1-190 g ^{235}U) the ^{252}Cf source background is larger than the IF signal so care must be taken in measuring this background.

4. System description and optimization

The AWCC shown in Fig.1 consists of a well-type HDPE moderator containing 42 3He tubes at 4 atm. pressure.[1] Measurements were made with both the ANTECH [7] and Canberra [8] AWCC systems

with no significant differences in their performance. However, the ANTECH AWCC has an attachment to the electronics junction box that contained a pulse de-randomizer to reduce the dead-time.

Fig. 1 Photo of one of the COE AWCC systems (left) with the 3He tubes removed (right) to show the HDPE moderator design.

To obtain optimum performance of the AWCC for low mass samples, thermal-neutron interrogation was used. The modifications to the AWCC included removing all Cd and the Ni annulus. The HDPE rings on both the top and bottom plugs were also removed to obtain a higher counting efficiency at the sample position. Figure 2 (left) shows the AWCC sample cavity with the Cd and HDPE rings removed from the bottom and top lid.

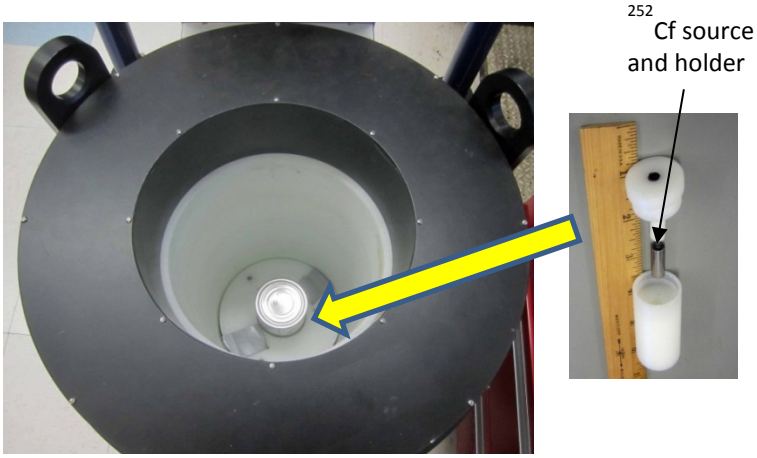

Fig. 2. Photo of the AWCC system with a sample can in the cavity (left) and the ^{252}Cf source holder that is inserted in the end plug (right).

Measurements were made to determine the optimum position for the ^{252}Cf source inside the holder (Fig. 2 right). The statistical precision in the doubles rate is a function of the neutron source coupling to the sample as well as the neutron background. To determine the optimum position for the source, the statistical uncertainty was measured at different depth positions for the ^{252}Cf inside the holder. The error was determined by the “sample mode” error evaluation in the INCC data collection software [9]. Each of the source configurations were measured for at least 30x20 s cycles and the spread in the doubles data

was compared for the different positions. Figure 4 shows the doubles rate and error versus the ^{252}Cf source position in the bottom end plug, and we see that the error reduces as the source gets closer to the sample. We operated the system with the source at the minimum separations distance (1cm) with the ^{252}Cf source at the top end of the holder.

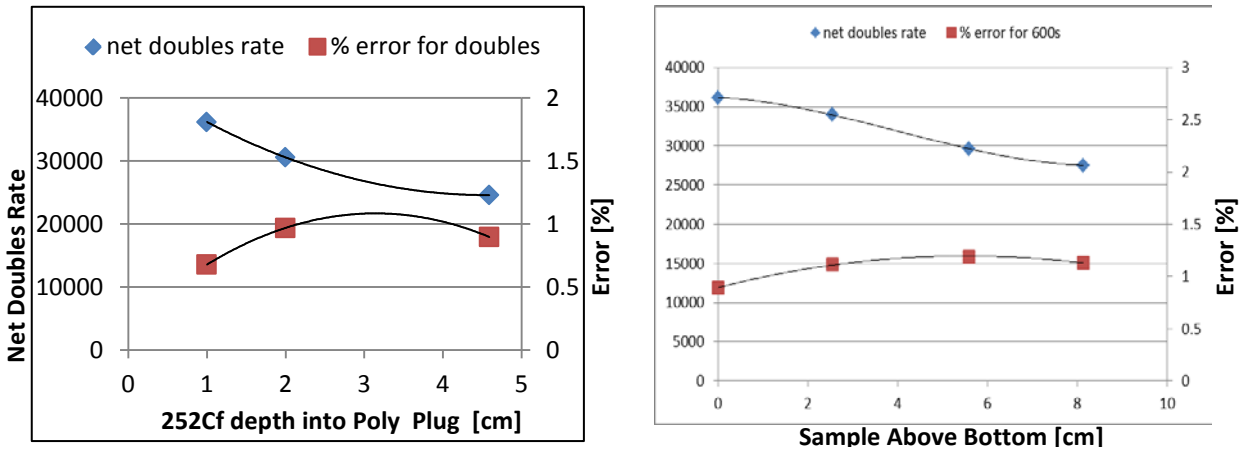

Fig. 3. The net doubles rate and statistical error as a function of the ^{252}Cf source depth into the HDPE end plug for a 600s measurement using a can of U_3O_8 powder (left) and statistical error as a function of the height above the bottom (right).

The doubles error for a 600s measurement was less than 1% for all of the measured positions. The sample measurements described above were used to optimize the configuration of the AWCC that were as follows:

1. No Cd liners or Ni annulus
2. Both HDPE rings on the end plugs removed
3. The maximum sample cavity height was the standard 20cm
4. Only one ^{252}Cf source positioned in the bottom plug (i.e. no source in the lid)
5. The ^{252}Cf source holder was set flush with the bottom end plug.

To evaluate the change in the doubles rate and error as a function of the height of the can above the cavity bottom, measurements were performed for different can heights. Figure 3 (right) shows the change in the doubles rate as a function of the sample height as well as the error in 600s for the different positions. The can used for the position optimization contained 186g of ^{235}U and had a diameter of 7.6cm and a height of 8.6cm containing a powder mass of 230g. The optimal sample position was determined to be sitting on the bottom of the sample cavity.

4.1 Detector Parameters Electronics Set Up

The neutron data was collected using a JSR-15 shift register [10] and a laptop computer. The INCC software was used with the HV at 1680V, pre-delay of 2.5 μs, gate of 128 μs. The dead time was measured using the 2 source method [3] with the combined rates of ~500,000 cps. Note that we used b = $a^2/4$ and multiplicity dead time = a/4. The results gave an a value of 0.757 μs for the Canberra units and 0.28 μs for the Antech detector.

5. Measurement Procedures and sample description

The samples that were used for the optimization study included the U_3O_8 powder mixtures of the type being supplied to the COE. All the samples contained 230g of powder with enrichments varying from 0.31% to 93%. The sample cans were 7.6cm diameter and 8.6cm tall. The enrichments ranged from 0.31% to 93% ^{235}U, and the ^{235}U mass varied from 0.0g to 181.1g.

The measurement procedure was to place the sample can on the HDPE bottom end plug and take a minimum of 30 cycles of 20s each for 600s total time. In some case much longer measurements were performed to better determine the statistical error. All errors in the tables have been normalized to 600s for comparison purposes. The singles and doubles backgrounds were measured with the blank (dummy) sample in the detector. The dummy sample had the same total mass as the calibration samples, but contained no fissile material. The room backgrounds were negligible because of the high source yield from the source FTC-CF-2494 (1.422E+06 n/s on 10/1/2015).

6. Measurement Results

Table 1 presents the calibration data and the statistical errors for a 600s measurement for the ANTECH AWCC. The doubles background was determined to be 81700cps and the singles was 378600cps by a long overnight measurement using a dummy sample that contained no ^{235}U. The doubles background was also measured for the empty sample cavity and the ratio of the sample dummy to the empty case was 1.029. The statistical error in the singles and doubles background was negligible because of the long measurement time. The first 3 samples in Table 1were measured twice on separate days to test the repeatability that was 1.6% in 600s.

U_3O_8 ID	^{235}U [g]	Cf gross D [cps]	Cf net D	Cf 600s sigma cps	Cf 600s sigma %	Cf net S
NBL-0075	181.09	119253	37553	425.6	1.13	38954
NBL-0074	105.22	114304	32604	359	1.1	34037
NBL-0073	38.98	103677	21977	474.4	2.16	23770
NBL-0075	181.09	118550	36850	501	1.36	38900
NBL-0074	105.22	113838	32138	416.7	1.3	34159
NBL-0073	38.98	104030	22330	416.7	1.87	23687
0005-20.06	39.1	103526	21826	326	1.49	23742
0006-52	102.4	112867	31167	425.1	1.36	33941
446-071	8.69	89114	7414	440.7	5.94	7858
295-072	5.75	86966	5266	416.8	7.92	5962
194-071	3.78	85640	3940	340.5	8.64	3235
En-0.71	1.38	83709	2009	352.5	17.55	1167
En-0.31	0.6	82500	800	389.5	48.69	500

Table 1. The ANTECH AWCC measured results for the U_3O_8 samples

We observe in the Table 1 that the doubles statistical error for a 600s measurement is ~ 1.1-1.8% for the mass range from 40-180 g ^{235}U. For mass values below ~ 10g, the error increases because of the low signal/background ratio. Note that the net doubles rate is almost the same magnitude as the net singles rate. The increase in the net doubles for the sample is a result of the time correlation between the ^{252}Cf counts and the IF reactions.

Figure 4 shows the doubles rate versus the ^{235}U mass both before and after subtracting the constant doubles background that was measured using the dummy sample. Fitting a 4th power polynomial through the data gives a zero mass intercept of 82461cps before the ^{252}Cf doubles background subtraction and 761cps after the background subtraction. This indicates that there is a fast-neutron IF component in the ^{238}U of about 761cps from the fast neutron fission in the sample that has no 235U. This component is only ~ 2-3% of the doubles rate for the higher mass samples, and it is built into the calibration function displayed on the graph.

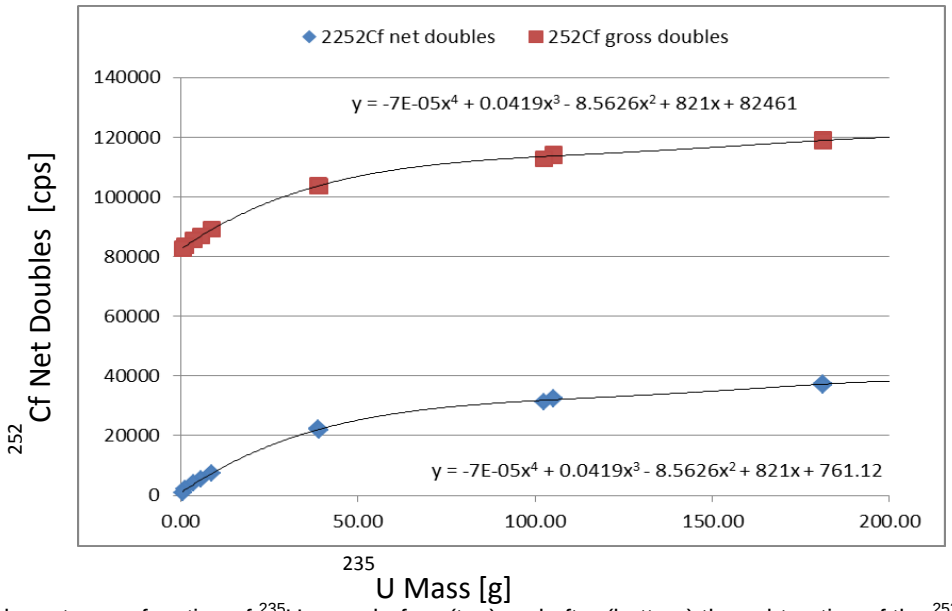

Fig. 4 The doubles rate as a function of ^{235}U mass before (top) and after (bottom) the subtraction of the ^{252}Cf background.

7. Comparison of AmLi neutron source with ^{252}Cf source interrogation

For each of the calibration sample measurements using ^{252}Cf, a similar measurement was made using the standard AmLi source MRC-95 for comparison purposes. The AmLi source was placed in the same position as the 252Cf source with the same thermal-neutron configuration of the AWCC. The same HV, gate, and pre-delay were used for the AmLi interrogation. It has been shown in the past that for neutron doubles counting, the doubles error is independent of the interrogation source strength for the case where the accidental rate dominates the statistical error [3]. Thus, the only changes were the lower neutron energy spectrum and the random source interrogation.

Table 2 presents the comparison of the ^{252}Cf results with the AmLi results after normalizing the ^{252}Cf source strength to the MRC-95 neutron yield (32620 n/s) at the time of the measurements (10/1/2015). The key observation is that the doubles rate from the normalized ^{252}Cf source is ~ 2.6 times higher per source neutron than for the AmLi source. The reason for the high net doubles rates for ^{252}Cf is that the IF reactions are time correlated with the background counts so the doubles tally in the coincidence gate gets the TCIF boost where **more than half of the net doubles originate from time correlated ^{252}Cf events.** Note that a singles background count that is time correlated with a singles neutron count from the IF in the 128us gate, results in a net doubles count for the signal. Figure 5 shows the net doubles rates after the normalization to the same source yield.

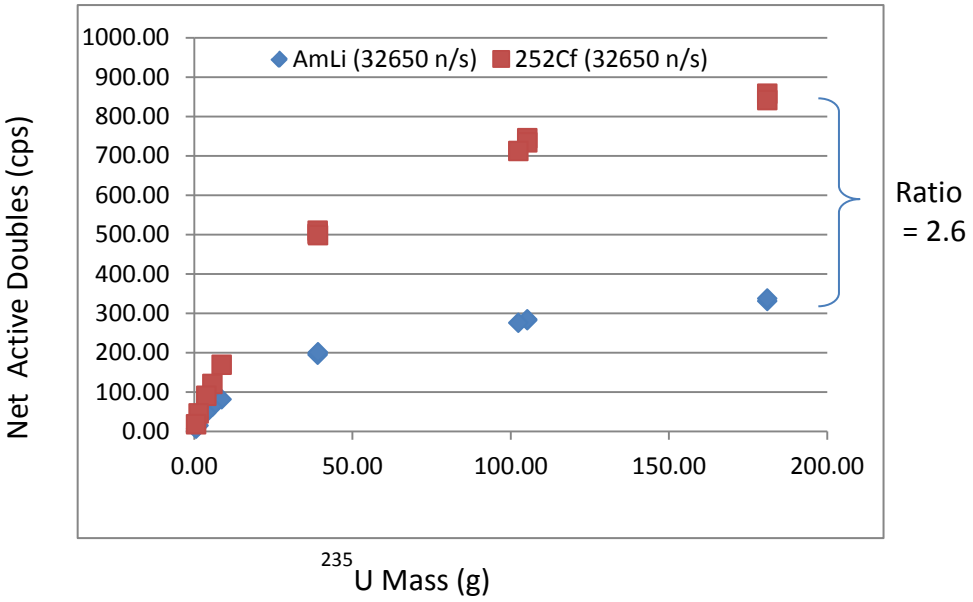

Fig. 5 Net doubles rate comparison for ^{252}Cf and AmLi after normalization to the same neutron interrogation strength.

^{235}U g g	AmLi Net S	AmLi net D	AmLi 600s D sigma %	Cf norm D 36250n/s	Cf 600s D sigma %	D Ratio Cf/AmLi
181.09	747	331.31	1.59	857.8	1.13	2.59
105.22	655	281.81	1.64	744.7	1.1	2.64
38.98	434	197.97	2.11	502	2.16	2.54
181.09	750	337.12	1.55	841.7	1.36	2.5
105.22	655	284.38	1.8	734.1	1.3	2.58
38.98	438	194.26	2.11	510	1.87	2.63
39.1	405	201.06	2.55	498.5	1.49	2.48
102.4	609	276.04	1.73	711.9	1.36	2.58
8.69	120	81.41	5.66	169.3	5.94	2.08
5.75	84	62.68	6.38	120.3	7.92	1.92
3.78	31	47.16	7.18	90	8.64	1.91
1.36	0	14.8	24.3	45.9	17.55	na
0.6	0	6.39	58.5	18.3	48.69	na

Table 2. Comparison of ^{252}Cf interrogation with AmLi random source interrogation

Another interesting result from Table 2 is that the statistical errors for the ^{252}Cf interrogation were about 30% lower than for the AmLi source interrogation in spite of the high ^{252}Cf doubles background where the signal/background ratio was ~ 1/2 for the ^{252}Cf source for the high mass sample (37553 cps versus 87700 cps in Table 1).

The theoretical statistical uncertainty for the time correlated doubles would be very complex, because the measured counts do not follow simple counting statistical theory. Thus, we have used the repeat sample based method to actually measure the spread in the data for the doubles errors in Table 2.

Table 2 shows that the Cf/AmLi doubles ratio is increasing from 1.91 to 2.6 in going from LEU samples to HEU (> 20% enrichment). This is caused by the change in the correlated coupling coefficient between the ^{252}Cf source and the sample. When the ^{238}U fraction is much larger than the ^{235}U fraction (0.31 to 4.45%) for the 5 lowest enrichment samples in Table 3, some of the thermal neutrons that provide the IF in the sample are lost to parasitic absorption in the ^{238}U. For the HEU, the fractional loss to ^{238}U becomes negligible, and the ratio of the Cf/AmLi doubles is rather constant at ~ 2.6 for the AWCC.

8. Summary

The conversion of the AWCC from the typical AmLi neutron interrogation source to a 252Cf source was necessitated by the lack of commercially available AmLi sources. This paper presented the detector configuration for optimizing the AWCC for using ^{252}Cf, and also the improvement in the statistical performance. After the optimization of the AWCC for the ^{252}Cf source use, the doubles statistical error was about 1.2% for a 600s measurement of a 100g ^{235}U sample. This was about 30% lower than for the AmLi source interrogation with both sources in the thermal-neutron mode. The sensitivity limit of the AWCC using ^{252}Cf was ~ 1g ^{235}U. We note that the statistical uncertainty in the doubles rate tends to increase for the calculated ^{235}U mass because of the slope of the doubles calibration curve for the higher mass samples. For ^{235}U mass values above ~ 500g, the AWCC can be used in the Cd liner mode to obtain better penetration of the samples.

The primary reason for the improved statistical performance for the modified AWCC is that the neutron emission from the ^{252}Cf source is time correlated to the IF reactions in the samples. The time correlated counts fall in the coincidence gate that is selected for the doubles counts. The time gate was extended from 64μs to 128 μs to account for the two thermalization intervals (one for the IF and one for the ^{3}He tube count).

The optimization and calibration of the AWCC was performed for the ANTECH AWCC detector. The other two AWCCs (from Canberra), that are included in the COE project, were cross calibrated for efficiency and performance with the ANTECH detector. All 3 AWCC units have the same HDPE design and matched 3He tubes (4 atm), and their operating parameters are the same except for the dead-time. The dead-time difference was a result of the de-randomizing buffer in the ANTECH junction box. The high neutron emission from the COE ^{252}Cf sources require a significant dead-time correction.

This paper shows that the ^{252}Cf sources are viable replacements for the AmLi sources that are no longer commercially available. The calibration function is a polynomial that is only valid within the calibration range 1-190 g of ^{235}U. When the unknown samples are measured with the same calibration function, any error related to the doubles background subtraction cancels in the measured ^{235}U mass result. The modification to the INCC software to support the use of the ^{252}Cf sources for the AWCCs is currently in progress [11].

9. Acknowledgements

This work was supported through the Office of International Nuclear Security (NA-21) under the Office of Global Materials Security (NA-21).

REFERENCES

[1] Howard O. Menlove, *Description and Operation Manual for the Active Well Coincidence Counter*, LA-7823-M, (May 1979).

[2] R. Schenkel, et. al., *"Calibration and Experimental Comparison of the Active Well Coincidence Counter and Phonid-II*", Euratom Report, EUR 10377 EN 1986.

[3] D. Reilly, N. Ensslin, H. A. Smith, Jr., and S. Kreiner, Eds., "*Passive Nondestructive Assay of Nuclear Materials* (Washington DC, United States Nuclear Regulatory Commission", NUREG/CR-5550, LA-UR-90-732 (1991).

[4] Menlove, H.O. S.H. Menlove, and C.D. Real, *"The Development of a New Neutron Time Correlated Interrogation Method for Measurement of ^{235}U Content in LWR Fuel Assemblies"*, Los Alamos National Laboratory Report , NIM-A, *Volume 701*, *11 February 2013*, *Pages 72-79*.

[5] Marlow, J.B., "The China Center of Excellence on Nuclear Security", American Nuclear Society Topical Meeting Advances in Nuclear Nonproliferation Technology and Policy Conference, September 25-30, 2016, Santa Fe NM

[6] Private communication with Martyn Swinhoe, Nov. (2015).

[7] AWCC produced by ANTECH Corporation, 9050 Marshall Ct, Westminster, CO, www.antech-inc.com

[8] AWCC produced by Canberra Industries, 800 Research Pkwy. Meriden, Ct., www.canberra.com/contact

[9] M. Krick, W. Harker, W. Geist, and J. Longo, "*INCC Software Users Manual*", LA-UR-1—6227, March 29 (2009).

[10] JSR-15 Shift Register electronic module produced by Canberra Industries, Meriden, CT. www.canberra.com/contact

[11] Private communication with Heather Nordquist and Martyn Swinhoe, Oct. (2015).

Field test of a full scale ^{3}He-alternative HLNC-type counter: High Level Neutron counter – Boron (HLNB)

D. Henzlova[1], H.O. Menlove[1], M. Tanigawa[2], Y. Mukai[2], H. Nakamura[2]

[1]Safeguards Science and Technology Group, Los Alamos National Laboratory, Los Alamos, NM 87545, USA
[2]Japan Atomic Energy Agency, Tokai-mura, Japan

Abstract:

Thermal neutron counters developed for deployment as non-destructive assay (NDA) instruments in the field of nuclear safeguards traditionally rely on ^{3}He-based proportional counting systems. ^{3}He-based proportional counters have provided core NDA detection capabilities for several decades and have proven to be extremely reliable with range of features highly desirable for nuclear facility deployment. Facing the depletion of ^{3}He gas supply and the continuing uncertainty of options for future resupply, Los Alamos National Laboratory (LANL) designed and built a ^{3}He-free full scale thermal neutron coincidence counter based on boron-lined parallel-plate proportional technology. The counter was designed as a direct alternative to High Level Neutron Coincidence counter (HLNC-II).

This paper provides a summary of performance evaluation of HLNB under realistic field conditions at Plutonium Conversion Development Facility (PCDF) of Japan Atomic Energy Agency (JAEA). The field test included a range of low to high mass MOX materials that represent realistic process samples and provided key insight on and validation of the feasibility of HLNB as a safeguards instrument in realistic facility environment. In particular, the results of verification measurements demonstrate that HLNB is capable to satisfy ITV expected for HLNC-II-type counter of 2.1% in 300 s measurement time.

Keywords: coincidence counting; ^{3}He alternatives; boron-lined proportional counters

1. Introduction

^{3}He gas-filled proportional counters have long been the cornerstone of safeguards detection system designs due to their reliability, robustness and high neutron detection efficiency. The latter is a key requirement of correlated neutron counting utilized in non-destructive assay of special nuclear materials (SNM). Over the past decade, a reduction of ^{3}He gas supply has been increasingly apparent [1,2] and prompted a widespread effort in development of various ^{3}He-free neutron detection technologies including plastic (typically ^{6}Li-coated) or liquid scintillators, and variety of designs of gas-filled boron-lined proportional counters [3-5]. Any such technology proposed for use in nuclear safeguards is presented with series of challenges that are specific to this type of application and include high neutron detection efficiency and optimum neutron thermalization characteristics while maintaining compact footprint. Other important aspects of nuclear safeguards technology development include reliability, low maintenance requirements, reproducibility and low sensitivity to gamma-ray backgrounds that can be significant especially when measuring high mass Pu-bearing materials [5,6]. All these aspects are driven by stringent requirements on technology deployment at nuclear facilities.

In order for a detection technology to be viable for safeguards use, its design features must provide performance characteristics essential for SNM assay. To address this need, LANL has developed a full scale thermal neutron coincidence counter (High Level Neutron Counter – Boron: HLNB) based on boron-lined parallel plate technology. The underlying boron-lined technology represents a well-established proportional technology that offers similar level of maturity as ^{3}He-based proportional counters making it a suitable candidate for development of a robust detection system [7]. The HLNB

was developed with design parameters similar to ^{3}He-based High Level Neutron Coincidence Counter (HLNC-II). The HLNB was first evaluated at LANL using available neutron and gamma-ray sources [8] and subsequently evaluated for operating parameters necessary for field deployment. This paper describes the key features of HLNB and its performance under realistic field conditions at Plutonium Conversion Development Facility (PCDF) of Japan Atomic Energy Agency (JAEA). The field test was performed using range of low to high mass MOX items (5 g Pu – 1.2 kg Pu) prepared specifically for this purpose in order to assess full HLNB functionality in Pu mass assay. Details of the activities performed and performance results are described in the following sections.

2. Physics design of HLNB

Detailed description of HLNB design can be found in [8]. Here we only summarize the key features. The HLNB counter is composed of six individual boron-lined detector modules manufactured by Precision Data Technology, Inc. (PDT) [7]. Each detector contains six boron-lined detection cells filled with Ar+CO_2 gas. The individual detection cells are interleaved with high density polyethylene (HDPE) plates for optimum neutron moderation. The entire system of cells and HDPE is hermetically sealed within an Al enclosure. The detectors tightly surround the sample cavity of 17.00 cm (6.69”) in diameter and height of 41.00 cm (16.14”). The top and bottom end plugs consist of aluminium core surrounded by HDPE. In addition, 1.27 cm (0.5”) thick HDPE slabs are added along the external sides of the detectors to boost the detection efficiency through neutron reflection. A view of the HLNB internal layout is shown in Figure 1.

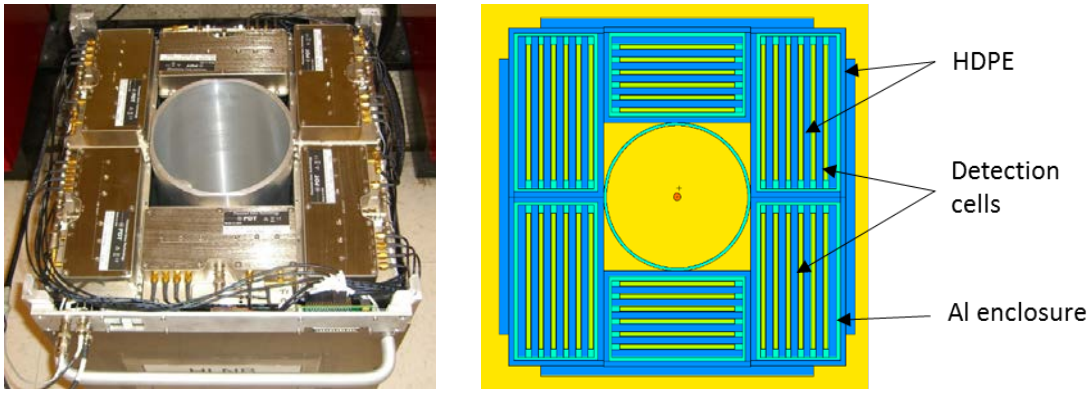

Figure 1: (left) Top view of the boron-lined detectors layout inside the HLNB along with associated wiring; (right) MCNP visualization of the HLNB internal structure.

The HLNB was designed as a direct replacement of a High-Level Neutron Coincidence Counter (HLNC-II) [9], which represents a safeguards standard, fielded in numerous nuclear facilities and used by the International Atomic Energy Agency (IAEA). The HLNB was developed to mimic the external dimensions of HLNC-II with identical size sample cavity. The key requirement was achieving performance (count rate capability and Pu assay uncertainty) similar to HLNC-II. A photograph of HLNB and HLNC-II side-by-side is shown in Figure 2.

Figure 2: HLNB (right) next to its ^{3}He-based reference HLNC-II. The HLNB LED display reflects the internal detector layout and allows for easy state-of-health assessment. The multi-pin connector is added for list mode acquisition.

The initial development of the HLNB dates back to 2012 and since its initial implementation, the detector has undergone series of dedicated tests at LANL to evaluate its key parameters relevant for nuclear safeguards applications. This rigorous testing also helped identify potential weaknesses of the initial design and allowed for further technical improvements and modifications that were performed on the system to improve its safeguards applicability. The current HLNB boron-lined detectors feature a sealed-cell concept with each individual detection cell hermetically sealed. The sealed-cell design allows for high degree of internal gas purification in order to prevent any potential contamination and to maintain its characteristics for extended periods of time. Such an approach is necessary to assure long term stability performance required in routine safeguards deployment. The individual sealed-cells are filled with C10 gas (Ar+CO_2 mixture) at sub atmospheric pressure. Therefore, good structural integrity of the cells is necessary to sustain pressure differential during handling and full system assembly at an atmospheric pressure. Once assembled, the detector module (with 6 sealed cells) itself is sealed in an external Al enclosure and filled with gas. This assures overall system robustness under variations in external atmospheric pressure. To provide the needed structural integrity of individual cells, a concept of corrugated surface was developed. In this concept the cell is manufactured in two identical halves and both boron-coated internal surfaces are corrugated. The two halves of the cell are then welded together and the internal corrugation provides an additional support through the contact of the individual ridges. Photographs of the internal corrugated layout for a single sealed-cell are shown in Figure 3.

Figure 3: Photographs of corrugated sealed-cell concept; (left) view of the corrugated boron-coated surfaces inside the cell; (right) finished sealed-cell.

The HLNB signal processing electronics is housed in a very compact junction box that is only 3.5 cm (1.5") tall. Each of the HLNB detectors is equipped with 3 amplifiers (each servicing two adjacent detection cells) making a total of 18 amplifiers in the entire system. The HLNB features a standard shift register compatible signal output with all the amplifiers OR'ed together. In addition, the HLNB is equipped with list mode data acquisition, which allows a direct read out of all the 18 amplifiers. The technique allows the recording of all of the HLNB channels, which can be analyzed for deadtime and dieaway information as well as provide monitoring of the state-of-health of the wholde system. HLNB list mode data is collected in PTR32-HV pulse train recorder unit [10]. The unit records time intervals between the consecutive neutron pulses in 10 ns increments and is capable to handle rates of up to 3 MHz of periodic pulses.

2.1. HLNB operating parameters

In order to prepare for the field trial measurements of Pu-bearing materials and to operate the HLNB as a coincidence counter, several operating parameters must be determined. The HLNB characterization and evaluation of operating parameters was performed at LANL using available neutron sources. The key operating parameters include operating HV setting, neutron detection efficiency (ε), die-away time (τ), pre-delay and gate width, dead-time correction parameters (A, B) and known-alpha calibration parameter (ρ_0). The listed parameters represent standard characteristics of a neutron coincidence counter used by INCC software [11] in SNM assay. The values of the individual parameters for HLNB are summarized and compared to HLNC-II in Table 1.

Detector	HV [V]	Pre-delay [μs]	Gate [μs]	ε	τ [μs]	ρ_0	A [μs]	B [μs^2]
HLNB	860	3	180	0.183	89.5	0.105	0.665	0.1105
HLNC-II	1680	4.5	64	0.175	43.0	0.103	0.768	0.2480

Table 1: Overview of HLNB and HLNC-II operating parameters

From Table 1, it can be seen that HLNB exceeds the detection efficiency of HLNC-II by 0.8% (a 4.6% increase), however, the die-away time of HLNB is about a factor of 2 longer than in case of the HLNC-II. It should be pointed out that the die-away time can be further improved by additional optimization of boron deposit thickness. In [12] it was demonstrated, using another PDT boron-lined detector, that recent improvement in boron coating technique leads to a ~40% improvement in neutron detection efficiency, and approximately a factor of two reduction in the die-away time.

3. Field trial of HLNB at PCDF

The field trial of HLNB was performed at Plutonium Conversion Development Facility (PCDF) of JAEA over a period of May –February 2016. The field trial represented a key milestone in the evaluation of HLNB performance and provided a unique opportunity to evaluate the overall performance of the newly developed system in conditions beyond well controlled laboratory environment with materials that were representative of realistic deployment conditions. Of key interest was the evaluation of transportability, ease of set-up and functionality in an operational facility with realistic backgrounds, noise interference and temperature and humidity conditions. The field trial measurements focused on range of items of operational interest that included medium to high mass MOX items. An overview of the available materials is provided in Table 2.

Pu mass [g]	^{238}Pu [%]	^{239}Pu [%]	^{240}Pu [%]	^{241}Pu [%]	^{242}Pu [%]	^{241}Am [%/Pu]	date	U [wt%]	Pu [wt%]
5-10	0.886	67.538	24.420	3.377	3.779	1.95	6.3.2015	43.75	41.72
50-1223	0.984	62.570	28.383	3.530	4.533	2.58	27.4.2015	43.61	41.50

Table 2: Overview of MOX items available for HLNB field trial measurements.

The measurements were performed in one of PCDF test process rooms with HLNB and HLNC-II detectors positioned side-by-side and separated by ~ 2 m distance. Each detector was connected to its own JSR-15 shift register. INCC was used for data acquisition and analysis in connection with JSR-15 to reflect realistic field assay conditions. HLNB data was also collected in list mode using PTR32-HV unit. List mode data was recorded for offline analysis with dedicated, LANL developed, software. Photograph of an experimental configuration is shown in Figure 4. Each MOX item was handled and inserted into the detectors by dedicated PCDF personnel. A reference swipe was taken and tested for every measured item to check for contamination.

Figure 4: HLNB and HLNC-II during field trial measurements. Photograph shows a PCDF operator taking swipe sample of a bagged small MOX container before measurement in HLNB.

MOX items that were prepared for the field trial measurements were enclosed in small stainless steel cans for the larger items and plastic containers for the low mass items and double sealed in a pair of plastic bags to prevent contamination of the detector surface. To assure reproducibility of field trial measurements, the items were placed on a fixed height lab jack located at the bottom of each detector. The height of the lab jack was set to 11.7 cm (4.6”) to assure the item positioning within the flat portion of the HLNB and HLNC-II counting efficiency. A photograph of pair of MOX items used in verification measurement (5 g Pu and 10 g Pu items were combined to obtain mass of 15 g Pu) is shown in Figure 5.

Additional MOX material was present in the process equipment in the room during the field trial campaign, however, no handling and processing was performed. To account for any variations in the material distribution, background measurements were repeated daily.

The performed measurements included initial post transportation state-of-health evaluation with a ^{252}Cf neutron source, high voltage plateau measurements, calibration using low to high mass MOX items (up to 100 g Pu), verification measurements and measurements with high mass MOX items (200 g and 1.2 kg Pu).

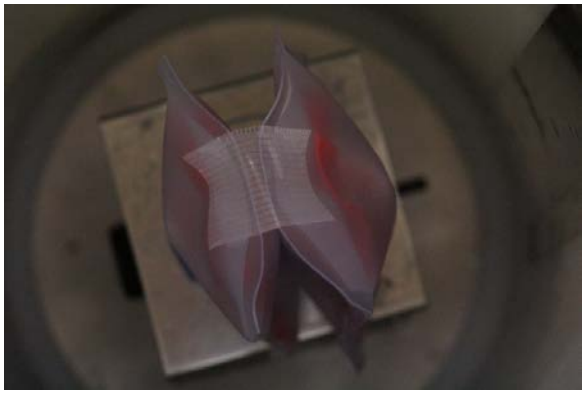

Figure 5: Photograph of two small MOX containers placed side-by-side on a lab jack inside the HLNB counter well.

3.1. Initial set-up and performance test

A JAEA provided ^{252}Cf source with neutron emission rate of 8.52x10^{4} n/s (on 1.5.2015) was used for post-transportation state-of-health assessment. The measurements focused on HV plateau curve and neutron detection efficiency for HLNB as well as HLNC-II and comparison of results with LANL reference measurements. The HLNB HV plateau data were recorded in list mode to obtain HV curve for each amplifier and evaluate any differences with respect to LANL reference measurements. Comparison of HV plateau curve measurements for individual HLNB amplifiers is summarized in Figure 6. The difference in the total counts between LANL and JAEA measurements is due to the different activity ^{252}Cf sources available at each location. The step decrease in the height of the plateau curves from individual HLNB outputs is a result of the increasing distance of the internal detector cells from the sample. Figure 6 illustrates that no significant deviation from reference measurements performed at LANL was identified in post-transportation evaluation performed at PCDF demonstrating robustness of the HLNB design. The count rate measured at operating HV was used to confirm unchanged detection efficiency.

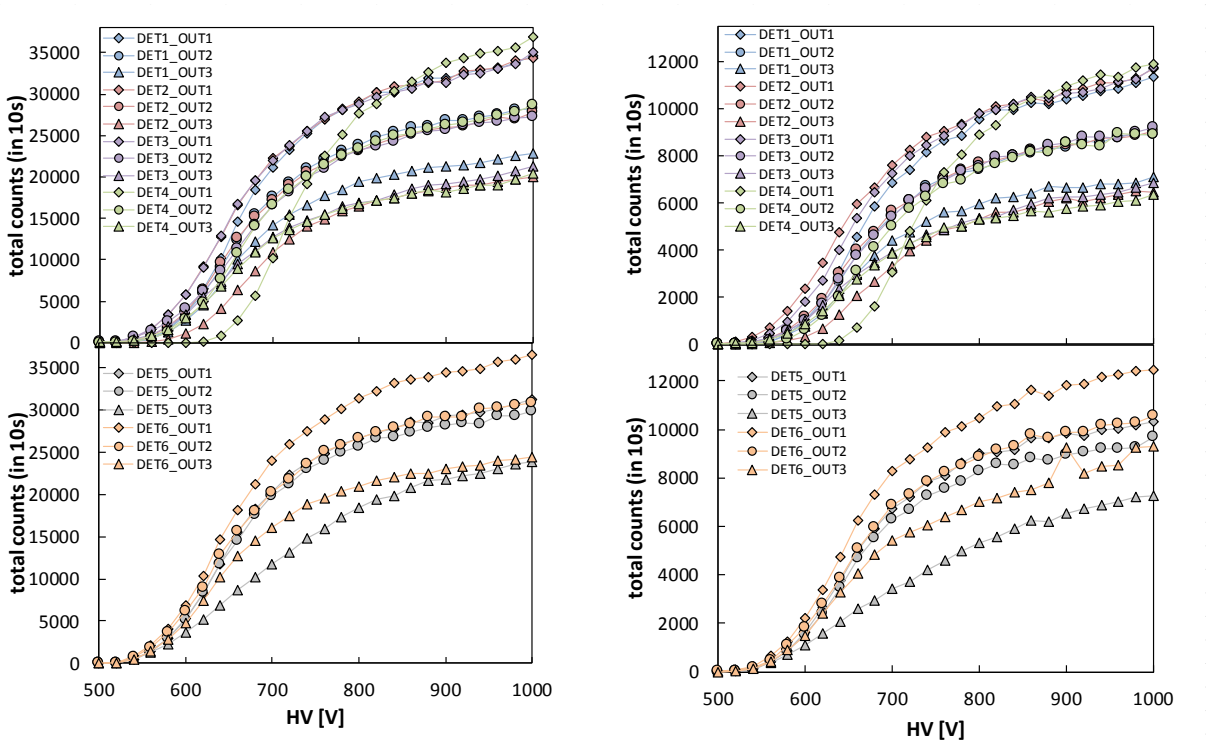

Figure 6: Comparison of HV plateau curves for individual HLNB amplifiers for detectors 1-4 (top) and detectors 5 and 6 (bottom); (left) measured at LANL; (right) post-transportation performance at PCDF.

3.2. MOX measurements

Measured MOX materials included small MOX items with mass corresponding to 5 g Pu - 10 g Pu, medium mass MOX items of 50 g Pu and 100 g Pu and high mass MOX items of 200 g Pu and 1.2 kg Pu with characteristics summarized in Table 2. The medium mass MOX items included two very similar 50 g Pu items, one was used for calibration and the other for verification measurements. A thin (1 mm) Sn foil was used inside the HLNB during the measurements of the high mass MOX items to remove low energy (60 keV from ^{241}Am) gamma-ray interference. It should be pointed out that similar effect is achieved in HLNC-II by its Cd liner. Note that the introduction of Sn foil does not affect the neutron detection efficiency due to its negligible thermal neutron capture cross section.

Calibration measurements were performed using passive calibration curve as well as known-alpha calibration methods in INCC. Two sets of calibration parameters were established for HLNB as well as HLNC-II, respectively; one for small MOX items with mass range < 20 g Pu and one for medium and high mass MOX items corresponding to mass range of > 20 g Pu. The division of calibration curves into two distinct mass ranges was motivated by the different encapsulation of the small MOX items (plastic container) and larger MOX items (stainless steel cans).

The MOX materials available for the calibration measurements included 5 g Pu and 10 g Pu for the small MOX items; and 50 g, 100 g, 200 g and 1223 g Pu for the medium and high mass MOX materials. The measurement times were kept the same in both detectors and corresponded to 1200 s. The measurements were performed in series of 20-30 s cycles that were used for statistical error estimation from the standard deviation in the repeat runs. The passive and known-alpha calibration parameters for HLNB and HLNC-II are summarized Table 3 and were used as input into INCC for verification measurements.

Calibration method and parameters		HLNB		HLNC-II	
		Small MOX	Medium /large MOX	Small MOX	Medium /large MOX
Known-alpha parameters	ρ_0	0.105		0.103	
	b	20.67	19.55	19.22	18.65
Passive calibration parameters	a	0.3639	0.0968	0.0171	0.0560
	b	22.6176	23.5515	20.3199	19.6920

Table 3: Overview of passive and known-alpha calibration parameters.

Figure 7 shows the multiplication corrected doubles rate measured for the medium and high mass MOX compared to the known-alpha calibration line. The observation that results of all items are well represented by the calibration fit confirms that the measurements were not affected by gamma-ray interference and that the operating HV of 860 V as well as Sn foil used with the high mass MOX items in HLNB provided adequate operating conditions for gamma-ray backgrounds from the full range of assayed materials.

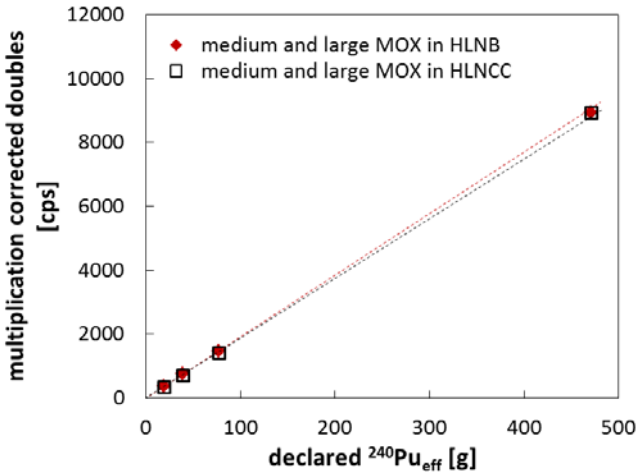

Figure 7: Multiplication corrected doubles versus declared ^{240}Pu effective mass for medium to high mass MOX items measured in HLNB (red diamonds) and HLNC-II (black open squares) compared to the known-alpha calibration for each detector.

Verification measurements were performed with materials that were not used for calibration. These materials included combination of 5 g Pu and 10 g Pu MOX items (equivalent of 15 g of Pu) and the second of the two 50 g Pu MOX items. The results of the verification measurements are summarized in Table 4 for 1200 s measurement time.

Analysis Method	Declared Pu mass [g]	HLNB				HLNC-II			
		Assay Pu mass [g]	σ	Declared-assay mass [%]	σ	Assay Pu mass [g]	σ	Declared-assay mass [%]	σ
Known alpha	15.0	15.06	0.04	-0.58	0.29	14.99	0.02	-0.08	0.15
	50.0	49.79	0.07	0.41	0.13	49.98	0.05	0.03	0.11
Passive calibration	15.0	15.24	0.11	-1.76	0.72	14.93	0.08	0.27	0.50
	50.0	49.85	0.25	0.29	0.49	50.44	0.21	-0.90	0.41

Table 4: Results of verification measurements in HLNB and HLNC-II.

The verification measurements indicate good performance of HLNB over the low-to-medium mass MOX range that is comparable to HLNC-II. Overall, the known-alpha calibration results in better accuracy in declared mass than passive calibration, because of the better statistical precision for known-alpha and the variability of the multiplication. The uncertainties of HLNB results for the mass range of the available MOX items reported in Table 4 are comparable to HLNC-II despite the longer die-away time of HLNB. The impact of longer die-away time is typically emphasized with increasing count rate due to increased contribution of accidental coincidences in the longer HLNB gate and therefore its effect on uncertainty is expected to affect predominantly higher mass items.

To provide further validation of the HLNB results a comparison with International Target Value (ITV) for HLNC-type counters is of interest. The HLNC-II ITV corresponds to 2.1% for 300 s long measurement of MOX with Pu content greater than 10% [13]. The measurements reported here correspond to 1200 s and although reduction of measurement time to 300 s would increase measurement uncertainties by approximately a factor of 2, the assay accuracy in Table 4 is largely determined by the overall calibration fit quality and therefore will be less affected by the measurement time reduction, especially if there is sufficient number of calibration points. Therefore, the HLNB (and HLNC-II used in the field trial) measurement results are projected to satisfy the ITV expectation for

equivalent 300 s measurement time. The HLNB performance thus confirms the expected performance of an HLNC-II equivalent system based on broad range of practical safeguards data.

4. Feasibility of HLNB as deployed safeguards system

The field trial of HLNB concluded development of a full scale prototype ^{3}He-free coincidence counter for nuclear safeguards applications. The development involved series of engineering challenges in manufacturing and mechanical and structural design that were driven by stringent requirements for routine deployment at nuclear facilities. In addition to key performance parameters that were evaluated during initial phases of the project, the full system build brought the attention to the key design parameters such as overall system robustness, reliability, ease-of-use and operation as well as ease of maintenance, that can only be addressed once the development moves into a full-scale system build. The latter represented an essential step in moving the technology into facility environment.

HLNB was developed and designed with these standards in mind and series of decisions and process modifications adopted along the way represented key shifts to satisfy these requirements. The field trial provided an essential insight on the performance of the system under facility conditions and helped answer questions on its transportability, ease-of-use and set-up. The extended time of the trial campaign required the JAEA personnel to acquire skills needed to operate the detector and provided insight on the operator training requirements. It is important to note that the PCDF facility staff has been able to fully operate the system after the initial joint measurements with LANL staff and less than half-day of training. The compatibility of the HLNB with the standard INCC software that is used by the IAEA, has made the system very user friendly for the inspectorates and facility staff.

The first activity of the field trial was dedicated to initial set-up and post-transportation state-of-health evaluation. This initial set-up required similar activities and efforts as HLNC-II, but with the addition of list mode data acquisition in the HLNB, which did not represent a significant added complexity. One of the differences between the HLNB and HLNC-II is the requirement of 12V supply for the HLNB operation, which, however, is typically incorporated into one of the standard shift register modules (AMSR, JSR-15 that provides the necessary 12V supply in a LANL-designed stand). The post-transportation state-of-health assessment revealed consistent performance of the HLNB in agreement with the reference LANL measurements. The post deployment efficiency was within ~ 1% of the efficiency prior to the field test. This provided a key demonstration of robustness of the HLNB structural and mechanical design.

Another key aspect of the field trial was an assessment of measurement times and the overall material handling and detector operation experience. The material handling and measurement times were maintained the same for HLNB and HLNC-II. The HLNB was equipped with list mode acquisition for additional level of detail that was essential for performance assessment of the system, however, is not strictly required for routine operation. Although measurement times during field trial corresponded to 1200 s, for routine operation a 300-600 s measurement would be adequate for the design basis materials used with the HLNC-II. Assuming the core application would utilize standard shift register electronics, the operation of HLNB fully mimics the operation of HLNC-II. A slight additional training is needed for the list mode operation. Nevertheless, since list mode (specifically PTR32 utilized with HLNB) was recently approved for use by IAEA, it can be anticipated that additional training on the operation of the device will become a part of regular inspector training exercises in the future. The JAEA personnel were trained to operate the HLNB using both, the shift register as well as the list mode data acquisition. The capability of JAEA personnel to perform the field trial measurements demonstrates the ease-of-use of the instrument under routine conditions.

In addition to the robustness and overall performance of HLNB, the reliability and ease of maintenance represent additional essential design aspects. The reliability and long term stability of HLNB was demonstrated throughout the 9 month long period that the instrument spent at PCDF with continuously consistent performance comparable to HLNC-II and without requiring any renormalization or modification of calibration parameters as can be confirmed in the presented results. The modularity of HLNB allows for ease of maintenance and repairs of potential faulty parts via a direct replacement of a full detector module. This feature represents an important consideration in the overall system maintenance requirements that is often overlooked in ^{3}He-alternative system designs.

The above observations along with the field trial measurement results discussed in previous sections indicate that HLNB is well positioned to provide a robust and reliable nuclear safeguards technology with characteristics similar to HLNC-II.

5. Conclusions

This paper provides a summary of performance evaluation of HLNB under realistic field conditions. The field trial measurements were performed at PCDF of JAEA and included range of low to high mass MOX materials that were prepared specifically for the purpose of the field trial and represent realistic process samples.

The field trial provided key insight on feasibility of HLNB deployment as a safeguards instrument in realistic facility environment. The HLNB proved to be a robust technology with no identified post-transportation issues and ease of set-up similar to HLNC-II. The dedicated state-of-health measurements with a ^{252}Cf source performed upon arrival of the detector to PCDF showed stable performance, in agreement with reference measurements performed at LANL prior to instrument shipment. The reliability and long term stability of HLNB was demonstrated throughout the 9 month that the instrument spent at PCDF performing consistently without the need of any renormalization or modification of calibration parameters. Agreement of HLNB assay results with HLNC-II for measurements acquired over this period of time provides further evidence of its long term reliability.

The field trial results indicate good performance of HLNB over the broad MOX mass range investigated (5 g Pu to 1.2 kg Pu) with uncertainties and accuracy that is comparable to HLNC-II. In particular, the results of verification measurements demonstrate that HLNB is capable to satisfy ITV expected for HLNC-II-type counter of 2.1% in 300 s measurement time. The known-alpha calibration results in better accuracy in declared mass than passive calibration for both instruments. Overall, the verification results serve as a first indication that HLNB is capable of similar performance in the same amount of measurement time as HLNC-II for the range of evaluated MOX items. Additionally, the agreement between HLNB and HLNC-II for the 200 g Pu and 1.2 kg Pu MOX items demonstrates feasibility of HLNB in assay of high mass items.

Improvements in the boron coating technology at PDT during the past year have demonstrated a ~ 40% increase in efficiency and a significant decrease in the die-away time compared with the sealed-cells in the HLNB [12]. Future units that incorporate the improvements could be expected to outperform the current unit as well as the HLNC-II.

6. Acknowledgements

This work was funded by the U.S. Department of Energy, National Nuclear Security Administration, through the Office of Nonproliferation and Arms Control. LANL authors would like to thank to JAEA personnel for their excellent and dedicated support during the field trial measurements, preparation stage and results consultation.

7. References

[1] Kouzes R.T., *The ^{3}He Supply Problem*, *Pacific Northwest National Laboratory Report*; PNNL-18388 (2009)

[2] Shea D.A., Morgan D., *The Helium-3 Shortage: Supply, Demand, and Options for Congress*, *Congressional Research Service Report for Congress* R41419 (2010)

[3] Pickrell M.M. et al., *The IAEA Workshop on Requirements and Potential Technologies for Replacement of 3He Detectors in IAEA Safeguards Applications*; *Journal of Nuclear Materials Management*; Volume XLI No. 2 (Winter 2013)

[4] Dolan J., Dougan A., Peranteau D., Croft S., *An International View on 3He Alternatives for Nuclear Safeguards*; *Journal of Nuclear Materials Management*; Volume XLIII No. 3 (Spring 2015)

[5] Henzlova D., Kouzes R., McElroy R., Peerani P. et al., *Current Status of ^{3}He Alternative Technologies for Nuclear Safeguards*; *Los Alamos National Laboratory Report* LA-UR-15-21201 ver3 (2015)

[6] Evans L.G., Henzlova D., Menlove H.O., Swinhoe M.T., Croft S., Marlow J.B., McElroy R.D., *Nuclear Safeguards ^{3}He Replacement Requirements*; *Journal of Nuclear Materials Management*; Volume XL Number 3 (Spring 2012)

[7] Henzlova D., Evans L.G., Menlove H.O., Swinhoe M.T., Marlow J.B., *Experimental Evaluation of a Boron-lined Parallel Plate Proportional Counter for Use in Nuclear Safeguards Coincidence Counting*; *Nuclear Instruments and Methods in Physics Research A* 697 pp. 114-121 (2013)

[8] D. Henzlova, H.O. Menlove, and J.B. Marlow, *Design and Performance of a 3He-free Coincidence Counter Based on Parallel Plate Boron-Lined Proportional Technology*; *Nuclear Instruments and Methods in Physics Research A* 788 pp. 188-193 (2015)

[9] Menlove H.O., Swansen J.E.; *A high-performance neutron time correlation counter*; *Nuclear Technology* 71, 497 (1985)

[10] http://www.iki.kfki.hu/radsec/groups/mcl_en.shtml.

[11] Krick M., Harker B., Geist W., Longo J., *INCC software users manual*; *Los Alamos National Laboratory Report* LA-UR-10-6227 (2010)

[12] Menlove H.O., Henzlova D., *Improvements in Boron Plate Coating Technology for Higher Efficiency Neutron Detection and Coincidence Counting Error Reduction*; *Los Alamos National Laboratory Report* LA-UR-16-26496 (2016)

[13] Zhao K. et al., *International Target Values 2010 for Measurement Uncertainties in Safeguarding Nuclear Materials*; *IAEA report* STR-368 (2010)

A Comparison of Approaches to Determine Dead Time Parameters Using a Boron-Coated-Straw High-Level Neutron Coincidence Counter

A.T. Simone[1, 2], S. Croft[2], A. Favalli[3], and J. P. Hayward[1, 2]

[1]University of Tennessee, Department of Nuclear Engineering, 308 Pasqua Engineering Building, Knoxville, TN 37996, USA.
[2]Safeguards & Security Technology, Nuclear Security and Isotope Technology Division, Oak Ridge National Laboratory, One Bethel Valley Road, PO Box 2008, MS-6166, Oak Ridge, TN 37831-6166, USA.
[3]Safeguards Science & Technology Group, Non-proliferation and Nuclear Engineering Division, Los Alamos National Laboratory, MS E540, Los Alamos, NM 87545, USA.

Abstract:

When characterizing a neutron coincidence counter for use in international safeguards, it is important to understand the dead time of the system. With current data acquisition in the form of shift register logic, there are several options to determine effective dead time model parameters. A customary approach consists of incrementally overwhelming the detection system with various sources to generate different count rates for analysis. An empirical fit to these data can then produce a dead time parameter. This method makes use of the expectation that the doubles to singles count rate ratio, after dead time correction, should remain fixed. In our measurements, we begin with a single ^{252}Cf source and successively combine it with 1, 2, 3, and 4 AmLi (α,n) sources. The time-correlated fission neutrons from the ^{252}Cf are detected by the neutron coincidence counter, and the random-in-time neutrons produced from the multiple AmLi sources provide excess counts to trigger on. Another recently reported approach [12] consists of utilizing the neutron-count number distribution, for a number of counting cycles, to permit a statistical analysis and subsequent determination the dead time along with a robust estimate of the statistical uncertainty. Moments of several orders can be used; therefore, several estimates of the effective dead time parameter are obtained. In the results reported here, two AmLi sources are measured simultaneously within the well of the counter for a number of cycles. We have selected 24 cycles of 300 s each, with predetermined timing gates, where detected neutron multiplicities can range up to approximately 10 neutrons per cycle. These two methods were tested at Oak Ridge National Laboratory using a Boron-Coated-Straw High-Level Neutron Coincidence Counter, but the methods are also applicable to ^{3}He counters. In this paper, we compare the results of these approaches and discuss the relevance of both.

Keywords: Dead time correction; boron-coated straws; high-level neutron coincidence counter; neutron coincidence counting; shift register

1. Introduction

Neutron coincidence counting is widely used in international safeguards applications for the nondestructive assay of nuclear material. Common thermal neutron coincidence and multiplicity counters take the form of an annular body filled with a moderator and populated with ^{3}He tubes, which surround a central well used for sample loading. When a sample undergoes fission, each event produces a simultaneous release of neutrons, the average number of which are characteristic of the sample's isotopics, which travel through the well of the detector and into the moderating body. These time-correlated neutrons are slowed in the moderator, spreading out this distribution over a longer period of time; this time is related to the neutron die-away time. The die-away time is characteristic of the geometry of the detector and not of the fissioning source, and it cannot be altered. These thermalized

neutrons are then captured in the ^{3}He tubes and can be detected, by software, in coincidence and higher order multiplicities using appropriate timing gates. The total number of neutron events measured is recorded as the singles count rate. The doubles count rate corresponds to two neutron events measured within a specified time gate, and the triples count rate corresponds to three neutron events within that gate. However, in addition to these fission neutrons, background and (α, n) neutrons can also be detected within these timing gates, generating artificial multiplicities.

Each neutron interaction produces a pulse in the electronics connected to the ^{3}He tube, and the tube system is then dead for some amount of time. This means that any neutrons captured during this dead period are not counted and do not contribute to the total neutron pulse train. The dead period is related to the processing and recovery time of the electronics used and applies to each of the tube and electronic systems and, because the signals from each are summed together in a total output, a total detector system dead time can be determined. For systems with several detector bank channel outputs, dead times for the individual channels can also be determined.

Neutron coincidence and multiplicity counting relies on the accurate measurement of these fission neutrons as a function of time to determine the quantity of nuclear material within the measured sample [1, 2]. These distributions of neutrons are perturbed due to this dead time, thereby influencing assay values. Because detection systems cannot be 100% efficient, nor will every emitted neutron travel towards the moderated detector body, corrections are applied for neutron losses. In addition, another correction for the dead time related losses in the system is required. This value must be well-known to accurately adjust the measured neutron multiplicity rates for the true multiplicity rates.

Previous work has been done to determine the dead time of neutron coincidence counting systems and to characterize how this affects the incoming neutron pulse trains. The long-standing and widely used approach is extended to higher order multiplicities by Dytlewski [3] and is applied to safeguards systems, including High Level Neutron Coincidence Counter designs [4, 5], assuming a paralyzable (or updating) dead time model. The paralyzable model assumes that not only will a neutron captured during the dead period of the tube not be counted towards the total neutron pulse train, but that neutron event will extend the dead period. Although this model has been assumed for neutron coincidence counting, it has not been fully verified. The common experimental approach to measure the dead time uses multiple ^{252}Cf sources of increasing strength to determine two dead time parameters, which will be explained in detail later. Another approach utilizes random-in-time neutrons produced by AmLi (α, n) sources— in conjunction with a single ^{252}Cf spontaneous fission neutron source— to increase the uncorrelated single neutron events while maintaining the doubles neutron rate; this method was employed for this paper. Many others have built upon these methods by deriving alternative approaches to singles dead time corrections [6, 7] and investigating the effect of correlation in the neutron pulse train due to varying sources [8, 9], while also trying to simplify the theory and expressions for easy adaptation. However, the final expressions and implementation of the theory to experiment are complex, and as a result have not been adopted in favor of older simplifications.

Using the approach laid out by Menaa [10], based on the theory outlined by Foglio Para and Bettoni [11], random-in-time neutrons produced by AmLi sources are used to obtain a neutron-count distribution. Then, using the methodology outlined in [12], a statistical analysis is performed on this distribution over many cycles. With this analysis, the dead time parameters for second, third, and fourth order factorial moments can be determined, enabling an inter-comparison of values from a single data acquisition. These multiple samplings also allow for a robust estimate of the statistical uncertainty.

The importance of this method from a safeguards inspection perspective relates to the availability of sources for in-field measurements; AmLi sources are present for active interrogation in neutron coincidence counters. Meanwhile, it is not uncommon for a facility under inspection to not have ^{252}Cf at that location. Compared to the traditional method, the AmLi sources allow for shorter acquisition times with similar precision, and they do not have to be replaced as frequently due to the long half-life of Am isotopes. This work summarizes both the traditional approach and the new statistical approach and compares the two using data obtained using a boron-coated-straw (BCS) High-Level Neutron Coincidence Counter (HLNCC) as a comparison between them.

2. Experimental Setup

The BCS HLNCC was built by Proportional Technologies, Inc. (PTI) as a prototype ^{3}He alternative neutron coincidence counter. This prototype was designed to meet the specifications and performance objectives set for evaluation against other systems at an international workshop searching for a drop-in ^{3}He replacement [13]. Because of this, the BCS HLNCC was built as an aluminum-encased cylindrical high density polyethylene (HDPE) body measuring 34 cm in diameter and 68.2 cm in height

(Figure 1a), preserving the dimensions of the ^{3}He-based HLNCC-II. The sample well is 17 cm in diameter and 41 cm in height and is sealed with top and bottom end plugs made of HDPE and aluminum. The main differences between the standard system and BCS system are a 6 kg increase in mass and the use of ^{10}B rather than ^{3}He for the neutron capture reaction.

The 18 ^{3}He tubes from the standard HLNCC-II were substituted for 804 ^{10}B straws, each measuring 4.4 mm in diameter, evenly dispersed throughout the HDPE body. The 96% enriched $^{10}B_4C$ coats a 2 μm thickness on the inside of aluminum or copper tubes, which are filled with a mixture of CO_2 (10%) and Ar (90%) at 1 atm [14-16]. The incident neutrons interact with the ^{10}B, releasing an alpha particle and ^{7}Li ion, which ionize the gas as they travel. Because this method of charge collection is similar to the method exploited in ^{3}He tubes, similar electronics and software can be used for both technologies. There are six detector banks, of 134 tubes each, connected and processed by six amplifiers. A conversion box consisting of inputs (Figure 1b), outputs (Figure 1c), and a field-programmable gate array (FPGA) module shapes the incoming pulses and amplifies them to produce the correct form for an output signal trigger to be used with shift register or list mode acquisition software (Figure 1d). An external power supply provides the +5 V needed for the detector.

Figure 1a-1d. Left to right: The BCS HLNCC showing (a) the six detector bank outputs; (b) the BCS HLNCC-specific conversion box containing electronics to shape and amplify the output signals, resting on the external power supply used for the +5 V; (c) the output signal cables of the conversion box; and (d) PTR-32. See text for details.

A list mode data acquisition system, Pulse Train Recorder-32 (PTR-32) [18], was used with the BCS HLNCC to bias, record, and analyze the neutron pulse train for each of the detector bank channels (Figure 1d). Because previous data taken with the PTR-32 have shown to be in agreement [19] with data taken with a JSR-15 shift register [20], the two were used interchangeably. PTR-32 can produce output files in a form similar to those output by the International Atomic Energy Agency (IAEA) Neutron Coincidence Counting (INCC) Program, including a neutron count distribution per every cycle recorded, in addition to neutron multiplicity analysis. PTR-32 can perform analysis using shift register logic when the user specifies predelay, gate width, and long delay time windows. As an added benefit, PTR-32 can perform this analysis for each individual detector channel connected to 1 of the 32 inputs on the board from a single measurement. The BCS HLNCC was biased to the standard setting of +850 V, and PTR-32 was set to analyze using the previously-determined optimal timing gates of 2 μs for the predelay, 48 μs for the gate width, and 4096 μs for the long delay for these measurements.

3. Traditional Dead Time Approach

As previously mentioned, the traditional and most commonly used approach for determining detector dead time was established decades ago, and extended to greater multiplicities by Dytlewski in 1990 [3], assuming a paralyzable dead time model. This methodology was then applied for use in neutron coincidence counters such as the ^{3}He- based HLNCC models [4, 5]. The combination of these

works derived the following equations for the doubles (D) and singles (S) dead time correction factors (CF):

$$CF_D = e^{\delta_R \cdot S_m} = e^{(a+b \cdot S_m) \cdot S_m} \quad (1)$$

$$CF_S = e^{\delta_T \cdot S_m} = e^{\frac{1}{4}(a+b \cdot S_m) \cdot S_m} = {CF_D}^{1/4} \quad (2)$$

Where δ_R is the dead time for the doubles, δ_T is the dead time for the singles, S_m is the measured singles rate, and a and b are the dead time parameters which are empirically determined for a specific detection system. Equation 1 represents the dead time correction factor for the doubles rate, and Equation 2 represents the dead time correction factor for the singles rate. The free parameters a and b are determined by a quadratic fit to doubles count rate data as a function of increasing singles rate. It is common for detectors of the same model to keep the ratio of a/b constant across all production, aiding in this analysis.

Data can be obtained using multiple ^{252}Cf sources of increasing strength, or with a single ^{252}Cf source in combination with random-in-time neutrons produced by AmLi sources to provide a range of count rates. The number and/or strength of the sources chosen should correlate with the full count range expected to be measured. Because the first method uses only ^{252}Cf point-like sources, there is no significant multiplication nor (α, n) contribution, and so the multiplicity ratios of triples to doubles (T/D), triples to singles (T/S), and doubles to singles (D/S) should all be constant and independent of the source strength once dead time corrected. This allows the dead time parameters to be determined and adjusted by minimizing the chi-squared value from each of these ratios.

For an uncorrelated neutron source, where the emitted neutrons have no time-dependent pattern (as a fissionable source would have), the (Reals + Accidentals) count rate should be approximately equal to the (Accidentals) count rate illustrated in the Rossi-Alpha distribution below (Figure 2). This means that there is a very low probability that emitted neutrons will be counted as false doubles or triples. The second experimental approach to the traditional method uses a number of AmLi sources with a single ^{252}Cf source to incrementally overwhelm the detection system to generate different singles count rates for a similar analysis. This method benefits from the convenience and availability of using one ^{252}Cf source, while still having the ability to determine the dead time corrections for both the singles rate and the doubles rate. This is the method used in this section for analysis.

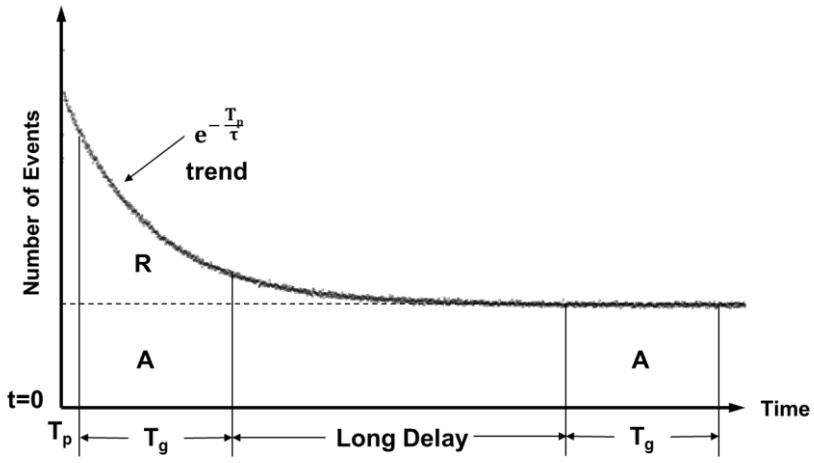

Figure 2. A Rossi-Alpha distribution illustrating the various gates used in shift register analysis and their chronological positions on the neutron pulse train.

A NIST-traceable ^{252}Cf source, with a detected neutron rate around 94,000 cps and 1.10% relative standard error, was placed in the center of the BCS HLNCC. Two different metal cans were used to hold the ^{252}Cf and the AmLi sources: the ^{252}Cf was placed just below the middle plane of the BCS for optimal efficiency, and a second, slightly taller, metal can was placed over this and served as a stand for the AmLi sources. The ^{252}Cf source and the metal cans remained stationary throughout the entire experiment to ensure that no associated systematic errors were introduced. Using the experimental setup described here, a 120 minute acquisition, using only the ^{252}Cf source, was

obtained to ensure good counting statistics on the doubles count rate. The total detector signal was collected along with the six individual channel neutron pulse trains, as a result of using the PTR-32. In this work, we only analyze the total detector signal, but the same procedure would apply when analyzing each of the channels. It was assumed that little difference would be registered between a measurement of the strong ^{252}Cf source and a measurement of the strong ^{252}Cf source with the addition of a single AmLi source; therefore, the next measurement taken was of ^{252}Cf with two AmLi sources. These two AmLi sources had measured strengths around 7300 cps with an uncertainty of 0.11%. Because of the greater count rate, the acquisition time for this data collection was reduced to 30 minutes. A third AmLi, with a measured strength around 10200 cps and an uncertainty of 0.11%, was then added. Data were taken again for 30 minutes. A fourth, and final, AmLi source, with similar strength to the third one was then added. For this run, the acquisition time was increased to 45 minutes to give a greater certainty of the count rate, as this is crucial for producing an accurate fit.

These files were then analyzed in PTR-32 with the standard 2 μs predelay, 48 μs gate width, and 4096 μs long delay in order to find the singles and doubles count rates for each of these runs. This method is the same as the analysis performed using a shift register. Figure 3 shows a plot of the ratio of doubles to singles count rates as a function of singles count rate with the empirical fit applied.

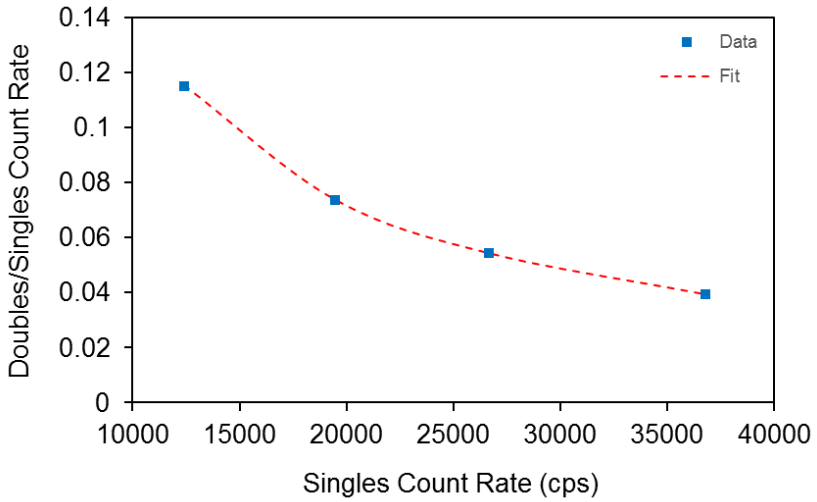

Figure 3. A plot of the measured Doubles to Singles count rate ratio as a function of the measured singles count rate. An empirical fit used to determine the dead time parameters is shown in red. The error bars are smaller than the markers.

The method described above is not robust under our experimental conditions, as it relies on the user to manipulate the terms by hand to produce the best fit. This method is also sensitive to the number of data points acquired, thereby increasing the total experimental time and number of sources needed for a more accurate result. Because of this, there can be several values which minimize the sum of squared errors of the deviation between the dead time corrected doubles to singles ratio to the uncorrected ratio with respect to a and b. For a set of standard counters, the ratio of b/a has typically been determined previously using a large number of ^{252}Cf sources; but for this new BCS HLNCC, there is no predetermined ratio. Instead, assuming that $b = \frac{a^2}{4}$, the fitting parameters were found to be $a = 6.53 \cdot 10^{-8}$ and $b = 1.066 \cdot 10^{-15}$, resulting in an average dead time of (0.0653 ± 0.0054) μs. The uncertainty in this value was determined through chi squared analysis and is relatively large due to the reasons discussed previously. Next, b was constrained to 0 and a was found to be $6.199 \cdot 10^{-8}$ producing a dead time of (0.0620 ± 0.0077) μs. The dead time values found are within error using the different empirical approaches, due to the insensitivity of the equations to b over a wide range of values.

A note to the reader: in the first work characterizing the BCS HLNCC [17], it was stated that the dead time parameters were $a = 0.55 \cdot 10^{-6}$ and $b = 0$ using ^{252}Cf sources. For the sources measured at PTI, these values were selected as the best fit for the D/S ratio allowing a constant value, independent of the source strength, once dead time corrected. However, only three sources of a limited count rate range were used, therefore influencing the accuracy of the fit. Also, these values applied to a measurement using only a single detector bank rather than the total six banks combined

for the total detector output. As expected, when the whole system was measured for this paper, the total detector dead time decreased.

4. Neutron Count Distribution Dead Time Approach

Menaa et al [10] outlined and experimentally justified an alternative method to the traditional approach. It was proposed that dead time could also be experimentally estimated using random-in-time neutrons produced by a source such as AmLi, to generate an uncorrelated neutron count distribution. The equations presented in [11], under the assumption of a paralyzable not-free (the system starts counting the initial neutron pulse while it is dead) detector, represent the mean value of the count distribution and the variance of that distribution. They are then used by Menaa et al. to derive expressions for the dead time, δ, in terms of the gate width, T_g, and the statistics of the neutron count distribution:

$$\varphi = 1 - \sqrt{1 - \left[\frac{\langle i\rangle - \sigma_i^2}{\langle i\rangle^2}\right]}\ ;\ \varphi = \frac{\delta}{T_g} \tag{3}$$

with $\langle i\rangle$ representing the mean value of the neutron count distribution as

$$\langle i\rangle = \frac{\sum_i i \cdot A_i}{\sum_i A_i} \tag{4}$$

and σ_i^2 representing the variance of the distribution as

$$\sigma_i^2 = \frac{\sum_i [i - \langle i\rangle]^2 \cdot A_i}{\sum_i A_i}. \tag{5}$$

Through simple measurement of an AmLi source, all necessary variables can be obtained in a short period of time.

Croft et al. [12] reviewed this method in detail, and built upon this work to extend the same methodology to higher order moments of the neutron count distribution. The expressions derived for the third and fourth reduced factorial moments,

$$\varphi = \frac{1}{2}\left[1 - \sqrt[3]{\frac{\langle i(i-1)(i-2)\rangle}{\langle i\rangle^3}}\right] \tag{6}$$

and

$$\varphi = \frac{1}{3}\left[1 - \sqrt[4]{\frac{\langle i(i-1)(i-2)(i-3)\rangle}{\langle i\rangle^4}}\right] \tag{7}$$

respectively, can all be determined from a single measurement. It was proven that the dead times determined from each of these expressions were consistent within counting precision. All three values are reported below.

Because the bias,

$$Bias = 100\left[\frac{\langle i\rangle_{R+A}}{\langle i\rangle_A} - 1\right], \%, \tag{8}$$

should be approximately zero for an uncorrelated neutron source, the neutron count distributions should be roughly equal between the (Reals + Accidentals), or (R + A), and the (Accidentals), or (A), gates (as illustrated in Figure 2). To test this theory, the (R+A) and (A) neutron count distributions were analyzed separately to produce individual dead time values, checked for bias, and then combined into a single 48 cycle data set for an additional dead time determination.

Twenty-four cycles of 300 s data acquisition runs were taken to randomly sample the neutron count distribution, produced by the AmLi sources previously listed, a large number of times. The AmLi sources were centered vertically and radially within the well to load an approximately even count rate on each of the six detector banks. Two separate acquisition runs were taken, one using two AmLi

sources for a combined measured singles count rate of approximately 14000 cps, and the other using all four AmLi sources for a combined measured singles count rate of 33500 cps. The optimal detector parameters were set at 2 μs for the predelay, 48 μs for the gate width, and 4096 μs for the long delay. The total neutron pulse train recorded in PTR-32 was exported to INCC format to produce the count distributions. As is customary with shift register electronics and INCC software, the neutron distributions in each of the cycles are reported as a function of multiplicity for both the (R+A) and (A) gates. These count distributions were analyzed using the second, third, and fourth order moment expressions to determine the dead time and the bias. The results are reported below in Tables I-III.

Number of Sources	δ(R+A) (μs)	±	δ(A) (μs)	±	δ(Combined) (μs)	±	Bias (%)	±
2	0.0669	0.0050	0.0657	0.0054	0.0663	0.0036	0.0008	0.0197
4	0.0641	0.0015	0.0652	0.0018	0.0646	0.0012	0.0060	0.0069
Average	0.0655	0.0052	0.0654	0.0057	0.0654	0.0038	0.0034	0.0209

Table I. Total detector dead time values calculated using the second order factorial moment

As expected, there is less uncertainty in the dead time calculated for the measurement using four AmLi sources rather than just two sources, due to better counting statistics. However, as is typical for in-field measurements, two AmLi sources may be more readily available and still provide accurate evaluations of the detector dead time. The bias is consistent with 0, the individually calculated dead time values are consistent within counting precision across sources, and therefore, the average dead time values between (R+A), (A), and combined gates are also in agreement.

Number of Sources	δ(R+A) (μs)	±	δ(A) (μs)	±	δ(Combined) (μs)	±
2	0.0639	0.0069	0.0723	0.0063	0.0681	0.0047
4	0.0632	0.0019	0.0635	0.0018	0.0634	0.0013
Average	0.0635	0.0071	0.0679	0.0065	0.0657	0.0049

Table II. Total detector dead time values calculated using the third order factorial moment

Number of Sources	δ(R+A) (μs)	±	δ(A) (μs)	±	δ(Combined) (μs)	±
2	0.0603	0.0111	0.0711	0.0086	0.0657	0.0072
4	0.0598	0.0029	0.0609	0.0026	0.0604	0.0020
Average	0.0600	0.0115	0.0660	0.0090	0.0630	0.0075

Table III. Total detector dead time values calculated using the fourth order factorial moment

As the ordered factorial moments increase, the uncertainty in the dead time parameter increases due to the lower precision of higher neutron multiplicities. Because an uncorrelated source is used, higher order multiplicities are not emitted, and therefore the probability of detecting one is low. Despite this, all three expressions result in values that are in agreement within counting precision. This result verifies, using another detector model than was used by Croft et al. [12], that this approach is robust and appropriate for estimating the dead time of a system.

5. Conclusion

The comparison of dead times determined from both the traditional and statistical methods are shown below in Table IV. The traditional approach values are reported for two different empirical fits where b was not free and when it was constrained to zero. The second order (R+A) and (A) combined gate average dead time value, obtained from both the two source and four source measurements, are reported for this comparison. The values are in agreement within uncertainties. It is evident that the uncertainty in the neutron count distribution analysis approach is much less than the uncertainty

associated with the traditional approach. This is due to the insensitivity of the equations to b over a wide range of values and the number of experimental data points used to find the empirical fit.

Method	δ (μs)	±
Traditional- $b=a^2/4$	0.0653	0.0054
Traditional- b=0	0.0620	0.0077
Statistical- 2 sources	0.0663	0.0036
Statistical- 4 sources	0.0646	0.0012
Statistical- Average	0.0654	0.0038

Table IV. Comparison of total detector dead time values using the traditional method and the statistical approach

Both methods have been previously used with ^{3}He-based neutron multiplicity counters, and are shown here to apply to BCS as well. The neutron count distribution approach allows for a quick, robust, and convenient way to determine the dead time of a system. The availability of AmLi sources in facilities also serves as another benefit to the traditional approach. Multiple dead time values can be calculated with a single data acquisition run using the higher order factorial moment expressions, allowing for a cross-verification.

In this work, it has been shown that both approaches return similar dead time values. We have discussed the underlying theories of both methods, while acknowledging many other works over the last few decades. This list is certainly not exhaustive, and it illustrates the revived drive to accurately, precisely, and easily represent detector dead times based on true physical models. A comparison was performed to show the capabilities of both approaches, while justifying this newly proposed analysis with another detector system. This statistical approach provides an experimentally determined approximation to the neutron multiplicity counter's dead time which may be more simple to grasp and implement, returning values with greater confidence due to the robust uncertainty calculations. Future work will include extending this analysis to each of the detector channels, in addition to quantifying the impact these dead time determinations have on the uncertainty in the final calculated mass values of an assay.

6. Acknowledgments

This work was sponsored by the U.S. Department of Energy (DOE), National Nuclear Security Administration (NNSA), Office of Nonproliferation Research and Development (NA-22).

7. References

[1] N. Ensslin, W.C. Harker, M.S. Krick, D.G. Langner, M.M. Pickrell, and J.E. Stewart, "Application guide to neutron multiplicity counting," Los Alamos National Laboratory Report LA-UR-98-4090, 1998.

[2] S. Croft, A. Favalli, D.K. Hauck., D. Henzlova, P.A. Santi, "Feynman variance-to-mean in the context of passive neutron coincidence counting*," Nucl. Instrum. and Meths. in Phys*. Res A686 (2012)136-144.

[3] N. Dytlewski "Dead-time corrections for multiplicity counters," *Nuclear Instruments and Methods in Physics Research Section A: Accelerators, Spectrometers, Detectors and Associated Equipment,* 305, no. 2 (1991): 492-494.

[4] M. S. Krick, H. O. Menlove, *The High-Level Neutron Coincidence Counter (HLNCC): User's Manual*, Los Alamos Scientific Laboratory Report LA-7779-M, June 1979.

[5] J. E. Swansen "Deadtime reduction in thermal neutron coincidence counter*," Nuclear Instruments and Methods in Physics Research Section B: Beam Interactions with Materials and Atoms* 9, no. 1 (1985): 80-88.

[6] S. Croft, L.G. Evans, D. K. Hauck, M. T. Swinhoe, P. A. Santi, “Testing an alternative singles rate dead time correction algorithm for use in neutron multiplicity analysis,” in: 52nd Annual Meeting of the Institute of Nuclear Materials Management, 17-21 July, 2011.

[7] L. G. Evans, M. T. Swinhoe, S. Croft, D. K. Hauck, and P. A. Santi, "Extension of ESARDA NDA Multiplicity Benchmark," 2011.

[8] W. Hage and D. M. Cifarelli, "Correlation analysis with neutron count distribution for a paralyzing dead-time counter for the assay of spontaneous fissioning material," *Nuclear science and engineering,* 112, no. 2 (1992): 136-158.

[9] D. K. Hauck, S. Croft, L. G. Evans, A. Favalli, P. A. Santi, and J. Dowell. "Study of a theoretical model for the measured gate moments resulting from correlated detection events and an extending dead time." *Nuclear Instruments and Methods in Physics Research Section A: Accelerators, Spectrometers, Detectors and Associated Equipment,* 719 (2013): 57-69.

[10] N. Menaa, S. Croft, S. C. Kane, S. Philips, M. Villani, and L. G. Evans. "Experimental Determination of the Multiplicity Deadtime Parameter," 2008.

[11] A. Foglio Para and M.M. Bettoni, “Counting statistics of nuclear detectors,” *Nuclear Instruments and Methods,* 70 (1969): 52-56.

[12] S. Croft, S. Cleveland, A. Favalli, R. D. McElroy Jr, A. T. Simone, "Estimating the Effective System Dead Time Parameter for Correlated Neutron Counting," submitted to *Nuclear Inst. and Methods in Physics Research, A*.

[13] Harwell Oxford, U. K., D. G. Energy, and France IRSN, "Current Status of ^{3}He Alternative Technologies for Nuclear Safeguards," 2015.

[14] J. L. Lacy, A. Athanasiades, L. Sun, C. S. Martin, G. J. Vazquez-Flores, and S. Mukhopadhyay, "Performance of a straw-based portable neutron coincidence/multiplicity counter," in Nuclear Science Symposium and Medical Imaging Conference (NSS/MIC), IEEE (2011): 529-532.

[15] J. L. Lacy, A. Athanasiades, C. S. Martin, L. Sun, and G. J. Vazquez-Flores, "Design and performance of high-efficiency counters based on boron-lined straw detectors," *Proceedings of the 53rd Annual Meeting of Institute of Nuclear Materials Management* (INMM), 2012.

[16] J. L. Lacy, A. Athanasiades, L. Sun, C. S. Martin, and G. J. Vazquez-Flores," A Straw Based HLNCC Multiplicity Counter with Improved FOM in Same Form Factor," *Proceedings of the 55th Annual Meeting of Institute of Nuclear Materials Management* (INMM), Atlanta, GA, 2014.

[17] A. T. Simone, S. Croft, R. D. McElroy Jr., L. Sun, J. L. Lacy, A. Athanasiades, and J. P. Hayward, "Performance of a Boron-Coated-Straw-Based HLNCC for International Safeguards Applications," submitted to *IEEE Transactions on Nuclear Science*, April 2017.

[18] "32-channel list mode instrument with channel number handling," Multi channel list mode instrument. Accessed April 05, 2017. http://www.iki.kfki.hu/radsec/groups/mcl_en.shtml.

[19] S. L. Cleveland, J. A. Chapman, S. Croft, and R. D. McElroy, Jr. “Comparison of Pulse Train Recorder Module (PTR) and Shift Register Multiplicity Measurements Using the Large Active Well Coincidence Counter (LV-AWCC),” *Proceedings of the 56th Annual Meeting of the Institute of Nuclear Materials Management*, July 12-16, 2015, Indian Wells, California.

[20] "Instrumentation." Instrumentation – CANBERRA Industries. Accessed April 05, 2017. http://www.canberra.com/products/waste_safeguard_systems/instrumentation.asp

The Characterisation of a Novel ^{6}LiF:ZnS Based Neutron Coincidence Counter

Hamid Tagziria[1], Mark Foster[2], Melissa Schear[3], Paul Blay[2], Shamilla Wijayasekara[2]

[1]European Commission, Joint Research Center, Nuclear Security Unit G.II.7, I-21027 Ispra, Italy

[2]Symetrica Security Ltd., Roman House, 39 Botley Road, Southampton, SO52 9AB, UK

[3]Symetrica Inc., 63 Great Road, Maynard MA 01754

Abstract:

LiF:ZnS technology, previously used in the nuclear security field has been successfully adapted by Symetrica Security (UK) to produce an effective neutron coincidence counter. A proof-of-concept system was tested alongside other US and European technologies during the "^{3}He Alternatives for International Safeguards Workshop and Inter-comparison Campaign" held in October 2014 at JRC Ispra.The system performed well as was reported to the 37th ESARDA symposium in Manchester and published in the ESARDA bulletin issue 53 (2015).

Subsequently, within an administrative arrangement with DG-ENER (Euratom) and JRC in Ispra, an upgraded Neutron Coincidence Counter based on this ^{6}LiF:ZnS technology was built. It comprised thirty-two low-profile thermal neutron detectors arranged in four banks of eight around a square sample cavity, with neutron reflectors included to improve the sensitivity profile and a cadmium lining to suppress background neutrons.

This paper describes the system and the results of measurements carried out at the JRC in Ispra to validate the Monte Carlo models, and to characterize the performance of the counter by measuring a number of important parameters such as absolute efficiency, die-away time, gamma-ray rejection efficiency and profile. The performance of the counter is compared to that of the commonly-deployed HLNCC-II which uses rare and expensive ^{3}He gas.

It was found that the ^{6}LiF:ZnS system had a superior absolute efficiency of 22.5% and a die-away time of 31.2µs. Gamma-ray rejection efficiency was measured to be better than 1:10^{7} for a Cs^{137} source at a dose-rate of 1.7mSv/hr at the surface of the sample cavity.

Keywords: NDA, Nuclear Safeguards, Neutron Coincidence Counting, LiF;ZnS

1. Introduction

Neutron coincidence counters (NCC) are essential tools in the non-destructive assay the material used in Nuclear Safeguards efforts. For the last few decades these systems have relied on ^{3}He proportional counters for thermal neutron detection However the future supply of ^{3}He has been recognised as a potential problem [1]. To address this a number of groups have conducted research into ^{6}Li and ^{10}B or organic scintillators as alternative detectors, whilst also exploring their potential to provide some additional capability. To facilitate this work, a number of benchmark tests have been carried out in the US and in Europe [2] and it has been found that useful systems have been developed using both isotopes. JRC Ispra and Symetrica Security Ltd have collaborated on development of a ^{6}LiF:ZnS based system by adapting technology originally developed by Symetrica for nuclear and Homeland Security purposes [3]. The new Neutron Coincidence Counter was designed utilising MCNP and a reduced-capability proof-of-concept detector was built and tested at the 2014 benchmark [4], and found to perform well. Whilst this instrument did not meet the specified performance targets, this was not expected and it did successfully prove the concept and provide essential information for the next stage of its development. The results of the 2014 benchmark tests are shown in **Table 1**.

	HLNCC-II	**PTI**	**Symetrica**	**GE Reuter Stokes**
Technology	^{3}He tubes	Multiple ^{10}B lined straws	^{6}Li loaded blades	Combined ^{10}B and ^{3}He proportional counter
Abs. Eff (%)	16.5	13.6	9.6	10.2
Die away time (s)	43.3	26	56.9	65.4
FoM	2.51	2.66	1.28	1.26

Table 1: Results of the 3He-free benchmark tests carried out in Ispra in 2014.

This paper presents the characterisation of the fully-instrumented NCC and the second stage of the development effort first presented by the authors in ESARDA Bulletin 39 in December 2015 [5] and presented at the ESARDA conference of that year.

2. System Description

The instrument being tested here is the first practical ^{6}LiF:ZnS based coincidence counter able to meet the required performance specification. It comprises thirty-two thermal neutron detectors (dubbed “blades” for their low profile) in a moderator matrix with readout electronics.

2.1. Thermal Neutron Detectors

The detection of thermal neutrons is achieved using a unique detector “blade” design utilising a pair of ^{6}LiF:ZnS screens sandwiching a wavelength-shifting PVT plate to create an active element having dimensions of 50 x 6 x 0.4cm. The scintillation light is collected by silicon photomultipliers and on-board electronics provide pulse-shape discrimination (PSD) to minimise the blades sensitivity to gamma-radiation. This circuit provides output neutron detections as TTL pulses. Each blade is self-contained and its calibration and PSD parameters may be set using a software interface. More detail can be found in Tagziria et al (2015) [5].

The application of a neutron/gamma discrimination threshold means that a fraction of those neutrons captured in the ^{6}Li will be missed, and the measurement of this “readout efficiency” is essential when designing the coincidence counter using Monte Carlo tools. Such a measurement was taken during the proof-of-concept development [5] and gave a value of 85.1 ± 2.9% (1σ).

- **Mass** = 430g
- **Dimensions** = 560 x 68 x 12 mm
- **Power requirement** = 9mA at 12V
- **Temperature range** = 10 to 30°C
- **Neutron detection signal =** +5V, 120ns TTL pulse

Figure 1: A photograph of a blade and some of their specifications.

For instruments that employ a large number of blades, the uniformity of efficiency is important. this was measured for the thirty-two blades produced for this development. A measurement jig was designed and the count rate when exposed to a moderated ^{252}Cf source was recorded for the same PSD parameters. The measurements are shown in Figure 2 and show good consistency over the set. The variation in sensitivity is due to small variations in the ^{6}LiF:ZnS screen thickness.

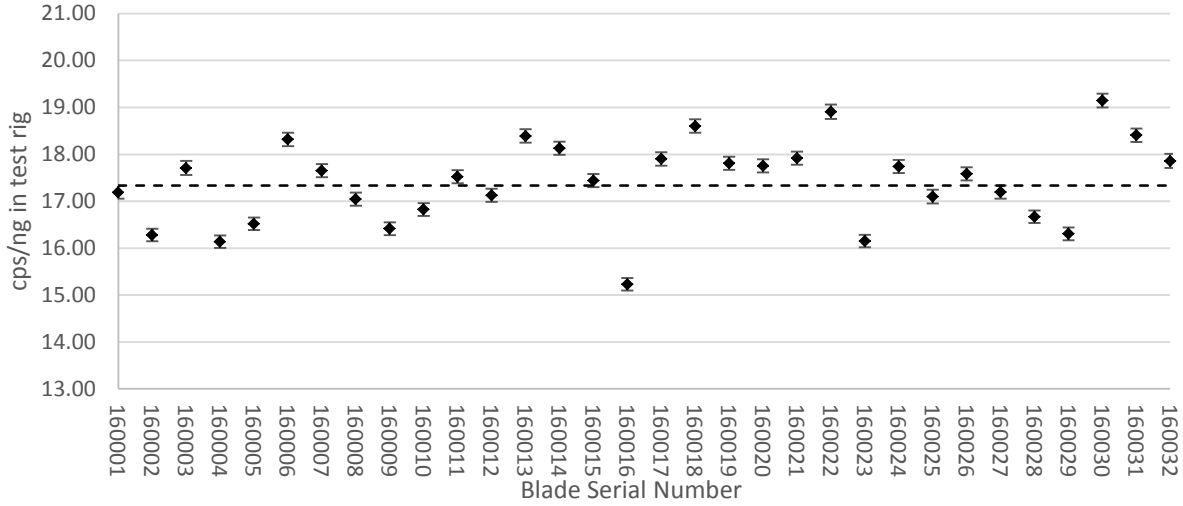

Figure 2: A plot of sensitivity for each of the thirty-two blades. Sensitivity is expressed in cps/ng of ^{252}Cf in the measurement jig. Error bars are shown at the 1σ level.

The mean of this distribution is 17.33 cps/ng and the standard deviation is 5.3%, which was deemed good enough for this development since the sensitivity of the blades is distributed randomly. If required, the neutron/gamma discrimination threshold could be used to further tighten the distribution by setting calibrating the blades to a specified sensitivity.

2.2. Instrument Design

Monte Carlo simulations were carried out to aid the design of an instrument suitable for neutron coincidence counting [5]. Thirty-two blades are arranged in four slabs of eight, surrounding a square sample cavity of 21x21x40cm. Each slab is made up of a HDPE moderator matrix lined on five faces by a 1mm-thick cadmium sheet which suppresses thermal neutron albedo from outside the instrument and prevents thermal neutrons from passing across the sample cavity thus leading to a longer die-away time. The top face is open to allow connectors and cables to pass whilst an aluminium cladding of 1mm avoids the need to handle cadmium. Neutron reflectors are included, in the form of four HDPE blocks to minimise loss of efficiency in the corners of the cavity. Similarly, HDPE and aluminium plugs play a similar role at the top and bottom of the cavity. Whilst this design is not expected to be offer optimised performance, it was selected for ease of manufacture.

Figure 3: Left: A photograph of the instrument with one slab removed showing its moderator and reflector design. Right: A photograph of the completed system including aggregator electronics and cabling.

Readout of the blades is achieved through four aggregator units (seen in the right panel of Figure 3) which power the blades, buffer their TTL outputs and then OR them into a single output. This allows the user to read each blade individually with coincidence-counting electronics such as the PTR-32 (EK Hungary) or to reduce the number of signals into a single output with the JSR-12 or JSR-14 (Canberra). Finally, a software interface is provided that allows the PSD parameters of the blades to be varied to trade off gamma-ray rejection with absolute efficiency.

3. Characterisation of the System

3.1. Performance Figure of Merit and Bias

The performance of the NCC has been quantified by measuring the absolute efficiency (ε) and die-away time (τ), and by calculating a figure-of-merit using the commonly used formula:

$$FoM = \frac{\varepsilon}{\sqrt{\tau}} \qquad (1)$$

Measurements were taken using a ^{252}Cf source of 1.81ng (4197n/s) placed at the centre of the sample cavity. Data was read out for each blade using a PTR-32 and analysed using its accompanying software on a Windows PC. Results are shown in **Table 2** compared to an HNLCC-II owned by JRC and the 8-blade proof-of-concept ^{6}LiF:ZnS instrument. Also given are the values as simulated in MCNP using the readout efficiency previously measured.

	HLNCC-II	8-Blade PoC	32-Blade Measurement	32-Blade MCNP Simulation
Abs. Eff (%)	16.5	9.6	22.5%	25.8%
Die away time (μs)	43.3	56.9	31.2	30.5
FoM	2.51	1.28	4.03	4.67

Table 2: Performance parameters of the instrument compared with an HLNCC-II benchmark and MCNP simulation.

The measured performance parameters of the instrument are encouraging and show a significant advantage over the HLNCC-II. They are also very close to the simulated values. The FoM is however a naïve measurement and other factors must be taken into consideration such as bias and gate fraction when optimal values for gate-width and pre-delay have been selected. These parameters have been investigated using an Americium-lithium source, the Rossi-alpha distribution for which is shown in **Figure 4**.

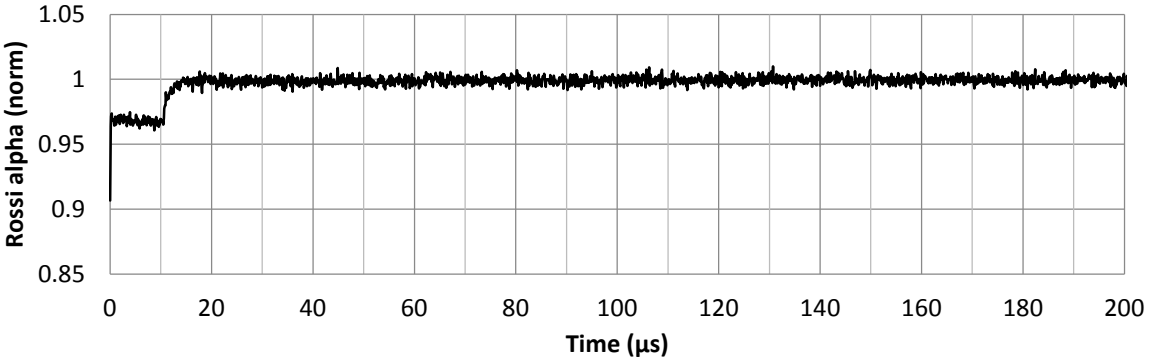

Figure 4: A Rossi-alpha distribution for an AmLi source taken with the completed NCC. Values have been normalised.

As in the proof-of-concept tests we can see a step in the distribution from 0 to 15µs which is caused by the dead-time of the blade that detected the first neutron. This represents a drop in efficiency during that time to 96.88% (31/32) of the maximum.

3.2. Selection of Operating Parameters

The doubles counting precision of the instrument depends on the acquisition gate structure. The goal of this analysis was to determine the optimal combination of pre-delay and gate-width settings which:

a. Minimizes the measurement bias of uncorrelated sources, such as AmLi or the uncorrelated component of PuO_2 sources.
b. Minimizes the relative statistical standard deviation in the measured doubles rate, $\sigma_{Doubles}$ (%), for correlated neutron sources.

The PTR-32 list mode acquisition data files were post-processed using the PTR-32 *Pulse Train Recorder* software [6] for varying combinations of pre-delay and gate-width settings in order to select the optimal gate structure. The determined pre-delay and gate-width settings are then used to determine the doubles gate fraction, f_d, for correlated neutron sources, and investigate its effect on the overall system performance.

3.2.1. Doubles Rate and Bias

The measured doubles rate from uncorrelated sources should ideally be zero in a non-biased counter. However, **Figure 5** shows the negative doubles rate recorded in the counter during the measurement of an AmLi source as a function of pre-delay. Doubles rates are negative regardless of pre-delay choice, but as the pre-delay is increased beyond ~15 us, the magnitude of the negative doubles rate diminishes and plateaus to a constant negative offset, where the effect of the diminished efficiency due to same-channel coincidences is less prevalent, as seen in Figure 4. The negative doubles rate represents a negative bias which was calculated as 100 R/A [7]. **Table 3** shows this bias as a function of pre-delay for various used gate-width settings for the same AmLi measurement. It is important to note that, for any tested gate-width, the negative bias appears to stabilize beyond 13us, making this value a logical choice for pre-delay. For a fixed 13-us pre-delay, the bias fluctuates with gate-width. Although the 39.6us gate-width demonstrates the lowest bias (-0.08%), the gate-width must be selected to reduce the doubles rate uncertainty, discussed in the following section. Later we discuss the effect of this untraditionally long pre-delay on the gate fraction.

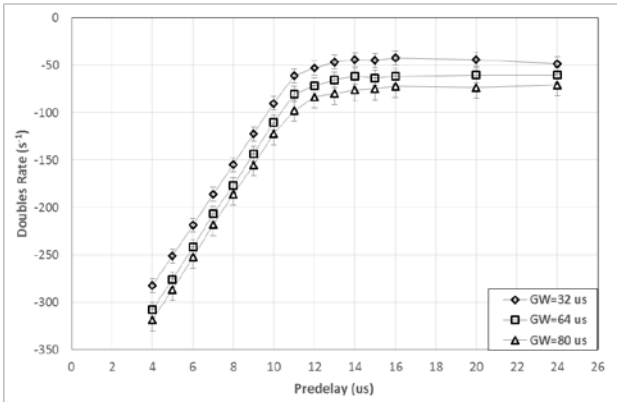

Figure 5: Negative Bias in Doubles rate as a function of pre-delay for various gate-widths for AmLi (singles rate of 31,923 cps, 1200s measurement)

GW (μs)	PD=12	PD=13	PD=14	PD=15
32	-0.20	-0.20	-0.2	-0.2
39.6	-0.16	-0.08	-0.08	-0.08
48	-0.13	-0.13	-0.13	-0.13
56	-0.17	-0.11	-0.11	-0.11
64	-0.10	-0.10	-0.10	-0.10
80	-0.12	-0.12	-0.12	-0.12

Table 3: Negative bias (%) as a function of pre-delay for various gate-width settings

3.2.2. Doubles Rate Uncertainty

Figure 6 shows the relative uncertainty in the doubles rate from a ^{252}Cf source vs. gate-width for pre-delay settings of 13μs and longer . The minimum uncertainty consistently occurs between gate-width settings of 30μs and 40μs. The optimal value of gate-width to minimize the relative error can be approximated by $GW = \tau(e^{\frac{GW}{\tau}} - 1)/2 \approx 1.257\tau$ [7] ,so the 39.6μs rule-of-thumb gate-width does fall within this minimum uncertainty range. The choice of 13μs for the pre-delay reduces the bias effect, while a 39.6μs gate-width reduces the relative uncertainty in doubles counting. Next we consider the effect of the gate structure on the doubles gate fraction.

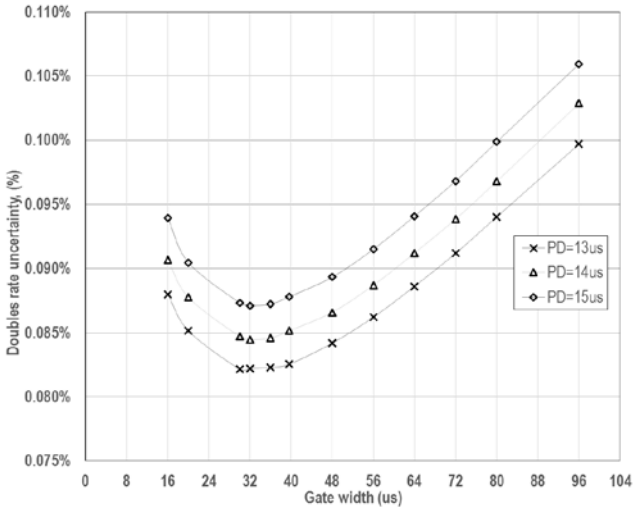

Figure 6: Doubles rate relative uncertainty as a function of gate-width for various pre-delays during 7200s measurement of ^{252}Cf (singles rate of 21,944 cps)

3.2.1. Gate Fraction and its Effect on Figure-of-Merit

The doubles gate fraction, or gate utilization factor, estimates the fraction of the coincidence signal that is measured by the counter. A typical HLNCC-II has a typical gate fraction of 0.696 [8]. The gate fraction increases with shorter pre-delay settings and longer gate-width values. The gate fraction is calculated using Equation 2.

$$f_d = \mathrm{e}^{\frac{-PD}{\tau}}(1 - \mathrm{e}^{\frac{-GW}{\tau}}) \qquad (2) \quad [7]$$

Table 4 shows the doubles gate fractions for varying gate settings for a ^{252}Cf source. For the prescribed pre-delay of 13µs and gate-width of 39.6µs, the gate fraction is 0.451 for this system, lower than that of the HLNCC-II, due to the longer pre-delay (13µs vs 4.5µs, respectively), and shorter gate-width (39.6µs vs 64µs, respectively) compared to HLNCC-II. The effect of this lower gate fraction on the overall system performance was factored into the FoM to give a more comprehensive performance comparison. Previous work suggests two alternative FoMs which include the gate fraction [9, 10], shown in Equations 4 and 5. The latter two are qualitatively similar as $FoM_3=(FoM_2)^2$. The results are summarized in Table 5. Even with the inclusion of the system's reduced gate fraction compared to the HLNCC-II, the Li-based NCC still shows a ~12% increase in performance over the traditional system.

$$FoM = \frac{\varepsilon}{\sqrt{\tau}} \quad (3), \quad FoM_2 = \frac{\varepsilon \cdot f_d}{\sqrt{GW}} \quad (4), \quad FoM_3 = \frac{\varepsilon^2 \cdot {f_d}^2}{GW} \quad (5)$$

GW (µs)	PD=12	PD=13	PD=14	PD=15
32	0.437	0.423	0.41	0.397
39.6	0.489	0.451	0.459	0.445
48	0.535	0.518	0.501	0.486
56	0.568	0.55	0.532	0.516
64	0.593	0.574	0.556	0.539
80	0.628	0.608	0.589	0.571

Table 4: Doubles gate fraction as a function of gate structure

Parameter	HLNCC-II	LiF:ZnS NCC
ε (%)	16.5	22.5
GW (%)	64	39.6
f_d	0.696	0.451
τ (µs)	43.3	31.2
FOM	2.51	4.03
FOM2	1.44	1.61
FOM3	2.06	2.60

Table 5: Overall system comparison

3.3. Axial and Horizontal Profile Measurements

An important characteristic of an effective neutron coincidence counter is a flat efficiency profile, with a large volume having the same absolute efficiency. This is a function of the whole counter design, especially the placement of neutron reflectors and moderators. To characterise this, two sets of measurements were taken: the first was to measure the axial profile with the source moving up along the centreline of the system, and the second to measure the horizontal profile by moving the source over a plane at the mid-height of the cavity. In both cases, the 1.81ng ^{252}Cf source was used. For the doubles measurement, a pre-delay and gate width of 15µs and 39.6µs were used.

3.3.1. Axial Profile

The axial profile (Figure 7) shows a considerable drop in absolute efficiency at each end of the sample cavity. If a limit of 5% were set on deviation in the doubles rate, then a small flat region of 10cm at the centre meets that requirement This compares unfavourably with the HLNCC-II. Future iterations of the design should include a change to the neutron reflector design to improve this.

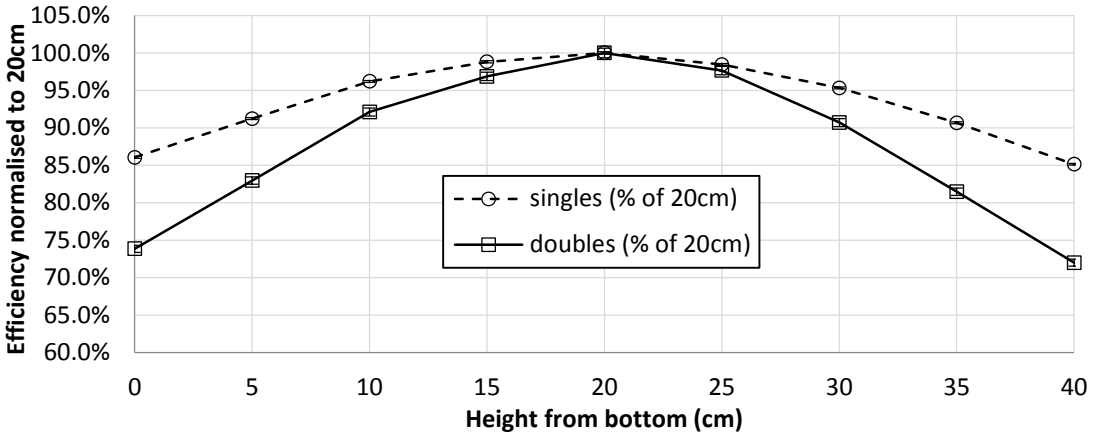

Figure 7: The axial profile of the system. Error bars are at the 1σ level.

3.3.2. Horizontal Profile

The horizontal profile was measured at a height of 20cm, supported on an aluminium stand. Figure 8 shows the variation of singles and doubles rates for a line going across the X-axis of the instrument, from the centre of one face to the centre of the other.

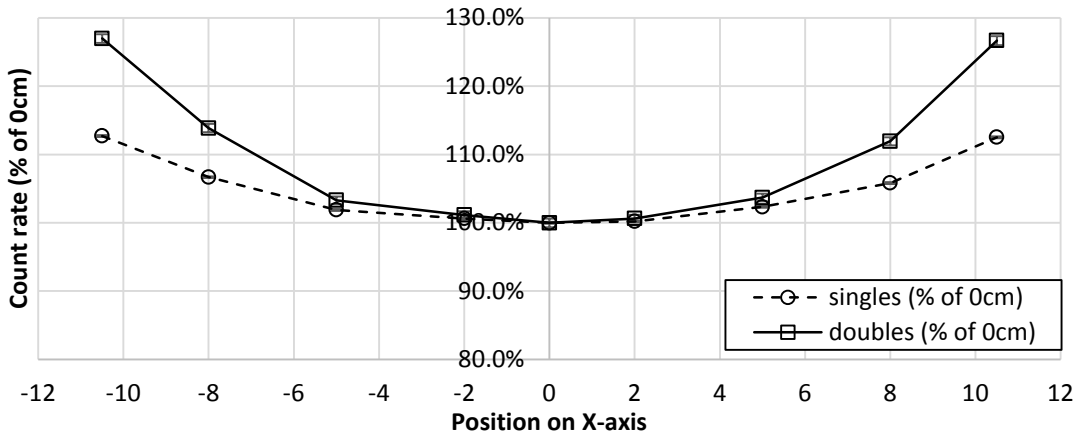

Figure 8: A plot of the singles and doubles rates, across the width of the sample cavity. Error bars are at the 1σ level.

This plot shows a large variation in both efficiency (represented by the singles rate) and doubles rate across the width of the sample cavity. If a limit of 5% were set on variation in doubles rate, then a flat area can be defined that is 10cm across, or ±5cm from the centre point.

A better response can be seen in Figure 9 as the source moves into the corners of the cavity with the largest deviation in doubles rate being 6.7 ± 0.57%. We can also see that the doubles rate starts to fall again in the corner whilst singles rate continues to rise. This is because a greater fraction of the detected neutrons have been partially moderated in the corner reflector before migrating into the slabs, leading to an increased die-away time. Die-away time at (8,8) was 31.8µs vs 30.9µs at (0,0), so the gate fraction there is slightly worse.

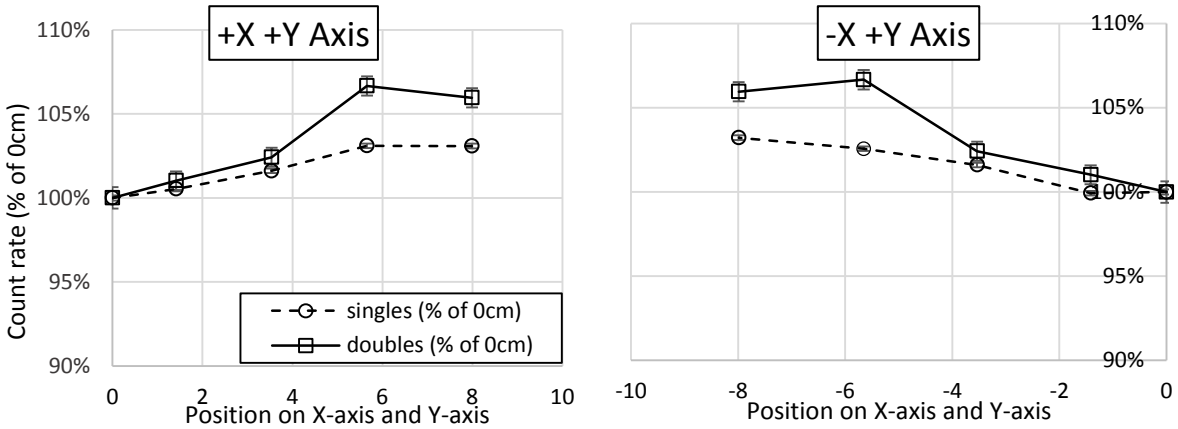

Figure 9: Singles and double rate as the source moves towards the +X,+Y corner (left) and the -X,+Y corner (right)

3.4. Gamma-Ray Rejection Measurement

Gamma-ray rejection (GRR) was measured by placing a ^{137}Cs source at the centre of the sample cavity and measuring the increase in counts above background. The activity of the source was 2.49 x 10^8 Bq and the dose at the surface of the sample cavity was calculated to be 1.73 mSv/hr. Gamma-ray rejection was calculated using the formula below and is expressed as the probability of a single gamma-ray causing a false neutron count.

$$GRR = \frac{G-B}{A \cdot R_B \cdot \Omega} \qquad (6)$$

Where A is the activity of the source in Bq, R_B is the branching ratio of the 662keV gamma ray (0.85), and Ω is the solid angle subtended by the detector as a fraction of 4π. In this case, only the solid angle of the slabs containing blades was used, giving $\Omega = 0.93$. G and B are the count rates during a ^{137}Cs exposure and background, respectively.

G was measured to be 32.49 ± 0.23 cps and B was measured to be 18.04 ± 0.18 cps. This gave a measurement of GRR = 7.33 x 10^{-8} ± 0.17 x 10^{-8} (1σ).

Another measurement was made of how the doubles signature for a fission source is affected by the presence of gamma-ray flux. To measure this, the same ^{137}Cs source and the 1.81ng ^{252}Cf were used, with the doubles rate measured with and without the gamma-ray flux being present. Using a pre-delay and gate width of 15μs and 39.6μs the following results were obtained:

	Doubles rate
^{252}Cf =	149.20 ± 0.59 cps
^{137}Cs + ^{252}Cf =	156.83 ± 0.86 cps
Ratio =	1.05 ± 0.01

Table 6: The measured doubles rate with and without a gamma-ray dose of 1.73mSv/hr.

This indicates that the introduction of the gamma-ray flux creates a significant positive bias. In practice, this can be reduced by raising the neutron/gamma discrimination threshold or by including a steel liner to reduce the surface dose.

3.5. Measurement with Plutonium Samples

Finally, the plutonium mass calibration function was measured, using a set of PuGa sources having the following isotopic composition:

Isotope	**Iso.Compo.wt %**	**rsd %**	**Specific Power mW/g (error)**	**Half Life (y)**
Pu-238	0.1336	0.04	567.57 (0.26)	87.74
Pu-239	75.6606	0.03	1.9288 (0.0003)	24119
Pu-240	21.4898	0.07	7.0824 (0.002	6564
Pu-241	1.9510	0.93	3.412 (0.002)	14.348
Pu-242	0.7651	0.38	0.1159 (0.0003)	376300
Am-241	1.86	0.02	114.2 (0.42)	433.6

Table 7: Isotopic composition of the PuGa samples used in this measurement.

The same measurement was performed with an HLNCC-II owned by JRC for comparison purposes. Figure 10 shows this data as well as data taken with the eight-blade proof-of-concept.

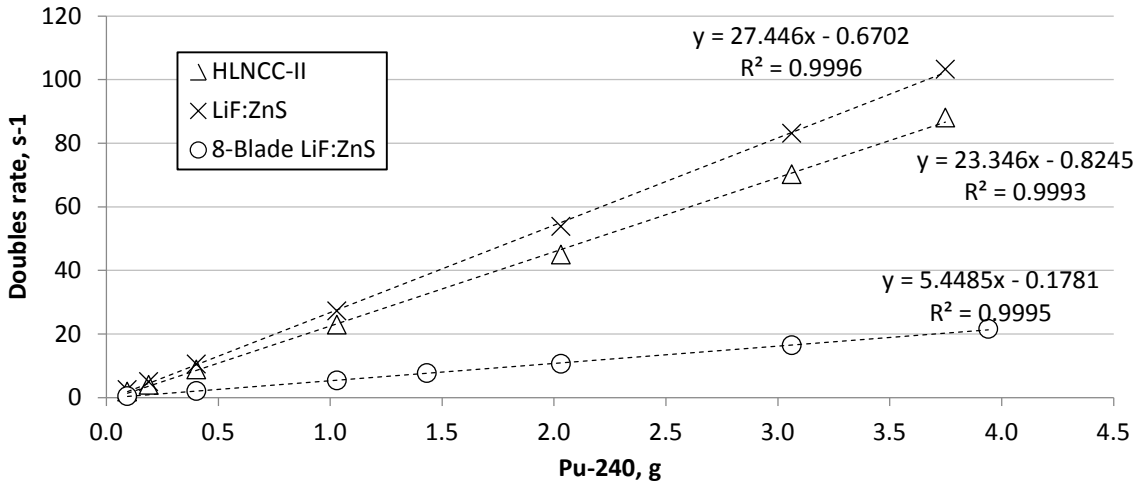

Figure 10: Plots of doubles rate as a function of 240Pu mass taken using PuGa samples. Statistical errors have been included but cannot be seen on this scale.

In the figure we see that the system has a linear relationship, as desired. The gradient of the 32-blade system is only somewhat steeper than the HLNCC-II because although it has a much higher absolute efficiency, this is moderated by the poorer gate-fraction caused by the long pre-delay. As in the 8-blade proof-of-concept a negative intercept is seen due to the negative bias remaining in the system.

4. Conclusions

This study relates to the first practical ^{6}LiF:ZnS NCC and has demonstrated that a system has been built that can be used for non-destructive assay in the field of nuclear safeguards. Good agreement was also observed between Monte Carlo models and measurements taken at JRC following validation of models during the first stage of this development [5].

It was found that the ^{6}LiF:ZnS system had a superior absolute efficiency of 22.5% and a die-away time of 31.2µs compared to 16.5% and 43.3µs for the HLNCC respectively. This achieved a figure-of-merit of 4.03 compared to the 2.51 of the HLNCC-II. In practical terms, this difference will allow a given doubles rate uncertainty to be achieved in less time and so improve throughput of samples. Gamma-ray rejection was measured to be better than 1:10^{7} for a ^{137}Cs source at a dose of 1.7mSv/hr at the surface of the sample cavity. The vertical and horizontal profiles of the counter are not optimal but are acceptable and can be improved with redesigned top and bottom reflectors, and an annular configuration. The validated Monte Carlo models will be used to make these improvements. Although a very small negative bias is observed even with the optimum pre-delay and gate-width, the plutonium mass calibration is rather linear.

There is scope for further development and improvements (both on the design and electronics) on aspects such as the imposition of a relatively long pre-delay by dead time and pulse pile-up effects in the blades, which is the main limitation on the performance of the instrument.

Acknowledgments:

The authors would like to acknowledge the support and funding from DG-ENER under AA no.33952 with the JRC. Discussions and collaboration with Peter Schwalback of DG ENER and the support of Arturs Rozite during the final testing of the NCC in PERLA are also acknowledged.

5. Legal matters

5.1. Privacy regulations and protection of personal data

The authors agree that ESARDA may print their names/contact data/photograph/article in the ESARDA Bulletin/Symposium proceedings or any other ESARDA publications and when necessary for any other purposes connected with ESARDA activities.

5.2. Copyright

The author agrees that submission of an article automatically authorises ESARDA to publish the work/article in whole or in part in all ESARDA publications – the bulletin, meeting proceedings, and on the website.

The author declares that their work/article is original and not a violation or infringement of any existing copyright.

6. References

[1] Kouzes RT. 2009. *The ^{3}He Supply Problem*. Technical Report PNNL-18388, Pacific Northwest National Laboratory, Richland, WA.

[2] Current Status of ^{3}He Alternative Technologies for Nuclear Safeguards, international measurement campaign and workshop on He3 alternatives for safeguards, at the JRC in Ispra October 2014, within a DOE-Euratom Action Sheet 47. Report LA-UR-15-21201 Ver. 2 , 2015

[3] G. Dermody, *A Scalable 3He--free neutron detector for multiple applications*. Presentation at the ESARDA Novel Approaches/Novel Technologies Working Group workshop held in Oxford in March 2014

[4] P. Peerani, C. Carrapico, B. Pedersen, V. Forcina, F. Rosas, A. Rosite, H. Tagziria, A. Tomanin, *Workshop on He-3 alternatives for safeguards applications*, presented at the 37th ESARDA symposium in Manchester May 2015

[5] H. Tagziria, M. Foster, M. Schear, D. Ramsden, G. Dermody, B. Pedersen, P. Peerani, P. Schwalbach, *Experimental Assessment of a 6LiF:ZnS(Ag) Prototype Neutron Coincidence Counter for Safeguards*, ESARDA Bulletin No.53, 2015, pg.30

[6] J. Huszti et al., *Pulse Train Recorder 32HV, Multichannel Neutron Coincidence Data Acquisition System Manual*

[7] D. T. Reilly, “Passive Nondestructive Assay of Nuclear Materials,” Office of Nuclear Regulatory Research, NUREG/CR-5550, Los Alamos National Laboratory Document LA-UR-90-732 (1990)

[8] P. Peerani, et al., Workshop on He-3 Alternatives for International Safeguards Benchmark Results Presentation, Ispra, 15-17/10/2014

[9] S. Croft, L. G. Evans, M. Schear, Optimal Gate Width Setting for Passive Neutron Multiplicity Counting, 51st INMM Annual Meeting, Baltimore, MD, 2010, LA-UR-10-04453

[10] J. Dolan, S. Croft, A. Dougan, D. Peranteau., An International View on ^{3}He Alternatives for Nuclear Safeguards, DOE NNSA report, May 2014

Session 08

Arms Control and Nuclear Disarmament

Verification II

Technical Challenges and solutions within the International Partnership for Nuclear Disarmament Verification (IPNDV)

H. Tagziria[a1], G. Kirchner [2] and P. Mazabraud [3]

[1] European Commission, Joint Research Center, Nuclear Security Unit G.II.7, I-21027 Ispra, Italy
[2] G. Kirchner, ZNF, Universität Hamburg, Germany
[3] Direction Générale des Relations Internationales et de la Stratégie, Ministère de la Défense, France

Abstract

The International Partnership for Nuclear Disarmament Verification (IPNDV) which was launched in March 2015 in Washington broadly aims to build international capacity amongst Nuclear Weapon States (NWS) and non-NWS, improve and broaden the understanding of the challenges faced with in nuclear disarmament verification and monitoring and finally provide international leadership by facilitating technical progress to meet these challenges. Following a short introduction to IPNDV (see also the presentation by US Nuclear Threat Initiative (NTI) at this symposium), this paper shall focus on the technical challenges in disarmament verification which heavily depends on Non-Destructive Analysis Techniques (NDA) combined with containment and surveillance and chain of custody which have been effectively used in nuclear safeguards and nuclear security for many decades. However boundary conditions and the need for information barriers to protect sensitive information make their application in nuclear disarmament verification that much more challenging.

Keywords: Disarmament Verification, NDA, Nuclear Safeguards, Chain of custody, information barriers

[a] Contact: hamid.tagziria@ec.europa.eu

1. Introduction

The International Partnership for Nuclear Disarmament Verification (IPNDV) [1,2] principally uses for its building blocks a number of initiatives such as the US-Russia monitoring and verification experience, the US-UK program on non-proliferation and arms control technology and the UK-Norway initiative [3] on nuclear warhead dismantlement verification.

IPNDV however differs from others in that it is focused on practical and technical activities and recognizes that 1) an effective verification underpins the all-important confidence, 2) that disarmament can only happen if verifiable and 3) that technologies (old and novel) are fundamentally needed for confidence in verification. The latter heavily depends on Non-Destructive Analysis Techniques (NDA) combined with containment and surveillance and chain of custody which have been effectively used in nuclear safeguards and nuclear security for many decades.

The IPNDV activities are organized around biannual plenaries (previously held in Washington, Oslo, Tokyo, Abu Dhabi and Berlin) and are principally focused on the work of the three working groups (WG):

- WG1: Monitoring and verification objectives
- WG2: On-site inspections
- WG3: Technical challenges and solutions

A number of much needed and useful joint group meetings were also organized.

The plenary sessions are generally attended by about 25 (invited) national delegations: the 5 UN Security Council's permanent members, about 11 or more EU Member states , about 11 non EU-NNWS and the EU/EEAS in addition to delegates from IAEA, VERTIC, CTBTO and OPCW.

While the IPNDV overall will be presented and described in the plenary of this ESARDA symposium and WG2 work described by Floyd et al. also in this event, this paper will focus on some aspects of WG3 work. For further details the reader is directed to references 1 and 2.

2. The IPNDV simple scenario:

In order to ensure further focusing of work and good progress towards IPNDV objectives, a simple scenario was agreed in Geneva in February 2016, although revisited and expanded on in subsequent meetings whereby:

- One NWS will dismantle one Nuclear Explosive Device (NED) and put the resulting components (nuclear material, explosives, etc.) into a temporary monitored storage at the dismantlement site.
- The inspecting party will consist of members from both NWS and non-NWS.
- Confidence in the completion of these activities is required by both the inspectors and governments.

The starting points of the scenario would be:

a) **To Confirm NED:** X quantity of either Pu or U with Y % of either Pu-239 or U-235; X and Y will depend on the NED, on what the NWS is willing to reveal and the accuracy of the equipment
b) **To confirm dismantlement of the NED:** Separation of the nuclear material (physics pack) and the High Explosive
c) **To Ensure Chain of custody:** from when inspectors confirm the item declared as an NED meets agreed characteristics until both HE and NM are in temporary monitored storage
d) **To ensure NM and HE remain within temporary monitored storage until the next stage of the dismantlement process:** arrangements must be made for how containers are moved and how the temporary storage will be monitored.

The diagram of Figure 1 drawn by the Japan delegation is to reflect the scenario.

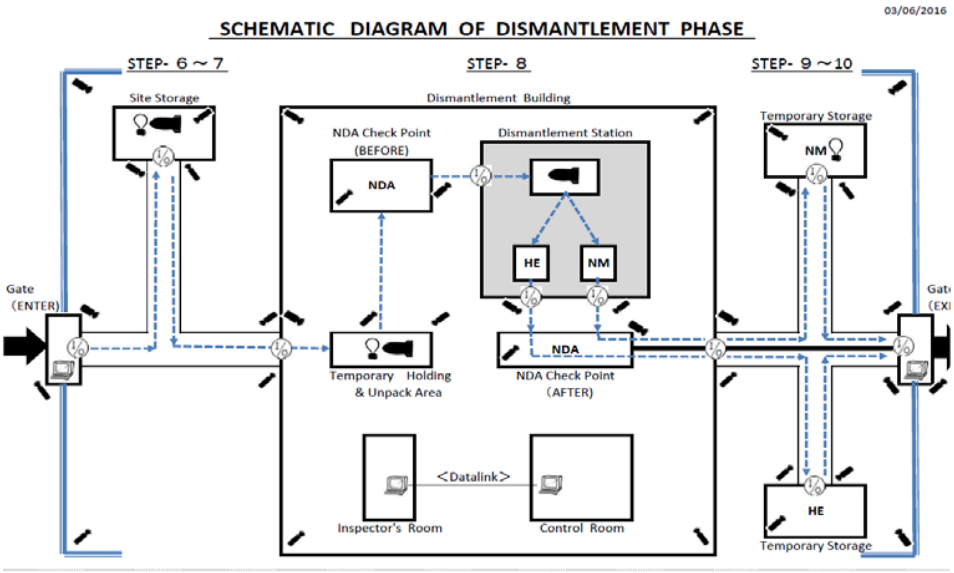

Figure 1: Schematic Diagram of a the dismantlement phase (by Japan delegation) based on the IPNDV simple scenario

3. Working Group 3: Technical challenges and solutions

In line with its terms of reference [1, 2] WG3 would examine and assess:

- How parties can confirm the presence or absence of nuclear warheads and relevant nuclear materials without revealing proliferation sensitive information;
- Effective methods and procedures for establishing and maintaining chain of custody for items at different stages in the nuclear weapons lifecycle; and
- Strategies and tools for software and hardware certification and authentication.

WG 3 thus endeavoured to map any existing and potential technical capabilities for the monitoring and verification of a nuclear weapon dismantlement process at its different stages, the associated level of confidence each technology can bring and finally draw a list that identifies capability gaps and weaknesses.

Ultimately the aim is to develop solutions for key technical challenges for Nuclear Weapons States (NWS) and Non-NWS related to nuclear disarmament verification, particularly issues focusing on nuclear warhead authentication, methods for establishing and maintaining chain of custody, and data and equipment authentication. Specific technologies and methods will be needed to support future arms control and disarmament initiatives. Nuclear warhead verification and monitored dismantlement of nuclear weapons in particular will require extensive collaboration, technology development, and testing. While significant contributions have already been made, this work has largely been focused within a handful of states and many issues remain unresolved. The WGs and IPNDV in general acknowledged the complete nuclear warhead lifecycle, but initial focus has been on the nuclear warhead dismantlement process and the monitored storage of nuclear materials resulting from dismantled nuclear warheads.

3.1. WG3's tool box of Potential Technologies

About 21 potential technology papers (or data sheets) now nearing completion have been developed and written by WG3 delegations which cover 3 main pillars of a dismantlement verification process. As no single technology would fit all purposes and stages, it is suggested that the technologies proposed should be seen rather as a tool box able to be picked from and adapted as to adequately address various aspects and stages of an agreed scenario which its possible variations (and development) in scope and within changing boundary conditions beyond the initial simple scenario.

1) Nuclear Materials
    a. High Resolution gamma spectrometry
    b. Gamma-ray imaging
    c. Passive neutron counting
    d. Pulsed neutron interrogation
    e. Active neutron interrogation
    f. Fast neutron imaging
    g. Muon Tomography
    h. Radiation templates

2) High Explosives (HE)
    a. Computed Tomography (X-ray imaging)
    b. Fast neutron interrogation (for HE identification)
    c. Nuclear quadrupole resonance spectroscopy (NQR)
    d. Raman spectroscopy (fingerprinting)
    e. X-ray backscattering imaging (for size and shape)
    f. Nuclear Resonance Fluorescence (NRF)

3) Chain of Custody:
    a) Facility Verification and change detection

b) 3D identification and containment
c) Surveillance
d) Accelerometers
e) Radiation detection
f) Tamper indicating seals and enclosures

More specifically for the Chain of Custody main pillars for surveillance, containment and identification:

Technology area	**Technology**
Surveillance	• Personal • Video • 3D Laser • Radiation portal monitors • Accelerometers • Radiation Detection • …
Containement	• TIDs and Seals • 3D Laser Change Detection System • Optical Change Detection Systems • Tamper indicating enclosure • …
Identification	• Radiation proof passive RFID • 3D Container identification • Tagging • ...

A number of the above technologies currently applied to nuclear safeguards and nuclear security (Non Destructive Analysis, 3D laser based, seals and tamper indicators..) were demonstrated by the Joint Research Centre in ISPRA to WG3 participants in May 2016.

3.2. Template of WG3 Technology Papers

Each paper or technology data sheet has been written based on a common template that provides the following information:

a. Physical Principle/ Methodology of Technology
b. Potential Monitoring Use Cases (e.g., chain of custody, nuclear material detection, explosives detection, etc.)
c. Physical Description of Technology
d. Time Constraints for verification
e. Technology Complexity
f. Infrastructure requirements
g. Technology Limitations
h. Information Collected by the Technology
i. Safety, Security, Deployment Concerns:
j. Technology Development Stage (or readiness level TRL)
k. Cost Estimate
l. Where/How the Technology Is Currently Used

m. Additional System Functionality
n. Examples of Equipment and References

4. Case study: Neutron Passive Counting

In essence within the simple scenario described above and the boundary conditions to be safeguarded by strong information barriers, the verification of attributes in nuclear disarmament for a Pu based device would ultimately seek to:

1) confirm the presence of Pu,
2) measure the ^{240}Pu to ^{239}Pu ratio (typically ≤ 0.1 for NEDs)
3) measure the mass of ^{240}Pu and
4) consequently extract the mass of Pu from steps 2) and 3) in order to verify whether the mass exceeds the agreed threshold.

4.1. Principles of neutron coincidence counting

Contemporary nuclear explosive devices (NED) or nuclear weapons primarily contain plutonium (Pu) with ≥ 90% of ^{239}Pu and/or Highly Enriched Uranium (HEU) with ≥ 20 % of ^{235}U (for which active interrogation is more suitable). In addition, the so called “primary” (or pit) may be made of Pu and/or HEU metal and as part of a “secondary” may also include extra fissile materials (in general HEU). It is expected that a nuclear weapon would contain about 8 kg of Pu (or ^{233}U) or 25 kg of ^{235}U in HEU. Passive Neutron Counting makes use of the neutrons emitted by spontaneous and induced fission processes in plutonium and uranium to measure the amount of nuclear material present. The very penetrating nature of neutrons facilitates this use by making it possible to measure neutrons from the entire item.

The neutrons from nuclear material are created by three processes:

- Spontaneous fission where the nucleus randomly separates into two fragments which then emit a distribution of neutrons and gamma rays.
- Induced fission where a fission event is driven by an incoming neutron interacting with the nucleus that then fissions.
- (α, n) reactions where lighter elements (^{18}O or ^{19}F for example) react with a decay α.

For well characterized material, the total or gross neutron counting rate is proportional to the mass of nuclear material present. The characterization requirement is substantial, however, and this approach is rarely used to quantify the mass of nuclear material as variations in the material composition and shape strongly affect the neutron rate. Neutron coincidence counting systems (both passive and active) have over many decades been successfully designed, adapted and used in safeguards for the accurate Non Destructive Assay (NDA) of Pu and Uranium containing items [4-6].

In essence, by measuring the correlated spontaneous fission rates of the item of interest, a passive neutron coincidence counter (2 neutrons correlated are counted) or a multiplicity counter (more than 2 neutrons in coincidence) once calibrated leads to the determination of the mass of plutonium provided the isotopic composition of the item is known (by e.g. gamma spectrometry) and that the other competing reactions and conditions are taken into account. For neutrons from either spontaneous fission (^{238,240,242}Pu isotopes) or induced fission (^{239}Pu and ^{235}U) are emitted almost simultaneously (in coincidence) and detected within a gate width in the range of 40 to 80 μs.

The train of electronic pulses produced by the neutron detector is recorded and their distribution in time is determined. Neutrons from background and from (α, n) reactions which must be accounted for are fortunately either uncorrelated or arrive randomly in time. Standard coincidence electronics such as the shift-registers or pulse train analyzers (or recorders) exploit this fact so that the detectors are insensitive to those unwanted neutrons.

In a traditional NCC the total neutron rates (Totals) and the time-correlated rates (called Reals or Doubles) are measured within a gate width of typically 64 μs (depending on counter) following a few μs pre-delay. By subtracting the accidental rates counted within the same gate width but 1000 μs later (i.e. once the fission neutron has died away) the pure correlated pulses are measured which leads to the determination of the plutonium mass and neutron multiplication (M) in the sample provided the ratio of random to coincidence neutrons (α) is known. The latter is not always easily known especially for impure samples or items for which information is restricted and/or whose chemical composition is unknown. This problem of more unknowns (^{240}Pu Mass, Neutron multiplication M and α) than equations is solved by using multiplicity counters with high efficiency which allow to measure the third order terms of the multiplicity distribution i.e. the Triplets rates (3 correlated fission neutrons) and subsequently extract the mass of ^{240}Pu equivalent (or effective).

Figure 2: Standard (HLNCC) neutron coincidence counter and coincidence electronics box

In summary, neutron coincidence counting is a well-established and powerful method used in nuclear safeguards to detect the presence of nuclear material and, provided the isotopic composition is known (by e.g. gamma spectrometry), is also used to determine the mass of Pu. It can be readily applied to nuclear disarmament verification, but only when agreed boundary conditions are respected and robust information barriers are installed. Monte Carlo simulation successfully also combined with measurements for the verification of nuclear material declarations [7-10] can also be envisaged within the disarmament verification regime.

5. Information barriers and boundary conditions

In applying one or more of the technologies from the toolbox above, the following attributes could be revealed:

1) Isotopic composition, the age and the mass of the fissile material
2) Design features of both the NED including the HE: geometry, density, reflectors, seals and tamper indicators etc..
3) Etc..

All these and more are classified and secret information thus requiring an ***Information Barrier*** (IB) to translate it into a standard unclassified information agreeable to all parties such as a binary yes/no (green/red light and perhaps also yellow).

IB systems thus principally aim to prevent the release of proliferative or other sensitive information. They provide the all-important confidence in:

1) the monitoring and verification of classified and sensitive items using measurements of high quality
2) protection of highly sensitive design information and thus alleviate concerns about security and non-proliferation

While the right definition of these attributes and by extension the definition and scope of the scenario the technologies are required to address is crucial, it is a political process as much as the declassification of the data allowed to be acquired. While disarmament is possible only if verifiable, the availability of verification technologies (including for chain of custody) combined with robust information barriers is fundamental in building confidence and advancing toward a process for disarmament. It is equally important that within this highly sensitive technical verification regime the role of “trust” and “confidence” is well understood by both the host and the inspecting parties.

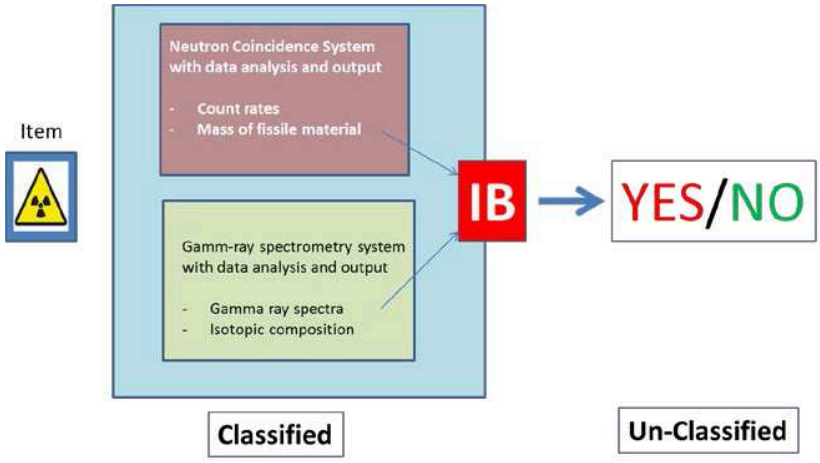

Figure 3: The application of information barrier (IB) to measurement of sensitive items

An example of information barrier was demonstrated in Oslo to IPNDV participants by the UK-Norway initiative [3] which uses gamma ray spectrometry for isotopic composition analysis. Another was shown in 2009 in VNIIF (Russia) to US observers for the Attribute Verification with Neutrons and Gamma rays (AVNG) system [11]. The latter combines an HPGe gamma spectrometer with a multiplicity neutron counter containing 164 ^{3}He tubes giving 30% neutron efficiency inside an AT-400R container (491 mm diameter and 503 mm in height).

Figure 3: An example of the IB box developed (in Phase III) by the UK-Norway initiative [3]

6. Conclusions

During the Abu Dhabi plenary of IPNDV, it was concluded that collective thinking on the broad goals, priorities and next steps have been advanced and several areas were identified as key for the next stages:

a) Further development and completion of technical and procedural papers to verify dismantlement (basic scenario)
b) One recurring theme was the need for practical activities such as technology demonstrations and exercises.
c) These practical and technical activities differentiate IPNDV from other disarmament efforts.

The US under-secretary of state Frank Rose concluded and stated that:

- Agreements must seek to maintain stability and confidence
- Effective verification underpins confidence
- Disarmament can only happen if verifiable
- Progress slow but no short cuts as of complex nature
- Disarmament desirable and feasible
- Technology development very important and new technology can be applied to verification
- Technologies fundamentally needed for confidence in verification
- Trust and Verify principle

In line with its terms of reference and planned activities, Working Group 3 has progressed well towards completing its deliverables. A toolbox of potential technologies applicable to all relevant stages of the nuclear disarmament verification process has been evaluated and papers describing the technologies developed.

As noted by various delegations, the need for practical activities such as technology demonstrations and exercises would be a natural and worthwhile next step for WG3 in particular and IPNDV in general. This was actually done within the trilateral initiative (IAEA, Russia, USA 1996-2002) in December 2001 at the JRC in Ispra (Italy). Eventually, when ready and adequate, an inter-comparison exercise could be organized such as the one performed for He-3 alternative neutron detection technologies for nuclear safeguards within DOE-EURATOM task sheet (47) at the JRC in Ispra in October 2014 combined with a workshop might be a format worth exploring.

As discussed in Nature by Rees et al [12], even at the pinnacle of the cold war US and Russian scientists constructively worked together on verification issues, technologies and approaches. Furthermore, scientists involved in disarmament and initiatives such as the IPNDV can draw inspiration from the fact that scientific collaborations has in the past helped negotiations and that science could eventually help paving the way forward to disarmament.

7. References

[1] http://www.ipndv.org
[2] http://www.nti.org
[3] UK - Norway initiative. http://ukni.info
[4] N. Ensslin, Principles of neutron coincidence counting in Passive NDA of Nuclear Materials, Editors D. Relly et al. Nureg/CR-5550 LA-UR-90-732 , 1991 p. 457-491
[5] Neutron Coincidence Instruments and Applications, H.O. Menlove in Passive NDA of Nuclear Materials, Editors D. Relly et al. Nureg/CR-5550 LA-UR-90-732 , 1991 p. 493-527

[6] W. Hage and Cifarelli, “Correlation Analysis with Neutron Count Distribution for a Paralysing Dead-Time Counter for the Assay of Spontaneous Fissioning Material”, Nucl. Sci. and Eng. 112, (1992) 136-138
[7] M. Looman, P. Peerani and H. Tagziria, Monte Carlo simulation of neutron counters for safeguards applications, Nuclear Instruments and Methods in Physics Research A 598 (2009) 542–550
[8] H. Tagziria and P. Peerani “Monte Carlo modelling of NCCs for Nuclear Safeguards” *International Conference on Mathematics, Computational Methods & Reactor Physics (M&C 2009)* Saratoga Springs, New York, May 3-7, 2009, American Nuclear Society, LaGrange Park, IL (2009)
[9] S. Vaccaro, I. Gaud, M.Vescovi, H. Tagziria, A. Smejkal and P. Schwalbach, “The forward-problem approach in Safeguards verification: directly comparing simulated and measured observables”, Proceedings of the 39th ESARDA, Dusseldolf May 16-18 May 2017
[10] M. Göttsche and G. Kirchner, Improving neutron multiplicity counting for the spatial dependence of multiplication: Results for spherical plutonium samples, Nuclear Instruments and Methods in Physics Research A 798 (2015) 99-106[11] AVNG (Attribute Verification with Neutrons and Gamma rays) with IB built by RFHC in VNIIEF Russia with support from LANL and LLNL (USA) within the Trilateral Initiative (IAEA, Russia, USA 1996-2002)
[12] M. Rees, B. Koppelman and N. Davison, “Scientific steps to nuclear disarmament”, in Nature Vol 465 20 May 2010

Acknowledgments:

This paper is based on work and discussions carried out with IPNDV in general and Working Group 3 in particular. All participating delegations are equally acknowledged.

Disclaimer
The views expressed in this paper represent only those of the authors not of IPNDV, any delegation country including the EU. IPNDV adopts a transparency policy whereby all documents are or would be posted on its portal and that of NTI from which, parts of this paper is inspired.

Disposition Verification of Non-Nuclear Warhead Parts as a New Approach to Verifying Dismantlement

Leesa L. Duckworth Ph.D.

Pacific Northwest National Laboratory
902 Batelle Boulevard P.O. Box 999, MSIN K8-50 Richland WA, 99354

Abstract:

Approaches for the verification of dismantlement of nuclear weapons have historically focused on the separation of High Explosives and Fissile Material. Proposed methods to prove separation and authenticity require measurements of features or characteristics of the Fissile Material and High Explosives, both in assembled and disassembled configurations, producing information commonly considered design information. Protection of this sensitive design information requires a universally approvable information barrier that does not yet exist.

While Fissile Material verification poses ongoing technical and policy challenges, non-nuclear disposition verification may provide a new approach to the challenge that is less encumbered by design sensitivity and operational security issues. Non-nuclear disposition verification focuses on the examination of dispositioned non-nuclear parts and pieces, integral to the assembly of the nuclear warhead. The approach utilizes forensic and spectroscopic techniques used commonly in environmental and safeguards applications, to look for evidence of material changes and activation products indicative of prolonged exposure to neutron fluence from Plutonium. As part of stockpile reduction, these parts would be expected to become excess and, as such, it is reasonable to expect that they will ultimately be dispositioned/destroyed. For the United States, a disposition processes already exist which effectively sanitizes the majority of these parts through physical destruction means (i.e. chopping, crushing shredding etc.), resulting in remnant products that can treated as general waste or recycled as raw materials. Because such processes are present, it would be reasonable to believe that a verification regime might take advantage of their existence to build confidence that dismantlement of a nuclear warhead has taken place. While the existence of these processes in the U.S. do not guarantee similar in treaty partner programs, there is a strong probability that something similar may exist. This paper will explore the feasibility of this novel approach to dismantlement verification.

Keywords: warhead; verification; Dismantlement; Non-Nuclear, Disposition

1. Introduction

Disposition verification as discussed in this paper draws upon foundational work in Safeguards [1], the Comprehensive Nuclear Test-Ban Treaty and Nuclear Forensics [2,3]. This study explores the utilization of technologies such as various NDA measurements, Mass Spectrometry and Ultratrace detection methods to identify neutron activation products in dispositioned parts, components and subassemblies and radiation induced material degradation associated with long term proximity to a source of weapons usable nuclear material. The techniques and capabilities that would be used to search for the presence of activation products or degradation in weapons materials are often used to assure longevity of parts in the stockpile, and have also been demonstrated successfully in emergency response, forensic and environmental applications, including looking at the impacts of radiation dose imparted as a result of the Fukushima disaster

This paper discusses a conceptual approach to disposition verification using established techniques that could provide a less sensitive means for providing confidence and verification that weapons have been dismantled. Because the disposition process is designed to destroy functions and features that would make the design of parts sensitive, disposition verification has the potential to serve as a

catalyst for verification activities that could include not only nuclear weapons states, but also non-nuclear weapons states.

2. Background

A weapon is comprised of many parts, components and subassemblies. Some of these components are nuclear; however the majority are simply mechanical or electronic (Figure 1). In addition to these components there is a significant amount of hardware, fixturing and casing material that is typically non-radioactive. The components that are part of the nuclear package have visual and physical (design) classification issues which can limit the options for verification. Non-Destructive Assay (NDA) measurements can provide detailed information on the mass, material composition and design configuration, but may provide too much information to make a host comfortable in the release of that information. To address this concern, such verification would probably require the addition of a trusted information barrier, a capability that does not currently exist for most NDA technologies.

The verification of dismantlement is expected to be an important component of future arms reduction treaties. Traditionally, dismantlement has focused on the separation of fissile material and high explosives (HE); however, the disposition verification approach considers dismantlement more broadly, to include "the removal of all subassemblies, components, and individual parts for the purpose of physical elimination of the nuclear warhead [4]." While there have been many approaches proposed for providing dismantlement verification, verification of physical dismantlement alone may not be sufficient. The traditional emphasis of dismantlement has been on the separation of fissile material and high explosives; non-nuclear parts and components have always been considered to be of lesser concern. As a result, multiple approaches to fissile material verification have been posited over the last several decades, but to date those approaches still encounter complexities relating to design sensitivities. While such complications exist with fissile material verification for dismantlement, the disposition verification approach discussed in this paper does not assume to be applicable to fissile material at this time. Instead this approach focuses purely on the non-nuclear parts, components and subassemblies that are required to complete the assembled nuclear weapon, and seeks to fill a gap in confidence that dismantlement of a nuclear weapon has actually been completed. Verified disposition of non-nuclear weapons parts has never been considered as part of dismantlement verification.

2.1. Components and their Significance

The inclusion of non-nuclear components (high explosives, electronic and mechanical parts/components not part of the nuclear package) in the disposition verification process could represent an important alternative or supplemental dismantlement verification approach for several reasons. First, the information security requirements associated with many non-nuclear components are generally lower than for the weapons usable nuclear material (WUNM) in the nuclear package itself. While the detailed characteristics of the WUNM are exceptionally difficult to share, even with a NWS treaty partner, the sharing of information on non-nuclear components, especially post-disposition, is likely to be more acceptable and less sensitive. Second, the disposition process for non-nuclear parts is typically conducted on site but in lower level security areas. This may make access to the remnant disposition materials for verification much less complicated and difficult.

Additionally, the proposed disposition verification approach could already take advantage of processes that currently exist instead of inserting invasive inspection processes that require changes in host operational behaviors, into the nuclear weapons production environment. The United States already has a disposition process for all nuclear weapons parts and the methodologies and pathways for disposition are well defined. Because disposition is a very common industrial practice, it would be reasonable to expect that other NWS have some sort of disposition process as well. Witnessed disposition practices were deployed during the Intermediate-Range Nuclear Forces treaty (INF) between the United States and Russia to verify destruction of the empty missile body [5]. Similarly the Conventional Forces in Europe (CFE) Treaty involved 22 states [6] with witnessed disposition of a variety of military armaments and equipment. Thus, there is some historic basis for witnessed disposition of military hardware and weapon components. Clearance and access of inspectors is considered a political decision and that will not be included in this paper, but access to disposition facilities for verification of non-nuclear component destruction could require less restricted access than that necessary for nuclear package SNM verification that may require access to the production facility

high security areas.The verified disposition of non-nuclear parts should provide increased confidence that a nuclear weapon was dismantled by helping verify reduction of parts and components required for the assembly of the weapon itself.

Figure 1. Example: B61 Weapons Parts

The dismantlement of a weapon can produce dozens of parts and up to hundreds of parts when hardware and support structure materials are included in the verification process. Depending upon the planned schedule and the parts/components or subassemblies that are included, a month-long dismantlement campaign could easily produce several hundred parts and components. While the disposition process for some parts and components may be simply to crush and submit for recycling, others components and subassemblies may require more time and steps prior to final disposition. If there is a quantity of parts that are all the same or follow the same disposition path, the host may prefer to disposition them *en masse*. However, as part of a regime, an inspector may prefer that disposition to be performed on an individual part by part basis within an agreed disposition regime. Because all of these items are routed to disposition in approved shipping containers, random selection for disposition verification may be a viable option. This could support the host's need for expedient disposition, but could also support monitored disposition verification needs for an inspector and provide the material content characterization by which to compare against future dispositions of the same component. Without disposition verification of non-nuclear parts and components, a gap exists that could allow for the retention of those parts for reintroduced into the stockpile at another point.

2.2. Disposition and its Pathways

As mentioned above a completed weapon is a combination of a number of different types of parts, components and subassemblies (figure 1.). In U.S. facilities, these items are handled and packaged independently for individual disposition. That disposition process may include reacceptance, repair, reuse or destruction, depending on the needs of the production activity. Similar disposition processes may exist in treaty partner facilities, and could be leveraged in a disposition verification approach. While not all disposition actions currently result is destruction, if a weapon system is being removed from the stockpile, destruction is a likely option for parts, components and subassemblies that will no longer be needed for the remaining stockpile. When these disassociated parts, components and subassemblies are no longer needed because the weapon is being removed from the stockpile, they are then routed for disposition.

Disposition is not an identical process for all items. Some components or subassemblies require further dismantlement before the resulting parts can be sent to final disposition. Nuclear components may be sent to other facilities for final disposition or disposal, while non-nuclear parts and components are typically dispositioned on site. The disposition process renders these unneeded items unusable,

and sanitizes them of all sensitive information. These parts, components or subassemblies are made up of a variety of different metals (both precious and non-precious), composite materials or plastics, and organic materials. The composition and characteristics of the item determine which method of disposition is applicable. Disposition approaches include but are not limited to methods such as shredding, chopping, melting, burning or detonation. These types of disposition processes produce remnant materials, the majority of which are then disposed of as either general waste or recycled. The disposition process of interest for this paper is circled in figure 2, below.

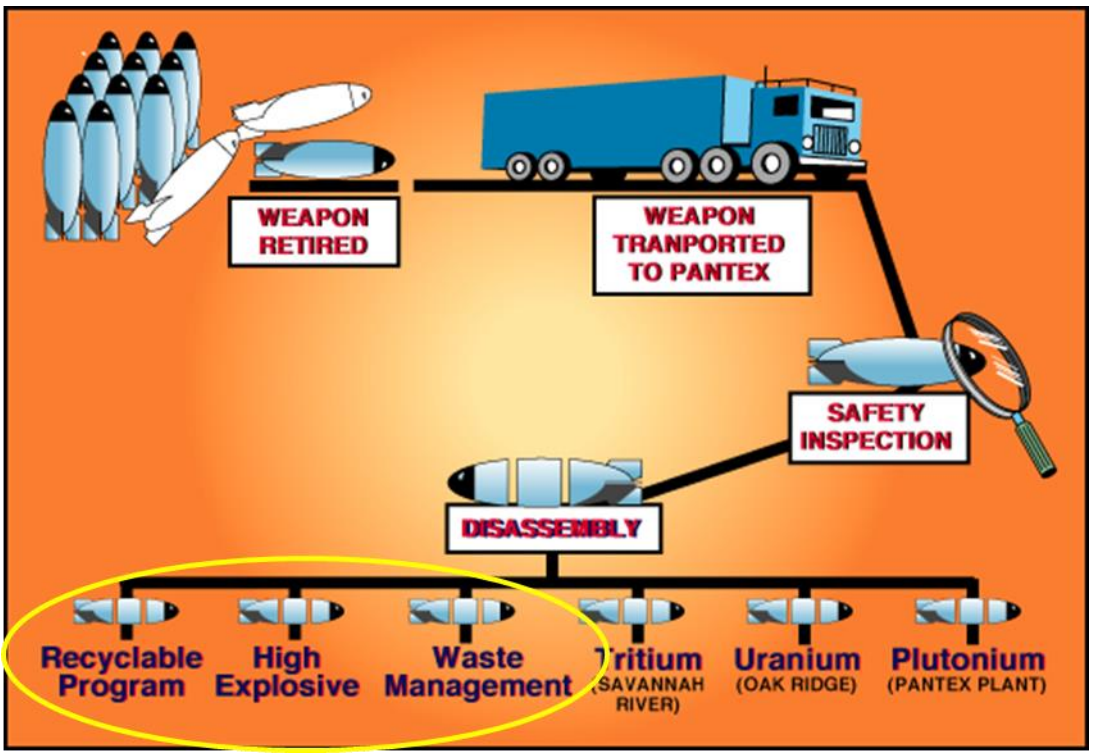

Figure 2. U.S. Dismantlement/Disposition process flow

3. Where and How Could Disposition Verification Happen

3.1. Disposition Verification Process

Disposition verification has three primary areas of focus: first, to confirm consistency of dispositioned materials over time; second, to confirm that the dispositioned material had been in the presence of a significant radiation source for a defined duration of time (size of source and warhead age or period of component presence determined, or bounded, by the host's declaration~ this may include deviation from overall age or presence of specific components due to maintenance); and third, to affirm that those items were recently removed from that source's presence (declared recent time window).

3.1.1. Confirming Consistency of Disposition Materials over Time

Confirming the consistency of dispositioned materials is a key element in ensuring that parts, components and/or subassemblies declared to have come from a specific category of treaty accountable items are consistent across each disassembled item type. In a broader treaty sense, this type of verification could confirm consistency in the type of weapon being dismantled as well. Confidence in this consistency would be expected to develop over time and with repeated verifications of the same dispositioned item(s). The over-time verifications could be performed in a variety of fashions including detailed visual inspections on every dispositioned item as it comes out of the disposition process and/or more detailed material inspections. Consistency may be achieved by witnessed disposition and detailed visual (and potentially physical in some cases) inspections of individual items shortly after dismantlement or verification of randomly selected pre-batched components, parts or hardware of the same types. While visual and physical inspection of

dispositioned materials are specifically applicable to this area of focus, there are additional techniques that could be deployed in support of the second and third areas of focus, which will also provide support for the development of confidence in the consistency of dispositioned products in addition to meeting the other two goals.

3.1.2. Confirm that the Dispositioned Material had been in the Presence of a Significant Radiation Source for a Defined Duration of Time

The proximity of most material to a radiation source for a long enough period of time will produce activation products within those elements as a result of exposure to neutron radiation. These neutron activation products are indicative of sustained exposure, but because of the way activation occurs, it does not support reconstitution of design information, and therefore is inherently protective of national security information. While these products may not be of sufficient quantity or strength to deter a host from disposing of the products in general waste (landfill) or sending their disposition products to recycling, their presence could prove invaluable for disposition verification. Rad hardening which prevents radiation damage to electronic components may prevent the generation activation products within the device itself, but external materials (brackets, housings etc.) may not have the same level of protection.

The decay of specific activation products would be expected to be fairly consistent across the same materials in similar locations within a warhead. Techniques that can be used to see these neutron activation products are dependent upon the quantity of activated product, and energy, mechanism and strength of the decay pathway. Some products may be of significant enough quantity and longevity of decay pathway to be readily seen using standard Mass Spec or other Techniques. Other products will be much less prevalent and could be revealed through the use of Ultratrace methodologies, helping to discern a history of both presence and duration in the presence of a radiation source. Ultratrace methods are broadly used in support of International Safeguards and nuclear forensics work as well as environmental characterization and emergency response. Therefore, a fieldable Mass Spec or Ultratrace system (one that could be set up in a field facility or the system that is currently deployed on the Mars rover) could be easily deployed to support identification. Any field facility would also have to have the capability of supporting appropriate sample preparation.

In addition to identifying the presence of the neutron activation products discussed in the paragraph above, there is also the potential for identifying degradation or chemical structural changes to organic materials including rubbers and plastics as a result of long term exposure to radiation fields within a sealed environment. Techniques such as physio chemical analysis, differential scanning calorimetry, infra-red spectroscopy and electron paramagnetic spectroscopy are some of the methods that can be used to discern characteristic changes to polymer materials that have been exposed to radiation over time in a sealed environment. While dose in open air may have a less significant effect on degradation, dose rates in a sealed environment can be 3 to 10 times higher for materials such as polyolefin, Polyether ether ketone (PEEK), Nylon and Polytetrafluoroethylene (PTFE), that are sensitive to oxidation [7]. A gas/air sample from the sealed environment could also contain outgassed chemical products indicative of radiation induced degradation, although the availability of such a gas/air sample may not be acceptable by the host. The ability of the inspector to witness a gas sampling process would have to be considered to support this type of verification.

3.1.3. Affirm that the Dispositioned Items were Recently Removed from that Source's Presence

In addition to knowing that the component, part or hardware was in the presence of the specified source for an extended (declared) period of time, it would also be valuable to discern that the exposure of the items ceased within the declared dismantlement window. While aging of the exposure would look at long-lived neutron activation products, the need to affirm recent dismantlement would require looking for the presence of much more short-lived neutron activation products. The reason affirmation of presence of short-lived products would be valuable, is that their presence would help provide confidence that the dispositioned item was recently part of the declared dismantlement, and not a part that has been on a shelf for months or years; another possible method to help verify dismantlement.

The identification and measurement of specific short-lived neutron activation products would be dependent upon the style or approach that would be utilized for disposition verification (immediate one-to-one disposition of items, or randomly selected items from batched products). Some very short-lived products will decay to the point that they can no longer be seen in minutes to hours, some in days, and others in weeks. In the case of random selection from batches, specific dates/times of dismantlement would be necessary for the randomly selected part, in order to determine expected level or presence of specific short-lived products. Batching processes which might include parts that had been stored for up to six months may provide limited value for this application, since many of the short-lived products may have decayed completely in the majority of parts.

4. Conclusion

While this approach still requires exploration, disposition verification may offer a number of options which could lead to the development of confidence over time while also protecting the most sensitive elements of the host's stockpile and lifecycle. Many U.S. non-nuclear components and parts are dispositioned by the host with a target of sanitization for release into a general waste or land fill. Because non-nuclear parts disposition may be conducted in lower security industrial areas, this option might provide more accommodating access for all treaty partners to engage in verification, and if the remnant materials are sufficiently insensitive for general release, their examination by even an NNWS partner, might be possible.

While the host might typically perform unmonitored disposition en masse (batched dispositions) for convenience, disposition processes could be designed such that individual items can be dispositioned as well. If this type of condition exists, it could potentially support both the continuous disposition of numerous parts and the disposition of randomly selected representative parts either from randomly selected full disposition verifications or from a ready batch of staged parts.

5. Acknowledgements

The authors would like to acknowledge the National Nuclear Security Administration's Office of Nuclear Verification who provided for the initial development and fleshing or of this concept, and have reviewed this paper and contributed to its completion.

6. References

[1] Glaser, Alexander, and Stefan Bürger. "Verification of a Fissile Material Cutoff Treaty: The case of enrichment facilities and the role of ultra-trace level isotope ratio analysis." *Journal of radioanalytical and nuclear chemistry* 280.1 (2009): 85-90.

[2] Healy, M. J. F. "A framework for the systematic realisation of phenomena for enhanced sensing of radiological and nuclear materials, and radiation." *Journal of Radiological Protection* 35.3 (2015): 649.

[3] Mayer, Klaus, Maria Wallenius, and Zsolt Varga. "Nuclear forensic science: correlating measurable material parameters to the history of nuclear material." *Chemical reviews* 113.2 (2012): 884-900.

[4] Innovating Verification: New Tools & New Actors to Reduce Nuclear Risks. Verifying Baseline Declarations of Nuclear Warheads and Materials. Nuclear Threat Initiative, July 2014.

[5] Treaty between the United States of America and the Soviet Union of Socialist Republics on the Elimination of Their Intermediate-Range and Shorter–Range Missiles (INF). U.S. Department of State, 1987. http://www.state.gov/t/avc/trty/102360.htm

[6] Included Belgium, Canada, Denmark, France, Germany, Greece, Iceland, Italy, Luxembourg, the Netherlands, Norway, Portugal, Spain, Turkey, the U.S., the UK, Bulgaria, Czechoslovakia, Hungary, Poland, Romania and the Soviet Union.

[7] Tavlet, Marc and Ilie, Sorin (1999), Behaviour of Organic Materials in Radiation Environment. IEEE Transactions on Nuclear Science. https://ab-div-bdi-bl-blm.web.cern.ch/ab-div-bdi-bl-blm/Radiation/Behaviour_of_organic_materials_in_radiation_environment.pdf

An Integrated Nuclear Archaeology Approach to Reconstructing Fissile Material Production Histories

Malte Göttsche[1], Baptiste Mouginot[2]

[1] Program on Science and Global Security, Princeton University, Princeton, NJ, USA
[2] Department of Engineering Physics, University of Wisconsin-Madison, Madison, WI, USA

Abstract:

Independent estimates assume that the world-wide civilian and military fissile material stocks amount to 500 tons of plutonium and 1,400 tons of highly-enriched uranium (HEU). To enable deep cuts in warhead arsenals, states will very likely need to verify declarations of fissile material stocks, as they could be used to build new nuclear weapons. One approach is nuclear archaeology, reconstructing the past production of those materials. Research has so far focused on specific measurements in reactors to assess past plutonium production, on deposits in gaseous diffusion plants and isotopics of depleted uranium tails to assess HEU production. For the large historical production of separated plutonium and HEU by Russia and the United States, uncertainties corresponding to large numbers of significant quantities remain with these techniques. A combination of measurements, fuel cycle simulations and reviews of records from past production activities could significantly reduce these uncertainties. This combination also would enable cross-checking information and measurement results for consistency. To demonstrate this approach, we conduct a case study. A declared production history is generated using the CYCLUS nuclear fuel cycle simulator. The simulation results are signatures resulting from the simulated history, some of which could in principle be measured. Assessing the isotopic compositions of waste streams, for example, can allow for cross-checking of declared fuel cycle histories. Based on this case study, the capabilities of the approach will be examined.

Keywords: nuclear archaeology; disarmament; fuel cycle simulations

1. Introduction

With the beginning of the Cold War, the United States and the Soviet Union launched their fissile material production (plutonium and highly enriched uranium, HEU) for military purposes. By the mid-1950s, both countries were already making ton-quantities of fissile material per year to supply their nuclear arsenals. They were soon joined by the United Kingdom (1951), France (1955), China (1964), and Israel (1965)—and later by India, Pakistan, and finally North Korea. According to independent estimates by the International Panel on Fissile Materials, there exist about 505 tons of plutonium and 1370 tons of HEU world-wide today [1].

Most large-scale fissile-material production programs were driven by a sense of urgency and typically shrouded in secrecy. It is generally believed that accounting for these military operations was poor. The fissile material production uncertainty is very large, and even states themselves have had difficulty reconciling production records with physical inventories. In the United States, for example,

estimated plutonium acquisitions exceeded the actual inventory by 2.4 tons, but it is not clear if this material ever existed [2].

These uncertainties will have to be understood and reduced as further progress toward nuclear disarmament is made. In particular, a solid understanding of fissile-material holdings is needed to achieve a meaningful degree of predictability and irreversibility of future arms-control initiatives. Speculations about unaccounted fissile-material stockpiles, possibly equivalent to hundreds of nuclear weapons, could make progress in this area very difficult. To this end, states must be able to verify the past fissile material production [3].

2. An integrated nuclear archaeology approach

In order to understand and reduce the uncertainties in the amount of produced fissile materials, new methods and tools must be developed that help reconstruct the past fissile material production history and enable verification. This is called nuclear archaeology, a concept introduced already in 1990 [4]. The state of nuclear archaeology research is at a low level despite its importance. Some initial research has been conducted on measurement concepts for nuclear archaeology in uranium enrichment plants [5]. The isotopic composition of the depleted uranium tails can be assessed, to determine whether HEU had been produced [6, 7]. Other techniques under development include quantitative estimates of the plutonium production in graphite-moderated reactors (GIRM) [6, 8, 9] and heavy water reactors [10] by examining the graphite moderator or structural reactor elements. By examining isotopic ratios of trace elements, the neutron fluence can be determined, which yields the total amount of plutonium produced in the reactor, assuming the reactor design to be fully known. Some further unpublished and perhaps classified research appears to have been conducted by U.S. government scientists [11]. Of all published research, only GIRM has been experimentally validated to a larger extent.

All past research results only deal with examining particular fuel cycle facilities in isolation. However, the nuclear archaeology toolbox could be much broader. Additional signatures could be sought. What is lacking is a systematic and integrated approach that ties together all available information – not only from measurements, but also from available records about the past fissile material production. Such an approach could be used to identify inconsistencies (for example between records and today's measurements), help understand the underlying reasons for the current uncertainties, and reduce them.

Some nuclear weapon states have a large number of nuclear facilities involved in the fissile material production. The operations of these facilities changed over time (e.g. changes in the power levels of the reactors), as did the complex material transfers between these facilities. For example, spent fuel has sometimes been reprocessed and used as feed in enrichment plants. Enrichment operations also had a level of complexity. For example, natural uranium has sometimes been enriched to low enriched uranium in one plant, which has subsequently been fed into another plant to produce HEU [12, p. 57].

To calculate the material flows in such complex fuel cycles, an integrated fuel cycle simulation tool would be very useful. Data on facility operations provided to the inspector or plausible assumptions could be used as input to simulate the nuclear materials as they pass through the fuel cycle. The simulation results of such forward-modelling would tell about the various signatures to expect from what is available today, for example the isotopic composition of different types of wastes (e.g. depleted uranium tails or radioactive reprocessing waste). It could then be checked whether information gathered today, such as waste measurements, are in agreement with the simulation results. In particular in more complex fuel cycles, various signatures are correlated, and examining

these correlations itself can provide information on the production history, e.g. to which extent reprocessed uranium was used for HEU production.

The joint evaluation of measurements and simulations based on provided data can potentially reduce the uncertainties of the fissile material estimates beyond what is possible based on either approach alone. Some documented data may be inaccurate, or different recorded data maybe inconsistent in itself, for example because of past inventory measurements with large uncertainties. Measurements today can perhaps help resolve such issues.

In the following, we first examine a tool that could be developed for the forward-modelling of complex fissile material production histories. Second, we use a case study to demonstrate the integrated nuclear archaeology approach.

3. Forward-modelling simulation tool

The forward-modelling simulation tool must be able to handle all relevant types of nuclear facilities. It must be able to calculate the composition and masses of nuclear materials at the different fuel cycle stages. To manage the complex fuel cycle histories, the code must provide for options to change facility operations over time, introduce new facilities and shut down old ones at specified times, and change the material flows between facilities. To realize this, discrete fissile material flows must be calculated, as opposed to continuous material flows resulting from a fuel cycle in a steady state.

The Cyclus fuel cycle tool [13] is an open source, agent based fuel cycle simulator. Fundamentally, the Cyclus simulator tracks the discrete flow of materials between facilities over time. It can also provide time series data such as material inventories, incorporating radioactive decay. Facilities are represented as agents. Each agent has its own unique and independent behaviour. The agents do not communicate directly with one another, but interact through the Dynamical Resource Exchange (DRE), which calculates the fissile material transfers between them.

At the beginning of each time step, each facility sends its own material requests to the DRE. The DRE then collects the corresponding bids made by the different facilities that have material to offer. Finally, the DRE solves the market problem by finding a solution that matches requests with bids, allowing the materials to flow between the different facilities. Each facility can specify requested quantities or compositions of materials, and they can decline trade if the offered materials do not meet its own requirements (e.g. regarding isotopic composition).

The Cyclus suite is offered as a pair of libraries: the Cyclus core contains the DRE as well as input and output interfacing, while the Cycamore library provides a basic set of nuclear facility agents. The separation between the simulation agents and the solver core provides flexibility and customizability. The Cyclus development team supports the development of the Cycamore plugins, which correspond to low fidelity archetypes that incorporate some physics [14]. If the Cycamore archetype suite does not capture a desired behavior, contributors can design their own specialized facilities as plugins.

For example, a modified version of the Cycamore enrichment facility has been developed for this research [15]. The original Cycamore enrichment facility allows enriching the uranium-235 content of a feed stream. All minor isotopes (those apart from uranium-235 and uranium-238, for example uranium-234 or uranium-236) are directly sent to the tails. This does not represent the physical reality, where also the minor isotopes are being enriched. To enable the tracking of additional isotopes, the new enrichment archetype allows for manually specifying the enrichment of isotopes other than uranium-235 and uranium-238 as well, and calculates the correct isotopic composition of the product and tails

streams. To enable this, the ratios of each isotope's product to feed enrichments must be specified manually.

Given a desired product mass $M_{product}$ and uranium-235 enrichment τ_p, as well as the specified uranium-235 content in the tails τ_t, the enrichment agent will first compute the required feed mass M_{feed} , which also depends on the uranium-235 enrichment of the feed τ_f, using

$$M_{feed} = M_{product} * \frac{\tau_p - \tau_t}{\tau_f - \tau_t}$$

The tails mass results from mass conservation. The concentrations of the specified minor isotopes in the product are then calculated based on their content in the feed and the specified enrichment ratios. The remaining minor isotope masses from the feed that are not in the product are transferred to the tails.

3. Demonstration of the integrated approach

In the following, we use a case study to provide an example of an integrated nuclear archaeology assessment, using more than one measurable signature, documentation provided to the inspector and forward-modelling to learn about the past fissile material production. For the purpose of clarity, we keep the case study simple. While complex fuel cycle computer simulations are not absolutely required in this simple case, a realistic nuclear weapons state case could be much more complex, in which case a complex simulation tool would be required to forward-model the fuel cycle based on the provided documentation.

For the case study (see Fig. 1), we assume a state used natural uranium to produce plutonium in reactors and a reprocessing plant (Fig. 1, path A) and HEU in a gaseous diffusion enrichment plant (path B). Because the state assumed limited access to natural uranium and wanted to maximize use of its natural uranium resources, it decided to enrich some of the reprocessed uranium (which still contains 0.6% to 0.7% uranium-235) to produce HEU (path C).

The principal goal is to determine how much HEU and plutonium the state produced, based on three pieces of information that were declared: the total amount of natural uranium used (208 tons), information on the reactors (full reactor designs known, specific power 4.45 W/gIHM and fuel burnup 300 MWd/t), and knowing the HEU enrichment (94%). Notably, to quantify the plutonium and HEU production, the material transfers corresponding to the paths A, B and C must be quantified.

While simplified, this case is relevant. For example, the United States released data on its history of natural uranium purchases, and further data on its nuclear program. [16]. This data has already been used to conduct a rough consistency test [17]. Also, at least the Soviet Union and the United States re-used their reprocessed uranium in reactors to produce more plutonium or in enrichment plants for the production of HEU [12, p. 57].

In the following, we propose an approach to solve this nuclear archaeology case study in three parts, combining measurements with forward-modelling.

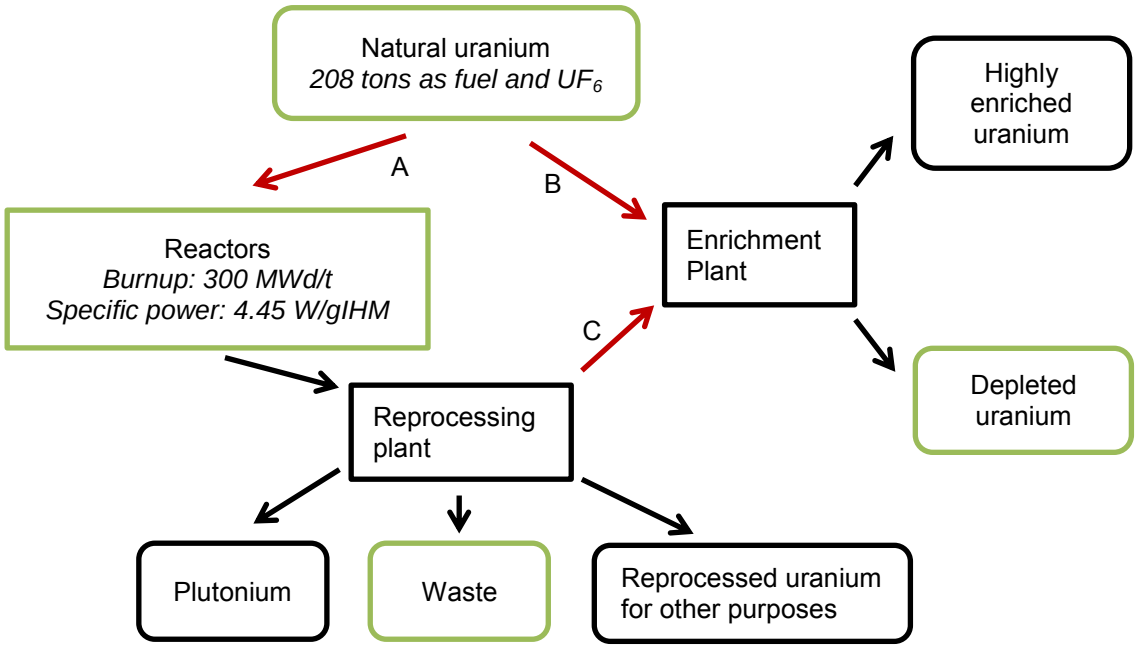

Figure 1: The fuel cycle of the case study. Certain knowledge from declared information or measurements exists for the materials and facilities marked in green. The italic text refers to information declared to the inspectors. The case study focuses on how to use the available data to gain information on the plutonium and HEU production, by quantifying the material transfers indicated by the red arrows, marked A, B and C.

i) The amount of produced plutonium and the required natural uranium (path A) can be determined by taking samples from structural components of the reactor cores for forensic analysis of trace elements.

ii) Confidence in the declared information can be increased by performing consistency-checks. As an example relating to the plutonium production part, the declared fuel burnup can be checked by forensic analysis of the radioactive (high-level) reprocessing waste (for example liquid waste using inductively coupled plasma mass spectrometry). Some plutonium remains in the waste – in particular from military reprocessing activities several decades ago [18]. The ratio of plutonium-239 to plutonium-240 indicates the fuel burnup, if the reactor design is known (see for example graphs in [19, p. 159]). It would be obtained by depletion calculations (forward-modelling). Because of the long half-lives, this signature is very little dependent on the time passed since the fuel discharge from the reactor, which may be unknown.

iii) To distinguish between HEU production from natural uranium feed (path B) and reprocessed uranium feed (path C), forensic analysis by thermal ionization mass spectrometry of samples taken from a number of depleted uranium tails containers could be used. Uranium-236 is produced from uranium-235 when irradiated in reactors, by capturing a neutron [12, p. 58]. Therefore, both HEU as well as the corresponding depleted uranium tails contain uranium-236, if the uranium had previously been irradiated. Given a reprocessed uranium feed, the concentration of uranium-236 in the depleted uranium tails depends on the uranium-235 enrichment of the produced HEU and the tails. It can be computed by using the matched abundance ratio or M* (M-star) cascade theory [20, 21, 22].

Natural uranium, in contrast, contains no uranium-236. Hence, the extent to which natural and reprocessed uranium were used can be determined by measuring the uranium-236 content.

5. Demonstration of the integrated approach: Results

i) Knowing the reactor design and the fuel burnup, infinite lattice depletion calculations using MCODE [23] were performed. The lattice used here corresponds to a reactor design similar to the Savannah River Site (USA) reactor, containing natural uranium slugs and lithium-aluminum alloy control rods. The MCODE simulations yield the isotopic composition of the spent fuel. The uranium isotopics of the spent fuel are shown in Table 1. The MCODE simulations also show that the reactors produced 0.25 g of plutonium per kg of uranium fuel.[1] In the future, a capability to perform such calculations could be integrated into Cyclus. For now, we have manually included the MCODE results in our Cyclus simulation.

Isotope	wt-%
Uranium-234	$5.30 \cdot 10^{-3}$
Uranium-235	0.678
Uranium-236	$5.13 \cdot 10^{-3}$
Uranium-238	99.312

Table 1: Uranium isotopics of the spent fuel

For the purpose of this paper, we assume (without actually assessing the ratios of trace elements in the reactors' structural elements) that it was successfully found that the reactors produced a total of 42 kg of plutonium, using 168 tons of natural uranium (path A). Given that the inspectors know that overall 208 tons of natural uranium were used for both plutonium and HEU production, they now know that 40 tons of natural (un-irradiated) uranium were used for HEU production (path B).

ii) The MCODE simulations show that, at 300 MWd/t, the plutonium isotopic ratio is $Pu-239/Pu-240 = 62.81$. If the forensic analysis of radioactive waste yielded this ratio, the measurement results would independently confirm the declared information that was used for forward-modelling.

iii) For a uranium-235 product enrichment of 94 wt-%, a tails enrichment of 0.3 wt-%, and the uranium-236 feed content from Table 1, we obtain a uranium-236 tails content of $3.85 \cdot 10^{-3}$ wt-% according to the M* cascade theory.[2] These values are used in the Cyclus simulation.

If the uranium-235 tails enrichment is unknown, it would be obtained from the forensic analysis of the tails. In this case study, it is 0.3 wt-%. Let us assume that the average uranium-236 content of the tails the inspectors measured is $2.14 \cdot 10^{-3}$ wt-%. At these values, the relative measurement uncertainties using Thermal Ionization Mass Spectrometry can be smaller than 10^{-3} [24], so the measurements have sufficient precision at these low concentrations. It can be deduced that about 44% of the enrichment feed was natural uranium, and 56% were reprocessed uranium. Thus, 50 tons of reprocessed uranium were enriched (path C). Note that it is necessary to measure the tails, *and* to know the uranium-236 content of the feed, which was obtained from forward-modelling based on the burnup data. Results would have been wrong, if the declared burnup had been wrong. By using forensic analysis of reprocessing waste, however, this cheating scenario could be excluded.

As the main purpose of the case study is only to demonstrate the nuclear archaeology concept in general, we have not conducted a comprehensive uncertainty analysis. The results are therefore preliminary.

[1] The results of the MCODE simulations are presented in order to demonstrate the proposed nuclear archaeology concept. We have validated the reactor model used for MCODE only to a limited extent.
[2] We have not compared the calculated uranium-236 concentrations against experimental values. Therefore, the computed concentration is used in this paper only to explain the described nuclear archaeology concept.

6. Conclusions

Using a case study, this paper has shown, how assessing several indicators of past fissile material production (here: isotopics of depleted uranium tails, isotopics of the reprocessing waste, and documentation provided to inspectors) can be used to study the consistency of data and deduce additional information that had not been provided. It has also shown the importance of combining computer simulations and measurements.

Cyclus provides a good framework for a fuel cycle simulation tool, as it calculates discrete fissile material flows and allows for changes in the fuel cycle design and facility operations over time. For example, a more complicated version of the case study would be a fuel cycle history with a much larger number of facilities with different operational characteristics each, changing over time.

The current facilities that exist as part of the Cycamore library have only very limited capabilities. To comprehensively use Cyclus in the nuclear archaeology context, such libraries must be significantly extended, for example allowing to use a wider range of operational parameters that might be part of provided documentation as simulation input.

Once the integrated nuclear fuel cycle code for nuclear archaeology has been developed, it must be validated, preferably against historical data. The code structure of Cyclus is modular, which facilitates validation: Facility agents can be programmed and implemented without changing other facility agents or the kernel. Therefore, specific extensions or new agents may not require repeated validations of the overall code, if the other parts have been previously validated.

With regard to the integrated nuclear archaeology approach, a robust uncertainty analysis of the gained information on the past fissile material production history will be central. For example, measurement uncertainties must be included. Uncertainties are also introduced by sampling strategies, e.g. from how many depleted uranium containers samples are taken, as isotopic ratios may vary between them. Information on past activities will be incomplete, which introduces uncertainties of the fuel cycle simulation results due to uncertainties of the input parameters. A study should be conducted comprehensively studying the various uncertainties and their propagation.

Overall, this approach can be able to identify errors (for example in the provided documentation) that would not have been found without consistency-checks, thereby possibly increasing precision of fissile material estimates. Also, it may enhance the capability to detect deliberate attempts to declare false or incomplete production histories. Such a widened nuclear archaeology approach could significantly contribute to enable a solid understanding of fissile-material holdings, thereby increasing predictability and irreversibility of future arms-control initiatives.

Acknowledgements

This project was funded by the U.S. Department of Energy’s Consortium for Verification Technology under Award DE-NA 0002534. The authors thank Meghan B. McGarry for the helpful discussions with regard to implementing the new enrichment archetype, and Julien de Troullioud de Lanversin for his support with the depletion calculations.

References

[1] International Panel of Fissile Materials, “Global Fissile Material Report 2015,” 2015.

[2] U.S. Department of Energy, “The United States Plutonium Balance, 1944-2009,” 2012.

[3] A. Glaser and M. Göttsche, “Fissile Material Stockpile Declarations and Cooperative Nuclear Archaeology,” in *FM(C)T Meeting Series, Verifiable Declarations of Fissile Material Stocks: Challenges and Solutions*, United Nations Institute for Disarmament Research Resources, 2017.

[4] F. v. Hippel, “Warhead and Fissile-material Declarations,” in *Reversing the Arms Race: How to Achieve and Verify Deep Reductions in the Nuclear Arsenals*, New York, Gordon and Breach Science Publishers, 1990.

[5] S. Philippe and A. Glaser, “Nuclear Archaeology for Gaseous Diffusion Enrichment Plants,” *Science & Global Security,* pp. 27-49, 2014.

[6] S. Fetter, “Nuclear Archaeology: Verifying Declarations of Fissile-Material Production,” *Science & Global Security 3,* pp. 237-259, 1993.

[7] M. Sharp, “Applications and Limitations of Nuclear Archaeology in Uranium Enrichment Plants,” *Science & Global Security 21,* pp. 70-92, 2013.

[8] C. Gesh, “A Graphite Isotope Ratio Method Primer - A Method for Estimating Plutonium Production in Graphite Moderated Reactors,” Richland, Washington, USA, 2004.

[9] B. Reid, D. Gerlach, P. Heasler and J. Livingston, “Trawsfynydd Plutonium Estimate,” Richland, Washington, USA, 2009.

[10] A. Gasner and A. Glaser, “Nuclear Archaeology for Heavy-Water-Moderated Plutonium Production Reactors,” *Science & Global Security 19,* pp. 223-233, 2011.

[11] T. Wood, B. Reid, C. Toomey, K. Krishnaswami, K. Burns, L. Casazza and L. Duckworth, “The Future of Nuclear Archaeology: Reducing Legacy Risks of Weapons Usable Material,” *Science & Global Security,* pp. 4-26, 2014.

[12] International Panel on Fissile Materials, “Global Fissile Material Report 2009: A Path to Nuclear Disarmament,” 2009.

[13] K. Huff, M. Gidden, R. Carlsen, R. Flanangan, M. McGarry, A. Opotowsky, E. Schneider, A. Scopatz and P. Wilson, “Fundamental concepts in the Cyclus nuclear fuel cycle simulation framework,” *Advances in Engineering Software 94,* 2016.

[14] R. W. Carlsen, M. J. Gidden, M. B. McGarry, A. C. Opotowsky, A. Scopatz and P. Wilson., ““Cycamore v1.3.0.” Figshare,” http://dx.doi.org/10.6084/m9.figshare.1427430.v1, 2015.

[15] B. Mouginot, ““CYCHT v0.1.0.” Figshare,” https://doi.org/10.6084/m9.figshare.4909334.v1, 2017.

[16] T. B. Cochran, W. M. Arkin, R. S. Norris and M. M. Hoenig, Nuclear Weapons Databook Vol.2, U.S. Nuclear Warhead Production, Cambridge, MA, USA: Ballinger, 1987.

[17] F. v. Hippel, “Consistency Tests for the Declarations of U.S. Fissile-Material Production,” *Science & Global Security 19,* pp. 1-14, 2011.

[18] R. Alvarez, “Plutonium wastes from the U.S. nuclear weapons complex,” *Science & Global Security 19,* 2011.

[19] International Panel on Fissile Materials, “Global Fissile Material Report 2010: Balancing the Books. Production and Stocks,” 2010.

[20] A. de la Garza, G. Garrett and J. Murphy, “Multicomponent Isotope Separation in Cascades,” *Chemical Engineering Science 15,* 1961.

[21] A. de la Garza, “A Generalization of the Matched Abundance-Ratio Cascade for Multicomponent Isotope Separation,” *Chemical Engineering Science 18,* 1963.

[22] H. G. Wood, “Effects of Separation Processes on Minor Isotopes in Enrichment Cascades,” *Science & Global Security 16,* 2008.

[23] Z. Xu, “Design strategies for optimizing high burnup fuel in pressurized water reactors,” Dissertation, Massachusetts Institute of Technology, Cambridge, MA, USA, 2003.

[24] S. Richter, H. Kühn, J. Truyens, M. Kraiem and Y. Aregbe, “Uranium hexafluoride (UF6) gas source mass spectrometry for certification of reference materials and nuclear safeguard measurements at IRMM,” *Journal of Analytical Atomic Spectrometry 28,* pp. 536-548, 2013.

Environmental effects on MCNP output and the consequences for arms control

Jennifer Schofield AWE,

Aldermaston, Reading, UK

Abstract:

The Monte Carlo N-Particle code, MCNP, is a well-known tool for investigating radiation transport and detector response. This work explores the capabilities and limitations of MCNP in the context of arms control. Future arms control disarmament verification activities may encounter a range of different environments and neutron backgrounds (for example inside a building at high altitude, as opposed to sea-level, dockside activities). Understanding the implications of these changes on the predicted response of detectors is important.

Two simulated neutron detectors (a boron straw and ^{3}He detector) are benchmarked against new experimental data taken in an average neutron background rate of 1.11 cps. The effect of differing background and consequences will be explored. The significance and effect of these results for arms control treaty verification will be discussed.

Keywords: MCNP; non-destructive assay; arms control; neutron detectors

1. Introduction

Arms control scenarios involving verification do not often explicitly consider the environment in which these measurements are taken [1]. There are many examples of existing treaties, such as New START, and exploratory initiatives, such as the AVNG (Attribute Verification by Neutron and Gamma ray assay using information barriers) system from the trilateral initiative, however few of these describe the verification environment in which measurements do/should take place. They instead tend to focus on the Detector:SNM dyad. It makes sense that arms control situations involving stored SNM might take place inside, although this doesn't necessarily tally for deployed systems. Equally test ban treaty nuclear forensics modelling considers a range of situations and environments. In brief a wide range of arms control environments should be considered.

This paper will discuss an experimental set-up and MCNP modelling results of two detectors with a californium source. The MCNP version used in the work is MCNP6.1.1 [2]. The work then presents various scenarios using these benchmarked detectors and a BeRP ball to simulate SNM (special nuclear material) [3]. The paper concludes by exploring what we can draw from these modelling results in the wider context.

The two detectors in this study are a helium detector and a boron coated straw detector. Helium-3 gas is a well-known and much utilised thermal neutron detector [4]. However, due to a global shortage and increased cost of helium, lithium and boron materials are also considered for detection purposes [5]. Boron is considered better than lithium as it has a larger cross section of 3840 barns (b) (although not as good as the 5330 b for ^{3}He) compared to 940 b for lithium [4]. Graph 1 shows the relative cross sections of importance for helium and boron from the ENDF nuclear cross section library. The close correlation means solid boron is therefore a good candidate substitute for helium gas, although this must be a thin layer in order to limit the stopping of particles in the boron. The following section describes the detectors and experimental and modelling set-up in more detail.

2. Experimental and modelling set-up

2.1. Experimental environment

As mentioned, two detector types were used in this study. Both are well suited to studying thermal neutrons due to their light ion content. As shown in Graph 1, the neutron absorption cross section increases with decreasing neutron energy. In the case of a helium-3 detector the reaction:

$$^{3}He + n \rightarrow p + {}^{3}H + Q(764\ keV)$$

describes neutron absorption. In contrast, boron can capture a neutron using one of two possible reactions:

$$^{10}B + n \rightarrow {}^{7}Li + \alpha + Q(2{,}792\ keV)$$

$$^{10}B + n \rightarrow {}^{7}Li^{*} + \alpha + Q(2{,}310\ keV)$$

For boron, 94 % of thermal neutron captures go down the excited lithium route.

The helium detector used was a Canberra ^{3}He type and for the boron, the boron coated straw type detector was chosen as it shows promise as an alternative to helium detectors [5]. For the experiments section a californium-252 source used, which had an activity of 163 kBq 127 days before the measurement.

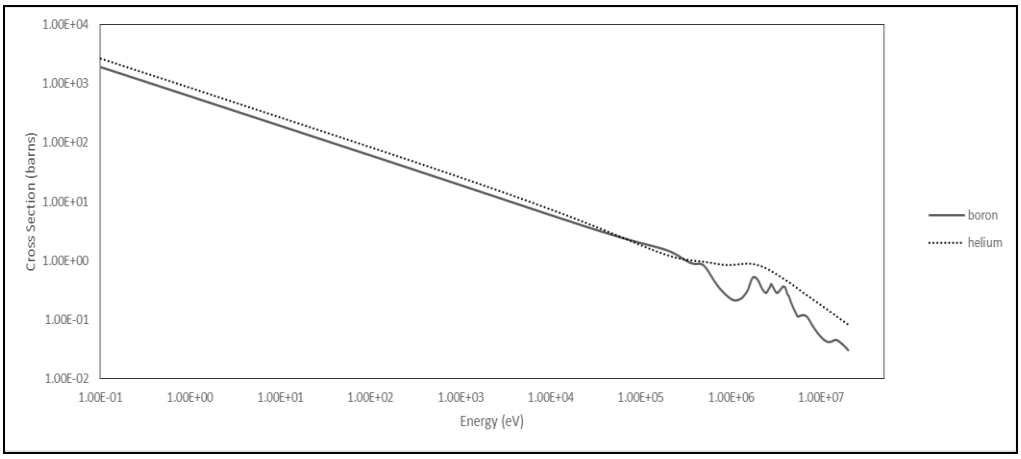

Graph 1: The (n,p) cross section for ^{3}He and the (n,alpha) cross section for ^{10}B according ^{10}B according to the ENDF/B-VII.1/Cross section library.

2.2. MCNP set-up

The MCNP version, MCNP6.1.1, was used in these simulations [2]. An F4 tally was used for the thermal neutron interactions with the ^{3}He gas and the ^{10}B solid. This flux tally was combined with an FM multiplier including the cross section for the (n,p) or (n,alpha) reaction to yield the correct number of interactions per source particle. Simulations were run at 1e6 or more source particles. Neutrons were run with NCIA (neutron capture ion algorithm) enabled, meaning light ion (He, Li and B) recoil physics and neutron capture is allowed. Analogue interactions of neutrons are also enabled. The LLNL fission model (enabled using the FMULT card) was used in both the initial experiment model and the arms control situations.

When benchmarking to experimental data a californium-252 source was used for neutron measurements due to ease and speed of obtaining data. However, when modelling future arms control situations, it was decided to use a BeRP ball in a case for a more complex simulation rather than elemental californium. The MCNP model of the BeRP ball used in this experiment is shown in Figure 1. This is based on the BeRP ball used by LLNL, as in reference [3]. A BeRP (beryllium reflected plutonium) ball is a subcritical ball of plutonium which can be used to represent SNM (special nuclear material). Specific details of this bare BeRP ball can be found in reference [3].

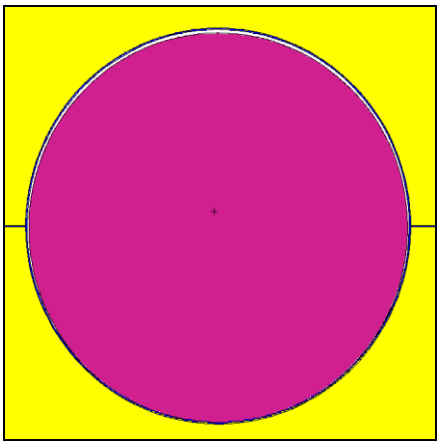

Figure 1: MCNP model of the BeRP ball from [3], used in this paper to model SNM.

3. Benchmark results

3.1. Helium detector results

The ^{3}He detector used for experimental measurements was a Canberra 64NH30 type, with a 30 cm active length and pressure of 10 bar [6]. This was used with an ORTEC ASPEC MCA, a Canberra HV supply and amplifier, a voltage of 1040 V was utilised. Counts were taken over 900 s for 2 different scenarios. Data was taken on Maestro software. The temperature, relative humidity and pressure were recorded using an Omega® detector during this experiment. They varied very little, between: 27.41 and 27.6 ^{o}C for the temperature, 33.26 and 35.47 % for the relative humidity, and 1020 and 1019 hPa for the pressure. These are all fairly uniform values and can be considered constant.

Two scenarios were considered, one simply with a high density polyethylene (HDPE) sleeve to moderate neutrons down to thermal energies, and one using an extra moderator block covering the whole of the active area of the detector.

Intrinsic neutron efficiency in this case is calculated as the number of charge pulses emitted by the detector as a ratio to the number of neutrons incident on detector calculated according to MCNP. There are some drawbacks to this approach as this doesn't fully take into account the geometry of the simulation however, as long as simulations maintain the same solid angle that the detector takes up, then the efficiency calculated here should be a good approximation.

Scenario	Experimental counts	MCNP Model counts	Efficiency
Source on top of the PE moderator	200,599 ± 2,074	1,522,890 ± 8,833	13 % ± 0.5 %
Source, placed next to detector with 3.5 cm thick PE shield moderator	190,134 ± 2,172	1,978,066 ± 10,484	10 % ± 0.5 %

Table 1: Experimental and detector results for helium tube with the californium-252 source. Correction factor for MCNP/efficiency of detector is shown.

The results shown in Table 1 illustrate the attenuating factor which should be applied to MCNP results when considering arms control situations in order to emulate the helium detector response. We can consider the efficiency to be 11.5 %. This agrees with previous descriptions of this detector as having 11% efficiency. The modelled neutron detector is shown in Figure 2.

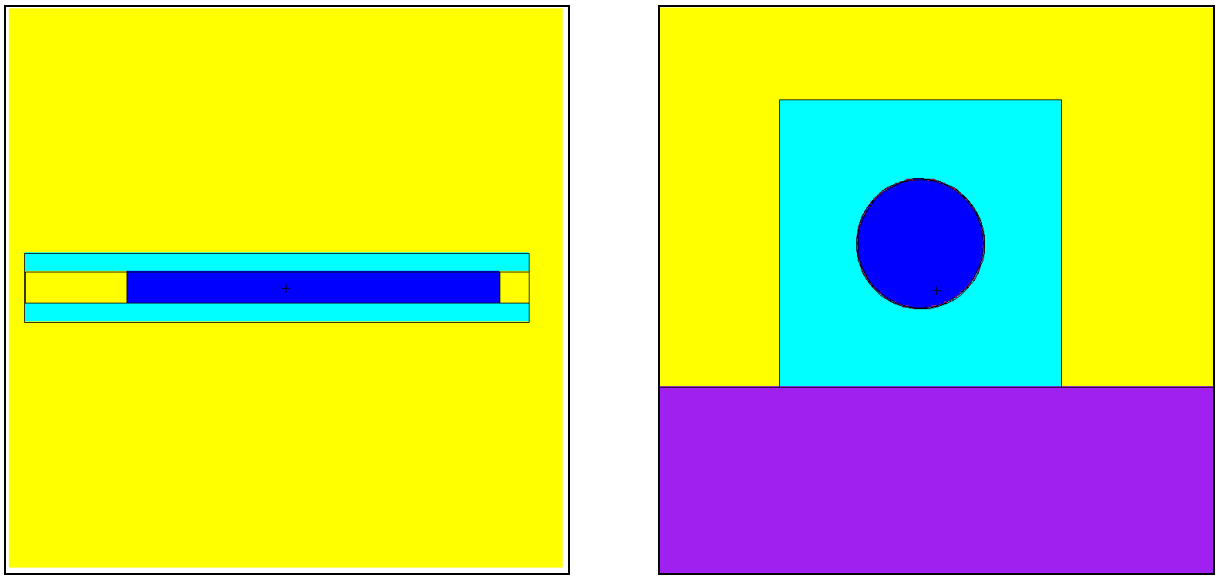

Figure 2: MCNP model of the helium detector. The inner helium (pressure 10 bar) is shown in dark blue, the moderator in light blue.

3.2. Boron detector results

The detector used is a boron coated straw detector from Proportional Technologies, Inc. (PTI) [7]. The detector is based on long, thin copper 'straws' with a 1.45 µm thick inner coating of boron carbide. The straw detectors are filled with a proportional gas mixture of carbon dioxide (10 %) & argon (90 %) with a tungsten anode wire through the centre, as with the helium detector, this detector operates at 1040 V. The detector was used in conjunction with 'NDMS' software provided by Proportional Technologies, Inc. (PTI).

The boron detector results were taken over a period of 180 – 360 seconds for several different runs, varying distance of the source to the detector and amount of moderation. Background counts were taken prior to the experimental run and were determined to be on average 1.11 cps (from a 960 second measurement). These are automatically subtracted from the detector measurement.

As shown in Table 2, the same attenuating factor can be derived for the boron straw detector as for the helium detector. It can be noted solely from number of counts that there is a difference in efficiency from a helium detector, even taking the time for measurement into account. The temperature, relative humidity and pressure were recorded during this experiment. Again there was little variation with measurements between: 25.3 - 25.2 ^{o}C for the temperature, 37.4 - 34.5 % for the relative humidity and 978 - 974 hPa for the pressure.

Scenario	Experimental counts	MCNP model counts	Efficiency
Source 100 cm from detector	18,199 ± 135	401,158 ± 1,845	6.24 % ± 0.5 %
Source 100 cm from detector with 4 cm PE shielding	20,270 ± 142	325,161 ± 1,756	4.54 % ± 0.5 %
Source 50 cm from detector	46,484 ± 216	791,907 ± 2,854	5.86 % ± 0.5 %
Source 50 cm from detector with 4 cm PE shielding	41,911 ± 205	473,964 ± 2,133	8.83 % ± 0.5 %

Table 2: Experimental and detector results for boron coated straw with californium-252 source. Efficiency of detector is shown.

From this (albeit shortened) benchmarking effort we are able to now situate our detectors in possible arms control environments and perceive the changes that are/aren't caused by

these situation variations. The boron detector is shown in Figure 3. The average efficiency is 6.4 %, this is expectedly lower than the efficiency found for helium. In fact, it fits relatively well with the expected efficiency of around 5 - 8 % for single layers of boron coated straws [8].

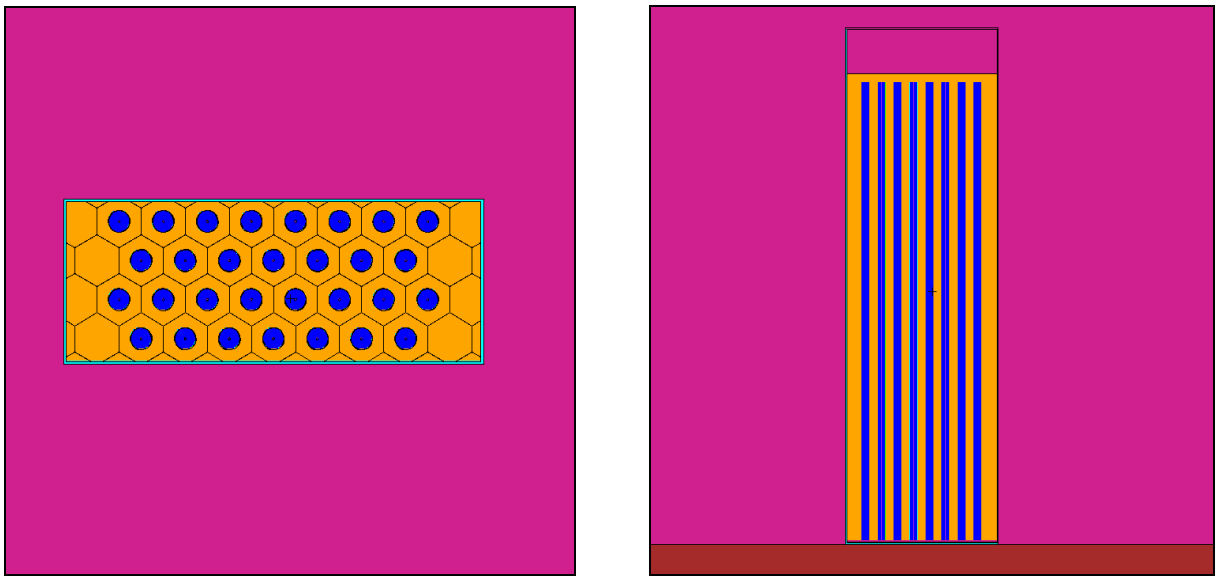

Figure 3: MCNP model of the boron coated straw detector used in this work. A series of straws are combined and encased in (orange) PE moderator.

4. Environmental changes

4.1. Background and height

Background radiation is a signal detected in a detector which does not pertain to the SNM/measurement object of interest in that experiment. Background radiation can come from a couple of areas: cosmic ray induced, NORM (naturally occurring radioactive material) and other sources which are not the source of interest at that time [9].

One of the main factors affecting background neutron flux is the height of the ground above sea level [10]. Background neutron flux has been shown to be proportional to ~exp(αZ) where Z is the altitude in metres above sea level. Alpha is a constant ranging from 0.7-1.01 [10,11]. Goldhagen also states that neutron rate at 3,000 metres is 11 times the rate at sea level [9].

It is obvious that background can have a significant effect, therefore, on the counts seen. In the case of the boron straw detector this can be overcome, as a background is acquired prior to the measurements being taken. However, in the case of the helium detector used here this is not the case – we can assume background counts are the same in both cases.

MCNP6.1.1 possesses a background source term which can be implemented when defining source particles [12]. This can be used to, for example, simulate the effect of cosmic muons on a detector to simulate a real world scenario. Background data is taken from several sources (the source of choice can be determined by the user) in order to make this assumption. In our case this was used – with solely neutrons simulated from a 'skymap' [12]. In future, deviations of this choice on results can be explored. It is possible that changes to the source background could affect the results of this background study.

As discussed, arms control situations could be wide ranging. We might expect activities to be confined to military bases – however this doesn't limit the height at which verification activities might take place, the world's highest military base is at a height of 6,000 m. This study will consider SNM at a height of 6,000 m and at sea level. Detectors will be modelled with no background, and solely background. The percentage difference will show how the different detectors are affected by differing

backgrounds. All responses are combined with the experimental efficiency found.

The result in Table 3 shows that the boron detector appears to be slightly less affected by the differing background. This result is expected to be 10 times higher for the higher background counts, closer to 10 % for high altitudes. A possible reason for this discrepancy could be an error in reproducing background rates (either from skymap or otherwise).

Detector	No background flux	% difference with high background counts	% difference with low background counts
Helium	7.36E-05	0.9028	0.8072
Boron	1.19E-03	0.4247	0.3978

Table 3: Effect of height on background counts.

4.2. Air composition – water environments

As described by Rosolem, the moderation of neutrons from background radiation can have a big effect [13]. This stems from the hydrogen in water vapour present in the atmosphere. The back scatter of neutrons can also be considered from SNM when there is sufficient water vapour/other sources of water in the area. Rosolem shows a 12 % change in neutron intensity according to humidity. This is not something often discussed by those who study the height effect of background neutron flux [10, 11] although it is mentioned by Goldhagen [9].

As previously, arms control can be expected to take place in several environments including bases with very different water environments. A naval submarine base could in the future have dockside verification activities taking place, whereas, there are realistic desert situations for arms control which will be significantly drier. An average precipitation could be something like 0.3 inches a month in these dry areas as opposed to a coastal base where we might expect considerably more rainfall. In this study two scenarios will be modelled: the BeRP ball on a dock with a layer of moisture on its case from high relative humidity, contrasted with the model in a completely dry environment.

In order to evaluate the amount of water that should be put into the system a global maximum measured by Dai [14] of p=23 g m^{-3} can be used. This can be combined with the equation:

$$IWV = pH [1 - \exp(-z/H)]$$

Where H is the water vapour scales height, 2.3 km according to Reitan [15] and z is the height in km. The IWV obtained is the equivalent mm of water if all the water vapour in the air were allowed to condense at a surface. This amount equals 229 g m^{-2} in the maximum case (and zero in the minimum case). This is put on both the BeRP ball case and the detector surface in the simulations.

Detector	Dry environment flux	Nearby ‘lake’ (% difference)	Absolute humidity (% difference)
Boron	0.0018	0%	3%
Helium	0.0001	0.41%	14.98%

Table 4: Results from different water vapour environments.

Table 4 shows the results from these different water vapour environments. The change for helium is much more noticeable. This is probably because of the small amounts of moderation in place. The additional water layer represents a significant addition in this case. Whereas there is already a large amount of polyethylene surrounding the boron.

4.3. PV=nRT – pressure and temperature changes

The pressure of the gas used, along with the active length, is known to have an effect on the efficiency of counts in the case of a helium tube [6]. This can be shown by a simple MCNP model, varying the pressure in the tube, shown in Graph 2. Higher pressures lead to a better efficiency. This can be followed through when discussing the temperature of the surroundings. The volume of the helium tube is fixed and therefore when the temperature increases, according to the ideal gas law, the pressure will also increase. Likewise, in colder climes, the pressure will be under that at normal operating temperatures.

As can be seen from the graph a logarithmic relationship is shown which has been portrayed elsewhere [6, 16]. We can define a relative correction which will apply to the detector efficiency at different pressures, shown in Table 5.

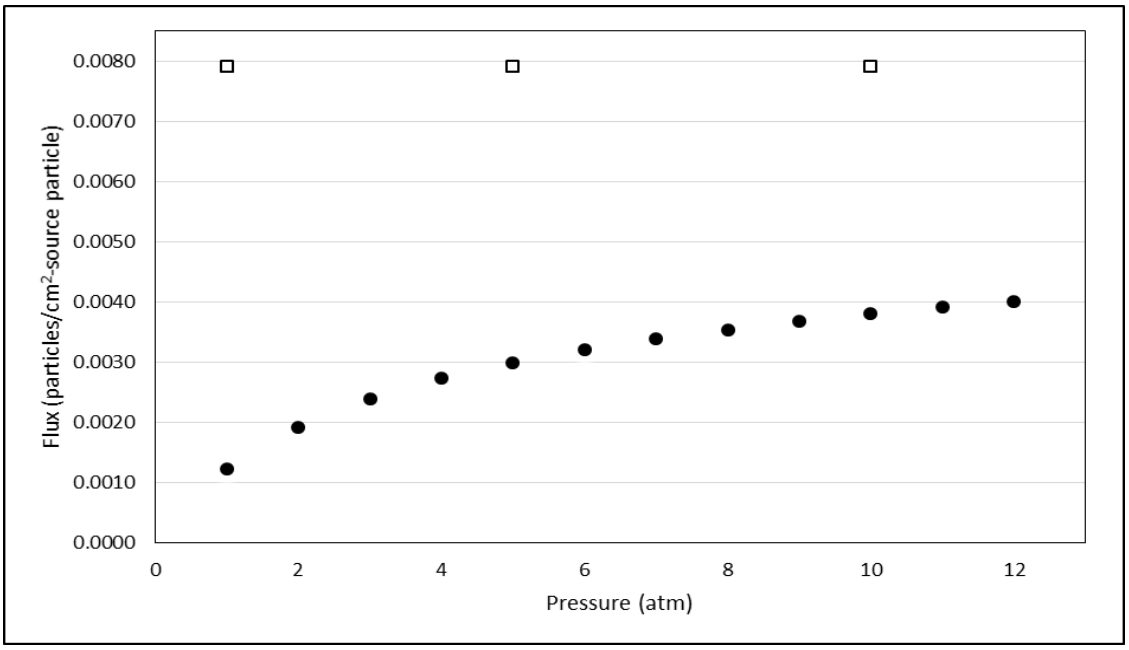

Graph 2: Increase in efficiency for helium tubes at greater pressures is shown clearly here for the black circles. The boron straw flux (open squares) doesn't change as a function of pressure.

Pressure (atm)	Correction
1	0.3231
2	0.5048
3	0.6273
4	0.7179
5	0.7885
6	0.8434
7	0.8903
8	0.9312
9	0.9677
10	1.0000
11	1.0300
12	1.0548

Table 5: Correction values for different atmospheres of pressure inside a helium detector tube.

In the case of the boron coated straw, we do not see a large difference in sensitivity due to pressure. This is because the method of signal production is not dependent on a gas for its functioning. This is also illustrated in Graph 2, which shows no change in the efficiency of our detector to changing air pressure.

Following the methodology of previous sections we can posit some extremes of temperature which these detectors might be used in. One of the coldest military bases have an average low of -24 ^{o}C and an extreme low of -53 ^{o}C. Hot areas will be in desert regions, it would not be impossible to imagine 43 ^{o}C for a verification activity in hot desert conditions.

When these extremes are taken into account we expect the boron straw to not be affected by this change in pressure (from 1 atm to 2 atm at the hotter end, falling to 0.4 atm at the lower end). In the case of helium, at 10 atm, a rise to a maximum of 12 atm can be expected, which we would predict to have a small positive effect on the efficiency of a detector of 5.5 %. The atmospheric pressure would fall to 7 atm within the tube for the very cold situations. This would lower the efficiency of the detector by almost 11 %, meaning measurements would have to be taken for significantly longer times in order to achieve the same precision. This implies a boron coated straw would be more robust in a range of pressure situations.

5. Conclusions

This study has shown that in a range of scenarios we would expect our two detectors to behave differently. The output from MCNP illustrates its ability to model useful comparisons for arms control situations. The results found in this study are limited for each effect (water, altitude etc.) and further work on atmospheric effects on likely detector responses should be undertaken. It is not considered in this study how other uncertainties in measurements would relate to these environmental effects. For example, the distance from source to detector.

The ideal verification scenario in terms of short measurement time and lowest background would be a measurement taken at a low altitude and high temperature for example at sea level during a hot summer's day. However even with this optimal scenario we do not expect this to have a large effect on measurements and therefore on arms control scenarios.

Further work should include taking more situationally accurate measurements with the SNM of interest. This will remove some of the uncertainty in the measurements modelled by MCNP. Measurements of a BeRP or other object in a variety of different scenarios would provide the required experimental data.

High gamma counts and how this might affect the detectors are not investigated in this work, but should be considered in future research. In addition, the timing responses of certain detectors using MCNP should be studied. This would be advantageous as it would allow investigatory experiments, such as the AVNG experiments, to be more closely related to the output.

6. Acknowledgements

The authors would like to acknowledge all those who have reviewed this work and contributed to its completion. In particular P. Arthur and C. Allwork for their help running experiments and R. Hughes for his help with MCNP6.1.1.

7. References

[1] Kondratov S. et al.; *AVNG system demonstration*; LA_UR-10-02420; INMM 51st annual meeting,
[2] Goorley T; *MCNP6.1.1-Beta release notes*; LA-UR-14-24680; 2014

[3] Percher C. M., Kim S. K.; *LLNL preliminary design for the BeRP ball with composite polyethylene and nickel reflection*; LLNL; Livermore; 2014
[4] Knoll, G. F.; *Radiation detection and measurement*; 4th edition; Wiley; 2010
[5] Simpson A. P. et al.; *A review of neutron detection technology alternatives to helium-3 for safeguards applications*; INMM 52nd annual meeting, California, 2011
[6] Canberra; *Helium-3 neutron detectors factsheet*; DC-01/03-73829A; France
[7] PTI Technologies, Inc. © 2017
[8] Lacy J. L.; Boron coated straw neutron detector; US7002159 B2 Patent; 2006
[9] Goldhagen P.; *Uses of cosmic ray neutron data in nuclear threat detection and other applications*; neutron monitor community workshop; Honolulu Hawaii; 2015
[10] UNSCEAR; *Sources and effects of ionizing radiation*; 1993 report; 1993
[11] Kowatari M.; *Altitude variation of cosmic-ray neutron energy spectrum and ambient dose equivalent at Mt. Fuji in Japan*; Journal of nuclear science and technology; 495; 2004
[12] Fensin M. L. and McKinney G. W.; *How to use the MCNP6 background source capability*; American Nuclear Society Winter Meeting; Washington DC; United States, 2008
[13] Rosolem R. et al.; *The effect of atmospheric water vapour on neutron count in the cosmic-ray soil moisture observing system*; American Meteorological Society; 2013
[14] Dai A.; *Recent climatology, variability, and trends in global surface humidity*; J. Climate; 19; 3589; 2006
[15] Reitan C. H.; *Surface dew point and water vapour aloft*; J. Appl. Meteor; 2; 776; 1963
[16] Kouzes R. T. et al.; *^{3}He neutron detector pressure effect and comparison to models*; PNNL 19110; PNNL; 2010

Novel Approaches and Synergies in Biological and Chemical Arms Control

Mirko Himmel

Centre for Science and Peace Research, University of Hamburg
Beim Schlump 83, 20144 Hamburg, Germany

Abstract:

The Biological and Toxin Weapons Convention (BTWC) was put into force in 1975 and bans the development, production, and stockpiling of bioweapons. The BTWC is thought to be a successful arms control treaty, because it paved the way for the complete world-wide disarmament of bioweapons. But there is one major shortcoming: the BTWC lacks a verification mechanism. Thus, biological arms control has a rather preventive, observational character without any inspection measures at hand. Confidence building within the BTWC regime relies on other instruments such as voluntary annual declarations, which proofed to be rather inefficient over time. It appears, that transparency regarding relevant member states activities has to be increased by alternative means. One solution is the development of a publicly applicable method to collect and analyze open source information with relevance to the BTWC in a structured, non-biased way. The Chemical Weapons Convention (CWC) was put into force in 1997 and complete disarmament of weapons stocks will not be finished before 2022. In the near future, the CWC regime is expected to see a shift towards a more preventive, observational role, too. Therefore, the use of open source information for compliance monitoring could be also beneficial for work under the CWC, ultimately creating synergies between biological and chemical arms control.

Keywords: biological; chemical; WMD; verification; monitoring

1. Ban and disarmament of biological and chemical weapons

The development and large-scale deployment of chemical weapons in the course of World War 1 was a critical moment in the (mis-)use of otherwise ground-breaking scientific and industrial achievements [1]. After the war, which is believed to have seen little military impact of chemical weapons on its outcome, disarmament of chemical (and the upcoming category of “bacteriological” weapons) has been discussed on the international level, but the leading nations could not find agreement on this. As minimal consensus, the Geneva Protocol of 1925 prohibited the use of these weapons against other treaty members. But a number of States Parties like France or the United Kingdom declared the right of retaliation in kind once they would be attacked with weapons prohibited by the Protocol. The United States of America as late major combatant nation of World War 1 and important promotor of pst-war disarmament negotiations changed the political attitude completely and postponed the ratification of the Geneva Protocol until 1975. Therefore, any country still had to face the prospects of chemical and biological warfare in future armed conflicts during the following decades.
It is important to note, that although there were concerns among military and political decision makers about the practicability of chemical and biological warfare – not to speak about the ethical implications – many nations kept their chemical weapons arsenal. Research & development was continued as well as testing activities and preparation of troops and the civilian population for large-scale biological and chemical weapons attacks.
During World War 2 chemical and biological weapons were not used on the European battlefields, but at varying degree by Japanese troops against Chinese troops and civilians; the latter being also victims of inhumane experiments with biological warfare agents [2]. At the beginning of the Cold War chemical and biological weapons were intensively studied in Western and Soviet labs. But in 1969 the

USA unilaterally declared the suspension of all offensive biological warfare preparations, a political movement which opened the ground for negotiating an international treaty aiming at the complete ban of a whole category of weapons of mass destruction: the Biological and Toxin Weapons Convention (BWC). The BWC was put into force in 1975 and shows currently 178 States Parties. The Convention prohibits the development, production, stockpiling, and transfer of any biological material intended to be used for hostile purposes. Furthermore, it calls all members to fully cooperate in the peaceful application of biotechnology. There is one major limitation of the BWC: the lack of any verification regime. Even nowadays there is no legally-binding mechanism implemented for continuous compliance monitoring, which is a rather odd phenomenon in the light of rapidly developing field such as biotechnology, biomedicine and the life sciences.
Chemical weapons were kept in the military arsenals during the whole Cold War. Their use in the case of sub-nuclear warfare activities or in combination with nuclear attacks, e.g. on the European battlefield in a potential armed conflict between NATO and Warsaw Pact forces, was always perceived as a real threat. Therefore, it was a major step forward when with the USA and the former Soviet Union the two major possessing countries agreed on the disarmament and complete ban of chemical weapons at the end of the 1980ies. In 1997, the Chemical Weapons Convention (CWC) was put into force. Currently, 192 countries are States Parties to the Convention, which is tremendous in numbers for an international arms control treaty. The importance of a mechanism for the verification of the treaty member's compliance with the provisions of the Convention, especially concerning certain production capacities for selected chemical compounds within the chemical industries, has been recognized early. Therefore, the CWC was from the beginning on equipped with an elaborated verification and inspection regime as well as an international body, the Organisation for the Prohibition of Chemical Weapons (OPCW), which was mandated to support the implementation of the CWC and to collect required data for compliance assessments by all States Parties.

2. Challenges of biological and chemical arms control

2.1. Special prerequisites of biological arms control

What do we know about potentially existing stockpiles of biological and chemical weapons? The complete destruction of biological weapons arsenals and the dismantling or conversion of associated testing and production facilities is mandatory in the course of the accession to the BWC. From a legal point of view one should now assume that all documented and declared bioweapons stockpiles have been successfully destroyed world-wide. But without any verification mechanism it remains difficult to assess the current situation. This is can be best understood when we look at the historical case of the Soviet Union's large-scale biological warfare programme, which has been continued and extended after (!) the ratification of the BWC [3]. National technical means used by Western intelligence services partially contributed to the disclosure of these illicit activities. But it required the reports by eyewitnesses (émigrés, whistle-blowers) to produce sound evidence that the Soviet Union was indeed in violation of the provisions of the BWC. With specifically designed verification and inspection measures (VIM) at hand, it might had been possible to penetrate the veil surrounding the many, many research, testing and production facilities of the Soviet BW programme. Of course, VIM will not necessarily provide in any case a detailed, forensically sound picture about an efficiently concealed state-driven biological or chemical weapons programme. But VIM could at least provide data and observational findings which could be used to promote political and scientific discussions about ambiguous activities of a BWC member state. Furthermore, VIM might also provide valuable hints for the intelligence community and (if made public) also for non-governmental observers allowing a deeper analysis of a given special situation. With the BWC lacking an agreed VIM, confidence building among States Parties (and towards a growing "global civil society") has to rely in part on surrogates such as Confidence Building Measures (CBM): annual, form-based declarations about selected facilities and activities, which submissions are just politically but not legally binding. In practice, they even proofed to be a rather weak source of information. Therefore, new approaches for confidence building such as a peer review mechanism ("transparent visits") are currently tested by some States Parties within the BWC regime [4].
Biological arms control is crucial to confidence building, because it provide facts required for compliance assessments. But arms control should not stick to conventional ideas and models about biological warfare programmes. To the opposite, it should be continuously developed further in order to be able to figure out what would be basic elements of a clandestine biological warfare programme and how to detected them - independently of the currently perceived demands by the BWC member

states. Of course, this mechanism should include also the continuous monitoring of BWC non-member states by the use of open source information (in addition to national technical means). In this respect, a non-discriminatory, unbiased and transparent analytical approach for accessing treaty compliance would be very beneficial. Such activities could even trigger the willingness of some countries to deliberately provide information in the open source information universe on the internet in order to foster public compliance monitoring.

2.2. Future perspectives of chemical arms control

Full disarmament of the last remaining large chemical weapons stockpiles in the USA and the Russian Federation is expected around 2023 and 2020, respectively. Once this goal has been achieved work of the OPCW is believed to be focused more on monitoring activities due to the then preventive character of the CWC.
But will this ever happen? Currently, toxic chemical substances are again frequently used in armed conflicts like the Syrian civil war, although at a much lower level than in full-scale chemical warfare scenarios of the past. But even these limited attacks already caused a number of dead and injured victims. For example, up to 1,400 people (mostly unprotected civilians) were found dead, when in August 2013 apparently Syrian governmental forces deployed the nerve agent sarin in Ghouta, East of Damascus. Furthermore, after Syria's (more or less enforced) accession to the CWC in October 2013 a number of doubts showed up about the completeness and accuracy of the mandatory declaration of the country's CW programme. By the work of the OPCW data assessment team Syria was coerced to submit additional information about previously undeclared research and production facilities. And still, there are a number of open questions concerning the types and total amounts of chemical weapons Syria might have had in possession [5].
In Iraq and in Syria militants of the so-called Islamic State (IS) allegedly used chemical agents such as mustard gas-like substances for a number of single attacks. It cannot be excluded, that some of these substances are not left-over from old Iraqi or Syrian chemical weapons stockpiles but chemical agents newly produced by IS specialists at seized research and production facilities [6]. After tedious international negotiations, UN-OPCW joint teams are investigating the aforementioned incidents in order to identify the chemical agents used and provide data which shall allow to determine who was responsible for these attacks. Therefore, the role of the OPCW in providing crucial scientific, technical and logistical support for inspection and fact finding missions cannot be underestimated.
Future chemical threats could stem from completely different classes of chemical compounds not covered by former chemical weapons programmes. Here, experts are already carefully looking at upcoming trends in the chemical and pharmaceutical industries, but also in biotechnology which could become more and more important in the production of chemical compounds formerly synthesized by classical procedures. Scientific and engineering expertise must be kept at hand for the analytical assessment of such novel trends. Therefore, it is a very likely scenario that the OPCW will keep its central role as supporting international body. But it should be (and hopefully will be) equipped with an extended mandate allowing OPCW experts to directly access open source information, process the raw data (e.g. results from a very focused scientific literature research, satellite imagery, business reports, patents etc.) and make it available for political decision making within the CWC regime. Analytical workflows for preventive chemical arms control will then be required which would share many similarities with those workflows already used in preventive biological arms control.

3. Novel approaches and synergies in biological and chemical arms control

Other than with nuclear weapons, the development of biological and chemical weapons will most probably go along with a reasonable number of wet lab-based cultivation/synthesis and pilot-production steps. This would include the repeated biochemical and biophysical testing of the obtain chemical compounds/biological agents. Lab-scale efficiency test will make use of with animals (or nowadays in some cases even cell culture material) might follow this first initial phase. These illegal activities are most difficult to detect, because the nature of the material (biological, chemical) used, the required equipment as well as the layout of the experiments might be quite similar if not identical to fully legitimate research and development activities. Therefore, preventive biological and chemical arms control must aim at shading some light on the intention behind certain types of experiments in selected research environments. This can be done most efficiently by the combination of many

different types of information and a cross-correlation between individual findings, but will in many if not all cases end up in an estimation of the intention, but no final proof.
The general structure of databases usable both for biological and chemical arms control could be the same: main fields of relevant activities (e.g., industrial activities; governmental activities (including public health measures as well as animal, plant and food security); civilian research and development activities; (defensive) military B/CW activities; civil protection activities). In this context, the term "activities" refers also to the type of work (one indicator) done at a specialised facility (part of the organisational model), which is provided for certain task (part of the system processes within the physical model). A summary of additional key elements of such a database is shown in table 1.

Database entries	Comments
Main Categories	Civilian research & development activities, military chemical and biological activities;
Sub-categories	Research on pathogenic microorganisms/toxins; production of selected vaccines; military biological and chemical weapons defensive research facilities;
Primary indicator	Self-explaining, no further knowledge required to understand its fundamental role within a putative B/C warfare programme (e.g., a biological threat agent)
Secondary indicator	Context-dependent meaning, further knowledge required to understand its role within a putative B/C warfare programme (e.g., biological research facility)
Descriptor	Allocates indicators to certain elements of the physical model
Physical model(s)	An assumption, how a B/C warfare programme would look like in a given context (country-based, time-dependent, conflict-dependent etc.)
Sub-model(s)	E.g., organisational pathways, system process flows etc.

Table 1: Key elements of a database usable for open source information gathering.

From table 1 it is getting evident, that the creation of groups of indicators representing certain materials, agents, installations etc. is forming the basis for the other elements mentioned (*Note:* An indicator is not a proof for illicit activities in the context of the treaties discussed here!). The associated value associated with an indicator just represent the findings of open source data collection. Indictors help to simplify the database structure, but there is still the need to integrate a huge variety of different types of information (names, addresses, geotags, imagery, tweeds, patent information, trade data, excerpts from news reports, measurement values etc.). The required integration and subsequent assessment can be done by a conventional analytical workflow, supplemented with additional working steps, as shown in the following:

Working steps	Comments
Selection of field of investigation	Main categories within the databse, e.g. biomedical research and development activities
Perform Search for relevant information by combination and permutation of appropriate search terms	Requires scientific, technical and military knowledge
Review of search results and removal of unreliable information	E.g. well-known conspiracy theories, prominent cases of false accusations, propaganda already detected and

	reported by others
Classification of obtained results in the course of database storage	Categories/classes have to be defined following a target-centric approach
Re-examination of database entries in the context of their corresponding category	Allows correction of the classification of database entries and the identification of missing research results (refers analyst back to step two)
Determination of (maybe even previously unknown) cross-connections between data sets by specialised database queries	Central part of the work with the aggregated data sets; try to remove any bias by using rival work hypothesis when performing analytical work
Generate topic-specific reports	E.g., tabular outputs; graphical outputs (country maps, network diagrams),

Table 2: Analytical workflow using open source information for biological and chemical arms control.

Repeated cycles of data collection, selection, and pre-analysis will result in reasonable amounts of aggregated information which might tend to become “invisible” due to the huge amount of data stored. Graphical outputs of results of database queries could make them visible again. Combined with several layers of cross-correlative analyses, this could highlight previously unknown interdependencies between individual indictors or groups of indicators. Especially in biological and chemical arms control this feature would be crucial due to potentially quite fragmented physical layouts of weapons programmes.
Ultimately, such analytical tools could become standard for the traceable, transparent data analysis required in preventive biological and chemical arms control. They would enable international arms control experts, but ideally also non-governmental actors sharing and discussing the obtained results.
Ideally, the results are subsequently be handed over to or grabbed by treaty member states in order to find a common understanding about certain compliance-relevant activities. In this respect, one first working example is the BioWeapons Monitor 2.0, which allows collecting and processing relevant data and provide analytical results usable for BWC compliance monitoring and transparency building [8].

4. Conclusions

Although biological and chemical arms control will look in the first instance on different threat agents and production principles, they share in common the (i) fragmented nature of illicit warfare programmes, (ii) similar or even identical sources of information, and (iii) comparable system process flows which all must be considered by a combined analytical workflow usable for compliance monitoring tasks. The CWC will most probably see in the mid-term future the increasing application of preventive chemical arms control measures. This treaty regime has already technical and political instruments implemented which could directly make use out of the data generated by open source information compliance monitoring approaches. With the BWC the situation is different. Biological arms control has currently a predominantly preventive function, but without any VIM capabilities. Frequently, a number of BWC States Parties, academic experts and non-governmental organizations urge the member states to address this shortcoming. But unfortunately, there is no indication that the political situation will change in the near future. Transparency building and compliance monitoring still has to be done outside the BWC. The use of open source information will be a practicable way to do so. But it could become part of a BWC “regime” in a broader context, because this work corresponds to analytical approaches anyways applied by intelligence services in those countries able to do so (“OSINT”; example: USA) and therefore will be recognized either as complementary, politically already usable information or simply as another source of open source information. And with no compliance monitoring mechanism within the treaty this work has to be done by other stakeholders. In one scenario, this could result in transformation of the treaty governance from the conventional, member states-centric approach towards a kind of public governmental partnership, where at least some BWC member states are in support of these monitoring activities by non-governmental actors and actively seeking for the information provided. Another scenario would of course be, that all information aggregated by public compliance monitoring activities has to be used solely outside the BWC regime. For example, in the case of grave concerns about compliance of selected BWC member states will

come up alarming news have to be published in social and mass media in order to get recognised. Experience frequently shows that this could make political decision making even more difficult.

5. Acknowledgements

Continuous support by G. Kirchner and G. Jeremias (Centre for Science and Peace Research, University of Hamburg) is greatly acknowledged. Part of the work was supported by the German Federal Foreign Office in order to perform a proof-of-concept study about the use of open source information for compliance monitoring.

6. References

[1] Tucker, JB: *War of Nerves: Chemical Warfare from World War I to Al-Qaeda*; Pantheon Books; New York; 2006.

[2] Geissler, E, Moon, JEvC; *Biological and toxin weapons: research, development, and use from the Middle Ages to 1945*; Oxford University Press; UK; 1999.

[3] Leitenberg M, Zilinskas, R; The Soviet Biological Weapons Program: A History; Harvard Univ. Press; Cambridge (MA), USA; 2012.

[4] Revill, J; *A peer-review mechanism for the biological and toxin weapons convention;* United Nations Institute for Disarmament Research (UNIDIR); New York and Geneva; 2013.

[5] OPCW; *Conclusions on the Outcome of Consultations with the Syrian Arab Republic Regarding its Chemical Weapons Declaration*; note by the Director-General to the 82nd session of the CWC Executive Council; document symbol: EC-82/DG.18; 2016.

[6] Quillen, C; *The Islamic State's Evolving Chemical Arsenal*; *Studies in Conflict & Terrorism*; vol 39; 2016; Taylor and Francis; USA; p. 1019-1030.

[7] Jeremias G, Himmel M; *Can Everyone Monitor the Bioweapons Convention? Bulletin of the Atomic Scientists*; Taylor and Francis; USA; vol 72; 2016; p 412-417.

[8] BioWeapons Monitor 2.0; Weblink: www.bwpp.org/monitor

Session 09

Destructive Analysis I

Uranium Microparticle Production: Support of IAEA's Analytical Capabilities

Alexander Knott [a, b, *], Ronald Middendorp [a], Ernesto Chinea-Cano [b], Laure Sangely [b], Martin Dürr [a], Stephan Vogt [b], Dirk Bosbach [a]

[a] *Forschungszentrum Jülich GmbH, Institute of Energy and Climate Research, Nuclear Waste Management and Reactor Safety (IEK-6), D-52428 Jülich*
[b] *International Atomic Energy Agency, Safeguards Analytical Services, Environmental Sample Laboratory (SGAS-ESL), A-2444 Seibersdorf*
[*] *Current address: European Commission, Joint Research Centre Karlsruhe, D-76344 Karlsruhe*

Abstract
The goal of a collaborative effort between the International Atomic Energy Agency (IAEA) and the Forschungszentrum Jülich GmbH (FZJ) is to produce monodisperse microparticles for nuclear safeguards applications in order to strengthen the IAEA's analytical capabilities to detect illicit nuclear activities.

These particles are intended to serve for quality control purposes and eventually as certified reference materials for mass spectrometry. Therefore, the principal requirement is the consistency concerning the number of uranium atoms per particle, but also a homogenous size distribution, a consistent isotopic composition and uniform particle morphology. This work focuses on different aspects of the particle production process, including (1) development and implementation of the particle generation process and (2) particle collection techniques as well as (3) substrate and sample preparation techniques for further analysis and (4) particle size distribution using scanning electron microscopy (SEM) and large geometry secondary ionization mass spectrometry (LG-SIMS) for determination of the isotopic ratios.

A working microparticle setup was developed and implemented at FZJ. The entire setup is designed as a closed system to mitigate the risk of contaminations. Monodisperse uranium oxide particles are generated by spray pyrolysis and particles are collected by inertial impaction on vitreous carbon substrates. Furthermore, substrates can be prepared in advance with reference marks to facilitate particle identification and relocation of single particles with high precision in different analytical instruments. Customizable reference marks were engraved using a laser micro dissection instrument (LMD). Collection efficiency assessment of two different inertial impactor designs, a one-stage inertial impactor and a modified cyclone impactor, are in agreement with the theoretical predictions. A consistent particle size distribution, a homogeneous morphology and the presence of uranium were confirmed using SEM-EDX. LG-SIMS analysis performed on single uranium microparticles confirmed consistency of the uranium isotopic ratios in comparison to the initial precursor solutions.

Keywords: Particle Production, LG-SIMS, Nuclear Forensics, Destructive Assay, Environmental Sampling

1. Introduction

Safeguarding nuclear facilities is the main objective of the International Atomic Energy Agency (IAEA). Its purpose is to verify compliance with existing legal multilateral safeguards agreements such as the non-proliferation treaty of nuclear weapons [1], the Additional Protocol [2] and others [i]. In order to ensure compliance the IAEA has implemented the concept of environmental sampling. Since its approval by the IAEA Board of Governors in 1995 it has proven to be the cornerstone of technical verification. Mass spectrometry is used to measure the isotopic composition with high accuracy. In nuclear safeguards and forensics high resolution mass spectrometers, e.g. Inductively Coupled Plasma Mass Spectrometry ICP-MS), Thermal Ionization Mass Spectrometry (TIMS) or Secondary Ionization Mass Spectrometry (SIMS) are commonly used to determine uranium isotope ratios [3, 4, 5, 6, 7, 8]. SIMS analysis offers the advantage of screening and isotope detection capabilities [9] and has a proven record in nuclear safeguards and forensics [10, 11, 12]. The implementation of a new generation of SIMS instruments offers higher resolution and higher transmission compared to conventional SIMS instruments [13]. The so-called large geometry SIMS (LG-SIMS) models, CAMECA IMS 1270, 1280 and 1280HR, are based on the basic principle such as the CAMECA IMS 3F-7F models but are equipped with a considerable larger magnetic sector field and improved ion optics [9, 14]. In nuclear safeguards and forensics samples are commonly taken as so-called swipe-samples on cotton. These cotton swipes contain minute quantities of material which carry an inherent signature of their production and release scenario. Generally, disposable one stage inertial impactors are used to transfer the particles from the swipes onto a vitreous carbon substrate [15, 16, 17, 18, 19]. SEM-energy dispersive X-ray spectroscopy (SEM-EDX) and LG-SIMS analysis are routinely used to assess the morphology, elemental and isotopic composition of these micro-particulates. QC-materials and (certified) reference materials (CRM) are indispensable for instrument calibration and method validation to ensure precise and reliable results. Currently, the availability of commercial U and/or Pu containing CRMs is limited to metals, powders and solutions. Monodisperse particles with a well-defined characteristics are needed to ensure and improve reliable data output. Single U and/or Pu containing particles with various isotopic compositions and sizes are needed. Homogeneous and monodisperse particles with a known number of atoms per particle are most suitable for instrument calibration and method validation; in particular for SIMS, TIMS or Laser Ablation ICP-MS (LA-ICP-MS) analysis. On the other hand, mixed particles sizes with different elemental and isotopic compositions are more suitable as a quality control material since they reflect actual field samples more accurately. In the end, that is why different monodisperse particle populations are intended to be blended and embedded into a more realistic dirt and dust matrix to imitate real swipe samples. This demand of a new generation of reference materials was already recognizes in the late 1990s. Since that time several particle production programs were initiated which yielded in mixed results: ranging from uranium micro-particulates to mimic real-life samples such as uranium doped glasses [20] or uranium-oxyfluoride particles [21] to polydisperse uranium/plutonium containing microparticles [22, 23, 24, 25, 26]. Erdmann et al. [27] and Stetzer [28] proved that monodisperse particles can be produced using a vibrating orifice aerosol generator (VOAG). Further studies on the correlation of the uranium mass content to the size distribution and particle density [29, 30] proved the potential of this approach, see Ranebo et al. [12]. Since the project was discontinued it was decided to take up this approach. In 2012 the Environmental Sample Laboratory at the Department of Safeguards (SGAS-ESL) at the IAEA decided to start a particle production program as part of a joint R&D project with the Institute of Nuclear Waste Management and Reactor Safety (IEK-6) at the Forschungszentrum Jülich GmbH (FZJ) in order to improve its analytical capabilities. This work is premised upon previous publications where the basics of particle production were already discussed [31]. A more detailed analysis will be given on how the particle size distribution and the final morphology dictate the overall scheme of the particle production setup. Therefore a more detailed insight will be given on the droplet-to-particle conversion process and the chronological succession of the setup. Finally a short assessment on the size distribution and morphology will be given as well as mass spectrometric analysis confirming the stability of the isotopic abundancy of the initial isotopic content.

i *Treaty of Rarotonga, Treaty of Tlatelolco, Treaty on a Nuclear-Weapon-Free-Zone in Central Asia (CANWFZ), Bangkok Treaty, Comprehensive Nuclear-Test-Ban Treaty, etc.*

1.1 Droplet-to-Particle Conversion

The goal of this project is to produce solid, homogenous micro particles: uranium oxides are therefore preferred over uranium salts such as nitrates or chlorides. Particles discussed in this paper are derived from dilute uranyl nitrate solution. Therefore it is necessary to convert the uranium nitrate particles to its subsequent oxides by thermal treatment. Additionally, calcinated particles offer a better chemical and mechanical stability than dried uranyl particles. Microparticle production via spray pyrolysis is a delicate matter: the final size, morphology and density are depended on many variables such as temperature profiles, dwell times, instrument configuration and precursor solution composition and concentration. These parameters dictate the setup configuration significantly.

The conditions during evaporation and decomposition of the uranyl nitrate solution play a key role in the formation of the final size and morphology [32]. This is particularly true for spray pyrolysis [33] [34] were the complex conversion from droplets-to-particles takes place in seconds.

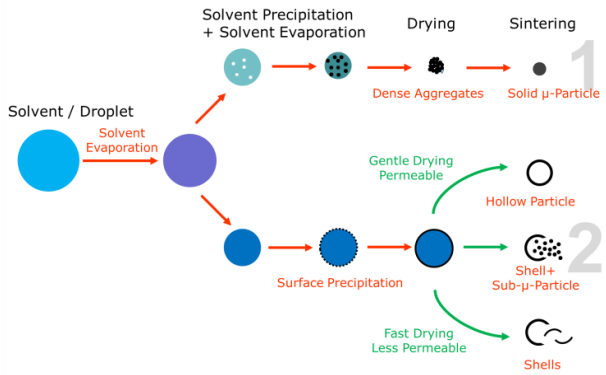

Figure 1: Schematics of droplet-to-particle conversion during thermolysis [35, 36].

This implies the following seven steps: (1) aerosol production, (2) evaporation, (3) dehydration, (5) nucleation, (4) thermal decomposition, (5) crystallization and oxidation, (6) cooling and (7) sampling. The nucleation process is the pivotal step in the production process. It is dictated strongly by the temperature profile and dwell time in order to yield solid and monodisperse particles. Reuge et al. [35] and Messing et al. [36] describe a basic conversion schematic for spray pyrolysis process. The formation of homogenous and solid particles is described as a competitive precipitation reaction. In order to yield in solid particles a homogeneous precipitation is needed. On the other hand a surface controlled precipitation leads to the formation of hollow or cracked-up species, see Figure 1. Depending on the permeability of the outer layer the evaporation pressure inflates the particles which can eventually cause them to disintegrate. Reuge et al. [35] and Gurav et al. [36] also mention that temperature profiles, dwell time, solvent composition and concentration are also contributing to some extend to the final size and morphology. SEM measurement, see Chapter 2.4, highlight the complexity associated with the nucleation process discussed in this paragraph.

1.2 Particle Collection – One Stage Inertial Impactor

Inertial impaction is a well-established and effective method to collect microparticles from an air flow. For this work a one-stage inertial impactor was used [15]. A sufficient number of particles can be collected directly onto a suitable substrate within a few minutes. Particles are impacted depending on their aerodynamic diameter, respectively by their inertia. The collection efficiency of a round one-stage impactor is dependent on factors such as the airflow, the length and distance of the entrance nozzle to the impaction plate and from interstage losses [37, 38]. An important component in the assessment of the impactor efficiency is the Reynolds number *"Re"*, the Stokes number *"Stk"* and the so-called cut-off diameter. *"Re"* describes the dynamic properties of the flow. *"Stk"* is a dimensionless number and it represents the ratio of the particle stopping distance, in a given flow to the characteristic dimension of an object in that flow. The most important parameter for an inertial impactor is the so-called cut-off diameter *"d_{50}"*. The cut-off diameter is defined as the threshold for the particle size where the collection efficiency is 50 %. There are physical limitation for the cut off diameter to a size range of about 0.2 - 0.3 µm [39].

$$d_{50} = \sqrt{\frac{9\pi\eta D Stk}{4V\rho_{Particle}x_C}} \qquad (1)$$

The cut off diameter of a round one stage impactor can be calculated using equation (1). *"D"* is the nozzle diameter of the impactor, *"η"* represents the dynamic viscosity

of air, *"v"* is the volume flow rate, *"x_C"* is the Cunningham slip correction factor to account for non-continuum effects, *"$\rho_{Particle}$"* is the particle density and *"Stk"* is the Stokes number.

1.3 Localization and Identification of Single Particles

In nuclear safeguards and forensics the identification and pinpointing of single particles of interest which are embedded into a large matrix is vitally important. A particle of interest can be defined as an entity which does not disintegrate while being observed [40]. The notion of a single particle however is an arbitrary definition because a particle may be homogenous for a specific property but heterogeneous by another. In our case, homogeneity of the morphology and the size distribution are the main criterions thus making particles identification simple. In this work particles were identified and pinpointed using microscopy (SEM or optical microscopy) with the help of references marks. Triangulation is a well-established method for single particle identification and relocation applied in nuclear safeguards and forensics related work, see Admon et al. [40].

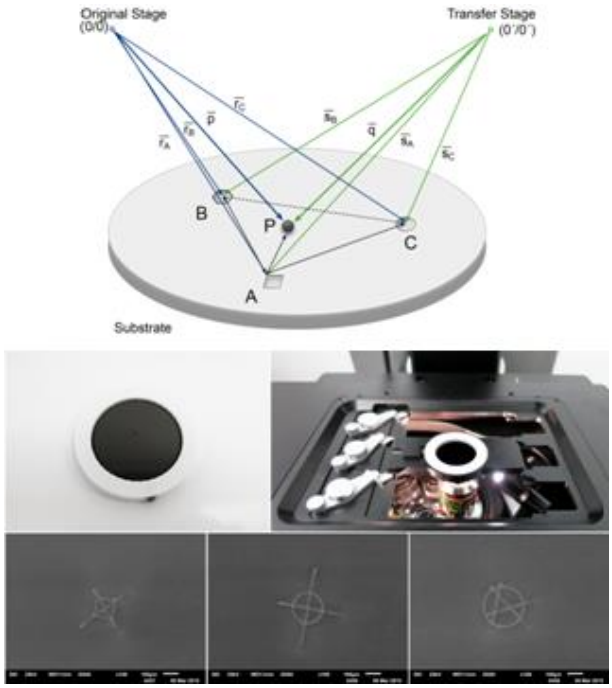

Figure 2: Top: vector diagram representing the triangulation method, see Admon, et al. 2005. Bottom: tailor-made reference marks engraved using a LMD system.

Figure 2 depicts a general schematic vector diagram of the triangulation method: with *"P"* the particle of interest, *"A, B, C"* are three non-collinear reference marks on the substrate, *"O and O`"* are the stage Cartesian coordinates system. This identification grid helped to relocate single particles of interest with appropriate precision in different instruments. The target coordinates of any given point can be calculated if the source coordinates are known. Commonly there are several ways of applying reference marks, (1) either by gluing some sort of a mesh or (2) by carving. This approach describes a new method to use a laser micro dissection (LMD) system to create precise tailor-made reference marks. Reference marks were defined in a custom excel sheet and then converted with Notepad++ and imported into the proprietary MMI software. The precision of this modified triangulation methodology is < 10.0 µm.

2. Experimental

2.1 Particle Production

Monodisperse uranium particles are produced by spray-pyrolysis (which is a four-step process) in a closed and sealed system, see Figure 3: (1) certified uranium solutions are diluted to hydro-alcoholic precursor solutions, (2) monodisperse aerosols are produced by a dedicated aerosol generator. All particles are carried throughout the system by carefully adjusted airstreams, (3) aerosol droplets are dried and calcinated in-stream to the subsequent uranium oxides and (4) collected from the system by inertial impaction.

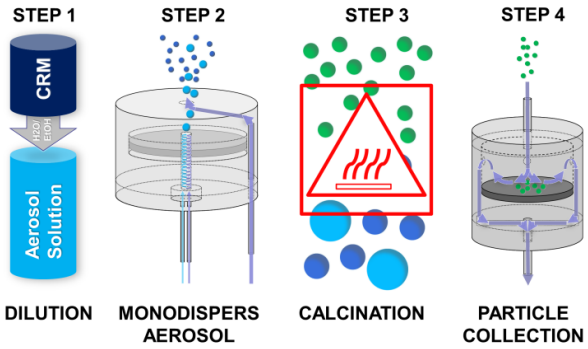

Figure 3: Schematic overview of the four step particle production process.

A vibrating orifice aerosol generator (VOAG, model 3450 TSI Inc.) was used to produce monodisperse aerosol droplets with a standard operating liquid feed rate "*Q*" of $Q = 1.392 \cdot 10^{-1}$ $cm^3 min^{-1}$, a 20 µm diameter orifice and a frequency "*v*" of $v \approx 70$ kHz. Particles are thermally converted in a furnace (Pressurized Air Heater, Dekati Ltd.) from uranyl nitrate to a corresponding uranium oxide. Uranium particles were produced from certified uranyl nitrate solution (IRMM-183) which was purchased from JRC-Geel [ii], see Table 1. Dilutions were prepared gravimetrically and volumetrically with ultrapure water (18.2 mΩ).

	Isotope Amount Ratio
n(234U)/n(238U)	$1.9755(22) \cdot 10^{-5}$
n(235U)/n(238U)	$0.0031257(16) \cdot 10^{-5}$
n(236U)/n(238U)	$1.48358(54) \cdot 10^{-5}$

Table 1: Isotope amount ratios of IRMM-183, re-certified values by Richter et al. (2005).

After adjusting the uranium concentration to about 200 $\mu g g^{-1}$ an equivalent volume of ultrapure ethanol (analytical grade, Merck Germany) was added. The uranium concentration of these solutions was determined by ICP-MS (Perkin Elmer, Sciex Elan 6100 DRC).

2.2 Setup Development

Particle production started in late 2012 with a preliminary setup. The system was operated with a uranium substitute, neodymium nitrate, to test the functionality of all components. The setup was comprised of an aerosol generator, a small furnace and a sampling unit. Over a period of three years the setup changed incrementally to adopt new features and to improve the particle generation process. The configuration of each component influences the particle size distribution, the morphology, the density and the crystal structure of the final particulates – some to a bigger extend than others. The following paragraph will depict these crucial components and the setup evolution until December 2014.

The aerosol generator was initially mounted upwards so that the aerosol particles had to travel against the force of gravity. Experiments performed at IEK-6 showed that the air flow is susceptible to turbulences caused by the shape of the tubing and the adjacent volumes. This resulted in a significant loss of particles inside the setup. Additionally, in the beginning the system was intended to be operated with two independent furnaces: (a) a small tubular furnace (Dekati Furnace) to preheat and dry the precursor droplets to mitigate stress induced cracks and then to transfer them directly to a (b) longer and hotter furnace (ThermConcept 4 zone furnace, max. temperature of 1100 °C) for the final calcination at temperatures between 600 - 900 °C. Both heating systems were installed in series. Initially it was considered that the second furnace was necessary to fully calcinated the aerosol particles. Depending on the temperature profile we expect to see mixed oxidation states of +V and +VI [41, 42]. Experiments showed that for uranyl nitrate hexahydrate solutions combined temperature profiles, including a preheating at around 600 °C and a calcination temperature well above 800 °C, tend to form hollow, inflated particles. During that time, it was difficult to produce monodisperse particles. Instead of generating only solid particles in the size range of ~ 1 µm, inflated and hollow particles as well as debris of these populations was generated simultaneously. SEM investigations showed that the intact and hollow particles would reach up to > 6 µm in diameter. These findings lead to the conclusion to focus on the adjustment of the temperature profile to yield solid particles. Experiments indicated that the small tubular furnace was sufficient. Micro Raman investigations showed that the small particles were predominantly made from U_3O_8 and to some lesser degree to UO_3, see Knott [43]. Initially, track etched polycarbonate filters (Whatman, Track Etched Nuclepore Filters) were used to collect particles. Further experiments revealed some major impairments compared to inertial impaction: (a) cumbersome sample preparation and post-processing procedures caused by curling of the filter, (b) low particle retention, (c) limited imaging capabilities inside SEM due to non-conductive surface and (d) charging effects which caused the particles to jump or move. A smooth, even and conductive surface was preferred. Hence it was decided to use inertial impaction to collect particles on vitreous carbon substrates (1" dia., Ted Pella Inc.).

[ii] *JRC-Geel: Joint Research Centre Geel formerly known as IRMM (Institute for Reference Materials and Measurements)*

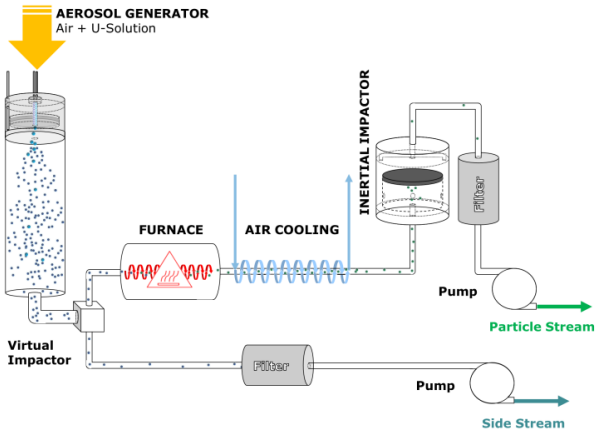

Figure 4: Schematic overview of the four-step particle production process.

This method is already well established in nuclear safeguards analytic and is applied to transfer a statistically significant number of particles from the swipes to a carbon substrate [15] which can be used almost directly for LG-SIMS analysis [9, 10]. It can be concluded that shorter dwell time and a more moderate temperature profile, with temperatures up to 600 °C, are sufficient to form solid uranium oxide particles. Additionally, it was decided to turn the VOAG upside down to use gravity and reduce the tubing to a minimum. Secondly it was decided to discard the four-zone oven to improve the particle collection process and to minimize the risk of unfavored particle species. These changes increased the particle yield significantly and made the overall process less prone to external influences. Between 2012 - 2015 various incremental steps were applied to modify and adopt the system to operate reliably. The size distribution is controlled online by an external optical sizer (Optical Particle Sizer 3330, TSI Inc.). In pursuance to reduce the combined air currents to a sufficient degree a component which is called a virtual impactor is used to generate two separate air streams. Each air stream is controlled separately by a pump. All air streams are directed into a ceramic Swagelok particle filter and discarded into the fume hood.

2.3 Particle Collection

2.3.1 One Stage Inertial Impactor

The inertial impactor used in this work was initially developed by Esaka et al. (2004) [15] to collect particles off swipe samples. But the design used in this work was changed and the cut-off diameter was never determined. Particles are generally collected at air flows in the range of 6 - 10 $lmin^{-1}$. The particle collection system at IEK-6 operates with combined airflows up to 32 $lmin^{-1}$.

Air Flow, [$lmin^{-1}$]	Substrate	Particle, [#]	Yield, [%]
Target	Si-Wafer	17211	-
4	Carbon	1354	8.27
10	Carbon	1174	6.98
15	Carbon	889	5.22
20	Carbon	759	4.41
25	Carbon	657	3.85
35	Carbon	519	3.01

Table 2: Overview of each airflow its corresponding substrate, number of particles collected and the yield.

Therefore, an airflow range of 4 - 35 $lmin^{-1}$ was chosen for the assessment. The aim of this assessment is to determine the cut off diameter, the radial distribution and the collection efficiency. For these experiments, certified soil matrix (Sigma Aldrich, Channel sediment, BCR-320R) was used. The soil matrix material is composed of finely ground polydisperse particles which have an irregular shape and geometry. Hence, the feret diameter was used to assess the particle size. 0.5 g of soil matrix was carefully grinded and transferred onto a cotton swipe. Particles were collected via inertial impaction directly onto a target substrate: Si wafer disk (Ted Pella Inc., 25.4 mm diameter). The number of particles on the target substrate was calculated with image acquisition software (FIJI) based on a composed large areal image; taken from multiple single optical microscopy images (Zeiss Axio Vision).

In total 17211 particles were counted on an area of about $4.0 \cdot 10^5$ μm^2. Image processing showed a consistent particle size distribution for each air flow throughout the whole investigated area ranging. For each air flow a theoretical cut off diameter *"$d_{50(theor)}$"* was calculated and compared against the measured cut off diameter *"$d_{50(meas)}$"* and their deviation *"Δ"* was recorded, see Table 2**.** As expected the cut off diameter decreases with increasing air flows.

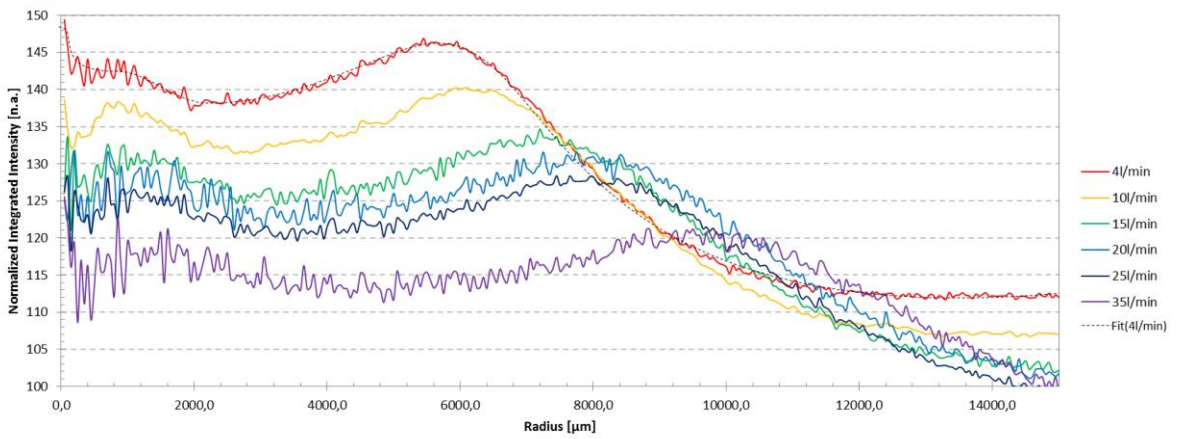

Figure 5: Radial distribution for all six air flows.

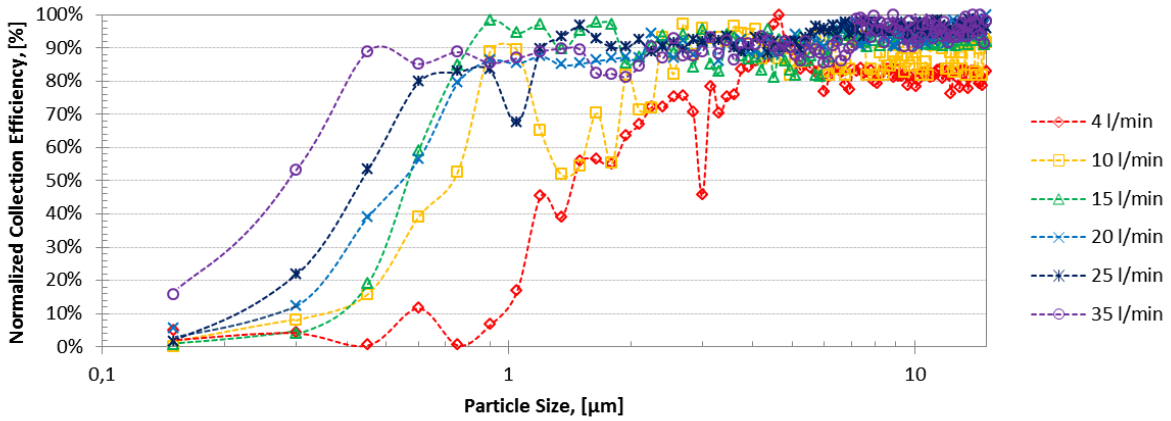

Figure 6: Normalized collection efficiency curves.

The number of particles collected decreases with increasing air flows due to blow-off effects and interstage losses. A higher air flow increases the number of particles impinging on the surface, but simultaneously a higher air flows also increases the probability of particles being detachment due to blow off- and re-entrainment effects [37, 38] as well as shear-, lift and drag forces caused by turbulences and pressure differences [44]. These effects substantiate in significant deviations between the measured and calculated cut-off diameters at low and high air flows, see Table 3. This investigation substantiated the prediction that the cut-off diameter decreases with increasing air flow and that the optimal working range is between 15 – 20 $lmin^{-1}$. The radial distribution of particles over an angle of 360° shows a distinct deposition pattern with one strong alleviation underneath the nozzle and a second slightly smaller deposition ring further away.

Air Flow, [lmin-1]	$d_{50(theor)}$ [µm]	$d_{50(meas)}$ [µm]	Δ, [%]
4	1.17	1.49	27.5%
10	0.71	0.78	9.86%
15	0.57	0.60	6.01%
20	0.48	0.45	6.05%
25	0.42	0.51	21.14%
35	0.34	0.39	13.70%

Table 3: Theoretical and measured cut-off diameters.

This deposition pattern is unique to this impactor design but it is also apparent that the radial distribution is linked to the air flow. The higher the airflow the more the second ring-like deposition moves further away from the center: for 4 $lmin^{-1}$ it is about 5800 µm, for 10 $lmin^{-1}$ it is 6150 µm, for 15 $lmin^{-1}$ it is 7200 µm, for 20 $lmin^{-1}$ it is 7750 µm, for 25 $lmin^{-1}$ it is 7900 µm and

for 35 $lmin^{-1}$ it is 9950 µm away from the center, see Figure 5. The collection efficiency was derived from the size dependent distribution and the data acquired from the radial profile distribution using FIJI. Figure 6 shows the normalized collection efficiency plotted against the particle size. Values for the measured cut-off diameters *"$d_{50(meas)}$"* were derived from this plot. An air flow of 15 $lmin^{-1}$ shows the most promising result.

2.3.2 Cyclone Impactor

Alternatively, to inertial impaction a cyclone impactor was designed at SGAS-ESL to ensure a sufficient particle collection yield. At the time the cyclone impactor was designed the inertial impactor could not deliver a sufficient collection yield because the combined air flows were too high due to the application of the four-zone furnace. Additionally, a cyclone impactor offers the advantage to collect particles directly into suspensions. Yet, this approach can facilitate and simplify the distribution of particles to various substrates. The first prototypes of the cyclone impactor were developed using 3D printing technology to test the basic functionality. Eventually a modified cyclone impactor with a conical body and a venture inlet was derived. The entire cyclone impactor consists of three components: (1) a venture nozzle with PTFE tubing, (2) cyclone body and (3) collection vessel. The venture nozzle is the inlet for the particle jet and is radially connected to the cyclone body. The collection vessel is threaded to the bottom of the cyclone body, see Figure 7. The venture nozzle is connected to the collection vessel with a PTFE tube to ensure water circulation. The collection vessel contains 5 ml MilliQ for circulation and dispersion. This inlet produces a fine aerosol water spray at air flows ranging from 20 - 135 $lmin^{-1}$. A jet of particles enters the venture nozzle is mixed with a spray of water. This mixture impinges tangentially on a conically shaped inner surface of a cyclone impactor. The Venturi nozzle serves the purpose to disperse a steady stream of water droplets to entrap the incoming particles and to increase the collection efficiency. The collection vessels are commercially available PTFE vessels with a thread and variable volume.

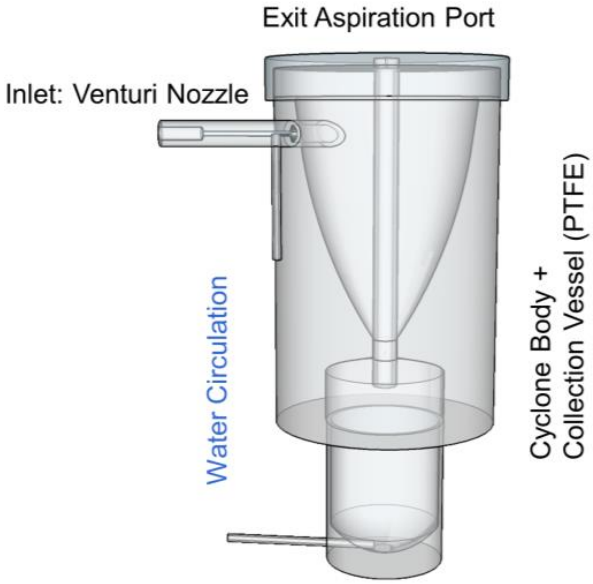

Figure 7: Left: Schematics of Cyclone Sampler. Right: Image of the Cyclone Sampler.

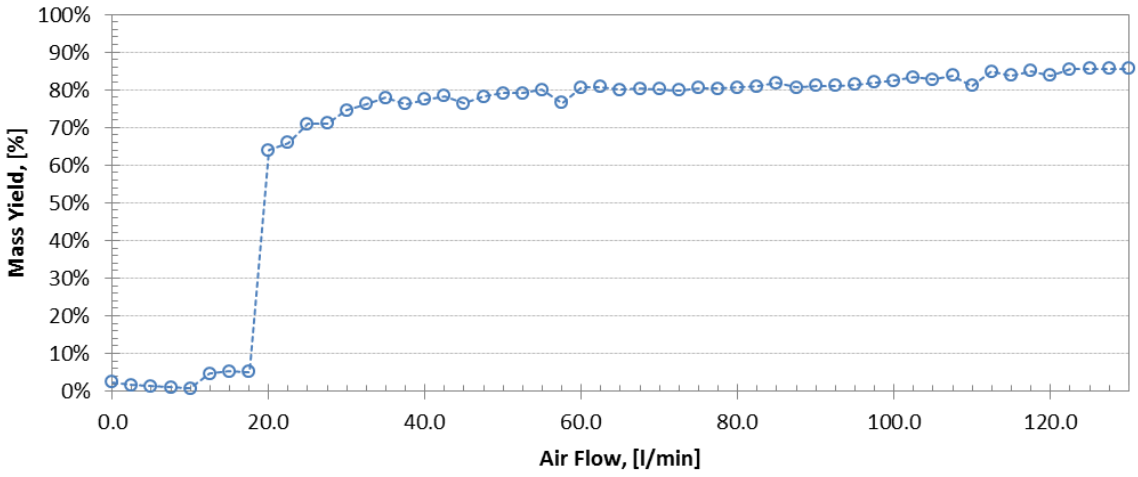

Figure 8: Collection efficiency of the cyclone sampler at various air flows.

For this assessment, PTFE vials purchased from VWR, Germany (V = 20 ml) where used. After impaction, the particles collected in the PTFE vessel and the air is diverted through the exit aspiration port. Finely ground certified soil matrix (Sigma Aldrich) was used to assess the collection efficiency. The collection efficiency, see Figure 8, was assessed by gravimetrical means at air flows between 0 – 130 $lmin^{-1}$.

Experiments also revealed that this cyclone design did not work above > 130 $lmin^{-1}$ due to turbulences: liquid is uncontrollably released through the exit aspiration port. A recommended operating range of 20 – 120 $lmin^{-1}$ can be derived, see Figure 8.

2.4 Particle Size

All six particle batches discussed in this work are produced from one CRNM (IRMM-183) by dilution with water and ethanol and are listed in Table 4 and Table 5. The focus of this chapter will be put on two distinct particle species that were observed during SEM analysis: (A) inflated and (B) solid particles. These solid particles are significantly denser than particle species (A). All particles were intended for a final particle diameter of around 1 µm. Initially a monodisperse size distribution could not be produced due to the formation of unfavored inflated species: batch (1) SG140521_02. After modifications to the setup, see Chapter 2.2, solid particles could be produced consistently on the following five batches: (2) SG141027_12A, (3) SG150312_05, (4) SG150401_14, (5) SG150413_03A and (6) SG150429_02. The particle size distribution and the aspect ratio were derived by using image acquisition software (FIJI) from stitched secondary electron (SE) images. This procedure was applied to obtain a statistical significant number of representative particles. All particles discussed in this chapter were identified as uranium containing entities with a Jeol JSM 6610 SEM which was equipped with an EDX detector by Oxford Instruments.

2.4.1 Inflated Particles

The inflated species on batch SG140521_02 were produced alongside a smaller number of solid particles. In total five distinct populations (solid, inflated and collapsed) in the size range from 0.67 to ≥ 9.3 µm were observed; on SG140521_02 - see Table 4. SEM investigations showed two distinct solid species with a mean diameter of 0.67 ± 0.50 µm and 1.35 ± 0.53 µm. These particles have cavities, pores and notches on the surface and are not perfectly spherically shaped, see Figure 11 (first and second from the left). To assess their geometry, the aspect ratio was determined using FIJI. It can be derived that the size and geometry of the solid species is not homogenous: Species (1) are small particles with a mean size of 0.67 ± 0.5 µm and an aspect ratio of 0.95 ± 0.05 and species (2) are solid particles with a mean size of 1.35 ± 0.53 µm and an aspect ratio of 0.77 ± 0.19 was derived.

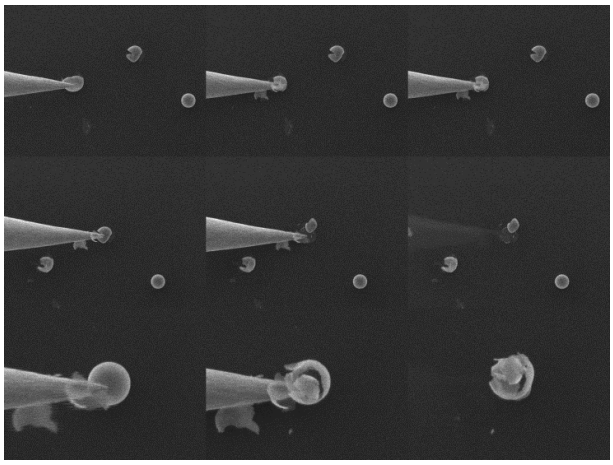

Figure 9: Typical hollow fragments and particles before (left) and after (right) destruction.

SEM investigations also showed that most of the particles were much bigger and hollow. Above 1.35 µm in diameter only hollow particles or debris of them was found. Species (3) and (4) are intact, hollow particles with a mean diameter of 4.61 ± 0.27 µm and 6.50 ± 0.53 µm respectively. These particles are spherically shaped which represented in a mean aspect ratio of 0.98 ± 0.02. Above 6.7 µm only collapsed shells, debris and aagglomerations were found.

SG140521_02	Ø [µm]	ΔØ [µm]
(1) solid species #1	0.67	0.50
(2) solid species #2	1.35	0.53
(3) inflated species #1	4.61	0.27
(4) inflated species #2	6.50	0.50
(5) debris + agglomerations	> 6.7 – 9.3	/

Table 4: Particle species of SG140521_02 and their corresponding mean particle size.

Due to the large amount of debris the mean diameter could not be determined satisfactory. For species (4) and (5) the highest number of particles was counted. SEM investigations on SG140521_02 confirmed that the clear majority of particles are hollow. In order to assess the inner structure a selected number of particles were cracked open with a motorized tungsten needle inside a Jeol SEM, see Figure 9. A more thorough and comprehensive study on the inner structure and the shell thickness is described by Knott [43]. Due to the formation of an outer shell the evaporation pressure inside the sphere causes the particle to inflate. If the evaporation pressure becomes too pronounced the spheres will collapse and form shells and debris, such as observed. The inflated species neither met the criteria of monodispersity defined by NIST [45] nor had a consistent morphology but they offer a helpful insight on the droplet-to-particle mechanics and demonstrate that higher temperature gradients tend to favor surface controlled precipitations, see Gurav et al. [33], Reuge et al. [35] and Messing et al. [36]. This observation only applies to dilute hydro alcoholic uranyl nitrate solutions. It can be concluded that the main parameters which govern the precipitation process during solidification are the temperature profile and the dwell time. Moreover, parameters such as air flow, uranium concentration and setup design have a less pronounced influence.

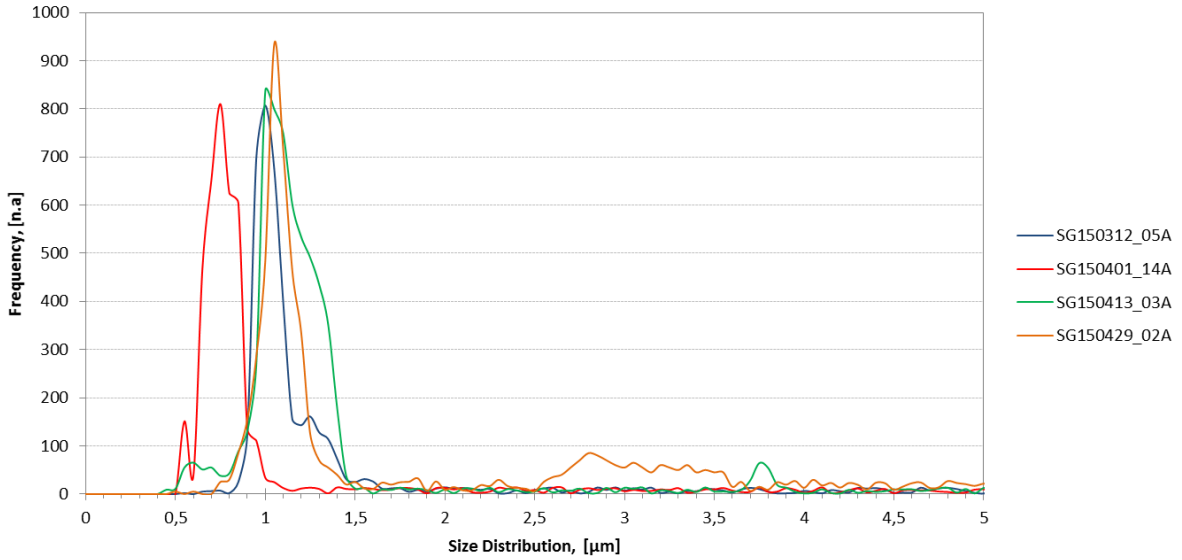

Figure 10: Size distribution of SG150312_05 (blue), SG150401_14A (red), SG150413_03A (green) and SG150429_02A (orange).

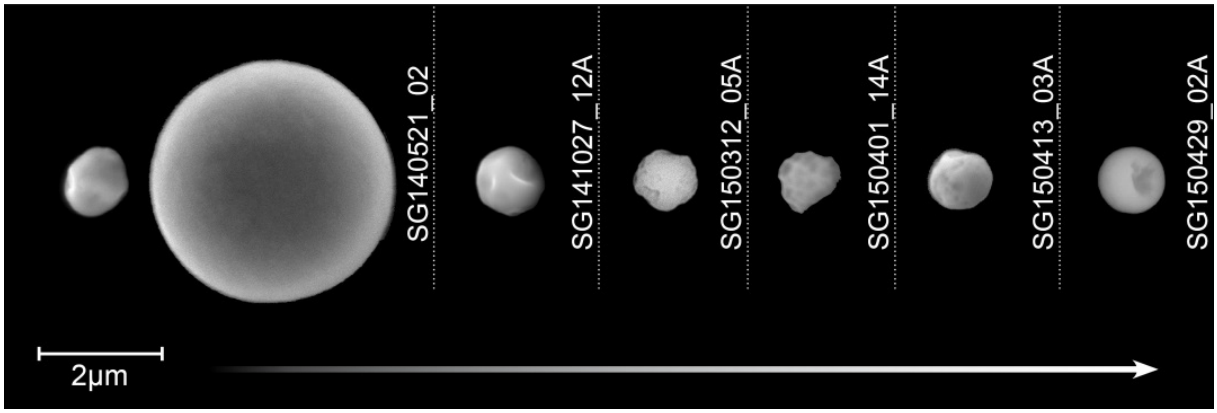

Figure 11: Overview of the particle evolution since May 2014 to April 2015. From left to right: inflated species and solid particle species.

2.4.2 Solid Particles

The presence of inflated species was a clear indication that the setup had to be modified and that the temperature profile had to be adjusted. The setup was changed subsequently to a configuration that is depicted in Figure 4. These modifications had a significant impact on the consistency of the particle characteristics. Five different batches were analyzed. Four different batches were intended for a mean final particle size of 1 µm and one for 0.85 µm. All particle batches show a consistent particle size distribution and are in good accordance with the calculated values, see Table 5. Particle analysis was performed using FIJI. All particle batches discussed in this paper are not yet monodisperse by NIST [45] definition.

	Ø [µm]	ΔØ [µm]
(1) SG141027_12A	1.37	0.19
(2) SG150312_05A	0.99	0.15
(3) SG150401_14A	0.85	0.15
(4) SG150413_03A	1.05	0.11
(5) SG150429_02A	1.02	0.10

Table 5: Mean particle size of solid particles from SG141027_12A to SG150429_02A.

SG141027_12A was the first particle batch towards consistent particle characteristics and was therefore investigated separately. A mean particle size of 1.37 ± 0.19 µm was derived. In total 2689 particles were measured on an area totaling 1430 x 1072 µm^2. A small doublet peak at 1.73 µm was detected with 1/6 of the intensity of the main peak. To a small degree inflated particles appear on SG141027_12A as well at 4.25 µm. For rest of the batches an area of ~ 4700 x 3500 µm^2 was investigated and no inflated species were detected. For SG150312_05 4497 particles were detected with a mean particle size distribution of 0.99 ± 0.15 µm. A small doublet tailing was measured at 1.25 ± 0.13 µm with about 1/5 of the intensity of the main peak. For SG150401_14A 5043 particles were analyzed with a mean size distribution of 0.85 ± 0.15 µm. Particles were intended to be around 0.8 µm in diameter. A small doublet tailing at 1.07 ± 0.11 µm with a signal of about 1/6 of the main peak was detected. SG150413_03A has mean diameter of 1.05 ± 0.11 µm for 7142 detected particles. No doublet peak could be identified. For SG150429_02A a similar picture can be drawn: 7505 particles were detected with a mean size distribution of 1.02 ± 0.10 µm, see Figure 10. These results highlight how the uranium concentration is vital for the adjustment of the final diameter. But it also shows that every parameter in the production process needs to be monitored carefully to ensure a reproducible outcome. Due to technical issues the liquid feed rate "*Q*" could not be established consistently which also lead to the formation of unwanted particle species, see batches SG140521_02 and SG141027_12A. It can be concluded that the particle size can be adjusted accurately by the precursor solution concentration if every step in the droplet formation process is controlled correctly. SEM investigations on the geometry revealed that these particles are not perfectly spherical. The outer surface of all investigated particles shows dents and cavities and an overview of the particle geometry and size is depicted in Figure 11. Since SG141027_12A was the first particle batch towards a more consistent quality it was investigated more thoroughly. Therefore, it was used in the following Chapter 2.5 to assess the isotopic composition of the final microparticles.

2.5 Isotopic Analysis

Isotopic amount ratios of n(^{234}U)/n(^{238}U), n(^{235}U)/n(^{238}U), n(^{236}U)/n(^{238}U) were measured on a CAMECA 1280 large geometry SIMS (LG-SIMS) at SGAS-ESL. In this investigation one representative batch (SG141027_12A) of solid particles will be discussed. All particles were measured with an ion probe current (IP) of IP = 50 pA and a beam raster size of 10 µm. Particles were directly measured from the C-substrate. Particles measured in this campaign all derived from one CRM: IRMM-183. Hence the isotopic composition of these particles was compared against the original composition to detect any anomalies. The isotopic ratios of n(^{234}U)/n(^{238}U), n(^{235}U)/n(^{238}U), n(^{236}U)/n(^{238}U) were compared against the re-certified values by Richter et al. [46].

Isotope Amount Ratio	
n(^{234}U)/n(^{238}U)	$1.9755(22) \cdot 10^{-5}$
n(^{235}U)/n(^{238}U)	$3.2157(16) \cdot 10^{-3}$
n(^{236}U)/U(^{238}U)	$1.48358(54) \cdot 10^{-4}$

Table 6: Re-Certified Isotopic Amount Ratios of IRMM-183, according to Richter et al. [46].

According to Richter et al. IRMM-183 was produced in 1987 along with a series of other uranium CRM's with various enrichment levels. Due to the progress in the development of mass spectrometers and procedures the certified values were to be updated. It is worth mentioning that Richter's data was derived from TIMS measurements on bulk quantities. Therefore, a better counting statistic can be derived which means a higher degree of accuracy and smaller corresponding uncertainties than for LG-SIMS measurements on minute quantities. These re-certified values were used a direct comparison. The scope of these measurements was to verify that no changes in the isotopic composition occur and to draw conclusions about the homogeneity of the particle morphology. For $n(^{234}U)/n(^{238}U)$ a mean isotope ratio of $n(^{234}U)/n(^{238}U) = 1.999 \cdot 10^{-5} \pm 1.333 \cdot 10^{-6}$ was measured which corresponds to a relative standard deviation (RSD) of 6.67 %. Richter measured an isotope ratio of $n(^{234}U)/n(^{238}U) = 1.976 \cdot 10^{-5} \pm 2.2 \cdot 10^{-7}$ with an RSD of 1.22%. For ^{235}U a much more precise result is expected due to better counting statistics and the results are in good agreement with this hypothesis: $n(^{235}U)/n(^{238}U) = 3.2189 \cdot 10^{-3} \pm 1.2991 \cdot 10^{-5}$ and a RSD of 0.40 %.

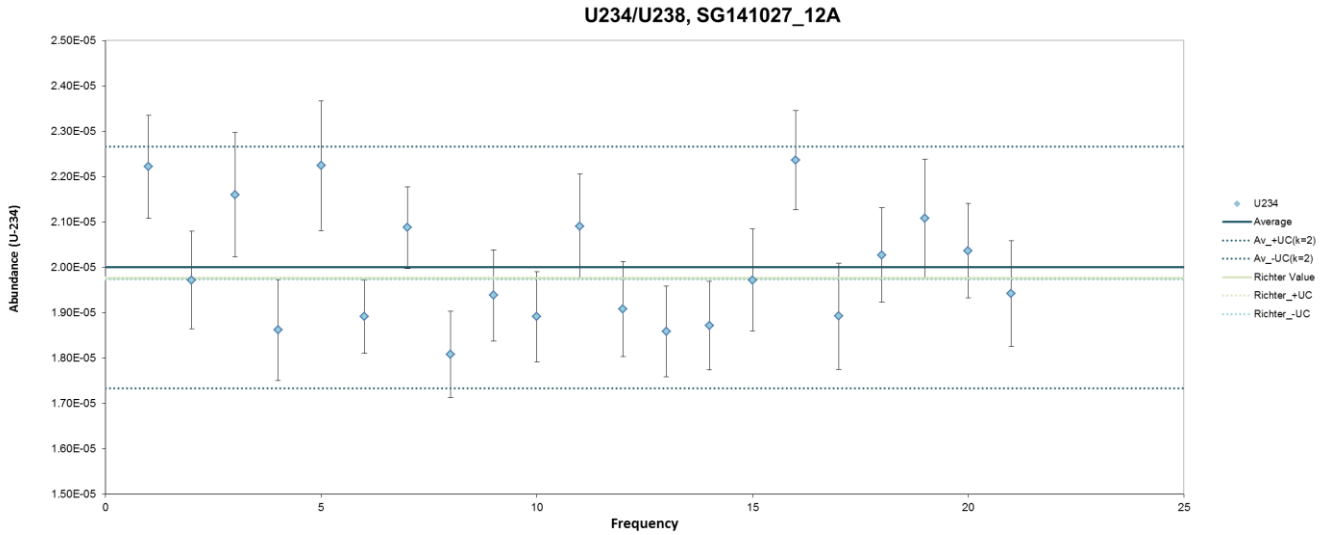

Figure 12: SG141027_12[a], $n(^{234}U)/n(^{238}U)$.

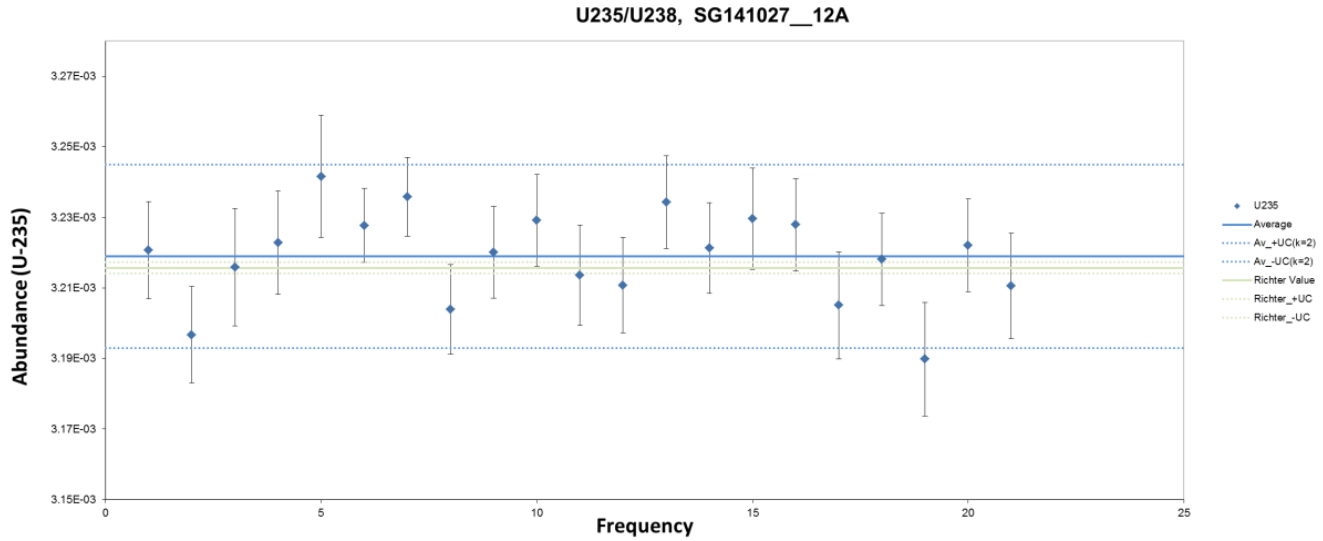

Figure 13: SG141027_12A, $n(^{235}U)/n(^{238}U)$.

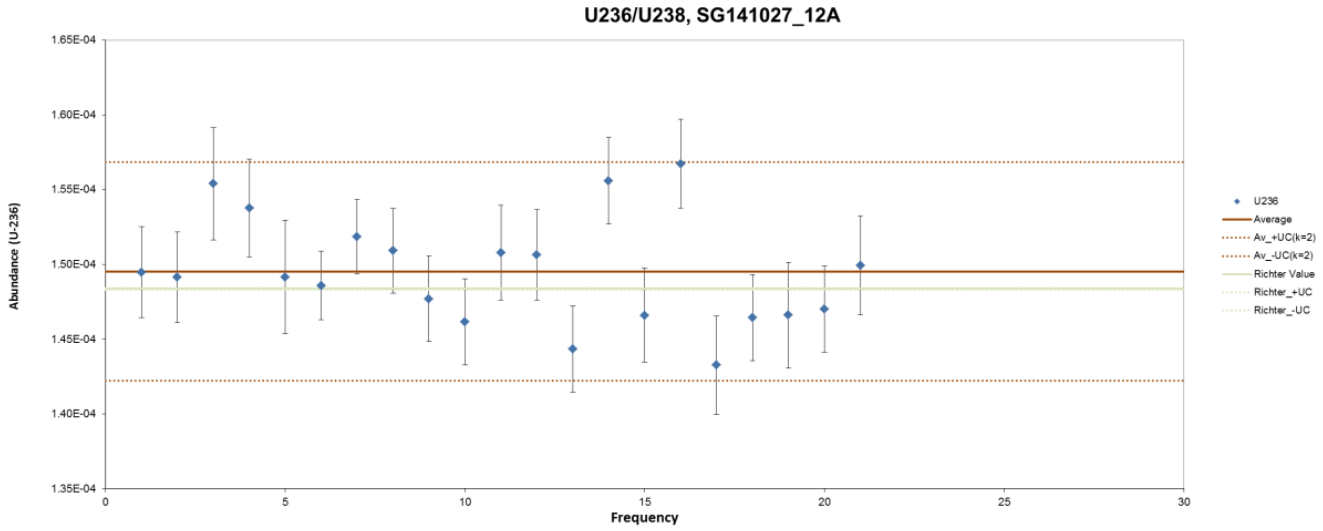

Figure 14: SG141027_12A, n(236U)/n(238U).

n(^{234}U)/n(^{238}U) SG141027_12A
Certified Value for $^{234}U/^{238}U$ ($1.9755 \cdot 10^{-5} \pm 2.2 \cdot 10^{-7}$), k = 2
Average $^{234}U/^{238}U$ ($1.9999 \cdot 10^{-5} \pm 1.3332 \cdot 10^{-6}$), k = 2 (STD, n = 21)
Rel. Std. Dev.: 6.67 %, Rel. Bias: 1.22 %
n(^{235}U)/n(^{238}U) SG141027_12A
Certified Value for $^{235}U/^{238}U$ ($3.2157 \cdot 10^{-3} \pm 1.6 \cdot 10^{-5}$), k = 2
Average $^{234}U/^{238}U$ ($3.2189 \cdot 10^{-5} \pm 1.2991 \cdot 10^{-5}$), k = 2 (STD, n = 21)
Rel. Std. Dev.: 0.40 %, Rel. Bias: 0.10 %
n(^{236}U)/n(^{238}U) SG141027_12A
Certified Value for $^{236}U/^{238}U$ ($1.48358 \cdot 10^{-4} \pm 5.4 \cdot 10^{-7}$), k = 2
Average $^{234}U/^{238}U$ ($1.4852 \cdot 10^{-4} \pm 3.6512 \cdot 10^{-6}$), k = 2 (STD, n = 21)
Rel. Std. Dev.: 2.44 %, Rel. Bias: 0.78 %

Table 7: Isotope Amount ratios on solid particles in comparison to Richter's data

This result is underlined by a small deviation to Richter's value, of only 0.10 %, and by the low standard deviation of the mean, see Table 7. For ^{236}U a mean intensity of $n(^{236}U)/n(^{238}U) = 1.49521 \cdot 10^{-4} \pm 3.65118 \cdot 10^{-6}$ was measured with a RSD of 2.44% and a standard deviation of the mean of $7.96754 \cdot 10^{-7}$. The deviation to Richter's value is about 0.78 %. It can be concluded that no deviation from the initial isotopic composition was detected. LG-SIMS measurements demonstrate that all solid particles show consistent and homogenous signals for all isotopes (^{234}U, ^{235}U, ^{236}U and ^{238}U), in particular for the minor isotopes ^{234}U and ^{236}U. The low variance of the measured data points indicates a consistent and homogenous morphology for all measured particles. This trend is in agreement with a significantly low deviation to Richter's data, ranging from only 0.10 - 1.22 % - see Table 7. Furthermore, it can be derived that the isotopic composition is independent from the particle size and morphology

3. Discussion and Conclusion

This work demonstrates the complexity associated with the production of monodisperse uranium microparticles made by spray pyrolysis. The final size and morphology is

governed by the setup itself, the production characteristics (i.e. liquid feed rate, temperature profile and dwell time) but more over by the uranium concentration. That is why the focus of this work is put on (a) the evolution of a working microparticle production setup and its vital components in the time period between 2012 and 2015 and (b) on a comprehensive analytical assessment to derive the size, morphology and isotopic composition. It can be concluded that the final particle size can be adjusted accurately by the uranium concentration of the aerosol solution. All parameters during the aerosol generation and the solidification and nucleation process must be monitored carefully to yield in solid uranium microparticles. The morphology control is not as straight forward. Depending on the conditions during the droplet-to-aerosol conversion the final particle size, morphology and density can significantly differ. Hence a smaller and more compact setup is favoured: a smaller dwell time in combination with temperatures up to 600 °C lead to the formation of solid uranium oxide particles.

Particle collection is an important issue. The collection system of choice needs to fulfil three basic requirements: (1) easy access, (2) mitigating the risk of cross contamination and (3) possibility to transfer single particles or bulk quantities easily to different substrates. And it needs to operate inside the existing air flow limitations. It could be demonstrated that inertial impaction fulfilled these requirements the best. A proprietary one stage inertial impactor was commonly used to collect particles. And its performance and cut-off diameter were characterized. It can be derived that theoretical collection efficiency and cut-off diameters are in good agreement with the measured values. Particles in the size range of a few micrometres can be collected efficiently. Only for very low and very high air flows a significant deviation for the cut off diameters was derived. Alternatively, particles can be collected directly into suspensions. A modified cyclone impactor was developed at SGAS-ESL to collect particles at high air flows. It can be concluded that this methodology is in good agreement with the theoretical values and it works for air flows in the range of 20 - 120 $lmin^{-1}$.

Particle identification and relocation is a vital step in nuclear safeguards and forensics. Single particles are to be measured and assessed in different instruments. Triangulation is commonly used in nuclear forensics to facilitate particles identification. The method depicted in this work describes a novel technique using a laser micro dissection system to engrave custom-made triangulation patterns as reference marks. With this method the precision of the relocation can be less than 10 µm, depending on the optical capabilities.

Six different particle batches were analysed in order to assess their size distribution, morphology and geometric characteristics. All particles discussed in this paragraph were identified as uranium bearing particulates with SEM-EDX. Chronologically, the first batch (SG140521_02) described in this work contained two specific particle species: (a) solid particles and (b) hollow, inflated particles. The existence of species (b) was not anticipated but it was used to highlight the complexity of the droplet-to-particle conversion. This specie consists of a wide range of different particulates: from inflated, intact species, to inflated broken particles, to debris and finally to agglomerations. That is why a broad size distribution of > 4.5 µm up to 9.2 µm could be observed. It can be derived that with increasing temperature profile (gradient and dwell time alike) particles tend to inflate. To demonstrate that the intact and inflated particles are hollow a selected number of particles were broken with a tungsten needle inside the SEM. Solid particle, from five different batches, were also investigated and showed a more coherent picture: (a) particles are not perfectly spherically shaped and (b) particle surface shows cavities and notches but (c) the particle size distribution is almost monodisperse. Over the time the size distribution became more consistent due to changes and monitoring devices in the setup. Solid particles are generated through a homogenous precipitation process which is in direct competition to a surface controlled precipitation. It can be concluded that the anticipated size distribution can be reproduced sufficiently, but a monodisperse size distribution could not be accomplished so far. Experiments also show that the final particle size is primarily controlled by the uranium concentration of the aerosol solution and the liquid feed rate (which is the volume/time unit that is pushed through the orifice [ml/s], see Berglund and Liu (1974)[47]; under normal working conditions.

Since these microparticles are intended to be used as a future CRM for SIMS analysis one exemplary batch (SG141027_12A) was used to confirm consistent isotopic composition. The measured isotopic ratios were compared against the re-certified values from IRMM-183 by Richter et al. [46]. For ^{234}U an isotope amount ratio of $n(^{234}U)/n(^{238}U) = 1.9755 \cdot 10^{-5} \pm 2.2 \cdot 10^{-7}$ with just a deviation of about 6.7 % to Richter's

value is measured. For the more abundant ^{235}U an $n(^{235}U)/n(^{238}U) = 3.2189 \cdot 10^{-3} \pm 1.2991 \cdot 10^{-5}$ with deviation of only 0.4 % is measured and for $n(^{236}U)/n(^{238}U) = 1.49521 \cdot 10^{-4} \pm 3.65118 \cdot 10^{-6}$ the deviation to Richter's value accounts to about 2.4 %. Furthermore, the variability of the measured isotopic amount ratios and its corresponding RSD's are a strong indication that the particle morphology is consistent throughout the entire particle batch.

It is worth noting that the particle production project is continued at IEK-6. Since December 2015 more improvements were implemented and new results are published, see Middendorp et al. [48].

4. Acknowledgements

I would like to acknowledge the IAEA's and FZJ's contributions to this project: This paper is a comprehensive excerpt of my doctoral thesis [43], which was partly funded by the Federal Ministry of Economic Affairs and Energy (BMWi) through the Joint Program on the Technical Development and Further Improvement of IAEA Safeguards between the Government of the Federal Republic of Germany and the IAEA under the GER SP Task A1961 and the International Atomic Energy Agency.

5. References

[1] INFCIRC/140, *IAEA* (1970).
[2] INFCIRC/540, *IAEA* (1997).
[3] S.F. Boulyga, J.S. Becker, *J. Anal. At. Spectrom.,* (2002), 17, 1143-1147.
[4] S. Boulyga, S. Konegger-Kappel, S. Richter, L. Sangely, *J. Anal. At. Spectrom.,* (2015), 30, 1469-1489.
[5] J.S. Becker, *J. Anal. At. Spectrom.*, (2005), 20, 1179-1184.
[6] S. Bürger, L. Riciputi, D. Bostick, S. Turgeon, E. McBay, M. Lavelle, *J. Mass Spectrom.*, (2009), 286, 70-82.
[7] S. Bürger, S. Balsley, S. Baumann, J. Berger, S. Boulyga, J. Cunningham, S. Kappel, A. Koepf, J. Poths, *Int. J. Mass Spectrom.,* (2012), 311, 40-50.
[8] T. Kuno, A. Ciurapinski, D. Klose, J. Cliff, O. Bildstein, S. Bulyha, D. Donohue, J. Poths, *IAEA,* (2008), SAL-IR 2008/07,1-33.
[9] P.M.L. Hedberg, P. Peres, T. Fanghaenel, K. Luetzenkirchen, K. Mayer, P. Meylemans, P. Schwalbach, M. Wallenius, *INMM Proceeding*, (2012), 1-6.
[10] P. Peres, P. Hedberg, F. Rabemananjara, J. Cliff, S. Littmann, N. Albert, C. Vincent, *Esarda Annual Meeting 2012*, (2012), 1-8.
[11] P. Peres, P.M.L. Hedberg, S. Walton, N. Montgomery, J.B. Cliff, F. Rabemananjara, M. Schuhmacher, *Surf. Interface Anal.,* (2012), 1-5.
[12] Y. Ranebo, P.M.L. Hedberg, M.J. Whitehouse, K. Ingeneri, S. Littmann, *J. Anal. At. Spectrom.*, (2009), 24, 277-287.
[13] G. Tamborini, M. Wallenius, O. Bildstein, L. Pajo, M. Betti, *Microchim. Acta*, (2002), 139, 185-188.
[14] Y. Ranebo, *JRC-ITU-TN-2008/09*, (2008), 1-30.
[15] F. Esaka, K. Watanabe, H. Fukuyama, T. Onodera, K.T. Esaka, M. Magara, S. Satoshi, S. Usuda, *J. Nucl. Sci. Technol.*, (2004), 41, 1027-1032.
[16] D. Donohue, A. Ciurapinski, J. Cliff III, F. Rüdenauer, T. Kuno, J. Poths, *Appl. Surf. Sci.*, (2008), 255, 2561-2568.
[17] F. Esaka, K. Esaka, C. Lee, M. Magara, S. Sakurai, S. Usuda, K. Watanabe, *Talanta*, (2007), 71, 1011-1015.
[18] F. Esaka, K. Watanabe, T. Onodera, C.G. Lee, M. Magara, S. Sakurai, S. Usuda, *Appl. Surf. Sci.*, (2008), 255, 1512-1515.
[19] F. Esaka, M. Magara, D. Suzuki, Y. Miyamoto, C.G. Lee, T. Kimura, *Talanta*, (2010), 83, 569-573.
[20] K. Raptis, C. Ingelbrecht, R. Wellum, A. Alonso, W.D. Bolle, R. Perrin, *Nucl. Instrum. Meth. A*, (2002), 480, 40-43.
[21] R. Kips, Ph.D. Thesis, *University of Antwerp and EC-JRC-IRMM,* (2007).
[22] T. Kärkelä, U. Tapper, R. Ziliacus, *VTT-R-07821-06*, (2006), 1-7.
[23] T. Kärkelä, U. Tapper, R. Ziliacus, *VTT-R-03335-07,* (2007), 1-12.
[24] R. Ziliacus, J.K.T. Hokkanen, U. Tapper, *VTT-R-10766-08,* (2008), 1-8.
[25] J. Hokkinen, U. Taper, R. Ziliacus, *VTT-R-100066-10*, (2011), 1-12.

[26] R. Taylor, J. Tushingham, *Department of Trade and Industry*, SRDP-R264, (2000), 1-25.
[27] N. Erdmann, M. Betti, O. Stetzer, G. Tamborini, J. Kratz, N. Trautmann, J. van Geel, *Spectrochim. Acta B*, (2000), 55, 1565-1575.
[28] B.O. Stetzer, Ph.D. Thesis, , *University Mainz*, (2001).
[29] M. Kraiem, S. Richter, N. Erdmann, H. Kühn, M. Hedberg, Y. Aregbe, *Anal. Chim. Acta*, (2012), 748, 37-44.
[30] Y. Ranebo, N. Niagolova, N. Erdmann, M. Eriksson, G. Tamborini, M. Betti, *Anal. Chem.*, (2010), 82, 4055-4062.
[31] A. Knott, M. Dürr, *ESARDA Bulletin*, 49, (2013), p. 40-45.
[32] T.T. Kodas, (1989), *Angew. Chem. Int. Edit.*, 28, 794-806.
[33] Y. Xiong, T.T. Kodas, *J. Aerosol Sci.*, (1993), 24, 893-908.
[34] A. Gurav, T.T. Kodas, T. Pluym, Y. Xiong, *Aerosol Sci. Tech.*, (1993), 19, 411-452.
[35] N. Reuge, B. Caussat, N. Joffin, J. Dexpert-ghys, M. Verelst, H. Dexpert, *AIChE J.*,(2008), 54, 394-405.
[36] G.L. Messing, S.C. Zhang, G.V. Jayanthi, *J. Am. Ceram. Soc.*, (1993), 76, 2707-2726.
[37] A.V. Marple, K. Willeke, *Atmos. Environ.*, (1976), 10, 891-896.
[38] B. Jurcik, H.C. Wang, *J. Aerosol Sci.*;(1995), 26, 1139-1147.
[39] D.S. Ensor, *Aerosol Sci. Tech.*, (2011), 1-21.
[40] U. Admon, E. Chinea-Cano, D. Wegrzynek, H. Aigner, A. Markowicz, D.L. Donohue, F. Ruedenauer, W. Costin, *Springer Science & Business Media B.V.*; (2009), 2nd Ed.; Chap. 2; 15-55.
[41] R.D. Kozlova, V.A. Matyukha, N.V. Dedov, *Radiochem.,* (2007), 49, 2, 130-134.
[42] S. Dash, M. Kamruddin, S. Bera, P. Ajikumar, A. Tyagi, S. Narasimhan, B. Raj, *J. Nucl. Mat.*, (1999), 264, 271-282.
[43] A. Knott, Ph.D. Thesis, *Ener. & Envir.*, (2016), 336, FZJ Jülich GmbH, RWTH-Aachen University.
[44] C. Misra, S. Kim, S. Shen, C. Sioutas, *J. Aerosol Sci.,* (2002), 33, 735-752.
[45] V.A. Hackley, C.F. Ferraris, *NIST SP 960-3*, (2001), 1-72.
[46] S. Richter, A. Alonso, W.D. Bolle, H. Kühn, A. Verbruggen, R. Wellum, P. Taylor, *Int. J. Mass Spectrom.*, (2005), 247, 37-39.
[47] R.N. Berglund, B.Y.H. Liu, Patent, 3,790,079, (1974).
[48] R. Middendorp, M. Dürr, A. Knott, F. Pointurier, D. Ferreira Sanchez, V. Samson, *Anal. Chem.*, (2017), 89 (8), 4721-4728.

Micro Particle Suspensions for Preparation of Reference Materials for Particle Analysis Methods in Safeguards

Ronald Middendorp, Martin Dürr, Irmgard Niemeyer, Dirk Bosbach

Forschungszentrum Jülich GmbH
IEK-6: Nuclear Waste Management and Reactor Safety
52428 Jülich, Germany
E-mail: r.middendorp@fz-juelich.de

Abstract:

In order to produce micro particle reference materials for nuclear safeguards particle analysis, a dedicated facility has been established at Forschungszentrum Jülich. This includes an aerosol-based particle production setup which is capable of producing uranium micro particles with consistent isotopic compositions and uranium contents. While the produced particles could be used as reference materials as obtained after production, further options for packaging the particles are being considered to simplify handling of the particles and to open new possibilities, such as the preparation of particle mixtures.

The transfer of the collected particles into a suspension bears several advantages. For example, particles in suspension stored in a bottle would be amenable to extraction of an aliquot, which could be dried on a substrate of interest, such as silicon wafers, glass-like carbon disks or cotton-swipes, to obtain test samples. Also, various suspensions could be mixed in different ratios followed by drying on the desired substrates to obtained particle mixtures of two or more different particle types. However, while the particles are dispersed in suspension, various reactions could have an influence on the stability of the micro particle property values. In order to assess the stability of uranium micro particles in a suspension, experiments have been conducted using synthetic powders and uranium micro particles. Our results from dissolution and uranium isotope exchange studies show that ethanol is a suitable medium for the storage of particles over a period of a few months. Using particles produced with the particle production setup at Forschungszentrum Jülich, particle suspensions have been produced by transfer of collected particles into ethanol and distribution on silicon wafers and cotton-swipes produced consistent results. It was demonstrated that the production of particle mixtures is feasible. It was also shown that particles in suspension could represent a suitable packaging for a particle reference material which permits a quick and flexible preparation of various types of test samples.

Keywords: Particle Analysis; Environmental Sampling; Reference Material; NWAL; Suspensions

1 Introduction

The destructive analysis of samples collected during inspections of nuclear facilities is one of the verification measures applied by the International Atomic Energy Agency (IAEA) to derive safeguards conclusions. One of the employed methods is particle analysis, which is based on the release of small amounts of microparticulate matter during all material handling processes. Such particles are collected via swipe samples taken during inspections of the nuclear facilities. The collected samples are sent to dedicated laboratories for analysis, which is typically performed using high accuracy micro-analytical tools, such as LG-SIMS. These methods are capable of measuring the isotopic composition of fissile elements within single microparticles. The capability to reveal the material handling history of inspected facilities has therefore become an important tool to detect undeclared activities in the inspected facilities.

Over recent years, great progress was achieved in the improvement of the measurement accuracy of isotopic composition of fissile elements within micrometer sized particles [1]. The analysis of individual

particles has progressed beyond the analysis of the major isotopes (e.g. ^{235}U and ^{238}U) towards the minor isotopes (e.g. ^{234}U and ^{236}U) which provide additional information, e.g. on the facility operations history.

Due to the improved measurement accuracy, quality assurance (QA) has become more stringent. Generally, the QA require various quality control (QC) measurements to be performed for the analytical method [2]:

1) Calibration;
2) Validation;
3) Quality control;
4) Proficiency testing.

Each of these measures requires a dedicated test material of high homogeneity and stability, which are generally described as reference materials (RMs) [3]. For calibration, validation and also proficiency testing, not only the stability and homogeneity of the material is of importance, the material is also characterized with respect to one or more property values to quantify the *true* value; i.e. the absolute value of the property with given uncertainty and traceability. Such materials are classified as certified reference materials (CRMs) and have strict requirements, as described in ISO Guide 34 [4].

Over the recent years, a setup has been established at Forschungszentrum Jülich [5-7] to produce micrometer sized uranium oxide microspheres, which are intended to be used for the various quality control measurements and are to be certified as CRM with respect to the uranium isotopic composition and uranium elemental content. The setup consists of an aerosol generator, after which the aerosol droplets are carried through an aerosol heater in which spherical particles are formed with a homogeneous size and shape. The obtained particles have been investigated in detail [7] and were shown to consist of triuranium octoxide (U_3O_8).

At present, the produced microparticles are collected using single-stage inertial impactors, which allow for the production of ca. 50 samples within a single run. The usage of such impactors does, however, have a number of limitations; the number of particles collected may differ between various production runs, the particles are deposited heterogeneously over the substrate and the production of particles mixtures under controlled conditions is not easily possible. Also, some applications require the production of more than 50 samples, which would require production of particles over multiple batches/days, which could lead to an expanded between-sample inhomogeneity.

This paper describes a method to transfer collected particles into particle suspensions. Such particle suspensions could then be mixed with similar suspensions containing different types of particles, for example different isotopic composition, which could then be distributed and dried over various substrates to prepare the final test samples. However, while in suspension, interaction of the particles with the solution could alter the properties of the particles. Therefore, a number of investigations were performed to determine whether and to what extend such interactions occur.

2 Particle Production at Forschungszentrum Jülich

The production of monodisperse uranium oxide microspheres with a nominal diameter around 1 µm at Forschungszentrum Jülich has been described elsewhere in detail [7]. The production is based on the formation of an aerosol from a dilute uranyl nitrate solution with the desired isotopic composition. The usage of uranyl nitrate was found to yield proper particles with a minimal amount of preparation [7], which would minimize the risk of cross-contaminations. The diluted solution is fed using a syringe pump through a vibrating orifice aerosol generator, where a monodisperse aerosol is formed. The volume of a single droplet can be calculated by dividing the volume flow rate Q by the oscillating frequency f applied to the generator. When the uranium content w and the density ρ of the feed solution are known, the amount of uranium contained in a single droplet m can be calculated according to equation 1.

$$m = Q / f \times w \times \rho \qquad (1)$$

The formed droplets are then guided with an air flow through an aerosol heater set to 500 °C; at 500 °C particles were found to be fully decomposed into uranium oxide whereas a further increase of the temperature causes the particles to deform, and a lower degree of monodispersity was obtained [7]. After cooling, the particles are collected using single-stage inertial impactors [8] onto glass-like carbon substrates. The collected particles were investigated by μ-XRD, μ-XANES and μ-Raman spectroscopy to identify the obtained chemical phase, all of these techniques resulted in an orthorhombic triuranium octoxide (U_3O_8) phase [7].

By using the single-stage inertial impactor, the produced particles can be collected on glass-like carbon substrates which, in turn, can be analyzed by SIMS without further handling, minimizing the risk of introducing any cross-contaminations. The usage of the inertial impactor does, however, cause an inhomogeneous deposition pattern of the particles on the substrate. An area with a diameter of 12 mm is deposited with particles where the particle loading density increases towards the outer rim of this deposition area and only few particles can be found at the center of the substrate (Figure 1).

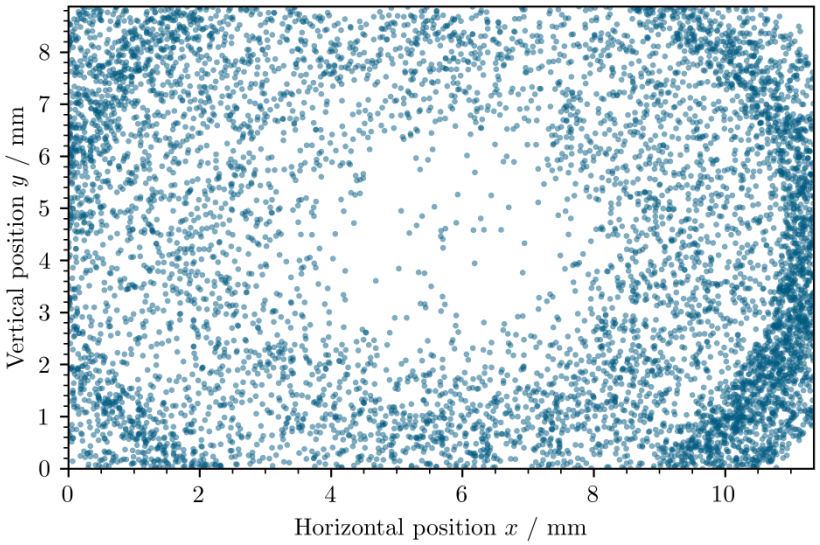

Figure 1: Spatial particle distribution of microparticles collected on a glass-like carbon disk using a single-stage inertial impactor, obtained from low-magnification SEM scans.

The number of particles collected can be controlled in a limited manner by varying the particle collection time; with an increasing collection time, the total number of particles increases. However, due to the intricacies of aerosol transport, the particle concentration of the air flow through the impactors may vary between different production runs and even between collections within a single production run.

3 Particle Suspensions

The previously described problems by using a single-stage inertial impactor can be overcome by using a suspension. When particles are dispersed in a solution, the particles are homogenized and aliquots of this suspension can be distributed for analysis, where each aliquot contains approximately the same number of particles. Such suspensions also increase the maximum number of samples which can be produced during a single batch. During normal operation, the number of samples which can be collected is limited by the liquid feed input reservoir, and lays around 50 samples. Once the reservoir is empty, the system needs to be interrupted to refill the reservoir before continuing. The particles properties between two such runs could therefore be different. Although similar limitations would be present when using suspensions, particles collected during multiple production runs could be homogenized, eliminating the between-sample inhomogeneity.

Particle suspensions could be produced by two methods; either the particles can be collected in a suspension directly or particles are collected using an inertial impactor and are subsequently transferred into a suspension. The former method has proven to be unsuccessful as the air flow

causes evaporation of the solvent during longer operation. Therefore, particles are collected using the single-stage impactors, typically onto silicon wafers due to the high degree of cleanliness and affordability. The silicon wafers can then be placed into a vessel filled with the selected medium and placed in an ultrasonic bath for a few minutes. The ultrasonic bath causes the detachment of particles from the surface into the medium, after which the silicon wafer can be removed.

The selection of the liquid medium has proven to be a critical step towards the production of particle suspensions due to the strong restrictions, as the medium should

1. Be of high purity to prevent significant cross-contaminations,
2. Not cause dissolution of particles within the required processing time,
3. Be suitable to detach the particles from the substrate and,
4. Not cause agglomeration of particles.

Previous investigations [9] have shown that ethanol is most suitable as liquid medium, as water and dimethyl formamide causes dissolution of the particles, n-hexane and n-decane prevent the detachment of particles from the substrate and 2-propanol causes increased agglomeration of particles.

In order to demonstrate the suitability of particle suspensions using ethanol as liquid medium, particles produced during the same run as the particles shown in Figure 1 were transferred into ethanol and were subsequently dried onto a glass-like carbon substrate. The temperature at which the samples were dried proofed to be a critical parameter, as with an increasing temperature agglomeration of particles was observed. The prepared samples were therefore placed in a glass Petri dish onto a heating plate set to 50 °C, the actual temperature at the surface of the substrate is, however, unknown. The prepared substrate was investigated by SEM, the obtained particle distribution is shown in Figure 2. The figure shows a much higher homogeneity compared to Figure 1 and shows the value of homogenizing the particles using a suspension. Although not yet quantified, the homogeneity between samples is also expected to be much higher compared to the direct collection.

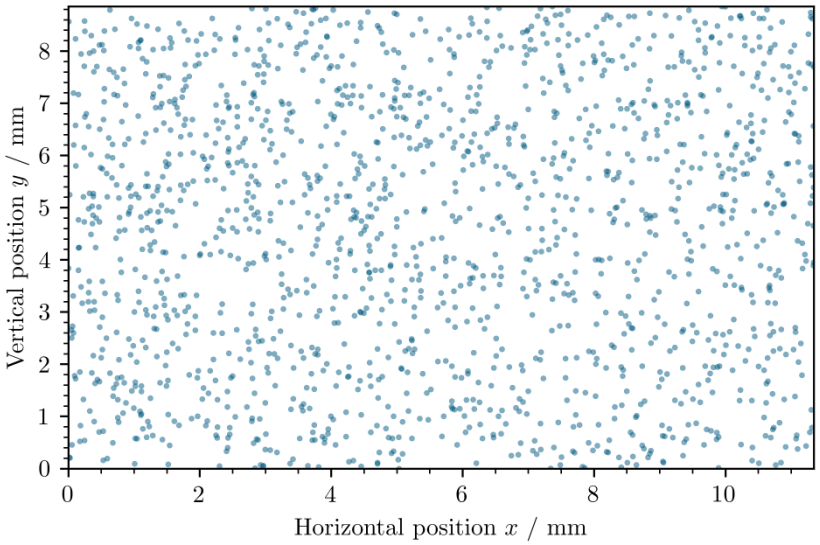

Figure 2: Spatial particle distribution of microparticles deposited on a glass-like carbon disk using an ethanol suspension, obtained from low-magnification SEM micrographs.

The prepared suspension also opens a number of new possibilities, such as the production of mixtures containing various types of particles. In order to demonstrate the possibility to produce particle mixtures, cerium particles were produced, which were subsequently transferred into an ethanol suspension. The cerium particle suspension was mixed with a uranium suspension, where the produced mixture was dried on a silicon wafer. The obtained wafer was then investigated by SEM/EDX where EDX spot measurements were performed on each identified particle to distinguish between uranium and cerium. Figure 3 shows collected EDX spectra of 12 randomly selected particles. The spectra show clear lines for either cerium (between 4.5 and 6 keV) or uranium (between 3.0 and 3.5 keV), no spectra containing both uranium and cerium were found. Of the 533 particles, 21 were identified as uranium particles and 509 were identified as cerium particles.

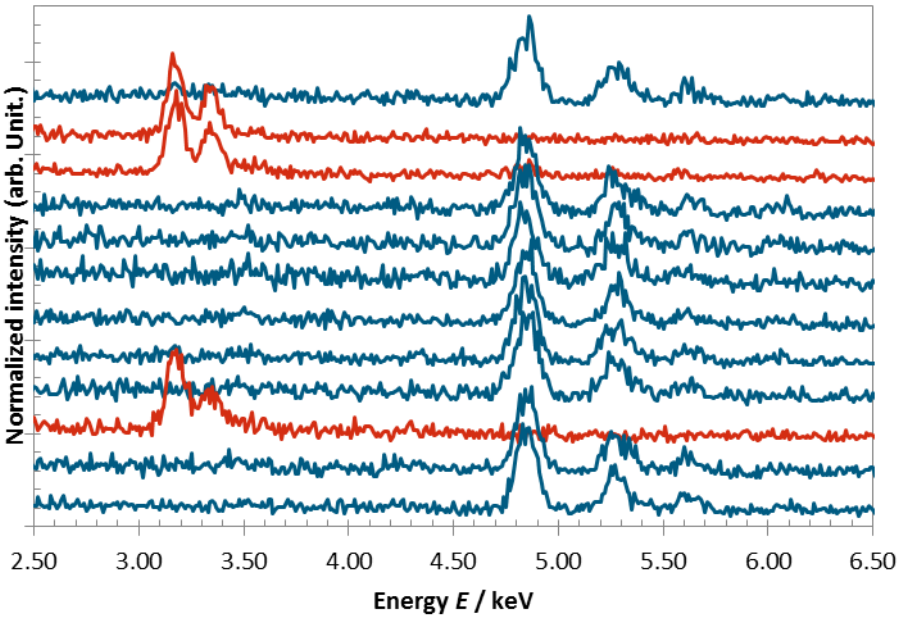

Figure 3: Measured EDX spectra of 12 randomly selected particles in a uranium/cerium mixture.

The prepared suspensions also expand the possibilities to prepare different substrates. When using the inertial impactor, only solid, flat substrates can be used, whereas the suspensions could be distributed over any type of substrate as long as the medium (ethanol) does not interact with the substrate. One such substrate would be cotton swipes, which are normally used to collect particles during inspections. To demonstrate the suitability of particle suspensions to prepare particle samples on such cotton swipes, an aliquot of the uranium/cerium mixture was dried on a small piece of cotton swipe. SEM/EDX analysis was complicated by the degradation of the swipe by the electron beam, even though both uranium and cerium particles could be identified. One of the collected SEM micrographs is shown in Figure 4, in which uranium are marked by a yellow circle and cerium particles with a red circle. The SEM/EDX studies show the possibility to deposit microparticles onto substrates which could not be used with the inertial impactors and open new possibilities for method optimization and quality control measurements in the nuclear safeguards particle analysis.

Figure 4: SEM micrographs of uranium (red) and cerium (yellow) particles transferred onto a cotton swipe from an ethanol particle suspension.

4 Stability of Particles in Suspensions

Although the previous section has shown the suitability of using particle suspensions as processing step and has shown some new possibilities with such suspensions, the suspensions could also have a negative impact on the particle property values. The produced particles are intended to be certified as a certified reference material with both the uranium isotopic composition and the uranium content as property values. Such certification does, however, not only require the property values to be quantified, but also required the determination of the expanded uncertainty, including contributions due to inhomogeneity and instability. During the storage of particles in a suspension, a number of effects could have an influence on the property values and/or the uncertainty of these values. For example, dissolution would decrease the uranium content, and exchange of uranium isotopes between particles and traces of natural uranium in the liquid medium would alter the composition. In order to assess these effects, various studies were undertaken.

The dissolution of particles was studied by storage of particles in an ethanol suspension for 365 days. After storage, an aliquot of the suspension was dried on a silicon wafer which was investigated by SEM. Figure 5 shows a collected micrograph of a particle compared with a micrograph collected of the sample before transfer into the suspension. Although the brightness/contrast differs slightly due to different SEM settings, no alteration of the particle could be observed. In contrast, strong signs of dissolution were observed for particles stored in water for only 16 days [9].

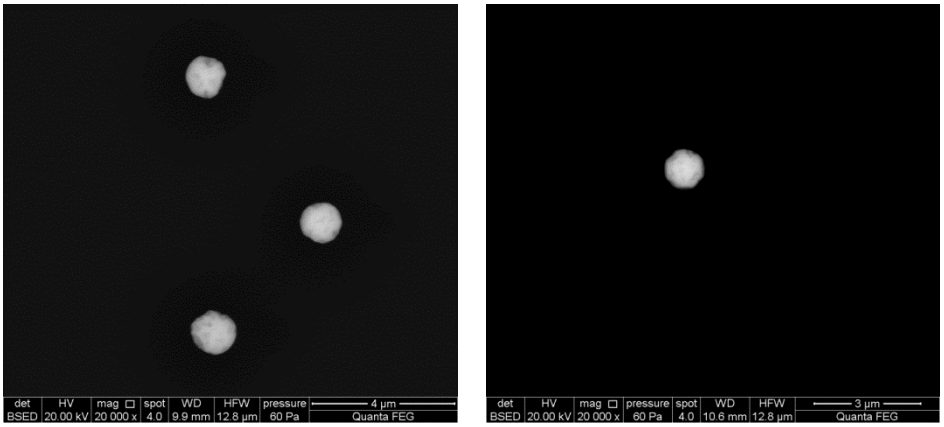

(a) *t* = 0 d **(b) *t* = 365 d**

Figure 5: Microparticles (a) before and (b) after storage in ethanol for 365 days.

A second effect which might be of significance to the produced particle property values is isotope exchange. When a particle suspension is prepared consisting of two or more particle populations with different isotopic compositions, exchange of uranium between particles could alter the isotopic composition of the particles. Although no information on such exchange is currently available, Johnston et al. [10] measured the exchange of oxygen between water and various uranium oxides, including U_3O_8. In order to assess whether such exchange occurs between particles, particles consisting of depleted uranium (DU) and low-enriched uranium (LEU) were produced and subsequently transferred into suspensions. The suspensions were distributed over a number of clean silicon wafers. One wafer containing DU particles and a wafer containing LEU particles were transferred into a vial to which ethanol was added. The sample was stored for a given time, after which both wafers were removed and separately dissolved in HNO_3 for Q-ICP-MS analysis. A schematic overview of the experimental setup is shown in Figure 6.

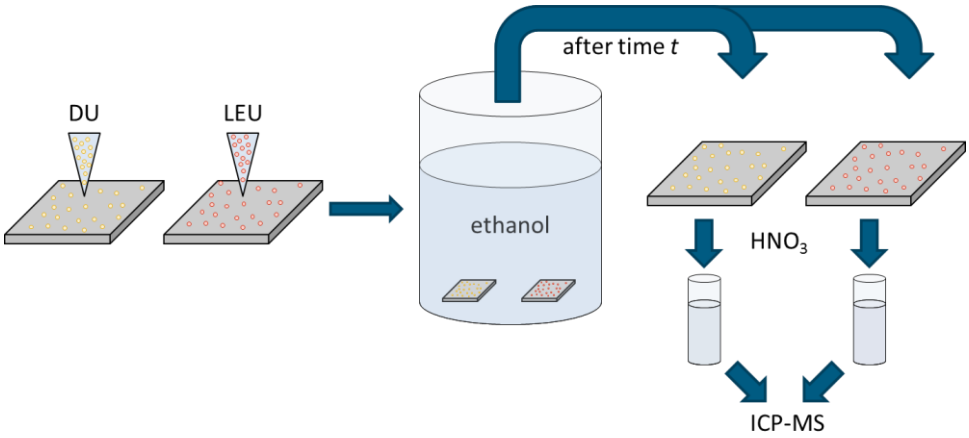

Figure 6: Schematic procedure to investigate the exchange of uranium between particles stored in an ethanol suspension.

The experiment aims to investigate the stability of the isotopic composition of particle mixtures stored in ethanol. Two distinct effects could occur; exchange between particles and traces of NU in the medium or exchange of uranium between particles. Figure 7 shows the measured isotope ratio of both the DU and LEU particles after storage for up to 202 days, although both particles do not show any significant change of the isotopic composition. Therefore, it can be concluded that no exchange occurs within the investigated timeframe.

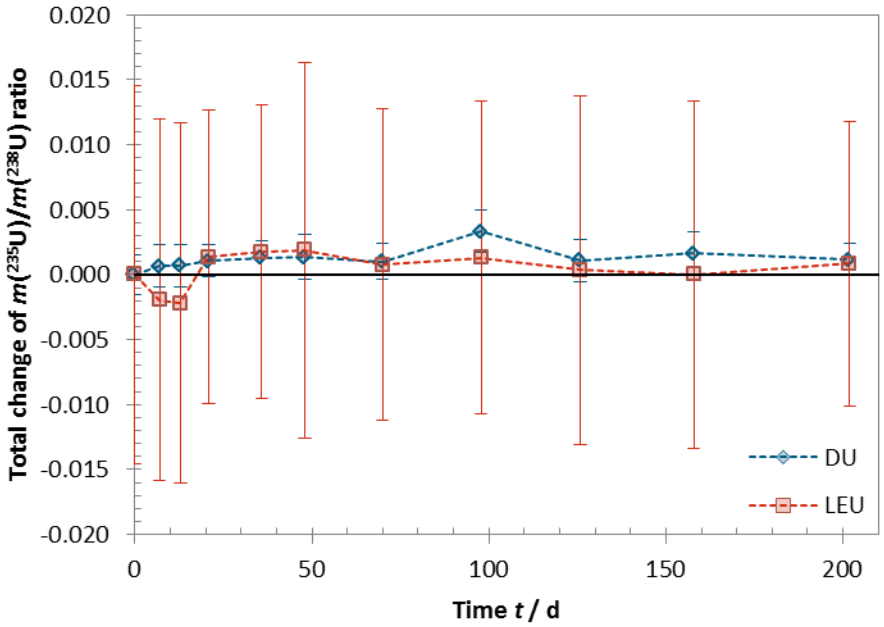

Figure 7: Measured change of the $m(^{235}U)/m(^{238}U)$ isotope ratio after storage in ethanol.

5 Summary and Outlook

This paper proposes a method to transfer produced uranium microparticles into an ethanol suspension, which could then be divided into multiple samples. The proposed method strongly increases the homogeneity of the particle distribution over the substrate. Also, the method reduces the spread of the total number of particles on different samples and allows the preparation of a larger number of samples, either from a single batch or combining multiple production runs. The particle suspensions also open new possibilities towards quality control materials for nuclear safeguards particle analysis. Mixtures of different particles could be prepared, as demonstrated with uranium and cerium particles, although mixtures of particles with different uranium isotopic compositions would also

be feasible. The suspensions also allow for a wider choice of substrates, such as cotton swipes, or a multitude of substrates with a single batch of particles.

In order to verify the stability of particles in ethanol, particles were stored for 365 days in a suspension, during which no alteration of the particle morphology was observed. Also, no exchange of uranium isotopes between different particles was measured after a period of 202 days. These studies show that even over multiple months' storage in suspension, the particles remain unaltered. As the transfer of particles into suspensions, possible mixing of different suspensions and distribution over a large number of substrates can be performed within a few days, particle suspensions offer a wide range of new possibilities to enhance the quality control measurements without affecting the property values.

6 Acknowledgements

We thank F. Sadowski and D. Schneider from Forschungszentrum Jülich for Q-ICP-MS analyses.

This work was supported by the Federal Ministry for Economic Affairs and Energy, Germany, through the German Safeguards Support Programme to the IAEA under task C.45/A1961 and through the Programme "Neu- und Weiterentwicklung von Safeguardstechniken und -methoden" (FKZ 02W6263).

7 References

[1] Boulyga, S., Konegger-Kappel, S., Richter, S., Sangely, L., *Mass spectrometric analysis for nuclear safeguards*, J. Anal. At. Spectrom., **30**, 1469, 2015.

[2] ISO 17025:2005 *General requirements for the competence of testing and calibration laboratories*, 2005.

[3] BIPM, IEC, IFCC, ILAC, ISO, IUPAC, IUPAP, and OIML. *International vocabulary of metrology - Basic and general concepts and associated terms*, volume 3. 2012.

[4] ISO Guide 34:2009 *General requirements for the competence of reference material producers*, 2009.

[5] Knott, A., Dürr, M.*, Production of monodisperse uranium particles for nuclear safeguards applications*. ESARDA Bulletin, **49,** 40, 2013.

[6] Middendorp, R., Knott, A., Dürr, M., *Preparation of Uranium Micro-Particles as Reference Material for Nuclear Safeguards*. ESARDA 37th Annual Meeting Proceedings, 448-497, 2015.

[7] Middendorp, R., Dürr, M., Knott, A., Pointurier, F., Ferreira Sanchez, D., Samson, V., Grolimund, D., *Characterization of the Aerosol-Based Synthesis of Uranium Particles as a Potential Reference Material for Microanalytical Methods*, Analytical Chemistry **89**, 4721, 2017.

[8] Esaka, F., Watanabe, K., Fukuyama, H., Onodera, T., Esaka, K. T., Magara, M., Sakurai, S., Usuda, S., *Efficient Isotope Ratio Analysis of Uranium Particles in Swipe Samples by Total-Reflection X-ray Fluorescence Spectrometry and Secondary Ion Mass Spectrometry*, Journal of Nuclear Science and Technology, **41**, 1027, 2014.

[9] Middendorp, R., Dürr, M., Bosbach, D., *The stability of uranium microspheres for future application as reference standard in analytical measurements*, Procedia Chemistry, **21**, 285, 2016.

[10] Johnston, F., Hutchison, D., Katz, J., *Oxygen exchange between uranium oxides and water*, J. Inorg. Nucl. Chem., 7, 392, 1958.

^{243}Am certified reference material for nuclear safeguards and security

Rožle Jakopič[1], Adelheid Fankhauser[1], Yetunde Aregbe[1], Stephan Richter[1], Marielle Crozet[2], Christophe Maillard[2], Cédric Rivier[2], Danièle Roudil[2], Maria Marouli[1], Faidra Tzika[1], Timotheos Altzitzoglou[1], Stefaan Pommé[1]

[1] European Commission, Joint Research Centre (JRC), Directorate for Nuclear Safety and Security, Retieseweg 111, 2440 Geel, Belgium
[2] French Nuclear and Alternative Energies Commission CEA, Nuclear Energy Division – CEA Marcoule
Research Department of Mining and Fuel Recycling ProCesses (DMRC)
BP 171, 30207 Bagnols-sur-Cèze cedex, France

Abstract:

The Joint Research Centre (EC-JRC, Geel, Belgium) and the Commissariat à l'Energie Atomique et aux Energies Alternatives (CEA/DEN, Marcoule, France) jointly prepared and certified a ^{243}Am spike reference material in compliance with ISO 17034. This reference material is needed for accurate mass spectrometry measurements of ^{241}Am in nuclear forensics, security and safeguards applications but also for the characterisation of radioactive waste. Nearly 600 units of this material were produced, each containing about 3.5 mL of dilute nitric acid solution with an Am mass fraction of 1.5 µg·g^{-1}. The reference material is certified for the ^{243}Am amount content by Isotope Dilution Mass Spectrometry (IDMS) using an in-house ^{241}Am spike, produced by beta-decay from highly enriched ^{241}Pu (99.3 %) material. The americium isotope amount ratios were certified by Thermal Ionisation Mass spectrometry (TIMS). Independent verification measurements were performed by alpha-particle spectrometry, high-resolution gamma-ray spectrometry for activity ratios, and alpha counting for the total massic activity of ^{241,243}Am.

Keywords: Americium; Certified Reference Material; Nuclear Safeguards; Nuclear Forensics; IDMS; TIMS; ISO 17034; ISO Guide 35

1. Introduction

In nuclear safeguards and security, accurate isotopic measurements are required in order to draw correct conclusions. The accuracy, reliability and traceability of such measurements depend heavily on suitable isotopic reference materials. There is a wide range of uranium and plutonium Certified Reference Materials (CRMs) for quality control, method validation and instrument calibration in mass spectrometry. On the contrary, the availability of americium reference materials is limited. Currently, there is no ^{243}Am spike reference material commercially available, although a CRM is indispensable for accurate mass spectrometry measurements of ^{241}Am in nuclear materials. Such material can be used in nuclear forensics to determine the 'model age' of a (seized) plutonium material, i.e. the time elapsed since its last chemical purification [1, 2, 3, 4]. Accurate measurements of elemental americium and isotopic composition are also needed for the management of nuclear waste, where ^{241}Am contributes via its daughter ^{237}Np to the long-lived radioactive waste [5].

The provision of nuclear reference materials is regularly addressed among reference materials providers and users, e.g. in the frame of the Working Group on Techniques and Standards for Destructive Analysis (WGDA) of the European Safeguards and Research Association (ESARDA), the International Atomic Energy Agency (IAEA), and the Nuclear Forensics International Technical

Working Group (ITWG). The need for an americium spike CRM was expressed at the 2014 IAEA Technical Meeting on Reference Materials for Destructive Analysis in the Nuclear Fuel Cycle and at the 2016 Nuclear Security Summit: Certified Reference Material Fact Sheet [6]. In order to fulfil this urgent need, a novel ^{243}Am spike material was jointly produced and certified by the Joint Research Centre of the European Commission (EC-JRC) in Geel (Belgium) and the Commissariat à l'Energie Atomique et aux Energies Alternatives (CEA/DEN) in Marcoule (France). The reference material was produced in compliance with ISO 17034 [7] and characterised for the ^{243}Am, ^{241}Am and total Am amount contents by Isotope Dilution Mass Spectrometry (IDMS) [8] and for the $n(^{241}\text{Am})/n(^{243}\text{Am})$ and $n(^{242m}\text{Am})/n(^{243}\text{Am})$ amount ratios by Thermal Ionisation Mass Spectrometry (TIMS). Furthermore, confirmation measurements of the certified values were performed by independent alpha-particle and gamma-ray spectrometry, as well as alpha-particle counting at a defined solid angle (DSA). Prior to release of this CRM, an inter-laboratory comparison (ILC) exercise using that same material has been organised by CEA/CETAMA.

The preparation and the characterisation of this ^{243}Am spike CRM will be presented in this paper. As the ILC exercise is still on-going, the certified values cannot be disclosed at this time. Therefore only the normalised results will be presented.

2. Preparation of the ^{243}Am reference material

Four mg of americium source material (88 % ^{243}Am and 12 % ^{241}Am) was made available by the CEA/L2AT (ATalante Analysis Laboratory). The solution was purified by TRU-Spec resin (Triskem International, Bruz, France) to remove the impurities and shipped to JRC-Geel for processing. The purified americium solution was diluted with 2400 mL nitric acid solution ($[HNO_3]$ = 1 M) to achieve an Am mass fraction of 1.5 $\mu g \cdot g^{-1}$. This Am concentration was considered suitable for various mass spectrometry measurements (e.g. TIMS, ICP-MS). The solution was allowed enough time to homogenise before being dispensed into pre-cleaned screw-cap ampoules. In total, 587 units were prepared, each unit containing approximately 5 μg of americium in nitric acid solution. Dilution of the original material and dispensing into ampoules were carried out in a dedicated glove box. The ampoules were packed in PVC bags and labelled. The major processing steps are depicted in Figure 1.

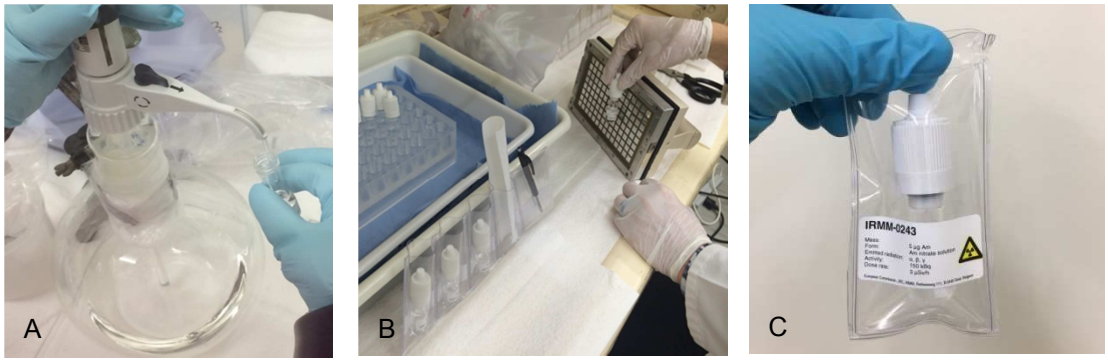

Figure 1: Preparation of ^{243}Am reference material: dilution and dispensing (A), packing and labelling (B and C)

3. Certification methodology

The ^{243}Am amount content was measured by Isotope Dilution Mass Spectrometry (IDMS). In IDMS, the amount of an element in the sample is determined on the basis of additions of known amounts of spike material of the same element, but with a significantly different isotopic composition from that of the unknown sample. By measuring the change in isotopic composition of the blend (sample-spike mixture), the unknown amount of the element in the sample can be determined [8].

The amount content of ^{243}Am (c_{243Am}) can be calculated using the following equation:

$$c_{243_{Am}} = \frac{R_y - R_b}{R_b - R_x} \cdot R_x \cdot \frac{m_y}{m_x} \cdot c_{241_{Am}}$$

Equation 1

where c_{241Am} is the ^{241}Am amount content (mol·g^{-1}) of the spike; m_x and m_y are the mass (g) of the sample and the spike, respectively; R_i is the isotope amount ratio $n(^{243}Am)/n(^{241}Am)$ in which index *i* takes the values x, y and b to represent the un-spiked sample, the spike and the blend, respectively.

The $n(^{241}Am)/n(^{243}Am)$ and $n(^{242m}Am)/n(^{243}Am)$ amount ratios were determined by Thermal Ionisation Mass Spectrometry (TIMS). The material was certified in compliance with ISO 17034 [7] and ISO Guide 35 [9]. Homogeneity assessment and characterisation (value assignment) measurements were combined and carried out on 18 randomly selected units representing the whole batch.

3.1 ^{241}Am in-house spike

In absence of a suitable ^{241}Am spike material for IDMS measurements of the ^{243}Am, an alternative approach was applied. The ^{241}Am spike material was produced from highly enriched ^{241}Pu (99.3 %) material available at JRC-Geel. The ingrown ^{241}Am, produced by the beta-decay of ^{241}Pu since the initial purification of the ^{241}Pu material, was used as spike for the measurement of the ^{243}Am by IDMS.

About 2 mg of ^{241}Pu material was purified to remove the daughter decay products growing in since the production of this material in 1991. This was accomplished by anion exchange separation (Biorad AG 1-X4 resin, 100-200 mesh) [10]. The purification procedure was performed three times; the final purification was carried out on 10 June 2014 at 15:10 CET (Central European Time), which marked the start of the Am in-growth (time zero). The completeness of the purification was confirmed by high resolution gamma-ray spectrometry. The purified plutonium material was diluted with 100 mL nitric acid solution ($[HNO_3]$ = 1 M) and characterised for the ^{241}Pu amount content and its isotopic composition by IDMS using a ^{242}Pu spike CRM (IRMM-049d) and by Triton TIMS, respectively.

The ingrown amount of the ^{241}Am in ^{241}Pu is calculated using the following equation:

$$c_{241_{Am}} = c^{o}_{241_{Pu}} \left[\frac{\lambda_{241_{Pu}}}{\lambda_{241_{Am}} - \lambda_{241_{Pu}}} \left(e^{-\lambda_{241_{Pu}} t} - e^{-\lambda_{241_{Am}} t} \right) \right]$$

Equation 2

where c^{0}_{241Pu} is the amount content (mol·g^{-1}) of ^{241}Pu in the spike solution at time zero, *t* (a) is the ingrowth time of ^{241}Am (time elapsed since time zero) and λ_{241Am} and λ_{241Pu} are the decay constants (a^{-1}) for ^{241}Am and ^{241}Pu, respectively. The half-lives and associated uncertainties used in the calculations were (14.325 ± 0.012) a (*k* = 1) [11] for ^{241}Pu and (432.6 ± 0.6) a (*k* = 1) [12] for ^{241}Am.

3.2 Spiking and chemical treatment

Spiking, chemical treatment and subsequent measurements were carried out about one and a half year after the purification of the ^{241}Pu material. During this period a sufficient amount of ^{241}Am had been produced for IDMS analysis. From each of the 18 selected units, an aliquot was taken for determination of the ^{243}Am content by IDMS and another aliquot for the determination of the isotopic composition by TIMS. The chemical treatment and subsequent measurements were spread over a period of 7 months. This approach was used in order to have different amounts of ingrown ^{241}Am in the blends for IDMS and to be able to assess the stability of the ^{243}Am solution during the certification campaign. Prior to the measurements, two purification steps were carried out to remove the ^{241}Pu from the in-grown ^{241}Am in the spike solution by means of UTEVA-spec (Triskem International, Bruz, France) and DGA extraction resins (Triskem International, Bruz, France), respectively [13, 14]. The chemical procedure is shown in Figure 2.

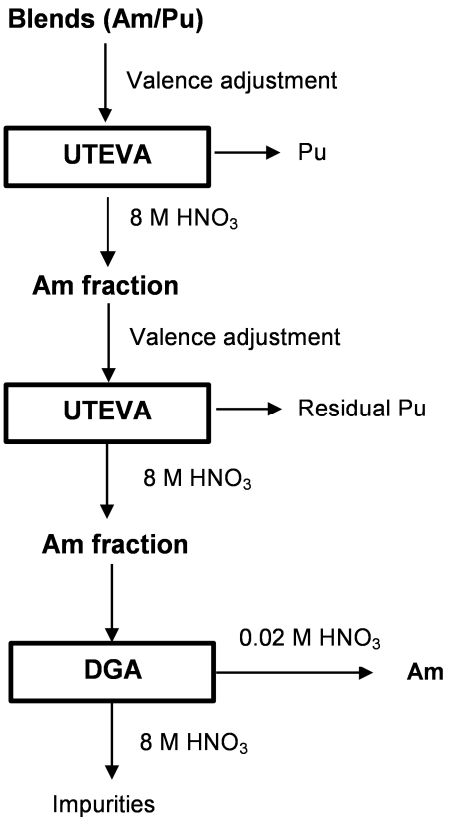

Figure 2: Purification of Am prior to isotope ratio measurement.

3.3 Isotope ratio measurement

Isotope ratio measurements were carried out using the total evaporation method on a multi-collector Triton Thermal Ionisation Mass Spectrometer (Thermo Fisher Scientific, Bremen, Germany), in a similar manner as routinely performed for uranium and plutonium samples of similar size. In the total evaporation method, the evaporation filament is heated up to maintain a steady intensity and measured until the whole sample is consumed. In this way, the fractionation effects in the ion source are minimized [15, 16, 17, 18, 19]. Degassed zone refined rhenium filaments (Thermo Fisher Scientific, Bremen, Germany) were used as ionization and evaporation filaments (double filament configuration). About 20 ng of americium as nitrate solution was deposited on an evaporation filament, dried down and mounted on a sample turret. All ion currents were measured simultaneously on Faraday cups.

For U and Pu a mass fractionation correction using measurements of a CRM on the same magazine is recommended following ASTM C1672-17 [20], but not mandatory. According to ASTM C1672-17, the relative bias for uncorrected $n(^{235}U)/n(^{238}U)$ and $n(^{242}Pu)/n(^{239}Pu)$ ratios is less than 0.05 % within 2 standard deviations (2σ) for ratios spanning 3 mass units. In the absence of a suitable Am isotopic standard, it was not possible to perform a mass fractionation correction for this project. Due to similarities in the chemical behaviour and similar ionization energies, it can be assumed that americium behaves similar to uranium or plutonium during the total evaporation measurement and that the bias statements for uranium and plutonium can equally be applied for americium. For the $n(^{243}Am)/n(^{241}Am)$ ratio the uncertainty component was calculated as 0.033 % (2 σ, for ratios spanning 2 mass units) and for the $n(^{242m}Am)/n(^{243}Am)$ ratio to 0.017 % (2 σ, for ratios spanning 1 mass unit).

3.4 Verification measurements

Independent verification measurements for the ^{243}Am and ^{241}Am amount contents and for the $n(^{241}Am)/n(^{243}Am)$ amount ratios were performed using radioactivity measurement methods.

High-resolution alpha particle spectrometry [21, 22, 23] was used to determine the $A(^{243}Am)/A(^{241}Am)$ activity ratio. The alpha source was prepared from the Am CRM solution by electrodeposition on a polished stainless disk with an active diameter of 18.6 mm and measured using a passivated ion-implanted planar silicon detector (PIPS®, 150 mm^2 active area, Mirion Technologies (MGPI) SA, France). The total Am activity per unit mass was determined by means of alpha-particle counting at a defined solid angle (DSA) [21, 24]. Gravimetrically quantified drops of americium solution were deposited on 34 mm glass plates and covered with 20 $\mu g \cdot cm^{-2}$ VYNS foils (polyvinylchloride-polyvinylacetate copolymer) to prevent material loss.

Two independent gamma-ray measurement campaigns were carried out, one in the underground laboratory 'HADES' [25] and one above ground in the radionuclide metrology laboratory at JRC-Geel. Point-like sources for gamma measurements were prepared gravimetrically by drop deposition on laminated plastic foils with a diameter of 34 mm. They were measured above ground using two coaxial HPGe gamma-ray spectrometers one of 35 % and the other of 90 % relative efficiency (Mirion Technologies (MGPI) SA, France). One gamma source was selected for ultra-low-level gamma-ray spectrometry measurements (ULGS) in HADES using the Ge-8 detector. The Ge-8 is a HPGe detector of type Broad Energy Germanium Detector (BEGe) with a relative efficiency of 20 % (Canberra). The activities of ^{241}Am and ^{243}Am were calculated based on the main gamma-ray peaks of the nuclides, i.e. the 59.54 keV line for ^{241}Am and the 74.66 keV line for ^{243}Am, respectively [26, 27, 28].

4. Results and discussion

4.1 Results of the characterisation of ^{241}Pu spike solution

The results of the characterisation of the purified ^{241}Pu solution are summarised in Table 1.

		Value	Uncertainty (k = 2)
Amount content	^{241}Pu [$mol \cdot g^{-1}$]	$8.1394 \cdot 10^{-8}$	$0.0053 \cdot 10^{-8}$
Isotope amount fractions	$n(^{238}Pu)/n(Pu) \cdot 100$	0.00097	0.00034
	$n(^{239}Pu)/n(Pu) \cdot 100$	0.00053	0.00018
	$n(^{240}Pu)/n(Pu) \cdot 100$	0.25741	0.00029
	$n(^{241}Pu)/n(Pu) \cdot 100$	99.29993	0.00052
	$n(^{242}Pu)/n(Pu) \cdot 100$	0.44116	0.00025

Table 1: Results of the characterisation of the purified ^{241}Pu solution

The values of the plutonium isotope amount fractions were found to be in agreement with the values from the certificate of the ^{241}Pu material from 1991. The value for the ^{241}Pu amount content was calculated from the mean of the 10 blends measured by IDMS. Each blend was measured in replicates on the Triton TIMS using the total evaporation method. The mass fractionation correction was based on the measurement of the IRMM-290/A3 Pu isotopic standard. The results of the IDMS measurements of the ^{241}Pu amount in the spike solution are shown in Figure 3.

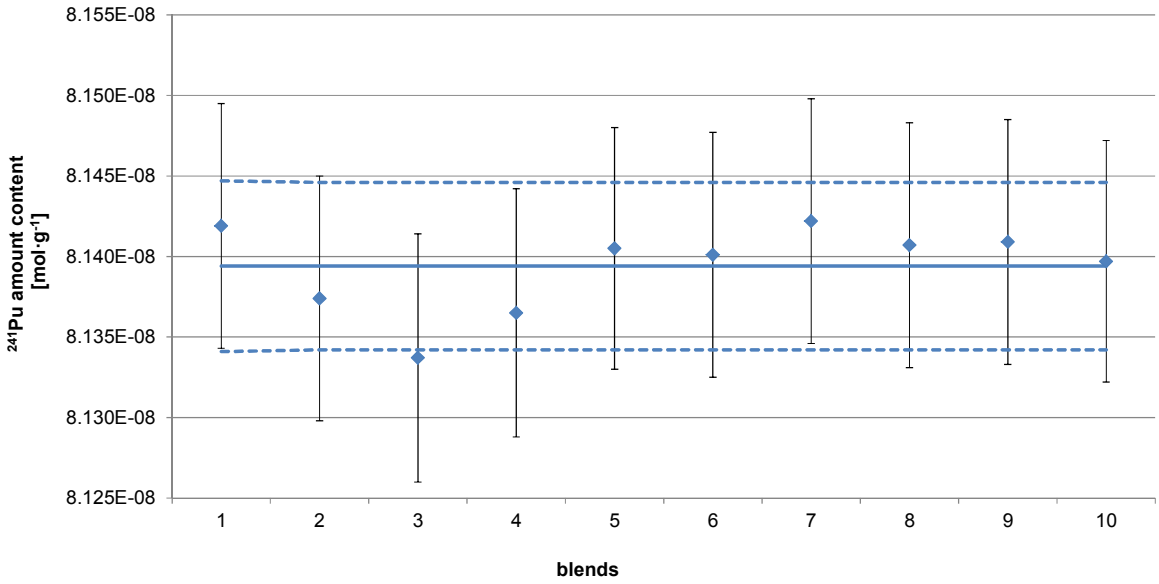

Figure 3: ^{241}Pu amount content in the purified ^{241}Pu solution established by IDMS of 10 blend solutions. The solid line represents the mean of the ten values, the dotted lines represent the expanded uncertainty (coverage factor, k = 2) of the mean.

4.2 Results of the verification measurements

Due to the on-going ILC exercise, only the normalised certified values are presented in this paper. The results of the verification measurements obtained by gamma-ray and alpha-particle spectrometry are shown in Figure 4. They are in agreement with the certified values within measurement uncertainty. Measurement uncertainties were estimated according to GUM [29] and mean values calculated by means of the power-moderated mean formalism [30].

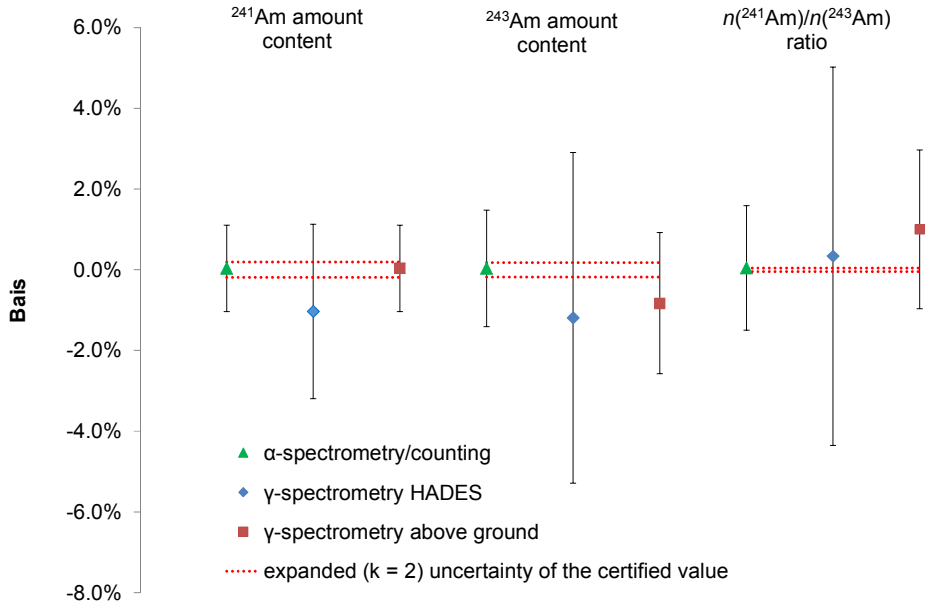

Figure 4: Results of the independent alpha-particle (triangles) and gamma-ray (diamonds and squares) measurements for the ^{241}Am and ^{243}Am amount contents and $n(^{241}\text{Am})/n(^{243}\text{Am})$ amount ratios expressed as relative differences from the certified value. All the measurement results are

shown with a relative expanded uncertainty (k = 2). Red dotted lines show the relative expanded uncertainty (k = 2) of the respective certified value.

The relative expanded uncertainty (k = 2) for the ^{243}Am amount content from the characterisation assessment was 0.20 %. The major sources of uncertainty come from the half-life of ^{241}Pu, the time of the ^{241}Am ingrowth and the amount content of the ^{241}Pu solution. The relative expanded uncertainties (k = 2) of the $n(^{241}\text{Am})/n(^{243}\text{Am})$ and $n(^{242m}\text{Am})/n(^{243}\text{Am})$ isotope ratios are 0.04 % and 1.0 % respectively.

5. Results and discussion

A novel ^{243}Am spike RM was prepared and certified for the amount content and isotope amount ratios. The material was produced in compliance with international guidelines. Certified values for the amount content and isotope amount ratios were established by IDMS and TIMS and confirmed by independent radioactivity measurements. The uncertainties associated with the certified values are fit for the purpose for this reference material. This material is available in dilute nitric acid solution with an americium mass fraction of about 1.5 ppm.

6. Acknowledgements

The authors would like to thank Carmel Hennessy, Frances Kehoe and Saskia Werelds from the JRC-Geel for support in the preparation of the reference material and Monika Sturm from the IAEA for support in separation chemistry and Am mass spectrometry. The authors would also like to thank the Laboratory for target preparation at JRC-Geel, which kindly provided the ^{241}Pu material.

7. Legal matters

7.1 Privacy regulation

I agree that ESARDA may print my name/contact data/photograph/article in the ESARDA Bulletin/Symposium proceedings or any other ESARDA publications and when necessary for any other purposes connected with ESARDA activities.

7.2 Copyright

The author agrees that submission of an article automatically authorises ESARDA to publish the work/article in whole or in part in all ESARDA publications – the bulletin, meeting proceedings, and on the website.

The author declares that their work/article is original and not a violation or infringement of any existing copyright.

8. References

[1] Wallenius M, Peerani P, Koch L, *Origin determination of plutonium material in nuclear forensics:* Journal of Radioanalytical and Nuclear Chemistry, 246, 2000, 317-321

[2] Nygen U, Rameback H, Nilsson C, *Age determination of plutonium using inductively coupled plasma mass spectrometry*: Journal of Radioanalytical and Nuclear Chemistry, 272, 2007, 345-510

[3] Wallenius M, Mayer K, *Age determination of plutonium material in nuclear forensics by thermal ionisation mass spectrometry:* Frasenius Journal of Analytical Chemistry, 366, 2000, 234-238

[4] Keegan RP, Gehrke RJ, *A method to determine the time since last purification of weapons grade plutonium:* Applied Radiation and Isotopes, 59, 2003, 137-143

[5] Chartier F, Aubert M, Pilier M, *Determination of Am and Cm in spent nuclear fuels by isotope dilution inductively coupled plasma mass spectrometry and isotope dilution thermal ionization mass spectrometry after separation by high-performance liquid chromatography*: Frasenius Journal of Analytical Chemistry, 364, 1999, 320-327

[6] 2016 Nuclear Security Summit: Certified Reference Material Fact Sheet: http://www.belfercenter.org/sites/default/files/legacy/files/nuclearmatters/files/2016_nss_certified_reference_material_factsheet.pdf?m=1461101302

[7] ISO 17034:2016: *General requirements for the competence of reference material producers:* International Organisation for Standardisation, Geneva, 2016

[8] Vogl J, *Characterisation of reference materials by isotope dilution mass spectrometry*: Journal of Analytical Atomic Spectroscopy, 22, 2007, 475-492

[9] ISO Guide35: *Reference materials – general and statistical principles for certification:* International Organisation for Standardisation, Geneva, 2006

[10] Jakopič R, Verbruggen A, Eykens R, Kehoe F, Kuhn H, Kushigeta J, Jacobsson U, Bauwens J, Richter S, Wellum R, Aregbe Y, *An inter-calibration campaign using various selected Pu spike isotopic reference materials*: Journal of Radioanalytical and Nuclear Chemistry, 286, 2010, 449-454

[11] Wellum R, Verbruggen A, Kessel R, *A new evaluation of the half-life of ^{241}Pu*: Journal of Analytical Atomic Spectroscopy, 24, 2009, 801-807

[12] Martin MJ, *Nuclear data sheets for A=241*: Nuclear Data Sheets, 106, 2005, 89-1558

[13] Vajda N, Kim CK, *Determination of ^{241}Am isotope: a review of analytical methodology*: Journal of Radioanalytical and Nuclear Chemistry, 284, 2010, 341-366

[14] Kazi ZH, Cornett JR, Zhao X, Kieser L, *Americium and plutonium separation by extraction chromatography for determination by accelerator mass spectrometry*: Analytical Chimica Acta, 829, 2014, 75-80

[15] Callis EL, Abernathey RM, *High precision isotopic analysis of uranium and plutonium by total sample volatilization and signal integration*: International Journal of Mass Spectrometry and Ion Process, 103, 1991, 322-327

[4] Richter S, Goldberg SA, *Improved techniques for high accuracy isotope ratio measurement of nuclear materials using thermal ionisation mass spectrometry:* International Journal of Mass Spectrometry, 229, 2003, 181-197

[17] Bürger S, Balsley SD, Baumann SD, Boulyga SF, Cunningham JA, Kappel S, Kopft A, Poths J, *Uranium and Plutonium analysis of nuclear material samples by multi-collector thermal ionisation mass spectrometry: quality control, measurement uncertainty, and metrological traceability:* International Journal of Mass Spectrometry, 311, 2012, 40-50

[18] Boulyga S, Konnegger-Kappel S, Richter S, Sangley L, *Mass spectrometry analysis for nuclear safeguards*: Journal of Analytical Atomic Spectroscopy, 30, 2015, 1469-1489, 2015

[19] Standard Test Method for Determination of Uranium or Plutonium Isotopic Composition or Concentration by the Total Evaporation Method Using a Thermal Ionization Mass Spectrometer, C1672-17, ASTM International

[20] Standard test Method for determination of uranium or plutonium isotopic composition or concentration by the total evaporation Method using a thermal ionization mass spectrometer, C1672-17, ASTM International

[21] Pommé S, Sibbens G, *Alpha-particle counting and Spectrometry in a primary Standardisation laboratory*: Acta Chimica Slovenica, 52, 2008, 111-119

[22] Pommé S, Marroyo BC, *Improved peak shape fitting in alpha spectra:* Applied Radiation and Isotopes, 96, 2015, 148-153

[23] Pommé S, *Typical uncertainties in alpha-particle spectrometry:* Metrologia, 52, 2015, S146-S155

[24] Pommé S, *The uncertainty of counting at a defined solid angle:* Metrologia, 52, 2015, S73-S85

[25] https://ec.europa.eu/jrc/en/research-facility/hades-underground-laboratory

[26] Hult M, Preusse W, Gasparro J, Kohler M, *Underground gamma-ray Spectrometry*: Acta Chimica Slovenica, 53, 2006, 1-7

[27] M. Hult, Low-level gamma-ray spectrometry using Ge-detectors, Metrologia, 44/4, S87-S94, Erratum at Metrologia 44/5, 425, 2007

[28] Kawrakow I, Rogers DWO, *PIRS-701: The EGSnrc Code System: Monte Carlo simulation of Electron and Photon Transport* : Ionizing Radiation Standards (NRC, Otawa, Ontario), 2003

[29] ISO/IEC 98-3: *Guide to the expression of uncertainty in Measurement (GUM 1995)*, International Organisation for Standardisation, Geneva, 2016

[30] Pomme S, Keightley J, *Determination of a reference value and its uncertainty through a power-moderated mean:* Metrologia, 52, 2015, S200-S212

Automated Clean Chemistry for Bulk Analysis of Environmental Samples for Safeguards

Brian W. Ticknor[1], Shalina C. Bottorff[1], Kayron N. Tevepaugh[1], Eddy H. McBay[1], Debra A. Bostick[1], Cole R. Hexel[1], Hwan Kim[2], Paul Field[2]

[1]Chemical Sciences Division, Oak Ridge National Laboratory, Oak Ridge, TN, United States
[2]Elemental Scientific Inc., Omaha, NE, United States

Abstract:

Sample preparation methods for mass spectrometry are being automated using commercial-off-the-shelf (COTS) equipment to shorten lengthy and costly manual chemical purification procedures. This addresses a serious need in the International Atomic Energy Agency's Network of Analytical Laboratories (IAEA NWAL) to increase efficiency in the Bulk Analysis of Environmental Samples for Safeguards program with a method that allows unattended, overnight operation. In collaboration with Elemental Scientific Inc., the prepFAST-MC2 was designed based on COTS equipment. It was modified for U/Pu separations utilizing renewable columns packed with Eichrom™ TEVA and UTEVA resins, with a chemical separation method based on the Oak Ridge National Laboratory (ORNL) NWAL chemical procedure. The original preFAST-MC2 system is currently installed in the Ultra-Trace Forensics Science Center at ORNL.

Initial verification experiments yielded small elution volumes, consistent elution profiles, ample separation, and good recovery without cross-contamination of the eluent. Separation of mixed U and Pu samples containing certified reference materials were analyzed by multi-collector inductively coupled plasma mass spectrometry (MCICPMS), and the isotope ratio results were well within data quality limits for the IAEA NWAL. The low blank levels allow the option of performing the chemical separations without the necessity of cleanroom infrastructure. Comparison of the amount of personnel time necessary for successful manual vs. automated chemical separations showed a significant decrease in hands-on time from 9.8 h to 35 min for 7 samples, respectively. Overall, the system will enable faster sample reporting times with reduced costs by limiting personnel hours dedicated to the chemical separation, and will ensure continued efficient and effective operation of the NWAL.

Keywords: automation, destructive assay, environmental sampling, safeguards

1. Introduction

Environmental swipes are one type of sample that the International Atomic Energy Agency (IAEA) may collect during inspections of facilities under safeguards to verify compliance with declared nuclear activities [1]. Bulk analysis is a particular form of destructive analysis that is performed on an entire swipe sample. It utilizes high precision mass spectrometry on purified samples to measure isotopic composition and concentration of actinide elements, particularly U and Pu that were collected on the swipe. Bulk analysis produces very accurate and precise data, but the chemical separations required to produce the purified samples are labor intensive and require significant laboratory infrastructure. The IAEA depends heavily on its Network of Analytical Laboratories (NWAL) to support the Bulk Analysis of Environmental Samples for Safeguards program. Timeliness and efficient sample processing are important for the NWAL laboratories. Typical characteristics of collected field samples are 1 ng to 10 mg U/swipe and <1 ng Pu/swipe. The Measurement Quality Goals set forth by the IAEA for the bulk analysis program are a ≤ 2% relative expanded uncertainty for $^{235}U/^{238}U$ and ≤ 20% for $^{234}U/^{238}U$ and $^{236}U/^{238}U$ at >10ng U and ≤ 20% for all Pu isotope ratios at >1pg at a 95% confidence level [2]. Multi-collector inductively coupled plasma mass spectrometry (MCICPMS) or multi-collector thermal ionization mass spectrometry (MCTIMS) are often employed for this analysis. However, these high precision instruments require highly purified actinide fractions, free from interferences such as

organics and heavy metals, to ensure the quality of the measurements. Current purification protocols include ashing samples individually in furnaces (or occasionally chemical leaching with acid), and then manually loading gravity-driven separation columns – a process that is both costly and time consuming. From start to finish, the manual purification chemistry takes between two and four weeks, and represents the longest single step in the analysis process for bulk environmental samples. The separation procedures are also typically carried out in certified International Standards Organization (ISO) cleanroom laboratories with heavily filtered air and high purity reagents to limit the contribution of background contamination to the measurement of nanograms or picograms of material that may be present in environmental samples. The installation and maintenance of cleanroom facilities represents a significant upfront financial investment and ongoing maintenance commitments that some laboratories may be unable to sustain.

Streamlining NWAL sample preparation methods for subsequent analysis by mass spectrometry using fully automated, commercial-off-the-shelf (COTS) equipment would address a serious need in the safeguards community by shortening lengthy and costly manual chemical digestion and purification procedures. Automating digestion and chemical separation, while still producing highly purified sample fraction, will offer significant time and cost savings to the IAEA without sacrificing data quality. Additional benefits may include lower and more consistent blank levels for U and Pu and the ability to achieve cleanroom level blanks without the infrastructure needs of ISO cleanrooms. Finally, the use of COTS equipment will allow an automated method to be quickly and economically transferred to and implemented by any NWAL laboratory (or prospective NWAL member), helping the IAEA globally execute standard operating procedures for isotopic purification while addressing the ongoing challenge of increasing efficiency and preventing sample backlogs.

These goals directly address high-priority Milestones 10.2 and 10.3 in the IAEA Long-Term R&D Plan (STR-375) [3] by developing new technologies and techniques that will improve the NWAL's ability to provide analytical services to IAEA. By supporting STR-375, this work also addresses the short-term needs described in the *Development and Implementation Support Programme for Nuclear Verification 2016–2017* (STR-382) [4]. Specifically, transfer of automated COTS technology to NWAL member laboratories supports SGAS-003, Analysis Support and NWAL Coordination, and especially the top priority to "Ensure efficient and effective operation of the NWAL" [4].

To this end, Oak Ridge National Laboratory (ORNL) has worked with Elemental Scientific Inc. (ESI) to customize their COTS sample preparation platform prep*FAST*-MC [5]. The prototype, dubbed prep*FAST*-MC2, has been installed at ORNL and closely mirrors the manual ORNL NWAL chemistry, but uses automation to perform chemical separations in unattended, overnight operation. The initial work has been described in more detail previously, [6], with those results summarized here and new data added where available. Specifically, ORNL has documented significant labor savings through use of this equipment without any associated impact to final data quality. As hoped, the blank levels achieved with the system point to the potential to operate as a portable cleanroom in laboratories lacking that infrastructure. Finally, ORNL is evaluating additional COTS technologies to enable efficiencies in other parts of the chemical processing of environmental swipe samples, which are also briefly described here.

2. Experimental

The prep*FAST*-MC2 prototype from ESI, installed in the Ultra-Trace Forensic Science Center at ORNL, is pictured in Figure 1 below. The heart of the system is a proprietary assembly of switching valves and syringe pumps that can perform precise and accurate column chemistry. The entire sample flow path is closed and is constructed from fluoropolymers, both of which serve to minimize the actinide blank levels from the system and ensure samples are handled as cleanly as possible. The system duplicates the ORNL NWAL procedure, which utilizes single-use prepacked Eichrom TEVA and UTEVA chromatographic resins to separate Pu and U, respectively, from the rest of the sample matrix. To automate this procedure, the prep*FAST*-MC2 is designed to use bulk TEVA and UTEVA resin that is packed and unpacked into two fluoropolymer columns (C1 - TEVA and C2 - UTEVA in expanded picture in Fig. 1). Packing and unpacking both columns before and after every separation ensures that each sample is exposed only to fresh, cleaned resin, and eliminates quality assurance concerns about the reuse of resin on environmental level samples.

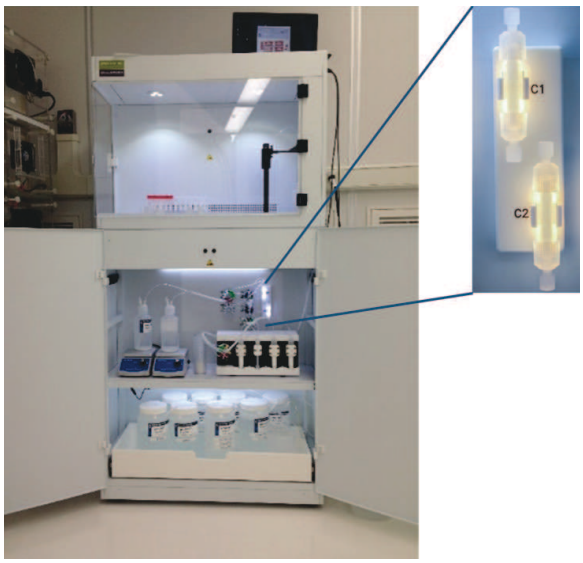

Figure 1. Installed prep*FAST*-MC2 at ORNL with TEVA (C1) and UTEVA (C2) columns in expanded picture.

The prep*FAST*-MC2 is housed in a plastic and powered coated metal frame, which makes it suitable for installation in a cleanroom (although a cleanroom is not required). The laboratory infrastructure requirements are minimal and are listed below.

- Space: 826 mm L × 430 mm W × 1625 mm H (from the floor)
- Power outlet within 3 m of instrument (120V/60Hz)
- Chemical exhaust with 69 mm ID to fit the back panel and a flow rate of 40 cubic feet per minute
- 5 bar of gas pressure (Ar or N_2)

Ultrapure reagents, including acids and American Society for Testing and Materials (ASTM) Type I (18.2 MΩ) water are recommended and were used in all studies at ORNL. The specifications for the resin used is listed below.

- UTEVA Resin: Eichrom; 50–100 µm; Part No. UT-B100-S
- TEVA Resin: Eichrom; 50–100 µm; Part No. TE-B100-S

Certified reference materials (CRMs), with known isotopic values, were used for the uranium and plutonium separation experiments. Specifically, New Brunswick Laboratory NBL-137 was used as the plutonium source and the Institute for Reference Materials and Measurements (now the Joint Research Center of the European Commission) IRMM-183 was used as the uranium source. Additionally, IRMM-57 (^{233}U) and an in house ORNL standard RAL-22 (^{244}Pu) were used as isotope dilution spikes to determine system blank levels and sample recoveries.

All mass spectrometric data presented here was collected on either a high-resolution inductively coupled plasma mass spectrometer (HRICPMS) or an MCICPMS. A ThermoScientific Element II (Bremen, Germany) was the HRICPMS used during the column calibration step to quickly scan column elution fractions for both U and Pu to verify separation and approximate recovery. It was also used for experiments evaluating the capacity of the automated system to remove contaminating elements such as Pb and Th, which might interfere with U and Pu measurements. A ThermoScientific Neptune *Plus* (Bremen, Germany) was used for all MCICPMS measurements. This instrument is typically utilized by ORNL for NWAL analysis of both U and Pu isotope ratios, and was used here to characterize the mixed CRM aliquots of U and Pu that were separated on the prep*FAST*-MC2.

3. Results and Discussion

3.1. Reproducibility of Resin Packing and Unpacking

The reproducibility of the prep*FAST*-MC2 in packing and unpacking resin into the columns for each separation proved a critical parameter in determining the reproducibility of the system to preform U and Pu separations. To quantify this, after a packing and unpacking run, the unpacked resin was collected, filtered, dried, and weighed. Repeated experiments gave a measurement of the reproducibility of the system within one day and over the course of three consecutive days. After optimization of the method, the daily average for the packing of the TEVA resin in column C1 was 0.556 ± 0.030 g and 0.601 ± 0.019 g for the UTEVA resin in column C2. This corresponds to daily variations of approximately 3 - 5%, which meets or exceeds the specifications that Eichrom quotes for its pre-packaged columns. The variation from one day to the next was slightly higher, on the order of 6 - 8%, but the performance of the system was still demonstrated to be suitable for highly reproducible actinide separations.

3.2. prep*FAST*-MC2 Column Calibration

The initial column calibration experiments were conducted using 5 ng of IRMM-183 and 2 pg of NBL-137, with the goal of verifying the elution profiles of the U and Pu respectively off the columns. The prep*FAST*-MC2 was run in a mode where the entire elution profile was collected in 1 mL fractions. These were then analyzed by HRICPMS to determine both the separation between the U and Pu elution and the recovery of the analytes. U and Pu were first run independently (and in replicate) to check the performance of each individual column, and then the full system performance was verified by the separation of mixed U and Pu samples.

Figure 2 is the elution profiles, as determined by HRICPMS analysis, for the U fraction (red downward triangles) and Pu (blue upward triangles) of a combined U/Pu sample. The figure shows narrow elution profiles for both elements, and demonstrates good separation between the U and Pu, with almost 20 mL of column wash volume separating the two. There is essentially no U present in the Pu fraction and vice versa. This calibration data allowed for the setting of the software parameters in the final method, notably the size of the fractions to collect to ensure complete recovery of the eluted analytes. The final collection volumes were 4 mL fractions for U and 8 mL fractions for Pu, compared to 5 mL and 12 mL respectively for the ORNL manual chemistry. The decreased aliquot size represents time savings for the acid dry down step that occurs before MCICPMS analysis.

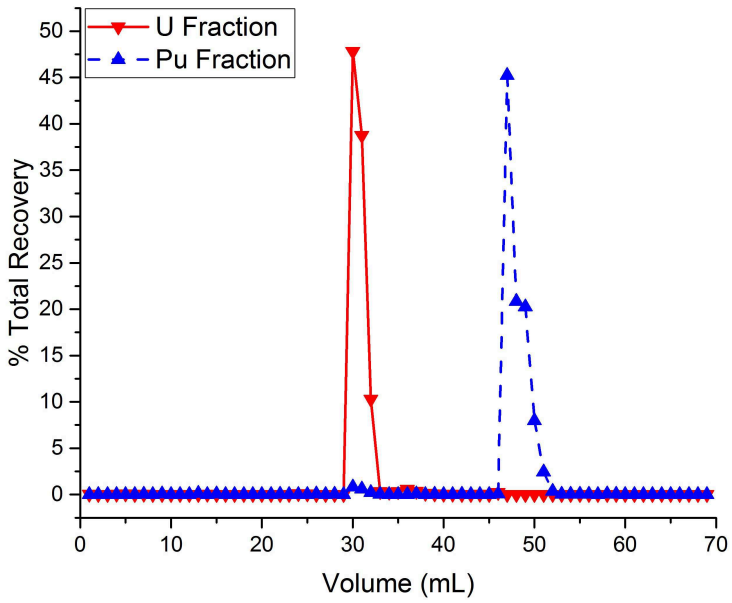

Figure 2. Combined UTEVA (red) and TEVA (blue) column calibration runs for U/Pu separations.

3.3. prep*FAST*-MC2 Blank Levels

Process blanks, or reagent blanks, are an important figure of merit for the prep*FAST*-MC2 as they represent the inherent actinide content background of system, in the absence of any intentionally added U or Pu, and thus contribute to the ultimate detection limits of the automated method. Because uranium is ubiquitous in the environment it is expected to be present in some small amount everywhere, even in cleanroom processes using ultrapure reagents. Additionally, the cotton swipes that make up the matrix for the environmental samples contains a small amount of uranium (~1-5 ng of U per swipe) that gets included in the bulk analysis measurement. The amount of Pu naturally occurring in the environment, however, is essentially nothing. For both U and Pu analysis, characterizing and minimizing the laboratory blank contribution to the final determination of both the isotope ratios and the total actinide content of a sample is extremely important.

Figures 3 and 4 below show the amount of U and Pu, respectively, measured by isotope dilution mass spectrometry in process blanks. The blue squares in both figures are the actual replicate data points, while the blue line is the average value and the black line is the average value for 2015-2016 from the manual separation chemistry in the ORNL cleanroom. The average amount of U in the process blanks from the automated chemistry is 15.03 ± 0.42 pg, compared to the cleanroom value of ~30 pg. The higher blank content of the cleanroom blanks also includes U acquired during the ashing process, a parameter not incorporated thus far in the budget of background contributors. The total amount of Pu, on average, is 0.00065 ± 0.00266 pg, compared to ~ 0.003 pg on average from the cleanroom.

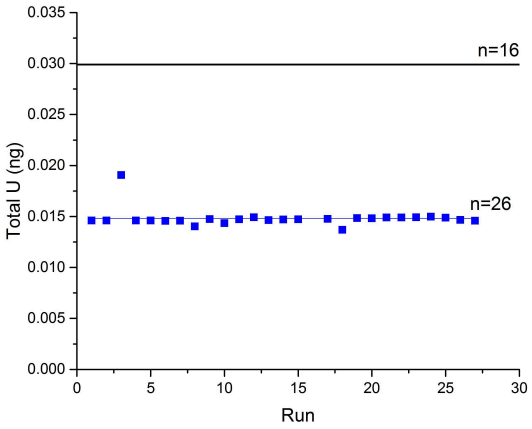

Figure 3. Average and total [U] in process blanks (blue squares) compared to the average value for ORNL manual chemistry for 2015-2016 (black line).

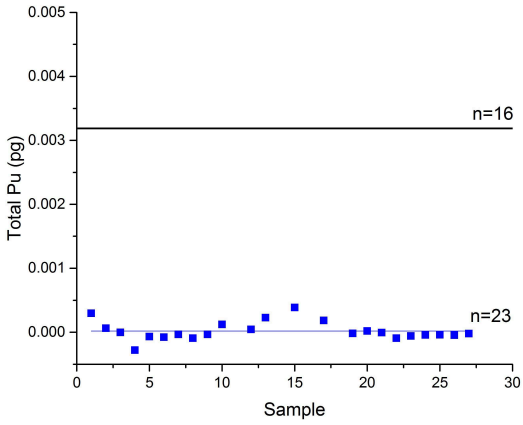

Figure 4. Average and total [Pu] in process blanks (blue squares) compared to the average value for ORNL manual chemistry for 2015-2016 (black line)

The goal of the automated system is to achieve blank levels approaching that obtained by the manual chemistry in a cleanroom, without the requirement of cleanroom infrastructure. The results shown here demonstrate that the goal is achievable. Additionally, the automation, with its completely closed sample lines, may prove to have a more consistent blank level than is achievable from the manual chemistry. Certainly, the data seen here indicated a high degree of reproducibility in the blank levels for both U and Pu. It is important to note that this data represents the initial condition of the unit, before appreciable amounts of U or Pu have been passed through it. However, the result is an important benchmark to document what a clean system is ultimately capable of.

3.4. Separation of Mixed Uranium and Plutonium Samples

Samples of mixed CRMs IRMM-183 and NBL-137 were separated by the prep*FAST*-MC2 in an automated, unattended mode. Initial experiments used ~45 ng of IRMM-183 and ~15 pg of NBL-137, interspersed with unspiked reagent blanks to verify the absence of sample carryover. Figures 5 and 6 show results for the major isotope ratios for U ($^{235}U/^{238}U$) and Pu ($^{240}Pu/^{239}Pu$), respectively, plotted

against the certificate values for these materials. The results show good agreement with certificate values, well within the targets set out by the IAEA [2], and they display a high degree of precision among replicate measurements. Good recovery is also observed, typically >85% for U and ~60% for Pu, on the order of that observed in the manual chemistry.

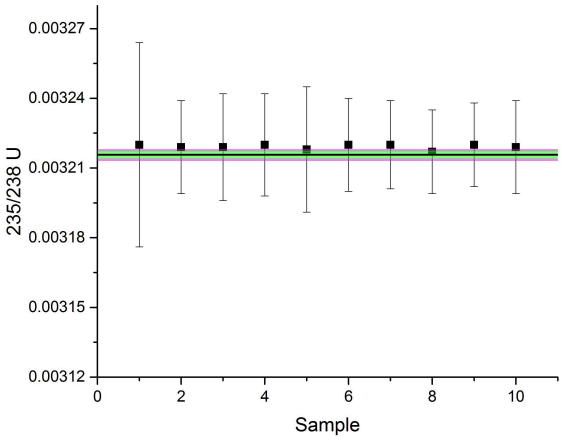

Figure 5. $^{235}U/^{238}U$ isotope ratios of U in separated samples compared to the IRMM-183 certificate value (black line).

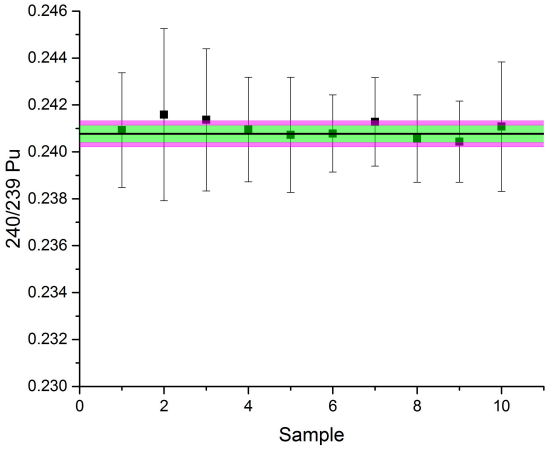

Figure 6. $^{240}Pu/^{239}Pu$ isotope ratio of Pu in separated samples compared to the NBL-137 certificate value (black line).

The blanks interspersed with the samples were also very clean, with a U content on average of 22 pg U/sample, and a Pu content on average of 0.0005 pg Pu/sample. Additionally, the isotopic content of the U in the blanks is natural abundance, while the samples, IRMM-183, are depleted in the $^{235}U/^{238}U$ ratio. Combined, the low total actinide content in the blanks, as well as the lack of depleted U present, both demonstrate the cleanliness of the system and confirm no carryover of sample from one separation into the next.

Recent experiments have been conducted to test the capability of the prep*FAST*-MC2 to successfully separate higher loadings of U and Pu, and especially to test samples with high U and low Pu (and vice versa). The same 2 CRMs were used, but in concentrations ranging from ~165 - 2 ng of U and ~150 - 3 pg of Pu. The results, even at these higher levels, showed ~99.8% removal of U from the Pu fraction and likewise a 99.9% removal of Pu from the U fraction, both of which are critical for a high-quality measurement by MCICPMS. At the highest Pu loading of 150 pg (extremely high for a typical environmental sample), when three samples were run consecutively, a very small amount of Pu (~13 fg) was present in the reagent blank immediately following the third sample. A second blank run after the first restored the Pu background to <1 fg. The finding suggests that the upper limit for Pu loading should be set at less than 150 pg to keep a low Pu background on the system. This will still encompass the vast majority of samples expected in the NWAL Bulk Analysis Program, and should be achievable with judicious aliquot sizing based on preliminary sample screening information. It also shows, however, that an occasional higher sample inadvertently loaded will not leave a permanent Pu background; it may simply require additional washing. Experiments to quantify recovery of extremely low Pu loadings (<1 pg Pu) are currently underway.

3.5. Separation of Heavy Metal Contaminates

Significant amounts of heavy metals such as W, Pt, Pb, and Th are known to create interferences in an ICP-MS plasma that can affect the measurement of U and Pu. Additionally, significant quantities of any metals may occupy binding sites in the resin columns and impact the successful purification of the U and Pu aliquots. To test this, elements either expected to be present in swipe samples in high abundance (Pb, Th) or elements, however rare, that are known to cause interferences in the ICPMS (Pt, Au, Bi) were spiked into samples and were separated on the prep*FAST*-MC2. The performance

was initially verified with blanks, and then the same contaminates were spiked into samples containing U and Pu CRMs. A fraction of each purified aliquot was measured by HRICPMS to quantify the removal of the contaminates, while the remainder was submitted for MCICPMS analysis to ensure no negative impact on the actinide isotope ratio determinations. The list of contaminates examined and their starting and final concentration in the CRM spiked samples is shown in Table 1. The results confirm that removal of all species in, even at significant quantities, is accomplished by the system for both the U and Pu containing fractions.

Element		U Fraction		Pu Fraction	
	Starting Concentration (ng/mL)	Final Concentration (ng/mL)	%Reduction	Final Concentration (ng/mL)	%Reduction
Zr	1000	17.0	98	0.4	100
Mo	1000	0.2	100	0.4	100
Ru	10	0.1	99	0.1	100
W	1000	0.2	100	0.2	100
Os	10	-0.3	103	-0.1	101
Pt	10	0.1	100	0.1	99
Au	10	0.2	98	0.1	100
Hg	10	0.2	100	0.2	100
Tl	10	-0.2	101	0.0	100
Pb	10000	0.8	100	0.6	100
Bi	1000	0.2	100	0.1	100
Th	5000	5.1	100	0.6	100

Table 1. Percent reduction of contaminant elements in U and Pu fractions by the prep*FAST*-MC2

3.6 Cleanroom Conditions

An important point to note with the results above is that all experiments were conducted with the prep*FAST*-MC2 located outside of a cleanroom. It was installed in standard laboratory, with ventilation for acid fumes but without the HEPA filtered air that constitutes an ISO certified cleanroom. The ability of the system to produce consistent reagent blanks on the order of (or even lower) than what results from the manual chemistry performed in a cleanroom is critical. It shows that the unit may be installed in a laboratory without the expensive infrastructure and personnel required to maintain an ISO certified cleanroom and still achieve comparable results.

The entirely closed fluoropolymer sample path, as well as the limited sample handling required and the smaller reagent volumes all contribute to the low blanks achievable with the automated system. Additionally, based on recommendations from ORNL staff, the second generation prep*FAST*-MC2 will have an attached ultra-low particulate air (ULPA) filter, which will ensure even cleaner air flows over the samples that sit open on the tray prior to being loaded onto the resin columns for separation, or when the final aliquots have been dispensed after separation.

A caveat to this, however, is that all the acid dry down steps still occur in specially designed boxes in the ORNL cleanrooms. The acid dry downs, alternatively called matrix conversions, are necessary and time-consuming steps occurring at several places in the sample preparation process. They serve to convert the analyte from one chemical form to another (as needed to change plutonium eluent from a chloride to a nitrate form in preparation for injection into the ICP-MS), to adjust analyte concentration, or to ensure complete mixing of a spike with the sample.

ORNL is currently evaluating COTS equipment that may serve to replace the dry down boxes and that can operate outside of a cleanroom. The EvapoClean® from Analab®, a sub-boiling distillation apparatus, is pictured in Figure 7 below. It is a 6 or 12 port vertical hotplate with programmable timer that can evaporate acids off from individual samples, each in a completely sealed fluoropolymer environment. The acid matrix of the sample is evaporated and then condensed into a separate vial,

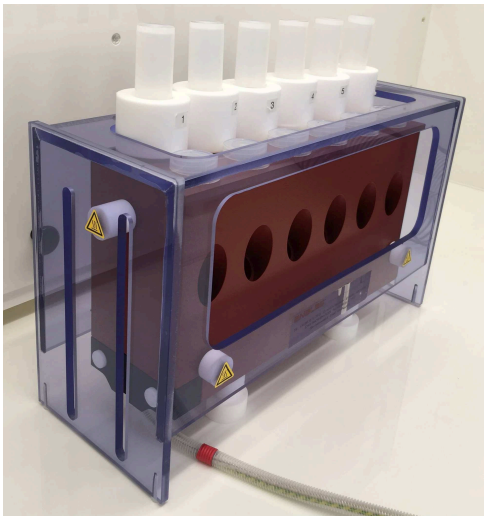

Figure 7. The Analab® EvapoClean® installed in a chemical hood at ORNL

while the analytes of interest (i.e. actinides in a sample) remain in the original vial. The sealed environment limits the exposure of the samples to lab air, which would enable the dry down step to move out of a cleanroom and into a traditional chemical laboratory. An additional benefit of the equipment is that it can simultaneously be used to reflux acid into labware (via the ports on top of the unit), either to clean new vials or to acid leach previously used vials for reuse. The dual use of the EvapoClean® enables both labware cleaning and sample dry downs to occur outside a cleanroom.

To measure the efficiency of analyte recovery, a 40-element cocktail with a concentration of 0.5 ng/g per element in 2% HNO3 was evaporated in the system, and 37 out of 40 elements were recovered at greater than 85%. Separate experiments were also conducted to specifically measure U and Pu recovery using CRM ~5 ng of IRMM-183 and ~3 pg of NBL-137. The results showed greater than 95% recovery for both U and Pu for 4 replicate samples. Testing continues at ORNL to document any time savings that may be gained by use of the EvapoClean® in place of the dry down boxes.

3.7 Documented Time Savings from Automation

Table 2 documents the time savings for the ORNL NWAL chemistry enabled using automation from the prep*FAST*-MC2 for a batch of 7 samples. This number was chosen because a typical set of swipe samples from the IAEA would include 5 samples, with the remaining two places occupied by laboratory blanks (a reagent blank and a swipe blank, for instance). The total time to manually process this set of samples, including multiple acid dry downs, is ~28 hours. Almost 10 hours of that requires hands-on labor from a chemist, the majority of which is the actual chemical separations (8 hours). The total time utilizing the automated system is approximately the same, ~27 hours. However, the total hands-on time for the entire sample set is ~35 minutes. A small amount of setup time is

Sub-Steps	Manual Chemistry		Automated System	
	Total Time (h)	Hands-on Time (h)	Total Time (h)	Hands-on Time (h)
Resin Cleaning	1.4	1.4	0.33	0.33
Misc. Setup	0.2	0.2	0.05	0.05
Chemistry	8	8	16.3	0
Dry Downs	18	0.2	10	0.2
Total	**27.6**	**9.8**	**26.68**	**0.58**

Table 2. Time comparison of ORNL NWAL manual chemistry and ESI prep*FAST*-MC2 automated system for a batch of 7 samples

required at the start of each run, and then the system will operate unattended, even overnight. The >90% reduction in manual labor required for the automated separations creates significant efficiency gains that can be realized without the addition of extra staff. Both the cost and the relatively small laboratory footprint make operation of multiple systems feasible, which would produce even greater gains. Two units in the same laboratory could operate simultaneously, doubling the throughput with a relatively modest increase in personnel effort. Additionally, the use of multiple systems would allow segregation by sample content, as is currently common in NWAL laboratories. A lab may utilize one unit for hot swipes and another for cold, minimizing the chance of cross-contamination between samples and eliminating concerns of carryover from one separation to the next.

4. Conclusions

The prep*FAST*-MC2 from ESI is a COTS automated sample preparation system that has been customized by ORNL to perform U and Pu separations on digested swipe samples in support of the IAEA's Bulk Analysis of Environmental Samples for Safeguards program. It packs and unpacks bulk Eichrom TEVA and UTEVA resins into columns for each individual sample purification. ORNL has characterized the reproducibility of the resin packing and the low blank levels achievable through automation without requiring housing in cleanroom space. The separation was verified by use of mixed U and Pu CRM samples and various concentration ranges. Heavy metal contaminates were also spiked into samples to ensure purification of the final U and Pu aliquots. The use of the prep*FAST*-MC2, along with other COTS equipment like the EvapoClean® from Analab®, create the opportunity to conduct cleanroom level separations without the expensive infrastructure. Documented time savings enabled by the automation reduce the hands-on time required for processing of a set of 7 samples from 9.8 hours to ~0.6 hours. The prep*FAST*-MC2 may be run in unattended, overnight operation, and the simultaneous use of multiple units would create even greater gains in efficiency.

5. Acknowledgements

This work is supported by the Safeguards Technology Development Program, Office of Nonproliferation and Arms Control, at the Department of Energy's National Nuclear Security Administration under contract DE-AC05-00OR22725 with UT-Battelle, LLC.

6. Disclaimers

This paper reflects the opinions and views of the authors only and is not intended to represent the views of their affiliated institutions nor the U.S. Government.

I agree that ESARDA may print my name/contact data/photograph/article in the ESARDA Bulletin/Symposium proceedings or any other ESARDA publications and when necessary for any other purposes connected with ESARDA activities.

7. References

[1] IAEA, *IAEA Safeguards Glossary; International Nuclear Verication Series No. 3*, International Atomic Energy Agency: Vienna, 2002; p. 78.

[2] IAEA, *Recommendations from the 2010 IAEA Technical Meeting: Bulk Analysis of Environmental Samples for Safeguards*. International Atomic Energy Agency: Vienna, 2010.

[3] IAEA, *IAEA Department of Safeguards Long-Term R&D Plan, 2012–2023; STR-375,* International Atomic Energy Agency: Vienna, 2013.

[4] IAEA*, Development and Implementation Support Programme for Nuclear Verification 2016–2017*;

STR-382, International Atomic Energy Agency: Vienna, 2016.

[5] Field, M. P. *prepFAST-MC™: Automating Sample Purification*. Elemental Scientific Inc.: 2014.

[6] Ticknor, B.W., Bottorff, S.C, Hexel, C.R., Tevepaugh, K.N., Bostick, D.A., *Automated Clean Chemistry for Bulk Analysis of Environmental Swipe Samples*, ORNL/TM-2016/662.

Recent technology developments for uranium and plutonium isotopic determination from small samples

Nicholas S. Lloyd [1], Cole R. Hexel [2], M. Paul Field [3]

[1] Thermo Fisher Scientific, Hanna-Kunath-Str. 11, 28199 Bremen, Germany. nicholas.lloyd@thermofisher.com
[2] Nuclear Analytical Chemistry and Isotopic Laboratories, Oak Ridge National Laboratory, One Bethel Valley Road, MS 6415, Oak Ridge, TN 37830. hexelcr@ornl.gov
[3] Elemental Scientific Inc., Omaha, Nebraska, USA. field@icpms.com

Abstract:

Uranium isotope ratio determination for nuclear forensic, nuclear safeguards and for environmental applications is challenging due to the large isotopic differences between different material types and because of the extreme differences in isotopic abundances. For some applications the total uranium quantities can be limited, or it is desirable to run at lower concentrations for radiological protection. Recent developments in inlet systems and detector technologies allow small samples to be analysed at higher precisions using MC-ICP-MS and TIMS.

Here we evaluate the combination of Elemental Scientific apex omega desolvation system with the Thermo Scientific NEPTUNE Plus MC-ICP-MS. The new inlet system is exceptionally stable and efficient with respect to sample transport to the ICP, and with respect to minimizing the $^{235}U^{1}H$ interference on ^{236}U. The highest ICP sampling efficiency is realized using the Thermo Scientific Jet Interface. The $^{235}U/^{238}U$ mass bias is typically stable to better than 0.01% RSD within an analytical session.

Thermo Scientific 10^{13} ohm amplifier technology allows small ion beams to be measured at higher precision on Faraday cups, offering an enhanced signal/noise ratio with a linear and stable response that covers a wide dynamic range (ca. 2 kcps – 30 Mcps). The baseline uncertainty on a 10-minute measurement is ca. 20-25 cps. 10^{13} ohm amplifiers are readily cross-calibrated at the 0.01% precision level. Thermo Scientific 10^{13} ohm amplifier technology can be applied to isotope ratio measurements for systems from Li to Pu using the Thermo Scientific NEPTUNE Plus MC-ICP-MS and TRITON Plus TIMS instruments.

For sub-nanogram quantities of LEU the ^{235}U can be measured with 10^{13} ohm amplifier technology instead of an ion counter. For nanogram sample amounts the minor isotopes ^{234}U and ^{236}U can be transferred from ion counters onto 10^{13} ohm amplifiers. Using 10^{13} ohm amplifier technology we were able to quantify $^{234}U/^{238}U$ ratios at the 0.1 % level with 25 ng sample amounts of natural isotopic composition.

Keywords: *MC-ICP-MS; TIMS; uranium; plutonium; isotopic*

1. Introduction

The use of Thermo Scientific 10^{13} Ω amplifier technology (Thermo Fisher Scientific (Bremen) GmbH, Germany) for multicollector mass spectrometry measurements was first described by Koornneef et al. [1]. 10^{13} Ω current amplifiers offer significant improvements over standard 10^{11} Ω amplifiers, especially with respect to signal/noise ratio, and allows low intensity ion beams to be measured more precisely than has previously been possible. 10^{13} Ω amplifier technology has been used for a variety of applications on the Thermo Scientific NEPTUNE *Plus* MC-ICP-MS and Thermo Scientific TRITON

Plus TIMS instruments [2]–[6], including uranium isotopic determination by modified total evaporation (MTE) [7]. For nuclear safeguards applications, 10^{13} Ω amplifier technology allows precise isotopic signatures to be obtained from smaller sample amounts. Here we illustrate the utility of the 10^{13} Ω amplifier technology for the determination of isotopic compositions of uranium and plutonium involving pg quantities of isotopes without the need for ion counters.

Figure 1 show a comparison of the dynamic range for the different detectors that are used for multicollector mass spectrometry measurements. The minor isotopes of uranium (^{234}U and ^{236}U), and the isotopes of plutonium are typically measured at ion beam intensities that are lower than the optimal dynamic range of the standard 10^{11} ohm amplifier. Ion counters are traditionally used for these measurements, however 10^{13} Ω amplifier technology offers advantages in terms of ease of use, detector lifetime, flexibility, dynamic range, linearity, stability and cross-calibration precision. Uncertainties approaching 0.01 % are achievable with 10^{13} Ω amplifier technology [5].

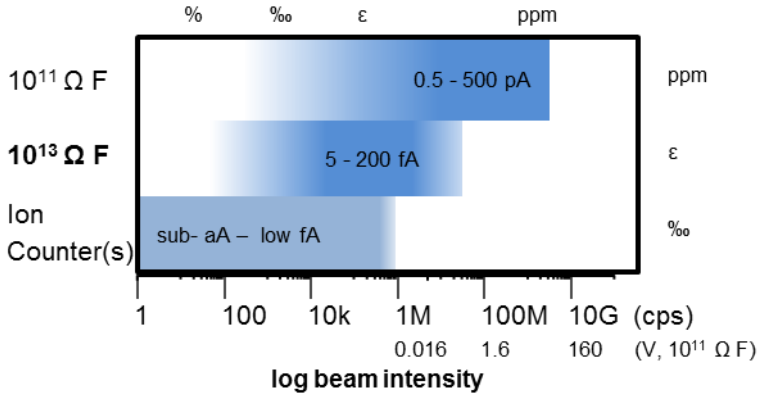

Figure 1: Dynamic range of different detector types (F = Faraday cup). The recommended detector(s) available for a given signal intensity are indicated by the intensity of shading. The counting statistic limit on precision for a 10 minute acquisition is indicated at the top, with typical limits for detector type on the right.

2. Uranium Isotopic Measurements Using MC-ICP-MS

A range of uranium isotopic reference materials were measured using a NEPTUNE *Plus* MC-ICP-MS equipped with Jet Interface option. An Elemental Scientific Apex Ω High Sensitivity Sample Introduction System (Elemental Scientific Inc., Omaha, USA) was used. This desolvating nebulizer offers sensitivity and stability with low oxide and low hydrides, and can be tuned remotely from the instrument PC. Uranium sensitivity was 1600 V/ppm at 119 µl/min uptake rate, and the hydride on *m/z* 239 was < 1 x10^{-6}.

The 10^{13} Ω amplifier were cross calibrated in a similar way to that described by Kimura et al. [4], comparing Nd isotope ratios measured using electronically cross-calibrated 10^{11} Ω amplifiers with those measured by 10^{13} Ω amplifiers. The precision of the cross-calibration measurements are within 0.01% (95% C.I.) and the cross-calibration measurements are recommended to be on a weekly basis. In contrast, ion counters require daily optimisation and within-run cross-calibration.

Each measurement included a half-mass off-peak baseline (100 seconds), followed by 7-minutes on-peak acquisition. Approximately 1.2 ml of sample solution was consumed per analysis, with 15 – 25 ng uranium required for an analysis.

The collector configuration used is shown in Table 1. The 10^{13} Ω amplifiers can be electronically switched between any of the Faraday cups as required for different applications.

Detector	L1	L2	C	H1	H2	H3
Amplifier	10^{13} Ω	10^{11} Ω	10^{13} Ω		10^{11} Ω	
Isotope	^{234}U	^{235}U	^{236}U		^{238}U	

Table 1: Collector configuration for uranium isotopic measurements. Detector C can be switched to an SEM with RPQ for the lowest quantification limits of ^{236}U. Comprehensive multi-ion-counting arrays are available for nuclear forensic applications, enabling precise measurements of sub-ng uranium sample quantities [8], [9].

Uranium isotopic determination was made by comparison to measurements of the uranium isotopic standard NBS U-010 (New Brunswick Laboratory, Argonne, USA). For every 4 'sample' measurements a blank and a standard measurement was made. The blank was < 0.01 %after a 10-minute wash. Ratios were corrected using the Richter & Goldberg [10] reference values, and their uncertainties are propagated through to the reported data.

2.1. Repeatability of uranium isotopic measurements.

Figure 2 shows the repeatability of ^{234}U/^{238}U and ^{236}U/^{238}U measurements of a 20 ng/g solution of NBS U-010. The mass bias stability of the measured ^{235}U/^{238}U ratio was 0.008 % RSD, with the measurements spanning 3-hours. Typical mass bias stability within an analytical session is within 0.01 % RSD. The ^{234}U/^{238}U and ^{236}U/^{238}U data were corrected using an exponential mass bias correction and the certified ^{235}U/^{238}U ratio. The values are within uncertainty of certified ratios, and within uncertainty of those obtained by Richter & Goldberg [10].

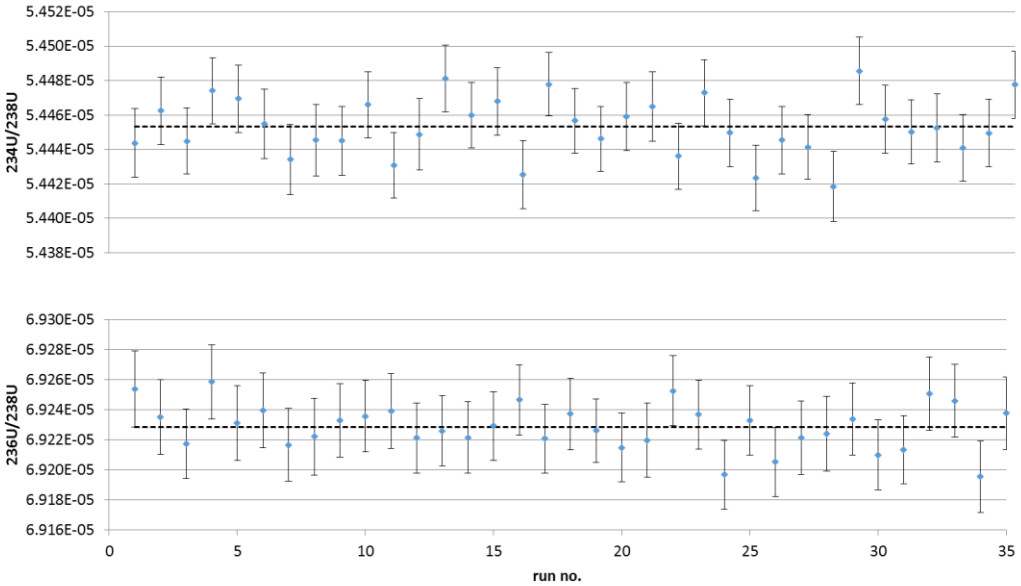

Figure 2: Repeatability of back-to-back measurements of a 20 ng/g solution of NBS U-010, with mass bias correction from ^{235}U/^{238}U. ^{234}U and ^{236}U were measured using 10^{13} Ω amplifier technology. The RSD for ^{234}U/^{238}U and ^{236}U/^{238}U are 0.03 and 0.02 % respectively, with no detector drift apparent in the datasets. Error bars on the data points are 2x standard error of the mean.

2.2. Reproducibility of uranium isotopic determinations.

Table 2 reports the data from *n=8* repeat measurements for each of 4 certified reference materials. The data for ^{234}U/^{238}U are plotted in Figure 3, expressed as deviation from certified reference value, and shows a good level of agreement for a range of isotopic compositions. NBS U-0002 is omitted for clarity, since the scatter is larger for the very lowest intensity ion beam (3.9 kcps).

n=8		$^{234}U/^{238}U$	$^{235}U/^{238}U$	$^{236}U/^{238}U$
NBS U-005	Mean	0.000021889	0.00491913	0.000047459
	SD	0.000000032	0.00000024	0.000000038
	RSD	0.15%	0.005%	0.08%
NBS U-0002	Mean	0.000001653	0.00017724	
	SD	0.000000042	0.00000016	
	RSD	2.5%	0.09%	
IRMM-184	Mean	0.000053230	0.00726026	<3.5E-7
	SD	0.000000049	0.00000016	
	RSD	0.09%	0.002%	
IRMM-183	Mean	0.000019824	0.00321731	0.000148529
	SD	0.000000050	0.00000019	0.000000037
	RSD	0.25%	0.006%	0.02%

Table 2: Reproducibility of uranium isotope ratio measurements for 4 certified reference materials. The ion beam intensity for ^{234}U ranges from 3.9 kcps for NBS U-0002 to 128 kcps for IRMM-184. The 3.5×10^{-7} quantification limit for ^{236}U was estimated from NBS U-0002.

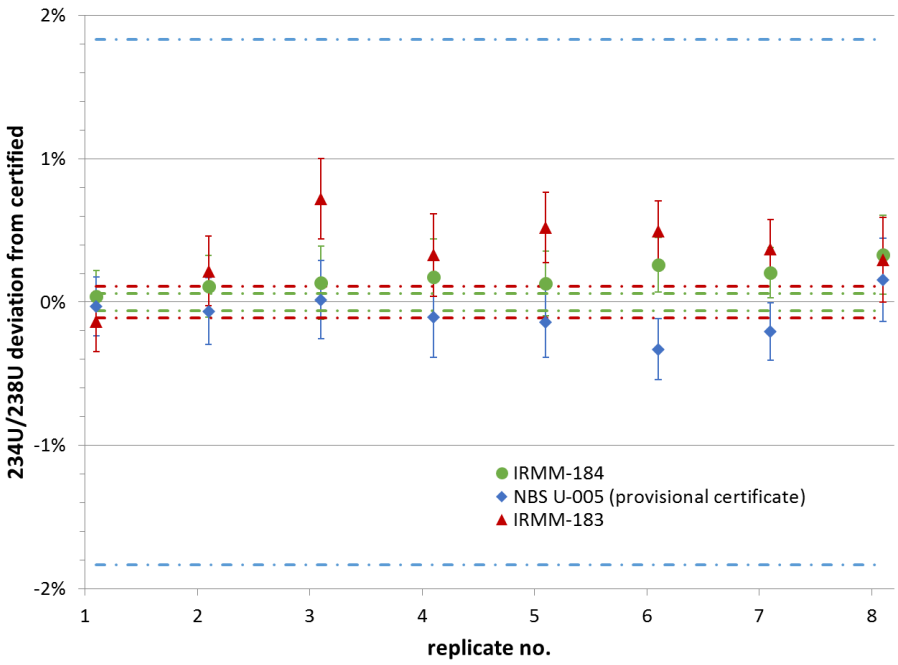

Figure 3: Accuracy and reproducibility of uranium isotope ratio measurements for 3 certified reference materials. The dotted lines indicate the 95 % C.I. intervals of the certified reference value. There is a good level of agreement with certified reference values.

2.3. Application

Solutions from individual uranium-oxide grains were re-measured using this setup and compared to data previously reported [11]. Sample amounts from 12.5 – 25 ng were available (equivalent to 15 – 20 µm diameter grains). Standards run at 12.5 and 25 ng/g concentration were within agreement of each other. The data are presented in Figures 4 & 5, and are significantly more precise than the previous analyses made using older instrumentation with an ion counter for the minor isotopes.

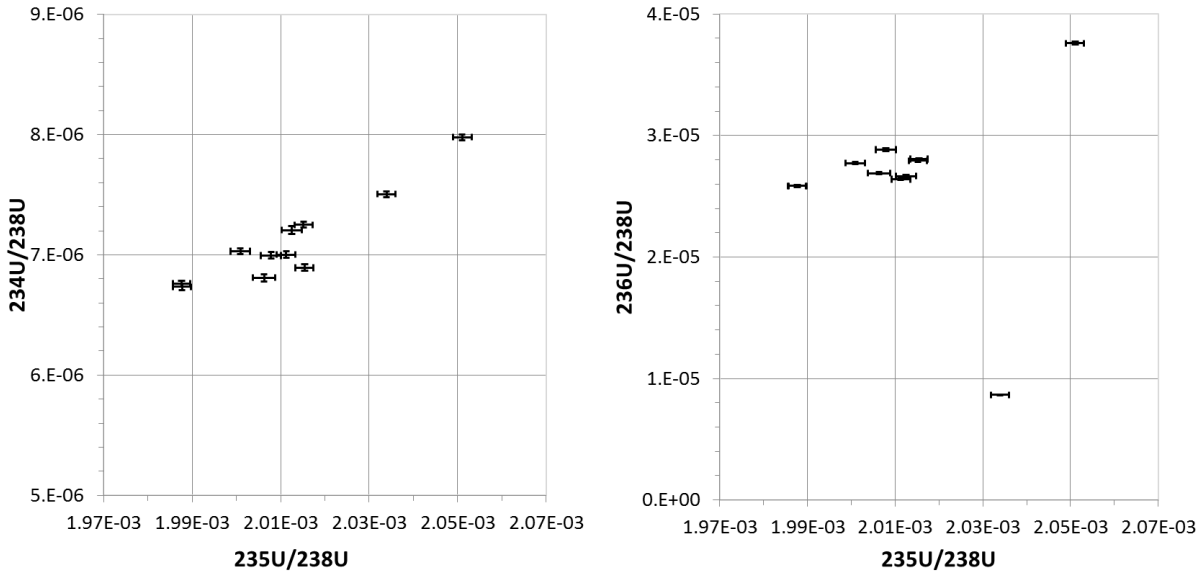

Figure 4: Solutions from individual uranium-oxide grains were re-measured using Faraday cups and the data are significantly more precise than previous data obtained using older instrumentation. The grains were isolated from dust and soil samples collected for an environmental case-study [12].

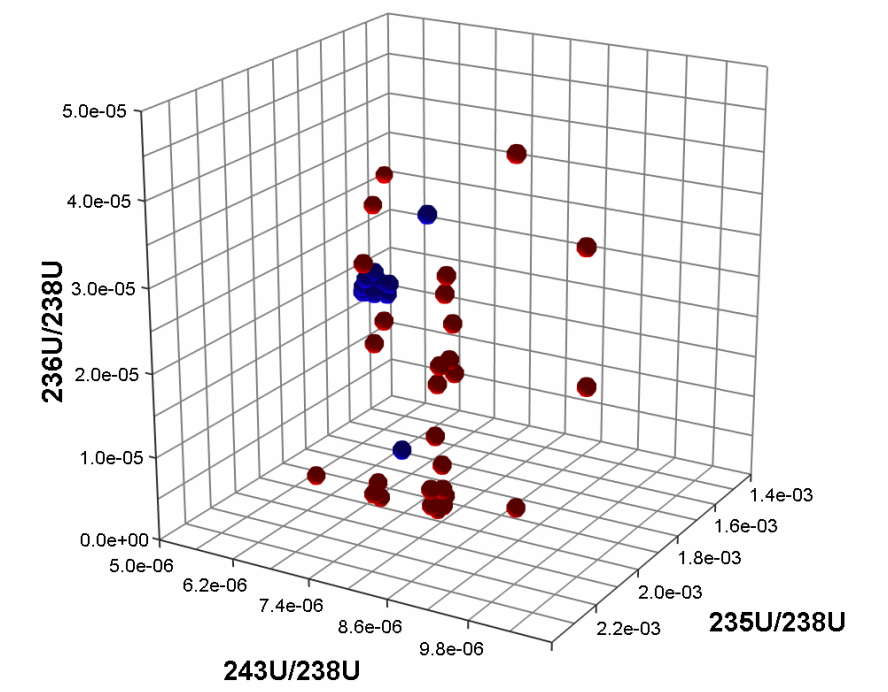

Figure 5: 3D plot of uranium isotopic signatures for the individual grains (blue dots) compared to a sub-set of PDGP tails assay data (red dots). The isotopic signatures of the individual grains can be explained through the mixing of batches of depleted uranium feedstock during processing and subsequent waste disposal at a site in Colonie, NY, USA [13].

3. Plutonium Isotopic Measurements Using MC-ICP-MS

The instrument setup for the plutonium isotopic measurements was similar to that used for uranium. Table 3 shows the collector configuration used for the plutonium measurements. An SEM ion counter was used for the ^{241}Pu measurements. Each measurement comprised 7.5 minutes on Line 1, followed by 100 seconds on Line 2. Approximately 1 ml of 6 pg/g plutonium solution was consumed for each

analysis. CRM 137 (New Brunswick Laboratory, Argonne, USA) was measured against IRMM-086 (Standards for Nuclear Safety, Security and Safeguards Unit, Geel, Belgium).

Detector	L2	L1	C	H1	H2
Amplifier	10^{13} Ω	10^{13} Ω	SEM	10^{13} Ω	10^{12} Ω
Line 1	^{239}Pu	^{240}Pu	^{241}Pu	^{242}Pu	^{244}Pu
Line 2			^{239}Pu	^{240}Pu	

Table 3: Collector configuration for plutonium isotopic measurements. A second line is included for the cross-calibration of the SEM ion counter used to measure ^{241}Pu. Multi-ion-counting arrays are available for nuclear forensic applications, enabling measurements of fg quantities of isotopes [8].

3.1. Reproducibility of plutonium isotopic determinations.

The data for the plutonium measurements is plotted in Figure 6. The data are within uncertainty of age corrected reference values. The repeatability (RSD) for ^{240}Pu/^{239}Pu and ^{241}Pu/^{239}Pu are 0.17 and 0.12 % respectively (from ca. 6 pg Pu). Ion beam intensity ranges on the 10^{13} Ω amplifier were from 22 kcps to 982 kcps (^{240}Pu and ^{239}Pu respectively from IRMM-086). The lower intensity ^{241}Pu beam was measured using an SEM (ca. 0.6 kcps for IRMM-086).

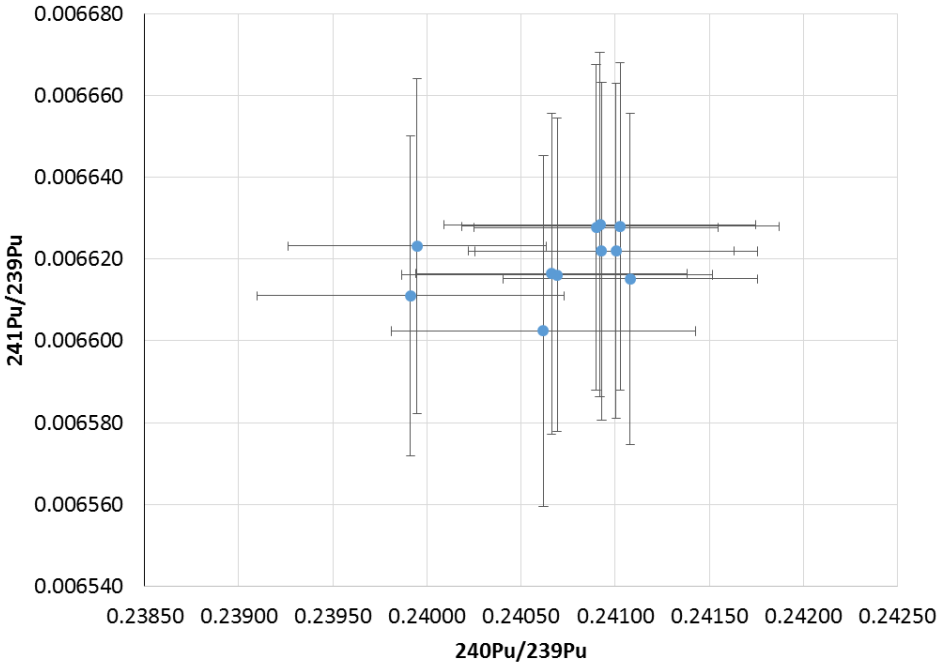

Figure 6: Reproducibility of plutonium isotope ratio measurements CRM 137 (6 pg Pu). There is a good level of agreement with age-corrected reference values. The RSD for ^{240}Pu/^{239}Pu and ^{241}Pu/^{239}Pu are 0.17 and 0.12 % respectively. ^{239}Pu and ^{240}Pu were measured using 10^{13} Ω amplifier technology, whilst ^{241}Pu was measured on an SEM ion counter. Prior to standardisation the RSD for ^{240}Pu/^{239}Pu from CRM 137 was 0.03 %; the low ^{240}Pu signal from the IRMM-086 standard limits precision.

4. Conclusions

Thermo Scientific 10^{13} Ω amplifier technology is shown to have utility for nuclear safeguards measurements of uranium and plutonium isotopic compositions. The combination of the Thermo Scientific NEPTUNE *Plus* MC-ICP-MS with Jet Interface option and the Elemental Scientific Apex Ω High Sensitivity Sample Introduction System delivers the sensitivity and stability required for obtaining precise and accurate isotope ratios from small sample amounts. The combination of new technologies enables precise isotope ratios to be measured from pg quantities of isotopes without the need for ion counters.

5. Acknowledgments

The solutions for the data presented in Section 2.3 were prepared at the NERC Isotope Geochemistry Laboratory and British Geological Survey. Gratitude is expressed towards Dr Matthew Horstwood (British Geological Survey), Dr Simon Chenery (British Geological Survey) and Prof. Randall Parrish (University of Plymouth). The plutonium measurements were made with the assistance of Eddie McBay and Brian Ticknor (Oak Ridge National Laboratory).

6. References

[1] J. M. Koornneef, C. Bouman, J. B. Schwieters, and G. R. Davies, “Measurement of small ion beams by thermal ionisation mass spectrometry using new 10^13 Ohm resistors.,” *Anal. Chim. Acta*, vol. 819, pp. 49–55, 2014.

[2] M. Klaver, R. J. Smeets, J. M. Koornneef, G. R. Davies, and P. Z. Vroon, “Pb isotope analysis of ng size samples by TIMS equipped with a 10^13 Ω resistor using a 207 Pb– 204 Pb double spike,” *J.Anal.At.Spectrom.*, vol. 31, pp. 171–178, 2015.

[3] A. von Quadt, J.-F. F. Wotzlaw, Y. Buret, S. J. E. Large, I. Peytcheva, and A. Trinquier, “High-precision zircon U/Pb geochronology by ID-TIMS using new 10^13 ohm resistors,” *J. Anal. At. Spectrom.*, vol. 31, pp. 658–665, 2016.

[4] J.-I. I. Kimura, Q. Chang, N. Kanazawa, S. Sasaki, and B. S. Vaglarov, “High-precision in situ analysis of Pb isotopes in glasses using ultraviolet femtosecond laser ablation multiple Faraday collector inductively coupled plasma mass spectrometry equipped with 10^13 Ω resistor high gain amplifier,” *J. Anal. At. Spectrom.*, vol. 31, pp. 790–800, 2016.

[5] J.-F. Wotzlaw, Y. Buret, S. J. E. Large, D. Szymanowski, and A. von Quadt, “ID-TIMS U-Pb geochronology at the 0.1 ‰ level using 10^13 Ω resistors and simultaneous U and 18O/16O isotope ratio determination for accurate UO2 interference correction,” *J. Anal. At. Spectrom.*, vol. 32, pp. 579–586, 2017.

[6] M. Pfeifer, N. S. Lloyd, S. T. M. Peters, F. Wombacher, B.-M. Elfers, T. Schulz, and C. Münker, “Tantalum isotope ratio measurements and isotope abundances determined by MC-ICP-MS using amplifiers equipped with 10^10 , 10^12 and 10^13 Ohm Ohm resistors,” *J. Anal. At. Spectrom.*, vol. 32, pp. 130–143, 2017.

[7] A. Trinquier and P. Komander, “Precise and accurate uranium isotope analysis by modified total evaporation using 10^13 ohm current amplifiers,” *J. Radioanal. Nucl. Chem.*, vol. 307, no. 3, pp. 1927–1932, 2016.

[8] S. Richter, S. Konegger-Kappel, S. Boulyga, G. Stadelmann, A. Koepf, and H. Siegmund, “Linearity Testing and Dead-Time Determination for MC-ICP-MS Ion Counters using the IRMM-072 Series of Uranium Isotope Reference Materials,” *J. Anal. At. Spectrom.*, vol. 31, pp. 1647–1657, 2016.

[9] S. F. Boulyga, A. Koepf, S. Konegger-Kappel, Z. Macsik, and G. Stadelmann, “Uranium isotope analysis by MC-ICP-MS in sub-ng sized samples,” *J. Anal. At. Spectrom.*, vol. 31, pp. 2272–2284, 2016.

[10] S. Richter and S. Goldberg, “Improved techniques for high accuracy isotope ratio measurements of nuclear materials using thermal ionization mass spectrometry,” *Int. J. Mass Spectrom.*, vol. 229, no. 3, pp. 181–197, 2003.

[11] N. S. Lloyd, R. R. Parrish, M. S. a. Horstwood, and S. R. N. Chenery, “Precise and accurate isotopic analysis of microscopic uranium-oxide grains using LA-MC-ICP-MS,” *J. Anal. At. Spectrom.*, vol. 24, no. 6, pp. 752–758, 2009.

[12] N. S. S. Lloyd, S. R. N. R. N. Chenery, and R. R. R. Parrish, “The distribution of depleted uranium contamination in Colonie, NY, USA,” *Sci. Total Environ.*, vol. 408, no. 2, pp. 397–407, 2009.

[13] N. S. Lloyd, R. R. Parrish, M. S. A. Horstwood, S. R. N. Chenery, and C. Bouman, “‘ Nuclear Forensic ’ application of LA -MC-ICP-MS,” in *IAEA Safeguards Symposium*, 2010, p. IAEA-CN-184/39.

Session 10

Spent Fuel Verification and Spent Fuel Transfer

Investigating the Cherenkov light production due to cross-talk in closely stored nuclear fuel assemblies in wet storage

Erik Branger, Sophie Grape, Peter Jansson, Erik Andersson Sundén, Staffan Jacobsson Svärd

Uppsala University, Uppsala, Sweden
E-mail: erik.branger@physics.uu.se

Abstract:
The Digital Cherenkov Viewing Device (DCVD) is one of the tools available to a safeguards inspector performing verifications of irradiated nuclear fuel assemblies in wet storage. One of the main advantages of safeguards verification using Cherenkov light is that it can be performed without moving the fuel assemblies to an isolated measurement position, allowing for quick measurements. One disadvantage of this procedure is that irradiated nuclear fuel assemblies are often stored close to each other, and consequently gamma radiation from one assembly can enter a neighbouring assembly, and produce Cherenkov light in the neighbour. As a result, the measured Cherenkov light intensity of one assembly will include contributions from its neighbours, which may affect the safeguards conclusions drawn.

In this paper, this so-called near-neighbour effect, is investigated and quantified through simulation. The simulations show that for two fuel assemblies with similar properties stored closely, the near-neighbour effect can cause a Cherenkov light intensity increase of up to 3% in a measurement. For one fuel assembly surrounded by identical neighbour assemblies, a total of up to 14% of the measured intensity may emanate from the neighbours. The relative contribution from the near-neighbour effect also depends on the fuel properties; for a long-cooled, low-burnup assembly, with low gamma and Cherenkov light emission, surrounded by short-cooled, high-burnup assemblies with high emission, the measured Cherenkov light intensity may be dominated by the contributions from its neighbours.

When the DCVD is used for partial-defect verification, a 50% defect must be confidently detected. Previous studies have shown that a 50% defect will reduce the measured Cherenkov light intensity by 30% or more, and thus a threshold has been defined, where a ≥30% decrease in Cherenkov light indicates a partial defect. However, this work shows that the near-neighbour effect may also influence the measured intensity, calling either for a lowering of this threshold or for the intensity contributions from neighbouring assemblies to be corrected for. In this work, a method is proposed for assessing the near-neighbour effect based on declared fuel parameters, enabling the latter type of corrections.

Keywords: DCVD; partial defect verification; Cherenkov light; Geant4; Cross-talk

1. Introduction

Irradiated nuclear fuel assemblies are commonly stored in water for radiation protection, as well as for decay heat removal. As a result of the interactions of the radiation emanating from the fuel assemblies with the surrounding water, Cherenkov light is produced. This Cherenkov light has frequently been assessed by safeguards inspectors, using the presence, characteristics and intensity of the Cherenkov light to verify that the object under study is an irradiated nuclear fuel assembly, and not some other non-fuel item.

The Digital Cherenkov Viewing Device (DCVD) is one of the tools available to safeguards inspectors to measure the Cherenkov light emissions from irradiated nuclear fuel assemblies in wet storage. The DCVD can be used for gross- as well as partial-defect verification [1]. The type of partial defect analysis under study in this paper relies on comparisons of the measured intensities to predicted

intensities, where removal or replacement of a fraction of the fuel rods will result in a lowered Cherenkov light intensity.

One of the main advantages of the DCVD is that the fuel assemblies do not have to be moved to an isolated area for measurement. A downside of measuring the assemblies where they are stored is that gamma radiation from closely stored assemblies can enter neighbouring assemblies and cause Cherenkov light emission there. This cross-talk, referred to as the near-neighbour effect, introduces a measurement error that is not compensated for in the currently deployed inspection procedure. The aims of this paper are: (i) to characterize and quantify the near-neighbour effect under selected fuel storage conditions, (ii) to identify how the near-neighbour effect affects the partial-defect verification procedure currently used, and (iii) suggest a method for its compensation.

1.1. Partial defect verification of used nuclear fuel using the DCVD

There are two methods used to detect partial defects in nuclear fuel assemblies with the DCVD. The first method uses image analysis to detect empty rod positions, and can be used to detect any removed rods in visible positions, as seen from the measurement position above the fuel. The second method is used to detect possible substitution of 50% of the fuel rods in an assembly. This method relies on the comparison of the measured intensity to a predicted intensity, based on operator-provided fuel declarations. In this analysis, the measured fuel assemblies are grouped by fuel type, so that each group contains fuels with the same physical design. For calibration within each group, the measured and predicted intensities are related by a linear fitting, as illustrated in Figure 1. As a result of this calibration, the predicted intensity values do not correspond to absolute measured intensity, but to a relative intensity of all fuel assemblies of the same type, and deviations from the group's linear fit call for further investigations of possible reasons. It is known from simulations that if 50% of the rods in an assembly are substituted with non-radioactive rods, the Cherenkov light intensity will be reduced by at least 30% [2]. Thus, if any measured intensity of an assembly is more than 30% lower than expected, a partial defect may be suspected.

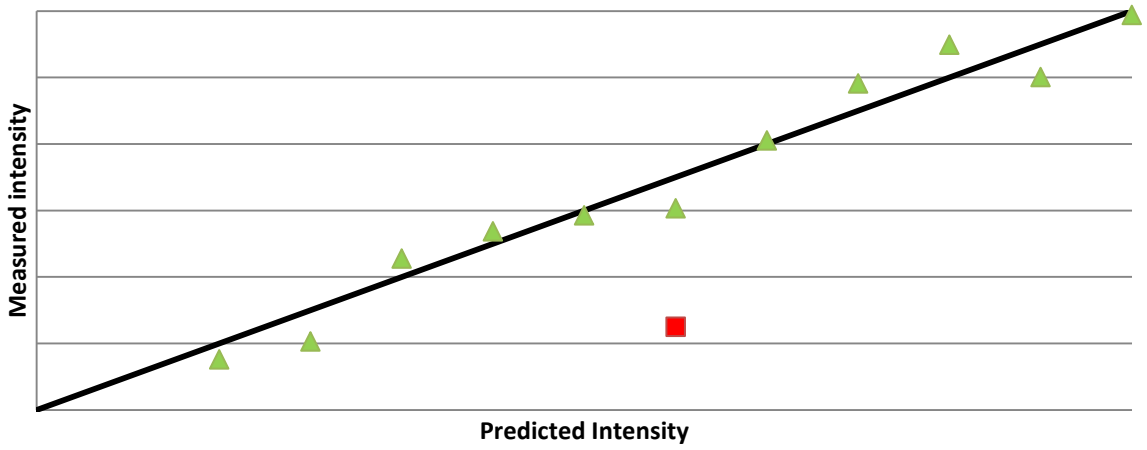

Figure 1 Illustration of the calibration procedure and partial defect verification method using the DCVD. For each fuel type, a linear fit is made between the predicted and measured intensity, where the fitted slope relates the predicted and measured intensity values. If any measured value deviates by more than 30% from the predicted (red square), a partial defect may be suspected.

Up until recently, the prediction method used was based on a parameterization of the Cherenkov light intensity as a function of burnup and cooling time in a BWR 8x8 configuration [3]. This method is currently being replaced by a new method [4], which more accurately considers the fuel irradiation history by calculating the inventory of fission products using ORIGEN [5], by considering the geometry of the fuel assemblies, and by including Cherenkov light intensity contributions from both gamma and beta decays [6].

1.2. DCVD measurements and the near-neighbour effect

During a measurement, the DCVD is typically mounted on the railing of a moveable bridge, looking down on the fuel storage pond. The fuel assemblies are typically stored densely enough that radiation from one fuel assembly may enter neighbouring assemblies and create Cherenkov light there. Due to the relatively long distance that the radiation must travel to reach a neighbour, only gamma-ray emissions are expected to contribute to the near-neighbour effect. The intensity of neutron emissions is too low in comparison to gamma emissions to contribute significantly, and the ranges of alpha and beta particles are too short to contribute. This work hence considers only Cherenkov light produced due to gamma-decays of fission products. The magnitude of the near-neighbour effect is a function of the distance between the fuels, the amount of storage rack material present in between the assemblies and the energy spectrum of the gamma-ray emissions, which depend on the fuel cooling time.

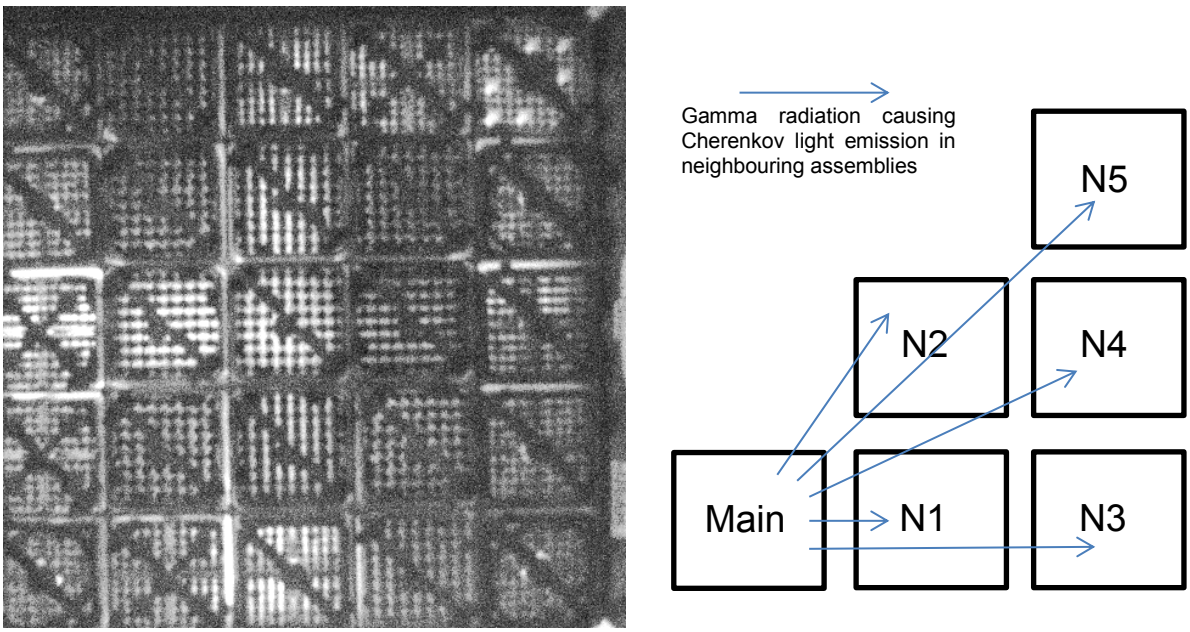

Figure 2 Left: DCVD image of 25 BWR fuels stored at the Swedish Central Interim Storage Facility for Spent Nuclear Fuel (Clab). Image courtesy of Dennis Parcey, Clab, and the Canadian Nuclear Safety Commission (CNSC). Right: For an active assembly emitting gamma radiation, called main, this paper analyses the Cherenkov light produced in the neighbouring assemblies, labelled N1 to N5, by gamma radiation originating from the main assembly. For symmetry reasons, all surrounding assemblies in a 5x5 grid may be defined using labels N1 to N5.

In Figure 2, an example is shown of the storage situation at the Swedish Central Interim Storage Facility for Spent Nuclear fuel (Clab), where 25 BWR fuels are stored in one fuel basket. The fuels are stored very close to each other, being separated by 4 mm of borated steel. At a reactor fuel pond, there is typically more distance in between the fuels for criticality safety reasons, and it is also more likely that fresh or low-burnup fuel is stored close to high-burnup fuel, which in turn may cause a significant near-neighbour intensity in the low-burnup neighbours. Low-burnup fuel will give rise to relatively low levels of gamma emission and consequently low levels of Cherenkov light, in comparison to high-burnup, short-cooled fuel. Accordingly, a large fraction of the gamma radiation in a low burnup fuel may have its origin in neighbouring high-burnup fuel, thus a significant fraction of the Cherenkov-light emission in the low-burnup fuel may be attributed to the near-neighbour effect. To be able to refer to the different neighbouring position in a storage rack, Figure 2 also labels the five neighbour positions considered in this work, where position N1 shares one side with the main assembly causing the near-neighbour effect in the studies, N2 shares a corner with the main assembly, and N3-N5 are one row/column further away. Other positions in a 5x5 grid may be referred to using these labels due to the symmetry of the storage situation.

2. **Definition and characterization of the near-neighbour effect**

In this work, the near-neighbour effect is studied in terms of the effect of one assembly emitting gamma radiation ("Main" in Figure 2) to its neighbours (N1-N5). The results will be presented as the ratio, NNR, of the Cherenkov light intensity in a neighbour ($I_{neighbour}$) produced by gamma radiation from the main assembly, as compared to the intensity in the main assembly itself (I_{main}), or

$$NNR = \frac{I_{neighbour}}{I_{main}} \quad (1)$$

Note that by this definition, the intensity I_{main} is caused only by fission product decays in the main assembly. For real measurements, this value is not accessible due to the near-neighbour effect, though I_{main} can be predicted using one of the available prediction models [3] [6]. Furthermore, this study is limited to gamma-ray and bremsstrahlung emission, whereas it has been shown that beta particles may increase I_{main} by 1-10%, depending on fuel assembly type, irradiation history and cooling time [4]. There are negligible beta particle contributions to $I_{neighbour}$ because of their short travel range in water.

2.1. Simulations

To characterize the near-neighbour effect, simulations were run for two different fuel assembly configurations, BWR 8x8 and PWR 17x17, and for two different fuel storage situations. The simulations were performed using a toolkit based on Geant4 [7], which is a further development of a previously used toolkit for simulating the Cherenkov light production in irradiated nuclear fuel [8].

The fuel assemblies were modelled including fuel rods and control-rod guide tubes for PWR, respectively a water channel and a fuel channel surrounding the rod configuration for BWR. The dimensions of the simulated fuel assemblies are given in Table 1. In addition, walls of a square steel storage rack were also included in the simulations. Vertically directed Cherenkov light was analysed in the simulations, since the DCVD will measure the vertical light component given the measurement situation with the DCVD situated above the fuel. Cherenkov light at an angle smaller than 3 degrees to the vertical axis was considered representative of the vertical light component in the simulations, and this value also allows for comparisons with earlier simulation results [8]. This angle is wide enough that sufficient statistics can be obtained in the simulations in reasonable time, while being narrow enough to represent the vertical component.

	BWR 8x8	PWR 17x17
Number of fuel rods:	63	264
Fuel pellet diameter [mm]:	10.44	8.18
Cladding thickness [mm]:	0.91	0.57
Rod centre to centre distance [mm]:	16.3	12.6

Table 1 Dimensions of the simulated fuel assemblies.

The fuel depletion code ORIGEN [5] was used to assess the gamma spectrum for fuel assemblies with burnups of 10, 20, 30 and 40 MWd/kgU, and cooling times ranging from 0.25 to 60 years. The initial enrichment was set to 2% in all cases. These fuel parameter sets were chosen to be comparable to earlier studies [3] [8] . Fuels with 10, 20 and 30 MWd/kgU burnup were simulated as irradiated for four cycles, where each cycle consisted of 312.5 days of irradiation and 46 days of cooling, for a total of 1250 irradiation days. The power levels for the three lower burnups were 8, 16 and 24 kW/kgU, respectively. For the 40 MWd/kgU case, the power level remained at 24 kW/kgU, and the fuel was irradiated for 5 cycles. Note also that the gamma spectrum provided by ORIGEN includes both gamma-rays from fission product decays as well as bremsstrahlung produced when beta-particles are stopped in the fuel material.

2.2. Effects of burnup and cooling time for BWR assemblies

Figure 3 shows results of the simulations of the near-neighbour effect for BWR 8x8 fuels with a burnup of 40 MWd/kgU, for the fuel storage situation shown in Figure 2, with a 4 mm steel wall separating the assemblies. As can be seen, the N1 position is most strongly affected by the near-neighbour effect, with an NNR up to 2.9% of the main assembly intensity. For the N2 position, the near-neighbour effect is weaker, however; the NNR value is affected by attenuation in the assembly at N1, and will differ if the N1 position is occupied or vacant (called “N2” respectively ”N2 only” in Figure 3). Accordingly, it is not only important to consider the properties of the emitting fuel assembly when estimating the near-neighbour effect; it is also important to consider which nearby positions that do not contain fuel to estimate the effect correctly. With N1 occupied, the intensity in N2 is up to 0.4% of the main assembly intensity, and with the N1 absent, it is up to 0.9% For the N3 position, if N1 and N2 are occupied the near-neighbour effect is at most 0.05%, and could be neglected. However, if N1 and N2 are absent, the near-neighbour intensity in N3 can be up to 0.5% (called “N3 only” in Figure 3), comparable to the intensity found at N2. The intensities in the N4 and N5 positions were found to be negligible in all cases simulated.

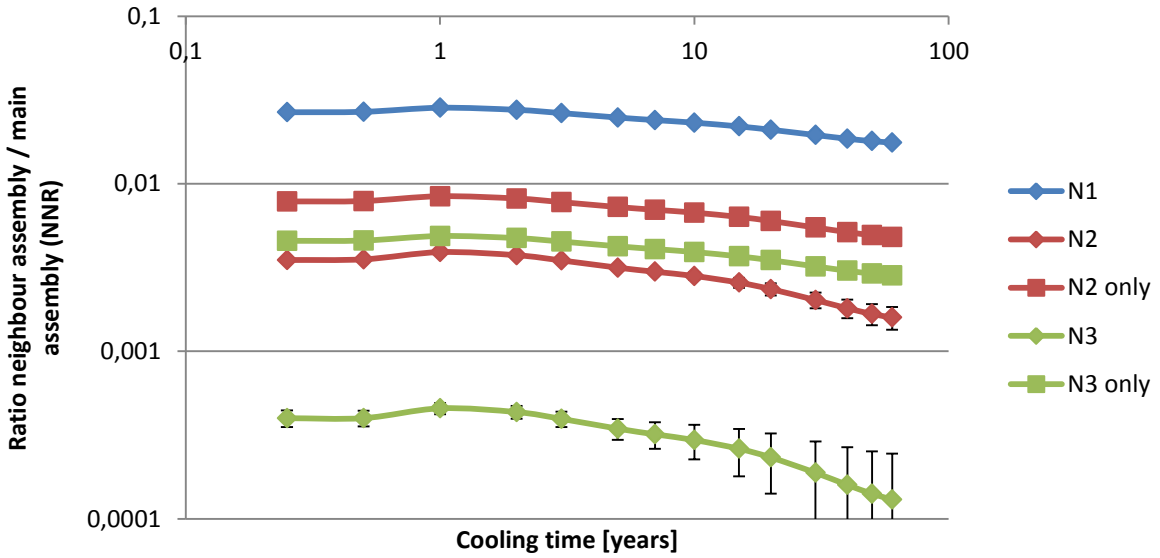

Figure 3 The magnitude of the near-neighbour effect as a function of cooling time, for BWR 8x8 assemblies. The N2 and N3 positions were simulated both for the situation that all neighbouring positions contained fuel (denoted N2 and N3, respectively), and for the situation that only two fuel assemblies were present, one at “main” and one at one neighbour position, (denoted “N2 only” and “N3 only”, respectively). Error bars denote 1 σ uncertainty.

As can also be seen in Figure 2, the near-neighbour intensity ratios NNR, (Eq. (1)), reach maxima at a cooling time of around 1 year. As an example, the N1 position has a maximum NNR value at 1 year of 2.9%, which decreases to 1.9% after 40 years cooling. This is due to the changing gamma spectrum of the fuel assembly with cooling time. For short-cooled fuel, several high-energy gamma-emitting isotopes are still present, which have relatively long range and thus contribute more to the near-neighbour intensity. As the fuel cools, the gamma emissions become dominated by the 662 keV emissions of Cs-137, which are of lower energy and has a relatively shorter range. As a consequence of the changing gamma spectrum with time, compensating for the near-neighbour effect will require assessing the gamma spectrum of all assemblies contributing to the measurable intensity at the event of measurement.

While the near-neighbour effect is noticeably affected by the cooling time, dependence on burnup is small, although a slight decrease with burnup is seen in the relative near-neighbour intensity at short cooling times. Note that while the near-neighbour intensity ratio changes little with burnup, the dependence of absolute Cherenkov light intensity on burnup is strong; high burnup implies high Cherenkov light intensity in both the fuel assembly emitting the radiation as well as in its neighbours.

2.3. Differences in the near-neighbour effect for BWR and PWR fuels

To investigate the differences in the near-neighbour effect for different fuel assembly configurations, the simulations in section 2.2 were complemented by simulations for a PWR case, where each PWR fuel was separated by a 5 mm steel wall, corresponding to closely stored fuel assemblies. In Figure 4, the ratios of NNR (see Eq. (1)) between BWR and PWR for the N1 and N2 positions are plotted, as a function of cooling time. The ratios are fairly flat at short cooling times, whereas for cooling times longer than 5 years, the near-neighbour intensity ratio, NNR, decreases more rapidly with cooling time for BWR as compared to PWR. Accordingly, the near-neighbour effect depends on the fuel assembly configuration, and thus a compensation procedure may have to take the fuel type into account. Furthermore, one may note that NNR is higher for BWR fuel than for PWR fuel (the ratios between the fuel types is >1), given that both assembly types are stored closely.

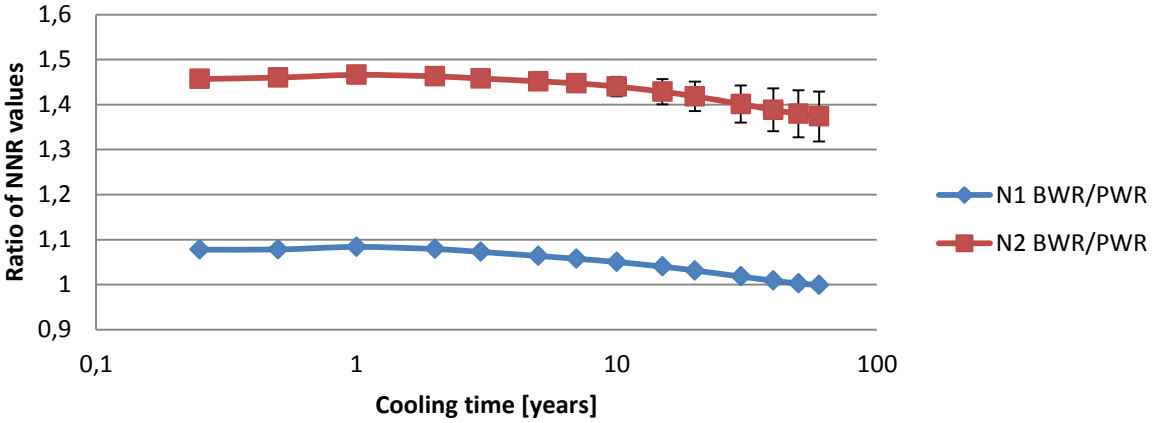

Figure 4 Ratio of NNR (see Eq. (1)) between BWR and PWR fuels as a function of cooling time, for the N1 and N2 neighbour storage positions. In the N2 case, all the N1 positions were occupied. Error bars denote 1 σ uncertainty, due to the Monte-Carlo nature of the simulations.

2.4. Effects of fuel assembly spacing

To investigate the dependence of the near-neighbour effect on the storage distance between fuel assemblies, the simulations in sections 2.2 and 2.3 were complemented with an additional more spacious storage geometry, which corresponds to the storage situation for BWR fuels at the Forsmark Nuclear Power plant, for comparison with the experimental results reported in [9]. In these simulations, each fuel assembly was surrounded by a 2.5 mm-walled square steel channel, similar to the storage rack found at Forsmark. For the PWR simulation, the same relative fuel distance, as compared to fuel size, was simulated as in the BWR case, and the same wall thickness (2.5 mm steel) was used. The results for each simulated configuration are presented in Table 2 for 1-year cooled 40 MWd/kgU burnup fuel.

Storage configuration	Fuel size [mm]	Wall thickness [mm]	Fuel assembly centre-to-centre distance, [mm]	N1 intensity ratio (NNR)	N2 intensity ratio (NNR)
BWR close	130	4.0	135	2.84 ± 0.03%	0.39 ± 0.02%
PWR close	215	5.0	220	2.60 ± 0.01%	0.26 ± 0.01%
BWR spacious	130	2.5 + 2.5	195	1.43 ± 0.02%	0.54 ± 0.02%
PWR spacious	215	2.5 + 2.5	322	0.63 ± 0.01%	0.18 ± 0.01%

Table 2 The near-neighbour intensity ratio (NNR in Eq. (1)) for two fuel types and two different fuel centre-to-centre distances. In the spacious simulations, each fuel was surrounded by a separate steel wall. In the simulations for the N2 intensities, the N1 positions were occupied. The uncertainties are due to statistics in the Monte-Carlo simulations, and are presented for the 1 σ level. The simulated fuel assemblies had a cooling time of 1 year and a burnup of 40 MWd/kgU.

As can be seen in Table 2, the near-neighobur intensity in N1 is smaller for the more spacious storage geometry. For position N2 in the BWR case, the intensity becomes higher. The reason is that the assemblies in N1 positions strongly attenuate radiation travelling between the Main and N2 position in the close storage configuration. In the more spacious storage configuration, the N1 fuels interfere less with the radiation from the Main assembly, leading to a net increase in the N2 intensity ratio, despite the increased distance between them. For the PWR case, the result in larger absolute distances in the spacious storage geometry lower the N2 intensity ratio. Had the simulated distance been smaller, it may have been possible to observe the same effects as for the BWR case.

3. **Comparison of simulations with experimental results**

In 2012, a series of measurements were conducted at the Forsmark nuclear power plant, where the near-neighbour effect was quantified for the N1, N2 and N3 fuel positions [9], when all other positions were vacant. This was done by; (i) moving one active fuel assembly (defined as “Main” in Figure 2) to an isolated location and measure it to record the I_{main} intensity of Eq. (1), and; (ii) place it relative to a fresh fuel assembly in the N1, N2 and N3 positions and measure the subsequent intensity increase in the fresh fuel assembly, corresponding to $I_{neighbour}$ in Eq. (1). For details on these measurements, we refer to [9]. Here, the measured configurations have been simulated to provide an experimental benchmark of the simulation procedure, as further described below.

3.1. Measured and simulated geometries

In the measurements, the active assembly was of one BWR 10x10 type, while the fresh fuel was a different BWR 10x10 design. The properties of the storage racks at the Forsmark plant are accounted for in Table 2, denoted “BWR spacious”. The irradiation histories of the fuel assemblies were made available to the authors, courtesy of the operator, Vattenfall.

In the simulations, the fuel irradiation histories were used to calculate the assemblies’ gamma emission spectra by means of the ORIGEN code [5]. Using these spectra, simulations were run for the Forsmark storage configuration. However, the fuels simulated were BWR 8x8, while the irradiated fuels measured at Forsmark were all 10x10, including several part-length rods. The reason for not simulating the 10x10 fuel type was that exact geometry data for that fuel type were unavailable. Still, because the outer dimensions are similar for BWR 8x8 and 10x10 fuels, the BWR 8x8 simulations may be considered to be representable also for 10x10 fuels.

3.2. Results

In Table 3, the simulated near-neighbour intensities are compared to the intensities measured at Forsmark [9]. The overall agreement is good, especially for the N1 position where the near-neighbour effect is the strongest. One may note that the N1 position is slightly underestimated, while the N2 and N3 positions are overestimated. The deviations may be explained by differences between the simulated and measured fuel assembly configurations, or by measurement uncertainties. Further investigations would be required to draw more solid conclusions on the deviations.

Another result of these simulations is that for fuel assemblies in this storage geometry, the N2 intensity is not much affected by the presence or absence of a fuel in the N1 positions. In the case of both N1 positions occupied, the simulated N2 NNR is 0.41 ± 0.01 %, and with the N1 positions vacant it increases to 0.43 ± 0.01 %.

Neighbour position	Measured neighbour intensity	Simulated neighbour intensity
N1	1.25%	1.16 ± 0.02%
N2	0.36%	0.43 ± 0.01%
N3	0.12%	0.18 ± 0.01%

Table 3 Comparison of the measured near-neighbour effect (data from [9]**)**, to a simulated near-neighbour intensity for a similar configuration, which was obtained using a gamma spectrum calculated with ORIGEN, taking into account the operator-declared fuel irradiation history. Simulation uncertainties are due to the Monte-Carlo nature of the simulations. Uncertainties in the measurements were not provided in [9].

4. **Detection limits in presence of the near-neighbour effect**

As mentioned in section 1.1, partial defect verification using the DCVD relies on the fact that a 50% substitution of rods with non-radioactive content will reduce the Cherenkov light intensity by at least 30%, which, accordingly, is taken as the limit for partial defect. Fuel assemblies where measured intensities are more than 30% lower than predicted are detected as being subject to partial defect, whereas other assemblies pass the inspection. This situation becomes slightly more complicated in presence of the near-neighbour effect, since the light being measured is partly caused by the fuel under study, and partly by the neighbouring fuels. As a consequence, the limit of 30% will be reduced when near-neighbour intensities influence the analysed data. This is shown in Figure 5, where the 30% intensity reduction is adjusted to also take into account the near-neighbour effect.

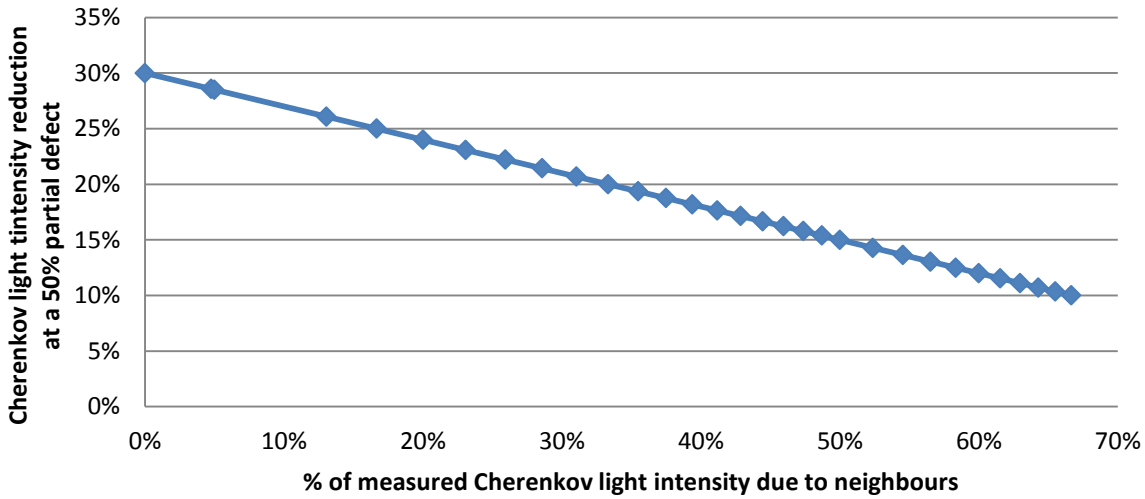

Figure 5 Calculated reduction of the 30% light intensity limit as a function of the near-neighbour intensity.

As a consequence of the data in Figure 5, the detection limit for partial defect at 30% lower intensity than expected would have to be lowered, unless the near-neighbour effect is corrected for. Lowering the detection limit would bring more stringent requirements on the accuracy of the models used for predicting the Cherenkov intensities as well as on the experimental precision that govern the accuracy of measured data in order to maintain the partial-defect detection capability. If the methods cannot meet these higher requirements, one must either allow a larger number of false alarms (using a lower threshold for partial defect according to Figure 5), or endanger the partial-defect detection rate (keeping the 30% intensity reduction threshold).

One situation where the near-neighbour effect would be particularly strong is when measuring a storage site with a population of neighbouring fuels with highly varying Cherenkov light intensities, due to largely varying burnups and cooling times. In such a situation, low-intensity fuel assemblies will be more strongly affected by the near-neighbour effect as compared to high-intensity ones. If the effect is not corrected for, the fuel intensity predictions will systematically underestimate the intensity of low-intensity fuels, while over-estimating the measured intensity of high-intensity fuels. Referring to Figure 5, considering a low-intensity assembly where as much as 50% of the intensity comes from neighbouring fuels, a diversion of 50% of its fuel rods may only cause a 15% decrease in measured intensity. It is doubtful that the current experimental and predictive methods may be further developed to offer the precision required for confident detection in such extreme cases, unless the near-neighbour effect is included in the analysis.

In conclusion, to avoid changing the detection threshold while maintaining the partial-defect detection capability, methods for correcting for the near-neighbour effect should be considered. Such correction methods are further discussed below.

5. **Methods for correcting for the near-neighbour effect**

In this section, two methods for correcting for the near-neighbour effect are presented. The basics of both methods are that each measured intensity can be expressed as a sum of the intensity from the assembly under study, I_0, and the intensities from its nearest neighbours:

$$I_{measured} = I_0 + \sum_i (I_i \cdot \varepsilon_i) \quad (2)$$

Here, ε_i denotes the ratio of the intensity that neighbouring assembly i emits in the studied assembly to the intensity it emits in its own position, (I_i). One may note that ε_i goes in the opposite direction compared to NNR defined in Eq. (1), but for symmetry reasons their values should be identical. The two methods presented below differ in how the ε_i are determined, where section 5.1 describes a method based on experimental data and section 5.2 describes a simulation-based method.

5.1. Least-squares fitting of experimental data

In [9], an experimental method to assess the near-neighbour effect was tested on a set of BWR fuel assemblies measured at Clab, under the conditions shown in Figure 2. The proposed method uses Eq. (2), limited to neighbours in relative positions N1 and N2 (referring to Figure 2). The method suggests collecting experimental intensities for the complete set of fuels in one storage rack and determining the ε_{N1} and ε_{N2}factors by performing a least squares fit of Eq. (2) for the experimental data set, based on predicted intensities. These fitted ε_{N1} and ε_{N2} can then be used to predict the measured intensity of an assembly, given a prediction of the intensity of the assembly and its neighbours, or alternatively to subtract the intensity caused by the near-neighbour effect from the measurements.

Ref. [9] presents values of ε_{N1} and ε_{N2} obtained from fitting of the experimental data set. In this work, simulations of the storage conditions at Clab for the assemblies under study have been performed to provide an independent evaluation of the deduced values. A comparison of the simulated and the experimentally fitted intensities from [9] is shown in Table 4.

Neighbour	Simulated ε_i	Fitted ε_i
N1	1.82 ± 0.05%	16%
N2	0.17 ± 0.02%	9.5%

Table 4 Comparison of the simulated near-neighbour intensity for closely-stored BWR fuels (as shown in Figure 2) and the fitted values reported in [9].

Table 4 shows poor agreement between simulated and fitted values, and the simulations suggest that the fitted values overestimate the near-neighbour effect by almost an order of magnitude. Considering the relatively good agreement between simulations and measurements shown in Table 3, there is reason to suspect that the fitting procedure may not be adequate to accurately quantify the near-neighbour effect. Probable reasons for this deficit are that the fit is based upon a rather small set of fuels, and that the equation system may be ill-conditioned, making it sensitive to stochastic noise. One may assume better results if larger data sets are used or if constraints are introduced on the near-neighbour intensities, based on expected ratios.

5.2. Simulation-based corrections

As shown in section 3, simulations can provide relatively accurate estimates of the relative intensities from neighbouring fuel. However, since the near-neighbour simulations are time-consuming, a method is needed to take the near-neighbour effect into account in a quicker way, which can be used by inspectors in the field. Here, a solution is suggested, where the near-neighbour effect is parameterised as a function of fuel geometry, fuel centre-to-centre distance, and gamma-ray energy. The parameterisation would be based on large simulations done in advance, allowing for fast deployment for in-field inspections.

Based on the results presented here, primarily the N1 and N2 positions would need to be considered when assessing the near-neighbour intensity, and only rarely will the N3 position be significant. Given the irradiation history, or at minimum the burnup and cooling time, of an assembly and all its neighbours, ORIGEN can be used to assess the gamma-ray energy spectrum of each fuel assembly. By binning the spectrum, it is possible to run simulations with initial gamma rays from each bin, to assess the near-neighbour intensity of gamma-rays of each energy. These simulations will have to be done for a large number of energy bins, for each fuel assembly configuration, and for several fuel centre-to-centre distances. The results will be the magnitude of the near-neighbour effect $\epsilon_{i,j}$for a fuel at neighbour position i and for gamma rays with energy in bin j. These simulations can be done in advance, and only have to be done once for each case.

To calculate the near-neighbour intensity at the event of measurement, the user selects the pre-calculated $\epsilon_{i,j}$ values applicable for the fuel type and storage situation applicable to the measurement situation. These values are combined with the calculated, binned gamma-ray emission spectra of the neighbouring fuels, based on the operator declared fuel declarations. If the binned spectrum of a fuel is given by S_j for bin j, the intensity caused by one neighbour at position i ($I_{neighbour,i}$) can then be calculated as:

$$I_{neighobur,i} = \sum_{j=1}^{\#\,bins} \epsilon_{i,j} \cdot S_j \qquad (3)$$

The total near-neighbour intensity contribution in an assembly is then the sum of the intensity of all present neighbours, each calculated using Eq.3. This value can either be added to a predicted assembly intensity I_0 to give a prediction of the measured intensity; alternatively it can be subtracted from the measurement to obtain an experimental value of assembly intensity I_0 without neighbours.

6. **Conclusions and outlook**

Fuel assemblies in wet storage are often verified using the Digital Cherenkov Viewing Device, which enables inspection without requiring the fuel to be moved to an isolated measurement location. Since the fuel assemblies are stored closely, gamma rays from one assembly may enter a neighbouring assembly and create Cherenkov light, the so-called near neighbour effect. This paper describes how simulations can be used to estimate the magnitude of the Cherenkov light intensity that occurs in a neighbouring position due to the near-neighbour effect. The simulations have been validated using experimental data. The near-neighbour effect will be particularly influential in cases where long-cooled, low-burnup fuels containing relatively low activity levels are stored next to short-cooled, high-burnup fuels containing relatively high activity levels.

It has been shown that the partial-defect detection limits may need adjustment unless the near-neighbour effect is corrected for. Two possible methods for such corrections have been described; one method based on experimental data and one simulation-based method. Building on the fact that simulations have proven capable reproducing experimentally recorded near-neighbour intensities, the latter method is recommended, and a methodology allowing for quick in-field use has been presented. The methodology is based on extensive, time-consuming simulations, which are done in advance to create parameterisations specific for storage configurations, assembly types and gamma-ray energies. These parameterisations may then be used for fast assessment during inspection.

While some experimental data is available regarding the near-neighbour effect, more is required to verify the simulations performed, and to assess the performance of the suggested method for predicting the near-neighbour effect. Knowing the accuracy of the near-neighbour prediction model will allow for higher limits to be set regarding what magnitude of near-neighbour effect can be tolerated in the measurements, which increases the partial-defect detection performance of the DCVD. Additional experimental data will also be useful for further refining the near-neighbour prediction model, which can further enhance the DCVD partial defect detection capabilities.

The studies presented in section 3 suggest that it may be possible to e.g. treat all BWR fuel assemblies as being identical with respect to the near-neighbour effect. Thus, it may be possible to simulate only a few selected fuel geometries of widely varying configuration, and use those

simulations to assess the near-neighbour effect for all fuel types. This would greatly reduce the amount of simulations necessary to perform to parameterize the near-neighbour effect, but further studies are required to assess what uncertainties are introduced by this simplification.

7. **Acknowledgements**

This work was supported by the Swedish Radiation Safety Authority (SSM), under contract SSM2012-2750. The computations were performed on resources provided by SNIC through Uppsala Multidisciplinary Centre for Advanced Computational Science (UPPMAX) under project p2007011.

8. **References**

[1] J. D. Chen et.al, “Spent fuel verification using a digital cerenkov viewing device,” 8:th International Conference on Facility Operations - Safeguards Interface, 2008.

[2] J.D. Chen et al., “Partial defect detection in LWR spent fuel using a Digital Cerenkov Viewing,” *Institute of Nuclear Materials Management 50th annual meeting,* 2009.

[3] S. Rolandson, “Determination of Cherenkov light intensities from irradiated BWR fuel,” IAEA task ID JNTA0704, SKI Report #: SE 1-94, 1994.

[4] E. Branger, S. Grape, S. Jacobsson Svärd, P. Jansson and E. Andersson Sundén, “Comparison of prediction models for Cherenkov light emissions from nuclear fuel assemblies (accepted manuscript),” *Journal of Instrumentation,* 2017.

[5] S. Bowman, L. Leal, O. Hermann and C. Parks, “ORIGEN-ARP, a fast and easy to use source term generation tool,” *Journal of Nuclear Science and Technology,* vol. 37, pp. 575-579, 2000.

[6] E. Branger, S. Grape, P. Jansson and S. Jacobsson Svärd, “Improving the prediction model for Cherenkov light generation by irradiated nuclear fuel assemblies in wet storage for enhanced partial-defect verification capability,” *ESARDA Bulletin,* vol. 53, 2016.

[7] Agostinelli, S, et al (the Geant4 collaboration), “Geant4 - a simulation toolkit,” Nuclear Inst. and Meth. in Physics Research Section A: Accelerators, Spectrometers, Detectors and Associated Equipment, Volume 506, Issue 3, 1 July 2003, Pages 250-303.

[8] S. Grape, S. Jacobsson Svärd and B. Lindberg, “Verifying nuclear fuel assemblies in wet storage on a partial defect level: A software simulaiton tool for evaluating the capabilities of the Digital Cherenkov Viewing Device,” Nuclear inst. and Meth. A, Volume 698, 11 January 2013, Pages 66-71, ISSN 0168-9002, 10.1016/j.nima.2012.09.048.

[9] D. Parcey, E. Sundkvist, J. Dahlberg, K. Axell, R. M Kosierb, B. Lindberg and S. Grape, “Determining the effect of adjacent spent fuel on Cherenkov light measurements,” in *Institute of Nuclear Materials Management symposium*, 2012.

Signatures from the spent fuel: simulations and interpretation of the data with neural network analysis

A. Borella[1], R. Rossa[1], C. Turcanu[1]

1) SCK•CEN, Nuclear Science and Technology unit,
Boeretang 200, B-2400 Mol, Belgium

Email: aborella@sckcen.be

Abstract:

In the last years, the safeguards verification of spent fuel assemblies by NDA has received increased interest also due to upcoming programmes for the geological disposal. During safeguards inspections one aims at verifying the completeness and correctness of operator declared data. One should then be able to draw conclusions on the fuel integrity and diversion of pins, as well as checking the consistency of operator declarations on initial enrichment, fuel type, burnup and cooling time. The verification of spent fuel is also important for safety aspects related to the storage of spent fuel.

The experimental observables associated to NDA of spent fuel assemblies are often a complex function of the characteristics of the fuel, its irradiation history and other variables related to the used measurement setup and devices; nowadays one often assumes that some of the variables are known to interpret the data and draw conclusions. To facilitate the interpretation of the data and draw more robust safeguards conclusions, an R&D effort is on-going at SCK•CEN and its results are given in this paper.

This work reports first about the efforts done at SCK•CEN on simulating detector response functions for different types of NDA instruments such as the Fork detector, the ForkBall detector and SINRD detectors. These responses are obtained from Monte Carlo model of the fuel and measurement setup. The spent fuel composition and radiation characteristics are taken from a spent fuel reference library developed in recent years.

A database of detector responses corresponding to 8400 cases with different fuel characteristics and irradiation parameters was then obtained. We explore the use of these simulated observables as input for data analysis algorithms aimed at uniquely characterizing the spent fuel and drawing safeguards conclusions. More specifically, we focus on the application of artificial neural networks due to their ability to generalize non-linear relationships. As a first step, cooling times smaller than 100 years were selected from the database, and several network configurations and training schemes were investigated.

Keywords: Spent fuel verification; Simulated observables; Data mining; Artificial neural network

1. Introduction

Spent fuel assemblies (SFA) are subject to verification of safeguards authorities due to their residual fissile material content. A direct measurement of the residual fissile mass is not possible with available technologies [1,2,3] and can only be estimated. The workhorses used during the verification of SFA are instruments such as the DCVD and the Fork detectors; these instruments allow to draw conclusions on the absence of gross defect in the fuel assemblies and verify the consistency of the operator declaration about fuel characteristics (e.g. fuel type, initial enrichment) and irradiation history (e.g. burnup and cooling time).

Considering the large amount of spent fuel in interim storage and the incipient opening of spent fuel repositories [4], there is an interest in developing NDA methodologies that could allow a more

quantitative assessment of the spent fuel assembly before its disposal. This interest is also shared by the regulatory authorities and fuel management bodies to comply with requirements related to the safe fuel disposal; the implementation-oriented R&D activities on deep geological disposal of spent fuel and long-lived radioactive waste has been emphasised in [5,6].

The traditional nuclear signatures of spent fuel in a Non-Destructive Assay, i.e. passive neutron, gamma emission and Cherenkov glow, are mainly due to minor actinides (e.g. Cm isotopes) and fission products (e.g. Cs isotopes). Their associated observables (i.e. measured counts or light) do not provide a direct measure of the residual fissile mass and are a complex function of several variables, such as irradiation history parameters. At the moment, none of the available methods allow a unambiguous determination of all the variables. Therefore, one typically supposes that one or more of such variables are actually known, so that the number of unknowns is reduced. An example of such case is the determination of the residual fissile content which can be estimated after the burnup of the fuel has been determined from the observables for example with a calibration procedure [7].

New NDA methods are being studied and developed in the last decade[3,8]. In an ideal scenario each method could generate one or more observables where each would allow the unique determination of the quantities of interest. However, this does not seem to be the case [9]. This situation therefore calls for a methodology to disentangle the quantities of interest from the observables.

In this framework, we carried out R&D work first to simulate observables associated to NDA equipment such as the ForkBall detector and SINRD. This work is described in Section 2, where the methodology developed at SCK•CEN to simulate observables is explained. Then, in Section 3 we focus on the interpretation of the data and the extraction of the quantities of interest from the simulated observables; we describe an approach based in neutral network analysis. The obtained results are presented and discussed; outlook and recommendation for future work are given.

2. Detector response function simulations

2.1. Methodology

Due to the limited accessibility of spent fuel [10], the development and optimization of measurements methods are carried out by means of numerical calculations, often based on Monte Carlo methods [11]. Studies with Monte Carlo methods are based on models including the geometry and composition of the measurements equipment, the measurement environment and the characteristics of the radiation source.

The determination of the spent fuel composition and the characteristics of the emitted radiation can be achieved by means of evolution and depletion codes such as Origen-ARP [12,13,14] and ALEPH2 [15]. In the last years, SCK•CEN developed a spent fuel library (SFL) and investigated the impact of different factors on spent fuel composition and emitted radiation. The characteristics of spent fuel depend on quantities such as fuel type, irradiation history and initial composition of the fuel. We focussed on 17x17 PWR fuel elements and studied the change of the neutron emission by varying parameters such as initial uranium enrichment (IE), average power level (AP), duration of the irradiation cycle (DIC) and cooling time between two complete irradiation cycles (CTIC), burnup (BU and cooling time (CT) after discharge [16,17]. The current version of the SFL contains information for Low Enriched Uranium (LEU) fuel with an initial enrichment between 2% and 5% and cases with Mixed Oxide (MOX) fuel with up to 10% of Pu.

The spent fuel library consists of entries, each corresponding to a specific irradiation case. In one entry the total neutron emission, total gamma emission, and the corresponding energy spectra are given. In addition, the abundances of 50 selected nuclides are present [10]. The data are generated in a format which is compatible with the one of an MCNP [18] input file.

The overview of the methodology developed for this study is presented in Figure 1. The used methodology relies on the development of an MCNP input file template of the measurement setup, including the fuel. The composition of the fuel and the description of the source term is then taken from the library for the desired cases, substituted in the template and the simulation is run. More information on the specific tallies is given in the next section where the considered detection system and associated

observables are described. The output file of the simulation is combined with the radionuclide abundancies and source term intensity obtained from the SFL to generate the database with signatures of the different fuel assemblies.

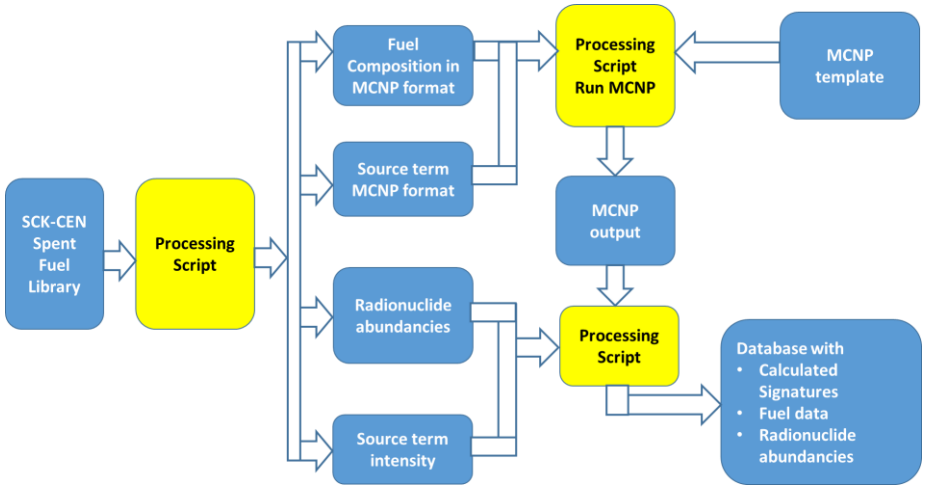

Figure 1: Overview of the methodology to generate simulated observables.

2.2. Considered detection systems

Two different types of equipment were considered. The first one is the so-called ForkBall detector [19]. This detector is designed for underwater measurements of SFA and includes features found in the Fork detector such as total neutron counts with fission chambers, total current obtained with ionization chambers and gamma-ray spectra obtained with a Cadmium Zinc Telluride (CZT) detector. The fission and ionization chamber are installed into cavities inside a polyethylene cylindrical arms wrapped with Cd. A variant without Cd was also considered.
The second detection systems implements the Self-Interrogation neutron resonance densitometry (SINRD) technique by carrying out measurements in dry conditions; this system features miniaturized fission chambers in the instrumentation channel of the SFA. The fission chambers are either bare or wrapped by neutron absorbing foils of Cd or Gd; additional details on the technique can be found in [8].

2.2.1. ForkBall detector

Separate simulations were carried out for neutrons and photons. In the neutron simulations for each entry of the SFL we determined the detection efficiency and the net multiplication factor both for the configuration with and without Cd around the polyethylene arms of the detector. The detection efficiency was estimated by multiplying to F4 tally by the (n,f) cross section of ^{235}U and amount of fissile material in the fission chambers (FM treatment).

While the neutrons simulations are straightforward and do not require a variance reduction technique, the gamma simulations associated to the CZT detectors require an ad-hoc procedure. Due to the presence of a shield and collimator used in the ForkBall, standard MCNP simulations are highly inefficient. A special procedure, described in [20], was therefore developed. The procedure splits the photon transport into two simulations. In a first simulation for a photon of given energy, the probability to reach CZT crystal is determined. A second set of simulations is done to determine the intrinsic detector efficiency that is the probability that an incoming photon deposits all its energy in the CZT crystal. These two quantities are then multiplied to obtain the overall full-energy detection efficiency, that is the probability that a photon of a given energy emitted by the fuel results in a full-energy peak in the crystal.
In first approximation, the overall full-energy detection efficiency does not depend on the fuel composition which still largely made up of Uranium and Oxygen. The obtained results are given in Fig. 2.

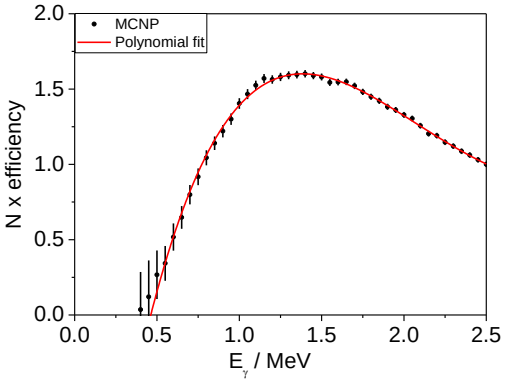

Figure 2: Normalised full-energy detection efficiency for the CZT detector in the Forkball detector.

The net peak count rate *c* due to a gamma ray of energy E_γ emitted by the radionuclide *i* is then given by

$$c(i, E_\gamma) = \varepsilon(E_\gamma) \times M_i \times A_i \times P(i, E_\gamma) \qquad (1)$$

Where

- $\varepsilon(E_\gamma)$ is the overall full-energy detection efficiency
- M_i is the mass of the radionuclide in the SFA
- A_i is its specific activity
- $P(i,E_\gamma)$ is the number of emitted gamma rays of energy E_γ per decay

2.2.2. Self-Interrogation neutron resonance densitometry

For the SINRD technique the response of different types of fission chambers in the instrumentation channel of the SFA was simulated by multiplying the F4 tally by the (n,f) cross section of the active material and amount of fissile material in the fission chambers (FM treatment). The presence of shielding material was also accounted for by the FM treatment. Table 1 gives the details of the modelled detectors; more details on the choice of detectors and filters thickness are given in [8].

Active material	Filter	Energy cutoff
^{238}U	---	---
^{235}U	---	---
^{235}U	1 mm Cd	~ 1 eV
^{239}Pu	0.1 mm Gd	~ 0.1 eV
^{239}Pu	1 mm Cd	~ 1 eV

Table 1: Active materials and filters for SINRD.

As indicated in [8], the chosen signatures are sensitive both to 239Pu and 235U in the fuel.

2.3. Data processing and results

The MCNP calculations provide observables (tallies) that are usually expressed per simulated source particles. To express the observables in absolute terms one has to take into account the source strength associated to the considered spent fuel element. This information is retrieved from the SFL and the value of the observable is determined for the considered case. Overall a database of observables and spent fuel characteristics is generated. Within the database other calculated information on the spent fuel is also included such as the content of fissile material and the multiplication factor. An excerpt of the database content is shown in Table 2.

BU	IE	CT	Neutron with Cd	Counts without Cd	SINRD	FAST/TH	CZT $^{134}Cs_1$	^{137}Cs	$^{134}Cs_2$	^{154}Eu
GWd/t_{HM}	%	y	cps	cps			cps	cps	cps	cps
5	2	5	1.0	1.2	0.026	0.009	22.2	425.2	38.4	3.2
10	2	5	6.3	6.9	0.031	0.010	88.3	847.3	153.2	12.9
15	2	5	31.3	34.4	0.037	0.009	187.3	1263.6	324.9	28.9
20	2	5	109.8	123.6	0.038	0.009	324.4	1677.7	562.7	51.2
25	2	5	284.2	317.0	0.041	0.009	485.4	2088.6	841.8	76.2
30	2	5	600.9	652.3	0.044	0.010	647.8	2490.3	1123.5	102.4
35	2	5	1088.2	1159.4	0.046	0.010	841.1	2893.2	1458.7	130.5
40	2	5	1711.4	1877.6	0.046	0.010	1041.0	3292.0	1805.4	157.4
45	2	5	2568.7	2793.7	0.047	0.010	1213.6	3679.9	2104.7	182.9
50	2	5	3559.5	3912.6	0.049	0.010	1420.1	4071.4	2462.8	208.8
55	2	5	4813.7	5240.8	0.049	0.010	1621.7	4459.6	2812.4	232.2

Table 2: Excerpt of the database. The signatures $^{134}Cs_1$ and $^{134}Cs_2$ denote the net peak areas at 605 keV and 796 keV respectively.

3. Neural network analysis

3.1. The use of Artificial Neural Networks as function approximators

Artificial neural networks (ANN) denote a class of computational models that emulate the functioning of the biological brain, by using a number of interconnected neural units (shortly, neurons or nodes). They have been widely used in machine learning and data mining, in particular owing to their capacity to work as universal function approximators, provided certain conditions are met by the network architecture [21].

An ANN can be described as a network in which each node *i* processes the *n* input units it is connected to through an activation function f_i :

$$y_i = f\left(\sum_{j=1}^{n}(w_{ij} \cdot x_j - \theta_i)\right) \qquad (2)$$

where y_i is the output of neuron *i*, $x_j$is the *j*-th input to node *i*, w_{ij} is the weight of the connection between input *j* and node *i,* and θ_i is the threshold (or bias) of the node.

Neural networks have a layer for input neurons, a layer for output neurons, and one or more inner layers of neurons, also called hidden layers. Leshno et al. [21] proved that a standard multilayer feedforward (i.e. without feedback loops) ANN with a locally bounded piecewise continuous and non-polynomial activation function can approximate any continuous function with any degree of accuracy. Feedforward networks used for function approximation problems have one or more hidden layers of nodes with non-linear activation functions (e.g. sigmoid) followed by an output layer of nodes with linear activation functions. This multilayer architecture allows the network to learn nonlinear relationships between input and output vectors.

Standard numerical optimisation algorithms can be used to optimise the network's performance function, often taken as the mean square error between the network's output and the network's target (real or simulated values of the function to be approximated). Various, gradient based or Jacobian based, learning algorithms [22] can be applied to adjust the weights and the biases of an ANN in a direction that optimises the performance function of the network. The most simple is the gradient descent algorithm, where the current vector $z^{(k)}$ of weights and biases is updated at each iteration *k+1* based on the current gradient g_k and the learning rate α_k, until the network converges:

$$z^{(k+1)} = z^{(k)} - \alpha_k \cdot g_k \qquad (3)$$

One of the fastest training algorithms for neural networks is the Levenberg-Marquardt optimization method [23], which was used for our application.

3.2 Spent fuel characterisation based on Artificial Neural Networks

In this work, we employ ANN's to explore the use of detector response values to characterize spent fuel in terms of initial uranium enrichment, burnup and cooling time. Simulated data are used to train and test different ANN architectures and learning algorithms. The MATLAB R2016b Neural Network Toolbox [24] was used for all data processing and analysis.

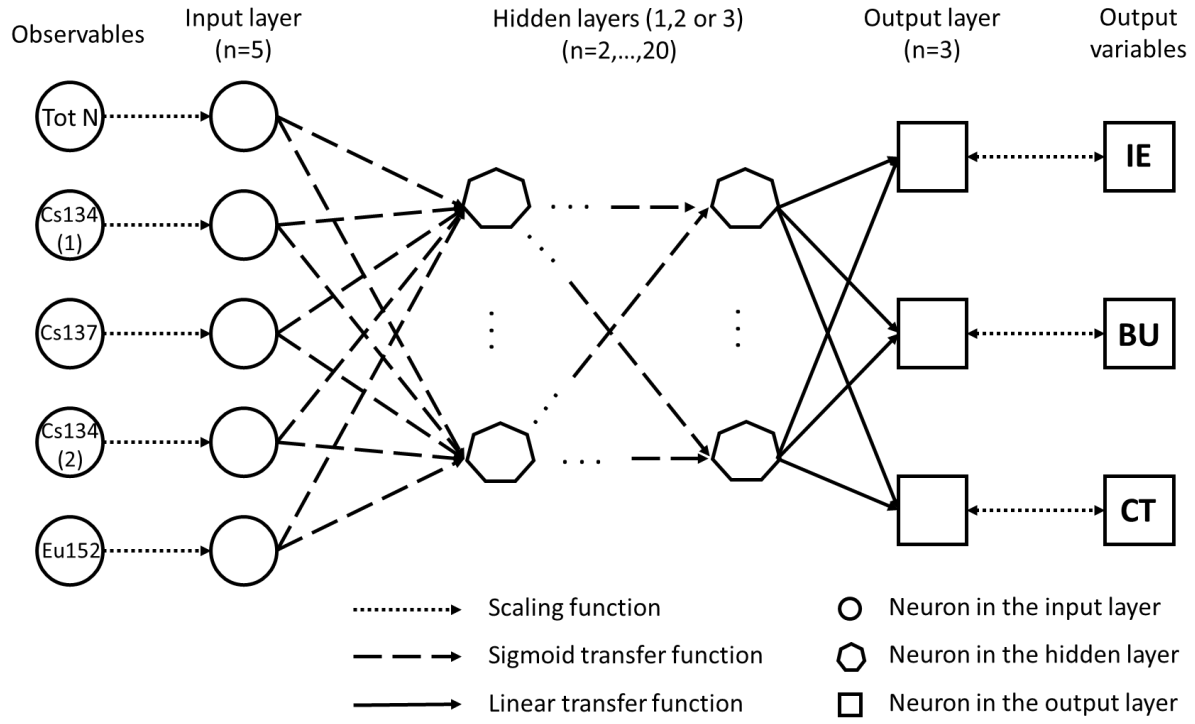

Figure 3: Artificial neural networks architecture implemented in this work.

The implemented ANN architecture is illustrated in Fig. 3. As observables, we considered total neutron counts for a Cd wrapped fission chamber and gamma rays spectroscopy data from ^{137}Cs, ^{134}Cs and ^{154}Eu. These data represent the variables in the input layer of the ANN. The BU, IE and CT represent the variables in the output layer of the ANN. While the BU and IE data were linearly spaced over their range, the CT data spanned several decades and had a logarithmical spacing. The natural logarithm was then taken to ensure that the resulting variable is uniformly distributed over its range. Both the values in the input layer (observable) and the one in the output layer (quantity to be predicted) were scaled between -1 and +1 before being fed to the network optimization algorithm.

The algorithm was tested on a subset of the database described in section 2.3. We considered data with fourteen burnup (BU) values (from 5 to 70 GWd/t$_U$ in steps of 5 GWd/t$_U$), initial enrichment (IE) of between 2.0% and 5.0% in steps of 0.5%, eleven values of cooling time (CT) from 1 day to 100 years. A total of 1078 cases were considered.

For the neurons in the hidden layers we used hyperbolic tangent sigmoid transfer functions whereas for the activation functions for the output neurons were linear. The quantity mean square error (*mse*) was used as target for minimisation. In the used *mse* each squared error contributes with the same importance as follows:

$$mse = \frac{1}{3N}\sum_{j=1}^{3}\sum_{k=1}^{N}\left(A_{k,j,calc} - A_{k,j}\right)^2 \qquad (4)$$

Where $A_{k,j,calc}$ is the value of the parameter as determined by the ANN in the output layer (Fig. 3), $A_{k,j}$ is the nominal value of the parameter. The index *j* runs over the IE, BU and CT output while *k* runs over the part of the database used for training. The calculation of the *mse* is done before the final scaling.

In the future we will define the performance in such a way that the percentage deviation enters in the definition of the quantity to be minimized rather than the absolute deviation. Note that the absolute variation in the logarithm of CT results already in a relative deviation on the CT.

The database of simulated observables and spent fuel characteristics is divided in two sets, corresponding to training and validation. The data in the training set are used to stop training if the network performance on these data fails to improve or remains the same for a predefined number of iterations. The Levenberg-Marquardt algorithm was used for training the network. The neural networks tested used up to three hidden layers.

3.3 Results

First we studied the impact of the number of neurons on the performance, assuming that all data set was used to train the network. The performance was then calculated on the whole database of N=1078 cases. We considered from 2 to 20 neurons per hidden layer, while the number of hidden layers went from one to three. The obtained results indicate that the performance increases in general with the number of neurons per layer and with the number of hidden layers. However, the improvement is marginal above 15 neurons, as shown in Fig. 4.

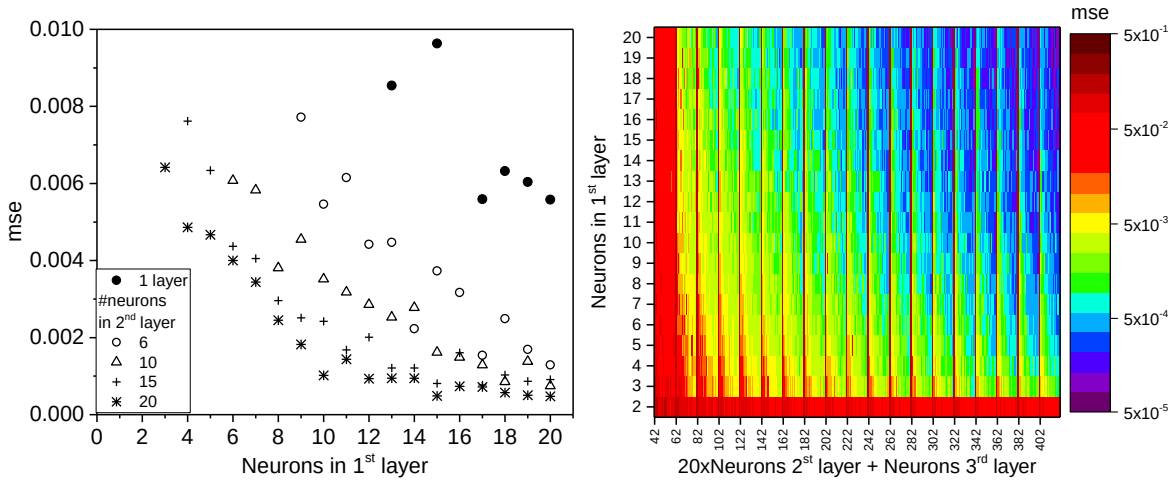

Figure 4: *mse* for ANN with one, two and three hidden layers as a function of the number of neurons. The *mse* in the right figure is limited to a maximum value of 0.01.

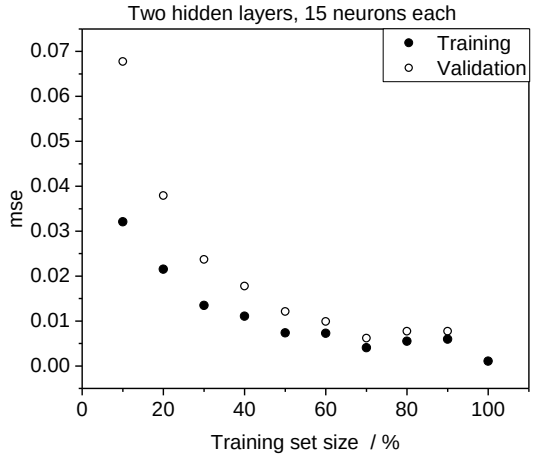

Figure 5: *mse* for ANN with two hidden layers as a function of the training set size. For both hidden layers the number of neurons was set to 15.

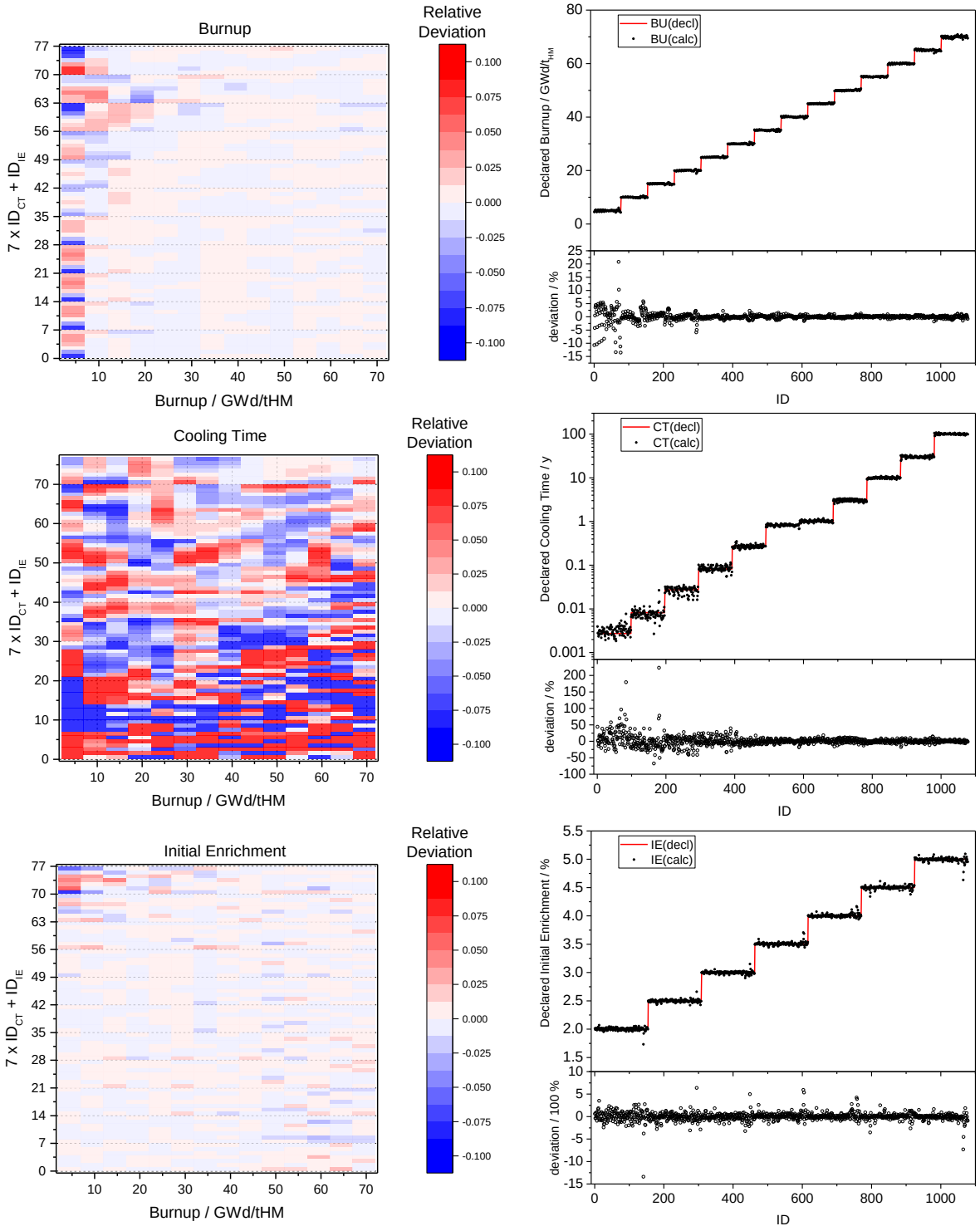

Figure 6: Deviations in the predicted values of BU, IE and CT for the considered cases. The results refer to an ANN with 3 hidden layers and 20 neurons per layer. See the text for explanation.

In addition, we carried out calculations by changing the fraction of data used for training from 10% to 100% in step of 10%. The rest of the data was used for validation. The number of neurons was 5, 10, 15 and 20 and we considered up to three hidden layers; both the performance on the training and the validation set were computed. The assignment of individual data to the training or validation set was done randomly by MATLAB.

In general, we found that the value of the performance changes if the calculation is repeated; this is due to the fact that in the current implementation the initial values of the weights and biases of the ANN are randomly assigned [25] and this is affecting the results. For each network configuration the calculations were repeated 20 times and the average performance was calculated with its standard deviation. For the case in which 100% of the data are used for training, we observed a standard deviation in the *mse* between 12 % and 25%. By reducing the share of the training set, the standard deviations are higher; this is due to the fact that choice of the data used for training is random and changes every time; consequently, the value of the performance is affected. In addition, it was found that also the share of the training and validation data sets is not a fixed number but fluctuates around its nominal values. The resulting spread on the performance should be kept in mind when comparing different performance values.

The performance on the training set was in general better than the performance on the validation set. The difference between them was increasing by reducing the size of the training set, as shown in Fig. 5., and by increasing the number of neurons in the last hidden layer.

In general the performance improves with the size of the training set and there is a clear difference between the performance obtained with 90% and 100% training; however, the improvement is marginal in the range 50% to 90%.

While it is of interest to identify which parameters affect the performance, it is also important to understand how performance values translate into deviation between calculated values and “real” values of BU, IE and CT. In Fig. 6, the % deviation on the value of BU, CT and IE are shown for the ANN with 3 hidden layers and 20 neurons per hidden layer with 100% training. In the plots on the left, the deviations are shown as a function of BU (X-axis) and IE and CT (Y-axis). The Y-axis is an identification number ID that is given by the formula $7 \times ID_{CT} + ID_{IE}$, where ID_{CT} and ID_{IE} range from 1 to 11 and 1 to 7 respectively and uniquely identify the case of CT and IE to which they refer. For the plots on the right the deviations are given as a function of an arbitrary case identified number (ID) that is used for a more straightforward representation; for each variable (BU, CT, IE) the ID is chosen such that the corresponding declared variable is monotonically increasing.

The results indicate that if 20 neurons and 100% of the data are used for training the ANN is capable of reproducing the value of BU within 3% for 96% of the cases, the value of IE within 2% for 98% of the cases and the value of CT within 10% for 87% of the cases. In a more realistic case, where only 50% of the data are used for training, the ANN is capable of reproducing the value of BU within 3% for 85% of the cases, the value of IE within 2% for 80% of the cases and the value of CT within 10% for 58% of the cases.

The reason why we obtain larger deviation on the CT when compared to BU and IE is not clear. The larger deviations at low value of CT can be related to the choice of observables which are less sensitive to CT smaller than 1 y.

4. Conclusions and outlook

In this work we first reported about a methodology developed to simulate detector response functions for different types of NDA instruments. A database of detector responses for 8400 cases with different fuel characteristics and irradiation parameters was then obtained. The use of the simulated observables as input for data analysis algorithms aims at uniquely characterizing the spent fuel and drawing safeguards conclusions. We explored the application of artificial neural networks due to their ability to generalize non-linear relationships on a subset of data corresponding to cooling times smaller than 100 years.

We studied the network performances in terms of mean square error as a function of the number of hidden layers, number of neurons in each hidden layer and share of the training data set. We could conclude that, within the range considered, the performances increase with the number of neurons, number of hidden layers and share of the training data set. The results show that, when all the data set is used for training, the ANN is able to predict the BU and IE within a few percent for most of the analysed cases, whereas CT is predicted with a larger deviation especially for values lower than 1y. The performance is significantly worse when a fraction lower than 50 % of the data set is used for training the ANN.

Future research will focus on improving the performance of the network with respect to the CT. In particular, we will investigate the possibility to selectively use data for training rather than randomly choose the data. We will investigate the impact of the initial weight values. We will also try to identify which additional observables (for instance the SINRD signatures) would result in an improvement of the performance. The impact of the range values of burnup, initial enrichment and cooling time on the performance will also be studied. The use of different performance functions will also be considered.

5. Legal matters

5.1. Privacy regulations and protection of personal data

"I agree that ESARDA may print my name/contact data/photograph/article in the ESARDA Bulletin/Symposium proceedings or any other ESARDA publications and when necessary for any other purposes connected with ESARDA activities."

5.2. Copyright

The authors agree that submission of an article automatically authorises ESARDA to publish the work/article in whole or in part in all ESARDA publications – the bulletin, meeting proceedings, and on the website.

The authors declare that their work/article is original and not a violation or infringement of any existing copyright.

6. References

[1] D. Reilly, N. Ensslin, H. Smith Jr. and S. Kreiner, *Passive Nondestructive Assay of Nuclear Materials*, NUREG/CR-5550, LA-UR-90-732, 1991

[2] *Coordinated Technical Research Meeting on Spent Fuel Verification Methods*, IAEA March 3-6 2003

[3] S. Tobin, H. Menlove, M. Swinhoe, M. Schear, *Next Generation Safeguards Initiative research to determine the Pu mass in spent fuel assemblies: Purpose, approach, constraints, implementation, and calibration*, Nuclear Instruments & Methods In Physics Research Section A, 2011, doi 10.1016/j.nima.2010.09.064

[4] Park W. S., et al., 2014. *"Safeguards by design at the encapsulation plant in Finland"*. Proceedings of the 2014 IAEA safeguards symposium.

[5] European Council Decision 2006/976/Euratom of 19 December 2006

[6] IGD-TP Implementing Geological Disposal of Radioactive Waste Technology Platform Strategic Research Agenda, www.igdtp.eu/index.php/documents/doc_download/14-strategic-research-agenda, 2011, ISBN 978-91-979786-0-6,

[7] Borella A., et al., *Spent Fuel Measurements with the Fork Detector at the Nuclear Power Plant of Doel*, 33rd ESARDA Annual Meeting, Budapest, Hungary, May 16-20 2011

[8] R. Rossa, *Advanced non-destructive methods for criticality safety and safeguards of used nuclear fuel,* PhD thesis at Université libre de Bruxelles, September 2016.

[9] S. Tobin et al., *Research into Measured and Simulated Nondestructive Assay Data to Address the Spent Fuel Assay Needs of Nuclear Repositories*, In: Proc. 57rd INMM Annual Meeting, Atlanta, Georgia, United States, 2016

[10] A. Borella, et al., *Extension of the SCK•CEN spent fuel inventory library*, 37th ESARDA Annual Meeting, 2015

[11] M.H. Kalos and P.A. Whitlock, Monte Carlo Methods. Volume I: Basics, John Wiley & Sons, NY 1986.

[12] S.M. Bowman , O.W. Hermann, L.C. Leal, C.W. Parks, ORIGEN-ARP, A Fast and Easy-to-Use Source Term Generation Tool, ORNL/CP-104231, Oak Ridge 1999

[13] I. Germina, et al. *Overview of ORIGEN-ARP and its Application to VVER and RBMK*. Oak Ridge National Laboratory, Oak Ridge, TN, 2007

[14] I. Gauld, S. Bowman, J. Horwedel, *Origen-ARP: automatic rapid processing for spent fuel depletion, decay, and source term analysis,* ORNL/TM-2005/39. January 2009

[15] A. Stankovskiy, G. van den Eynde *ALEPH 2.2 A Monte Carlo Burn-up Code,* SCK•CEN-R-5267, September 2012

[16] R. Rossa., et al., *Development of a reference spent fuel library of 17x17 PWR fuel assemblies*, ESARDA BULLETIN, No. 50, December 2013

[17] A. Borella, M. Gad, R. Rossa, K. van der Meer, *Sensitivity Studies on the Neutron Emission of Spent Nuclear Fuel by Means of the Origen-ARP Code*, In: Proceeding of the 55th INMM Annual Meeting, Atlanta, Georgia, United States, July 2014.

[18] MCNP6 Users Manual - Code Version 6.1.1 beta, LA-CP-14-00745, June 2014.

[19] A. Borella, et al., *Advances in the Development of a Spent Fuel Measurement Device in Belgian Nuclear Power Plants*.- In: Symposium on International Safeguards, Linking Strategy, Implementation and People, Book of Abstracts, Presentations and Papers, 2014, IAEA, Vienna, Austria, p. 272

[20] A. Borella, et al., *A Method To Determine Detector Response Functions In A Heavily Shielded Environment And Application To Spent Fuel Measurements With Cadmium Zinc Telluride Detectors*, In: MC2015 - Joint International Conference on Mathematics and Computation (M&C),Supercomputing in Nuclear Applications (SNA) and the Monte Carlo (MC) Method, Nashville, United States, 2015

[21] Leshno, M., Lin, V. Y., Pinkus, A., & Schocken, S., *Multilayer feedforward networks with a nonpolynomial activation function can approximate any function*, Neural networks, 6(6):861-867, 1993.

[22] Hagan M.T., Demuth H.B., Beale M.H., *Neural Network Design*, Boston, MA: PWS Publishing, 1996.

[23] Hagan, M.T., and M. Menhaj, *Training feed-forward networks with the Marquardt algorithm*, IEEE Transactions on Neural Networks, Vol. 5, No. 6, 1999, pp. 989–993, 1994.

[24] https://www.mathworks.com/products/neural-network.html

[25] MATLAB documentation, *init* function

Detection of fuel pins diversion with the self-indication neutron resonance densitometry technique

R. Rossa[1], A. Borella[1], P.-E. Labeau[2], N. Pauly[2], K. van der Meer[1]

1) SCK•CEN, Belgian Nuclear Research Centre, Boeretang, 200, B2400 Mol, Belgium

2) Université libre de Bruxelles, Avenue F.D. Roosevelt, 50, B1050 Brussels, Belgium

Email: rrossa@sckcen.be

Abstract

The verification of spent fuel assemblies is among the activities conducted during the safeguards inspections, and several non-destructive assay techniques are being developed to improve the accuracy of existing methods. Among other techniques, the self-indication neutron resonance densitometry (SINRD) relies on the passive neutron emission from the spent fuel assemblies. Previous research conducted at SCK•CEN found that the optimal configuration was obtained with the fuel kept in air and surrounded by a polyethylene slab.

The SINRD technique was proposed mainly for the direct quantification of the ^{239}Pu mass in spent fuel, whereas this contribution is focused on the potential to detect the diversion of fuel pins from a spent fuel assembly. First, the detector responses of several fission chambers placed in the guide tubes of a PWR 17x17 fuel assembly were calculated with the Monte Carlo code MCNPX. Different fissile material coatings (e.g. ^{239}Pu, ^{238}U) were taken into account to consider detectors mostly sensitive to thermal and fast neutrons. In addition, the response to ionization chambers was modelled for the detection of gamma-rays. Fuel assemblies with material compositions corresponding to different initial enrichment, burnup, and cooling time were modelled to evaluate the sensitivity of the detector responses to the fuel irradiation history.

The detector responses were calculated also for several diversion scenarios where fuel pins from a complete fuel assembly were replaced with dummies made of stainless steel. The diversions ranged from 15% to 50% of the total pins. The detector responses obtained from the diversion cases were compared to the values for the complete fuel assemblies to determine the capability of SINRD to detect the diversion of fuel pins. Promising results were obtained by combining the responses of the different detector types.

Keywords: SINRD, spent fuel, NDA, partial defect, Monte Carlo

1 Introduction

The technical objective of nuclear safeguards is to ensure the detection of the diversion of nuclear material from peaceful applications to the manufacture of nuclear weapons (IAEA, 1972).

Safeguards inspections are carried out by the International Atomic Energy Agency (IAEA) in the countries signatories of the Non-Proliferation Treaty (NPT) (IAEA, 1970). Since most of nuclear material placed under safeguards is in the form of spent fuel, the verification of this material is of major interest for the IAEA (IAEA, 2013).

However, the measurement of spent fuel presents many challenges due to its very high radiation emission and decay heat. Currently the spent fuel verification is performed with non-destructive assay (NDA) techniques such as the digital Cherenkov viewing device (DCVD) (Chen et al., 2003), (Chen et al., 2009), (Branger et al., 2014), the spent fuel attribute tester (SFAT) (Arit et al., 1995), (Honkamaa et al., 2003), and the Fork detector (Rinard et al., 1988), (Borella et al., 2011). In addition, many other NDA techniques are under development to improve the accuracy of the verification (Tobin et al., 2011).

This contribution is focused on the capabilities of the self-indication neutron resonance densitometry (SINRD) (Menlove et al., 1969) for the detection of diversion from a spent fuel assembly. The basic principle of SINRD is described with the Monte Carlo models used in the study. Then the overview of the simulations is given, considering both complete fuel assemblies and diversion scenarios, and the capabilities of SINRD for this application are discussed. Finally the conclusion are presented with an outlook on future research.

2 Description of the SINRD technique

The self-indication neutron resonance densitometry is a non-destructive assay technique that relies on the passive neutron emission of spent nuclear fuel (LaFleur, 2011), (LaFleur et al., 2015), (Rossa et al., 2015), (Rossa, 2016).

The basic principle of SINRD is described in Figure 1. The total cross-section for neutron-induced reaction of ^{239}Pu is plotted with the transmission of a neutron flux through samples containing different percentages of ^{239}Pu. The transmission values were calculated with Monte Carlo simulations considering a sample of ^{239}Pu with density and dimensions equal to a PWR fuel pin. It is evident from the figure that the attenuation of the neutron flux is related to the amount of ^{239}Pu in the sample. The SINRD technique aims at measuring the attenuation of the neutron flux around the 0.3 eV region due to the presence of ^{239}Pu in the fuel assembly. The neutron detection in the 0.3 eV region is enhanced by using a fission chamber with ^{239}Pu as fissile material, according to the self-indication principle (Fröhner et al., 1966).

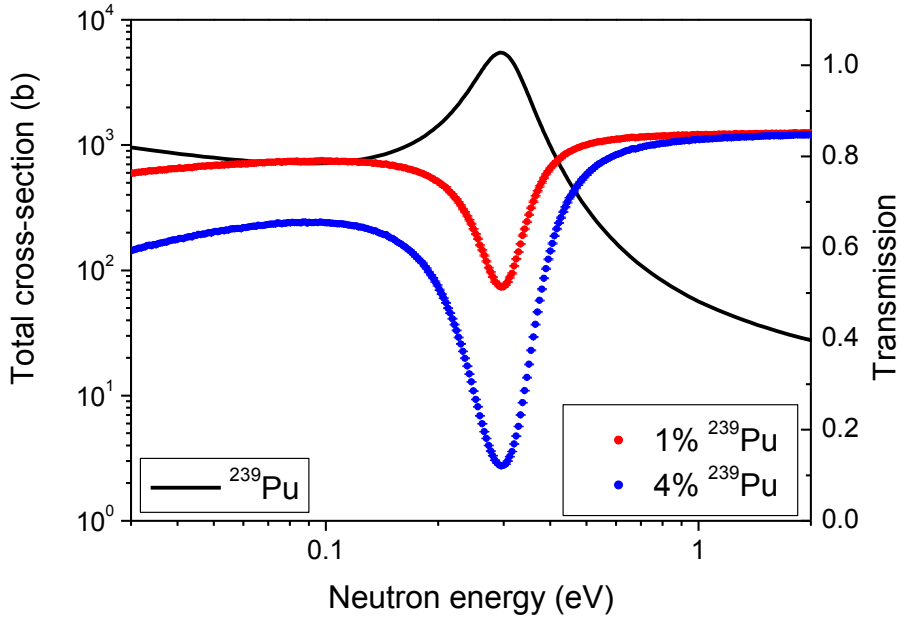

Figure 1: *Total cross-section of ^{239}Pu and transmission of a neutron flux through samples containing ^{239}Pu. The cross-section values were obtained from the ENDF/B-VII.0 data library, whereas the transmission was calculated with Monte Carlo simulations.*

The neutron flux in the 0.3 eV energy region is estimated with SINRD by taking the difference between the neutron counts of two ^{239}Pu fission chambers. One detector is covered by a thin Gd filter, whereas the other detector is covered by a Cd filter. These materials were chosen because they have a cutoff in the neutron absorption below and above 0.3 eV, respectively.

In addition, the thermal neutron flux and fast neutron flux were estimated in this work by calculating the response of a bare ^{239}Pu fission chamber and ^{238}U fission chamber, respectively.

The approach for the study of the SINRD technique was extended in this paper by calculating the response of ionization chambers for the detection of gamma-rays. The multiple insertion of neutron and gamma-ray detectors in a fuel assembly was proposed for the PDET detector (Ham et al., 2009), (Ham et al., 2015), and can be beneficial also for the SINRD technique.

3 Model developed for the study

3.1 Monte Carlo model

The capability of SINRD for the detection of partial defects was investigated in this article with Monte Carlo simulations. The Monte Carlo code MCNPX v.2.7.0 (Pelowitz, 2011) was used to simulate a PWR 17x17 fuel assembly stored in air and surrounded by a 12-cm slab of polyethylene to ensure neutron moderation. The model of the fuel assembly is shown in Figure 1. The fuel geometry chosen for the simulation contains 264 fuel pins and 25 guide tubes. These are used for the insertion of control rods during the reactor operation and provide enough room for neutron or gamma-ray detectors once the fuel is discharged.

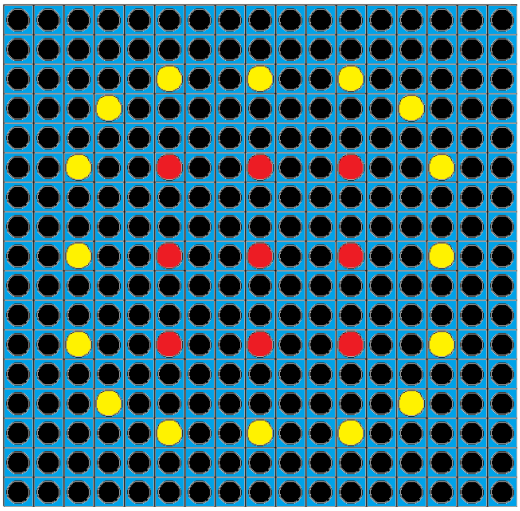

Figure 2: *MCNPX model of the fuel assembly used for the study. The fuel pins are depicted in black, the peripheral guide tubes in yellow, and the central guide tubes in red.*

3.2 Calculation of the neutron detectors counts

The total counts of the neutron detectors (N_{bare}) were calculated with Formula (1) as the product between the coefficient C_N, the incoming neutron flux (φ_N) and the microscopic cross-section (σ_{DET}) of the active material in the detector itself. The coefficient C_N was calculated with Formula (2) as the product between the amount of fissile material in the detector (n_{fiss}), the total neutron emission from the spent fuel assembly (N_E), and the measurement time (t). The Photonis CFUE43 fission chamber (Photonis, 2017) was taken as reference design, but the active length was increased to 2 m to obtain a fissile material mass of 263.89

mg (Rossa, 2016). The total neutron emission was taken from the reference spent fuel library (Rossa et al., 2013), whereas the measurement time was set to one hour.

The neutron flux (φ_N) and the microscopic cross-section (σ_{DET}) included in Formula (1) are a function of the incoming neutron energy E_N. The neutron flux was obtained from the MCNPX simulations and accounts also for the multiplication effect. The cross-section values were taken from the ENDF/B-VII.0 nuclear data library (Chadwick, 2006) and averaged over 600 logarithmically-interpolated energy bins between 10^{-9} and 20 MeV. The fission cross-sections of ^{239}Pu and ^{238}U were used to model detectors sensitive mainly to thermal and fast neutrons, respectively.

$$N_{bare} = C_N \int_{E_N} \varphi_N(E_N)\ \sigma_{DET}(E_N)\ dE_N \qquad (1)$$

$$C_N = n_{fiss}\ N_E\ t \qquad (2)$$

The presence of a thin Gd or Cd filter around the ^{239}Pu fission chamber was accounted for with Formula (3), where n_{fil} and σ_{fil} are the atom density and cross-section of the filter.

$$N_{fil} = C_N \int_{E_N} \varphi_N(E_N)\ \sigma_{DET}(E_N)\ e^{-n_{fil}\sigma_{fil}(E_N)}\ dE_N \qquad (3)$$

The neutron counts in the energy region close to 0.3 eV were calculated as the difference between the counts of two fission chambers, one covered by a Gd filter and one covered by a Cd filter.

The uncertainty of the neutron counts for the different detectors was estimated as the square root of the corresponding neutron count.

3.3 Calculation of the gamma-ray detectors response

The gamma-ray detector response (P) was calculated with Formula (4) as the product between the coefficient C_P, the gamma-ray flux (φ_P) and the response function of the detector (f_{DET}). The coefficient C_P is the product between the total photon emission from the spent fuel assembly and the measurement time. The total photon emission was taken from (Rossa et al., 2013) and the measurement time was set to one hour as for the neutron measurements.

The photon flux (φ_P) and response function (f_{DET}) were obtained from MCNPX simulations and are function of the incoming gamma-ray energy E_γ. The photon flux was calculated in the guide tubes with the model of the spent fuel described in Section 3.1, whereas the response function was obtained by modelling the detector alone as an aluminum cylinder filled with nitrogen. The transport of both photons and electrons was simulated to obtain the response function (f_{DET}), which was calculated as the energy deposition tally (F6 type) in the gas-filled cavity. The energy range of the source term was divided into 23 bins from 50 keV to 5 MeV, and separate simulations were performed defining the source with a uniform histogram distribution over a single energy bin.

$$P = C_P \int_{E_\gamma} \varphi_P(E_\gamma)\ f_{DET}(E_\gamma)\ dE_\gamma \qquad (4)$$

The statistical uncertainty of the gamma-ray detector response was neglected since ionization chambers are normally operated in current mode and reach a stable signal well within the considered measurement time.

4 Overview of the performed simulations

4.1 Complete fuel assemblies

The simulations performed for this study considered both complete fuel assemblies and assemblies with diverted pins. In the case of a complete fuel assembly the fuel pins are identical in material composition and source strength, and these characteristics were taken from the reference spent fuel library (Rossa et al., 2013), (Borella et al., 2015). The sensitivity of the detector responses to the fuel irradiation history was evaluated by considering fuel assemblies with material composition and source strength corresponding to:

- initial enrichments: 2.0, 2.5, 3.0, 3.5, 4.0, 4.5, and 5.0%;
- burnup: 5, 10, 15, 20, 30, 40, and 60 GWd/t_{HM}.

4.2 Diversion scenarios

In the diversion cases the fuel pins were replaced by dummies made of stainless steel with the same dimensions of a fuel pin. The diversion scenarios are shown in Figure 3 and the replaced pins were between 50% and 15% of the fuel pins in a fuel assembly. The diversion scenarios were symmetrical since it resulted from previous work as the most challenging pattern to detect (Sitaraman et al., 2009), (Rossa, 2016).

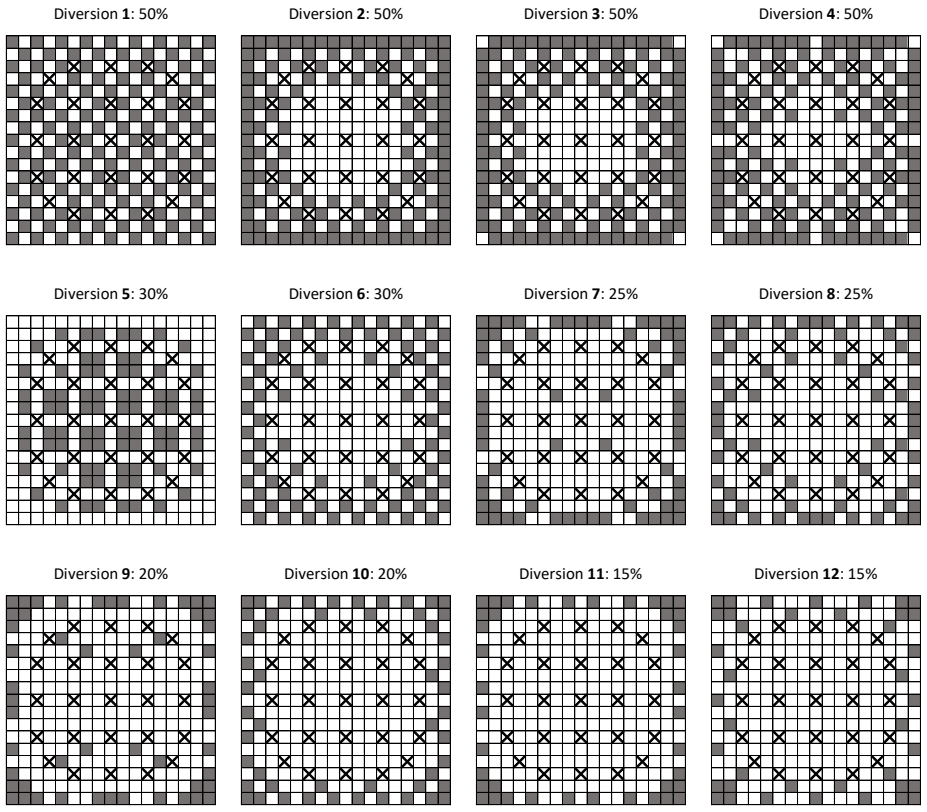

Figure 3: *Overview of the diversion scenarios. The fuel pins are depicted in white, the dummy pins in grey, and the guide tubes with crosses.*

For the simulations with the diversion scenarios the fuel pins had a material composition and source strength corresponding to fuel with:

- 2% initial enrichment and 30 GWd/t_{HM} burnup;
- 3.5% initial enrichment and 10, 30, or 60 GWd/t_{HM} burnup;
- 5% initial enrichment and 30 GWd/t_{HM} burnup.

In all simulations included in this contribution the fuel pins had a cooling time of 5 years.

5 Results

5.1 Complete fuel assemblies

For each simulations in this study the detectors responses calculated according to the approach described in Sections 3.2 and 3.3 were normalized to the value obtained in the central guide tube. In addition, the guide tubes were divided for this study into 16 peripheral and 9 central guide tubes depending on the geometrical location in the fuel assembly. The two groups are identified in Figure 1 by different colors. The average detector responses were calculated in the two guide tubes groups.

The average detector responses obtained in the cases with complete fuel assemblies were used to establish a reference band associated to each type of detector response (i.e. thermal neutrons, resonance region neutrons, fast neutrons, gamma-rays). The low and high boundaries are reported in Table 1 for the nine central guide tubes and for the sixteen peripheral guide tubes. In order to obtain the low boundaries for the neutron detectors in Table 1, the minimum detector responses obtained in the whole set of complete fuel assemblies were further decreased by the 1-σ value to account for uncertainty. Similarly the high boundaries were obtained by increasing by 1-σ the maximum values obtained for each detector type. The boundaries for the gamma-ray detector were taken as the minimum and maximum detector responses obtained in the whole set of complete fuel assemblies.

Both boundaries for thermal and resonance region neutrons are lower for the central guide tubes compared to the peripheral guide tubes, whereas the opposite occurs for fast neutrons and gamma-rays. In general the width of the reference band is larger for peripheral guide tubes compared to central guide tubes, and it is significantly larger for neutron than for gamma-ray detectors.

Table 1: *Normalized detector responses calculated for the complete fuel assemblies for thermal neutrons, neutrons around the 0.3 eV region, fast neutrons, and gamma-rays. The low and high boundaries are given for the nine central guide tubes and the sixteen peripheral guide tubes.*

	Central guide tubes		Peripheral guide tubes	
	Low boundary	High boundary	Low boundary	High boundary
Thermal neutrons	1.153	1.263	1.695	2.298
Resonance region neutrons	1.122	1.271	1.576	2.290
Fast neutrons	0.862	1.090	0.802	0.977
Gamma-rays	0.985	0.987	0.904	0.912

5.2 Diversion scenarios

The average detector responses obtained for the diversion scenarios were compared to the reference bands shown in Table 1, and the values that fell outside these bands signaled possible diversion cases. Figures 4-7 show the normalized detector responses calculated for the diversion scenarios for the different

detector types. The results are the average values for the nine central guide tubes and for the sixteen peripheral guide tubes.

The results for the thermal neutron detectors show that most of the diversion cases fall within the reference band of the complete fuel assemblies. Only for diversion with fuel with 5% initial enrichment the detector responses are above the high boundaries both for central and peripheral guide tubes.

Considering the detectors measuring neutrons around the 0.3 eV resonance region (Figure 5), most of the diversions with fuel assemblies with initial enrichment of 5% fall outside the reference band. In addition, also some scenarios with 50% of replaced pins from fuel with 3.5% initial enrichment and burnup larger than 30 GWd/t have values above the reference band.

The results for the fast neutron detectors show that for all diversion scenarios the average values for the central guide tubes are within the reference band. The average detector responses for the peripheral guide tubes are lower than the reference band for some scenarios with 50% and 30% of replaced pins. In all cases there is not a significant difference due to the fuel irradiation history.

Figure 7 shows that for all diversion scenarios the average responses of the gamma-ray detectors are outside the reference band of the complete fuel assemblies. The peripheral guide tubes are the most affected by the replacement of fuel pins. As in the case of fast neutron detectors, the irradiation history of the fuel assembly does not influence significantly the results. By comparing the different detector types, the gamma-ray detectors show a larger variation due to the fuel pins diversion compared to the neutron detectors.

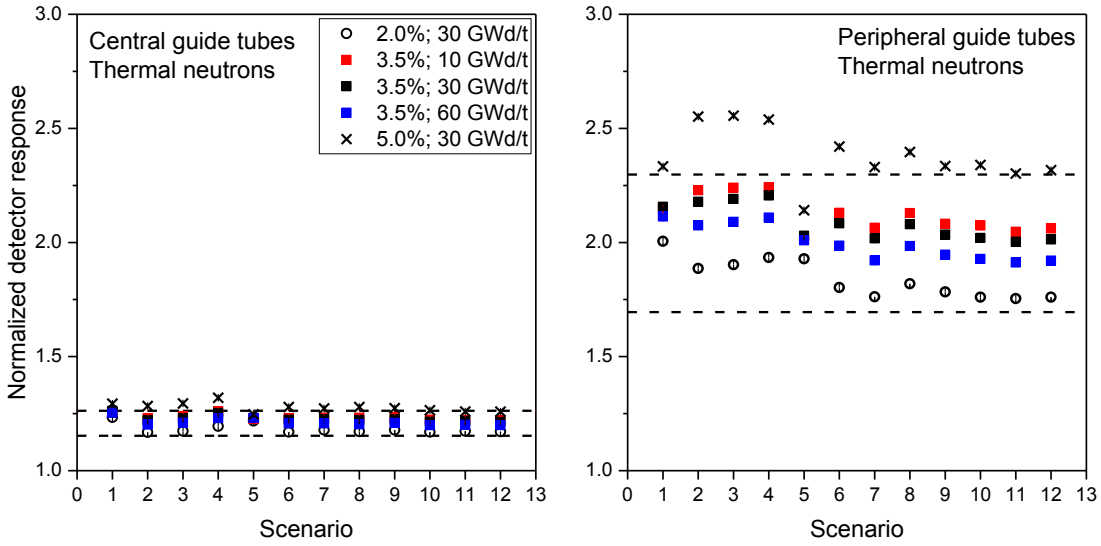

Figure 4: *Normalized detector responses for thermal neutrons in the different diversion scenarios. The average value for central guide tubes (left), and peripheral guide tubes (right) are shown. The lower and upper boundaries for the cases with complete fuel assemblies are also reported.*

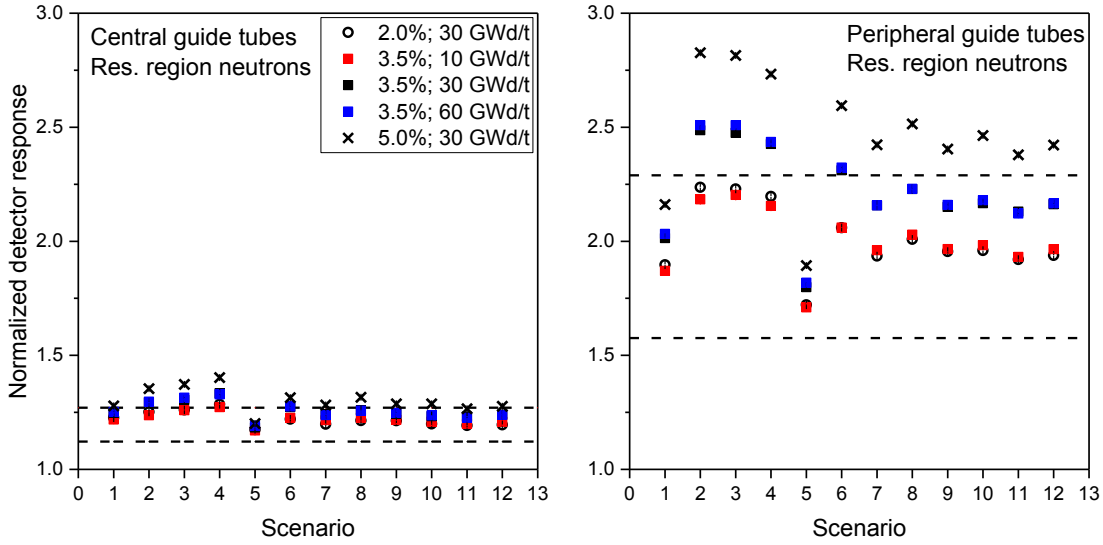

Figure 5: *Normalized detector responses for neutrons around the 0.3 eV resonance region in the different diversion scenarios. The average value for central guide tubes (left), and peripheral guide tubes (right) are shown. The lower and upper boundaries for the cases with complete fuel assemblies are also reported.*

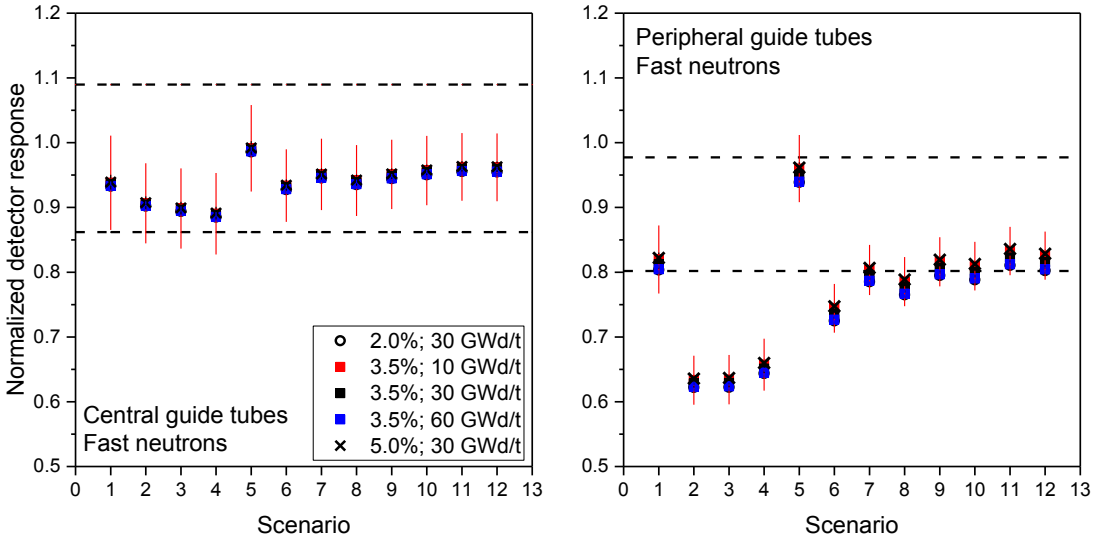

Figure 6: *Normalized detector responses for fast neutrons in the different diversion scenarios. The average value for central guide tubes (left), and peripheral guide tubes (right) are shown. The lower and upper boundaries for the cases with complete fuel assemblies are also reported.*

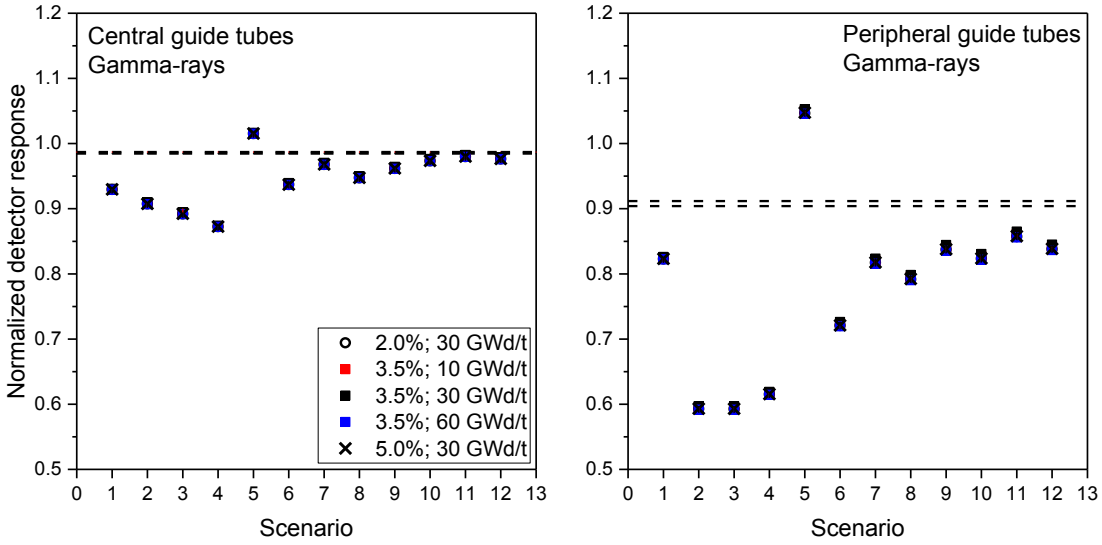

Figure 7: *Normalized detector responses for gamma-rays in the different diversion scenarios. The average value for central guide tubes (left), and peripheral guide tubes (right) are shown. The lower and upper boundaries for the cases with complete fuel assemblies are also reported.*

6 Conclusions

The capabilities of SINRD to detect the diversion of fuel pins from a complete assembly were investigated in this paper. The neutron and gamma-ray fluxes were estimated in the guide tubes of a PWR fuel assembly to mimic the use of multiple detectors during the measurements. The response of detectors sensitive mainly to thermal neutrons, neutrons with energy around 0.3 eV, fast neutrons, and gamma-rays were considered.

A first series of simulations concerned complete fuel assemblies with different irradiation histories to estimate the influence of initial enrichment, burnup, and cooling time on the detector responses. The results from the complete fuel assemblies were used to identify a reference band of values obtained for complete fuel assemblies. The values calculated for the diversion scenarios were then compared with the reference bands of each detector type, and the values that fell outside the reference bands were an indication of diversion.

The peripheral guide tubes in almost all scenarios were the most affected by the fuel pins diversion and were outside the reference bands for multiple detector types. For all diversion scenarios the average gamma-ray detector response for the guide tubes was outside the reference band, whereas for some diversion cases with 50% and 30% of replaced pins also the values for neutron detectors were outside the reference bands. Overall the gamma-ray detectors showed a larger change due to the diversion of pins compared to the neutron detectors.

Future work will continue the assessment of the SINRD technique for the detection of fuel pins diversion by considering additional diversion scenarios and other approaches to the data analysis. The comparison among different NDA techniques for the same diversion scenarios is also foreseen.

7 Legal matters

7.1. Privacy regulations and protection of personal data

"I agree that ESARDA may print my name/contact data/photograph/article in the ESARDA Bulletin/Symposium proceedings or any other ESARDA publications and when necessary for any other purposes connected with ESARDA activities."

7.2. Copyright

The authors agree that submission of an article automatically authorises ESARDA to publish the work/article in whole or in part in all ESARDA publications – the bulletin, meeting proceedings, and on the website. The authors declare that their work/article is original and not a violation or infringement of any existing copyright.

References

Arit R., et al., 1995. "SFAT in physical inventory verification of spent LWR fuel". Proceedings of the 17th ESARDA annual meeting.

Borella A., et al., 2011. "Spent fuel measurements with the Fork detector at the nuclear power plant of Doel". Proceedings of the 33rd ESARDA annual meeting.

Borella A., et al., 2015. "Extension of the SCK•CEN reference spent fuel inventory library". Proceedings of the 37th ESARDA annual meeting.

Branger E., et al., 2014. "Improved DCVD assessments of irradiated nuclear fuel using image analysis techniques". Proceedings of the 2014 IAEA safeguards symposium.

Chadwick M. B., et al., 2006. "ENDF/B-VII.0 next generation evaluated nuclear data library for science and technology". Nuclear data sheets, volume 107, issue 12.

Chen J. D., et al., 2003. "Cherenkov characterization of BWR assemblies using a prototype DCVD with a back-illuminated CCD". Report prepared for the Canadian safeguards support program and the Swedish support program (CSSP Report 2004-01-01, SKI Report ISRN SKI-R-03/45).

Chen J. D., et al., 2009. "Partial defect detection in LWR spent fuel using a digital Cerenkov viewing device". Proceedings of the 50th INMM annual meeting.

Fröhner F. H., et al., 1966. "Accuracy of Neutron Resonance Parameters from Combined Area and Self-Indication Ratio Measurements". Proceedings of the Conference on Neutron Cross Section Technology, P. Hemmig (ed.), CONF-660 303, Washington D.C. (1966) Book 1, pp. 55-66.

Ham Y. S., et al., 2009. “Development of a safeguards verification method and instrument to detect pin diversion from pressurized water reactor (PWR) spent fuel assemblies phase I study”. Lawrence Livermore National Laboratory technical report LLNL-TR-409660.

Ham Y. S., et al., 2015. “Partial defect verification of spent fuel assemblies by PDET: principle and field testing in interim spent fuel storage facility (CLAB) in Sweden”. Proceedings of the 2015 ANIMMA conference.

Honkamaa T., et al., 2003. “How STUK verifies spent nuclear fuel - and why?” Proceedings of the 25th ESARDA annual meeting.

International Atomic Energy Agency (IAEA), 1972. “The structure and content of agreements between the Agency and States required in connection with the treaty on the nonproliferation of nuclear weapons”. INFCIRC/153 (corrected).

International Atomic Energy Agency (IAEA), 1970. “Treaty on the non-proliferation of nuclear weapons”. INFCIRC/140.

International Atomic Energy Agency (IAEA), 2013. “IAEA department of safeguards long term R&D plan, 2012-2023”. STR-375.

LaFleur A. M., 2011. “Development of self-interrogation neutron resonance densitometry (SINRD) to measure the fissile content in nuclear fuel”. Ph.D. dissertation at Texas A&M University.

LaFleur A. M., et al., 2015. “Analysis of experimental measurements of PWR fresh and spent fuel assemblies using self-interrogation neutron resonance densitometry”. Nuclear Instruments and Methods Section A, 781 (2015) 86-95.

Menlove H. O., et al., 1969. “A resonance self-indication technique for isotopic assay of fissile material”. Nuclear applications, volume 6, 401-408.

Pelowitz D., editor, 2011. “MCNPX user’s manual version 2.7.0”. Los Alamos National Laboratory LA CP 11-00438.

Photonis, 2017. http://www.photonis.com/nuclear/products/fission-chambers-for-in-core-use/.

Rinard P. M., et al., 1988. "Safeguarding LWR spent fuel with the FORK detector". Los Alamos National Laboratory report LA-11096-MS.

Rossa R., et al., 2013. "Development of a reference spent fuel library of 17x17 PWR fuel assemblies". ESARDA Bulletin n. 50.

Rossa R., et al., 2015. "Investigation of the self-interrogation neutron resonance densitometry applied to spent fuel using Monte Carlo simulations". Annals of Nuclear Energy 75 (2015) 176-183.

Rossa R., 2016. “Advanced non-destructive methods for criticality safety and safeguards of used nuclear fuel”. Ph.D. dissertation at Université libre de Bruxelles ULB.

Sitaraman S., et al., 2009. "Symmetric pin diversion detection using a partial defect detector (PDET)". Proceedings of the 50th INMM annual meeting.

Tobin S. J., et al., 2011. "Next generation safeguards initiative research to determine the Pu mass in spent fuel assemblies: purpose, approach, constraints, implementation, and calibration". Nuclear Instruments and Methods in Physics Research A 652 (2011) 73-75.

An Integrated 3S Model for Safeguards for International Transport of Spent Nuclear Fuel

Maikael Thomas, Adam Williams, Katherine Jones, Doug Osborn, Elena Kalinina, Brian Cohn, M. Jordan Parks, Amir Mohagheghi
Global Security Programs, Sandia National Laboratories
Albuquerque NM USA
[mthomas; adwilli; kajones; dosborn; eakalin; bcohn; mjparks; ahmohag]@sandia.gov

Abstract:

The international transport of spent nuclear fuel (SNF) provides a novel challenge to the safeguards community considering the expected significant frequency in such shipments and increasing complexity of multimodal routing. We have developed a notional transportation case study, grounded in real case data, capturing the complex, socio-technical security, safety and safeguards (3S) factors influencing an SNF shipment that traverses several international boundaries while using various transportation modalities (e.g., roads, rail, and water). Our research focuses on using system-level analysis techniques (e.g., dynamic probabilistic risk assessment, DPRA) to analyze these complex risk factors influencing SNF transportation from an integrated 3S perspective in an attempt to identify possible advantages and efficiencies.

As it fits within the integrated 3S approach, this paper focuses specifically on the modelling and analysis of safeguards for the international transportation of SNF. Using our notional transportation case study, we modelled the various stages of SNF transport as states within a Markov Chain using the Brookhaven National Laboratory-developed PR-CALC software. The resultant model identifies distinct safeguards approaches and intrinsic barriers at each state of the SNF shipment, which then determines the probability of the SNF moving to one of several proliferation states: a 'state' of diversion detected, a 'state' of diversion failure, or a 'state' of proliferation success. Initial results from the Markov Chain model are encouraging in that they provide a clear description of how safeguards can be applied to an international SNF shipment—suggesting improvements over current best practices. We then situate this new safeguards model in an integrated 3S perspective by exploring the interplay with models for security and safety of the international SNF transportation (using DPRA as the integrating framework). Ultimately, our work aims to help identify where safeguards concepts, approaches, and technologies could be improved to bolster the international safeguards regime among an expected (and significant) increase in international SNF transports.

Keywords: 3S, transportation, spent nuclear fuel, risk complexity, Markov models

1. Introduction

The growing global interest in nuclear energy programs and high costs associated with the storage of spent nuclear fuel (SNF) has increased the demand for transport to offsite locations. In the U.S. alone, shipments are expected to reach over 12,000 by the year 2055 [1]. Shipments to reprocessing facilities or storage sites may employ different transport modalities (e.g., train, boat, rail) and travel long distances, perhaps crossing international borders. As the shipment progresses, the SNF may face a variety of socio-technical influences (e.g., protesters, terrorists, national policies, economic constraints, or geopolitical pressures) that challenge traditional approaches to managing risk. From a nuclear safeguards perspective, managing these risks is guided by a State's export obligations via its Comprehensive Safeguards Agreement (CSA) with the IAEA for the international shipment of SNF. Prior to a shipment, the State will send identifying information about the shipment cask and its origin, material composition, expected shipment dates, and the destination [2]. The increased demand to ship SNF internationally may present opportunities for proliferators to divert nuclear materials—especially considering how casks are transferred between various transportation modalities and across multiple geopolitical and maritime borders. How these characteristics of international SNF transportation

challenge safeguards effectiveness is compounded when the influence(s) of safety and security concerns along international transportation routes are also considered.

As such, the international transport of SNF presents unique challenges in the areas of security, safety, and safeguards (3S). Traditionally these challenges are assessed and analyzed independent of one another, which can lead to compartmentalized descriptions (and a segmented understanding) of the international SNF transportation risk space. Recent work by Williams, et. al. [3] suggests that applying an integrated 3S-based complex risk perspective may improve the overall design and analysis of SNF transportation.

In this paper, we model applied safeguards (e.g., containment seals) and intrinsic barriers (e.g., heat and radiation characteristics of the SNF) of a hypothetical SNF transportation case study using an analytical technique based on Markov chains. Our model is evaluated with software named PRCALC (created at the Brookhaven National Laboratory [4]) which computes the probabilities of proliferation success, diversion detection, and diversion failure at a given stage in the model. Some PRCALC inputs and results are subsequently used in a novel analysis called Dynamic Probabilistic Risk Assessment (DPRA) to assess the complex risk perspective of the integrated 3S.

2.Transportation Case Description & Scenario

A regional map of our hypothetical SNF transport case study is shown in Figure 1 below (NOTE: A more complete description of this case study is provided in [5]), and includes the following fictitious nations:

- **Zamau**, a non-weapons state signatory to the Treaty on the Non-Proliferation of Nuclear Weapons (NPT) with a fairly robust nuclear enterprise that provides 12% of national electrical power [SNF origin];
- **Famunda**, a non-weapons state signatory to the NPT with rampant governmental corruption and no developed safeguards system [SNF transit country]; and,
- **Kaznirra**, a non-weapons state signatory to the NPT & Additional Protocol with a well-developed nuclear enterprise interested in making Site B a regional SNF repository [SNF end destination].

The SNF shipment route spans these three hypothetical countries and travels first via rail (the grey path), then barge (the dark blue path), and finally road (the orange path).

We included a variety of SNF characteristics to represent a wide range of realistic SNF factors—including the need to understand how SNF from the variety of reactor types currently used in existing nuclear power plants (and fuel usage strategies) affect safeguards. In addition, these SNF configurations influence the attractiveness of the SNF to state actors (e.g., quantity of Plutonium, Pu) and the ease of handling the SNF cask (e.g., radioactivity and thermal heat). Within our hypothetical case description of international SNF transportation, we consider different SNF characteristics, including:

- PWR and BWR reactor types with 24 and 52 fuel rods per assembly, respectively
- Three burnup values of 40, 50, and 60 GWD/MTU
- Four fuel ages after discharge of 5, 10, 20, and 50 years

The SNF cask has generic characteristics and its construction is consistent with International Atomic Energy Agency (IAEA)-certified AREVA TN-Series dual purpose casks used for storage and transportation. In this hypothetical case, the SNF cask has a passive metal containment seal applied by the Site A facility operator under video surveillance by the IAEA. Prior to shipment, the country of Zamau sends the IAEA the SNF and cask attributes as part of its CSA. Further, Zamau has responsibility for the SNF shipment until the recipient state Kaznirra assumes custody [2].

This train is dedicated to SNF transport and includes an onboard security force that protects the SNF (per international best security practice). The rail car itself has a protective canopy and buffer/escort cars, meeting the US AAR S-2043 standard for trains to carry high-level radioactive waste, including SNF [5]. Given the relatively low track class (i.e., standards dictating railroad track quality) of Zamau's expansive railway network [6] and the fact that train derailments are the most common type of rail incident [7], for this paper we include this event in our scenario to explore the safeguards repercussions within a complex risk context.

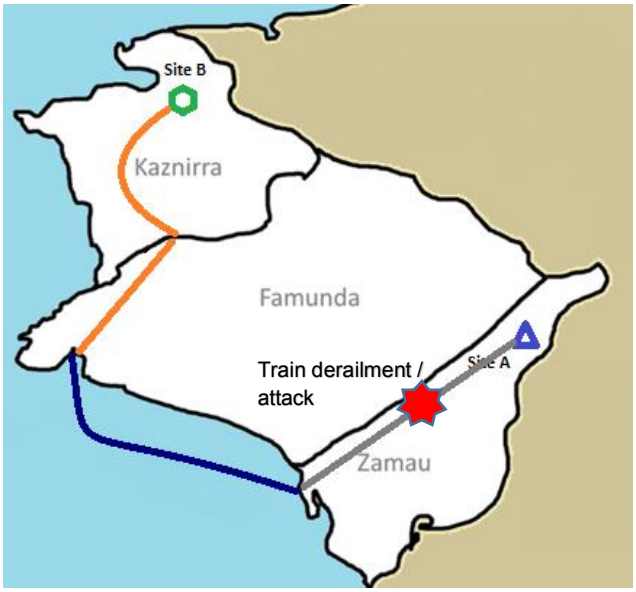

Figure 1: Regional (and route) Map of Spent Nuclear Fuel Transport

More specifically, a 40-foot section of track is removed, causing the train to derail (Figure 1). The derailed train is then (opportunistically) attacked by a state actor posing as a terrorist organization. During the attack, the train's security force engages the attackers in a short firefight. In this scenario, if the attack is thwarted, the SNF shipment continues to its destination. However, if the attackers are successful, they quickly divert one significant quantity (SQ) of Pu from the fuel assembly, replace any missing material with dummy fuel rods, re-apply the containment seal and create a radiological release by detonating TNT attached to a fuel rod to make the diversion appear to be an act of terrorism. Lastly, the remains of the SNF assembly in the cask will eventually be shipped back to Site A and Zamau will send a special report to the IAEA detailing the incident. An IAEA inspector will subsequently inspect and examine the SNF shipment cask at Site A.

3. Markov Model in PRCALC

The complexity facing safeguards in this scenario suggest the importance of maintaining continuity and the quality of knowledge (beyond current best practices) along international SNF transportation routes. In a manner similarly aimed at maintaining continuity and quality of nuclear material knowledge, Denning suggested Markov chain models as a method to assess scenarios for proliferation resistance [7]. A Markov model breaks a time-variant scenario into discrete stages (or states) using a directed graph with transition parameters defining the probability of advancing to the next stage. Future and past states of the Markov process are considered independent of the present state. In addition, this method can compute probabilistic measures that account for a wide range of uncertainties found in the complexity inherent in maintaining safeguards obligations in the international transportation of SNF.

The train derailment/attack scenario, described in the previous section, is shown as a Markov model in Figure 2. The model starts where the SNF cask is loaded onto the train in the country of Zamau—the 'Loaded on train at Site A' stage. Next, the train travels (under anticipated normal conditions) to a seaport (the 'Travel on Train' stage). (NOTE: A more complete Markov Chain Model would also have a branch illustrating the state descriptions associated with SNF traveling along the desired path to its destination. We truncated the model in this paper for clarity.) However, the train derails and is subsequently attacked by the Zamau state actors posing as terrorists (the 'Derail/Attack Train' stage). At this point in the scenario, the model offers two possibilities: the attack on the derailed train can be either successful or thwarted. For this paper, we do not consider the 'Attack Thwarted' stage from a safeguards point of view because there is no unique opportunity for proliferation. In the 'Attack Successful' stage, the adversaries divert enough SNF to contain one SQ of Pu and subsequently cause a radiological release to create the appearance of a terrorist act. From here, the Markov model accounts for three safeguards outcomes:

- the diversion may eventually be detected by safeguards inspectors under current safeguards best practices due to the applied safeguards measures —the '**Diversion Confirmed**' stage;
- the diversion could fail, because of the SNF intrinsic barriers—the '**Diversion Failure**' stage; or,
- the adversaries overcame both the applied safeguards measures and intrinsic barriers to gain the SNF without detection—the '**Diversion Success**' stage.

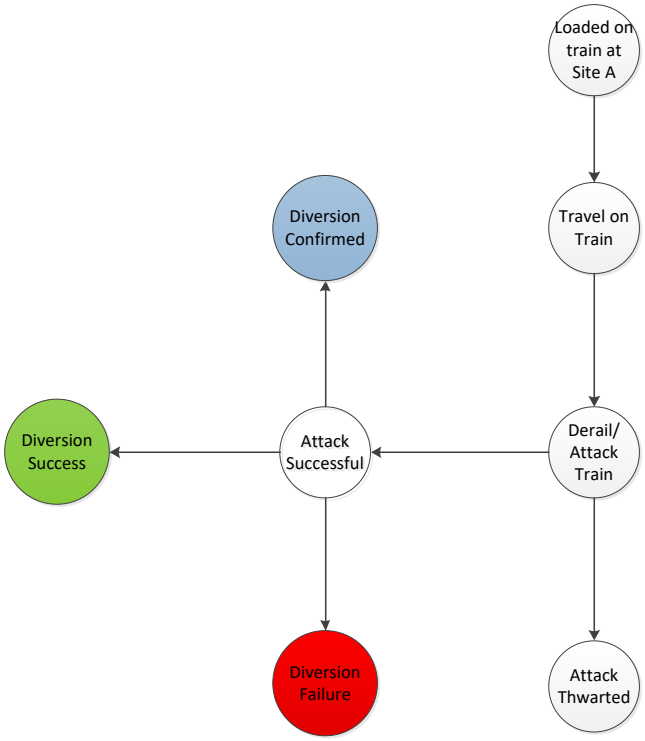

Figure 2: Markov Model for Train Derailment / Attack

Our model applies safeguards measures which help safeguards inspectors more quickly detect a diversion of SNF. The scenario narrative after the attack is that the cask will return to Site A. During the next safeguards inspection, our model assumes the inspector will check the seal applied to the cask and send it to a laboratory for analysis. Another modeling assumption is that the inspector will also perform a visual inspection of the fuel assembly. In this scenario, the State actor takes measures to conceal their diversion by tampering with the seal to access the SNF and the use of dummy fuel rods. Given the (assumed) sophistication and maturity of Zamau's state-level safeguards system, we assume their concealment activities are effective 80% of the time. The average inspection period T_I, inspection time to discover an anomaly T_{DA}, and time to confirm the anomaly T_{VA} are all used to compute the time to detect a diversion T_D. Table 1, below, gives the average times, as defined by Yue [4], for our scenario safeguards measures. Per the logic of PRCALC (and international best practices in safeguards), increasing the number and effectiveness of applied safeguards, increases the likelihood that inspectors will detect a diversion (ideally in a timely manner).

Table 1: Applied Safeguards and Factors to Compute the Time to Detect Diversion

Safeguards Approach	T_I	T_{DA}	T_{VA}	$T_D = T_I + T_{DA} + T_{VA}$
Visual Inspection	52 weeks	Days	Quickly	53 weeks
Passive Seal	3 months	Days	2 weeks	13 weeks

Intrinsic barriers related to international SNF transportation are natural fuel and/or transportation mechanism (e.g., cask) characteristics that work to delay a successful proliferation and increase the likelihood of failure. IN PRCALC, the delay time associated with these intrinsic barriers, along with the rate of diversion, directly affects the amount of time it takes to divert the SNF, which affects the

probabilities of proliferation success and failure. We added a fixed intrinsic barrier delay to the model to represent the detrimental qualities of the SNF (e.g., SNF heat, toxicity, and radiation) as well as the physical barriers associated with the cask and train design. Before material can be successfully diverted, the proliferators will need to overcome these barriers. As with applied safeguards, increasing the number and effectiveness of intrinsic barriers, prolongs the proliferation time and increases the likelihood of proliferation failure.

We input the Markov model into the PRCALC software along with information from this scenario describing the applied safeguards measures, the intrinsic barriers, and SNF/cask characteristics. We consider 24 SNF cask configurations, including SNF from PWR and BWR reactors as well as different fuel age and burnup values as shown in Table 2. Note that these parameters affect the mass of Pu in the SNF shipment, a key parameter in PRCALC. As represented in our model, the software outputs three time-variant probabilities: 1) the diversion detection, 2) the diversion failure, and 3) the proliferation success.

Table 2: Spent Fuel Characteristics for reactor type, age, and burnup values

Age (years)	**5**	**10**	**25**	**50**	**5**	**10**	**25**	**50**	**5**	**10**	**25**	**50**
Burnup, GWD	**60**	**60**	**60**	**60**	**50**	**50**	**50**	**50**	**40**	**40**	**40**	**40**
PWR												
Pu per assembly (kg)	3.95	3.85	3.67	3.53	3.66	3.56	3.37	3.24	3.31	3.22	3.05	2.93
Pu in cask (kg)	94.8	92.5	88.1	84.8	87.8	85.5	81.0	77.8	79.5	77.4	73.4	70.5
BWR												
Pu per assembly (kg)	1.85	1.81	1.73	1.67	1.72	1.68	1.60	1.54	1.55	1.51	1.45	1.40
Pu in cask (kg)	96.6	94.3	90.0	86.8	89.6	87.5	83.4	80.4	80.7	78.9	75.4	72.9

4. Results

We ran the 24 configurations for the SNF shipment derailment/attack scenario for the 'Attack Successful' stage of our Markov model. The peak output probabilities of diversion detection, diversion failure, and proliferation success are given in Table 3. These probabilities all start at zero at time t=0, but grow over time based on the SNF characteristics, diversion rate, safeguards, and intrinsic barriers. The PRCALC simulation terminates when these probabilities no longer significantly change. For our scenario and configurations, PRCALC stopped simulation after 50 – 60 weeks of time. We found that the probability of diversion detection remained constant across all configurations because the value T_D (time to detect a diversion) is computed solely on the selected safeguards measures, which remained static across the 24 configurations for the SNF.

However, the calculations for the probabilities of diversion failure and proliferation success are dependent upon the amount of Pu contained in, and the rate of diversion from, a fuel assembly (and therefore the cask) as well as the time delay caused by the intrinsic barrier. Note that the selection of a fixed intrinsic barrier value for all configurations is a simplifying assumption. As the SNF ages it becomes easier to handle because the SNF becomes less radioactive and thermally hot. Overall, despite the differences in reactor type, age, and burnup values, there were only small differences in the probabilities of diversion failure and proliferation success (Table 3). Both of these probabilities are computed based on the total amount of Pu, compared to one SQ, in the transport cask, and the goal of the proliferators in our scenario is to divert one SQ. As such, shipments that contain more Pu are more likely to experience a higher diversion failure probability but also more likely for proliferation to succeed. This is because the amount of time needed to divert the material decreases as the amount of Pu in the cask

increases. Yue showed that diversion time is used to compute both diversion failure and proliferation success, and a decrease in this time drives an increase in these probabilities [4].

Table 3: Probabilities of Diversion Detection, Diversion Failure, and Proliferation Success for the 24 configurations

Reactor Type / Burnup (GWD) / Age (years)	**$P_{(Diversion\ Detection)}$**	**$P_{(Diversion\ Failure)}$**	**$P_{(Proliferation\ Success)}$**
PWR / 60 / 5	0.496	0.00282	0.00470
PWR / 60 / 10	0.496	0.00275	0.00459
PWR / 60 / 25	0.496	0.00262	0.00437
PWR / 60 / 50	0.496	0.00252	0.00421
PWR / 50 / 5	0.496	0.00261	0.00436
PWR / 50 /10	0.496	0.00254	0.00424
PWR / 50 / 25	0.496	0.00241	0.00402
PWR / 50 / 50	0.496	0.00232	0.00386
PWR / 40/ 5	0.496	0.00237	0.00395
PWR / 40 /10	0.496	0.00230	0.00384
PWR / 40 / 25	0.496	0.00218	0.00364
PWR / 40 / 50	0.496	0.00210	0.00350
BWR / 60 / 5	0.496	0.00287	0.00479
BWR / 60 / 10	0.496	0.00281	0.00468
BWR / 60 / 25	0.496	0.00268	0.00446
BWR / 60 / 50	0.496	0.00258	0.00431
BWR / 50 / 5	0.496	0.00266	0.00444
BWR / 50 /10	0.496	0.00260	0.00434
BWR / 50 / 25	0.496	0.00248	0.00414
BWR / 50 / 50	0.496	0.00239	0.00399
BWR / 40/ 5	0.496	0.00240	0.00401
BWR / 40 /10	0.496	0.00235	0.00392
BWR / 40 / 25	0.496	0.00224	0.00374
BWR / 40 / 50	0.496	0.00217	0.00362

Figure 3 illustrates how the probability of detection of the 'Attack Successful' stage varies with time for a given configuration. The more time that passes after the diversion, the greater the likelihood the safeguards inspectors will discover the diversion. After 10 weeks have passed, the diversion detection and confirmation probability reaches about 25%, and after 50 weeks the probability stabilizes at roughly 50%. It takes almost one year to reach its highest probability of detection because of the average detection times of 13 weeks for the seal and 53 weeks for a visual inspection. Also, our assumed concealment effectiveness factor of 80% serves to further delay the discovery of diversion.

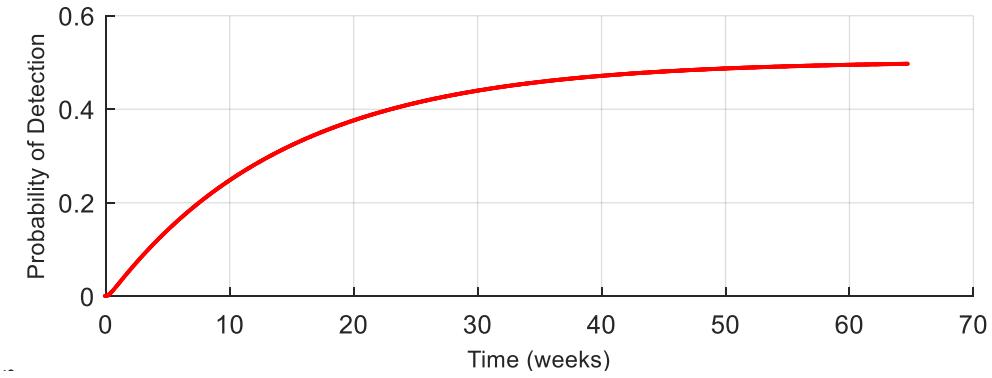

Figure 3: Probability of Diversion Detection versus Time for the 'Attack Successful' stage

Figure 4 illustrates the time varying probabilities of diversion failure and proliferation success for a PWR configuration with 25 year age 60 GWD/MTU burnup. For all of the configurations, these

probabilities stabilize after one to three weeks of time, which is a much shorter time period than for the probability of detection. This shorter time period is attributable to the large amount of Pu in the transport cask, a quick diversion rate, and the model selection of a fixed intrinsic barrier that does not cause significant delay to proliferation. However, selecting intrinsic barriers that cause more time delay will correspondingly increase the probability of diversion failure.

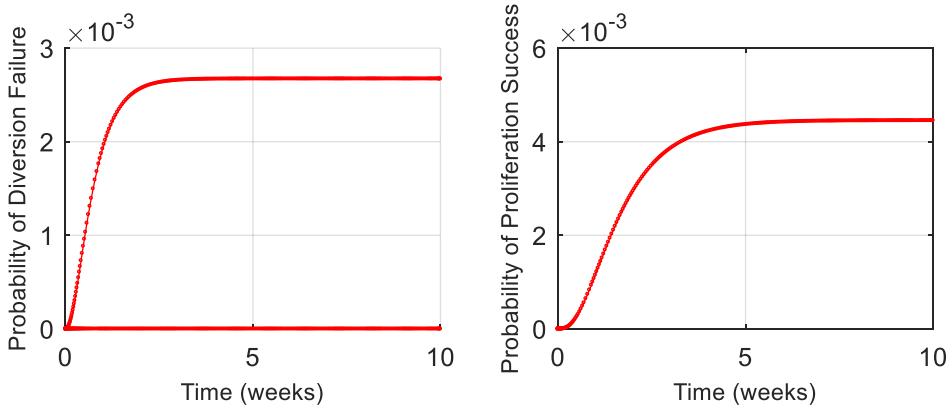

Figure 4: Probability of diversion failure and proliferation success for PWR with 60 GWD Burnup and 25 year age for the 'Attack Successful' stage

5. 3S Integration using DPRA

Dynamic probabilistic risk assessment (DPRA) is an extension of traditional PRA methods that investigates both the aleatory (e.g., arising from stochasticity in the process) and epistemic (e.g., arising from the model) uncertainties in complex systems by varying key parameters during simulations [3]. We use a software program called ADAPT, which is designed to investigate the uncertainty space of complex systems through the use of dynamic event trees (DETs) [6]. In ADAPT, DET analysis begins at time t = 0 in the system and continues until a set of pre-determined conditions (known as branching rules and relating to either time-dependent or system physics-dependent phenomena) are met. At this point, the computer model stops and reports the condition that ended the run, and, based on the reason given, generates multiple modified models in order to reflect the possible system evolutions based on system parameters (e.g., edit rules). This process continues until all of the possible system evolutions have been investigated with a variety of PRA-related values (e.g., probability of occurrence) being reported for each branch/modified DET model.

For our scenario, ADAPT evaluated how three independent safety (RADTRAN), security (STAGE) and safeguards (PRCALC) analysis techniques interact to more fully address the uncertainty (and complexity) within our SNF transportation scenario. In order to investigate all three models together, ADAPT modifies all of the models jointly using the output(s) of some as the input(s) of others. This is done through edit rules which describe how the system changes based on scenario parameters (e.g., the state of the casks before vs. after the derailment)—and results in various new branches that compose the DET. In ADAPT, when a predetermined state has been reported, the edit rules then alter the input file by replacing selected variables with different parameters reflecting the changed status of the system (e.g., integrity of the mechanical safeguards seal before vs. after the derailment).

DPRA is designed to look at the behaviors of specific scenarios—hence our hypothetical scenario that involves the interactions between safety, security and safeguards considerations. For example, in the scenario there is a branch point based on whether the railcar is still on the track. A traditional safeguards scenario would not cause the train to go off-track, but the ability of both applied safeguards and intrinsic barriers to meet safeguards obligations would certainly be affected. If Zamau were to sign the Additional Protocol, a safeguards-related branch point could determine whether or not Zamau is in 'good standing' with the IAEA regarding its obligations—where 'good standing' may result in reduced scrutiny over the initial application of the mechanical safeguards seal on the cask at the point of origin. DPRA—via ADAPT—provides a mechanism for exploring higher fidelity models of these classes of interactions. To further evaluate the sensitivity of safeguards in this scenario, ADAPT will

be used to simulate various orders of the integration between the three previously mentioned codes (e.g., RADTRAN to STAGE to PRCALC, STAGE to RADTRAN to PRCALC). [NOTE: At the time of this publication, the ADAPT-related PRCALC results were not complete, and thus could not be reported.]

6. Conclusion

Traditional safeguards approaches struggle to handle the complexities introduced in the international transportation of SNF and mitigate the risk of diversion of nuclear material. Integrated 3S, complex risk approaches offer a new analytical framework to address this gap. Our focus in this paper is on the safeguards 'S' using a Markov chain model, which supports the reorientation of safeguards towards a focus on the continuity *and* quality of nuclear material knowledge, which can improve current best practice (e.g., 'check-in/check-out' system).

Results from analyzing 24 SNF configurations of our hypothetical scenario showed that the transport SNF characteristics, applied safeguards, and intrinsic barriers are all important factors in calculating proliferation measures. PRCALC computed quantitative values for probabilities of detection, diversion failure, and proliferation success. In this scenario (and across all modeling assumptions), the probability of diversion success is approximately twice as high as the probability of diversion of failure. Combined with a 50% (at best!) probability of detection after 53 weeks, the challenges of current safeguards approaches to the international transportation of SNF are evident. For example, these results could lead to more conscientious physical barrier design for the transport cask and rail car. Since the 24 SNF configurations do not change appreciably in the amount of Pu being transported, the attractiveness and challenges to proliferators do not vary significantly. Given the similarity in trends across these configurations—and in the context of the expected significant increase in international transportation of SNF—emphasis on Pu context for adversarial attractiveness may need to be reconsidered. Lastly, we demonstrated the following with this complex systems approach to safeguards:

- how meeting well-established reporting requirements may be insufficient to meet international safeguards obligations (and needs!) for international SNF transportation;
- how accounting for a 'per system state' safeguards approach may improve the continuity and quality of knowledge of the nuclear material over the current international best practice (where the safeguards responsibility is on the country of origin until the SNF is delivered and 'checked in' to the destination country's inventory); and,
- the importance of accounting for the relationships between safeguards and security (e.g., what 'intrinsic barriers' can the physical security design provide), as well as between safeguards and safety (e.g., how can safety inspections of SNF be leveraged as applied safeguards).

Our future research will focus on the integration of all 3S, using the results of this paper as well as safety and security results published elsewhere [1]. We will further develop and refine other SNF transport scenarios. The defined model inputs and outputs will lend better understanding to the interdependences between the 3S, and help to better define complex risk. An integrated 3S, complex risk approach (grounded in systems theory) provides a new concept for framing—and new approaches for applying—more efficient and effective safeguards in rapidly changing, dynamic implementation environments.

7. Acknowledgements

Sandia National Laboratories is a multi-mission laboratory managed and operated by National Technology and Engineering Solutions of Sandia, LLC., a wholly owned subsidiary of Honeywell International, Inc., for the U.S. Department of Energy's National Nuclear Security Administration under contract DE-NA0003525.

SAND 2017-4690 C

8. References

1. Kalinina, E., et. al., “Transportation of Spent Nuclear Fuel from Reactor Sites in the US—What Will It Take?”, IHLRWM 2015 (Proc. of ANS International Conf., Charleston, SC, 2015).
2. Ritchie, I., “Technical and Administrative Preparations Required for Shipment of Research Reactor Spent Fuel to Its Country of Origin”, IAEA/ANL Regional Training Course, Jan 13-24, 1997, Argonne, USA.
3. Williams, A., et. al., “Preliminary Results from a System-Theoretic Framework for Mitigating Complex Risks in International Transport of Spent Nuclear Fuel”, INMM 2016, (Proc. Annual Meeting. Atlanta, GA., 2016).
4. Yue, M., et. Al., “A Markov Model Approach to Proliferation-Resistance Assessment of Nuclear Energy Systems”, Nuclear Technology, Vol. 162, April 2008.
5. Performance Specification for Trains Used to Carry High-Level Radioactive Material. Car Construction Fundamentals and Details, AAR Manual of Standards and Recommended Practices, Standard S-2043 (effective 2003 revised 2008).
6. Williams, A., et. al., “A New Look at Transportation Security: A Complex Risk Mitigation Framework for the Security of International Spent Nuclear Fuel Transportation”, IAEA International Conference on Nuclear Security, Dec 5-9, 2016, Vienna, Austria.
7. Abkowitz, M. and Bickford, E., “Development of Rail Accident Rates for Spent Nuclear Fuel Rail Shipments”, WM2017 Conference, March 5-9, 2017, Phoenix, Arizona, USA.
8. Denning, R., et al., “Guidelines for the Performance of Nonproliferation Assessments,” *Trans. Am. Nucl. Soc.*, **87**, 365 (2002); see also PNNL-14294, Pacific Northwest National Laboratory (2003).

Session 11

Training and Knowledge Management

Training and Qualification Plan for U.S. Nuclear Regulatory Commission's International Safeguards Analysts

United States Nuclear Regulatory Commission

Bruce W. Moran, Peter Habighorst and David H. Hanks

U.S. Nuclear Regulatory Commission
Washington, D.C.

ABSTRACT

Training and qualification plans are developed for the primary skills required of U.S. Nuclear Regulatory Commission (NRC) staff to ensure that they can effectively and correctly perform their job responsibilities. To ensure that NRC's International Safeguards Analysts, Import and Export Analysts, and Nuclear Materials Management and Safeguards System (NMMSS – U.S. nuclear materials database) Analysts have the necessary knowledge and skills to perform their job responsibilities a training and qualification plan was developed for these areas of expertise. Such a plan is especially important during periods when changes in staffing occur. Brainstorming was performed to determine what information is necessary for performing the international analyst job responsibilities. From this list, two general objectives for the training and qualification were identified: (1) Effectively represent NRC and U.S. interests in domestic and international meetings on nonproliferation issues, and (2) Ensure NRC and its licensees comply with international treaties and agreements. Each of these general objectives was further characterized through the development of sub-objectives. Each of the sub-objectives was assessed to determine performance metrics that would need to be met at the basic, intermediate, or comprehensive level. The importance of the sub-objectives was then prioritized based on the staff member's primary area of responsibility – international safeguards analysis, import and export analysis, or NMMSS analysis. Assessment questions were developed to assist the qualification panel in assessing a candidate. The training and qualification plan was linked to locations in the public internet and NRC-intranet where training resources could be found. Information on training courses, seminars, and meetings that could assist the candidate in developing their skills, as well as on-the-job training opportunities, were also linked to the plan. Where training materials were not already available, they are to be developed.

BACKGROUND

The U.S. Nuclear Regulatory Commission (NRC), like many other organizations in the nuclear field, is placing increasing importance on ensuring that knowledge is transferred to newer staff who are replacing those who are retiring or otherwise leaving the organization. One aspect of the NRC's program is the establishment of training and qualification plans that identify what information must be transferred to newer staff for them to become qualified to perform assigned activities.

NRC's international safeguards staff require some knowledge of a variety of technical disciplines and government policy. For example, international safeguards implementation requires accountants, auditors, information management specialists, statisticians, information and trade analysts, mathematicians, chemists, physicists, chemical engineers, nuclear engineers, international policy analysts, and lawyers, among others. While it is typically necessary for persons to be experts within a given discipline, some knowledge of all of the disciplines is useful to have a full understanding of how the discipline relates to the global nonproliferation policies and practices. The Training and Qualification Program for NRC's staff assigned to international safeguards related activities – International Safeguards Analysts, and Nuclear Materials Management and Safeguards System

(NMMSS) Analysts – addresses each of the primary knowledge areas and prioritizes them for the different disciplines.

PLAN DEVELOPMENT:

Brainstorming: The beginning activity for developing the International Safeguards Training and Qualification Plan began with a "brainstorming" to identify the primary topics and information that an NRC international safeguards staff person would need to know. This information was then organized into a hierarchical outline structure and reviewed to identify apparent gaps in the information.

Objectives: After conducting the "brainstorming" exercise, an objectives-based analysis was performed to determine the knowledge and skills that the new international safeguards analyst would need to have to be qualified to independently represent the NRC in U.S. Government and international meetings and in meetings with NRC and Agreement State licensees. The learning objectives are listed in Table 1.

Performance metrics: For each of the objectives, performance metrics were determined that defined abilities and knowledge that the new international safeguards analyst should possess to be qualified. The performance metrics were prioritized for each of the technical specialties to establish the level of knowledge needed by that specialty to be qualified – basic, intermediate, or comprehensive knowledge. In addition, for each performance metric, example questions were developed to assist the qualifications review panel in assessing whether the new staff person has the necessary ability or knowledge. The performance metrics are listed in Table 1.

Training activities: For each training objective and its associated performance metrics, training activities were identified in three categories: suggested reading, training courses and conferences, and on-the-job training. We identified that there already exists a large body of training materials and courses that have been established in the United States, most by the U.S. Department of Energy, its national laboratories, and its contractors. Some have also been established by universities and other non-government organizations. The assembled list of training resources provides options that can be used by the new international safeguards analyst in developing a training plan. On-the-job training, where experienced and new international safeguards staff work together to address the international safeguards and nonproliferation tasks of the NRC, remains a critical component of the knowledge transfer.

Identifying Available Resources: Links were provided in the qualification card to public internet and NRC-intranet locations for information used to establish newer staff knowledge baseline. In particular, the IAEA guidance for State compliance with safeguards obligations (IAEA Service Series 21 and associated Safeguards Implementation Practice guides). Mentor assignments for newer staff also serves to improve assimilation of large amounts of information and practicality of analysis being performed.

SUMMARY:

To ensure that it has qualified International Safeguards Analysts, Import and Export Analysts, and NMMSS Analysts for the future, NRC has developed a training and qualification plan to assist new international safeguards staff in determining the knowledge and abilities that they need to know, and what the resources are to assist them in gaining that knowledge and abilities. The training and qualification plan also assists NRC managers in their assessment as to whether the new staff meets the levels of performance necessary to be considered qualified. NRC began to implement the training and qualification plan in 2016 to guide the development of new staff selected for the international safeguards team.

Table 1. International safeguards staff training objectives and performance metrics

Objective	Performance metric
A. Effectively represent NRC and U.S. interests in domestic and international meetings on nonproliferation issues	1. Ability to develop, present, and defend NRC positions (both verbally and in writing) 2. Ability to provide acknowledged technical expertise to discussions 3. Ability to understand other Federal agency interests and motivations 4. Ability to understand International Atomic Energy Agency (IAEA) and IAEA Department of Safeguards interests and motivations 5. Ability to understand other countries or groups of countries interests and motivations 6. Ability to differentiate policy and technical perspectives in discussions and provide options to meet both needs
A.1. Understand U.S. and international nuclear nonproliferation policy and objectives and the history of their implementation	1. Knowledge of the Nuclear Nonproliferation Treaty and international perspectives on its content 2. Knowledge of the IAEA's Statute, structure and operations, including the structure and practices of the Department of Safeguards 3. Knowledge of the US-IAEA safeguards agreements and protocols to those agreements (e.g., additional protocol and small quantities protocol) 4. Knowledge of other agreements that establish safeguards obligations, such as project supply agreements, and nuclear weapon free zones 5. Knowledge of the routine bilateral, multilateral, and international (e.g., IAEA Board of Governors and IAEA General Conference) coordination meetings 6. Knowledge of differences in nonproliferation objectives among IAEA, U.S., and other countries 7. Knowledge of IAEA safeguards implementation at NRC-licensed facilities 8. Knowledge of IAEA safeguards implementation at U.S. Department of Energy (DOE) facilities 9. Knowledge of IAEA safeguards implementation during the U.S. Atomic Energy Commission
A.2. Understand interagency roles and responsibilities	1. Knowledge of the roles of Federal agencies in meeting those objectives (e.g., U.S. National Security Council, U.S. Department of State, DOE, U.S. Department pf Defense, U.S. Department of Commerce, NRC) 2. Knowledge of the roles of the interagency coordination committees – Subgroup on IAEA Safeguards in the U.S. (SISUS), Subgroup on Safeguards Technical Support (SSTS), Subcommittee on International Safeguards and Monitoring (SISM), IAEA Steering Committee (ISC), Interagency Policy Sub-committee (Sub-IPC) 3. Knowledge of the DOE national laboratories, and other major DOE facilities and their roles in supporting nonproliferation and international safeguards activities
A.3. Understand international nonproliferation obligations	1. Knowledge of the model safeguards agreements (INFCIRC/66, 153, 540) 2. Knowledge of international export control guidance (INFCIRC/207 and 254) 3. Knowledge of IAEA guidance for State compliance with safeguards obligations (IAEA Service Series 21 and associated Safeguards Implementation Practice guides) 4. Knowledge of the Hexapartite Agreement and bilateral agreements for the import of enrichment technology to the U.S. (URENCO States and Australia)

Objective	Performance metric
B. Ensure NRC-licensees comply with international safeguards treaties and agreements	1. Knowledge of U.S.-specific safeguards agreements (INFCIRC/288, INFCIRC/288/Add. 1, INFCIRC/366), protocols to the agreements, subsidiary arrangements, and facility attachments 2. Knowledge of the resulting obligations that affect NRC licensees 3. Knowledge of regulations impacting international safeguards implementation (e.g., 10 CFR 75 and 810) 4. Knowledge of licensee facilities and operations to determine effective, efficient, and practical means to meet the international obligations
B.1. Understand the design and operations of reactors and other nuclear fuel cycle facilities	1. Knowledge of how all types of nuclear facilities operate 2. Knowledge of classified, sensitive and proprietary aspects of fuel cycle processes 3. Knowledge of how fuel cycle processes could be misused for proliferation purposes 4. Knowledge of the global nuclear fuel cycle and nuclear trade
B.2. Understand NRC's safety, physical security, and information security requirements for licensing nuclear facilities	1. Knowledge of Atomic Energy Act of 1954 (as amended) and Energy Reorganization Act of 1974 (as amended) 2. Knowledge of NRC licensing requirements for reactors (50), fuel cycle facilities (10 CFR Part 35, 40, 70, 72, and 76), Agreement States (10 CFR Part 150), and physical security (10 CFR Part 73) 3. Knowledge of classified and sensitive technology protection (10 CFR Part 95 and 810)
B.3. Understand nuclear material control and accounting	1. Knowledge of nuclear materials control and accounting 2. Knowledge of NRC regulations for material control and accounting (10 CFR Part 74) 3. Knowledge of the content and structure of a fundamental nuclear material control plan 4. Knowledge of nuclear material measurements and statistical evaluations 5. Able to develop a conceptual nuclear materials accounting system for a facility
B.4. Understand concepts of IAEA safeguards implementation	1. Knowledge of State-level concept for IAEA safeguards implementation 2. Knowledge of additional protocol content and related guidance 3. Knowledge of IAEA model safeguards approaches for each type of fuel cycle facility 4. Knowledge of safeguards verification procedures, techniques and equipment 5. Knowledge of the safeguards by design concept
B.5. Understand and be able to implement actions that must be undertaken by NRC and licensee facilities to ensure compliance with IAEA safeguards obligations	1. Able to add or remove a licensee facility from the Eligible Facilities List 2. Able to compile and submit annual and quarterly additional protocol declarations on licensee sites and locations 3. Able to review and advise licensees on completion of design information questionnaire and additional protocol declarations 4. Able to facilitate access to licensee installations under both safeguards agreement and additional protocol (e.g., design information verification, scheduled inspection, random inspection, or complementary access) 5. Ability to coordinate interagency actions associated with a design information verification, inspection or complementary access at a licensee installation 6. Able to perform acquisition/diversion path analysis for a nuclear facility 7. Able to determine safeguards objectives at facility and State levels 8. Able to develop safeguards verification options for a facility

Objective	Performance metric
	9. Able to assess effectiveness and efficiency of safeguards approach and the associated safeguards measures
B.6. Understand NRC's requirements for licensing exports of nuclear equipment and material	1. Knowledge of export and import licensing requirements and review processes 2. Ability to perform export license review, including using Congressional Research Service Reports 3. Knowledge of the requirements of foreign regulatory agencies (e.g., European Commission, Australia, Canada, etc.)
B.7. Understand foreign obligations and obligation tracking	1. Knowledge of the foreign obligation reporting requirements (transaction and inventory) applicable to licensees and DOE sites. 2. Knowledge of the U.S. Nuclear Materials Management and Safeguards System (NMMSS) actions to track foreign obligations 3. Knowledge of current agreements for cooperation and associated administrative arrangements. 4. Knowledge of the Government-to-Government exchange process for establishing foreign obligations 5. Knowledge of the NMMSS actions that go into the preparation of the annual inventory of foreign obligated nuclear materials in the USA
B.8. Understand and be able to manage NMMSS database to ensure completeness and correctness of U.S. nuclear material accounting reports for NRC licensees	1. Knowledge of the domestic and international reporting requirements in 10 CFR Parts 40, 50, 62, 70, 72, 74, 75, 76, and 150) 2. Knowledge of Code 10 of the U.S. Subsidiary Arrangements 3. Knowledge of NMMSS processes for receiving and reviewing material accounting reports 4. Trained and certified as Contracting Officer Representative 5. Able to review correctness and completeness of U.S. accounting declarations to the IAEA 6. Ability to lead reconciliation of differences between IAEA and U.S. data

EUSECTRA training centre - Practice and experience

János Bagi, Jean Galy, Indra Krevica

European Commission, Joint Research Centre, Karlsruhe, Germany

Abstract:

The European Commission has dedicated large efforts to address the fight against illicit trafficking of nuclear and other radioactive materials by supporting its States and partner countries to strengthen Nuclear Security by enhancing their capabilities in prevention, detection and response. The Joint Research Centre (JRC) supports EU policy strengthening nuclear security in providing a broad range of trainings on radiation detection and response to front line officers, trainers and experts. The courses include border detection, train-the-trainers, equipment maintenance, national response plans, nuclear forensics core and advanced capabilities, radiological crime scene management and nuclear security awareness.

One of the main focuses of the Nuclear Security Training Centre (EUSECTRA) of the JRC is the training of front line officers from Member States. Dedicated training consists of theoretical lectures, demonstrations, hands-on and table-top exercises. The training curriculum was developed by the Border Monitoring Working Group, (BMWG) and based on "The Systematic Approach to Training" (SAT) methodology. Practical exercises under realistic conditions are considered as the most important and most effective part of the courses. Thus, in our facility training areas simulate realistic environment and professional scenarios, namely airport conditions and border crossing point. The training program offers a unique opportunity for trainees to see and experience actual materials and commodities, as EUSECTRA is one of the few places in the world where a wide range of samples of plutonium and uranium of different isotopic compositions can be used for training in detection, categorization and characterization together with a large portfolio of dedicated instrumentation.

Since the inauguration of the training centre, a number of courses were carried out, hundreds of front line officers were trained and a lot of experience was gained by the EUSACTRA staff. We use this experience and also the feedbacks of the trainees to enhance the training methodology. In this paper we would like to share our experience and practices in implementing radiation detection trainings.

Keywords: Nuclear security; Detection; Identification; Nuclear materials

1. Introduction

Nuclear and other radioactive materials have many benefits in nuclear industry and many other areas. At the same time, such materials represent a notable threat to people and environment if they are out of control or get into inadequate hands. Radioactive sources of high activity have the potential to cause a serious radiological incident. Nuclear materials also can be used for malicious acts. Nuclear smuggling events and radiological incidents happened in the last decades have established that the threat is real and that the illicit trafficking, inadvertent movement and unauthorized use of such material persists [1]. Therefore, within the framework of nuclear security architecture, certain measures have been implemented to prevent, detect and response to such incidents.

- Prevention involves physical protection of nuclear and radioactive facilities, accountancy, administrative control and inspection on such materials.
- Detection of materials out of control requires radiation detection infrastructure at airports, seaports and border crossing point, and can be achieved through an instrument alarm or information alert.
- Response involves confirmation, identification, assessment of the situation and health risk, measures to protect the health of the personal and the population and secure the material. Such response measures are typically defined in the national response plan and based on or harmonised to the recommendations of the International Atomic Energy Agency. The grade of response depends on the severity of the individual situation [2].

For law enforcement organizations, the term detection has a much broader meaning than detecting radiation from radioactive material by a portal monitor -or by any other instrument- or by information alert. Before the national response protocol is initiated, it must be confirmed that the alarm is real and generated by radioactive material out of control. Front line officers (FLOs) also have to determine, or at least, to estimate the radiological hazard and carry out measures for their own personal safety. These steps can be considered as initial response to instrument alarm or information alert. It is slightly overlapping with the response measures, but carried out at lower level [3].

Identification of radioactive materials and radiological hazard assessment require dedicated expertise. Only experts with scientific background and experience can carry out an adequate assessment. Detailed and accurate analysis of such materials shall require accordingly laboratory conditions and proper experimental set up. Time is another important factor. The preparation of the measurement, the acquisition and the evaluation of the results can last for hours or days. On the contrary, at border check points laboratory conditions cannot be provided, there is a time pressure and the measurements have to be carried out by front line officers such as customs, police, border guards or security officers, who are in principle not in position to do such work. Therefore, investigation of an instrument alarm requires special equipment, straightforward but well-defined response protocol and trained front line officers.

The European Nuclear Security Training Centre (EUSECTRA) to address these concerns provides, among others, such dedicated training for front line officers. Over the past few years, many courses were provided and, consequently, experience is accumulated that we continuously use to enhance the quality and effectivity of the training courses. This paper focuses on mainstreaming to share experiences and good practices among international and national organisations active in the field of nuclear security training.

2. The role of front line officers in nuclear security

Detection and interdiction of radioactive and nuclear material emerges as a crucial duty of the customs and other border management to perform a vital community protection role in terms of preventing international terrorism, in addition to their "traditional" fiscal role in terms of tax collection, and their environmental and social role in terms of protecting public health and cultural heritage. In that respect, FLOs play an essential role in detection of material out of control as they are the first facing the case and they have to initiate the national response. They have to be able to operate radiation detectors, to understand the information provided by the equipment, to conduct secondary inspection with hand-held devices, to maintain their personal radiation safety and to make "detain or release" decision. They also have to understand the principles of radioactivity, radiation detection and the general context of nuclear threat and security, even if very deep knowledge is not required.

3. The European Nuclear Security Training Centre (EUSECTRA)

The European Nuclear Security Training Centre (EUSECTRA) was specifically established by the Joint Research Centre (JRC) of the European Commission to complement the national training efforts and to support the member states of the European Union other countries in nuclear security. Based on the unique combination of scientific expertise, specific technical infrastructure and special nuclear materials available at the premises of the JRC in Karlsruhe, Germany and Ispra, Italy, EUSECTRA provides nuclear security training courses, such as radiation detection at border, train-the-trainers, mobile emergency response (i.e., MEST), reach-back, creation of national response plans, nuclear forensics, radiological crime scene management, nuclear security awareness and sustainability of a national nuclear security posture. The Centre serves also as platform for knowledge transfer and for networking experts.
EUSECTRA is one of the few places in the world that can provide realistic scenarios including special nuclear material. The training program offers a unique opportunity for trainees to get experience in detection and identification of plutonium and uranium of different isotopic compositions.

4. Objectives of FLOs training

The main goal of the training is to get FLOs able to adjudicate and response to radiation alarm and to determine whether it is caused by material out of control.
To accomplish this goal the following main learning objectives are identified:

- FLOs will understand
  - the threat of illicit trafficking of nuclear and other radioactive material,
  - the role of their role in countering this threat,
  - the steps of response process to radiation alarm.
- They will be able to
  - review instrument alarms,
  - use radiation detection equipment,
  - carry out secondary inspection,
  - maintain their personal radiation safety,
  - distinguish innocent and threat material,
  - initiate national response.

The training is performance-oriented with the focus on hands-on exercises supported by lectures, case studies and table-top exercises. The curriculum was developed in an international coordination effort of the Border Monitoring Working Group using the Systematic Approach to Training (SAT) methodology.

5. Practice and Experience

5.1. Preparation

Preparation for a course has to start with the logistic in weeks or even months before the training occurs. Although the general training material is ready and the practical scenarios are worked out, the presenters, who are typically not the developers of the lectures, need time to prepare themselves. The trainers also have to check the training facilities and the equipment, revise the training materials and prepare the training aids. It is also worth to studying the nuclear profile, the radiation detection infrastructure and the operational protocol of the country.
The typical training course consists of 5 days. Lectures are generally given in the morning and hands-on exercises carried out in the afternoon. According to our observations the most effective period for lectures is the first 2 days. The trainees are bright and alert, motivated and pay huge attention to the lectures. Thus, these 2 days are the best to provide the audience with the most important information. On the other side, on the first day they are typically the less proactive. On the last day the situation is actually just the opposite. They are very proactive but after 4 days can pay less attention to the lectures. This is important aspect to be taken into account when making the agenda.

5.2. Lectures and exercises

There is a logical sequence of lectures and exercises, that has to be kept. The first lecture is an overview on the general context of and the FLOs role in nuclear security.
It is particularly important that the trainees receive all necessary information prior to the exercises. Before they take the equipment in their hand on the first afternoon, they have to receive an matching introduction, which is accordingly given on the first morning.
The operational response protocol to an instrument alarm is the most essential part of the training. It describes step by step what the front line officers have to do in the case of an instrument alarm. They receive the lecture on Monday or Tuesday, and then they have to carry out hands-on exercises. Even if there is a general recommendation from the IAEA, the protocol is country and situation dependent. Thus, before the course it is worth to studding the protocol of the given country, to consult with its national atomic authority and, if possible, to invite and involve a national expert in the course.
Some lectures are interactive involving a multiply-questionnaire about the key points. Each trainee is equipped with a clicker and can provide her answer anonymously. The benefit of such practise is that it keeps the trainees attention, makes them thinking and the trainer gets a feedback immediately if the audience understood the discussed point.
In the second half of the course there are also many case studies presented and discussed step by step. The main objective of these studies is to learn and share good practices from previous cases.

Some of them are also interactive and the trainees have to decide what they would do in a given situation. It not just keeps the audience attention but also generates a discussion. The participants are also encouraged to present their cases during the discussion.

The hands-on exercises have to be as realistic as possible involving entire detection equipment, real radioactive and nuclear materials and real-life scenarios and professional situations. The practical section is divided into four modules: (a) introduction to detection equipment, (b) pedestrian portal monitor exercises, (c) vehicle portal monitor scenarios, and (d) computer-based alarm evaluation activity. The practical exercises are complemented with a table top exercise (TTX) where nuclear security detection infrastructure and tactic can be challenged. Typically the trainees are split into 3 working groups and 3 exercises are running simultaneously at 3 different locations. This pattern is, obviously, dependent of the number of participants. This specific set up requires lot of resources, preparation and manpower, but it is still the most effective way of training. The group size has a huge influence on the effectiveness. The working groups should not be larger than 8 persons since it would be difficult to keep everyone active. There are always very active trainees who would like to play the main role and others who would like simply to stay in the background. The trainers have to pay attention to that. The smaller the group the higher the effectivity, but it would require more main manpower and, as the groups have to work separated, more training rooms and equipment. 5-7 people in a group is a good compromise. Each trainee can get a dedicated task, they can rotate the roles, and the trainer can follow their personal activities.
There is a wide range of radiation detection equipment from different producers. In our training centre we have a number of different devices. In most cases we can provide the trainees with that they use at their duty station with few exceptions. Anyway, the international standards on nuclear security equipment ensure that the principals of operation are the same for all devices. If custom officers learn how to operate one device, they are able to use any other.

5.3. Language barriers

Language barrier is a real challenge for the trainers and has a strong effect on the effectivity. In an international training centre as EUSECTRA that provides training not just within the European Union but worldwide, this is an essential aspect to take into account. In many cases, the English practice of the front line officers is good enough to receive the training in English. However, they may need strong support to understand the lectures. The most important tool remains the actual presentations and consequently the individual slides. Preparing and giving lectures has its own science and practice, here we would like point out that we find especially important for our training: First of all, the bullet points of the lecture should particularly simple and clear. Either using just keywords or too complex messages degrades the comprehension. The speaker has to follow the bullet points more strictly than for native speakers and to use more common words that convey the message in simpler terms. Otherwise the audience might lose the line. It is especially important for the lectures involving instructions. In practical exercises it is easier to overcome the language barrier. The instructor can tell and demonstrate what the trainees have to do and see immediately if the message has arrived to the trainees.
Many lectures may include scientific and technical explanations and typically given by trainers with scientific background. Scientists have their own specific terms and phrases that the front line officers might fail to understand. Even the most qualified technical experts and well-crafted course materials can fail to have impact if they do not communicate to the participants in terms that they can understand. This is another language barrier to be considered.
In many instances, interpretation is than needed. In this case all lectures and training materials are translated to native language. The speaker may use English but the audience can see the translated lecture and listen to the interpretation. The disadvantage of using interpretation is that the trainer loses direct contact to the trainees. Interpretation is particularly difficult for practical exercises. Involving a national expert is very beneficial in such a situation, as they know the legal, scientific and technical background and can support the trainer.

5.4. Course evaluation

After the course is completed the effectiveness of the training has to be evaluated. The evaluation is based on the observation of the trainers and the feedback of the trainees. During the exercises the instructor can observe directly the FLOs performance development and identify difficulties and

possible improvements immediately. Directly after the course trainers identify what is needed to improve performance and determine how the course could be better done.
Additionally, the facilitators may use breaks and other opportunities to poll participants informally about their response to the activity as well as to give feedback to facilitators/trainers on techniques that might improve effectiveness.
The trainees also have the opportunity to evaluate and rate the course anonymously using a multiply choose questionnaire. This feedback is very valuable in helping us to refine the training program.

6. Summary

A large series of nuclear security courses for front-line officers, trainers and experts have already been provided involving participants from many countries within and out of the European Union. The basic radiation detection training to front line officers is the most demanded within the EUSECTRA training portfolio. Since its official launch, EUSECTRA has hosted trainees in Karlsruhe and Ispra from over 70 different countries, including more than 1000 front line officers from all around the world, which have benefited from the training provided.
Based on the feedback provided by the trainees and their respective national authorities it can be concluded that the course fulfils its objectives. EUSECTRA trainings are indeed repeatedly acknowledged by trained countries to be beneficial in terms of enhancing preparedness, detection of and response to nuclear security events. EUSECTRA's unparalleled training opportunities lead to a steadily increasing demand for training sessions. Yet, the EUSECTRA team is very committed to improve efficiency, and gives effort to continuously enhance quality of the trainings at all levels.

7. References

[1] IAEA Incident and Trafficking Database (ITDB)
[2] Response to events involving the inadvertent movement or illicit trafficking of radioactive materials, IAEA-TECDOC-1313
[3] Detection of Radioactive Materials at Borders, IAEA-TECDOC-1312, Vienna (2002).

Education and Training on Nuclear Safeguards and Non-Proliferation in EC JRC under ESARDA TKM WG

Kamel Abbas[(1)], Véronique Berthou[(2)], Pascal Daures[(3)], Willem Janssens[(2)], Paolo Peerani[(4)] and Francesco Raiola[(1)]

[(1)] European Commission, Joint Research Centre, Nuclear Safety and Security Directorate, Nuclear Security Unit, Ispra, Italy
[(2)] European Commission, Joint Research Centre, Nuclear Safety and Security Directorate, Ispra, Italy
[(3)] European Commission, EuropeAid, Development and Cooperation, Brussels
[(4)] European Commission, Joint Research Centre, Nuclear Safety and Security Directorate, Nuclear Decommissioning Unit, Ispra, Italy

Abstract:

Nuclear safeguards and non-proliferation are generally absent from academia curricula in nuclear science and technology. To fill this gap, the Working Group on Training and Knowledge Management of ESARDA developed a dedicated specialized course, which is organized on yearly basis by EC JRC in Ispra (Italy). Since the first course in 2005, 16 editions of the course with 40 to 60 students have been successfully organized. This compact course is open to master degree students, in particular nuclear engineering students, but also to young professionals and International Relations/Law students. It aims at complementing nuclear engineering studies by including nuclear safeguards and non-proliferation in the academic curriculum. The course addresses aspects of efforts to create a global nuclear non-proliferation system and how this system works in practice: The Treaty on Non-proliferation of Nuclear Weapons, safeguards technology, and export control. Also regional settings, such as EURATOM Treaty, are presented and discussed. The course deals in particular with technical aspects and application of safeguards: i.e. how to implement the safeguards principles and methodology within the different nuclear facilities. Therefore, the course presents an overview on inspections techniques, ranging from neutron/ gamma detectors, to design information verification, to environmental sampling, etc. Students attending the course and passing an examination, consisting on a multi-choice questionnaire and a written assay, are awarded three credits according to the ECTS (European Credit Transfer System) in their university curriculum.

The paper presents the experience of 16 years' experience of ESARDA course by also pointing out on it evolution during these years. Moreover, due the success of the course and the need of such initiative to be implemented out of Europe, DG DEVCO has funded, the program of this last development will be also presented.

Keywords: Safeguards, Non-Proliferation, Education, Training, ESARDA

1. Introduction

The knowledge retention issue in the nuclear field was acknowledged by the OECD in 2000. The United Nations study on disarmament and non-proliferation education (2002) made detailed recommendations for urgently required improvements. In fact, nuclear safeguards and non-proliferation are generally absent from academia curricula in nuclear science and technology. Moreover, teaching in the Nuclear Safeguards field is indeed strongly influenced by national history so the objective of the ESARDA course is to provide homogeneous material in Nuclear Safeguards and Non-Proliferation matters at the European and international level.

ESARDA, the European Safeguards Research and Development Association (Ref. 1), which is nowadays considered more and more as European forum/think tank in safeguards, non-proliferation and related fields

reacted to these shortcomings with a strategy to tackle the problem and created a Working Group on Training and Knowledge Management (ESARDA TKM WG) to setup academic course modules to an internationally recognised reference standard. The objectives of the ESARDA TKM WG are to promote nuclear safeguards and non-proliferation education and training in general and to setup and yearly organise the so-called ESARDA Course on nuclear safeguards and non-proliferation.

Since 2005 the Nuclear Security Unit, Nuclear Security and Safeguards Department, Nuclear Safety and Security Directorate, Joint Research Centre Directorate General of the European Commission in collaboration with ESARDA TKM WG collaboration has yearly organised the ESARDA Course. The last edition was organised in April 2017. In the following chapters an overview of the course is given including duplications of the course out of Europa. In fact, due to its success and the need of such initiative to be implemented worldwise, EC DG DEVCO funds the organisation of the course in several regions to enhance awareness of nuclear safeguards and non-proliferation.

2. Organisation of ESARDA Course

The course is organised yearly in Ispra by JRC Nuclear Security Unit and features a full five-days program with lectures and practical exercises by international experts in the field of nuclear safeguards and non-proliferations. The course includes visits to JRC Ispra safeguards laboratories. The session preceding the closing ceremony of the week course is dedicated to the evaluation of course in which a multi-choice exam is performed by the students and then discussed in a plenary. This exam contains questions on each of the topics dealt in the week. After that, a feedback on the course is asked to the students not only on the on the content of each of the lectures but also on the lecturers. In addition to examination performed during the ESARDA course, the students attending the course have a possibility, on their voluntary basis, to make an exam consisting on an online multi-choice questionnaire and a written assay. Then, if they pass they are awarded three credits according to the ECTS (European Credit Transfer System) in their university curriculum. Up to 2 best essays can be selected for being published in the ESARDA Bulletin or for being presented in the poster session at the ESARDA Symposium.

The closing ceremony of ESARDA Course is dedicated to the delivery of participation certificates and closing addresses by the organisers and the participants. No course fee is requested to the registries.

This compact course is open to master degree students, in particular nuclear engineering students, but also to young professionals and International Relations / law students. It aims at complementing nuclear engineering studies by including nuclear safeguards and non-proliferation in the academic curriculum. The basic aim of the course is to stimulate students' interests in safeguards and non-proliferation. The course addresses aspects of the efforts to create a global nuclear non-proliferation system and how this system works in practice: The Treaty on Non-proliferation of Nuclear Weapons (NPT), safeguards technology, and export control. Also regional settings, such as EURATOM Treaty, are presented and discussed. The course deals in particular with technical aspects and application of safeguards; i.e. how to implement the safeguards principles and methodology within the different nuclear facilities. Therefore, it creates an overview on inspections techniques, ranging from neutron/gamma detectors, to design information verification, to environmental sampling, etc.

The course material, consisting of a complete set of presentations and literature is provided to the participants which is also posted on the webpage of ESARDA. It also contains a link to the portal of NuSaSET (Nuclear Safeguards & Security Education and Training) (Ref 2) being an international initiative of the INMM (Institute for Nuclear Material Management), ESARDA and IAEA. This portal provides support to professionals in the field of Nuclear Safeguards and Security, specifically to promote the provision of training and education of students.

As course material, the syllabus book of ESARDA Course (Figure 1) is also distributed to the participants. A new edition of the book is being under elaboration that will contain news chapters such as nuclear trade regulation, the utility of open-sources, monitoring and verification applications, nuclear security in context of international law and concepts. Additionally, few chapters will be updated such as those on DA and NDA techniques sued for safeguards and history of the evolution of safeguards and its international regulations.

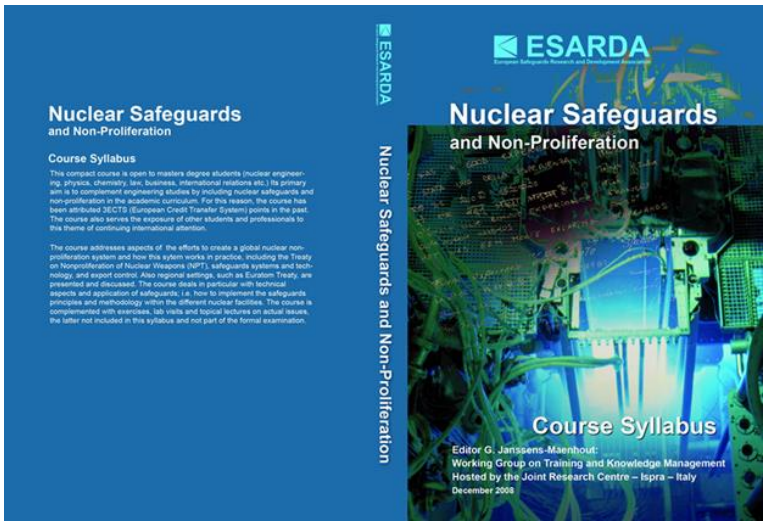

Figure 1: ESRDA Syllabus edition 2008, a new edition is being prepared

3. ESARDA Course Content and Participation

The major topics covered in the course are presented below.
Introduction: evolution of the Non Proliferation Treaty - regime, safeguards, international control regimes in theory and practice. and present trends in the nuclear non-proliferation efforts.
What is safeguarded: nuclear material that is subject to nuclear safeguards and related safeguards goals (significant quantity, timeliness and detection probabilities).
Where: nuclear fuel cycle from mining to final repository, focussing on enrichment in the front-end and reprocessing in the back-end.
Legal framework: overview on international and regional Non-Proliferation Treaties and established Institutions and Organisations.
Verification methodology: nuclear material accountancy principles and statistics of auditing.
Inspection tools: overview on inspector tools and their use to verify the nuclear activities (Destructive and Non-Destructive Assay, Containment/Surveillance); additional safeguards measures under the Additional Protocol (complementary access, satellite imagery, environmental sampling) and how they are applied in field (storage facility, process facility, enrichment facility, research institute, spent fuel transfer).
Nuclear security: physical protection, import/export control of dual-use items, combating illicit trafficking, nuclear forensics.
Non-proliferation: collection/analysis of open source data and case studies. Collection of open source data and demonstration of some case studies (Iraq, 1993).

Approximately 60 students participate in each course with a majority from Europe. Figure 2 presents some information of the last ESARDA course (16th edition) held from 3rd to 7th April 2017 with a comparison on the participation with respect to the 15th edition. Lecturers are offered by JRC, EURATOM, IAEA, JAEA, DoE and many other organisations of EU Members States including other ESARDA members.

Apart from students, the course is typically attended by professionals from:
- Nuclear inspectorates (IAEA and EURATOM)
- National authorities
- Research centres
- International organisations
- Operators of nuclear facilities

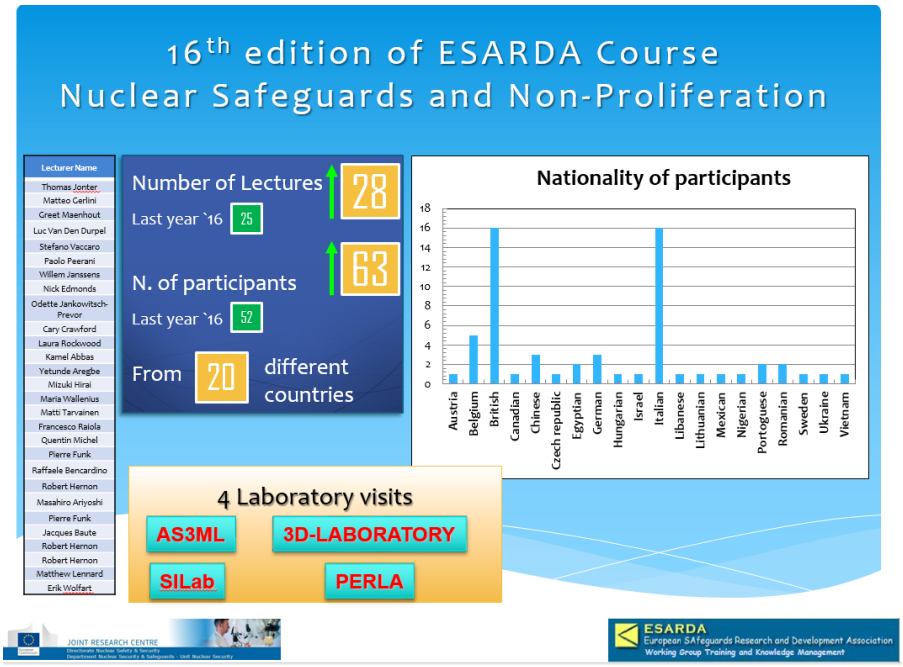

Figure 2: Participation to the 16th edition of ESARDA Course held in Ispra on April 3rd-7th 2017

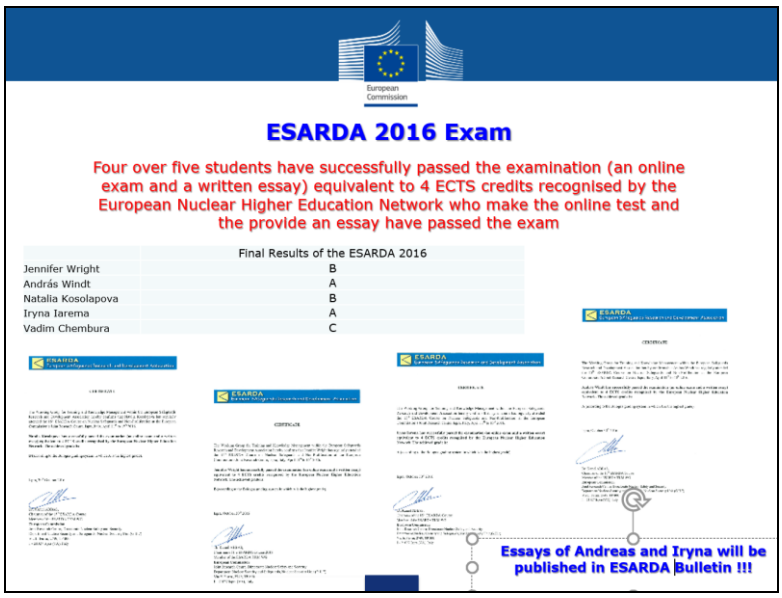

Figure 3: Results of the exam of the 15th edition of ESARDA Course: Four over the five students that have made the exam have successfully passed.

4. Towards the implementation of ESARDA course worldwide

An Administrative Arrangement was signed between JRC and DEVCO in 2016 (Figure 4) in view of provision by JRC of educational courses of nuclear safeguards and non-proliferation, world-wide, based on the ESARDA course experience at JRC Ispra in the last 15+ years. Those course participants shall be adequately selected by the country beneficiaries in the perspective that some of the participants shall be future organisers of safeguards courses in their respective countries. The latter will enhance the suitability of the EU outreach effort in this field. Similarly, the planned creation of an “Educational Network” (i.e. bringing together future organisers for such safeguards courses across countries and regions) should support sustainability.

The project aims in a first instance at providing an academic basis for an educational course in a limited time of a week of classroom teaching. The academic recognition will be a duty of the partner country. In Europe this was achieved in the past by adding to the course itself the duty for the students to write an essay and take an exam (for a total of 3 ECTS points). It will depend on the specific universities and countries on how this can be translated outside Europe. In case academic recognition cannot be achieved under this project, the integration of the course in existing training packages and training centres will be aimed at. The course is so structured to ensure to the participants a good basis for performing safeguards activities and also for ensuring transfer of acquired knowledge in their countries which contributes to the sustainability of the project achievements.

In agreement with DEVCO, the first contacts are already taken with two countries namely Algeria for north Africa Region and South Africa for south Africa region. The organizational work for the course in north Africa has started and it is planned for the end 2017 or beginning 2018. Other targeted regions will follow such as Iran, Vietnam, Jordan, Kazakhstan, Georgia and Philippines, … The choice of countries is discussed/agreed with DEVCO in line with updated country or region priorities.

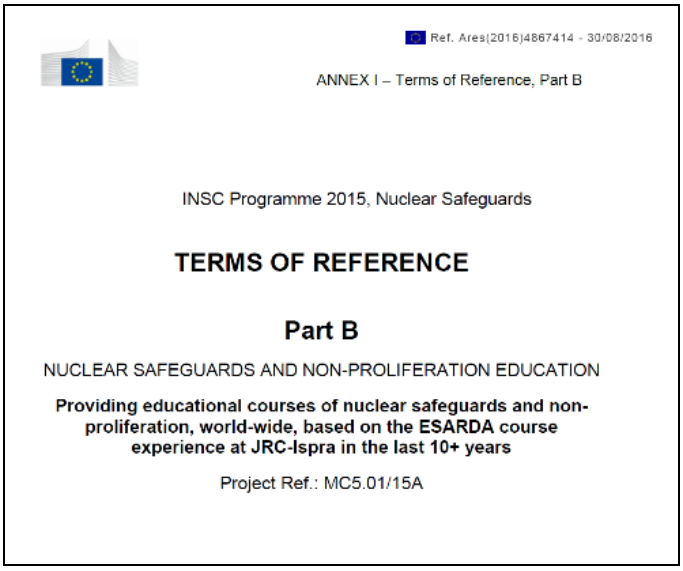
Ref. Ares(2016)4867414 - 30/08/2016

ANNEX I – Terms of Reference, Part B

INSC Programme 2015, Nuclear Safeguards

TERMS OF REFERENCE

Part B

NUCLEAR SAFEGUARDS AND NON-PROLIFERATION EDUCATION

Providing educational courses of nuclear safeguards and non-proliferation, world-wide, based on the ESARDA course experience at JRC-Ispra in the last 10+ years

Project Ref.: MC5.01/15A

Figure 4: Administrative Arrangement for Provision of Safeguards Education worldwide

5. Conclusion

ESARDA as a whole is playing an important role as an European forum/think tank in safeguards, non-proliferation and related fields. Additionally, its symposiums and meetings of its WGs make support successfully the mission of the association. ESARDA Course is well established and successfully organised over 16 years. Due to its success and the need promote safeguards and non–proliferation Training & Education networking, sustaining competences, ESARDA Course is presently under way being implemented worldwide.

References

1. ESARDA: https://esarda.jrc.ec.europa.eu/
2. NUSASEThttp://www.nusaset.org/index.php?option=com_content&view=article&id=137&Itemid=130

The JRC Advanced Safeguards Measurement, Monitoring and Modelling Laboratory

Claudio Bergonzi, Luc Dechamp, F. Littmann, Giovanni Mercurio, Patrice Richir, Vitor Sequeira, Erik Wolfart, Willem Janssens

Nuclear Security Unit, Directorate Nuclear Safety and Security,

Joint Research Centre, European Commission, Ispra, Italy

ABSTRACT

The innovative aspect of the Advanced Safeguards Measurement, Monitoring and Modelling Laboratory, AS3ML, subject of this paper, is that it aims to complement the classical approach of implementing nuclear safeguards by providing an innovative method to monitor the process of sensitive facilities such as Gas Centrifuge Enrichment and Nuclear Fuel Reprocessing plants and/or deploy innovative / smart sensors and technologies.

AS3ML endeavors to enhance the "traditional safeguards measures" by the focus on and analysis of (other) process parameters, that may be used to understand & monitor better the whole plant.

Some of new technologies investigated include: Indoor localization (RFID, UWB, Laser positioning), 2D/3D Camera, ID (OCR) of cans, Investigative Inspector, pulse shape generator to simulate Gamma and Neutron detectors

The AS3ML is conceived as an R&D location, test bed, demo facility and training centre for innovative safeguards approaches where researchers, inspectors (and operators) can conceive and analyse different approaches (including competing technologies) for safeguarding nuclear facilities.

The paper will describe techniques and approaches, not currently used in routine safeguards applications, including some recent return of experience on deploying AS3ML based approaches for a new way of safeguarding a plutonium storage location and an enrichment facility.

Keywords : safeguards, modeling, process monitoring, innovative sensors, mass/volume

1. Introduction

JRC started the development, a couple of years ago, of a new laboratory, baptized Advanced Safeguards Measurement Monitoring and Modelling laboratory (AS3ML), with the main scope to both modernize safeguards implementation and provide a test-bed, demo-site and training facility to look at new approaches, use of operator data, advanced sensors and innovative process monitoring technologies.

This paper describes the current state of the laboratory, provides some examples of recent achievements and developments and an outlook on the future projects planned in AS3ML.

The AS3ML is conceived as an interconnection of a number of distinct areas, each representative for a specific type of fuel cycle facility, but at the same time offering the opportunity to test out the use of certain techniques typically deployed in other areas. Another major emphasis lies on the tools used to enhance the inspector's analysis and interpretation skills to deal with multiple sensors, comparison between process modelling and measurement and diagnosis of anomalies in general.

2. The Mini-process/TAME/Mass-volume area

Reprocessing plants (RP) are among the most sensitive ones in the nuclear fuel cycle and safeguards inspectorates have always invested large effort to control them. JRC has an historical competence in supporting Euratom and IAEA inspections in reprocessing plants like La Hague, Sellafield and Rokkasho.

In particular the TAME laboratory is especially dedicated to the development and validation of techniques used to monitor and account solutions of nuclear material in RPs and to train inspectors. The TAME facility is equipped with full-scale vessels similar to those installed in RPs and is located in the same hall of AS3ML.

A demo and training area for simulation of processes in RPs is included in the AS3ML and has been equipped with reduced-scale vessels of different shapes (cylindrical, conical, slab, annular, harp,…) connectable with a choice of transfer systems (pumps, gravity, syphon,…). This allows reproducing and playing a broader variety of scenarios in management of solutions and associated monitoring techniques and to test the software used to monitor the process and train the inspectors in the review of data.

Some R&D components associated to this is the development and validation of software for automated calibration of mass/volume measurement devices and for the tank calibration verification by continuous flow mode (upgrade of to VOLCAM.NET program).

The signals to be monitored in such processes are pressure and temperature, from the pressure values the level and density values are then derived (trough calibration curves). New measurement devices are developed using the latest technologies in term of industrial data acquisition (OPC, Ethercat) and data transmission (OPC UA, data authentication and encryption).

This new hardware makes largely use of Ethernet as a communication channel. The use of “Power over Ethernet” (PoE) will be tested in order to determine the advantages and disadvantages. It could help to simplify the design of future installation and so reducing also the wiring cost.

The use of industrial standard for performing data acquisition using PLC is also one of the objectives of the facility. PLC code for acquiring the data could be written using the IEC 61131-3 standard then exposed them using the IEC 62541 (OPC UA also known as IIoT) standard and using IEC 61508 (EtherCAT) standard to collect data from other real time devices. Some of those norms have been investigated to evaluate their advantage or disadvantage for a deployment for safeguard purpose and deployed in real facilities such as THORP, La Hague UP2 and UP3. The IEC 61131-3 standard is used to perform the data acquisition making use of IEC 61508 (EtherCAT). Further investigations are needed for IEC 62541 (OPC UA).

Figure 1: Picture of the facility performing multiple solution transfer processes with different types of tanks (cylindrical, annular, slab, conical and others) and transfer systems (pumps)

3. Test and validation of software for data acquisition and analysis

The monitoring software tool, called DAI (Data Analysis and Interpretation) has been developed by JRC upon request of the EURATOM inspectorate and was initially specifically designed for process monitoring in RPs, even though its modularity and flexibility allows nowadays its use for monitoring most of the safeguards-relevant processes in all the nuclear facilities. This monitoring tool does more than just supervision: it interprets the signals and verifies the consistency and coherency with predefined criteria and without intervening in the process. These criteria are based on the design characteristics of the recipients and transfer mechanism.

In the case of the solution process in a reprocessing plant, the signals are visualizing the solution properties (temperature, density) and tank levels. The change in tank level of the feeding tank is cross-checked against the corresponding change in tank level of the communicating process tank and the software verifies the coherency in total mass transferred. In particular the start of a transfer has to be recognized appropriately and that with the appropriate signal profile, that differs for siphon transfer and mechanical pumping. DAI is continuously monitoring/tracking nuclear material flow through a reprocessing plant, while verifying by cross-correlation if the total mass transferred is arrived at its destination in the tank downstream.

The JRC's software package for Process monitoring consist several modules:

1. The data acquisition: to collect the data for the data historian (local buffering).
2. The data historian: allow real-time registering of data with timestamp (dead band and compression).
3. The data analysis kernel (DAI): to analyse and interpret the data collected from the process control sensors and actuators. The central task of the DAI kernel is the recognition of exploited process cycles with the objectives to survey in real time the correct operation of the production process, to diagnose abnormal situations and to evaluate the process performance indicators and inventory balances of the batch cycles in real time.
4. The relational database with results.

The numerical simulation of Gas Centrifuge Enrichment Plants presents many important challenges:

1) Fluid properties: uranium hexafluoride is a heavy gas, having a density about 10 times larger than air;
2) Flow conditions: the system works at low pressure (around 500 Pa) and with extremely small flow rates, in the order of micrograms per seconds;
3) System complexity: plants contains hundreds or thousands of centrifuges;
4) Physical complexity: the isotope separation process takes place into centrifuges spinning at hypersonic velocities.

A system level fluid-dynamic approach was designed and implemented using the advanced CFD software tool FloMASTER®. In order to model the complexity of the system, a bunch of custom components were implemented into the library. The most important one is the component capable to model a single centrifuge or a single stage of the cascade by providing the separative power of the centrifuge as a function of gas flow rate and the number of centrifuges in the stage (see Figure 2).

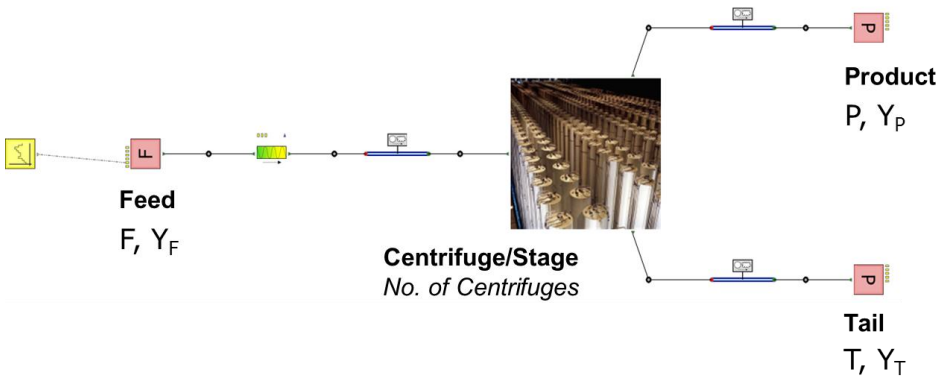

Figure 2: System Level 1D FloMASTER Computation Fluid Dynamics model of Centrifuge/Stage

The numerical simulations performed with a complete network cascade model show that a system level approach is capable to model the main features of an uranium enrichment cascade plant on workstations in times ranging from few seconds to few hours depending on the length of the simulated times. In addition the simulations supply a reliable estimation of the cascade separation performances under normal and off - normal conditions. In particular it is possible to analyze the transient behavior of the centrifuges cascade physical parameters in case of material diversion and/or misuse activities. An example is illustrated in Figure 3 where are showed the transient curves corresponding to the stages product assays in case of a small addition of undeclared feed for an 11 stage cascade composed of “Rome” type centrifuges.

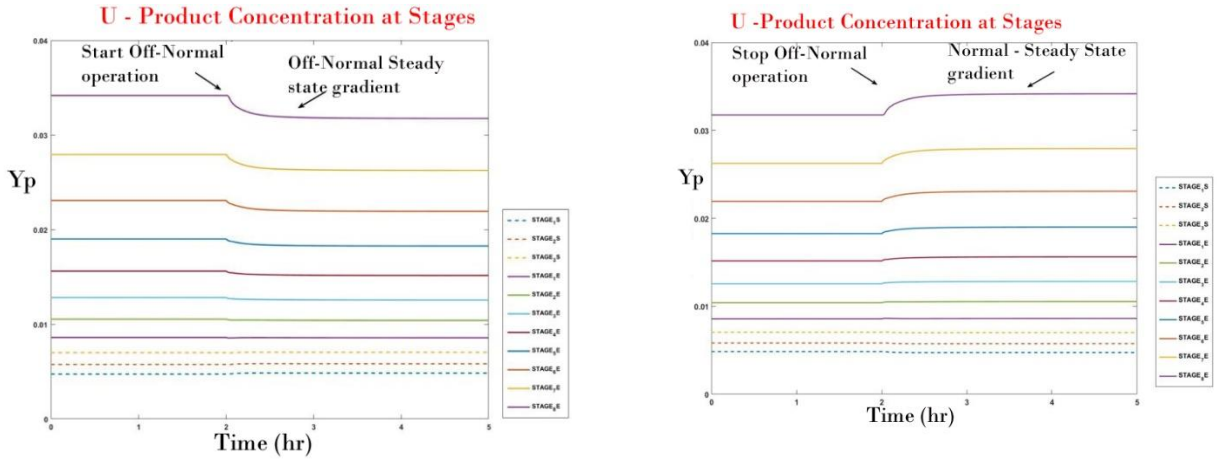

Figure 3: Stages product assays transient effects in case of undeclared addition of UF6 feed (Off – Normal condition) and successive restoration of UF6 normal feed (Normal condition) at the input stage.

4. Local and remote inspector offices

Future safeguards will make use more and more of unattended monitoring systems coupled with remote data transmission, provided that secure data transmission is granted.

In order to test the data communication tools and protocols and to demonstrate the functionalities of the remote monitoring software, AS3ML will host two offices that will act respectively as the Local Inspector Office at the facility and the Inspectorate Headquarter.

The equipment of the office areas will basically consist on high-end servers for collection and storage of data from the different other areas of the AS3ML, workstations for data retrieval and analysis from the inspectors, large screens to project synoptic of the facilities (with HD and 3D capabilities) and, when applicable, replicas of facility control rooms.

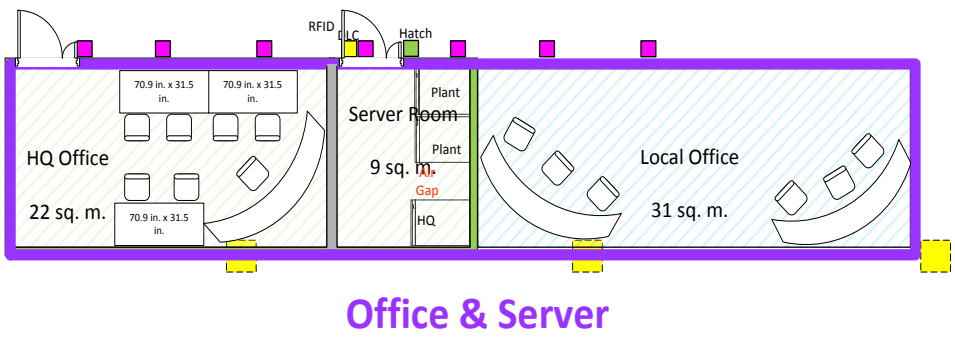

Figure 4: Layout of the inspector offices area

The main requirements for the data transmission systems include:

- The devices in the process should be able to communicate state-of-health and data to clients in the local office
- Flexibility in adding/removing devices to/from the data transmission system
- Monitors with Graphical User Interfaces (GUI) should allow displaying the facility layout and verifying the status of devices at the local office
- The Headquarter Office should allow viewing the status of the process and access to a (limited) set of operator approved data
- Communication between facility and local office and between local and HQ offices should include authentication features
- Data communication between local and HQ offices shall have integrity strength to be managed by public internet (encryption)
- Communication protocols should be compatible with international standards and make use as much as possible of proven industrial tools

OPC-UA (IIoT), MQTT, AMQP) (MQTT = Message Queuing Telemetry Transport, AMQP Advanced Message Queuing Protocol, OPC-UA = OPC Unified Architecture (OPC UA) is an industrial M2M communication protocol for interoperability developed by the OPC Foundation. It is the successor to Open Platform Communications (OPC).

Figure 5 shows a generic scheme of a data transmission system including the main protocols used for data exchange (OPC-UA, MQTT and AMQP)

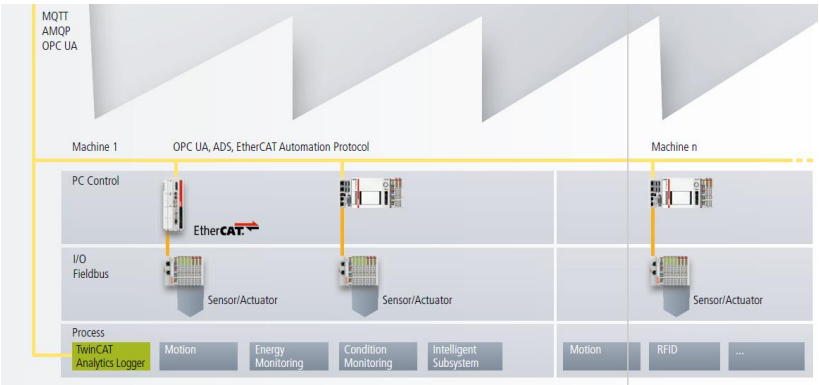

Figure 5: From sensor to headquarter Data transmission system

Figure 6 shows the use of data agent to provide Data to public or Private Cloud making use of any of the transmission protocol OPC-UA, MQTT or AMQP

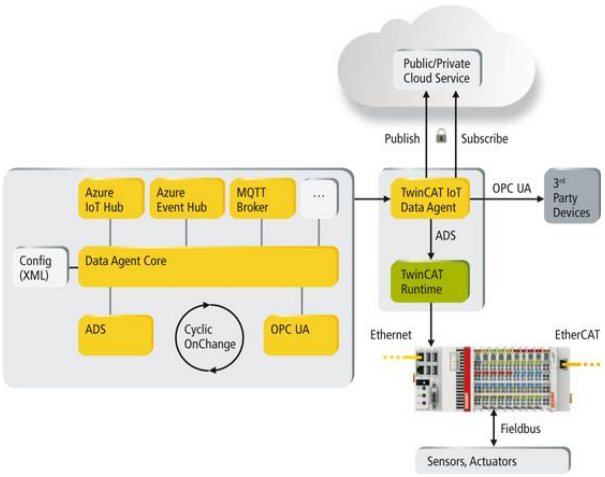

Figure 6: From sensor to CLOUD

5. The spent fuel pond area

Spent fuel ponds are the most sensitive part of nuclear power plants from a safeguards perspective and pose very specific needs in terms of safeguards. The fuel, once it has been used in the nuclear reactor, has to be kept in water to cool down before it can be removed and put in dry storage casks. Spent fuel is kept under strict control to avoid diversion, and the spent fuel ponds are constantly under video surveillance to detect undeclared activities.

In some cases, for example in CANDU reactors, the small size of the spent fuel element and the plutonium contained in it require an even more strict control. In the AS3ML is a small pond filled with water containing various mock-ups of the spent fuel racks with a platform, which is used to simulate a spent fuel pond and a bridge moving above where operators and inspectors can go to install and read seals.

This facility gives a great opportunity to train inspectors from Euratom and/or IAEA and facility operators, on a one-to-one scale mock-up of an underwater storage, on the use of the ultrasonic sealing systems developed by JRC. This is particularly relevant for the JRC CANDU (in use in Romania – Cernavoda and Pakistan – Karachi) or the JRC La Hague (France) Sealing Systems, underwater ultrasonic sealing systems that require the handling of long tools to deploy the seal over the stacks containing the spent fuel (see figure 7). It is used as well to test new prototypes, as the one developed for ABACC to be deployed in Argentina, at Atucha nuclear plant. The facility can be used also to train people over the use of other instruments, with the aid of a Cherenkov Effect simulator, that produce a light emission similar to spent fuels.

On the side of the pool two mock-ups of dry storage casks have been installed and reproduce how the casks are sealed. These mock- ups are used to train inspectors on the use of Ultrasonic Optical Sealing Bolts, a new dual technology seal expressly designed by JRC for dry storage sealing. UOSB combines wire sealing (passive, like COBRA or active, like EOSS, RMSA or AOLS) with ultrasonic seals (see figure 8)

A recent achievement, in addition to all training sessions done on underwater and dry storage ultrasonic sealing system is the validation of the prototypes used for ABACC. The first prototype designed for the sealing of Atucha spent fuel pond, has been tested in the pond area. A mockup of the hangers was designed and validated the correct fitting of the locking mechanisms first in air and then in water (figure 9). It later happened that the prototype brought to Argentina fit perfectly well with the real hangers. The final design which will be tested in second half of2017 has been fine tuned in the same pond as well. For training purposes, even a copy of the pond and a mock up of the hangers was build to train inspectors and operators in Buenos Aires.

Real spent fuel pond in Karachi, with racks sealed by JRC ultrasonic sealing bolts

Mock–up of the Kanupp sealing racks (on the right) with associated handling tools

Figure 7: Spent fuel pond in reactor and mock-up in AS3ML

Real CONSTOR dry storage cask in Ignalina (Lithuania) with Ultrasonic Optical Seal Bolts

Mock–up of the CONSTOR cask used for training of inspectors

Figure 8: Sealing of casks for dry storage of spent nuclear fuel

Test of a ABACC sealing system prototype in the pond

Mock–up of the hangers and test in air of ABACC prototype

Figure 9: Specific tool development for use by ABACC

6. The interim/final storage area

The storage area is conceived to test technologies and methodologies applicable to any kind of itemised facility, such as fabrication plants, nuclear material storages, reactors, interim and final storage of spent fuel, etc. The storage area is equipped with different types of technologies that can be used to identify, authenticate, localize and follow movements of items containing nuclear material in a plant, including radiation detectors, surveillance equipment, weighing scales and identification and localization devices.

The storage area aims to support the development of integrated containment and surveillance systems, such as the ‘Unattended Combined Measurement System’ (UCMS) that was developed for monitoring the plutonium storage at the Magnox plant. It is also used to investigate concepts for the integrated analysis of data coming from different sensors and systems.

Some of the technologies that are being developed, evaluated and demonstrated in the AS3ML storage area are the following:

Identification And Authentication

RFID: Radio Frequency Identification (RFID) has been used in various industrial and commercial applications for many years. The tags, which are attached to the objects of interest, modulate an electro-magnetic field that is emitted by a reader and generate a unique response. The latest generation of tags allows authentication and encryption with passive tags.

3D laser for container identification.

JRC develops systems for the identification and authentication of nuclear material containers using accurate 3D measurements of the container surface. For example, LMCV (laser surface mapping for containment verification) has been developed for the identification and authentication of dry storage containers. It uses triangulation-based laser scanning to acquire surface profiles of the container welds with micrometer accuracy which are used as a unique signature of the container, figure 10.

Figure 10: LMCV mounted on dry storage casks in Canada during a field trial.

Localization and Tracking.

Localization of nuclear items and handling equipment is fundamental for the detection and tracking of safeguards relevant events in nuclear (storage) facilities. Commercial Indoor Position Systems use either radio- frequency (RF) and/or ultrasonic signals and require the installation of an infrastructure (beacons) in the facility. AS3ML will be used to demonstrate the use of the techniques in different application scenarios and investigate the suitability and limitations of the available products.

Laser Positioning systems can be used for precise localization of items of interest and could be used for monitoring the declared movement of UF6 cylinders in an enrichment plant. The feed, product and tail material are contained in large and heavy containers that are moved using a special dedicated loading machine. Monitoring the movements of the loading machine can be a way to double check the declared movements of cylinders and therefore the transfers of nuclear material.

7. Surveillance

AS3ML has been used during the development and testing of various safeguards surveillance devices, in particular related to 2D and 3D laser systems: Laser curtains use laser scanners measuring the position of objects within a 2D plane. They allow detecting movements of pre-defined objects (i.e. according to size and shape) within a specified area of interest, see figure 11. Event detection based on laser scanners is more robust than change detection based only on optical imagery and is typically used to trigger optical surveillance cameras. Laser curtains are used for example in the UCMS in Sellafield and for monitoring movements over a fuel pond in La Hague.

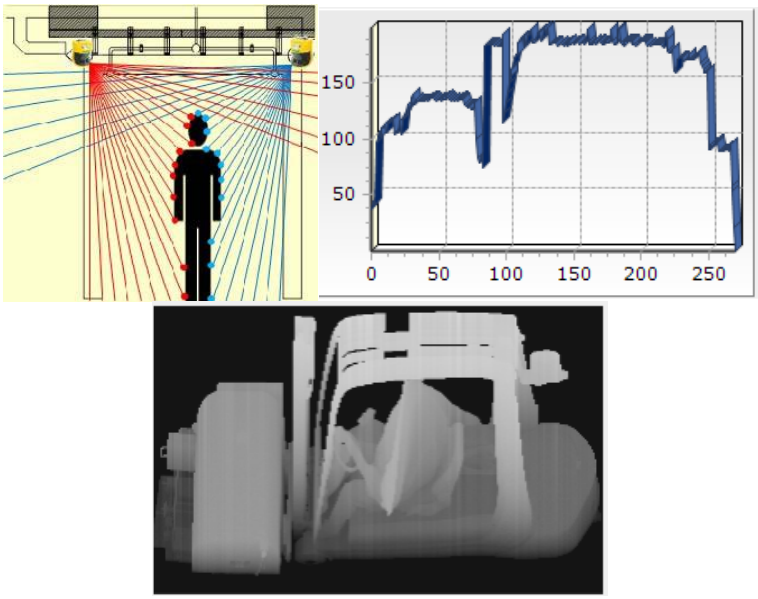

Figure 11: detection principle by the laser curtain. Profile and reconstructed profile of a forklift truck as used in the UCMS.

Considering the long development cycles in nuclear safeguards, the design of the future surveillance system will be starting soon. Optical surveillance cameras will remain the core of safeguards surveillance system. However, many other relevant sensor types are becoming available and a future system should be able to support multiple sensors and be flexible enough to integrate new sensors types as they become available. The following design principles should guide the developments of the future surveillance system (see figure 12): i) It uses a modular approach where the common requirements are separated from the sensor itself. ii) The hardware design is based on OEM components and is owned by the inspectorates. iii) The surveillance device is compatible with the existing infrastructure for remote data transmission and, for example, supports remote configuration and health checks. iv) The surveillance device supports different deployment scenarios (i.e. stand-alone with local data storage, networked with and without remote data transfer. JRC will support the development through the design, prototype development and evaluation phase as presented in a dedicated paper “Containment and Surveillance Systems – reflections on future technologies” in this 2017 ESARDA meeting.

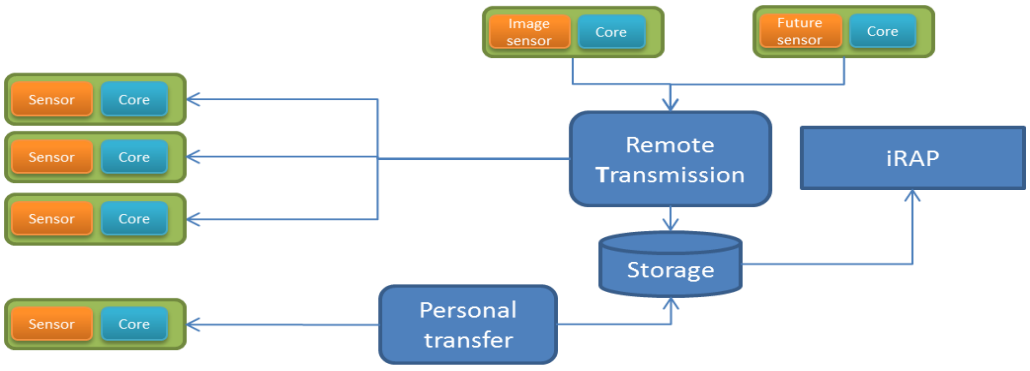

Figure 12: Proposed structured of data gathering, transfer and storage.

8. Simulation

Since the use of real nuclear material is not foreseen within AS3ML, the signal of radiation detectors will have to be simulated. Neutron counter and gamma spectrometer surrogates are under

development that will be able to reproduce the signal of a real instrument as a function of position and type of the item containing the nuclear material.

9. Outlook

The AS3ML laboratory continues to be equipped and expanded, both based on innovative R&D results and on return of in-field implementation of new safeguards approaches. AS3ML offers itself as a testbed for new methodologies to be validated and thus is open for both safeguards inspectors, national authorities and nuclear fuel cycle facility operators.

Session 12

Destructive Analysis II

Certification of Ultra-High Purity Pu-244 for Safeguards Applications

Marianne Fisher[1], Arden Dougan[1], Ross Williams[2], Anagha Iyengar[3], Kerri Treinen[2]

[1]U.S. National Nuclear Security Administration (NNSA)'s Office of International Nuclear Safeguards, [2]Lawrence Livermore National Laboratory, [3]Oak Ridge National Laboratory

Abstract:

Following nearly 25 years of negotiation, preparation, and collaborative efforts between the U.S. Department of Energy (DOE), the International Atomic Energy Agency's (IAEA) Department of Safeguards, and the Russian Scientific Research Institute of Experimental Physics (VNIIEF), the U.S. National Nuclear Security Administration's (NNSA) Office of International Nuclear Safeguards is finalizing production and certification of ultra-high purity plutonium-244 (Pu-244). This newly fabricated Pu-244 material will support the IAEA Network of Analytical Laboratories' (NWAL) need for a better Pu spike material for low-level analyses to address international nuclear safeguards challenges. Before the end of 2017, this joint effort will have produced and certified the highly-enriched Pu-244 (99.98% purity), thereby enabling accurate measurements of Pu in environmental samples and providing more than a century's supply of Pu-244 certified reference material (CRM) for nuclear safeguards, nuclear forensics, and other scientific purposes. This paper seeks to provide an overview of the historical origins of the cooperation, a timeline of the Pu-244 production, and its applications in support of IAEA safeguards.

Keywords: Plutonium, Pu-244, Safeguards, Certified Reference Material, Network of Analytical Laboratories

1. Background

Currently, Lawrence Livermore National Laboratory (LLNL) is fabricating ultra-high purity plutonium-244 (Pu-244) reference material for use in bulk environmental sample analyses for safeguards. Pu-244 is used by many members of IAEA's Network of Analytical Laboratories (NWAL) as a spike isotope for quantification of Pu content, but stocks of this essential spike are nearly exhausted. Although discussions on fabrication of new sources of ultra-high purity Pu-244 began in 1991, technical preparations did not begin between the U.S., Russia, France, and the IAEA until more than a decade later. Following nearly 13 years of work, the Pu-244 fabrication project is expected to be completed in 2018, with a new Pu-244 reference material expected to supply the needs of the IAEA NWAL for many decades.

In 2005, NNSA/DOE agreed to supply a small quantity of plutonium dioxide containing about 17.5 atom % Pu-244 to the IAEA, who subsequently negotiated an agreement with the Russian Federal Nuclear Center — Institute of Experimental Physics (VNIIEF) to perform a two-phase electromagnetic separation to increase isotopic purity of the supplied material for the fabrication of a high-purity Pu-244 certified reference material (CRM). As it stands, 60% of the CRMs that will be produced in the US will be sent to the IAEA and 40% will be retained by the United States for domestic use. The feed material containing 0.5 g Pu was delivered to VNIIEF in 2012, initiating the fabrication process.

The first pass through the mass separator produced approximately 10 milligram (mg) of intermediate product. This product was sampled by the IAEA and a small quantity was shipped to LLNL in April 2013

for measurement of the isotopic composition. Both the U.S. and Russian measurements of the Pu-isotopic composition were in agreement – the Pu-244 content had increased to 98.86%. This product material was used to feed the second round of separation, and test samples were received and analyzed at LLNL in January 2015.

Results were reported to the IAEA in early 2015 that the Pu-244 content was > 99.98 atom%. The entire sample of the final product, denoted FP-33-2, was received at LLNL in May 2015 along with all residue and waste from VNIIEF. Approximately 800 micrograms (µg) of final product were recovered. As of 2017, 190 reference material units have been prepared from this material. This high-purity Pu-244 will be extremely valuable to the safeguards analytical community for the analysis of environmental Pu and will improve analyses of very low-level Pu in safeguards environmental samples.

1.1 Historical Context

In April 1991, the needs of nuclear reference materials in the international safeguards community were assessed and discussed at the IAEA. The IAEA's Safeguards Information Management division noted requirements for rare CRMs, especially those which would enhance measurement of plutonium concentration and isotopic composition. The meeting resulted in an agreement to fabricate ultra-high purity Pu-244 spikes, and VNIIEF offered its capability to perform the required separation for a low cost using an S-2 electromagnetic mass separator that can provide highly enriched isotopes,[1,2] Following this, VNIIEF made improvements to the performance of the separator through modification of the ion source and isotope collector design and optimization of the material recovery procedures, all of which increased the feed utilization efficiency and the product yield [1]. The main stated goals of the project were to obtain 100 mg of 99.5% Pu-244 for production of reference materials for nuclear material accountancy measurements and 1 mg of 99.99% Pu-244 for production of the isotopic spike required for environmental sampling (ES) analysis.

The US, IAEA, and Russia agreed to and implemented the processing of 0.5 g of the source 'FP-33' material to the IAEA for transfer to and separation at VNIIEF on the conditions that the performance of the VNIIEF installation, and that the IAEA would oversee sampling and verification of the separation products. DOE also undertook the responsibility, upon return of the separation products, to produce certified reference materials and provide 60% portion of the finished product to the IAEA for use in nuclear safeguards and forensics applications [2]. Based on the agreed upon conditions and goals between all parties, the IAEA and VNIIEF negotiated a contract for separation of the FP-33 sample and production of highly-enriched Pu-244. In February 2012, the 0.5 g test portion of the source material was delivered to VNIIEF, and the work began after nearly 20 years of negotiations and arrangements.

In early 2012, VNIIEF converted the provided FP-33 plutonium dioxide into trichloride, a working substance for electromagnetic separation, and used the feed in several batches. After separation of each batch, individual isotope fractions were extracted from the ion collectors, and dispersed material inside the separator was recovered and returned to feed. By October 2012, VNIIEF completed separation of the FP-33 test portion, and claimed that the primary product contained over 98.86 % Pu-244. In November 2012, the IAEA arranged for sampling of the initial separated product and applied seals to the containers with aliquots intended for verification measurements. The IAEA tasked two members of NWAL to perform these analyses: V. G. Khlopin Radium Institute (KRI) in St. Petersburg, Russia, and LLNL. By April 2013, the results of the verification were found to be consistent and confirmed successful completion of the initial test separation.

Following this, the parties involved proceeded with further purification of the test separation product, aiming to obtain 500 µg of 99.99% Pu-244 that would suffice for production of isotopic spikes for ES analysis. To maximize the amount of product, VNIIEF agreed to recover additional residues of the material derived from FP-33 and perform an extra cycle of separation; this work generated an additional 0.7 mg of ~97.8% Pu-244, which later was combined with the test separation product to feed the second phase of separation.

In February 2014, VNIIEF was authorized to proceed with the second phase of separation using the combined first phase product: approximately 10 mg of Pu. In August 2014, VNIIEF reported that the separation work was completed. In October 2014, the IAEA collected samples of the final product and supervised the plutonium nitrate solution being evaporated to dry salt to facilitate its safe transportation. The results of the verification analysis performed by LLNL on this final product sample became available in January 2015 and confirmed the values reported by VNIIEF. The isotopic purity of the final product was > 99.98% Pu-244, falling slightly below the target for isotopic enrichment, however the yield (880 µg) far surpassed the expected value given that only 0.5 grams of starting material was used.

The shipment of all the final product and waste materials associated with the mass separation at VNIIEF arrived at LLNL in May 2015. The bulk of the high purity material was contained in two 25 milliliter glass volumetric flasks: 1) Flask FP-33-2-A, containing 792 micrograms, and 2) flask FP-33-2-B, containing 7.5 micrograms. During 2014, a dedicated laboratory was constructed for the preparation of CRMs in a new mass spectrometry facility at LLNL. The laboratory was outfitted with a class 100 laminar flow fume hood, a balance table and analytical balances, a high-purity water system, and a high-precision liquid dispensing system. A study of plutonium background in this laboratory was conducted through sampling and analysis of environmental swipes. The analytical detection limit was approximately 1 femtogram, and no environmental Pu was detected.

During 2015 and 2016, the Pu-244 was prepared for the CRM. These steps included: transfer of the material from the two glass flasks and verification that the isotopic composition of each was identical; combination of the two and purification of the plutonium; verification that the post-purification isotopic composition had not changed; preparation of a master solution and dispensing of 190-5 milliliter aliquots of that solution into pre-weighed 30 milliliter fluorinated ethylene propylene (FEP) bottles. The mass of the master solution that was dispensed into these units was measured individually and each is expected to contain approximately 110 nanogram of Pu-244.

In 2015, Los Alamos National Laboratory (LANL) prepared a gravimetric Pu-239 standard from CRM 126A Pu metal standard for use as one of the spikes for isotope dilution mass spectrometry (IDMS) measurements of the Pu-244. This material was received by LLNL in September 2015. The other IDMS spike used was a unit of IRMM-086 Pu standard already available at LLNL, and a dilution of this was prepared in 2016. The Pu-239 content of these two standards has been certified by national metrology institutes (United States and European Union, respectively), and will be used in the certification of the molar content of Pu-244 in the CRM units. To achieve this, a random sample of 12 units were selected for spiking with the Pu-239 standards. Six were spiked with CRM 129A and six with IRMM-086. In addition, two special aliquots of the master solution (each 3 x 5 milliliter) were prepared at the mid-point of the unit dispensing process. Each of these is expected to contain approximately 330 ng of Pu-244. These special units were also spiked with the Pu-239 standards and were equilibrated, dried, re-dissolved, and each was split into three samples.

Per an action sheet signed between DOE and Commisariat à l'Énergie Atomique (CEA, Île de France) in 2015, three laboratories will oversee mass spectrometric analyses of the IDMS mixtures: LLNL, LANL, and CEA. Each lab will analyze two units spiked with CRM 126A, two units spiked with IRMM-086, two of the special units described above, and one un-spiked unit to determine the isotopic composition [3].

1.1.1 Pu-244 as a CRM

Performance of the IDMS method strongly depends on the quality of the isotopic reference materials used – both purity of isotopic tracers and as well as precision of their certified values. The isotope which is the least abundant in the sample analyzed is preferable for use as an isotopic tracer (spike). The most common isotope dilution tracers for plutonium mass spectrometry are based on the Pu-242 isotope generated in small quantities in commercial nuclear reactors. However, for ES application it is often required to reliably quantify Pu-242 itself; this is near-impossible when such a spike is used.

Pu-244 was recognized as the most suitable spike for low-level mass-spectrometric measurements of plutonium, allowing for accurate determination of all isotopes from Pu-239 to Pu-242 [4, 5]. However, the currently available reference materials based on Pu-244 are few and lack the isotopic purity required for ES analysis. These include New Brunswick Laboratory (NBL) CRM-131 (former NBS SRM-996) and Central Bureau for Nuclear Measurements (CBNM) IRM-042/IRM-042a which were all certified in the 1980s and have Pu-244 content just under 98%, and Pu-242 impurity slightly over 1.3%.

Due to the need for an updated and more accurate CRM, the new high-purity Pu-244 is being prepared at LLNL for use in bulk environmental sample analyses for safeguards. When used as a spike, the low abundances of the other Pu isotopes in this new material will enable higher precision measurements of Pu-240/Pu-239 in the sample to be made at lower concentrations. There is a strong need for high-purity isotopic spikes at the IAEA, as typical analysis of environmental samples involves, among other techniques, bulk measurement of plutonium amount and isotopic composition by means of mass spectrometry with isotope dilution.

1.2 Historical Technical Considerations

During the early 1970s, 86 plutonium targets were irradiated in a high neutron flux reactor at the Savannah River Site (SRS) in the United States with the primary objective of producing gram quantities of Californium-252 (Cf-252). Until now, 65 of the original 86 irradiated targets remain unprocessed and are stored at SRS; their total inventory is several hundred grams of plutonium containing about 20 g of Pu-244, which constitutes the majority of the existing global inventory of Pu-244 [6, 7, 8].

By the mid-1980s, a total of 21 irradiated targets were processed in several batches at the Oak Ridge National Laboratory (ORNL) to recover Cf-252 along with curium, berkelium, and einsteinium byproducts. A plutonium fraction with ~17% Pu-244 was also recovered and partially electromagnetically separated in the ORNL calutrons to produce ~2 g of 98.5% Pu-244, designated for U.S. DOE research programs. A later reworking of another part of the plutonium fraction produced 1 g of ~97.8% Pu-244 for safeguards programs; this material ultimately was certified as Standard Reference Material (SRM)-996 [9].

When different options were considered for producing a new stock of material highly enriched in Pu-244, the remaining residues from the initial production campaigns, containing 14.2 g of plutonium (of which ~17% was Pu-244), were judged to be the most suitable feed for an electromagnetic separation path, a route which would not involve reprocessing of additional irradiated targets. Even this least expensive option, however, would have only produced material with 94.3% Pu-244 and was estimated to have cost about $5M in 1986 dollars (more than double that amount if considered in 2017 dollars). With a lingering need for ultra-high purity Pu-244, various routes to fabricate the specialized Pu-244 material were explored, and talks with the IAEA and other international partners in the early 1990s led to work that began in the mid-2000s.

1.2.1 Applications in Support of Safeguards

Analyses of bulk environmental samples taken for safeguards purposes by the IAEA require measurement of femtogram to attogram levels of Pu isotopes. Pu-244 is used by the IAEA's Network of Analytical Laboratories as the spike isotope for isotope dilution measurement of the Pu content of these samples. The present stocks of Pu-244 used by the NWAL contain relatively high levels of the other Pu isotopes, correction for which results in elevated detection limits for Pu and elevated uncertainty on the measurement of Pu isotopic ratios. Use of the new high purity Pu-244 reference material will increase confidence in the results supplied by the IAEA NWAL for safeguards evaluations and will supply the needs of the IAEA NWAL for decades to come.

The isotopic purity of the newly fabricated Pu-244 material is greater than 99.98 % Pu-244, with 0.0040 % Pu-240 and 0.0012 % Pu-239. This purity is significantly greater than other Pu-244 spikes currently used by the NWAL. As is known, such high-purity Pu-244 would be extremely valuable to the safeguards analytical community for the analysis of environmental Pu.

1.2.2 How does Ultra High Purity Pu-244 Compare?

NBL's CRM 131 (NBS SRM 996), the current go-to standard, is only 97.87 % Pu-244, also containing 0.68 % Pu-240 and 0.034 % Pu-239, respectively. However, this CRM is no longer available to the public. The figure below shows the error magnification that occurs using the new spike vs. CRM 131. Detection limits of state-of-the-art analytical laboratories are in the femtogram range. For the parameters shown, the $^{240}Pu/^{239}Pu$ ratio can be measured in one femtogram of Pu at about 10% uncertainty using the new ultra-high purity spike, whereas it could not be measured at all using the CRM-131 spike (uncertainty > 100%). When used as a spike, the low abundances of the other Pu isotopes in the newly fabricated Pu-244 CRM will enable higher precision measurements of Pu-240 and Pu-239 in the sample to be made at lower concentrations, and will increase the confidence in the results for safeguards evaluations. Further, assuming that analysis of one swipe sample can require up to 10 pg of Pu isotopic spike, and with a tenfold margin introduced to account for various QC measurements, one CRM unit containing 0.1 µg Pu-244 will be sufficient for analysis of 1000 samples, which covers the IAEA annual needs.

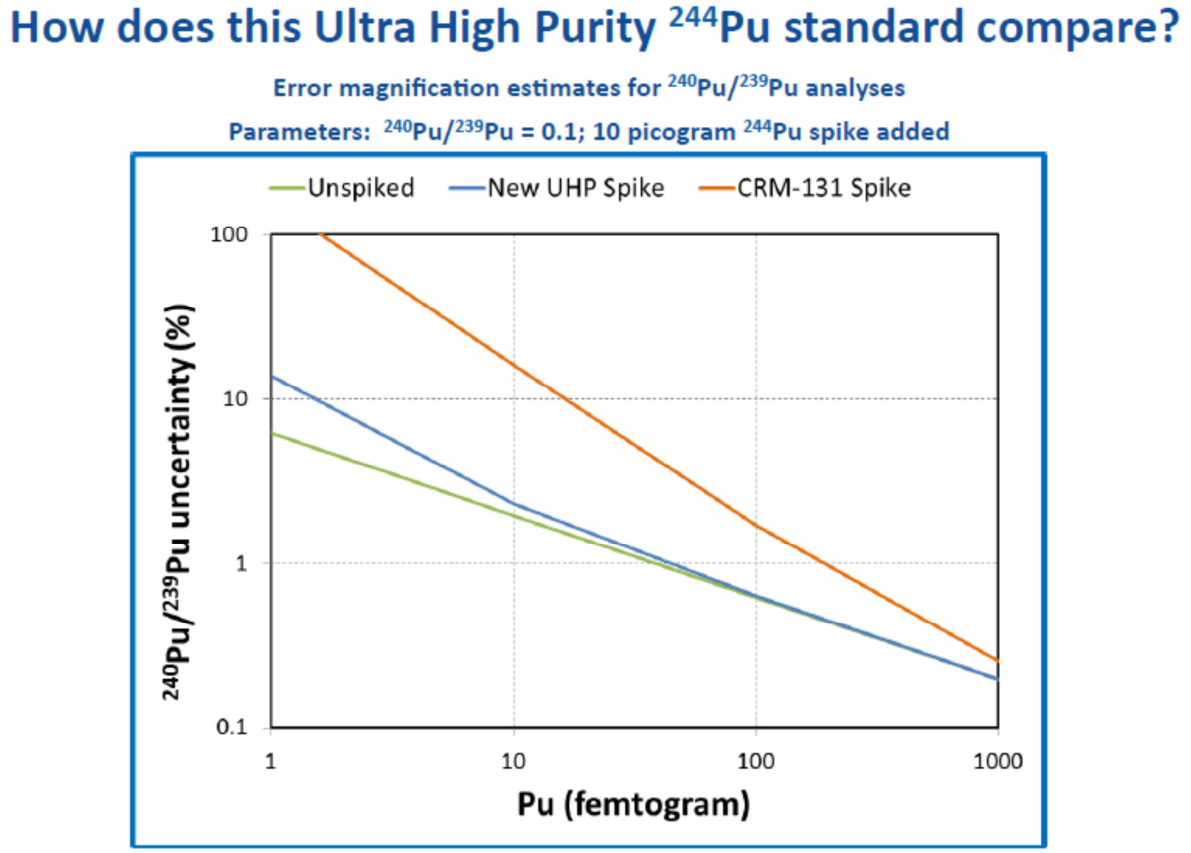

Table 1: Error magnification that occurs using the new spike vs. CRM 131.

2. Current Developments

In 2017, LLNL will send samples of Pu-244 and the IDMS mixtures described above that are needed for the certification measurements to CEA and LANL. The three labs (LLNL, LANL and CEA) will analyze the samples and report results with uncertainty budgets to LLNL and NIST, who will make independent

calculations of the mole content of the Pu-244 units. Upon completion of the measurement and reporting requirements, LLNL intends to compile the data and report these results to CEA and LANL. The final analysis report will be sent to NIST for review and evaluation relative to the certification criteria of the institute, and if acceptable, NIST will file the certification report for further review.

2.1 Quality Assurance Protocols

The limited supply of this irreplaceable material warranted an elevated level of care to produce a high-quality Certified Reference Material while minimizing the potential for degrading or otherwise wasting the material. At LLNL, Quality Assurance Protocols were enacted to ensure the integrity of the Pu-244 material in its preparation as a CRM, including but not limited to:

- Balance and weight sets calibrated annually (ISO 17025) [10];
- Balance linearity checks;
- Detailed experimentation to demonstrate quality control (e.g., viability of using H_3PO_4 as a fixative; evaporation potential from standard units);
- Laboratory environmental monitoring system measures temperature, humidity, and barometric pressure (for buoyancy correction);
- Use of ultra-high purity acids
- Screening all prepared reagents for Pu and other interfering isotopes;
- Detailed notes and records management;
- Control charts for Quality Control samples maintained for Multicollector-Inductively Coupled Plasma Mass Spectrometer (MC-ICP-MS) instruments;
- Analytical plans shared with NIST colleagues prior to execution;
- Staff training, good housekeeping, etc.

These protocols, among others, were used to ensure the safety, security, and integrity of the samples throughout their lifecycle.

To date, the National Institute of Standards and Technology (NIST) provided metrological oversight of this project, assisted in the development of the project plan and has observed or approved all work performed at LLNL. NIST will also evaluate the results provided by the analytical laboratories for the IDMS mixtures and will determine whether those results, along with the preparation and analysis plans and other documentation of the work done at LLNL and LANL, are suitable to allow the certification to proceed. Ultimately, it is expected that the units will bear NIST labels and certificates.

3. Upcoming Developments

It is expected that the analyses at LLNL, LANL and CEA will be completed before August 2017, and the reports will be sent to both NIST and LLNL for independent evaluation and comparison. Standard statistical methods will be used to evaluate any bias between laboratories, any bias between results from the two Pu-239 standards used, and to determine if there are any outliers. The results of this evaluation will determine whether any additional verification measurements will be needed. Upon completion of this evaluation, the units will be labeled and prepared for shipping and storage in heat-sealed Mylar bags. In early 2018, these units could be distributed with “provisional” certificates of analysis as needed, and the final certificates would be sent when available later in the year.

4. Conclusion

Following decades of preparation and collaborative work across several continents, mass separation of several hundred micrograms of Pu-244 was completed recently under the direction of the IAEA at the VNIIEF. The U.S. Department of Energy had originally provided 0.5 grams of FP-33 plutonium material to the IAEA, which transferred the material to VNIIEF in Russia for isotopic separation under the terms of a 2005 Memorandum of Understanding. The product of the first pass of the material through the isotope separator at VNIIEF was 98.86 atom % Pu-244. The second and final pass through the separator produced a high-purity product that was measured at LLNL to be greater than 99.98 atom % Pu-244, and is being fabricated at LLNL as a CRM. Upon completion of the fabrication, it is expected that 60% of the prepared units are intended to be returned to the IAEA. The CRM is expected to be a valuable asset to the IAEA Network of Analytical Laboratories for use as an isotope dilution spike to measure environmental Pu for nuclear safeguards.

Acknowledgements

The authors would like to thank the IAEA, NIST, CEA, VNIIEF, NNSA/DOE, among others, for decades of successful, collaborative support on the fabrication effort. Further, a significant portion of this work was supported by DOE-NNSA's Office of Nonproliferation and Arms Control.

Disclaimers

This paper reflects the opinions and views of the authors only and is not intended to represent the views of their affiliated institutions nor the U.S. Government.

I agree that ESARDA may print my name/contact data/photograph/article in the ESARDA Bulletin/Symposium proceedings or any other ESARDA publications and when necessary for any other purposes connected with ESARDA activities.

References

[1] Deron, S and Vesnovskii, S, *Development of technology for high purity ^{244}Pu Production by Method of Electromagnetic Separation;* Volume 438. Nuclear Instruments and Methods in Physics Research. Section A, Accelerators, Spectrometers; 1999. 20–22.

[2] Memorandum of understanding between US DOE and IAEA concerning supply of feed material FP-33 for separation of high-purity Pu-244 (2005).

[3] Action Sheet between US DOE and CEA of France for Cooperation on Analyses of ^{244}Pu for Certification of a New Reference Material (2015).

[4] Deron, S and Vesnovskii, S, *Development of technology for high purity ^{244}Pu Production by Method of Electromagnetic Separation;* Volume 438. Nuclear Instruments and Methods in Physics Research. Section A, Accelerators, Spectrometers; 1999. 20–22.

[5] Bigelow, JE and et al. *Preparation of additional supplies of ^{244}Pu*. Meeting on Nuclear Reference Material Needs & Availability, IAEA Consult; Antwerp, Belgium; 1985.

[6] Croff, A and et al. *Production, Uses, Supply, and Demand of Heavy Actinide Isotopes*. Fifth Topical Meeting on Spent Nuclear Fuel and Fissile Materials Management; Charleston, South Carolina; 2002.

[7] Goldberg, S and et al. *Efforts to save ^{244}Pu in Mark 18A Targets for use in International Safeguards Measurements, IAEA-SM-367/5/01/P.* IAEA Safeguards Symposium; Vienna, Austria; 2001.

[8] Robinson, S and et al. *Processing and Disposition of Special Actinide Target Materials.* Waste Management Conference; Phoenix, Arizona; 2013.

[9] Bigelow, JE and et al. *Preparation of additional supplies of ^{244}Pu.* Meeting on Nuclear Reference Material Needs & Availability, IAEA Consult; Antwerp, Belgium; 1985.

[10] *ISO/IEC 17025: General requirements for the competence of testing and calibration laboratories.* International Organization for Standardization; 2005. https://www.iso.org/standard/39883.html

Innovative Developments in Destructive Analysis for Safeguards

A. D. Dougan[1], A. M. Krichinsky[1], A. P. Belian[1], M. N. Fisher[1]

[1]NNSA Office of International Nuclear Safeguards

Abstract

The U.S. Department of Energy/National Nuclear Security Administration's (DOE/NNSA) Office of International Nuclear Safeguards is sponsoring the development of innovative technologies applicable to nuclear materials safeguards. In particular, one primary area of development applies to destructive analysis (DA) methods and technologies of uranium- and plutonium-bearing materials. This paper will discuss trends in sample acquisition, prioritization, pretreatment and analysis, some of which focus on mass spectrometry. For instance, ongoing work in the DOE/NNSA DA portfolio covers the testing of several improved ion sources for mass spectrometers and options to collect uranium hexafluoride in solid form for shipment, all in addition to overviews of several planned field tests. Stakeholders in destructive analysis should be encouraged by the improvements underway that can lead to more efficient processes in this traditionally costly and time-consuming aspect of safeguarding nuclear materials.

Keywords: safeguards, development, destructive analysis, mass spectrometry, calibration standards.

1. Introduction

The mission of the Safeguards Technology Development (SGTech) Program is the development and application of tools, technologies, and methods that improve the effectiveness and efficiency of international nuclear safeguards in support of the International Atomic Energy Agency (IAEA) at both the facility and state levels. SGTech focuses its initiatives on refining, adapting and testing existing or emerging technologies and methods, to employ these techniques or tools in the near-term (within 3-to-5 years) for IAEA safeguards applications or for manufacture by commercial vendors.

Safeguards technologies can be categorized in various ways, but the SGTech Program portfolio breakdown is typically organized within the following profiles:

- Destructive Analysis (DA);
- Nondestructive Analysis;
- Containment and Surveillance;
- Standards and Infrastructure;
- Data Management.

This paper focuses on SGTech efforts at improving the efficiencies in its first portfolio, Destructive Analysis, which encompasses measurement technologies and methods that alter samples in the process of characterizing them. Several DA technologies under development across DOE laboratories are intended to improve efficiencies of analyzing environmental (or "swipe") samples (ES), often conducted in the IAEA Network of Analytical Laboratories (NWAL), while other improvements are intended for application in the field (such as during sample acquisition). This paper also will touch on standards being produced to maintain and improve current DA capabilities.

2. Current DA development projects

For safeguards applications, DA techniques serve two general purposes:

1. Analyze nuclear material to quantify declared inventory;

2. Analyze ES to detect undeclared nuclear activities.

Most of the SGTech focus addresses the second of these purposes, developing technologies for analyzing ES, although some initiatives support analyzing declared nuclear material as well. A correlated goal is to produce techniques that are field-ready or provide for portable solutions to aid inspectors in supporting DA.

2.1 Improve efficiency and effectiveness of current methods

Mass spectrometry (MS), a technique in support of DA, is a key analysis technique in the IAEA program for bulk analysis of ES. The current method for analysis of swipe samples utilizes high-precision, multi-collector, mass spectrometry to produce highly accurate and precise isotopic data. Two SGTech-supported projects, such as the cart-portable MS system and automated clean chemistry system, involve the application of MS in safeguards.

2.1.1 Cart-portable mass spectrometry system – a downsized benchtop mass spectrometer for enrichment measurements

In response to growing difficulties in transporting gaseous UF_6 samples from inspection sites to analytical laboratories, there is interest in deploying an MS capability in enrichment facilities. To address this need, Oak Ridge National Laboratory (ORNL) is downsizing and modifying a benchtop MS system based on a Thermo Scientific Quadrupole-Ion Trap MS so that the system can be nearly self-contained (now requiring only hood ventilation and electric power) and be transported on a hand cart [1]. (See Figure 1.) Three improvements are particularly notable, and are discussed below.

Figure 1. Cart Portable Mass Spectrometer (left) and Sample Manifold (right) in a 6-foot-wide hood.

Downsizing: Although it retains its benchtop cabinet, key internal parts (most notably, the vacuum chamber) have been downsized to about ¼ its original size. This not only reduces the device's weight by almost half (from 68 kg to 36 kg), it also allows commensurate reductions in much of the infrastructure such that some external supporting components and added features could be included within the benchtop cabinet. The added features include purges and gas-absorbers intended to protect internal components most vulnerable to fluoride corrosion. An outcome of this downsizing effort is a major reduction of the vacuum pumping system which demands most of the electric power needs for MS.

Combining CO_2 with UF_6: Originally, CO_2 was added simply to UF_6 to dilute the corrosive effects of the fluorides present; however, it was found that introducing the mixture of gases also improved the ionization efficiency which, typically, is the first step upon feeding a sample into an MS system.

Automating gas sample mixing: Initial tests mixing CO_2 and UF_6 demonstrated a need to closely control the mixture to ensure reproducible results. To achieve this, a sample manifold (SM) was designed, fabricated and tested, with subsequent tests demonstrating the intended reproducibility. The sample

manifold included P-10 bottles for upper- and lower-range calibration gases, mixing chambers for calibration gases and sample gases, exterior connections for sample bottles, and a programmable logic controller for single-touch operation of vacuum pump-down, gas mixing, introduction, purging and shutdown. Interestingly, the SM can be a beneficial add-on to any MS system used for analyzing corrosive gases.

So far, and without comprehensive optimization of feed-gas mixing ratios, the cart-portable MS system has demonstrated a precision of <1%, with a measured variation of 0.5% to 0.8%, over 1 hour of sampling (that is, it approaches international target values for isotope dilution mass spectrometry).

2.1.2 Automated clean chemistry system – an automated sample preparation system for MS

Samples are prepared for MS by extensive purification procedures to isolate actinide elements from commingled materials, thereby reducing interferences and minimizing matrix effects. For ES – where entire sample contents are analyzed, not just portions thereof – preparations include 'ashing' [or a total destruction the sample substrate (typically, a cloth swipe)], dissolution of the contents, separation of actinides to avoid confounding results due to presence of isobars, matrix reduction and conversion (acid dry-downs), and sample spiking with well-known tracer isotopes (for concentration measurement). These preparations are time-consuming, repetitive and require chemical experts to manipulate samples before introduction into a mass spectrometer. By automating this process, ORNL will simplify, streamline, reduce the possibility of contamination, and reduce costs and errors [2]. (See Figure 2.)

Figure 2. Commercially available, operational sample preparation system. Upper cabinet shows the clean sample manipulation enclosure. Open doors on lower cabinet reveal reagent storage (bottom shelf) and, on the upper shelf, resin reservoirs (left), syringe pumps (right) and columns and mixing valves (mounted on the wall behind the syringe pumps).

Cleanroom-level enclosure: Analyses of ES – intended to identify and quantify only trace amounts of materials on swipe samples – require that analyses and their preparations be conducted in cleanrooms certified to International Standards Organization (ISO) criteria. Commercially available, automated, sample-preparation systems allow incorporating enclosure options capable of emulating cleanroom processing environments without the infrastructure of a typical, ISO-certified cleanroom. This option was included in the U-Pu separations system discussed below, and demonstrated to be an effective cleanroom alternative as evidenced by blank-sample results, obtained using the enclosed system located in a regular chemical laboratory, that equaled or surpassed blank-sample levels determined by manual chemistry performed in a Class 100 cleanroom. [It is noted that this encouraging performance was achieved on a new system vented to a radiological hood; its ability to maintain that cleanliness is yet to be confirmed.]

U-Pu separations: The first achievement in this area involves separating low concentrations of uranium and plutonium from "ashed" swipes. This separation uses a previously developed ion exchange column-separations system, equipped with a proprietary assembly of valves and pumps that control sample flow throughout the process. System testing demonstrated very good performance as evidenced by sample content determination (well within IAEA data quality limits) and no cross-contamination between samples (based on alternate blank-sample runs). A significant decrease in *hands-on* chemists' time from 9.8 hours to 0.6 hours was demonstrated for a seven-sample run when the amount of personnel time necessary for successful manual was compared respectively to automated chemical separations. This documented reduced labor commitment translates to a significant cost savings per sample. Overall, the system will enable faster sample reporting times at reduced costs by limiting expert-personnel hours dedicated to the chemical separation.

The commercial U-Pu separations system has other cost- and labor-saving options which are under current investigation; these include automated spiking of tracers used in isotope dilution mass spectrometry (IDMS), and an integrated barcode reader for high fidelity sample tracking.

Automating other sample preparations: Other commercially-available off-the-shelf (COTS) equipment is being evaluated this year for potential time and cost savings for ES preparation include:

- Rapid matrix reduction and conversion – multiple dilutions and evaporations intended to adjust concentration or to convert the acid form automatically, rather than occupying a chemist during several hours of processing;
- Microwave ES swipe ashing – a microwave oven system equipped with an automatic sampler (for interfacing directly with the U-Pu separations system) to replace the protracted, labor-intensive furnace ashing or acid digestion.

2.2 Adapt new techniques to DA applications

In safeguards, DA encompasses sample acquisition, sample preparation, sample analysis, data evaluation, and results reporting. Currently, the SGTech program is adapting technologies addressing the first three aspects of the DA process: sample acquisition, preparation, and analysis described briefly below.

2.2.1 NuGoo – a gel coating for environmental sampling of porous surfaces

NuGoo is a UV-curable, peelable coatings being developed by the Los Alamos National Laboratory (LANL) to improve the efficiency of ES acquisition – especially where only trace amounts of material present [3]. These coatings also promise to enable sampling surfaces not amenable to current swipe-sampling techniques – that is, porous surfaces such as meshes (e.g., fabrics) or cracked solids (such as wood grains, corroded metal, etc.). Liquid gels are being combined with additives that chemically target and affix analytes, and allow for extraction from surfaces. Rapid curing using a pocket ultraviolet LED lamp makes this an attractive option to swipe sampling.

The NuGoo sampling process takes about two minutes, only slightly longer than swipe sampling – but is expected to be well worth the gains in efficiency. (See Figure 3.) It involves applying a stencil (to aid in peeling) and the gel coating; waiting for a short period to allow analytes to loosen from the surface and migrate into the uncured gel; curing the gel with a pocket UV LED lamp (~30 seconds); and peeling the stencil and cured gel. Preliminary testing indicates sampling efficiencies >50%. With increased efficiency, commensurately improved actinide detection sensitivity is anticipated.

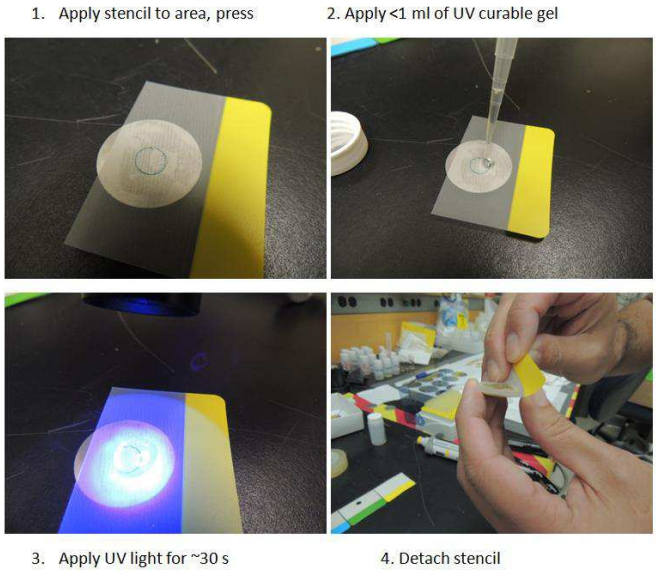

Figure 3. NuGoo in use.

2.2.2 DNDG – Delayed-Neutron/Delayed-Gamma (DNDG) screening of ES

The IAEA has expressed interest in using J-swipes for ES of hot cell interiors. Because of the anticipated, high activity levels for these samples, they cannot be analyzed in NWAL laboratories (which specifically focus on ES analysis) due to their extreme sensitivity to elevated backgrounds. To address the need for analyzing J-swipes with isotopic specificity, ORNL is combining the results of delayed gamma (DG) counting with delayed neutron (DN) counting [4].

J-swipes are 1½-inch-diameter swipes currently used by inspectors as Pre-Inspection Check Samples (PICS) of their clothes. Currently, PICS are analyzed by DN counting – a highly sensitive method (currently capable of picogram detection levels) which detects neutrons emitted upon decay of neutron-rich fission products formed in the sample during irradiation. DN counting infers the presence of fissile material which is quantified in terms of the equivalent mass of ^{235}U. However, it does not provide fissile isotope specificity. This lack of specificity is sufficient for PICS, but is not adequate for ES intended to provide specific evidence of undeclared nuclear activity.

DG counting provides insight into the presence of specific fissile isotopes based on the profile of fission products (FP) present and the photons emitted after irradiation. Fission results in a bimodal distribution of lighter and heavier FP that depends on the parent fissile isotope. This distribution is shifted somewhat – more notably for the lighter FPs than for the heavier ones – to an extent that the ratio of the yield of a light fission fragment to a heavy fission fragment is parent-isotope specific. (See Figure 4.) When combined with the equivalent mass of ^{235}U, specific quantities can be determined for individual fissile isotopes present in a sample. This combined method will provide a new technique for inspectors to determine undeclared activities in hot cells.

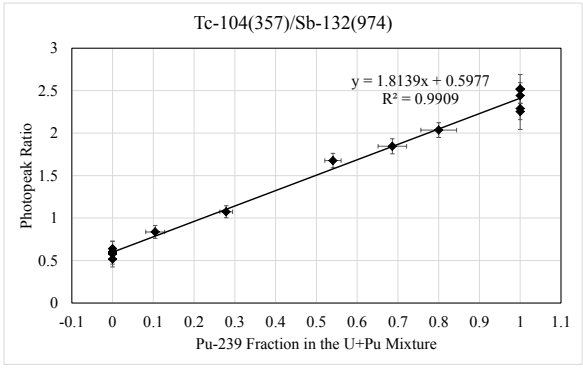

Figure 4. Graph showing linearity of photopeak ratios for 357keV and 974 keV photons from ^{104}Tc and ^{132}Sb, respectively, when plotted against ^{239}Pu fraction in a U-Pu mixture.

2.3 Improve data analysis methods

The IAEA's analysis of ES requires data interpretation and analysis using expertise in reactors and facilities. One of SGTech's projects applies to DA and is aimed at improving the way data are analyzed.

INDEPTH – an Inverse Depletion Theory (INDEPTH) code

The current interpretation of ES analyses rely on expert knowledge to *manually* identify the best matches of predicted data to measured data. The INDEPTH code – which was developed by ORNL and uses search routines that automatically pair irradiation history and fuel design parameters to measured data – is being adapted to interpret analytical results from ES [5]. Automatically matching the irradiation history and fuel design parameters to ES measurements will help analysts characterize irradiated nuclear material and verify its origin with greater speed and confidence.

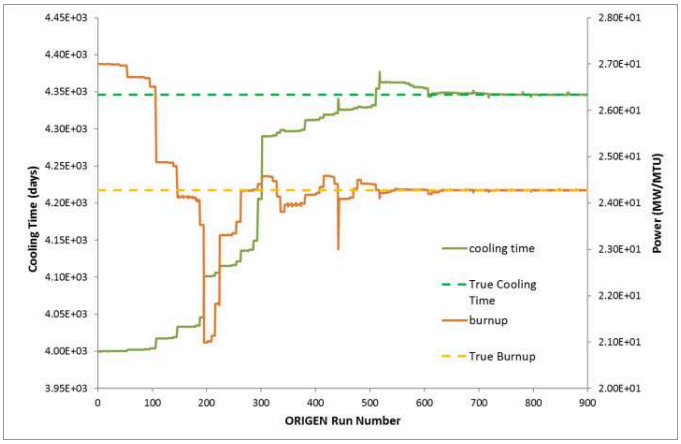

Figure 5. ORIGEN isotope depletion and decay code generates scenarios which help interpret ES data.

Adaptations for ES include a user-friendly graphical user interface, streamlined inputs and outputs tailored to IAEA's ES mission, and a thorough validation of the results using a set of realistic scenarios and measured data. The modified version of INDEPTH will help IAEA scientists to meet verification requirements using analytical results provided by the Network of Analytical Laboratories (NWAL), and to identify undeclared nuclear activities.

2.4 Provide calibration standards for maintaining or improving capability

Standards are a crucial component for instrument calibration and benchmarking to aid in maintaining instrument performance thereby ensuring consistency from one analysis to the next, and for identifying and eliminating bias between laboratories performing similar analyses on samples. SGTech is involved in the production of two types of standards, including 1) spike standards that are added to liquid samples as part of the protocol for IDMS, and 2) particle standards used to analyzing microscopic particulate material by secondary ion MS.

2.4.1 Spike standards

Two sets of spike standards are being produced at the Lawrence Livermore National Laboratory (LLNL) to increase confidence in the results supplied by the IAEA NWAL for safeguards evaluations. These standards are being produced using ultra-pure ^{244}Pu and ^{233}U materials to improve the precision of trace plutonium and uranium analyses in ES respectively [6]. (See Figure 6.) In 2016, a dedicated laboratory was established at LLNL for preparing reference materials (RM). This year, approximately 200 µg of >99.98%-pure ^{244}Pu were processed into 190 RM units, with each unit containing approximately 100 ng of pure ^{244}Pu material. Sample units were selected and prepared (by ^{239}Pu spike addition) for independent evaluation at two other laboratories; these units will be analyzed later this year. Standard statistical methods will be used in evaluating the results to identify any bias between laboratories or between results from the two ^{239}Pu standards used, and to determine if there are any outliers. In 2018, the analytical results and statistical analysis for the ^{244}Pu RM units will be evaluated by the certifying authority – the National Institute of Standards and Technology (NIST) – leading up to their issuing the ^{244}Pu RM certification. Also next year, a nearly identical process will begin for producing ^{233}U RM for certification, although these units will likely contain close to 1 mg of this pure isotope.

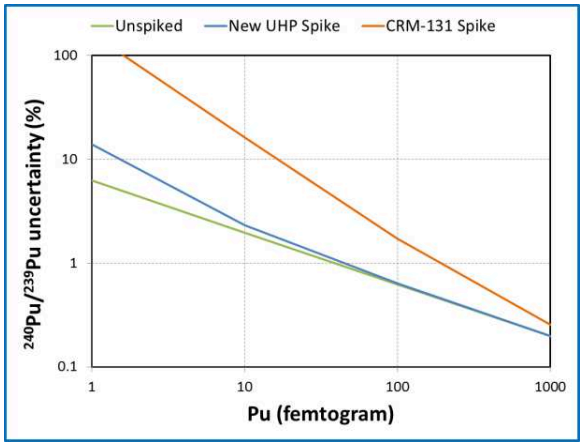

Figure 6. Graph showing improvement in IDMS precision for trace (femtogram-level) plutonium in ES using the new UHP spike (blue line) when compared with the current spike (CRM-131; red line).

2.4.2 Calibrated particles

To meet the growing demand for a reliable and universal approach to generating U particle reference material, two techniques are being tested: 1) chemical formation, and 2) printing technology. The proposed chemical pathways allow the fabrication, purification and stabilization of colloidal dispersions of actinide material to within a fixed particle-size range. Pacific Northwest National Laboratory (PNNL) and LANL are exploring different synthetic approaches for particle creation are being evaluated, tested and then optimized for producing particulate material of monodispersed size, singular composition and density, uniform morphology and tailored isotopic abundances [7]. (See Figure 7.)

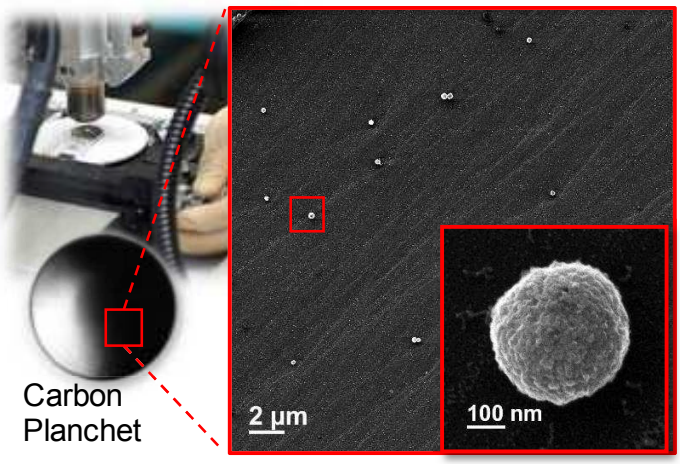

Figure 7. Progressively enlarged images of monodispersed particles deposited on a carbon planchet.

An inkjet printing technique is being developed at LANL to create depositions of particulates of known mass, in known locations with separations of 10-20 micrometers. The basic technology involves a COTS piezoelectric MEMS (microelectromechanical systems) printer to deposit known concentrations of solutions on a silicon or carbon substrate with known volume, in the 1-10 picoliter range, and then in the sub-picoliter range. Developing this technology requires precise volume and position control for deposited droplets, and the development of a basic methodology to control and optimize depositions. Depositions will be characterized in terms of physical properties such as diameter, thickness and uniformity.

3. Upcoming Technology Competitions

When different techniques promise to achieve the same or similar improvement in efficiency, then a side-by-side challenge provides a convenient method for evaluating the relative merits of one technology over another, if they are at similar points in their maturity and if they can be tested under similar circumstances. SGTech has used this competitive approach in the past, and is preparing to do so in two areas of the DA cycle: sample acquisition and MS feed ionization.

3.1 Innovative UF_6 Sampling Techniques

Sampling, shipping, and analyzing UF_6 gas poses many logistical and technological challenges. Investment in sampling technologies to mitigate said challenges has resulted in three similar pathways – all using the controlled hydrolysis of corrosive UF_6 gas to a solid and relatively benign uranyl fluoride. (See Figure 8.) Argonne National Laboratory (ANL) is developing an alumina-pellet approach called HORUS, a Handheld Operation for Rapid Uranium Sampling, which is based on the Cristallini method of the Brazilian-Argentine Agency for Accounting and Control's (ABACC's), while LANL's PADDA (Planar Alumina-based Deposition for Destructive Analysis) uses a commercially available anodized alumina disc to collect and stabilize milligram quantities of UF_6 [8]. PNNL's Single-Use Destructive Assay (SUDA) sampler uses a thin film of zeolite on a disc substrate to collect and stabilize milligram quantities of UF_6 [9]. The three UF_6 DA sampling technologies will be tested side-by-side in a competition taking place in two phases: first using only depleted UF_6 (DUF_6) as a test run, and the second using uranium at a variety of enrichments. Each technology will be evaluated based on criteria such as compatibility with facility operations, ease of transport, suitability for analysis by various methods, and cost.

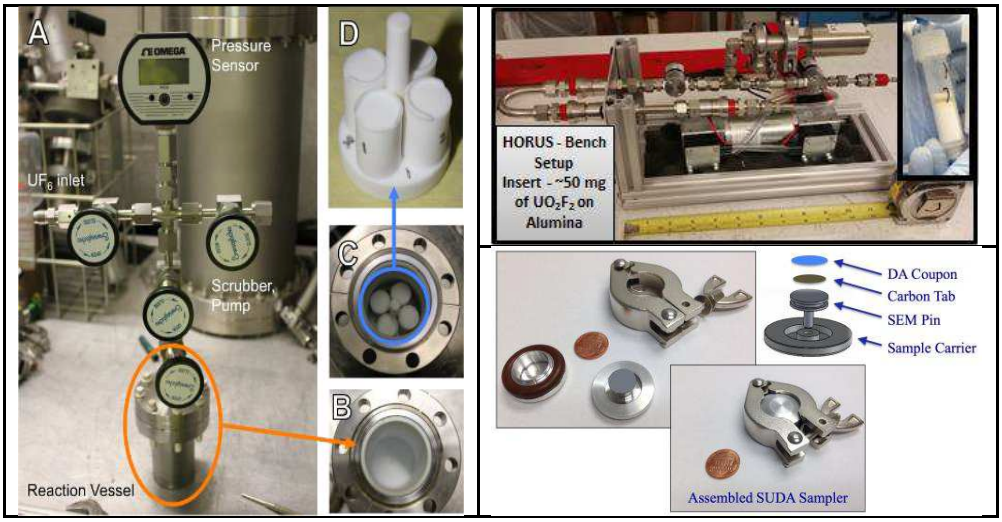

Figure 8. Three UF_6 gas sampling devices are being tested competitively: LANL's PADDA (left), ANL's HORUS (upper right), and PNNL's SUDA sampler (lower right).

3.2 Innovative MS Ion Source Technologies

As part of the effort to create a more-portable mass spectrometer (MS), three ionization systems (also referred to as ion sources) were developed at LANL and PNNL over several years. (See Figure 9.) Laser ablation/ionization (LAI; at LANL) uses a laser to desorb and ionize uranium samples from a planar sample surface (e.g., planchet) [10]. Atmospheric pressure glow discharge (APGD; at PNNL) ionizes a liquid sample in a plasma formed between two electrodes near the MS sampling cone [11]. Substrate-enhanced laser desorption and ionization (SELDI; at PNNL) uses pretreated planchet to enhance laser energy utilization in ablating and ionizing the sample absorbed onto the surface [12]. Development of these systems is coming to a decision point for which competitive performance testing is warranted to facilitate down selection to the best-performing technology.

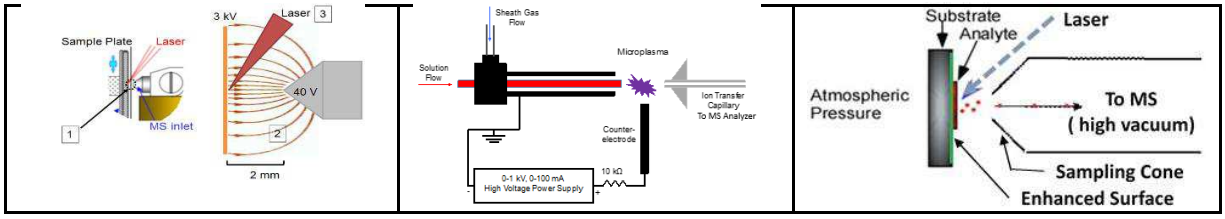

Figure 9. Three MS ion source technologies are being tested for UF_6 analysis: LANL's LAI (left), LS-PNNL's APGD; and PNNL's SELDI.

Field testing of each ion source is to be conducted on two different benchtop MS platforms for a comprehensive performance comparison that considers MS system differences. Several performance measures will be used to compare the ionization techniques including: efficiency of pure ions production; results accuracy, precision, bias and relative standard deviation; limits of detection; analysis time; and the amount of sample needed to achieve reported results. The competition is scheduled to be conducted early in FY2018.

4. Concluding Summary

The SGTech mission focuses on achieving measureable improvements in international safeguards by adapting emerging or existing technologies to address a safeguards function within a relatively short period. The main customer of these improvements is the IAEA with a particular focus on efforts to

improve efficiencies and effectiveness in all aspects of safeguards inspections, to ease the burden on inspectors in the field, and to improve confidence in drawing safeguards conclusions. The projects mentioned above showcase technology development in the destructive analysis area. Similar efforts are being pursued in nondestructive analysis technologies, containment and surveillance, and data management.

5. Acknowledgements

The authors acknowledge the dedicated efforts by scientific and engineering staff at Argonne National Laboratory, Los Alamos National Laboratory, Oak Ridge National Laboratory, and Pacific Northwest National Laboratory in developing the state-of-the-art technologies mentioned in this report. These efforts also involve collaborations with the other U. S. Government institutions, universities and private corporations. Some of these technologies resulted from earlier research sponsored by the Defense Nuclear Nonproliferation Office of Research and Development (NA-22) in the U.S. Department of Energy/National Nuclear Security Administration (DOE/NNSA). The technology development reported herein is supported by the Office of Nonproliferation and Arms Control (NA-24).

6. Legal matters

6.1 Privacy regulations and protection of personal data

I agree that ESARDA may print my name/contact data/photograph/article in the ESARDA Bulletin/Symposium proceedings or any other ESARDA publications and when necessary for any other purposes connected with ESARDA activities.

6.2 Copyright

The authors agree that submission of an article automatically authorizes ESARDA to publish the work/article in whole or in part in all ESARDA publications – the bulletin, meeting proceedings, and on the website.

The authors declare that their work/article is original and not a violation or infringement of any existing copyright.

7. References

[1] Thompson C.V. and Whitten W.B.; *FY16 Safeguards Technology Cart Portable Mass Spectrometer Project Final Report;* ORNL/TM-2017/70; Oak Ridge National Laboratory; Oak Ridge, TN; February 2017.

[2] Ticknor B.W., Bottorff S.C., Tevepaugh K.N., McBay E.H., Bostick D.A., Hexel C.R., Kim H., Field P.; *Automated Clean Chemistry for Bulk Analysis of Environmental Samples for Safeguards*; 39th ESARDA Symposium on Safeguards and Nuclear Non-Proliferation; Düsseldorf, Germany; May 2017.

[3] V. Henzl, R. Lakis, K. Koehler, and D. Desimone; *Safeguards Technology Development – Complementary Access Tools Report (Final Report)*; Los Alamos National Laboratory internal report LA-UR-16-24034.

[4] Croft, S., Venkataraman, R., McElroy, R.D., Knowles, J., Glasgow, D.; *DN/DG Screening of Environmental Swipe Samples: FY2016 Report*; ORNL/TM-2016/748; Oak Ridge National Laboratory; Oak Ridge, TN; January 2017.

[5] Grogan B.R. and Richards S.M., *Verifying Safeguards Declarations with INDEPTH: A Sensitivity Study*; Proceedings of the International Conference on Mathematics & Computational Methods Applied to Nuclear Science & Engineering; Jeju, Korea; April 2017.

[6] Fisher M.N., Dougan A.D., Williams R., Iyengar A., and Trienen K.; *Certification of Ultra-High Purity Pu-244 for Safeguards Applications*; 39th ESARDA Symposium on Safeguards and Nuclear Non-Proliferation; Düsseldorf, Germany; May 2017.

[7] Barrett C.A. and Abheier N.C. Jr; *UO_2 Particle Standards: Synthesis, Purification & Planchet Preparation*; PNNL-25271; Pacific Northwest National Laboratory; Richland, WA, USA; March 2016.

[8] Esteban A., Cristallini O., Perrotta J.A.; *UF_6 Sampling Method using Alumina*, Proceedings of the Institute for Nuclear Materials Management 49th Annual Meeting; Nashville, TN; 2008.

[9] Anheier N.C., et. al; *A new approach to enrichment plant UF6 destructive assay sample collection and analysis*; Presented at the Eighth INMM/ESARDA Joint Workshop Building International Capacity; Grand Teton, WY; October 2015.

[10] Judge, E.J., Dirmyer M.R., Campbell K., Stark P.C., Yoshida T.M., and Leibman C.P.; *Laser Ablation ICP-MS Comparison and Evaluation for IAEA Safeguard Use*; LA-UR-15-28705; Los Alamos National Laboratory; Los Alamos, NM, USA; October 2015.

[11] Hoegg E., Marcus R.K., Barinaga C., Hager G., Koppenaal D., and Hart G.; *Stability and Precision of a Liquid Sampling - Atmospheric Pressure Glow Discharge Ion Source Interfaced with a Orbitrap Mass Analyzer*; poster presented at SciX2016: The 43rd Annual North American Meeting of the Federation of Analytical Chemistry and Spectroscopy Societies; Minneapolis, Minnesota, USA; September 2016.

[12] Barinaga C.J., Carman A.J., Hager G.J., Hart G.L., Hoegg E.D.; *Feasibility of a Fieldable Mass Spectrometer: FY 2015 Year-end Report*; PNNL-24842; Pacific Northwest National Laboratory; Richland, WA, USA; October 2015.

Towards novel field-deployable instrumentation for UF_6 enrichment assay – an overview of existing and emerging technologies

George C.-Y. Chan, John D. Valentine, and Richard E. Russo

Lawrence Berkeley National Laboratory, 1 Cyclotron Road, Berkeley, CA 94720, USA.

Abstract:

Uranium hexafluoride (UF_6) is the uranium compound typically involved in uranium enrichment processes. As the first line of defense against proliferation, accurate determinations of the uranium isotopic ratio (or enrichment) in UF_6 are critical for materials verification, accounting and safeguards. Currently, mass spectrometry (MS) is the most sensitive measurement technique for analysis of stable and long-lived isotopes. However, current MS techniques require too much infrastructure and operator expertise for field deployment and operation. In-field isotopic analysis of UF_6 has the potential to substantially reduce the time, logistics and expense of bulk sample handling by allowing for an 'informed' choice of samples to be sent to a central laboratory for further definitive analysis by standard techniques.

It is common that the next generation of analytical instruments is driven by technologies that are either currently available or just now emerging. Therefore, a comprehensive and in-depth review is conducted on state-of-the-art and emerging technologies for field enrichment analysis of UF_6. These technologies are evaluated based on their competitive advantages and current limitations for in-field UF_6 enrichment assay. The objective of the study is to identity the most promising technologies that can be used for development of the next-generation, field-deployable instrument for providing rapid, accurate, and precise UF_6 enrichment assay. In this paper, we provide an overview of instrument options, discuss their limitations, and examine the main gaps between needs and capabilities for their field use.

Keywords: uranium hexafluoride; enrichment assay; mass spectrometry; optical spectrometry

1. Introduction

Uranium hexafluoride (UF_6) is arguably the most important uranium compound in the nuclear fuel cycle, particularly for uranium isotope enrichment. The enrichment of the ^{235}U isotope in UF_6 is a necessary major step in the production of fuel for most nuclear power plants. As nuclear fuel cycle technology becomes more prevalent around the world, international nuclear safeguards and interest in UF_6 enrichment assay has been growing. As the first line of defense against proliferation, accurate analytical techniques to determine the uranium isotopic distribution in UF_6 are critical for materials verification, accounting, and safeguards at enrichment plants.

Currently, the International Atomic Energy Agency (IAEA) monitors the production of enriched UF_6 at declared facilities by collecting between 1–10 g of gaseous UF_6 into a sample bottle, which is then transferred and tamper-sealed in an approved shipping container. The sample is shipped under chain of custody to a central laboratory [e.g., IAEA's Nuclear Materials Analysis Laboratory (NMAL) in Seibersdorf] for high-precision isotopic assay by mass spectrometry (MS) [1, 2]. The logistics are cumbersome and the analysis is costly, and results are not available for some time after sample collection. In addition, new shipping regulations are making it more difficult to transport UF_6 [2]. The IAEA is challenged to develop effective safeguards approaches at enrichment plants while working within budgetary constraints [3].

There is one on-site enrichment-assay technique, termed COMbined Procedure for Uranium Concentration and Enrichment Assay (COMPUCEA), which offers exceptional analytical capabilities with typical combined (systematic and random) measurement uncertainty around 0.25% relative [4, 5]. COMPUCEA combines energy-dispersive X-ray absorption edge spectrometry and gamma-ray spectrometry to measure uranium elemental content and ^{235}U enrichment, respectively. The method is

already in use in inventory verification campaigns at European LEU fuel fabrication plants [4]. Currently, the method is utilized only for solid samples and is not yet applied to UF_6 enrichment assay. IAEA is exploring extending the COMPUCEA system to in-field UF_6 enrichment determination [6]. Major shortcomings of the method are its comparatively complicated sample preparations, and its hours-long measurement time for each sample.

For off-site U-enrichment measurements, MS is currently the most sensitive analytical technique; however, current MS techniques require too much infrastructure and operator expertise for field deployment and operation. In-field UF_6 enrichment assay has the potential to substantially reduce the time, logistics and expense of bulk sample handling by allowing for an 'informed' choice of samples to be sent to a central laboratory for definitive analysis by standard laboratory techniques.

The objective of the present study is to identify the potential, viable technologies that are likely to culminate in an expedited development of the next generation of field deployable instrumentation for rapidly determining UF_6 enrichment. One common approach to project the next generation of chemical instrumentation is to track the current trends and to extrapolate them [7]. This approach, albeit somewhat conservative, has been demonstrated with a fair degree of reliability in the fields of analytical science and chemical instrumentation [7]. Therefore, an extensive literature review on existing and emerging technologies for UF_6 enrichment assay is performed, and the competitive advantages and current limitations of different analytical techniques are compared. Based on the results of the review, requirements and recommendations for development of the next-generation field-deployable instrument for UF_6 enrichment assay are addressed.

2. Methodology

Current analytical techniques for UF_6 enrichment assay are based on one of three scientific principles: radiometry, mass spectrometry, and optical spectrometry. In this study, a comprehensive list of UF_6 enrichment-assay methods is reviewed and evaluated. COMPUCEA [4, 5] is a radiometric technique and serves as a benchmark for on-site U enrichment assay. Evaluated mass spectrometric techniques include: gas source mass spectrometry (GSMS) [8], thermal ionization mass spectrometry (TIMS) [9], inductively coupled plasma mass spectrometry (ICP-MS) [9, 10], multi-photon ionization mass spectrometry [11, 12], UF_6 molecular mass spectrometry with portable mass spectrometer [13], laser ionization mass spectrometry [14], surface-enhanced laser desorption and ionization (SELDI) [2], liquid sampling-atmospheric pressure glow discharge mass spectrometry (LS-APGD-MS) [15-17], and atmospheric-pressure solution-cathode glow-discharge mass spectrometry (AP-SCGD-MS) [18]. Techniques based on optical spectrometric principles include: optical atomic emission with argon afterglow discharge or ICP [19-21], glow discharge optogalvanic spectroscopy [22], laser-ablation laser induced fluorescence [23], laser ablation absorbance ratio spectrometry (LAARS) [24, 25], atomic beam tunable diode laser absorption [26], tunable laser infrared (IR) absorption [27, 28] and its high performance version with quantum cascade laser [29], and laser induced spectrochemical assay for uranium enrichment (LISA-UE).

GSMS, TIMS and ICP-MS are included to enable comparison with laboratory techniques. Otherwise, all other techniques should be directly compared with COMPUCEA for their potential to serve as an alternative field-based enrichment assay technique. Each technique is compared against seven criteria. Because of page limit, it is not feasible to describe, even briefly, all the reviewed techniques in great detail. Therefore, only those analytical techniques, according to published literature results, that so far show the highest potentials for UF_6 enrichment assay as alternatives for TIMS or multi-collector (MC)-ICP-MS will be emphasized.

2.1. Assessment criteria

The seven assessment criteria are: meeting predefined target of analytical accuracy and precision (two separate criteria), meeting relaxed target of accuracy and precision (two criteria), simultaneous ^{235}U and ^{238}U measurement, measurement time, and overall ease of operation and system complexity. The IAEA published international target values (ITVs) [30] for a wide variety of measurement techniques for nuclear material accountancy and safeguards verification. The ITVs are considered to be achievable values in routine measurements and are uncertainties to be considered in judging the

reliability of analytical techniques applied to the analyses of nuclear materials [30]. GSMS, TIMS and MC-ICP-MS are the only three MS systems listed under destructive analysis (DA) techniques [30]. Although more techniques (five) are listed under the category of non-destructive analysis (NDA), it is notable that measurement uncertainties from NDA techniques are much larger – typically more than an order of magnitude larger – than the three MS-based DA techniques [30].

To evaluate the analytical accuracy and precision of a candidate analytical technique, reported analytical figures of merit are compared to the ITVs of TIMS and MC-ICP-MS [30], which serve as comparison references. For these MS systems, the *u(r)* and *u(s)* (i.e., random and systematic uncertainties, respectively) ITVs are the same, and they are 0.5% (relative) for depleted U (^{235}U < 0.3% abundance), 0.2% (relative) for uranium with ^{235}U abundance between 0.3% and 1%, 0.1% (relative) for LEU (1% < ^{235}U < 20%), and 0.05% (relative) for HEU (^{235}U > 20%) [30]. The IAEA ITVs define the strict target for analytical accuracy and precision for all analytical techniques under evaluation. Because the IAEA ITVs are intended for more established techniques, to better gauge the potential of emerging techniques that are still under active development, an additional set of performance criteria is set by relaxing the target values by 10× (i.e., 5% relative for depleted U, 2% relative for samples with ^{235}U between 0.3% and 1%, and so on). In case the emerging technique is so new that experimental data are not yet available specifically for uranium, projected or extrapolated values from very similar techniques sharing the same scientific principle are used.

2.2. Importance of simultaneous measurement and signal correlation in isotope-ratio determination

Signal correlation is crucial in defining the accuracy and precision of isotope-ratio measurements, and thus, its importance needs to be stressed. So far, none of the analytical techniques ***directly*** measure the ^{235}U/^{238}U ratio. Instead, all available techniques indirectly gauge the ^{235}U/^{238}U ratio through separate measurements of the signals from ^{235}U and ^{238}U. All measurements unavoidably contain noise. The relative error in the ratio of two signals, *x* and *y*, could be larger or smaller than those in the individual signals (i.e., a further degradation or an improvement in measurement precision); the outcome is heavily dependent on the correlation of noise in the two signals. To illustrate the importance of signal correlation, computer simulated signals with both correlated and uncorrelated noise components have been generated and are shown in Figure 1 below. Individually, the precisions of the two signals, *x* and *y* [relative standard deviations (RSD) ~ 20%] are rather unacceptable for many situations. However, because the two signals are highly correlated – that is signal dips and peaks occur at the same time for the two signals, the noise is greatly reduced in the ratio *x*/*y* (RSD ~ 1.5%). These highly correlated signals are usually achievable only when the two signals are acquired simultaneously, as repeatedly proven in the literature [31-33]. Signal correlation typically greatly degrades for sequential measurements (i.e., when signals *x* and *y* are measured one by one, sequentially in time).

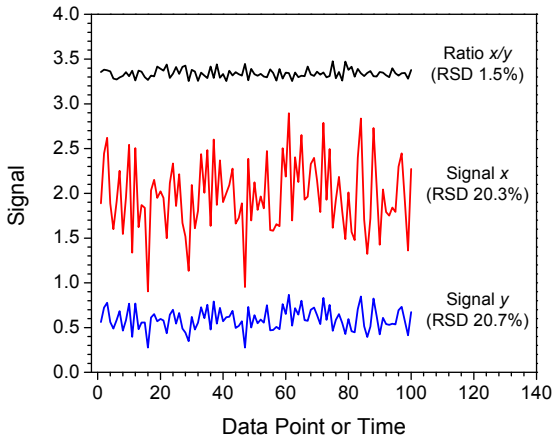

Figure 1: Two simulated signals, x and y, and the resultant signal ratios (x/y), demonstrating the importance of correlated noise and simultaneous measurement in improving the signal (isotopic) ratios.

It should be noted that not all noise sources are correlated in nature. One well-known source of uncorrelated noise, which is particularly relevant to isotopic analysis, is counting statistics (also known as Poisson noise). In an ideal case in which all other noise sources are eliminated, precision of isotopic analysis is then governed by counting statistics. Because radiometric techniques usually do not have other noise sources, their precisions are largely limited by counting statistics. For a truly simultaneous ICP mass spectrometer, it has been shown that isotopic-ratio precision close to counting-statistics limit is achievable [34]. Accordingly, one criterion on evaluation of a candidate analytical technique is on its capability to perform truly simultaneous measurement for ^{235}U and ^{238}U.

3. Results and Discussion

3.1. Results of performance assessment

Table 1 summarizes the performance of the benchmark laboratory-based techniques (GSMS, TIMS, and MC-ICP-MS), the benchmark field technique (COMPUCEA), and the four emerging techniques that show promising potential for in-field UF_6 enrichment assay. The assessment results are color coded. For analytical accuracy and precision, a "green" rating indicates meeting the stated criteria, a "yellow" rating represents not meeting the criteria but is within 3× the target (i.e., marginally fail), and a "red" rating denotes not meeting the criteria even if the target is relaxed by a factor of 3. The metric "simultaneous ^{235}U and ^{238}U measurements" summarizes if the ^{235}U and ^{238}U measurements are performed in truly simultaneous (green), quasi-simultaneous (yellow) or sequential (red) fashions. The metric "measurement time" refers to typical measurement time. Techniques rated "green" typically require less than 10 minutes for one measurement. Techniques that typically require more than 10 minutes but less than one hour are rated "yellow", and those requiring more than one hour are rated "red". Finally, the metric "overall ease of operation" reflects the overall complexity of the measurement procedures (including sample-preparation procedures) and instrument operation (e.g., turn-key *versus* complicated systems), as well as general robustness of the instrument and the technique.

Table 1: Assessment summaries of benchmark and promising techniques for UF_6 enrichment assay. Box with diagonal hatch indicates guestimate from scientific principle. A question mark indicates that information either is not yet available or is insufficient for estimation.

	Analytical Performance					Operation	
	Accuracy meets target	Precision meets target	Accuracy within 10× target	Precision within 10× target	Simultaneous ^{235}U and ^{238}U measurements	Measurement time	Overall ease of operation
GSMS							
TIMS							
MC-ICP-MS							
COMPUCEA					Note 1		
LS-APGD-MS (with Orbitrap MS)	?		?				
AP-SCGD-MS (with Orbitrap MS)	?	?	?	?			
LAARS							
LISA-UE			?	?			

Note 1: Signal correlation for measurement-noise reduction through simultaneous ^{235}U and ^{238}U measurement does not apply in COMPUCEA because the isotopic assay is performed through radiometric counting (gamma ray), in which the dominated noise source is counting statistics.

3.2. Benchmark techniques – GSMS, TIMS, MC-ICP-MS and COMPUCEA

The benchmark techniques will be briefly discussed in this section, whereas the details of each promising emerging technique will be individually discussed in the following sections. Overall, all the three benchmark, MS-based techniques offer outstanding analytical performance but demanding operation in terms of measurement time as well as expertise in instrument operation. All MS-techniques comprise two essential components – an ionization source and a mass analyzer. The mass analyzer responds only to ions (charged particles) but not neutrals; thus, an ionization source is required to convert the neutral (uncharged) sample to charged ions. The mass analyzer separates and measures the charged ^{235}U and ^{238}U atoms/molecules according to their different mass-to-charge ratios.

Gas source mass spectrometry (GSMS) accepts gaseous UF_6 samples directly for enrichment-assay measurements. Because of the homogeneity of gaseous samples, it is currently the most sensitive and precise measurement technique [35]. However, its drawback for UF_6 analyses is its long measurement time. The long measurement cycle is related to memory effects due to the corrosive and reactive nature of gaseous UF_6, which can be compensated only by multiple measurements alternating between the sample and two calibration standards. As a result, the duration for one measurement cycle is about 5 hours [35]. For TIMS measurements, samples are usually presented as a solution and deposited onto the TIMS filament for electrothermal vaporization as well as ionization. Measurement precision for TIMS is slightly lower than GSMS because the sample on a TIMS filament becomes isotopically inhomogeneous due to fractionation during the measurement process [35]. MC-ICP-MS employs a high temperature (>6000 K) inductively coupled plasma – requiring high power (~1.5 kW) – as the atomization and ionization source. The MC-designation refers to the specific type of mass analyzer, a multi-collector. The MC-mass spectrometer is a double-focusing system consisting of an electrostatic sector and a magnetic sector in which ions are separated according to their mass-to-charge ratio and focused onto a focal plane. The MC-system allows the operator to position several detectors at different positions along the focal plane of the mass spectrometer [36] for simultaneous collection and measurement of several masses.

A joint-laboratory study [37] compared U-isotopic ratio measurements by GSMS, TIMS and MC-ICP-MS. For a UF_6 sample with ^{235}U at natural abundance, the RSDs were 0.012%, 0.025% and 0.060%, respectively [37]. Sample throughput is about 1-2 samples/day for GSMS, increases to 5-10 samples/day for TIMS and further increases to around 20 samples/day for MC-ICP-MS [37].

The COMPUCEA technique, developed at the Institute for Transuranium Elements (ITU), is a transportable analytical system for on-site uranium concentration and enrichments assays [5]. Its application specifically for UF_6 enrichment assay is still under development by the IAEA [6], although its use on LEU-oxide samples is considered routine. In fact, IAEA has published an ITV for COMPUCEA – 0.4% *u(r)* and 0.2% *u(s)* for ^{235}U enrichment in LEU oxides [30]. ITVs for other enrichment levels (i.e., DU, NU and HEU oxides) are not published [30].

The COMPUCEA technique is based on energy-dispersive X-ray absorption edge spectrometry and gamma-ray spectrometry. Before presented to X-ray and gamma-ray measurements, the solid sample needs to undergo some laborious preparation steps. Briefly, the solid sample is quantitatively transformed into a uranyl nitrate solution, which involves sample digestion in 8 M nitric acid and subsequent dilution to 3 M acidity with a target U concentration about 190 g/L [5]. The solution is first characterized for its density and temperature [5]. During the process, standard laboratory tools (e.g., portable density meter, glass-ware, chemicals, hot plate, weighing balance) and operators' facilities (e.g., fume hood) are used [5].

The solution sample is then measured by X-ray and gamma-ray spectroscopy. Typically, for an LEU sample, three replicates of each measurement type are performed; acquisition of each X-ray and gamma-ray spectrum takes about 1000 s and 2000 s, respectively [5]. For a natural U sample, the time is increased to 5000 s for each gamma-ray counting [38]. Data treatment is not very straightforward because the two measurements are interdependent. Specifically, the X-ray measurement needs the knowledge of the enrichment to accurately convert the measured uranium concentration into mass fraction, whereas the gamma measurement needs the uranium concentration as input to correct for self-attenuation effect [38]. Therefore, data evaluation is made in an iterative manner. Furthermore, the sample parameters (including solution density, sample volume, and bottom

thickness of sample container) need to be taken in account [4]. Software has been developed for automatic data acquisition and analysis for the in-field COMPUCEA measurement system [5].

The analytical performance is impressive for an on-site measurement. For LEU samples, the achievable combined uncertainty (*u(r)* and *u(s)*) is typically around 0.25% relative [4, 5] (published ITV for combined uncertainty is 0.45% [30]). According to a recent IAEA report [6], the adaptation of the chemical preparation steps for COMPUCEA determination of UF_6 enrichment is currently being studied by IAEA and with the European Commission. As chemical transformation of UF_6 to uranyl nitrate solution is comparatively simple compared with its oxide counterpart, it is anticipated that the COMPUCEA method will be available for on-site UF_6 enrichment assay in the very near future. The drawback of the method is the relatively long counting time, especially for natural (3×5000 s) and depleted uranium, and its labor intensive sample preparation process.

3.3. Emerging mass-spectrometric techniques

3.3.1. Liquid sampling-atmospheric pressure glow discharge mass spectrometry

Liquid sampling-atmospheric pressure glow discharge mass spectrometry (LS-APGD-MS), under joint development from Clemson University and Pacific Northwest National Laboratory (PNNL) [15-17], is the most well characterized emerging mass-spectrometric technique, especially for the determination of uranium isotopic ratio. The glow discharge is a microplasma (volume ~ 1 mm^3) formed by imposing a low direct-current potential (typically several hundred volts) between the surface of an electrolyte solution (e.g., 2% nitric acid) and a metallic counter electrode [39, 40]. The supporting electrolyte solution flows at atmospheric pressure out of a small (~ 100 μm) glass capillary housed within a slightly larger metal capillary, between which cooling gas is passed [40]. The normal operating parameters include liquid electrolyte flow rates of 5–100 μL/min, cooling gas (typically helium or argon) flow rate of < 1 L/min, and power consumption of < 40 W [16].

Currently, the researchers coupled this LS-APGD ionization source to a high-resolution mass spectrometer (the Orbitrap). Hoegg *et al.* [15, 16] recently discussed various aspects of the LS-APGD and Orbitrap combination for uranium isotopic analyses, including optimization of various operating parameters (both for the discharge and the Orbitrap), preliminary analytical figures of merit, and known limitations. U-containing sample was introduced in a solution form and mixed with the supporting electrolyte. The researchers reported that the dominant U-species in the mass spectra was UO_2^+, and little U^+ or UO^+ were detected [15].

Based on published results [16], the reported analytical precision is encouraging, and is, so far, the best in all the emerging techniques reviewed. For an analytical session, each contained ten sets of data acquisitions, precisions in the $^{235}U/^{238}U$ ratio ranged from 0.41% to 1.67% RSD [16]. The sample was introduced in the form of a uranium solution (5 μg/mL, with natural isotopic abundance) [16].

Although the LS-APGD, in its present form, would not directly accept gaseous UF_6 for analysis, a two-step reaction to transform UF_6 to a uranium solution is well established and regarded as a somewhat standard procedure [8]. The two-step reaction involves hydrolysis of UF_6 to UO_2F_2 ($UF_6 + 2\ H_2O \rightarrow UO_2F_2 + 4\ HF$), followed by conversion to nitrate salt with nitric acid ($UO_2F_2 + 2\ HNO_3 \rightarrow UO_2(NO_3)_2 + 2\ HF$).

One potential drawback of the LS-APGD-MS technique for UF_6 enrichment assay is memory effect, which has been documented in several reports [2, 16, 41]. The cause(s) for the memory effect is not well characterized, but it was suggested that material deposited on the capillary counter-electrode and/or the mass spectrometer capillary interface could be the source [2, 41].

3.3.2. Atmospheric-pressure solution-cathode glow-discharge mass spectrometry

Atmospheric-pressure solution-cathode glow-discharge mass spectrometry (AP-SCGD-MS), currently under development jointly at Rensselaer Polytechnic Institute and Indiana University [18], is identical in scientific principle to the LS-APGD-MS reviewed in the last section but different in design for the generation of the microplasma discharge. The AP-SCGD is a direct-current plasma sustained directly

on the surface of a flowing liquid electrode (typically at a rate of 1–2 mL/min), supported in ambient air without the need for a cooling gas or other gas flows [18]. Power of AP-SCGD is ~ 70 W (normally < 100 W) [42], and is generally slightly higher than that of the LS-APGD. A distinct difference between AP-SCGD and LS-APGD is that AP-SCGD sustains on a flowing liquid cathode, with the liquid in excess, whereas LS-APGD operates in a total consumption mode in which all the electrolyte solution is consumed [15]. An advantage of the total consumption in LS-APGD is that no chemical waste solution is generated. Although the excessive flow of electrolyte generates chemical waste for AP-SCGD, the continuously self-renewing liquid surface of the flowing solution cathode potentially minimizes memory effects. In terms of instrument setup, footprint and operation requirements, AP-SCGD shares many similarities with LS-APGD.

Although not yet characterized for its performance on isotopic analysis, the AP-SCGD demonstrated a significantly better detection limit than the LS-APGD as an ionization source for atomic mass spectrometry [18]. The latest work on AP-SCGD [18], reported the analytical performance of this source coupled to an Orbitrap mass spectrometer for atomic and molecular mass spectrometry. Specific for uranium solution samples, the reported detection limit in AP-SCGD was 0.8 ng/mL with UO_2^+ as the measuring ion [18], whereas estimated detection limits for the LS-APGD were greater than 25 μg/mL for U^+ and less than 1 μg/mL for UO_2^+ [17]. As detection limit is related directly to sensitivity and/or background noise, the significantly better (lower) uranium detection limit for the AP-SCGD implies that it offers higher sensitivity and/or lower background noise than the LS-APGD. As both factors are important for isotopic ratio measurements, the AP-SCGD should be considered as a candidate emerging technology meriting further evaluation of its full potential for uranium isotopic assay.

3.3.3. Is Orbitrap suitable as field-deployable mass spectrometer?

In the two emerging mass-spectrometric techniques covered above, both research teams employed Orbitrap mass spectrometer. Given the impressive isotopic-ratio precisions and detection limits achievable by the two techniques, one might think that the problem of looking for the next generation of field-deployable instrument for UF_6 enrichment assay is solved. Unfortunately, the current technology of the Orbitrap mass spectrometer makes it inappropriate to serve as a field-deployable instrument [2]. A comment from the LS-APGD-MS research team [2] is that "*Although a conveniently available instrument for this work* (the LS-APGD-MS)*, it* (the Orbitrap) *is not one that would be appropriate for the type of in-field work envisioned by the potential user."* To elaborate, although the Orbitrap is a benchtop instrument, it is rather large and heavy (490 pounds [43]). Also, the requirement for environmental conditions for the Orbitrap mass spectrometer is quite demanding. For instance, according to the pre-installation manual of the Orbitrap [43], the optimum operation temperature is between 18°C to 21°C and temperature fluctuations of 1°C or more over a 10 minute period can affect performance. There are also rather strict requirements for humidity and vibration controls [43].

It should also be noted that the high resolution offered by the Orbitrap likely contributes to the impressive analytical figures of merit reported for the LS-APGD-MS, as it is documented that several low-intensity, non-uranium ions remain after collision-induced dissociation (CID, a process to dissociate and reduce background ions in the mass spectrometer) and require the high-resolution capability of the Orbitrap to resolve them [17]. If the Orbitrap is replaced by a more fieldable (and very likely lower resolution) mass spectrometer, it is currently unknown how such replacement would affect the analytical accuracy and precision. Clearly, there is a need to couple, characterize and evaluate the LS-APGD and AP-SCGD (and possibly other similar glow-discharge variants) to a mass spectrometer that is more field-deployable and preferably capable of performing truly simultaneous measurements.

3.4. Emerging optical-spectrometric techniques

3.4.1. Laser ablation absorbance ratio spectrometry

Laser ablation absorbance ratio spectrometry (LAARS), currently being developed at PNNL, is an all-optical technique for uranium isotopic assay. Its working principle is based on the isotopic shifts in atomic transitions between ^{235}U and ^{238}U atoms, and employs atomic absorption as the measurement means. The technique employs three lasers – one for ablation sampling and two for simultaneous

measurements of the relative abundances of ^{235}U and ^{238}U [24]. Laser ablation creates free uranium atoms from a solid sample, and these atoms are then probed by diode laser through atomic absorption. Measurements are conducted in a reduced-pressure environment to reduce spectral-line broadening.

The Niemax research group in 2002 [44] is probably the first to report measurements of uranium isotope ratios in solid samples through combination of laser-ablation sampling and diode-laser atomic absorption (before the technique was coined as LAARS). Liu *et al.* [44] utilized two diode lasers – one tuned specifically for ^{235}U absorption and the other for ^{238}U. This two-diode-lasers approach allows *simultaneous* measurements of the two U isotopes leading to measurement precision of 1.1% RSD for a pure uranium-oxide sample with ^{235}U at natural abundance [44]. Reported accuracy for the $^{235}U/^{238}U$ ratio was within 5% (relative) for a uranium mineral sample (i.e., an impure sample) at natural isotopic abundance.

The LAARS setup developed at PNNL [24, 25] is similar to that reported by Liu *et al.* [44] in many aspects. For example, LAARS also employs two diode lasers to simultaneously measure the relative abundances of ^{235}U and ^{238}U [24]. However, it should be stressed that the atomic transitions employed by LAARS [24] and those by Liu *et al.* [44] were different. The exact probing wavelengths in LAARS were not disclosed but it was mentioned that its two diode lasers operated at ~ 405 nm and ~ 415 nm [24], whereas the absorption lines at 682.6736 nm and 682.0768 nm were used for ^{235}U and ^{238}U, respectively, in the work of Liu *et al.* [44]. In both cases, the probed transitions for ^{235}U and ^{238}U are from different atomic transitions [24, 44].

Specific for UF_6 enrichment assay, LAARS employs a tailored solid thin-film sorbent to convert gaseous UF_6 to uranyl fluoride through a hydrolysis reaction [45]. Data from a presentation dated October 2014 [45] showed that accuracy and precision can achieve 0.1% ^{235}U enrichment. Specifically, for three UF_6 samples with ^{235}U abundances at 0.725%, 3.982% and 5.119%, the reported *relative* bias with frequency-locked probe lasers were 10%, 0.8% and 0.3%, respectively [45]. Reported relative precisions for these three UF_6 samples were 8.3%, 1.5% and 1.5%, respectively [45]. The latest result [46] demonstrated improvements in both accuracy and precision. For a sample with ^{235}U abundance at 5.119%, relative bias and precision were about 0.1% and 0.6%, respectively.

Measurement time for LAARS is fast and is typically around 10 minutes [24]. The overhead for sample preparation is also minimal; the reaction time for the conversion of gaseous UF_6 onto the solid thin-film sorbent is several minutes [24]. Because wavelength selectivity for the two isotopes comes from the narrow-bandwidth diode laser, an optical spectrometer is not needed, which further reduces the footprint of the instrument.

From its operating principle, the LAARS instrument might need slightly more demanding environment control. The two diode lasers need to be perfectly aligned with each other so that the two laser beams are probing identical volumes of the plasma plume generated by the ablation laser. Thus, a high level of mechanical robustness (e.g., anti-vibration, thermal expansion control) is likely required. Also, emission wavelength of a diode laser is very sensitive to temperature, the diode laser is mounted onto a Peltier element-operated heat sink and the temperature is precisely monitored and controlled [47]. Even with precise temperature control, the diode laser needs active feedback and frequency locking to minimize wavelength drift. Overall, the LAARS instrumentation set up is moderately complex, which could potentially be a drawback in its adaptation as an in-field instrument.

3.4.2. Laser induced spectrochemical assay for uranium enrichment

Laser induced spectrochemical assay for uranium enrichment (LISA-UE) is in a very early stage of development (starting October 2016), and is a joint effort between Lawrence Berkeley National Laboratory (LBNL) and Oak Ridge National Laboratory (ORNL). It is an all-optical technique for uranium isotopic assay and, in fact, is an extension of the well-known laser induced breakdown spectroscopy (LIBS) technique to low-pressure gaseous UF_6 samples. Like LAARS, its principle is based on the isotopic shifts in ^{235}U and ^{238}U atomic transitions. Instead of utilizing atomic absorption, LISA-UE employs atomic emission as the measurement means. It is known that isotopic shifts for some uranium atomic emission lines can reach tens of picometers and are large enough to be readily measured with an optical spectrometer even under ambient pressure and comparatively high

temperature (e.g., 5000 K) [48]. In fact, atomic emission spectrometry has a long history of being utilized for uranium isotopic analysis [49, 50]. Recently, Kracher *et al.* [19, 20] validated isotopic analysis of ^{235}U and ^{238}U in depleted, natural and enriched uranium with ICP-atomic emission spectrometry, and further extended the analysis to other U-isotopes like ^{233}U.

The LISA-UE system is targeted for direct analysis of gaseous UF_6 samples, although a solid sample (e.g., UF_6 absorbed on a solid substrate) also can be used. Specifically for gaseous UF_6 samples, a small gas chamber with optical access couples directly to a UF_6 cylinder/pipeline valve for sampling. Through the optical port, a pulsed laser beam is focused into the UF_6 gas sample and the laser–gas interaction then creates a transient high temperature plasma excitation source. This high-temperature plasma is capable of breaking down the chemical bonds in the sample, converts it into its constituent atoms, and promotes a portion of these atoms into their excited states. These excited states, through radiative decay, emit photons that are characteristic of its elemental and isotopic identities. When this transient plasma starts to cool (typically after several microseconds), molecules form through recombination. It has recently been reported that resulting molecular emissions also carry isotopic information [51]. The technique is potentially applicable to both off-line and on-line measurements.

There are some marked contrasts between LAARS and LISA-UE. Only one ablation laser is required in LISA-UE whereas LAARS needs three lasers [24]. Similar to the LAARS ablation laser, there are no constraints on the LISA-UE laser wavelength, and a laser with nanosecond (or shorter) pulse width is required in both cases. Plasma emissions in LISA-UE are collected by single set of light-collection optics for simultaneous ^{235}U and ^{238}U measurement, which also inherently guarantee that an identical plasma emission volume is probed. Furthermore, one potential advantage of employing emission over laser absorption is that a large collection of spectral lines (atomic) and bands (molecular) are emitted from the laser induced plasma, which can be simultaneously measured with a multi-channel optical spectrometer. As many of these spectral features carry the isotopic information of the sample, multiple emission-line/band measurement has been shown through simulations to improve analytical precision [51].

As LISA-UE is in a very early stage of development, its analytical capabilities are not yet known. However, it is anticipated that emission measurements on a collection of spectral features likely offers advantage over single line-pairs commonly employed in absorption measurements. For example, it has been shown through computer simulation that the use of a chemometric algorithm from a collection of spectral features provides several times improvement in the precision of ^{235}U abundance compared to those measurements utilizing only a single pair of emission lines [52]. In simulation, the ultimate precision was about 0.11% in absolute ^{235}U abundance for multiple line analysis [52], with signals accumulated from 10 laser pulses. Clearly, further improvement in precision can be achieved through more signal accumulation (i.e., accumulating signal from more than 10 laser pulses), although it is also anticipated that computer simulation probably offers the best-case scenario. The anticipated measurement time is a few minutes for each UF_6 sample. Commercial, field-deployable LIBS instruments for direct solid-sample analysis are readily available. Although these commercial systems are not specifically designed for gaseous samples, modification for handling gaseous samples is feasible. The size, as well as power requirements, of the components can be readily fit into a field-deployable instrument. While it is extremely early in the development cycle, the LISA-UE instrumentation set up – with a single laser excitation source and a single set of light-collection optics – is likely to be the simplest among all the techniques discussed above, which is advantageous as an in-field instrument.

4. Outlook

To summarize, a comprehensive and in-depth review was conducted on state-of-the-art and emerging technologies for field enrichment analysis of UF_6. All techniques were assessed for their potential to serve as an alternative for laboratory-based mass spectrometry. The evaluation was comprised of seven criteria, broadly defined: measurement characteristics and analytical capability, measurement time, and overall ease of operation and system complexity.

In terms of both analytical performance and sample throughput, the LS-APGD-MS is currently the best in all the emerging techniques reviewed. The AP-SCGD-MS, although currently utilized only for elemental analysis and not yet for isotopic measurements, already exhibits its pronounced sensitivity

advantage for uranium detection. Unlike the ICP, these glow-discharge ion sources use microplasmas which allow operation under low power and low gas flow (if a plasma gas is ever needed) — and, thus, are highly field deployable. The technical challenge to transform them into the next generation field-deployable UF_6 enrichment-assay instrument, perhaps, relates to identifying and coupling to a multi-channel field-deployable mass spectrometer that, through simultaneous measurement, can maintain the current achievable analytical figures of merit.

Some emerging techniques based on optical spectrometric techniques are also promising. LAARS shows its promise with a relative bias of 0.1% and relative precision of 0.6% for a LEU (5.119% ^{235}U) sample. LISA-UE is a new development and is based on well-established atomic emissions (LIBS). All of these emerging technologies show potential to be the next generation of rapid, field deployable instrumentation for UF_6 enrichment assay.

5. Acknowledgements

This work was performed under the auspices of the U.S. Department of Energy by Lawrence Berkeley National Laboratory under Contract DE-AC02-05CH11231. The project was funded by the Safeguards Technology Development Program in the U.S. Department of Energy/National Nuclear Security Administration's (DOE/NNSA's) Office of Nonproliferation and Arms Control (NPAC).

6. References

1. Anheier N., Cannon B., Martinez A., Barrett C., Taubman M., Anderson K., and Smith L.E.; *A new approach to enrichment plant UF_6 destructive assay sample collection and analysis;* PNNL-SA-112353, Pacific Northwest National Laboratory, 2015.
2. Barinaga C.J., Hager G.J., Hoegg E.D., Carman A.J., and Hart G.L.; *Feasibility of a fieldable mass spectrometer FY 2015 year-end report;* PNNL-24842, Pacific Northwest National Laboratory, 2015.
3. Smith L.E., and Lebrun A.R.; *Design, modeling and viability analysis of an online uranium enrichment monitor; in 2011 IEEE Nuclear Science Symposium Conference Record;* 2011, p 1030-1037
4. Erdmann N., Amador P., Arboré P., Eberle H., Lutzenkirchen K., Ottmar H., Schorlé H., van Belle P., Lipcsei F., and Schwalbach P.; *COMPUCEA: A high performance analysis procedure for timely on-site uranium accountancy verification in leu fuel fabrication plants; ESARDA Bulletin;* 43; 2009; 30-39
5. Berlizov A., Schachinger A., Roetsch K., Erdmann N., Schorlé H., Vargas M., Zsigrai J., Kulko A., Keselica M., Caillou F., Unsal V., and Walczak-Typke A.; *Feedback from operational experience of on-site deployment of bias defect analysis with COMPUCEA; J. Radioanal. Nucl. Chem.;* 307; 2016; 1901-1909
6. International Atomic Energy Agency; *Development and implementation support programme for nuclear verification 2016-2017;* STR-382, International Atomic Energy Agency (IAEA), 2016.
7. Hieftje G.M.; *The future of plasma spectrochemical instrumentation. Plenary lecture; J. Anal. At. Spectrom.;* 11; 1996; 613-621
8. Mialle S., Richter S., Hennessy C., Truyens J., Jacobsson U., and Aregbe Y.; *Certification of uranium hexafluoride reference materials for isotopic composition; J. Radioanal. Nucl. Chem.;* 305; 2015; 255-266
9. Boulyga S., Konegger-Kappel S., Richter S., and Sangely L.; *Mass spectrometric analysis for nuclear safeguards; J. Anal. At. Spectrom.;* 30; 2015; 1469-1489
10. Ardelt D., Polatajko A., Primm O., and Reijnen M.; *Isotope ratio measurements with a fully simultaneous Mattauch-Herzog ICP-MS; Anal. Bioanal. Chem.;* 405; 2013; 2987-2994
11. Okada Y., Kato S., Satooka S., and Takeuchi K.; *Measurements of U-235/U-238 isotopic ratio in the photoproduct UF_5 by multiphoton ionization and time-of-flight mass spectrometry; Appl. Phys. B;* 62; 1996; 515-519
12. Armstrong D.P., Harkins D.A., Compton R.N., and Ding D.; *Multiphoton ionization of uranium hexafluoride; J. Chem. Phys.;* 100; 1994; 28-43
13. Whitten W.B., Reilly P.T.A., Verbeck G., and Ramsey J.M.; *Mass spectrometry of UF_6 in a micro ion trap; in 7th International Conference on Facility Operations: Safeguards Interface;* Charleston, SC; 2004; Paper 345-349

14. NNSA Office of Nonproliferation and Arm Control; *Safeguards technology factsheet - portable mass spectrometry working group (MSWG);* 2016.
15. Hoegg E.D., Barinaga C.J., Hager G.J., Hart G.L., Koppenaal D.W., and Marcus R.K.; *Preliminary figures of merit for isotope ratio measurements: The liquid sampling-atmospheric pressure glow discharge microplasma ionization source coupled to an Orbitrap mass analyzer; J. Am. Soc. Mass Spectrom.;* 27; 2016; 1393-1403
16. Hoegg E.D., Barinaga C.J., Hager G.J., Hart G.L., Koppenaal D.W., and Marcus R.K.; *Isotope ratio characteristics and sensitivity for uranium determinations using a liquid sampling-atmospheric pressure glow discharge ion source coupled to an Orbitrap mass analyzer; J. Anal. At. Spectrom.;* 31; 2016; 2355-2362
17. Barinaga C.J., Hager G.J., Hart G.L., Koppenaal D.W., Marcus R.K., Jones S.M., and Manard B.T.; *Toward a fieldable atomic mass spectrometer for safeguards applications: Sample preparation and ionization; in 12th Symposium on International Safeguards: Linking Strategy, Implementation and People (IAEA-CN-220);* Vienna, Austria; 2014; Paper S08-08
18. Schwartz A.J., Williams K.L., Hieftje G.M., and Shelley J.T.; *Atmospheric-pressure solution-cathode glow discharge: A versatile ion source for atomic and molecular mass spectrometry; Anal. Chim. Acta;* 950; 2017; 119-128
19. Krachler M., and Carbol P.; *Validation of isotopic analysis of depleted, natural and enriched uranium using high resolution ICP-OES; J. Anal. At. Spectrom.;* 26; 2011; 293-299
20. Krachler M., and Wegen D.H.; *Promises and pitfalls in the reliable determination of U-233 using high resolution ICP-OES; J. Anal. At. Spectrom.;* 27; 2012; 335-339
21. Zamzow D., Murray G.M., Dsilva A.P., and Edelson M.C.; *High-resolution optical-emission spectroscopy of uranium hexafluoride in the argon afterglow discharge; Appl. Spectrosc.;* 45; 1991; 1318-1321
22. Barshick C.M., Shaw R.W., Young J.P., and Ramsey J.M.; *Evaluation of the precision and accuracy of a uranium isotopic analysis using glow-discharge optogalvanic spectroscopy; Anal. Chem.;* 67; 1995; 3814-3818
23. Smith B.W., Quentmeier A., Bolshov M., and Niemax K.; *Measurement of uranium isotope ratios in solid samples using laser ablation and diode laser-excited atomic fluorescence spectrometry; Spectrochim. Acta Part B;* 54; 1999; 943-958
24. Boyer B.D., Anheier N., Cable-Dunlop P., and Sexton L.; *Incorporation of new, automated environmental sampling systems into safeguards approaches;* LA-UR-13-28412, Los Alamos National Laboratory, 2013.
25. Bushaw B.A., and Anheier Jr N.C.; *Isotope ratio analysis on micron-sized particles in complex matrices by laser ablation-absorption ratio spectrometry; Spectrochim. Acta Part B;* 64; 2009; 1259-1265
26. NNSA Fact Sheet; *Fieldable atomic beam laser spectrometer for isotopic analysis;* 2016.
27. Berezin A.G., Malyugin S.L., Nadezhdinskii A.I., Namestnikov D.Y., Ponurovskii Y.Y., Stavrovskii D.B., Shapovalov Y.P., Vyazov I.E., Zaslavskii V.Y., Selivanov Y.G., Gorshunov N.M., Grigoriev G.Y., and Nabiev S.S.; *UF_6 enrichment measurements using TDLS techniques; Spectrochim. Acta Part A;* 66; 2007; 796-802
28. Grigor'ev G.Y., Lebedeva A.S., Malyugin S.L., Nabiev S.S., Nadezhdinskii A.I., and Ponurovskii Y.Y.; *Investigation of $^{235}UF_6$ and $^{238}UF_6$ spectra in the mid-IR range; Atomic Energy;* 104; 2008; 398-403
29. NNSA Fact Sheet; *Spectroscopic mathods for ultra-low isotopic analysis of proliferant material;* 2016.
30. Zhao K., Penkin M., Norman C., Balsley S., Mayer K., Peerani P., Pietri C., Tapodi S., Tsutaki Y., Boella M., Renha Jr. G., and Kuhn E.; *International target values 2010 for measurement uncertainties in safeguarding nuclear materials;* STR-368, International Atomic Energy Agency (IAEA), 2010.
31. Hieftje G.M.; *Emergence and impact of alternative sources and mass analyzers in plasma source mass spectrometry; J. Anal. At. Spectrom.;* 23; 2008; 661-672
32. Meija J., and Mester Z.; *Signal correlation in isotope ratio measurements with mass spectrometry: Effects on uncertainty propagation; Spectrochim. Acta Part B;* 62; 2007; 1278-1284
33. Grotti M., Todoli J.L., and Mermet J.M.; *Influence of the operating parameters and of the sample introduction system on time correlation of line intensities using an axially viewed CCD-based ICP-AES system; Spectrochim. Acta Part B;* 65; 2010; 137-146
34. Schilling G.D., Ray S.J., Sperline R.P., Denton M.B., Barinaga C.J., Koppenaal D.W., and Hieftje G.M.; *Optimization of Ag isotope-ratio precision with a 128-channel array detector coupled to a Mattauch-Herzog mass spectrograph; J. Anal. At. Spectrom.;* 25; 2010; 322-327

35. Richter S., Kuhn H., Truyens J., Kraiem M., and Aregbe Y.; *Uranium hexafluoride (UF_6) gas source mass spectrometry for certification of reference materials and nuclear safeguard measurements at IRMM; J. Anal. At. Spectrom.;* 28; 2013; 536-548
36. Wieser M., Schwieters J., and Douthitt C.; Multi-collector inductively coupled plasma mass spectrometry, in Isotopic analysis - fundamentals and applications using ICP-MS, 1st ed., Wiley-VCH Verlag, (2012) p 77-91
37. de Oliveira O.P., de Bolle W., Alonso A., Richter S., Wellum R., Ponzevera E., Sarkis J.E.S., and Kessel R.; *Demonstrating the metrological compatibility of uranium isotope amount ratio measurement results obtained by GSMS, TIMS and MC-ICPMS techniques; Int. J. Mass Spectrom.;* 291; 2010; 48-54
38. Erdmann N., Albert N., Amador P., Arboré P., Eberle H., Lutzenkirchen K., Ottmar H., Schorlé H., van Belle P., Lipcsei F., Schwalbach P., Jung S., and Lafolie R.; *COMPUCEA 2nd generation performance evaluation;* IAEA-CN-184/316, International Atomic Energy Agency, 2010.
39. Quarles C.D., Carado A.J., Barinaga C.J., Koppenaal D.W., and Marcus R.K.; *Liquid sampling-atmospheric pressure glow discharge (LS-APGD) ionization source for elemental mass spectrometry: Preliminary parametric evaluation and figures of merit; Anal. Bioanal. Chem.;* 402; 2012; 261-268
40. Marcus R.K., Quarles C.D., Barinaga C.J., Carado A.J., and Koppenaal D.W.; *Liquid sampling-atmospheric pressure glow discharge ionization source for elemental mass spectrometry; Anal. Chem.;* 83; 2011; 2425-2429
41. Carado A.J., Quarles C.D., Duffin A.M., Barinaga C.J., Russo R.E., Marcus R.K., Eiden G.C., and Koppenaal D.W.; *Femtosecond laser ablation particle introduction to a liquid sampling-atmospheric pressure glow discharge ionization source; J. Anal. At. Spectrom.;* 27; 2012; 385-389
42. Schwartz A.J., Ray S.J., and Hieftje G.M.; *Evaluation of interference filters for spectral discrimination in solution-cathode glow discharge optical emission spectrometry; J. Anal. At. Spectrom.;* 31; 2016; 1278-1286
43. Thermo Fisher Scientific; *Exactive™ series: Exactive™ and Q Exactive™ preinstallation requirements guide;* Revision A - 1288110, 2011.
44. Liu H., Quentmeier A., and Niemax K.; *Diode laser absorption measurement of uranium isotope ratios in solid samples using laser ablation; Spectrochim. Acta Part B;* 57; 2002; 1611-1623
45. Anheier N., Cannon B., Martinez A., Barrett C., Taubman M., Anderson K., and Smith L.E.; *A laser-based method for onsite analysis of UF_6 at enrichment plant;* PNNL-SA-105776, Pacific Northwest National Laboratory, 2014.
46. NNSA Safeguards Technology Factsheet; *Laser ablation absorption ratio spectroscopy (LAARS);* PNNL-SA-123926, 2017.
47. Niemax K., Zybin A., Schnurer-Patschan C., and Groll H.; *Semiconductor diode lasers in atomic spectrometry; Anal. Chem.;* 68; 1996; A351-A356
48. Chan G.C.Y., Choi I., Mao X., Zorba V., Lam O.P., Shuh D.K., and Russo R.E.; *Isotopic determination of uranium in soil by laser induced breakdown spectroscopy; Spectrochim. Acta Part B;* 122; 2016; 31-39
49. Burkhart L.E., Stukenbroeker G., and Adams S.; *Isotope shifts in uranium spectra; Phys. Rev.;* 75; 1949; 83-85
50. Edelson M.C., and Fassel V.A.; *Isotopic abundance determinations by inductively coupled plasma atomic emission spectroscopy; Anal. Chem.;* 53; 1981; 2345-2347
51. Mao X., Chan G.C.-Y., Choi I., Zorba V., and Russo R.E.; *Combination of atomic lines and molecular bands for uranium optical isotopic analysis in laser induced plasma spectrometry; J. Radioanal. Nucl. Chem.;* 312; 2017; 121-131
52. Chan G.C.Y., Mao X., Choi I., Sarkar A., Lam O.P., Shuh D.K., and Russo R.E.; *Multiple emission line analysis for improved isotopic determination of uranium – a computer simulation study; Spectrochim. Acta Part B;* 89; 2013; 40-49

Alternative nuclear certified reference materials for safeguards and industry

SANCHEZ HERNANDEZ Ana María[a], TOTH Kalman[b], AREGBE Yetunde[b], BANIK Nidhu Lal[a], BAUWENS Jeroen[b], BUDA Razvan[a], BUJAK Renata[b], CARLOS MARQUEZ Ramón[a], CASTELEYN Karin[a], DUINSLAEGER Lily[a], HENNESSY Carmel[b], JAKOPIC Rozle[b], KEHOE Frances[b], VAN BELLE Pieter[a], ZULEGER Evelyn[a]

[a] JRC G.II.6 Nuclear Safeguards and Forensics
Hermann-von-Helmholtz-Platz 1, 76344 Eggenstein-Leopoldshafen, Germany
JRC Directorate G - Nuclear Safety and Security
[b] JRC G2 Standards for Nuclear Safety, Security and Safeguards
Retieseweg 111, 2440 Geel, Belgium

Abstract:

Large-Sized Dried (LSD) spikes are Certified Reference Materials (CRMs) used in nuclear safeguards for accurate determination of nuclear material inventories by Isotope Dilution Mass Spectrometry (IDMS). They are a metrological quality tool to meet the existing requirements for reliable accountancy and verification measurements (IAEA STR-368).
LSD spikes are produced by drying down accurately weighed quantities of uranium and plutonium nuclear reference solutions into vials. The dried deposits are not stable over time. To keep the spikes integrity and to prevent unintended losses of material, the CRMs need to be protected with a matrix or coating material. This substance is a critical component for the quality and long-term stability of these CRMs.
IDMS relies on the mechanical integrity of the spikes; they need to be robust during transport and storage for their guaranteed life-time. The main requirements for coating materials are good adherence to glass, mechanical stability, resistance to radiation and long term stability. The material should furthermore, not interfere with the preparation and mass spectrometric measurements.
Under the project "Innovative nuclear CRMs for EURATOM safeguards and industry" (INS-CRM), the JRC Directorate G for Nuclear Safety and Security examines alternative substances for coating spikes. The main candidate is CarboxyMethyl Cellulose (CMC) which seems to meet the requirements mentioned above. The goal of the project is to find the right methodology and composition for the preparation of the coatings. Additionally, the mechanical integrity needs to be proven under simulated transport and radiation conditions, and finally the spikes shelf life will be determined. Furthermore, to understand better the interaction between the matrix and the actinides, the structure and chemical properties have to be investigated using different analytical techniques. It is also planned to test several U/Pu ratios for CRMs suitable for different sample types. This paper reports on the current status of the project.

Keywords: Safeguards, Spikes, Coating, IDMS, ITV2010.

1. Introduction

The European Commission is responsible for the control of all civil fissile nuclear material in the European Union, EURATOM Treaty Chapter VII: *The European Commission shall satisfy itself that nuclear material is not diverted from intended uses* [1]. One of the JRC core activities is supporting EURATOM safeguards (DG ENER), the International Atomic Energy Agency (IAEA), and industry with metrological quality control tools and top notch analytical service.

Large-Sized Dried (LSD) spikes are Certified Reference Materials (CRMs) used in Nuclear Safeguards and industry. They are a metrological quality tool for nuclear plant operator and safeguards laboratories for accurate determination of nuclear material inventories by Isotope Dilution Mass Spectrometry (IDMS). Using high quality spikes in IDMS as one of the primary measurement techniques provides accurate and traceable measurement results (IAEA/ESARDA International Target Values, ITV) [2]. In particular, the IRMM-1027 series of LSD spikes are certified for the mass of ^{235}U, ^{238}U and ^{239}Pu per unit and the uranium and plutonium isotope amount ratios [3]. The spikes are covered with a thin layer of the organic substance cellulose acetate butyrate (CAB) to preserve integrity of the dried nitrates. The quality and reliability of the LSD spikes determine the accuracy of the fissile material accountancy of irradiated nuclear fuel at the EURATOM on-site laboratories and at reprocessing plants. The EURATOM laboratories operated by DG JRC on behalf of DG ENER, are located at the reprocessing plants in Sellafield, UK and La Hague, France. Both laboratories are instrumental in providing independent assurance to the European Commission that nuclear material is not diverted from its declared use.

The main requirements for suitable coating materials are good adherence to glass, mechanical stability, good complexation properties, resistance to radiation and long-term stability. The material should not interfere with the preparation/chromatographic separation steps and mass spectrometric measurements. The preparation of spike CRMs should furthermore allow the production in large batches in compliance with ISO Standard 17034 to fulfil the demands for fissile material control by safeguards authorities and plant operators [4].

Currently the CAB coated IRMM-1027 LSD spikes provided by JRC-Geel have a shelf life of 3 years. Customers, however, require a longer shelf life. Therefore the optimization of the preparation of the organic layer with embedded uranyl- and plutonium nitrate as well as investigations on new types of coatings have been undertaken as a joint endeavour by the JRC-Geel and JRC-Karlsruhe. Different approaches have been used to address these goals:

1. Use of carboxymethyl cellulose sodium salt (CMC) foam as coating material [5].
2. Improvement of the mechanical properties of the CAB film by using plasticizer [6].
3. Reconditioning of CAB spikes by treatment with phosphoric acid (H_3PO_4).

The well-defined objective and the limited granted time span render this project a project of mainly experimental nature. In addition, several characterisation techniques such as X-ray diffraction (XRD), Scanning Electron Microscopy (SEM) with Energy Dispersive X-Ray Analysis (EDX) and Transmission Electron Microscopy (TEM) are applied with the aim to better understand the binding mechanism and distribution of the U and Pu in nitric systems.

2. CMC

CMC is the sodium salt of carboxymethylcellulose [7]. It is produced from cellulose, which is made water-soluble by introducing carboxymethyl groups along the cellulose chain. CMC is formed by the reaction of cellulose with chloroacetic acid and sodium hydroxide.

The applications of CMC in many areas, particularly in food industry, are well known, but there are not many studies on the interaction of CMC with nuclear materials. According to the experimental research carried out by the JRC [5] with actinides embedded in CMC, the material shows properties which make this substance a very good candidate to be used as coating material for the LSD spikes. Some of these properties are listed below:

- CMC is a powder that dissolves in water or nitric acid solutions. For the envisaged application, a nitric acid solution is required for several reasons. Most important is to create a coating that embeds the nuclear material, which at the same time, impedes the formation of plutonium colloids [8, 9]
- When the CMC solution is dispensed and dried, it builds a foam, see Figure 1. Over time and during storage the structure changes starting with carboxylic acid formation; nevertheless, the product remains stable. The final product depends on the used protocol for the preparation and final composition of the CMC solution (composition in terms of CMC and nitric acid concentration)
- The final product tends to remain fixed on the walls and at the bottom of the vials

- The foam appears to offer a good adsorption capability for the dried U and Pu nitrates; the U and Pu element distribution within the foam appears homogenous as demonstrated by SEM studies [5]
- The final product quickly dissolves in nitric acid solution

Figure 1. Formation of CMC-foam from the mother solution to different stages of maturation.

2.1. CMC solution and coating preparation

The first part of the project has been mainly dedicated to define the parameters for the optimal composition of the CMC solution, the working range and the protocol for the production of the CMC mother solution.

The objective has been to produce a robust product suitable for production on a large scale. In particular, production and treatment under the special conditions required for the preparation of nuclear CRMs (i.e. working in glove boxes).

2.1.1. CMC protocol

During the production and evaluation of the foams prepared during the first stage of the project, it was realized that the protocol for the preparation of the CMC solution has a strong influence on the quality and the ageing of the final product.

Preliminary tests performed [5] used a solution in the form of a gel with high viscosity which was very difficult to dispense into vials. The concentration of CMC was limited by the solubility of the CMC in water to about 5 % CMC. Another drawback of this protocol was that during the drying process the solution had a tendency to produce a very thin ring of dried of dried CMC on the wall of the vial; this ring is liable to produce flakes and thus nuclear material could be dispersed.

Several protocols have been checked until the final one met the following requirements:

- CMC starting solution easy to prepare
- CMC solution in liquid form easy to dispense
- Reasonable foam production repeatability
- Good quality of the foam
- Better control of the foam formation time (drying time)

The drying time of the solution, produced using the current protocol, varies between 24 and 72 hours depending on the drying temperature applied on the heating device. Setting up variable temperatures depending on the drying stage (evaporation phase or formation of foam) allows reducing the drying time; the maximum temperature during the foam formation phase should not exceed 45 °C.

2.1.2. Heating device – Foil Heater

An appropriate hot plate has been developed in collaboration with the workshop of the JRC.G.1 - JRC Sites Radioprotection and Security Unit (Figure 2). The design has been tailored considering the main requirements for the production of LSD spikes in large batches and in particular the requirements of the JRC-Geel facilities.

Heat is provided by a flexible thermofoil heater; several manufactures (Minco, Termya, Synomas) provide these heaters with the required features: Polyimide material, 101.6x101.6 mm, with pressure-sensitive adhesive, Voltage 24V, Watt density 0.39 W/cm^2, *Teflon* leads and insulated connection

points. The operational range to dry down the coating solution is between 7.5 V and 9 V depending on the equipment set up. An aluminium plate has been adapted to the foil heater in order to better disperse the heat which in return provides for a homogeneous surface temperature. The temperature gradient has been thus reduced from about Δ 10 °C to Δ 2 °C.

The heating element is enclosed in an outer casing made of polycarbonate with UL94 V-0 certification. The heat output is negligible. The external-surface temperature of the foil heater enclosure is below 60 °C which is acceptable for the use inside a glove box. An outlet in the casing is connected to the ventilation system to remove acid fumes. The hotplate has inserts allowing secure placement of spike vials. Three heating devices have been connected in series. The power supply and the temperature control unit are located outside the glove box. Temperature sensors placed on the foil heater are connected to the control unit. The cabling is ensured via feed-through "LEMO" connectors.

The construction has been installed at the JRC-Karlsruhe and the JRC-Geel facilities for the preparation of the spikes.

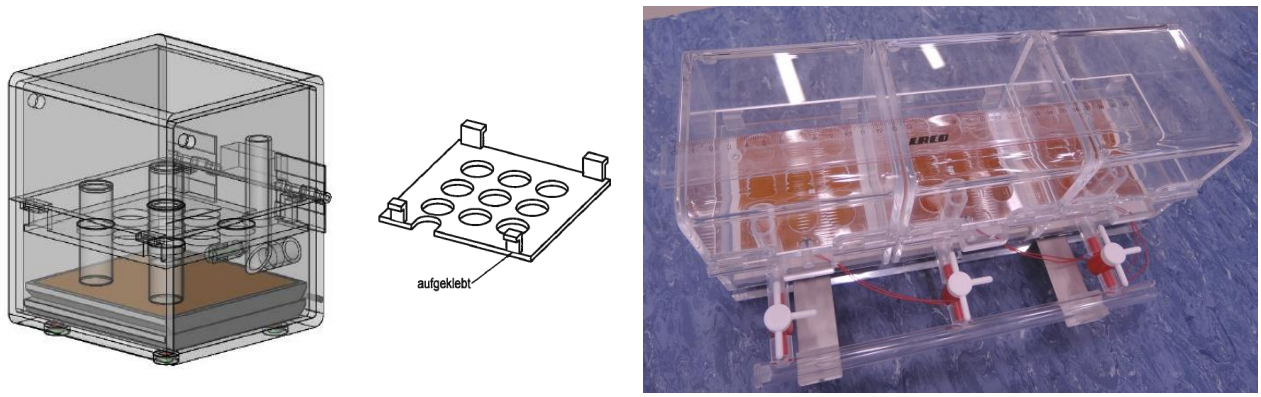

Figure 2. Chamber foil heater developed at the JRC-Karlsruhe.

2.1.3. Optimisation of the CMC coating

With the aim to find the most suitable composition, different concentrations of CMC and HNO_3 and different viscosity of CMC have been tested on a set of cold tests (inactive samples without nuclear material). Furthermore, the influence of different environmental parameters has been also evaluated. The four main variables which have been controlled are summarised more concretely below:

- Concentration of CMC in mass fraction, from 6 to 17 %
- CMC viscosity (Low viscosity – CMC LV, High viscosity – CMC HV)
- HNO_3 molarity from 1 to 6 mol/L
- Environmental parameters (temperature, humidity and environmental acidity)

To test the CMC behaviour under different environmental conditions, samples have been produced outside and inside glove-boxes and in different laboratories at JRC-Karlsruhe and JRC-Geel facilities.

The main indicators used for the evaluation of the foam are the quality (in terms of development, colour and height of the foam), the ageing of the product and finally the resistance to the mechanical tests. The height of the foam should be limited in order to avoid material dispersion and to concentrate all material at the bottom of the vessel. A homogeneous white colour on the fresh foam indicates that the foam has been properly developed and that the product has not been over-heated.

As a result of the tests performed with non-active samples the protocol for the preparation has been improved. The working range has been defined for the different laboratories, considering that the final composition required depends on the environmental conditions mentioned before.

The concentration of HNO_3 is a deciding factor for the quality of the coating. A minimum of molarity of nitric acid is required for the formation of the foam, but an excess has a negative impact on the quality of the foam: higher foams and faster degradation presumably because of the unreacted acid.

In order to incorporate the typical amount of nuclear material of the LSD spikes in the coating matrix, the minimum mass of CMC per vial was ascertained [5]. The concentration of CMC is limited by the concentration of nitric acid; the foam will not be fully developed with an excess of CMC.

Regarding the CMC viscosity, based on our experimental results, the low viscosity CMC is preferred for the preparation of spikes; it has also a higher degree of substitution which, together with the lower molecular weight, facilitates the dissolution in water based systems.

According to the tests done at JRC-Geel and JRC-Karlsruhe, the optimal nitric acid concentration varies in a range between 2 and 3 mol/L (depending on the laboratory environmental conditions) for a mass fraction of 10-11 % LV CMC. The amount of CMC solution dispensed in the vials has been fixed at 1.5 mL; this quantity has been adjusted in such a way that the actinides complexation capacity is maintained with respect to the previous tests [5] and the content of nitric acid can be kept as low as possible. Also this volume of solution is large enough to cover all remainings of nuclear material that might be sorbed on the walls of the vials in the previous step of drying the spiking material.

2.1.4. Ageing and transport simulation tests

The non-active CMC vials have been visually inspected (ageing test) monthly during the first 6 months and then every 3 months in the first year after the production. Furthermore, mechanical tests have been performed 6 months after the production of the sample.

According to the visual inspections carried out, the most changes due to ageing take place during the first 5-6 months. Afterwards the product is more stable and suffers less modifications.

Considering the constraints of working in a nuclear facility, some transport conditions have been simulated. The following tests have been performed:

- Vibration test using a laboratory shaker at 1500 rpm for 6 hours
- Low temperature test (-15°C) for 8 hours
- Elevated temperature (43-45 °C) for 8 hours

The outcome of these ageing and transport simulation tests is very promising. The integrity of the matrix produced with the most optimal protocol and exposed to the transport simulation tests has not been affected. The structure of the CMC does not change and no flakes or cracks could be detected.

Furthermore, a collaboration with the Centrum voor Polymer & Materiaaltechnologie (CPMT) of the Ghent University in Belgium has been established under this project. Experimental techniques commonly used in polymer research will also be applied with the aim to discover more about the chemical and mechanical properties of the organic substances evaluated under this project. Apart from alpha and gamma radiations degradation is also caused by the presence of nitric acid that induces hydrolytic cleavage of the etheric bonds of CMC. Blank CMC foams will be analysed by gel permeation chromatography (GPC) to assess the effect of nitric acid on the molecular weight and to evaluate the degradation process.

2.2. CMC active spikes

In order to test the coating capabilities and to check that the material meets the requirements, several sets of spikes with different ratios of nuclear materials have been produced. Some of the samples will undergo the same tests as the non-active CMC: exposition to elevated and low temperature, resilience during simulated transport and irradiation conditions. Finally, in order to confirm the reliability of the spikes, several samples from every set will be analysed for the concentration of the U and Pu by IDMS. Figure 3 summarizes the sets of samples and tests envisaged; for sets 4 and 5 different tests will be performed on the same spikes. The U/Pu concentration determination by IDMS is the last test for some of the vials from sets 3, 4 and 5 as this step is destructive.

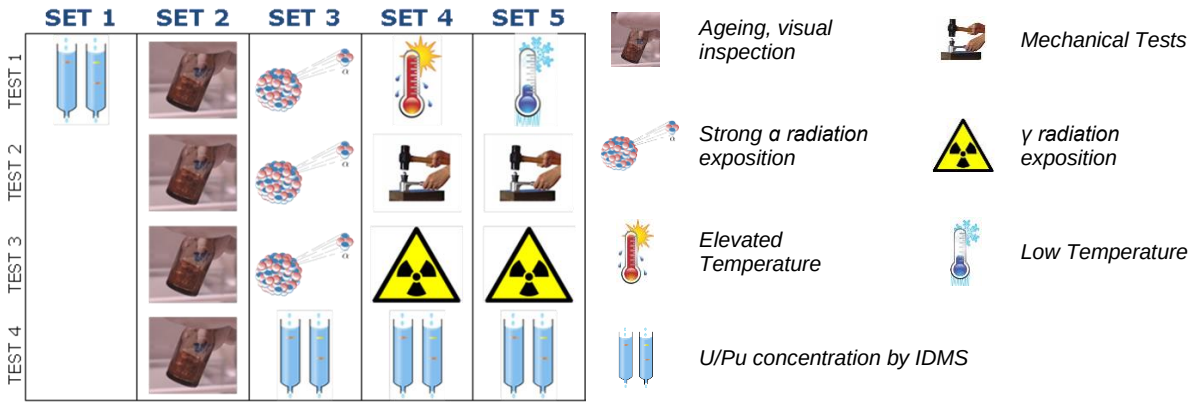

Figure 3: Outline of the different tests to be done.

Set 1 will serve to determine any possible interferences of the coating with the actinide and fission product chromatographic separation and mass spectrometry measurements. The JRC-Karlsruhe will follow the procedure routinely used for the verification of spikes produced by external customers of the Analytical Service [10], using the chromatographic separation on resin UTEVA®: Eichrom [11]. In the case of the JRC-Geel the anion exchange method (Bio-Rad AG1-X4 100-200 mesh resin) [12] is used for the actinides separation.

For the evaluation of the stability of the CMC the full kinetic and thermodynamic processes of the chemical reactions need to be ascertained for the desired shelf life of at least five years. The ageing and long-term stability of the spike will be evaluated using about 30 vials (Set 2) of the internal reference materials prepared (see Table 1, SPK1-6), capped and kept in a glove-box. For this it is necessary to visually inspect the samples monthly during the first 6 months and every 2-3 months for the lifetime of the samples.

The timespan of the project does not cover the entire period. Nevertheless, several specific tests have been performed to simulate as much as reasonable possible the behaviour of the products over longer periods of time under the influence of internal and external factors like intrinsic radiation or exposure to heat variations and vibrations.

In order to understand the influence of radiolysis stemming from the alpha-emitting Pu in the CMC foam, a third series (Set 3) of 34 vials with nuclear material high enriched in ^{238}Pu (strong alpha emitter) has been loaded. These samples are also kept in a glove-box and visually inspected periodically. A few vials have been coated with CAB in order to compare the influence of the self-irradiation and the ageing in the two coating materials.

In addition, for the assessment of the robustness, influence of temperature and irradiation 2 more sets of samples (Set 4 and Set 5) will be processed and exposed to high and low temperature and resilience tests. Also the Hot Cell facilities of the JRC-Karlsruhe will be used to expose the CMC covered spikes to about 1Sv/h dose rate of gamma rays radiation. As part of the testing several vials of the Set 4 and 5 will be examined in order to assess the influence of the experiments on the CMC foam after the elapsing of carefully chosen periods of time

Another goal of the project is to introduce various U/Pu ratios suitable for different sample types; the present U/Pu ratio ~25:1 is a compromise. To achieve measurement uncertainties below the ITVs for the large range of samples currently measured, the spikes need to be provided with different U/Pu ratios. To this end, various laboratory internal reference materials have been produced and characterized for the different tests. Seven spike solutions with mainly different U concentrations (Pu concentration is maintained stable except for SPK7 as explained below) and variable U/Pu ratios have been produced (Table 1):

SPIKE RATIOS			
	Ratio U/Pu	Pu (mg)	U (mg)
SPK1	25	2	50
SPK2	8	2	16
SPK3	100	2	200
SPK4	Pure U	-	18-50
SPK5	Pure Pu	2	-
SPK6	1	2	2
SPK7	Pu-238	0.06	-

Table 1: Preparation of spike solutions and U/Pu amount per vial.

The isotopic composition of the U and Pu solutions from SPK1 to SPK6 is comparable to the current LSD spikes IRMM-1027 [3]. The quantity of Pu in the spikes is also comparable to the LSD spikes, 2 mg Pu per vial and the amount of U has been adjusted in order to reach the desired U/Pu ratio.

The spike SPK7 has been prepared in order to check the self-irradiation and radiolysis influence (Set 3). SPK7 contains only Pu with a different isotopic composition, elevated relative mass fraction of ^{238}Pu (^{238}Pu/Pu 73.32 ± 0.21 % [*k*=2] 23/03/2016). The amount of Pu dispensed is calculated in such a way that the radioactivity in 1 month in this spike is equivalent to the radioactivity over 6 months in one of the IRMM 1027 series LSD spikes [3].

34 SPK7 spikes have been dispensed and coated in the facilities of the JRC-Karlsruhe, 10 CAB, 12 CMC LV and 12 CMC HV. Figure 4 shows the ageing of three SPK7 spikes covered with CAB, CMC LV and CMC HV respectively:

Figure 4: SPK7 spikes coated with CAB and CMC LV and HV.

In all the CAB spikes, the coating starts to react and to form small bubbles around the areas where the nuclear material and consequently the radioactivity are concentrated. Nevertheless, the spike SPK7 without uranyl nitrates is not representative the real LSD spikes but serves as described above for understanding the influence of the self-irradiation effects in a limited time span; the CAB coating dissolves partially the Pu nitrates and the nuclear material is not homogeneously dispersed in the coating. The presence of U in spikes plays a key role for the dissolution of the material in the CAB

solution before drying down. In the case of the CMC, the solution totally dissolves and incorporates the dried Pu nitrates before creating the foam. The CMC ageing is comparable to the non-active samples. Therefore, the influence of the self-irradiation in the case of the CMC is not significant for the time of observation.

For the coating of the spikes from SKP1 to SPK6, initially the composition of the CMC solution chosen to prepare the active spikes was the one optimised during the tests with the non-active samples. However, while producing the CMC foams with the different ratios, we have appreciated that the nitric acid concentration can be customised according to the amount of nuclear material, but always in the range of 2-3 mol/L HNO_3; higher amounts of nuclear material require less HNO_3 concentration which could enhance the long-term stability of the spikes.

One of the main outcomes of these active tests is the confirmation of the high complexation capacity of the CMC. This property allows the production of spikes with different U/Pu ratios using higher amounts of nuclear material. Figure 5 shows a spike SPK3, U/Pu ratio 100 with 200 mg of U and 2 mg of Pu, before and after being coated with CMC solution. Besides, due to the characteristics of the drying process of the CMC, the possible remaining material fixed on the walls of the vials is incorporated and dissolved in the solution before the formation of the foam, see Figure 6.

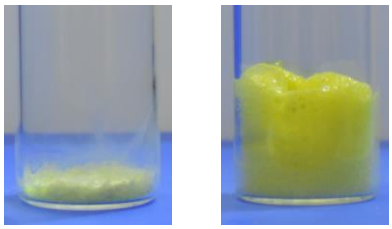

Figure 5: Picture on the left dried SPK3 spike (without CMC) and on the right the same spike coated with CMC.

Figure 6: Dried test spike with some nuclear material on the tube walls.

So far no disturbances during spike dissolution, actinides separation and mass spectrometry measurements could have been observed due to the present of CMC coating. The tests have been carried out for Set 1 spikes.

Furthermore, in order to verify that the final product does not depend on the CMC material manufacturers two materials from different producers are being tested with the same production protocol at the moment. Figure 7 shows CMC spikes from the different sets of ratios coated with CMC from the following producers: *Calbiochem* [13] in the first row and *Alfa Aesar* [14] in the second row of pictures:

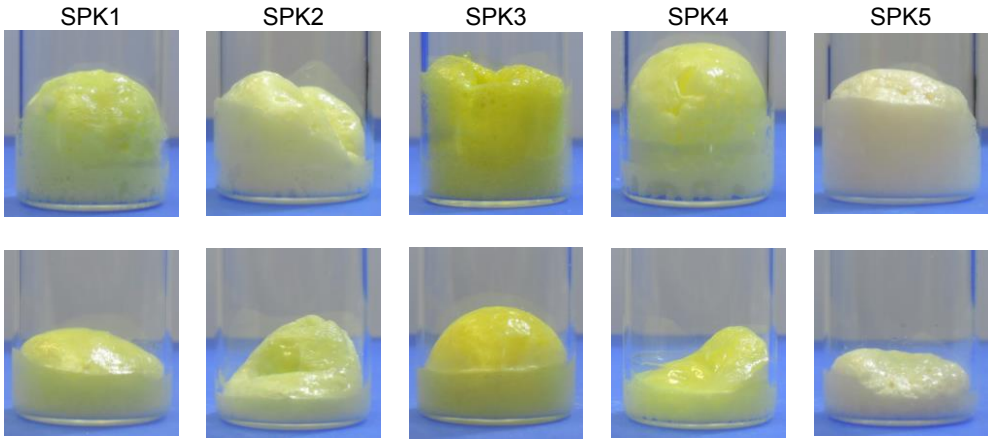

Figure 7: Different spikes and ratios coated with *Calbiochem* CMC (first row) and *Alfa Aesar* (second row).

The first impression is that the coatings produced with both materials meet the requirements in terms of foam quality. Further investigations are undergoing on the coatings produced with the second material.

2.2.1. Additional analysis techniques

In order to complement the experimental results and to understand better the behaviour of the coatings, further investigations are planned to be applied using the following techniques:

- GPC for polymer molecular weight and polydispersity analysis
- Thermo Gravimetrical Analysis (TGA) and Differential Scanning Calorimetry (DSC) for thermal analysis
- Mechanical testing for tensile stress and tensile strain behaviour
- SEM-EDX, TEM, imaging techniques used to analyse morphology, defects, etc.
- Nuclear Magnetic Resonance spectroscopy (NMR) for chemical structure
- XRD and X-ray Absorption Spectroscopy (XAS) for molecular structure
- Molecular modelling

CMC foams containing REIMEP17A U/Pu material [15] were subjected to SEM/EDX investigations [5] and the distribution of both U and Pu was proven to be homogeneous. Additional preliminary analyses with TEM have been performed on CMC foam contacted with nuclear material with U/Pu ratio ~20 (~2 mg Pu), and the diffraction of the resulted figure shows a perfectly amorphous material, with no rings or single diffraction spots which could be assigned to any crystallinity (see Figure 8).

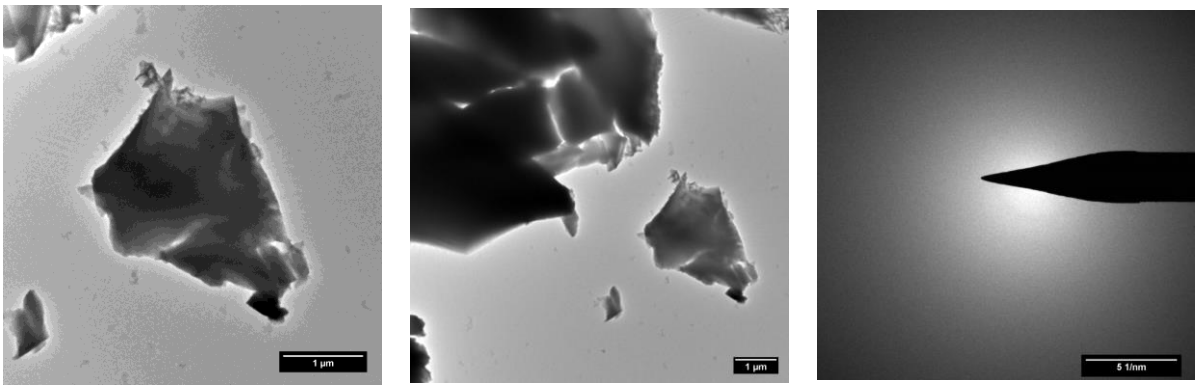

Figure 8: Low resolution bright field images of typical particles on the CMC –U/Pu material in the first and second pictures from the left. Last picture demonstrates by electron diffraction the typical amorphous appearance.

3. CAB

Cellulose acetate butyrate (CAB) has been applied as the organic matrix of LSD spikes for the last 16 years. It was the successor of the 'THF spikes' due to its better solubility in nitric acid and easy preparation procedure. CAB is cellulose derivative partially esterified with acetyl and butyryl groups where the ratio of –OH/acetyl/butyryl functional groups differ (see Figure 9). Depending on the degree of substitution, the ratio of the different functional groups and the degree of polymerization the physical and chemical properties of the polymer can be altered. Commercially available CABs are usually characterized by their butyryl content, given as wt%, and this value can vary between ~17-55% (the hydroxyl content of the CABs is typically low < 2 wt%).

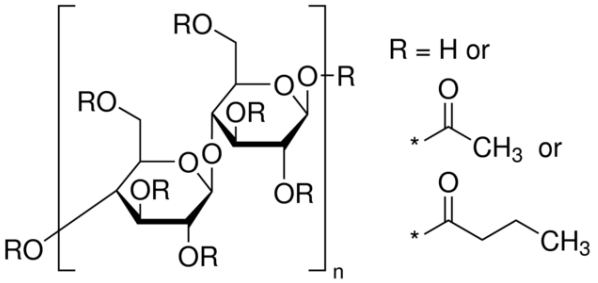

Figure 9: Chemical structure of cellulose acetate butyrate (source: Sigma-Aldrich [16])

First CAB with 17 wt% butyryl content (CAB-17) was used with metallic spikes as well as on the LSD spikes [17]. Films made of CAB are strong but they do not stretch appreciably. The least flexible films are obtained with CAB-17 within the CAB family due to the low butyryl content. This layer tends to chip and flake after about two years of storage, which did not meet anymore the demand from the end-users. Hence, the CAB-17 was replaced with CAB-35 and later with a 9 to 1 mixture of CAB-35 and CAB-50 [6]. Currently, the shelf life of LSD spikes coated with any of the latter two organic matrixes is 3 years. In order to further prolong the shelf life to at least five years we made the following efforts:

1) Increasing flexibility and attempt to delay flaking by the addition of plasticizer
2) Reconditioning of the flaked CAB coated spikes by H_3PO_4

3.1. Use of plasticizer (CAB+DIOP)

Plasticizers are commonly used additives of CAB to increase strain or modify other physical properties. The effect of the type and amount of plasticizer on the mechanical properties of the CAB film has been widely studied [18]. Based on those finding we decided to test only a few plasticizers including dioctyl phthalate (DIOP) which have the most beneficial effect on the mechanical properties.

CAB has very high tensile strength (comparable to artificial bone) but it is very stiff. The use of only a mass fraction of 10 % of DIOP plasticizer increased the flexibility of solvent cast CAB films by ~40% while the tensile strength dropped less than 15% (Figure 10). The flexibility improvement is supposedly even higher with the addition of 20 or 30% DIOP which is important because the stress strain gradually decreases with polymer degradation. The preservation of a relatively high elongation could potentially lead to retarded brittleness and flaking.

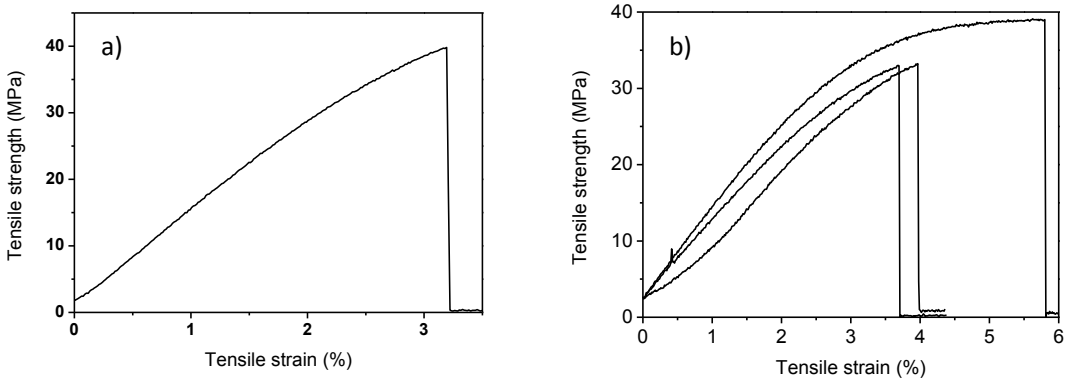

Figure 10: Stress-strain curve of solvent cast films made of a) CAB-35 and b) CAB-35 + 10 % DIOP

The use of plasticizer did not alter the appearance, chemical separation process or IDMS results of the spikes. Several spikes are currently undergoing long-term (i.e. five years) stability experiments.

3.2. Reconditioning with H_3PO_4

The CAB coating on LSD spikes undergoes degradation due to alpha and gamma radiation from U and Pu, acid hydrolysis induced by HNO_3 and the formation of minute air bubbles during solvent casting and/or chemical reactions. All these combined effects lead to discoloration, crack formation

and finally flaking and then the certified value cannot be guaranteed any more. It is worth reconditioning existing spikes before they reach this stage and thus to prolong their shelf life. Therefore, we decomposed the remaining organic matrix with 8 mol/L HNO_3 at 50-60°C and once the spike was dried we added 1 mol/L H_3PO_4. The water was evaporated at 100-120°C by increasing the temperature stepwise and an orange to green amorphous product was obtained (Figure 11). This product has a tendency to become a viscous liquid after 1-2 months of storage. Nonetheless, flaking will never occur, there is less chance for the active material to 'escape' and this spike could be used for many more years if handled properly. Moreover, it can be heated up again before use or in case of need to recreate the amorphous solid form. With the selected phosphoric acid concentration the most likely formed products are: $UO_2HPO_4 \times H_2O$ and $Pu(HPO_4)_2 \times H_2O$ (although at higher temperature an oxidation state change of U and/or Pu might occur) [19]. The structure will be further investigated by XRD and UV-Vis.

There is a different but much [illegible] H_3PO_4 is directly applied on the organic cover at the sam[illegible]ct is a dark brown to black foam. The main advantages o[illegible]rs to prepare and it is more environmentally friendly as m[illegible]s in the vial. The stability of the foam is under evaluation a[illegible]

Figure 11: Appearance of CAB coated spike before and after reconditioning with H_3PO_4. (In practice it is better to recondition the spikes before any flaking occurs)

Both, the improved CAB spikes and the reconditioned ones will undergo the same studies and will be analysed using the same characterisation techniques and equipment as applied to the CMC spikes.

4. Conclusions

The first stage of an exhaustive study has been done on the new options proposed for coating LSD spikes. For CMC, which has the potential to become the successor in the future of the currently used CAB, the protocol for the preparation of the coating solution has been optimised according to the production requirements. The molarity of the nitric acid solution and solid content of the coating has been also defined. It needs to be pointed out that the protocol for preparation and application of any organic layer also depends on environmental conditions and needs therefore to be adapted to the respective laboratory ambient conditions.

During the coating of the LSD test spikes with CMC some good and promising properties of this material have been discovered: CMC is a good choice for coating spikes even when the nuclear material is unevenly dispersed on the lower part of the vial walls. CMC has a high U/Pu complexation capacity allowing the production of spikes with a wide range of U/Pu ratios.

Over time, the CMC foam suffers a transformation which depends on the initial concentration, possibly leading to a final product similar to a viscous gum. Nevertheless, it preserves the same desired properties as the foam: the final product has good adherence to the glass and keeps the material at the bottom of the vial. It has no tendency towards crack formation and flaking off. It can be thus concluded that CMC can ensure the integrity of the spike over long periods of time.

The distribution of actinides within the matrix is homogeneous as shown by SEM-EDX results. This property provides for an even distribution of the radioactivity in the foam volume which in turn prevents the development of local damages due to the formation of hot-spots. Furthermore, according to the tests done providing an accelerated alpha irradiation, the self-irradiation and radiolysis seems not to be significant for the time of observation.

CMC spikes have additional beneficial properties for the final user. As the CMC final product tends to be sticky, the risks of losing any spike material when opening the vial in a hot cell or glove box is very low. Besides, the CMC coated spike dissolves almost instantly in HNO_3. Until now, no interferences during actinide separation or mass spectrometry measurements have been observed. CMC is used also in the food industry so it is not a harmfull material. Thus it can be easily handled in laboratories posing no hazards during the handling under fumehoods as provision for larger sets of spike preparation campaingns.

In parallel it was shown that the currently used CAB coating can also further be optimized towards longer shelf life (aiming at least 5 years). As the main problems are brittleness and flaking the effort is focused on boosting flexibility and producing defect-free films. Even relatively low level of plasticizer additive (i.e. 10 % DIOP in mass fraction) can increase elongation by up to ~40%, while the long term stability of such spikes is yet to be tested.

The reconditioning of discoloured or cracked CAB based LSD spikes where the certificate has expired is also possible with the use of phosphoric acid. The appearance of the reconditioned spikes can differ depending on whether or not the remaining organic layer was destroyed prior to the addition of phosphoric acid. Although, this process requires additional effort from the end-user the initial experiments suggest that the shelf life of the spikes can be increased. Moreover, if one considers the administrative burden related to the transport of nuclear materials spike reconditioning of 'old' spikes may offer significant advantages in fissile material accountancy of irradiated nuclear fuel.

5. Acknowledgements

The INS-CRM project is being carried out jointly by JRC-Geel and JRC-Karlsruhe as an exploratory research project of the JRC. Therefore the INS-CRM project team would like to express their acknowledgement to the JRC Scientific Committee and the Directorate A5 Scientific Development for their support and for providing the necessary resources.

The authors would like to acknowledge the colleagues of the JRC.G.II.6 unit for their contribution in providing nuclear material for the preparation of the spikes and for the characterisation performed in the Analytical Service. They would like to thank in particular to Martin Vargas Zuñiga and Sebastien Mialle for their contribution to the spikes characterisation.

The authors would like to thank as well the Workshop team of the JRC.G.1 Unit for their ideas and development of equipment needed for the project. We would like also to acknowledge our colleagues of the JRC.G.I.3 Unit for their contribution with the SEM/EDX analysis, Oliver Dieste Blanco, Thiery Wiss and Bert Cremer.

The authors would like to thank Stephan Richter for the idea to use phosphoric acid on LSD spikes and Ulf Jakobsson for the IDMS analysis of test samples, both JRC-Geel.

6 Legal matters

6.1. Privacy regulations and protection of personal data

In order to comply with the European Directive 95/46/EC as approved by the European Parliament and the Council of Ministers on the 24th October 1995 relating to the protection of individuals with respect to the processing of data of personal nature and on the free circulation of such data, it is necessary that you provide us with written consent. Feel free to use the example below as a template:

"I agree that ESARDA may print my name/contact data/photograph/article in the ESARDA Bulletin/Symposium proceedings or any other ESARDA publications and when necessary for any other purposes connected with ESARDA activities."

6.2. Copyright

The author agrees that submission of an article automatically authorises ESARDA to publish the work/article in whole or in part in all ESARDA publications – the bulletin, meeting proceedings, and on the website.

The author declares that their work/article is original and not a violation or infringement of any existing copyright.

6.3. Disclaimer

Authors who intend to include a disclaimer should do so at the end of the article and should ensure that it is as concise as possible.

7. References

[1] *Treaty establishing the European Atomic Energy Community (Euratom Treaty)*; Rome (Italy); 1957.

[2] IAEA; *International Target Values 2010 for Measurement Uncertainties in Safeguarding Nuclear Materials*, IAEA-STR-368, 2010.

[3] Jakopič R., Aregbe Y., Richter S., Zuleger E., Mialle S., Balsley S. D., Repinc U., Hiess J.; *Verification Measurements of the IRMM-1027 and the IAEA Large-Sized Dried (LSD) Spikes*; *J Radioanal Nucl Chem;* 2017; 311:1781-1791.

[4] ISO 17034:2016; *General Requirements for the Competence of Reference Materials Producers;* 2016.

[5] Carlos R., Buda R., Lützenkirchen K., Sánchez Hernández A., van Belle P.; *Stabilisation of Uranium/Plutonium dried spikes with a cellulose matrix, Proceedings of 37th ESARDA Symposium on Safeguards and Nuclear Non-Proliferation*, Manchester, UK, 19-21 May 2015; 498-505.

[6] Buják R., Delva L., Erkoç M., Bauwens J., Jakopič R., Vincze L., Aregbe Y., Cardon L.; *Long-term stability of cellulose acetate butyrate thin films for nuclear certified reference materials*, *Journal of Radioanalytical and Nuclear Chemistry*; January 2017, Volume 311, Issue 1, pp 877-886.

[7] HERCULES Incorporated; *AQUALON® Sodium Carboxymethylcellulose: Physical and Chemical Properties;* Technical report, 1999.

[8] Neck V., Altmaier, Seibert A., Yun JI., Marquardt CM., Fanghänel Th.; *Solubility and redox reactions of Pu(IV) hydrous oxide: Evidence for the formation of* PuO_{2+x}*(s, hyd)*; *Radiochimica Acta*; Volume 95; 2006; p 193-207.

[9] Walther C., Rothe J., Brendebach B., Fuss M., Altmaier M., Marquardt CM., Buechner S., Cho H-R., Yun J-I., Seibert A.; *New insights in the formation processes of Pu(IV) colloids*; *Radiochimica Acta*; Volume 97; 2009; p 199-207.

[10] Van Belle P, Zuleger E; *Procedure for the verification of large scale U/Pu dried spikes*, Technical Note JRC-ITU-TPW-2009/22; 2009.

[11] Richir P., Brandalise B., Apostolidis C., Molinet R., and Mayer K.; *Development of a robotized separation method for U-Pu samples using UTEVA resin; Proceedings of the International Workshop on the Application of Extraction Chromatography in Radionuclide Measurement*, Geel, Belgium; 1998.

[12] Jakopič R., Bauwens J., Buják R., Eykens R., Hennessy C., Kehoe F., Kühn H., Richter S., Aregbe Y.; *Preparation and certification of Large-Sized Dried (LSD) spike IRMM-1027o*; EUR 25857 EN, 2013.

[13] Merck Millipore, Calbiochem - Carboxymethylcellulose, Sodium Salt, Low Viscosity; https://www.merckmillipore.com/DE/en/product/Carboxymethylcellulose%2C-Sodium-Salt%2C-Low-Viscosity---CAS-9004-32-4---Calbiochem,EMD_BIO-217277

[14] Alfa Aesar - A18105 Carboxymethylcellulose sodium salt; *Product specification;* https://www.alfa.com/en/prodspec/A18105

[15] Jakopič R., Aregbe Y., Buják R., Richter S., Buda R., Zuleger E.; *Results of the REIMEP-17 interlaboratory comparison for the measurement of the U and Pu amount content and isotope amount ratios in the synthetic input solution*; *European Commission Report EUR 26667 EN;* 2014.

[16] Sigma Aldrich – Cellulose Acetate Butyrate; http://www.sigmaaldrich.com/catalog/product/aldrich/419044?lang=en&region=BE

[17] Raptis, K., Alonso, A., Ingelbrecht, C., Verbruggen, A., Wellum, R.; *The Preparation of metal spikes for IDMS of reprocessing input solutions; Proceedings of 21st Annual ESARDA Meeting,* 1999, 598-592.

[18] a) Luqman M.; (ed.), *Recent Advances in Plasticizers; Chapter 8*, Intech, 2012; b) Ouajai S., Shanks R.A.; *Macromol; Mater. Eng.*, 2009, *294*, 213–221.

[19] a) Vesely V., Pekarek V., Abbrent M.; *J. Inorg. Nucl. Chem.*; 1965, *27*, 1159-1166; b) Morss L.R., Edelstein N., Fuger, J.; (Eds.), *The Chemistry of the Actinide and Transactinide Elements; 4th ed.*, Sprieger, 2010.

Nuclear Material Characterisation for Transport and Storage

ZULEGER Evelyn[1], BROSSARD Corinne[1], BRAGEA, Mihaela[1], HEIN Herwin[1], HOLZHÄUSER Michael[1], LÜTZENKIRCHEN Klaus[1], MANFRÈ Laura[2], RAUSCH Nicole[1]

European Commission, Joint Research Centre, Directorate for Nuclear Safety and Security, P.O. Box 2340, D-76125 Karlsruhe, Germany

Nucleco S.p.A., Via Anguillarese, 301 - 00123 Roma, Italy

Abstract:

Nuclear material which has been used for R&D purposes at a given facility generally must be shipped back to the legal owner or sent for disposal. The various efforts required to prepare nuclear material for the purpose of an off-site shipment include conditioning and characterisation. Subsequently, the material can be fed into the nuclear fuel cycle or be stored for a longer term.
At the JRC Karlsruhe, a conditioning facility has been installed for such purposes. It consists of a chain of three glove-boxes, a set of pellet crushers and various furnaces. Uranium and plutonium materials can be effectively handled as appropriate for commercial transport containers.
In addition to crushing, mixing and oxidation, nuclear material has to be properly characterized. Usually, information on the uranium and plutonium concentration, the isotopic composition and the amount of fission products is required, as well as the water content and transport related sensitive impurity contents such as beryllium, fluorine, chlorine and oxygen. Techniques to meet these requirements include Thermo-gravimetric Analysis, High-Resolution Gamma Spectrometry, Hybrid-Kedge Densitometry, Thermal-Ionisation and Inductively-Coupled Mass Spectrometry. This paper focuses on a description of the analytical measurements carried out for material characterisation.

Keywords: waste, nuclear material, conditioning, transport, storage, analysis, kedge, impurities, ICP-MS, TIMS.

1. Introduction

Nuclear material which has been used for scientific purposes at a R&D facility must in general either be shipped back to the legal owner or sent for disposal. One example is nuclear material removal actions in the frame of the global threat reduction initiative (GTRI) [1]. In any case the material has to be conditioned, repackaged and characterised. The requirements for transport such as mass, composition, transport devices are defined in the IAEA safety standard SSR-6 [2]. In addition to transport regulations depending if the material is fed back to the nuclear fuel cycle or stored for a longer term, national and/or site license requirements have to be fulfilled. The technical strategy set up at the JRC Karlsruhe to prepare nuclear material for transport or storage is described in the following chapters, using the expertise of the various units of the JRC Karlsruhe to build up a unique facility for conditioning, repackaging and using the analytical capabilities to characterize the material for the requested assays and isotopic compositions. For example, non-oxidized nuclear material needs to be pre-oxidized. All material is required to be thermally stabilized at a minimum of 950 °C. An additional stringent licensing requirement for nuclear transports is the moisture content, which often has to stay below 0.5 wt% of the nuclear material. Especially for nuclear accountancy purposes the isotopic vector as well as the assay content of the nuclear material has to be well known. Depending on the history and future of the material the absence of alkaline earths, chlorides and other trace elements have to be demonstrated. The first of such campaigns at JRC Karlsruhe has been successfully performed in 2016 [3] and the experience gained is the basis of this paper.

2. Conditioning of samples

In order to prepare such material a conditioning facility has been installed as an essential component in the elimination of non-irradiated legacy waste and materials in the next decades. This facility can handle large, but still laboratory sized, batches, typical for transport containers due to the innovative solutions eliminating nuclear criticality risks implemented. It is composed of three glove boxes with a pellet crusher, mixer, and a furnace included. The boxes are adapted for the requirements of having a pre-oxidizing atmoshere in the furnace and glove box operation under inert gas atmosphere for safety reason and to eliminate water pick up by the samples even under short storage times.

During the first campaign, different types of material had to be treated. Pu-oxides, MOX, oxidized U/Pu powder, U-Pu nitrides and carbides, as well as U-Pu alloys and metallic HEU have been selected. Some containers were filled with only one sample, others with several. Also short fuel pins belonged to the campaign and has to be opened and the material therein prepared for relocation.

The containers had to be checked for outside contamination, and for integrity of the packages. Prior to opening, the packages had to be bagged into a glove box and the content verified against the accountancy of fissile material (NMA) sheets. In cases when several sub-containers are found inside the containers, each was treated individually. Organic material and any sort of metal or plastic had to be removed, U and Pu powder and pellets are weighed into trays. Pellets and material larger than 2 mm are transferred to a pre-weighed crusher tray and crushed with a Retsch Jaw Crusher for approximately 5 minutes to a grain size smaller than 2 mm. Afterwards the tray is weighed again to make sure all material is removed from the crusher and the accountancy updated.

2.1. Pre-oxidation of metals and alloys

One requirement for conditioning was that non oxidized material had to be oxidized. This was performed using an leak-tight Linn High Therm VMK-80 muffle furnace (Figure 1). For safety reasons only small batches (≤ 100 g) are treated in one run. For the pre-oxidation of metallic material, an Ar/O2 gas inlet with flow rate of approx. 2 L/min is used. The material can only be introduced to the stabilisation and packaging process if the grain size after pre-oxidation is ≤ 2 mm. The grain size is verified by visual inspection.

2.2. Thermal stabilization of the oxidized material

Another requirement was to thermally stabilize the oxides at a temperature of at least 950°C for more than 2 hours, guaranteeing that all material has been stabilized in an oxidizing atmosphere.
The leak tight Linn High Therm VMK-80 muffle furnace (Figure 1) consists of Inconel chamber, where the oxidising atmosphere is provided via gas inlet. The oxidising atmosphere supplied is compressed air with <100 ppm H_2O from JRC-Karlsruhes central gas system.

The original cooling plates of the muffle furnace with a total water content of more than 12 litres had to be modified in order to comply with laboratory internal regulations (maximum 3 litres of water in the glove box) (Figure 1). Copper tubes were soldered on copper plates and installed as replacement of the former cooling. The amount of cooling water was reduced to less than 1,5 Litre in the glove box, while cooling performance actually improved. In addition, the door was modified with the purpose to improve the temperature profile of the muffle furnace.

The furnace chamber is flushed by compressed air (approx. 21% O_2, flow rate 2 L/min) only during the heating process. When the heating is off, before and after the thermal treatment, an automatic 3/2 way valve is switching to Argon (Argon 5.6; flow rate 2 L/min) to flush the chamber and to protect the purified inert glove box atmosphere from oxygen when the furnace door is opened.

To guarantee that the funace provides a minimum temperature of 950°C to all material in the tray, an acceptance test was performed using a CeO_2 bed to simulate a Pu oxid bed. Cu wires distributed in this bed are used to demonstrate that the oxidizing atmoshere reached all the material introduced into the oven. Therefore the stabilisation was performed at a temperature of 1050°C for 4 hours. Again careful weighing of the empty and filled trays had to be performed in order to guarantee that no material was lost.

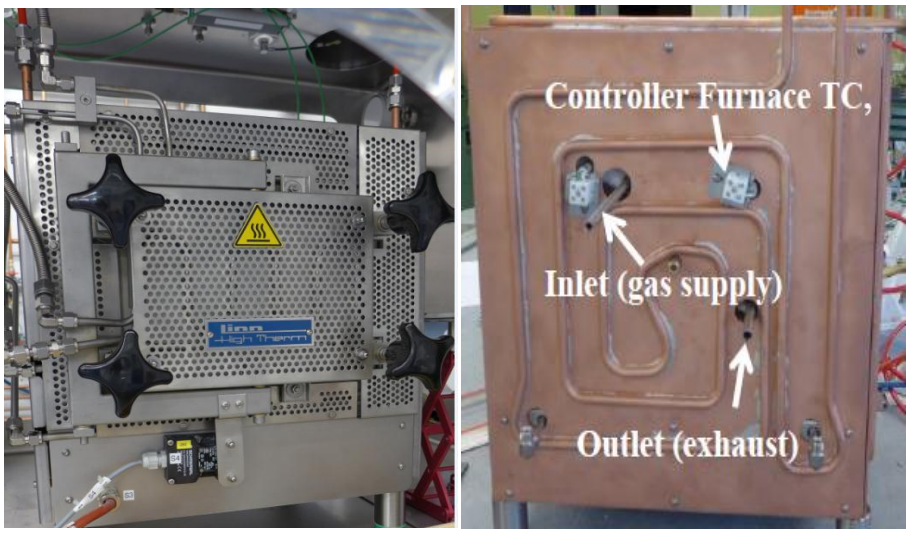

Figure 1: LINN VMK-80 leak-tight muffle furnace. Left: front door showing the inlet for cooling water. Right: Modification of the cooling plate; this set-up reduces the volume of cooling water to 1.5 L. The outlet was used to insert the thermocouples for the furnace acceptance test.

2.3. Mixing, subsampling and packaging

Prior to taking sub samples for analysis the material has to be mixed. Therefore, batches of maximum 800 g are filled in a mixing vessel (see Figure 2), while weighing the container empty and filled. The vessel is then shaken for 5 minutes to guarantee homogeneity of the material.
Four sub samples are filled in pre-weighed sample containers under a relative humidity of less than 40% (water content was kept below 10 ppm) and forwarded to the different analytical steps.

The main sample content is filled under the same conditions and careful weighing into a slip-lid container (SLC). This container is bagged out of the glove box and then packed into an Al transport container for internal transport. In a final step the SLC is packed into an outer screw lid container (OSC 18 cm height, 11 cm diameter), waiting to be loaded into the transport package 9975 (Figure 3). However, this could only be done after full gamma spectrometry verification had been performed using ISOCS (see 3.2).

Figure 2: The Mixer used for homogenisation of the material.

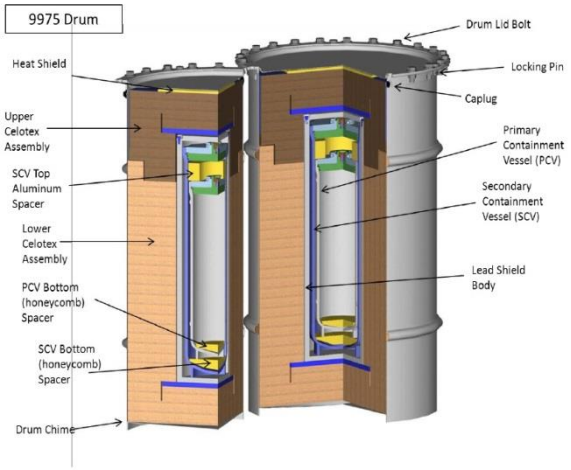

Figure 3: 9975 shipping package (Photo taken from Kerry A. Dum)

3. Analytical Methods

Prior to the transport a verification of the accountancy has to be performed, as well as a consistency check with the limits defined in transport regulations. It is important to note that the detection limits of the methods described must be low enough to meet the mass limits specified for the transport container 9975.

Quantitative information on the water content and several other impurities are requested by the receiver and the transport authorities. Thermogravimetry was used to determine the water content. Gamma spectrometry has been used to provide the U and Pu isotopic composition as well as Be, F and fission products. Other impurities like Al, B, Li, Mg, Na, ^{244}Cm, ^{243}Am and ^{232}Th have been analysed by Inductively Coupled Plasma Mass Spectrometry (ICP-MS). U and Pu assay was performed by Hybrid Kedge densitometry and the isotopic composition by Thermal Ionization Mass Spectrometry TIMS). Many of the analytical laboratories of the JRC Karlsruhe worked together to provide the characterisation of the stabilized nuclear material using destructive and non-destructive methods. Details are given below.

3.1. Determination of the water content by Thermogravimetry (TGA)

One requirement for transport and of receivers of nuclear material is a moisture content below 0.5wt % after the samples have been conditioned in a furnace at 1050°C. TGA Analysis to 1000°C with an inert cover gas is used for measuring the moisture content. Therefore, from every batch of material 2 representative samples are determined using a Netzsch 449C Jupiter TGA housed in a glove box (Figure 4).

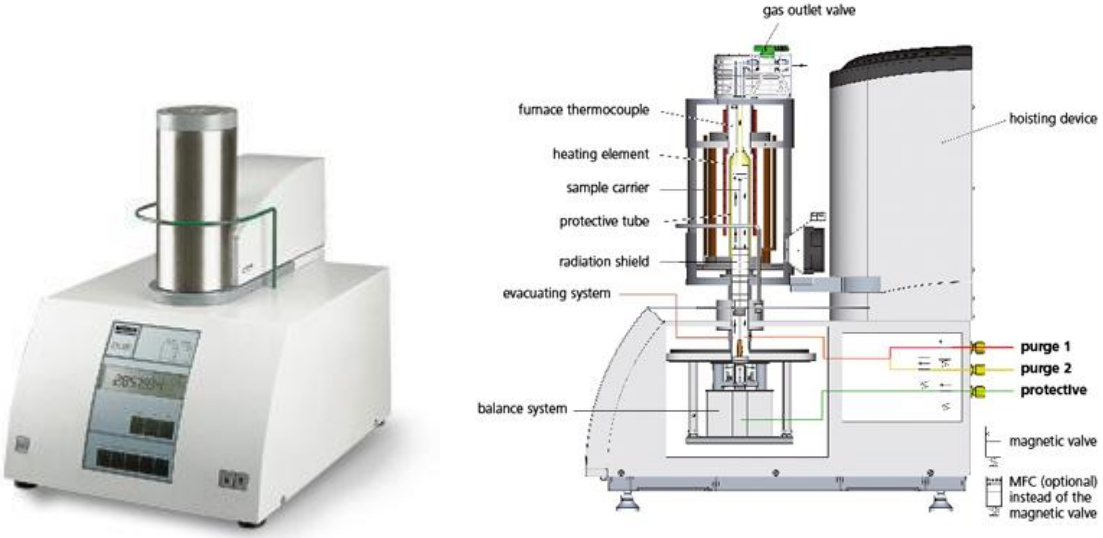

Figure 4: Netzsch 449C Jupiter thermogravimetric analyzer

To assure that the TGA is working properly a temperature calibration and a weight loss checks have to be performed. The temperature calibration is done before each measurement campaign, starting by measuring the melting point of Ag metal (961.78 °C) which is close to the required max temperature of 1000°C. The temperature calibration measurements are achieved under the same conditions as the sample measurement under Argon atmosphere, and with a heating rate of 20°C/min.

To assure that the weight measurement is correct a control measurement with $CaC_2O_4.H_2O$ is made after the second sample measurement of each batch, again performed under the same conditions as the samples. A control chart for the measurement of the $CaC_2O_4.H_2O$ guarantees correct weight measurements. The Standard deviation of the method has been determined performing 15 measurements with the heating program used for the analysis of samples. The heating program is as follows: step 1 a stabilization time of 15 minutes, step 2 heating up to 1000°C with 20°C/min., step 3

cooling with 20°C/min to room temperature. During the entire run Argon (>5 ppm H2O) from the central gas supply is flushed through the instrument at a flowrate of 60 ml/min.

Before the measurements are done a blank measurement has to be performed so that the influence of the buoyancy effect can be eliminated. A representative sample (2 – 3 g) is taken after good mixing with the tumbler out of the main batch, from which two 400-600 mg sub samples are taken.

All the weight loss is reported as moisture. When both samples give a result < 0.42wt% and are close to each other, then this proves that the moisture contained in the batch is below the requested 0.5wt%. The higher of the two measured values is reported.

3.2. Characterisation of fission products and of the U, Pu isotopic composition by Gamma spectrometry

Different approaches have been taken to verify the isotopic composition of U and Pu as well as the impurities Be, F and fissions products. Firstly, bulk samples have been analysed to quantify the radiological content of the sample. Secondly, high resolution gamma spectrometry has been employed to analyse parameters where the bulk sample analysis could not guarantee that the limits for the transport containers 9975 as well as the transport license requirement are respected (Table 1) or additional information to verify the decay products such as ^{232}U are needed.

Table 1: Analytical parameters for radionuclides: minimum detectable quantities, mass limits for 9975 transport container, mass limits for the transport license, and uncertainties

Radio-nuclide	Determined by	Min. Detectable Activity [Bq]	Min. Detectable Mass [g]	Limits for 9975 [g]	Limits Transport licence [g]	Uncertainty [%]
Pu-238	PC/FRAM	1.42E+10	0.022	34		>7
Pu-239	Genie 2000	6.50E+06	0.003	4400	660	± 2 to 4
Pu-240	PC/FRAM	5.63E+06	0.001	2200		± 2 to 4
Pu-241	PC/FRAM	1.94E+11	0.051	188.9		± 2 to 4
Pu-242	PC/FRAM	-	-	2200		>7
Am-241	PC/FRAM	1.24E+03	0.00001	188.9 (in combination with Pu-241)		± 3
Am-243	Genie 2000	1.98E+05	0.00003	1.00		± 5
Np-237	PC/FRAM	4.72E+04	0.002	220		± 3
Th-232	Genie 2000	9.48E+03	2.3	4400	100	± 5
U-235	Genie 2000	1.07E+03	0.013	4400	1300	± 4.5
U-238	Genie 2000	5.67E+04	4.558	4400		± 4.5
U-232	Genie 2000	6.10E+08	0.0007	0.00044 (not in fresh)		-
U-233	Genie 2000	3.20E+08	0.9	427	(0.103 expected)	-
Be-9	dedicated analysis	-	Method 1: 0.005 Method 2: 0.150	0.9		-
F-19	dedicated analysis	-	Method 1: 0.7 Method 2: 2.0	9.7		-

3.2.1. Gamma spectrometry of bulk samples using ISOCS

The samples have been used for the radiological characterization with gamma spectrometry. Table 1 shows the detection limits and uncertainties of the measurements. The characterization is performed for each sample in two steps:

1. The quantitative determination of the Plutonium and Uranium and other gamma-emitting radionuclides, such as ^{232}Th, ^{243}Am, ^{137}Cs, ^{154}Eu; using the OSC container as described in 2.3;
2. The determination of impurities due to light elements (Beryllium and Fluorine), using a separate subsample of approximately 2 g.

Each step needed a dedicate gamma spectrum and also a dedicated detector calibration performed by means of the ISOCS (In Situ Object Counting System) system developed by Canberra. The system had a liquid nitrogen cooled REGe (Reverse Electrode Germanium) high-purity germanium detector in coaxial geometry with 40% of relative efficiency.

For the assay of Plutonium and Uranium, the gamma analysis was focused on the energy range 100 – 1000 keV. The “bulk” spectrum (i.e. the spectrum collected on the entire sample) was acquired for 3 hours with a distance detector-sample of 1 meter, the detector collimation of 30° and a few mm-thick absorbers. The geometry setup was defined in order to keep the dead time lower than 10%. The gamma spectrum was collected by a multi-channel analyser covering the energy range of interest. The bulk sample was measured in a double steel-made containment in cylindrical geometry.

The analysis was performed using the Genie 2000 software by Canberra to assess the mass of the ^{239}Pu, ^{235}U and ^{238}U isotopes and to determine the other gamma emitting radionuclides.
The setup characteristics were entered into the Geometry Composer software for the efficiency calculation. The historical data were used for the evaluation of the matrix composition (in particular about the Plutonium and the Uranium content).

The determination of the absolute ^{239}Pu, ^{235}U, ^{238}U mass was combined with the analysis of the Pu isotopic composition performed with the software PC/FRAM developed by LANL [4]. The Pu isotopic composition computed using PC/FRAM was combined with the mass of ^{239}Pu computed using Genie2000 to calculate the mass of the other Plutonium isotopes (^{238}Pu, ^{240}Pu, ^{241}Pu, ^{242}Pu), as well as the mass of ^{241}Am and ^{237}Np.

The gamma spectrometric assay of Beryllium and Fluorine was performed with a small sub-sample of 2 grams collected from the bulk sample during the finalization of the treatment process. Due to the homogenization process, the sub-sample could be considered as representative of the bulk material.

The assay was prepared to yield a minimum detectable activity which would satisfy the limits imposed by the competent authorities for transport.

The Beryllium content was evaluated for the sub-sample studying the 4.4 MeV photons emitted due to the following reaction:

$$\alpha + {}^{9}_{4}\mathrm{Be} \rightarrow {}^{12}_{6}\mathrm{C}^{*} + \mathrm{n}$$

$${}^{12}_{6}\mathrm{C}^{*} \rightarrow {}^{12}_{6}\mathrm{C} + \gamma(4.4\ \mathrm{MeV})$$

Two independent methods were used to extrapolate the Beryllium mass from the detected counts at 4.4 MeV, one based on a theoretical approach and the second one based on an experimental calibration.

Theoretical approach: The rate of events was computed from the alpha activity of the source and a number of nuclear reaction parameters (cf. [5]).

Experimental approach: it is based on a calibration performed at LANL [6] which relates the number of counts of the 4.4 MeV energy line with the mass of Be obtained by chemical analysis. The data were collected on samples of plutonium dioxide with small contaminations due to light elements. The Be concentration depends on the 4.4 MeV gamma counts according to

$$\mathrm{x(ppm)} = \mathrm{b} \cdot \mathrm{N^{A}}$$

where $\mathrm{x(ppm)}$ is the Be concentration from the chemical analysis, N is the “normalized” net area at 4.4 MeV and A and b are fit parameters. For Beryllium, the calibration gives A=0.813 and b=33651.

The two methods are independent and so both were used comparing and integrating the results.

A Fluorine containing sample can emit gamma rays in a similar way according to

$$\alpha + {}^{19}_{9}\mathrm{F} \rightarrow {}^{22}_{11}\mathrm{Na}^{*} + \mathrm{n}$$

$${}^{22}_{11}\mathrm{Na}^{*} \rightarrow {}^{22}_{11}\mathrm{Na} + \gamma(891\ \mathrm{keV})$$

The two methods presented for the Beryllium estimation have been adapted and used for the assessment of Fluorine. With the experimental method, the calibration parameters are A=1.029 and b=741310.

3.2.2. High resolution gamma spectrometry

High resolution gamma measurements are used to provide information which could not be delivered by the bulk sample measurements.

a) ^{232}U content to give information about the decay matrix
b) Gamma spectra to define if Am is present as a decay product or as surface contamination

The ^{232}U content was restricted in the container validation to 0.00044 g per batch (= per transport container) as it decays to ^{208}Tl, which is a hard gamma ray emitter (2,6 MeV), in order to comply with maximum dose levels at the container surface of 2 mSv/h.

The ^{232}U content of the samples was measured by high-resolution gamma spectrometry, using the radiation from the short-lived daughter products of ^{232}U, ^{212}Bi and ^{208}Tl. To account for the buildup of these isotopes from the possibly present ^{232}Th, the gamma radiation from the ^{232}Th daughter ^{228}Ac was also monitored. To avoid problems with calibration for absolute activity measurements, the ^{232}U mass was measured relative to the mass of ^{238}U. Then the ^{232}U content of the samples was obtained by multiplying the ^{232}U/^{238}U mass ratio with the ^{238}U content of the samples known from mass spectrometry. The procedure for the gamma-spectrometric measurement of the ^{232}U/^{238}U ratio in uranium samples is given in detail in [7].

Clarification regarding presence of Am has been required. Sometimes ^{241}Am had been observed in gamma spectra of the original samples. In such cases the sub-samples have been leached with acid until they have lost more than 10% of their mass. Then they have been re-measured with a planar HPGe detector. In all the leached sub-samples where the ^{241}Am gamma peak could be observed in the spectra, its relative intensity (vis-a-vis U isotopes) decreased at least 6 fold in comparison with the relative intensity of the ^{241}Am peak in the original sub-samples' spectra. Therefore, it was concluded that ^{241}Am is a surface contaminant.

3.3. Destructive Analysis

3.3.1. Dissolution and sample preparation

The representative sample (2 – 3 g) taken from the main batch after thorough mixing with the tumbler is dissolved in various media. MOX (mixed Uranium – Plutonium oxides), and pure Plutonium samples are dissolved overnight in an acid mixture of 14 M nitric acid : 0.1 M hydrofluoric acid, using about 6 ml of mixture per g of sample at 80°C. Then the solution is adjusted to the required final conditions for further dilution and analysis. Pure Uranium samples are dissolved overnight in 5 ml 8M nitric acid per gram of sample at 80°C.

Suitable amounts for determining the U and Pu assay by Hybrid K-edge/XRF densitometry are 0.5 to 1 grams of plutonium oxides and 5 (± 2) grams of MOX. The solutions have been further diluted for chromatographic separation prior to mass spectrometry.

3.3.2. U and Pu assay by Hybrid K-edge/XRF densitometry (HKED)

The U and Pu content of the samples had to be analysed with good precision and in a timely manner. The combination of K-Edge Densitometry with X-ray fluorescence, the so called Hybrid K-Edge (HKED) [8] has been used for this purpose. This instrument is using a single X-ray source for the K-edge absorption and the fluorescence excitation. The combination of the two techniques allows the simultaneous and quantitative determination of Uranium and Plutonium. A filtered and collimated X-ray beam with cut-off energy of about 150 keV passes through a solution along a well-defined path length. Its transmission energy ("K-edge") spectrum is measured and later analysed. The step-like decrease of the transmitted X-ray intensity (Figure 5) beyond the K absorption edge is a measure of the uranium or plutonium concentration in the sample in terms of g/l.

The K-edge instrument needs a series of carefully characterized solutions of uranium and plutonium to establish a calibration curve. These solutions, in turn, are calibrated by an IDMS measurement (see below).

For the purpose described here, the range of calibrations has been extended as compared to safeguards applications to cover the full expected range of uranium/plutonium ratios.

In order to deliver results in g/g, one needs to determine the density of the solutions under investigation to compare the measurement results obtained by the different techniques. The X-ray fluorescence spectrum, taken at the same time as the K-edge spectrum, is used to determine U/Pu ratio.

The analyses are performed with a combined uncertainty <1% (K=2) for solutions with a U concentration between 100 g/l and 300 g/l [9].

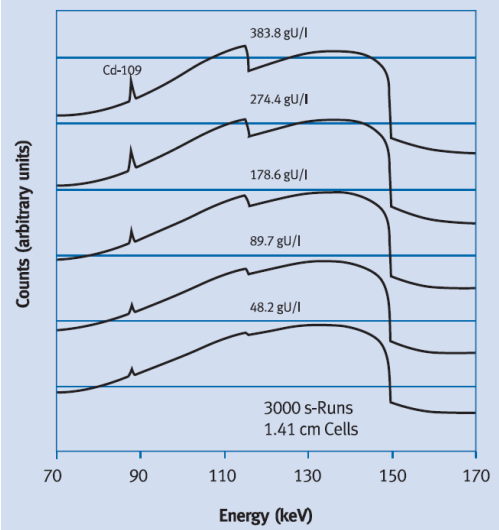

Figure 5: X-ray transmission spectra for uranium solutions with concentration from 48.2 to 383.8 g/l. The count rate is shown as a function of incident X-ray energy. The K absorption edge with the step-like intensity decrease is at 115.6 keV [9]

3.3.3. U and Pu assay and isotopic composition determination by thermal ionisation mass spectrometry (TIMS)

Thermal Ionization Mass Spectrometry (TIMS) (Figure 6) is widely applied for isotopic measurements in nuclear analytical laboratories and suitable for practically all types of material. However, the sample is required in liquid form, to allow conversion to the appropriate species. For many sample types an additional purification of the sample is needed either to remove matrix effects and in the case of Uranium and Plutonium samples to avoid interferences on different masses. Therefore, a separation step has to be performed using the chromatographic separation technique on resin (UTEVA®: Eichrom, Figure 7). In addition, an alpha spectrometric analysis is performed to provide an

approximate Pu concentration to the TIMS analyst. The sample is then deposited onto a filament from which it is evaporated once being introduced in the mass spectrometer. These “vapors” are then atomized and ionized at a hot surface, from which the name “thermal ionization” is derived. The ions are subjected to acceleration by applying a high voltage and subsequent mass separation (e.g. ^{234}U, ^{235}U, ^{236}U, ^{238}U, ^{238}Pu, ^{239}Pu) by means of a magnetic field. An appropriate detection system allows the measurement of ratios of ion beam intensities. The isotope abundances are derived from these ratios using the total evaporation method [10] using a mass spectrometer Thermofisher Triton. In order to determine the Uranium and/or the Plutonium content Isotope Dilution Mass Spectrometry (IDMS) is performed.

Figure 6: Thermal Ionisation Mass Spectrometer Triton connected to a glove box for U-Pu analysis

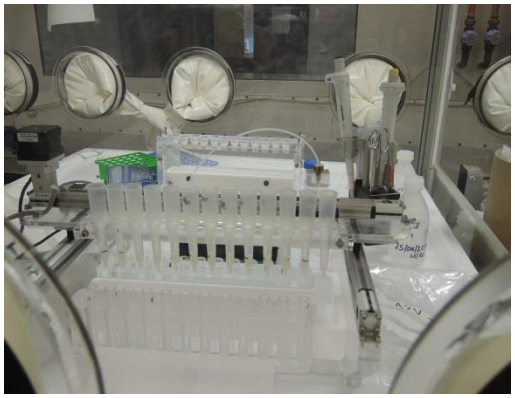

Figure 7: Chromatographic separation by UTEVA®: Eichrom UTEVA

Again samples are dissolved and diluted to a suitable concentration. For a precise determination of the analyte concentration in the samples the IDMS method requires a pre-spiking of the sample. By addition of a known amount of the analyte with a validated isotopic composition (spike) a very precise determination of the concentration for the sample is performed. The isotopic composition of the spike is chosen to be as different as possible from the expected isotopic composition of the sample. Where necessary, samples undergo the above described chromatographic separation from fission/decay products and other interferences.

Standards of known composition are regularly prepared in parallel to the samples for the verification of the method. The uncertainty of the Uranium and Plutonium content analysis is less than 0.2 % (combined uncertainty K=2). The Uranium isotopic composition for material with enrichments between 0.3 and 20% ^{235}U as well as the Pu isotopic composition for material with ^{239}Pu composition between 50 and 80 atom % are analysed with an uncertainty of less than 0.1 % (combined uncertainty K=2) [11].

3.3.4. Impurity determination by inductively coupled plasma mass spectrometry (ICP-MS)

Inductively coupled plasma mass spectrometry is an analytical method that can determine the content of more than 70 elements in different matrices with low level of detection, as well as the isotopic composition of elements [12]. The elements are atomised and ionised by a high-frequency plasma. After extraction the ions are separated in the mass spectrometer according to their mass-to-charge ratio. Quantitative determination is possible using an appropriate standardisation method.

For the transport and storage of material the absence of earth alkaline chlorides and other trace element concentrations had to be demonstrated. Therefore, the content of Al, Mg, Be, B, Na, Li and Th have been determined as well as the ^{244}Cm and ^{243}Am content. In one case also the Th isotopic composition was requested.

However, the sample is required in liquid form, and as the ICP-MS is a very sensitive technique and the possibility of contaminating the samples is high, all materials have to be dissolved in high purity acids and all material which is brought in contact with the sample needs to be pre-cleaned in high purity acids and dissolved in high purity grade acids. Therefore, sample aliquots of about 300 mg are

dissolved in high purity aqua regia (hydrochloric acid/nitric acid 3:1 v:v) + 0.05 M hydrofluoric acid and further diluted with high purity 5% nitric acid to:

- reach a maximum concentration of 100 µg/g TDS (total dissolved solids) in order not to overload the plasma and to minimise quenching of elements in the low mass range and
- reach a concentration, where none of the elements of interest produce count-rates >$2x10^9$ cps.

As an internal standard Rh (Inorganic Ventures) is added to compensate for possible instrument drift and a two point calibration is used, prepared from multi element standards containing all elements to be analysed except for Am, Ac, Cm and Pu. As no element standards exist and the behaviour in ICP-MS can be considered the same as for U and Th, the evaluation is made based on the U and Th calibration curve. For quality control a control sample is prepared from different certified reference material. A blank is produced from the used high purity nitric acid and taken into account for result preparation.

The samples are analysed with a ThermoFinnigan Element 2 (Figure 8). Table 2 provides the detection limits of the elements requested. The measurements have been performed with a total expanded uncertainty of less than 12 % rel. (combined uncertainty K=2), confirmed by participation of proficiency tests.

Table 2: Detection limits of the requested Elements by ICP-MS

Isotope	g/l
Li7	25-420x10^{-6}
Be9	9-100x10^{-6}
B11	50-3000x10^{-6}
Na23	280-1100x10^{-6}
Mg24	7-25x10^{-6}
Al 27	110-520x10^{-6}
Ac223	200-600x10^{-12}
Th228	2x10^{-9}
Th230	200-1000x10^{-12}
Th 232	0.7-100x10^{-9}
Pu242	400-900x10^{-12}
Am243	2.2-0.13x10^{-9}
Cm244	600-850x10^{-12}

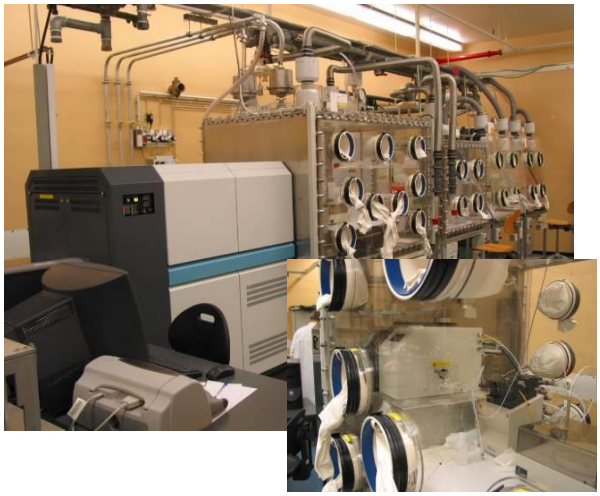

Figure 8: ICP-MS Thermofinnigan Element 2

The samples are analysed with a ThermoFinnigan Element 2. Table 2 provides the detection limits of the elements requested. The measurements have been performed with a total expanded uncertainty of less than 12 % rel. (combined uncertainty K=2), confirmed by participation of proficiency tests.

3.3.5. Quality control and Uncertainty estimation

All methods described are controlled via control charts, prepared measuring certified reference material (CRM) or reference material traceable to CRMs. Uncertainty calculations are done in accordance with the ISO “Guide to the Expression of Uncertainty in Measurement” and EURACHEM/CITAC Guide "Quantifying Uncertainty in Analytical Measurement". As uncertainty the expanded uncertainty with a coverage factor k = 2 is commonly stated.

4. Conclusions

Technical infrastructure has been built up at JRC Karlsruhe to condition nuclear material like legacy waste for transport, but also for medium or long term storage. It consists of 3 glove boxes with

equipment for pre-oxidation, thermal stabilisation, mixing, sub-sampling and packaging of the materials. Analytical techniques deployed for nuclear safeguards and forensic purposes or for the study of nuclear material properties were used for elemental and isotopic characterisation of the conditioned samples. The infrastructure described can be used for similar needs also in the future.

5. Acknowledgements

The authors acknowledge valuable contributions by Co Boshoven, Rachel Eloirdi, Michael Hauer, Sven Pfirrmann, Chris Selfslag for material conditioning, Matthias Schulz for transport preparation, Fillipo Gagliardi (Nucleco) for gamma measurements and Analytical Service for providing the nuclear material analyses. In addition we acknowledge Martin Vargas-Zuñiga and Artur Mühleisen for review of this paper.

6 Legal matters

6.1. Privacy regulations and protection of personal data

In order to comply with the European Directive 95/46/EC as approved by the European Parliament and the Council of Ministers on the 24th October 1995 relating to the protection of individuals with respect to the processing of data of personal nature and on the free circulation of such data, it is necessary that you provide us with written consent. Feel free to use the example below as a template:

"I agree that ESARDA may print my name/contact data/photograph/article in the ESARDA Bulletin/Symposium proceedings or any other ESARDA publications and when necessary for any other purposes connected with ESARDA activities."

6.2. Copyright

The author agrees that submission of an article automatically authorises ESARDA to publish the work/article in whole or in part in all ESARDA publications – the bulletin, meeting proceedings, and on the website.

The author declares that their work/article is original and not a violation or infringement of any existing copyright.

6.3. Disclaimer

Authors who intend to include a disclaimer should do so at the end of the article and should ensure that it is as concise as possible.

7. References

[1] B. Obama, „https://www.whitehouse.gov/the-press-office/remarks-president-barack-obama-prague-delivered“.

[2] IAEA, „ Safety Standards for protecting people and the environment. Regulations for the Safe Transport of Radioactive Material, Specific Safety Requirements, No. SSR-6. http://www-pub.iaea.org/MTCD/publications/PDF/Pub1570_web.pdf,“ Vienna, 2012 Edition.

[3] whitehouse, „https://www.whitehouse.gov/the-press-office/2016/04/01/fact-sheet-nuclear-material-removal“.

[4] T. Sampson, „Plutonium isotopic analysis using PC/FRAM,“ Report LA-UR-03-4403, Los Alamos National Laboratory, 2007.

[5] J. L. Boles, R. S. Hafner, L. E. Fisher, „ Neutron Source Strength Estimates From (α, n) Reactions

in Binary Mixtures of Actinide Particles and Light Element Particles," in *ASME 2005 Pressure Vessels and Piping Conference, Report UCRL-CONF-212717*, 2005.

[6] J. E. Narlesky, E. J. Kelly, L. A. Foster, „A calibration to predict the concentrations of impurities in Plutonium oxide by prompt gamma analysis," LA-14258, Los Alamos National Laboratory Report, 2005.

[7] J. Zsigrai, T. Cong Nguyen, A. Berlizov, „Gamma-spectrometric determination of 232U in uranium-bearing materials.," *Nuclear Instruments and Methods in Physics Research ,* Bd. B 359, p. 137–144, 2015.

[8] H. Ottmar, H. Eberle, The Hybrid K-Edge/ K-XRF Densitometer: Principles- Design- Performance, KFK 4590. http://open.fzk.de:81/de/fzk_ber_frm_html, 1991.

[9] K. Casteleyn, L. Duinslaeger, et al., „The Euratom Safeguards On-Site Laboratories at the Reprocessing Plants of La Hague and Sellafield," JRC reference Report 59608, European Commission, Karlsruhe, 2011. https://ec.europa.eu/jrc/en/publication/reference-reports/euratom-safeguards-site-laboratories-reprocessing-plants-la-hague-and-sellafield (accessed on 28 April 2017).

[10] Romkowski, M. Franzini, S. Koch, L., „Mass-spectrometric analysis of sub-nanocurie samples of uranium and plutonium.," in *ESARDA Symposium*, London, 1987.

[11] E. Zuleger, K. Casteleyn, L. Duinslaeger, K. Mayer, P. Richir, P. van Belle, „Accuracy and Precision Achieved in Thermal Ionization Mass Spectrometry of Uranium and Plutonium in a Safeguards Analytical Laboratory under Routine Conditions.," in *45. INMM Annual Meeting*, Orlando, 2004.

[12] „ASTMC1287-03- EN – STM for Determination of Impurities in Uranium Dioxide by Inductively coupled plasma mass spectrometry.".

Session 13

Non-destructive Analysis: Tomography

Outcomes of the JNT 1955 Phase I Viability Study of Gamma Emission Tomography for Spent Fuel Verification

Staffan Jacobsson Svärd[1], L. Eric Smith[2], Timothy A. White[2,7], Vladimir Mozin[3], Peter Jansson[1], Peter Andersson[1], Anna Davour[1], Sophie Grape[1], Holly Trellue[4], Nikhil Deshmukh[2], Erin A Miller[2], Richard S. Wittman[2], Tapani Honkamaa[5], Stefano Vaccaro[6], James Ely[7]

[1]Uppsala University, Uppsala, Sweden
[2]Pacific Northwest National Laboratory, Richland, WA, USA
[3]Lawrence Livermore National Laboratory, Livermore, CA, USA
[4]Los Alamos National Laboratory, Los Alamos, NM, USA
[5]STUK – Radiation and Nuclear Safety Authority, Helsinki, Finland
[6]European Commission, Directorate General Energy, Directorate Euratom Safeguards, Luxembourg
[7]International Atomic Energy Agency, Vienna, Austria

Abstract:

The potential for gamma emission tomography (GET) to detect partial defects within a spent nuclear fuel assembly has been assessed within the IAEA Support Program project JNT 1955, phase I, which was completed and reported to the IAEA in October 2016. Two safeguards verification objectives were identified in the project; (1) independent determination of the number of active pins that are present in a measured assembly, in the absence of a priori information about the assembly; and (2) quantitative assessment of pin-by-pin properties, for example the activity of key isotopes or pin attributes such as cooling time and relative burnup, under the assumption that basic fuel parameters (e.g., assembly type and nominal fuel composition) are known. The efficacy of GET to meet these two verification objectives was evaluated across a range of fuel types, burnups and cooling times, while targeting a total interrogation time of less than 60 minutes.

The evaluations were founded on a modelling and analysis framework applied to existing and emerging GET instrument designs. Monte Carlo models of different fuel types were used to produce simulated tomographer responses to large populations of "virtual" fuel assemblies. The simulated instrument response data were then processed using a variety of tomographic-reconstruction and image-processing methods, and scoring metrics were defined and used to evaluate the performance of the methods.

This paper describes the analysis framework and metrics used to predict tomographer performance. It also presents the design of a "universal" GET (UGET) instrument intended to support the full range of verification scenarios envisioned by the IAEA. Finally, it gives examples of the expected partial-defect detection capabilities for some fuels and diversion scenarios, and it provides a comparison of predicted performance for the notional UGET design and an optimized variant of an existing IAEA instrument.

Keywords: Spent nuclear fuel assemblies; Partial defect verification; Gamma-ray emission tomography

1. Introduction

The accurate verification of declarations about the fissile content of spent fuel is central to the International Atomic Energy Agency's (IAEA) safeguards of facilities handling and storing irradiated fuel. IAEA safeguards approaches for used fuels that are being transferred to difficult-to-access storage and that have a design allowing disassembly call for verification using a partial-defect or best-available method [1]. At present, IAEA's authorized instruments for attended partial-defect detection have limitations in terms of independence, defect sensitivity, and implementation flexibility. Furthermore, there is no authorized instrument for unattended partial-defect detection in spent fuel. Accordingly, the IAEA has expressed a need for "more sensitive and less intrusive alternatives to existing NDA instruments" for partial-defect detection [2].

Passive gamma-ray emission tomography (GET) is attractive for addressing partial-defect detection because it has the potential to non-destructively image the spatial distribution of the active fuel material in the assembly structure, and extract numerical data on individual fuel pins, without the need for any operator-declared information or disassembly of the fuel. Advantage is taken of the high level of radioactivity in used nuclear fuel in a two-step procedure:

(i) The gamma radiation field around a fuel assembly, at a selected axial level, is collected using one or several gamma-ray detector elements in a large number of positions relative to the fuel, and;
(ii) The internal source distribution in the fuel is reconstructed based on the recorded data, using tomographic algorithms.

In both steps, one may identify a multitude of alternative approaches, e.g. in terms of choice of detector set-ups and measurement schemes (step i) and choice of data analysis and reconstruction algorithms (step ii). In addition, for the case when the assay result is an image, there is a variety of image-analysis methods that may be applied to draw conclusions on the individual fuel pin level.

As described in this paper, reconstructed images and pin-wise data may be used directly to draw conclusions on possible pin diversion. Measured gamma-ray source concentrations can also be strongly correlated to fuel parameters such as burnup (BU) and cooling time (CT), thereby achieving more specificity than other partial-defect detection methods. Further, tomographic assessment at multiple axial locations along the assembly length enables axially resolved pin-level assay (as opposed to volume-integrating assay). Finally, GET is viable in both wet and dry measurement environments, and in either unattended or attended modes, thus offering operational flexibility.

The IAEA attention to the GET technique began in the 1980's, leading to the development and testing of small-scale systems in multiple field campaigns on BWR and PWR fuel items [3]. Building on those efforts, the JNT A 1510 project began in 2003 and was completed in late 2015. Under JNT 1510, a full-scale, transportable tomography system based on IAEA's user requirements for underwater application was designed, fabricated, and field-tested [4]. This system is referred to as PGET (Passive Gamma Emission Tomography) and is used in attended mode.

In parallel to the IAEA-led efforts, a Swedish project for validating core simulators for pin-power distributions led to the construction of a heavy (30-metric tons) tomographic device, which was used for measurements on short-cooled (2-4 weeks) BWR fuel assemblies [5], [6]. As a consequence, the project also covered studies of the safeguards aspects of this technique [7]. During recent years, international nuclear research institutes have also gained interest in the application of tomographic techniques on complete fuel assemblies [8], [9]. Leveraging from the relatively large pool of knowledge and expertise that is now available on GET, the JNT 1955 Phase I project was launched by the IAEA in 2013 and was reported in 2016 [10]. This paper accounts for its main outcomes.

2. Scope of the JNT 1955 Phase I project

The JNT 1955 Phase I project was carried out 2013-2016 by the IAEA Member States Support Programs of the United States, Sweden, Finland and European Union, under the leadership of the IAEA. It was intended to complement previous IAEA projects on the GET technique, e.g. by considering unattended GET and an extended range of fuels and implementation scenarios.

Verification Objective	Description	Assumptions
1	Independent determination of the number of active pins that are present in a measured fuel assembly.	No a priori information about the assembly is available.
2	Quantitative assessment of pin-by-pin properties, for example the activity of key isotopes or pin attributes such as cooling time (CT) and relative burnup (BU).	Basic fuel parameters (e.g., assembly type, geometry and nominal fuel composition) are known.

Table 1: Verification Objectives covered in the JNT 1955 Phase I project.

At the project start-up, two Verification Objectives were identified, as defined in Table 1, where only Objective 1 may be considered addressed by the already existing PGET device. With these Verification Objectives in mind, efforts were made within the following areas:

- **GET performance analysis framework:** A modelling and analysis framework was developed for partial-defect detection capability evaluation, including a procedure for simulating tomographic data for selected experimental setups, fuel types, diversion and implementation scenarios;
- **GET instrument design:** The design of a "universal" GET instrument (UGETv1) was developed, intended to support the full range of verification scenarios envisioned by the IAEA;
- **Reconstruction and analysis methods:** A set of tomographic reconstruction and analysis methods were identified, described and demonstrated;
- **Proposed metrics for GET partial-defect sensitivity:** Metrics for quantifying the partial-defect detection capability of alternative GET approaches on selected diversion cases were suggested;
- **Quantitative performance predictions:** Quantitative performance predictions were made for the PGET and UGETv1 instrument designs, for a set of different fuel types, fuel parameters and diversion scenarios;
- **Inspection procedures:** An envisioned inspection procedure was presented.

Due to the extent of the work, each area is only covered superficially in the coming sections of this paper, while details may be found in [10].

3. GET performance analysis framework

One important outcome of the JNT 1955 project is the creation of a modelling and analysis framework for the evaluation of GET partial-defect-detection performance, which can be applied to various GET instrument designs, fuel assembly types and parameters, diversion scenarios and analysis methods. A flowchart describing this framework is illustrated in Figure 1. It provides end-to-end capability to assess tomographer performance for nuclear fuel assay, and could be considered a new, standing capability for the international safeguards community.

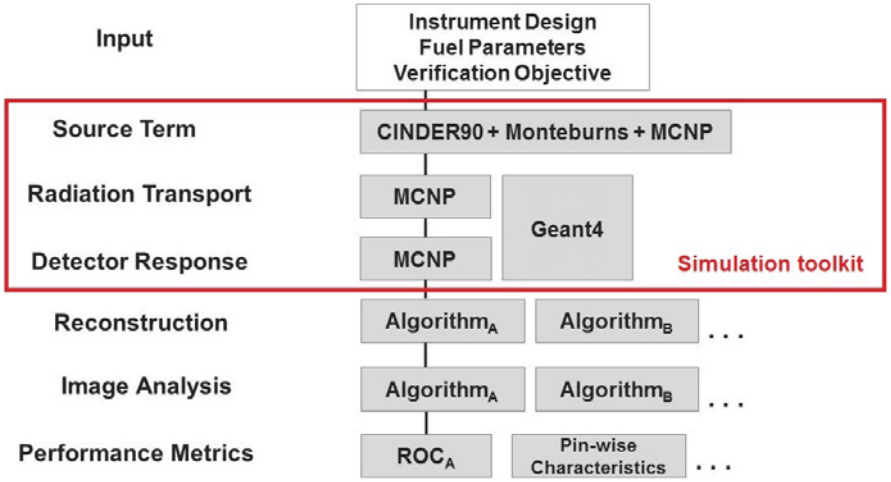

Figure 1: Flowchart describing the developed modelling and analysis framework for GET performance evaluation.

The inputs are the specifics of the fuel to be analyzed, the instrument design, including data-collection schemes such as the set of angular and lateral detector element positions used, and the conditions under which the analyses are made (e.g. the level of access to a priori information), which governs what tomographic reconstruction and analysis methods that are applicable. (Verification Objectives 1 and 2 presented in Table 1 are examples of such conditions.) The framework allows for the deployment of various reconstruction and analysis methods as well as various metrics of performance.

The heart of the framework is the simulation toolkit, marked in red in Figure 1. Here, a brief overview of the simulation procedure is presented, and the reader is referred to ref. [10] for more details;

1. First, pin-by-pin gamma-ray source terms for each fuel type and fuel parameter set under study are calculated using a combination of codes and methods, as described in refs. [11] and [12].
2. Second, the Monte Carlo N-Particle (MCNP) transport code [13] is used for transport of emitted gamma quanta from the fuel to the surface of the detector elements, taking into account the specifics of the studied fuel geometry (including possible pin diversions) and the device design. This is done pin-by-pin and energy-by-energy to get single-pin flux data for the complete set of detector element positions, which can be added together to form complete assembly data. In this summation, pin-wise weights are applied according to the source terms calculated in the first step. (In this way, the results from the time-consuming transport calculation can be re-used when changing pin-wise fuel parameters.) In this work, alternative simulations using the Geant4 code [14] have also been performed to benchmark the MCNP simulations, as described in section 7.2.
3. Third, separate Monte Carlo calculations of the detector response are performed, taking into account the complete gamma-ray flux into the detector elements, at all energies, while also considering detector specifics (e.g. energy resolution). Consequently, performance of different detector types in the same setup can be assessed using the same data from the first two steps.

This three-step simulation procedure allows for the creation of tomographic data for large virtual assembly populations, in terms of; (i) varying pin-by-pin BU, and; (ii) varying sets and levels of statistical noise. The former variation responds to the fact that authentic fuel assemblies have a pin-by-pin variation in BU, which may be as large as ±20% under normal operation. The latter variation allows e.g. measurement time to be accounted for. Altogether, analyses of large assembly populations, with these variations included, enable the deployment of statistical performance metrics, as discussed in section 6.

4. GET instrument design

A basic requirement for a GET device is spatial selection capability, so that a well-defined region of the fuel contributes to the gamma-ray intensity in a certain detector element position. This capability is typically achieved using heavy collimators, which shield the detector elements while allowing radiation to enter through well-defined slit openings. The choice of detector as well as collimator material and dimensions depend on a number of factors such as;

- Fuel properties, e.g. BU, CT and size: Highly radioactive fuel (short CT, high BU, large mass) generally requires better shielded detector elements to avoid high levels of background radiation;
- Requirements on isotopic selectivity: Detector elements with high energy resolution and spectroscopic data collection may be required to select specific gamma peaks, in particular for Verification Objective 2. Also, high full-energy peak efficiency will enable more efficient subtraction of background from scattered gamma rays, and thus enhanced data quality;
- Spatial resolution requirements: Long and narrow collimator slits enable higher spatial resolution;
- Count-rate management: The collimator slit dimensions should preferably be large enough to allow for high counting rates in order to reduce measurement time, while staying within acceptable limits for the selected detector type in terms of count-rate saturation;
- Time requirements: Assay time can be shortened by using many, tightly-packed, detector elements as well as using detectors with high-count-rate capability.

Altogether, there is a strong inter-dependence between these design factors. As an example, detector elements offering high full-energy peak efficiency are generally relatively large, implying that a relatively small number of detectors will fit into the device, thus leading to longer assay times. Accordingly, instrument design will include a trade-off between e.g. time and precision.

The device design performed in this work was informed by two previous underwater designs, PGET [4], which was constructed in the JNT 1510 project to deliver on Verification Objective 1 for relatively long-cooled fuel, and PLUTO [6], which was constructed in Sweden to deliver pin-wise power in short-cooled fuel, a task similar to Verification Objective 2. The resulting notional Universal GET design (UGETv1) was developed to meet both Verification Objectives 1 and 2. The PGET and UGETv1 designs are illustrated in Figure 2, and their respective properties are listed in Table 2. A more thorough presentation of the UGETv1 design considerations can be found in refs. [10] and [15].

As described in section 7, performance evaluations have been carried out for the PGET and UGETv1 designs. In short, the main differences between these designs are; (i) PGET uses CdTe detectors with limited spectroscopic capability, while UGETv1 uses LaBr scintillator detectors to provide spectroscopic full-energy gamma-ray peak analysis, and; (ii) PGET uses relatively light collimation, while additional shielding is included in UGETv1 to manage count rates for more short-cooled fuels (CT down to 1 year). As a result of these design selections, PGET allows for tightly-stacked detector arrays that offer rapid data collection in a rotate-only geometry, while the fewer number of LaBr detectors in UGETv1, which offer isotopic-specific data, require both rotation and translation of the detector arrays to record complete intensity projections, leading to longer assay times.

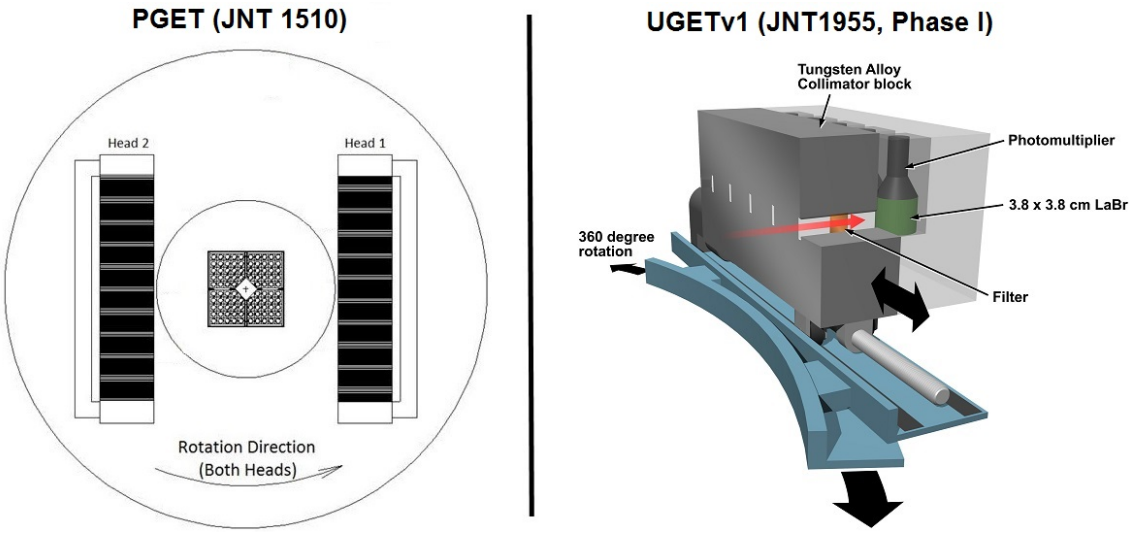

Figure 2: The two device designs analysed in section 7. **Left:** The existing PGET device, which was constructed in the JNT1510 project. It is based on two large arrays of small, non-spectroscopic CdTe detectors in a rotate-only geometry. **Right:** A single detector head of the notional UGETv1 design, developed in this work. The full instrument would include four heads, 8 spectroscopic LaBr detectors in each, in a translate-rotate geometry. The devices are not to scale.

Design parameter	PGET*	UGETv1
Maximum object diameter	30 cm	37.5 cm
Number of detector heads	2	4
Number of detectors per head	104	8
Detector type	CdTe	LaBr
Detector dimensions	Cuboid: 10×5×2 mm^3	Cylindrical: 38x38 mm
Spectroscopic analysis	Broad ROI	Peak analysis
Collimator slit length	100 mm	200 mm
Collimator slit width	1.5 mm	1.5 mm
Collimator slit height	Tapered 70→10 mm	10 mm
Detector (and slit) pitch	4 mm	46 mm
Number of lateral steps per angular projection for 2 mm sampling	- (rotation only)	23

* PGET parameters reflect design under JNT 1510. During 2016, PGET was refurbished, changing the design slightly.

Table 2: Parameters of the JNT1510 PGET and the JNT 1955 Phase I UGETv1 device designs.

5. Reconstruction and analysis methods

There are a variety of algorithms available for emission tomography, which over the years have been developed and applied mainly for medical applications. However, a nuclear fuel assembly, with its highly inhomogeneous mix of strongly gamma-ray attenuating materials (such as uranium dioxide) and less attenuating materials (such as water or air), is a challenging object for tomographic measurement and reconstruction. If not taken into account in the reconstructions, gamma-ray attenuation will strongly influence the resulting representation of the source distribution. In this work, options from the two main classes of tomographic reconstruction algorithms; analytic and algebraic [16], have been explored for use on nuclear fuel assemblies. Analytic methods, such as filtered back-projection (FBP), typically use the Fourier transform, while the algebraic methods express the reconstruction in terms of an equation system, allowing for detailed modelling of e.g. attenuation when defining the equation system's weight matrix (the system matrix). The quantitative capabilities of some analysis methods when applied on emission data from nuclear fuel assemblies are presented in ref. [17].

5.1. Image reconstruction and image analysis for Verification Objective 1

For Verification Objective 1, the number of fuel pins present should be determined without assuming any *a priori* information on the fuel. The route taken in this case is to reconstruct an image of the axial cross section of fuel, based on the collected sinogram of a fuel assembly (i.e. the collected intensities in a set of angular and lateral detector element positions relative to the fuel). See Figure 3. This image is then further analysed to deduce pin-wise data and allow for counting of the fuel pins.

Most image reconstructions in this work have been done using an FBP algorithm without attenuation correction [16]. Some reconstructions have also been done using an algebraic method, including the spatial response of the collimator-detector system and a gross model for gamma-ray attenuation in the object when defining the system matrix [17]. The spatial response function of the UGETv1 design for 1274 keV gamma rays is presented in Figure 4. The corresponding ideal response function used in FBP analysis is a single-valued line integral at Y=0. The more realistic physics representation shown in Figure 4 is achieved using no prior fuel information, thus fulfilling the assumptions for Objective 1.

Once the image is obtained, image analysis methods are required to extract pin-by-pin data, here called "pin scores". The most fundamental image analysis is to aggregate the reconstructed activities of multiple pixels in a "neighbourhood" centred on each pin location, as illustrated in Figure 5. However, irregularities that may arise from e.g. assembly torsion and pin dislocations may call for more advanced methods. A toolkit of such methods has been developed for analysis of fuel assembly images [18]. As part of the JNT1955 Phase I project, these methods were demonstrated on experimental tomographic images, proving functional on disturbed geometries [10].

Examples of analysis results for PGET and UGETv1 are given in section 7 for two combinations of methods; (i) FBP reconstruction and fundamental image analysis; and (ii) algebraic reconstruction and advanced image analysis. All analysis codes used can be made available to the IAEA.

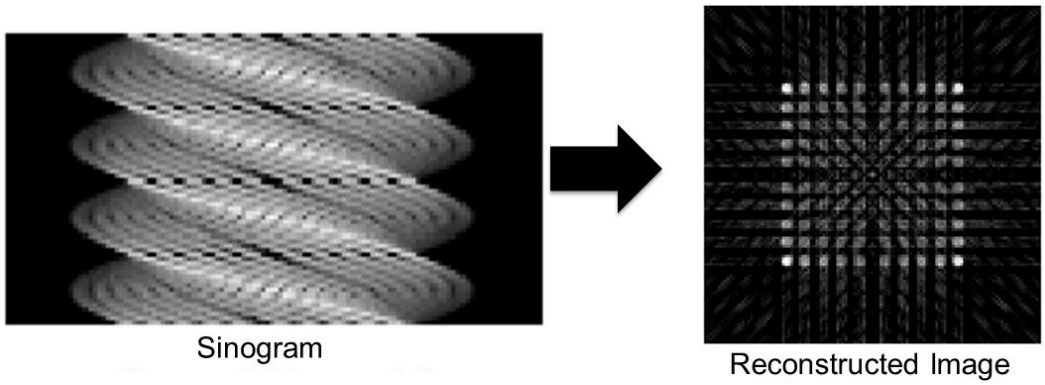

Figure 3: Tomographic data may be presented as a sinogram, with intensities as a function of lateral detector element position (horizontal axis) and angular position (vertical axis). Image reconstruction methods transform sinogram data into images of gamma-ray emission intensity, which are further analysed to deduce pin-wise data.

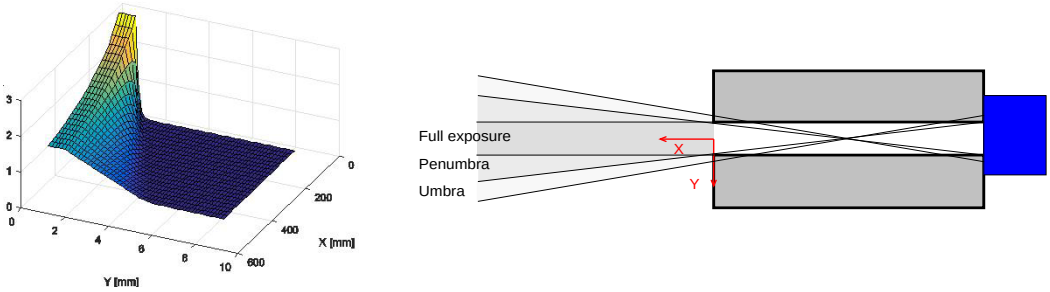

Figure 4: An example spatial response function (a.u. on the z axis) of the UGETv1 device design, used in algebraic reconstructions (left figure). The origin (X,Y=0) of the response function is centred at the front of the slit opening, and only positive Ys are presented. The function takes into account the physical properties of the measurement system (e.g., in terms of finite collimator slit width and gamma-ray transmission through the collimator material), which give rise to significant contributions from penumbra and umbra regions (right figure).

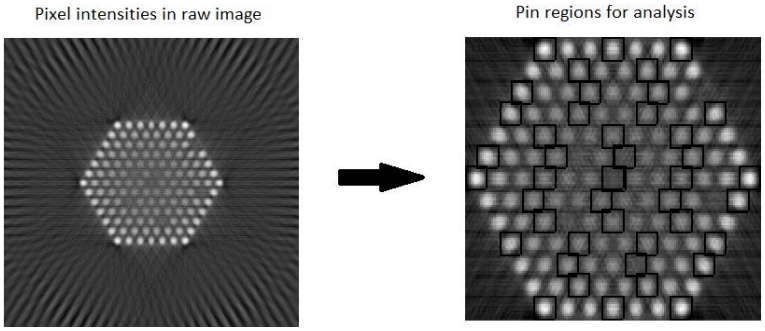

Figure 5: Example reconstructed image of simulated data for a VVER-440 assembly (left). The most fundamental image analysis is the aggregation of pixel intensity values in beforehand-defined pin-centred quadratic regions (right). A toolkit of more advanced image-analysis methods have also been developed to search the image for pins, being capable of adapting to possible irregularities in the geometry, as presented in ref. [18].

5.2. Pin-activity reconstruction for Verification Objective 2

For Verification Objective 2, pin-wise fuel properties should be determined under the assumption that information on the fuel and its geometry is available. This opens a possibility to apply detailed modelling of the fuel configuration using algebraic methods, enabling a level of detail not accessible using analytic methods. In the work on Objective 2, three different alternatives have been used for defining a detailed system matrix in algebraic reconstructions, for which software can be made available to the IAEA; (Results obtained using the two latter methods are presented in section 7.4.)

- **MCNP-generated matrix:** For simulation data obtained using MCNP (see section 3), the same transfer function as was used to create the data may be used to reconstruct the modelled source distribution. While being “unrealistically perfect” for the simulated data set, this approach enables analyses of the sensitivity to stochastic noise, added to the simulated data. For experimental data, one may also envisage the use of MCNP or similar Monte Carlo codes to model the system matrix, however, such a procedure would be excessively slow for “new” measured cases.
- **Ray-tracing:** The reconstruction toolkit TOMOPACK, with established use for reconstructions of tomographic data from the PLUTO [5] and Halden [9] devices, where %-level precision of pin-wise data has been demonstrated, is essentially based on ray-tracing and is thus suitable for analysis of spectroscopically-analysed full-energy-peak data. This modelling comprises the following features; (i) modelling of the instruments spatial response function, see Figure 4; (ii) modelling the full-energy gamma-ray transport through the detailed 3D configuration of fuel pins, taking the axial symmetry into account, and; (iii) adaption of the pixel pattern to fit the object.
- **RADSAT-based matrix:** The Radiation Detection Scenario Analysis Toolbox (RADSAT) [19] combines 3-D deterministic transport through the measurement geometry with a stochastic model for detector response. Its use for tomography is somewhat exploratory, but it offers the capability to generate object-scatter contributions in the system matrix coefficients, for each pin, which may be essential for the analysis of data with low full-energy peak specificity, such as that of PGET.

6. Proposed metrics for GET partial-defect detection capability

For Verification Objective 1, so-called receiver operator characteristic (ROC) curves are suggested to provide metrics of the partial-defect detection capability, since they can be used to understand the trade-off between probability of detection (PD) and probability of false alarm (PFA). ROC analysis is used in many fields; a standard reference from imaging sciences relevant to this work can be found in [20]. In the present case, the pin scores obtained from a measurement (calculated as described in Section 5.1) can be plotted as histograms, one histogram for the pins present and another for missing (or replaced) pins. In the ROC analysis, a threshold value is selected, so that pin scores above the threshold are defined as present pins, while scores below the threshold are defined as non-fuel objects. If the two histograms do not overlap, perfect detection of missing pins without any false alarms can be realised. If the histograms overlap, then false alarms and/or non-detected missing pins will occur, depending on the threshold. By varying the threshold, the tradeoff between detection and false alarm can be quantified. An example of how the pin-score distributions for missing and present pins can be used to generate a ROC curve is given in Figure 6. When selecting an acceptable false alarm rate (setting the threshold), the ROC curve will give the corresponding probability of detection.

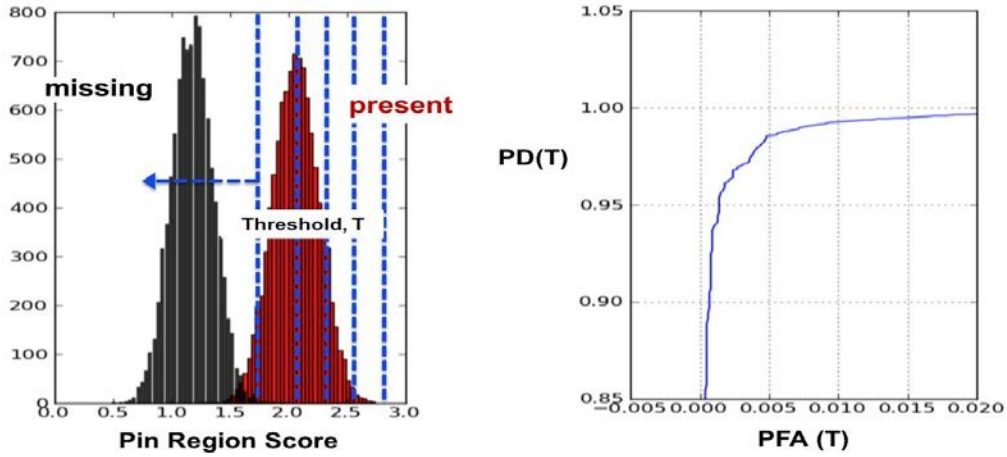

Figure 6: Pin-score distributions for missing and present pins (left) can be used to calculate the probably of detection (PD) and probability of false alarm (PFA) as a function of threshold, T, in terms of a ROC curve (right).

For Verification Objective 2, the metric used in this work (see e.g. section 7.4) is simply the agreement of reconstructed pin-wise isotopic activities with the simulated source distribution, expressed as a relative difference, or “fractional error”. At the event of inspection, pin-wise data measured using a benchmarked methodology may be used to verify operator-declared data (in case such are available on the individual pin level) or to evaluate consistency among the population of pins in an assembly at a level within the demonstrated precision.

7. Quantitative performance predictions of PGET and UGETv1 device designs

Using the modelling and simulation framework described in section 3, the expected performance of two device designs has been analysed; the existing PGET device and the notional UGETv1 device (see section 4). The reconstruction tools described in section 5 have been deployed, as well as the performance metrics described in section 6.

7.1. Analysed cases

Since the number of imaginable GET implementation alternatives and diversion scenarios are exceedingly large, and a vast amount of time is required for simulating each foreseeable case, a comprehensive study of all possibilities would not be manageable. Consequently, this study was limited to a relatively small set of implementation and pin-diversion scenarios, fuel types and parameters, and gamma-ray energies used for assay, according to the following;

Implementation scenarios: The matrix of implementation scenarios (including fuel CTs), deployment constraints and target measurement times considered in this work is presented in Table 3. The notional UGETv1 device covers a CT range from 1 to 40 years, while PGET is not applicable for CTs as short as 1 year. Measurement times up to approximately 60 minutes were assumed acceptable. Only underwater assay was studied.

Pin-diversion scenarios: Three partial defect scenarios were considered; (i) Pin removal without any substituting materials, i.e. with water replacing the pins; (ii) Pin replacement with depleted-uranium pins (replicates low- or no-activity containing high-density substitute), and; (iii) Pin replacement with fuel pins of the same construction but lower BU (replicates material diversion between reactor cycles). However, as described in [10], scenario (ii) poses the least tomographically challenging case. Focusing on the more challenging cases, only results from scenarios (i) and (iii) are presented here.

Fuel types, parameters and pin configurations: Three fuel types were studied, for which the simulated fuel pin configurations are illustrated in Figure 7; (i) SVEA-96S BWR fuel with 96 fuel pins, of which 5 were diverted; (ii) VVER-440 fuel with 1 water channel and 126 fuel pins, of which 6 were diverted, and; (iii) PWR 17x17 fuel with 25 water channels and 264 fuel pins, of which 11 were diverted. Due to gamma-ray attenuation, it is more challenging to tomographically measure fuel types with large and dense pin configurations, where information obtained from central fuel pins is scarce. Accordingly, BWR fuel poses the least challenging configuration and PWR poses the most challenging. Fuel BUs from 10 to 40 GWd/MTU were analysed in order to span typical values encountered in commercial power industry.

Gamma-ray energies: The gamma-ray source terms will depend on the fuel parameters; short-cooled assemblies will contain short-lived as well as long-lived fission products and higher total activity, while the gamma-ray spectrum emitted from long-cooled assemblies (CT>30 years) will be dominated by ^{137}Cs. All simulations covered a large number of gamma emitters and energies, but in the tomographic analyses only a few energy regions were selected (taking detector characteristics into consideration), corresponding to specific gamma-emitting fission products. The gamma-ray energies under study in this work are presented in Table 4. For each gamma-ray energy, relevant stochastic noise levels corresponding to assay time, BU and CT, were included in the statistical analyses of each simulated fuel type. The noise levels were given by Poisson statistics, based on simulated absolute intensities.

Implementation Scenario	Cooling time (years)	Deployment constraints
Routine verification of old fuel being transferred to a geologic repository	40	Attended or unattended
Routine verification of fuel being transferred to dry storage	5	Attended or unattended
Random verification of in-pool inventory	1	Attended

Table 3: Description of GET implementation scenarios considered in this work. The hardware configurations studied were the existing PGET device and the notional UGETv1 design (see section 4), for both Verification Objective 1 and Objective 2.

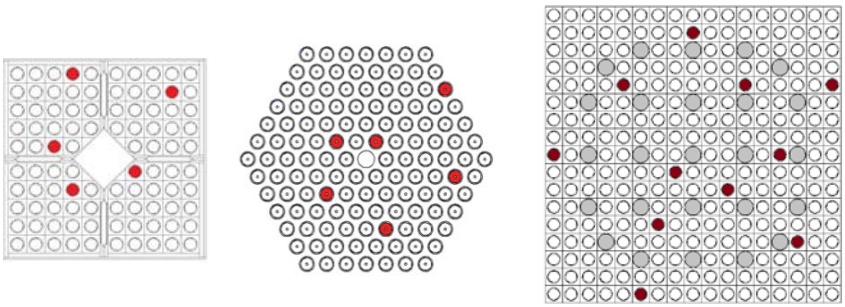

Figure 7: Map of the simulated diverted pin locations (in red) in the three assembly types under study: five for BWR (left), six for VVER-440 (middle) and 11 for PWR (right). In addition, VVER fuel by design includes one central water channel and PWR fuel includes 25 water channels (marked in grey).

Isotope	Energy, MeV	Half-life	Relevant CT range
^{137}Cs	0.662	~30 y	up to 100-150 y
^{134}Cs	0.605	2.1 y	up to 10 y
	0.796		
^{154}Eu	0.723	8.5 y	up to 25–30 y
	0.873		
	0.996		
	1.005		
	1.274		
^{144}Pr (^{144}Ce)	2.186	285 d	up to 5 y

Table 4: Characteristic fission products and associated gamma-ray emissions from spent fuel in the 0.4-2.5 MeV energy region.

In general, the higher gamma-ray energies in Table 4 facilitate tomographic assay, since their higher penetrability enables more information to be obtained from the assemblies' innermost sections. However, also the emission intensity is important. For ^{154}Eu, the highest energy (1.274 MeV) is also the most intense and thus the most useful. One should note that for relatively long-cooled fuel (CT between 30 and about 100 years), only the long-lived, lower-energy gamma emitter ^{137}Cs is abundant enough to be measured.

7.2. Simulation and benchmarking

The simulation toolkit described in section 3 was used to create tomographic data for sets of virtual fuel assemblies for the cases accounted for above. Following the procedure described in section 3, "single-pin base sinograms" were weighted and added together to comply with isotopic contents due to selected pin-wise BU and CT. Accordingly, high statistical quality of these calculated "single-pin base sinograms" was critically important for reducing systematic effects in the large sets of derived virtual assemblies that were used to assess performance evaluation. A particular concern was the sampling of pin contributions from the inner regions of the assembly, where gamma-ray self-shielding and line-of-sight obstructions are severe, leading to few sinogram counts. However, the calculation scheme did not allow for statistical analyses of individual single-pin sinograms. Instead, an estimate of precision emanating from the base data was achieved based on two separate, independent simulations of a "difficult" case (low gamma-ray energy from ^{137}Cs in a large PWR fuel configuration). The resulting reconstructed source concentrations for central fuel pins, obtained in identical reconstructions of the simulated data sets, matched within 3% [10], constituting a measure of the precision of the base data and thus defining a limit of the achievable precision in the tomographic analyses of pin-wise source contents. One may note that implications of counting statistics, due to e.g. variations in detector count rate or measurement time, may be evaluated at a higher level of precision by investigating the statistical spread obtained when adding such variations to the base data.

In order to ensure that the simulation-based conclusions drawn on PGET and UGETv1 performance for various fuel parameters and measurement times were correct, the Monte Carlo simulations were verified and validated in multiple ways;

- Gamma-ray source terms and detector response calculations (simulation steps 1 and 3) were evaluated using experimental data from measurements performed at the Clab interim storage facility for spent fuel in Sweden. This benchmark included relative peak intensities for a large number of gamma peaks as well as peak shape and level of Compton-scattered background;
- The Monte Carlo-based gamma-ray transport (simulation step 2) was evaluated using tomographic data from the PLUTO device [5]. Both simulated gamma-ray projections as well as properties of reconstructed images were evaluated;
- The MCNP model of the PGET device was evaluated using experimental PGET data;
- A model of the PGET device was also developed in the alternative Monte Carlo simulation tool Geant4, and the Geant4 simulations were evaluated using experimental PGET data, and;
- The MCNP model of the notional UGETv1 device was evaluated in inter-code simulation comparisons to an independent Geant4 model.

All evaluations were considered satisfactory, thus providing confidence in the comparisons made between expected instrument performance for the existing PGET and the notional UGETv1 devices. Details on the evaluations can be found in ref. [10].

7.3. Results for Verification Objective 1: Independent pin counting

As accounted for in section 5.1, the approach for Verification Objective 1 was to use tomographic data in different types of image reconstructions, and perform image analysis on the reconstructed images to independently count the number of fuel pins. Two alternative analysis routes were taken:

- **Analysis Route 1:** Basic analytic FBP image reconstruction, followed by basic image analysis (summing sets of pixel values said beforehand to represent each fuel pin). While not allowing for inclusion of spatial response or gamma-ray attenuation in the reconstruction, nor adaption to possible dislocation or torsion of the fuel in the image analysis, this route enabled automated analysis of large populations (up to 1,000) of simulated assemblies with varying BU distributions and stochastic noise. Consequently, this route enabled ROC curve analyses, as described below.

- **Analysis Route 2:** Algebraic image reconstruction and analysis, including modelling of the device's spatial response function and homogeneous gamma-ray attenuation in the image reconstruction as well as more advanced image analysis tools to identify and quantify pin-shaped objects in the reconstructed image. This route was not automated and thus smaller populations of assemblies could be analysed (up to 10), excluding ROC curve analyses of the results.

Apart from demonstrating the methods' capabilities to distinguish diverted fuel pins from present pins, one important aspect of these studies was to compare the performance of the PGET and UGETv1 devices.

Examples of quantified pin-wise ^{154}Eu activities when applying the two alternative analyses routes on simulated UGETv1 data for short-cooled PWR fuel assemblies with missing pins, offering a challenging diversion scenario for the most challenging fuel type of the three under study, are presented in Figure 8. As seen in the figure, the FBP reconstruction (which does not take gamma-ray attenuation into account) calculates lower pin activities in the assembly interior than in its periphery, whereas a more leveled response is given by the model-based algebraic reconstruction (which takes gamma-ray attenuation into account). In agreement with ref. [17], model-based reconstruction seems to allow for better separation between fuel pins and missing pins respectively water channels. However, one should also note that the simulation for the latter does not include any pin-BU variation.

ROC curve formalism (see section 6) was used to compare the expected performance of the existing PGET device with that of the notional UGETv1 device. For both devices, perfect energy and efficiency calibration of detector elements was assumed in the simulations. The evaluations were based on automated FBP reconstruction and summation of pixel values (Analysis Route 1) for sets of 1,000 virtual fuel assemblies with a BU variation within ±20% and stochastic noise corresponding to a 60-minute assay for UGETv1 and a 10-min assay for PGET. The results for the three fuel types under study with fuel parameter sets {BU=20 GWd/MTU, CT=5 years} respectively {BU=10 GWd/MTU, CT=40 years} are presented in Figure 9. For the sets with CT=5 years, the 1274-keV radiation from ^{154}Eu was analysed, while the 662-keV radiation from ^{137}Cs was used for the sets with CT=40 years.

The ROC curves in Figure 9 indicate that PGET offers more confident or similar capability of detecting missing pins as UGETv1. However, one should also note that no ROC analyses have been made for Analysis Route 2, which might offer different detection capability according to the results in Figure 8. The detection capability is further discussed in section 7.5.

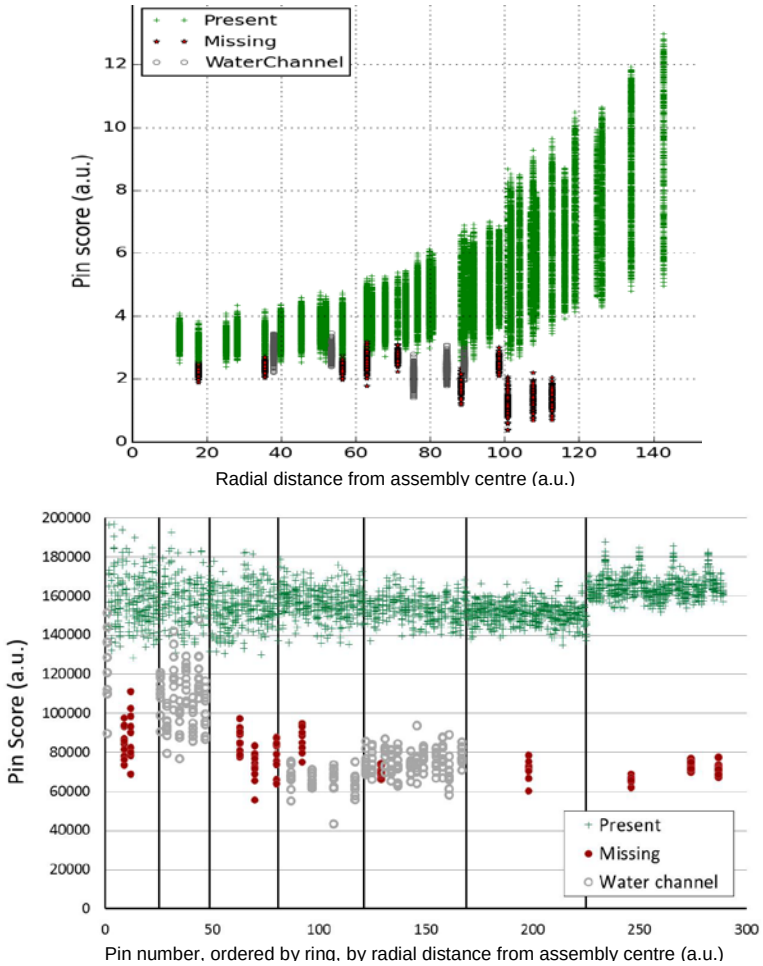

Figure 8: Pin-scores for present and missing pins, simulating the deployment of the UGETv1 device on sets of PWR assemblies (BU=40 GWd/MTU, CT=1 year) using the 1275 keV emission from ^{154}Eu. The upper figure accounts for simple FBP reconstruction and pixel summation on a set of 100 virtual assemblies with ±20% pin-wise BU variation. The lower figure accounts for model-based algebraic reconstruction and image analysis on a set of 10 virtual assemblies with no pin-wise BU variation. Both data sets include stochastic noise.

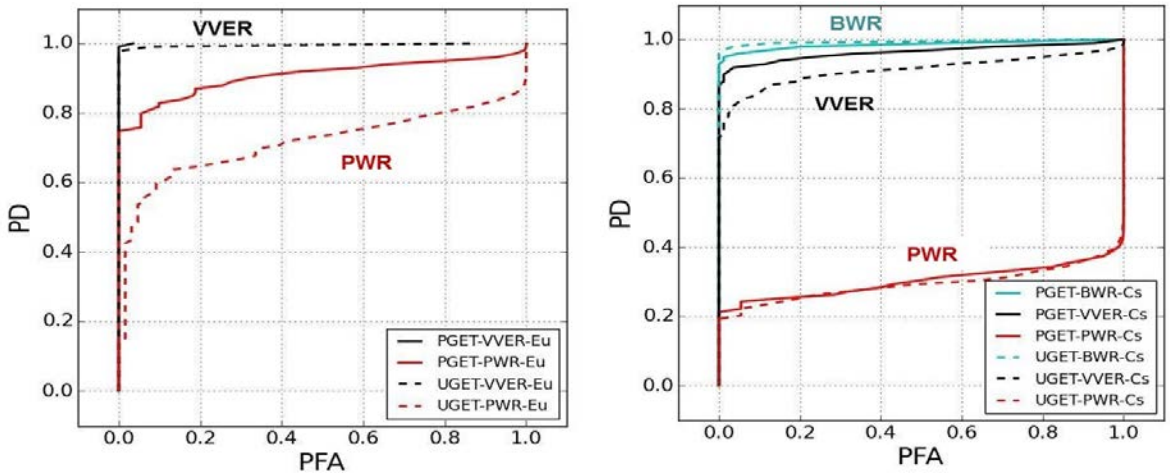

Figure 9: Predicted detection sensitivity of a single missing pin (i.e., bias defect) for perfectly-calibrated PGET and UGETv1 for BWR, VVER and PWR fuels, deploying simple FBP reconstruction and pixel summation. **Left:** Nominal BU of 20 GWd/MTU and 5 year CT with assay based on ^{154}Eu. (BWR performance is even higher than VVER and therefore not shown.) **Right:** Nominal BU of 10 GWd/MTU and 40-year CT with assay based on ^{137}Cs.

7.4. Results for Verification Objective 2: Pin-wise fuel properties

Verification Objective 2 assumes availability of the fuel-geometry information needed to enable the detailed algebraic reconstruction methods described in section 5.2. Using these methods, pin-wise isotopic contents are reconstructed (rather than images as in Verification Objective 1). The quality of the results, i.e. the precision of the calculated pin-wise isotopic contents, will depend on the fidelity of the algebraic system matrix. If spectroscopic full-energy peak analysis is applied, such as in the notional UGETv1 design (see section 2.2), full fidelity may be provided by full-energy transport calculations (ray tracing). If the collected data comprises significant scattered components, which may be the case for the PGET design, the calculations may require the inclusion of gamma-ray scattering as well. However, the more detail that is included in the calculations, the longer the execution time, which may make the most detailed calculations, such as MCNP, prohibitively long.

The results from three types of analyses are presented below;

1. Pin-wise isotopic-content reconstructions using the ray-tracing toolkit TOMOPACK, applied on simulated data for the notional UGETv1 device design for PWR fuel assemblies;
2. Pin-wise isotopic-content reconstructions using the RADSAT toolbox, which includes calculations of gamma-ray scattering components, applied on simulated data for the notional UGETv1 device design and the existing PGET device.
3. Estimation of pin-wise BU and CT, based on measured pin-wise isotopic contents.

For a complete description of all analyses performed, we refer to [10].

7.4.1. Ray-tracing-based reconstruction models

Simulations of UGETv1 assay of PWR fuel assemblies with 11 fuel pins missing (see Figure 7) have been analysed using the TOMOPACK ray-tracing-based reconstruction toolkit. In the simulations, the assemblies contained uniform pin-wise isotopic contents, and sets of 10 virtual assemblies were analysed for each case under study. Results for a short-cooled (1 year), high-BU PWR assembly (40 GWd/MTU) with 11 fuel pins missing are presented in Figure 10. Reconstructed relative pin-by-pin isotopic contents of ^{137}Cs, ^{134}Cs and ^{154}Eu are presented in terms of the fractional error from the simulated values, ordered ring-by-ring from the fuel assembly centre to the periphery. In the presented cases, the level of statistics in the analysed data sets corresponds to 40 minutes total assay time. Since a prerequisite for Verification Objective 2 was a priori known fuel geometry, activities are only reconstructed in present fuel pins and not in water channels or positions of missing pins.

For all three isotopes in Figure 10, precision is high in peripheral fuel pins and up to about 10% (1 σ) in central fuel pins. Systematic deviations are generally smaller than a few %, except for the most central sections, where insufficient sampling of single-pin base sinograms may disturb the analysis (see section 3). The best and most stable results are obtained for ^{154}Eu, which emits the highest gamma-ray energy (1274 keV) and thus offers the highest escape fraction from the assembly centre.

The TOMOPACK ray-tracing toolkit was also used for reconstructing the pin-wise content of ^{137}Cs based on simulations of long-cooled (40 years) low-BU (10 GWd/MTU) PWR fuel. In this “difficult” case (low source concentration, low gamma-ray energy, large-sized fuel), longer measurement times would be required to obtain good statistics, and approximately 2 hours total assay time would give similar results as presented in Figure 10 (top).

7.4.2. Reconstruction models including scattered components

The RADSAT-based reconstruction approach offers an attractive path to analysis of PGET performance, in particular when broad energy windows are deployed so that object scatter constitutes a significant portion of the sinogram signal. Here, RADSAT has been used to analyse simulated data for both the UGETv1 and the PGET device. Data sets from 100 virtual VVER assemblies were studied, including ±20% variation in pin BU and six tampered fuel pins with 50% of the average BU value (replicating material diversion at about mid-life of the fuel). Figures 11 and 12 show the results for pin-by-pin quantification of the ^{137}Cs and ^{154}Eu concentrations in VVER fuel with two sets of fuel parameters; {BU=20 GWd/MTU, CT=5 years} respectively {BU=10 GWd/MTU, CT=40 years}.

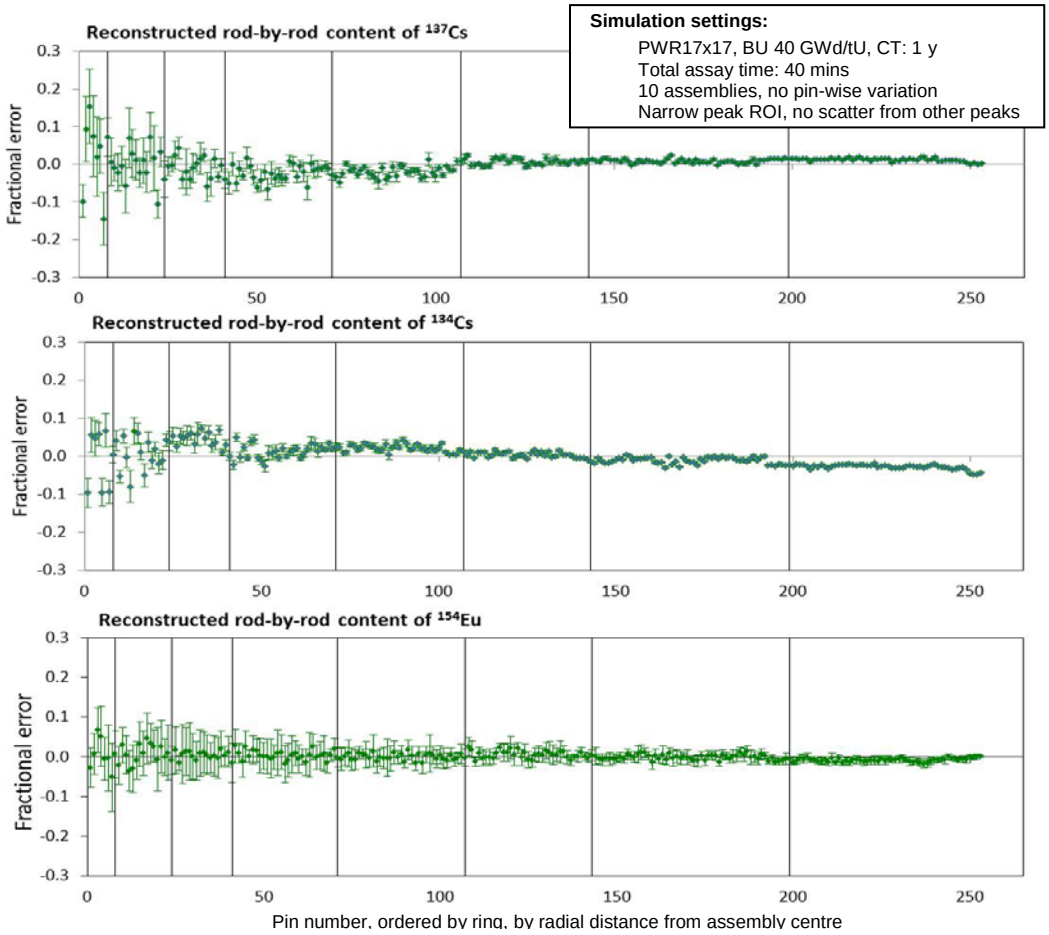

Figure 10: Results obtained in TOMOPACK reconstructions of simulated data for short-cooled, high-BU PWR 17x17 fuel assemblies in the suggested UGETv1 device design, presented as mean values of fractional error in reconstructed pin-by-pin isotopic contents obtained in analyses of 10 datasets, including error bars corresponding to ±1 σ confidence intervals. All pins were assigned equal isotopic contents in the simulations. The analyses were based on full-energy gamma peaks at 662 keV (^{137}Cs), 796 keV (^{134}Cs) respectively 1274 keV (^{154}Eu).

As seen in Figure 11 (top) and Figure 12 (top), RADSAT calculates activities in normal fuel pins within a few percent for all VVER fuels under study, when applied on simulated data for the UGETv1 device. Statistical uncertainty is smaller in the assembly periphery (as expected), but also in the inner sections precision is in the order of a few percent. Some systematic deviations may be identified, but these are also on the few-percent level. Performance is good also for tampered fuel pins, although their content of ^{154}Eu is generally slightly overpredicted and the statistical uncertainty is higher than for normal fuel pins. Accordingly, one would expect these tampered fuel pins to be confidently detected. In addition, a short-CT (1 year), high-BU (40 GWd/MTU) fuel was studied, giving similar results for ^{154}Eu assay using UGETv1 as presented in Figure 11 (top). (For this short-cooled fuel, only UGETv1 assessment was covered because PGET cannot manage the high count rates encountered for such fuel.)

In the analyses of simulated data for the PGET device, there is a systematic overprediction of the activities in normal fuel pins, which increases towards the assembly centre. The tampered fuel pins are strongly overpredicted, especially for the ^{154}Eu assessment in Figure 11 (bottom), which would complicate their detection.

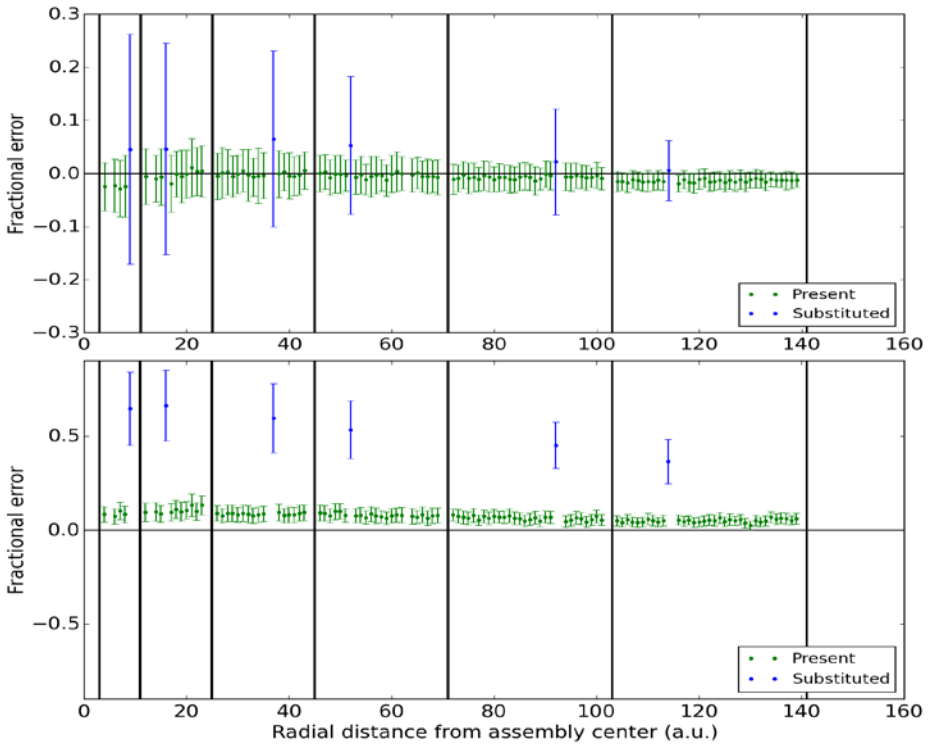

Figure 11: Fractional error, relative to true values, for pin-by-pin ^{154}Eu activity reconstruction with RADSAT-based system matrix using UGETv1 (top panel) and PGET (bottom panel). The 100-assembly population assumed VVER fuel with nominal BU of 20 GWd/MTU, 5-year CT, and ±20% pin-wise BU variation. Tampered pins (blue), have a nominal activity half that of the present pins (green).

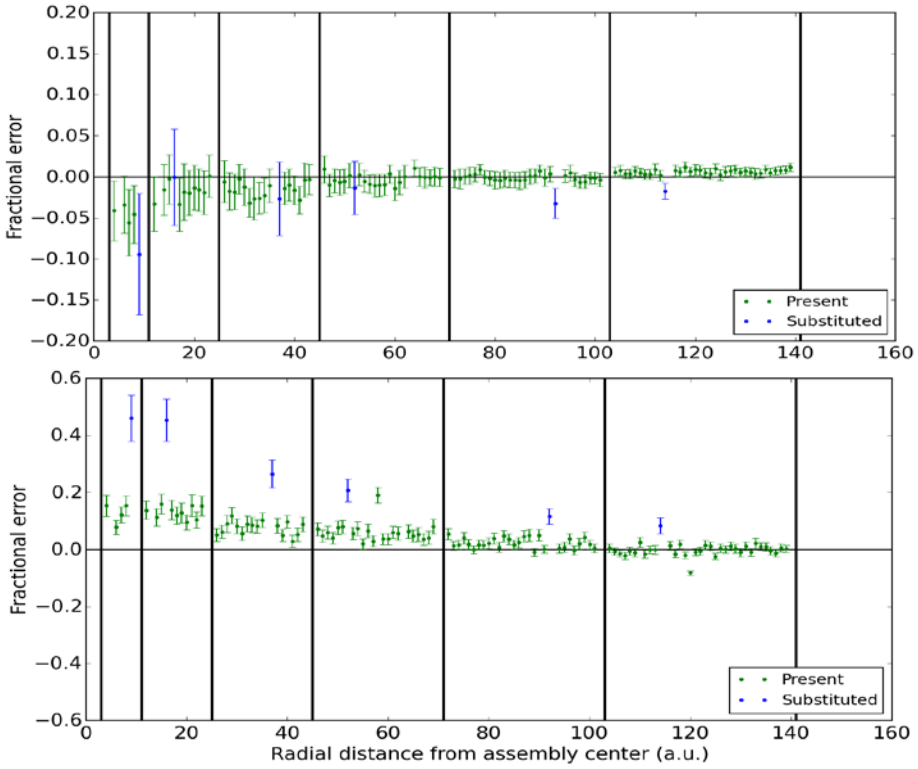

Figure 12: Fractional error, relative to true values, for pin-by-pin ^{137}Cs activity reconstruction with RADSAT-based system matrix using UGETv1 (top panel) and PGET (bottom panel). The 100-assembly population assumed VVER fuel with nominal BU of 10 GWd/MTU, 40-year CT and ±20% pin-wise BU variation. Tampered pins (blue), have a nominal activity half that of the present pins (green).

7.4.3. Pin-wise BU and CT determination

Gamma-ray spectroscopy is an established technique to characterize nuclear fuel, and several studies have been made to establish correlations between full-energy peak intensities of gamma rays from ^{137}Cs, ^{134}Cs and ^{154}Eu, recorded in gamma-scanning measurements of nuclear fuel assemblies, to fuel parameters such as BU and CT [21]. In a similar manner, tomographically measured pin-wise activities of these isotopes may be used to determine BU and CT on the single-pin level. These pin-wise fuel parameters may, in turn, be used to control the consistency of the population of fuel pins in an assembly or even to verify operator-declared data, if available on the single-pin level. However, such data are not typically provided to the IAEA today in spent fuel declarations.

As described in [10], the investigations performed in this work lead to the following conclusions;

- For short-cooled fuels, analysis of the quotients of the tomographically measured pin-wise contents of ^{134}Cs and ^{154}Eu would offer the smallest statistical uncertainty in the determination of pin-wise BU and CT, using the methods in [21], when these isotopes are available (i.e. at CT<10 years).
- At intermediate CT (10 to 30 years), the quotient of ^{154}Eu and ^{137}Cs can be used, with slightly larger statistical uncertainties.
- At long CT (>30 years), only ^{137}Cs will be available. However, ^{137}Cs can still give a direct measure of the fuel BU, provided that all fuel pins have the same CT. Consequently, the precisions demonstrated in e.g. Figure 10 (top) or Figure 12 (top) give a direct measure of the achievable precisions in pin-wise BU determination.

Considering a 40-minute assay using the notional UGETv1 device, the simulations and ray-tracing-based analyses in this work (see section 7.4.1) show that even for the innermost sections of PWR fuel assemblies with CT=1 year and BU=40 GWd/MTU, the pin-wise BU and CT may be determined with statistical uncertainties below 6% and 0.4 years, respectively, based on the quotients of the pins' ^{134}Cs and ^{154}Eu contents. However, one should note that this represents the highest achievable precision, which requires that systematic uncertainties are eliminated. For more information, we refer to [10].

7.5. Discussion on predicted UGETv1 and PGET performance

As seen in Figure 9, the evaluations on Verification Objective 1 indicate that PGET performance would exceed that of UGETv1 for most analysed cases. The reason is mainly the larger number of detector elements in PGET, which leads to more efficient data collection and thus to better counting statistics during a fixed measurement time. Assuming an operationally tolerable false alarm rate of approximately 0.05 (1 false alarm per 20 assemblies), these findings indicate that Analysis Route 1 (FBP reconstruction and summation of pixel values) would achieve a probability of detecting a single missing pin, at any location in the assembly, that is greater than 0.80 for VVER and BWR fuels, with both devices, regardless of BU and CT. However, the evaluation also indicates that the single-missing-pin performance for both devices would be low for PWR fuel (due to its large physical dimension and relatively tight fuel-pin spacing). Referring to Figure 8, one should note that alternative analyses, such as Analysis Route 2 (algebraic reconstruction and advanced image analysis) may perform better, albeit efforts must be made to automate it for use in unattended mode.

As seen in Figure 11 and 12, the evaluations on Verification Objective 2 indicate superior performance of the UGETv1 device as compared to PGET, contrary to Objective 1. The reason is the capability of UGETv1 to select full-energy gamma, which enables the analysis of isotope-specific data. However, one may expect that smaller energy windows (for example 630-680 keV instead of 400-700 keV for ^{137}Cs, which was simulated here), may help to reduce the systematic bias in the application of PGET to Objective 2. More investigations of object-scatter effects, as a function of energy-window width in PGET, is needed. For UGETv1, a potential to deduce pin-wise BU and CT in short-cooled PWR fuel with statistical uncertainties below 6% respectively 0.4 years, has been indicated even for central pins.

Finally, one should note that PGET is not operational at CTs down to 1 year due to count-rate saturation of the detector elements in the high gamma flux from short-cooled fuel, while UGETv1 was designed to be operational also at short CTs. For Verification Objective 1, results obtained when applying Analysis Route 1 on UGETv1 data at CT=1 year shows that a probability >95% for detecting a single missing fuel pin would be achievable for all three fuel types under study, assuming a tolerable false alarm rate of 0.10. For more detailed information of these analyses, we refer to [10].

8. Envisaged inspection procedure

The envisioned inspection procedure, identified and refined as part of the JNT 1955 Phase I project can be outlined according to the following:

A. Baseline inspection procedure, performed on-site, either automatically in case of unattended use or by an inspector in the case of attended use:
    1. Tomographic measurement
    2. Online image reconstruction
    3. Online image analysis
    4. On-site initial integrity statement

B. If undeclared removal/replacement is suspected:
    5. Detailed pin-activity reconstruction based on current fuel type and position in device. (No additional measurement required.)

The last step (B.5) reflects the functionality of Verification Objective 2, at least if operator-declared information is used for the detailed modelling. However, it may also be envisaged that geometric information is extracted directly from reconstructed images in step A.2, without any need for operator-declared data. Such a possible procedure ("Verification Objective 1.5") is also discussed below.

9. Conclusions, discussion and outlook

According to this and previous studies, GET has the potential to provide bias-defect sensitivity in most fuel verification scenarios, a significant improvement over IAEA's current partial-defect capabilities using a Fork-based system or Digital Cerenkov Viewing Device. The IAEA also possesses a GET measuring device for attended use (PGET), which was refurbished during 2016, introducing e.g. new detector elements to provide adequate efficiency and energy calibration. The current study covers analyses of expected PGET performance assuming high-fidelity calibration (but with detailed device design before refurbishment) for a variety of fuel types and fuel parameter sets. However, there may still be room for improvements in terms of e.g. optimisation of energy windows used for selecting the detected gamma rays to be analysed, which can be a subject for future studies.

In this study, a "Universal" GET design has been developed ("UGETv1"), which is capable of supporting the full range of fuel characteristics considered in this study, but that versatility comes at a price in terms of both assay time and instrument lifecycle cost. (For cost estimates, see [10].)

A set of tomographic reconstruction algorithms have been identified, described and used, which may find use in the application of GET for safeguards. For Verification Objective 1 (counting of fuel pins without any prior information on the fuel), image reconstruction algorithms have been presented, which are complemented by image-analysis methods to count the number of fuel pins present in the measured assembly. For Verification Objective 2 (determination of pin-wise fuel properties, making use of prior information on e.g. fuel geometry), algebraic methods have been suggested that include detailed modelling of the gamma-ray transport through the fuel configuration.

Among the outcomes of this work is the creation of a simulation and modelling framework, which provides end-to-end capability to assess tomographer performance for nuclear fuel assay, and could be considered a new, standing capability for the international safeguards community, available on request. It is modularised to allow for studies of expected performance of various GET measurement device designs for a variety of fuel types, fuel properties and data analysis methods.

For Verification Objective 1, it was found that the PGET and UGETv1 devices exhibit, in general, comparable performance despite their very different designs, but PGET achieves that sensitivity in shorter assay times. The higher collection efficiency of PGET elevates its performance over UGET for cases where the signal coming from interior pins is particularly weak (e.g., PWR assemblies), while UGET achieves high performance for the shortest-cooled fuels that cannot be measured by PGET. These comparative findings are based on an analytic FBP reconstruction; however, results may vary with other reconstruction methods. Among the conclusions drawn for Objective 1 were namely that algebraic reconstruction including modelling of system's intrinsic response function and uniform

attenuation gave the most promising results in terms of separation between fuel pins and background. Prior work has also indicated that image analysis and algebraic reconstruction methods offer the potential robustness to issues such as misalignment of assemblies, bowing of individual fuel pins, non-functioning detector elements, irregular measurement positions etc.

For Verification Objective 2, predicted performance for PGET was lower than for UGETv1, primarily because significant object-scatter contributions in PGET's wide energy windows perturb a relatively small full-energy peak signal. Smaller energy windows might offer improvements in Objective 2 performance for PGET, but more studies are needed to quantify this potential. It may also be envisaged that geometric information may be extracted from reconstructed Objective 1-type images, to be used in Objective 2-type analyses without any need for operator-declared data. The project team and stakeholders have discussed the potential for such a procedure ("Verification Objective 1.5"), but analysis of such an approach was beyond the scope of this study.

Finally, one may note that the performance metric used for Verification Objective 1 relates to bias defects, i.e. diversion of single fuel pins. If the performance metric were defined for higher defect levels (e.g. 5% or 10% of the pins instead of the <0.5% bias defect at the event of 1 missing pin out of 264 pins in a PWR assembly) the ROC curves are expected to look considerably better also for PWR fuels. This is an area for future work.

10. Acknowledgements

U.S. participation in the JNT 1955 Phase I project has been funded by the U.S. Support Program to the International Atomic Energy Agency (IAEA) and the National Nuclear Security Administration's Office of Nonproliferation and Arms Control. Uppsala University's contributions were funded by the Swedish Radiation Safety Authority (SSM) via the Swedish Support Program to the IAEA under contracts SSM2013-85-9, SSM2014-94, SSM2015-99, SSM2016-130, and activity number 3060152-08. The computations performed by Uppsala University were partially performed on resources provided by Swedish National Infrastructure for Computing (SNIC) through Uppsala Multidisciplinary Center for Advanced Computational Science (UPPMAX) under projects p2013091, snic2013-1-296, snic2014-1-203, and snic2014-1-392. Finnish participation was supported by the Finnish Support Program to the IAEA, financed by Finnish Foreign Ministry. The contribution by the European Commission was financed through the regular European Commission budget.

The project team appreciates the guidance of IAEA's James Ely, Misha Mayorov, and Alain Lebrun.

11. References

[1] International Atomic Energy Agency; *Special Criteria for Difficult-to-Access Fuel Items*; SG-GC-Annex-04; IAEA; 2009.

[2] International Atomic Energy Agency; *IAEA Department of Safeguards Long-Term R&D Plan, 2012-2023*; STR-375; IAEA; 2013.

[3] Lévai F, Desi S, Czifrus S, Feher S, Tarvainen M, Honkamaa T, Saarinen J, Larsson M, Rialhe A and Arlt R; *Feasibility of gamma emission tomography for partial defect verification of spent LWR fuel assemblies*; STUK-YTO-TR-189; Finnish Radiation and Nuclear Safety Authority, STUK; 2002.

[4] Honkamaa T, Levai F, Turunen A, Berndt R, Vaccaro S, and Schwalbach P; *A Prototype for passive gamma emission tomography*; IAEA Safeguards Symposium; 2014.

[5] Jacobsson Svärd S, Håkansson A, Bäcklin A, Osifo O, Willman C and Jansson P; *Non-destructive Experimental Determination of the Pin-power Distribution in Nuclear Fuel Assemblies*; Nuclear Technology, 151(1):70-76; 2005.

[6] Jansson P, Jacobsson Svärd S, Håkansson A and Bäcklin A; *A Device for Non-destructive Experimental Determination of the Power Distribution in Nuclear Fuel Assemblies*; Nuclear Science and Engineering 152(1):76 86; 2006.

[7] Jacobsson Svärd S, Håkansson A, Bäcklin A, Jansson P, Osifo O and Willman C; *Tomography for partial-defect verification - experiences from measurements using different devices*; ESARDA Bulletin, 33:15-25; 2006.

[8] Baird B; *Quantitative analysis of the fission product distribution in a damaged fuel assembly using gamma-spectrometry and computed tomography for the Phebus FPT3 test*; Nuclear Engineering and Design, 262:469-483; 2013.

[9] Holcombe S, Jacobsson Svärd S and Hallstadius L; *A novel gamma emission tomography instrument for enhanced fuel characterization capabilities within the OECD Halden Reactor Project*; Annals of Nuclear Energy, (85):837–845; 2015.

[10] Smith LE, Jacobsson Svärd S, Mozin V, Jansson P, Miller E, Honkamaa T, Deshmukh N, White T, Wittman R, Trellue H, Grape S, Davour A and Vaccaro S; *A Viability Study of Gamma Emission Tomography for Spent Fuel Verification: JNT 1955 Phase I Technical Report*; PNNL-25995, Pacific Northwest National Laboratory, USA; 2016.

[11] Trellue HR, Fensin ML, Richard JR, Galloway J and Conlin JL; *Description of the Spent Nuclear Fuel Used in the Next Generation Safeguards Initiative to Determine Plutonium Mass in Spent Fuel*; LA-UR 11-00300, Los Alamos National Laboratory, USA; 2011.

[12] Mozin V and Tobin S; *DGSDEF: Discrete Gamma-ray Source DEFinition code*; LA-CC-10-083. Los Alamos National Laboratory, USA; 2010.

[13] Pelowitz DB; *MCNPXTM User's Manual. Version 2.6.0*; NM LA-CP-07-1473 Los Alamos National Laboratory, USA; 2008.

[14] Agostinelli A et.al.; *Geant4 a simulation toolkit*; Nuclear Instruments and Methods in Physics Research Section A, 506:250–303; 2003.

[15] White TA, Jacobsson Svärd S, Smith LE, Mozin VV, Jansson P, Davour A, Grape S, Trellue N, Deshmukh NS, Wittman RS, Honkamaa T, Vaccaro S and Ely JH; *Passive Tomography for Spent Fuel Verification: Analysis Framework and Instrument Design Study*; ESARDA Symposium, Manchester, UK; 2015.

[16] Kak AC and Slaney M; *Principles of Computerized Tomographic Imaging*; IEEE Press, ISBN 0-85274-349-1, Piscataway, NJ, USA; 1988.

[17] Jacobsson Svärd S, Holcombe S and Grape S; *Applicability of a set of tomographic reconstruction algorithms for quantitative SPECT on irradiated nuclear fuel assemblies*; Nuclear Instruments and Methods in Physics Research Section A, 783:128–141; 2015.

[18] Davour A, Jacobsson Svärd S, Andersson P, Grape S, Holcombe S, Jansson P and Troeng M; *Applying image analysis techniques to tomographic images of irradiated nuclear fuel assemblies*; Annals of Nuclear Energy, 96:223-229; 2016.

[19] Shaver MW, Smith LE, Pagh RT, Miller EA, and Wittman RS; *The Coupling of a Deterministic Transport Field Solution to a Monte Carlo Boundary Condition for the Simulation of Large Gamma-Ray Spectrometers*; Nuclear Technology 168(1):95-100; 2009.

[20] Metz CE; *Basic Principles of ROC Analysis*; Seminars in Nuclear Medicine; 8(4):283-298; 1978.

[21] Jansson P. *Studies of Nuclear Fuel by Means of Nuclear Spectroscopic Methods*; PhD thesis, Uppsala University, Sweden. Retrievable at http://urn.kb.se/resolve?urn=urn:nbn:se:uu:diva-2057; 2002.

Detection of Fuel Pin Diversion via Fast Neutron Emission Tomography

A. Iyengar[1,2], P. Hausladen[1], J. Yang[1], L. Fabris[1], J. Hu[1], J. Lacy[3], A. Athanasiades[3]

[1]Oak Ridge National Laboratory; [2]The University of Tennessee-Knoxville Bredesen Center, [3]Proportional Technologies, Inc

Abstract:

Oak Ridge National Laboratory is developing a new capability to perform passive fast neutron emission tomography of spent nuclear fuel. The goal of this capability is to detect vacancies or substitutions of individual fuel pins in spent nuclear fuel assemblies for international safeguards applications, such as verifying the integrity of an assembly prior to transfer to "difficult to access" storage. Emission tomography uses collimation to isolate activity along "lines of response" through an object. By combining many collimated views through an object, the neutron emission from each fuel pin can be mathematically extracted and an image of the fuel assembly can be constructed. However, performing fast-neutron imaging is challenging for the very reason that it is desirable, namely, that fast neutrons penetrate a good deal of shielding and are consequently difficult to collimate and measure with high resolution. For spent fuel, additional challenges include the modest neutron source strength and the overwhelming gamma-ray emissions. While the International Atomic Energy Agency (IAEA) is presently investigating the use of passive gamma emission tomography for the same application, it is useful to investigate neutron emission tomography because fast neutrons better penetrate larger fuel assemblies and because fast neutrons (originating primarily from curium-244 which is mainly produced at the end of the exposure cycle) may be sensitive to replacement fuel pins that are subsequently irradiated. In the present work, we present a novel collimator concept that will enable rapid transaxial tomographic imaging of spent nuclear fuel using the spontaneous fast neutron emissions from the fuel. Initial design simulations of an imager based on this collimator indicate sufficient resolution to identify individual fuel pins. Employing such a collimator, the resulting imager can be sufficiently compact, efficient, and radiation resistant to make fast neutron emission imaging practical.

Keywords: safeguards, fast neutrons, tomography, imaging, spent fuel, non-destructive analysis

1. Introduction

Due to the thousands of metric tons of heavy metal being discharged from nuclear reactors globally, countries like Finland and Sweden are taking the lead to develop underground repositories to store their used nuclear fuel [1][2]. The International Atomic Energy Agency (IAEA) has developed safeguards approaches under integrated safeguards for encapsulation plants and geological repositories [3]. Spent fuel safeguards rely primarily on material containment and surveillance techniques along with item counting and non-destructive assay (NDA) verification measurements [4]. These types of measurements are required before spent fuel assemblies are transferred to long-term dry storage, final disposal at a repository or, in general, to other facilities where they are not easily accessible [2].

The majority of plutonium safeguarded by the IAEA is contained in spent nuclear fuel from light water reactors (LWRs). The LWR fuel assemblies are safeguarded as items, where absence of diversion is only confirmed when all items are accounted for after their integrity is verified. All nuclear material in LWR fuel assemblies used to remain in the same items during the whole irradiation lifetime of the fuel assemblies. However, since the 1980's, most LWR operators can replace leaking rods during planned refuelling outages and as a result, a small population of assemblies has rods stripped out or replaced [5]. Several attempts have been made by the IAEA and its Member States to develop technologies to detect diversions of pins from a spent fuel assembly and to determine whether pins have gone missing or have been replaced with dummy or fresh fuel pins. This mode of verification is known as partial defect detection [1]. The IAEA partial defect test addresses a diversion scenario where irradiated pins are

extracted from the fuel assembly or the pins are replaced with un-irradiated material, and no subsequent irradiation after the fuel rod substitution is envisaged. The current policy of the IAEA is to carry out a partial defect test on all easily dismountable spent fuel that is being transitioned to storage where re-verification would be impossible or difficult, such as in dry storage casks, or repositories [4].

The unit of special nuclear material (SNM) in a reactor is a nuclear fuel assembly made up of an array of fuel rods. For example, a four-loop pressurized water reactor (PWR) Westinghouse reactor core has 193 fuel assemblies, a third of which is replaced approximately every 12-18 months depending on the reactor design and operating history [6]. The instruments currently approved and in use for the partial defect testing of spent fuel for verification before transfer to dry storage are the fork detector (FDET), and the digital Cerenkov viewing device (DCVD) [7-8]. For these devices, the performance criteria for verifying the integrity of a spent fuel assembly means detecting a diversion of 50% of the material in an assembly with high confidence (90%) [5]. The DCVD is less accurate in measuring fuel with long cooling times, low burnup, or in dirty pool conditions [1]. The DCVD also cannot detect a single replaced fuel rod and is limited in scenarios in which random pins are missing since adjacent fuel pins can cause the device to register a false negative [1] [7]. FDET measurements use both the passive neutron and gamma emissions from the spent fuel assembly to characterize it and cannot be employed to independently verify pin diversion [8]. FDET relies upon the facility operator's declared data to conduct verification of spent fuel assemblies before the fuel is transferred to dry storage casks [7]. According to the IAEA, a major weakness of both the DCVD and FDET is that the detection probability is insignificant for carefully designed low-level diversions of a few fuel rods in each fuel assembly within a large population [5].

The IAEA in conjunction with some Member State Support Programs is presently supporting the development of a Passive Gamma Emission Tomography (PGET) system for partial and bias defect detection in spent fuel [7-8]. This technique has been demonstrated to be capable of resolving individual fuel pins in smaller fuel assemblies. It is envisioned that fast neutron emission tomography could be used in the same situations for larger fuel assemblies where gamma emission tomography would have difficulty resolving individual pins towards the center of the assembly. The neutron tomography system could be built into a facility – such as one handling fuel before sending it to a repository – or could be built into a cask-like container that could be housed at each facility or shipped to various sites.

The objective of the work described in this paper is to develop a new passive NDA capability for detecting the diversion of single fuel pins (rods) from nuclear spent fuel assemblies using neutron emission tomography before the fuel is moved to difficult to access storage. The results of the tomographic measurements are correlated to the measured neutron flux originating from each fuel pin within a square or hexagonal-lattice fuel assembly, and an image of the cross section of the assembly is generated. This pin-by-pin accounting is predicted to provide a robust check on the integrity of a fuel assembly against pin removals or substitutions prior to transfer to difficult to access storage.

2. Overview and System Concept

The intent of the present work is to develop the capability to perform fast neutron emission tomography of spent nuclear fuel. In this way, the integrity of fuel assemblies can be verified using the measured neutron emission rate from each fuel pin in the assemblies.

Most readers are familiar with the notion, if not the details, of computed tomography (CT) from medical physics where x-ray CT has been commonplace for decades. Similarly, emission tomography such as positron emission tomography (PET) and single photon emission computed tomography (SPECT) see wide diagnostic use. In each form of CT, projection data from many angles are used to reconstruct cross-sectional images of patients for diagnostic purposes. The crucial elements of this process are that measured data divide the object (patient) into "lines of response," and multiple views through the object are mathematically combined to estimate an image. Here, a "line of response" refers to a path through the patient (or other object) along which an observable (such as activity) can be integrated. For passive neutron imaging, collimation is used to isolate such paths, or lines of response, through the fuel assembly, and neutron counts in a detector correspond to an integral of neutron activity along the corresponding path. Fast neutron tomography having the desired resolution is possible provided each line of response sufficiently isolates a path through the object, the object is sampled with a sufficient number of lines of response, and there are a sufficient number of views through the object to invert

measured data to form an image. Previously, ORNL demonstrated the ability to perform fast neutron emission tomography of small arrays of fresh plutonium mixed oxide rods [9].

Unfortunately, performing fast-neutron imaging is challenging for the very reason that it is desirable, namely, that fast neutrons penetrate a good deal of shielding. As a result, they are difficult to collimate and measure with fine spatial resolution. For spent fuel, additional challenges stem from the modest neutron source strength and the overwhelming gamma-ray emissions. In general, attributes that maximize one desirable characteristic are in conflict with other desirable characteristics. The extreme gamma dose rates require a collimator construction that manages the gamma dose on detectors and detectors that are exceptionally gamma blind. While polyethylene or borated polyethylene are suitable materials for the collimation of fast neutrons, they do little to reduce gamma ray dose rates. Typically, the most gamma blind detectors function via neutron capture reactions that require neutron moderation and a corresponding detector size to achieve this. The modest neutron source strength of spent fuel prescribes efficient use of the available neutrons, such as by placing detector close to the fuel, but the need to manage dose rates, have effective collimation, and use moderated (larger) detectors all prescribe the opposite. Efficiency also prescribes measuring all lines of response simultaneously, but removing material from the collimator for additional slits reduces the effectiveness of the remaining slits. Despite these challenges, the use of a novel collimator concept appears to make it possible to construct an imager having sufficient resolution to identify individual fuel pins while also keeping the imager sufficiently compact, efficient, and radiation resistant to be practical.

In the remainder of this section, example lines of response will be shown for a single collimator slit, the novel “modified parallel slit collimator” will be introduced, and the neutron source term per fuel rod will be estimated.

2.1. Example Lines of Response

Tomographic imaging depends on isolating lines of response through an object. For neutron emission tomography, that means that the neutron counts that are recorded in each detector correspond primarily to those originating along a known path through the object. These lines of response are achieved via collimation. To illustrate the concept of a line of response, a series of simulations were performed using a collimator consisting of an annulus of material with a single 3 mm wide slit cut in it. A schematic diagram of this geometry is shown in Fig. 1 (a). MCNP6 Simulations were performed with a ^{244}Cm point source placed at the 17^2 locations corresponding to a grid separated by the pin pitch of a 17×17 PWR fuel assembly (however, note that no assembly was present in the simulations.) For each simulation, the neutron counts were tallied at the exit of the slit via the FMESH card with the F4 tally for calculating neutron flux through a cell. The resulting image in Fig 1. (b) shows the neutron counts associated with each source location for a collimator thickness of 15 cm. In this image, there is an identifiable path through the inspection volume that contributes more counts, but significant contributions remain from all the source positions. Similarly, Fig. 1. (c) shows the counts associated with each source location for a collimator thickness of 30 cm. Here, almost all response is limited to a particular path across the inspection volume, but the larger collimator thickness reduces the total intensity.

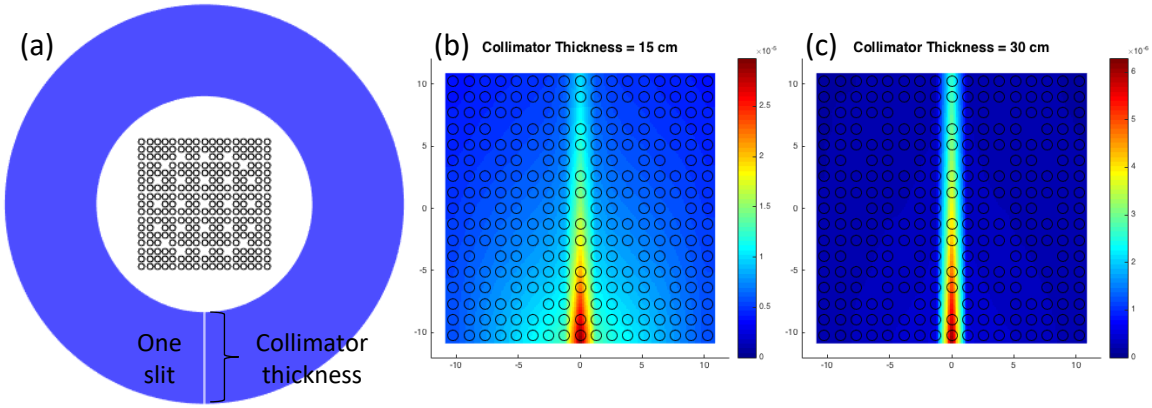

Figure 1: Example lines of response for a detector counting neutrons that exit a single 3 mm wide collimator slit, shown (a) as a schematic diagram. The results of a ^{244}Cm point source simulated at each assumed fuel pin location are shown (b) for a 15 cm thick collimator and (c) for a 30 cm thick collimator.

2.2. The Modified Parallel Slit Collimator

The intent of the present work is to make a functional equivalent to a parallel slit collimator that can be used for large detector pixels in close proximity to the fuel. To reconstruct with resolution sufficient to identify individual fuel pins, it is desirable to oversample each fuel pin approximately three times giving, for a conventional parallel slit collimator, a total of about 100 slits spaced across 35 cm. It is recognized that a conventional parallel slit collimator (due to the required detector element size or the efficiency of the collimator) can only work by reducing the number of slits and scanning the apparatus to achieve the required resolution. While this solution is acceptable for the more numerous gamma rays, an increase of an order of magnitude (or more) in measurement time due to the necessity to scan would be unacceptable for neutrons. Instead, the required spacing between slits (and detector elements) is achieved by rotating the position of each slit through a known angle so that the detectors around the outside of the collimator annulus are equally spaced. In this way, the essential function of the collimator is enabled and correspondence to the parallel slit collimator is maintained, that is, isolating lines of response along particular chords across the central volume of the annulus.

To illustrate, imagine a parallel slit collimator that is part of the annulus of shielding. In the example shown in Fig. 2 (a), 20 slits are shown for ease of viewing. These slits are spaced too closely to modulate neutrons effectively, and in addition, this geometry would require small (mm scale) neutron detectors. Instead, the detectors can be moved farther apart by rotating each slit through a known angle to place the detectors at equiangular points around the outside of the collimator circle, as shown in Fig. 2 (e). Now, each slit is looking at the same line of response as it originally was, but for a different rotation of the object. For tomography, measurements will be made from angles spaced around $360°$, so an equivalent set of views will be acquired for the rotated slits as for the original ones.

An advantage of this collimator design is that the fuel and detectors can remain stationary, and only the collimator need rotate. As a result, fuel-detector positioning does not have to be made very precisely provided there is no relative motion during the measurement. Note that the proximity to the fuel dictates that the detectors need to tolerate substantial radiation fields.

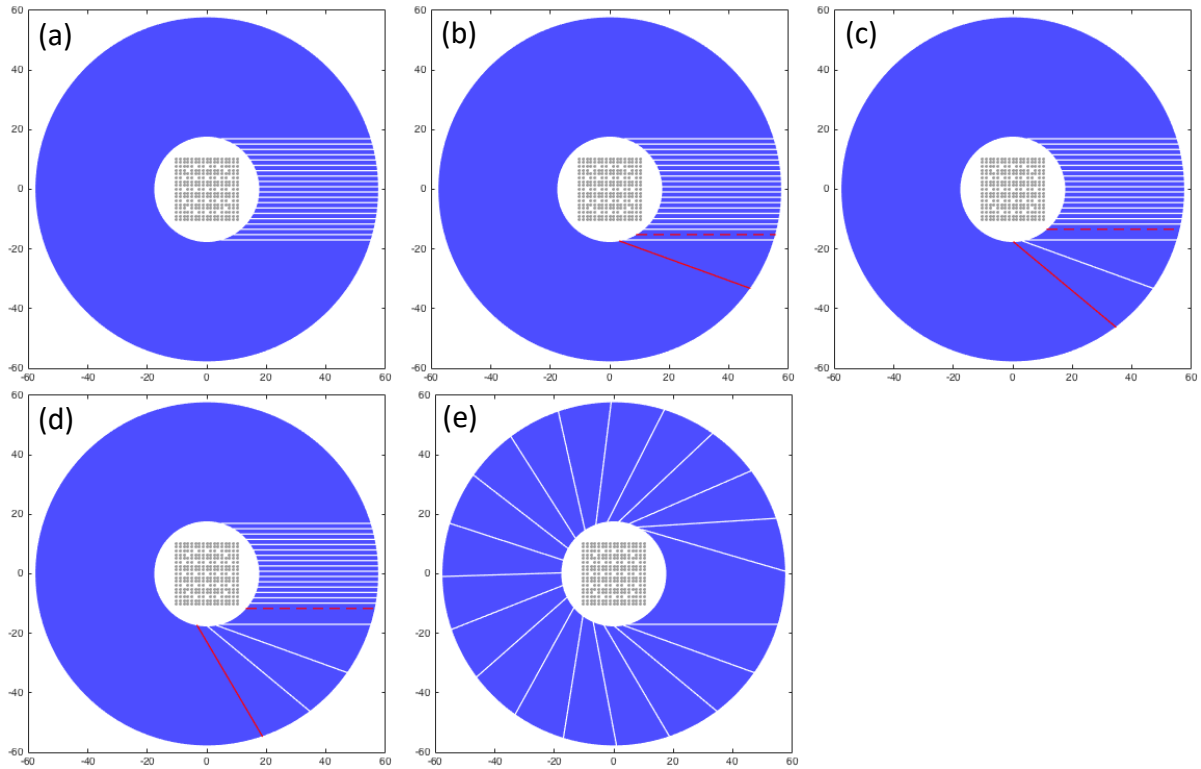

Figure 2: The modified parallel slit collimator is equivalent to the parallel slit collimator shown in (a). Then, in (b)-(d), each slit is rotated from the dashed to the solid red line so that after rotation, the resulting slits are (e) spaced equally around the circle. Each slit still inspects the same chord of the inspection volume.

2.3. The Neutron Source Term

Neutron emission from spent nuclear fuel is dominated by the spontaneous fission of ^{244}Cm, which has a half-life of 18.2 years and a neutron production rate of 1.64×10^{7} neutrons s^{-1} $gram^{-1}$ [10]. A plot of the neutron rate (per meter per fuel rod) from spontaneous fission of ^{244}Cm in spent fuel having 3% initial enrichment, 2 years of cooling, and the prescribed exposure is shown in Fig. 3 [11]. Note that for most commercial fuels the source strength per meter of fuel rod will exceed 10^{5} n/s. Note also that this emission rate is many orders of magnitude lower than the gamma ray emission rate.

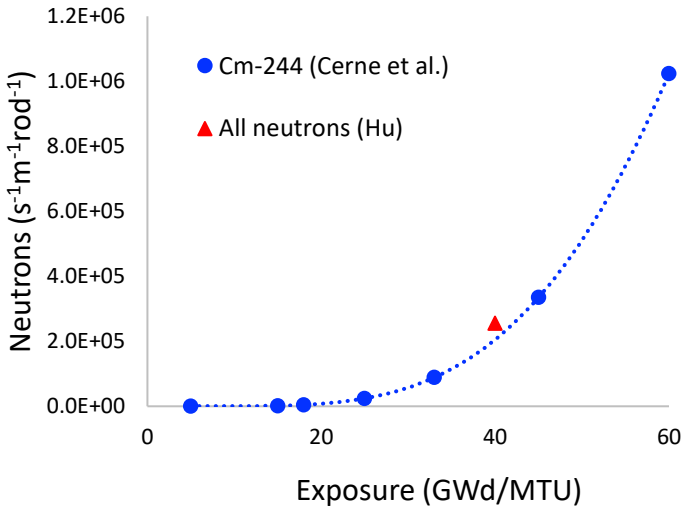

Figure 3: Neutron rate per fuel rod due to Cm-244 as a function of exposure within an average commercial PWR (shown for 3% initial enrichment and 2-year cooling time) [13].

3. The Baseline Imager Design

At the present stage of development, a baseline design for the fast neutron tomographic imager has been identified. The baseline design was driven by the need to have:

- The neutron detector (due to its inherent properties and shielding by the collimator) sufficiently gamma-blind so that it can operate in close (50-60 cm) proximity to the spent fuel.
- The combination of the collimator and detector sufficiently able to isolate lines of response through the assembly to enable resolving individual fuel pins.
- The combination of the collimator and detector have sufficient efficiency to measure most assemblies in minutes.
- The combination of the collimator and detector is sufficiently compact and robust to ship and use in an operational environment.

The baseline design consists of an annular collimator that fits around a spent fuel assembly, as shown in Fig. 4. The innermost 10 cm of the collimator is constructed of stainless steel (shown in green) for gamma ray shielding and structural integrity. Surrounding the stainless steel, there is a further 35 cm of collimator constructed from borated polyethylene (shown in yellow). The collimator has one hundred 3-mm-wide slits in it, each terminating on a detector (shown in gray). The 3-mm width was chosen because it is approximately the same as the slit spacing, so a larger slit width will be sampling some of the same activity as the neighboring slits. Each detector is wedge-shaped in cross section and has an active length of 1 m; it is composed of a high-density polyethylene (HDPE) moderator with 23 boron straws embedded in the moderator. There is an additional 5 cm of borated polyethylene shielding on the outside of the detectors.

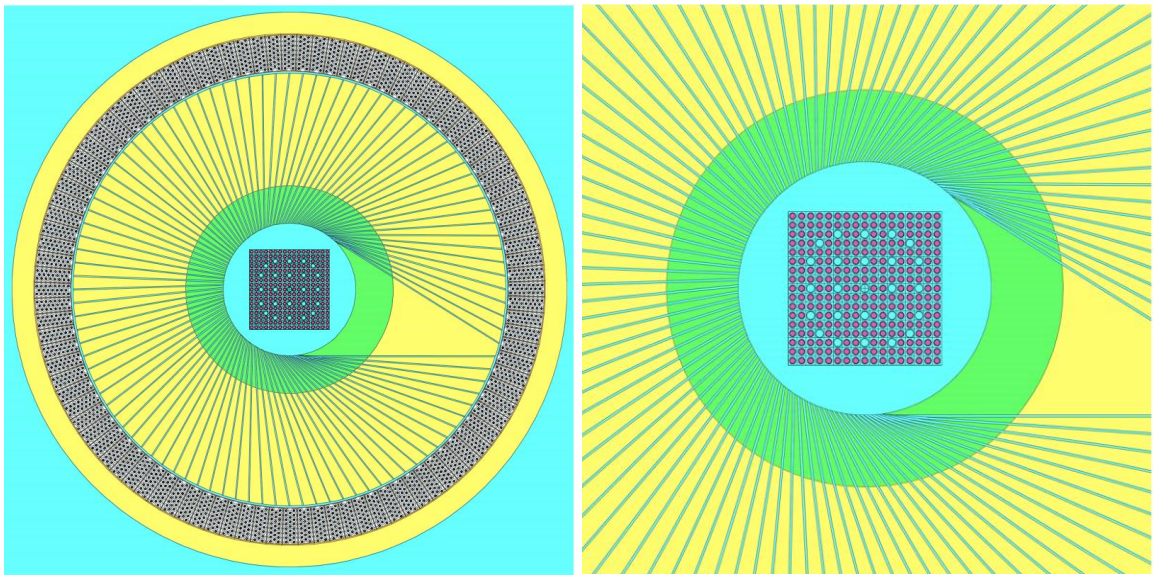

Figure 4: 2D view of the collimator: stainless steel (green), borated poly (yellow), and neutron detectors around.

Once the baseline design is determined, aspects of the design can be varied in order to further optimize it. In the remainder of this section, the detectors will be described, dose rate calculations will be described to identify configurations consistent with the capability of the detectors, signal to noise estimates will be described to identify a metric for identifying better imager configurations, and an example image reconstruction will be performed to identify that the imager response has sufficient resolution to resolve individual fuel pins.

3.1. The Detectors

Based on the geometry of the collimator, the imager requires 100 detectors (one at the outer radius of each collimator slit). Each detector is roughly wedge-shaped and approximately 1 m tall to intercept a reasonable fraction of the neutrons from the fuel assembly. The ideal detector for such an application would be perfectly gamma blind but highly efficient to fast neutrons. In choosing a commercially-available solution, ^{10}B straws were found to be the best combination of gamma blindness, efficiency, and cost per volume instrumented. The ^{10}B straws in this project are manufactured by Proportional Technologies, Inc. (PTI). ^{10}B tubes or straws rely on thermal neutron capture, and thus require moderation of the fast neutrons. By incorporating boron in the collimator and placing a Cd thermal-neutron filter between the collimator and detector, the imager still responds primarily to fast neutrons.

For this application, it was desirable to maximize neutron efficiency while minimizing gamma-ray efficiency. In practice, minimizing gamma-ray efficiency corresponds to minimizing the number of boron straw detectors per readout channel, thereby minimizing gamma-ray pileup. To investigate the most favorable configurations of boron straws, the efficiency was calculated as a function of $^{10}B_4C$ coating thickness and the straw spacing in a high-density polyethylene matrix. When calculating the efficiency of the boron straws, the overall detection efficiency is the product of the absorption fraction, the wall escape efficiency (WEE), and the threshold efficiency (TE). The absorption fraction is obtained from simulation (MCNP). The wall escape efficiency is the fraction of reaction products that escape the $^{10}B_4C$ coating, and enter the gas, where they can be counted. This number is a function of the $^{10}B_4C$ coating thickness, T, (in μm). The threshold efficiency is the fraction of events counted above the discriminator threshold. For the straw detectors, this has been found to be around 0.95.

An image of the various wedge detector geometries simulated are shown in Fig. 5; the results from the efficiency studies as a function of boron carbide thickness is shown in Fig. 6. The option with a coating thickness of 1.4 μm and a straw pitch of 1.2 cm yielding 23 straws per detector for a total of 2300 straws was chosen because it provided 97.5% the efficiency of the most efficient configuration while using the least number of straws, thus making it more economical and less gamma sensitive.

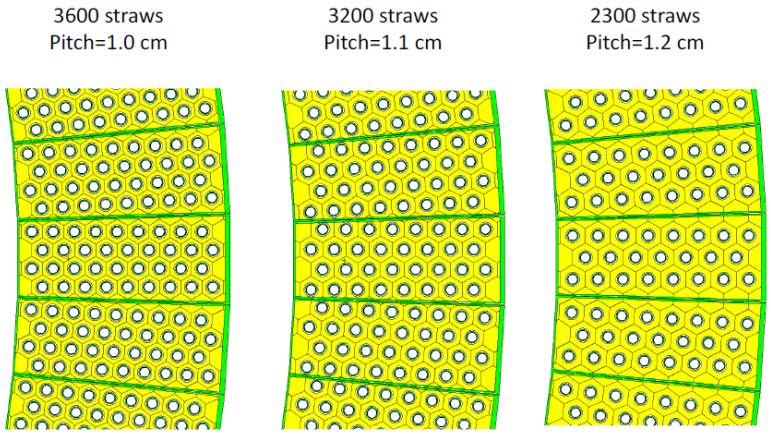

Figure 5: Various wedge and straw geometries simulated by PTI.

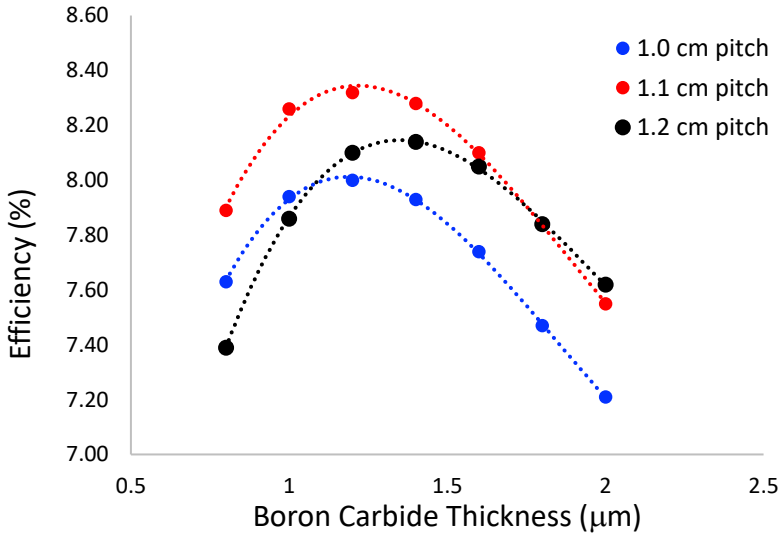

Figure 6: Efficiency as a function of boron carbide coating thickness for the four different straw geometries simulated by PTI.

3.2. Dose Rates

For the gamma calculations, a 17 x 17 PWR fuel assembly with an exposure of 48 GWd/MTU and a cooling time of 1 year was simulated to estimate the dose to which the detectors may be exposed. The gamma source intensity after 1 year of cooling time was 4.03×10^{16} photons/sec. The MCNP F6 tally (in the unit of MeV/g) was used and conversion factors were used to convert from MeV/g to rad to Roentgen. A 3D configuration of the collimator and neutron detectors around a typical fuel assembly is shown in Fig. 7. The boron straw detectors are thought to be robust to radiation fields up to 1000 R/hr when instrumented on a straw-by-straw basis.

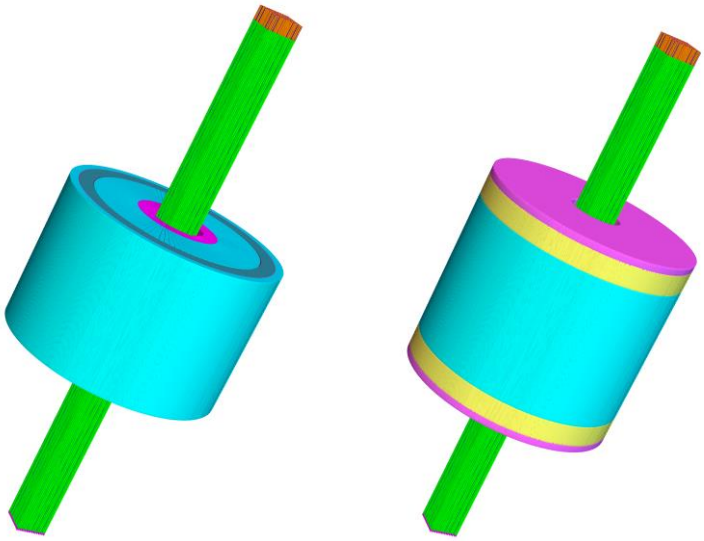

Figure 7: 3D configuration of the collimator and neutron detectors around a typical fuel assembly (green). The imager is shown (left) without and (right) with stainless steel (pink) and borated polyethylene shielding (yellow) at the top and bottom of the imager to shield from the fuel above and below.

Gamma simulations were performed to estimate the amount of shielding that would be needed at the top and bottom of the imager that would otherwise be directly visible to the spent fuel assembly as seen in Fig. 7 on the left. The purpose of the simulations was to determine a composite (borated polyethylene and stainless steel) shield sufficient to minimize the contribution of the fuel assembly outside the active imaging region. For this purpose, the minimum thickness of stainless steel to bring the dose at the detectors down to a reasonable value was found to be 10cm. Likewise, the thickness of the borated polyethylene for the neutron shielding on the top and bottom of the imager was calculated by using an absorption reaction rate tally in the ^{10}B straws to estimate the reaction rates in the boron straw detectors. The minimum thickness of borated polyethylene that would shield the detectors from the neutrons originating from either end of the fuel assembly was found to be 20cm.

Once suitable shielding on the top and bottom of the collimator was identified, the properties of the collimator itself were investigated. For this purpose, various combinations of stainless steel and polyethylene have been investigated as shown in Table 1.

Stainless Steel (cm)	Borated Polyethylene (cm)	Total Collimator Thickness (cm)
5	35	40
5	40	45
5	45	50
5	48	53
5	50	55
10	30	40
10	35	45
10	40	50
10	45	55

Table 1: Simulation case studies for the imager designed to fit into two different commercially available spent fuel casks. Also shown are the various combinations of stainless steel and polyethylene simulated.

For the case with 10cm stainless steel and 30cm borated poly, gamma dose rates for various collimator slits widths have been estimated. A slit width of 3mm was used to calculate the dose for all subsequent studies. The gamma dose rates at all 2,300 straw locations are shown in Fig. 8. Simulations showed that the highest gamma dose rates occur at detector 19, but the dose rates are still within the limits of what the straws can handle. The highest dose calculated in the straws is less than 500 R/hr, which is much lower than the 1000R/hr upper limit.

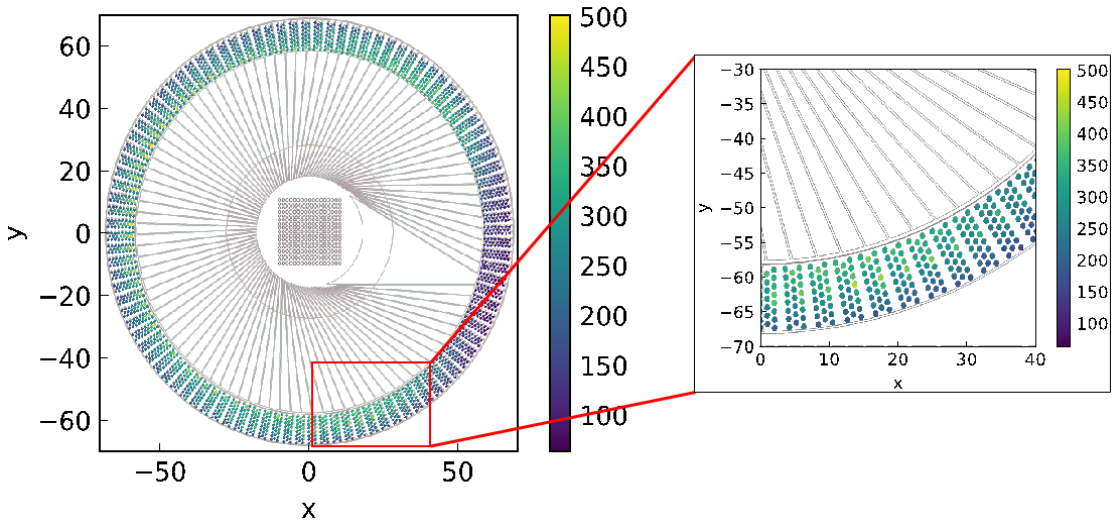

Figure 8: The gamma dose rate distribution for all 2300 detector locations for the case of 3mm slit widths

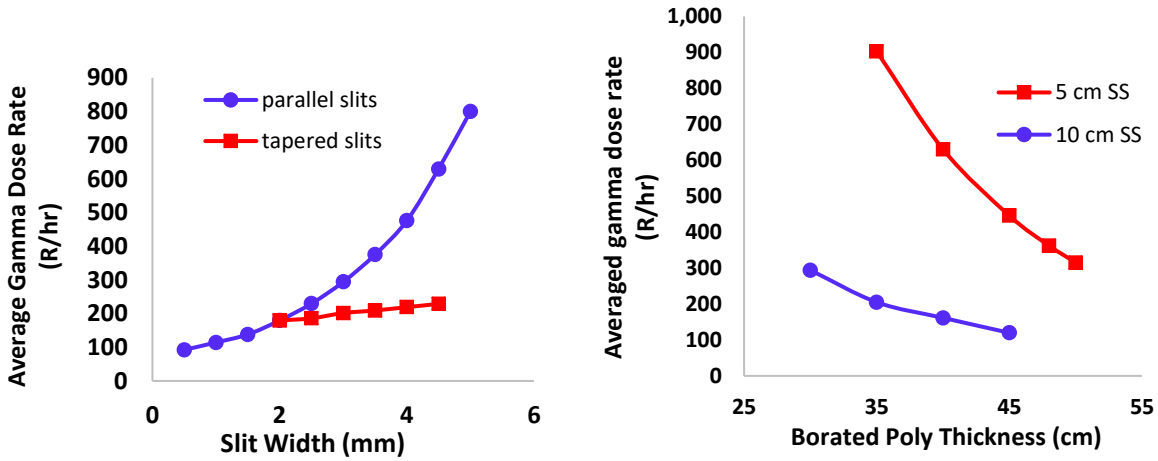

Figure 9: (Left) Gamma dose rates averaged over a total of 23 detectors in wedge 19 for parallel and tapered slits. (Right) Gamma dose rates averaged over detector 19 for 5 cm and 10 cm of stainless steel (SS) and varied thicknesses of borated polyethylene.

The dose rates at detector #19 when the slit widths are changed or tapered are shown in Fig. 9 on the left. The gamma dose rates increase exponentially as the slit width increases when parallel; however, when tapered, the dose rate increases at a much lower rate and is lower at larger slit widths. With a 3mm slit width, the gamma dose rates at detector #19 for a collimator consisting of 5 cm and 10 cm of stainless steel towards the center and various amounts of polyethylene are shown on the right in Fig. 9. These results show that gamma dose rates can be limited to a 200-300 R/hr by having the innermost 10 cm of the collimator constructed from stainless steel.

3.3. Imager Response and Signal to Noise

The various cases in Table 1 were simulated using MCNP6's F4m Tally function to generate a reaction rate for the neutrons interacting with ^{10}B in each of the 100 wedge-shaped detectors. This reaction rate when plotted as a function of detector number, is called the "point spread function." For each case, an isotropic ^{244}Cm source was simulated at the center of the cavity in air as shown in Fig. 10. The detectors are numbered clockwise from detector #1, which corresponds to the detector wedge facing the bottom tangent collimator slit.

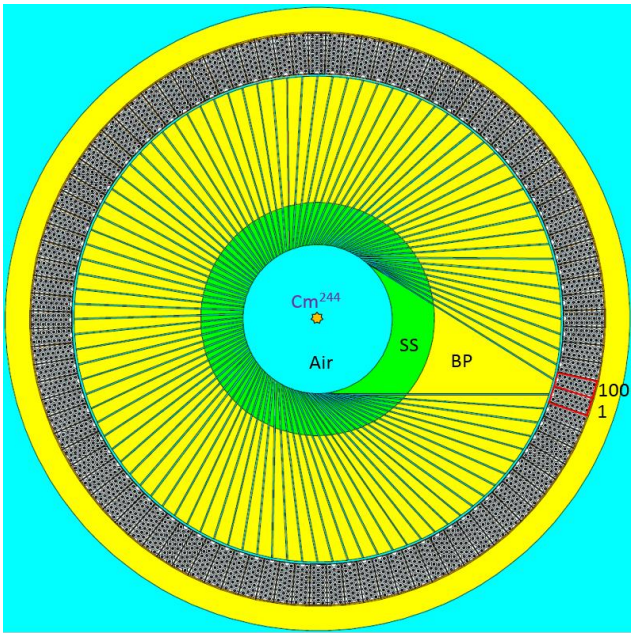

Figure 10: The MCNP geometry used to simulate the point spread functions. There are 100 slits in the collimator made up of stainless steel (SS), and borated polyethylene (BP). The nomenclature for numbering the wedges is also shown with the 1st and 100th wedges highlighted in red.

The point spread function for the case of 10 cm stainless steel and 35 cm borated polyethylene is shown in Fig. 11. Here, the peak at detector 50 is as expected for the position of the source. The design of the collimator is intended to maximize the signal (peak) and suppress the background (areas to the sides of the peak).

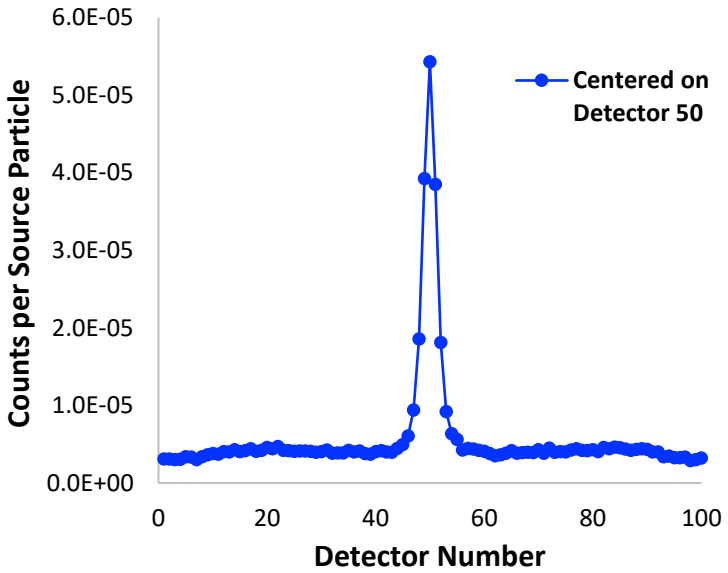

Figure 11: An example point spread function for the collimator having 10 cm (SS) and 35 cm borated polyethylene (BP).

When varying the dimensions of the collimator, as the thickness of borated polyethylene increases, the background counts in the point spread function decreases. However, the peak counts decrease as well. With a basic understanding of the contribution of the different collimator components, signal to noise ratio (SNR) calculations of the nine potential designs were performed to identify an optimal combination. The SNR was calculated for each of the point spread functions above to a sample problem where a single pin in a sample 17 x 17 PWR fuel assembly is missing. Fig. 12 shows the geometry using 10 cm stainless steel and 35 cm borated polyethylene for which the reconstruction was attempted and SNR

calculated. In this fuel assembly simulation, the red circles represent fuel rods, white circles the empty channels, and the dark gray circle signifies the missing rod.

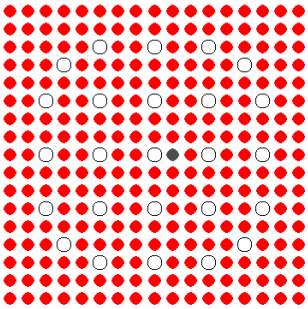

Figure 12: Assumed geometry of a 17 x 17 PWR fuel assembly used to calculate the SNR response of the full imager with 1 fuel pin missing (black)

Each pin in the assembly will have a unique contribution to the sinogram associated with it, which is calculated by summing the activities along a line. First, assuming all 264 pins are present, each point spread function was applied to a full assembly, and accounting for the fuel pin location, 264 sinograms were generated by summing up the activities in lines. The sinogram for the fuel assembly with the missing rods was found by subtracting the calculated sinogram from two pins located in the missing fuel pins' location from the calculated sinograms from 264 pins as seen in Fig. 13.

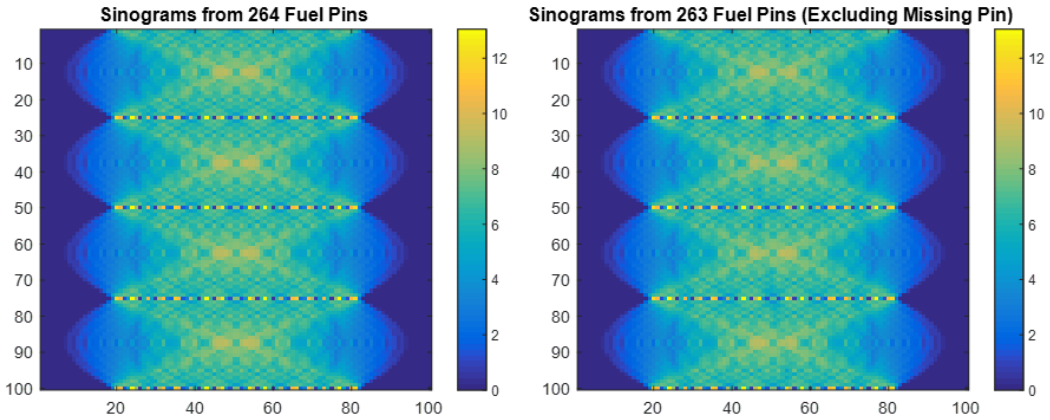

Figure 13: Sinograms as seen by 100 detectors for a full 17 x 17 PWR fuel assembly with 264 rods (left), and one with only 262 rods (right).

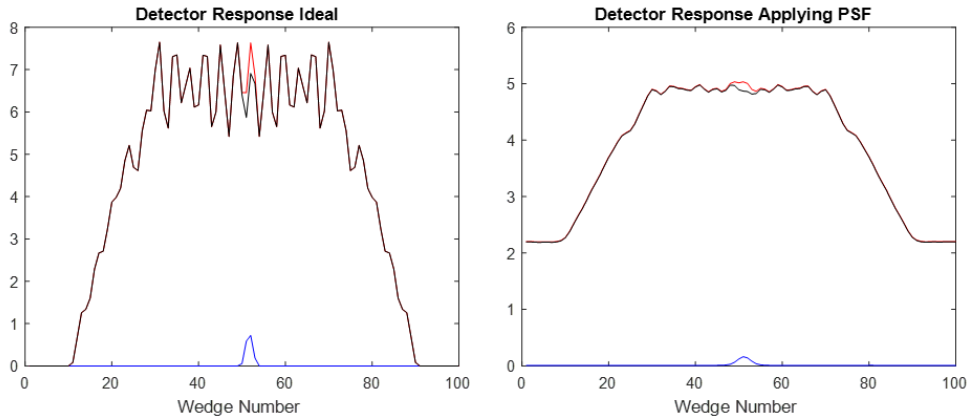

Figure 14: The ideal detector responses (left) and after applying a point spread function (PSF) to account for scatter and background (right) are shown here. The blue line is the expected signal from the missing rod if it were present in the fuel assembly. The red line is the signal from the missing rod plus the signal from the other 263 rods, and the black line is the signal from only the 263 rods.

From Fig. 14, we see that separating the expected signal from a missing pin from the signal from a full up assembly is non-trivial since the signal from the missing rod (red line) is barely above the signal from the 263 other rods. Fig. 15 shows the relative SNR values calculated for the cases in Table 1. This calculation assumes 2.55×10^5 n/s/m/fuel rod.

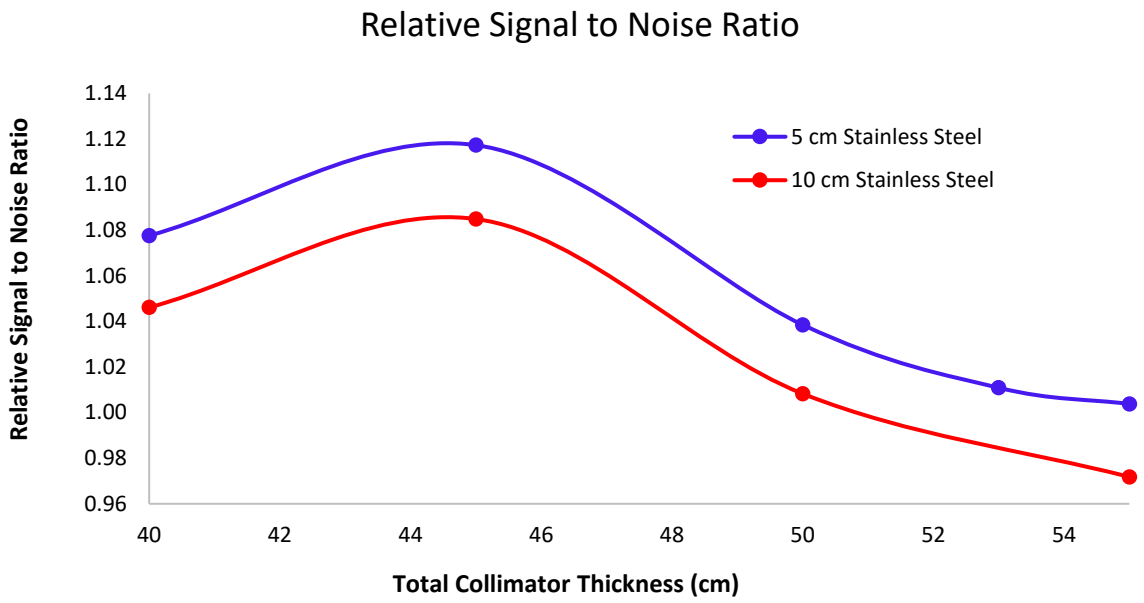

Figure 15: Signal to noise ratios are presented here for all 10 cases identified in Section 3.4.

Note that these SNR values are calculated for a 1 s measurement time. The SNR scales as a function of the square-root of time. From the SNR calculations, a first order approximation of what the optimal thickness of collimator is for a 3-mm slit width due to the peak at a total thickness of 45cm. It should be noted that this analysis does not account for the effects of scatter and self-attenuation that emitted neutrons would experience within the spent fuel assembly. This is expected to reduce the signal to noise further, and would increase the measurement time.

While the present work has achieved an incomplete understanding of the behaviour of a fast neutron imager, the predicted resolution and efficiency are capable of resolving individual fuel pins or vacancies in an assembly. A reconstructed image for a geometry with one missing fuel pin is shown in Fig. 16. The simulated data for this image was generated simply by applying the point spread function to a forward projection of an idealized 17 x 17 fuel assembly with a single pin missing without accounting for scattering or self-attenuation. The image was reconstructed using maximum likelihood expectation maximization that included knowledge of the point spread function in Fig. 11. Fig. 16 shows preliminary results that will change when factors such as self-attenuation and scattering are accounted for. In the reconstruction, the missing pin is clearly visible, indicating that there are sufficient counts and resolution, which shows that this method is promising.

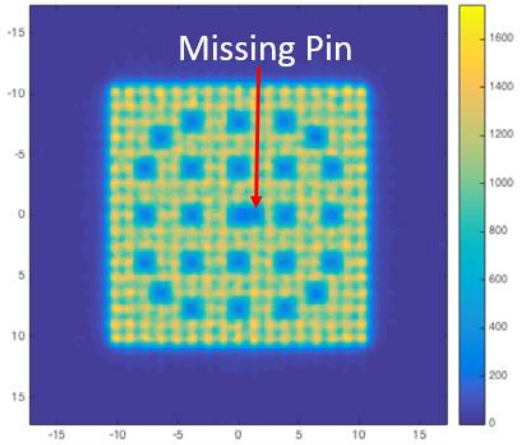

Figure 16: Reconstructed image with one missing fuel pin.

4. Future Work

Although a preliminary design basis for the imager has been identified, more parametric studies need to be implemented to converge on a final imager design. One of the parameters currently being optimized is the collimator slit width for various borated poly and stainless steel combinations. In conjunction, the use of tapered slits will be investigated to see if the efficiency and resolution can be optimized. First order simulations show that the detector concept works and that a pin-by-pin reconstruction can be achieved. Future simulations will include the effects of neutron scattering within the fuel assembly and self-attenuation to see how this affects the image reconstruction. Revised SNR values will be calculated once the additional parameters have been incorporated, and a final design will be decided upon. Additionally, once the PTI detectors are procured, a thorough performance evaluation under a high gamma environment will be conducted.

5. Conclusions

ORNL has utilized existing expertise in fast neutron imaging to demonstrate to first order a new capability to detect diversion of fuel pins from spent nuclear fuel assemblies based on passive fast neutron emission tomography for international safeguards applications. Simulations thus far show that this has the potential to detect single fuel pin diversion. The Monte Carlo simulations performed showed that it is possible to isolate activity along lines of response using emission tomography. The line of response simulations helped identify a minimum collimator thickness consisting of borated polyethylene and stainless steel, and gamma measurements helped identify the minimum amount of stainless steel shielding necessary above and below the detection system to shield the detectors from the length of the fuel assembly. Commercially available ^{10}B straws that can withstand the high gamma rate environments that the imager will be subject to were identified as the best detectors for this application. Results show that the detector concept identified in this paper works, and that a pin-by-pin image reconstruction of a 17 x 17 PWR fuel assembly can be achieved, and a missing fuel pin can be discerned. The first order simulations accounting for detector efficiency show that a good SNR value can be achieved in a relatively quick time (25sec). Once the scattering of neutrons within the fuel assembly is accounted for, this measurement time will increase. A final imager design will be decided upon once a few remaining parameters are optimized based on the notional imager design described in this paper.

6. Acknowledgements

This work was done under the support of the U.S. Department of Energy, Office of Defense Nuclear Nonproliferation R&D in the National Nuclear Security Administration.

7. References

[1] Ham, Y., et al. "Partial defect verification of spent fuel assemblies by PDET: Principle and Field Testing in Interim Spent Fuel Storage Facility (CLAB) in Sweden", *Advancements in Nuclear Instrumentation Measurement Methods and their Applications (ANIMMA), 2015 4th International Conference*, IEEE, 2015.

[2] Hildingsson, Lars, and Camilla Andersson. "Safeguards Aspects Regarding a Geological Repository in Sweden", IAEA Symposium on International Safeguards Vienna, 2014.

[3] IAEA, Department of Safeguards, Model Integrated Safeguards Approach for a Geological Repository, 03-SG-PR-1306, IAEA, 2011-02-10.

[4] Gauld, I.C., et al. “In-field performance testing of the fork detector for quantitative spent fuel verification”, in ESARDA Symposium 2015, Manchester, UK, 2015.

[5] Lebrun A., Zykov S. “Status of NDA techniques in use for IAEA verification of light water reactor spent fuel”, Proceedings of 55th INMM Annual Meeting, 2014.

[6] “Pressurized Water Reactor (PWR) Systems”, Reactor Concepts Manual, USNRC Technical Training Center.

[7] Honkamaa, Tapani, et al., "A Prototype for passive gamma emission tomography," IAEA Safeguards Symposium, 2014.

[8] “Safeguards Techniques and Equipment: 2011 Edition”, IAEA Verification Series No. 1 (Rev. 2), Vienna, 2011.

[9] Hausladen, P. A., Matthew A. Blackston, and R. J. Newby. "Demonstration of Emitted-Neutron Computed Tomography to Quantify Nuclear Materials." ORNL/TM 357 (2011).

[10] Fast, James E., et al. *Spent Nuclear Fuel Measurements*. No. PNNL-23561. Pacific Northwest National Laboratory (PNNL), Richland, WA (US), 2014.

[11] S. P. Cerne, O. W. Hermann, R. M. Westfall, “Reactivity and Isotopic Composition of Spent PWR Fuel as a Function of Initial Enrichment, Burnup, and Cooling Time”, Oak Ridge National Laboratory Report ORNL/CSD/TM-244 (1987).

PNNL-SA-125791

Hybrid Gamma Emission Tomography for the Verification of Unirradiated Fuel: A Viability Study

EA Miller[1], LE Smith[1], Vladimir Mozin[2], RS Wittman[1], LW Campbell[1], MA Zalavadia[1], NS Deshmukh[1]

[1]Pacific Northwest National Laboratory
[2]Lawrence Livermore National Laboratory

Abstract:

Current International Atomic Energy Agency (IAEA) methodologies for the verification of fresh low-enriched uranium (LEU) and mixed oxide (MOX) fuel assemblies are volume-averaging methods that lack sensitivity to individual pins. Further, as unirradiated fuel assemblies become more and more complex (e.g., heavy gadolinium loading, high degrees of axial and radial variation in fissile concentration), the accuracy of current IAEA instruments degrades and measurement time increases. Particularly in light of the fact that no special tooling is required to remove individual pins from modern fuel assemblies, new capabilities for the verification of unirradiated (i.e., fresh LEU and MOX) assemblies are needed to ensure that fissile material has not been diverted. Passive gamma emission tomography has demonstrated potential to provide pin-level verification of spent fuel, but gamma-ray emission rates from unirradiated fuel emissions are significantly lower, precluding purely passive tomography methods. The work presented here introduces the concept of Hybrid Gamma Emission Tomography (HGET) for verification of unirradiated fuels, in which a neutron source is used to actively interrogate the fuel assembly and the resulting gamma-ray emissions are imaged using tomographic methods to provide pin-level verification of fissile material concentration. This paper describes the status of a viability study on the HGET concept, including: envisioned use-case scenarios and corresponding definitions of fuel assemblies; modeling framework based on Monte Carlo and deterministic transport methods, and its validation; quantitative assessment of candidate HGET signatures with a focus on prompt fission gamma rays and delayed fission gamma rays; a nominal HGETv1 instrument design; candidate HGET-specific tomographic reconstruction methods that fully incorporate declared information; and examples of simulation-based predictions of HGET performance.

Keywords: safeguards; fuel verification; gamma emission tomography

1. Introduction

Current IAEA methodologies for the verification of fresh LEU assemblies at fuel fabrication facilities utilize active neutron interrogation with neutron coincidence counting; verification of fresh MOX fuel utilizes passive neutron coincidence counting with gamma-ray spectroscopy for Pu isotopics. These volume-averaging methods are not capable of individual-pin sensitivity and as fuel assemblies become more complex (e.g., heavy gadolinium loading, and axial variation in boiling water reactors [BWRs]), their accuracy degrades and measurement times increase. Particularly in light of the fact that no special tooling is required to remove individual pins from modern fuel assemblies, the IAEA needs new capabilities for the verification of unirradiated fuel assemblies that can provide high-precision fissile-mass quantification, ideally at the single-pin level. The IAEA has documented the need for new unirradiated-fuel verification tools in the IAEA Department of Safeguards Long-Term R&D Plan [1]. Other potential users of a new fuel verification tools include EURATOM, and State regulators.

PNNL-SA-125791

Passive gamma-ray emission tomography (GET) is a promising candidate for verification of item integrity in fuel assemblies because it has the potential to directly image the spatial distribution of the active fuel material, without the need for operator-declared information [2]. In this sense, it is an absolute, rather than comparative verification method. In addition, the relative intensity of gamma-ray signatures can be used to verify declared attributes on a pin-by-pin basis (e.g., burnup in irradiated fuels; uranium enrichment or plutonium isotopics in unirradiated fuels). The viability of GET for the detection of missing pins in irradiated fuels, where relatively intense, higher-energy gamma emissions are available, appears promising based on findings of a recent IAEA study [3] and ongoing testing of a prototype passive GET instrument by the IAEA.

For unirradiated fuels with relatively weak and lower-energy emissions, the ability to see interior pins with purely passive tomography is less clear. The use of active neutron interrogation to stimulate gamma-ray emission can provide additional signal intensity for emission tomography, here referred to as Hybrid Gamma Emission Tomography (HGET). There are several candidate signatures for hybrid (i.e., tomographic imaging of an active interrogation signature) assay of unirradiated fuels, including prompt capture gamma rays in the isotopes of interest (e.g., 1.28 MeV from ^{235}U); prompt fission gamma rays (continuum peaked at ~ 1 MeV); and delayed gamma rays from short-lived fission products (discrete lines generally from 1 to 7 MeV).

Each of the candidate signatures above has been studied previously, and sometimes in combination, for the assay of both irradiated and unirradiated fuels. For example, delayed-gamma methods have been studied for the direct assay of fissile isotopes in irradiated fuels [4, 5], but the delayed-gamma methods studied to date provide no spatial information about the origin of the signatures and therefore, localized neutron moderation effects and self-attenuation can produce biases in fissile isotope quantification. In addition, the high passive background in spent fuel forces the use of only the higher-energy (> 3 MeV) delayed-gamma signatures, while the most intense signatures are presented at lower energies. In unirradiated fuels, these more-intense, lower-energy delayed-gamma signatures are accessible, but information about their location of origin in the fuel assembly is needed.

To the authors' knowledge, no prior work has demonstrated the ability to provide spatial information about the origin of the candidate signatures and therefore, verify fuel characteristics at the pin level. In the HGET concept, it is postulated that the collection of these candidate signatures through a tomographic lens will support pin-by-pin verification of fissile materials in the assembly.

Here we describe an ongoing modeling-based viability study of the HGET concept. This paper discusses potential IAEA use cases and implementation approaches, a novel method for modeling instrument response that couples Monte Carlo and deterministic transport methods, candidate signatures, and a method for extracting fissile isotope concentrations on a pin-by-pin basis. Example results for pin-level verification of fissile isotope concentrations in MOX fuel assembly are presented. The paper concludes with a discussion of the ongoing and planned analyses that are needed to more fully assess the viability of the HGET concept for safeguards verification.

2. Potential Use Cases in International Safeguards

The use case for an HGET instrument by safeguards inspectorates is presumed to be consistent with how current IAEA instrumentation is used for the verification of unirradiated fuels. For fresh LEU fuel, the IAEA uses the Uranium Neutron Coincidence Collar (UNCL); for MOX fuel the Passive Neutron Coincidence Collar (PNCL). Both instruments use neutron coincidence signatures to verify the total uranium or plutonium in the assembly--additional information about each method can be found in [6], with IAEA's International Target Values (ITVs) for verification of unirradiated assemblies in [7].

For fresh LEU fuel, the UNCL is used to measure the mass density of ^{235}U at a given axial location of the assembly. It is assumed that the ^{235}U is the only fissile isotope in the assembly and therefore, that all induced fission comes from ^{235}U. This localized ^{235}U mass density is translated to total ^{235}U mass for the assembly using an active length measurement (e.g., gamma scanning). The ITV for determination of total ^{235}U mass in an LEU assembly is 4.5% (one-sigma relative), assuming relatively low gadolinium (Gd) content. Count times are not specified in the ITV document, but information provided by other sources indicate that

measurement times for UNCL, on fuels with relatively low Gd concentration, are approximately one hour to reach the desired statistical uncertainty. Systematic uncertainties for high-Gd assemblies can be 10 or more times higher.

For MOX fuel, the PNCL is used to measure the mass density, at a given axial location, of the Pu isotopes with appreciable spontaneous fission yields (^{240}Pu dominates). High-resolution gamma-ray spectroscopy on exterior pins of the assembly is then used to infer the linear density of total Pu. An active length measurement (e.g., gamma scanning) is employed to translate that value to total Pu for the assembly. The ITV for determination of total Pu mass in a MOX assembly is 3.2% (one-sigma relative). Count times are not specified in the ITV document, but information provided by other sources indicates that measurement times are typically on the order of 15 minutes.

The use cases and ITVs for UNCL and PNCL provide useful context for the HGET viability study, and are the basis for the assumptions that were adopted to guide the first phase of this study:

- Verification of unirradiated fuel will occur in an air environment and the operator will position the fuel assembly in such a way that the HGET collar will assay one or more vertical segments of the assembly. As with UNCL and PNCL, it is assumed that some form of active-length measurement will inform the translation from the HGET-measured ^{235}U and total Pu linear densities to a ^{235}U and total Pu assembly mass value. Note that the HGET gamma-spectrometer array, operating in purely passive mode, could provide an active-length measurement similar to what is performed today using a handheld gamma-ray detector. (This assumes that the operator moves the fuel assembly through the HGET collar.)
- Total measurement time for HGET verification of unirradiated fuel assemblies should be on the order of 1-2 hours. While today's measurements may be shorter in duration for many fuel types, the fact that HGET will provide pin-by-pin verification of fissile content encourages a broader window of assay-time acceptability for the first phase of the study.
- The physical dimensions and mass of HGET should be comparable to existing IAEA instruments: for example, the JCC-71 PNCL/UNCL instrument sold by Canberra weighs approximately 40 kg [8]. A maximum neutron moderator/reflector weight of 100 kg was enforced during the design study, on the logic that this represented a reasonable size for a mobile instrument deployed at a fuel fabrication or reactor facility.

3. MOX Fuel Assembly as Initial Case Study

While the HGET study is also investigating low-enriched uranium (LEU) fuels with and without burnable poisons, an initial use case was defined for a pressurized water reactor (PWR) assembly of 17x17 pins with mixed oxide (MOX) fuel. PWR fuel is at the more-challenging end of the continuum of fuel types under safeguards in terms of neutron and gamma-ray attenuation, due to its relatively dense pin-array geometry and overall large dimension. The age since separation for the reactor-grade Pu was assumed to be 5 years, an upper limit in terms of occupational health hazards (after about 5 years enough ^{241}Am has grown in to make handling difficult; this process has little impact on the amount of fissionable material for the HGET measurement), and the composition is shown in Table 1.

Generally speaking, the composition of MOX fuel pins varies with pin position. An IAEA technical report, provides Pu concentrations of each pin type in an example MOX assembly, as shown in Figure 1 [9]. Note that the overall Pu concentration varies from pin to pin but the relative Pu isotopics, as defined in Table 1 is consistent across all pins.

PNNL-SA-125791

		MOX	LEU
Atom	Isotope	Atom Fraction (X3)	Atom Fraction (X3)
U	234	5.20×10^{-5}	3.12×10^{-3}
U	235	6.81×10^{-4}	4.05×10^{-2}
U	238	9.39×10^{-1}	9.60×10^{-1}
Pu	238	1.36×10^{-3}	
Pu	239	3.21×10^{-2}	
Pu	240	1.52×10^{-2}	
Pu	241	7.06×10^{-3}	
Pu	242	4.21×10^{-3}	
O	16	2	2
	density (g/cc)	10.4538	10.4538

Table 1. Initial composition (before decay) of the fuel assembly definitions used in the HGET viability study (atom fractions displayed are 3x the total atom fraction, such that the U/Pu isotopes add to approximately 1).

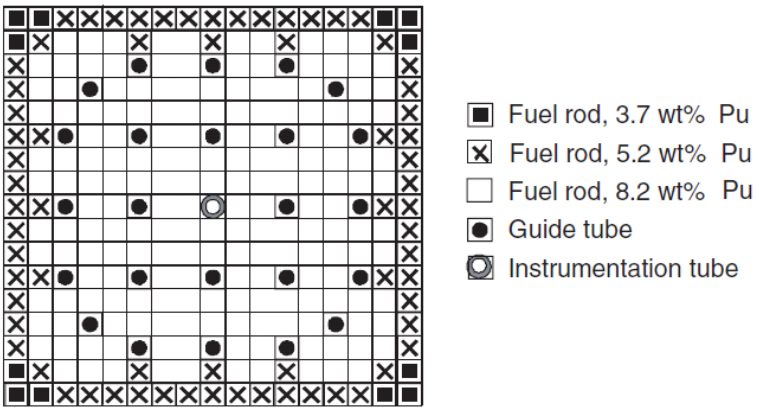

Figure 1. PWR MOX assembly design of the 17x17—24 type with assembly averaged plutonium concentration of 7.2 wt% Pu. (From [9])

4. Overview of HGET Modeling Methods

An overview of the HGET modeling methods is given in Figure 2 below. Neutron transport was performed using MCNP6 and the calculated fission rates in the fuel pins were used to generate the prompt- and delayed-gamma source terms. Those gamma-ray source terms were then used as input to a separate calculation for the transport of the photons out of the assembly and into the detector. Gamma-ray transport through a highly attenuating assembly can be prohibitively time-consuming with pure Monte Carlo methods. The gamma-ray transport was performed using a deterministic transport by the discrete-ordinates package Attila [10]. More detail on the HGET modeling method and validation can be found in [11].

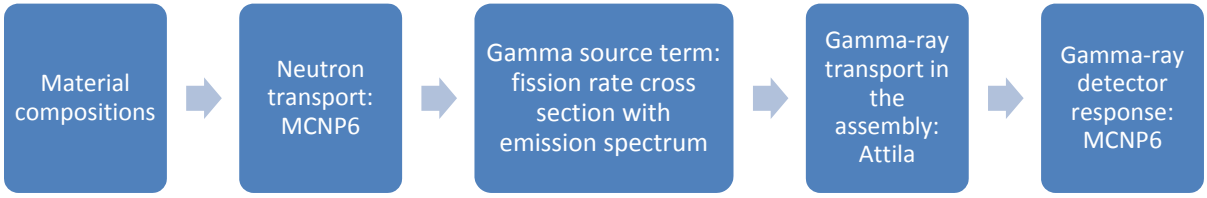

Figure 2. Schematic of HGET modeling approach for modeling neutron-induced gamma-ray signatures and detector response functions.

5. Candidate HGET Signatures

Gamma emission tomography is based on detecting gamma emissions selectively, sensitive to both their location and their angle of incidence. Detection of inner pins can be very difficult, since radiation from these pins must pass through a considerable distance of dense fuel. Gamma rays with energies of less than 500 keV have a very low probability of escaping from inner pins to the outside. Penetration increases with increasing energy to a broad maximum at around 3 MeV to 4 MeV, beyond which the pair production mechanism of absorption causes penetration to decrease. Isotopic specificity is also desirable; if a gamma-ray emission is uniquely tied to a given isotope (e.g., fissile isotope or fission product), it will likely be more useful in characterizing the fissile content of the assembly. Finally, methods based on excessively complex signatures may be difficult to implement, limiting their utility.

An order-of-magnitude comparison of typical spent-fuel assay signatures, to the candidate signatures for HGET assay of a nominal MOX fuel assembly is given in Table 2. The actively induced count rates were estimated using the neutron-gamma modeling methods described in the previous section, and the nominal HGETv1a design described later that employs a commercial, off-the-shelf deuterium-tritium (D-T) neutron generator producing approximately 10^8 n/s at 14.1 MeV.

Technique	Emission rate (γ/pin/cm/s)
Spent fuel, 1 year CT, ^{154}Eu 1274 keV	1 x 10^8
Spent fuel, 30 year CT, ^{137}Cs 662 keV	5 x 10^9
^{239}Pu 414 keV	5 x10^3
Prompt fission > 1000 keV	1 x10^4
Delayed gamma individual lines	< 2 x10^1
Delayed gamma at 1 s, > 1000 keV Delayed gamma at 1000s, > 1000 keV	4 x 10^2 5 x 10^3
Prompt capture gamma, U	Uncertain, ~1 x10^2
Prompt capture gamma, Pu	<1 x10^3
Activation gammas > 500 keV	Uncertain, small

Table 2. Order-of-magnitude comparison of signal intensities from passive tomography of PWR spent fuel variants (top three entries) and HGET for unirradiated MOX fuel. HGET signatures highlighted in gray are the most promising in terms of absolute emission intensity.

Clear from Table 2 is that the passive Pu emissions from unirradiated MOX fuel are many orders of magnitude less than from spent fuel, and have low penetrating power. The actively induced signatures offer

somewhat higher intensities and importantly, their higher energies offer the promise of greater penetrability through the fuel assembly. Delayed gamma signatures are more complex, due to their time dependence, and no individual lines are observed with sufficiently high emission intensity for tomography. It is possible that a delayed gamma-ray signature summed over broad energy windows could be imaged – but fissile-isotope specificity would be lost. The assay of other activation products to infer fuel composition offers little promise both because of low intensity and limited direct connection to the fissile material that is the focus of IAEA verification. Given that no isotope-specific signatures are high enough in intensity for direct fissile isotope assay, the most useful signature for verifying the integrity of fuel assemblies and total fissile content appears to be the prompt fission gamma rays, possibly in combination with the delayed gamma rays. The relatively high production of these signatures at energies above 1 MeV is key, although still four orders of magnitude below emission rates typical of spent fuel.

This large gap in emission intensity points to the need for the development of HGET-specific tomographic designs and methods, for example neutron moderation and reflector designs that are efficient for inducing fission in the assembly, detector and collimator designs that balance gamma-ray collection efficiency with spatial resolution for imaging, and tomographic reconstruction methods that wring as much information as possible from the collected data by relying heavily on the declared, *a priori* information about the pin assembly geometry. These topics are discussed in the sections below.

6. Nominal HGET Design

A wide range of source/moderator/reflector designs and materials (e.g., poly, graphite, hydrided DU) were considered in the early stages of the HGET v1 design study. Both a D-D and a D-T neutron generator were considered; the lower energy neutrons from D-D produce a smaller background of ^{238}U fissions but D-D generators are generally significantly lower in achievable intensity, given similar form factors. The metrics for evaluating the various designs were: 1) uniformity of thermal and epithermal flux across the assembly cross-section, 2) total fission rate induced in the MOX fuel definition, and 3) relative contributions of fissile and ^{238}U fission. Several of the early designs were discarded based on these metrics; Figure 3 (left) depicts the design that demonstrated considerable promise: HGETv1a. Figure 3 (right) shows the low-energy fission rate distributions for the HGETv1a designs, with an assembly present (each pixel in the image corresponds to an individual pin). Immediately evident is a relatively high fission rate on the generator side of the assembly, in the outer row of pins. The neutron self-shielding effect, which depresses the fission rate on the interior of the assembly due to interactions between the neutrons and the fuel pins, is also clear. The overall effect is a gradient of approximately 10X between the fission rates at the outermost to innermost pins – although if the outer row of pins is neglected, the fission rate in the rest of the assembly is within a factor of ~3X and has a predictable gradient structure, with no highly localized changes on the interior of the assembly.

For the collection of the prompt and delayed gamma rays produced by the induced fissions, an array of highly collimated gamma detectors is rotated around the assembly to build up the tomographic projection data, as a function of both energy and angle. A number of potential collimator/detector combinations are possible, but the nominal HGET design assumes a configuration founded on the IAEA's original Passive Gamma Emission Tomographer (PGET), as described more fully in [3] and depicted in Figure 4 below. Though PGET is intended for verification of spent fuel, a variant on PGET tailored for unirradiated fuels would benefit from a high degree of familiarity among tomography practitioners and the potential for leveraging of hardware components (e.g., detector arrays, pulse-processing electronics).

PNNL-SA-125791

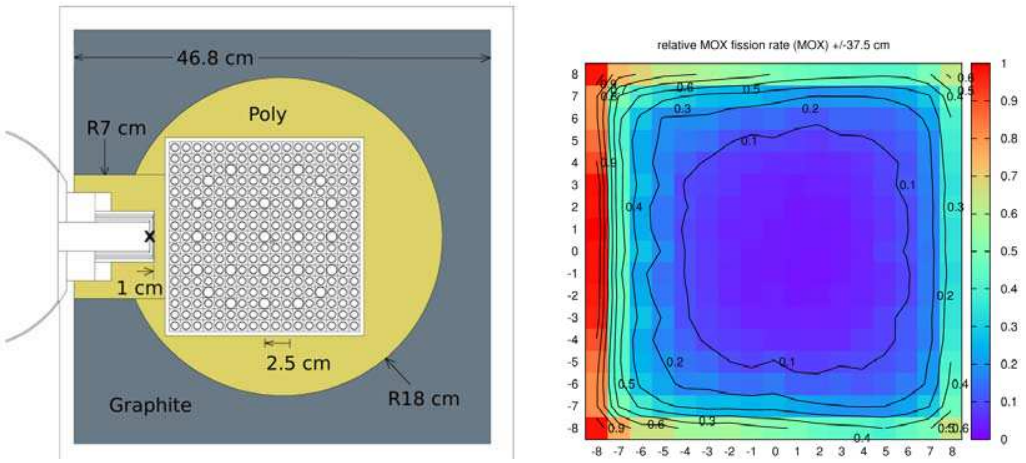

Figure 3. Left: Cross-section of the HGETv1a instrument geometry including a D-T generator (far left), a PWR assembly, and a combination of poly and graphite moderator/reflector. Right: Mapping of fission rate induced by low-energy neutrons, assuming the HGETv1a design (each pixel represents one fuel pin).

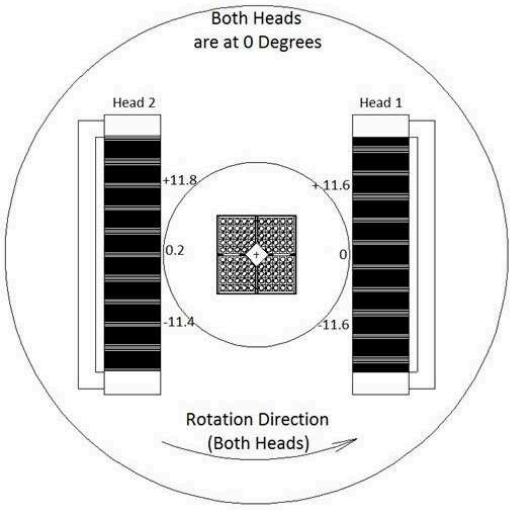

Figure 4. Rendering of the IAEA's PGET instrument design showing a vertical view of the detector heads containing 104 CdTe detectors in each head (right) [3].

The central challenge in designing the HGET collimator/detector combination is to increase the collection efficiency significantly while preserving sufficient spatial resolution to resolve individual pins. To increase the collection efficiency for HGET gamma-ray signatures, the aperture's field of view was opened significantly in the horizontal and vertical directions. These adaptations produce an increase of approximately 30X compared to the PGET collimator.

$Bi_4Ge_3O_{12}$ (BGO) was chosen as the nominal gamma-ray spectrometer material for the HGETv1a design. Although it has significantly poorer energy resolution than other candidates such as NaI(Tl), CZT or $LaBr_3$, energy resolution is not expected to be critical for the broad energy windows for collection of prompt-fission and delayed-gamma signatures. BGO's high density and atomic number translate to high stopping power for higher-energy gamma rays, whilst maintaining a relatively small form factor that can support a highly arrayed detector arrangement like the one used in PGET. Importantly, BGO is a very common material for positron emission tomography systems used in nuclear medicine, which means that large arrays of relatively

small voxels are readily available in the commercial market. The BGO detector is observed to give a factor of three improvement in intrinsic efficiency for the collection of gamma-rays above 1 MeV, when compared to the CdTe detectors employed in the original PGET device.

The combination of higher collimator efficiency (~30 X) and greater intrinsic detector efficiency (~3X) results in an overall HGET gamma-ray collection efficiency that is approximately two orders of magnitude higher than the original PGET design, thereby helping to recover a significant portion of the signal discrepancy (several orders of magnitude) between the spent fuel applications for which PGET was originally designed and the HGET scenarios for unirradiated fuels.

7. Reconstruction and Analysis Methods for HGET

The simplest approach to tomographic reconstruction is filtered backprojection, which solves analytically for the distribution of emissions, assuming that measurements are spaced at equal angles and that attenuation is minimal. This approach has the advantage of being both fast and requiring few assumptions about the system [12], and has been successfully used to locate missing pins in spent nuclear fuel [3]. However, since FBP in its simplest form makes no assumptions about attenuation, it cannot correct for the highly attenuating pins that block emissions from the center of the assembly. This leads to a reconstructed image which is systematically lower in intensity inside the assembly.

The case of fresh fuel is different from the spent fuel application in two important ways. First, the emission intensity is much lower, indicating that without other modifications a much longer measurement time will be needed. Second, emission intensity is a function not only of fuel composition, but also of illumination by the neutron field. Achieving a high and relatively uniform flux of thermal neutrons in the center of a large assembly is difficult, as discussed previously. The difference in counts at the detector from inner pins to outer pins is already large in passive emission tomography, but neutron interrogation adds another significant gradient, on the order of 10X, between inner and outer pins. Reconstructing a dataset with such an extreme gradient results in poor image quality.

While the HGET application is challenging from the reconstruction standpoint, it is decidedly different from other tomographic applications (e.g., nuclear medicine) in that it is fundamentally a confirmatory measurement of the operator's declaration about the assembly (as opposed to a blind test in which nothing about the object is known). This means that *a priori* information about a declared assembly, perhaps after initial verification via FBP, can be used to extract as much information as possible from each collected gamma ray and thereby improve the quality of the resulting image reconstruction. There are a number of ways to incorporate this information, but one straightforward approach is to assume a declared assembly geometry and solve for average emission values for each pin. Mathematically, this is phrased as measurement data (g_α) with α as the sinogram angle/offset index according to

$$g_\alpha = \sum_k H_{\alpha k} f_k \tag{1}$$

where f_k is the reconstructed activity estimate, here with k as the pin index, and $H_{\alpha k}$ is the model-based system response matrix, in this case the detector response to each possible emitting pin in the presence of attenuation due to the whole assembly. This approach is described more fully in [3][11]. Reconstructing at the level of individual pins, rather than over a series of pixels, incorporates the assembly geometry and greatly decreases the number of unknowns, regularizing the inverse problem. This results in much lower relative statistical error, but contingent upon the accuracy of the model.

The model-based tomographic reconstruction methods translate the collected gamma-ray signature into the emission intensity of prompt and delayed fission gammas in each pin, and therefore the pin-wise fission rate. Next, the pin-by-pin fission rate produced by the tomographic inverse problem must be translated to the verification parameter of interest: fissile-material concentration. De-tangling the fissile concentration from the fission rate must recognize that fission from non-fissile isotopes, most notably ^{238}U, can contribute significantly to the total induced fission rate, but the concentration of the non-fissile isotopes is not the IAEA

verification parameter of interest. Such a translation can be complex since the fission cross-sections for the fissile and fissionable isotopes are highly dependent on incident neutron energy (including resonance structures and threshold reactions), and the neutron energy spectrum varies by pin location—due to attenuation from surrounding pins and attenuation within the pin of interest due to its own fissile loading. The methods used to translate total fission rate in a pin into fissile-isotope concentrations in that pin are beyond the scope of this paper but are described fully in [11].

8. Example Performance Prediction Results

In the early rounds of performance prediction studies, only the prompt-fission gamma-ray signal has been considered, and a straightforward model-based reconstruction on a pin-by-pin basis was used to bound the tomography inversion problem. The primary question to be addressed was: Based on the HGET v1a design, the "MOX A" assembly definition, anticipated operator declarations, and simulated prompt-gamma signatures, can reasonable statistical uncertainties be achieved for fissile-mass concentration on a pin-by-pin basis within 1-2 hours? The end-to-end HGET analysis process is shown in Figure 5 for this MOX A case study and reflects the discussions in the previous sections of this paper. In the example case-study results presented in Figure 6, it is assumed the operator declares the Pu isotopics for each pin

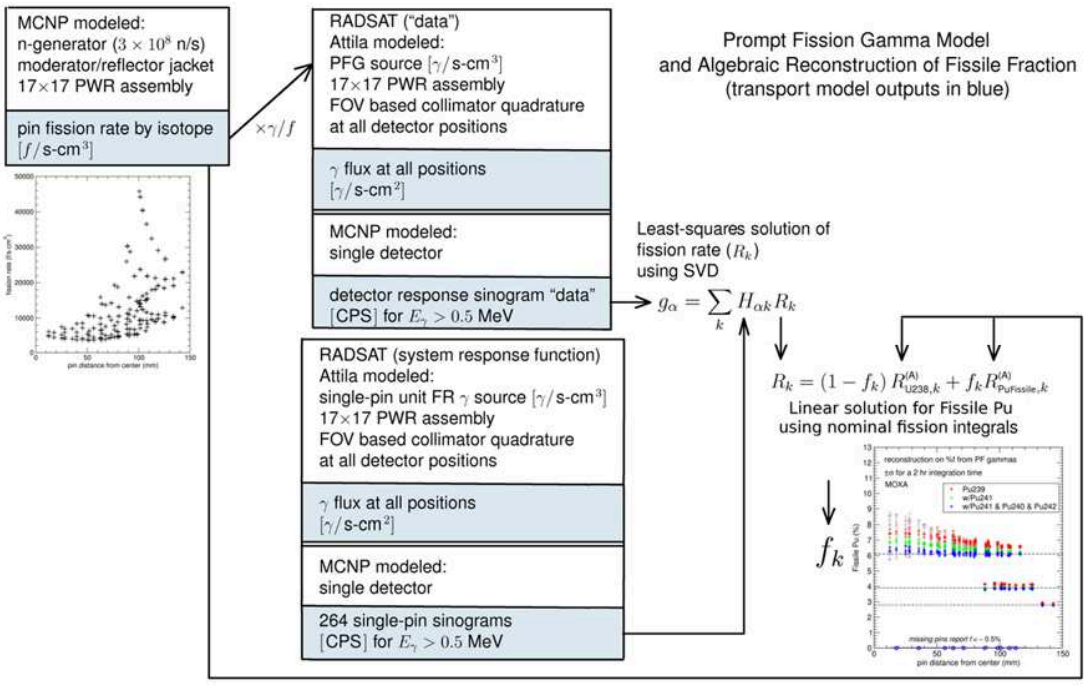

Figure 5. Overview of HGET performance-prediction methodology (assuming a PWR MOX assembly) that begins with forward calculations of induced fission rate (upper left) and culminates in quantification of fissile Pu concentration in each pin (lower right).

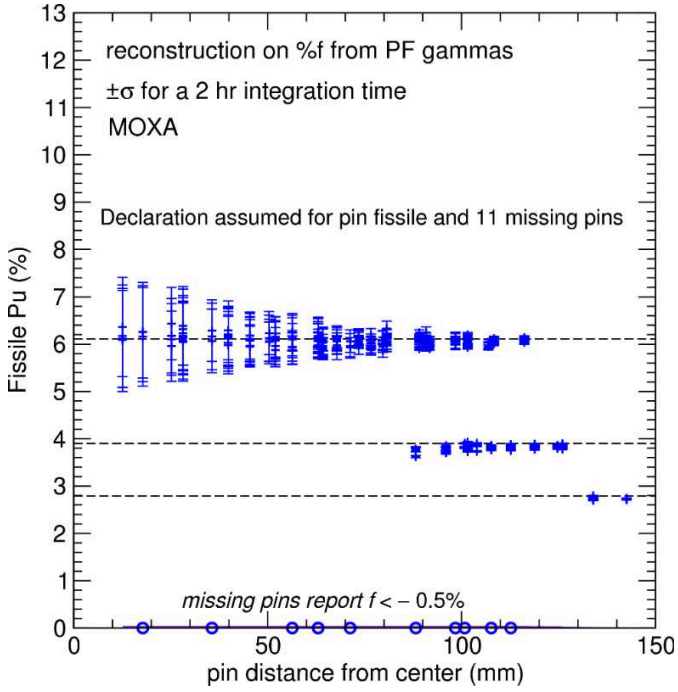

Figure 6. Example results for the determination of Fissile Pu (^{239}Pu + ^{241}Pu) fraction in MOX A, when incorporating assembly geometry and Pu isotopics data in the analysis process. Calculated values are based on 2-hour total assay time; one-sigma error bars on statistical uncertainty are shown. Dashed lines are the actual fissile fraction (^{239}Pu + ^{241}Pu) for the three Pu loading levels. (Note that Pu isotopics are identical for all loading levels).

The preliminary results shown in Figure 6 indicate that: given a careful system design, a COTS portable neutron generator and reconstruction and analysis algorithms that fully acknowledge operator-declared information about the assembly, HGET has the potential to verify fissile-mass concentration on a pin-by-pin basis in total assay times of approximately 2 hours for a representative PWR MOX assembly. These initial performance estimates assumed that assembly type, missing-pin locations and Pu isotopics were accurately declared by the operator and incorporated in the analysis process. Under those assumptions, the relative standard deviation of the fissile-Pu quantification was less than a few percent for most pins, but approached 20% for the interior pins. The uncertainty in fissile concentration is small compared to the reconstructed contrast for the 11 missing pins.

9. Summary and Next Steps

While the initial HGET performance predictions presented in this paper are encouraging, they were generated using simulated data that does not include background terms, assuming full availability and accuracy of declared data for the assembly of interest, and assuming a near-perfect system response function in the tomographic reconstruction. Considerably more analysis is needed to more fully understand the potential of HGET and its viability for IAEA verification scenarios. The highest priority is the extension of the feasibility analysis to LEU, and to LEU with burnable poisons (Gd rods). The case of Gd loading in particular is challenging for coincidence counting assay, and the possibility of using the high-energy and high-intensity gamma rays from Gd to account for the burnable poisons offers potential advantages for HGET in overcoming the burnable poison effects. The performance predictions presented here were performed using only the prompt-gamma signature but delayed-gamma signatures become significant as the active-interrogation measurement progresses, and could be included in the reconstruction algorithms as a smoothly varying time dependent term. Continued study of HGET-specific reconstruction algorithms, particularly those that can identify the perturbation patterns created by missing pins and have robustness to

imperfections in the system response function (e.g., undeclared or inaccurately declared missing pins), is needed. Perhaps most importantly, the HGET viability study needs to move into empirical space. The challenges of high-fidelity simulation for this relatively complex active interrogation approach (for which even basic cross-section data are not always available), and the inability of simulations to accurately capture the background terms that may arise in this active-interrogation scenario, strongly encourage proof-of-principle laboratory measurements using a representative tomographic device and objects (e.g., LEU fuel rodlets), to benchmark the predictive modeling tools and guide refinement of the nominal HGET instrument design.

10. References

[1] IAEA: Vienna, Austria; *IAEA Department of Safeguards Long-Term R&D Plan, 2012-2023*. 2013.

[2] Svard, S.J., et al., *Gamma-ray Emission Tomography: Modeling and Evaluation of Partial-Defect Testing Capabilities*, in *2014 IAEA Symposium on International Safeguards*. 2014.

[3] Smith, L.E., et al., *A Viability Study of Gamma Emission Tomography for Spent Fuel Verification: JNT 1955 Phase I Technical Report*. 2016, Pacific Northwest National Laboratory: Richland, WA. p. 197.

[4] Campbell, L.W., L.E. Smith, and A.C. Misner, *High-Energy Delayed Gamma Spectroscopy for Spent Nuclear Fuel ASsays.* IEEE Transactions on Nuclear Science, 2011. **58**(1).

[5] Mozin, V., et al., *Delayed gamma-ray spectroscopy for spent nuclear fuel assay.* Journal of Nuclear Materials Management, 2012. **40**(3): p. 78-87.

[6] *Safeguards Techniques and Equipment: 2011 Edition*, in *International Nuclear Verification Series*. 2011: Vienna, Austria. p. 162.

[7] Zhao, M., et al., *International Target Values 2010 for Measurement Uncertainties in Safeguarding Nuclear Materials.* ESARDA Bulletin, 2012. **48**: p. 3-24.

[8] Canberra Industries, I. 2011 [cited 2016 December 1]; Available from: http://www.canberra.com/products/waste_safeguard_systems/pdf/JCC-71-72-73-SS-C38898.pdf.

[9] Bairiot, H., et al., *Status and Advances in MOX Fuel Technology*, in *Technical Reports Series*. 2005, International Atomic Energy Agency: Vienna, Austria. p. 179.

[10] Wareing, T.A., J.M. McGhee, and J.E. Morel, *ATTILA: A Three-Dimensional, Unstructured Tetrahedral Mesh Discrete Ordinates Transport Code.* Transactions of the American Nuclear Society, 1996. **75**.

[11] Miller E A,Smith L E,Wittman R S,Campbell L W,Deshmukh N S,Zalavadia M A,Batie M A,Mozin V V . *Hybrid Gama Emission Tomography (HGET): FY16 Annual Report,* Pacific Northwest National Laboratory, 2017.

[12] *Emission Tomography: The Fundamentals of PET and SPECT*. 1 ed. 2004: Elsevier Academic Press. 576.

Cosmic-ray muon tomography for safeguards applications

Guangliang Yang[1], Tony Clarkson[1], David Ireland[1], David Mahon[1], Ramsey Al Jebali[1], Scott Lumsden[1], Claire Neilan[1], Ralf Kaiser[1], Craig Shearer[2], Matthew Ryan[2]

[1] SUPA, School of Physics and Astronomy, University of Glasgow, Kelvin Building, University Avenue, Glasgow G12 8QQ, Scotland, UK
[2] National Nuclear Laboratory, Central Laboratory, Sellafield, Seascale, Cumbria CA20 1PG, England, UK

Abstract:

Cosmic-ray muon tomography uses naturally-occurring muons to detect the presence of high-Z material within shielded containers. The fundamental physics of muon tomography is that the RMS width of the deflection angle and/or the lateral displacement of muons within a material is dependent on the Z of the material. Muon tomography systems work just like a CT scanner in the medical field that can reveal information about the inside of a target. Muon tomography works by measuring the deflection angle and or the lateral displacement of each individual muon, and inversely calculates the radiation length of the target materials inside the image area. The deflection angle and lateral displacement can be calculated from the trajectories of muons, which can be measured by suitably-positioned sensitive detectors. One advantage of muon tomography is the super-penetrative ability of the muon, which allows it to image large, shielded objects like spent nuclear fuel canisters. Therefore, it is perfect for safeguards applications. In this paper, detailed Geant4 simulations have been carried out to investigate the factors that will affect the performance of a muon tomography detector for use within safeguards. The capability of a Muon Tomography system is successfully demonstrated through this detailed simulation study that highlights the image quality achievable and the imaging time required for a spent fuel canister.

Keywords: muon tomography; multiple scattering; spent fuel canister; Geant4

1. Introduction

Cosmic-ray Muon Tomography was invented by scientists in the Los Alamos National Laboratory about a decade ago[1], which is based on the multiple scattering of muons. It can be used to detect the presence of high-Z material within shielded containers by using naturally-occurring muons. There are active studies for its application in many areas, such as, detecting high Z materials in shipping containers for border security control[2], examining damaged nuclear reactor cores[3], and other applications demonstrated by publications[4-9]. One advantage of Muon Tomography is the super-penetrative ability of the muon, which allows it to image large, shielded objects like spent nuclear fuel canisters.

The fundamental physics of muon tomography is that the RMS width of the deflection angle and/or the lateral displacement of muons within a material is dependent on the Z of the material. According to the Moliere theory[10], the scattering angle distribution follows a roughly Gaussian distribution for the centre part and with a rather heavy tail. The width of this Gaussian distribution of scattering angle can be well described using the Rossi formula[11], which has the following form,

$$\sigma = \frac{15MeV}{p\beta}\sqrt{\frac{t}{L_0}} \qquad (1)$$

where σ is the RMS width of the Gaussian distribution, t is the path length, p is the particle momentum, β is the particle velocity and the L_0 is the radiation length (unit in length), which can be described as:

$$L_0 = \frac{716.4 g cm^{-2} A}{\rho Z(Z+1)\ln(\frac{287}{\sqrt{Z}})} \qquad (2)$$

We can rewrite the equation (1) as,

$$\sigma^2 = \left(\frac{15MeV}{p\beta}\right)^2 \frac{t}{L_0} \qquad (3)$$

The equation (3) links the multiple scattering width to the radiation length, which is further dependent on the atomic number Z, as can be seen from the equation (2). However, the equation (3) only works for single material. In reality, we are more interested in complex materials. Schultz et al. developed a relationship between the variance of scattering angle and the radiation lengths for complex materials in reference[12], which can be shown as,

$$\sigma^2 = \sum_i \left(\frac{15MeV}{p_i\beta_i}\right)^2 \frac{t_i}{L_{0i}} \qquad (4)$$

From equation (4) it can be seen that the variance of the muon scattering angle equals to the integral of the inverse of the radiation length along the muon path. With a large number of muon measurements from different angles and different positions, we will get a system of equations. If the variance of the scattering angle can be obtained accurately, the radiation length can be inversely reconstructed by solving this linear system of equations by using algebraic methods. However, as the muon multiple scattering is a stochastic process, we can only directly measure the scattering angle for each muon, but we need to know the expected variance of scattering angle along each muon path. To overcome this difficulty, Schultz opted to use the Maximum likelihood method for the image reconstruction[12]. They first used the Newton method to get the Maximum likelihood estimator, later they developed a Maximum likelihood Expectation Maximization (MLEM) method[13]. In reference [12], Schultz also showed that the lateral displacement of each individual muon can be used for the image reconstruction, and the image reconstructed using both the angle and lateral displacement information has better quality.

The deflection angle and lateral displacement can be calculated from the muon trajectories, which can be measured by suitably-positioned sensitive detectors. Since the muon is a charged particle, there are quite a large number of detector techniques can be used for obtaining the muon striking position, such as the drift chamber[2], scintillating fibre trackers[14], GEM [15] and RPC detector [16] etc.

Using the muon tomography technique for safeguards application has drawn considerable interests in the recent years[17-20]. This is because it can provide a viable way to verify the nuclear spent fuels for deterring potential diversion to plutonium reprocessing, and to monitor the health of casks to prevent failures. Due to the heavy shielding of the spent fuel canisters, techniques like neutron and gamma ray imaging are struggling to provide enough information for the above purpose [21]. On the other hand, because of the high penetrative capability of cosmic ray muon, muon tomography is the most suitable technique for this purpose.

The first experiment using muon tomography to verify the contents of dry storage casks was carried out by Durham et al.[17]. They used a pair of drift detectors to measure a MC-10 dry storage cask from the side; their result proved that muon tomography is capable to detect missing fuel assembly. However their measurement failed in providing the exact locations of the missing fuel elements because it can only produce the integrated density along the measuring direction. In a recent study, Poulson et al who used a cylindrical detector and the filter-backproject(FBP) algorithm for image reconstruction provided a clear 2 D horizontal section image of a dry storage cask, where exact locations of each fuel assemblies can be identified[20]. However, in their simulation, ideal detector with perfect resolutions is used, which is not available in a practical application. In this paper, studies by using a scintillating fibre detector with a MLEM image reconstruction method are used to investigate the application of muon tomography for the nuclear safeguards. We focused on the study how the detector arrangement will affect the reconstructed image, and the effect of the detector resolution on the image quality. The effects of factors like the voxel size, muon number etc. on the image quality are studied in this paper as well.

2. Muon tracking detector design

The tracking detectors should be positioned in such a way that the striking positions of incoming and outgoing muons can be measured, and subsequently the trajectories can be determined from the measured striking positions. Since the cosmic ray muon is isotropic in azimuth and falls off approximately with (cos(theta))2, where theta is the angle from the zenith[20], an optimal detector set up will require to have a 4pi coverage to order to be able to detect muons for all possible directions. For the application in the dry storage casks, we assume that it is difficult or impossible to put detectors directly above and below the casks due to the heavy weight of the casks and the casks have circular shape in the horizontal sections, therefore, a cylindrical detector that fits around the outside of the cask will be ideal. However, it will be difficult to construct such a cylindrical detector, because it needs curved detector elements. The cost to build such a system will also be prohibitive. Instead a pair of planar detectors which were placed on the opposite sides of the imaging volume will be more cost effective and easier to build. However, a planar detector with limited width can't cover the whole range of azimuthal angle, therefore such a system has to be operated in several azimuthal angles separately to cover the whole angle range.

The planar detector has four modules, the effective area of each module has a size of 2.8 m by 4.2 m. For each planar detector module, there are two orthogonal layers of tracking elements. While the cylindrical detector has only one circular module with two rings of detectors. The inner ring has a diameter of 2.8 m, while the outer ring has a diameter of 3.4 m. The position of the detect relative to the dry storage cask can be find in figure 1.

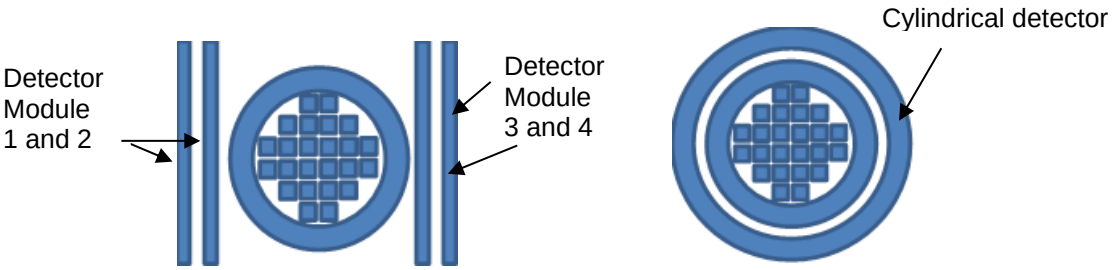

Figure 1: sketches of the planar and cylindrical detector systems.

3. Geant4 simulation

To verify the effectiveness of the detector system and to optimize the design, detailed Geant4 simulation have been carried out. Geant4 is a scientific software tool-kit which is developed by CERN[23]. It has been widely used in the high energy, nuclear and accelerator physics, as well as studies in medical and space science areas. In the past, we had compared the Geant4 simulation results with the experimental results for the performance of our muon tomography prototype detector[14]. Our results show that the Geant4 simulation agrees very well with the experimental results. Therefore, using Geant4 simulation to verify the detector design is technically reliable.

Plastic scintillator fibres with various diameters from 2mm to 32mm are used in the simulation. These scintillator fibres are placed in the grooves made on the Rohacell plate which is rested on aluminium plates for further support. The technique for making the plastic scintillator fibres detectors for use for the muon tomography application can be found in reference [14].

For the planar detector system, to cover the whole azimuthal angle range, the detector system has to be rotated by a fixed angle step around vertical z axis until it return to its original position, while at each angle, a fixed number muon is generated by the muon generator.

In the imaging volume, a partially loaded Westinghouse MC-10 cask was simulated. In the simulation, the MC-10 has a 25 cm thick steel wall, and an aluminium basket to holds the fuel assemblies in the centre of the cask. 20 out of 24 of the aluminium basket holder slots filled with pressurized water reactor fuel assemblies and leaves 4 of them empty; a neutron shielding layer and 24 fins for heat transfer. Each fuel assembly contains 204 fuel rods, 20 control rod guide tubes, and one instrument tube. The

fuel rods are filled with UO2 and surrounded by a zirconium alloy cladding. The control rods and instrument tube were simulated an empty cladding, with no fuel present. The dimensions and geometry of the MC-10 cask and the water pressure fuel assembly used in the simulation was found in reference [24, 25].

4. Results

Both the cylindrical detector and the planar pair detector can't cover the full 4pi solid angle, therefore it is not possible to detect the incoming and outgoing muon tracks for all the muons that are going through the casks; some of the muon will interact with only part/or none of the tracking detectors, therefore were ignored by the analysis software. It is estimated that there will be around 4 to 5 million muons passing the planar detectors with valid incoming and outgoing tracks in one day. The true momentum is used in the image reconstruction for each individual muon. A MLEM method is applied for the image reconstruction. This reconstruction method was detailed in paper[13].

The imaging volume is divided into voxels. The x and y dimensions of the voxel are in the range from 5 mm to 40 mm, while the z dimension is 6000 mm. The reason for using a very large vertical voxel size is because there is very little materials variation along the vertical direction for the vertical dry storage casks. With a larger voxel, more muon will be gathered in one voxel therefore better statistics can be achieved.

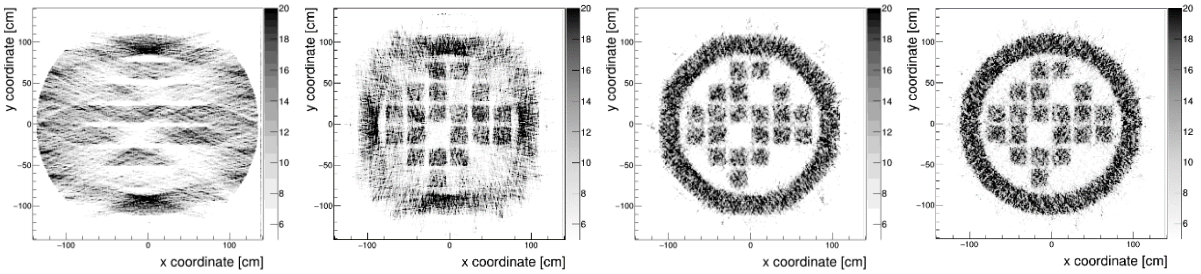

Figure 2: section images for each angular settings, from left to right, the angle steps 180 degrees, 90 degrees, 45 degrees, 22,5 degrees.

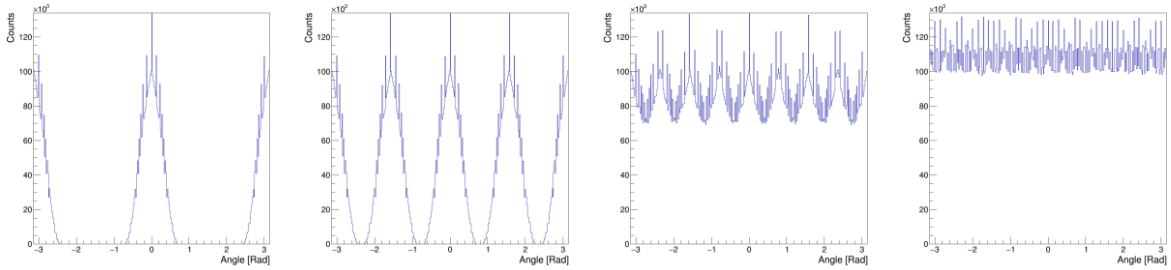

Figure 3: angular distribution for each angular settings, from left to right, the angle steps 180 degrees, 90 degrees, 45 degrees, 22,5 degrees

In figure 2, horizontal section images reconstructed from different planar detector settings are shown. From the left to the right the rotation angle steps are 180 degrees, 90 degrees, 45 degrees and 22.5 degrees. It can be seen that with a 22.5 rotation angle step, the horizontal section image of the cask has been correctly reconstructed; all the important features of the cask can be seen. Each individual fuel assembly can be clearly distinguished between each other and missing assemblies can be easily identified. For the images reconstructed with larger rotation angle steps, there are large distortions. The bigger the rotation angle step, the bigger the distortion. The distortion of the reconstructed image is a common problem for muon tomography, it often appears as vertical smearing problem, as for most of the muon tomography applications planar tracking detector were placed on top and underneath of the target. This problem is similar to the limited angle problem in the medical imaging field. In figure 3, the azimuthal angle distribution of muons used in the image reconstruction are shown. It can be seen that for larger rotation angle steps, the muon angle intends to concentrate in a few directions, while with smaller rotation angle step, there is a more uniform azimuthal angle distribution.

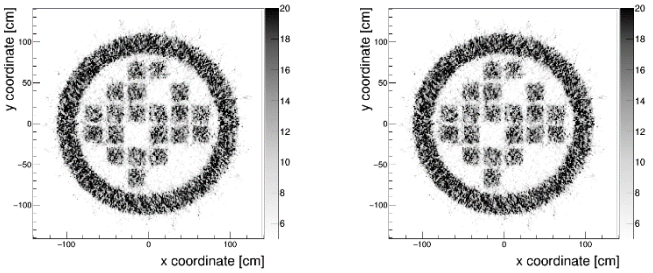

Figure 4: images reconstructed from data simulated with the planar (left) and cylindrical (right) detectors.

In figure 4, the horizontal section images of the storage cask are shown for cylindrical detector and for a planar detector with a rotation angle step of 22.5 degrees. It can be seen that both images correctly revealed the inner structure of the modelled cask. They looks identical. In the simulation, the fibre size was 2mm.

In figure 5, image reconstructed with detectors equipped with different fibre size are shown, it can be seen , that with the increase of fibre size, the quality of reconstructed image is decreasing slightly. With the fibre diameter of 16mm, the fuels assembly can still be seen. Our study shows that the fibre diameter can be further increased to 32 mm, however, the imaging voxel size have to be increased to match the fibre size. A larger fibre size can significantly reduce the number of electronics channels, therefore a save to the cost, but it also means it lost the ability to see small features.

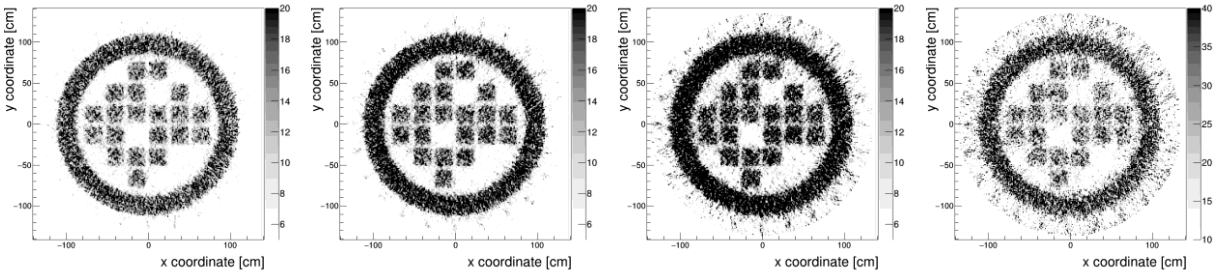

Figure 5: image quality vs scintillator fibre size, from left to right, the fibre size are 2mm, 4mm, 8mm,16mm diameters.

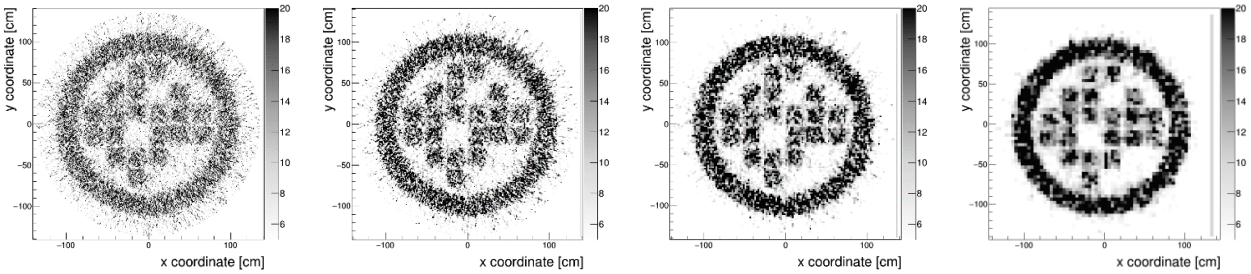

Figure 6: image quality vs voxel size, from the left to the right, the pixel sizes are 5mmx5mm, 10mmx10mm, 20mmxmm, 40mmx40mm.

The voxel size can affect the image quality as well. In figure 6, section images reconstructed with different voxel sizes are shown. All these images are reconstructed with the same number of muons. It can be seen, that although the main feature of the image can still be seen in the image with a 5mm by 5 mm pixel size, the background noise can be seen increased dramatically. The image with a 40 mm by 40 mm pixel size shows the smallest back ground noise. However, further increasing the pixel size, the partially occupied pixel elements will reduce the image quality.

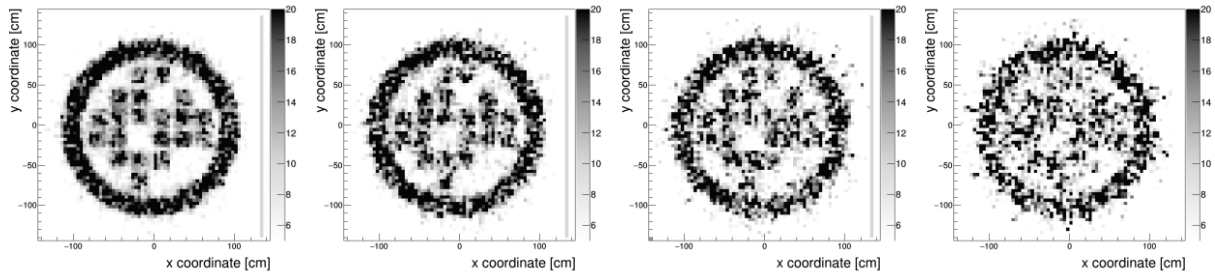

Figure 7: image quality vs muon number. From left to right, muon numbers are, 1.12M, 560K,208K,140K.

In figure 7, the images reconstructed with different muon numbers are shown. It can be seen that with the decrease of muon number, the image quality is decreasing. The boundary of each fuel assembly can be clearly identified with around one million muons. Missing fuel assembly can be confirmed with only a few hundreds of thousands muons with naked eyes. However, it should be mentioned that the above simulation was carried out with the full knowledge of the momentum for each muon. Technically, it is very difficult to measure the muon momentum accurately, and cost effective method is needed to measure the muon momentum. Without the muon momentum information, high quality image can still be obtained with increased muon numbers. In figure 8, a section images reconstructed with 32 and 6 million muons are shown, which are reconstructed without using the true momentum information, and the data was simulated with a 2 mm diameter fibre.

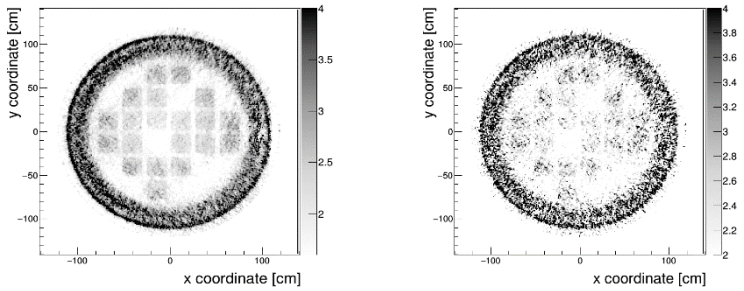

Figure 8: image reconstructed with 32 million muons and 6 million muons (from left to right) without using true momentum in image reconstruction.

5. Conclusions

The study about the application of muon tomography for nuclear safeguards is carried out. By considering the capability of cosmic muon tomography and the feature of vertical dry storage cask, the effect of detectors position and arrangement had been studied. GEANT4 simulations of muon imaging of a partially loaded dry storage cask show that missing fuel assemblies can be located with high confidence. This will help determine the diversion of spent fuel assemblies without opening the cask.

6. Acknowledgements

The authors gratefully acknowledge Sellafield Ltd., on behalf of the UK Nuclear Decommissioning Authority, for their continued support and funding of this project.

7. References

[1] K.N. Borozdin et al., “Surveillance: Radiographic imaging with cosmic-ray muons”, Nature 422 (2003) 277.

[2] C.L. Morris et al., “Tomographic Imaging with Cosmic Ray Muons”, Sci. Global Secur. 16 (2008) 37.

[3] K. Borozdin et al., “Cosmic ray radiography of the damaged cores of the fukushima reactors”, Phys. Rev. Lett. 109, 152501 (2012).

[4] G. Jonkmans et al., “Nuclear waste imaging and spent fuel verification by muon tomography”, Annals of Nuclear energy 53, 267–273 (2013).

[5] J. Gustafsson, “Tomography of Canisters for Spent Nuclear Fuel Using Cosmic-ray Muons”, Master’s thesis, Uppsala University, Uppsala, Sweden (2005).

[6] A. Clarkson et al., “Characterising encapsulated nuclear waste using cosmic-ray muon omography”, 2015 JINST 10 P03020 [arXiv:1410.7192].

[7] S. Pesente et al.,” First results on material identification and imaging with a large-volume muon tomography prototype”, Nucl. Instrum. Meth. A 604 (2009) 738.

[8] J. M. Durham, 1,a E. Guardincerri, 1 C. L. Morris et al, “ Tests of cosmic ray radiography for power industry applications”, AIP ADVANCES 5, 067111 (2015).

[9] E. Guardincerri, J. M. Durham, C. Morris et al, “Imaging the inside of thick structures using cosmic rays”, AIP ADVANCES 6, 015213 (2016)

[10] G. Moli`ere, “Theorie der Streuung schneller geladenen Teilchen II Mehrfach- und Vielfachstreu-ung,” Z. Naturforschg. 3A (1948) 78-97

[11] Bruno Rossi, “High-Energy Particles”, Prentice-Hall, New York (1952).

[12] L. Schultz, “Cosmic ray muon radiography,” Ph.D. dissertation, Portland State Univ., Portland, OR, 2003

[13] L. Schultz, S. Gary, N. Konstantin et.al., "Statistical reconstruction for cosmic ray muon tomography." IEEE transactions on Image Processing 16, no. 8 (2007): 1985-1993.

[14] A. Clarkson et al., “Geant4 simulation of a scintillating-fibre tracker for the cosmic-ray muon tomography of legacy nuclear waste containers,” Nuclear Instruments and Methods in Physics Research A 746, 64 – 73 (2014).

[15]Kondo Gnanvo a, n , Leonard V. Grasso III a , Marcus Hohlmann et al., “Imaging of high-Z material for nuclear contraband detection with a minimal prototype of a muon tomography station based on GEM detectors”, Nuclear Instruments and Methods in Physics Research A 652 (2011) 16–20.

[16] P. Baesso, 1 D. Cussans, C. Thomay and J. Velthuis, “Toward a RPC-based muon tomography system for cargo containers”, 2014 JINST 9 C10041

[17]] J. M. Durham et al., “Cosmic ray muon imaging of spent nuclear fuel in dry storage casks,” Journal of Nuclear Materials Management 44, 3 (2016).

[18] S. Chatzidakis, C. Choi, and L. Tsoukalas, “Interaction of cosmic ray muons with spent nuclear fuel dry casks and determination of lower detection limit,” Nuclear Instruments and Methods in Physics Research A 828 (2016) 37 –45

[19] S. Chatzidakis et al., “A bayesian approach to monitoring spent fuel using cosmic ray muons,” Trans. Am. Nucl. Soc. 111, 367–370 (2014).

[20] D. Poulson, J. M. Durham, E. Guardincerri, C. L. Morris, J. D. Bacon, K. Plaud-Ramos, D. Morley, A. Hecht, “Cosmic ray muon computed tomography of spent nuclear fuel in dry storage casks”, arXiv:1604.08938 [physics.ins-det]

[21] K. P. Ziock et al., “Radiation imaging of dry-storage casks for spent nuclear fuel,” IEEE Nuclear Science Symposium Conference Record , 1163–1167 (2005).

[22] J. Beringer et al. (Particle Data Group), “Review of particle physics”, Phys. Rev. D86, 2012

[23] GEANT4 collaboration, S. Agostinelli et al., GEANT4: A simulation toolkit, Nucl. Instrum. Meth. A 506 (2003) 250.

[24] M. A. McKinnon et al., “The mc-10 pwr spent-fuel storage cask: testing and analysis,” Electric Power Research Institute Report NP-5268 (1987).

[25] http://www.nrc.gov/docs/ML0136/ML013650469.pdf

Muon Tomography for spent nuclear fuel control

Paolo Checchia[1], Franco Gonella[1], Andrea Rigoni[2], Sara Vanini[2], Gianni Zumerle[2]

[1]INFN sezione di Padova Padova Italy
[2]Department of Physics and Astronomy, University of Padova, Padova, Italy

Abstract:

At present no validated methods to verify the content of Dry Storage Containers exist. The investigation profiting of cosmic muons may constitute a very effective method to detect or exclude the presence of spent fuel bundles. The layout of a possible detector and the techniques to provide the relevant information are described. A specific proposal to evaluate effects of surrounding radioactivity on detector performance is presented.

Keywords: muons tomography; spent fuel control; muon detectors

1. Introduction

Cosmic rays at sea level consist mainly of charged elementary particles called muons. Muons are produced by the decay of several types of very short-lived elementary particles, created in the upper part of the atmosphere by the interactions of primary cosmic rays, mainly protons or alpha particles, with atoms or molecules. Primary cosmic rays originate from galactic processes and thus their flux on earth is constant and isotropically distributed. At sea level the muon flux is about $10^4/m^2$/minute, with maximum intensity in the vertical direction and an approximate dependence on the zenith angle θ as $\cos\theta^2$. The cosmic muon energy spectrum is quite broad, with an average value of several GeV/c^2. Energetic muons can cross very thick layers of dense materials since they do not undergo nuclear interactions.

The use of the highly penetrative properties of cosmic-ray muons to explore inaccessible volumes has been proposed in the past [1], [2] and recently many efforts have been produced to demonstrate the potential of muon tomography in many application fields [3],[4]. A detailed review of possible applications can be found in [5].

2. Spent nuclear fuel inspection with cosmic muons

In the particular case of the dry storage containers (DCS), the approach to explore their content can profit of different physical processes occurring when muons cross the container. Firstly, since all the charged particles travelling in a medium loose energy as a function of the medium density, a fraction of muons is stopped inside the container. In addition, depending on the density and the atomic number of the crossed material, the muon trajectories undergo detectable deviations from the initial direction (multiple Coulomb scattering). These phenomena would give a three-fold information on the content of the material inside the hidden volume provided a set of muon detectors could be installed around the container. In detail, cylindrical detectors can be placed around the lateral surface of the containers. They should measure the position and direction of the muons entering in the container. They should

also measure position and direction of the particles that exit crossing the lateral surface of the container as shown in Figure1.

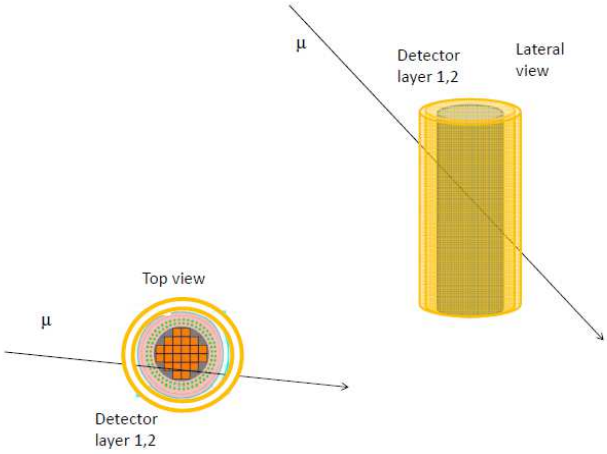

Figure 1: Sketch of a Muon Tomography station (not in scale) Top and lateral view.

With this configuration it is possible to know: i) the most probable path of muons that pass through the container; ii) most probable path of muons that should exit from the lateral surface but are absorbed; iii) the scattering angle of the passing-through muons.
The first two items contain a complementary information. Indeed the abundance of passing-through particles is connected to spatial regions with light material (e.g. air), while the absorbed particles are located in correspondence to dense regions. In case of an inhomogeneous material distribution (e.g. because a fuel bundle is missing) the first set of data would show an excess of particles with a path crossing a large fraction of the light material region. At the opposite, the absorbed particles whose trajectory points to the light material region would be less copious, since they have a smaller probability to stop inside the container.
The measurement of the muon scattering angle allows to determine a two or three-dimensional image of the container. The image reproduces the spatial distribution of a quantity, the linear scattering density, that is roughly proportional to the product of the material density times its atomic number. This method requires a complex formalism and noise filtering techniques as described in [6] , [7].
In more detail, to obtain a three-dimensional distribution of the material linear scattering density in the inspected volume, the space is divided into finite volume elements called voxels. The density is assumed to be uniform in the single voxel. It is important to stress that the particular geometry of the inspected volume and the well-known shape of the fuel bundles, allow the choice of voxels with vertically-elongated geometry. This results in a small size set of voxels, high statistics as regards muons per voxel, and low inspection time required.

2.1. Results with simulated data

It is possible to produce a realistic simulation of an inspection system and to obtain simulated cosmic-muon data in a situation similar to the one sketched above. The simulation software chain is based on GEANT4 package that is designed for modeling a broad range of particle processes and their interaction with matter and it is used in a variety of applications, including High Energy Physics (HEP), nuclear physics experiments, astrophysics, space science and medical physics [8]. In the present environment, the simulation includes the generation of cosmic-muon spectrum, the description of the muon detectors and the tracking of muons through a DCS. Several sets of data can be produced simulating different detectors and different containers. For each configuration, datasets with the presence of all the foreseen fuel bars and others with missing bars can be produced.
.
Using GEANT4, a complete CASTOR® container with and without a missing bar placed in different positions has been simulated. The simulation includes a cylindrical detector placed around the CASTOR, covering its entire lateral surface. The detector is composed by 8 layers of cylindrical drift tubes. Figure. 2 shows the top view sketch of the simulated CASTOR.

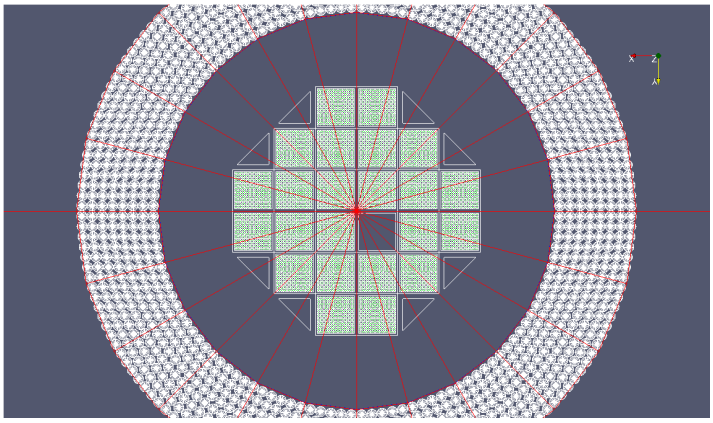

Figure 2: Top- view of a drift tube detector placed around a CASTOR® container with a missing fuel bar.

Preliminary results about the detection of a missing bar in a CASTOR container, for simulated samples corresponding to one to three hours of cosmic-muons data taking, are shown in Figure 3. On the left there is the reconstructed CASTOR density average along vertical axis, obtained using absorbed muons information. The right image shows the same set of data when muons passing through the container are analyzed. The missing bar is clearly visible with both techniques. Given the large size of CASTOR containers, comparable or even better results can be reasonably expected for other types of containers. These results are based on the simulation of a DCS without any nuclear activity and radioactivity emission. In real case, canisters with spent nuclear material emit gamma and neutrons that could interfere with the cosmic muons detection.

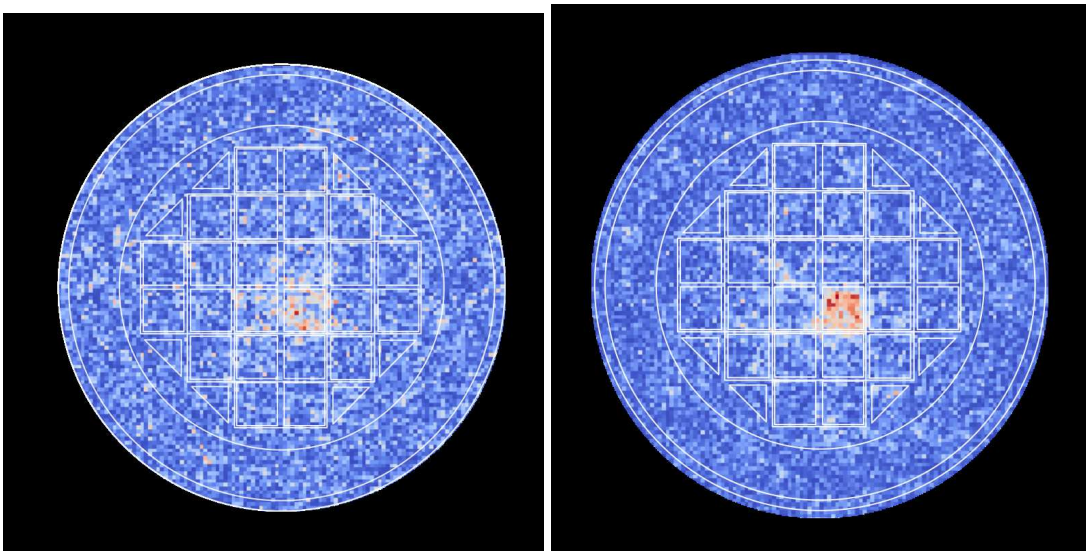

Figure 3: Top-view of the reconstructed CASTOR® density, averaged over vertical axis, obtained using absorbed muon (left) and passing-through muon information (right). The simulated container has one missing bar.

3. An operative proposal

While the perspectives of a system based on cosmic-muon tracking used to provide an effective control are encouraging, several concerns could arise from the environmental radioactivity in proximity of a DCS and the consequences on the muon detector response.

3.1. Detector layout for canister inspection

It has been shown that one of the cheapest way to provide muon detection with good tracking capability and large area coverage is based on drift tube technology [9],[10],[5].
As sketched in Figure 2, an ideal detector could be realised by several circular layers of drift tubes surrounding the cylindrical container. Muons crossing the tubes before entering the container and, if not absorbed, after exiting, release with large efficiency a hit in each crossed tube. It is then possible to have a good tracking of particles with a hit multiplicity that can be as large as twice the number of circular layers.
However, the presence of an intense radioactivity produced inside the container and reaching the detector can induce a number of signals with a frequency and an occupancy that could, in principle, spoil the detector performance. To quantify this effect it is necessary to quantify the activity and the impact of its components on the detector. It is therefore not straightforward to clarify this point until several details will be available.
In any case, even if it has been demonstrated that the proposed type of detectors can be operative in presence of high radioactivity, the best way to prove their response in problematic environmental conditions is to perform a dedicated test.

3.2. A detector for a dedicated test

The proposed test consists in producing a small prototype of drift tube detector with a reasonable number of channel to measure properly a cosmic muon track and sufficiently light to be moved and transported in proximity of a DCS. The detector should be capable to self trigger the data recording in the event of a muon passage. Once positioned in proximity of a DCS, the response of the prototype in presence of the radioactivity could be easily monitored. In particular, it could be proved that the tracking capability is maintained even with the coincidence of several additional hits induced by photon conversion or nucleon interactions in some of the tubes of the detector.

The design of such a prototype is shown in Figure 4 and consists of 8 layers of 8 drift tubes each for a total of 64 channels. Each drift tube is realised with a 50 mm diameter Al tube, 1.5 mm thick and a length of 2 meters. The tubes are equipped with a 100 μm anodic wire, connected to a High Voltage supply (~3000 V), to produce a radial electric field and the necessary multiplication of the charges released by incident muons. The collected signal is then amplified and shaped by the front end (FE) electronics and then processed (time digitalization, trigger and remote transmission) by the readout block.The tubes are operated with a gas mixture (Ar85%/$CO_2$15%) that should not present any safety issue.

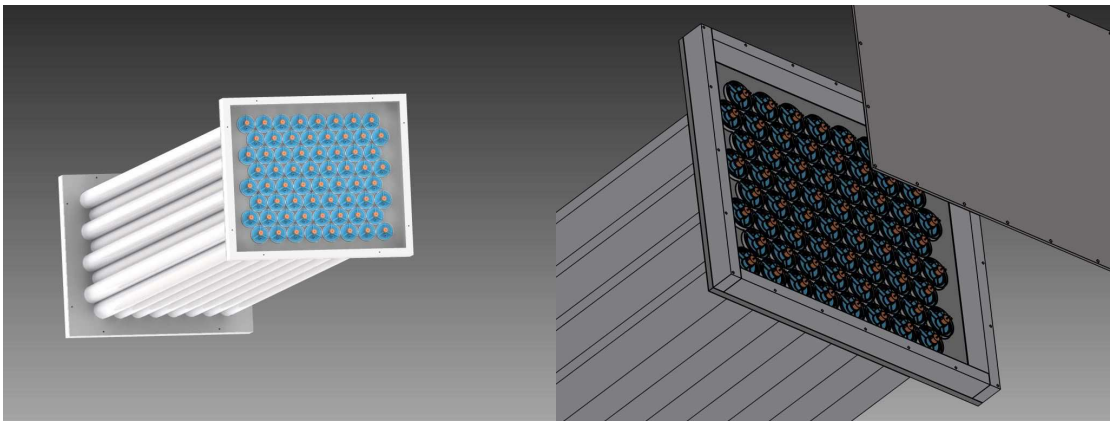

Figure 4: schematic view of a drift tube prototype detector (left). A detail of the front-end side of the tubes (right).

The total size of the prototype, including mechanical supports, would be about 0.6 m x 0.5m x 2 m, with a total mass of about 100 kg. A sufficient number of tubes have been produced so far by the Padova group in the INFN national laboratory of Legnaro (LNL), as shown in Figure 5. To complete the prototype, it is then sufficient to assembly the cells and to equip the detector with HV and FE electronics and to complete the gas distribution system. A read-out system based on field-programmable gate array (FPGA) circuits installed in the detector and remote data transmission to an on-line computer is foreseen. The whole electronic chain has been developed for the muon chambers produced for the CMS experiment at CERN-LHC [11] and is available to realize the prototype.

The time needed for an “on site” test would require a couple of days for far (low radioactivity) and near DCS data taking.

Figure 4: set of 2m long drift tubes produced in LNL INFN laboratory.

4. Conclusions

The volume reconstruction using cosmic muons represents a promising technique for spent nuclear fuel control inside Dry Storage Canisters. It could ensure an effective inspection of the content of disposal canisters after closure. Remaining doubts about the detector capability to operate in presence of radioactivity can be quickly understood with a simple test in proximity of a real canister. A detector prototype for this kind of tests is proposed.

5. Acknowledgements

The authors would like to acknowledge the important help received from Paolo Peerani and Hamid Tagziria, respectively, at the early and at the present stage of this work. This work has been supported by the INFN_E project of INFN.

8. References

[1] E.P. George, *Cosmic rays measure overburden of tunnel*, *Commonwealth Engineer* (1955) 455.

[2] L.W. Alvarez et al., *Search for Hidden Chambers in the Pyramids*, *Science* **167** (1970) 832.

[3] K.R. Borozdin et al., *Surveillance: Radiographic imaging with cosmic-ray muons*, *Nature* **422** (2003) 277.

[4] S. Pesente et al., *First results on material identification and imaging with a large-volume muon tomography prototype*, *Nucl. Instrum. Meth.* **A 604** (2009) 738.

[5] P. Checchia, *Review of possible applications of cosmic muon tomography, JINST* **11** C12072 (2017)

[6] L.J. Schultz et al., *Statistical reconstruction for cosmic ray muon tomography*, *IEEE Trans. Image Process.* **16** (2007) 1985.

[7] M. Benettoni et al., *Noise reduction in muon tomography for detecting high density objects*, 2013 *JINST* **8** P12007

[8] GEANT4 Collaboration, "*GEANT 4 – a simulation toolkit*", *Nucl. Instrum. Meth. A* **506** (2003) 250

[9] https://www.decisionsciences.com/

[10] http://mutomweb.pd.infn.it:5210/

[11] CMS collaboration, *The CMS experiment at the CERN LHC*, 2008 *JINST* **3** S08004.

Session 14

Evaluation

Evolution of Verification Data Evaluation under the State-Level Concept

C. Norman, J. Baute, R. Binner, M. Nikkinen, A. Walczak-Typke

International Atomic Energy Agency (IAEA)
Wagramer Strasse 5, A-1400 Vienna, Austria

Abstract

Every year, thousands of days are spent by IAEA inspectors in nuclear fuel cycle (NFC) facilities and other sites around the world. A large portion of this time is used for carrying out in-field measurements by various non-destructive assay (NDA) techniques and for taking environmental samples (ES) and/or destructive analysis (DA) samples. Comparably intensive resources are needed to maintain continuity of knowledge (CoK) on the verification data collected through these activities by means of a range of sophisticated containment and surveillance (C/S) systems. The IAEA collects, authenticates, quality controls, maintains and evaluates a large body of verification data and compares them with State declarations to support two of the main objectives of safeguards under the State-level concept (SLC), that is: the detection of diversion of nuclear material and of undeclared production or processing of nuclear material at declared facilities and locations outside facilities (LOFs).

In recent years, the NFC Information Analysis Section of the Safeguards Department Division of Information Management (SGIM-IFC), which is in charge of the evaluation of verification data, has been faced with a number of challenges: the first and most demanding is the need to evolve facility-based evaluation concepts to innovative, consolidated concepts that can integrate different types of information and support credible State-level safeguards conclusions, the second is the increasing volume and diversification of verification data to be evaluated given static resources, and the third is the need to keep abreast of modern methodologies and technologies with a view to ensure optimal effectiveness and efficiency.

This paper reviews the conceptual and methodological issues associated with these challenges and the approach that was applied to address them while taking advantage of the corresponding development opportunities. It presents the overall strategy adopted as well as the supporting project plan and the progress made to date in the related project components, with a special emphasis on the implementation of data visualization tools.

Keywords: evaluation; State-level Concept; methodology; diversion detection; visualization.

1. Introduction

The main mission of the IAEA Department of Safeguards is to provide credible assurances that States are abiding by their safeguards obligations. Since the safeguards system was strengthened after the discovery of a clandestine nuclear weapon programme in Iraq in the early 1990s and its legal authority was subsequently reinforced by the additional protocol (AP) in 1997, the nature and sources of information collected and evaluated by safeguards experts have extensively diversified and the volume of material to be researched has considerably increased. The Division of Information Management provides the Department of Safeguards with services of data processing, secure information distribution, information analysis and knowledge generation and consists of teams of

professionals specialized in the analysis of different types of information plus a team in charge of information integration. These specialists play a critical role in the work of the Division of Operations' State evaluation groups (SEGs) in identifying, analysing and consolidating safeguards-relevant information from all sources to draw independent, non-discriminatory and soundly based conclusions for all States having concluded a safeguards agreement (Fig. 1).

All-source safeguards-relevant information falls in three broad categories:

- Information declared by States, which consists in nuclear material accountancy (NMA) reports and reports submitted to the IAEA pursuant to the AP to the States' safeguards agreements.
- Information resulting from verification activities, e.g. results of NDA measurements, DA samples and environmental samples (ES), seals verification, surveillance review and other verification activities.
- Information from open sources (OS) such as, for example, media, scientific publications, IAEA and public databases, trade import/export information and commercial satellite imagery.

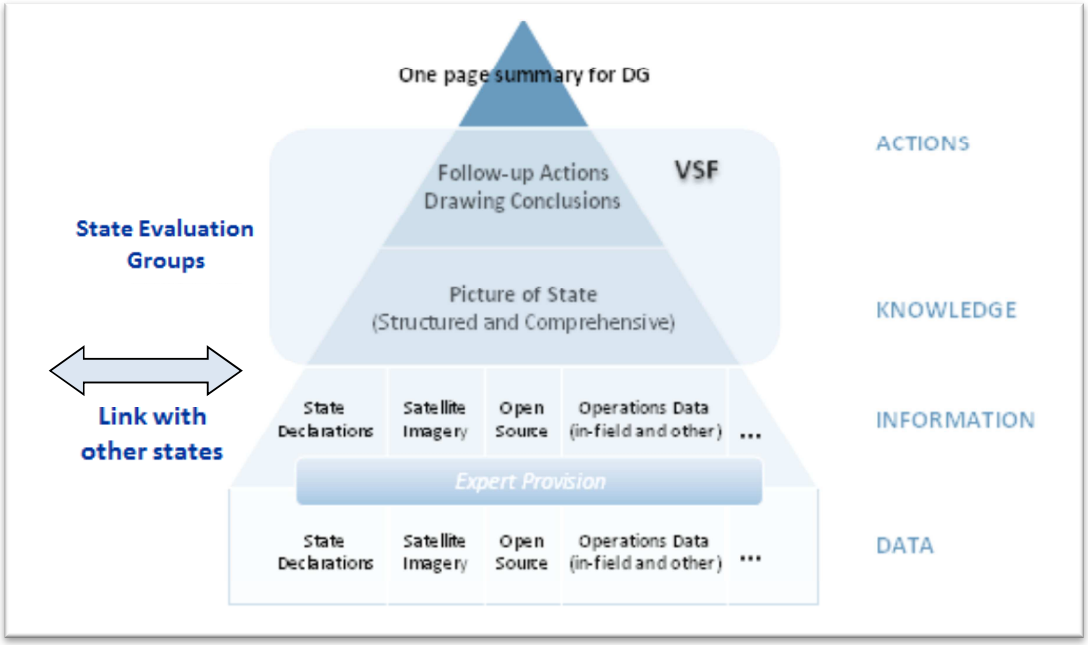

Fig.1: All Source safeguards-relevant information analysis – from data to actions [3]

The organizational structure of the Division of Information Management reflects these categories, which correspond to different analytical competencies. Besides the Integration and Coordination Team, it comprises four specialized Sections: the Declared Information Analysis Section whose role is self-explanatory, the State Factor Information Analysis Section in charge of general OS information analysis, the State Infrastructure Analysis Section specialized in geospatial information and satellite imagery analysis and the Nuclear Fuel Cycle (NFC) Information Analysis Section which collects, performs quality control of, stores, and evaluates results from in-field NDA measurements and from ES and DA samples to compare them with State declarations.

This paper will focus on the activities of the NFC Information Analysis Section. Its objective is to describe the challenges and opportunities encountered in this area from the evolution of the safeguards landscape and concepts, from the need for enhanced efficiency to cope with an ever increasing volume of data under static and sometimes reduced resource conditions, as well as from the progress made in information technology (IT) and data processing and evaluation methodologies. Section 2 below describes the strategy that was developed to address these challenges in a consistent, integrated and synergic manner, while utilizing state-of-the art IT tools and innovative data analysis and presentation. It will review the progress accomplished to date as well as future development plans.

2. Verification data evaluation and its evolution under the State Level Concept

Every year, thousands of days are spent by IAEA safeguards inspectors in NFC facilities and other sites around the world. A large portion of this time is used for carrying out in-field measurements by various NDA techniques and for taking ES and/or DA samples. Comparably intensive resources are needed to maintain CoK on the verification data collected through these activities by means of a range of sophisticated C/S systems. The IAEA collects, authenticates, quality controls, maintains and evaluates a large body of verification data. In this context, the specific mission of the NFC Information Analysis Section, as illustrated in Fig. 2 below is defined as follows: *to contribute to the Department's provision of credible safeguards conclusions through the evaluation of verification data from samples (ES, DA) and in-field measurements (NDA) and their comparison with State declared information in order to detect and deter diversion and undeclared activities at declared facilities and sites.*

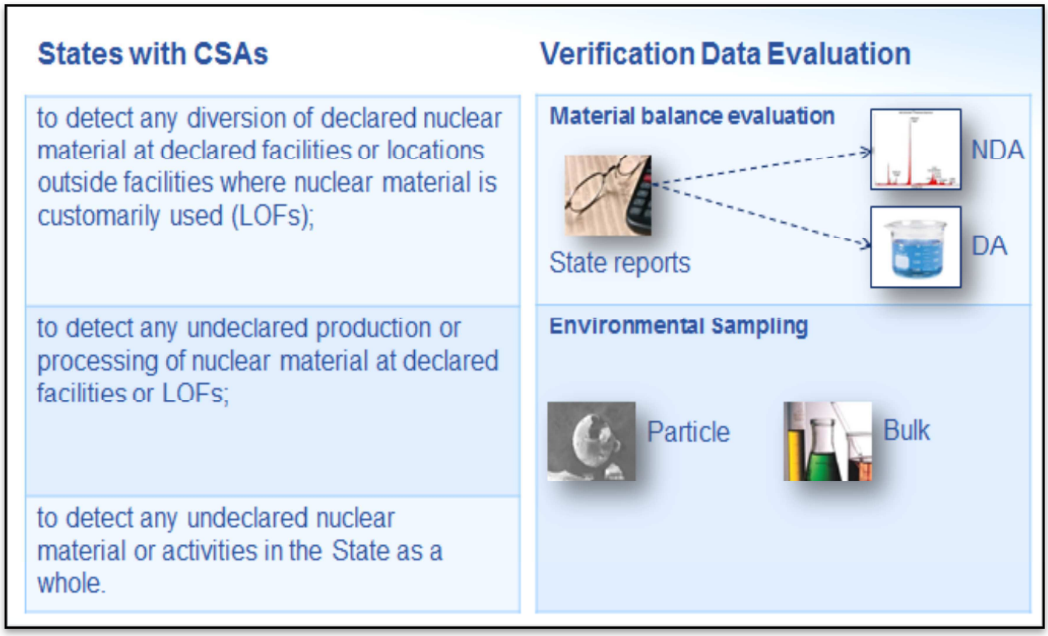

Fig.2: Role of verification data evaluation in supporting safeguards objectives under the State-level concept (example: States with a CSA).

2.1. ES data evaluation – detection of undeclared nuclear material and activities.

Fig. 2 shows that the role of ES data evaluation is different from that of NDA and DA data evaluation and that it requires different expertise profiles. Its purpose is to confirm that NFC facilities are operated as declared, that there are no undeclared nuclear materials or activities in these facilities and, within the limits of its implementation modalities, that there are no undeclared nuclear materials or activities in the State as a whole. The principle of ES rests on the premise that nuclear processes release traces of nuclear and other material that constitute a signature of these processes and that can be transferred to samples collected at appropriate places. The characteristics of materials found on swipe samples (e.g. isotopic ratios, association with radionuclides or other elements) are compared with those predicted by specialized process modelling tools. Particle analysis methods rely on the detection and measurement of individual nuclear material bearing particles on the sample while bulk analysis methods involve the analysis of an entire swipe sample - in this case, the analytical results represent average values associated with the nuclear material contained within the sample [7].

ES was implemented in the context of strengthening the effectiveness of the safeguards system following the discovery of Iraq's clandestine nuclear weapons programme in the aftermath of the 1991 Gulf War. Its feasibility and detective power were established through a series of field trials in the context of the *Programme 93+2* with the support of Member States. Analytical laboratories that would later form the basis of the present international network of analytical laboratories (NWAL)

demonstrated their capability to perform the extremely low-level radiochemical and isotopic measurements needed for the analysis of environmental samples. The field trials also showed that swipe sampling is the preferred method and it is now the standard, although other types of samples may be collected according to the technical objective pursued. For example, small quantities of ore or other compounds are collected for material characterization as described below.

Since 1995, ES samples have been taken at locations where IAEA inspectors have access during inspections and design information verifications (DIV) and, following the approval of the Additional Protocol by the IAEA Board of Governors in 1997, ES can be taken at a broader range of locations in States where an AP is in force. ES has expanded over the years to include all NFC facility types and the number of ES collected increased steadily to reach the current number of up to ~400 samples per year. Sub-samples are distributed to the NWAL, which presently includes 21 laboratories in 8 States in addition to two European Commission Joint Research Centers and the IAEA safeguards analytical laboratory (SAL) in Seibersdorf, Austria.

ES continues to evolve through scientific and technical developments supported by Member States' laboratories in close collaboration with the IAEA. IAEA International technical meetings are held every year, alternatively focusing on bulk or particle analysis, to review technological advances, among other objectives, and to discuss potential developments with representatives of the NWAL. For example, age dating makes it possible to establish the chronology of certain processes based on the isotopic composition of plutonium bearing particles. Age dating of uranium bearing particles based on thorium in-growth would require an improvement of the sensitivity of laboratory analyses but is also of high interest for potential future applications. Another promising development field is nuclear material characterization (aka impurity analysis), which associates samples of ore and other uranium compounds with signatures in terms of the trace elements they contain (for example lanthanides). These signatures, compared with global databases currently being populated, can be used to determine the origin of these materials by applying specialized statistical algorithms. Trace element fingerprints can also provide information about processes the material may have undergone. More generally, stable chemical elements in nuclear material bearing particles could reveal chemical signatures associated to processes such as reprocessing or enrichment. The feasibility and technical requirements of such evaluation methods are currently being investigated. An existing routine application of impurity analysis is to determine if the purity of the material sampled is suitable for fuel fabrication or isotopic enrichment and hence, if it should be subject to nuclear material accountancy measures under article 34 (c) of INFCIRC/153 (Corr.).

Since they have been developed in the wake of the strengthened safeguards system and in synergy with the evolution of safeguards concepts in the last decades, ES evaluation processes and deliverables are well integrated in the present SLC system. ES evaluation reports are delivered to Operation Divisions at both sample and State level according to increasingly performant time targets. Weekly performance indicators are regularly issued to monitor the timeliness of the process and the number of ES samples evaluated in different categories. The ES evaluation processes are effectively and efficiently supported by a state-of-the art ES database, automated report generation tools and regularly upgraded expert NFC modelling tools. This advanced IT environment makes it possible to compare the characteristics of isotopic species found in samples with those predicted by theoretical models and with isotopic species observed at other facilities worldwide. However, the unique expertise necessary for ES evaluation is very rare and its application to safeguards requires a long on-the-job training period. Therefore, a well-thought-out long-term recruitment and training plan is needed to maintain an adequate level of professional capacity and capability in the ES evaluation area.

2.2. DA and NDA data evaluation – detection of nuclear material diversion.

For their part, the NDA and DA data resulting from inspectors' verification sampling plans and combined with bulk measurements, i.e. weight and volume measurements, are compared with the State's NMA reports to detect diversion through the material balance evaluation (MBE) process. MBE is a complex analytical activity which assesses all quantitative declared information and verification results. In particular, at bulk handling facilities (BHF) where material is processed in loose forms (gases, liquids, powders) complex measurement systems are needed to establish the flows and inventories of material. The conclusions regarding material balances rest on resource-intensive statistical and metrological analyses based on the estimation and propagation of measurement uncertainties into uncertainties associated to balance statistics in order to determine if the BHF

operators' imbalances and the differences between nuclear material amounts declared by operators and measured by inspectors can plausibly be explained by legitimate measurement errors and, hence, to conclude on the absence of diversion from these facilities.
In contrast with ES data evaluation, MBE was developed at a much earlier stage of the safeguards' history and is rooted in the criteria-driven, facility-based approach which has long underpinned the IAEA's conclusions. While MBE principles and methodologies remain generally valid in the framework of a State-level evaluation, their scope (previously restricted to material balance areas (MBA) within facilities) needs to be expanded to the analysis of the nuclear material flows, inventories and balances of the whole State, taking into account the increasing use of random inspection schemes in State level approaches (SLA) and the implications for the statistical analysis of data collected according to these patterns. In addition to this undertaking, which poses a number of methodological challenges, new approaches are needed to optimize the distribution of limited MBE resources, to align them with the State-level technical objectives (TO) that are identified through the acquisition path analysis (APA) performed by the SEGs and to consolidate and compare MBE results with information from other sources. Last but not least, considerable progress was made in the field of IT and statistical methodologies since MBE was first developed several decades ago, and the migration of the safeguards Departmental IT platform under the Modernization of Safeguards Information technology (MoSaIc) project provides a unique opportunity to adapt and evolve methodologies and to integrate them into new software tools.

An additional and stringent practical challenge is to effectively address these development needs under a static budget with a small group of statistical analysis professionals whose primary mission is to deliver timely input to safeguards approaches, evaluations and conclusions for all States with extended NFCs, including a substantial support to priority mandates like the IAEA verification activities under the Joint Comprehensive Plan of Action (JCPOA) in Iran. Furthermore, evolving evaluation approaches and processes make it necessary to regularly communicate and collaborate with stakeholders within and outside the Safeguards Department through the organization of training and liaison actions. A fruitful project to evolve safeguards verification data evaluation must therefore rest on a well-structured and synergic strategy, based on a clear long-term development plan and taking into account manpower limitations while making the best use of available extra-budgetary support, e.g. in the form of Member State Support Program (MSSP) human resources and expertise. The strategy implemented by the NFC information analysis Section since its creation in July 2011 and illustrated schematically in Fig. 3 is articulated around a set of components whose common objective is to promote and provide new types of evaluation reports designed to effectively support the work of SEGs in drawing sound safeguards conclusions:

Fig.3: Organization and components of the NFC Information Analysis Section strategy to evolve verification data evaluation under the State-level concept

Quite evidently, the starting point of any strategy, as represented in the top of the diagram is to ensure sufficient human resources (HR) both in terms of manpower and expertise. The first implementation phase of the project therefore consisted in rebuilding a team of competent statistical data evaluators after the Safeguards Department capability and capacity in this field had virtually vanished following retirements and rotation of long-standing specialized staff. This was achieved through an extensive recruitment and training campaign completed in 2013 and 2014. However, maintaining adequate staffing, based on a regularly reviewed succession plan, remains a continuous effort, given the current shortage of adequate expertise on the world market.

In order to address the methodological component of the project and to foster new ideas, a biennial Technical Meeting (TM) on Statistical Methodologies for Safeguards was initiated to establish an overview of the methodological landscape in this field, gather worldwide expertise in addressing current gaps and questions, draft recommendations and build a network of specialists to remedy the lack of internal resources by identifying potential MSSP support tasks. The first meeting was held in Vienna in October 2013 and detailed recommendations were prepared around the high-level structure represented in Fig.4 below, which distinguishes to establish an overview of the methodological landscape in this field, gather worldwide expertise in addressing current gaps and questions, draft recommendations and build a network of specialists to remedy the lack of internal resources by identifying potential MSSP support tasks..

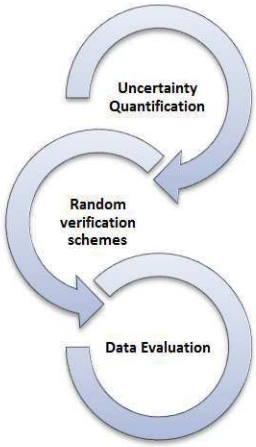

Fig.4: Three high-level interconnected methodological development areas as identified during the 1st TM on Statistical Methodologies for Safeguards (Vienna, October 2103).

Considerable progress, described in numerous publications [10], was made to date in the first two areas (uncertainty quantification and random verification schemes) and led to the preparation of several new safeguards technical reports (STR), thanks to extensive MSSP support in the form of cost free experts (CFE) and individual support tasks. The next phases planned include the harmonization of uncertainty quantification terminology between safeguards partners (evaluators, facility operators, laboratories) in preparation of the periodic review of international target values (ITV -2020) as well as a methodological consolidation of random inspections schemes. These topics will be the focus of the 3rd TM in October 2017. On completion of the prerequisite methodological work on uncertainty quantification and random verification schemes, the final phase will consist in reviewing and upgrading data evaluation methodologies which constitute the cornerstone of the overall project.

In parallel to the methodological review, evaluation processes and procedures are being adapted to the Departmental organisation which supports the work of the SEGs under the State-level concept. Process improvements were implemented in coordination with Operation Divisions in order to optimize both timeliness and quality based on available resources. Direct collaboration with inspectors in the framework of State-level approaches have significantly increased as well as in-field integration of evaluator expertise through their participation in inspections and design information verification (DIV) activities. This has greatly improved communication and collaboration between inspectors and evaluators and, in some cases, has allowed the resolution of long-standing issues. Quality control (QC) continues to be an essential

component of the data evaluation activities and is now implemented both at the level of source data and to the evaluation process and the resulting conclusions, by systematic peer-review, and by an additional review by inspectors in charge of facilities and States to ensure that all in-field and operational information has been taken into account.

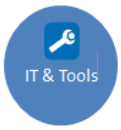

In the context of the re-engineering and integration of safeguards databases and software under the MoSaIc project and their migration into the secure integrated safeguards environment (ISE), all legacy software that was developed over the last decades to support statistical analysis, e.g. sampling plans, verification performance evaluation, analysis of DA sample results, and MBE, are also being re-engineered and integrated under the Statistical Testing, Evaluation and Planning for Safeguards (STEPS) project. The STEPS project is designed to take into account both methodological and best practise developments and is expected to substantially increase the efficiency of the evaluation processes through the automation of calculations, QC checks and report generation.

In the framework of the State-level concept, Operations inspectors and safeguards analysts need to understand and consolidate conclusions from many different sources of information. A structured programme of seminars is organised by the NFC Information Analysis Section to ensure effective communication with safeguards analysts from different areas and with Operation inspectors. These seminars address the mathematical rationales underlying safeguards verification strategies as well as the statistical treatment of the quantitative data declared by NFC facility operators and collected by Operations inspectors. Their objective is to present the mathematical and statistical methodologies applied in safeguards in a clear and progressive way, using a minimum of formalism and with special emphasis on practical examples taken from everyday safeguards experience.

In addition to training and regular liaison with IAEA partners, a valuable measure in monitoring the quality of NMA and verification data is a trilateral liaison framework [11] with the SRA and facility operators to discuss MBE results for the elapsed material balance period, review trends in material balance statistics, investigate their causes and agree upon recommendations and possible remedial actions. When available, DA sample results from three laboratories (IAEA, SSAC, facility operator) are also examined to identify biases and compare analytical uncertainties. Using not only IAEA's and operators' measurement results but also the SRA's results can help to investigate the source of significant pairwise differences of DA sample results. The cooperation of SRAs and facility operators with the IAEA in the framework of trilateral liaison meetings provides a useful mechanism to remedy any issue related to the quality of the operator's measurement systems before it becomes a safeguards concerns, thereby promoting a proactive rather than reactive approach. This considerably enhances safeguards effectiveness and efficiency since the root cause of NMA issues may be difficult to establish at a later point, when their effects on the material balance have reached a safeguards significant threshold. In several instances, yearly trilateral liaison meetings organized between the IAEA, SRA and plant operators have noticeably improved the operators' accounting procedures and/or measurement performance. In addition, trilateral meetings considerably improve the communication between safeguards partners by fostering direct contacts between IAEA, SRA experts and facility staff specialized in NMA and by making it possible to maintain continuity of knowledge on complex technical files in case of rotation of responsible staff on all sides. Given their in-depth knowledge of industrial processes, operational conditions and accounting systems, nuclear fuel cycle facility operators are often the most knowledgeable when it comes to identifying the source of procedural or measurement issues. A regular dialogue with them is an important confidence building measure that improves their understanding of safeguards objectives and practices and engages them to willingly cooperate in ensuring the performance of the facility's accounting and measurement system.

As was commented above, the bases for evolving DA, NDA and MBE data evaluation reports and designing new report types were laid by the NFC Information Analysis Section as a keystone and convergence point since the strategy described in this paper was first implemented. However, the deployment of new reports is progressive and depends on the development stage of the project components described above. The central challenge is to design a concept addressing the complexity of MBE at State level while *optimizing its effectiveness* at detecting diversion and/or misuse at *key points* of the State nuclear fuel cycle. This paragraph describes some of the main guiding principles, i.e. a) evolution from a facility oriented approach to a State-level approach b) integration of the *Physical Model* [8], as a backbone of

the method, to support flow analysis and information consolidation; c) use of modern *visualization tools* to extract significant facts and patterns and identify potential inconsistencies in growing volumes of data.

The table in Fig. 5 compares the main features of the new data evaluation reports with the former facility-oriented concept:

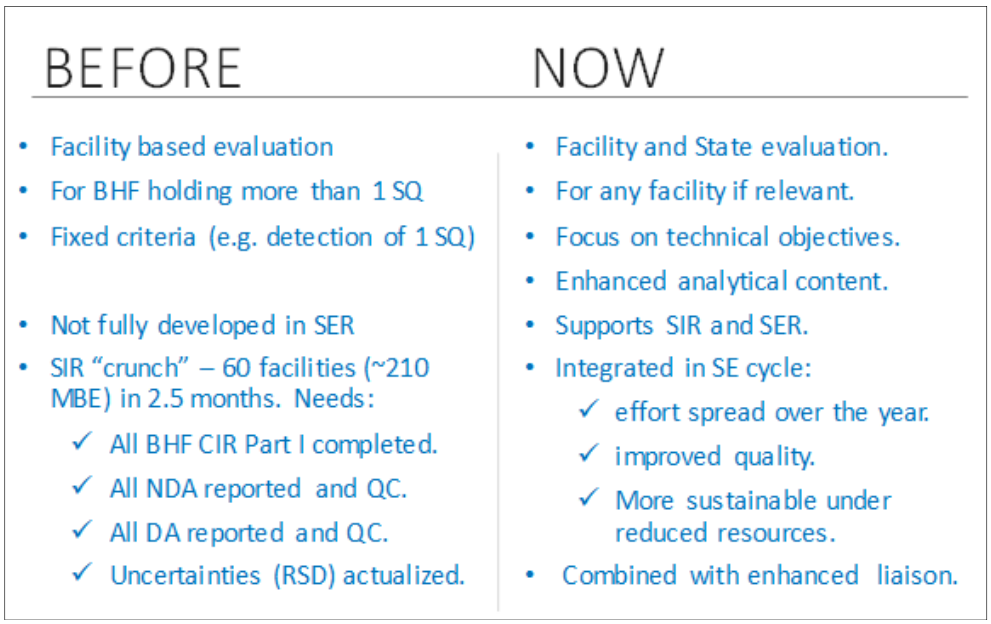

Fig.5: Evolution from a facility oriented approach to a State-level approach

In addition to providing a solution to resource limitations related to internal processes and timetables, the highlight of this new evaluation approach is that it is in line with one of the main tenets of the SLC, i.e. it addresses specific technical objectives (TO) resulting from the SEGs' APA and makes it possible to focus analytical resources on these TO as opposed to systematically checking a certain number of predetermined criteria. For example, while MBE evaluation was performed in the past for BHF holding more than one significant quantity (SQ) only, it can now be performed at any facility in agreement with the SEG if this is considered relevant to an identified acquisition path. Conversely, although it is important to mention that all large BHF will continue to be subject to MBE, the thoroughness of the evaluation may be adapted to prioritize analytical resources in case diversion during a given material balance period was covered by effective and conclusive measures (e.g. C/S), making MBE redundant, or in case the effectiveness of MBE is insufficient (e.g. low detection probabilities due to very large material flows/inventories).

The key principle of the method consists in visually representing nuclear material flows on a backdrop structure based on the Physical Model (PM) as shown in Fig 6. It can be outlined as follows:

- Facilities are represented by boxes grouped according to their function in the State nuclear fuel cycle (stages of the PM).
- For a period that can be customized by the user, nuclear material flows between facilities are visualized by solid curves whose colour represents material types and whose width is proportional to their magnitude (normalized in SQ), which can be read from the tick marks on the PM separation lines.
- Beginning and ending inventories are represented according to the same scale convention.
- Flows into and out of the States are symbolized by ellipses.

The APAs developed by SEGs identify paths, steps and the corresponding TOs which involve diversion or misuse of nuclear material at declared facilities. This makes it possible, as described above, to align data evaluation efforts with the results of the APA, taking into account the other safeguards measures foreseen by the SLA. In addition, operational links between facilities that can

influence specific MBE statistics and their trends are emphasized and integrated in the data evaluation. Initial trials performed in collaboration with SEGs demonstrated that the interest of the nuclear material flow diagrams underlying this method –referred to as Sankey diagrams[1] or "Snakeys" in reference to their sinuous appearance (Fig.6 below) - go beyond data evaluation and can usefully support the general work of SEGs, *inter alia*, the APA itself. The method has now evolved from the key elements described above to include a number of interactive features which support the current Departmental evolution from paper to electronic deliverables. In addition, the original concept is designed to integrate other types of relevant information (e.g. APA, SLA as well as ES, NDA and DA verification results). It is envisioned that, in future, it could serve as a possible portal to safeguards information in a State seen from a nuclear material perspective.

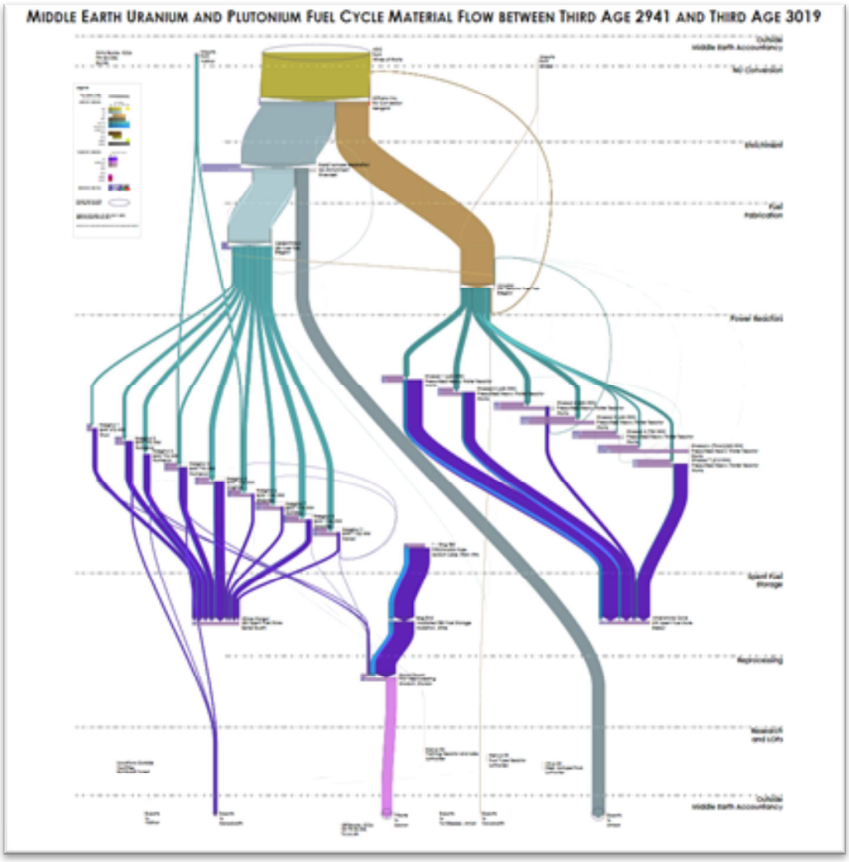

Fig.6: Snapshot of a nuclear material flow "Snakey" diagram for a hypothetical State

3. Conclusion

A structured, comprehensive and synergic long-term strategy is implemented by the Department of Safeguards' Division of Information Management NFC Information Analysis Section to evolve the evaluation of verification data in order to ensure the integration of its concepts, methods and processes into the SLC framework while optimizing its effectiveness in detecting undeclared nuclear material and activities and diversion of nuclear material at declared facilities. The present paper presents the complementary and mutually supporting components of this strategy, which converge towards the promotion and provision of new types of data evaluation reports designed to better support the work of SEGs.

[1] Sankey diagrams are named after Irish Captain Matthew Henry Phineas Riall Sankey, who used this type of diagram in 1898 in a classic figure (see panel on right) showing the energy efficiency of a steam engine (from Wikipedia)

An essential and innovative feature of this new generation of safeguards data evaluation reports is that it utilizes the power of modern IT, which allows interactivity, supports the Department's evolution to secure electronic deliverables and takes advantage of data visualization to complement the limited capacity of the human brain to extract useful and relevant information from large volumes of data.

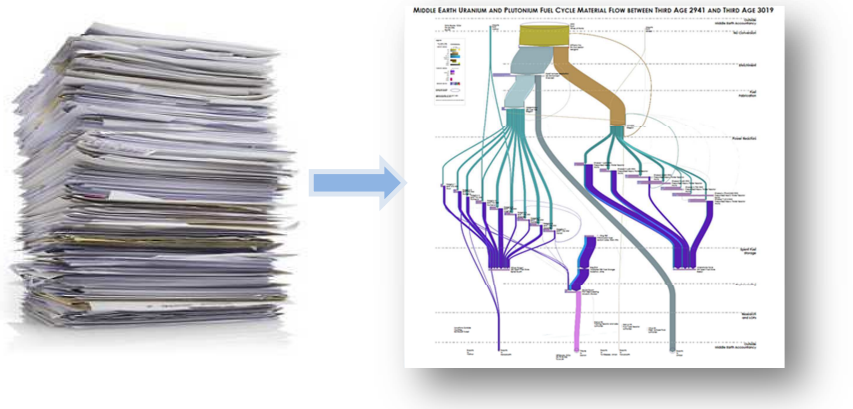

Fig.7: Data visualization can help analyze and understand large volumes of data

References

[1] Norman, C, M. Barletta, and M. Ferguson; *Collaborative Analysis in Support of State Evaluations*, IAEA-CN-184/268; Symposium on International Safeguards: Preparing for Future Verification Challenges; IAEA-CN-184/268; International Atomic Energy Agency, Vienna, Austria, 1-5 November 2010.

[2] Ferguson, M, and C. Norman; *All-Source Information Acquisition and Analysis in the IAEA Department of Safeguards;* In Proceedings of the INMM 52nd Annual Meeting, in Palm Desert, California USA, July 17-21, 2011.

[3] Baute, J. *Information Management Supporting the Evolution of the State-Level Concept*,in Proceedings of the INMM 53th Annual Meeting, Orlando, Florida, USA, July 15-19, 2012.

[4] C. Norman, M. Barletta, M. Ferguson; *Collaborative Analysis in Support of State Evaluations;* in proceedings of the IAEA International Safeguards Symposium, Vienna, 1-5 November 2010.

[5] C. Norman, K.Zhao, J. Baute; *Nuclear fuel cycle verification data and the state evaluation process: challenges and opportunities;* in proceedings of the INMM, 54th annual meeting in Palm Desert, California, USA; July 14-18th 2013.

[6] J. Baute, C. Norman, R.Binner, A. Walczak-Typke, F. Caillou, K. Zhao, E. Bonner*; Dynamic Exploratory Visualization of Nuclear Fuel Cycle Verification Data in Support of the State Evaluation Process*; in proceedings of the INMM, 56th annual meeting in Indian Wells, California, USA, July 12-16th 2015**.**

[7] IAEA; *Safeguards Technical Report -348 - Environmental sampling for safeguards,* Vienna, November 2011.

[8] IAEA; *Safeguards Technical Report -325 – Making use of the Physical Model,* Vienna, December 2000.

[9] International Atomic Energy Agency; *The Structure and Contents of Agreements between the Agency and States in Connection with the Treaty on the Non-Proliferation of Nuclear Weapons*, INFCIRC/ 153 (Corrected).

[10] C.Norman, T.Krieger, R. Binner, E. Bonner, N.Peter, C. Portaix, S. Richet, A. Walczak-Typke, J. Wüster, K. Zhao; *Outcome and Perspectives from the first IAEA International Technical Meeting on Statistical Methodologies for Safeguards;* in proceedings of the IAEA International Safeguards Symposium, Vienna, 20-24 October 2014.

[11] C. Norman, S. Iso, R. Binner, K. Zhao and C. Portaix*; Role and successes of trilateral liaison frameworks (IAEA -SSACs/RSACs - Nuclear Fuel Cycle Facility operators) in monitoring the quality of the operator's Measurement and Accounting Systems;* in proceedings of the IAEA International Safeguards Symposium, Vienna, 20-24 October 2014.

SAND2017-3795 C

Brain Science and International Nuclear Safeguards: Implications from Cognitive Science and Human Factors Research on the Provision and Use of Safeguards-Relevant Information in the Field

Zoe N. Gastelum, Laura E. Matzen, Heidi A. Smartt, Karl E. Horak, Eric M. Moyer, Matthew E. St. Pierre

Sandia National Laboratories
Albuquerque, New Mexico, USA

Abstract:

Today's international nuclear safeguards inspectors have access to an increasing volume of supplemental information about the facilities under their purview, including commercial satellite imagery, nuclear trade data, open source information, and results from previous safeguards activities. In addition to completing traditional in-field safeguards activities, inspectors are now responsible for being able to act upon this growing corpus of supplemental safeguards-relevant data and for maintaining situational awareness of unusual activities taking place in their environment. However, cognitive science research suggests that maintaining too much information can be detrimental to a user's understanding, and externalizing information (for example, to a mobile device) to reduce cognitive burden can decrease cognitive function related to memory, navigation, and attention.

Given this dichotomy, how can international nuclear safeguards inspectors better synthesize information to enhance situational awareness, decision making, and performance in the field? This paper examines literature from the fields of cognitive science and human factors in the areas of wayfinding, situational awareness, equipment and technical assistance, and knowledge transfer, and describes the implications for the provision of, and interaction with, safeguards-relevant information for international nuclear safeguards inspectors working in the field.

Keywords: safeguards; inspection; cognition; information

1. Introduction

In today's information age, more safeguards-relevant data is available for International Atomic Energy Agency (IAEA) nuclear safeguards inspectors than ever before. Inspectors are not only responsible for an increasing number of nuclear facilities as the number of safeguarded facilities continues to grow around the world, but more information about those facilities is available. This increased information availability is in part due to enhanced reporting requirements under the Additional Protocol, but also due to the unprecedented growth in availability and diversity of open source information. Providing this information alone will not support more effective safeguards inspections. More important, for both the traditional and emerging sources of information that can be used to support IAEA safeguards inspections, is the actionable provision of that information – providing the right information, in the right format, at the right time.

Since at least the 1990s, proposals have been brought forward to provide advanced information technology platforms for IAEA safeguards inspectors. Some of these proposals, such as deploying Agency laptops with inspectors, have become a reality and now a norm. Other proposals such as the integration of mobile touch screen devices like tablet computers or smart phones into inspection information collection or documentation, or the use of 3D holographic displays, have been more futuristic and less likely to be deployed near-term [for example, references 1, 2, 3]. Meanwhile, new software products have been developed or commercially procured by the Department of Safeguards to support information collection, analysis, and processing both at Headquarters and in the field [4, 5, 6, 7, 8]. While these tools appear to have preliminary positive results, there has been little evidence of

SAND2017-3795 C

formal assessments of how these tools impact a safeguards inspector's or analyst's cognition of the safeguards information being presented.

In this paper, we will explore unique insights from the cognitive science and human factors communities as they apply to international safeguards inspector use of, and interaction with, information during in-field activities. To identify the cognitive science and human factors principles most relevant for international nuclear safeguards activities, we first catalogued the most common safeguards activities conducted in the field. We then documented procedures for commonly used equipment or activities, and the information available to inspectors while conducting those activities. General categories of safeguards activities included, for example, destructive sampling, visual observation, and the use of safeguards equipment for non-destructive measurements of radioactive materials. From the catalogue of in-field safeguards activities and their relevant information environments, a list of relevant cognitive science and human factors concepts was assembled which included the following areas of study:

- Wayfinding;
- Inattentional blindness;
- Situational awareness;
- Equipment troubleshooting; and
- Knowledge transfer.

In addition to these cognitive science and human factors concepts relevant for safeguards tasks, a few common themes were identified that span across safeguards activities, including operation in one's non-native language, exhaustion, stress due to time constraints, and operation in industrial environments. While these factors were also considered relevant to effective execution of international safeguards activities in the field, their pervasiveness and the difficulty to ameliorate them within international safeguards inspection scenarios led to removal from consideration in this aspect of our research.

In this paper, we will describe each of the selected cognitive science and human factors areas of study in turn, including a discussion of their relevance to safeguards activities and the current understanding of best principles or practices that may influence how to interpret their findings for international nuclear safeguards.

2. Application of Cognitive Science and Human Factors Literature to International Nuclear Safeguards

Cognitive science and human factors are scientific fields that study human behavior, activity, and learning from two distinct perspectives. For the purposes of this research, cognitive science studies human thought, learning, and mental organization related to how individuals interact with and understand information related to international nuclear safeguards inspection activities. Human factors, on the other hand, studies human interactions with a system (such as a safeguards procedure or piece of equipment) and can impact how individuals act in their physical environment based upon information they are provided. Thus, both disciplines can provide unique insight into effective and efficient means to provide information to international nuclear safeguards inspectors working in the field.

2.1. Wayfinding

Wayfinding is a form of spatial cognition in which people determine where they are in an environment and how to navigate to where they want to go [9]. Wayfinding can include navigation by map, landmarks, or verbal/written directions outdoors or indoors.

2.1.1. Wayfinding for International Safeguards

When safeguards inspectors move from one part of a facility to another, they must rely on their wayfinding skills to effectively navigate a nuclear site or facility. This includes both indoor and outdoor navigation. For outdoor navigation, inspectors can have access to GPS, maps with landmarks, or other aids. But indoors, inspectors rely on a facility map or their own mental map of the facility based

on previous experience. Even if they are being escorted by an operator, inspectors should be aware of where they are so that they can efficiently go from one area to another within a facility and ensure that they are being taken to the correct location. They should also be able to note if routes taken at a site or facility appear circuitous or seem to avoid areas that were previously on the regular route (which may be cause for follow-up questions).

2.1.2. Theoretical Background of Wayfinding Research

Some prior studies have potential relevance for international nuclear safeguards inspections. Several studies [10, 11, 12] have attempted to compare wayfinding using paper maps to wayfinding using mobile maps or GPS devices. These studies have had mixed results, with some finding that users took longer to reach their destinations when using a paper map [11] and others finding that participants took longer when using GPS [12]. The generalizability of the results of these studies is limited by factors such as small sample sizes [10], small screen sizes on the electronic devices [12], and inexperience with mobile maps on the part of the participants [12]. In the years since these studies took place, increasing familiarity with mobile maps and GPS among the general population could lead to very different results. However, one finding that is likely to hold true is that mobile map users tend to have a poorer understanding of the overall layout of the area in which they are navigating [10]. A paper map provides participants with an overview of the area, an aspect of navigation that is often absent when people navigate using point-to-point directions provided by a navigation app. This finding indicates that safeguards inspectors may have very different mental models of a facility if they learn its layout by walking through it as opposed to studying blueprints or diagrams. This in turn may influence how they navigate through a site or facility and how they notice changes or discrepancies.

Another area of wayfinding research that applies directly to the safeguards domain addresses indoor navigation. This is an area of interest for researchers who are trying to understand how to help people navigate through complex buildings, such as hospitals, transportation hubs, or large shopping centers. While navigation apps and mobile maps have been widely adopted for outdoor use, these tools typically fail for indoor environments, where GPS does not work (due to signal weakness) and navigation landmarks such as street names and numbers are absent. Researchers have attempted to address these problems by developing indoor navigation systems that use waypoints rather than continuous information about a person's location. For example, Mulloni, Seichter and Schmalstieg [13] demonstrated a system that provides turn-by-turn directions from one waypoint to another. In another study, Mulloni et al [14] used a similar system in which localization markers were used to help attendees navigate during a conference. Trilateralization from Wi-Fi transmitters is also a possible solution [see 15].

These navigation techniques might be applicable within the safeguards domain to help inspectors navigate a complex facility. However, in any application of navigation aids, it is important to note that there are substantial individual differences in terms of how people navigate [16]. Indoor navigation systems must be designed so that they are robust to individual differences in the users' spatial abilities and navigation preferences. Furthermore, indoor navigational aid deployment would require approval and cooperation from the facility operator regarding placement of such markers, maintenance of their integrity, and the use of mobile technologies to engage or interpret them.

2.2 Inattentional Blindness

Inattentional blindness, also known as "change blindness" or "perceptual blindness", is the concept that the changing of certain stimuli, considered to be in plain sight, is missed by an observer. Studied to a relatively large extent within the academic psychological research community, it has sometimes been relegated to a status of marginal importance due to the historical difficultly ability of drawing practical inferences from the research results [17]. However, human observers' tendency to miss changes that occur right in front of them has been demonstrated repeatedly [18, 19].

2.2.1 Inattentional Blindness and International Safeguards

The discovery of Iraq's nuclear weapons program the early 1990's led to a shift in international nuclear safeguards from the verification of solely the correctness of a state's declaration, to verification of both the correctness and *completeness* (i.e., no undeclared nuclear activities) of the declaration. This led to a change in expectation that safeguards inspectors would become more investigative, and the

SAND2017-3795 C

incorporation of multiple visual observation and detection of anomaly tasks required as part of safeguards inspection activities. However, inattentional blindness research indicates that even highly focused safeguards inspectors may miss key information from their environment. For example, one of the most well-known examples of inattentional blindness is from an experiment conducted by Daniel Simons and Christopher Chabris [20], in which the researchers documented a sustained period in which test subjects asked to count the number of ball passes between a select group of individuals failed to notice the presence of someone dancing in a gorilla suit in the scene. The experiment calls into question whether international safeguards inspectors focused on one type of data collection in the field might inadvertently miss critical information that could indicate anomalous or undeclared activities at a facility or site under IAEA safeguards.

2.2.2. Theoretical Background of Inattentional Blindness Research

Recent research in the field of inattentional blindness has focused on humans in real-world contexts rather than laboratory studies. This research is showing that change blindness occurs often and in many circumstances in the real-world. One such study demonstrated that many observers failed to notice when a conversation partner was replaced in the middle of a real-life interaction [21, 22]. These research efforts have established that attention is needed to see change, and that we possess a finite ability to focus our attention on our environment. Therefore, changes to semantically central items in a scene are detected faster than changes elsewhere [18] which suggests that we assign preferential attention to certain objects based on context [23]. While attention is required for conscious change perception, the focus of our attention can change frequently while viewing a scene. If a change occurs in the scene, we may miss it despite actively viewing the scene [24, 25].

Various studies in change detection have shown that only about four items can be monitored at a time. This supports other research which implies we possess only one mechanism for the formation and maintenance of coherent visual attention, primarily concerned with the perception of objects [26]. This research may have implications on how safeguards inspectors divide tasking within an area of a nuclear facility in order to limit over-burdening the brain's visual observation capacity.

Additionally, scene representation plays a large part in our ability to visually attend to objects, and we only attend to what we need from the scene for the task at hand [25], reinforced by our experience with the stimuli being viewed. We usually do not need to mentally represent all the objects around us at any given time in order to make sense of our environment. Rather, we need only to represent the objects, and properties of those objects, involved in a task at hand. Thus it is possible that we operate with a dynamic representation of a scene that is highly sensitive to the demands of the current task and the expectations of the observer [27]. For safeguards inspectors working in the field, therefore, their mental models will appropriately shift between broad site-level understanding and smaller, more detailed visual representations needed to complete specific safeguards verification tasks.

Other studies in inattentional blindness indicate that the amount of knowledge or familiarity an individual possesses about the objects in any given scene influences their ability to detect changes to that object [28]. For example, social drug users are more likely to detect changes to drug paraphernalia in photographs than are non-drug users [29] and American football experts are better able to spot changes to football scenes than are novices [30]. This has also been demonstrated regarding change detection with people [21], for objects described to individuals about scenes they view afterwards [18], and objects of interest to the observer [31]. This means we detect changes much more easily for objects we are familiar with or are told are of importance in a particular scene. In this context, international nuclear safeguards inspectors would be expected to have higher than average change detection capabilities in nuclear facilities they are familiar with, but may still suffer from inattentional blindness to changes in a facility when focusing on a specific task or area not associated with the change.

2.3 Situational Awareness

Situational awareness is the term used to describe a person's understanding of "what is going on" [32, 33]. This topic has received considerable research attention over the past three decades because it is a crucial component of human performance in any dynamic situation. According to the most widely-used model of situational awareness, to perform efficiently humans must be able to 1) perceive the

important things in their environment, 2) understand them, and 3) be able to predict what will happen next [32].

2.3.1. Situational Awareness for International Safeguards

The highly investigative and observational nature of international nuclear safeguards activities, combined with a potentially hazardous working environment, makes inspector situational awareness crucial for their ability to safely and effectively observe anomalous or unusual activities during the course of their on-site activities. Inspectors must be aware not only of their current task at hand, but the operation of a nuclear facility or site that provides broader context to their safeguards verification activities.

2.3.2 Situational Awareness Theory

A variety of methods have been employed for improving situational awareness. Experience is a key component of situational awareness, with more experienced individuals generally exhibiting higher levels of situational awareness [34]. Thus, training and knowledge transfer can directly influence situational awareness. The way in which information is presented to an individual also has significant impact on situational awareness, which has led to a great deal of research on how to visualize information for rapid consumption by the user [35, 36, 37, 38].

In general, the design of a system has a substantial impact on situational awareness. A well-designed system or tool should present the user with the right information at the right time and in the right format to support the components of situational awareness: perception, comprehension, and projection. The details of these tasks are often domain-specific, so many researchers have focused on developing methodologies for understanding situational awareness within a specific operational context such as cyber defense [35], emergency medicine [39] and law enforcement [40].

Though situational awareness has not been explicitly studies in relation to international safeguards inspections, the techniques outlined above could be applied to understanding the components of situational awareness for different types of inspection activities. Once these components have been identified, new technologies such as data visualizations or enhanced training techniques could be developed to improve inspectors' situational awareness.

2.4 Equipment Troubleshooting

Humans interact with systems such as technical equipment on a regular basis, most commonly via intuitive action/reaction modes. This is especially true for people who are frequent users of the equipment. However, when equipment malfunctions or breaks, use of that equipment can quickly become frustrating. User guides are not always straightforward or available, and often require the user to know the specific problem with the equipment in order to troubleshoot it effectively. Troubleshooting is a form of problem solving in which users "diagnose faulty systems and take direct, corrective action to eliminate any faults in order to return the systems to their normal states" [41].

2.4.1 Equipment Troubleshooting for International Safeguards Equipment

IAEA safeguards inspectors use a large variety of safeguards equipment depending on the activity they will be carrying out in the field, and facility-specific requirements. Some equipment is brought with the inspector or shipped from IAEA headquarters, while other safeguards equipment is stored on-site. While an inspector might only use a limited number of pieces of equipment for a specific safeguards inspection, there are many types of equipment that they might use over the course of their safeguards activities at different facilities or for different inspection types. In cases where maintenance is scheduled or an especially challenging piece of equipment will be used, a technician may accompany the inspector. However, inspectors often encounter equipment failure or malfunction during the course of routine use of equipment that they are required to resolve in the field.

2.4.2. Theoretical Foundations of Equipment Troubleshooting

Research in novice troubleshooting strategies tends to focus on structured representations of the system in which large parts of the problem space can be discounted early on [42]. (This "pruning of

SAND2017-3795 C

the search tree" is much like the selective search carried out by expert chess players.) The representation of the system as a functional hierarchy can be used to facilitate their troubleshooting in some cases [43, 44, 45].

Kurland and Tenney posit that documentation provided for troubleshooting can be too difficult for a novice to extract, leading to information overload. In other cases, documentation might not be available. According to research conducted by Schaafstal [42] and Kurland and Tenney [46], challenges facing novice troubleshooters can come from one of two areas: 1) their limited experience with and understanding of the system, or 2) lack of a systematic approach in which robust and flexible troubleshooting strategies are applied for goal-oriented problem solving. Both Shaafstal et al [42] and Jonassen and Hung [41] stress the importance of a training regimen for troubleshooting that includes both a systematic understanding of the equipment at hand as well as a system-independent strategy for troubleshooting that prevents information overload and ensures a consistent troubleshooting approach across systems. For international safeguards inspectors, this will require training both on the safeguards equipment the inspectors will use in the field and equipment troubleshooting strategies that are equipment-agnostic.

2.5 Knowledge Transfer

Knowledge transfer refers to sharing information and experience across different teams or parts of an organization [47]. This includes knowledge that individuals or teams have gained through experience, as well as routines and procedures that have been developed over time [48]. Institutional knowledge resides in many places, including individuals, organizational structures, operating procedures, institutional culture, tools and technologies, and in the interrelationships created by combining individuals, tasks, and tools [47]. When one team hands off work to another, or when people move in or out of an organization, transferring knowledge is crucially important for maintaining continuity. Similarly, as new forms of institutional knowledge are acquired, they must be disseminated through the organization in order to improve the performance of the organization as a whole.

2.5.1 Knowledge Transfer for International Safeguards

Knowledge transfer is a critical component of international safeguards inspection activities, to ensure that facility subject matter expertise is passed from experienced to newer inspectors, as well as the transfer of information learned from in-field inspection activities from one inspector (or inspection team) to another. While most of the research regarding knowledge transfer has related to shift workers who have brief periods of overlap, IAEA safeguards inspector knowledge transfer poses a new challenge due to the amount of time between inspector visits to a facility. In this case, knowledge is being transferred mostly through paper or electronic documentation (though some may occur via in-person briefs before an inspection). Due to travel time and the potential for multiple inspections at different facilities or countries to occur in a single trip, an in-person brief may take place days or weeks before visiting the facility. Further, some information may be left at IAEA headquarters with only notes taken into the field to avoid potential loss or exposure of sensitive information (significantly increasing reliance on memory).

2.5.2. Theoretical Background of Knowledge Transfer

Knowledge transfer has been studied in shift work environments, such as manufacturing environments [48], hospitals [49], and nuclear power plants [50]. Handoffs between shifts are crucial for maintaining continuity and preventing duplication of effort in which different teams are independently trying to solve the same problems [48]. Failures of knowledge transfer between shifts have been identified as key components in industrial accidents [51, 52] and medical errors [53]. Research on knowledge transfer in these domains has identified key strategies that are used to facilitate the handoff of information (Patterson et al., 2004) and handoff checklists that could be applied to a variety of domains [52].

Face-to-face meetings are often used to transfer knowledge from one shift to the next, but this transfer can also occur via *boundary objects*. Boundary objects are artifacts that support the translation of information from one group to another, allowing disparate groups to communicate and work toward common goals [54, 55]. Bosua and Venkitachalam [48] explored the use of boundary objects in shift handovers. Of the three shift environments studied, only one had a system for codifying knowledge

SAND2017-3795 C

and making it easily available to all shifts. The culture of codifying and transferring knowledge facilitated handoffs from one team to the next.

The safeguards domain shares some features with shift work environments, such as the need to transfer knowledge from one inspection team to the next. However, it also differs from shift work environments in several key ways. For example, shifts in a hospital setting occur back-to-back, allowing different teams to overlap and share information during the transition between shifts. In contrast, there may be weeks or months between facility inspections and different teams of inspectors may not meet face-to-face. This introduces additional challenges, such as the need for robust boundary objects that can adequately transmit knowledge from one team to the next, as well as the need to account for changes that may occur between inspections. While international safeguards inspectors do complete extensive documentation regarding their in-field inspection activities, the format of this information may or may not support effective knowledge transfer between teams. The question remains as to how safeguards-relevant knowledge from inspections at a specific site is best transferred from one team to the next.

3. Conclusions

Some of the cognitive science and human factors disciplines related to mechanisms by which international safeguards inspectors interact with information in the field are well studied, such as interior and outdoor wayfinding using various navigational aids. Others, such as knowledge transfer, are well studied in specific situations but do not currently capture significant nuances for international safeguards application space. Over the next three years, researchers at Sandia National Laboratories will develop and execute human performance experiments on mechanisms for the effective provision of information for safeguards inspection-like scenarios. We will seek to measure accuracy, timeliness, and situational awareness of test subjects performing safeguards-relevant activities and suitable proxies dependent upon the type, quantity, and provision mechanism of information to which test subjects have access. In this way, the project team seeks to have both an impact on the state of understanding in the cognitive science and human factors fields, as well as provide meaningful and actionable results that can be implemented to support international safeguards inspectors working in the field.

4. Acknowledgements

The work described in this paper is funded by Sandia National Laboratories' Laboratory Directed Research & Development office.

5. References

1. DeLand, S, Blair, D and Horak, K; *Mobile Computing for On-Site Inspection; Proceedings of the Annual Meeting of the Institute of Nuclear Materials Management*; Indian Wells, CA, USA; 2015.

2. Gastelum, ZN, Henry, MJ, Burtner, ER, Doehle, JR, Zarzhitsky, DV, Hampton, SD, LaMothe, RR, Nordquist, PL; *The Development of an Example Precision Information Environment for International Safeguards Use Cases; Proceedings of the Annual Meeting of the Institute of Nuclear Materials Management*; Indian Wells, CA, USA; 2015.

3. Gastelum, ZN, Brotz, JK, Le, TD, Whalen, RT, Bolles, JC; *Proposed Use Cases for Augmented Reality for Nuclear Nonproliferation Verification and Training; Proceedings of the Institute of Nuclear Materials Management;* Atlanta, GA, USA; 2016.

4. Steinmaus, K, Norman, C, Ferguson, M, Rialhe, A, Baute, J; *The Role of the Geospatial Exploitation System in Integrating All-Source Analysis; Proceedings of the Annual Meeting of the Institute of Nuclear Materials Management*; Palm Desert, CA, USA; 2013.

SAND2017-3795 C

5. Vilece, K, Norman, C, Baute, J, Giaveri,cG, Kiryu, M, Pellechi, M; *Visualization of Environmental Sampling Results at Inspected Facilities; Proceedings of the Annual Meeting of the Institute of Nuclear Materials Management*; Orlando, FL, USA; 2012.

6. Norman, C, Baute, J, Binner, R, Walczak-Typke, AI, Aillou, F, Zhao, K, Bonner, E; *Dynamic Exploratory Visualization of Nuclear Fuel Cycle Verification Data in Support of the State Evaluation Process; Proceedings of the Annual Meeting of the Institute of Nuclear Materials Management*; Indian Wells, CA, USA; 2015,.

7. Crowley, J, Gagne, D, Calle, D, Murray, J, Kirkgoeze, R, Moser, F; *Computational Methods for Physical Model Information Management: Opening the Aperture; Proceedings of the 2014 Symposium on International Safeguards: Linking Strategy, Implementation and People;* Vienna, Austria; 2014.

8. IAEA; *The Modernization of Safeguards Information Technology: Completing the Picture;* 2017. https://www.iaea.org/sites/default/files/17/01/mosaic.pdf

9. Raubal, M, Egenhofer, M; *Comparing the complexity of wayfinding tasks in built environments; Environment & Planning B*; 25; 1998; 895-913.

10. Willis, KS, Hölscher, C, Wilbertz, G, Li, C; *A comparison of spatial knowledge acquisition with maps and mobile maps*; *Computers, Environment and Urban Systems; 33*; 2009; 100-110.

11. Lee, W, Cheng, B; *Effects of using a portable navigation system and paper map in real driving; Accident Analysis and Prevention;* 40; 2008; 303-308.

12. Ishikawa, T, Fujiwara, H, Imai, O, Okabe, A; *Wayfinding with a GPS-based mobile navigation system: A comparison with maps and direct experience; Journal of Environmental Psychology; 28;* 2008; 74-82.

13. Mulloni, A, Seichter, H, Schmalstieg, D; *Handheld augmented reality indoor navigation with activity-based instructions; Proceedings of MobileHCI*; 2011.

14. Mulloni, A, Wagner, D, Schmalstieg, D, Barakonyi, I; *Indoor positioning and navigation with camera phones; Pervasive Computing*; 2008; pp. 22-31.

15. Shchekotov, M; *Indoor Localization Method Based on Wi-Fi Trilateralization Technique*; *Proceedings of the 16th Conference of Fruct Association*; Oulu, Finland; 2014.

16. Lawton, CA; *Strategies for indoor wayfinding: The role of orientation*; *Journal of Environmental Psychology;16;* 1996; 137-145.

17. Simons, DJ, Rensink, RA; *Change blindness: past, present, and future; TRENDS in Cognitive Science;* Vol. 9; No. 1; 2005.

18. Rensink, RA, O'Regan, JK, Clark, JJ; *To see or not to see: The need for attention to perceive changes in scenes*; *Psychological Science*; Vol. 8; Issue 5; 368–373.

19. Simons, DJ, Levin, DT; *Change blindness*; *Trends in Cognitive Sciences;* Vol 1; Issue 7; 1997; 261–67.

20. Simons, DJ, Chabris, CF; Gorillas in our Midst: *Sustained Inattentional Blindness for Dynamic Events; Perception*; Vol 28; Issue 9; 1999.

21. Simons DJ, Levin DT. *Failure to Detect Changes to People during a Real-World Interaction; Psychonomic Bulletin & Review*; Vol 5; Issue 4; 1998; 644–49.

22. Levin, DT; Simons, DJ, Angelone, BL, Chabris, CF; *Memory for Centrally Attended Changing Objects in an Incidental Real-World Change Detection Paradigm; British Journal of Psychology;* Vol 93; Issue 3; 2002; 289–302.

SAND2017-3795 C

23. Kelley, TA, Chun, MM, Chua, K-P; *Effects of scene inversion on change detection of targets matched for visual salience; Journal of Vision*; Vol 3, Issue 1; 2003; 1–5.

24. Williams, P, Simons DJ*; Detecting changes in novel, complex three-dimensional objects; Visual Cognition*; Vol 7; Issue 1-3; 2000; 297–322.

26. Rensick, RA; *Seeing, sensing, and scrutinizing; Vision Research;* Vol 40; 2000; 1469 – 1487.

27. Rensick, RA; *Change Detection*; *Annual review of Psychology*; Vol 53; 2002; 245 -77.

28. Archambault, A, O'Donnell, C, Schyns, PG; *Blind to Object Changes: When Learning the Same Object at Different Levels of Categorization Modifies its Perception; Psychological Science*; Vol 10; 1999; 249–255.

29. Jones, BT, Jones, BC, Smith, H, Copley, N; *A Flicker Paradigm for Inducing Change Blindness Reveals Alcohol and Cannabis Information Processing Biases in Social Users; Addiction;* Vol 98; 2003; 235–244.

30. Werner, S, Thies, B; *Is 'Cange Blindness' Attenuated by Domain-Specific Expertise? An Expert-Novices Comparison of Change Detection in Football Images; Visual Cognition*; Vol 6; 2000; 163–173.

31. Shore DI, Klein, RM. The Effects of Scene Inversion on Change-Blindness. *Journal of General Psychology;* Vol 127; Issue 1; 2000; 27-43.

32. Endsley, M R; *Toward a Theory of Situation Awareness in Dynamic Systems; Human Factors;* Vol 37; 1995; 32-64.

33. Endsley, M; *Theoretical Underpinnings of Situation Awareness: A Critical Review; Situation Awareness: Analysis and Measurement* (Eds. Endsley, M, Garland, D); Erlbaum; Mahwah, NJ, USA; 2000; 3-32.

34. Underwood, G, Ngai, A, Underwood, J; *Driving Experience and Situation Awareness in Hazard Detection; Safety Science*; Vol 56; 2013; 29-35.

35 D'Amico, A, Kocka, M; *Information Assurance Visualizations for Specific Stages of Situational Awareness and Intended Uses: Lessons Learned; IEEE Workshop on Visualization for Computer Security*; 2005; 107-112.

36. Feibush, E, Gagvani, N, Williams, D; V*isualization for Situational Awareness; IEEE Computer Graphics and Applications*; Vol 20; Issue 5; 2000; 38-45.

37. Kim, YJ, Hoffmann, CM; *Enhanced Battlefield Visualization for Situation Awareness; Computers & Graphics;* Vol 27; Issue 6; 2003; 873-885.

38. Toet, AI, Jspreert, JK, Waxman, AM, Aguilar, M; *Fusion of Visible and Thermal Imagery Improves Situational Awareness; Displays;* Vol 18; 1997; 85-95.

39. Sapateiro, C, Antunes, P; *An Emergency Response Model toward Situational Awareness Improvement; Proceedings of the 6th International ISCRAM Conference;* Gothenburg, Sweden; 2009.

40. Datcu, D, Lukosch, S, Lukosch, H, Cidota, M; *Using Augmented Reality for Supporting Information Exchange in Teams from the Security Domain; Security Informatics;* Vol 4; 2015.

41. Jonassen, DH, and Woei H; *Learning to Troubleshoot: A New Theory-Based Design Architecture*; *Educational Psychology Review;* Vol. 18; No. 1; 2006; 77-115.

42. Schaafstal, A, Maarten, J, van Berlo, M; *Cognitive Task Analysis and Innovation of Training: The Case of Structured Troubleshooting*; *Human Factors*; Vol 42; No. 1; 2000 75-86.

SAND2017-3795 C

43. Bereiter, SR, Miller, SM; *A Field-Based Study of Troubleshooting in Computer-Controlled Manufacturing Systems; IEEE Transactions on Systems, Man, and Cybernetics*; Vol 19, 1989; 205–219.

44. Egan, DE, Schwartz, BJ; *Chunking in Recall of Symbolic Drawings; Memory and Cognition*; Vol 7; 1979; 149–158.

45. Rasmussen, J; *Information Processing and Human-Machine Interaction: An Approach to Cognitive Engineering*; Elsevier; Amsterdam; 1986.

46. Kurland, LC, Tenney, YJ*; Issues in Developing an Intelligent Tutor for a Real-World Domain: Training in Radar Mechanics; Intelligent Tutoring Systems: Lessons Learned* (Eds Psotka, J, Massey, LD, Mutter, SA); Psychology Press; Hove, UK; 1988; 119–180.

47. Argote, L, Ingram, P; *Knowledge Transfer: A Basis for Competitive Advantage in Firms*; *Organizational Behavior and Human Decision Processes;* Vol. *82;* 2000; 150-169.

48. Bosua, R, Venkitachalam, K; *Fostering Knowledge Transfer and Learning in Shift Work Environments; Knowledge and Process Management;* Vol. 22; 2015; 22-33.

49. Kerr, MP; *A Qualitative Study of Shift Handover Practice and Function from a Socio-Technical Perspective; Journal of Advanced Nursing*; Vol. 37; 2002; 125-145.

50. Patterson, ES, Roth, EM, Woods, DD, Chow, R, Gomes, JO; *Handoff Strategies in Settings with High Consequences for Failure: Lessons for Health Care Operations*; *International Journal for Quality in Health Care;* Vol. 16; 2004; 125-132.

51. Lardner, R; *Effective Shift Handover: A Literature Review; Offshore Technology Report - Health and Safety Executive OTO*; 1996.

52. Wilkinson, J, Lardner, R; *Pass it on! Revisiting Shift Handover after Buncefield; Loss Prevention Bulletin;* Vol 229; 2012; 25-32.

53. Cook, RI, Woods, DD, Miller, C; *A Tale of Two Stories: Contrasting Views of Patient Safety; National Health Care Safety Council of the National Patient Safety Foundation at the AMA*; 1998.

54. Star, SL, Griesemer, JR; *Institutional Ecology, 'Translations' and Boundary Objects: Amateurs and Professionals in Berkeley's Museum of Vertebrate Zoology; Social Studies of Science;* Vol 19; Number 3; Issue 1907-39; 1989; 387-420.

55. Trompette, P, Vinck, D; *Revisiting the Notion of Boundary Object; Revue d'Anthropologie des Connaissances;* Vol 3; 2009; 3-25.

The forward-problem approach in Safeguards verification: directly comparing simulated and measured observables

S.Vaccaro[1], I. Gauld[2], M. Vescovi[3], H. Tagziria[4], A. Smejkal[1], P. Schwalbach[1]

[1]European Commission, Directorate General Energy, Directorate Euratom Safeguards, Luxembourg

[2]Oak Ridge National Laboratory, Oak Ridge, TN, USA

[3]iScience, Milan, Italy

[4]European Commission, Directorate Joint Research Centre, Directorate Nuclear Safety & Security, Ispra, Italy

Abstract:

Physical verification by NDA in nuclear safeguards implies typically the adoption of an inverse-problem approach. This is, indeed, the definition of a problem, in which we use physical observables to deduct other physical quantities, which in our case are contained in the operator's declaration. A typical example is the Plutonium mass, measured using Pu isotopics and neutron coincidence doubles counts, linked to the Pu 240 effective mass by a calibration.

An alternative approach has been recently proposed and is now close to the in-field deployment by the Euratom Safeguards Directorate of European Commission's DG ENER. In fact, the detailed knowledge of the physical processes that are taking place in the sample and within the detector allows computing the amount of the measured observable, by modelling the physical system as it results from the operator's declaration, in a forward-problem approach.

The present paper describes the first two examples of the forward-problem approach's application to actual real-life safeguards verification. The first example deals with a Monte-Carlo-based modelling tool that has been developed to enable the inspectors to perform an improved verification of fresh fuel assemblies by neutron coincidence collar (NCC), taking into account the growing complexity of the fuel's design. The second example shows how the verification of spent fuel is improved regarding the false alarm rate and the partial defect detection capability, by the integration of the automated review package iRAP and the modelling by the Oak Ridge transmutation code (ORIGEN).

The potential applications of the new approach are not limited to the two described in this article, which, however, represent relevant proofs of concept of the potential that a change of perspective in verification by NDA may generate.

Keywords: NDA, Forward problem, Spent Fuel, Fresh Fuel, ORIGEN, Neutron Coincidence Collar

1. Introduction

In 2017, Euratom Safeguards celebrates its 60th anniversary – the legal being the Euratom Treaty, signed in Rome on March 25, 1957. During this long history, a number of field practices, approaches and methods have been developed, consolidating Euratom inspectorate position as one of the reference institutions in the international Safeguards community.

An essential component of the conformity controls, which allow the inspectors to draw independent conclusions, is the Credibility Control, linking the declarations by the nuclear operators to the physical reality, as observed by the inspectors. The physical verifications, that the inspectors carry out in order to perform a credibility control, often consist in the measurement of physical quantities, related to the declared nuclear material properties, by Non-Destructive Assay (NDA).

The advantage of NDA measurements is the possibility to perform the necessary verification, without excessive interference with the operator's industrial process and without alteration of the nuclear material under assay, its physical form or its container. However, one drawback of NDA methods is the not always obvious interpretation of discrepancies, because of an imperfect estimate of measurement uncertainty, especially caused by the difficult quantification of uncertainty in the instrument calibration. Moreover, for the measurement methods used in NDA verification, an appropriate metrological traceability is made impossible by the non-existence of reference materials of the same type, quantity range and physical form of the samples to be measured.

The growing availability of technologies allowing high performance calculations, since the late 1990s, has allowed tackling these limitations of the NDA methods, by using physical-model-based simulation to define the instruments' calibration, starting from a detailed knowledge of the physical system defined by the instrument, the sample and by their mutual interactions. In this perspective, although modeling was used to overcome some of its limitations, simulation did not change the traditional calibration approach, relating an observable physical quantity (for instance, a neutron or gamma count rate) to the values of the quantity of interest (for instance, the quantity of nuclear material).

More recently, a further step has been taken, by using real-time simulation to predict directly the observable physical quantities, which are then compared with the measurement results [1][2]. This different forward-problem approach, has allowed overcoming some limitations of the traditional calibration approach in particularly complex cases. The following paragraphs will describe its consequent practical and conceptual implications.

2. Inverse and Direct problems: definition and application to Nuclear Safeguards Measurements

During verification, as in every measurement operation, we establish a relation between two different abstract spaces. One, which we define as Model Space ($\mathcal{M}$), contains all the knowledge we have from the physical system, defined by a set of parameters including the information contained in the operator declaration. The other abstract space, which we define as Data Space ($\mathcal{D}$), consists of the data from the observable quantities.
The general measurement problem is defined by the following relationship:

$$d = \boldsymbol{G}(m)$$

where $d \in \mathcal{D}$, $m \in \mathcal{M}$ and $\boldsymbol{G}$ is a generic operator linking explicitly the observed data and the model parameter.
In other terms, the general measurement problem is about establishing a relationship linking the causes (the physical theory leading to the model parameters) and the effect (the observed data). As shown in Figure 1, the direction we choose interpreting this link determines whether we are dealing with a direct (forward) or with an inverse problem.
The inverse problem approach will be, then, the one starting from the measured data (e.g. correlated neutron flux) to determine one or more *unknown* parameters (e.g. fissile material mass and/or isotopic composition) defining the physical system under observation. Those parameters subject to verification are thus not measured directly, but they are rather the result of inversion algorithms solving complex equations, deriving the unknowns from the measured observables.

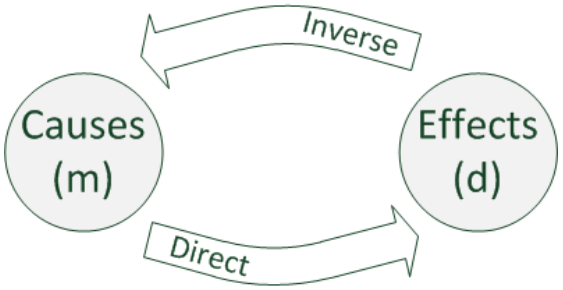

Figure 1. Schematic representation of direct and inverse problems

The inverse problem approach will be, then, the one starting from the measured data (e.g. correlated neutron flux) to determine one or more *unknown* parameters (e.g. fissile material mass and/or isotopic composition) defining the physical system under observation. Those parameters subject to verification are thus not measured directly, but they are rather the result of inversion algorithms solving complex equations, deriving the unknowns from the measured observables.

Figure 2 schematically represents the inverse problem, in the specific case of nuclear safeguards verification: the measured data go through a model, in order to deduct the unknowns, which are eventually compared to the declared values in the verification phase. One of the implications of this process is that measurement uncertainties on the initial observables need to be propagated throughout the inversion model, which is not trivial from the mathematical point of view.

Sometimes, to simplify the model, assumptions like "infinite thickness" of the samples need to be taken or the model is replaced by empirical calibration curves. These latter suffer from a critical drawback: the Certified Reference Materials of the same type (i.e. in size, weight, matrix, fissile mass, package form) do not exist; therefore, selected samples from the operator's facility are used for calibration. In this way, measurement's metrological traceability not directly possible (sometimes indirect traceability can be established, e.g. by help of destructive assay of samples). Interpreting discrepancies in the verification results is then only possible with the intervention of experts in the specific measurement technique, who are able to assess uncertainties including knowledge from additional information sources.

Moreover, the inverse problem can represent a case of *ill-posed* problem in the sense of Hadamard [3], where the *well-posedness* conditions are that

a. A solution exists;
b. The solution is unique;
c. The solution's behavior changes continuously with the initial conditions.

In particular, we can immediately understand why the condition b. is not met in a simple practical case: two fuel assemblies with different ^{235}U masses, but different location of burnable poison rods, may give the same (i.e. statistically comparable) double neutrons count rate, if measured in a thermal-mode neutron collar. In this case, thus, the solution of the observed data inversion is not unique.

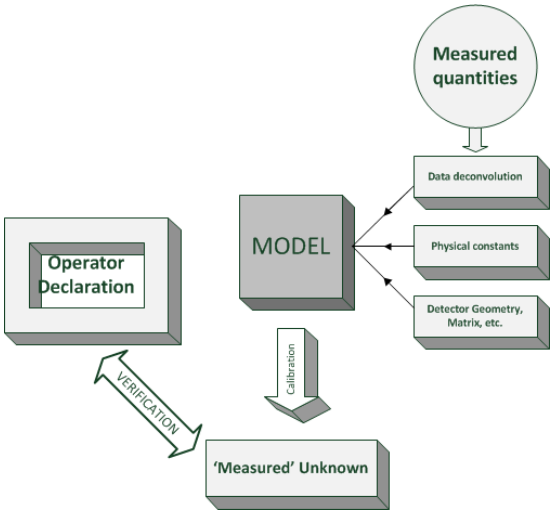

Figure 2. Schematic representation of the inverse problem as applied to nuclear safeguards verification.

On the other hand, the choice of a forward problem approach would start from the modeling of the physical system involved in the measurement, where the quantities of interest (e.g. fissile material mass/isotopic composition) become parameters of the model. As shown in Figure 3, the operator's declaration will then identify specific values of the mentioned parameters, while the model will predict the observable's quantities under these specific conditions. The verification phase will then consist in the direct comparison of the measured versus the predicted observables. The whole verification task becomes, in this way, a typical *hypothesis testing* exercise, in which a predicted quantity undergoes a direct comparison with its experimental value, under

the hypothesis defined by the operator declaration.

We can then observe that a forward problem approach avoids the most difficult aspects of the mathematical inversion (deconvolution algorithms, non-unique solution, experimental error propagation), which are no longer needed in the verification task. At the same time, using the same set of information available and the same set of data, the credibility of the verification conclusion is not affected. Even in a forward-problem approach, though, one can still postulate other operator declarations that could result in the same or similar predicted quantities (within measurements and model uncertainties). However, we have to keep in mind that the primary task of the inspectorate is to verify the declarations provided by operator, not necessarily role to develop the declared parameters independently.

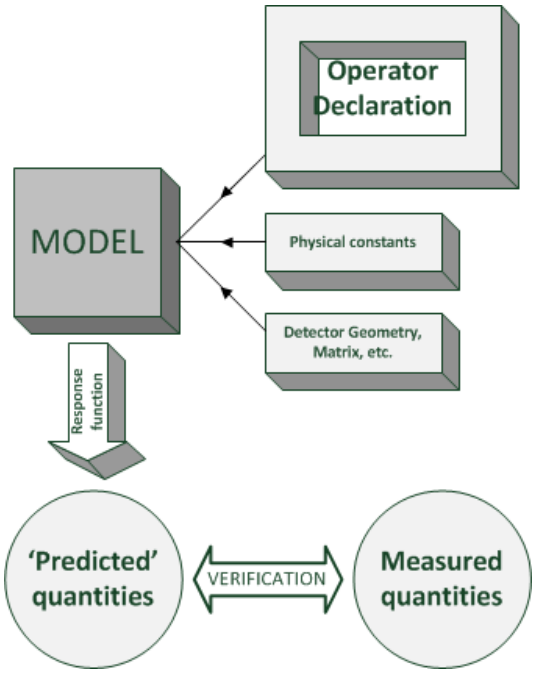

Figure 3. Schematic representation of the forward problem as applied to nuclear safeguards verification.

3. Euratom field-ready inspection tools using a forward-problem approach

Euratom Safeguards directorate makes use of Monte Carlo modeling in several deployed instruments, thus overcoming the issues with lack of reference materials and metrologically traceable calibration standards [4][5]. The improved computing capabilities and some specific verification issues have recently suggested that a forward problem approach with real-time simulation can improve the current verification practices. Clearly, every model needs to be appropriately benchmarked against well-characterised reference materials.

3.1. XFuelBuilder tool for Fresh LWR Fuel verification

Fresh fuel verification by Neutron Coincidence Collar (NCC) poses difficulties, in particular due to the increasing optimization of fuel performance, resulting in greater complexity of fuel design. In particular, fuel producers optimize the fuel assemblies by the use of strategically located burnable poison-enriched rods and by pins that have a variation in ^{235}U enrichment both axially and radially in the assembly.

In order to allow the inspectors to cope with this complexity, European Commission's Joint Research Centre and iScience have developed for Euratom Safeguards inspectorate *XFuelbuilder*, a tool based on the Monte Carlo simulation of NCC measurements. *XFuelbuilder* is in fact a software package, with a user friendly graphical interface, that allows the inspector to prepare a MCNP-PTA input in a simple visual way and then run the simulation of the fuel + collar physical system.

XFuelbuilder includes already the built-in models of the NCCs used by Safeguards inspectorates, both in thermal and fast mode configuration. The inspector can retrieve a stored assembly model or add a new pin or assembly design. Once chosen the collar type, the fuel design and the collar position along the fuel's active length, the inspector can run the simulation, thus obtaining the Reals, the Accidentals and the Totals as he or she would do in any neutron measurement. These values are then easily compared with the measured data, acquired by NCC assay of the assembly. Figure 4 describes the data flow of the whole verification task.

XFuelbuilder, choosing a forward-problem approach, is not affected by the already mentioned ill-posedness of the NCC verification problem and will be a user friendly tool for the inspector. At the same time, it is capable to integrate many of the declared fuel details in the verification itself. Moreover, this approach is going to improve practical aspects of NCC verification, usually needing a passive measurement before the active one, in order to

take into account for the 238U spontaneous fission correlated neutrons. While this two-phase process obliges the inspector to deploy and remove the source and is a practical limit to the possibility to make such measurements as unattended, in *XFuelbuilder* both induced and spontaneous fission are taken into account. Then only the active measurement needs to be done, thus giving the inspectorate the possibility of unattended measurements.

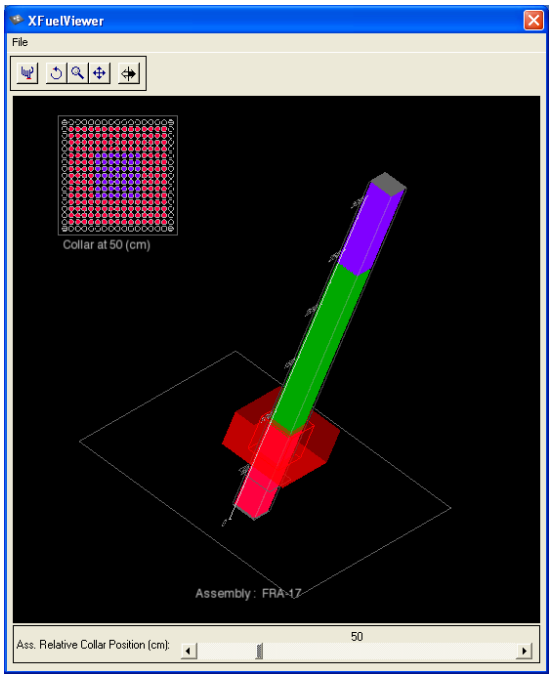

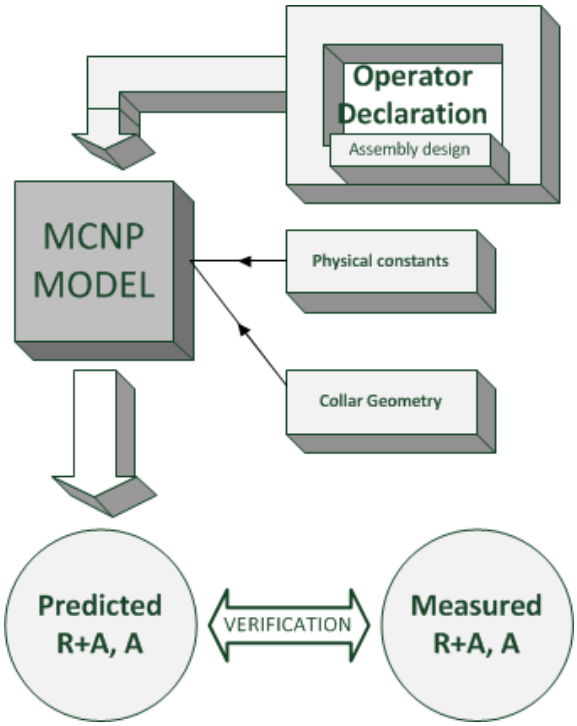

Figure 4. Screenshot and data flow of XFuel Builder

3.2. iRAP-ORIGEN method for improved Fork detector measurement results evaluation

Spent-fuel is one of the big challenges for NDA. In fact the high neutron and gamma activity from irradiated assemblies make it extremely difficult to measure and quantify fissile material in a simple and direct way. Although some promising methods may address this issue in the future [8], the FORK detector is at present the workhorse for the verification of fuel in preparation of intermediate/long term or final, geological storage, where recovery (and re-measurement) is practically not possible. In FORK detector verifications, safeguards inspectors measure the neutron and total gamma fluxes from an irradiated fuel assembly to check its consistency with the declared burn up, initial enrichment and cooling time of the assembly itself.

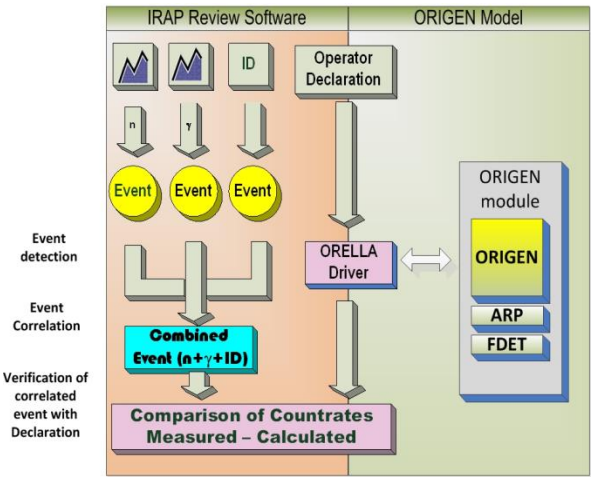

Figure 5. Data flow of an iRAP-ORIGEN Verification

Euratom Safeguards is presently field testing a data evaluation tool [9][10], based on the integration of the review code iRAP (joint development of Euratom and IAEA) and the ORIGEN code (Oak Ridge Isotope GENeration), part of the package SCALE developed by Oak Ridge National Laboratory [11]. The iRAP-ORIGEN integration has been developed and improved under various Action Sheets on the EC-US DOE agreement in the field of nuclear material safeguards R&D.

The iRAP-ORIGEN tool allows, on the one hand, to process unattended FORK measurements, extract the assembly neutron and gamma signature. On the other hand, a simulation combining an ORIGEN irradiation and depletion calculation, using the operator's declarations as input data, and a Monte Carlo computed detector response function compute the expected values of the same signature. The data flow of the complete process is explained in
Figure **5**.

This tool has already proven to be accurate in in taking into account the factors, which may influence the neutron and gamma signatures of spent fuel (e.g. cooling between irradiation cycles, within-assembly neutron multiplication). iRAP-ORIGEN is also ready for unattended measurements evaluation and is proving particularly inspector-friendly in installations where remote data transmission is available. The tool helps inspectors and operators making the data reception from the operator, the measurement and the evaluation a fast and seamless process, minimizing risks of clerical errors and false alarms, reducing the need for re-verification and provides better timeliness for inspectors.
Finally, still remaining a rather simple and limited technique, this improved version of FORK measurements is complementary to other techniques, aimed at the assembly integrity verification, like tomography [13], or aimed at other types of fuel characterization, like Passive Neutron Albedo Reactivity (PNAR) [8].

4. Conclusions

A forward-problem approach, consisting in real-time simulations using declaration data as parameters in a model that predicts directly measured observables, may be helpful in nuclear safeguards NDA verification, especially in cases where calibration can hardly take into account the complexities of the specific sample.

Euratom Safeguards Directorate, in partnership with research institutions such as the European Commission's Joint Research Centre and the Oak Ridge National Laboratory, has already developed tools, which are ready to bring this *hypothesis testing* approach into every day's inspection activities. The first two application fields are the verification of fresh LWR fuel by Neutron Coincidence Collar and the verification of irradiated fuel assemblies by FORK detector.

The forward-problem approach is also an opportunity for resource optimization, as it can be very well integrated in a remote data infrastructure, which allows performing the computational part of the verification at the headquarters.

References

[1] Zykov, *Technical Challenges and Technological Gaps in IAEA Safeguards*, in: Proceedings of the 56th annual meeting of the Institute for Nuclear Material Management, July 12-16th 2015, Indian Wells, USA;
[2] Peerani *et al.*, *Real-time simulation of neutron counters*, Radiation Measurements 43 (2008) p 1506–1510;
[3] Hadamard, J., *Sur les problèmes aux dérivés partielles et leur signification physique*, Princeton University Bulletin, Vol. 13 (1902), p. 49-52;
[4] Looman, M., Peerani, P., Schwalbach, P., *Calibration with Monte Carlo calculations of a neutron collar for the verification of FRM-II fuel elements*, in: Proceedings of the 25th Annual Symposium on Safeguards and Nuclear Material Management, 13–15 May 2003, Stockholm, Sweden;
[5] Peerani, P., Looman, M, *Computational modelling of NDA instruments for nuclear safeguards* in: Proceedings of the 24th Annual Symposium on Safeguards and Nuclear Material Management, 28–30 May 2002, Luxembourg, p. 131–137;
[6] Peerani et al., *A user-friendly tool for easy and fast in-field Monte Carlo simulation of neutron collars*, in: Proceedings of 37th ESARDA Symposium on Safeguards and Nuclear Non-Proliferation, Manchester, UK, 19-21 May 2015
[7] Tagziria et al., *XfuelBuilder for the Analysis of Simulations and Measurements of fresh fuel assemblies using neutron coincidence collars by nuclear inspectors*, current conference.
[8] S.J. Tobin *et al.* , *Technical Cross-Cutting Issues for the Next Generation Safeguards Initiative's Spent Fuel Nondestructive Assay Project*, Journal of Nuclear Materials Management 40(3), p.18-24, 2012.
[9] S. Vaccaro, J. Hu, J. Svedkauskaite, A. Smejkal, P. Schwalbach, P. De Baere and I. C. Gauld, *A New Approach to Fork Measurements Data Analysis by RADAR-*

CRISP and ORIGEN Integration, IEEE Transactions on Nuclear Science 61, 4, 2014.

[10] I. Gauld, J. Hu, P. DeBaere, S. Vaccaro, P. Schwalbach, H. Liljenfeldt, and S. Tobin, *In-Field Performance Testing of the Fork Detector for Quantitative Spent Fuel Verification*, Proceedings of the 37th Annual Meeting ESARDA Symposium 2015, Manchester.

[11] S. M. Bowman, *SCALE 6: Comprehensive Nuclear Safety Analysis Code System*, Nuclear Technology 174(2), p 126–148, May 2011.

[12] S. Vaccaro, I. C. Gauld, J. Hu, P. De Baere, P. Schwalbach, A. Smejkal, A. Tomanin, C. Demartini, A. Sjöland, S. Tobin, D. Wiarda, *Advancing the Fork Detector for Quantitative Spent Nuclear Fuel Verification*, in preparation.

[13] T. Honkamaa, F. Levai, A. Turunen, R. Berndt, S. Vaccaro, and P. Schwalbach, *A Prototype for Passive Gamma Emission Tomograph, IAEA Symposium on International Safeguards*, IAEA CN-220/129, 2014.

Session 15

Containment & Surveillance

Containment and Surveillance Systems – reflections on future technologies

Gunnar Boström, Vitor Sequeira, Erik Wolfart

European Commission, Joint Research Centre
Directorate for Nuclear Safety and Security, Ispra, Italy

Abstract:

Euratom Safeguards is currently implementing in the field the Next Generation Surveillance System (NGSS), close to 700 units are to be installed in the next years.

This paper deals with the time after NGSS. It is time to design the technology that follows, to discuss the requirements for containment and surveillance systems in a broader sense, to study the very volatile general technical environment and select options for further development.

With the growth of the security markets, with the advent of autonomously driving cars, with increasing threats in cybersecurity, with the appearance of more intelligent, smart sensors using various physical technologies beyond optical vision, opportunities can be envisaged and analysed for applicability. This may allow more efficient and effective safeguards implementation, and ideally, could contribute to an opening of the market and help reducing cost.

At the same time, a growing number of facilities particularly at the back end of the fuel cycle turn static and new facility types appear. These pose their own challenges and may call for revised inspection approaches utilizing non image based sensors.

Keywords: Containment and surveillance, remote transmission

1. Introduction

Inspectorates are constantly being challenged with decreasing funding, personnel, inspection days and mission budget and therefore need to increase the efficiency and effectiveness of safeguards activities. At the same time, new equipment must be developed to replace old technologies which have come close to their end of life cycle.

In order to make safeguards more effective and efficient, we need to increase the number of sensors connected together with an intelligent and automated event extraction. The “integrated Review and Analysis Program” (iRAP) is a joint development project by IAEA and DG-ENER with constantly increasing functionalities [1]. Adding the automated data transfer using techniques such as RADAR and Rainstorm is building a very cost-optimized solution.

Could we not in the (near) future have even more unattended equipment in place, which observes the processes transmitting relevant data to a local storage? Automated processes could identify events and assist the nuclear inspectors to confirm declared operations and to analyse situations that are potentially safeguards-relevant. The unattended systems could be based on a combination of dedicated components and OEM modules.

The above scenario would require a larger amount of unattended sensors that have the capacity to transmit data automatically to a central store. Today’s nuclear safeguards uses an increasing amount

of unattended systems, primarily surveillance cameras and a few other connected devices deployed in enrichment and reprocessing facilities [2].

An integrated review tool, correctly configured and where relevant data is provided, is able to extract a list of relevant events and provide, if necessary and available a limited-sized video sequence over the time of the events. The strength of such a tool is the efficiency with which the inspector would work, i.e. the activity of the inspector is focused on the events and not on all the time in between events.

With a constantly increasing threat from cyber-attacks, new safeguards tools must be able to seamlessly follow the latest advancement in cyber security to ensure the authenticity of all safeguards relevant data and be able to handle future cyber-attacks.

The valid lifetime for dedicated safeguards equipment is very long because the development time and validation process of new devices is both long and expensive. The development of new equipment from idea to final fully functional system can take 5 to 10 years, sometimes even longer. Often, safeguards equipment cannot be updated, changed or replaced because other comparable or better equipment neither exists nor can be developed in a reasonable amount of time.

Whenever new safeguards equipment is designed, it is necessary to consider future technology trends and synergies with other industrial branches. By thinking out of the box, one can potentially gain strengthened detection capacities and effectiveness.

Where allowed by the operator and local authorities, the devices can send data to headquarters or local site-offices without interaction from inspectors or technicians. The data can be processed automatically and benefits can be identified both for inspectors but also for operators and state inspectorates. With this in mind, the future safeguards tools must enable secure remote data transmission and centralized control.

2. Next Generations Surveillance System (NGSS)

The NGSS is currently deployed in large scale substituting old DCM-14 cameras and other commercially available systems such as FAST/NICE. The output video stream files from the camera can be handled by both the Safeguards review station GARS, by iRAP but also by new emerging video-review tools such as VideoZoom [3] or, in its most basic form, any MPEG enabled video-application. NGSS implements important features such as multiple asymmetric crypto-keys for authentication, enabling joint-use and third party installation and maintenance.

The primary components, i.e. the imaging sensor and the processing DSP, acquire the images and implement scene-change detection. This detection capacity means that the camera can by itself react to scene changes, tag the event and change the image storage frequency. The camera can also trigger and/or be triggered by external sources via electrical interfaces.

The subsequent video review tool can list all events that have been detected by the scene-change detection and that have been triggered via electrical or network-based connections. In some cases NGSS still returns large amounts and long sequences of video data. Generally, it is a very time-consuming task for the inspectors to perform an efficient and effective analysis of long video-streams.

3. Innovative Sensors for Safeguards Surveillance systems

When considering a future generation of surveillance systems, what kind of additional tools and sensors can be added? Since the time from an idea to final deployment is very long, it is now time to start thinking of a successor for NGSS. Currently, the commercial market is designing new generations of advanced sensors that did not exist some years ago. Some sensors, which may be essential for safeguards in 10 years from now, have potentially not even been launched commercially.

The design of a future safeguards surveillance system should consider commercially available or open modules while keeping the global aim of a robust system with long term guaranteed operational lifespan in mind. Finding adequate devices may be very challenging because of the special conditions in which safeguards equipment operates and the requirement thereby put on them. Still, new emerging tools, sensors and OEM platforms could be part of a new generation of safeguards systems.

Apart from the basic CMOS/CCD light sensitive sensor, what additional sensors could be of interest to design the future system? A list drawn today cannot be fully comprehensive, since future intelligent sensors are not known. Trying to answer the question, we can start with a few sensors that appear in existing nuclear safeguards equipment, which could also be of interest in a modular sensor system.

3.1. LIDAR sensors

Lidar (Light Detection and Ranging) is a sensor which uses electromagnetic waves in the near- or visible spectra to measure distances. These sensors have the capacity to measure the near surrounding in 3 dimensions. They have already entered into the consumer market and the first smart-phones equipped with solid-state sensors with active light enabled 3D capacity are commercially available [4].

How would this help future surveillance systems? In the area of design information verification/Building Technical characterization (DIV/BTC) or containment verification, LIDAR technology is already a key-player. Several nuclear safeguards systems use these sensors to draw conclusions; Static 3D scanners are used for accurate change detection [5] and mobile scanning equipment is used for large scale mapping/change detection and for indoor-localization[6].

But what can they do for a Surveillance system? As previously mentioned, video-review is a crucial but fairly time-consuming activity. A large amount of image sequences may be visualized to identify declared activities and an inspector must maintain focus to potentially also find what not searched for, i.e. potential non-declared activates.

A safeguards surveillance system combining LIDAR and optical cameras could be designed in such a way that an event is triggered whenever something physically happens in a pre-defined area of interest. One could neglect changes in the image-scene such as shadows, light changes etc. and concentrate on actual movements.

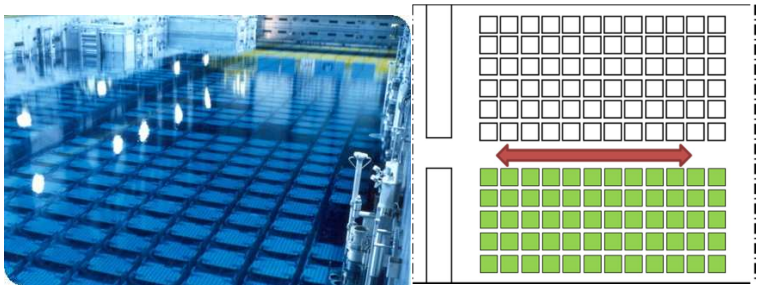

Figure 1: Left: Image of Interim storage pond in La Hague, France (image from Areva Webpage), Right: concept pond with green baskets under surveillance and red arrow indicating daily movement of equipment with traversal crane.

Figure 1 shows a surveillance image and a schematic drawing of a spent fuel pond. The surveillance camera is placed to overlook the stored bins where no changes are to take place. The allowed movement of the traversal crane with a bin-carrier introduce changes in the camera image. The crane will also introduce small waves which make the reflection of illumination to flicker on the water surface. In such a situation, an image-based scene change detection will have difficulties to perform well.

By introducing a 2D or 3D based laser scanner we do not need to rely only on the camera image. The additional sensor will map in Cartesian dimensions a plane parallel to the water surface above the bins; and any interference with a device, rod or traversal crane can be detected and consequently an image sequence event can be stored. There are several other examples where an added proximity sensor would assist and provide robustness, efficiency and effectiveness to a safeguards camera.

3.2 Radiation sensors

Both neutron and gamma detectors are playing an important role for triggering a safeguards camera when relevant scenarios occur. Most probably, future safeguards cameras would integrate such sensing capacities and, based on need, assist in the triggering of events.

3.3 Other sensors

Considering that we discuss future technologies, why not broaden the concept? Many commercial sensors (e.g. pressure gauges, noise sensors, scales, temperature and pyroelectric sensors and ID-readers) could be of interest. And last but not least, the sensors which are not even commercially available yet.

4. Introducing the concept of a “Remote Safeguards Device”

Some basic requirements apply to any unattended safeguards device installed in a nuclear facility: it must be able to withstand power-outages for days, store data locally and have tamper-proof enclosures. It also needs to support secure remote transmission and control.

A future remote safeguards device should have a modular design where a ‘core module’ implements the basic capabilities. One or more sensors can be connected to the core module and placed in the tamper-indicating housing. As discussed above, the new design should be able to handle future sensors within some reasonable limit.

In figure 2, the blue box lists the capabilities of the core module that are required for the installation in a nuclear site. All the functionalities for command and control exists; a modular CPU for decision making and logics, exchangeable memory module, battery-backup, remote communication for control and data-extraction. The core module must be equipped with a state-of-the-art protection for cyber-attacks as well as configurable encryption logics for digital encryption and data-authentication. Other modules needed for the execution, i.e. the ‘extra sensors’, are added as needed via a pre-defined

electrical, logical and physical interface. This enables a concept where several sensors can interact within the same tamper-proof enclosure as a single smart device.

From a maintenance point of view, the concept should allow an external actor to perform on-site activities. An installation of a pre-configured device and basic maintenance such as battery-change and memory-card substitution should be allowed by design. This would mean that safeguards organizations significantly could reduce mission costs and manpower. It would also be a clear benefit for the operator, which would not need to plan, organize and host visits on the site.

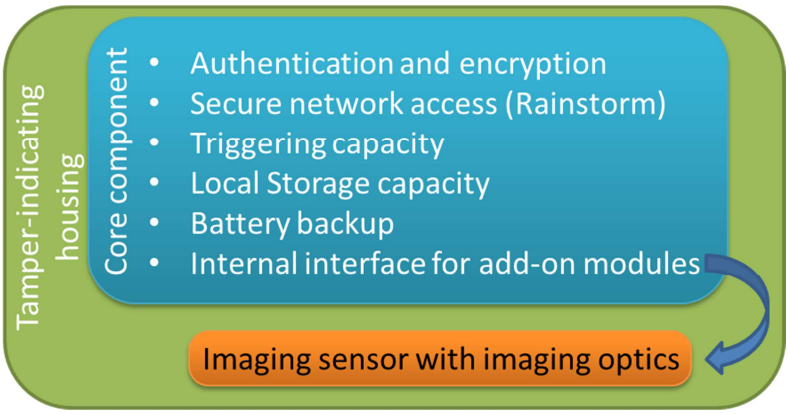

Figure 2: Schematic design of a new base unattended system with capacity to attach sensors using an internal interface

For sure, the imaging sensor will in most cases be used to enable an 'inspector's eye' in case of events. But the core modules could also be used as a future remote data acquisition module in an extended RADAR architecture.

Ideally, the design is based on existing components that are offered openly by the electronics industry or where intellectual property rights (IPR) can be guaranteed for nuclear safeguards. A realistic scenario would probably be to use a dedicated and optimized inner core component together with added outer OEM or semi-commercial components. By using an existing open operating system and maintaining an open architecture, we would meet the nuclear safeguards community concerns and requests regarding IPR and cost-optimizations. This would demand a high level of cooperation and openness between a few major players in the design and potential development phase.

4.1 How the concept fits into current and future remote data transmission paradigm

The ever-increasing need and request for remotely connected devices lead to the concept for unified approaches. Both remote transmission of data from device to headquarters or local servers can be implemented with this modular architecture. Streamlining the remote transfer enabling a Rainstorm [7] connection in the core module would immediately enable the strength of a compressed and adaptive network connection to a large amount of devices.

Once implementing the remote connection capacity with the core module, all systems will inherit the same communication interface and thereby unify both data transfer and control logics.

Figure 3 shows the data transfer scheme for a site that has several connected systems based on the concept device. As seen, different devices can connect to remote transmission software with standardized means for data transfer or optionally connected to data consolidators like RADAR. In cases where there is no remote transmission available, data can be hand-carried using digital memories.

The same concept for unification applies to control and command. An established unified way to communicate state of health and to read/update configuration can be implemented in the common core module which greatly simplifies control software.

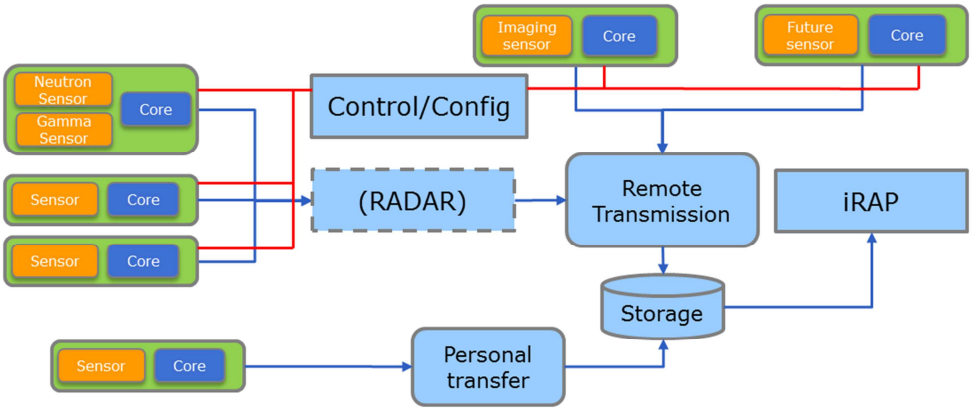

Figure 3: The concept safeguards surveillance system in a future remote data transmission scenario. The blue arrows show the direction of data-transfer. The red lines indicate flow of command and control.

4.2 Concept usage

Future safeguards will require future technologies and new ideas. Currently, the safeguards community is facing new challenges such as an increase in dry storages and geological repositories. New sensors and systems are entering the arena that need to be managed regarding both installation and configuration but also related to remote data and status transmission.

This happens at the same time as efficient work-procedures are under discussion. Remote safeguards with less mission days as well as more effective inspections are requested.

The remote devices installed should generate a minimal footprint in volatile memory for normal situations, but when an event can be identified, higher framerates, more information and extended datasets can be accepted. The only issue is, who is deciding what is an event and when does it happen?

Sample case 1:
If we can detect an object physically entering an area of safeguards interest, we would robustly be able to consider this as a safeguards relevant event. For a safeguards camera, adding a 2D/3D laser-based proximity sensor, we would achieve a more effective analysis following an efficient posterior review. Such system in the new concept would be based on a combination of an imaging sensor and a 2D/3D sensor.

Sample case 2:
In a transfer hall or loading cell, observation of loading events is requested. The presence of nuclear material would be detectable with either a small gamma or neutron detector. By coupling the presence of nuclear material to the imaging sensor, we would achieve a very powerful surveillance system within a single tamper-proof case enabling effective and efficient posterior image review where events would reveal relevant movements.

Sample case 3:
Monitoring dry-storage casks in a spent fuel storage is a fairly static operation. Very few or no movements occur over long periods. In this case, potentially no imaging capacity would be needed. Why would we need to generate video-files that show a static scenario? Instead, a 2D laser would be able to monitor the casks and in case movements occur; an item tracking file could be extracted. An optional still image could be acquired to document the event. Furthermore, adding a radiation sensor could add essential information to an event data set.

Sample case 4:
Pressure, temperature, light, pyroelectric, weight, position, item counters, ID readers or other sensors already applied to a material-process by an operator could be used to confirm a normal operation. The sensor data could be bypassed in a core module with copy functionality as described by Thomas et. Al

[8], where the data transmission is read but not logically interfering with the data flow. The data copied would then be authenticated and transmitted accordingly.

Sample case 5-:
Today we might not care for sound, ambient temperature and light sensors or other currently not known sensors. In the future, there may be the need for a combination of such sensors. We cannot design and implement the future sensors but we can to as large degree as possible make space for them and allow a smooth integration into the future generations Remote Safeguards Device.

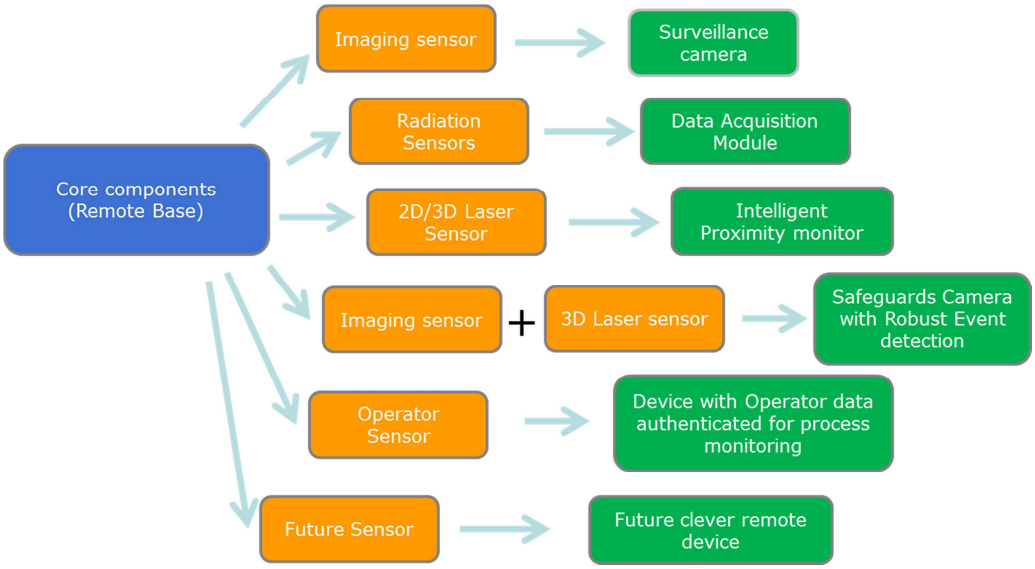

Figure 4: The base unattended system with a few conceptual sensors and there indicated use-cases.

Figure 4 describe in a single image a few realistic sensors and their indicative use which can be part of a future toolbox of devices ready to be deployed in the field when deemed necessary. The Orange boxes define a few sensor architectures which could be relevant. The green boxes briefly describe the potential use of such configurations.

5. Summary

The development of a new safeguards device is a long process and it is therefore time to start the discussion of a post-NGSS safeguards surveillance system. In this paper we introduce the concept of a Remote Safeguards Device which would be a modular device with the capacity to host different sensors in a tamper-proof case. We have identified core features that are needed for any future device such as remote transmission, effective and clever decision making. We propose that the common features are implemented in a core module which can be extended with one or more sensors according to the needs of the specific use case.

The design should be open and based – as much as possible – on COTS and open-source technology. The proposed concept could increase safeguards efficiency and effectiveness as it would reduce time and costs of the development; facilitate sensor integration and remote monitoring; and reduce the inspector's workload for routine activities. In order to design a new safeguards device a large amount of preparatory work is needed. This paper proposes a new concept and further analysis and discussions are needed.

Acknowledgements

The authors would like to thank J. Pekkarinen, K. Schoop and P. Schwalbach, EC Directorate Euratom Safeguards, for interesting discussions and comments.

References

[1] Smejkal A et.al., “Automated Processing of safeguards data: Perspective on software requirements for a future ‘All in One Review Platform’ based on iRAP”, Proceedings of 37th ESARDA Annual Meeting, Manchester, 2015

[2] Schoop K. at. al., “Progress and Status of Remote Data Transmission in EURATOM Safeguards”, Proceedings of 37th ESARDA Annual Meeting, Manchester, 2015

[3] Versino C. at. al., “Evaluation of a Surveillance Review Software based on Automatic Image Summaries”, Symposium on International Safeguards: Linking Strategy, Implementation and People vol. IAEA-CN-220 p. Page 224 - Paper IAEA CN220 #195

[4] http://www3.lenovo.com, Smartphone ‘Phab 2 Pro’

[5]Oddou J. et. al., “The Application of 3D Laser Scanning techniques for the efficient Safeguarding of fairly static storage facilinatural, depleted and reprocessed uranium“, INMM 51st annual meetings proceedings, July 2010

[6] Wolfart E. et. Al. “Mobile 3D Laser scanning for Nuclear Safeguards”, ESSARDA Bulletin nr. 53, December 2015.

[7] Morgan K. et. Al. , “Real-time And INtegrated STream-Oriented Remote Monitoring (RAINSTORM) Interface“, INMM Proceedings 2012.

[8] Thomas M. at. al., “Enhanced Data Authentication System: Converting Requirements to a Functional Prototype”, 35th ESARDA Symposium proceedings, 2013.

Sealing Systems in German Spent Fuel Storage Facilities

Katharina Aymanns[1], Arnold Rezniczek[2], Astrid Jussofie[3], Irmgard Niemeyer[1]

[1]Forschungszentrum Jülich GmbH
IEK-6: Nuclear Waste Management and Reactor Safety52425 Jülich, Germany

[2]UBA Unternehmensberatung GmbH
52134 Herzogenrath, Germany

[3]GNS Gesellschaft für Nuklear-Service mbH
45127 Essen, Germany

Abstract:

This paper describes the current issues related to sealing devices in the German on-site spent fuel dry storage facilities (SFSFs) and investigates options for improving techniques in order to achieve better radiation protection and occupational safety during safeguards verification of spent fuel casks stored in SFSFs.

In the context of Germany's energy transition, the eight still operating reactors will be successively disconnected from the power grid by the end of 2022 at the latest. The nuclear material of all power reactors has to be removed prior to decommissioning of the reactor building. The defueling of reactors increases the handling operations at these sites especially by the temporary higher number of cask loadings. Accordingly, the number of transfers of these loaded casks (dual purpose: transport and storage casks) from the reactor to the SFSF will further increase as well. By end of 2027, it is foreseen that all spent fuel assemblies will have been loaded into casks. After their transfer to SFSFs, the SFSFs will have a static inventory of more than 1,000 casks, because no receipts or shipments are expected following the final reactor shut down. The spent fuel packed in casks will be stored in interim dry storages for several decades until a repository for heat generating high level waste is available. The casks may be difficult to be accessed; especially the seals attached at the protection plate on top of the approx. 6 meter high casks. A seal verification that involves the replacement of the seal will require more time and will lead to a higher radiation dose for both inspector and storage staff than easier in-situ verification or seal verification by remote data transmission (RDT). Given this situation optimization of safeguards concepts and sealing systems devices applied is needed. Solutions are required to ease the verification of the casks and to minimize the exposure of the inspectors and storage staff.

Keywords: spent fuel management, spent fuel storage facilities, sealing systems

1. Introduction

Following the nuclear accident at Fukushima in March 2011, the German Government decided to immediately shut down eight of the 17 operating nuclear power plants (NPPs) and to completely phase out the use of nuclear energy for electricity production. The decisions have a significant impact on spent fuel management in Germany. After shut-down of another reactor in 2015, the eight remaining NPPs will be successively taken from the power grid by the end of 2022 at the latest. On 23 July 2013, The German Federal government entered an Act into force on the site selection process for a deep geological repository for high level radioactive waste, including spent fuel assemblies and vitrified waste [1]. This act does not specify a specific host rock type but it determines a selection of a final repository site until 2031. The repository site selection procedure should be transparent and science-based. Potentially suitable areas should be narrowed down, step y step, on the basis of

scientific criteria for the best possible safety for a period of one million years. Furthermore, the selection procedure includes public participation. A commission was set up to prepare the site selection procedure and in July 2016, the commission submitted a final report including their recommendations for the German Federal Parliament (*Bundestag*). [2] The recommendations of the commissions were included in the Act on the further development of the site selection act, which entered into force on 16 May 2017 [3].

The site selection will be followed by the licensing procedure for the construction, operation and decommissioning of the repository. The decision of phasing out the production of nuclear energy provides some safeguards challenges in Germany. The defueling of reactors has a major impact on the time schedules and frequency of spent fuel handling operations in reactors, storage facilities and their associated safeguards activities. Due to the defueling of the reactors the amount of cask transfers dramatically increases. Therefore the need for long-term reliable unattended Safeguards (SG) measures must be put in place to preserve the continuity of knowledge (CoK).

This paper describes the current issues related to sealing devices in the German on-site dry spent fuel storage facilities. The Research Centre Jülich set up a project on this issue. The next step in this project is to investigate options for improving techniques in order to minimize the radiation exposure of the inspectors and storage staff as well as occupational safety for verification of spent fuel casks stored in SFSFs.

2. Spent Fuel Storage Facilities in Germany

Due to the defueling of reactors, the number of transfers of loaded casks (dual purpose: transport and storage casks) from the reactor to the SFSF are increasing. Accordingly the spent fuel cask inspections for safeguards are also rising.
By the end of 2027, all spent fuel assemblies are foreseen to be loaded into dual purpose casks. Once the transfer of all loaded casks to the SFSFs is complete, the SFSFs will have a static inventory of more than 1,000 casks because no receipts or shipments are expected following the final reactor shut down. Germany's former plan to store spent fuel in central dry storage facilities at Ahaus and Gorleben had to be abandoned due to the prohibition of spent fuel transports on public traffic routes. In this context, 12 new decentralized on-site interim dry storage facilities were constructed and licensed for the storage of spent fuel assemblies. The assemblies are loaded in dual purpose casks for transport and storage - CASTOR® V-casks. The licensed storage period of all German SFSFs is limited to 40 years beginning with the emplacement of the first spent fuel containing cask in the storage building. The licensed mass of heavy metal (HM) in the on-site dry SFSF varies between 450 Mg and 2,250 Mg and amounts to 3960 Mg (Ahaus) and 3800 Mg (Gorleben). The storage capacities of the on-site dry SFSFs range between 80 and 192 CASTOR® V-casks [7].

The construction of the 12 on-site dry SFSFs is based on three different concepts: the STEAG, the WTI and the tunnel concept. They were constructed as storage halls from steel concrete (at the Neckarwestheim site in the form of storage tunnels). The STEAG concept has been applied at six North German sites at Brokdorf, Krümmel, Brunsbüttel, Grohnde, Lingen and Unterweser. The WTI concept has been applied at the five sites at Biblis, Philippsburg, Grafenrheinfeld, Isar and Gundremmingen located in the southern part of Germany. The tunnel concept at Neckarwestheim was developed as a special solution due to site-specific conditions [4].

In addition to the two central SFSFs and the twelve on-site dry storage facilities, two local interim dry storage facilities at Greifswald (ZLN) and Jülich are operated in Germany [4].

STEAG Design:

The design characteristics of the STEAG concept (designed by the company STEAG encotec GmbH) include a one-nave building with thick concrete structures (Figure 1). The wall thickness is about 1.2 m and the roof thickness is about 1.3 m. The gap between each cask in X-direction is approximately 55 cm [4].

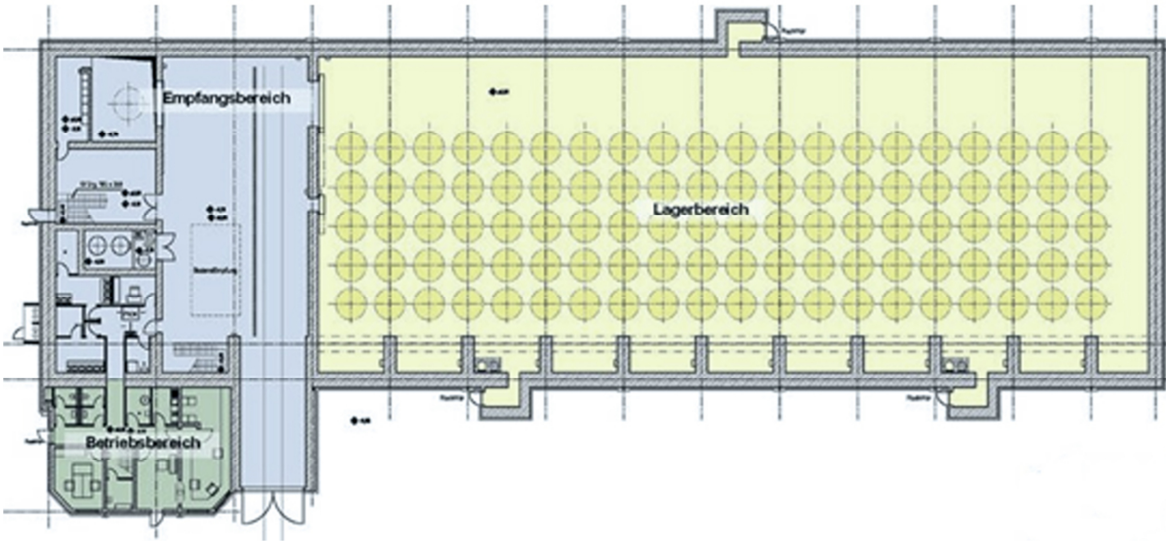

Figure 1: SFSF built as STEAG Concept [4]

WTI Design:

The WTI concept (designed by the company of consulting engineers Wissenschaftlich-Technische Ingenieurberatung GmbH) is a two-nave building with two separate storage halls; the wall thickness is around 0.85 m, respectively, and the roof thickness about 55 cm (Figure 2). The gap between each cask in X- direction is approx. 50 cm [4].

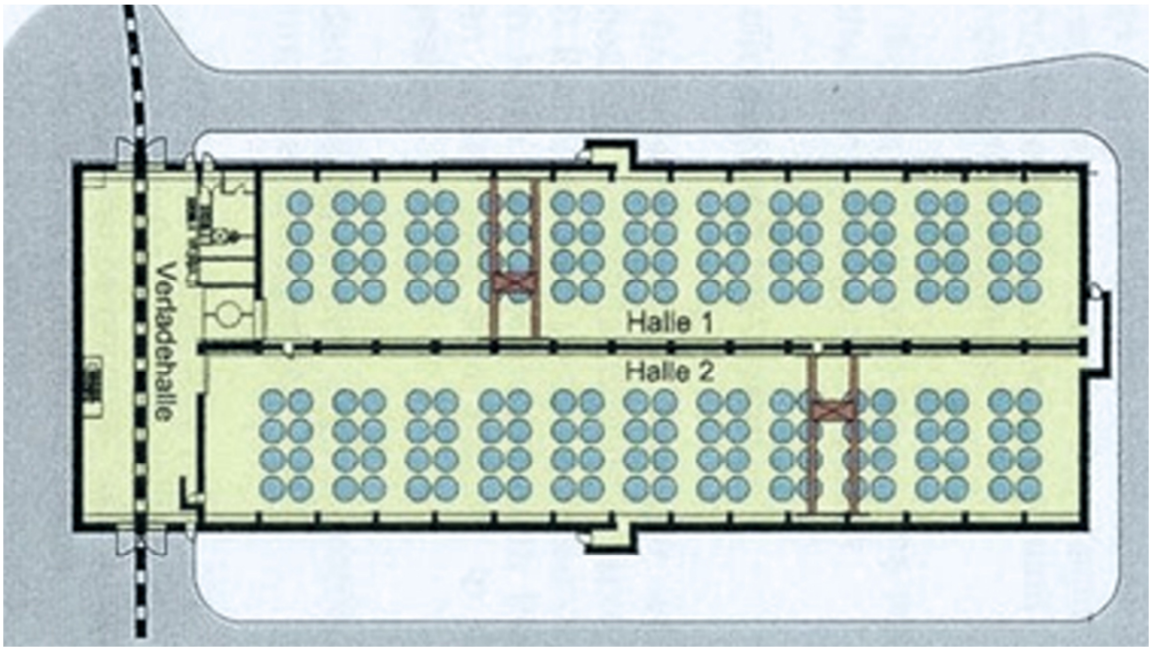

Figure 2: SFSF built as WTI Concept [4]

Tunnel Design:

The tunnel storage was designed to the specific on site geological conditions. The facility consists of an entrance building, which is arranged aboveground, two tunnel tubes running parallel in east-western direction, which are connected at their ends by a tunnel, and an exhaust air system and an escape construction (Figure 3). The gap between each cask in X-direction is approx. 44 cm [4].

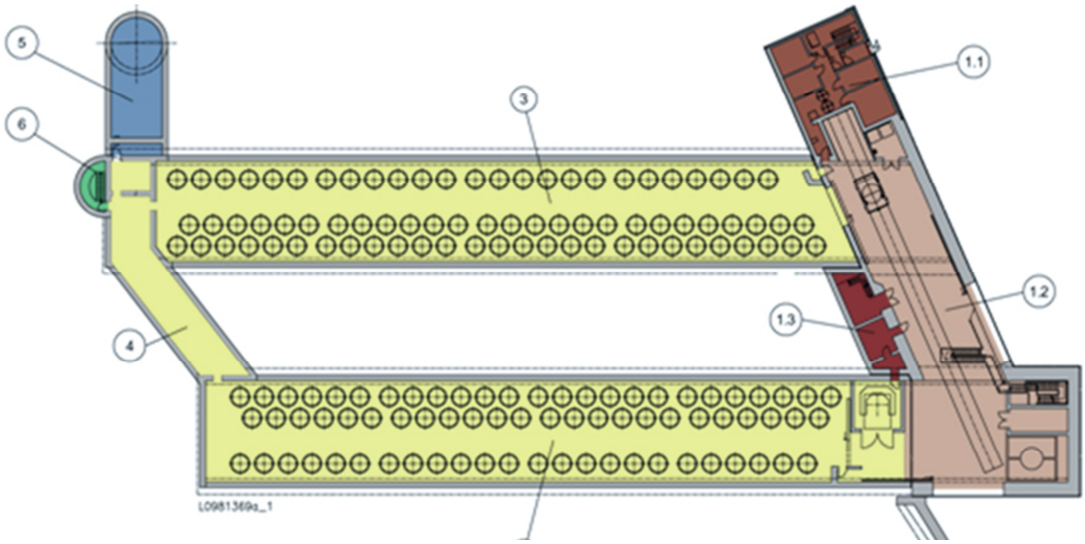

Figure 3: SFSF built as tunnel concept [4]

The dense packing of casks can be seen on the three layouts of the SFSFs. Due to this arrangement; casks cannot be moved between other casks without more ado. Cask movements over the other casks are not allowed. If a cask has to be transferred into the maintenance room (located inside the entrance area), all casks in the rows in front of this cask have to be transferred individually to a buffer area first in order to allow the movement of the selected cask.

3. Safeguards Implementation in German Spent Fuel Storage Facilities

The IAEA has drawn the 'broader conclusion' for Germany in March 2009 for the first time. The implementation of integrated safeguards started with in 2010. This was also the starting point for implementing integrated safeguards in the German SFSFs. Since the IAEA concluded on the absence of undeclared nuclear material and activities in Germany, the safeguards objectives changed. The requirements to timeliness for spent fuel verification and detection probability were lowered; the quarterly routine inspections were replaced by randomly performed inspections with a short notice of 24 h and a probability of occurrence of 20 percent in a given facility. The inspection-interval for physical inventory verification (PIV) continues to take place annually.
Regarding the long-term storage of spent fuel in SFSFs, any safeguards inspection plan for the dry interim storage should be ruled by two main aspects. First, CoK of the nuclear material flow by C/S measures from the reactor to the storage facility and during the storage period should be maintained. Second, verifying the nuclear inventory of the casks by counting and identification should involve an evaluation of the C/S system and, as a back-up, non-destructive-analysis (NDA) measures on the CASTOR®-casks as appropriate in the hypothetical worst case where all safeguards measures, seals and surveillance fail [5, 8]. In order to avoid this worst case, different sealing systems are applied for cask sealing in combination with camera surveillance.

For states under integrated safeguards, such as Germany, the IAEA requires maintaining CoK during transport of CASTOR® V-casks to their storage position and during their long term storage. Due to the inaccessibility of the nuclear material during interim dry storage, casks loaded with spent fuel should be under dual containment and surveillance (C/S). In order to meet this requirement, two independent sealing systems using different physical principles are applied by IAEA and EURATOM during long-term storage, mostly supplemented by surveillance. Three different types of sealing systems (see Table 1) are currently used at German SFSFs.

Code	Equipment name	Description/ Application
CAPS	Cap seal (metallic)	Cap seal is used with several types of containment. After removal the verification of seals is only possible at IAEA Headquarters.
Cobra	Fibre optic general purpose seal	Fibre optic seal; reflective particles incorporated in the seal body provide unique identifier; in situ verifiable
EOSS	Electronic optical sealing system	Reusable seal consisting of a fibre optic loop and electronical seal. Light pulses monitor the loop, and every opening and closing of the seal is stored in the seal. A dedicated reader is used to verify the seal.

Table 1: Sealing Systems used in German SFSF [6]

The loading and transfer of CASTOR® V-casks is not always as straight forward as desirable due to the drying process necessary before the seal can be applied. The residual moisture in the cask has to meet special criteria and the time needed to reach these criteria is difficult to predict. Practical experience shows a range from 10 to 100 hours. To avoid inspectors having to remain on-site or on-call while the casks dry, the IAEA and EURATOM proposed an approach to delegate the task of applying the seals to the operator when the inspectors are not present. After the spent fuel has been loaded into the cask the operator provides the cask sealing by using the COBRA seal, the electronic seal EOSS and the EOSS seal interface. This procedure is recorded by installed safeguards video surveillance. The EOSS seal interface guides the operator through the sealing procedure and confirms its successful termination as a storable message. [7]. Casks that were sealed by the operator in the reactor and transported to the storage facility are there verified after finishing the loading campaign by the two inspectorates of EURATOM and IAEA; at the same time the EOSS seals are replaced by metal seals or Cobra seals. Some SFSFs use Cobra seals as group seals. In one SFSF individual CASTOR casks are sealed by COBRA seals and additionally groups of those casks are connected by a single EOSS seal as a group seal.

5. Discussion and Outlook

The verification of sealing systems currently used at German SFSFs is a very arduous and time consuming task due to the spatially limited storage configuration.
Seal verification or seal renewing that involve the replacement of the seal on the top of the casks lead to a higher radiation dose for both inspector and storage staff than the easier in-situ verification or seal verification by RDT. Work safety rules do not allow unsecured movements between casks and thus enforce time consuming positioning of persons for each cask separately. Near the casks the radiation level is higher than elsewhere. The principle guideline for radiation protection „As Low As Reasonably Achievable“ (ALARA principle) calls for a reduction in the duration of stay in this environment as far as possible. Efforts should be made to minimize the dose rate for inspectorate and staff in this area for example by using RDT systems.
At present, apparently no convincing approach for safeguarding of static SFSF in the long run exists. Given this situation, there is an urgent need to optimize the safeguards concept and to tailor the sealing devices to the specific conditions of an interim SFSF in a static operation. Solutions are required to ease the verification of the casks and to minimize the exposure of the inspectors and storage staff. Therefore, it is important to review suitable current and future sealing systems as well as

alternative available technologies, such as laser based systems or neutron monitors, and evaluate pros and cons of their application to safeguarding spent fuel storage casks in the German SFSFs.

6. Acknowledgements

This work was supported by the Federal Ministry for Economic Affairs and Energy, Germany, through the German Safeguards Support Programme to the IAEA and the programme "Neu- und Weiterentwicklung von Safeguardstechniken und -methoden" (FKZ 02W6263).

7. References

[1] Gesetz zur Suche und Auswahl eines Standortes für ein Endlager für Wärme entwickelnde radioaktive Abfälle und zur Änderung anderer Gesetze (Standortauswahlgesetz – StandAG) vom 23. Juli 2013 (BGBl. I 2013, Nr. 41, page 2553)

[2] Kommission Lagerung hoch radioaktiver Abfallstoffe - Abschlussbericht: Ein faires und transparentes Verfahren für die Auswahl eines nationalen Endlagerstandortes, 5. Juli 2016

[3] Gesetz zur Fortentwicklung des Gesetztes zur Suche und Auswahl eines Standortes für ein Endlager für Wärme entwickelnde radioaktive Abfälle und anderer Gesetze vom 05.05.2017 (BGBl. I 2017, Nr. 26, issued on 15th May 2017, page 1074

[4] „Dezentrale Zwischenlager, Bausteine zur Entsorgung radioaktiver Abfälle“, Bundesamt für Strahlenschutz, Salzgitter, Germany, 2005

[5] Jill Cooley „Integrated Safeguards – Current Status of Development and Plans for Implementation”, Department of Safeguards, International Atomic Energy Agency, Vienna, Austria, IAEA-SM- 367/3/01

[6] „Safeguards Techniques and Equipment: 2011 Edition”; International Nuclear Verification Series No. 1 (Rev.2), International Atomic Energy Agency, Vienna, Austria, 2011

[7] A. Jussofie, R. Graf, W. Filbert, “German Approach to Spent Fuel Management”, IAEA-CN-184/30; Symposium on International Safeguards: Preparing for Future Verification Challenges, Vienna, Austria, 2010

[8] A. Jussofie, K. van Bevern, M. Hahn, W. Trautwein, “Germany’s Accelerated Exit from Nuclear Energy: Challenges and Perspectives with regard to Safeguards” IAEA-CN-220/ Symposium on International Safeguards: Linking Strategy, Implementation and People, Vienna, Austria, 2014

EU/ABACC Cooperation: Strengthening Safeguards Capabilities through implementing new technologies

Use of Ultrasonic Sealing System as a Containment System at Spent Fuel Storage

Aníbal Bonino[1], Geraldo Renha[1], Sonia F. Moreno[1], Luis Machado[1], François Littmann[2], Bernie Wishard[3], Sebastian Vigile[4], Leonardo Pardo[4]

[1] Brazilian-Argentinean Agency for Accountancy and Control (ABACC), Rio de Janeiro, Brazil, [2] European Commission – Joint Research Centre (JRC), Ispra, Italy, [3] International Atomic Energy Agency (IAEA) – Safeguards Technical Service (SGTS), Vienna, Austria, [4] Argentinean Regulatory Authority (ARN), Buenos Aires, Argentina

Abstract:

A sealing system has been designed by JRC/ISPRA in cooperation with ABACC and the IAEA in order to account for the difficulties in accessing spent fuel located in lower layers of spent fuel ponds.

The system consists of mechanical parts with an ultrasonic seal as containment measure combined with a surveillance system. The objective of the sealing arrangement is to maintain continuity of knowledge on nuclear material stored in the lower racks of the spent fuel ponds by preventing undeclared removal of this material. It will also introduce advantages by lowering the re-verification requirements at Physical Inventory Verifications (PIVs) and in case of surveillance failure.

For this application, ultrasonic seals have the necessary characteristics since they are designed to be attached underwater, they are very resistant to harsh environments like storage pools, they are easy to apply and they can be regularly verified. The verification of ultrasonic seals does not involve the replacement of cables or seals, thus improving inspector's productivity and decreasing the burden on the plant operator.

A six-month field trial will be conducted at the spent fuel storage at the *Central Nuclear de Atucha 1* (CNA1) – *Presidente Juan Domingo Perón,* after which ABACC and the IAEA will be able to assess whether the system meets the necessary requirements for safeguards use.

The overall impact on safeguards is discussed through a general approach to this facility. The key components of a possible safeguards approach that considers the implementation of this specific ultrasonic design are also briefly discussed.

Keywords: Nuclear Safeguards, International Cooperation, Ultrasonic seals, Containment System, Spent fuel storage.

1. Introduction

The *Central Nuclear de Atucha 1* (CNA1) is an on-load refuelling Pressurized Heavy Water Reactor (PHWR), where the spent fuels are stored in a closed packet way, in two layers at the storage pool, not allowing an easy way to verify the entire pool when it becomes necessary. More specifically, in case of fuel element verification, the accessibility of nuclear instrumentation to the lower layer of spent fuel is very complex and time consuming.

One way to maintain the Continuity of Knowledge (CoK) on the nuclear material at the spent fuel pond is to apply surveillance and containment measures at racks where these fuels are stored. It is important to guarantee that ABACC and IAEA maintain the CoK over multiple layers of the spent fuel storage with application of seals on fuel elements, racks or hangers.

The Ultrasonic Seals (US) have been used for this type of containment [1] [2] and they are already approved for safeguards use by both the IAEA (responsible for the implementation of the Nuclear Non-Proliferation Treaty – NPT) and by the European Commission's DG-Energy (responsible for the implementation of the EURATOM Treaty).

ABACC and the European Commission engaged into a collaborative project on strengthening the safeguards capabilities using the ultrasonic sealing system as containment and its general application [3]. ABACC and ARN evaluated the benefits of this system to be consolidated in a specific use on the spent fuel storage at CNA1 in Argentina.

The IAEA/ABACC approval process for application of this technology should go through evaluation of diversion scenarios considering the vulnerability aspects of the project and improvements required. The results of a field trial at the spent fuel storage planned for 2017 will support the final approval of the system, after which ABACC and the IAEA will be able to assess whether the system meets the necessary requirements for safeguards use.

2. Safeguards system based on containment and surveillance

The proposed sealing system already tested in CNA1 pond consists of a stainless steel bar attached on each external hanger of the fuel elements support devices. This attachment is provided by means of ultrasonic seals, in this way when the bar is installed, it disables any possibility to remove the fuel elements from the specific hanger, without breaking the seals.

The objective of the sealing arrangement at CNA1 is to maintain the CoK of the nuclear material stored in the lower and upper racks of the Spent Fuel (SF) ponds by preventing undeclared removal of this material. The dual system considered for these ponds consist of the ultrasonic seal system as containment and surveillance system based on the Next Generation Surveillance System (NGSS).

The IAEA contracted the development of the NGSS system to replace the DCM-14 cameras. NGSS basic level consists of a single camera taking, authenticating, and storing surveillance data.

The system will be applied in order to avoid item counting of the SF stored in the lower racks in the ponds during the annual Physical Inventory Verification (PIV) as well as their re-verification in case of surveillance failure.

The re-verification of spent fuel assemblies (SFAs) in tightly configurations in storage ponds is a challenge at the Atucha site since SFAs are stored in two layers in the spent fuel pond. A prototype Spent Fuel Neutron Counter (SFNC) has been used since November 2002 in verifying long decayed spent fuel stored in the upper layer.

The original SFNC which was developed and tested at the site jointly by the IAEA and ABACC used a fission chamber that was lowered into the gap among four adjacent fuel assemblies. In

fact, provided that a safe and reliable access of the neutron detector can be gained to the entire length of the assemblies in the lower level, the verification of the fuel in the lower layer could be done exactly in the same manner as the verification of the fuel in the upper layer. This has, so far, not been attempted, mainly because of the difficulty, seen in lowering the neutron detector between fuel assemblies of the upper and lower layer.

A specific project was signed in collaboration with Department of Energy (DoE) for developing a spent fuel gross defect system at CNA1 [4]. The objective was to develop a comprehensive database for the SFAs at both natural U and enriched 0.85w% covering the range of cooling times and burn-up present. An algorithm uses this database to predict expected signals when coupled with the SFNC at any location in the pond.

Although part of a project for optimizing the re-verification of spent fuel assemblies in the pond, the activity itself is still time consuming, so ABACC/IAEA are considering the containment project using the ultrasonic seals as a back-up component for surveillance, only in case of failures of these two components the re-verification would be applied.

3. Ultrasonic seals project

ABACC has agreed with JRC/ISPRA on a project of containment of Spent Fuel in Complex Storage Environment in 2012. The ultrasonic technology was chosen with a potential for future joint use with IAEA.

The requirements for the ultrasonic sealing system are mainly based on:

- CoK is guaranteed when sealing spent fuel pond;
- Seals on fuel elements, racks or hangers, guarantee knowledge over multiple layers of spent fuel storage;
- Ultrasonic seals are designed to be attached underwater, they are resistant to harsh environments, they are easy to apply and they can be regularly verified;
- Verification does not involve the replacement of cables or substitution of the seal, nor does it require the movement of spent fuel;
- This improves inspector’s productivity, takes due care of radiation, safety considerations and decreases the disturbance to the plant operator;
- Seals technology are already used in other countries.

For this project a specific agreement with Argentinean National Authority (ARN) was signed and it considers training in the use of "Ultrasonic Seals" for the containment of spent fuels located in a complex storage environment and difficult to access for verification for safeguards purposes and their application in power reactor installations - demonstration of practical application in the CNA1.

3.1 Preliminary design

The first design was based on a sealing bar with two locking mechanisms, to be inserted over the hangers. The locking mechanisms were put instead of the two lateral extreme spent fuel rods as shown in Figure 1.

The seal bolt is tightened outside of the pond, by the inspector. The mechanism is spring loaded, once clamped on the hanger it can’t be removed without first breaking the seal, opening the locking mechanism.

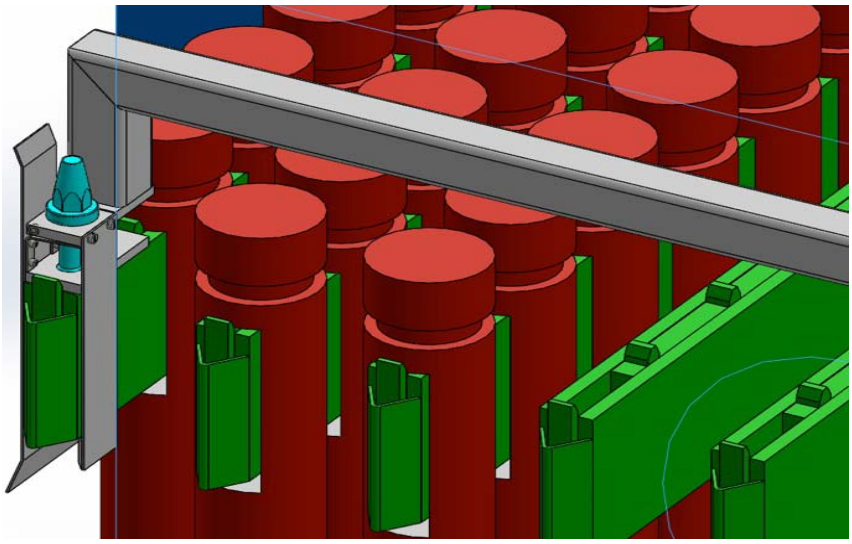

Figure 1: Close 3D view of the bracket locked on the hanger

This solution was not acceptable since the spent fuel storage positions blocked significantly reduces the SFAs storage capacity of the pond.

3.2 Alternative solution: locking with fuel bundle in position

The idea was to still use a bar with two locking mechanisms but the triangular tip of the two lateral hangers will be used, freeing the two positions for spent fuel assemblies. The seal bolt would be tightened underwater to close the locking systems by pushing rods under the triangular tips.

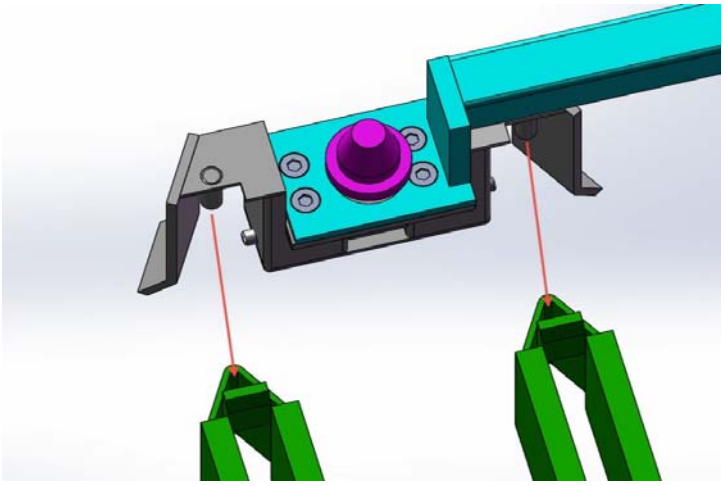

Figure 2: View of the two centering pins and associated positions on the racks

On the following Figure 3, we can see how the system was working.

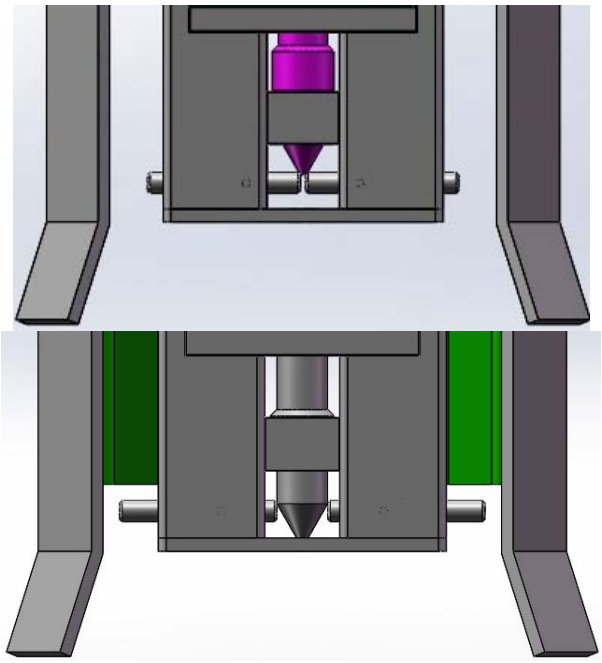

Figure 3: Unlocked, seal high, pins retracted (top) versus locked, seal in lower position, pins extracted (bottom)

3.3 First infield mission in Atucha

The first mission was done in June 2015 at CNA1 and ABACC/JRC took the opportunity to have access to a hanger outside of the pond (Figure 4) and they were able to discuss changes in the design.

Figure 4: View of the hangers outside of the pond

3.4 Proposed third design and associated prototype

Following the first mission and the comments received by Atucha's operators and ABACC technical staff, JRC updated the design accordingly and the locking mechanism fitted on only one triangle on each extremity of the hangers (and not two as on the previous design), in order to cope with the relative variability of the distance between two successive individual beams of the hangers.

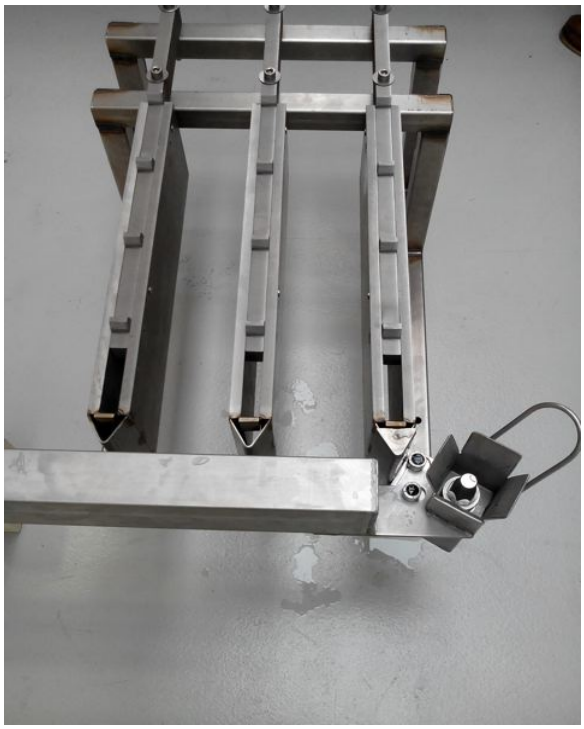

Figure 5: Mock up of the hangers and view of the locking system

3.5 Second infield mission in Atucha - Ultrasonic seals tests at the spent fuel pond

JRC and ABACC returned to Atucha in November 2015 with a foldable locking system with 4 m bar (cut in four separate 1 m bars), several locking mechanisms, two seals & tools. The equipment was tested on various elements outside CNA1 and the overall prototype system on the spare hangers. After this first step the bar and locking devices were tested in CNA1.

The bar was raised from the center with the crane and located on the first row of fuels in the pool five as shown in Figure 6. The plug-in process was easier than expected and the assistance from the steel bar ends practically was not required. The steel bar has a water tight design providing a low weight when it is submerged in the pond. The sealing bar was mounted over the hangers, seals tightened and then broken. Following the tests performed with the first prototype of sealing bar and locking mechanisms, ABACC and JRC validated the principle of locking on the triangular tip of the hanger on CNA1 hangers (underwater storage pond).

As shown in Figure 7 the system was attached and locked properly, when the steel rod is installed it disables any possibility to remove the fuel elements in the complete hanger.

Figure 6: Ultrasonic system installation with operator assistance in CNA1

Figure 7: Close view of sealing bar of hangers into the pond

4. Jointly Safeguards Approach and Scenarios

Based on the successful results obtained after spent fuel pond tests in Atucha and the training with inspectors and operators, ABACC contacted IAEA in 2016 to propose a common approach to use this technology.
After discussion of different diversion possible scenarios pointed out by the IAEA from the lower racks, the project [4] was improved to take into account these new considerations, it can be

seen from Figure 8 an example of these changes related to the locker system. A joint ABACC-IAEA procedure on the verification has been discussed based on the criteria for On-Load reactors [5], so that part of the spent fuel under dual C/S; both C/S systems should be evaluated as follows:

1. The surveillance system to be serviced and reviewed, during Physical Inventory Verification and interim inspections;
2. The ultrasonic seals to be verified with low detection probability and the containment to be examined, including visual observation on the integrity of the metal bars, during Physical Inventory Verification inspection.

The nuclear material subject to the dual system (C/S) is Pu and U contained in the SF from the nuclear power plant at Atucha (RAI1) which is stored in racks.

Figure 8 – Locking mechanism (new on the left and first model tested in CNA1 on the right)

Upon filling up the lower rack with SF, the upper rack will be staked on the lower one as a cover of the lower rack; the upper rack will be immobilized with the metal bar and sealed as described above. The diversion would require possibly tampering of the respective metal bars and removal or displacement of the associated upper racks allowing access to the lower levels. IAEA/ABACC identified improvements to be done and technical solutions have been discussed with JRC and a possible final schematic sealing system with protective arms should be applied during field trial, as presented in Figure 9.

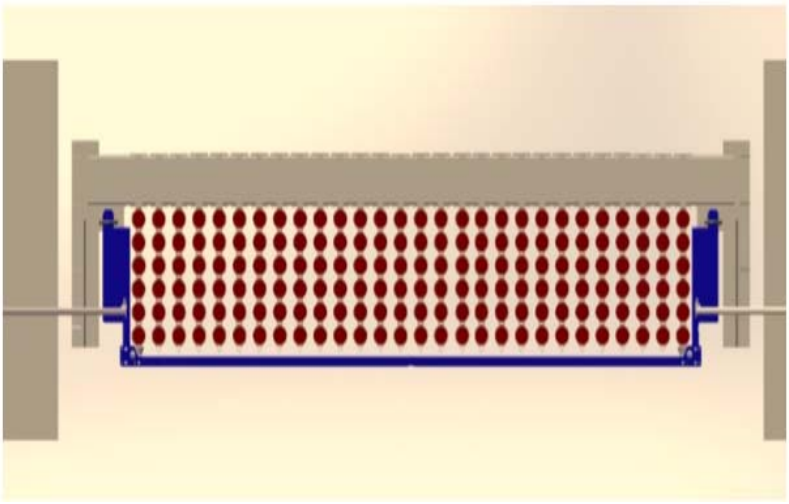

Figure 9: Schematic sealing system with protective arms.

5. Field Trial Perspective

The main purpose of sealing using ultrasonic technique is to maintain the CoK and avoid re-measurement. This is particularly important when applied to SF storages. ABACC, together with national authority and operator in Argentina, have been discussing the application of ultrasonic seals technologies, and, in particular, on how their use improves safeguards inspections without affecting operational tasks and turning activities less intrusive and more efficient.

Besides technical developments, safeguards approaches and scenarios should be discussed among all parties before ultrasonic seals system deployment. The parties involved are the state through ARN and the international safeguards agencies, ABACC and IAEA in order to ensure ultrasonic seals containment system success during safeguards implementation.

IAEA has been engaged in the evaluation process of the ultrasonic seal specific application for the CNA1 through the Safeguards Technical Service (SGTS) and different tasks need to be performed before final approval of the system.

The field trial, as part of the final IAEA/ABACC approval process, should start during the second semester of this year when JRC will be able to fabricate bars, seals and locking mechanisms to apply at least in one pond considering the final ABACC and IAEA remarks on the project. Meanwhile ABACC/ARN/IAEA would agree on the SF ponds selection, the procedures for evaluation of the system during the field trial and the final approval process for this ultrasonic sealing containment.

The use of new technologies in safeguards is important to enhance their effectiveness and efficiency. In this particular case, any future application of ultrasonic technology should be developed and implemented in such a way to allow joint use application between ABACC and IAEA, so the results from the containment provided by the ultrasonic seals during the field trial shall permit that ABACC and IAEA approve the technology for specific safeguards use in CNA1.

6. References

[1] M. Chiaramello, M. Sironi, F. Littmann, P. Schwalbach, V. Kravtchenko, *"JRC CANDU Sealing Systems for Cernavoda (Romania) and Upcoming Developments",* ESARDA BULLETIN, No. 44, June 2010, pp 29-39.

[2] Y. Lahogue, F. Littmann, S. Synetos, J. Lupo, V. Piron, M. Sironi*, "Developments in the deployment of Ultrasonic Bolt Seals at the storage ponds of a large reprocessing plant",* Book of Abstracts, Presentations and Papers of Symposium on International Safeguards: Linking Strategy, Implementation and People, Vienna – 20/24 October 2014, p. 120.

[3] J. Goncalves, F. Littmann, V. Sequeira, M. Sironi, O. Peixoto, S. de Almeida and S. Fernandez Moreno,"*EU - ABACC Cooperation: Strengthening Safeguards Capabilities*", Conference Proceedings of 37th ESARDA Symposium on Safeguards and Nuclear Non-Proliferation, Manchester, UK, 19-21 May 2015, pp.91-98.

[4] S. Sitaraman, Y. S. Ham, N. Gharibyan, O. J. M. Peixoto and G. Diaz, "*Methodology and Software for Gross Defect Detection of Spent Nuclear Fuel at the Atucha-I Reactor* – Nuclear Technology, October 2015, pp. 74-83.

[5] F. Littmann, A. Guarino, E. Lanza, G. Selvagio, P. Tebaldi, JRC Technical reports *"ABACC Project Ultrasonic Bolt Sealing System Description of Final technical Design"* – JRC/ISPRA, November 2016.

[6] International Atomic Energy Agency*, "Safeguards Criteria On-Load Reactors (OLRs)",* SG-SMC-02.

Energy Harvesting for Increased Safeguards Equipment Battery Life

Ross Hymel
Unclassified Unlimited Release, SAND2017-4965 C

Sandia National Laboratories (SNL)
PO Box 5800, Albuquerque, NM USA 87185-1373
E-mail: rwhymel@sandia.gov

Abstract:

Most unattended safeguards equipment (e.g. electronic seals) use some form of battery—traditionally an expensive, bulky and, oftentimes, hazardous lithium battery. The limited charge-life of these batteries necessitates periodically replacing them or the equipment they power (if batteries are not field-replaceable) to prevent total battery discharge and potential loss of continuity of knowledge. These maintenance cycles present a significant monetary cost to a safeguards inspectorate and demand on in-field inspector time, as well a potential increase in personnel exposure to radiation.

One approach to increasing the operational lifetime of this equipment is known as energy harvesting: the process by which energy is replenished by collection and storage from external source(s). The replenished, stored energy can be used to supplement the energy available from the initial battery charge. This paper examines energy harvesting via photovoltaic (PV) cells, both monocrystalline and amorphous, and the cells' associated performance in converting energy across the entire infrared to UV spectrum, including both indoor and outdoor lighting conditions. It then explores the system architecture required for energy harvesting as well as the design trade-offs available. Finally, this paper assesses the performance of a prototype system incorporating this type of energy harvesting in a real-world application.

Keywords: safeguards, containment, batteries, energy harvesting

1. Introduction

Modern unattended safeguards equipment (e.g. seals) incorporates many low-power electronic circuits, which are typically powered by expensive and toxic lithium thionyl chloride ($LiSOCL_2$) batteries. The limited life of these batteries necessitates their periodic replacement. This replacement must be performed before total battery discharge to avoid potential loss of continuity of knowledge. Thus, the effective battery capacity becomes significantly less than the actual usable capacity. Additionally, such maintenance can be a radiological hazard to personnel, as well as a monetary burden to a safeguards inspectorate.

Energy harvesting, a commercially available technology, could extend the operational life of battery-powered equipment to achieve significant efficiencies for safeguards deployments. Energy harvesting involves scavenging and storing ambient energy sources, such as solar, thermal, and kinetic for use in low-power electronic applications. While the amount of scavenged energy per unit time may be small, it most often comes from a source that will not be depleted throughout the deployment of the harvesting device. The best-known energy harvesters are solar panels and wind turbines.

Recently, far-field wireless energy harvesting has become a commercially available option. Far-field wireless energy harvesting provides consistent, predictable, and un-tethered power over distances up to 50 feet. This process converts radio frequency (RF) energy, both intentionally emitted and ambient, into usable direct current (DC) power. Incorporating far-field wireless energy harvesting into safeguards equipment can significantly extend the equipment's battery life and perhaps make it indefinite. Furthermore, additional functionality can be added to safeguards equipment without

lowering its operational life expectancy. This type of energy harvesting was previously explored, and the results can be found in Reference 1.

Alternatively, should RF harvesting not be permitted or desired, photovoltaic-based harvesting is a promising substitute. Photovoltaic (PV) cells are semiconductor devices that convert incident photons directly into electricity via the photovoltaic effect. These cells come in several types depending on the underlying crystalline structure and include amorphous, polycrystalline, and monocrystalline. Recent advances in monocrystalline panel technology enable such cells to convert up to 22% of ambient light energy into usable electric power. Should cost be the overriding factor, cheaper, but less efficient, amorphous cells are also an option.

This paper explores the benefits and drawbacks of integrating energy harvesting into a chosen safeguards seal: the Remotely Monitored Sealing Array (RMSA). Specifically, it examines the usage of commercially-available PV cells, amorphous and monocrystalline, detailing the pros and cons of each type as well as the in-system performance.

2. Photovoltaic energy harvesting overview

Figure 1 shows a simplified diagram of a PV-based energy harvesting system.

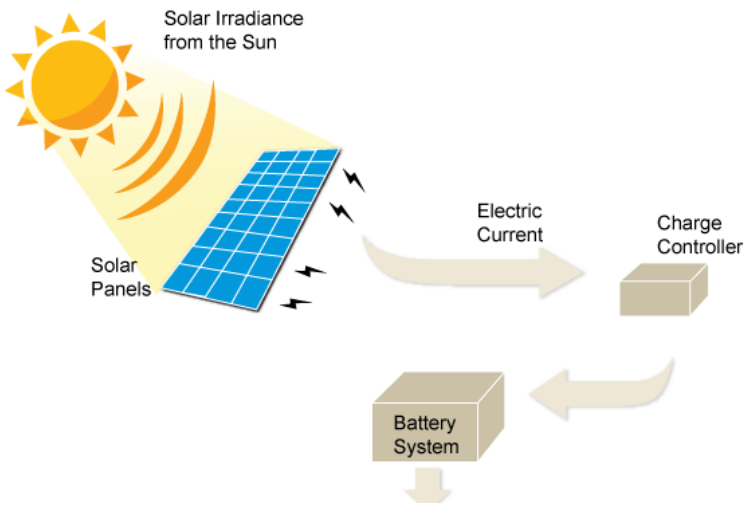

Figure 1: PV-based Energy Harvesting System (image courtesy http://lifefreeenergy.com)

Such a harvesting solution typically contains four main components. First, a source of photonic energy, such as the sun, must be available. While solar irradiance is the preferred form of energy, providing up to an order of magnitude more photonic energy per unit of collector area than indoor lighting, the PV system itself is only weakly constrained to the form and strength of lighting. Certain cells are optimized for operation under specific light intensities – for example, indoor cells that must not experience greater than 1000 lux illumination. Also, all cells have a varying efficiency across wavelength and will produce a larger signal output based on the spectral content of the lighting source. This non-ideal behaviour is known as external quantum efficiency and will be discussed later.

Next, a small PV cell must be exposed to the photonic energy. When irradiated, a PV cell behaves analogously to a current source. As irradiation increases, so too does the amount of charge available for collection. Such cells are self-limiting; as the attached electronic load increases, the output voltage of the cell drops, finally reaching its short circuit current (I_{SC}) at a zero-ohm load. Similarly, as electronic load decreases, the output voltage of the cell rises, eventually reaches its open circuit voltage (V_{OC}). All points in between are characterizable and form the cell's I-V curve. Figure 2 displays an example I-V curve for an IXYS brand solar cell. The blue line plots the cell's voltage and current under fixed lighting conditions but with an electronic load that varies incrementally from 0 to ∞ ohms.

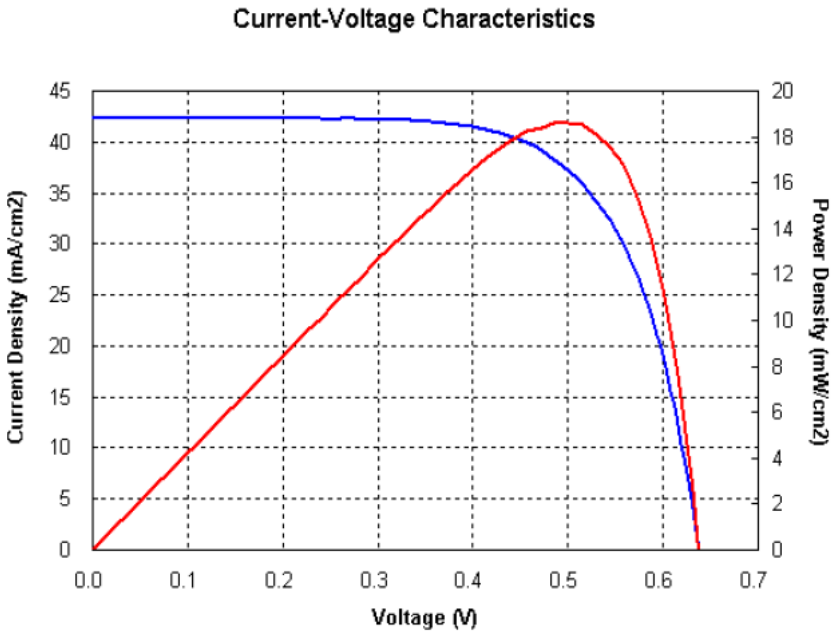

Figure 2: Representative I-V Curve (image courtesy http://ixys.com)

As can be seen, even under fixed illumination, the power available from the cell varies based on the electronic bias point of circuit. The red line plots the variation of power available from the cell under different loads. There is clearly a point of largest power, known as the maximum power point (MPP), and, for solar cells, it typically occurs at 80% of the open circuit voltage.

Because the energy delivered by the cell must be collected in a very specific manner to optimize the available power, a specialized circuit is needed that can properly bias the cell at its MPP as well as convert the low voltage energy into a more usable form. The charge controller in Figure 1 is this element. Even for indoor lighting, the illumination levels, and thus the charge generated by the cell, will vary significantly throughout the day. The charge controller must dynamically vary the impedance presented to the cell in order to maintain operation at the MPP. Furthermore, most electronic systems require a constant, well-regulated voltage to operate correctly. The charge controller must also employ a voltage converter to transform the varying input voltage into a constant, predictable output voltage.

Lastly, solar cells are not able to store energy. Should the cell generate energy in excess of what is required for the load, this additional energy would be lost. While such an approach may be tolerable in a simple system where the lighting conditions are known and continuous, a more advanced system will employ some form of energy storage. This energy storage allows the system to continue to operate without depleting the primary batteries when the photonic source is diminished or removed, for example at night when the lights are turned off. Here, the primary batteries serve to power the unit upon start-up (while secondary batteries are charging) and when secondary battery power is depleted due to lack of photonic energy.

Many forms of energy storage are available, including rechargeable batteries and supercapacitors. Each have different charging methods, such as constant current or constant voltage, and the previously mentioned charge controller must be able to provide the appropriate form. Also, each type of energy storage has different capacity, cost, and self-discharge, so care must be taken when down-selecting for an application.

2.1. PV cell evaluation

For this study, three PV cells were evaluated, each cell having varying characteristics and use cases. Their measured parameters are listed in

Table 1. All cells were first tested using white light at an intensity of 1.0 sun (1000 W/m^2). They were then retested using ambient room lighting (10 W/m^2). For each test, the load presented to the cell was varied such that the voltage across the cell increased from 0 (zero) V to an open circuit indication in 0.01 V increments.

	AM-5902CAR	**AM-1816CAR**	**SLMD121H10L**
Crystal Type	Amorphous	Amorphous	Monocrystalline
Intended Use	Outdoor	Indoor	Dual
I_{SC} (1000 W/m^2)	58.6 mA	3.55 mA	35.7 mA
V_{OC}	7.86 V	6.24 V	6.64 V
P_{MAX}	254 mW	5.26 mW	173 mW
Fill Factor (FF)	0.550	0.00526	0.728
I_{SC} (10 W/m^2)	202 µA	227 µA	132 µA
V_{OC}	5.1 V	5.2 V	3.46 V
P_{MAX}	600 µW	770 µW	264 µW
Fill Factor (FF)	0.582	0.653	0.577
Size	8.72 in^2	8.50 in^2	2.28 in^2
Unit Cost (quantity 10)	$23.06	$9.56	$11.81

Table 1: Evaluated PV Cell Parameters (0.1 Sun)

I_{SC} is the current through the cell when the cell is shorted, i.e. the voltage across the cell is zero. This number represents the maximum amount of current the cell can deliver, and, for a cell with moderate resistivity, is relatively flat even as the voltage increases up to the MPP.

V_{OC} is the voltage across the cell when the cell is open circuited, i.e. the current through the cell is zero. This parameter will influence the choice of charge controller, as the value must not be so low that the charge controller fails to start-up and not so high that the charge controller is damaged. Please note that no power can be extracted from the cell in either I_{SC} or V_{OC} conditions.

P_{MAX} represents the maximum power the cell can deliver and is easily calculated by tracing the I-V curve and using the equation P = I*V. As previously mentioned, power will be zero at the I_{SC} and V_{OC} points, with maximum power occurring at some point in between, usually 80% of V_{OC}.

Fill factor (FF) measures the quality of a solar cell. An ideal solar cell's I-V curve is a flat square, with vertex at (I_{SC}, V_{OC}). For such a cell, P_{MAX} = I_{SC} * V_{OC} = P_T (theoretical power) resulting in a FF of 1. Actual cells operate below this point due to losses such as internal resistance and diode effects. Fill factor is graphically represented in Figure 3, and is the ratio of P_T to P_{MAX}.

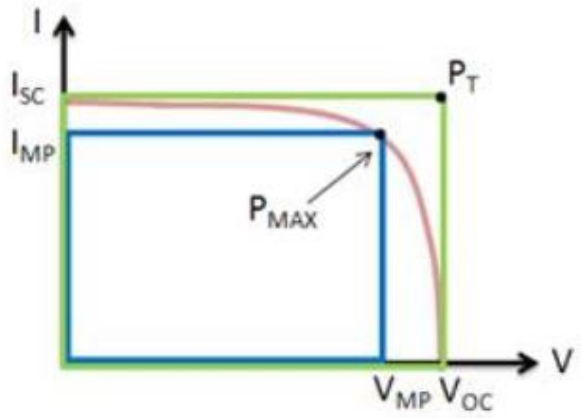

Figure 3: Graphical illustration of FF (image courtesy http://ni.com)

For all electrical parameters listed above (I_{SC}, V_{OC}, P_{MAX}, and FF), a higher number is better. However, size and cost must also be considered when selecting a cell. For both indoor and outdoor lighting conditions, the SLMD121H10L has the greatest electrical performance per square inch. If cost is the overriding factor, the SLMD121H10L should be used outdoors while the AM-1816CAR should be chosen for indoor applications.

The above measurements were taken under uniform, white light conditions (400 nm to 700 nm). Realistic lighting conditions will not be so evenly distributed across all spectral wavelengths. A measure of the cell's response versus frequency is known as the external quantum efficiency (EQE). This metric is the ratio of the number of charge carriers collected by the cell versus the number of photons incident on the cell. An ideal cell will have a quantum efficiency of 100% across all wavelengths. Actual cells will have optical losses due to recombination effects. Figure 4 plots the measured EQE of all three cells across the infrared (IR) (700 - 1100 nm) to ultraviolet (UV) (< 400 nm) spectrum in 10 nm increments.

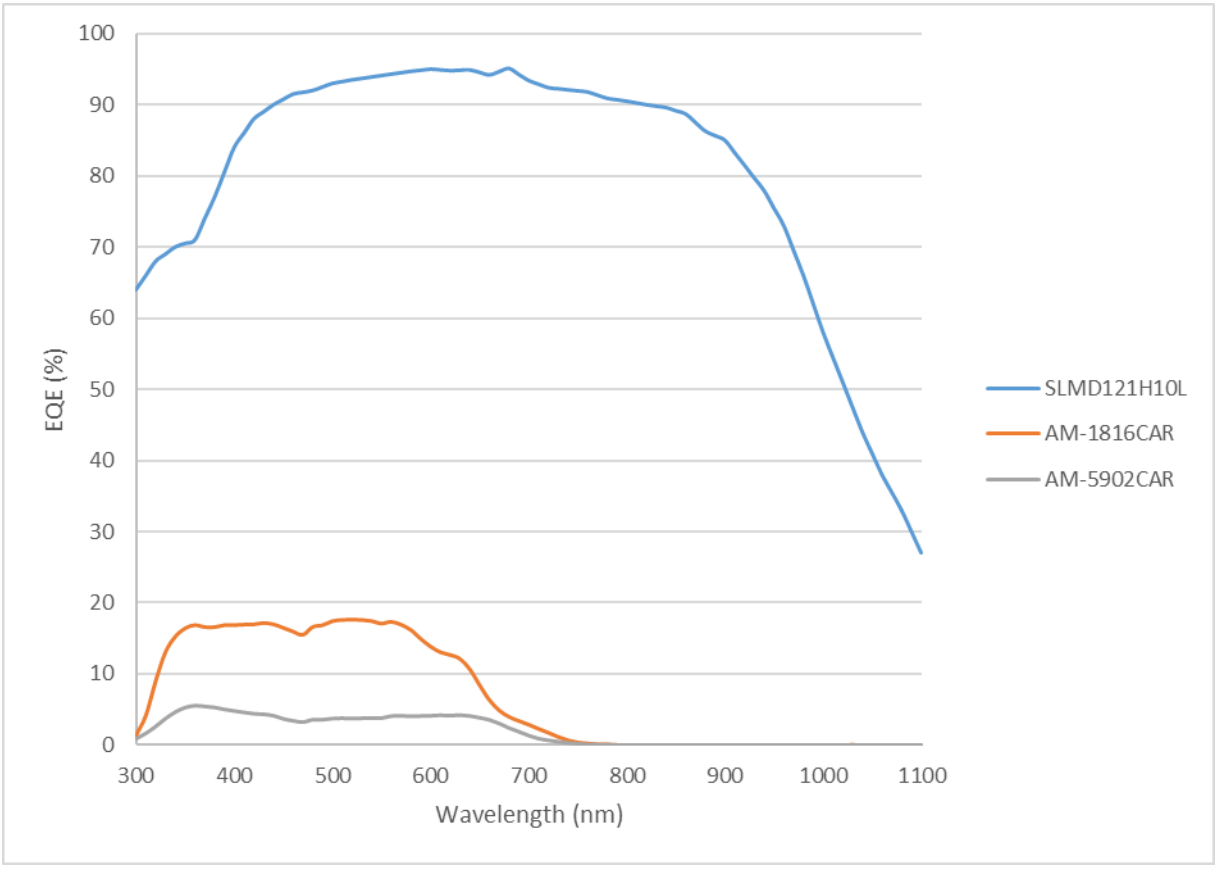

Figure 4: EQE measurements

The advantages of monocrystalline cell construction are evident in this Figure 4. The SLMD121H10L can operate across the entire spectral range, while the two amorphous cells are limited to the 300 nm to 600 nm visible portion. This larger area of operation will result in increased power conversion efficiency when operated in the presence of infrared and ultraviolet light, especially outdoors. [Note that the magnitude of increased efficiency is not fully evident in the Table 1 values since they were determined only for the visible portion of the spectrum.] Further, the quantum efficiency is significantly higher, allowing a much smaller cell to be used for similar energy harvesting results.

Lastly, monocrystalline cells have less temperature dependence than other types. In general, the voltage output of a cell will decrease with increasing temperature. While this effect occurs in monocrystalline cells, the net effect is less severe than in amorphous and polycrystalline cells. For the

above tested cells, the monocrystalline will experience a -0.03 %/K degradation in V_{OC} while the amorphous cells will undergo -0.3 %/K, an order of magnitude larger impact.

3. Charge controller and energy storage

The circuit topology for collecting and storing charge generated by the solar cells can take on many forms depending on the objectives of the system. The options include battery replacement, battery extension, and tiered architectures, which are explained below.

The first option is the complete removal of system batteries. By calculating the load requirements of the attached system over the course of a lighting cycle (usually one full day), the designer can size a PV cell arrangement such that it will provide enough harvested energy to fully power the system over the entire cycle, with enough margin for off-normal events, such as clouds. Unfortunately, this option is unusable in the schema, as batteries (or other large capacity storage) must always be present in a secure system such as a seal. Otherwise, an adversary could turn of the lights or cover the cells with opaque material to force the equipment to power down since harvestable energy is no longer present.

The second option is to increase the lifetime of the primary batteries by only powering the system from them when the energy harvester is not available. This option necessitates the same load requirement analysis as the battery removal option, but, rather than eliminating the batteries, significantly increases the time period between battery replacements.

For this evaluation, a tiered architecture was chosen consisting of a primary battery, a secondary storage unit, and the energy harvester. See Figure 5. During normal operation, solar energy is harvested and stored in the secondary storage unit. This unit must be carefully sized such that it can fully power the system during the course of the lighting cycle where no solar energy is present. On initial power-on, the attached load is powered by the primary battery (Line 2 is connected to Line 3 in Figure 5). Once the harvester has fully charged the secondary storage, the charge controller switches the power source from the primary batteries (Line 3) to the secondary storage (Line 1). The harvester will continue to replenish this secondary storage so long as solar power is available. If solar re-charging is not available, the system will continue to run from the secondary source until the attached load drains it below a specified threshold, at which point system power will revert back to the primary batteries (Line 3). Figure 5 presents a simplified representation of this tiered architecture.

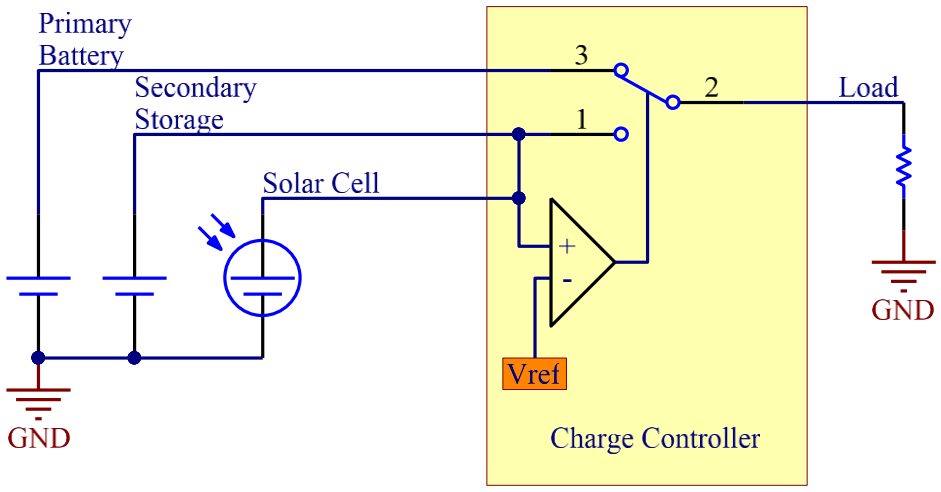

Figure 5: Tiered architecture block diagram

Besides being able to seamlessly switch between primary and secondary power (break-before-make), the charge controller must also be capable of several other important functions. These include:

- Programmable prevention of secondary storage over- and under-voltage to prevent damage or irreversible depletion, respectively
- Cold-start operation at extremely low levels of input voltage from the harvesting element (< 0.5 V) for start-up at low light levels
- Wide input voltage range (0.1 V to 5 V ideal) allowing for operation with many different kinds of PV cells
- Maximum power point tracking for optimal energy extraction
- Low quiescent current (< 1 µA ideal) to maximize energy delivery to the load

Several devices meet these criteria, including the ADP5091 from Analog Devices, the SPV1050 from STMicroelectronics, and the BQ25505 from Texas Instruments. For this evaluation, the BQ25505 was chosen as it has the lowest quiescent current (325 nA typical) and start-up voltage (330 mV). These two parameters are most important, as they will minimize the drain on the primary batteries and allow for operation in very low lighting conditions. Additionally, the part has a wider input voltage and power range, allowing its use with most outdoor cells.

4. Seal Integration

To integrate PV energy harvesting into a safeguards seal such as RMSA, only minor modifications must take place. First, the PV cells must be mounted to the case and electrically connected to the base seal hardware. Because these cells require exposure to ambient light, they must be mounted externally. Fortunately, existing RMSA cases already support both external and internal antenna configurations. Instead of installing an external antenna, the existing antenna mounting can be used for connecting the PV cell(s). These cell(s) are in turn soldered to a custom printed circuit board (PCB) and attach via a standard SMA connector. Once the cells are attached, the external connector is cabled internally to the base hardware as an antenna would be. This approach minimizes cost, as it requires no retooling of the case or RMSA manufacturing process. Figure 6 shows the fully assembled RMSA with lid both open and closed. For this work, the SLMD121H10L PV cell was chosen, for reasons mentioned in the PV cell evaluation section; two PV cells are needed for maximum system lifetime under indoor lighting conditions. Full testing results are presented in the next section.

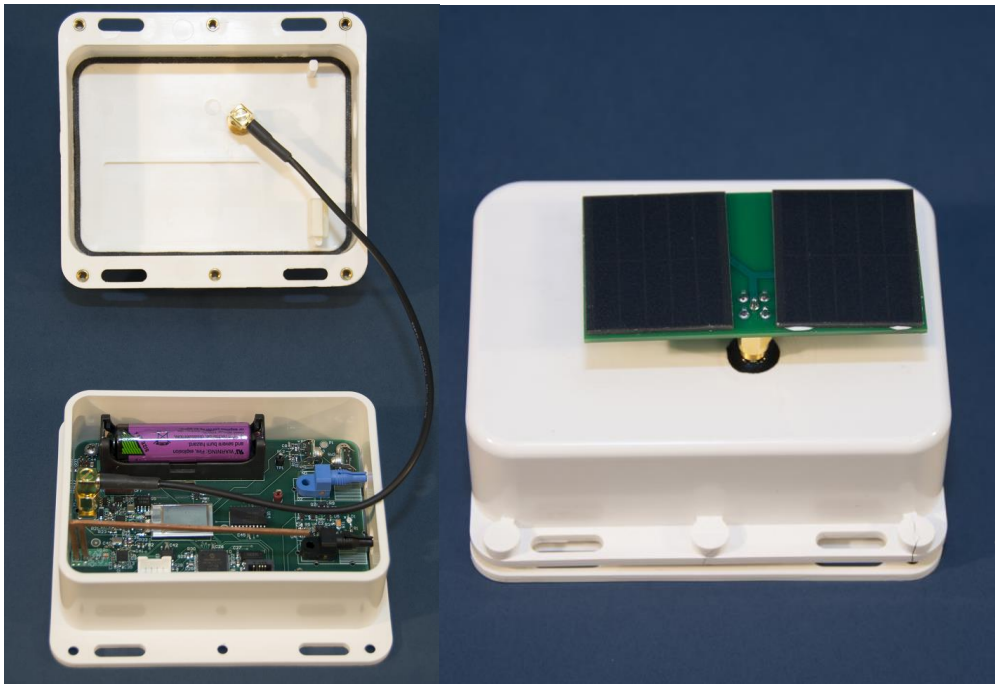

Figure 6: Fully assembled unit with lid open and closed

As previously mentioned, batteries must still be contained within the unit to prevent external tampering and seal power-down. Nevertheless, because ambient PV energy is so abundant, the base hardware for this instantiation contains only one battery rather than the standard two. This reduction offsets the cost of the second attached SLMD121H10L PV cell. Additionally, because the design is a tiered architecture, a secondary storage unit is included. This unit is carefully sized to match the power needs of the attached system and the lighting cycle. An EDLC supercapacitor is once again the preferred storage medium [1]. Given that the RMSA requires a quiescent current of ~20 µA and an operating voltage of 2.5 V – 3.6 V, and assuming a typical warehouse environment with artificial lighting available for at least 12 hours a day, a fully charged supercapacitor must contain at least 660 mF of capacitance to fully power the system without requiring switchover to the primary battery. The nearest value commercially available is 470 mF, which is used in this design, allowing for 8.6 hours of continuous operation without any available solar energy when fully charged.

For this work, no modification of the RMSA firmware is necessary. However, should further diagnostics be desired, such as the amount of charge on the secondary storage, the hardware connections on the base design would require no alteration. Only the firmware would require change, notably to digitize such an analog measurement and then add it to the periodic State-of-Health message.

5. Performance

To measure the performance of the system, three different lighting types were evaluated. The types chosen are representative of what might be present in an indoor environment and include LED, fluorescent, and incandescent. Each type of lighting contains different spectral power distribution curves that characterize the power emitted per wavelength of light.

For each lighting source, the harvester was placed a fixed distance away, corresponding to a given illumination level. The illumination level and color of the light was measured using a spectrometer; the test was repeated four times at different illumination levels. For these tests, light illumination was measured in lux. If watts is preferred, lux may be converted using the following equation

$$P(w) = \frac{E_{V(lx)} * A_{(m^2)}}{\eta_{(\frac{lm}{W})}}$$

Where P is the power in watts, E_V is the illuminance in lux, A is the area in square meters, and η is the luminous efficacy in lumens per watt. For typical lighting, η is 15 for tungsten incandescent, 60 for a compact fluorescent, and 30 for a white LED.

The results for each type of lighting are shown below, as is the spectral output of each light type. The Y axis in each figure represents the current harvested by the device in amps, while the X axis is the measured illumination level in lux. The figure also plots the average current required by an RMSA.

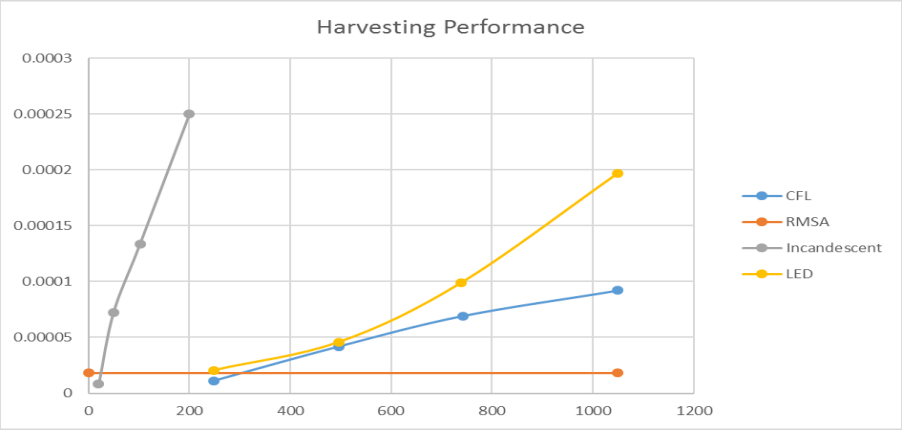

Figure 7: Harvesting Results

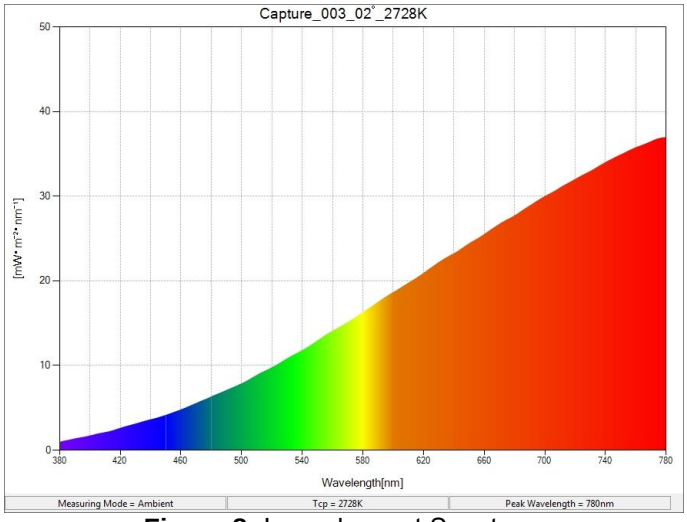

Figure 8: Incandescent Spectrum

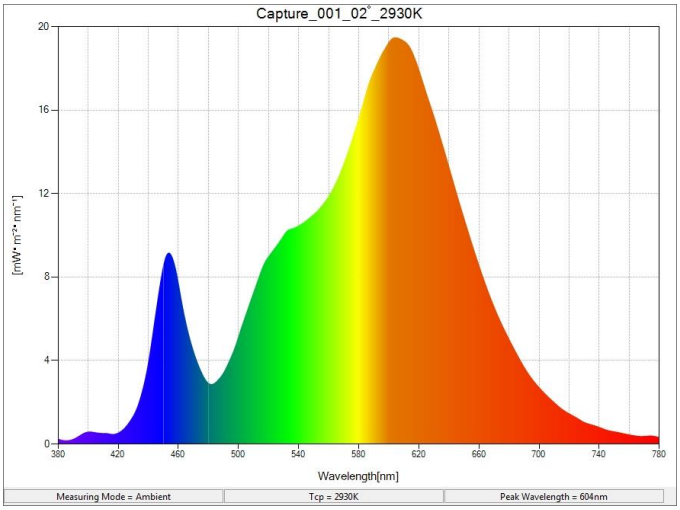

Figure 9: LED Spectrum

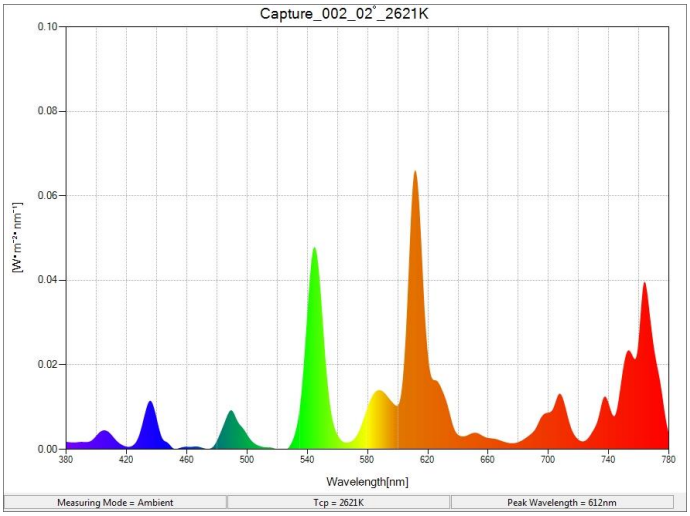

Figure 10: Fluorescent Spectrum

As shown in Figure 7, for illumination levels above ~30 lux for incandescent and ~250 lux for fluorescent/LED, the harvester is able to fully power a single RMSA. Incandescent light is clearly superior, as it provides the whitest output of the three lighting styles resulting in less required illumination. Also, these required illumination levels are low and easily attainable indoors. For reference, in a setting with two overhead 40W fluorescent bulbs, the illumination level directly underneath at a distance of seven feet is ~500 lux. Likewise, a single 40W incandescent bulb will provide ~30 lux at a distance of five feet.

6. Conclusions

There are many different options and architectures available to integrate PV-based energy harvesting with a safeguards instrument, such as a seal. It is up to the designer to match the power requirements of the system to the power available over the course of a lighting cycle. This paper has shown that ~$25 of monocrystalline cells coupled to a $10 PCB assembly can provide enough power, even in sparsely lit indoor areas and regardless of lighting type, to fully power a safeguards instrument, such as RMSA. Further, by using a tiered architecture, this system permits almost 9 hours of downtime within the lighting cycle without having to tap into the primary battery's charge. So long as the cells are not installed in overly dusty or dirty areas, the system will provide self-sustainable operation that is only limited by the lifetime of the electronic components and not the battery.

7. Acknowledgements

The author gratefully acknowledges funding support from the Safeguards Technology Development Program in the US Department of Energy/National Nuclear Security Administration's Office of Nonproliferation and Arms Control.

Sandia National Laboratories is a multi-mission laboratory managed and operated by National Technology and Engineering Solutions of Sandia, LLC., a wholly owned subsidiary of Honeywell International, Inc., for the U.S. Department of Energy's National Nuclear Security Administration under contract DE-NA0003525.

8. References

[1] Hymel, R; *Far-Field Wireless Energy Harvesting for Increased Safeguards Equipment Battery Life*: Proceedings of the Institute for Nuclear Material Management Annual Conference; 2016.

Session 16

Non-destructive Analysis: Neutron II

Development of Active Neutron NDA Techniques for Nuclear Non-proliferation and Nuclear Security

Yosuke Toh[1], Akira Ohzu[1], Harufumi Tsuchiya[1], Kazuyoshi Furutaka[1], Fumito Kitatani[1], Masao Komeda[1], Makoto Maeda[1], Masatoshi Kureta[1], Mitsuo Koizumi[1], Michio Seya[1]
Jan Heyse[2], Carlos Paradela[2], Willy Mondelaers[2], Peter Schillebeeckx[2]
Tatjana Bogucarska[3], Jean-Miche Crochemore[3], Giovanni Varasano[3], Kamel Abbas[3] and Bent Pederson[3]

1Japan Atomic Energy Agency (JAEA)
Tokai-mura, Naka-gun, Ibaraki 319-1195, Japan
2 Joint Research Centre – Geel
Retieseweg 111, B - 2440 Geel, Belgium
3 Joint Research Centre – Ispra
Via E. Fermi, 2749, 1-21027 Ispra (VA), Italy

Abstract:

In 2015, the Japan Atomic Energy Agency (JAEA) and the Joint Research Centre (JRC) of the European Commission collaboration started to develop an active neutron NDA system for nuclear non-proliferation and nuclear security. To the best of our knowledge, no established technique exists that allows us to accurately *determine the amount of Special Nuclear Materials (SNM) and Minor Actinides (MA) in high radioactive nuclear materials, such as spent fuel, nuclear fuel for nuclear transmutation, melted fuel debris from the damaged reactors and others. The collaboration aims at contributing to the establishment of an innovative Non-Destructive Analysis (NDA) system using a D-T pulsed neutron source for various applications. We utilize several active neutron NDA techniques, namely Differential Die-Away Analysis (DDA), Prompt Gamma-ray Analysis (PGA), Neutron Resonance Capture Analysis (NRCA), Neutron Resonance Transmission Analysis (NRTA) and Delayed Gamma-ray Analysis (DGA). All of these techniques have advantages and disadvantages. The different methods can provide complementary information which is particularly useful for nuclear non-proliferation and nuclear security. In this project, we have developed a combined NDA system, which enables the measurements of DDA and PGA, at NUclear fuel Cycle safety Engineering research Facility (NUCEF) in the JAEA Tokai-site. Numerical calculations have been performed to study the effects of the rather long pulse width (10μs) of the D-T neutron source on the NRTA measurements.*
In this paper, we will introduce our project and report the recent progress of developments, especially in NRTA, DDA and PGA.

Keywords: active neutron technique, differential die-away, neutron resonance transmission analysis, prompt gamma-ray analysis, delayed gamma-ray analysis

1. Introduction

Obviously, nuclear material accountancy (NMA) is of fundamental importance for nuclear safeguards and security. However, to the best of our knowledge, there is no established technique that enables us to accurately determine the amount of Special Nuclear Materials (SNM) and Minor Actinides (MA) in high radioactive nuclear materials, such as spent fuel, MA transmutation fuel and others. At least, much work needs to be done before a viable instrument is installed in place. The decommissioning of nuclear power plants produces a number of radioactive waste drums that contain SNM. The conventional passive γ-ray techniques cannot handle such waste drums. In particular, melted fuel debris from the damaged reactors at the Fukushima Daiichi nuclear power plant is difficult to apply the current NMA, because the debris contains nuclear fuel, fission product and structural materials such as concrete, metal and control rod. The Japan Atomic Energy Agency (JAEA) and U.S. Department of

Energy (DOE) provided recommendations for measurement systems of the fuel debris [1-3]. Neutron Resonance Densitometry (NRD), which was developed in a collaboration Action Sheet-1 (2012-2015) between Japan Atomic Energy Agency (JAEA) and the Joint Research Centre of the European Commission (JRC), was also proposed for the quantification of U and Pu isotopes in particle-like melted fuel debris [4,5]. NRD is very promising and allow us to determine the amount of ^{235}U and ^{239}Pu in particle like debris in melted fuel within 2% [6,7]. However, NRD is suitable for a rather thin sample, and is hard to apply for thick lava-like fuel-containing materials.

2. R&D project and active neutron techniques

The Japan Atomic Energy Agency (JAEA) and the Joint Research Centre (JRC) of the European Commission collaboration Action Sheet-7 (2015-2017) started to develop an active neutron NDA system for nuclear non-proliferation and nuclear security [8]. Figure 1 shows schematic outline of the "Development of active neutron NDA techniques" project. The collaboration aims at contributing to the establishment of an innovative non-destructive analysis (NDA) system using a D-T pulsed neutron source for various applications. Several active neutron NDA techniques, namely Differential Die-Away Analysis (DDA), Prompt Gamma-ray Analysis (PGA), Neutron Resonance Capture Analysis (NRCA), Neutron Resonance Transmission Analysis (NRTA) and Delayed Gamma-ray Analysis (DGA) have been developed in the collaboration. Table 1 shows the basic principles of the active neutron interrogation techniques that will be used in the project. All of these techniques have advantages and disadvantages. The different methods can provide complementary information which is particularly useful for quantification of SNM and MA in high radioactive nuclear materials. In this project, we have developed a combined NDA system, which enables the simultaneous measurements of DDA and PGA, at NUclear fuel Cycle safety Engineering research Facility (NUCEF) in the JAEA Tokai-site. Numerical calculations have been conducted to study the effects of the long pulse width (10 μs) of D-T neutron source on the NRTA measurements. The project is built in two phases: 1) Development and experimental validation of simulation tools that are used to optimise the design of the system. In addition, the quality of the nuclear data and models that are needed for data processing and analysis, are verified. 2) Modelling, design and construction of a prototype system for measurements in a MA-Pu fuel conversion facility as part of nuclear transmutation activities.

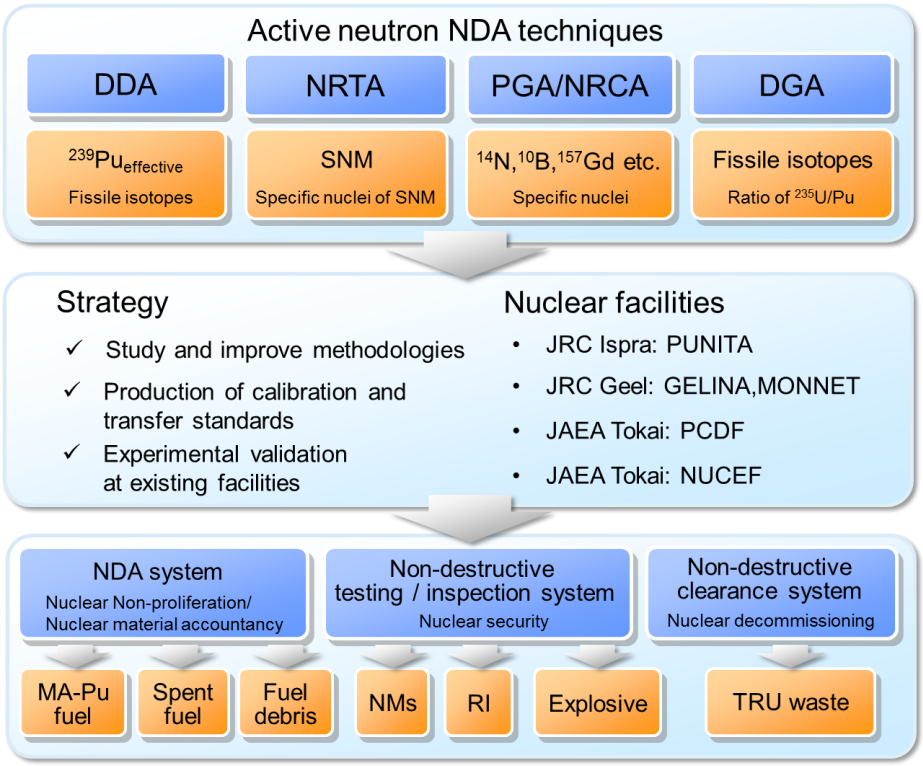

Figure 1. Schematic diagram of JRC – JAEA collaboration: Action Sheet -7.

NDA methods	Principles	Quantities of interest
DDA	Interrogation by a pulsed neutron Detection of induced prompt fission neutrons Correction of matrix effect	Total fissile content
NRTA	Irradiation by a moderated pulsed neutron beam Detection of neutrons transmitted through a sample Analysis of transmission spectrum	U and Pu contents
PGA/NRCA	Irradiation by a (pulsed) neutron beam Detection of prompt γ rays from (n,γ) reactions Analysis of γ-rays/TOF spectrum	Specific nuclides contents (N as explosive, B as neutron absorber, etc.)
DGA	Irradiation by a (moderated) neutron Detection of delayed γ rays from fission products Analysis of γ-rays spectrum	$^{235}U/^{239}Pu$ $^{241}Pu/^{239}Pu$

Table 1: Non-destructive analytical methods and quantities of interest.

2.1 DDA

The DDA technique detects fission neutrons, and it can determine very small amounts of the fissile mass, such as ^{235}U and ^{239}Pu. A D-T or D-D pulsed neutron generator is usually used for sample interrogation. A short pulse width (typically about 10 μs) is suited for DDA measurements. The prompt fission neutrons are detected in thermal neutron detector modules, and can be separated from the interrogation neutrons and background signals. The DDA technique has been investigated and developed for many years. Several different hardware and methodologies have been proposed. The most common method of DDA uses a thermal neutron for sample interrogation because the fission probability remains constant during the interrogation period. On the other hand, JAEA-DDA utilizes fast and epi-thermal neutrons for interrogation. There are differences between conventional DDA and JAEA-DDA in many ways, such as methodology, hardware and software. The project involves the exchange of the results of scientific and technical research for the DDA technique, as well as the exchange of information arising from the collaboration.

2.2 NRTA

NRTA is an NDA method which uses the energies of resonances to identify nuclides (elements) by the time-of-flight technique [9]. NRTA can be used to quantify almost all medium and high-Z elements and considered as one of the most accurate NDA techniques to quantify the amount of SNM and MA. In fact, NRTA was applied to quantify ^{235}U and ^{238}U in an U_3O_8 reference sample that was enriched to 4.5 at% in ^{235}U [10]. The difference between the experimentally determined areal densities of ^{235}U and ^{238}U and the reference values was less than 1%. The research collaboration Action Sheet-1 successfully demonstrated the technical feasibility of applying NRTA for the determination of the amount of SNM in particle-like debris generated in a severe nuclear accident [5,6]. However, to be compliant with the requirements for a compact NRTA system further development is needed. It is assumed that the compact NRTA system uses a D-T neutron source which has a 10 μs pulse width.

2.3 PGA / NRCA

PGA is one of the most efficient NDA techniques [11,12]. It utilizes neutron capture γ rays, which are characteristic of each particular nuclide. These provide the means to identify and quantify the elemental constituents of a sample. Thus, PGA has been used as a rapid, non-destructive method for performing both qualitative and quantitative multi-elemental analysis and is well acknowledged to be especially valuable for the measurement of light elements such as H, B, N, Si, S, and Cl, as well as Cd, Gd, Sm, and Hg which have large neutron capture cross sections. Therefore, PGA is utilized for the quantification of neutron absorber and particularly useful for the detection of explosives, because the most typical high explosive materials contain nitrogen.
The principle of NRCA is essentially similar to that of NRTA [9]. It differs from NRTA in that it detects γ rays that are emitted in neutron resonance capture reactions. In general, NRCA has a better detection limit compared to NRTA for most elements. However, for high radioactive nuclear materials, NRCA may lose the advantage in the detection limit because the γ rays from radioactive materials increase the background in the γ-rays spectrum.

2.4 DGA

DGA typically utilizes delayed γ rays emitted from the fission products in the neutron induced reactions. It seems to be a very promising NDA method for the spent nuclear fuels. The mass distribution of the fission products is correlated with the mass of the fissile nuclei, such as ^{235}U, ^{239}Pu and ^{241}Pu. Therefore, the intensities of individual gamma-ray peaks in the DGA spectra allow us to determine the ^{235}U/^{239}Pu and/or ^{241}Pu/^{239}Pu ratio. The DGA experiments have been performed using the Pulsed Neutron Interrogation Test Assembly (PUNITA) at the JRC-ITU (Ispra) [13].

3. Experimental and simulation studies

Monte Carlo simulation programs, such as PHITS [14] and MVP [15], which have been developed by JAEA, was utilized to develop DDA, NRTA, PGA/NRCA and DGA methods, and to construct and evaluate the prototype system which is combined with DDA and PGA. In addition to the simulation programs, the resonance analysis program REFIT [16] is used in the development of NRTA and NRCA. Experimental measurements have been conducted at the JRC Geel site Linear Accelerator (GELINA) and the PUNITA facility at the JRC Ispra site. In the developments of DDA, 1) the effects of the fast and thermal neutron uniformity in the sample cavity were evaluated, 2) the selections of neutron reflector material and the optimization of thickness of the neutron moderator and neutron shields, etc. were investigated, 3) quantitative determination of matrix effects was conducted. In the developments of PGA, 1) the neutron and γ-ray shields, the γ-ray collimators and the layout of γ-rays detector system were optimized, 2) the quantitative and qualitative estimation of explosive (nitrogen) was performed, 3) the setup was reconfigured to accommodate a high count-rate detector: $LaBr_3$(Ce) scintillation detector and a high energy resolution detector: HPGe detector. In the developments of DGA, 1) the detector setup was optimized for the measurements of high energy γ rays, 2) nuclear data of high energy delayed γ rays emitted by the radioactive fission product were obtained and evaluated.

3.1 Progress on NRTA

The most promising method in terms of the low-background measurements for high radioactive nuclear materials would be the NRTA method because the detector of NRTA can be located farther away from the high radioactive samples. NRTA is a well-established method to obtain accurate nuclear data, such as the total neutron cross section, the resonance parameters, and plays a key role in NRD which was developed in the collaboration Action Sheet-1. As already described above, NRTA allows us to accurately quantify the amount of SNM and MA. The current NRTA system requires a large accelerator to produce the intense pulsed neutron beam. Therefore, the aim of the project is to develop a compact system for NRTA with a DT tube. We have conducted a simulation for a prototype NRTA system, which is shown in Figure 2 [17].

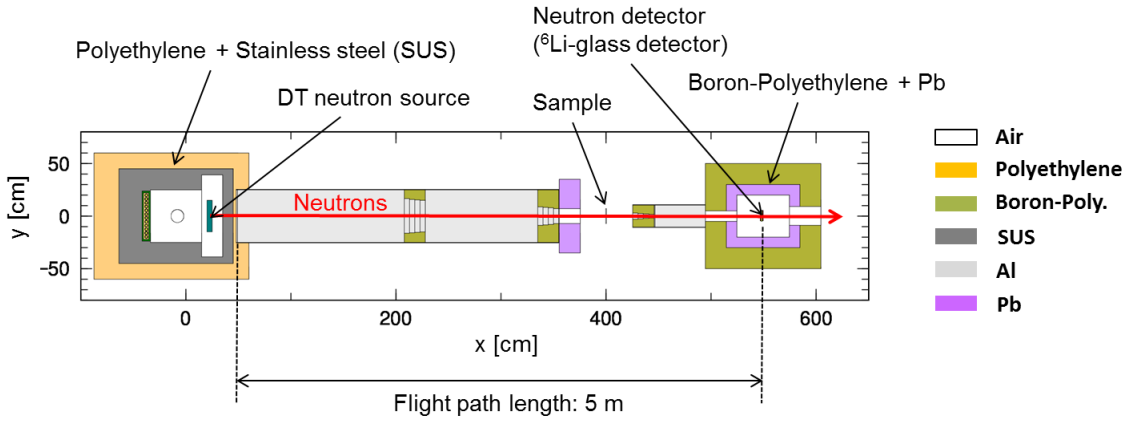

Figure 2. Schematic view of a compact NRTA system.

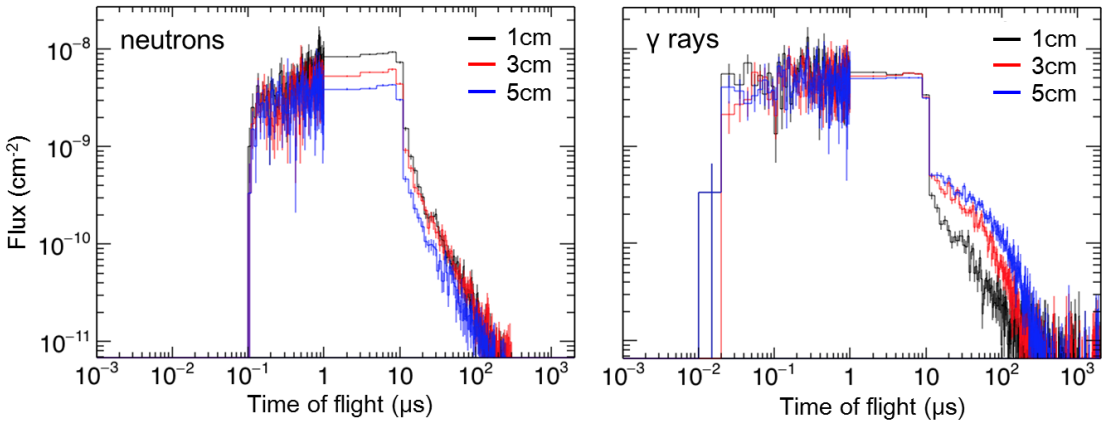

Figure 3. The fluxes of neutrons and γ rays at the detector position are calculated with MCNP. The black, red and blue lines show the results with 1cm, 3cm and 5cm thick moderators, respectively.

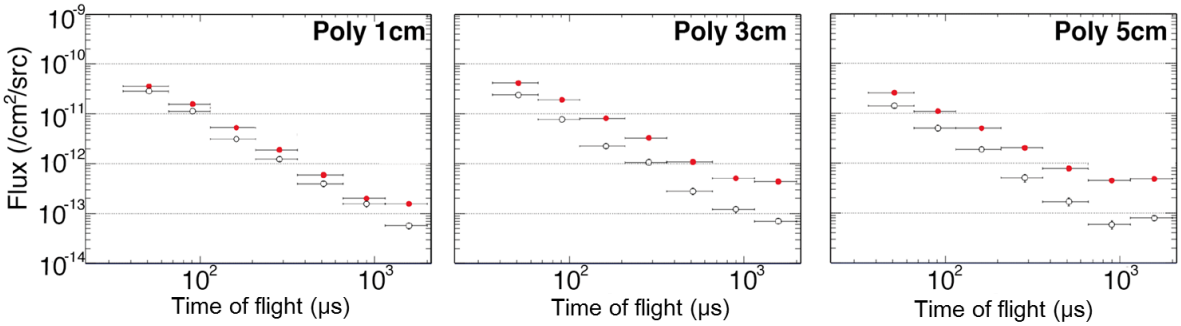

Figure 4. The fluxes of direct (red) and scattered (white) neutrons at the detector position.

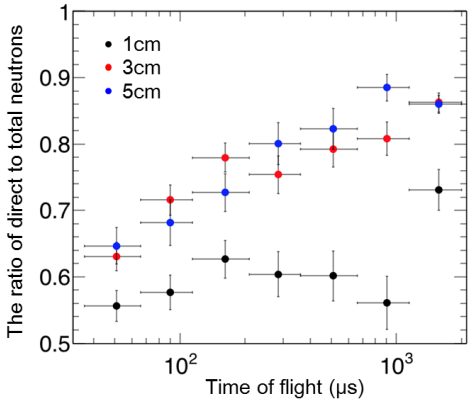

Figure 5. The ratio of direct to total (direct+scattered) neutrons at the detector position.

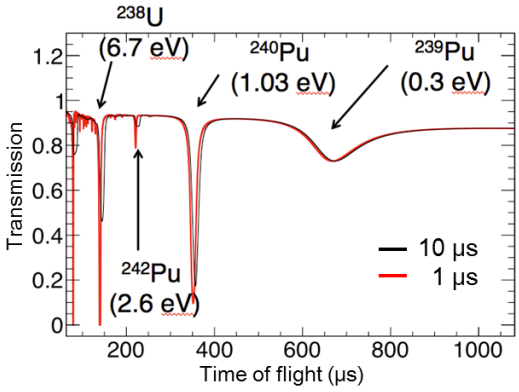

Figure 6. The NRTA spectra of spent fuel by 1μs and 10μs pulse width neutron beams.

In the prototype system, a polyethylene and a stainless steel are used as a neutron moderator and a reflector, respectively. We optimized the thickness of the neutron moderator between the DT neutron generator and the flight path tube with MCNP simulation [17,18]. The fluxes of neutrons and γ rays at the detector position are calculated (See Fig. 3). Since the pulse width of DT neutron generator is 10 μs, we have to utilize a time of flight of over 10 μs in NRTA measurements. Considering that the γ rays are one of the main sources of background interference, the moderator thickness of 1cm and 3cm can be accepted as candidates. The main issue in this study is to achieve a good ratio of direct to scattered neutrons because a compact NRTA system that has a short flight path is rather hard to avoid the scattered neutrons. Here, a scattered neutron is defined as a neutron scattered by reflector and / or shield in the neutron source part, and a direct neutron goes directly into the moderator from

the DT neutron source. The scattered neutrons fly relatively long length compared to the direct neutrons. Therefore, the scattered neutrons will disturb the time-of-flight (NRTA) measurements. Figure 4 shows the fluxes of direct and scattered neutrons at the detector position for the flight times ranging from 36 to 2000 μs (corresponding to 0.03 to 100 eV). The highest fluxes of the direct and scattered neutrons can be obtained by the 3cm and 1cm polyethylene moderators, respectively. The ratios of direct to total (direct + scattered) neutrons are shown in Figure 5. The ratio of 3cm thickness has nearly the same value as that of 5cm. Therefore, the 3cm polyethylene moderator is considered as the leading candidate among the polyethylene moderators [17].

The establishment of a compact NRTA system that can accurately quantify SNMs in spent fuel is the major goal of the project. We performed a simulation study for a spent fuel measurement with a compact NRTA system that utilizes a neutron source (1μs, 10μs pulse widths, $5x10^8$ n/s) and has a flight path length of 5m. Figure 6 shows the NRTA spectra of the spent fuel sample which has a diameter of 10cm and a thickness of 1cm. We assumed that the measurement time was 800s. The resonance dips of ^{238}U, ^{239}Pu, ^{240}Pu and ^{242}Pu were observed in both spectra. The difference in the pulse width has negligible effects on the dips of ^{240}Pu (1.03eV) and ^{239}Pu (0.3eV), which exist in low energy region. Although the dips in high energy region, especially ^{242}Pu, are significantly affected, we can obtain reliable results from these dips [17].

3.2 Prototype system (DDA and PGA)

A prototype system for measurements in a MA-Pu fuel conversion facility was developed and installed at NUCEF in the JAEA Tokai-site. Figure 7 shows a photograph of the prototype system: Active-N (mark II) and the transparent view. Active-N consists of two individual measurement systems which are DDA and PGA. A D-T pulsed neutron source as the interrogation source was installed in the sample cavity. The neutron generator can produce a 14 MeV neutron flux of 1.0×10^9 n/sec. The pulse width and the repetition rate are usually set to 10 μs and 100 Hz, respectively. The cross-cut views of Active-N are shown in Figure 8. The neutron generator is placed near the side wall of neutron reflector. The detector bank is mounted at the opposite side wall. As mentioned above, JAEA-DDA utilizes fast and epi-thermal neutrons for interrogation. Therefore, the inside walls are covered with

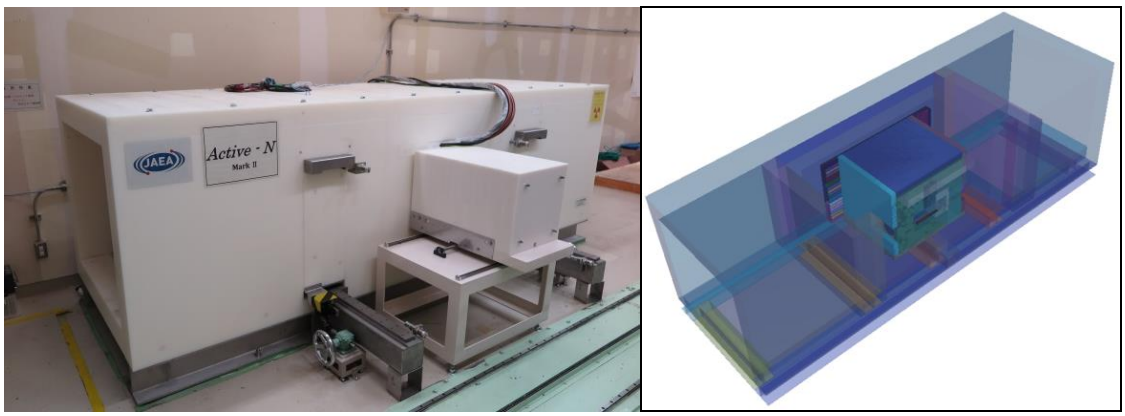

Figure 7. The photograph of the prototype system: Active-N (mark II) and the transparent view.

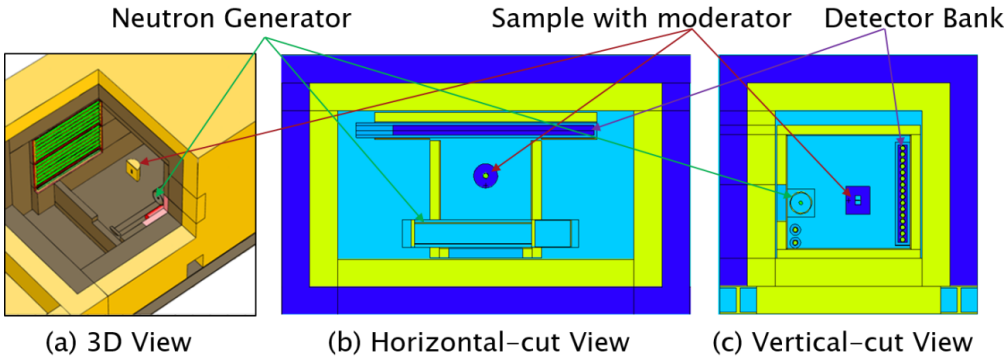

Figure 8. The cross-cut views of the prototype system: Active-N (mark II).

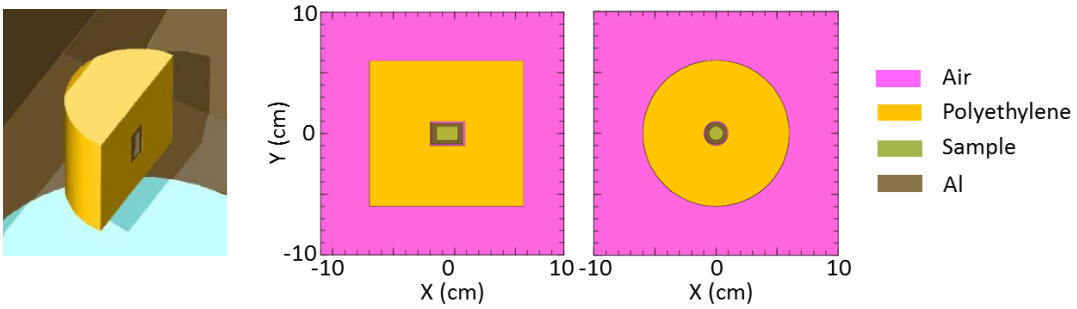

Figure 9. The neutron moderator which surrounds the sample is utilized for small samples.

boron rubber to supress the thermal neutron in the cavity. The interrogation with fast neutrons has a significant advantage for the measurement of large samples, such as 200L waste drums because of good spatial uniformity in detection sensitivity [8]. However, the JAEA-DDA method is not appropriate for small samples because fast neutrons are difficult to be thermalized in such small samples. Therefore, the moderator, which surrounds the sample (see Fig.9), is used to slow down the neutrons to around thermal energy(0.025eV), and can drastically improve detection limit of JAEA-DDA measurements for small samples. The Monte Carlo calculations were conducted to find the optimum thicknesses of the moderator for a vial bottle (ϕ26 x 40mm). Figure 10 shows three simulated DDA spectra of Pu (0.1-15g) for three different values of the moderator thickness a) 3cm, b) 6cm, c) 10cm. The corresponding measuring time is 600 seconds. As the moderator thickness increases, the die-away (decay) time also increases because the die-away time mainly reflects a neutron mean lifetime in the moderator (and sample). The results of simulations (Fig.10b)) show that in the most ideal case, the prototype system will be capable of detecting 0.1g of Pu. The relationship between the number of detected fission neutron counts and ^{239}Pu mass for different moderator thicknesses is shown in figure 11. The simulation results indicate that there is an optimal value (around 5-7cm) for the thickness of the moderator.

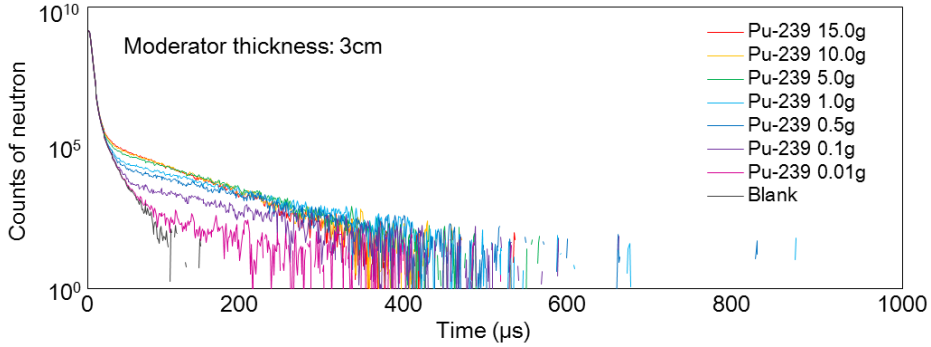

Figure 10a. The simulated DDA spectra of Pu (0.1-15g) with moderator thickness of 3cm.

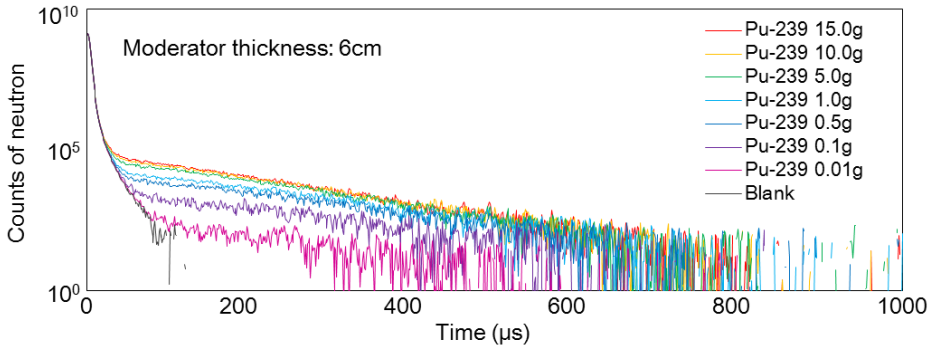

Figure 10b. The simulated DDA spectra of Pu (0.1-15g) with moderator thickness of 6cm.

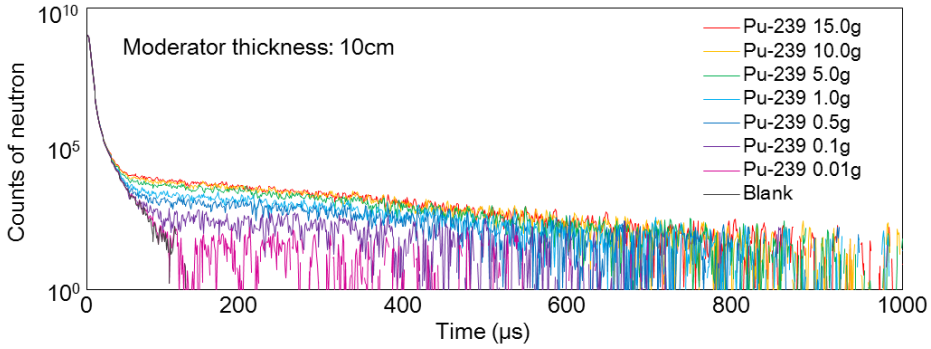

Figure 10c. The simulated DDA spectra of Pu (0.1-15g) with moderator thickness of 10cm.

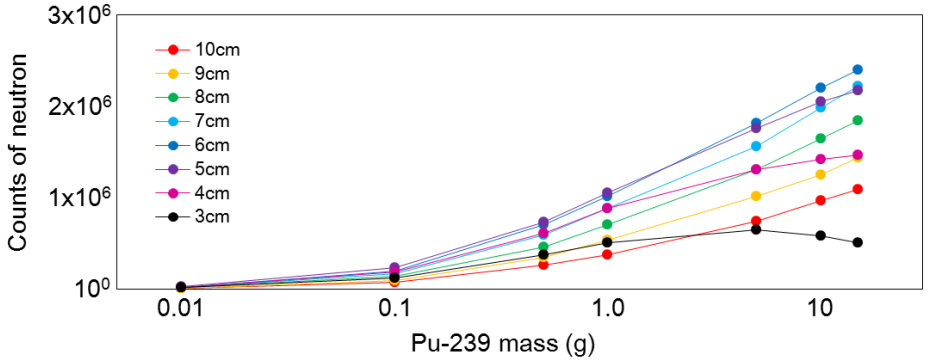

Figure 11. The relationship between the number of detected fission neutron counts and ^{239}Pu mass for different moderator thicknesses.

A dirty bomb is an explosive radiation dispersal device that combines explosives, such as dynamite, with radioactive materials. Most dirty bombs are very hard to release enough radiation materials to kill people with radioactivity. However, it could produce mass panic, and require time consuming and expensive cleanup operations. Detecting explosives can be very dangerous due to the hazard of explosion and toxic materials. Therefore, the developments of non-destructive inspection methods are important for the detection of explosives. Most of explosives are organic compounds or mixtures consisting of hydrogen, carbon, nitrogen, and oxygen, especially containing a relatively high percentage (by weight) of nitrogen. The ratios of nitrogen to carbon and oxygen are also used as the indicators. PGA is considered a useful tool in a non-destructive inspection process of explosives as described above because PGA can detect these light elements, which are used as the indicators. We conduct simulation experiments to verify the effectiveness of PGA in our prototype system for the detection of nitrogen. In this simulation, we used a slightly different system configuration, which is called as Active-N (Mark I). In Figure 12, we show the spectrum of the nitrogen obtained from the simulations using MCNP [18]. The excited ^{15}N nucleus, formed in ^{14}N(n, γ)^{15}N reaction, emits a number of γ rays (1678, 1885, 3678, 5269, 5533 and 10829 keV etc.). The 10.8 MeV γ ray peak of nitrogen was clearly observed in the spectrum.

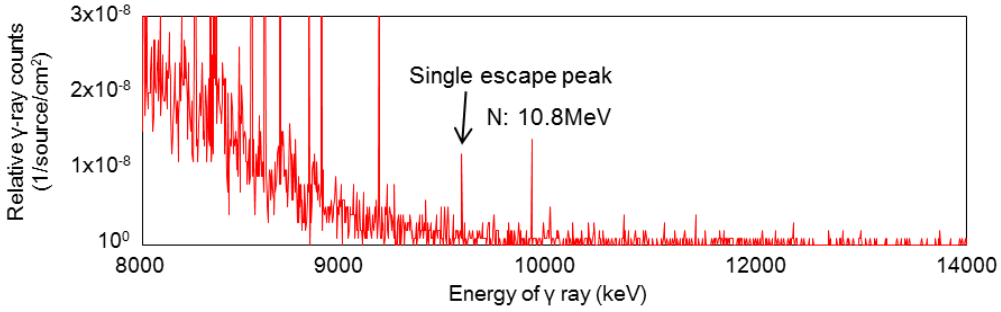

Figure 12. The energy spectrum of the prompt γ rays emitted in the ^{14}N(n, γ)^{15}N reaction.

4. Summary

JRC – JAEA collaboration AS-7 started to develop an active neutron NDA system for nuclear non-proliferation and nuclear security. The collaboration aims at contributing to the establishment of an innovative non-destructive analysis (NDA) system for the quantification of SNM and MA in high radioactive nuclear materials, such as spent fuel, MA transmutation fuel, fuel debris etc. Several active neutron NDA techniques, namely DDA, PGA/NRCA, NRTA and DGA have been developed. We have conducted a simulation for a compact NRTA system. It seems reasonable to conclude that the compact NRTA system can quantify the amounts of ^{238}U, ^{239}Pu, ^{240}Pu and ^{242}Pu in spent fuel. The combined NDA system, which enables the simultaneous measurements of DDA and PGA, has been developed at NUCEF in the JAEA Tokai-site. The Monte Carlo calculations were conducted to find the optimum thicknesses of the moderator and showed that in the most ideal case, the prototype system would be capable of detecting 0.1g of Pu. The 10.8 MeV γ ray peak of nitrogen was clearly observed in the PGA spectrum obtained from the simulation. Thus, PGA with the combined NDA system will be able to detect explosive materials. In the near future, we will have DDA and PGA experiments with the combined NDA system at NUCEF in JAEA.

5. Acknowledgements

We would like to acknowledge the Japanese government (MEXT; Ministry of Education, Culture, Sports & Technology).

6. References

[1] Heinberg C et al.; *The Status of the Japanese Project on Material Accountancy of Fuel Debris and U.S.-Japan Cooperation on Survey of Technologies for Nuclear Material Accountancy at Fukushima Daiichi Nuclear Power Plant*; Proceedings of INMM 55th Annual Meeting; Atlanta, Georgia, USA; 20-24 July 2014.

[2] Nagatani T et al.; *Recommendations for Measurement Systems for Nuclear Material Accountancy of Fukushima Daiichi Fuel Debris: Neutron Technologies*; Proceedings of INMM 55th Annual Meeting; Atlanta, Georgia, USA; 20-24 July 2014.

[3] Tomikawa H et al.; *Recommendations for Measurement Systems for Nuclear Material Accountancy of Fukushima Daiichi Fuel Debris: Gamma Technologies*; Proceedings of INMM 55th Annual Meeting; Atlanta, Georgia, USA; 20-24 July 2014.

[4] The Hague Nuclear Security Summit Communique; http://www.nss2016.org/past-summits/2014/; 2014.

[5] Harada H et al.; *Proposal of neutron resonance densitometry for particle like debris of melted fuel using NRTA and NRCA*; Proceedings of the 35th ESARDA symposium on Safeguards and Nuclear Non-Proliferation; Bruges, Belgium; 28-30 May 2013.

[6] Schillebeeckx P et al.; *Development of neutron resonance densitometry at the GELINA TOF Facility*; ESARDA Bulletin 50; 2013; p9 – 17.

[7] Schillebeeckx P et al.; *Neutron resonance Spectroscopy for the characterisation of materials and objects*. JRC Science and Policy Reports. European Commission,
Joint Research Centre Institute for Reference Materials and Methods, Report EUR 26848-EN; 2014.

[8] Kureta M et al.; *JAEA − JRC Collaboration on the Development of Active Neutron NDA Techniques*, Proceedings of 37th ESARDA Symposium on Safeguards and Nuclear Non-Proliferation, Manchester, UK; 2015; p111-120

[9] Postma H and Schillebeeckx P; *Neutron Resonance Capture and Transmission Analysis*; Encyclopedia of Analytical Chemistry (John Wiley & Sons Ltd); 2009; p1-22.

[10] Schillebeeckx P et al.; *Neutron Resonance Spectroscopy for the Characterisation of Materials and Object*, Report EUR 26848 EN.

[11] Rossbach M; *Multielement prompt gamma cold neutron activation analysis of organic matter*; Anal. Chem.; 63; 1991; p2156−2162.

[12] Ember P et al.; *Improvement of the capabilities of PGAA by coincidence techniques*; Appl. Radiat. Isot.; 56; 2002; p535−541.

[13] Koizumi M et al.; *Development of a $LaBr_3$ scintillation detector system for neutron resonance densitometry (NRD)*; Proceedings of INMM 55th Annual Meeting; Atlanta, Georgia, USA; 20-24 July 2014.

[14] Sato T et al.; *Particle and Heavy Ion Transport code System, PHITS, version 2.52*; Journal of Nuclear Science and Technology; 50[9]; 2013; p 913-923.

[15] Nagaya Y et al.; *MVP/GMVP II: General Purpose Monte Carlo Codes for Neutron and Photon Transport Calculations based on Continues Energy and Multigroup Methods*; JAERI 1348; 2005.

[16] Moxon M and Brisland J; *GEEL REFIT, A least squares fitting program for resonance analysis of neutron transmission and capture data computer code*; AEA-InTec-0630; AEA Technology; October 1991.

[17] Tsuchiya H et al.; *Development of active neutron NDA techniques for nonproliferation and nuclear security (2) Study on a compact NRTA system*, Proceedings of INMM 57th Annual Meeting; Marriott Marquis, Atlanta, GA, USA; 24-28 July 2016.

[18] T. Goorley, et al.; *Initial MCNP6 Release Overview*; Nuclear Technology; 180; 2012; p298-315.

Comparison between simulation and experimental results for neutron flux in DDA systems

Makoto Maeda[1], Masao Komeda[1], Akira Ohzu[1], Masatoshi Kureta[1], Yosuke Toh[1], Tatjana Bogucarska[2], Jean M. Crochemore[2], Giovanni Varasano[2], Bent Pedersen[2]

1 Japan Atomic Energy Agency
Tokai-mura, Naka-gun, Ibaraki 319-1195, Japan
E-mail: maeda.makoto@jaea.go.jp
2 Joint Research Centre Ispra
Via E. Fermi, 2749, 1-21027 Ispra (VA), Italy

Abstract:

JAEA and EC/JRC have been carrying out collaborative research for developing new non-destructive assay techniques that can be utilized for quantifying high radioactive special nuclear materials such as spent fuel and next generation minor actinide fuels. In the research, accuracy of Monte Carlo simulation is important since it is utilized for design and development of a demonstration system of next-generation Differential Die-Away (DDA) technique in JAEA. In order to evaluate the accuracy, neutron fluxes in the sample cavity of the PUNITA device which utilizes JRC type DDA technique and the JAWAS-T device which utilizes JAEA type DDA technique were measured. The neutron flux in the target sample placed in the PUNITA sample cavity was also measured. The measurement results were compared with the simulation results. In this presentation, we report on comparison results for the neutron flux obtained by experiment and simulation.

Keywords: Monte Carlo simulation; Differential die-away; Neutron flux

1. Introduction

Japan Atomic Energy Agency (JAEA) and European Commission Joint Research Centre (EC/JRC) have conducted collaborative research to develop a technique that can be utilized for quantification of high radioactive special nuclear materials such as next generation minor actinide fuels. In the collaborative research, JAEA has been developing the integrated system Active-N which consists of some active neutron techniques. In the study of a Differential Die-Away (DDA) technique[1], which is one of the techniques to be involved in the Active-N, JRC type and JAEA type[2-5] DDA techniques are compared to develop a next generation DDA. The DDA technique is one of the active neutron NDA techniques. The DDA technique interrogates an object of interest with neutrons to induce fission reactions and estimates amounts of nuclear materials by measuring the induced fission neutrons. The JRC type DDA technique utilizes thermal neutrons, which are moderated in the measurement system especially a graphite liner, as the interrogation neutrons. If a matrix of the sample has strong moderation and/or absorption effect on neutrons, the interrogation neutrons are absorbed by the matrix and also fission neutron is moderated and absorbed by the matrix. Thus, for such samples, the JRC type DDA technique has a large difference in the detection efficiency between internal and external parts. On the other hand, the JAEA type DDA technique utilizes fast neutrons as the interrogation neutrons and thermalize the interrogation neutrons by a matrix of the sample to induce the fission. In the central part of the sample, thermal neutron flux is higher and detection efficiency for the fission neutron is lower and thus position dependence of the detection efficiency for the fissile material is improved. However, additional moderator is required in the measurement of small sample.

An accuracy of a Monte Carlo simulation is important since performance of the system is estimated and optimized by using the Monte Carlo simulation, in design of the Active-N. Thus, measured and

simulated neutron flux distributions were compared to evaluate the accuracy of the simulation. We obtained the neutron flux distributions in the sample cavities of the Pulsed Neutron Interrogation Test Assembly (PUNITA) [6,7] which is a demonstration system of the JRC type DDA technique and the JAEA Active Waste Assay System – Tokai (JAWAS-T) which is a demonstration system of the JAEA type DDA technique by measurement and simulation. Furthermore, in the PUNITA, the neutron flux in the standard sample placed in the sample cavity was also obtained.

2. Experimental apparatuses

2.1. PUNITA

Figure 1 shows the PUNITA which is a demonstration system of the JRC type DDA technique. The PUNITA is designed for experimental studies in NDA methods for nuclear safeguards and security. A D-T neutron generator and a He-3 counter for thermal flux monitor are placed in a central sample cavity. The dimensions of the cavity are 50×50×80 cm^3. The cavity is surrounded by a graphite liner with a thickness of 20.5 cm. The graphite liner is surrounded by a polyethylene layer for radiation shielding. Fission neutron counter modules are located in each of six sides behind the graphite liner. In the each module, 16 He-3 counters of 3040 torr and 100 cm length are embedded in polyethylene covered with cadmium which is thermal neutron absorber. On each of the vertical four sides, eight He-3 counters of 3040 torr and 50 cm length, nominated source monitors, are embedded in the polyethylene shield behind the fission neutron counter modules. In the measurement, 14 MeV neutrons are emitted by the D-T neutron generator and a large number of thermal neutrons are generated by moderation in the graphite liner. The thermal neutrons induce fission in a sample and the total amount of fissile materials in the sample is estimated by measuring the fission neutrons by the fission neutron counter modules. The PUNITA has achieved very low detection limit by using high thermal neutron flux and high neutron detection efficiency with 96 He-3 counters.

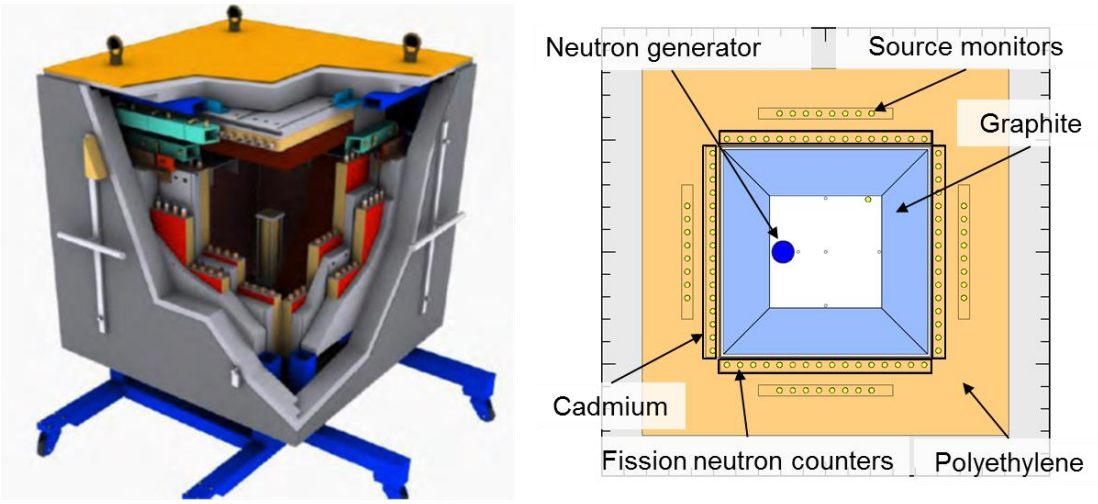

Figure 1: PUNITA system. Left side figure shows cutaway drawing of the system. Right side figure shows horizontal cross sectional view of the system.

2.2. JAWAS-T

Figure 2 shows the JAWAS-T which is a demonstration system of the JAEA type DDA technique. The JAWAS-T has been developed for measuring fissile materials in 200 L nuclear waste drums. The JAWAS-T has a central sample cavity with a size of 90×90×105 cm^3. A D-T neuron generator, a He-3 counter for thermal neutron flux monitor and three fast neutron detector modules are placed in the sample cavity. There are two types of the modules. One has 14 He-3 counters and the other has 8 He-3 counters. In the both modules, He-3 counters of 3040 torr and 100 cm length are embedded in polyethylene layer covered with a cadmium sheet. The sample cavity is covered with a 2 mm thick cadmium liner to prevent inflow of thermal neutrons generated outside of the cavity. The cadmium liner

is surrounded by a 30 cm thick graphite layer, a 10 cm thick polyethylene layer, and a 10 cm thick borated polyethylene layer in order from the inside to outside for radiation shielding. In the measurement, the drum placed on the stage is moved to the centre of the sample cavity as shown in Figure 2 and irradiated by 14 MeV fast neutrons from the D-T neutron generator. The fast neutrons moderated to thermal neutrons by matrix of the drum and the thermal neutrons induces the fission. During the measurement the drum is rotated to make the neutron flux uniform.

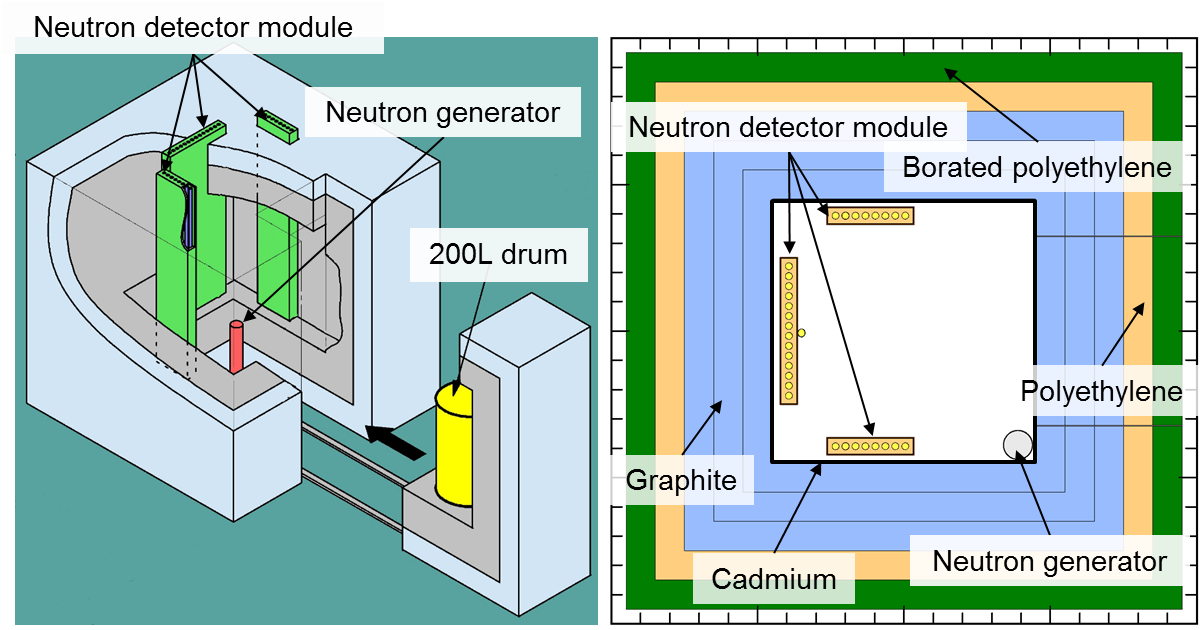

Figure 2: JAWAS-T system. Left side figure shows schematic drawing of the system. Right side figure shows horizontal cross sectional view of the system.

2.3. Standard sample

Figure 3 shows a standard sample fabricated for measurement of the neutron flux in the matrix. The sample has a cylindrical shape with a diameter of 120 mm and a height of 127 mm. The sample has 5 holes for the small He-3 detector to measure the neutron flux. Each hole is assigned alphabet and the sample is irradiated by D-T neutrons from A and B side as shown in Figure 3 (c). The sample can be separated into two parts at the centre and a Pu source can be set to measure the neutron flux with and without the Pu source as shown in Figure 3 (a) and (b). Three samples were made of different materials which have different cross sections for neutron: polyethylene which has a large scattering cross section, stainless steel which has a relatively high absorption cross section, and lead which has a small total cross section. The samples were tested only in the PUNITA.

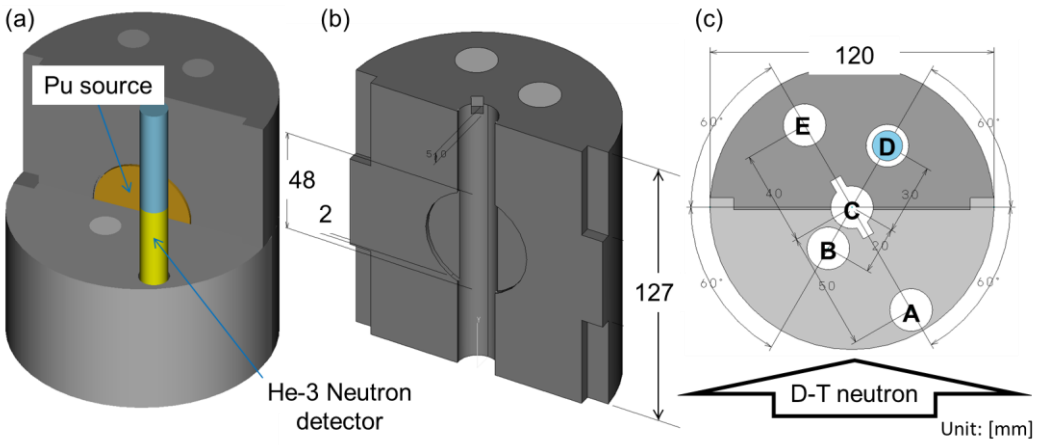

Figure 3: Standard sample for measurement of neutron flux in the matrix. (a) and (b) are schematic drawing of the sample. (c) shows an arrangement of measurement position and direction of D-T neutron.

3. Comparison between experimental and simulation results

3.1. Neutron flux distributions in the sample cavities of the JAWAS-T and the PUNITA

The experimental and simulation results for neutron flux distributions in the sample cavity were compared in the PUNITA and the JAWAS-T. In the PUNITA, the neutron flux is measured by small He-3 counter in each position shown in Figure 4 (a). A position A is the nearest to the D-T neutron generator and a position B is the centre of the cavity. The others are defined by moving the detector to five sides from the centre except the position A. The small He-3 counter with gas pressure of 760 torr, diameter of 1.27 cm, and length of 7.62 cm was used. The neutron flux is defined by an integral from 0.6 ms to 2.0 ms of the neutron counts of the small He-3 counter since the neutron counts of this time region are dominated by thermal neutron counts, or interrogation neutron counts in the PUNITA. Then, a relative neutron flux distribution is evaluated by normalizing the neutron flux of each position by that of the position A. In the JAWAS-T, a small He-3 counter with gas pressure of 190 torr, diameter of 2.5 cm, and length of 12.5 cm was used. Measurement positions are shown in Figure. 4 (b). As is the case in the PUNITA, a position A is the nearest to the D-T neutron generator and a position B is the centre of the cavity. The others are defined by moving the detector to six sides. Total neutron counts were defined as the neutron flux, since it is hard to distinguish the interrogation neutrons in the JAEA type DDA. In the simulation, both systems are modelled and the He-3 counter is set in each positon. A neutron capture reaction in the He-3 counter is simulated by a Monte Carlo simulation code PHITS ver.2.82[8] with JENDL 4.0[9].

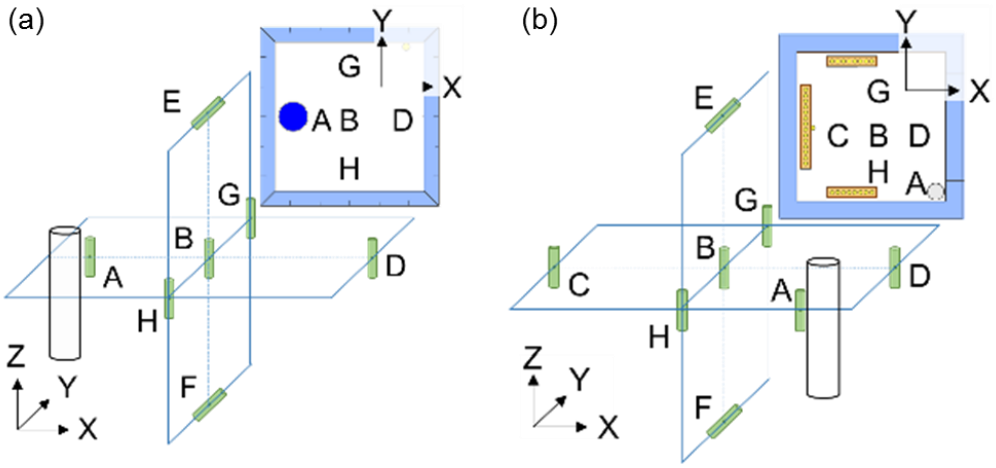

Figure 4: Schematic view of the measurement positions in both systems.

Figure 5 shows the positon dependence of a C/E value which is defined as a ratio of the results obtained by the simulation and the experiment in each system. The C/E value is 1.00 in the position A since the flux of this position is used for normalization. The C/E was less than 1.00 in every position except the position A in both systems. The largest discrepancies between the experiment and the simulation results are observed in the position D with the C/E value of 0.84 in the PUNITA and the position H with the C/E value of 0.87 in the JAWAS-T.

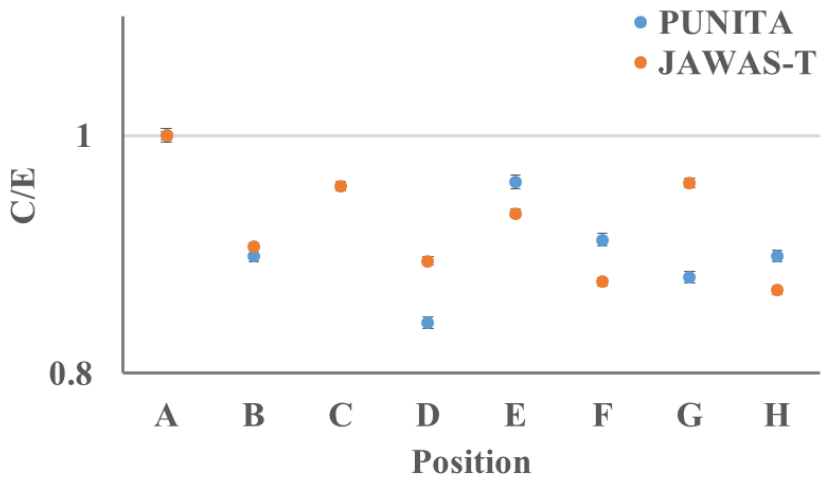

Figure 5: A positon dependence of a C/E value for neutron flux in both systems.

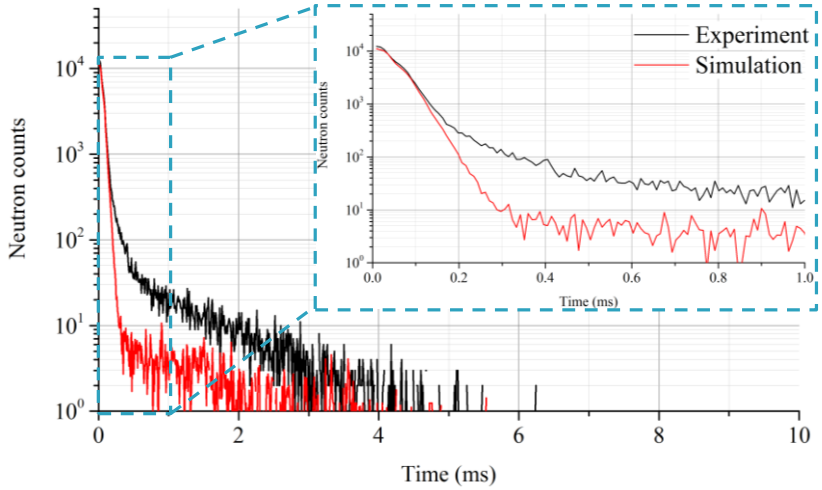

Figure 6: Comparison between measured and simulated time distributions of neutron counts in the position B in the JAWAS-T.

In the JAWAS-T, to investigate the reason for the discrepancies, time distributions of neutron counts in the position B were obtained as shown in Figure 6. Since the simulation results are obtained in the unit of 1/source, the results are normalized by source neutron intensity of 3.0×10^{10} evaluated by the activation method using an aluminium sample. In Figure 6, the discrepancy is observed after 0.1 ms. Since the neutron flux in this time region is dominated by thermal neutrons in the JAWAS-T, the thermal neutron flux distribution was simulated by PHITS as shown in Figure 7. Each panel shows the neutron flux in each time intervals of those between 0.1 and 0.2 ms, 0.2 and 0.5 ms, 0.5 and 1.0 ms, 1.0 and 2.0 ms, 2.0 and 5.0 ms, and 5.0 and 10 ms. Two lines in the right side of each panel in Figure 7 are gaps in the cadmium liner for the moving part of the stage for the drum. As shown in Figure 7, the thermal neutron flux in the sample cavity after 0.1 ms is dominated by inflow of the thermal neutrons generated by moderation in the graphite layer. The reason of the large discrepancies is that the size and the position of the gaps are not incorporated accurately in the model of the simulation.

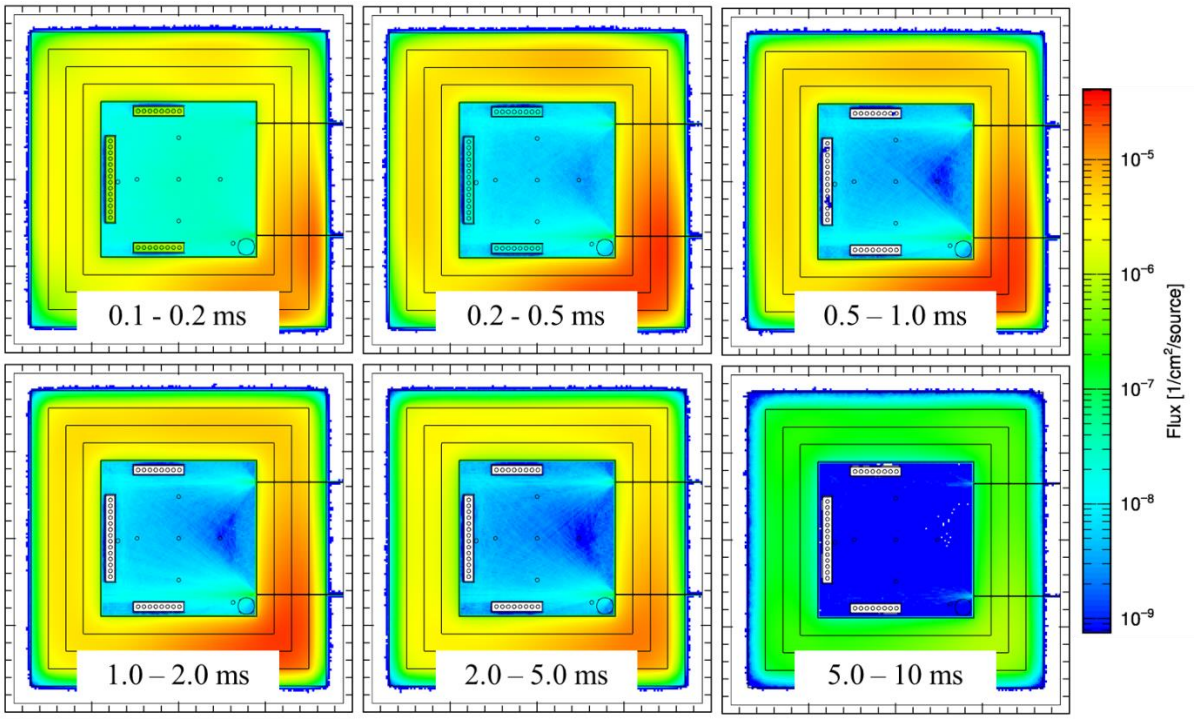

Figure 7: Time variation of the thermal neutron flux in the JAWAS-T.

3.2. Neutron flux distributions in the standard sample placed in the PUNITA

The experimental and simulation results for neutron flux distributions in the standard samples are compared in the PUNITA. Neutron flux is measured by using the same He-3 detector as described in section 3.1 at each position shown in Figure 3 with and without Pu source. As is the case in section 3.1, the neutron flux is defined by an integral from 0.6 ms to 2.0 ms of the neutron counts of the small He-3 counter. Then, a relative neutron flux is evaluated by normalizing the neutron counts of each measurement by those of the measurement without standard matrix. The neutron counts of He-3 detector are simulated by PHITS ver.2.82 with JENDL 4.0 and compared with experimental results. Comparison results represented in the C/E are shown in Figure 8 (a), (b), and (c) for polyethylene, stainless steel, and lead, respectively. In Figure 8 (d), plots represent average value and bars represent maximum and minimum values of the C/E for each sample. The simulation underestimates the neutron fluxes in the polyethylene and the lead samples especially in a farther position from the neutron generator. Because of a longer neutron path in the standard sample at the farther position, effect of the thermal neutron scattering is considered to be the cause of the underestimation. Since there are no S(α,β) data for lead and poor data for polyethylene, an accuracy of the simulation can be improved with more accurate S(α,β) data.

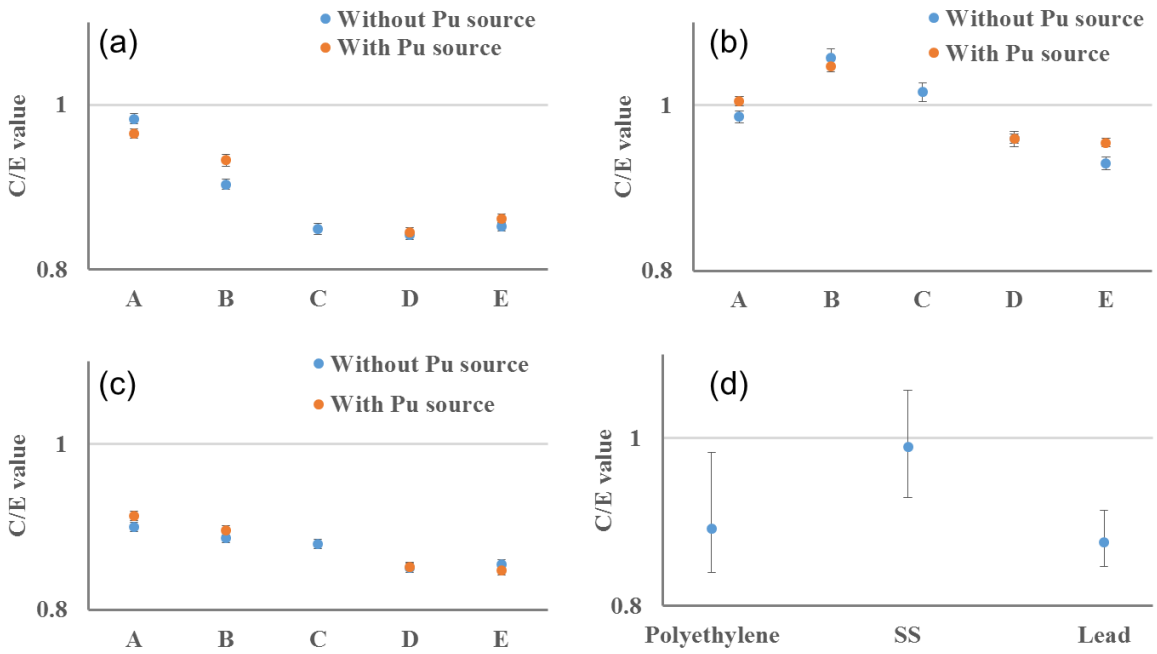

Figure 8: Position and material dependence of the C/E values for the neutron flux in the standard samples. (a), (b), and (c) show the results with a matrix of polyethylene, stainless steel, and lead, respectively. (d) shows the averaged C/Es for each material.

4. Summary

In this research, we have measured and simulated the neutron flux distributions in the sample cavity of the PUNITA and the JAWAS-T and the neutron flux distributions in the standard samples placed in the PUNITA and compared measurement and simulation results. For the neutron flux distribution in the sample cavity, the simulation underestimates the neutron flux. There are rooms for improvement in the both models for the simulation, and thus an accuracy of the simulation can be improved. For the neutron flux distribution in the standard sample, the simulation underestimate the neutron flux in the polyethylene and the lead samples. The underestimation seems to be due to low accuracy of S(α,β) data for thermal neutron scattering law.

In the design of the Active-N which is the demonstration system of the next generation DDA technique, to improve the accuracy of simulation, the gap of the moving part is covered with thermal neutron absorber to prevent the inflow of thermal neutrons.

5. Acknowledgements

This work was done under the agreement between JAEA and EURATOM in the field of nuclear materials safeguards research and development. This work is supported by JSGO/MEXT.

6. References

[1] W. E. Kunz, J. D. Atencio, J. T. Caldwell, ‘‘A 1-nCi/g Sensitivity transuranic waste assay system using pulsed neutron interrogation’’, LA-UR-80-1794, Los Alamos Scientific Laboratory (1980).
[2] M. Haruyama, A. Ara, M. Takase, “High-sensitivity detection of fissile materials in a waste drum by direct interrogation of 14 MeV Acc neutrons” Transactions of the Atomic Energy Society of Japan, 43(4], 397-404 (2001) [in Japanese].
[3] M. Haruyama, M. Takase, H. Tobita, T. Mori, “High-sensitivity detection by direct interrogation of 14 MeV Acc neutrons, (I) Uranium-contained metal matrix in a waste drum” Transactions of the Atomic Energy Society of Japan, 3(2], 185-192 (2004) [in Japanese].

[4] M. Haruyama, H. Tobita, M. Takase, T. Mori, “High-sensitivity detection by direct interrogation of 14 MeV Acc neutrons, (II) Uranium-contained cloth matrix in a waste drum” Transactions of the Atomic Energy Society of Japan, 6(1), 65-72 (2007) [in Japanese].
[5] M. Haruyama, M. Takase, H. Tobita, “Improvement of Detection Limit in 14 MeV Neutron Direct I nterrogation Method by Decreasing Background”, J. Nucl. Sci. Technol., 45(5), 432-440 (2008).
[6] A. Favalli, B. Pedersen, “Design and characterization of a pulsed neutron interrogation facility” Rad. Prot. Dos., 126(1-4), 74-77 (2007).
[7] A. Favalli, H.-C. Mehner, J.-M. Crochemore, B. Pedersen, “Pulsed neutron facility for research in illicit trafficking and nuclear safeguards” IEEE Trans. Nucl. Sci., 56(3) 1292-1296 (2009).
[8] T. Sato, K. Niita, N. Matsuda, S. Hashimoto, Y. Iwamoto, S. Noda, T. Ogawa, H. Iwase, H. Nakashima, T. Fukahori, K. Okumura, T. Kai, S. Chiba, T. Furuta and L. Sihver, Particle and Heavy Ion Transport Code System PHITS, Version 2.52, J. Nucl. Sci. Technol. 50(9), 913-923 (2013).
[9] K. Shibata, O. Iwamoto, T. Nakagawa, N. Iwamoto, A. Ichihara, S. Kunieda, S. Chiba, K. Furutaka, N. Otuka, T. Ohsawa, T. Murata, H. Matsunobu, A. Zukeran, S. Kamada, and J. Katakura: "JENDL-4.0: A New Library for Nuclear Science and Engineering," J. Nucl. Sci. Technol. 48(1), 1-30 (2011).

Simulation study of neutron moderator in a delayed gamma-ray measurement system using a 14 MeV D-T neutron source

J. Takamine, F. Rossi, D.C. Rodriguez, M. Koizumi, M. Seya,

Integrated Support Center for Nuclear Security and Nuclear Nonproliferation
Japan Atomic Energy Agency, Tokai, Japan

Abstract:

Methods to determine the ratios of fissile nuclides (e.g U-235, Pu-239, and Pu-241) contained in nuclear materials (NM) are required for nuclear nonproliferation and security. At the Japan Atomic Energy Agency (JAEA), we are developing a delayed gamma-ray spectroscopy (DGS) system using a compact, pulsed neutron, deutrerium-tritium (D-T) generator. It is important to develop moderators suitable to decrease the 14-MeV energy of neutrons produced by the D-T generator into the thermal region for the purpose of increasing the possibility of fission reactions. The design of the neutron moderator system that consists of tungsten, graphite, and polyethylene is being developed using MCNP6. We present here the results our study of the time dependence and spatial and energy distributions of the neutron fluence in the system.

Keywords: Delayed gamma-ray; Nuclear nonproliferation and security; 14-MeV neutron; Neutron moderator; MCNP

1. Introduction

Measurement methods of nuclear materials (NM) such as purified NM (e.g. MOX fuel) and non-purified NM with high radioactivity (e.g. spent fuel, vitrified waste, melted fuel from reactor accidents, and next-generation fuel cycle materials) have been studied for the purpose of nuclear security and nonproliferation in the world. Especially, the spent and melted fuels irradiate very strong gamma rays and neutrons. Since it is quite difficult to distinguish gamma rays irradiated from fissile nuclides in these NM from intense passive gamma rays from fission products, current NDA methods are not effective to quantify the fissile nuclide.
In the Japan Atomic Energy Agency (JAEA), delayed gamma spectrometry (DGS) [1-3] using 14MeV D-T neutron generator (D-T generator) [4,5] is under development to remove this deficiency. The D-T generators have the advantages of being more compact and cost effective than the photo-neutron sources of large particle accelerators. The generators also have higher intensity and are also easier to handle than radioactive isotope (RI) sources such as Cf-252 and Am-Be. Since D-T neutrons are high energy (14 MeV), it is important to develop moderators suitable to decrease the energy of the neutrons into the thermal region for the purpose of increasing the possibility of fission reactions in the fissile nuclides of interest (e.g U-235, Pu-239, and Pu-241). If a moderator consisting of only low-Z materials is applied for the D-T generators, it is presumed that many of the fast- and high energy-neutrons are released from the moderator, because of the low elastic scattering cross-section at 14 MeV.
In the DGS technique, delayed gamma rays derived from the fission products produced from thermal fission is used to determine the ratio of fissile isotopes. The fission cross-section of U-238 is close to other isotopes above ~2 MeV, very different compared to the thermal region. Most NM of interest, such as spent fuel, contain high U-238 densities for which the fission reactions by fast neutrons are not negligible [3]. Additionally, decreasing fast- and high energy-neutrons contributes to prevent High pure germanium detector from being damaged. It is necessary to moderate as many 14-MeV neutrons as possible to the thermal region.
In previous research [3,4], we demonstrated that combinations of tungsten, graphite, and polyethylene were appropriate as the moderator materials for 14-MeV neutrons by analysing simple spherical and more realistic cylindrical models using MCNP6. Neutron multiplication reactions are occurring between

nuclei in tungsten, and reducing the kinetic energy of the 14-MeV neutrons to evaporation spectrum with the most probable energy from 1 to 2 MeV. These lower-energy neutrons can then be slowed down by polyethylene and reflected by graphite easily.
Effectiveness of the moderator model is confirmed by comparing energy spectrum of multiple MCNP6 models. For the purpose of understanding contribution each region in the model, spatial distributions of neutron flux respective energy regions were also visualized. Since the time distribution have information specific to materials such as ability of moderation, time distribution measurements of thermal neutron counts using He-3 detectors were also simulated using MCNP6.
We present here the results our study of the time dependence, spatial and energy distributions of the neutron fluence in the system.

2. Calculation model

As mentioned above, it is necessary to moderate as many 14-MeV neutrons as possible to the thermal region for improved fissile quantification. In this section, we demonstrate that combinations of tungsten, graphite, and polyethylene are appropriate as the moderator materials for 14-MeV neutrons by analysing simple spherical models and more realistic cylindrical models using MCNP6. In this research, more details of the realistic moderator system than previous research are analysed to understand how well each region of the system contribute to slowing down or reflection of neutrons and making plans of future experiments. X-Z and X-Y sectional views of the model are shown in Figure 1.

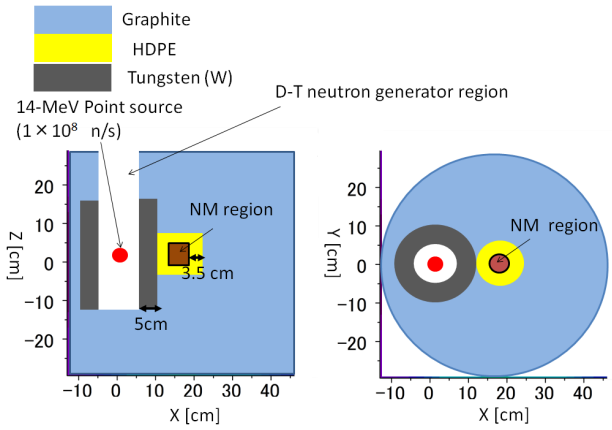

Figure 1. X-Z and X-Y sectional views of the realistic moderator model consisting of tungsten, HDPE and graphite. Each part has a cylindrical shape.

Each region is cylindrical shape. The hollow space in the cylindrical tungsten is where the D-T neutron generator would be positioned. The 14-MeV neutrons are emitted isotropically from the source position with neutron yield of 10^8 [n/s] based on a SODERN generator [5]. NM region is void, which is surrounded by high-density polyethylene (HDPE). We evaluate the quality of the moderation by comparing the neutron flux within the NM sample region. We call the modal WPC below.

3. Comparison of energy spectrums

To confirm the contribution of tungsten, HDPE, graphite in WPC, four moderators based on WPC but lacking one or two regions are considered. The four models are: W has only tungsten region, WP has only tungsten and HDPE regions, PC has only HDPE and Graphite regions, WC has tungsten and Graphite regions. Neutron energy fluxes in the NM region are compared in Figure 2. Integrated values below 0.5 eV (thermal), above 1MeV (fast) and (red line) the thermal/fast ratio are shown in Table1.

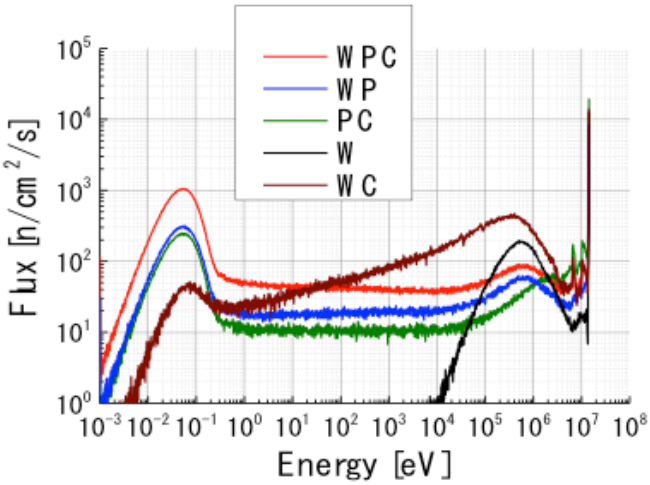

Figure 2. Neutron energy spectrums in the NM regions of WPC, WP and PC calculated by MCNP6

	< 0.5eV (Thermal) [n/cm^2/s]	> 1MeV (Fast) [n/cm^2/s]	Thermal/Fast
WPC	1.7×10^5	2.20×10^4	7.77
WP	4.96×10^4	1.76×10^4	2.86
PC	4.00×10^4	3.82×10^4	1.05
W	0	2.29×10^4	0
WC	9.04×10^3	3.62×10^4	0.25

Table 1. Integrated flux of WPC, WP, PC, WC, and W for neutrons with energies below 0.5 eV (thermal) and above 1MeV (fast) and the ratio between these values.

A large peak in the W spectrum is shown around 500keV. Neutron multiplication reactions seem to occur between nuclei in tungsten and reduce the kinetic energy of the 14-MeV neutrons.
Adding HDPE effectively reduces the energy as seen by comparing the W and WP spectra. Many of the neutrons with most probable energy of 500keV are moderated by HDPE well, since the peak intensity is decreased and continues energy neutrons are seen from thermal to fast region. There is a large peak below 0.5eV not only in WP spectrum but also others except for W. The difference between WPC and WP mean that intensity of total energy neutrons are increased by reflection effects of Graphite. Especially, thermal neutron flux of WPC is 3.43 times higher than that of WP as shown in Table 1. On the other hand, fast neutron flux of WPC is only 1.25 times higher than that of WP. The graphite region contributes to increase thermal / fast ratio. The difference between WPC and PC means that tungsten reduces over 2 MeV neutrons and increase below 1MeV neutrons. The thermal flux of WPC is over four times higher than that of PC, and fast neutron flux of WPC is 0.57 of PC as shown in Table 1. The difference between WPC and WC means that moderation power of graphite is not enough to slow down neutrons derived from multiplication reactions in tungsten. HDPE surrounding NM region moderates neutrons above 1MeV well and increases neutrons below 0.5eV well as shown in Table1. Since Thermal/Fast of WPC (7.77) is much more than others, we consider that each region in WPC contributes to increase Thermal/Fast well.
Physical dimensions of tungsten, HDPE and Graphite regions were decided by parametric surveys, the weight and effective cost. In this paper, these results are omitted for simplicity.

4. Spatial distributions

In section 3, it was shown that each region in WPC contributed to increase Thermal/Fast by compared WPC with some systems. In this section, neutron spatial distributions of three energy regions of WPC are observed, for the purpose of visual confirmation for effectiveness of the whole of WPC. The three regions are: above 10MeV (High energy), from 0.1 to 10 MeV (Fast), below 0.5eV (Thermal). X and Y direction of spatial meshes in the distributions are divided for every 10mm. Z direction is only one region from -25mm to 25 mm, centered on the source position. Spatial distributions with the three energy regions are shown in Figure 3.

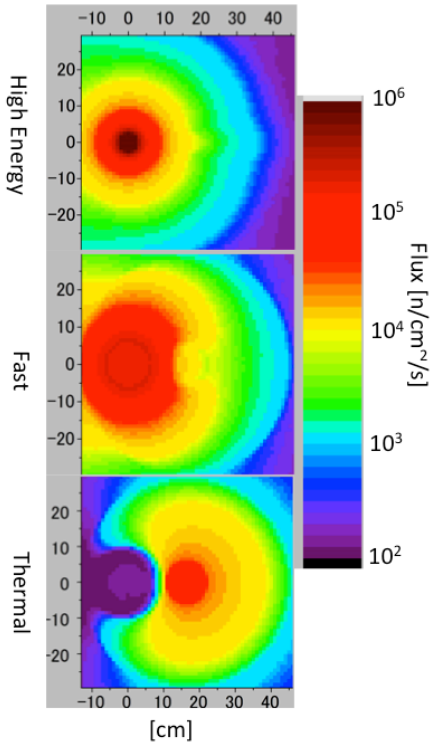

Figure 3. Spatial distributions with the three energy regions. The three regions are: above 10MeV (High energy), from 0.1 to 10 MeV (Fast), below 0.5eV (Thermal).

Horizontal and vertical axes in Figure 3 are X and Y in Figure 1. As shown in High energy of Figure 3, the neutrons above 10MeV are decreased in tungsten region rapidly by effects of multiplication and inelastic reactions. In graphite region, the neutrons are decreased slower than tungsten. Fast energy of Figure 3 shows that intensity of the neutrons from 0.1 to 10MeV becomes the maximum by effects of multiplication reactions and inelastic reactions in tungsten region. The neutrons are decreased rapidly by high moderation power of HDPE region. Thermal of Figure 3 shows a thermal energy neutrons distribution. The neutrons are spread entirely but concentrated especially in HDPE and NM regions. From above results, it is understood that each region in WPC contributes to increase Thermal/Fast well.

5. Time distribution of neutron flux

Though the neutron energy can be estimated by simulation codes, it is difficult to know energy of the neutrons using simple detection systems. Detectors using neutron capture reaction such as He-3 detectors can measure time distribution of thermal neutrons that are directly related to the specific materials. In this section, He-3 gas with pressure of 4 atm is filled with NM region in WPC, WP, PC, and WC. The time distribution measurements of capture reaction number are simulated. The time of

releasing the 14MeV neutrons and time bins are set to 0 sec and 10 μ sec respectively. These results are shown in Figure 4.

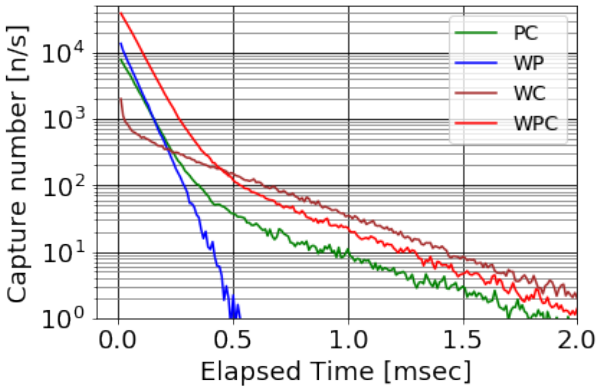

Figure 4. Time distributions of neutron capture number in the He-3 regions of WPC, WP, PC and WC.

As shown in Figure 4, lines of WPC and PC consist of a fast and slow decay component, and we consider that each component is caused by the reactions of hydrogen atoms and carbon atoms. Since slowing down of neutrons in WP and WC seems to be caused by hydrogen or carbon atoms, these plots consist of one component of fast or slow. Exponential approximations were performed by

$$C(t) = \alpha \cdot \exp\left(-\lambda_{fast} \cdot t\right) + \beta \cdot \exp\left(-\lambda_{delay} \cdot t\right)$$

Where C is counts, t is elapsed time in μsec, α and β are constants of the two exponential components, λ_{fast} and λ_{delay} are decay constants of the two components. The constants derived from the fittings are shown in Table 2. The α and β of WPC are about 5 and 4.2 times of PC, which are caused by multiplication effect of tungsten. λ_{fast} and λ_{delay} of WPC are about 1.02 and 1.2 times of PC. We consider that comparatively high absorption cross-section of tungsten put the effect on HDPE and carbon regions. The α of WPC are about 2.9 times of WP, which is caused by graphite reflections. We conclude that by influencing the neutron time distribution of each system and comparing these coefficients of exponential fitting results, it is possible to ascertain the influence of each region on thermal neutrons.

	α	λ_{fast}	β	λ_{delay}
WPC	$4.50E\times10^4$	14.6	$3.38E\times10^2$	2.81
PC	$8.94E\times10^3$	14.4	$8.92E\times10^1$	2.37
WP	$1.57E\times10^4$	18.2	–	–
WC	–	–	$6.92E\times10^2$	3.11

Table2. Constants derived from the exponential fittings of neutron capture time distributions in He-3 detectors

6. Summary

A neutron moderator system consisting of tungsten, HDPE, and graphite was designed for a delayed gamma-ray measurement system using a 14 MeV D-T neutron source by simulations using MCNP6. For the purpose of evaluation of the effectiveness, energy spectrums in the sample region of the system were compared using different combinations of the three material components. Each region of the system contributed to increase thermal neutrons entering the nuclear material region while the tungsten and HDPE decrease the 14-MeV and fast neutrons. However, it is difficult to measure neutron energy actually with simple measurement system. For preliminary study of experimental

evaluation, time distributions of neutron counts in He-3 detectors in the moderator system were compared using different combinations of the three material components. The time distributions were fit with double-exponential functions to account for the fast and delayed periods, and the coefficients were compared. Since the coefficients showed moderation and absorption effects of each part well, we concluded that evaluation of the system using the method is possible experimentally.
In the future, a moderator design of more detailed experimental environment will be performed. The effectiveness of the moderator system will be verified by measurement experiment of time dependent.

Acknowledgements

This technological research and development was supported by the Japanese government (MEXT).

References

[1] Douglas Chase Rodriguez, Jun Takamine, Mitsuo Koizumi, et al., “Utilizing Delayed Gamma Rays for Fissionable Material Measurement in NDA,” In 37th Annual Meeting of the European Safeguards Research & Development Association, EUR-27342, May 2015.
[2] D.C. Rodriguez et al., “Active Neutron NDA Techniques for Nuclear Non-proliferation Applications (3) Development of Delayed Gamma-ray Spectroscopy - Preliminary Monte Carlo Studies”, Proceedings INMM Japan Chapter 36th Annual Meeting, Tokyo, Japan, October 2015.
[3] J. Takamine et al., ”Active Neutron NDA Techniques for Nuclear Non-proliferation Applications (5) Development of Delayed Gamma-ray Spectroscopy - Design Study of a moderator for a 14-MeV D-T Neutron Source”, Proceedings INMM Japan Chapter 36th Annual Meeting, Tokyo, Japan, October 2015.
[4] <http://www.thermoscientific.com>
[5] http://www.sodern.com/sites/en/ref/home.html

Field trial of KM200 Electronics in the JRC PUNITA Facility

Kiril Ianakiev[1], Metodi Iliev[1], Martyn Swinhoe[1], Bent Pedersen[2], Giovanni Varasano[2], Tatjana Bogucarska[2], Ludwig Holzleitner[3], Paul De Baere[4], Stefano Vaccaro[4], Marc Couland[4]

[1]Los Alamos National Laboratory, Los Alamos, NM 87545
[2]European Commission, Joint Research Centre, Nuclear Security Unit, Via Enrico Fermi 2749, 21027 Ispra (VA), Italy
[3]European Commission, Joint Research Centre, Nuclear Safeguards and Forensics Unit, P.O. Box 2340, 76125 Karlsruhe, Germany
[4]European Commission, DG Energy, Directorate E – Nuclear Safeguards, L-2920 Luxembourg

Abstract:

In this paper we present the joint efforts of the partners under Action Sheet (AS) #59 "Cooperation on Improved Techniques for High Count Rate Non-destructive Assay Measurements" to conduct comparison testing of a high counting rate preamplifier developed at LANL with the currently installed PUNITA electronics in a pulsed, high neutron flux environment. Two of the PUNITA analogue channels (one close and one far away from the neutron generator) were upgraded with the LANL-fabricated KM200 analogue electronics. In addition, remote switching of KM200 amplifier inputs and detector outputs allowing a newly developed LANL method for self-calibration of counting loss compensation to be applied. Side by side comparison of raw count rate data was made with the KM200 and original PUNITA electronics for a wide range of neutron flux intensities and different numbers of detectors per KM200modules. .
The experimental data were analyzed to obtain the dependence of output versus input count rates and the corresponding dead-time (DT) loss error for a wide range of count rates. The comparison results indicated that the configuration with four preamplifiers per module will expand the count rate capabilities about 10 times while the configuration with two preamplifiers will expand the existing count rate capabilities about 5 times. The LANL DT correction method will expand further the count rate capabilities in both cases. The abrupt drop in the corrected data noticed at extremely high rates may suggest a gain shift due to a space charge effect.
The data analysis confirmed that dead-time losses in the He3-based neutron counters fit to the non-paralyzable DT model, rather than the paralyzable DT model currently used by the community, but the equivalent DT at high counting rates is a few times higher than that measured at low counting rates.

Keywords: preamplifiers; high signal rates; neutron counting; active interrogation; DDA

1. Introduction

Non-destructive Assay (NDA) techniques for nuclear safeguards often require acquisition systems capable of handling high signal count rates. In recent years, a general need has emerged to improve the existing detector analogue electronics for better performance in these high count rate applications. Recent examples of this need include an increasing emphasis on direct measurement of spent nuclear fuel (SNF), a need to measure accurately fissile material within samples exhibiting high (α,n) reactions, and measuring high neutron fluxes in pulsed neutron interrogation systems with safeguards applications. In the last example, prompt neutron and gamma emissions from a sample are the most intense signatures that can be used to accurately quantify the material. So far, the use of prompt emissions has, to some extent, been hampered by the difficulty in acquiring meaningful signals during, or immediately after, the burst of neutrons from the interrogation source. Currently available electronics for processing gamma-ray and neutron signals (mainly based on Amptek A-111 and PDT10) perform poorly due to saturation of the electronics in the high flux environment. In the case of

Differential Die-Away assay (when applied to SNF, nuclear waste, etc.), a majority of the signal of interest occurs immediately after the interrogation, and decays exponentially thereafter, typically resulting in that portion of the signal being lost to saturation. Better electronics are needed for DDA of spent fuel measurements due to the combination of gamma-rays and neutrons from SNF as well as the 14-MeV neutron burst from the neutron generator).

Pursuant to the Agreement between the European Atomic Energy Community (Euratom) and the United States Department of Energy (DOE) in the field of Nuclear Material Safeguards and Security Research and Development, signed 2 November 2010 (AS #59), the National Nuclear Security Administration (NNSA) and Euratom will undertake a cooperative effort to improve the performance and reliability of NDA Measurements in applications including high counting rate situations. The US DOE has developed new (KM200) high count rate electronics for proportional counters [1, 2, 3].

This paper describes the activities and results related to the requirements of Task 1 – field trial of KM-200 electronics for improvement of Differential Die-Away (DDA) assay at the Pulsed Neutron Interrogation Test Assembly (PUNITA) of the European Commission's Joint Research Centre (JRC) [4,5]. By this cooperative effort, the U.S.-designed preamplifiers can be evaluated in a controlled environment involving active interrogation allowing a comparison of measurement results for U and Pu standards with previous measurements acquired with standard DDA electronics at PUNITA.

The safeguards objective achieved by the testing campaign of the KM200 at PUNITA is to demonstrate the superior count-rate capabilities of this circuit compared with the standard amplifier circuits for proportional counters as used in a variety of safeguards instruments. The tests involved the installation of KM200 amplifiers, developed by Los Alamos National Laboratory (LANL), in the PUNITA pulsed-source facility in order to assess the effectiveness of the KM200 for safeguards purposes. A new self-calibration method (also developed by LANL) for correcting DT losses in pulsed neutron experiments, was implemented and tested.

With the KM200 enabling measurement in the period closer to the neutron generator (NG) burst, this enhancement should allow:

- Significantly better counting statistics to be obtained on the signal component from detected fission neutrons (thus lowering the limit of detection) without prolonging the measurement time
- Better accuracy in safeguards verification measurements for samples of high neutron count rates because of the reduced dead-time (DT) of the KM200.
- Evaluation of KM200 count rate capabilities in wide range of neutron flux conditions that that are difficult to achieve with radioactive neutron sources

The self-calibration method for DT correction was implemented simply by changing the numbers of tubes per amplifier. This change accommodates higher tube neutron incident rates and uses that information for a quantitative comparison basis for dead-time losses. Furthermore, it allows an assessment of the performance improvement versus installation cost, and speeds-up the testing time for different measurements (i.e., since there is no need to open the junction box and change the HV circuitry).

2. Description of the neutron detection system of the PUNITA facility and experimental setup

JRC's PUNITA laboratory incorporates a main detection system composed of 96 ^{3}He proportional counters called fission neutron counters (designed to detect fission neutrons). These detectors are grouped into 24 modules. Each module includes a junction box containing one amplifier unit connected to four ^{3}He tubes (Figure1).

The PUNITA system is excited with a short neutron pulse from a neutron generator (NG). After a short thermalization period, the NG pulse produces a thermal neutron flux in the detectors that, by design, decays exponentially over a nominal 10 ms period (Figure2). Further detail is given in [4, 5].

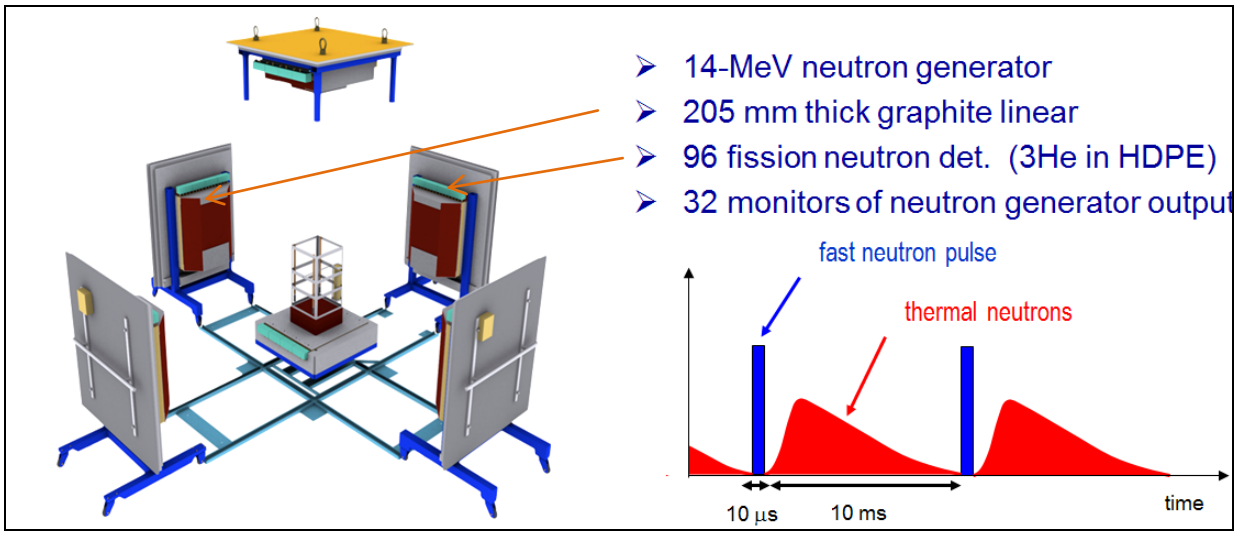

Figure 1: PUNITA depiction (expanded view).

The detector response is a convolution of neutron interactions from the generator flux and the exponential die-away response determined by the graphite moderator and neutron absorbers in the system's walls. The detectors and moderators in the wall are shielded from the thermal neutrons coming from inside the cavity. The signal in the detectors follows an exponential decay as long as the dead-time losses are negligible, and the electronics are not saturated.

Besides fitting each detector with a dedicated amplifier, a faster response amplifier circuit (providing less DT effect in the neutron counters) could benefit the PUNITA detection system by producing a faster return to the exponential decay of the counts from the neutron pulse.

3. KM200-UPGRADE OF PUNITA Electronics

3.1. KM200 electronics

The KM200 front-end electronics is a modular and flexible technology [1, 2] that can interface with a broad range of thermal neutron detectors and other applications. It consists of a set of customizable circuit boards that can be used in new detector systems or as retrofit for existing ones. The customization consists of adapting the time constants and the gain in the KM200s for the specific application and user requirements, such as a more universal KM200-FAST and KM200-SLOW designed to works with all typical multiplicity counter tubes, or one optimized to have minimal dead time for a specific detector. The latter is likely for extreme application requirements such as an SNF DDA instrument, the IAEA Vitrified Waste Coincidence Counter, gross neutron measurements in fork detector, etc.

3.2. KM200 retrofit design

The installation of four KM200 preamplifiers (one per tube) with low DT compared to the single PUNITA preamplifier – serving four ^{3}He tubes with time constants similar to the PDT-10A developed by Canberra – would improve substantially the count rate performance, but will require higher installation cost. In order to measure the level of improvement versus the installation cost, separate measurements with different (two or four preamp) in the box must be performed. Rewiring the connection in the junction box requires extensive and time consuming assembly and disassembly work on the detectors in the PUNITA instrument. Additionally, we will not know the magnitude of DT losses immediately following the burst, which are inevitable to some degree. Therefore, we have installed one relay that allows remote reconfiguration of the pre-amp so that measurements can be performed in the planned time frame. An additional advantage of the relay installation is that we can compare the measured count rates with incident neutron rates in the tube by using a newly developed by LANL self-calibration method for correction of DT losses [3]. A detailed description of the dead time calibration and compensation method and proof of principle results are reported in [6] .The

additional hardware burden for implementing this remote-reconfiguration method is minimal (installation of only one mechanical relay with dual switching contacts per junction box).

The PUNITA retrofit design (Figure 2) consists of four KM200 amplifiers (one per tube) mounted on a redesigned ground plate (preamplifiers on the top and HV circuitry with switching relay on the bottom) for each junction box. This design allows a drop-in replacement of the exiting ground plate which should ease the potential full replacement of PUNITA electronics without any mechanical work in the existing enclosures, and eases testing and troubleshooting the entire assembly outside the PUNITA detector.

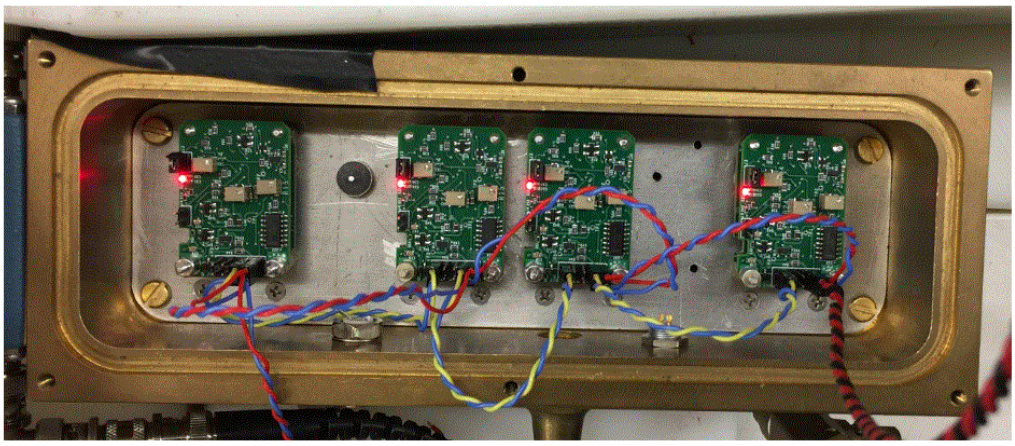

Figure 2: Top view of KM200 electronics installed in the junction box. The 5X2 header connector of KM200 was used for power and TTL signal daisy-chain connections

3.3. Initial testing at LANL

PUNITA staff communicated that their ^{3}He tubes have Ar+CH_4 gas admixture similar to detectors used in the HLNCC counters. Unlike the universal KM200-FAST preamplifier developed to work with both Ar+CH4 and CO2 gas admixtures [2], the KM200 was optimized to minimize the DT for this particular tube fill. The plateau curves of individual and daisy-chained preamplifiers – after gain matching and double pulsing filter optimization, as shown in Figures 3a and 3b – provided uniform performances, with plateaus beginning at about 1600 V and having width of about 150V. The time interval analysis in Figure 3c shows uniform performance for all tubes with this version of KM200 having about 30% reduced DT compared to the KM200-FAST preamplifier reported in [2]. The hump in the Time Interval Histogram (TIH) at around 500 ns is due to some double pulsing that is acceptable for single rates counting of DDA application.

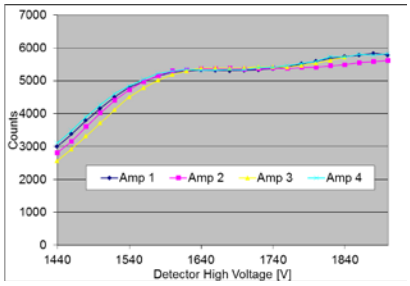

Figure 3a: Matched plateau characteristic for the first module four KM200 set.

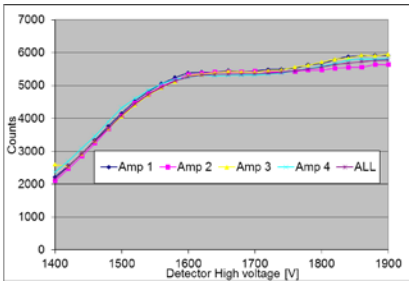

Figure 3b: Matched plateau characteristic for the second module four-KM200 set.

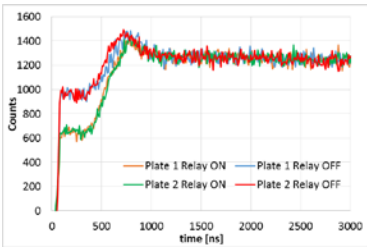

Figure 3c: Time interval analysis with one detector per amplifier (relay OFF) and two detectors per amplifier (relay ON)

4. Testing of PUNITA and KM200 electronics

4.1. Test plan and experimental setup

Understanding the combined, quantitative effect of implementing KM200s and the dead time self-calibration and compensation method on precise active interrogation measurements would require a larger-scale effort and a full upgrade of electronics and analysis algorithms. LANL and the JRC believe that the simple upgrade of two of the PUNITA analogue channels – one close to and one far from the NG, as shown in Figure 4. – and a simple set of experiments with the NG located at different distances from detectors A4 and B1 will provide a sufficient indication of improvement for making further implementation decisions. The location variations are necessary to overcome the limited range of the NG burst intensity allowing the evaluation of the KM200 electronics for a wide range of input count rates. We have to stress that this sort of study is possible only in a versatile, pulsed neutron research facility such as PUNITA.

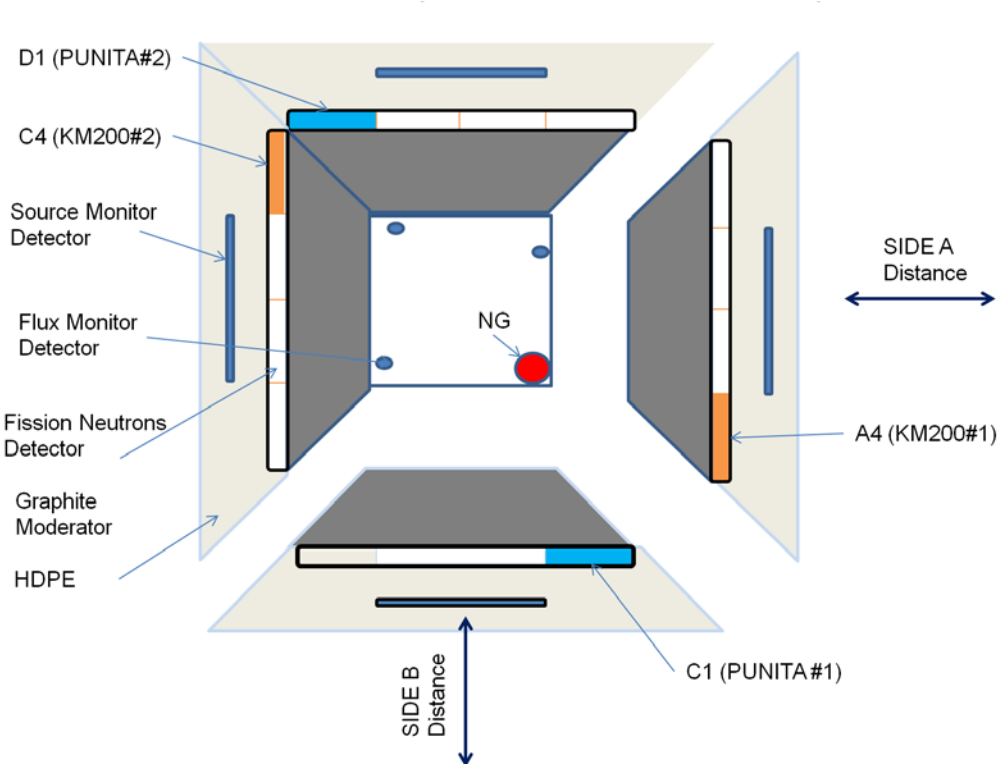

Figure 4: Layout of comparison testing experiment where the inensity of incident neutron flux is changed by the changing the distances from the neutron generator by moving Side A and Side C. The blue modules contain PUNITA electronics, the orange modules - KM200 electronics

4.2. Setup of KM200 parameters and evaluation of KM200 and PUNITA responses to NG bursts

This activity determines saturation limits of the electronics for a 100% and 200% load per amplifier at different settings of the NG and compares the KM200 and PUNITA amplifiers: The original PUNITA 4 bar (Ar+CH4 gas admix) ^{3}He tubes (LND, Inc. have lower operating voltage, likely due to its respectively thinner (0.001") anode wire than those commonly used in multiplicity counters, i.e., Reuter Stokes 4 bar ^{3}He tubes with Ar+CH4 and 0.002" anode wire. The combination of relatively low stopping power of 4 bar gas and slower charge collection of tubes with thin anode wire leads to higher fluctuations in the charge collection time and commensurately excessive double pulsing effect when short shaping time is used. The plateaus of the KM200 electronics upgraded module C4 taken before and after the setup is shown on Figure 5.

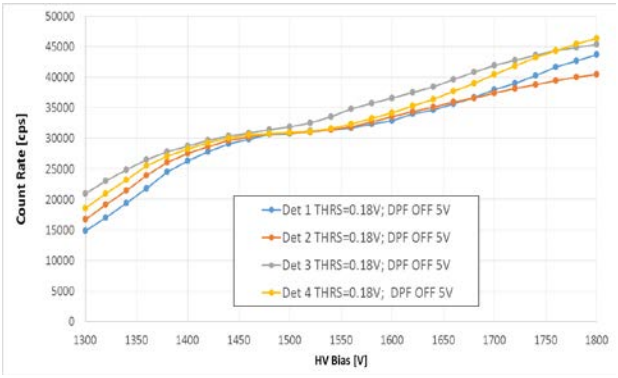

Figure 5a: Initial plateaus for LND tubes taken with uniform settings of KM200 electronics (DPF=OFF, threshold 0.18V).

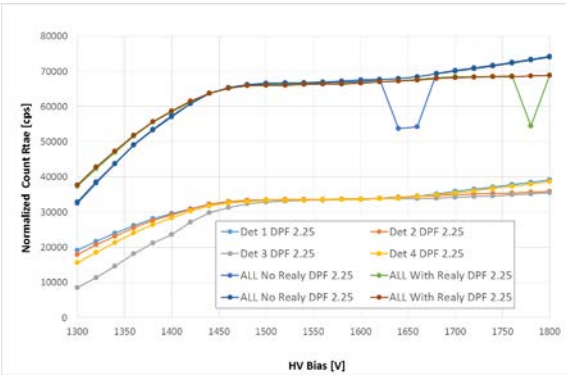

Figure 5b: Plateaus for LND tubes after gain matching and DPF optimization. Upper curves: all preamps output for one and two preamplifiers per tube configurations (with a bad-performing Tube #3). Lower curves: plateaus of individual preamps.

Unlike the Reuter Stokes tubes, the LND tubes show very high spread of gain and plateau length (Figure 5a). The plateaus after gain matching show reasonable plateau even with bad performing tube #3.

4.3. Experimental data

The accelerating voltage of the NG was reduced about 15% in order to reduce the intensity of fast neutrons burst and avoid deep saturation of the first stage observed during preliminary measurements. According to the setup on Figure 4, two sets of data (one with Relay Off and one with Relay On) were taken for each position of the modules A4 and B1. The count rate data (Figure 6) from A4/B1 modules close to the NG and C4/B1 modules far from the generator taken with closed PUNITA represent the data of normal operating conditions.

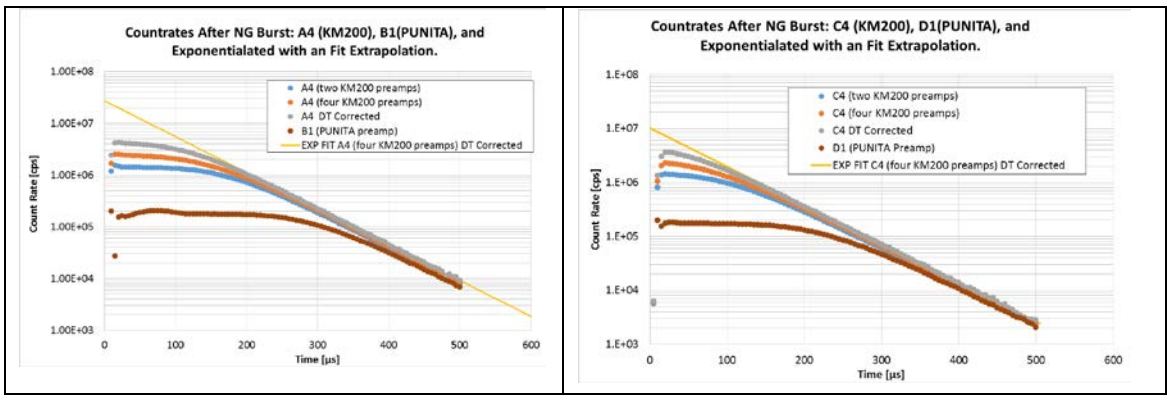

Figure 6: Count rate response-tested electronics measured at closed PUNITA. Left: A4 (KM200) and B1 (PUNITA) modules. Right: Positions C4 (KM200) and D1 (PUNITA).

5. Data analysis

Thanks to PUNITA's single exponential thermal neutron die away time, count rate extrapolation can be made even in the period immediately after the NG burst, where dead-time loses are very large or the electronics is in saturation. The count rate response form NG burst shown on Figure 6 indicates substantially better count rate performance of KM200 electronics, but does not allow quantifying the DT losses versus input count rates. Therefore the following data analysis was performed. We have selected a region of time with low DT losses for the measured data and used an exponential fit to extrapolate these data to the region with substantial DT losses. We used this exponential fit as an

input count rate Nin (zero DT losses) in order convert the time dependence of count rate measurements from Figure 6 to the well-known output (measured) versus input count rate.

The plotted (Figure 7) count rates (especially from slower PUNITA pre-amplifier) flatten at counting rates many times the value $1/\tau_d$, where τ_d is the shaper dead-time (about 2μs) and have behaviour much closer to the system with non-paralyzing dead-time ($N_{out}=N_{in}/(1+N_{in}*\tau_{np}$) with maximal asymptotic count rate $N_{max}=1/\tau_{np}$ rather a system with paralyzing dead-time ($N_{out}=N_{in}*\exp(-N_{in}*\tau_p)$) with maximal rate $1/(\tau_p *e)$ at count rate $1/\tau_p$, where τ_p is paralyzable dead-time, τ_{np} is non-paralyzable dead-time, N_{in} is the incoming count rate, and N_{out} is the measured count rate.
Using the two most severe DT cases (PUNITA and two KM200 amplifiers) we can estimate an equivalent non-paralyzing dead-times as follows: PUNITA amplifier τ_{np} = 5.6 μs and KM200 preamplifier τ_{np} = 1.4 μs (asymptotic count rate divided by two to find the count for single amp). We have to stress that the obtained equivalent non-paralyzing DTs are over 2 times higher than the DTs measured at low count rates by the TIH (see data in Figure 3c). The observed DT behaviour is consistent with our prior measurements. More detailed analysis and explanation of the phenomena can be found in [6].

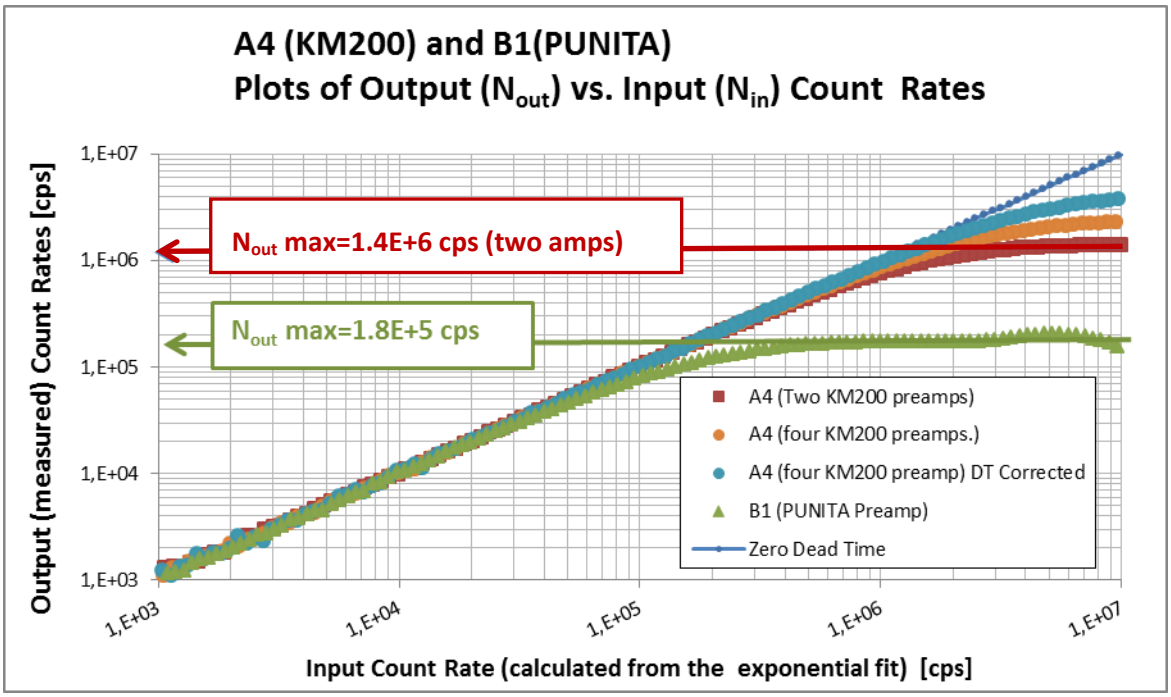

Figure 7: Plot of measured versus input count-rates. The extrapolated exponential fit (in blue) represents a zero DT system. The horizontal arrows point toward the maximal count rate for each measurement

We have used the obtained dependency between the input and measured count rates to calculate the relative counting losses as $(N_{out}-N_{in})/N_{in}$ plotted in Figure 8.

The plot on Figure 8 indicates that an upgrade with four preamplifiers will expand the count rate capabilities about 10 times where the upgrade with two preamplifiers per module will expand the current count rate capabilities about 5 times.

The DT correction method will expand further the count rate capabilities in both cases. The abrupt drop in the corrected data may suggest a gain shift due to space charge effect. Operation away from the plateau knee could mitigate this problem.

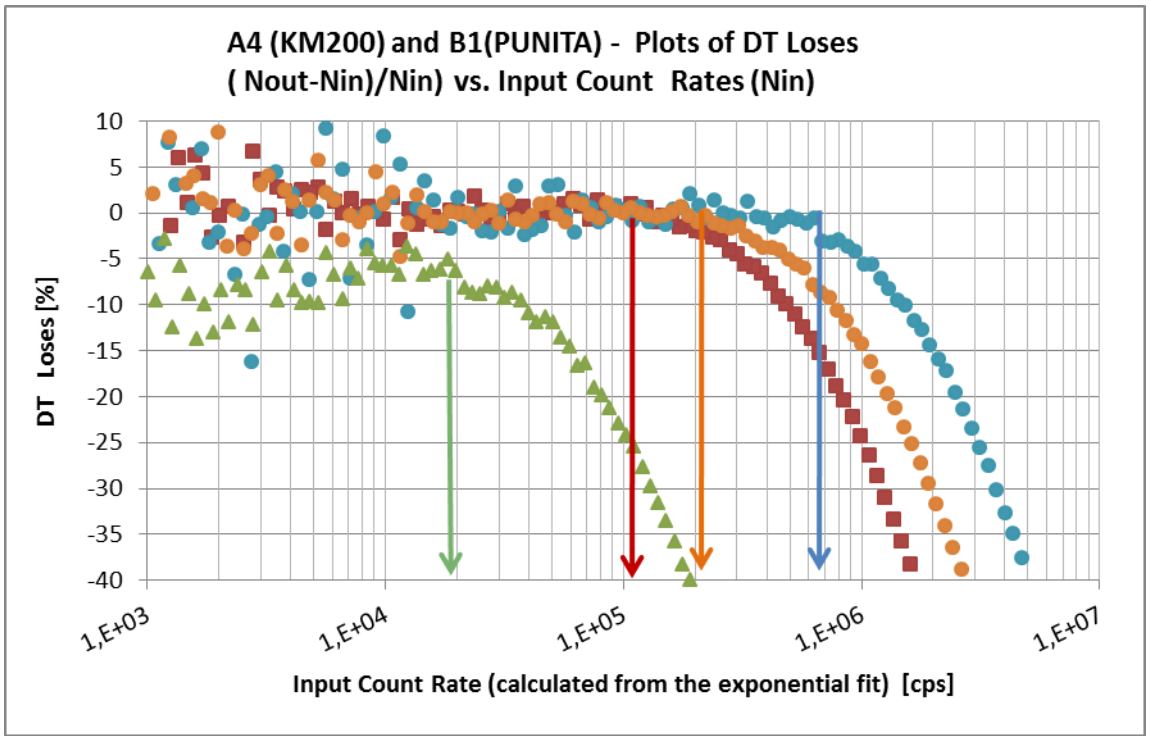

Figure 8: DT losses error versus input count rate for the current PUNITA instrument, green plot. PUNITA: Red – two KM200 preamplifiers per module; Orange – four KM200 preamps for module; Blue – four KM200 preamplifiers per module DT corrected

6. Discussion of possible next steps

There are three future testing options for KM200 electronics in EURATOM safeguards assays:

- Multiplicity counting. The AWCC coincidence counter was selected as a preferable candidate for testing of KM200 electronics because of its higher detection efficiency and number of tubes per amplifier than HLNCC-II. The need of sources or nuclear material that provides substantial DT for comparison testing of current and KM200 electronics was outlined. Measurements using different numbers of detectors per amplifiers (use of relay) will provide not only the DT losses correction, but also will allow testing the counter at 2x DT using the same source).

- Gross neutron measurements with FORK detector. The exceptional stability of KM200 amplifier and ability for remote threshold sensitivity control will allow neutron measurements of all type spent fuel assemblies without tedious recalibration.

- Full PUNITA upgrade. A decision to fully upgrade PUNITA electronics would allow analytical measurements to be performed.

7. Acknowledgements

The authors would like to thank the DOE and EURATOM headquarters for bold support of this research and presentation to the ESARDA conference. The project was funded in part by the Office of International Nuclear Safeguards in the U.S. Department of Energy/National Nuclear Security Administration's (DOE/NNSA's) Office of Non-proliferation and Arms Control (NPAC).

8. References

[1] Ianakiev, K, M. Iliev, M, Swinhoe, M, and Johnson, N, *High Count Rate Thermal Neutron Detectors;* IAEA Safeguards Symposium, Vienna, 2014

[2] Iliev, M; Ianakiev, K, Swinhoe, M, *KM200 Front-End Electronics for Thermal Neutron Detectors*; INMM 57th Annual Meeting, 2016-07-24/2016-07-28; Atlanta, Georgia, United States

[3] Ianakiev, K, Iliev, M, Swinhoe, M, *High Count Rate Thermal Neutron Detectors and Electronics*; Provisional Patent Application Serial No. 62/411,898

[4] Favalli, A, Pedersen, B, *Design and Characterization of a Pulsed Neutron Interrogation Facility*; Radiat. Prot. Dosimetry (2007) 126 (1-4):74-77

[5] Favalli, A, Mehner, H-C, Crochemore, J-M, Pedersen, B, *Pulsed Neutron Facility for Research in Illicit Trafficking and Nuclear Safeguards*; IEEE TNS, Vol. 56, No. 3, June 2009

[6] Ianakiev, K, Iliev, M, Swinhoe, M, LaFleur, A, Lee, Ch, *Self-calibration Method for correction of counting losses in neutron counting systems;* ESARDA Symposium, Dusseldorf, 2017

Self-calibration Method for Dead Time Losses in Neutron Counting Systems

K. D. Ianakiev[1], M. L. Iliev[1], M. T. Swinhoe[1], A. M. LaFleur, Chaehun Lee[1, 2]

Affiliation: 1 Los Alamos National Laboratory, Los Alamos, NM 87545

Affiliation: [2]KAERI, Republic of Korea

Abstract:
Most of the safeguards assay for quantitative characterization of SNM (mass, multiplication, random neutron contribution) are based on neutron measurements and rely exclusively on the counting information from very efficient, but slow He-3 proportional tubes. The response of neutron detection systems is inevitably affected by Dead Time (DT) losses that are generally caused by very complex and convoluted processes, which are difficult to take into account for corrections (for example, the DT losses for bipolar shapers differ from those of unipolar shapers). Therefore an empirical approach for calculating the DT losses assuming exponential (paralyzing) DT using measurements with two Cf-252 sources with known activities was established as current practice for many safeguards neutron counting systems. The availability of a very wide range of such Cf-252 calibration sources becomes the limiting factor for extending the deadtime correction calibration over a sufficient dynamic range to reach the conditions of real measured material.
In this paper we present a novel self-calibrating method for the determination and correction of deadtime losses that uses directly the neutron signal from real measured material. The count rate from the material is measured with two configurations of the preamplifiers: a standard configuration of the preamplifiers and tubes, corresponding to a nominal (100%) load per preamplifier and a second "deadtime measurement" configuration, where every two neighbouring clusters of He-3 tubes are connected together to a single preamplifier, corresponding to 200% load per preamplifier. A proof of principle DT calibration measurement over a wide dynamic range exceeding 10^6 reactions/sec using a 14 MeV neutron generator, demonstrated experimentally the viability of this method. The method produces the DT correction factor at every measured counting rate. The results show the very important observation that the correction factor does not fit with either fully paralyzing or fully non-paralyzing dead time models. Using either model could lead to substantial deadtime correction errors. Explanation of DT behaviour and implementation aspects of this method in typical safeguards neutron systems (already in use or to be built) such as differential dieaway, coincidence and multiplicity counting will be discussed.

Keywords: neutron counting losses; dead time models; dead time correction; self-calibration; KM200

1. Introduction

The analytical measurements using pulse mode radiation detection systems rely on proportionality between incident and recorded radiation events. That proportionality is limited by the inevitable counting losses due to: a) random time distribution and intensity of the incident radiation events and b) the minimum response time of the detection system to process and record two separate detection events, called Dead Time (DT). The DT in a typical gamma spectroscopy measurement system has two components: a) one from the duration of shaped pulses resulting from convolution between the detector current pulse *I(t)* and time response (weighting function W(t)) of the selected pulse processing electronics and b) electronics time to detect the pulses above the event threshold, measure (typically the ADC measurement time) and record the amplitude of the pulse. Because the emphasis of gamma spectroscopy instrumentation is on preserving the energy information, unipolar shaping with time constant much longer than detector current pulse is used for better noise and ballistic deficit suppression. In order to correct these losses two DT loss models are conventionally applied: a) paralyzing DT model Nmeas=Nin*exp(Nin*Td), where Td is a deadtime constant used to

correct the losses due to pile-up of superimposed unipolar pulses that prevents a new event being detected and recorded before the pile-up pulse goes below the event discriminator threshold and b) non-paralyzing DT model $N_{meas} = N_{in}/(1+N_{in}*T_d)$ used to correct the time for a pulse amplitude measurement process that is triggered by the event discriminator signal. These two models have similar behaviour at incident rate where DT losses are relatively low ($N_{in}* T_d << 1$) but very different behaviour at elevated rates and high DT losses [1, 2]. The uniform pulse shape due to time constants longer than the detector pulse and low busy time amplitude dependence due to very low event detection threshold (set just above the noise) provided a good match with constant extension of the DT of the paralyzing model. Therefore the paralyzing DT model combined with very effective pile-up rejection became an industry standard for correction of DT losses in gamma spectroscopy.
On the contrary, the emphasis in neutron counting systems is to preserve the counting information from the 3He detector despite the long (microseconds) and very fluctuating shape of the current pulse (see Fig 1a). Therefore with almost no exceptions the signal processing of existing electronics (Amptek-11, PDT, KM200) is based on bipolar shaping with time constant much shorter than duration of detector current pulse in order to reduce the dead time [3] as it is shown on Fig 1b.

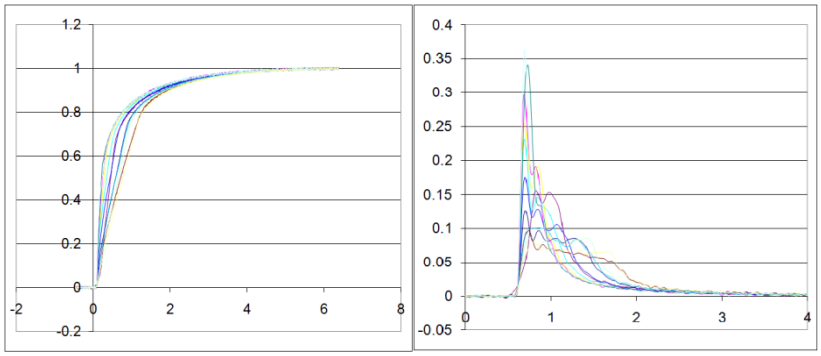

Fig. 1a. Normalized charge pulses (left) and corresponding current pulses. The fluctuation of charge collection time (left) result in very wide amplitude and duration of the current pulses (right)

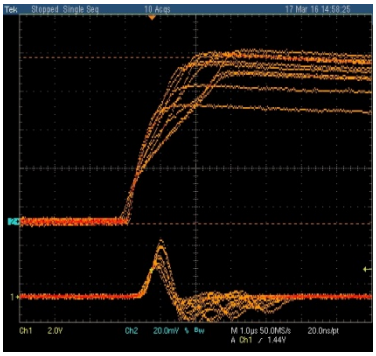

Fig.1b Charge pulses (top) of N2 gas fill He3 tube and corresponding bipolar output pulses from KM200-SLOW shaper [4]

The fluctuation of differentiated current pulse causes artificial parasitic triggering (the so called double pulsing effect). This effect is the main factor governing the selection of time constant as a trade-off between dead time and minimal amount of artificial pulses. We would like to stress that the average value of a bipolar pulse is zero (the areas of positive and negative lobes are equal). This leads to substantial differences in high count rate behaviour between unipolar and bipolar shapers:

- The pulse pile-up spectrum in a unipolar shaper is superimposed on the right (higher energy) versus the original spectrum while the pile up in the spectrum from a bipolar shaper is superimposed in both directions versus the original non-pileup spectrum.

- The pile-up of unipolar pulses causes updating dead time and is described very well with the exponential dependence of the paralyzing DT model (zero output at Nin*DT >>1). **Because the bipolar pulse has zero average value, the average value of superimposed bipolar pulses also will be zero regardless of the input counting rate.** The intuitive implication is that the paralyzing DT model would not describe well the DT behavior of a bipolar shaper at elevated DT.

2. Description of the neutron detection system of the PUNITA facility and experimental setup

As described in the previous section, the DT losses in neutron counting systems are very complex and convoluted processes, which are difficult to take into account for corrections. Therefore an empirical approach for calculating the DT losses assuming exponential (paralyzing) DT using measurements

with two Cf-252 sources with known activities was established as current practice for many safeguards neutron counting systems [5].

The following equations are used to calculate the deadtime corrected singles (S_C) and doubles (D_C) rates:

$$S_C = S_M e^{\frac{\delta S_M}{4}} \quad (1)$$

$$D_C = D_M e^{\delta S_M} \quad (2)$$

where S_C and D_C are the true singles and doubles rates, S_M and D_M are the measured singles and doubles rates, respectively, and δ is the total deadtime coefficient given by:

$$\delta = \left(A + B \cdot S_M \cdot 10^{-6} \right) \mu s \quad (3)$$

where A and B are constants. The dead-time parameter B is approximated as $B = A^2/4$. These standard deadtime correction parameters (A and B) are applied to the singles and doubles rate for both coincidence and multiplicity analysis. The triples deadtime correction uses the multiplicity deadtime parameter. The multiplicity deadtime parameter was approximated as A/4.

It is important to note that there are several measurement methods that can be used to establish A and B for a particular detector system.

1) ***Doubles to Singles Ratio*** – measure the singles and doubles rates from at least 4 ^{252}Cf sources that span a large range in activity, plot ln(D/S) versus Singles rate, and use a quadratic curve to fit the data and determine A.
2) ***Source Intensity Ratio*** – measure a strong and a weak ^{252}Cf source with very well-known neutron yields, set the ratio of the deadtime corrected doubles rates equal to the known ratio of ^{252}Cf yields, and iteratively solve the equation for A.
3) ***Paired Source*** – measure 2 high yield ^{252}Cf sources separately and then together, set the deadtime corrected doubles rate from measuring sources together equal to the sum of the deadtime corrected rates from measuring the sources separately, and iteratively solve the equation for A.

The system deadtime is affected by properties of detector (e.g. polyethylene design, detector fill gas) and by the signal processing electronics (e.g. number of preamps, shaping time). The deadtime loss of neutron pulses increases as higher count rate, and it can be corrected empirically [6,7,8]. These techniques can provide excellent results for measurement samples with count rates in the range of the calibration sources used. But applications such as spent fuel, plutonium waste and MOX storage canisters, uranium and trans-uranium ingots, etc. often require operation at count rates many times the count rate of the empirical calibration. The reliance of the present deadtime calibration method on a single measurement point therefore introduces potential limitations, such as:

- It is difficult to find and measure Cf-252 sources in the entire dynamic range of the detection system.
- The count rates and neutron correlation characteristics of Cf-252 calibration source are different from those of measured SNM.
- The last but not least, the dead time behavior of bipolar shapers used in the ^{3}He electronics can differ from that calculated based on the simple assumption of paralyzing DT model with a fixed deadtime constant even at low or moderate count rates.

3. Self-calibration method for counting loss correction

In order to address the listed above challenges, LANL has developed a new self-calibrating method for the determination and correction of dead time losses that uses the neutron signal from real measured material directly [9]. It is based on measuring the same incident reaction rate in the detector (count rate) from the material, N_{in}, with two configurations of preamplifiers: a standard configuration of preamplifiers and tubes, corresponding to a nominal (100%) count rate load per preamplifier and

second “dead time measurement” configuration, where every two neighbour clusters of detectors are connected together to a single preamplifier, corresponding to 200% load per preamplifier. An illustration of the described measurement is shown on Figure 2.

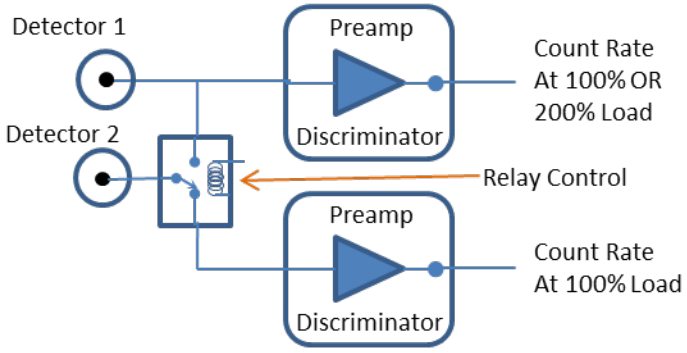

Figure 2. Illustration of detector switching method for dead time self-calibration. When the relay switch at the preamps’ input is in initial position, both channels see normal count rate load ($N_{100\%}$). When the relay is switched, the bottom preamp sees no detector signal and the top sees double the count rate load ($N_{200\%}$). The TTL output of both preamplifiers are summed in OR circuitry.

The expression for the dead time constant (t_D) and the corrected input count rate per channel (N_{IN}) can be found using the following analysis:
First assuming the dead time in the system is paralyzing:

$$N_{100\%}(sum\ of\ two\ channels) = 2 \times N_{IN}\, e^{-N_{IN}\, t_D} \quad => \frac{N_{100\%}}{2 \times N_{IN}} = e^{-N_{IN}\, t_D} \qquad /4/$$

$$N_{200\%} = 2N_{IN}\, e^{-2N_{IN}\, t_D} \quad => \frac{N_{200\%}}{2N_{IN}} = (e^{-N_{IN}\, t_D})^2 \qquad /5/$$

Where, $N_{100\%}$ is the measured count rate when one detector is connected to one amplifier, and $N_{200\%}$ is the measured count rate when two detectors are connected to one amplifier.
Observing that $e^{-N_{IN}\, t_D}$ is present in both expressions, we can eliminate the t_D unknown and simplify:

$$\frac{N_{200\%}}{2N_{IN}} = \left(\frac{N_{100\%}}{2N_{IN}}\right)^2$$

Solving for N_{IN}, we get an expression for the incoming count rate that involves only measured quantities:

$$N_{IN} = \frac{{N_{100\%}}^2}{2N_{200\%}} \qquad /6/$$

We can also solve for the value of the paralyzing dead time.

$$t_D = \frac{-2N_{200\%}}{{N_{100\%}}^2} \ln\left(\frac{N_{200\%}}{N_{100\%}}\right) \qquad /7/$$

Secondly we can apply the same method with the assumption of non-paralyzing dead time. In this case the measured count rates are:

$$N_{100\%} = N_{IN}(1 - N_{100\%}\, t_D) \text{ and } N_{200\%} = 2N_{IN}(1 - N_{200\%}\, t_D). \qquad /8/$$

Then, $\frac{N_{100\%}}{N_{200\%}} = \frac{1 - N_{100\%}\, t_D}{2(1 - N_{200\%}\, t_D)}$.

In the above equation $t_D$is the only unknown, so solving for $t_D$gives

$$t_D = \frac{2}{N_{200\%}} - \frac{1}{N_{100\%}}. \qquad /9/$$

Substituting t_D in the equation /5/ and solving N_{IN} for gives

$$N_{IN} = \frac{N_{100\%} N_{200\%}}{2(N_{200\%} - N_{100\%})}.$$

4. FNEM detector and DT calibration using classical dual source method

The classical paired source DT correction method was used to calibrate a new a detector developed at KAERI called the Fast Neutron Energy Multiplication (FNEM) detector. This detector utilizes both FNEM and passive neutron albedo reactivity (PNAR) methods. FNEM consists of two rings of three ^{3}He tubes where 1 ring is located close to the sample cavity and the other ring is located far from the sample cavity (see Figure 3). The FNEM method is sensitive to the induced fission rate by fast neutrons and PNAR is sensitive to the induced fission rate by thermal neutrons. The total induced fission rate is proportional to the amount of fissile material in the sample being measured.
The efficiency for each ring of the FNEM detector was measured to be ~6.7% for the inner ring and ~0.75% for the outer ring. Since the FNEM method is based on multiplication (induced fission) in the measured sample, this detector was designed to measure high count rate samples (>1 x 10^{6} n/s) and thus understanding the DT correction is essential to its calibration and characterization [10].

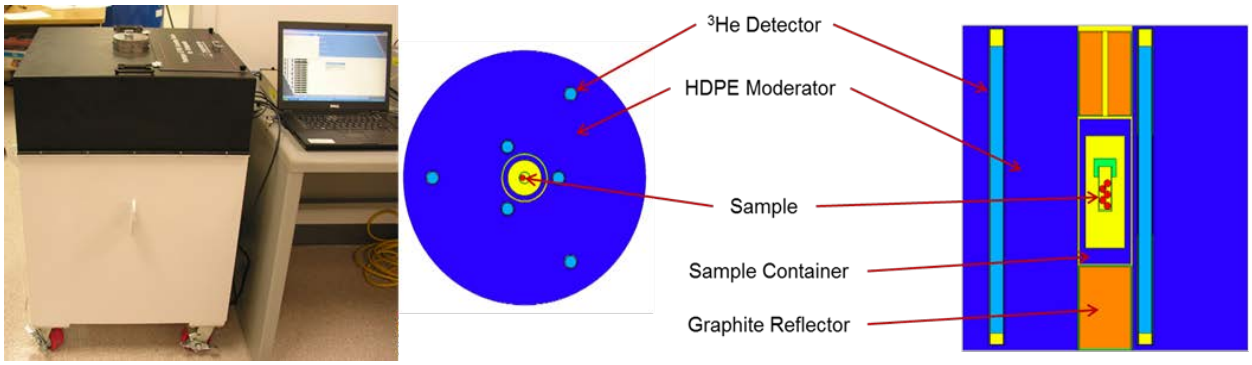

Figure 3. Picture and schematic of FNEM detector.

Using the paired source method described earlier in this paper, the DT coefficients (A and B) for FNEM were measured using two Cf252 sources with intensities of 1.57×10^{6} n/s and 1.55×10^{6} n/s at LANL. The iteratively calculated coefficients for dead time were 2.147×10^{-6} for A and 1.152×10^{-12} for B, which were then applied in the INCC software. The fractional count loss of the inner ring was determined to be about 6.3% and 12.1% for the 0.12 and 0.25 MHz count rates, respectively. It should be noted that the incident neutron rate used for deadtime measurement corresponds to about 3% of the maximum expected emission from a high count rate multiplying sample.

5. DT calibration using neutron generator and LANL self-calibration method

Because the exponential non-paralyzing Dt model may not fit the real behaviour of bipolar shaper of PDT-110A well, the extension of the calibration from two Cf252 sources by about 30 times may lead to substantial count rate (respectively SNM mass) correction error. Therefore, we have used a neutron generator placed in the centre of the FNEM cavity as a neutron source with variable intensity of neutron flux. It should be noted that unlike the radioactive sources , we don't know the exact value of the NG neutron flux.
The neutron flux was controlled by changing the neutron generator's acceleration voltage and beam current, which provides a dynamic range greater than a factor of 10. Two types of measurements were performed: one with PDT-110A and another with KM200 electronics with a switching relay that allows us to measure $N_{100\%}$ and $N_{200\%}$. The KM200 electronics were mounted on an aluminium junction box that contains the HV and a switching relay circuitry. The preamps were gain matched and the plateau characteristics were tested in both switching configurations to make sure that the additional capacitance does not change the threshold. We switched only the top two detectors (#1 and #3) in the first ring of the FNEM shown on Fig.3. During the first measurement, each detector was connected to its own preamplifier. We recorded the individual count rates to make sure that each detector sees roughly the same count rate. We used the average of the count rates of detector 1 and detector 3 to represent $N_{100\%}$. The second measurement was performed with detector #3 disconnected from preamplifier 3 and connected to preamplifier 1 which provided the count rate in DT measurement condition $N_{200\%}$.

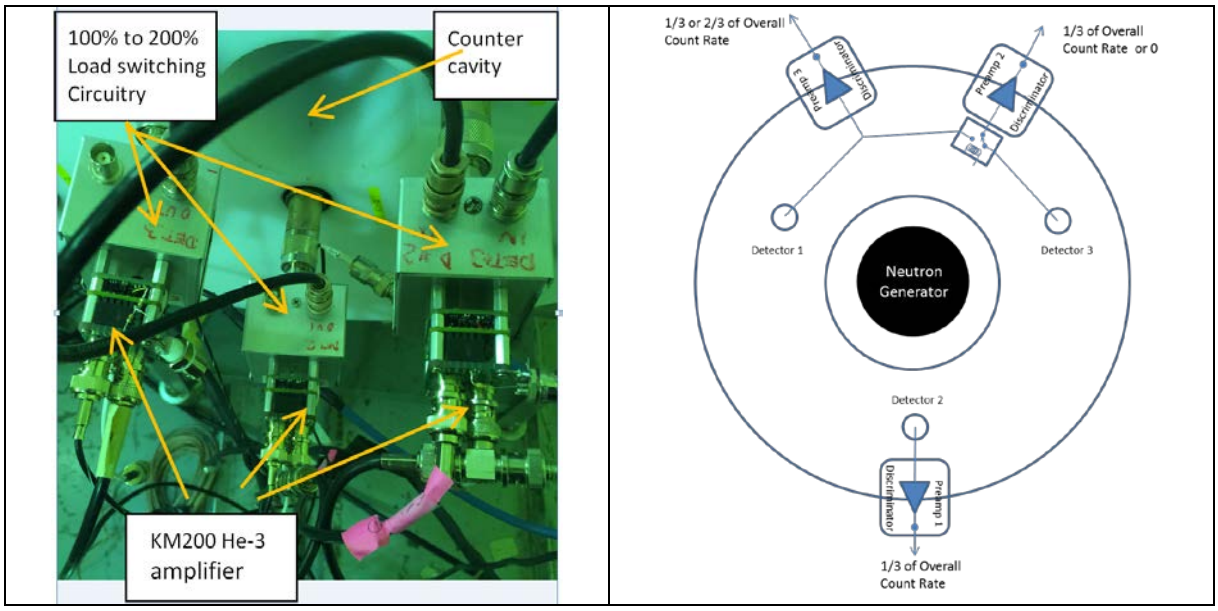

Fig.3 Left: Top view of FNEM with preamplifiers and switching boxes installed on inner ring of tubes. Right simplified switching diagram.

The count rates $N_{100\%}\ and\ N_{200\%}$, corresponding to one and two tubes per amplifier, were measured for each intensity setting of the neutron generator. The load per amplifier and count rate data for each were recorded using a JSR-15 shift register. Using the analytical expressions derived in section two based on paralyzing dead time, we have calculated the incident neutron rate N_{IN} per amplifier. The measured count rates for PDT-110 (one tube per amplifier) and KM200 (one and two tubes per amplifier) are plotted in Fig 4.
The corrected output count rate Nout=Nin is used to calculate the dead time losses and corresponding dead time td based on the paralyzing DT model. In order to compare these results we also calculated and compared the KM200 and PDT-110A dead time using classical empirical and self-calibration methods for correction of counting losses.; . The plot on Fig.5 compares the calculated DT behaviour for:

- PDT dead time from the paired source calibration (see section 2) calculated as 1.62 μs for 40 000 cps, and 1.54 μs for 83000 cps input count rate per tube;
- PDT-110A dead time using NG versus input count rate from self-calibration method ;
- KM200 dead time using NG and self-calibration method.

The results plotted in Figure 5 show significant dead time reduction (about 30%) between the calibrated and extended range of count rates as well as good consistency in PDT dead time behaviour using paired ^{252}Cf source and NG. The deduced dead time constant (td) shows a reduction in value for higher count rates. This is a clear indication that the real dead time losses do not follow the exponential dependency of the paralyzing DT model. The correction of counting losses using equations /6,7/ for non-paralyzing DT model provided even higher dead time constant dependence with positive slope. Therefore we used the correction data based on paralyzing DT that has lower dead time deviation at the maximal count rate range and thus fits better for that particular case.

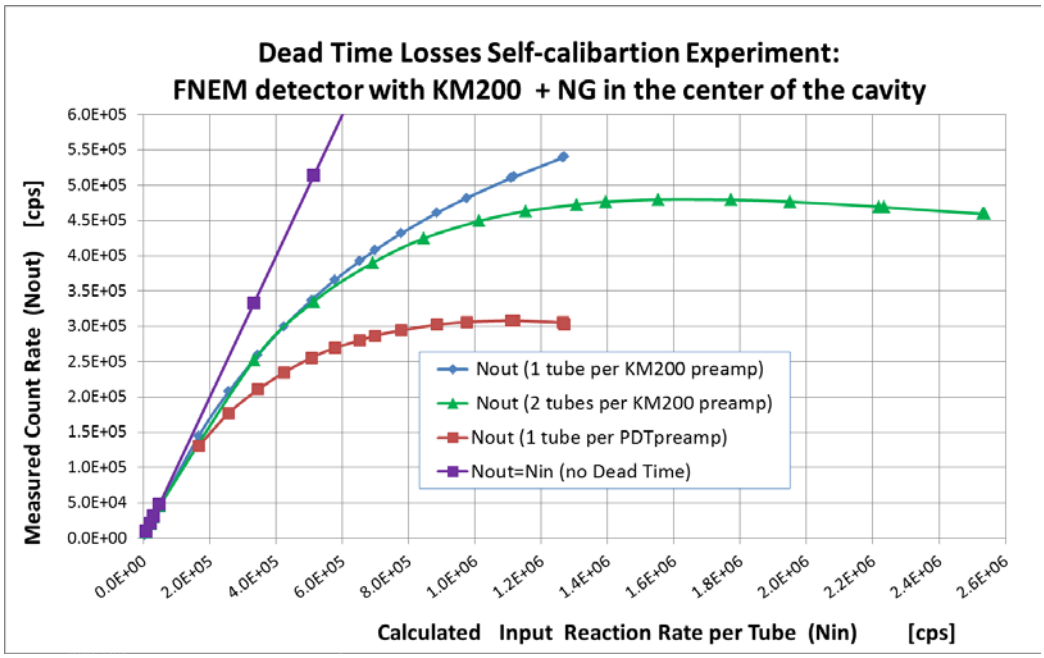

Figure 4. Measured count rates per amplifier versus (determined) input count rates for the KM200 at $N_{100\%}$ (blue) condition, KM200 at $N_{200\%}$ condition (green) and PDT110A amplifier (red) connected to one detector. The purple line represents represent the corrected count rate (Nout=Nin).

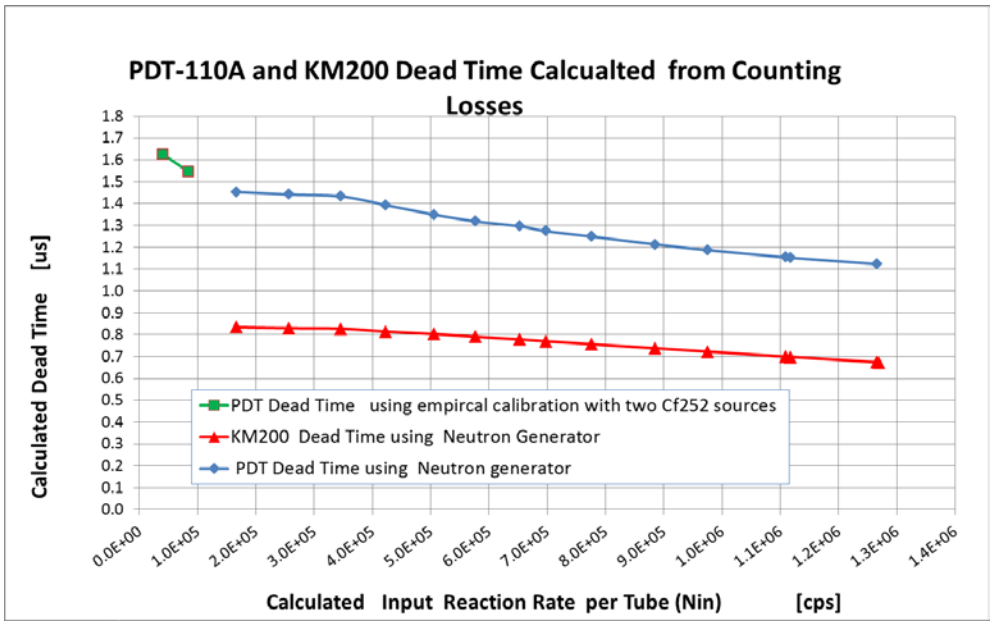

Figure 5. DT versus input reaction rate. Green: PDT-110A DT using a pair of ^{252}Cf sources [10]. Blue: PDT-110A DT using a NG and empirical method for correction of counting losses. Red: KM200 dead time using NC and self-calibration method for correction.

It should be noted that neither the non-paralyzing nor the paralyzing models are accurate over a wide dynamic range of incoming neutron count rate. Therefore, it is necessary to perform dead time calibration near the intensities of the target measured source. This is where the proposed calibration method is most valuable. It does not rely on the extrapolation of a priori calibration at lower intensity. In order to explore and explain the count loss trend at higher count rates we ran the neutron generator in pulsed mode where the constant output emission rate is increased in reverse proportion to the generator duty cycle. The snapshots of the unipolar (current pulse) and bipolar (shaper output)

signals from KM200 amplifiers, recorded at 10% duty cycle and maximum intensity of the neutron generator are shown on Fig. 6. The estimated incident rates for that setting is about 13×10^6 cps (10 times higher than maximum count rate from continuous output testing shown on fig.4.

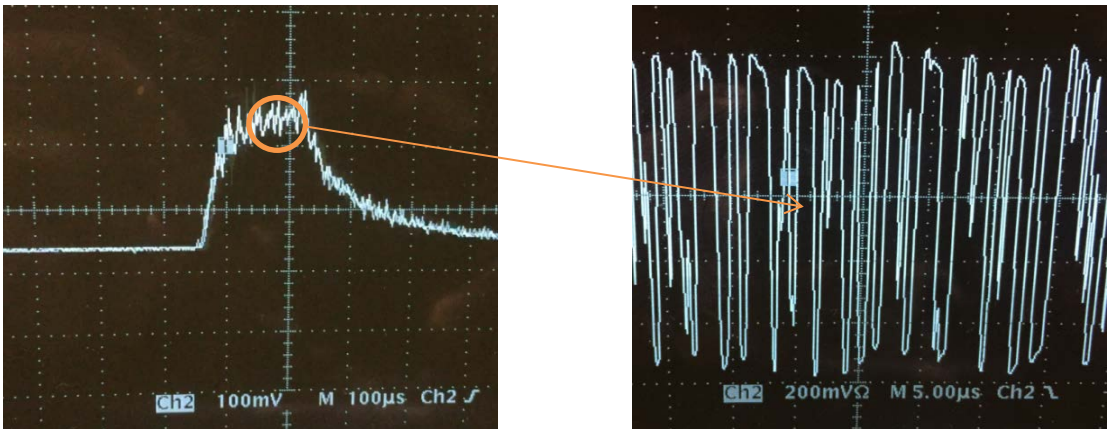

Fig. 6 Left: unipolar (current pulses) Right: The bipolar pulse output shown in expanded time scale

The pile up of detector current pulses appears as a single fluctuating pulse that does not reach the base line during the entire duration of the neutron generator pulse, consistent with the updating paralyzing dead time model. In contrast, the bipolar pulses pile-up in both directions and thus cross the baseline despite the severe pile-up (20+ pulses during the duration of shaper pulse) and thus continue to count. Because of the random phase of the pile-up the superimposed signal looks much wider than singe bipolar pulses shown on Fig.1b.

6. Implementation aspects of this method and in typical safeguards neutron systems

6.1. Active interrogation

Fission neutron detectors used in the pulsed active interrogation systems such as DDA assay for measuring of SNM have to operate at very wide dynamic range of incident count rates and thus are subject of severe counting losses. Implementation of faster tubes and electronics can improve the counting capabilities and allow analysis closer to the burst, but will not eliminate all of the counting losses. The implementation of this self-calibration method could further expand this capability by using simple switching circuitry without extensive retrofitting of existing electronics. The DT losses can be characterized by one time calibration that can give values that can be used for routine measurements. Because the DDA assay relies on singles rate measurements, DT losses are smaller and the accuracy of the calibration is not as critical as for assays based on neutron coincidence counting. Initial testing of this method in JRC PUNITA active interrogation system at JRC-Ispra will be reported in [11].

6.2. Neutron coincidence counting

Unlike singles rate measurements, neutron coincidence counting is very sensitive to the counting losses as the DT losses error of singles propagates with power 2, 3 etc, to the double, triples moments. The currently used DT loss calibration works well for low DT losses where the paralyzing DT model does not deviate much from the experimentally observed behavior of the DT losses. But an applications such as coincidence assay for measuring high mass plutonium canisters, spent fuel , etc, that are expected to operate at higher DT losses the current practice for calibration with low activity 252Cf sources may lead to substantial errors.

Here the measured count rates (S,D,T etc.) for the two hardware configurations (standard – i.e. 100% load and dead time – i.e. 200% load) can be used to extract and correct for dead time losses. Two possible methodologies are envisioned: a) extrapolate dead time free count rates from the slope of the measured count rates for 100% and 200% load; b) iterative procedure to extract and correct for dead time losses. The former approach relies on linearity of the count rate variation with preamplifier

load, which will be explored and confirmed experimentally. For more complex situations, where nonlinearities in count rate variation with preamplifier load are observed, the iterative approach will be used. The iterative approach is foreseen to use the ratios (e.g. $\frac{S_{100\%}}{S_{200\%}}; \frac{D_{100\%}}{D_{200\%}} \frac{T_{100\%}}{T_{200\%}} \frac{Q_{100\%}}{Q_{200\%}}$) for singles, doubles, triples and quads, that, if properly dead time corrected, should not depend on the load per preamplifier. We will use this fact to develop the iterative calibration procedure, where the initial estimate of dead time correction will be used to extract initial dead time corrected count rate ratios for both preamplifier loads. The dead time correction estimate will then be further iterated until close agreement between the dead time corrected ratios for 100% load and 200% load measurements is achieved.

We would like to stress that the proposed method and hardware implementation is applicable for all currently used preamplifiers (such as Amptek A-111) electronics for both shift register and list mode data acquisition.

7. Conclusion

We have presented a new hardware based method for the determination of counter dead time. This method can use the counting rates from actual unknown samples in order to determine the dead time correction constants and thus avoid the problem of extrapolating dead time coefficients determined at low counting rates to high counting rates. The hardware is relatively easy to retrofit to many existing neutron detectors. We have demonstrated the method for singles counting and shown that the dead time behaviour of typical neutron detector systems does not follow either paralyzing or non-paralyzing model precisely, but the paralyzing model is closer. The method can also be used for doubles and triples and higher moments of multiplicity counters.

8. Acknowledgments

Office of International Nuclear Safeguards in the U.S. Department of Energy/National Nuclear Security for their support for presenting this work at ESARDA conference.

8. References

[1] G. F. Knoll. “Radiation Detection and Instrumentation” -3rd ed., New York, NY: Wiely & Sons, 2010

[2] R. Jenkins, R. W. Gould, D. Gedcke. “Quantitative X-rays Spectroscopy”, New York, NY: Marcel Dekker, Inc., 1995

[3]. K. Ianakiev, M. Iliev, M. Swinhoe and N. Johnson “High Count Rate Thermal Neutron Detectors “High Count Rate Thermal Neutron Detectors “IAEA Safeguards Symposium, Vienna, 2014

[4]. Iliev, Metodi; Ianakiev, Kiril Dimitrov, Swinhoe, Martyn Thomas “KM200 Front-End Electronics for Thermal Neutron Detectors”, INMM 57th Annual Meeting, 2016-07-24/2016-07-28 (Atlanta, Georgia, United States)

[5] N. Ensslin, W. C. Harker, M. S. Krick, D. G. Langner, M. M. Pickrell, J. E. Stewart, “Application Guide to Neutron Multiplicity Counting,” LANL, Los Alamos, NM, LA-13422-M, November 1998.

[6] H.O. Menlove, M.T. Swinhoe, J.B. Marlow, et al., “Mini-Epithermal Neutron Multiplicity Counter (Mini-ENMC) Manual,” Los Alamos National Laboratory Report, LA-14350-M (2007).

[7] L. Holzleitner, M.T. Swinhoe, “Dead-time correction for any multiplicity using list mode neutron multiplicity counters: A new approach – Low and medium count-rates,” Radiation Measurements 46 (2011) 340-356.

[8] A. M. LaFleur, et al. “Characterization and performance evaluation of a new passive neutron albedo reactivity counter for safeguards measurements”, Radiation Measurements 61 (2014) 83-93.

[9]. K. Ianakiev, M. Iliev, M. Swinhoe, HIGH COUNT RATE THERMAL NEUTRON DETECTORS AND ELECTRONICS; Provisional Patent Application Serial No. 62/411,898;

[10] Hee Seo, et al. “Development of prototype induced-fission-based Pu accountancy instrument for safeguards applications”, Applied Radiation and Isotopes Volume 115, September 2016, Pages 67–73

[11] K. D. Ianakiev[1], M. L. Iliev[1], M. T. Swinhoe[1], B. Pedersen[2], G. Varasano[2], J. Crochemore[2], T. Bugucarska[2], L. Holtzlightner[2], P. De Baere[3,] S. Vaccaro[3], M. Couland[4,] « Field trial of KM200 Electronics in the JRC PUNITA Facility” , 39th ESARDA Conference, 15th-18th May 2017, Dusseldorf, Germany

Session 17

Nuclear Security

NEUTRON GENERATION BY LASER-DRIVEN PROTON SOURCES

M.Roth[1,2], V. Bagnoud[3], C. Barty,[4] M.A.M. Bourke,[5] K. Falk[6], A. Favalli[5], J. Fernandez[5], D. C. Gautier[5], S. Glenzer,[7] C. Haeffner,[4] D. Henzlova[5], J. Hornung[1], M. Iliev[5], W. Leemans,[8] A. Losko[5], I. Kishon[9], A. Kleinschmidt[1], M. Mocko[5], S. Palaniyappan[5], I. Pomerantz[9], V. Schanz[1], G. Schaumann[1], C.W. Siders,[4] M. Swinhoe[5], A. Tebartz[1], S. Vogel[5], F. Wagner[3], G. Wurden[5]

[1]Institute for Nuclear Physics, Technische Universität Darmstadt, Darmstadt, Germany
[2]Facility for Antiproton and Ion Research in Europe GmbH (FAIR GmbH)
[3]Helmholtzzentrum für Schwerionenforschung – GSI, Darmstadt, Germany
[4]Lawrence Livermore National Laboratory, Livermore, California, USA
[5]Los Alamos National Laboratory, Los Alamos, New Mexico, USA
[6]Institute of Physics of the ASCR, ELI-Beamlines, Prague, Czech Republic
[7]SLAC National Accelerator Laboratory, Menlo Park, California, USA
[8]Lawrence Berkeley National Laboratory, Berkeley, California, USA
[9]The School of Physics and Astronomy, Tel-Aviv University, Tel-Aviv, 69978, Israel

Abstract:

Ultra-intense lasers have demonstrated the capability of accelerating short pulses of intense ion beams. These ion beams have been used to generate short bursts of neutrons by irradiating a converter in close distance to the source, making this scheme a very compact and bright source of neutrons up to more than 100 MeV in energy. Using novel laser ion acceleration mechanisms directed beams of neutrons can be generated, which increases the brightness of these sources compared to previous attempts. We review the recent research and present experimental data using a mechanism based on relativistic transparency to drive the most intense laser driven neutron source and use them for first applications.

Keywords: Laser; neutron sources; active interrogation; non-destructive testing

1. Introduction

There is a growing need for small and medium sized neutron sources of high brightness [1] and ranging from thermal to multi-MeV particle energies. Applications include basic research, the use in material sciences and further industrial and medical applications. Since the advent of ultra-intense lasers the acceleration of intense ion beams has been one of the most exciting fields of research over the last decade. Those laser systems can accelerate ion beams using fields six orders of magnitude above the highest conventionally available fields and therefore have reduced the required accelerator length from meters to sub-millimeters.
The basic concept of laser driven neutron sources is to replace large conventional accelerator structures by compact laser driven ion sources and use a small converter design to form a compact neutron source. Thus one combines the large cross section for neutron evaporation and related nuclear processes with the spatial and temporal advantage of a laser driven source.
The most widely used mechanism had been discovered in 1999 and is known as the target normal sheath acceleration (TNSA) [2,3]. This mechanism is based on the charge separation at the rear surface of thin, micrometer-sized solid foils and results in short bursts of ions up to energies of 60 MeV in an exponential spectrum [4]. The ion beams usually contain protons as the predominant species as those have the highest charge to mass ration and are accelerated most efficiently by the quasi electro-static potential.
The short pulse duration of the ion beam results in a short burst of neutrons with highest brightness and allows for techniques not accessible with conventional drivers.

2. Prior research

Shortly after the discovery of laser driven proton beams by the TNSA mechanism those have been used to generate neutrons. Early experiments include the Li(p,n)Be reaction [5] and obtained 3x10^8 n/sr^{-1} using the CLF Vulcan laser in the UK and 70 J of laser energy. They also observed an anisotropy with an increased yield in the backward direction towards the laser.

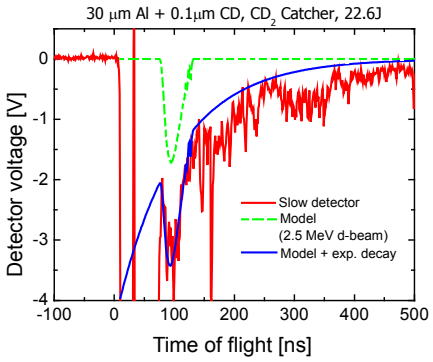

Fig. 1: one of the first nTOF measurement for neutron generation by laser driven deuterons (2000) at LULI. The neutron peak at 2.45 MeV is clearly visible in the decaying signal caused by the x-ray flash.

Experiments of our group at the LULI laser system in 2000 resulted in 4x10^8 neutrons using the d-d fusion reaction when irradiating a deuterated plastic block with deuterons (see Fig.1). A clear mono-energetic peak at 2.5 MeV was observed, which was boosted in energy in the forward direction by the beam fusion kinetics.
In 2010 Higginson et al. continued the work on neutron production using the LLNL TITAN laser system [6] and obtained 1.8x10^9 n/sr^{-1} using LiF as a converter and 120 J of energy. They calculated those numbers to be sufficient enough for neutron resonance spectroscopy as a possible application. A year later the same group succeeded in getting 8x10^8 n/sr^{-1} via the same reaction using 360 J of laser energy on the same facility [7]. This time they also increased the neutron energy up the 18 MeV and observed a forward peaked intensity distribution. At a smaller laser system, but at a high repetition rate, the university of Michigan also obtained a directed neutron emission up to 1x10^8 n/sr^{-1}, energies up to 16 MeV and a conversion efficiency of 10^{-5} from laser to neutron energy using 10^{21} W/cm^2 pulses [8]. Here the group used a deliberate deuterium contaminant layer at the rear surface to enhance the neutron production via the TNSA mechanism. As all the cross sections and the directionality of the emitted neutrons are energy dependent and the use of deuterium instead of protons is advantageous due to the additional neutron present in the latter a novel mechanism was investigated to enhance the neutron emission.

3. Relativistic Transparency

Relativistic transparency occurs, when the motion of the electrons in the laser results in an increased inertia caused by the relativistic mass increase as the electrons approach the speed of light. As the electrons are no longer able to follow the laser oscillation and their number is decreasing due to the expulsion by the ponderomotive force of the laser the target becomes transparent for the laser frequency. So a target becomes relativistic transparent when $N/\gamma \leq 1 < N$ with $N = n_e/n_{cr}$ the normalized target electron density, $n_{cr} = m_e\omega_0^2/(4\pi e^2)$ the critical electron density and $\gamma=(1-(v/c)^2)^{-½}$.
At this point the laser interacts with the entire target volume and efficiently accelerates the bulk material [9]. In contrast to the TNSA now all the ions are accelerated, which opens the possibility to use the most efficient neutron conversion reaction.
Two important developments were required to experimentally confirm this new mechanism, the reliable production of sub-micrometer free standing target foils [10,11] and the enhancement of the laser contrast, i.e. the ratio of unwanted light prior to the main pulse [12,13,14]. This mechanism, the so-called Break Out Afterburner (BOA), has been predicted using large scale 3D simulations on the first PFLOP computer at the Los Alamos National Laboratory (LANL) [15,16] and has meanwhile experimentally demonstrated at several laser facilities.

4. Neutron production

The most promising neutron generating reactions are the p(Be,xn)B reactions, widely used in conventional accelerator driven sources [17,18]. A highly efficient converter is therefore made of beryllium, where the length of the converter matches the range of the incoming ion beams. To further enhance the converter performance and to increase the directionality the Be converter is often surrounded by a cylinder of tungsten. If initially the proton beams is replaced by a deuteron beam the additional neutron generating breakup reaction of the deuteron yields a directed neutron beam in addition to the isotropic Be(p,n)B reaction.

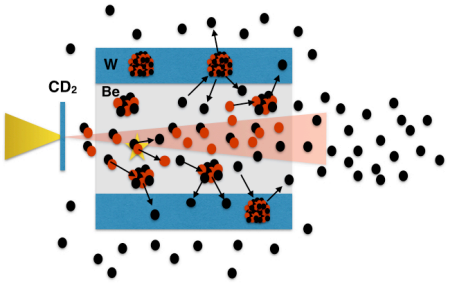

Fig. 2: nuclear reactions in the converter. In addition to the energy loss there are breakup reactions, nuclear excitation via (d,xn), (p,xn) and (n,xn) reactions in Be and W. The tungsten cylinder also reflects some of the neutrons back into the forward emission cone.

The conversion of the incident ion beam into neutrons therefore is governed by the following processes (see Fig.): 1. breakup of the deuteron as it enters the converter material, 2. neutron emission due to the Be(p(d), xn)B processes according to the energy dependent cross sections, 3. energy loss of the ions inside the converter material, 4. pre-compound reactions in the converter material for the highest neutron energies, 5. neutron scattering and W(n,xn)W reactions in the tungsten wall of the converter casing.

5. Recent Experiments

Whereas initial experiments on neutron production using the TNSA mechanism have resulted in neutron numbers that made them suitable for resonance spectroscopy, a higher conversion efficiency is needed for more demanding applications.
Recently, our group used the BOA mechanism to generate an intense beam of energetic deuterons from the bulk of deuterized plastic foils at the LANL Trident facility. The BOA mechanism also offers the possibility to efficiently accelerate ions independent of their charge to mass ratio, preferential for accelerating deuterons [19]. Different converter materials were tested, starting with copper and then changed to an encapsulated beryllium target, about 5 mm behind the plastic foil. The BOA mechanism required a precise target thickness control as if the target is too thin the target becomes transparent too soon, before the laser pulse reaches maximum intensity and the interaction is inefficient. If the target is too thick the regime of relativistic transparency cannot be reached and the ions are accelerated by the less favorable TNSA mechanism [20] (see also Fig. 5). A typical experimental setup is shown in Fig. 3. A short focal length off-axis parabolic mirror (e.g. F/1.5) is used to focus tens of Joules of one micrometer laser light of a few hundreds' femtosecond pulse. The on-target focus is a few µm in radius ($1/e^2$-condition, containing >60% of the laser energy) with a peak intensity of up to $1x10^{21}$ W/cm^2. The laser pulse duration and beam parameters have to be carefully recorded during the whole campaign. Thin, free-standing, plastic (CH_2) and deuterized plastic (CD_2) foils with thicknesses from 200 nm to 3.2 µm were then used to generate proton and deuteron beams.

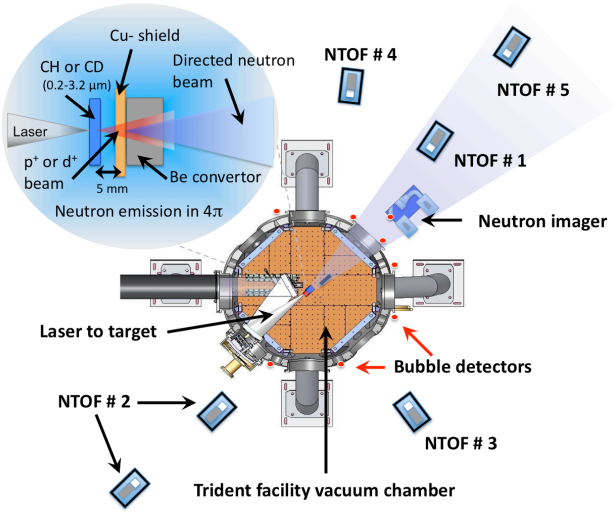

Fig. 3: Experimental setup at the LANL TRIDENT facility. The accelerator length in this case was 5 mm to the converter (upper inset). The neutron emission was monitored with NTOF detectors and bubble detectors in different directions to get energy resolved, absolute, spatial neutron distribution function.

Evaluation of the neutron generation performance requires detailed knowledge of the driver in terms of energy distribution, particle numbers and energy content, as well as beam divergence. Ideally one uses several independent diagnostics to characterize the driving ion beam for these parameters including an ion Wide Angle Spectrometer (iWASP) [21], Radiochromic Film Imaging Spectroscopy (RIS) [22] and Nuclear Activation Imaging Spectroscopy (NAIS) [23]. During the experiments at LANL in 2012, the optimum target thickness was approximately 650 nm for the CH and CD targets at which peak energies of up to 150 MeV have been measured for protons and deuterons, respectively. With thinner or thicker targets, particle energies and numbers drop rapidly (for more details, see Ref. [24]).
Neutrons can be measured using activation techniques in different materials (In, Cu, Ag), neutron time-of-flight (nTOF) methods in different directions, neutron imaging camera systems [25,26] and BTI bubble detectors[1,2] [27]. Details about our experimental setup can be found in [28].
According to the requirements in the previous chapter, the neutron converter has to have a sufficient length according to the stopping range of the deuterons, but not too long in order not to scatter or absorb too many neutrons in the desired forward direction.
Laterally, the converter can be limited in order to maintain a small source size, e.g. for point projection imaging using high energy neutrons, but this reduces the total amount of neutrons, as the ion beam diverges and more deuterons start to miss the converter material.
The neutron yield and distribution is made of two parts. a) The 4π emission of neutrons from the $^{9}Be(p,n)^{9}B$ reaction for lower energetic protons and the $^{9}Be(p,2n)^{8}B$ reaction at higher proton energies. b) the forward peaked emission from the breakup if deuterons were used.

[1] See http://www.bubbletech.ca for BTI, Bubble Technology Industries.

[2] F. Smecka and M. Hajek,
AIAU Paper No. 2007-27607, Technische Universität Wien, 2007.

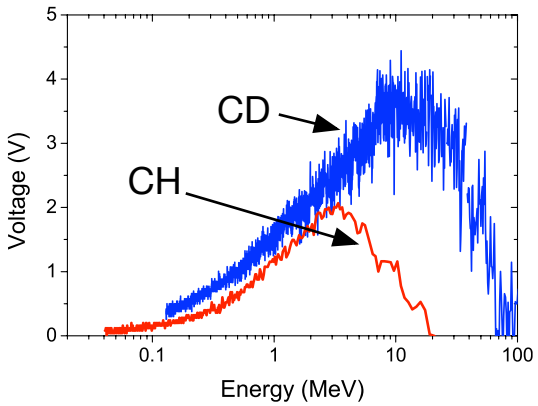

Fig. 4: Neutron spectra from a 400 nm CH foil and a 480 nm CD foil, measured with an nTOF detector.

As can be seen in Fig. 4 the efficiency in forward neutron emission as well as the neutron energy strongly increases with the use of deuterium instead of protons. For the deuteron breakup experiments we have measured almost one percent conversion efficiency and around 0.2 percent for the proton reaction.
Fig. 5 shows a result that clearly demonstrates the difference of efficient deuterium acceleration if the thickness of the target matches the optimum for the BOA mechanism with a strongly peaked neutron emission in the forward direction (0°).

6. Results

So far, recent experiments have measured record neutron yields close to 3 x 10^{10} n/sr (data from 2014, to be published soon), energies well exceeding 100 MeV and a strongly directed neutron beam [29,16]. It is important to note that due to the compact generation of the neutron beam and the ultra-short pulse duration of the driving ion beam the neutron pulse is extremely short. As the ion beam is generated and accelerated within a few picoseconds and the total length of the system, accelerator and converter structure is less than 15 cm the total pulse duration is only a few nanoseconds for the entire pulse. In fact for the ion energies between 100 MeV and 4 MeV (e.g. required for activation) the pulse in forward direction has a total length of 6.5 ns.

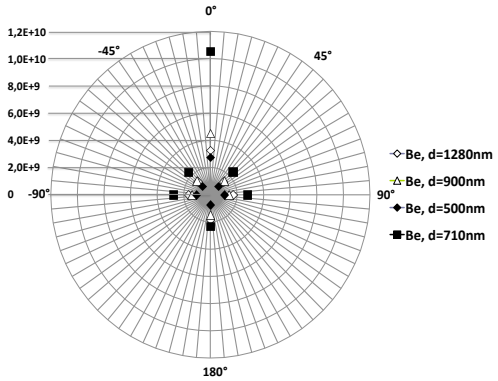

Fig. 5: Neutron production from different targets. Whereas the isotropic part is not that much sensitive, the efficient deuteron acceleration is strongly correlated to the target thickness. In this case for 10^{21} W/cm² at TRIDENT 710 nm was close to the optimum fort he BOA mechanism. The neutron emission exceeds 1x10^{10} n/sr.

But more important, the pulse duration for the beamed neutron part originating from the deuterium breakup is different as the neutron emission closely follows the initial deuterium kinetics. Thus the pulse is strongly chirped in energy having an excellent time to energy correlation and resembling the initial ps pulse duration. This would allow for excellent energy resolution for fast neutron resonance spectroscopy as one possible application.

7. Applications

The high brightness, directionality and compact format of the neutron source opens up a multitude of applications.

Radiography with neutrons.—With such an intense, directed and ultra-short neutron beam available a first laser-driven neutron image of a structured object was demonstrated [29]. The main detector for neutron radiography was a fast scintillating fiber array gated neutron imager, developed by LANL for fusion experiments at the National Ignition Facility (NIF) [26]. Neutrons, impacting into a 5 cm thick fiber array generate light that is transported through the fibers, down collimated by a coherent fiber taper, amplified by a gated micro-channel plate and finally detected in a high resolution cooled CCD camera. The scintillator is also sensitive to the large number of x-rays being produced during the initial laser target interaction. With a decay constant (1/e) of 2.5 ns, the x-ray contribution can be used for radiography or excluded from the measurement choosing a specific timing. Moreover, gating the detector well past the decay of the scintillating light caused by the prompt x rays and limiting the gate width allows for easy selection of the neutron energies, which is of special interest as this allows for the radiography of material imaging different neutron energies similar to recently observed neutron bursts using electrons as a driver [30], but with much higher neutron numbers. By varying the delay between the laser pulse and the exposure window of the imager, one is able to distinguish between the contribution of instantaneous hard-x-ray emission from the primary target and the exposure due to neutrons from several discrete energy intervals.

As right behind the converter material the neutron flux is around 10^{20} N/(cm^{2}s) the source is an excellent tool for tests on neutron damage of materials.

One application that has recently been tested successfully is the active interrogation of sensitive nuclear material using neutron activation. This application can serve in security and safeguarding environments as well as to detect nuclear material that has been lost, buried or is not directly accessible (e.g. due to destruction in accidents).

Nuclear, fissile material is exposed to the short burst of neutrons and the subsequent neutron emission is detected. Because of the short pulse duration the secondary neutron emission can be monitored shortly after the probe pulse and therefore very early in the exponentially decaying signal. Moreover, the delayed neutrons from the subsequent decay chain can be monitored as well as the response to thermal and epithermal neutrons, thus allowing for the detection of different isotopes, like ^{235}U,^{238}U and ^{239}Pu. A first experiment has been carried out in 2012 and 2014 and will be published elsewhere. This method of detection is quite insensitive to high Z shielding and therefore can be used in real environments, like container transport or behind radiation shielding.

8. Summary

The generation of neutrons using laser driven ion beams has made significant progress in the recent years. The initial experiments using the TNSA mechanism to drive an ion beam have been followed by new acceleration mechanisms based on relativistic transparency of solids with the advantage of selected ion species at very high brightness. Using the most favorable reaction of deuterium on beryllium high brightness neutron sources driven by laser systems of a few Joules of energy have been realized and the unique neutron beam characteristics have been measured. First applications like neutron radiography, the test of detector systems and the use in active interrogation have opened the field to those compact sources. As this states the very early results of this new technique and given the rapid development of short pulse laser systems this will become an exciting field of research with many useful applications.

9. References

[1] I. Anderson et al., Report of a technical meeting held in Vienna, 18–21 May 2004 (IAEA, 2005).

[2] S. P. Hatchett, C. G. Brown, T. E. Cowan, E. A. Henry, J. S. Johnson, M. H. Key, J. A. Koch, A. B. Langdon, B. F. Lasinski, R. W. Lee, et al.: Phys. Plasmas **7** (2000) 2076.

[3] S. C. Wilks, A. B. Langdon, T. E. Cowan, M. Roth, M. Singh, S. Hatchett, M. H. Key, D. Pennington, A. MacKinnon, and R. A. Snavely: Phys. Plasmas **8** (2001) 542.

[4] R. A. Snavely, M. H. Key, S. P. Hatchett, T. E. Cowan, M. Roth, T. W. Phillips, M. A. Stoyer,

E. A. Henry, T. C. Sangster, M. S. Singh, et al.: Phys. Rev. Lett. **85** (2000) 2945.
[5] K. L. Lancaster, S. Karsch, H. Habara, F. N. Beg, E. L. Clark, R. Freeman, M. H. Key, J. A. King, R. Kodama, K. Krushelnick, et al.:Phys. Plasmas **11** (2004) 3404
[6] D. P. Higginson, J. M. McNaney, D. C. Swift, T. Bartal, D. S. Hey, R. Kodama, S. Le Pape, A. Mackinnon, D. Mariscal, H. Nakamura, et al.: Phys. Plasmas **17** (2010) 100701.
[7] D. P. Higginson, J. M. McNaney, D. C. Swift, G. M. Petrov, J. Davis, J. A. Frenje, L. C. Jarrott, R. Kodama, K. L. Lancaster, A. J. Mackinnon, et al.: Phys. Plasmas **18** (2011) 100703.
[8] C. Zulick, F. Dollar, V. Chvykov, J. Davis, G. Kalinchenko, A. Maksimchuk, G. M. Petrov, A. Raymond, A. G. R. Thomas, L. Willingale, et al.: *Proc. SPIE 8779, Laser Acceleration of Electrons, Protons, and Ions II; and Medical Applications of Laser-Generated Beams of Particles II; and Harnessing Relativistic Plasma Waves III* (SPIE, 2013) p.87790N.
[9] L. Yin, B. J. Albright, D. Jung, R. C. Shah, S. Palaniyappan, K. J. Bowers, A. Henig, J. C. Ferńndez, and B. M. Hegelich: Phys. Plasmas **18** (2011) 063103.
[10] V. Liechtenstein, V. Jaggi, E. Olshanski, J. A. Scheer, P. Wurz, and S. K. Zeisler: Nucl. Instr. Methods A **613** (2010) 429.
[11] S. Palaniyappan, B. M. Hegelich, H. C. Wu, D. Jung, D. C. Gautier, L. Yin, B. J. Albright, R. P. Johnson, T. Shimada, S. Letzring, et al.: Nat. Phys. **8** (2012) 763.
[12] S. H. Batha, R. Aragonez, F. L. Archuleta, T. N. Archuleta, J. F. Benage, J. A. Cobble, J. S. Cowan, V. E. Fatherley, K. A. Flippo, D. C. Gautier, et al.: Rev. Sci. Instrum. **79** (2008) 10F305.
[13] F. Wagner, C. P. Joao, J. Fils, T. Gottschall, J. Hein, J. Korner, J. Limpert, M. Roth, T. Stöhlker, and V. Bagnoud: Appl. Physics B **116** (2014) 429.
[14] F. Wagner, S. Bedacht, A. Ortner, M. Roth, A. Tauschwitz, B. Zielbauer, and V. Bagnoud: Opt. Express **22** (2014) 29505.
[15] L.Yin, B. J. Albright, B. M. Hegelich, and J.C.Fernandez : Laser Part. Beams **24** (2006) 291.
[16] D. Jung, L. Yin, B. J. Albright, D. C. Gautier, S. Letzring, B. Dromey, M. Yeung, R. Hörlein, R. Shah, S. Palaniyappan, et al.: New J. Phys. **15** (2013) 023007.
[17] R.E. Heft and W.F. Libby: Phys. Rev. **100** (1955) 799.
[18] S. Wittlestone: J. Phys. D **10** (1977) 1715.
[19] L. Yin, B. J. Albright, B. M. Hegelich, K. J. Bowers, K. A. Flippo, T. J. T. Kwan, and J. C. Fernández: Phys. Plasmas **14** (2007) 056706.
[20] B. M. Hegelich, I. Pomerantz, L. Yin, H. C. Wu, D. Jung, B. J. Albright, D. C. Gautier, S. Letzring, S. Palaniyappan, R. Shah, et al.: New J. Phys. **15** (2013) 085015.
[21] D. Jung, R. Hörlein, D. C. Gautier, S. Letzring, D. Kiefer, K. Allinger, B. J. Albright, R. Shah, S. Palaniyappan, L. Yin, et al.: Rev. Sci. Instrum. **82** (2011) 043301.
[22] F. Nürnberg, M. Schollmeier, E. Brambrink, A. Blažević, D. C. Carroll, K. Flippo, D. C. Gautier, M. Geißel, K. Harres, B. M. Hegelich, et al.: Rev. Sci. Instrum. **80** (2009) 033301.
[23] M. M. Günther, J. Schütrumpf, A. Britz, K. Vogt, K. Sonnabend, and M. Roth: Fusion Sci. Technol. **61** (2012) 231.
[24] D. Jung, L. Yin, B. J. Albright, D. C. Gautier, S. Letzring, B. Dromey, M. Yeung, R. Hörlein, R. Shah, S. Palaniyappan, et al.: New J. Phys. **15** (2013) 023007.
[25] C. R. Christensen, C. W. Barnes, G. L. Morgan, M. Wilke, and D. C. Wilson: Rev. Sci. Instrum. **74** (2003) 2690.
[26] G. P. Grim, G. L. Morgan, M. D. Wilke, P. L. Gobby, C. R. Christensen, and D. C. Wilson: Rev. Sci. Instrum. **75** (2004) 3572.
[27] R. H. Olsher, T. D. McLean, M. W. Mallett, L.L. Romero, R. T. Devine, and J. M. Hoffman: Radiat. Prot. Dosim. **126** (2007) 326.
[28] D. Jung, K. Falk, N. Guler, O. Deppert, M. Devlin, A. Favalli, J. C. Fernandez, D. C. Gautier, M. Geissel, R. Haight, et al.: Phys. Plasmas **20** (2013) 056706.
[29] M. Roth, D. Jung, K. Falk, N. Guler, O. Deppert, M. Devlin, A. Favalli, J. Fernandez, D. Gautier, M. Geissel, et al.: Phys. Rev. Lett. **110** (2013) 044802.
[30] I. Pomerantz, E. McCary, A. R. Meadows, A. Arefiev, A. C. Bernstein, C. Chester, J. Cortez, M. E. Donovan, G. Dyer, E. W. Gaul, et al.: Phys. Rev. Lett. **113** (2014) 184801.

Changes to the ^{252}Cf neutron spectrum caused by source encapsulation

R. Weinmann-Smith[1,2], S. Croft[3], M.T. Swinhoe[1], , A. Enqvist[2]

[1]Safeguards Science and Technology Group (NEN-1), Nuclear Nonproliferation Division, Los Alamos National Laboratory, NM 87545, USA
E-mail: swinhoe@lanl.gov , rweinmann@lanl.gov

[2]Nuclear Engineering Department, University of Florida, Gainesville, FL 32611, USA
E-mail: enqvist@mse.ufl.edu

[3]Safeguards and Security Technology, Nuclear Security & Isotope Division, Oak Ridge National Laboratory, One Bethel Valley road, Oak Ridge, TN 37831, USA
E-mail: crofts@ornl.gov

LA-UR-17-22582

Abstract: *Lightly encapsulated ^{252}Cf sources are commonly used to characterize and calibrate neutron detectors for safeguards applications without much attention being paid to what it means for the encapsulation to be neutronically "light". In this work we quantify the impact of encapsulation on both the neutron spectrum and neutron intensity. We find that a 1.3 mm shell of copper reduces the mean energy by about 1 %. Thus encapsulation can be used to deliberately adjust the mean energy to match, for example, that of the spontaneously fissile Pu nuclides. The spectrum cannot be matched perfectly however and so the influence of encapsulation on a particular system calibration is case specific. We demonstrate using encapsulation to match the Pu neutron detection efficiency for a common safeguards detector, the Active Well Coincidence Counter.*

Keywords: NDA; Monte Carlo; Prompt Fission Neutron Spectrum, ^{252}Cf, encapsulation

1. Introduction

Monte Carlo modeling is a well established way to make performance estimates of neutron assay systems for safeguards [1]. The models may be benchmarked against experimental results obtained using sealed sources containing ^{252}Cf, which is a convenient source of spontaneous fission neutrons, as a surrogate for the materials of interest. Often a correction is needed to allow for the difference between the energy spectrum of the ^{252}Cf neutrons and the neutron emission spectrum of interest. For a lightly encapsulated ^{252}Cf source the prompt fission neutron spectrum from ^{252}Cf may be approximated reasonably well by simple analytical shapes. For instance in ISO 8529 [2] a Maxwellian distribution with a temperature parameter of 1.42 MeV corresponding to a mean energy of 2.13 MeV is recommended. Fröhner [3] makes the case for the next simplest macroscopic representation, namely the Watt spectrum, with a temperature parameter equal to 1.175 MeV and the fragment kinetic energy per nucleon parameter of 0.359 MeV corresponding to a mean energy of approximately 2.122 MeV. The meaning of light encapsulation is, however, not quantified in the literature. Presumably the Amersham X1 capsule [4] would qualify. This is a cylindrical assembly about 10 mm long and 7.8 mm

in diameter with a combined wall thickness of roughly 1.6 mm of stainless steel. But it is well established that even such a modest capsule perturbs the angular distribution from what would otherwise be a near perfect isotropic pattern coming from the small amount of ^{252}Cf source material inside into a anisotropic distribution with near cylindrical symmetry about the axis of the capsule [4,5]. When calibrating a fluence measuring device correction factors for the anisotropic emission of the source must be made [4-7]. Less well known is the impact on the neutron spectrum caused by neutron interactions in the source encapsulation. Whether the difference between a 1 mm and a 3 mm stainless steel container, or some other jacketing material, matters or not clearly depends on the detailed response function of the system. However, the lack of general guidance on what constitutes a lightly encapsulated source and the general neglect of the effect of encapsulation on the neutron spectrum in the scientific literature means it is difficult to make an informed judgment. In this work we take a step to resolving this dilemma by analyzing the effect of encapsulation on a specific system.

In Section 2 we present a simple analysis justifying why encapsulation needs to be considered in neutron metrology and establishing that for common source types spectral indices might be expected to exhibit a linear behavior with wall thickness. In Section 3 we draw on published results taken from a report [8] in which the authors were deliberately trying to moderate the spectrum of ^{252}Cf and ^{241}Am/Be(α,n) sources as an alternative to using accelerator facilities to obtain a variety of spectra for calibration of neutron dosimetry instruments. In particular we show how the mean energy from ^{252}Cf surrounded by spherical shells scales roughly linearly with shell thickness. In real situations we are concerned with the full energy distribution, as modified by all reaction channels, and also with potential losses and gains to the number of neutrons emerging per initial source neutron. This was studied in Section 4 through a series of Monte Carlo simulations using the Los Alamos MCNP6 code [9, 10]. The effects of spheres of common materials were simulated, along with some common commercial encapsulations. Finally the spectrum modification was coupled to the Active Well Multiplicity Counter (AWCC) [11] detection efficiency, and the source encapsulation was modified to match the detection efficiency of ^{240}Pu. Manufactured cylindrical encapsulation was measured for verification.

2. A simple analysis

We might intuitively expect that simple spectral indices of the emergent neutron spectrum will vary linearly with the thickness of the encapsulation when the thickness is small. Consider as an example how the mean energy for a point emitter located at the centre of a thin spherical shell of encapsulating material will shift as a function of shell thickness under the approximation that the only reaction of significance taking place is elastic scattering. Because of the assumption that the source is lightly encapsulated the probability, p_s, that a neutron will scatter on its way out is given, to first order, by

$$p_s = \Sigma_s t \ll 1$$

where Σ_s is the macroscopic scattering cross section of the shell material and t is its thickness.

Thus, a fraction $(1 - p_s)$ of neutrons emerge without scattering and without suffering any energy loss. The neutrons that do scatter will lose on average an energy of half the amount of the maximum energy that can be transferred to the target nucleus as recoil kinetic energy under the additional assumption that the scattering is isotropic in the center of mass reference frame. Thus, we can write the mean fractional neutron energy loss, f, as

$$f = \frac{2A}{(1+A)^2}$$

where A is the ratio of the mass of the target nucleus to that of the rest mass of the neutron. For an element we may take, to a good approximation, A to be numerically equal to the molar mass in g.mol^{-1}.

The mean energy of the scattered neutrons, $\bar{E}_s$, is consequently lower than the mean energy, $\bar{E}$, of the emitting source and can be expressed as

$$\bar{E}_s = \bar{E}(1-f) = \bar{E}\left(1 - \frac{2A}{(1+A)^2}\right)$$

The mean energy of the emerging spectrum of neutrons, $\bar{E}_{ext}$, is formed from the contributions of both the unscattered and scattered neutrons and becomes

$$\bar{E}_{ext} = (1-p_s)\,\bar{E} + p_s\bar{E}_s = (1-p_s)\,\bar{E} + p_s\bar{E}\left(1 - \frac{2A}{(1+A)^2}\right)$$

which upon rearrangement and substitution yields

$$\bar{E}_{ext} = \bar{E}\left(1 - \frac{2A}{(1+A)^2}\Sigma_s t\right)$$

This formula predicts that for an idealized scattering capsule the mean emergent energy will fall linearly with wall thickness. Real capsules can drop energies more effectively through inelastic processes and other channels such as (n,2n) interactions. The latter is also an example of a neutron gain process, in contrast (n,α) interactions are an example of a neutron loss process. Although we did not consider these kinds of interaction in the simple view presented, for a thin wall, the basic idea remains sound. Thus, we anticipate the ratio between the emergent mean energy and that of the ideal unencapsulated source to trend roughly as follows

$$R = \frac{\bar{E}_{ext}}{\bar{E}} = 1 - bt$$

where b is a coefficient specific to the composition and density of the wall material.

3. Illustration using literature data

Hsu and Chen [8] performed a series of calculations in which ^{252}Cf was placed at the center of spheres of various radii and of various materials to see if they could create reference spectra that would be useful for calibrating health physics instruments. Spheres of radius 25.4, 50.8, 76.2, 101.6, 153.2 and 20.32 mm were selected. Twelve materials were studied Be, graphite, Al, Fe, Cu, Pb, LiD, H_2O, D_2O, polyethylene $(CH_2)_n$, glass and concrete. Neutron spectra at 500 mm from the center were computed. The results are presented graphically and are difficult to interpret. Gains and losses are not quantified. The mean energy as a function of wall thickness is given numerically only in the case of copper. With zero wall thickness the mean energy is given as 2.54 MeV. This is far higher than the generally accepted value of about 2.12 to 2.13 MeV [2,3]. However, by forming the ratio of the emergent spectrum to the initiating spectrum we expect that this apparent bias will be largely suppressed. The results of our analysis are summarized in Table 1.

Table 1: Summary of results taken from [8] for the case of ^{252}Cf at the center of Cu spheres

Sphere Radius (mm)	Mean Energy Ratio, R	Fit $R = e^{-bt}$
0	1.0000	1.0000
25.4	0.8228	0.8182
50.8	0.6692	0.6694
76.2	0.5433	0.5477
101.6	0.4449	0.4481
153.2	0.2957	0.2981
203.2	0.1992	0.2008

Also shown in Table 1 is the result of a fit to the data of the form

$$R = e^{-bt}$$

which reduces to the linear form ($R \approx 1 - bt$) expected for thin shell walls when $bt \ll 1$. In the present case the exponential fit produces an excellent fit across the whole range of spheres modeled with $b = 0.0079\, mm^{-1}$. This is also evident from Figure 1. It is also apparent from Figure 1 that a copper sphere with a radius greater than about 10 or 20 mm cannot be considered thin in the context of our earlier simple theoretical development. A radius (wall thickness) of a few mm falls in the linear range and we see that to get a 1% shift in mean energy requires a wall thickness of about $0.01/0.0079 = 1.27$ mm of Cu; this equates to a shift of about 21 keV in the mean energy. For the HLNCC-II (ref), a common thermal well counter with a single ring of ^{3}He filled proportional counters, the fractional change in detection efficiency in the vicinity of 2 MeV is about 17% per MeV [12]. Thus a 21 keV reduction in mean energy translates into a projected relative increase in efficiency of about 0.36% (from about 0.1750 counts per neutron to about 0.1756 counts per neutron. This is a change which is readily measureable.

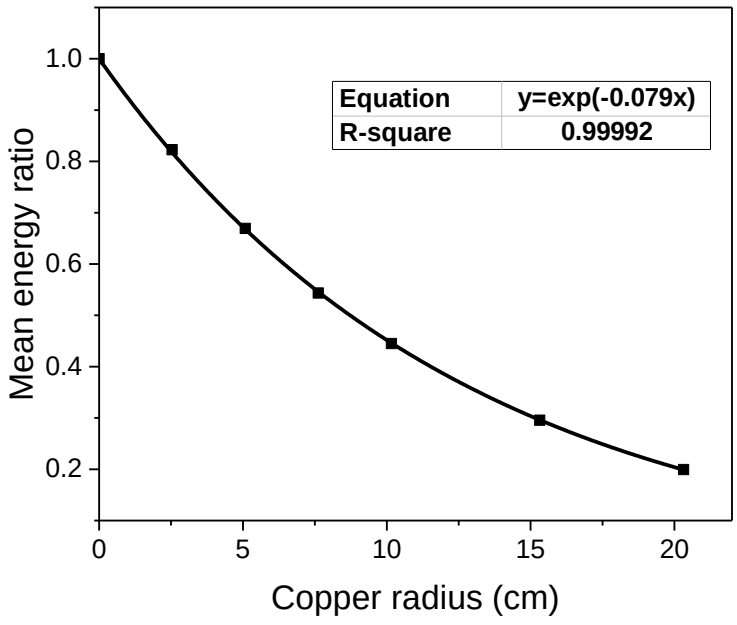

Figure 1. Plot of mean energy ratio, R, as a function of moderator radius, t, taken from [8] for the case of ^{252}Cf at the center of Cu spheres along with the fitted result as listed in Table 1.

4. Detailed modeling

Although instructive the results of Hsu and Chen are not in a form and do not cover the range of interest relevant to our present discussion – which is the use of lightly encapsulated sources typical of those obtained from a variety of vendors and used routinely in safeguards laboratories. For this reason we performed a series of focused Monte Carlo simulations. These calculations give not only the mean energy shift but the shape of the spectrum and also allow losses and gains to be tallied.

The model used the MCNP6 default energy spectrum of ^{252}Cf with a mean energy of 2.13 Mev, starting at a point source at the origin. The energy was tallied over a sphere centered at the origin with a radius of 300 mm. Figure 2 shows the average energy of neutrons crossing this sphere as a function of thickness of copper. The mean energy of prompt fission neutrons from ^{240}Pu spontaneous fission, again using the default MCNP6 energy spectrum is 1.93 MeV. Using the exponential relationship shown in Figure 2, we would require a sphere of 13.9mm copper thickness to produce an average energy equal to that of a notional bare ^{240}Pu source.

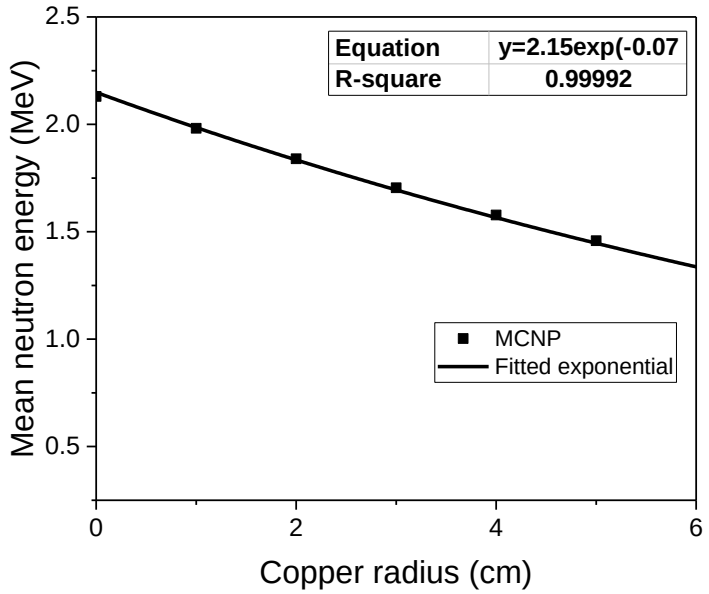

Figure 2. Mean Energy of neutrons escaping from a ^{252}Cf in a copper sphere as a function of radius (1 cm = 10 mm)

Figure 3 shows a comparison between the Hsu results [8] and our MCNP6 results. The agreement is very good at all thicknesses.

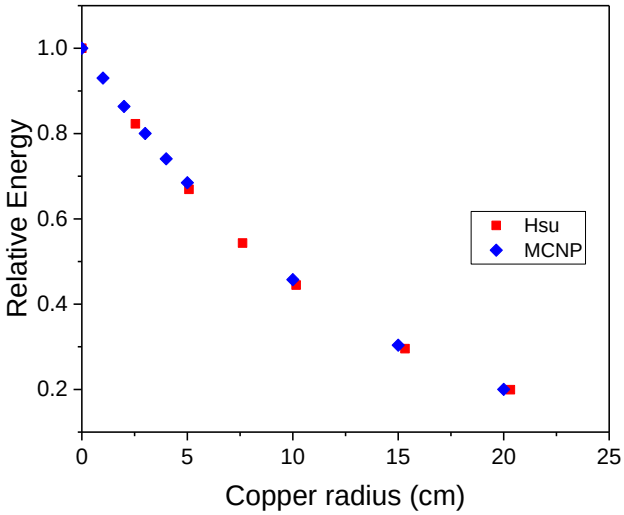

Figure 3. Comparison of our MCNP calculations and the results of Hsu et al interpreted as a relative energy to remove the obvious mean energy discrepancy in that work.

Table 2 shows the gains, losses, net neutrons, and average energy, for spheres of the materials calculated in MCNP for thicknesses between 1 and 20 cm. The gains, losses, and net values are per source neutron. Lead has the least effect on the average energy while polyethylene has the most. Beryllium's (n.2n) reaction causes a 6.5% increase in emitted neutrons at a thickness of 15 cm. Stainless steel has a negligible net intensity effect but a potentially significant energy effect at the thicknesses of common encapsulations.

Table 2. Effects of spherical encapsulation of various materials on a Cf-252 source

Aluminum (cm)	1	2	3	4	5	10	15	20
Gains	6.28E-7	1.22E-6	1.73E-6	2.22E-6	2.64E-6	4.25E-6	5.71E-6	6.66E-6
Losses	3.82E-4	7.50E-4	1.11E-3	1.45E-3	1.79E-3	3.33E-3	4.70E-3	6.00E-3
Net	1.00E+0	9.99E-1	9.99E-1	9.99E-1	9.98E-1	9.97E-1	9.95E-1	9.94E-1
Average energy(MeV)	2.07E+0	2.02E+0	1.96E+0	1.91E+0	1.85E+0	1.58E+0	1.32E+0	1.08E+0
Beryllium (cm)	1	2	3	4	5	10	15	20
Gains	3.07E-2	5.87E-2	8.41E-2	1.07E-1	1.28E-1	2.02E-1	2.43E-1	2.65E-1
Losses	2.00E-2	3.83E-2	5.50E-2	7.05E-2	8.50E-2	1.37E-1	1.78E-1	2.28E-1
Net	1.01E+0	1.02E+0	1.03E+0	1.04E+0	1.04E+0	1.06E+0	1.07E+0	1.04E+0
Average energy(MeV)	2.00E+0	1.87E+0	1.74E+0	1.60E+0	1.47E+0	8.78E-1	4.79E-1	2.48E-1
Concrete (cm)	1	2	3	4	5	10	15	20
Gains	8.84E-7	1.47E-6	2.06E-6	2.72E-6	3.21E-6	1.04E-5	6.38E-4	5.81E-3
Losses	9.42E-4	1.85E-3	2.74E-3	3.61E-3	4.48E-3	1.27E-2	4.96E-2	1.38E-1
Net	9.99E-1	9.98E-1	9.97E-1	9.96E-1	9.96E-1	9.87E-1	9.50E-1	8.62E-1

Average energy(MeV)	2.05E+0	1.97E+0	1.88E+0	1.80E+0	1.71E+0	1.29E+0	9.21E-1	6.41E-1
Copper (cm)	1	2	3	4	5	10	15	20
Gains	5.19E-5	9.91E-5	1.42E-4	1.82E-4	2.14E-4	3.25E-4	3.82E-4	4.07E-4
Losses	2.22E-3	4.61E-3	7.22E-3	1.01E-2	1.32E-2	3.48E-2	7.05E-2	1.25E-1
Net	9.98E-1	9.95E-1	9.93E-1	9.90E-1	9.87E-1	9.65E-1	9.30E-1	8.75E-1
Average energy(MeV)	1.98E+0	1.84E+0	1.70E+0	1.58E+0	1.46E+0	9.75E-1	6.47E-1	4.26E-1
Heavy Water (cm)	1	2	3	4	5	10	15	20
Gains	8.53E-4	1.64E-3	2.38E-3	3.06E-3	3.69E-3	6.20E-3	7.85E-3	8.92E-3
Losses	7.43E-4	1.44E-3	2.16E-3	2.69E-3	3.24E-3	5.46E-3	7.03E-3	8.39E-3
Net	1.00E+0	1.00E+0	1.00E+0	1.00E+0	1.00E+0	1.00E+0	1.00E+0	1.00E+0
Average energy(MeV)	1.98E+0	1.83E+0	1.68E+0	1.54E+0	1.40E+0	8.54E-1	5.02E-1	2.91E-1
Iron (cm)	1	2	3	4	5	10	15	20
Gains	3.25E-5	6.05E-5	8.59E-5	1.10E-4	1.31E-4	2.03E-4	2.43E-4	2.61E-4
Losses	8.69E-4	1.70E-3	2.56E-3	3.41E-3	4.28E-3	8.90E-3	1.40E-2	2.05E-2
Net	9.99E-1	9.98E-1	9.97E-1	9.97E-1	9.96E-1	9.91E-1	9.86E-1	9.80E-1
Average energy(MeV)	2.02E+0	1.91E+0	1.80E+0	1.70E+0	1.60E+0	1.18E+0	8.79E-1	6.77E-1
Glass (cm)	1	2	3	4	5	10	15	20
Gains	7.80E-7	1.34E-6	2.14E-6	2.84E-6	3.53E-6	6.15E-6	8.30E-6	9.46E-6
Losses	1.23E-3	2.43E-3	3.62E-3	4.78E-3	5.92E-3	1.12E-2	1.59E-2	2.00E-2
Net	9.99E-1	9.98E-1	9.96E-1	9.95E-1	9.94E-1	9.89E-1	9.84E-1	9.80E-1
Average energy(MeV)	2.09E+0	2.04E+0	1.99E+0	1.95E+0	1.90E+0	1.65E+0	1.39E+0	1.14E+0
Graphite (cm)	1	2	3	4	5	10	15	20
Gains	0.00E+0	0.00E+0	0.00E+0	0.00E+0	0.00E+0	0.00E+0	0.00E+0	0.00E+0
Losses	1.37E-4	2.66E-4	3.87E-4	5.01E-4	6.09E-4	1.06E-3	1.42E-3	1.92E-3
Net	1.00E+0	1.00E+0	1.00E+0	9.99E-1	9.99E-1	9.99E-1	9.99E-1	9.98E-1
Average energy(MeV)	2.08E+0	2.02E+0	1.96E+0	1.90E+0	1.84E+0	1.50E+0	1.17E+0	8.67E-1
Water (cm)	1	2	3	4	5	10	15	20
Gains	0.00E+0	0.00E+0	0.00E+0	0.00E+0	0.00E+0	6.62E-8	1.99E-8	1.99E-8
Losses	3.28E-4	8.30E-4	3.11E-3	1.14E-2	3.06E-2	3.06E-1	6.25E-1	8.17E-1
Net	1.00E+0	9.99E-1	9.97E-1	9.89E-1	9.69E-1	6.94E-1	3.75E-1	1.83E-1
Average energy(MeV)	1.94E+0	1.75E+0	1.57E+0	1.41E+0	1.25E+0	6.93E-1	3.79E-1	2.08E-1

Lead (cm)	1	2	3	4	5	10	15	20
Gains	5.24E-4	1.01E-3	1.46E-3	1.88E-3	2.27E-3	3.80E-3	4.81E-3	5.45E-3
Losses	2.62E-4	6.06E-4	9.46E-4	1.25E-3	1.13E-3	2.98E-2	4.51E-3	6.31E-2
Net	1.00E+0	1.00E+0	1.00E+0	1.00E+0	1.00E+0	1.00E+0	1.00E+0	9.99E-1
Average energy(MeV)	2.07E+0	2.00E+0	1.94E+0	1.88E+0	1.83E+0	1.56E+0	1.33E+0	1.14E+0
Lithium Deuteride (cm)	1	2	3	4	5	10	15	20
Gains	7.71E-4	1.45E-3	2.07E-3	2.62E-3	3.11E-3	4.84E-3	5.82E-3	6.35E-3
Losses	1.89E-3	4.65E-3	9.46E-3	1.35E-2	2.03E-2	1.00E-1	2.71E-1	4.78E-1
Net	9.98E-1	9.96E-1	9.93E-1	9.88E-1	9.81E-1	9.02E-1	7.32E-1	5.25E-1
Average energy(MeV)	1.95E+0	1.77E+0	1.61E+0	1.44E+0	1.29E+0	7.06E-1	3.62E-1	1.79E-1
Polyethylene (cm)	1	2	3	4	5	10	15	20
Gains	0.00E+0	0.00E+0	0.00E+0	0.00E+0	0.00E+0	0.00E+0	0.00E+0	0.00E+0
Losses	8.30E-5	9.10E-4	7.62E-3	2.98E-2	7.39E-2	4.81E-1	7.83E-1	9.14E-1
Net	1.00E+0	9.99E-1	9.92E-1	9.70E-1	9.26E-1	5.19E-1	2.17E-1	8.59E-2
Average energy(MeV)	1.89E+0	1.66E+0	1.44E+0	1.25E+0	1.08E+0	5.02E-1	2.34E-1	1.12E-1
304 Stainless Steel (cm)	1	2	3	4	5	10	15	20
Gains	3.28E-5	6.29E-5	8.88E-5	1.12E-4	1.32E-4	2.06E-4	2.43E-4	2.64E-4
Losses	1.47E-3	2.91E-3	4.34E-3	5.77E-3	7.18E-3	1.45E-2	2.39E-2	3.87E-2
Net	9.99E-1	9.97E-1	9.96E-1	9.94E-1	9.93E-1	9.86E-1	9.76E-1	9.61E-1
Average energy(MeV)	2.01E+0	1.89E+0	1.78E+0	1.67E+0	1.57E+0	1.13E+0	8.23E-1	6.10E-1

While the previous information is interesting academically, most source encapsulation encountered is standard manufactured capsules from source vendors. Variations in the capsules are introduced through spacers in the source cavity void, inner and outer capsules of different materials, and the inclusion of threaded studs or other modifications. 304L Stainless steel is the most common capsule material in our experience, but Zircalloy-2 is also used.

Physical information about the capsules as simulated is described in Table 3. The A3026 capsule is provided by Eckert & Ziegler [13]. The FTC capsules are provided by Frontier Technology Corporation [14], where s denotes a shorter version of the capsule. The FTC 10 capsules are single encapsulation. The FTC 100 capsule is the second encapsulation that surrounds a FTC 10 capsule and both were included in the simulations. FTC 10 and FTC 100 are the equivalent of Savannah River National Laboratory's SR-Cf-1X and SR-CF-100 capsules respectively. X1 capsules are provided by Amersham,

now known as QSA [15]. Table 3 shows the physical characteristics and Table 4 shows the gains, losses, net, and average energy of the spectrum. Simulations demonstrated a negligible difference between 304 and 304L SS, which is to be expected as only the concentration of carbon atoms (less than 1% overall) change.

Table 3. Common encapsulation's physical characteristics

Capsule	Material	Mass (g)	Outer diameter (cm)	Outer length(cm)
A3026	304 SS	18.4	0.942	3.6
FTC 10s	304L SS	1.7	0.551	1.19
FTC 10	304L SS	2.9	0.551	2.46
FTC 100	304L SS	15.9	0.942	3.76
Amersham X1	SS	3.1	0.782	0.98

Table 4. Common encapsulation's effects on the emergent neutrons

Capsule	Gains	Losses	Net	Average energy
A3026	1.8154E-5	7.5632E-4	9.9926E-1	2.0668E+0
FTC 10s	5.6432E-6	2.2208E-4	9.9978E-1	2.1115E+0
FTC 10	5.1108E-6	2.0717E-4	9.9980E-1	2.1128E+0
FTC 100	1.4108E-05	5.7600E-04	9.9943E-1	2.0825E+0
Amersham X1	1.0115E-5	4.4757E-4	9.9956E-1	2.0997E+0

Figure 4 shows the launch spectra of bare ^{240}Pu and bare ^{252}Cf together with the calculated spectrum from a point ^{252}Cf source inside a 13.9 mm radius sphere of copper. Although the mean energy can be easily matched, the spectra show that the shape of the tailored spectrum is non-the-less significantly different from that of ^{240}Pu. Whether this is important depends on the nature of the measurement configuration and the objectives of the experiment. For detectors with non-linear response functions matching the average energy is insufficient to match the measurement efficiency.

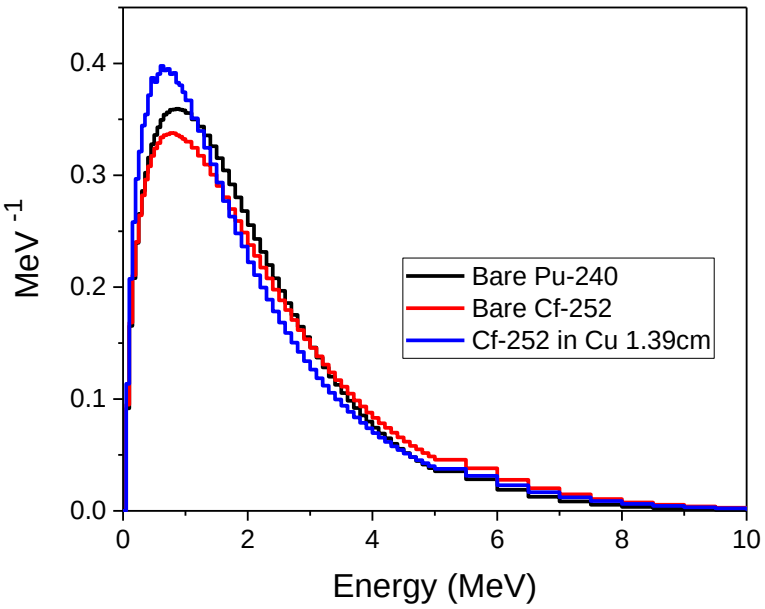

Figure 4. Normalized Spectra from bare ^{240}Pu, bare ^{252}Cf and ^{252}Cf within a 13.9mm copper sphere

A complete analysis of the effects of encapsulation is detector specific. The Active Well Coincidence Counter (AWCC) was simulated to find the encapsulation of ^{252}Cf necessary to match the ^{240}Pu efficiency and measurements were made to verify the simulations. A series of measurements were taken with cylindrical encapsulation of varying wall thicknesses of stainless steel, copper, and polyethylene. The encapsulations are shown in Figure 5. The ^{252}Cf source was A7-869 in the A3026 capsule. First, the exit spectra of the capsules were simulated. Then the measured and simulated ring ratios of the AWCC were compared. The AWCC non-linear detection efficiency as a function of neutron energy was simulated. Finally the AWCC measured and simulated efficiencies are compared, and an estimation of the encapsulation to match ^{240}Pu efficiency is given.

The AWCC can operate in thermal mode without thermal neutron absorbers or in fast mode with cadmium liners and a nickel reflection ring. In fast mode the sample cavity cadmium liner reduces the count rate in high mass samples and the cadmium liners of the interrogation source ensure a high energy interrogation flux for better penetration of large samples. In this study the fast mode was used. The cadmium liners absorb neutrons below about 0.7 eV.

The exit ^{252}Cf spectra from the capsules is shown in Figure 6, where the legend refers to the number of 0.5cm shell thicknesses. The results show that increasing encapsulation amplifies the change in spectrum. The strong thermalization efficiency of polyethylene is demonstrated by the increasing flux at lower energies, indicating a relatively bimodal distribution compared to the other materials. The absorption resonances in copper at 0.002 MeV and other energies can be seen.

Figure 5. Encapsulations with wall thicknesses of 0.5cm

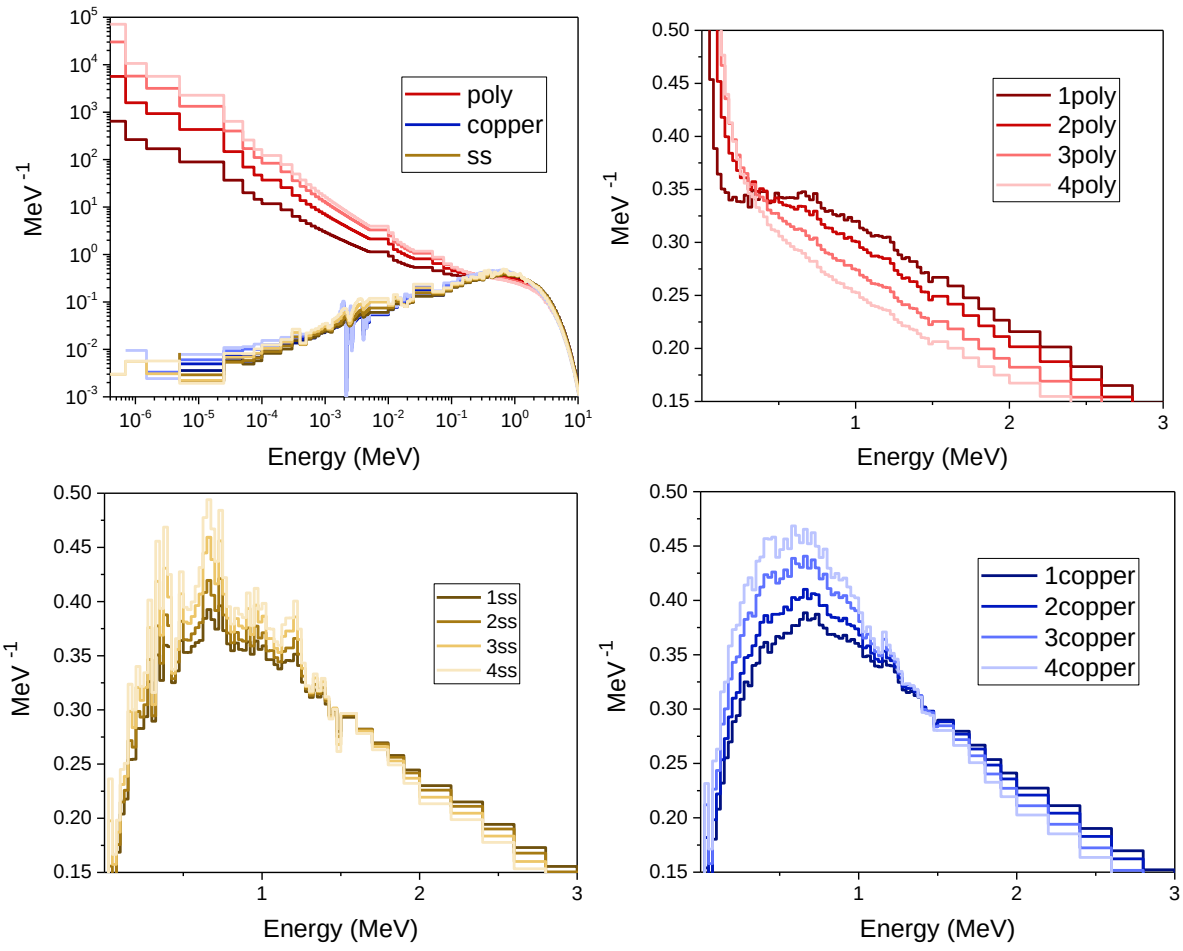

Figure 6. Exit spectra of encapsulation for the number of 0.5cm shell thicknesses. Note the log-log scale in the first figure. Individual materials are shown in a range of 0-3 MeV on a linear scale.

The AWCC has two rings of ^{3}He detectors at different depths of polyethylene, so as neutrons in a specific energy range are moderated their detection efficiency by one ring goes up while the other goes down, dampening the change in overall detector efficiency. This effect is more pronounced in neutron detectors with more rings, while single ringed neutron detectors such as the HLNCC-II [16] are more susceptible to changes in the source energy spectrum.

The ratio of the neutron counts of the two AWCC rings indicates the mean detected neutron energy. The ratio is spectrum dependent, two different spectra with the same average energy will not yield the same ring ratio. This spectral dependence occurs because the ring ratio energy dependence is nonlinear. The measurements and simulations of the ring ratio were compared to verify the accuracy of the simulations. The values were normalized to the ratio of only the standard A3026 source encapsulation to remove bias in the simulation of the detector. The results are shown in Figure 7. The relative statistical uncertainty was too small to clearly plot and was less than 0.02% for measurements and 0.09% for simulations. The measurements and simulations agree within 2 standard deviations for all cases except the 2cm shell thickness of copper. The strong agreement demonstrates that the simulation accurately simulates the measurement.

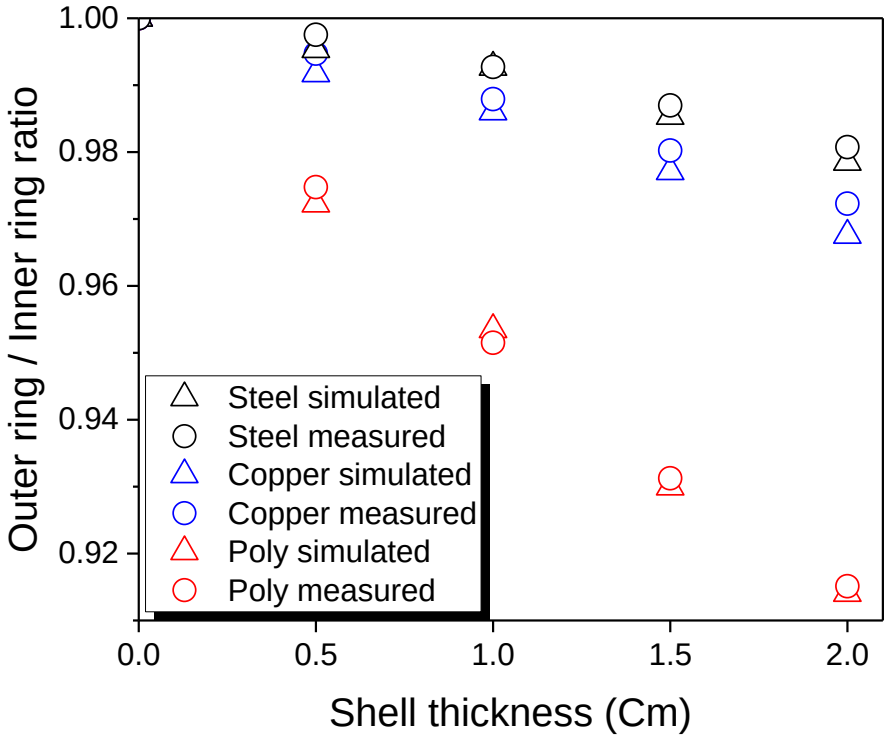

Figure 7. Measured and simulated AWCC ring ratios relative to the bare A7-869 source for various encapsulations

The AWCC response function demonstrates how a mean energy does not directly correspond to the efficiency. A spectrum of neutrons half at 0.5 MeV and half at 2.5 MeV will have a lower efficiency than neutrons at their average of 1.5 MeV. The response function was simulated and is shown in Figure 8. The peak efficiency is around 1.2 MeV. The inner ring has a higher efficiency due to geometric considerations and its peak energy is about 0.6 MeV while the outer ring peak energy is about 2.1 MeV.

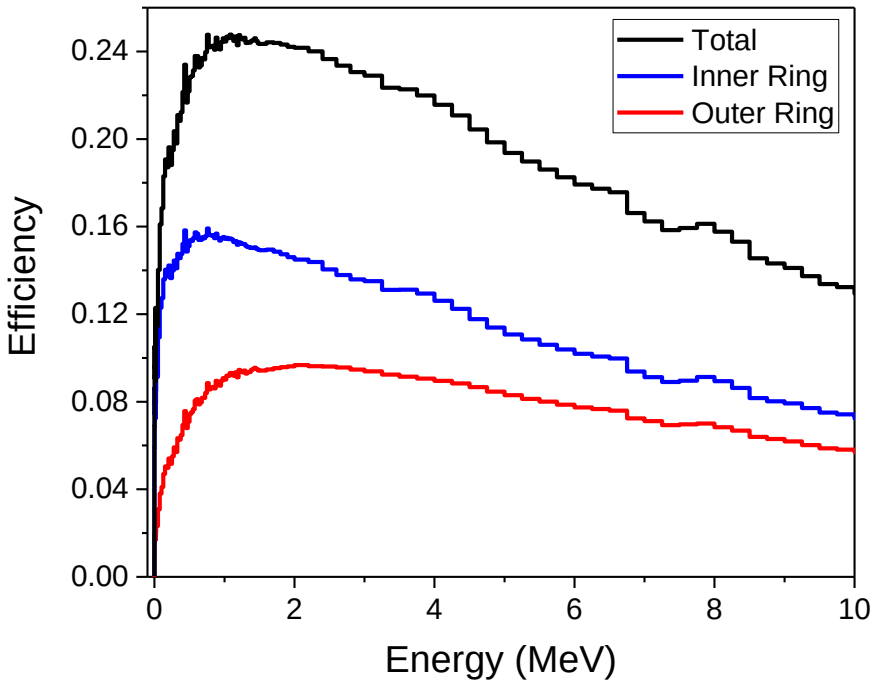

Figure 8. AWCC response function

Finally, the efficiency can be compared between the measurements and simulations to demonstrate the encapsulation's effect on the detector response. This efficiency is modified by all reaction channels and is a more accurate detector response than average energy. The result of this is shown in Figure 9 and is normalized to the efficiency of the A7-869 source in the A3026 capsule. The relative uncertainties were 0.07% for the simulations and 0.02% for the measurements, which are too small to appear in the figure. The strong agreement gives confidence to simulations of samples that were unable to be measured, namely a bare ^{240}Pu source and a bare ^{252}Cf source. The simulations of these give relative efficiencies of 0.992 and 0.980, which differ by an absolute efficiency of 0.27%. To give a bare ^{252}Cf source the same efficiency as ^{240}Pu, it can be encapsulated. The simulations demonstrate that surrounding it with A3026 encapsulation gives a relative efficiency of 1 and an additional 0.5cm of polyethylene gives a relative efficiency of 0.986, which differ from ^{240}Pu by 0.008 and -0.006 and differ by absolute efficiencies of 0.18% and -0.13%. A shell thickness of 0.35cm gives a relative efficiency of 0.992 and an absolute efficiency difference of 0.004% which is within one sigma uncertainty.

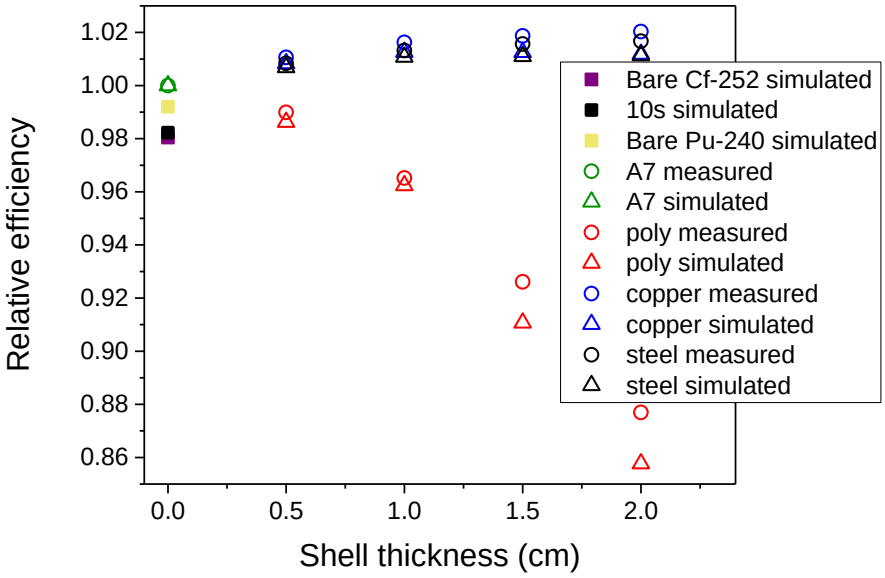

Figure 9. Simulated and measured efficiencies normalized to the A7-869 source in A3026 encapsulation

5. Conclusion

A few mm of metallic encapsulation influences the energy spectrum emerging from ^{252}Cf to a degree that is measurable in safeguards systems. This also means that the average energy of a point ^{252}Cf spontaneous fission neutron source can easily be tailored to match any lower value. This is a useful feature to exploit when using ^{252}Cf to measure the neutron detector efficiency as a surrogate for Pu sources in cases where the detector response is a simple function of energy. The modified spectrum however shows significant differences from a Pu spectrum with the same average energy and thus is unlikely to be adequate for detectors with strongly non-linear energy efficiency profiles. In non-linear response detectors such as the Active Well Coincidence Counter, Monte Carlo simulations can be used to calculate the encapsulation needed. In the AWCC a cylindrical encapsulation of polyethylene around an A7-series source with a wall thickness of 0.35cm will match the efficiency of a bare ^{240}Pu pure fission source. Conversely, this information shows the effects of unwanted encapsulation and guides the user towards a decision about an encapsulation being ‘neutronically light’.

Acknowledgements

This work was sponsored in part by the U.S. Department of Energy (DOE), National Nuclear Security Administration (NNSA), Office of Nonproliferation and Verification Research and Development (NA-22). This work was funded in part by the Consortium for Verification Technology under Department of Energy National Nuclear Security Administration award number DE-NA0002534.

References

[1] Croft, S., Favalli, A., Swinhoe, M.T. and Rael, C.D., State of the art Monte Carlo modeling of active collar measurements and comparison with experiment, Proc. 52nd Annual INMM Meeting, Palm Desert, CA, USA, July 2011

[2] International Organization for Standardization, Reference neutron radiations -- Part 1: Characteristics and Methods of Production, ISO 8529-1:2001-02-01(E), see also ISO 8529-1:2001/Cor 1:2008(F) which provide a typographical correction to Table A.4 the ^{241}Am-Be(α,n) spectrum. (2001)

[3] Fröhner, F.H., Evaluation of 252Cf prompt fission neutron data from 0 to 20 MeV by Watt spectrum fit, Nuclear Science and Engineering 106 (1990) 345-352.

[4] Bardell, A.G., Burke, M., Hunt, J.B., Tagziria H., and Thomas, D.J., Anisotropy of emission from radionuclide neutron sources, National Physical Laboratory report CIRM 24, ISSN 1369-6793. Dec. 1998.

[5] Tsujimura, N., Yoshida, T., and Momose, T., Calculations of anisotropy factors for radionuclide neutron sources due to scattering from encapsulation and support structures, Radiat. Prot. Dosim. 126(1-4) (2007) 168-173.

[6] Hawkes N.P., Freedman R., Tagziria, H., and Thomas D.J., Measurement and calculation of the emission anisotropy of an X1 252Cf neutron source, Radiat. Prot. Dosim. 126(1-4) (2007) 78-82.

[7] Roberts N.J., Jones L.N., Wang Z., Liu Y., Wang Q., Chen X., Luo H., Rong C., Králik M., Park H., Choi K.O., Pereira W.W., da Fonseca E.S., Cassette P., Dewey M.S., Moiseev N.N., and Kharitonov I.A., International key comparison of measurements of neutron source emission rate (1999-2005) – CCRI(III)-K9.AmBe, Metrologia Tech. Suppl. 06018, 48 (2011) 35pp.

[8] Hsu, H.-H. and Chen, J., Moderation of neutron spectra, Los Alamos National Laboratory report LA-UR-97-0749.

[9] Pelowitz, D.B.(Editor), MCNPX User's Manual, Version 2.7.0 Los Alamos National Laboratory report, LA-CP-11-00438 (2011).

[10] Pelowitz, D.B.(Editor), MCNPX 2.7.0 Extensions, Los Alamos National Laboratory report, LA-UR-11-02295 (2011).

[11] HO Menlove, Description and operation manual for the active well coincidence counter, Los Alamos Scientific Laboratory report LA-7823-M, (1979).

[12] Croft, S. and Chard, P.M.J., Neutronic characterization of plutonium oxide reference samples at Harwell, Proc. 15th Annual ESARDA Symp. on Safeguards and Nuclear Material Management, Rome, Italy, 11-13 May 1993. Report ESARDA 26 EUR 15214 EN CEC, Luxembourg, (1993)511-519.

[13] Eckert & Ziegler, available at http://www.ezag.com (accessed on April 4th, 2017).

[14] Frontier Technology Corporation, available at http://www.frontier-cf252.com (accessed on April 4th, 2017).

[15] QSA Global Inc., available at http://www.qsa-global.com/californium-252/ (accessed on April 4th, 2017).

[16] HO Menlove and JE Swansen, A high-performance neutron time correlation counter, Nucl. Technol . 71(1985)498-505

SNM Detection by Fission Signatures Induced by a Low-energy Neutron Source

Aharon Ocherashvili[2], Giovanni Varasano[1], Eric Roesgen[1], Arie Beck[2], Jean-Michel Crochemore[1], Tatjana Bogucarska[1], Bent Pedersen[1]

[1]Joint Research Centre, European Commission
Directorate Nuclear Safety and Security
Nuclear Security Unit
Via E. Fermi 2749, Ispra 21027 (VA), Italy

[2]Physics Department
Nuclear Research Center Negev
P.O. Box 9001, 84190 Beer-Sheva, Israel

Abstract:

The identification of fast neutron interactions in liquid scintillation detectors, by means of the pulse shape discrimination method (PSD), has been demonstrated by many to be a valid technology both as an alternative to standard neutron detectors and as a direct detection method of fast neutrons. We have previously reported on the use of this technology combined with a pulsed neutron source for the detection of coincident prompt fission neutrons in multiple liquid scintillation detectors. The intention is to develop this technique into a method for detection of special nuclear materials (SNM) in cargo containers. In this paper we present a more detailed investigation of the effectiveness of two and three fold coincidences in observation intervals of 40 nanosecond duration. The observation of prompt fission neutrons and photons in such coincidence events is a strong indicator for the presence of fissile materials.

We use a pulsed 14-MeV neutron source in a graphite assembly as external neutron source. In the time period of 60-125 μsec after the 14-MeV neutron burst practically only low-energy source neutrons persist. These source neutrons are not identified as neutrons in the PSD analysis whereas the induced fast fission neutrons are. Interrogation by only low-energy neutrons is achieved by time-gating the acquisition. The use of a neutron source with an energy component above cadmium cut-off is to assure detection of fissile materials which are deliberately shielded against an external thermal neutron source. The paper shows the experimentally obtained sensitivities of the method to the detection of uranium samples.

A scaled-up system based on the same detection principle as in the laboratory experiments is proposed based on Monte Carlo calculations. The performance prediction of the scaled-up system applied to the case of air cargo containers is discussed.

Keywords: SNM detection; neutron generator; PSD analysis; induced fission

1. Introduction

Passive and active non-destructive assay (NDA) methods have potential in practical applications as a means to detect special nuclear materials (SNM). The prompt emission from fission of neutrons and γ-rays appear to be useful signatures for the detection of SNM in shielded containers. One reason for this is that a component of the prompt γ-rays from fission are of high energy and thus very penetrating and difficult to deliberately shield from detection. Furthermore identifying the detected radiation to be originating from fission events is evidence of the presence of SNM in the object under investigation.

To this end it is useful to arrange the detection system to take advantage of the fact that during the fission event multiple prompt γ-rays and neutrons are emitted simultaneously [1-3].

Using an external neutron source to induce fission extends the usefulness of this detection method to apply not only to spontaneous fissile elements but also to elements with a cross-section for neutron induced fission. Pulsing of the external neutron source can provide further advantages to be exploited in the detection method. This includes the fact that by proper timing (gating) of the detection period with respect to the neutron emission from the external source, the object can be interrogated by a low energy (epi-thermal or thermal) neutron flux only, providing the possibility to distinguish the fast fission neutrons from the low energy source neutrons in the neutron detection system [4].

In the present work we study thermal neutron interrogation and epi-thermal neutron interrogation separately. The thermal interrogation provides a strong prompt fission neutron signal proportional to the fissile mass [4]. In the epi-thermal interrogation the response is harder to interpret due to the larger proportion of gamma detection events during slowing-down of the source neutrons. The epi-thermal interrogation however is important from a nuclear security point of view as these neutrons will to some degree penetrate any thermal neutron shield purposely placed around an object containing fissile material. An instrument used in practice should apply a combined thermal and epi-thermal interrogation regime.

2. Experimental setup

The Pulsed Neutron Interrogation Test Assembly (PUNITA) of the Joint Research Centre is designed for experimental studies in non-destructive analysis (NDA) methods for nuclear safeguards and security. Figure 1 shows a cross section of PUNITA and the positioning of the detectors used in this work. The facility is composed of a large graphite liner surrounding a central cavity of volume 50x50x80 cm^3. The (D-T) pulsed neutron generator, the sample under investigation and the scintillation detectors used for coincident detection are located inside the cavity. In total 96 one metre long ^{3}He neutron detectors are embedded in polyethylene modules and shielded by cadmium (fission neutron counters in Figure 1). In the present experiments these detectors are used as reference detectors of the prompt fission neutrons.

In Figure 1 is also indicated, as source monitors, bare ^{3}He neutron detectors which are used to normalize detector readings in all experiments to the same total neutron emission from the generator target. The neutron generator (Model A-211 from Thermo Fisher Scientific Inc.) is pulsed at 100 Hz which is chosen based on the average thermal neutron lifetime in the graphite/cavity configuration. The generator is able to produce short and intense bursts of neutrons with no neutron emission between bursts. This fact, together with the very short duty-cycle of one per mille, allow separation of the neutron interrogation into a fast/epi-thermal period from zero to 85 μs, and a thermal period from 250 μs to 9 ms, respectively [4].

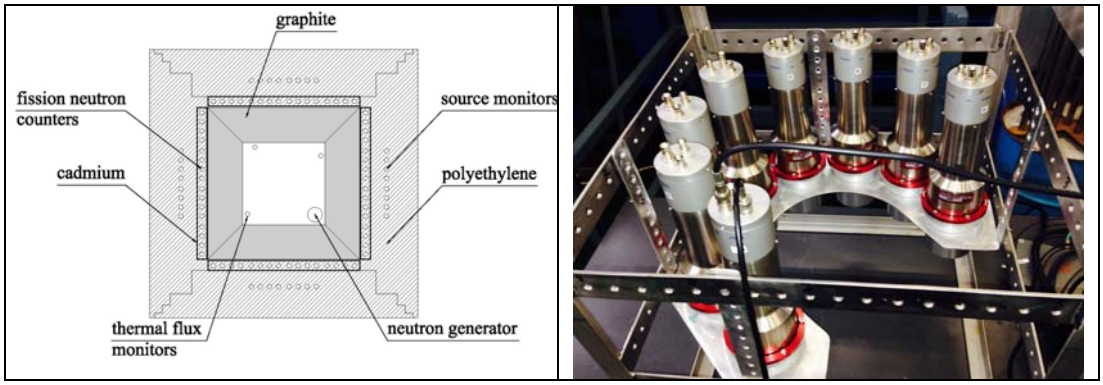

Figure 1: Sketch of PUNITA showing the permanently mounted neutron detectors and the neutron generator mounted inside the sample cavity (left picture). The right hand picture shows the positioning of the eight liquid scintillation detectors within the sample cavity of PUNITA.

The performance of scintillation detectors with respect to γ/n discrimination in the PUNITA facility is described in [4]. Due to the very fast response of the scintillation detectors the effect of the neutron generator burst can be followed in detail [5]. The liquid scintillation detectors used in this work are of the type EJ-309 from Eljen Technology (www.eljentechnology.com). The anode output of the photomultiplier is connected directly to a signal digitizer. The signal digitizers used in this work are from Signal Processing Devices Sweden AB (http://spdevices.com/). Figure 2 shows the triggering and data processing scheme used in these experiments. A detection event includes storage of a waveform from each of the eight detectors.

The fact that the detection of fast prompt neutrons from fission is done in multiple (eight) detectors allows for counting not only single neutrons, which may be subject to misinterpretation in the PSD analysis and detection of fast generator neutrons in case of epi-thermal interrogation, but also detection of multiple neutrons from the same fission event in short observation intervals referred to hereafter as two or three fold coincidence events. Events of coincident neutrons are a strong signature of a detected fission event.

Searching for fast neutron detections in the multi-detector setup can mean searching through tens of thousands single events, and two-fold or three-fold coincidence events. These events are stored in each experiment for off-line analysis. We use MATLAB [6] to perform the PSD analysis (n/γ discrimination) and plot the coincidences according to their multiplicity (two-fold or three-fold coincidence events) and kind (γ-γ, γ-n, n-n, etc.). In case of single event triggering about 98% of stored single events were γ-rays. The two-fold or higher order coincidences have a much higher fraction of neutron signals thus reducing the amount of data necessary to identify a significant quantity of detected neutrons. For the coincidence experiments we used a (software) coincidence gate of 30 ns.

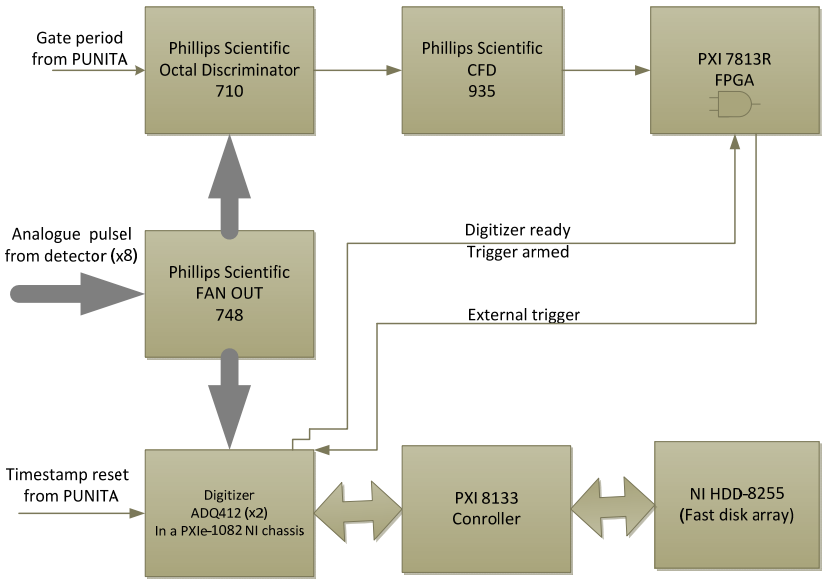

Figure 2: Block diagram of the data processing for digitizing and storing detection events on the eight scintillation detectors (lower half). The trigger system (upper half) allows to limit acquisition to a given part of the PUNITA pulse period, and to select single-signal, 2-fold coincidence, 3-fold coincidence etc. trigger events.

3. Experiments at the PUNITA facility

By adjusting the data recording period following the neutron generator burst (Figure 2, "Gate period from PUNITA") the data acquisition can be tailored to a certain neutron energy range. By means of slowing down in the graphite, the thermal flux caused by the 14-MeV source neutron pulse peaks at about 250 μs after the 14-MeV neutron burst [7]. Whereas thermal source neutrons persist for several milliseconds, the fast sources neutrons as detected in the scintillation detectors (through PSD analysis) are only visible for some tens of μs. Figure 3 shows the ratio of detected neutrons to all signals as function of time following the generator pulse at time zero.

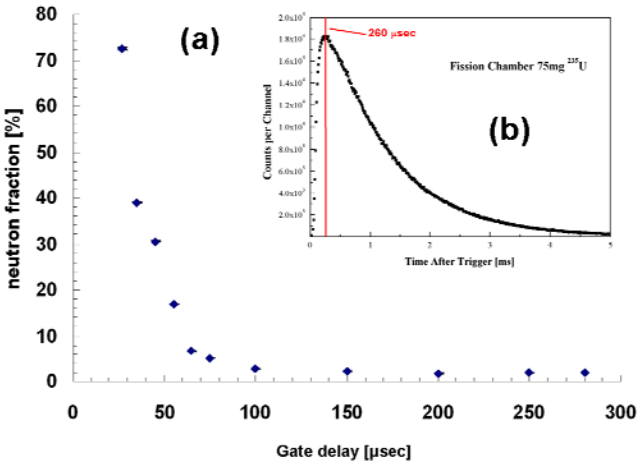

Figure 3: Fraction of the neutron signals to all signals as function of the time following the n-generator burst (a). The insert, picture (b) shows the time behaviour of the thermal flux in PUNITA.

The fast source neutrons disappear within few tens of μs indicating the presence of epi-thermal source at least beyond the first 100 μs of the PUNITA time cycle. This assumption was supported in Monte Carlo simulations.
For the study of both thermal and epi-thermal interrogation a series of five CBNM low enriched uranium samples (and an empty container) of same total mass but variable enrichments from 0.31% to 4.46% ^{235}U was used to vary the fissile mass.

3.1. Experiments with epi-thermal neutron interrogation

For the purpose of studying epi-thermal neutron interrogation a 95 μs period (from 28 μs to 123 μs after the 14-MeV neutron burst) was investigated. The result for total neutron counting (single neutrons) as function of fissile ass is shown in Figure 4 below. In the analysis, the 95 μs period was sub-divided into three. The earlier period (28-59 μs) does not show a response depending on the fissile mass. The reason is likely due to source neutrons still being observed as fast neutrons in the detectors.

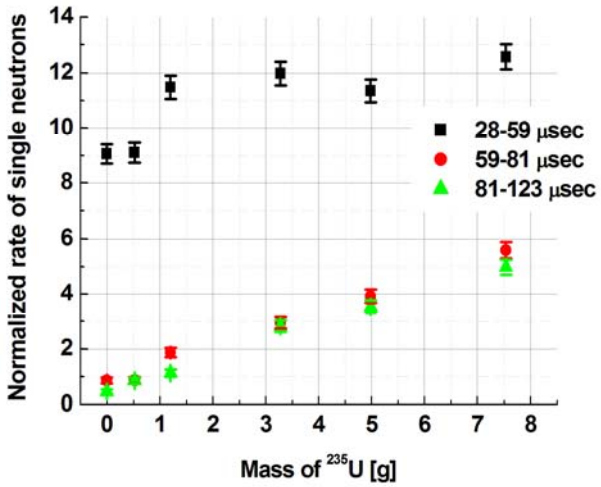

Figure 4: Detected normalized rate of single neutrons in three time periods

Also two and three fold coincidences (trigger scheme of Figure 2) were recorded in the epi-thermal range. These coincidence signals however were dominated by gamma detection events and gave

poorer counting statistics and linearity as function of fissile mass than the single neutron detection events shown above.

3.2. Experiments with thermal neutron interrogation

Although the total neutron flux caused by the 14-MeV neutron pulse decays exponentially over time, the thermal flux only peaks at 250 μs after the fast pulse, and the number of thermal neutron induced fissions is still significant partly due to the higher fission cross-section at thermal energy.

Many series of experiments were carried out to study the sensitivity to ^{235}U mass as function of coincidence trigger level (single signal trigger, two-fold coincidence trigger, three-fold coincidence trigger etc.). We found that three-fold coincidence events had the best sensitivity to fissile mass. This means that events were counted where three signals or more (from the eight detectors) were found within a period of 30 ns, and at least one signal had a neutron PSD value i.e. coincidence events of the types (γ, γ, n), (γ, n, n) or (n, n, n). As an example Figure 5 shows the response of recorded three-fold coincidences as function of ^{235}U mass.

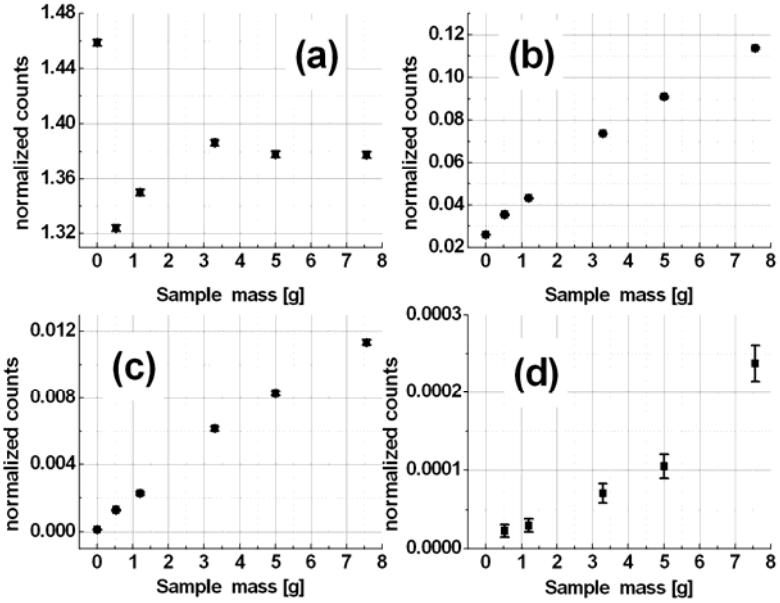

Figure 5: Example of three-fold coincidences as function of fissile mass of types : a: (γ, γ, γ), b: (γ, γ, n), c: (γ, n, n), d: (n, n, n).

Figure 5 shows that pure gamma coincidences (a) are not dependent of the fissile mass. In any of the types of coincidences including a neutron however, the linearity with fissile mass is visible although counting statistics deteriorate when multiple neutrons are selected.

4. Monte Carlo simulations of a scaled up device for cargo containers

The experiments described above essentially applies equipment which can be acquired without exceptional requirements and budget. The main components are readily available off the shelf, including the neutron generator, the graphite envelope, and liquid scintillation detectors. Also the signal analysis is done using commercial signal digitizers.

In order to estimate the performance a scaled up facility based on the same detection principle as applied experimentally in the PUNITA facility, we carried simulations using MCNP6 [8] of both PUNITA and a technically feasible installation that could be housed in a standard 20-foot shipping container. The two performance of the installations were compared by devising a figure of merit as the product of

the thermal neutron flux at the position of the fissile material and the prompt fission neutron detection efficiency in the detector configuration:

FOM = [thermal-n flux] x [detector n-efficiency]

We did not model the light output from the scintillation detectors for the estimation of the neutron detection efficiency in MCNP. Instead we tracked the proton kinetic energy following neutron scattering interactions. We assumed a (conservative) proton energy of 700 keV as the detection threshold considering the need to clearly distinguish neutrons in the PSD analysis. The MNCP model corresponding to the PUNITA experiment (Figure 1) is given in Figure 6.

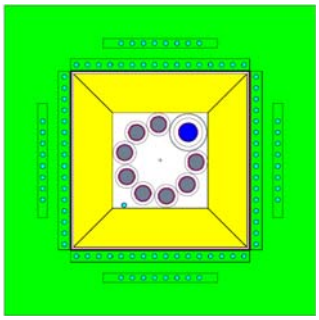

Figure 6: The MCNP input model of the experiment in PUNITA. The picture shows the position of the neutron generator (blue), the scintillation detectors (gray), and the graphite block (yellow,) polyethylene (green). Uranium samples were placed in the centre of the cavity.

The scaled up device is a hypothetical instrument intended to be operated in airport cargo handling areas (non-public area). The purpose of this device is to assay standard Unit Load Devices (ULDs) for air cargo transportation. The geometry of Figure 4 would be sufficient to interrogate a socalled LD1 device designed for Boeing 474-400 cargo of dimensions: 234 x 153 x 163 cm (4.9 m^3). As a standard matrix for this volume we used the MCNP material cellulose ($C_6H_{10}O_5$) with a density of 0.15 g/cm^3, yielding a total (cargo) mass of 735 kg.

The MCNP input geometry is depicted in Figure 7. The geometry includes 24 liquid scintillation detectors (four in each wall) of dimensions 7” x 7”, and a single neutron generator, of same operation parameters as PUNITA, located in the floor below the assay object. The device would fit a 20-foot standard transport container.

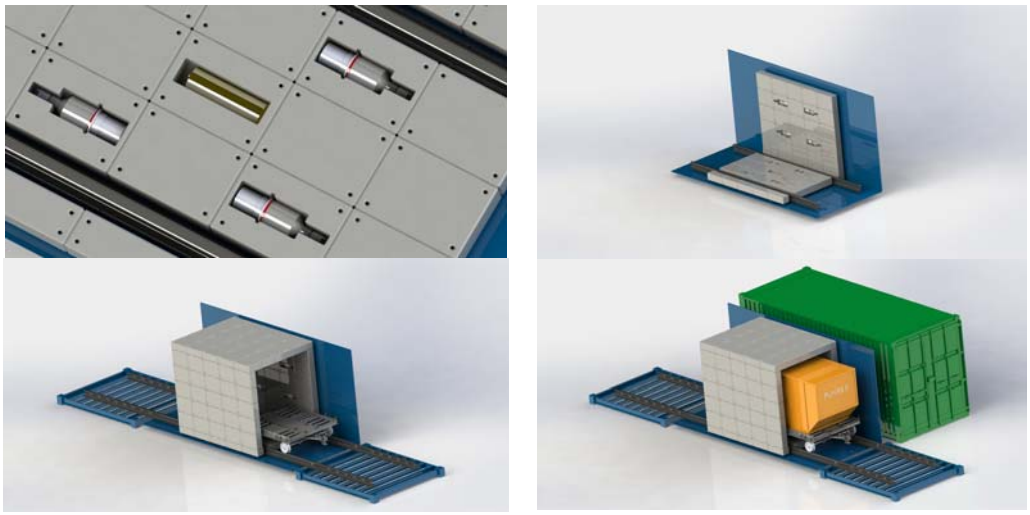

Figure 7: Model of scaled up device for assay of air cargo containers. The detectors are embedded in the graphite walls, floor and ceiling. The n-generator centered in the floor. The entire device fits into a standard 20-foot transport container (green).

The MCNP calculations of the scaled up device showed not surprisingly the lowest FOM value for the centre position of the sample volume. The comparison of the MCNP simulations of the PUNITA experiment to the scaled up device described above, the following parameters are derived:

Geometry comparison “ULD device / PUNITA”:

- moderator volume ratio 11.9
- sample cavity size ratio 31.7
- detector volume ratio 21.8
- neutron generator same (1x 10^8 /sec, 100 Hz pulsing)

Preliminary simulation results “ULD device / PUNITA”:

thermal n-flux ratio, centre pos.	$\varphi_{th,ULD\ device} / \varphi_{th,PUNITA} = 0.00606 \pm 0.000238$
fission neutron det. efficiency	$\varepsilon_{n,\ ULD\ device} / \varepsilon_{n,\ PUNITA} = 0.379 \pm 9.94 \times 10^{-4}$
FOM ratio	1/436 ± 1/11065

Based on the (conservative) estimate of a detection limit in the PUNITA configuration of 0.52 g ^{235}U in a 100 second measurement, using the 3-fold neutron coincidences as signature, the detection limit of the “ULD device” described above would be approximately a factor 436 higher or equivalent of 228 g ^{235}U.

5. Conclusions

In the present work we have investigated a detection method for special nuclear material based on a pulsed neutron source of neutrons inducing fission is fissile isotopes, and the detection of fast prompt fission neutrons as a signature of the presence of fissile material. The advantage of this method is that low-energy neutrons do not produce a neutron signature in the liquid scintillation detectors, while the neutron energy is sufficiently high for the neutrons to pass through thermal neutron shielding, and induce fission in fissile isotopes. The best suited energy range of the source neutron is selected by varying the delay of interrogation with respect to the pulse of 14-MeV neutron from a generator embedded in a strongly moderating detection assembly.

Based on Monte Carlo simulations of experimental results of the prompt fission neutron response, a scaled up instrument of the same detection principle could be able to detect at the limit a few hundred grams of ^{235}U in a measurement time of 100 seconds.

More work is needed to better interpret the response of epi-thermal neutron interrogation.

6. References

[1] Enqvist A, Flaska M, Dolan J L, Chichester D L, Pozzi S A; *A combined neutron and gamma-ray multiplicity counter based on liquid scintillation detectors;* Nucl. Instr. Meth. A; 652; 2011; p 48-51.

[2] Pozzi S A, Clarke S D, Flaska M, Peerani P; *Pulse-height distributions of neutron and gamma rays from plutonium-oxide samples*; Nucl. Instr. Meth. A; 608(2); 2009; p 310-315.

[3] Clarke S D, Flaska M, Pozzi S A, Peerani P; *Neutron and gamma-ray cross-correlation measurements of plutonium oxide powder*; Nucl. Instr. Meth. A; 604(3) 2009; p 618-623.

[4] Ocherashvili A, Roesgen E, Beck A, Caspi E N, Mosconi M, Crochemore J-M, Pedersen B; *SNM detection by means of thermal neutron interrogation and a liquid scintillation detector*; JINST, 7 CO3037; 2012.

[5] Ocherashvili A, Mosconi M, Crochemore J-M, Beck A, Roesgen E, V. Mayorov, Pedersen B; *Fast neutron coincidences from induced fission as a method for detection of SNM*; ESARDA Bulletin, Issue No 49, July 2013, p 42-51.

[6] MATLAB 7.0 and Statistics Toolbox 7.1, The MathWorks, Inc., Natick, Massachusetts, United States.

[7] Favalli A, Mehner H-C, Crochemore J-M, Pedersen B; *Pulsed Neutron Facility for Research in Illicit Trafficking and Nuclear Safeguards*; IEEE Transactions on Nuclear Science; 56(3); 2009; p 1292-1296.

[8] X-5 Monte Carlo Team Diagnostics Applications Group Los Alamos National Laboratory; *MCNP – A general Monte Carlo N-Particle Transport Code, Version 5, Volume I: Overview and Theory;* LA-UR-03-1987; 2003; Los Alamos National Laboratory.

The Illicit Trafficking Radiation Assessment Program (ITRAP+10) for Detection Equipment in Nuclear Security

S. Abousahl [2], C. Carrapico [1], G. Eklund[1], V. Forcina[1], M. Goncalves [2], M. Marin-Ferrer [1], A. Ossola [1], J. Paypen [3], P. Peerani [1], F. Raiola [1], R. Rossa [1], F. Rosas [1], A. Rozite[1], A. Tomanin [1] and H. Tagziria [1a]

[1] European Commission, Joint Research Centre , Nuclear Safety and Security Directorate G, Nuclear Security Unit G.II.7 , Ispra (Italy)
[2] European Commission, Joint Research Centre , Directorate A, Brussels (Belgium)
[3] European Commission, Joint Research Centre, Directorate G, Unit G2, Geel (Belgium)

Abstract

The European Commission's (EC) Joint Research Centre (JRC) was entrusted by DG-Home to carry out a far reaching ITRAP+10 programme aiming to assess the performance of 8 main families of off-the-shelf instruments for the detection of nuclear and other radioactive materials. Over 170 instruments from EU Member States (MS) companies and from the USA were tested (from 2011 to 2014) against international standards (IEC, ANSI) and the IAEA's NSS1 recommendations. The work was performed in collaboration with the US DoE/DNDO and the IAEA. In 2015, ITRAP+10 Phase II was launched by the EC and being implemented by the JRC with the goals to test the Mobile and Transportable Radiation Monitors (MTRM) family of instruments (in controlled and real environmental conditions) for the first time, build testing capacity within the EU MS and contribute to International standardization and certification of detection equipment.

Keywords: ITRAP, Nuclear Security, Detection, Illicit Trafficking, Standards

[a] Contact (Technical manager): hamid.tagziria@ec.europa.eu

1) Introduction:

Since the breakup of the soviet Union in 1991 the world has seen a dramatic increase in incidences of illicit trafficking of nuclear material and other radioactive material (NRM) which led the IAEA to conduct from 1997 to 2001 the first ILLICIT TRAFFICKING RADIATION ASSESSMENT PROGRAM (ITRAP) aiming to test and evaluate the performance of handheld and pocket radiation detection equipment in nuclear security. As the IAEA's Incident and Trafficking Database (ITDB) shows, the situation was further exacerbated following the 9/11 terror attacks which resulted in a number of nuclear summits, international conferences, national and international plans and initiatives to reinforce the fight against the illicit trafficking of NRM as well as strengthen international treaties and agreements (Amm. CPPNM, JCPOA, UN1718). The drive to establish a sound nuclear detection architecture which incorparates a number of fundamentals, one of which most importantly, is adequate detection by instrument with all its prerequisites including standardization, has ever since been internationnally recognised and actively pursued.

Within the framework of the European Commission's (EC) CBRN action plan adopted in 2009, its Joint Research Center was entrusted by DG-HOME to carry out a far reaching ITRAP+10 programme aiming to assess from 2011 to 2014 the performance of the most families of commercially available NRM detection instruments and test them against international standards.

Extensive data was collected and managed using a client-server based Data Collection System (DCS) the results of which were subsequently communicated to standards committees and to participating commercial companies thus helping them to improve the performance of their products.

EC funded projects such as SCINTILLA (FP 7) hugely benefited from ITRAP for its well recognized success in developing, testing and benchmarking alternatives to ^{3}He-based detection systems for difficult to detect NRM. In June 2015, C-BORD which is an H2020 project was launched bringing together 22 EU commercial companies, research centers, universities and end users to develop systems to detect illicit trafficking in containers at borders, some of which will be tested within the ITRAP test bed facilities at the JRC.

In 2015 ITRAP+10 Phase II was launched by the European Commission with the scope to 1) test the rest of detection systems or technologies which are either novel (eg. He-3 alternatives) or simply not previously tested such as the mobile systems 2) build testing capacity in EU member states and 3) provide feedback to participating industry and to international standards

This paper aims to describe the testing and measurement campaigns carried out at the JRC in Ispra (Italy) within ITRAP+10.

2) Test bed facility at the JRC in Ispra

a. Dynamic tests with sources:

These are carried out using the test bed facility shown in figure 1 which has the following characteristics:

- 27 m long conveyor/rail
- Speed varying from 0.02 to 3. m/s
- 10 to 300 cm vertical elevation of source
- With/without moderator
- Various shielding arrangement
- 2 source mounting options: automatic and manual for testing with heavily moderated or shielded sources
- Data Collection system (DCS) described below

Figure 1 : Dynamic test bed facility at the JRC in Ispra

b. Static testing on purpose built irradiators

In another laboratory at the JRC in Ispra two purposely built irradiators (shown in figure 2) are installed with the following specifications:

- 2 separate irradiators for neutron and gamma sources
- Full control of exposure time and duration

- Complete record of instrument's response
- Extensive data collection and management using a client-server based Data Collection System

Figure 2: neutron and gamma irradiators at the static test bed facility at the JRC in Ispra

c. The Data Collection System (DCS)

A client-server based Data Collection System (DCS) shown in figure xxx was developed by DNDO and implemented at the JRC Ispra the acquisition and management of data within ITRAP+10. Eight different databases have been created to accurately record any single piece of information that could help to analyse the results. This allowed a quality assured collection and management of vast amount of data (pictures, spectra etc) during these extensive testing campaigns.

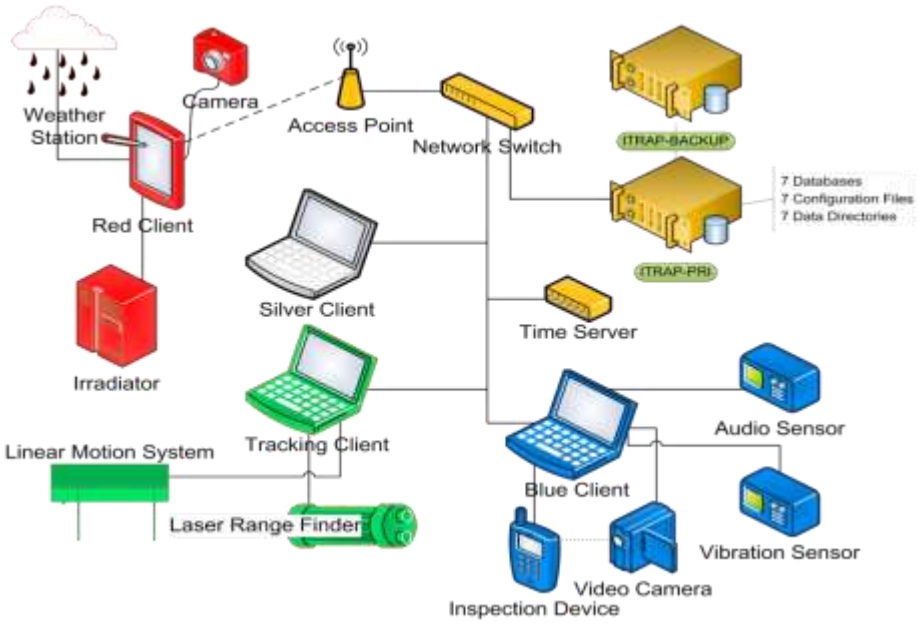

Figure 3: Schematic of the Data Collection System (DCS) at the JRC 's ITRAP facility in Ispra

3) ITRAP+10 Phase I:

a. Introduction

From 2010 to 2013 the performance of the following 8 families of commercially available NRM

detection instruments was assessed and the instruments tested against international standards (IEC, ANSI) and IAEA's NSS1 recommendations, in collaboration with the US DOE/DNDO and IAEA:

1. Personal Radiation Detectors (PRD),
2. Spectroscopic Personal Radiation Detectors (SPRD),
3. Radioisotope Identifiers (RIID),
4. Gamma Search Detectors (GSD),
5. Neutron Search Devices (NSD),
6. Radiation Portal Monitors (RPM),
7. Spectroscopic Radiation Portal Monitors (SPRM),
8. Personal Radiation Scanner (PRS).

About 170 instruments were tested at the following laboratories in the EU and the USA using the same test procedures:

1. EC JRC Ispra (all except mobile, done in Phase 2)
2. DNDO - Pacific Northwest National Laboratory (RID)
3. DNDO: Savannah River National Laboratory and Global Testing Laboratory (PRD)
4. DNDO - Oak Ridge National Laboratory (RPM)

Following extensive data analysis and it was concluded that although most detection technologies performed well and fit the purpose, no one instrument or category fully passed all the standards tests and can fit all purposes. This implies that there is room for improving instruments (in some cases) or/and the international standards in others. The vast amount of test data collected was made available, in the shape of suitably targeted reports, to manufactures allowing them to assess and improve performance of their equipment and to international standards committees as feedback and input for improving standards. A full report was made available to the general public in early 2016 by the European Commission and the US Homeland Security [2].

b. **Conclusions of ITRAP+10 Phase I assessment**:

- None of the instruments tested under ITRAP+10 passed the complete set of tests
- This fact implies that:
  - The standards need to be updated to meet the limitations of the actual technology.
  - In some cases Instruments need to be improved
- Vast amount of test data available for improvement of detector technology and revision of standards
- Numerous Reports including Public report no. EU 27958 (25 Jan 2016)
- Testing against standards assesses well for detectors performance even if testing is under controlled conditions.

However, it is important to note that much progress and improvements have been achieved in last 4-5 years and since e.g. the RPM tests in 2012 as demonstrated within SCINITLLA (FP7) and CBORD (H2020) EU projects for instance. The following case is most indicative of that.

Data collected for instance at the Port of Antwerp (Belgium) in 2005 where 10000 to 15000 trucks transit daily past RPM reported between 100 and 200 innocent alarms per day (1.1 to 1.4 %).

Data collected (2359 alarms) at the same port of Antwerp from June to Nov 2013 with systems developed within the SCINTILLA Eu FP7 project reflect the great progress made whereby:

- RPM with PVT NORM identification: 80% reduction in nuisance alarms
- Spectroscopic RPM (with NaI identification): 98% reduction.
- 8800 alarms (normal PVT RPM N42.35 compliant) would be reduced to 1400 and 100 respectively
- While still able to reliably identify threat and medical sources

4) ITRAP+10 Phase II

a. Introduction

The JRC was entrusted in 2015 by DG-Home to carry out Phase II of ITRAP+10 with the aim to:

a) test the remaining families of instruments (mobile and transportable) at the ITRAP facility of the JRC in Ispra and in real external environmental conditions.
b) build the capacity of a selected consortium of EU laboratories to test and (ultimately) certify nuclear security detection equipment through the provision by JRC of testing procedures and the organization of a round robin exercise based on a set of representative instruments (PRD, RID and SRPM) which had been thoroughly tested in Ispra.
c) ITRAP+10 phase II also aims to make good strides and contribution towards improving international standards and generally move towards certification of nuclear detection equipment for nuclear security.

b. Measurements and Testing at the JRC

Figure 4 shows a panoramic view of the dynamic testing facility during the testing campaign of mobile and transportable systems also shown being tested in external environments (Figure 5)

Figure 4 : Testing of mobile and transportable detection instruments in dynamic ITRAP facility at the JRC

Figure 5 : Testing of mobile and transportable detection instruments in external environments

c. Round Robin Exercise for capacity building in EU member states

The transfer of know-how to EU Member States' laboratories will be ensured through a round robin exercise (Figures 6 and 7) whereby:

5) A limited but representative set of instruments will be circulated namely:
    a. Personal Radiation Detectors (PRD) – IEC 62401

   b. Radioisotope Identifiers (RID) – IEC 62327
   c. Spectrometric Radiation Portal Monitor (SRPM) – IEC 62484
6) Test procedures have been developed and validated at the JRC and provided to a consortium of participating EU laboratories
7) Testing of instruments to be carried out at the JRC in Ispra
8) Testing of the equipment by the consortium of Eu laboratories using the same procedures
9) Results will be compared with those of reference measurements by the JRC in Ispra and if meaningful between different laboratories (including JRC)

PRD RID Pedestrian sRPM

Figure 6: Three categories of instruments taking part in the round robin exercise

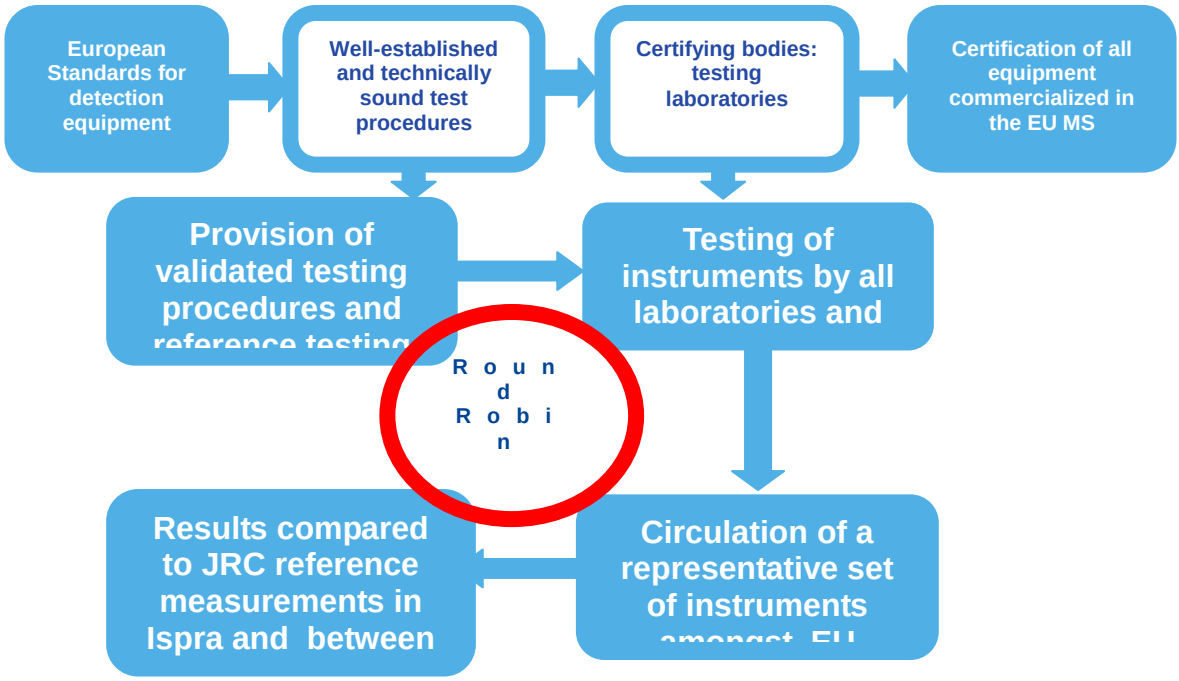

Figure 7: Schematic representation of the round robin exercise

The consortium of participating EU laboratories funded by DG-Home is composed of:

- IRSN (France)
- CEA (France)
- EK (Hungary)
- FhG-INT (Germany)
- Seibersdorf Lab (Austria)

Testing within the round robin exercise (coordinated by France Expertise and implemented by the JRC) is planned to start in September 2017 as agreed during the kick off meeting held in Paris on 5 May 2017 and will be completed by the end of 2018.

10) Summary and Conclusions:

- Over 180 off-the-shelf radiation detection instruments commercialized in EU and USA were assessed against international standards within ITRAP+10 from 2011 to 2016.
- A detailed picture of the state-of-the-art technologies was obtained for all families of detectors (including mobile and transportable)
- Full reports were provided to the companies about their own equipment thus contributing to improve performance and technologies.
- Feedback provided to international standards committees and to IAEA to improve standards and progress towards certification.
- Capacity building and knowledge transfer to EU Member States within ITRAP+10 Phase II through a round robin exercise
- User laboratory access benefited EU member states and international partners and collaborators
- Strong EU contribution to enhancing nuclear security within the EU-CBRN action plan
- No single detector technology or category
    - fits all purposes *(not to be confused with «does not fit the purpose» which fortunately is not the case as these are two totally different statements)*
    - passes all standards tests which implies that either the technology or (and) the standards need to be improved
- Assessment within ITRAP+10 of all families contributed to R&D of detection technology and to standardization
- Major progress made within projects such as SCINTILLA (FP7) and C-BORD (H2020); EU consortia projects: industry, research centers and universities, end users..
- New He-3 free technologies now available and tested
- Good progress with communication tools and formats but much more needs be done.
- Most are N42.42 compliant but variations can create difficulties
- Newest detectors able to communicate with: USB, Bluetooth; WiFi; satellite phone via USB, 3G and web interface…
- Many new technologies and much progress made since ITRAP+10 phase I as regards instrument performance, He-3 alternatives, methods and algorithms.

11) References

[1] ITRAP +10 test campaign summary report, 25 Jan 2016, EUR publication no. 27958 https://ec.europa.eu/jrc Available from EU Bookshop (http://bookshop.europa.eu)

[2] The ITRAP+10 summary report is also made available by the U.S. Department of Homeland Security – Domestic Nuclear Detection Office with the following identifiers:
Guidance: DHS SCG DNDO-001.1, 12/12 Document Number: 200-ITRAP-124860V1.0

Acknowledgements
The funding of the EC's DG-Home is acknowledged

Session 18

Process Monitoring

Cyber Security and the Future of the Nonproliferation Regime

Jacob Benz
Pacific Northwest National Laboratory
PO Box 999, MSIN K8-50
Richland, WA 99352

Abstract

As the nonproliferation regime continues to expand throughout the world, attention needs to be paid to cyber security. Cyber security is much more than the detection and prevention of malware and cyber-attacks. In the context of nonproliferation, cyber security is the implementation of tools and techniques to ensure the integrity and authenticity of equipment, infrastructure, and data being generated. This is important because the data is used to provide evidence of treaty compliance, whether it be the Nuclear Non-Proliferation Treaty (NPT) or a future arms control regime. As an example, in international safeguards there is a push for increased use of unattended and remote monitoring to ease the resources burden on the IAEA due to the ever expanding number of monitored countries and facilities. Therefore, new equipment is being developed to facilitate such monitoring activities. Additionally, existing equipment is being modified to accommodate uses beyond its original intended use. In each case, there is the potential to inadvertently introduce vulnerabilities into the system which did not exist previously. By integrating cyber security into this development process, it may be possible to identify and mitigate these vulnerabilities before they can be exploited. The same concerns are present in arms control as well. Equipment which may be proposed for use in a future regime may be jointly designed or an existing commercial technology. While each case has specific advantages and disadvantages, the cyber security concerns remain the same; to generate and maintain trust and confidence in the authenticity and integrity of the equipment throughout the regime. This paper will identify and explore the cyber security challenges which exist in the nonproliferation regime, and will highlight the many ways cyber security can and should be integrated into current and future international safeguards and arms control regimes.

Keywords: Cyber Security, Authentication, Treaty Verification, Arms Control

1. The Role of Data in the Nonproliferation Regime

Globally, the nonproliferation regime is expanding to accommodate new states, facilities, missions, and challenges. This is occurring in the face of stagnant or shrinking resources and budgets. As an example, the International Atomic Energy Agency (IAEA) has significant responsibilities in the 191 countries party to the NPT. In 2014, the IAEA spent the equivalent of 13,000 calendar days performing inspections and monitoring over 193,000 significant quantities (SQs) of material with a budget of 126.4M euros [1]. In 2015, these numbers increased to 13,248 calendar days monitoring 200,110 SQs with a budget of 130.7M euros. In order to meet the increased demand on resources, additional efforts have spent to strengthen the effectiveness and efficiency of safeguards through modernizing technologies for attended and unattended systems, and improving the performance and security of information systems. These efforts have resulted in less in-field inspection days in certain states, but increased evaluation activities at IAEA headquarters, some of which is due to the increased application of unattended or remote monitoring of facilities and activities [2].

Nuclear arms control is a successful strategic tool to increase stability between two or more competing countries. The best examples of this are the multiple nuclear arms control and reduction treaties implemented between the United States and Russia (and the USSR). These negotiated treaties include the use of agreed tools and procedures to confirm the agreed limits, reductions, or

eliminations of treaty accountable items. Historically, the treaties between the US and Russia have focused on strategic nuclear capable submarines, intercontinental ballistic missiles, and nuclear-capable bombers. Counting of these treaty accountable items is a fairly straight-forward process due to the size and lack of mobility of the delivery vehicles. Previous treaties have also included a limit on the number of deployed nuclear warheads. However, these limits are based more on attribution, attributing a specific number to a delivery vehicle or counting shrouded items on a launcher such as an ICBM, rather than true accounting of nuclear warheads. Technical radiation-based measurements to confirm the authenticity of a shrouded item on a re-entry vehicle are limited to only those bumps declared not to be a nuclear warhead. In fact, only the Intermediate Nuclear Forces (INF) Treaty allows radiation-based measurements to confirm the authenticity of a treaty accountable item [3]. As future treaties look to transition treaty accountable items from delivery vehicles and launchers to nuclear warheads, alternative tools and approaches employed to confirm treaty obligations may need to be developed. There has never been a regime where the main treaty accountable item has been a nuclear warhead. Therefore well-developed and vetted tools and approaches to gain high confidence in the equipment and data used to provide evidence that a treaty partner is meeting its agreed obligations remain in their infancy.

To minimize the risk to data authenticity and integrity, cyber security should become a key consideration in any evaluation of the efficiency and effectiveness of new technology and modernized infrastructure. Cyber security is much more than the detection and prevention of malware and cyber-attacks or protecting one's computer. In the context of nonproliferation, cyber security is the implementation of tools and techniques to ensure the integrity and authenticity of equipment, infrastructure, and data being generated and used to provide evidence of treaty compliance, whether it be the Nuclear Non-Proliferation Treaty (NPT) or a future arms control regime.

1.1. International Safeguards

The IAEA has a legal obligation to draw independent conclusions to determine whether a country is meeting its safeguards obligations and the state's nuclear fuel cycle enterprise is used exclusively for peaceful purposes. This is a significant challenge given the breadth and depth of facilities and infrastructure among the 191 parties to the Nuclear Nonproliferation Treaty (NPT), and hence the need to make efficient and effective use of technologies and information systems. However, the use of and reliance on unattended/remote monitoring technologies and modernized information systems within the international safeguards regime adds additional risk to the collected, transmitted, and stored data ultimately used to provide evidence of compliance.

Historically, IAEA inspections involved the use of technologies which were developed in-house or by trusted support programs. These technologies were developed specifically to IAEA specifications and ultimately were controlled, used and maintained by the IAEA. Data were either stored locally in protected enclosures and retrieved by inspectors, or digitally signed if possible and sent via a virtual private network (VPN) to IAEA headquarters. Moving to today and the future, missions have expanded and resources have not kept pace. Future IAEA monitoring is moving to identify more efficient ways to perform inspections and make independent safeguards determinations. The long term IAEA Research and Development (R&D) Plan identifies a number of desired solutions. Including the increased use of commercial-off-the-shelf (COTS) products, use of operators' systems and equipment, and secure communication between the field and headquarters to facilitate the use of unattended and remote monitoring technologies [4].

The move away from on-site inspections requires additional trust and increases the potential risk to technical equipment, infrastructure, and data. As this move occurs, the technologies and infrastructure transition from IAEA inspectors' control to the State's through the increased reliance on unattended/remote or potentially joint use technologies where the equipment is resident in the State's facilities and the data must travel through the State's network and communication infrastructure. One example of how this has been done recently is given in Figure 1. Generated data, either digitally signed at the source or protected via tamper-indicating conduit, are stored locally at a trusted IAEA equipment cabinet (represented by the dark box on the left of Figure 1. Once data have reached an

IAEA equipment cabinet it can be secured and transmitted, in this example, using a wireless router and VPN, through State infrastructure and transmission lines, to the European Commission and ultimately IAEA headquarters [5].

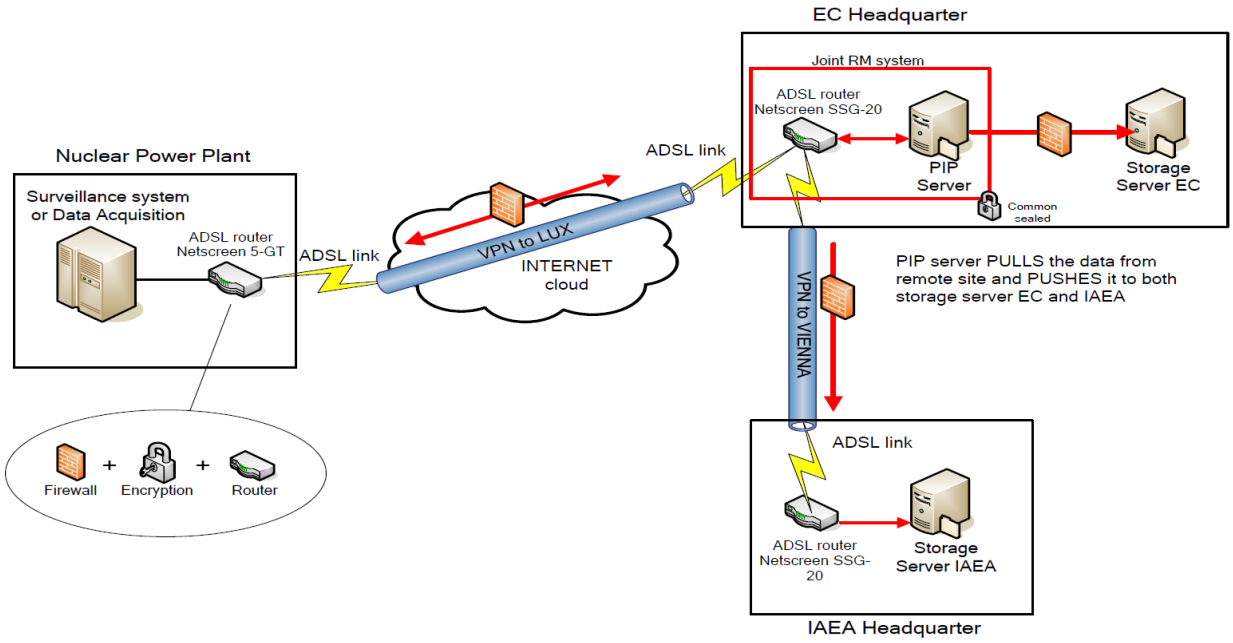

Figure 1: Remote Data Transmission Scheme for Routine Data Transfer [5]

The data flow described in Figure 1 highlights the reliance on the infrastructure through which the data travels. The IAEA has been monitoring countries since the NPT entered into force in 1970. Over the last 47 years, equipment and infrastructure have been put into place in State's facilities for monitoring purposes, and at the IAEA in Vienna for collection, analysis, and evaluation. Technology has continued to evolve based on newer technology, more efficient implementation, and identification of vulnerabilities. However the IAEA has been slow to catch up. In 2013, the IAEA implemented a program called the Modernisation of Safeguards Information Technology (MoSaIC) project. The intent of the program is to begin to upgrade and replace aging and vulnerable equipment. As of 2014, they were just in the planning stages of how to move forward on the project [6].

1.2. Arms Control

The same issues and concerns present in international safeguards, with respect to technologies and data, apply to arms control regimes where data are used to provide evidence of compliance to treaty objectives and to detect potential subversive activities. Therefore it is imperative that data can be trusted, e.g. to confirm integrity and authenticity.

As the transition of treaty accountable items move toward warheads, and measurements are performed to determine presence and identity of special nuclear material in support of treaty verification objectives, the needs for confidence in equipment and data increase significantly from current practice. The National Nuclear Security Administration recently published a report on the technical collaboration efforts between the U.S. and U.K. in the area of arms control. One of the key lessons learned states "An overarching lesson learned is that the ability to strike a balance between information protection and information sufficiency is key to an effective monitoring and verification regime. A monitoring party must be able to obtain sufficient data to confirm declarations, while a host party must have assurances that their most sensitive information is protected throughout the monitoring and verification process." [7].

The balance between information protection and sufficiency is a difficult issue which is a current area of technical research and development in arms control. It applies to all aspects of technology and approaches considered for use in potential future monitoring regimes. The challenge moving forward is not simply developing new widgets or technologies, but developing trust and confidence in proposed existing widgets or technologies, and striking the right balance between information protection and sufficiency. The methods by which these challenges are addressed are via inspector-focused authentication and host-focused certification:

- Authentication: A process by which a monitoring party to a treaty or agreement obtains confidence that the information reported by the monitoring equipment accurately reflects the true state of a monitored item and that the monitoring equipment has not been altered, removed, or replaced and functions such that it provides accurate and reproducible results at all times [7]
- Certification: A process by which a monitored party to a treaty or agreement assures itself that an inspection/monitoring system meets required safety and security requirements and will not divulge classified or proliferative information to a monitoring party [7]

2. The Role of Cyber Security in the Nonproliferation Regime

Typically, when cyber security is mentioned, first thoughts focus on issues like malware, ransomware, or denial of service attacks. While these are very important aspects of cyber security and are challenges facing the country in many sectors, e.g. critical infrastructure, financial, and commercial, they are less of a concern facing the nonproliferation regime. The area of cyber security with the greatest impact on the nonproliferation regime is Information Assurance, which is defined by the National Institute of Standards and Technology (NIST) as “measures that protect and defend information and information systems by ensuring their availability, integrity, and authentication, confidentiality, and non-repudiation.” [8]. These concepts are described visually in Figure 2. While these concepts are easily defined, the implementation of these principles in equipment and security procedures is complex. Each of these must work together to mitigate potential attacks, yet not make the equipment or procedures so cumbersome or onerous as to make them unusable. The remainder of this section will introduce these areas of Information Assurance and describe how they interact with and impact the nonproliferation regime in the context of new equipment or approaches.

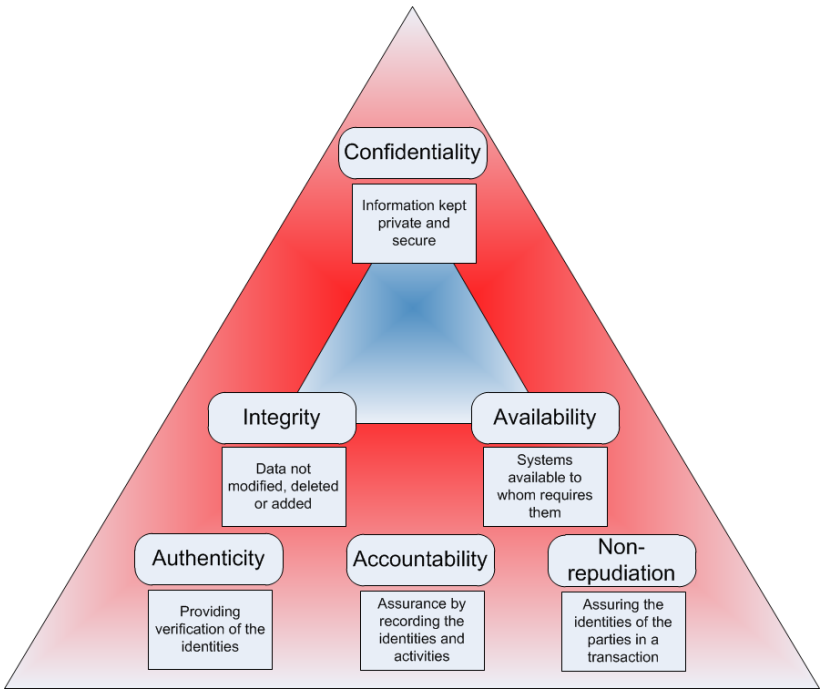

Figure 2: CIA Triad of Computer Security[1]

[1] http://geraintw.blogspot.com/2012/09/cia-infosec.html

2.1. Availability

Availability ensures timely and reliable access to information and information systems [9]. In a traditional cyber security context, denial of service attacks are one example of impacts to the availability of systems. The importance of availability varies by the importance of the component, equipment, or process, and loss of availability can vary from a nuisance to catastrophic consequences. For example, loss of availability to safety systems in critical infrastructure can result in extreme danger to the public or loss of life.

This concept becomes extremely important in the context of remote monitoring. Successful implementation of remote monitoring depends on being able to remotely access data upon request. If access is denied and the information becomes unavailable, then all benefits gained through remote monitoring may be lost and continuity of knowledge over safeguarded material or facilities may also be lost. The result of which is expending significant resources to reestablish continuity of knowledge. When the IAEA considers new equipment or how to safeguard a new facility, an assessment of where and how it will be used is performed. This identifies requirements and defines use cases within which the equipment must function properly. It also likely defines the safety and security requirements on the equipment and potentially the output data. Part of this evaluation process should also consider the importance of the availability, or loss of availability, of the equipment or data on the ability to draw safeguards conclusions. As a specific example, consider the impact if a database containing a state's Additional Protocol declaration or facility inspection results on the IAEA's ability to make informed decisions on a state's compliance. This can be a real issue with the desire to move toward information driven safeguards.

An example impact from availability, in arms control, is the loss of opportunity to monitor a treaty accountable item (TAI) or process. Consider a monitored dismantlement regime with a portal monitor serving the function of monitoring declared pathways in an unattended mode, e.g. inspectors are not standing outside the dismantlement cell while dismantlement occurs. If the portal monitor fails, and the data is unavailable, then confidence that no diversion or substitution occurred may not be possible, as the host could not reassemble the TAI for a do-over and the inspectors have no evidence that no subversion occurred. This represents an extreme case which could result in the potential consequence of the inspection team not counting the dismantlement toward the host's treaty obligation.

One lesson learned from the above examples is the need for defense in depth. Availability impacts the usability of the equipment, process, or data. If the loss of any of these negatively impacts a regime, or the ability to provide evidence of compliance, then careful thought must be given to how to mitigate loss of availability.

2.2. Confidentiality

Confidentiality is preserving authorized restrictions on information access and disclosure, including means for protecting personal privacy and proprietary information [9]. As highlighted in the definition, confidentiality includes confidentiality of data and privacy concerns. Privacy is very important in terms of protecting personally identifiable information (PII). This is one of the main areas of concern for the public and private sectors and often times the target of hackers. Phishing campaigns and malware are typically focused on gathering this type of information to allow an attacker to gain access to one's accounts or steal one's identity.

Within the nonproliferation regime, data confidentiality plays a much larger role and is a bigger concern. Data confidentiality assures that information is not available to unauthorized persons. Safeguards data may contain sensitive, proprietary, or export controlled information. The results of the data collected are not meant for public viewing or release and therefore must be protected from unauthorized access. This is true whether the data is at rest or in transit. IAEA databases contain confidential safeguards information and analysis data on every monitored country. The impact of someone gaining unauthorized access to modify or remove the data could be severe as it may alter the independent conclusions drawn by the IAEA as mandated in their charter.

As indicated in Figure 1, the IAEA currently uses VPNs and encryption to protect data confidentiality. However, it is important to keep in mind that the use of VPNs by themselves may not guarantee confidentiality, as evidenced by the widely publicized breach discovered in some Juniper Networks VPNs in 2015 [10]. The use of symmetric cryptography, with secret keys, is a robust technique to aid confidentiality. The challenge though is that the secret keys absolutely must be protected. If they are stolen or compromised then all confidentiality is lost. Key management can be difficult and unwieldy if there is a proliferation of equipment or procedures requiring inspectors to maintain a large number of different keys. Public key encryption is another robust method to provide confidentiality, however it too is reliant on the security of encryption algorithm, security over the private key, and the overall security of the procedure or protocol in which encryption is utilized. One of the strengths of public key encryption is that it can be employed to ensure that a message can only be viewed by the intended recipient, and also to provide confidence that a message came from the expected source. This dual role makes it useful to maintain both confidentiality and integrity.

Data confidentiality is a very serious issue for the host in any potential arms control regime. As the treaty accountable items move from delivery vehicles to warheads, the sensitivity of the data at risk significantly increases. The host will likely want to limit access to data as well as the quality of any data collected or released. One way this is accomplished is through the use of Information Barriers, which separates sensitive data from the very simple output necessary for verification. Data confidentiality is also the reason why the host may require review of all data prior to release to ensure that unagreed information is not made available or accidentally disclosed to unauthorized persons. Future techniques and technologies should consider how to balance confidentiality with the ability to provide sufficient evidence of treaty compliance.

2.3. Integrity

Integrity involves guarding against improper information modification or destruction including ensuring information nonrepudiation and authenticity [9]. Loss of integrity of equipment or data can have catastrophic impacts. For example, consider the ramifications if medical records were altered or could not be trusted to be authentic. Another more recent example of potential impacts due to loss of system integrity can be seen in the hacking of computer systems of presidential candidates and political parties [11].

Loss of integrity within the nonproliferation regime may be the most damaging to overall confidence and is an ongoing challenge. Equipment and data are used together to provide evidence of compliance. Within international safeguards, the IAEA has the obligation to ensure peaceful use of nuclear material and facilities. Equipment and data play key roles in gathering evidence to allow these conclusions to be drawn throughout the world. Unauthorized and undetected loss of integrity can affect global confidence in the IAEA. The evidence (and therefore the data and systems) must be demonstrably authentic, and should be sufficiently robust to ensure information nonrepudiation.

In the context of integrity, there are both adversarial and non-adversarial threats facing the international safeguards regime. Adversarial threats include nation-states and insiders. In both cases, it may be possible to corrupt or modify equipment, infrastructure or data to alter safeguards data to hide or modify evidence of non-compliance or attempted cheating. Specific examples may include before lens tampering, targeting cables or transmission pathways (wired or wireless) or modifying data on computers and databases. Just these few examples highlight the potential difficulty of maintaining integrity, as well as the importance of the effort. As the IAEA considers developing new equipment, adopting procedures for facility remote monitoring, or upgrading new infrastructure either in the field or at headquarters, consideration for equipment and data integrity must be at the forefront. Non-adversarial threats tend to be the infrastructure itself, both at the IAEA and in the field. IT infrastructure has been in place at the IAEA since the 1970s and infrastructure in many states may also be decades old. Lack of upgraded infrastructure may leave data vulnerable to attacks, and it also may not be able to support remote monitoring technologies and data due to bandwidth and capacity challenges.

Similar issues and concern exist in arms control as well. The host party has an obligation to protect sensitive and classified national security information. One way this may be achieved is through

managed access and the use and control of host-provided equipment as part of a monitoring regime. Because of these constraints, the inspecting party would have limited access to the equipment, and the data may be reviewed by host security prior to release to the inspecting party. Therefore, the challenge is to develop equipment, procedures, and manage data such that integrity throughout the entire process can be confidently achieved. The processes used by the host and inspecting parties are Certification and Authentication, respectively, as defined earlier. These processes can be complex, resource intensive and at times incompatible. However, as the collected and agreed data is one of the key pieces of evidence regarding whether or not treaty obligations are being met, it forms the cornerstone of current research and development efforts to identify techniques and technologies to develop monitoring solutions to confirm current and future arms control regimes.

Technical solutions to maintain confidence in data integrity include, as examples, digital signatures and public key cryptography. Proper use provides a mechanism to allow users to have confidence in the authenticity or origin of data, and confidence that the data has not be substituted or modified through transit from the source to the user. Digital signatures provide a robust mechanism to generate and maintain confidence in the integrity and authenticity of data, as well as means to ensure nonrepudiation of the data. Therefore, new equipment or procedures being considered in either international safeguards or arms control should consider the inclusion or use of digital signatures and public key cryptography. Data that is not or cannot be signed requires alternative methods for maintaining confidence in its integrity and authenticity. One example is through the use of tamper indicating conduit to protect data cables. These cable runs can be long, expensive to secure, and are detrimental to the growth of remote monitoring, in the case of international safeguards, due to the need to inspect the integrity of the conduit. Within arms control, the use of digital signatures could ease the inspection team's concern over host review prior to release to the inspection team, and ease the burden of chain of custody over the data throughout the process.

3. Conclusion

The growing expectations and roles asked of the nonproliferation regime, in the presence of stagnant or even decreasing resources is a huge challenge facing the future of the regime. One potential solution to address this challenge is to utilize COTS or joint use equipment and take advantage of modern technology and information systems. Another complementary solution is to rely more heavily on unattended or remote monitoring systems to replace or minimize the need to spend large amounts of time in the field. The consequence of these solutions is a greater reliance on technology and information systems.

Data and information, equipment, and information systems are used extensively in the nonproliferation regime to generate, analyze, and store evidence of treaty compliance. One aspect of cyber security, information assurance, is specifically focused on ensuring the confidentiality, integrity, and availability of equipment, data, and information systems. These concepts form the foundation of computer security and techniques and technical solutions have been implemented successfully over the past few decades. The objective of this paper was to introduce the concepts of the CIA triad and introduce how they may be applied within the nonproliferation regime. A few examples have been highlighted in this paper to identify the issues and challenges facing the nonproliferation regime now and in the future. It also highlighted a few technical solutions utilized in information assurance to provide for confidentiality, integrity, and availability of data, equipment, and information systems. As new technologies, processes, and infrastructure are developed and deployed to provide more efficient and effective monitoring, the solutions already proven successful in information assurance could be integrated into the nonproliferation regime.

Explicit consideration of the CIA concept within the nonproliferation regime may highlight issues or concerns which may not be realized otherwise, e.g. through piecemeal evaluation. The triad are at times competing, but a robust and secure infrastructure or piece of equipment requires the balance of all three. This process has been successfully demonstrated in cyber security, and looking toward the future, it can help ensure a trusted and robust nonproliferation regime.

References

[1] International Atomic Energy Agency, "IAEA Safeguards Serving Nuclear Nonproliferation," June 2015. [Online]. Available: https://www.iaea.org/sites/default/files/safeguards_web_june_2015_1.pdf.

[2] International Atomic Energy Agency, "Safeguards Statement for 2015," 31 August 2016. [Online]. Available: https://www.iaea.org/sites/default/files/16/08/statement_sir_2015.pdf.

[3] US Department of State, "Treaty Between The United States Of America And The Union Of Soviet Socialist Republics On The Elimination Of Their Intermediate-Range And Shorter-Range Missiles (INF Treaty)," 8 December 1987. [Online]. Available: https://www.state.gov/t/avc/trty/102360.htm. [Accessed 9 February 2017].

[4] International Atomic Energy Agency, "IAEA Department of Safeguards Long Term R&D Plan, 2012 - 2023," Vienna, 2013.

[5] K. Schoop, P. Schwalback, J. Levert, G. Basso, M. Boella and D. Korosec, "Development in Implementation of Remote Data Transmission," in *Symposium on International Safeguards - Preparing for Future Verification Challenges*, Vienna, 2010.

[6] International Atomic Energy Agency, "Safeguards Implementation Report, Appendix A: Safeguards Statement for 2014," IAEA, Vienna, 2015.

[7] U.S. National Nuclear Security Administration, U.K. Ministry of Defense, Joint U.S. - U.K. Report on Technical Cooperation for Arms Control, 2015.

[8] R. Kissel, "Glossary of Key Information Security Terms," May 2013. [Online]. Available: http://nvlpubs.nist.gov/nistpubs/ir/2013/NIST.IR.7298r2.pdf.

[9] W. a. B. L. Stallings, Computer Security Principles and Practice Second Edition, Prentice Hall, 2012.

[10] L. Mandaro, "FBI said to probe breach of Juniper Networks VPN software," 19 December 2015. [Online]. Available: https://www.usatoday.com/story/tech/news/2015/12/19/fbi-investigates-juniper-networks-breach-hack-vpn-encrypted/77642450/.

[11] Department of Homeland Security, "Joint Statement from the Department of Homeland Security and Office of the Director of Nationl Intellegience on Election Security," 7 October 2016. [Online]. Available: https://www.dhs.gov/news/2016/10/07/joint-statement-department-homeland-security-and-office-director-national.

Viability of an Unattended Verification Station for UF_6 Cylinders: Phase I Findings

LE Smith[1], KA Miller[2], BS McDonald[1], JB Webster[1], MA Zalavadia[1], JR Garner[3], SL Stewart[3], SJ Branney[4], LC Todd[1], NS Deshmukh[1], HA Nordquist[2], JA Kulisek[1], MT Swinhoe[2]

[1]Pacific Northwest National Laboratory
[2]Los Alamos National Laboratory
[3]Oak Ridge National Laboratory
[4]Savannah River National Laboratory

Abstract:

In recent years, the International Atomic Energy Agency (IAEA) has pursued innovative techniques and an integrated suite of safeguards measures to address the verification challenges posed by the front end of the nuclear fuel cycle. Among the unattended instruments currently being explored by the IAEA is an Unattended Cylinder Verification Station (UCVS), which could provide automated, independent verification of the declared relative enrichment, ^{235}U mass, total uranium mass, and identification for all declared uranium hexafluoride (UF_6) cylinders in a facility (e.g., uranium enrichment plants and fuel fabrication plants). Under the auspices of the United States and European Commission Support Programs to the IAEA, a project was undertaken to assess the technical and practical viability of the UCVS concept. Phase I of the UCVS viability study was centered on a long-term field trial of a prototype UCVS system at the Westinghouse Fuel Fabrication Facility in South Carolina, USA. A key outcome of the study was a quantitative performance evaluation of two nondestructive assay (NDA) methods being considered for inclusion in a UCVS: Hybrid Enrichment Verification Array (HEVA), and Passive Neutron Enrichment Meter (PNEM). This paper will provide context for the UCVS and potential implementation concepts, a description of the UCVS prototype design, and an overview of the long-term field trial at a fuel fabrication facility. Selected field-trial results and interpretation are presented, including the performance of PNEM and HEVA for the verification of declared enrichment and ^{235}U mass in over 200 "typical" Type 30B cylinders. Example results from a modeling study provide a preliminary assessment of sensitivity to material-substitution scenarios, for the as-fielded NDA methods.

Keywords: international safeguards; uranium enrichment; nondestructive assay; gamma-ray; neutron

1. INTRODUCTION

The International Atomic Energy Agency's (IAEA's) current enrichment-plant safeguards approaches include attended weighing and nondestructive assay (NDA) of a subset of the plant's cylinder flow and inventory, collection of bulk uranium hexafluoride (UF_6) samples for destructive analysis, and environmental sampling for subsequent laboratory analysis. New safeguards measures that are more effective and cost-efficient than contemporary measures are needed, particularly for modern high-capacity plants [1][2]. Detection of prominent misuse scenarios could be improved at enrichment plants if the IAEA could monitor 100% of material flows and periodically calculate independent uranium and ^{235}U mass balances for the facility. However, human and financial resources preclude continuous inspector presence at the facility to measure all of the material flow, using today's attended methods.

Unattended instruments capable of continuously monitoring material flows, and of performing the routine and repetitive measurements previously performed by inspectors, without additional burden to operators, are central to the new safeguards approaches being considered by the IAEA. One of the instrumentation concepts being considered is an Unattended Cylinder Verification Station (UCVS). UCVS units would be located at key intersections of cylinder movement between material balance areas,

or at the operator's accountancy scales (to take advantage of the facility's cylinder weighing operations) and would autonomously verify 100% of the declared cylinder flow in the facility. The station could include technologies for cylinder identification, NDA of the cylinder contents, load cells, camera surveillance, and data transmission to an on-site computer or inspectorate headquarters. The NDA components of the UCVS would support several measurement objectives, including unattended, independent assay of cylinder enrichment (E_{235}) and ^{235}U mass (M_{235}) for product, feed, and tails cylinders [3][4]. UCVS units would be owned and operated by the IAEA, but the data streams could be shared with the operator (e.g., for process control) or other regulatory body in conformance with IAEA requirements for shared-use instruments. A notional UCVS is illustrated in Figure 1.

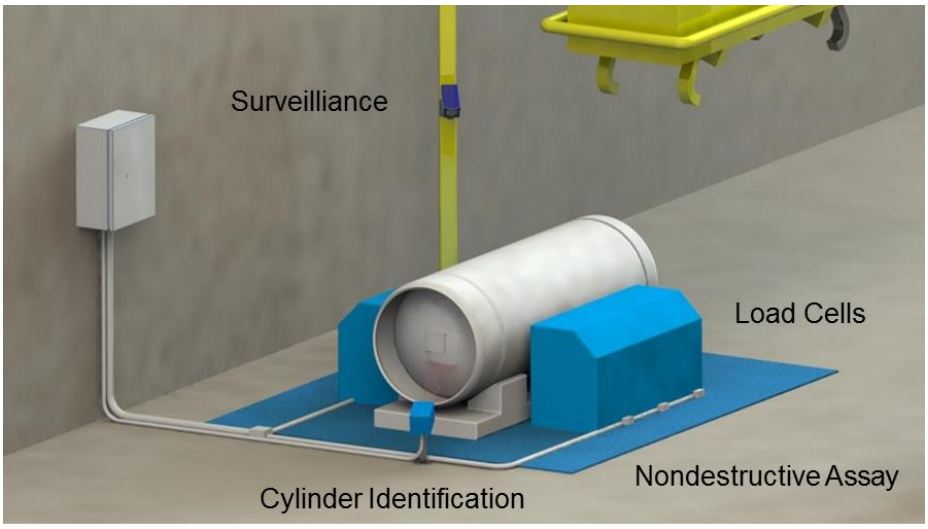

Figure 1. Concept of an integrated UCVS that includes unattended NDA instrumentation (blue panels), load cells, camera surveillance, and cylinder identification technology.

If the potential of the UCVS concept can be realized, such an instrument could significantly enhance the efficiency of IAEA's safeguards approaches at large-capacity enrichment plants, while simultaneously improving effectiveness for deterring and detecting diversion of material from declared flow. A UCVS could also provide benefits to the operators, for example: easing and expediting the release process for product cylinders; reducing the need for sampling and mass spectrometry for process control; and cylinder tracking.

The technical and operational viability of the UCVS concept has been under evaluation under the auspices of the United States and European Commission Support Programs to the IAEA. The centerpiece of UCVS Phase I was a long-term field trial of a prototype UCVS system at the Westinghouse Fuel Fabrication Facility (WFFF) in South Carolina, USA. This paper begins with a description of an example UCVS implementation concept and the UCVS prototype design. An overview of the field trial and selected analysis results is then provided, along with example results from the modeling study that complemented the field trial.

2. IMPLEMENTATION CONCEPT AT ENRICHMENT FACILITY

An example of how a UCVS might be implemented in an enrichment facility is shown in Figure 2, for unblended Type 30B product cylinders. UCVS tracking would begin as the empty cylinder is transferred from the storage material balance area (MBA) to the process MBA (steps 1 and 2). This initial scan would verify that the cylinder is indeed empty by industry standards (i.e., some residual "heel" material often remains in a cylinder labeled as empty). After the product cylinder is filled and homogenized in the process MBA, a UCVS scan is performed during the transfer back to the storage MBA (steps 3 and 4). In this scan of the full unblended product cylinder, the UCVS would independently measure E_{235}, M_{235}, and M_U, and store these data in a way that supports automated comparison to operator declarations of those parameters. A collection of distinguishing characteristics (e.g., gamma-ray peak ratios and spatial variation) for each filled cylinder, labeled here an "NDA Fingerprint", would also be collected and

archived during this scan [4]. Product cylinders would remain in the storage MBA until the operator is ready to ship the cylinder off-site. As the cylinder is removed from the storage MBA for shipment, the UCVS would re-verify the declared parameters and confirm the consistency of the NDA Fingerprint with previous scans. These UCVS data could be reviewed and approved by a remotely located inspector (e.g., at IAEA headquarters). This automated confirmation process could enable an expedited cylinder release process for facility operators (steps 5 and 6), when compared to today's approaches that involve routine interim inspections and on-site inspector measurements.

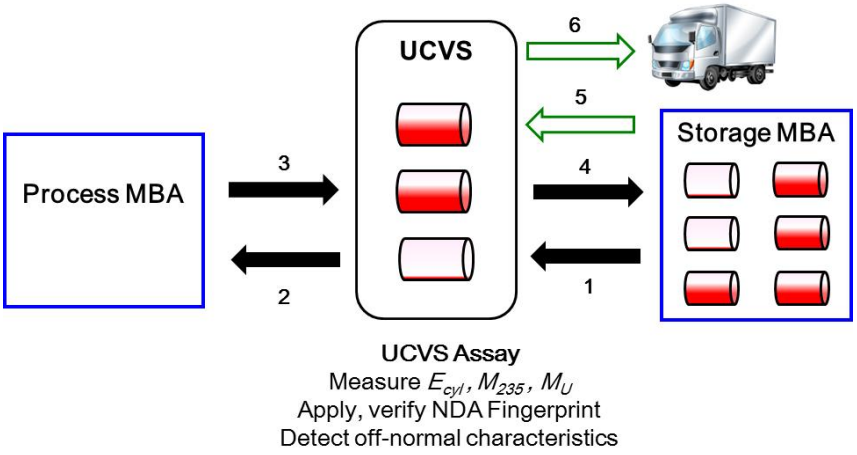

Figure 2. Conceptual overview of how an unblended product cylinder could be verified and released from an enrichment facility using a UCVS.

3. CANDIDATE NDA METHODS

At the inception of UCVS Phase I, the IAEA identified two candidate NDA methods for UCVS, both of which were developed under support from the U.S. National Nuclear Security Administration, Office of Nonproliferation and Arms Control: the Hybrid Enrichment Verification Array (HEVA) and the Passive Neutron Enrichment Meter (PNEM).

HEVA uses an array of NaI(Tl) spectrometers with specially designed collimators to simultaneously measure the direct 186-keV signature from ^{235}U, and via high-energy gamma rays induced by neutrons in ^{56}Fe and the NaI(Tl) itself, the total neutron emission rate from the cylinder [5][6]. The 186-keV signature provides direct measure of E_{235}. Under assumptions of known ^{234}U/^{235}U relationships in the plant, the total neutron signal can be calibrated to total M_{235} in the cylinder. In the Phase I field trial, three HEVA modules were positioned along one side of the cylinder (Figure 3, top), each module consisting of a 7.5-cm × 7.5-cm cylindrical NaI(Tl) spectrometer coupled to a Canberra Osprey digital photomultiplier tube base, and surrounded by a cylindrical collimator that includes iron and polyethylene layers to enhance neutron-to-gamma conversion [7]. Nonproprietary data acquisition and analysis software was developed.

PNEM employs polyethylene-moderated ^{3}He neutron detectors to measure the singles and doubles neutron count rates from the cylinder [8][9]. The singles counts come primarily from the ^{234}U and under an assumption of known ^{234}U/^{235}U behavior, allow determination of ^{235}U mass, a method used by the Uranium Cylinder Assay System (UCAS) deployed by the operator at a Japanese enrichment plant [10]. PNEM extends beyond singles neutron counting to use the coincidence (i.e., doubles) neutron signature that arises from induced fission in ^{235}U, thereby allowing quantification of E_{235}. The PNEM hardware consists of two polyethylene-moderated detector pods, each containing 12 ^{3}He tubes at a pressure of 10 atm. Data acquisition and analysis are based on pulse processing electronics from Precision Data Technology (PDT), a Canberra JSR-12 shift register, and standard IAEA software for unattended monitoring systems: Multi-Instrument Collect (MIC), Radiation Review, and the IAEA Neutron Coincidence Counting software (INCC).

4. UCVS PROTOTYPE DESIGN

The UCVS team, in consultation with the IAEA, Euratom, and Westinghouse, developed a field prototype design consistent with field-trial objectives (see below), the IAEA's preliminary user requirements, and the characteristics of the field-trial deployment location. A depiction of the UCVS field prototype is given in Figure 3 (top). The HEVA and PNEM modules were aligned alongside and below the cylinder support, respectively; load cells were mounted under the cylinder support. Two surveillance cameras were integrated, one with a large field of view to survey the entire field trial location (i.e., the Next Generational Surveillance System, NGSS, in Figure 4) and the other with a field of view focused on the cylinder nameplate (to support confirmation of operator-declared data and troubleshooting). An environmental-sensor package provided temperature, humidity, and dew-point data. A push-button allowed the facility operator to indicate when the cylinder occupancy began, and the associated timer display informed the operator when the 7-minute minimum occupancy period had elapsed. A data acquisition cabinet, filled with components representative of (but not always identical to) the IAEA's Unattended Monitoring Systems was located inside a utility building near the assay platform.

The UCVS software architecture was composed of individual data acquisition modules for each sensor type (Figure 3, bottom). Raw data files and state-of-health information were saved to the local data acquisition computer and a server hosted at PNNL retrieved the raw data daily. No real-time analysis of the raw data was performed in Phase I; all interpretation and analysis beyond state-of-health monitoring of the instruments was performed in post-processing. No digital signing of the data was performed but a virtual private network (VPN) tunnel was used for transmission and IAEA's Get RAINSTORM software was used for data retrieval, consistent with IAEA's current remote monitoring processes [11].

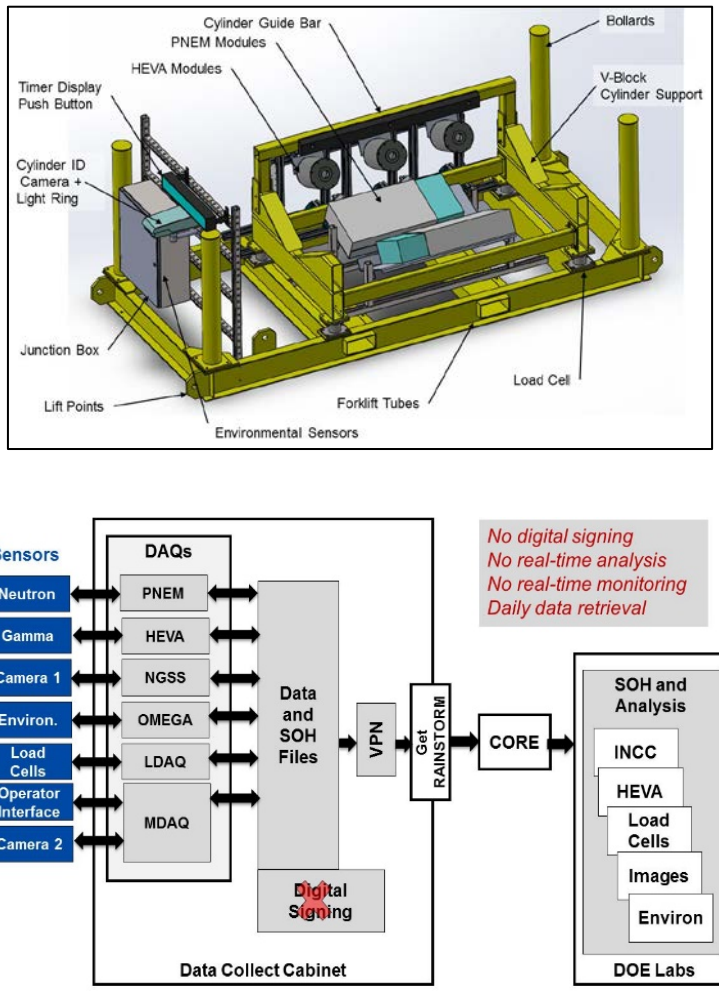

Figure 3. Top: Depiction of the UCVS field prototype. Bottom: Schematic of the UCVS software architecture.

5. FIELD TRIAL OVERVIEW

A visualization of the UCVS prototype as it was deployed at WFFF in April 2015 is given in Figure 4, along with a photo of cylinder placement on the prototype platform. In the nominal cylinder scanning sequence used in the field trial, a cylinder was lifted by crane from the transportation overpacks (located on the vehicle trailer located approximately 3 meters from the UCVS prototype) onto the UCVS cylinder platform. After the occupancy period was complete, the cylinder was loaded by crane onto the operator's accountancy scale, which was located approximately 2 meters from the UCVS platform. A fork truck removed the cylinder from the accountancy scale before processing the next cylinder on the UCVS prototype. The intended full-cylinder handling procedure was not always observed, with the most significant impacts being that cylinders were sometimes left on the accountancy scale, or near the UCVS prototype, during the UCVS occupancy. For a number of occupancies, these nearby background source terms significantly perturbed the PNEM and HEVA signals. Analysis of the raw NDA signatures and camera images was used to identify and remove significantly perturbed occupancies from the cylinder populations used for the viability analysis presented in this paper.

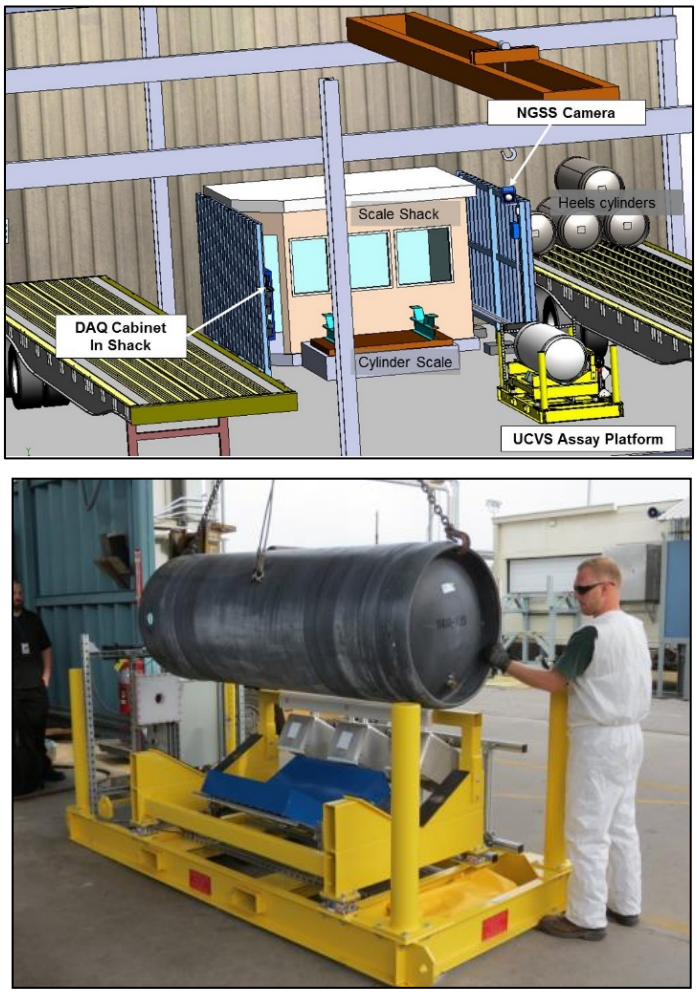

Figure 4. Top: UCVS prototype location at WFFF. The trailer on the left typically contains incoming (full) cylinders in transportation overpacks. The trailer on the right is periodically filled with empty (but with heels) cylinders. Bottom: Placement of a Type 30B cylinder on UCVS using an overhead crane.

During the course of the 8-month field trial, over 300 cylinder occupancies were recorded. Approximately 60 of those were repeated assays of the same cylinder to inform the viability of the NDA Fingerprint concept, several were used for benchmarking simulations, approximately 15 were shown to be perturbed by nearby cylinder movements, and another 14 were not analyzed due to a data acquisition failure. With these reductions, the number of occupancies corresponding to "Typical" cylinders filled to licensed capacity was 229. This population was labeled "Typical All." It consists predominantly of cylinders produced in URENCO enrichment facilities but also includes cylinders from a conversion plant (natural

enrichment) and centrifuge facilities in China and Russia. Subpopulations of the typical cylinders were also defined to support quantitative investigation of facility-specific effects on the fidelity of cylinder assay, particularly as it pertains to the $^{234}U/^{235}U$ behavior and ^{234}U-derived signatures collected by PNEM and HEVA. Characteristics of the subpopulations are summarized in Table 1.

	Shipping Facilities	Number of Cylinders	Range of Enrichment (wt%)	Most Common Enrichments (wt%)
Typical All	Multiple centrifuge enrichment facilities, one conversion facility	229	0.71 to 4.95	2.5, 4.4, 4.95
URENCO All	URENCO's USA, Capenhurst, Almelo and Gronau facilities	166	1.5 to 4.95	4.0, 4.4, 4.95
URENCO A	URENCO USA	66	2.5 to 4.95	4.0, 4.4
URENCO B	URENCO Capenhurst	50	1.5 to 4.95	2.5, 4.95
AREVA All	Multiple enrichment facilities of unknown characteristics	34	1.5 to 4.4	2.6, 3.2

Table 1. Overview of the Type 30B "typical" cylinder populations analyzed in this study.

6. EXAMPLE FIELD TRIAL FINDINGS

A key technical objective in UCVS Phase I was quantifying the precision with which the NDA methods under test (e.g., HEVA and PNEM) could assay the cylinder-verification parameters important to the IAEA, particularly the declared enrichment and ^{235}U mass. The typical-cylinder occupancies, nominally seven minutes in duration, provided the raw PNEM and HEVA data needed to define the calibration relationship between each NDA signature, or combinations thereof, and the operator's declarations for E_{235} or M_{235}. The precision of the PNEM- and HEVA-determined enrichment and ^{235}U mass values is reported as the relative difference to the declared values, expressed in relative standard deviation (RSD). Six NDA signatures were calibrated and evaluated: traditional 186-keV ($HEVA_T$), non-traditional singles neutron ($HEVA_{NT}$), $HEVA_{hybrid}$, singles neutron ($PNEM_S$), doubles neutron ($PNEM_D$) and $PNEM_{hybrid}$. The hybrid signatures for quantifying cylinder enrichment are a simple averaging (i.e., equal weighting) of the other two signatures for each NDA method, under an assumption that the total uranium mass is known (e.g., from the UCVS load cells or operator declarations). Previous work has indicated that the integration of signatures with a low degree of statistical correlation in their uncertainties can provide more precise and revealing verification results than either signature independently [5][6], and that hypothesis was examined further in this study.

A summary of the PNEM and HEVA results for the assay of E_{235} is given in Table 2 and Figure 5. The field-measured uncertainties for one-time assay of typical cylinders are compared to the IAEA's International Target Values (ITVs) for uncertainty in the assay of UF_6 in cylinders using handheld spectrometers. The ITVs are based on gamma-ray spectrometers using the traditional enrichment meter analysis technique, a 5-minute count time, a well-calibrated instrument with negligible systematic bias, and the use of wall-thickness corrections using ultrasonic tools.

	Typical All (229)	URENCO All (166)	URENCO A (66)	URENCO B (50)	AREVA All (34)
ITV		**5.4 (HPGe)**	**5.8 (NaI)**		
$HEVA_{hybrid}$ E_{235}	5.4	4.3	3.5	3.5	4.3
$PNEM_{hybrid}$ E_{235}	10.6	4.9	1.9	3.4	5.0
$HEVA_T$ E_{235} (186-keV)	5.5	5.3	5.9	4.4	5.8
$PNEM_D$ E_{235} (Doubles)	14.8	5.7	2.4	4.9	7.6

Table 2. Relative standard deviation (σ_E , in %) of measured enrichment values, as compared to operator declarations. HEVA and PNEM results are shown for five populations (cylinder counts in parenthesis) and two analysis approaches: hybrid and single-signature. IAEA's International Target Values (ITV) for product-cylinder assay using high-resolution and medium-resolution handheld spectrometers are noted. Results are reported for cylinder enrichments greater than 1.5 wt%.

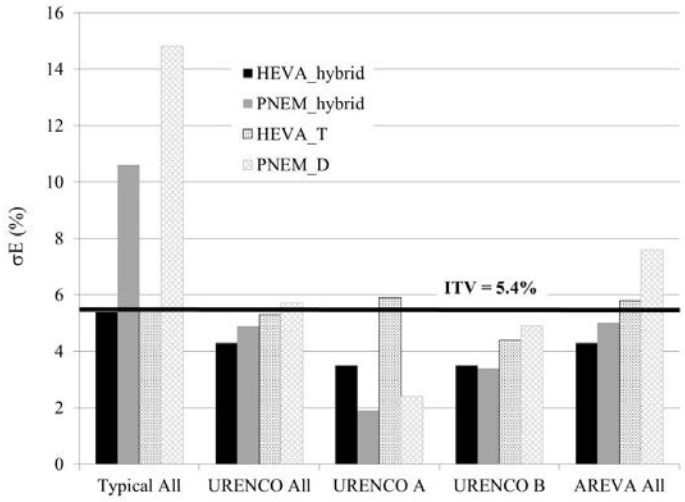

Figure 5. Relative standard deviation (σ_E , in %) from the operator's declared values for cylinder enrichment, for HEVA and PNEM for the cylinder populations analyzed in the field trial. The ITV for high-resolution spectrometers is shown for comparison.

A summary of the PNEM and HEVA results for the assay of M_{235} is given in Table 3 and Figure 6. ITVs for M_{235} are not available because the handheld devices used today measure only a small portion (<0.1%) of the UF_6 volume in the cylinder and are therefore not capable of assaying the absolute mass of ^{235}U in the cylinder.

	Typical All (229)	**URENCO All (166)**	**URENCO A (66)**	**URENCO B (50)**	**AREVA All (34)**
UCVS Target Values			**3.0**		
$HEVA_{NT}$ M_{235} (Singles)	7.6	5.7	3.0	2.6	5.4
$PNEM_S$ M_{235} (Singles)	7.4	4.8	2.1	2.9	3.4

Table 3. Relative standard deviation (σ_M , in %) from the operator's declared values for ^{235}U mass. HEVA and PNEM results are shown for five populations of Type 30B cylinders (cylinder counts in parentheses). IAEA's target values, as given in the UCVS user requirements, are also shown.

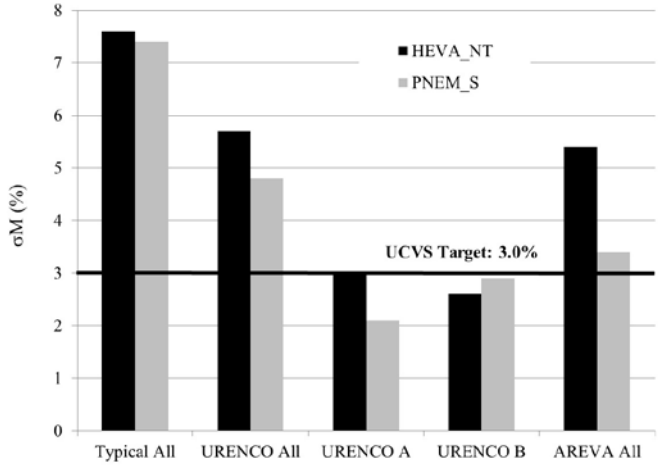

Figure 6. Relative standard deviation (σ_M , in %) from the operator's declared values for ^{235}U mass, for HEVA and PNEM for the cylinder populations analyzed in the field trial. The IAEA target value for ^{235}U mass assay is shown for comparison.

Additional field-trial results and interpretation for the candidate NDA methods, including preliminary findings on the viability of the NDA Fingerprint (not discussed in this paper) can be found in [12][3].

7. EXAMPLE MODELING RESULTS

As a complement to the long-term field trial of the two NDA methods, Monte Carlo N-Particle (MCNP) simulation studies were performed to more fully characterize the neutron and gamma-ray signatures collected by PNEM and HEVA, and to support analyses of material-diversion sensitivity for scenarios that are not easily measured. Simulations of different material substitution scenarios were combined with the field-measured RSD values to provide an estimate of partial-defect sensitivity for the full-volume, neutron-based $PNEM_S$ and $HEVA_{NT}$ signatures. The average of the field-measured RSDs for the two largest facility-specific calibration populations, URENCO A and URENCO B, was taken as representative of the uncertainty for the one-time assay of typical cylinders (σ_{typ}). The σ_{typ} values for $PNEM_S$ and $HEVA_{NT}$, as calculated from Table 3, are 2.5% and 2.8%, respectively.

The geometry used for the partial-defect scenarios is shown Figure 7. In this example scenario, depleted UF_6 (DUF_6) has replaced a portion of the low-enriched UF_6 ($LEUF_6$) in the interior of the cylinder such that there is a uniform thickness *L* of $LEUF_6$ surrounding the diverted material. This geometry was chosen because it represents the most difficult scenario to detect based on a traditional (e.g., enrichment meter method) gamma-ray measurement taken uniformly around the cylinder walls and, thus, provides a conservative estimate of detection probability in that it maximizes reliance on neutron detection.

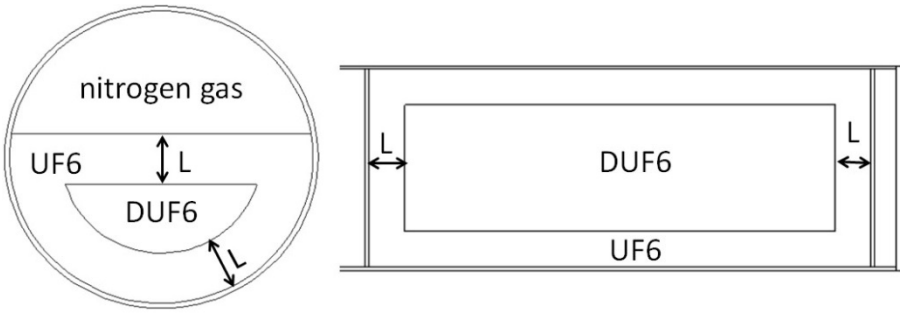

Figure 7. Schematic of the partial-defect scenario in which $LEUF_6$ in the center of the cylinder is replaced with DUF_6. The dimension *L* is varied to create partial defects of varying relative mass fractions.

Performance predictions for partial-defect detection were calculated in terms of the probability of detection at a given false alarm rate for various levels of diverted material. A false alarm rate of 1% was enforced by defining alarm thresholds above and below the mean net counts expected for a cylinder filled with material enriched to the declared value, assuming a normal distribution: $\mu \pm 2.58\ \sigma_{typ}\ \mu$, where μ is the expected, mean count rate for a cylinder with no material diversion.

The probability of detection for each mass fraction level of diverted material is determined using the probability density function (again, assuming a normal distribution) of the count rate for the corresponding cylinder with diverted material (see Figure 8). For the DUF_6 substitution scenario, the fraction of the probability density function of the diverted cylinder that falls below the lower alarm threshold, which is set based on the distribution of the cylinder with no diversion, is the detection probability.

The probability-of-detection curves for $PNEM_S$ and $HEVA_{NT}$ for the DUF_6 substitution scenario are shown in Figure 8 for a 1% false alarm rate. The results indicate that PNEM can detect mass defects of greater than 8% with greater than 90% confidence in the one-time cylinder assay scenario. HEVA sensitivity is somewhat lower, at approximately 15% for the same confidence level. The reasons for superior PNEM sensitivity include a marginally lower uncertainty for singles neutrons (2.5% versus 2.8% for HEVA) and higher spatial sensitivity over the cylinder region in which the material substitution occurred.

Additional modeling and simulation results, as well as interpretation related to the design and implementation of UCVS, can be found in [12][14].

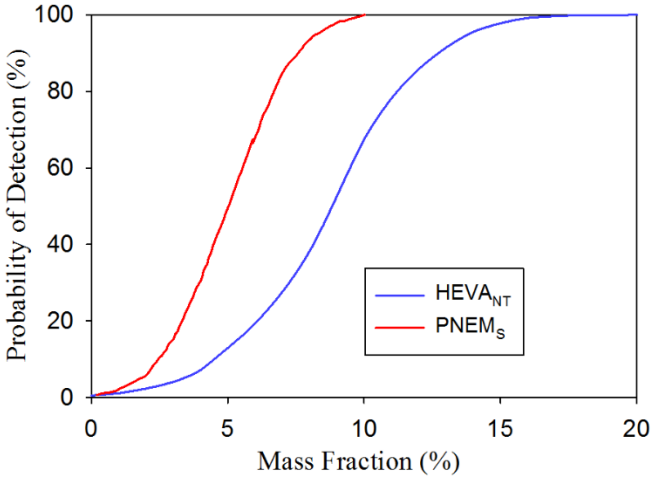

Figure 8. Probability-of-detection curves for $PNEM_S$ and $HEVA_{NT}$ for the DUF_6 substitution scenario.

8. CONCLUSION

The UCVS Phase I field trial was completed on schedule and achieved the objectives defined by project stakeholders. The functionality and reliability of the integrated UCVS prototype was encouraging: it operated in continuous unattended fashion for over eight months in an outdoor environment. The raw data collected during the trial, for various subpopulations of typical Type 30B cylinders, have supported comparative analyses of the candidate NDA methods for the one-time assay of cylinder enrichment and ^{235}U mass, and compared to performance for today's handheld devices. Both HEVA and PNEM demonstrated the ability to accurately and precisely assay E_{235} in a full-volume fashion, using the hybridization of NDA signatures. Both methods have the potential to provide assay precision comparable to or better than IAEA target values for handheld devices, without the need for wall-thickness corrections using an ultrasonic instrument. PNEM and HEVA precision for ^{235}U mass assay, using total neutron signatures, were comparable over all populations, consistent with the fact that both are collecting essentially the same signature. Both methods offer the potential for full-volume assay of ^{235}U mass. This would represent a new capability to safeguards inspectorates and support a significant improvement in the ability to detect material substitution and removal scenarios, as illustrated in the modeling-based results presented here.

The findings and lessons learned from the Phase I field trial will inform a follow-on phase in which the NDA methods will be refined and the integrated prototype platform evolved toward the IAEA's vision for an unattended cylinder verification station. The next phase of the study is expected to include, for example, the assay of a broader range of cylinder enrichments and Type 48 cylinders, and place a greater emphasis on collection of data from repeated cylinder assays—to inform the viability of the NDA Fingerprint concept. In addition, emphasis will be placed on demonstrating fully unattended operation (e.g., automated occupancy detection), analysis, and reporting. The iRAP software, currently being developed by Euratom and IAEA, was not ready for deployment in Phase I but will likely be included in Phase II.

9. ACKNOWLEDGEMENTS

Funding for this work has been provided by the U.S. National Nuclear Security Administration's Office of International Nuclear Safeguards (NA-241) and the U.S. Support Program to the IAEA. The IAEA and Euratom have provided oversight and invaluable guidance to the project from its inception. The UCVS team is indebted to Westinghouse and the staff at the Westinghouse Fuel Fabrication Facility for supporting this measurement campaign, from the early planning stages through the final reporting.

10. REFERENCES

[1] Cooley JN, *Model Safeguards Approach and Innovative Techniques Implemented by the IAEA at Gas Centrifuge Enrichment Plants.* INMM Annual Meeting Proceedings. 2007.

[2] Lebrun AR, et al., *Improved Verification Methods for Safeguards Verifications at Enrichment Plants*. Proceedings of the ANIMMA Conference. 2009.

[3] International Atomic Energy Agency, *Unattended Cylinder Verification Station (UCVS) User Requirements*. SG-UR-12186. IAEA Department of Safeguards. 2013.

[4] Smith LE, Lebrun AR, Labella R, *Potential Roles of Unattended Safeguards Instrumentation at Centrifuge Enrichment Plants*. Journal of Nuclear Materials Management (42). 2013.

[5] Smith LE, Mace EK, and Misner AC, *Signatures and Methods for the Automated Nondestructive Assay of UF_6 Cylinders at Uranium Enrichment Plants.* IEEE Transactions on Nuclear Science (57). 2010.

[6] Smith LE, Jordan DV, Kulisek JA, McDonald B, Mace EK, *Viability of UF_6 Cylinder Verification using the Hybrid Enrichment Verification Array.* Journal of Nuclear Materials Management (43). 2015.

[7] Zalavadia MA, Smith LE, McDonald BS, Kulisek JA, Mace EK, Deshmukh NS, *Hybrid Enrichment Verification Array: Module Characterization Studies*, PNNL-25066. Pacific Northwest National Laboratory. 2016.

[8] Menlove HO, Swinhoe MT, and Miller KA, *A More Accurate and Penetrating Method to Measure the Enrichment and Mass of UF_6 in Storage Cylinders Using Passive Neutron Self-Interrogation*. INMM Annual Meeting Proceedings. 2010.

[9] Miller KA, Menlove HO, Swinhoe MT, Marlow JB, “A New Technique for Uranium Cylinder Assay Using Passive Neutron Self-Interrogation.” Proc. IAEA Symposium on International Safeguards. 2010.

[10] Miller KA, et al., *The Uranium Cylinder Assay System for Enrichment Plant Safeguards*. Journal of Nuclear Materials Management (39). 2010.

[11] Morgan K and Brunhuber C, “Evolution of RAINSTORM,” Proc. IAEA Symposium on International Safeguards. 2014.

[12] Smith LE, Miller KA, et al., *Viability Study for an Unattended UF_6 Cylinder Verification Station: Phase I Final Report*, PNNL-25395. Pacific Northwest National Laboratory. 2016.

[13] Smith LE, KA Miller, et al., *An Unattended Verification Station for UF_6 Cylinders: Field Trial Findings.* Submitted to Nuclear Instruments and Methods in Physics Research, A. April 2017.

[14] Miller KA, Kulisek JA, et al., *Viability of an Unattended Verification Station for UF_6 Cylinders: Monte Carlo Modeling Studies.* In preparation for Nuclear Instruments and Methods in Physics Research, A.

Status of Safeguards R&D on pyroprocessing related facilities at KAERI

Ho-Dong Kim, Se-Hwan Park, Seong-Kyu Ahn, Hee Seo, and Byung-Hee Won

Korea Atomic Energy Research Institute, Daejeon

Daedeok-daero 989-111, Yuseng-gu, Daejeon, 305-353 Republic of Korea
E-mail: khd@kaeri.re.kr

Abstract:

The Republic of Korea (ROK) has implemented the Safeguards By Design (SBD) concept in nuclear fuel cycle facilities. Since the early 1990s KAERI (Korea Atomic Energy Research Institute) has developed several nuclear fuel cycle facilities for research activities on spent fuel treatment. Such facilities include the DUPIC Fuel Development Facility (DFDF), the Advanced spent fuel Conditioning Process Facility (ACPF), and the PyRoprocessing Integrated inactive DEmonstration facility (PRIDE). PRIDE is an engineering-scale R&D facility, handling non-irradiated depleted uranium and surrogates to develop and test key technologies for pyroprocess. The data obtained from this facility will be used to evaluate the feasibility of pyroprocessing facility in the future. DFDF consists of one concrete hot cell used for the technology development of the DUPIC (Direct Use of Pressurized Water Reactor Fuel in CANDU) fuel fabrication as well as for voloxidation of irradiated PWR spent fuel rod cuts to produce feed material for the electrolytic reduction process in ACPF. ACPF consists of two interconnected hot cells with two shielded rear doors for material transfer designed for research on electrolytic reduction of spent oxide fuel into the metallic form. Pyroprocessing related facilities which contain less than one significant quantity of nuclear material but which utilize technologies and equipment related to the electrochemical recycling of spent fuel have been treated as category III by the IAEA. The demands for robust safeguards applied to pyroprocessing facilities require the IAEA to develop new safeguards measures and techniques. The KAERI's safeguards R&D will provide the IAEA and the international community with credible assurances regarding a State's fulfilment of its safeguards obligations.

Keywords: SBD; Safeguards Approach; Safeguards Measures; Nuclear Fuel Cycle; Pyroprocessing

1. Introduction

Since the early 1990s, KAERI has developed safeguards systems of several nuclear fuel cycle facilities for research activities on spent fuel treatment. Such facilities include the DUPIC Fuel Development Facility (DFDF), the Advanced spent fuel Conditioning Process Facility (ACPF), and the Pyroprocessing Integrated inactive DEmonstration facility (PRIDE). These facilities are now being used as facilities to develop and evaluate the pyroprocessing concept. Pyroprocessing related facilities which contain less than one significant quantity of nuclear material but which utilize technologies and equipment related to the electrochemical recycling of spent fuel have been treated as category III by the IAEA.

As part of a cooperative effort with the IAEA to find a safeguards approach for the pyroprocessing facility, the ROK designed a Reference Engineering-scale Pyroprocessing Facility (REPF) and developed a safeguards system for the REPF that was reviewed by the IAEA. The IAEA plans to test the safeguards measures of REPF in KAERI pyroprocessing facilities through member state support program (MSSP) with ROK. The REPF is being upgraded to REPF+, which include the scale-up of the pyroprocessing facility and U/TRU fuel fabrication process. KAERI has developed a simulation program, Pyroprocessing Material flow and MUF Uncertainty Simulation (PYMUS) to assess the nuclear material accountancy system of the REPF. The PYMUS is under improvement to include the function of the statistical analysis of Near Real Time Accountancy (NRTA).

KAERI is developing an advanced safeguards system, including nuclear material accounting technologies and new safeguards approach for pyroprocessing facilities in parallel with the process technology development and facility design. This paper addresses the main features of the safeguards R&D status of pyroprocessing facilities at KAERI.

2. Safeguards Systems of Nuclear Fuel Cycle Facilities at KAERI

According to the “Agreement for Cooperation between the Government of the Republic of Korea and the Government of the United States of America Concerning Peaceful Uses of Nuclear Energy” revised in 2015, KAERI has been using DFDF for preparing the feed material (porous pellet or fragment) from the spent PWR fuel generated in domestic nuclear power plants for the ACPF electrolytic reduction process. The ACPF at KAERI has been refurbished for the demonstration of the pyroprocessing technologies related to the electrolytic oxide reduction process of the PWR spent fuels. The safeguards approaches for the DFDF and ACPF have been developed, that include neutron counters and containment and surveillance equipment with a process and radiation monitoring system. The ACPF can provide a valuable opportunity to test various types of safeguards equipment for nuclear material accountancy, containment and surveillance, as well as process monitoring. At the moment, there are two types of safeguards equipment at the ACPF, i.e., ASNC (ACP Safeguards Neutron Counter) and ALIM (ACP LIBS Monitoring system) [1].
The ASNC, based on the passive neutron coincidence measurement technique, measures the amount of 244Cm. The amount of nuclear material in the ACPF can be determined by using the Cm balance technique, which multiplies the measured 244Cm amount by the Pu/244Cm or 235U/244Cm ratio to calculate the amount of nuclear material of interest (Pu or 235U). This ratio can be obtained by a destructive analysis, gamma-ray spectroscopy, or burnup-code calculation.
In a previous study [2], the ASNC was installed in a hot cell of the ACPF and tested successfully with spent fuel rod cuts. However, its inner structure, with a horizontally-laid geometry, becomes deformed over the course of many years due to the weight and the ductility of the leaden gamma-ray shield. To address this problem, the ASNC was to be redesigned for a vertically-standing geometry based on the MCNP simulation and irradiation test results as shown in Figure 1.

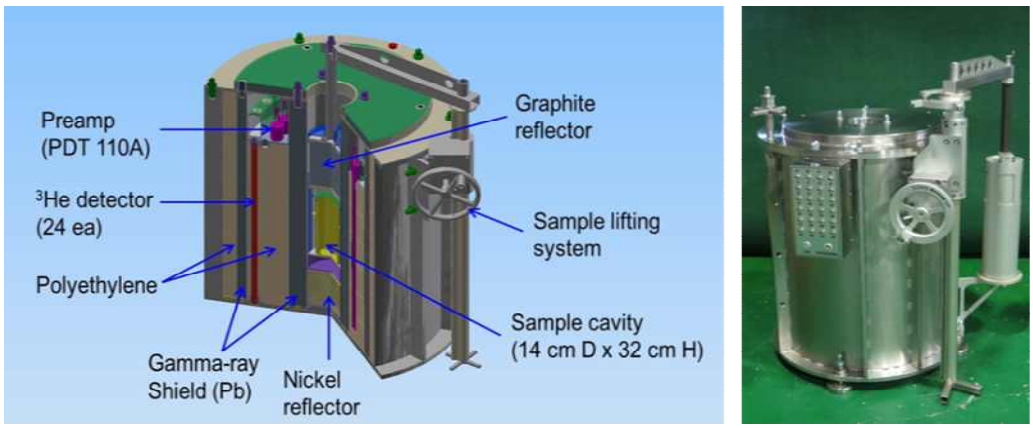

Fig. 1. Modified ACP Safeguards Neutron Counter

The detection efficiency profile of the ASNC in the axial and radial directions was measured for a 252Cf standard source in order to characterize the system and verify the MCNP model. Ideally, a good system shows the same efficiency regardless source locations, resulting in low measurement error. The system showed flat response in terms of the measured efficiency, as shown in Fig. 2. In addition, the simulated results showed excellent agreement with the measured data, which confirmed the accuracy of the MCNP model for the measurement system. The modified ASNC will be tested with the spent fuel rod cuts for calibration and with the input and output materials of oxide reduction process for evaluation of the performance.
LIBS was recognized as a promising technique because material can be analysed without the careful sample preparation. The use of LIBS based on the fiber optics is a benefited applications of LIBS to hot cell environment by delivering the laser energy to the target and by collecting the plasma light. The Fiber-Optic LIBS (FO-LIBS) system to measure the Pu/U ratio of the process material of ACPF has installed at air cell of ACPF, and the performance will be tested as the spent fuel will be introduced to ACPF.

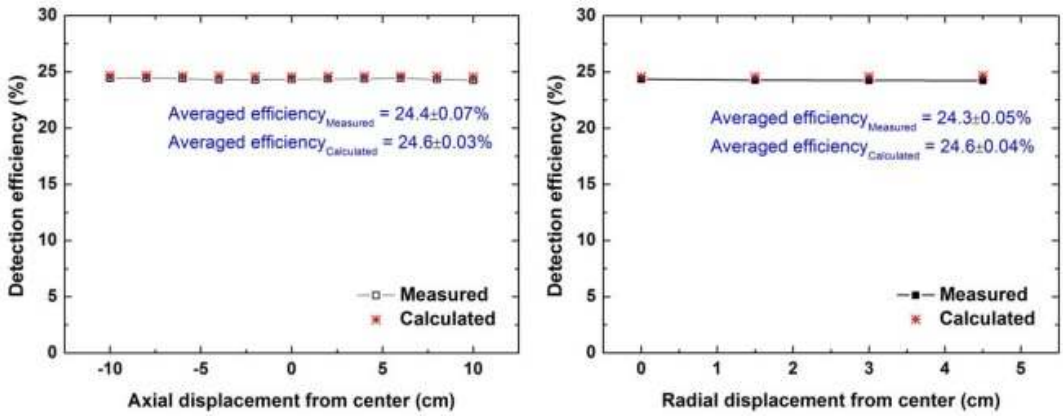

Fig. 2. Detection Efficiency Profile of the ASNC

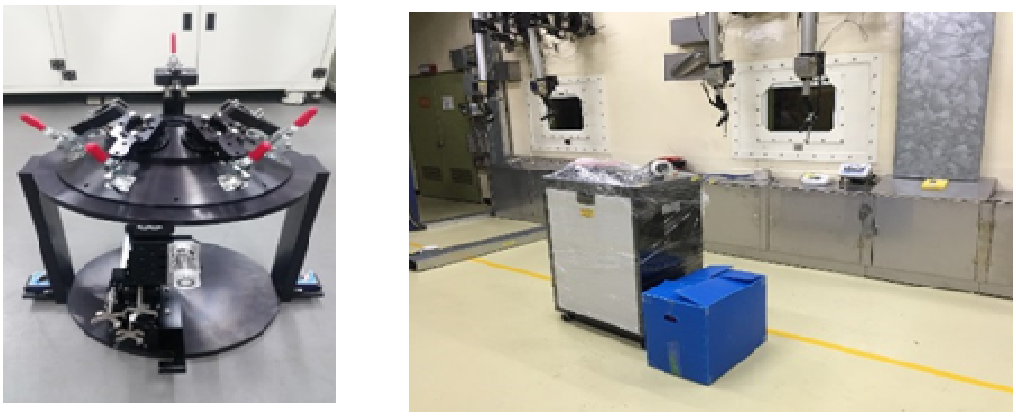

Fig. 3. LIBS installed at ACPF

PRIDE is an engineering-scale R&D facility, handling non-irradiated depleted uranium (DU) and surrogates to develop and test key technologies for pyroprocessing prior to the development and construction of an engineering-scale facility. The demands for robust safeguards applied to pyroprocessing facilities require the IAEA to develop new measures and techniques to complement the more traditional safeguards systems. The bus bar system, together with portal radiation monitors, were selected and installed in the PRIDE facility to support IAEA safeguards implementation in this facility [3].

Process monitoring data such as voltage, current, temperature, and humidity are collected from the process equipment. Most of parameters relevant to the PRIDE safeguards are collected, and they are displayed and provided to the IAEA. PRIDE facility will be used for the testing how to develop the safeguards signature of process monitoring data, containment and surveillance (C&S) device, and the training of IAEA inspectors on the engineering-scale pyroprocessing facility

Fig. 4. Front view and working area of the PRIDE facility

3. Safeguards System of Reference Engineering-scale Pyroprocessing Facility

The ROK was working closely with the IAEA under the ROK's MSSP to develop a model SG approach for a REPF. REPF design is part of the IAEA's effort to develop an effective safeguards approach for pyroprocessing facilities. As a result of the project, a model Design Information Questionnaire (DIQ), a model Facility Attachment (FA) and a model SG approach were prepared [4].
The concept of the REPF is now being revised to 30 MTHM throughput facility, REPF+, to investigate the scale-up effect of the safeguards. One of key features of REFP+ is the allowance of nuclear material mixing between campaigns, whereas the material mixing was limited in the REPF. A simulation program, PYMUS, has been developed to analyze the nuclear material flow and calculate the MUF uncertainty [5]. The PYMUS is being upgraded to evaluate the detection probability based on the statistical test for the various diversion scenarios.
Based on the experience with the ROK MSSP, the IAEA is well on the way to establish effective safeguards for future engineering/commercial scale pyroprocessing facilities.

4. Conclusions

KAERI has developed several nuclear fuel cycle facilities (DFDF, ACPF and PRIDE) for research activities on spent fuel treatment. The ROK designed the REPF through IAEA MSSP and developed a safeguards system for the REPF that was reviewed by the IAEA. KAERI is developing an advanced safeguards system, including nuclear material accounting technologies and new safeguards approach for pyroprocessing facilities in parallel with the process technology development and facility design.
The application of Safeguards by Design (SBD) to these efforts will contribute to improving non-proliferation and safeguards technology so that pyroprocessing technology can be realized in the future. It is expected that the deployment of these safeguards technologies would be useful for the advanced nuclear fuel cycle.

5. Acknowledgments

This work was partly supported by the National Research Foundation (NRF) grant funded by the Ministry of Science, ICT & Future Planning, Republic of Korea (No. 2017M2A8A5015084).

6. References

[1] H. Seo et al., "Development of ACP Safeguards Neutron Counter (ASNC)," KAERI/TR-6594/2016, pp.1-29 (2016)

[2] T. H. Lee et al., "Hot-test Results of the Advanced Spent Fuel Conditioning Process Safeguards Neutron Counter for PWR Spent Fuel Rods," Nucl. Technol. 176, 147-154 (2011)

[3] W. Bekiert et al., "Safeguarding Pyro. Related Facilities in the ROK', Proceedings of IAEA Safeguards Symposium (2014)

[4] H.D. Kim, H.S. Lee, D.Y. Song, T.H. Lee, B.Y. Han, S.K. Ahn, and S.H. Park, "Application of safeguards-by-design for the pyroprocessing facilities in the ROK', JNMM, Vol. XL(4), 24 (2012)

[5] H. S. Shin, B. Y. Han, S. K. Ahn, J. S. Seo, and H. D. Kim, "Development of a Simulation Program for the Pyroprocessing Material Flow and MUF Uncertainty", Proc. of INMM 52th, California, USA (2011)

Feasibility study of advanced technology for Pu with FP solution monitoring
- Overview of Research Plan and Modelling for Simulation-

Megumi Sekine[(1)], Takuya Matsuki[(1)], Satoshi Suzuki[(1)], Masafumi Tanigawa[(1)], Takeshi Yasuda[(1)], Atsushi Yamanaka[(1)], Koichi Tsutagi[(1)], Hironobu Nakamura[(1)], Hirofumi Tomikawa[(1)]
LaFleur Adrienne Marie[(2)]、Browne Michael Charles[(2)]

[(1)]Japan Atomic Energy Agency (JAEA)
[(2)]Los Alamos National Laboratory (LANL)

Abstract:

The IAEA has proposed in its long-term R&D plan, the development of technology to enable real-time flow measurement of nuclear material as a part of an advanced approach to effective and efficient safeguards for reprocessing facilities. To address this, JAEA has designed and developed a neutron coincidence based non-destructive assay system to monitor Pu directly in solutions which is after purification process and contains very little fission products (FPs). A new detector to enable monitoring of Pu in solutions with numerous FPs is being developed as a joint research program with U.S. DOE at the High Active Liquid Waste (HALW) Storage Facility in Tokai Reprocessing Plant.
As the first step, the design information of HALW tank was investigated and samples of HALW was taken and analyzed for Pu concentration and isotope composition, density, content of dominant nuclides emitting gamma ray or neutron, etc. in order to develop a Monte Carlo N-Particle Transport Code (MCNP) of the HALW tank. In addition, gamma ray source spectra simulated by Particle and Heavy Ion Transport code System (PHITS) was developed by extracting peaks from the analysis data with germanium detector. These outputs are used for the fundamental data in the MCNP model which is then used to evaluate the type of detector, shielding design and measurement positions. In order to evaluate available radiations to measure outside the cell wall, continuous gamma ray and neutron measurement were carried out and the results were compared to the simulation results. The measurement results showed that there are no FP peaks above 3 MeV.
This paper presents an overview of the research plan, characteristics of HALW, development of source term for MCNP, simulation of radiation dose from the HALW tank and radiation measurement results at outside of cell wall.

Keywords: Pu monitoring, High level liquid waste, Reprocessing facility, Non-distractive analysis

1. Introduction

The IAEA has proposed in its long-term research and development (R&D) plan[1], development of improved tools and techniques to enable real-time flow measurements technology of nuclear material including Pu as an advanced approach to conduct reprocessing safeguards effectively and efficiently. The solution monitoring and measurement system (SMMS), which has been installed for continuous monitoring for reprocessing safeguards, can only monitor density, temperature and level of solution. Thus, direct Pu monitoring in the solution by SMMS is impossible. At JAEA, we have already designed and developed a neutron coincidence based non-destructive assay (NDA) system[2] to directly monitor pure Pu solution after extraction and purification. It has been confirmed that a total measurement uncertainty of less than 6% could be achieved, which could be applied as a partial defect verification.
In the reprocessing plant, Pu including FP is being stored as inventory or retained waste. The Pu including FP has an extremely high radiation dose rate making it difficult to access and it's a challenge to develop a technology for monitoring of Pu with FP. Establishment of monitoring technology is important in order to increase transparency of material control and accountability (MC&A). Thus, JAEA has initiated development of a new technique to monitor Pu with FP, through a joint research program under the United States Department of Energy (US DOE) and the Ministry of Education, Culture,

Sports, Science and Technology (MEXT) of the Japanese government.

2. OVERVIEW

2.1 Plan[7]

Although the most suitable test area is the input accountability tank or first extraction process, the JAEA's Tokai Reprocessing Plant (TRP) is no longer operating. Since HALW solutions contain both Pu and FP, the HALW tank (Fig. 1) was selected as the place where the technology will be developed and tested under this R&D program. The HALW tank is shielded by a concrete cell and it is possible to place detectors at the inside/outside of the concrete cell. Figure 1 shows the image of the Pu monitoring technology development. The purpose of the R&D is the development of a detector that can monitor Pu solutions containing FP.

The development is carried out under cooperation with U.S. national laboratories: Los Alamos National Laboratory (LANL) and Lawrence Livermore National Laboratory (LLNL). At first, the radiation (type and intensity) from the HALW is characterized and measurement technology is selected. Then, appropriate detector is designed and developed. The optimized detectors are tested and evaluated at the HALW tank with changing liquid level as shown in Fig. 1. This technology has the potential to be applied to real time monitoring for the entire reprocessing plant.

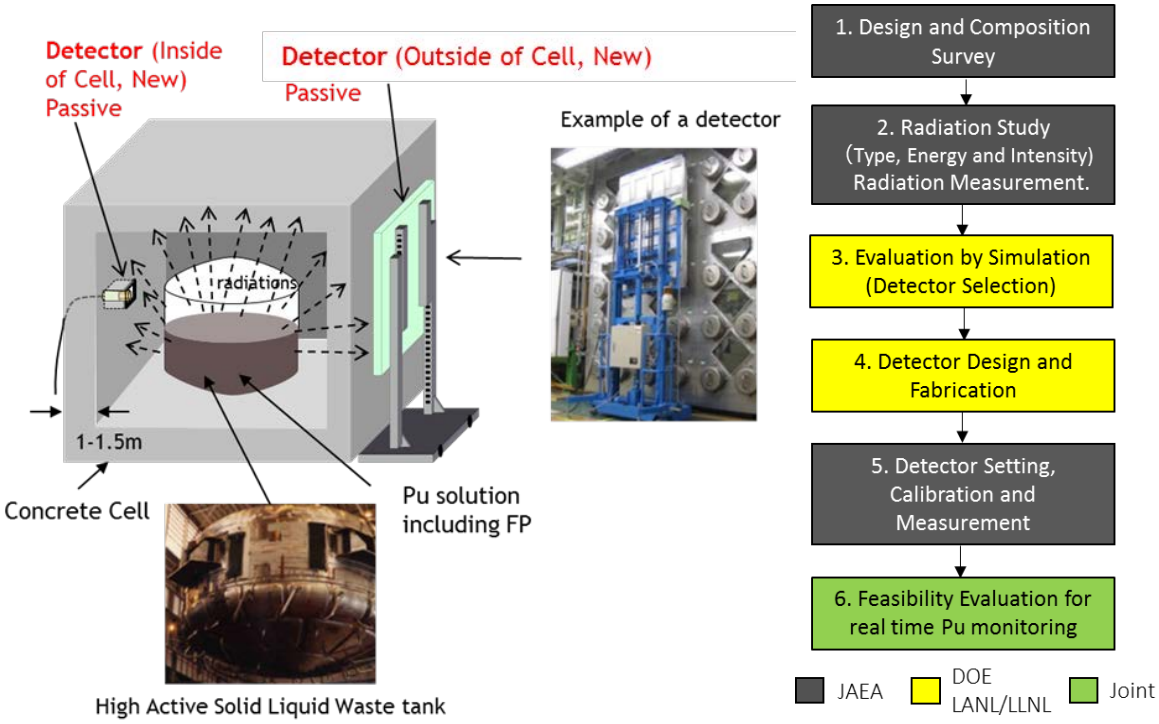

Fig. 1 Image of Pu direct monitoring technology development

The study of development of a new technique to monitor Pu with FP is being carried out from 2015 to 2017. The timetable for the project is shown in Table 1.

Table 1 Timetable for establishment of Pu monitoring system (Japanese fiscal year)

2015	**1. Design information and composition survey of HALW(JAEA)** The design information for HALW tanks and concrete cells was reviewed to develop a simulation model. Radiation (type and intensity) using alpha spectra and gamma spectra, and composition using mass analysis were investigated to develop an input file for simulation. Using HALW analysis data of gamma spectra and neutrons, the radiation dose rate in HALW tank was estimated for the input file for simulation. **2. Radiation study (JAEA)** Gamma rays and neutrons were continuously measured outside of the concrete cell, where the HALW is located, to study placement of the detector and radiation characteristics. The detectors used were high purity germanium (HPGe) detector for

	gamma rays and six He-3 tubes for neutrons [3].
2016	**2. Radiation study (JAEA/LANL)** Gamma rays were continuously measured inside of the concrete cell, where the HALW is located, to study placement of the detector and radiation characteristics. **3. Evaluation by simulation (LANL/LLNL)** LLNL made a common model and simulate gamma rays to benchmark ion chamber measurements help JAEA with gamma detector design. LANL will use this common model to simulate the neutron flux from the HALW tank to support the neutron detector design development.
2017	**2. Radiation study (JAEA/LANL)** Neutrons will be continuously measured inside of the concrete cell, where the HALW is located, to study placement of the detector and radiation characteristics. **4. Detector design and fabrication(JAEA/LANL/LLNL)** Based on the analysis data, simulation analysis results, and preliminary measurement results at the inside and outside of the concrete cell, candidate technologies and Pu monitoring algorism will be considered. The test detector will also be optimized and designed. **5. Detector setting, calibration and measurement(JAEA/LANL/LLNL)** Detector test with changing high level liquid waste amount. **6. Feasibility evaluation for real time Pu monitoring(JAEA/LANL/LLNL)** The test detector will be demonstrated at HALW tank to validate its measurement capabilities.

In the implementation of this technology development, JAEA has received the support of LANL/LLNL based on the implementing arrangement between MEXT and DOE concerning cooperation in the field of nuclear energy-related research and development.

3. The results of composition research of HALW

3.1. Analytical tools for HALW solution

Composition research of HALW for our target HALW storage tank (V35) which has the highest concentration of Pu in HALW tanks at TRP was conducted. Especially, Gamma-ray spectrum was measured in high energy range (up to 10 MeV). Figure 2 shows experimental setup of gamma-ray spectrometry. HPGe [COAXIAL TYPE Ge Detector (GC2020), CANBERRA] and multi-channel pulse height analyzer (MCA) [DSA1000, CANBERRA] connected to HPGe was used for gamma-ray spectrometry. Figure 3 and 4 show photos of HALW sample bottle and picture of experimental setting for gamma-ray measurement. HPGe detector and HALW sample is surrounded by Pb introducing to cut environmental gamma-ray. In order to reduce dose rate, sampled 1 [ml] HALW solution was diluted with nitric acid of same acid concentration to one million times because too high dose rate cause high dead time. Other analyzed items and methodologies are shown in Table.2.

Fig. 2 Experimental setup

Fig. 3 Measurement chamber and sampling bottle

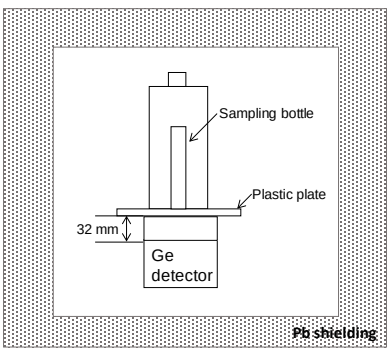

Fig. 4 Image of inside of the measurement chamber

Table 2 Analysed items and methodologies

Analytical item	Unit	Methodology
Acid conc.	mol/L	Neutralization Titration with NaOH (*Hiranuma COM-1600*)
Density	g/cm^3	Density meter (*Anton-paar DMA-35*) oscillating U-tube type
Cm conc.	Bq/mL	*SEIKO EG&G* using detector *"alpha duo"*
Pu conc.	mg/L	Spectrophotometry using cerium nitrate with sludge dissolution by HF
U conc.	g/L	Spectrophotometry(*Shimazu UV-2450*) using TOPO - Ethyl acetate - Dibenzoylmethane (DBM)
Gamma measurement	Bq/mL	Canberra using detector *GC-2020*
Pu isotopic composition	wt%	Mass spectrometer(*Thermo TRITON*) with sludge dissolution by HF, TEVA resin for Pu separation
U isotopic composition	wt%	Mass spectrometer(*Thermo TRITON*) with sludge dissolution by HF, U-TEVA resin for U separation

3.2. Results of gamma-ray and neutron of HALW solution [6]

The gamma-ray spectrum from HALW solution was measured and shown in Fig.5. It is used for source file of MCNP simulation. However, the measured spectrum didn't show any of our target gamma-rays in high energy region [4,5]. We estimated neutron yield in V35 with calculation based on alpha spectra and show it in Table 3. The neutron yield can then be used in the input file for simulations.

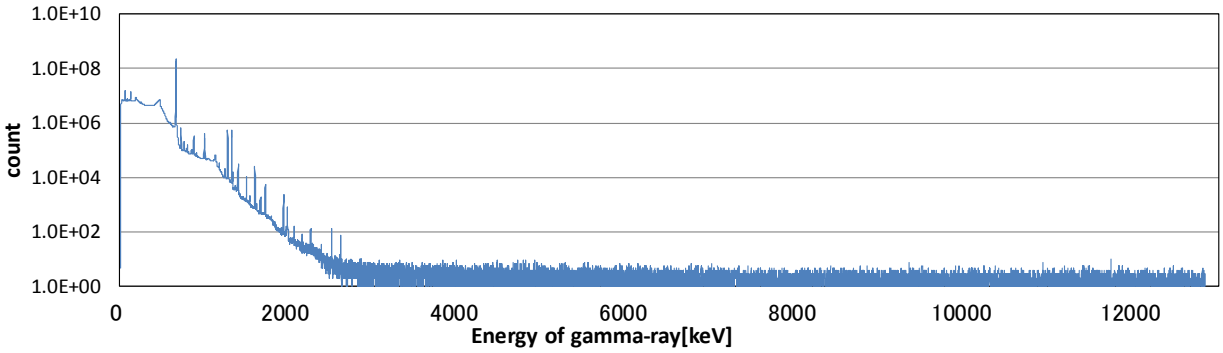

Fig.5 measured gamma-ray spectrum (Measurement time: 550000 [sec])

Table 3 Neutron generation yield in V35

Nuclide	Neutron yield [n/sec]
^{244}Cm	*1.09×10^9*
^{240}Pu	8.24×10^6
^{242}Pu	2.10×10^6
^{238}Pu	8.47×10^5
^{241}Am	1.22×10^4

4. Development of irradiation source input file in HALW tank

4.1. Gross count of each peaks

It was necessary to estimate the absolute gamma-ray counts emitted from HALW sample for the

gamma-ray source data in the MCNP simulations. Key points for making source data were (1) Evaluation for gamma-ray energy emitted from HALW sample, (2) Peak count quantity, (3) Estimation for emitted gamma-ray quantity. After, we conducted more precise energy calibration for the gamma-ray spectrum and made peak count estimation. Then we calculated the attenuation ratio in the analysis geometry. As shown in Fig.6 each peak spectrum was cut with straight line in red. The gross counts from each peak was estimated with this original spectrum as shown in Fig.7.

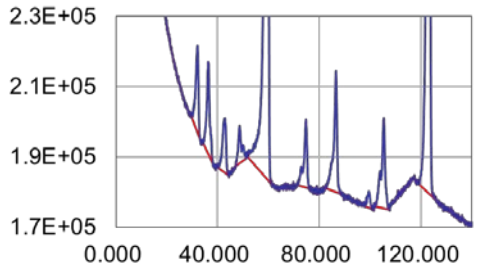

Fig.6 cutting spectrum with straight line (gross)

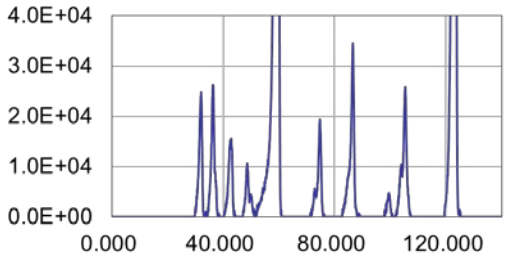

Fig.7 Net count of each peak

4.2. Calculation of Attenuation ratio by PHITS model

In order to confirm how well the HPGe detector could detect gamma rays at the inside of the measurement chamber, a model of the measurement chamber was developed as shown in Fig.8. Because the attenuation ratio of each peaks was different by each gamma-ray energy, we calculated attenuation ratio of each gamma-ray in analysis geometry by PHITS code [9]. The attenuation ratio multiplied to net counts (Fig.7), then gamma ray amounts at V35 tank by the each energy were calculated as shown in Table 4. The Bq values were converted to Ci to compare ORIGEN results. The evaluated absolute gamma-ray intensities were on the same order as ORIGEN and the analysis value as shown in Table 5. We succeeded to create gamma ray source file for simulation.

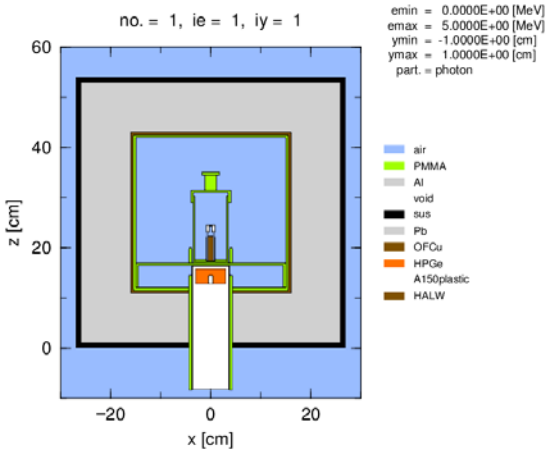

Fig.8 Model of the measurement chamber

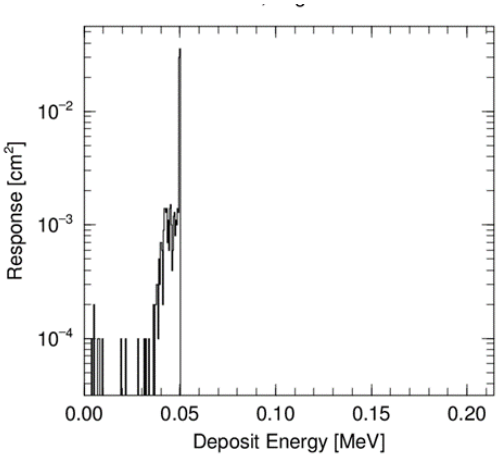

Fig.9 Case of the attenuation ratio of 50 [keV]

Table.4 Net counts, attenuation ratio, total gamma ray amounts at V35 tank

Nucleus	Energy [keV]	net counts	Attenuation ratio (PHITS) [deposit/source]	count/mL (Sample bottle)	Measurement time[s]	Bq/mL	Bq(V35)
241Am(Ci)	59.54	8.23E+06	6.084E-02	1.352E+08	5.615E+04	2.41E+07	1.85E+15
154Eu(Ci)	123.07	6.48E+06	5.785E-02	1.120E+08	5.615E+04	1.99E+07	1.53E+15
134Cs(Ci)	604.80	1.00E+05	1.432E-02	6.983E+06	5.615E+04	1.24E+06	9.56E+13
137Cs(Ci)	661.66	2.94E+08	1.343E-02	2.191E+10	5.615E+04	3.90E+09	3.00E+17
134Cs(Ci)	795.95	7.77E+04	1.144E-02	6.794E+06	5.615E+04	1.21E+06	9.31E+13

Table. 5 Evaluated absolute gamma-ray quantity, ORIGEN and analysis value

Nucleus	Evaluation value [Ci]	ORIGEN calculation value [Ci]	Analytical value [Ci]
241Am(Ci)	1.85E+15	4.40E+15	1.31E+15
154Eu(Ci)	1.53E+15	5.03E+15	-
134Cs(Ci)	9.56E+13	1.61E+14	-
137Cs(Ci)	3.00E+17	2.66E+17	6.23E+16
134Cs(Ci)	9.31E+13	1.61E+14	-

5. Results of gamma and neutron measurements on the outside surface of HALW cell

5.1. Experimental setting

The gamma-ray spectrum and neutron flux were measured outside of the concrete cell. Figure 10 shows the measurement point for the gamma-ray spectrum and neutron measurements. We chose two tanks (these call for V35, V36) for these measurements. V36 tank has only nitric acid and is a spare tank. The result from V36 was compared to the other results. V35 tank has HALW. Figure11 shows measurement setup outside the concrete cell. There is 1.9[m] thickness concrete between detector and HALW tank in outside wall of HALW cell measurement. The largest solid angle point was selected for measurement point that is the same level of HALW tank liquid height.

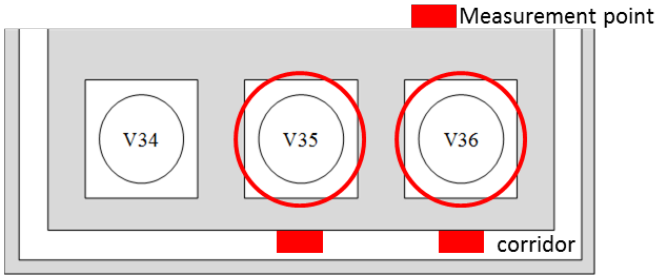

Fig.10 Measurement point (floor plan)

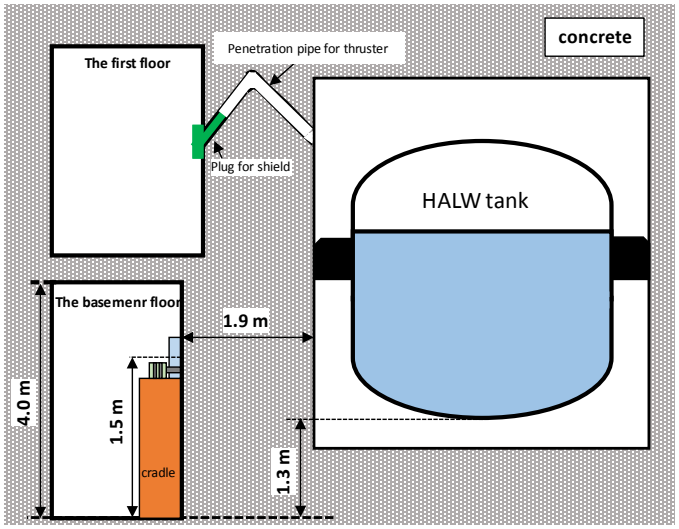

Fig.11 Measurement setup (cross section view)

Two detectors were used for the gamma-ray and neutron measurements. One was HPGe [GMX50-83-A ORTEC] for gamma-ray measurements and its energy range was up to 10 [MeV]. The other was six He-3 tubes in high density polyethylene to measure neutrons (singles rate). Figure 12 and 13 show the HPGe and six He-3 tubes detector setup[1].

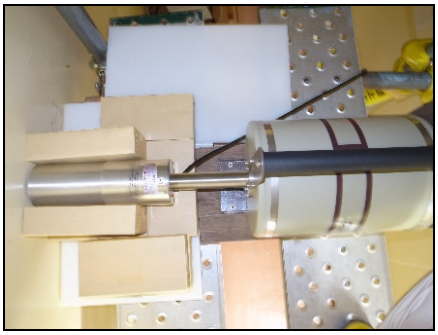

Fig.12 HPGe

Fig.13 Six He-3 tubes

5.2. Result of gamma-ray measurement.

Regarding to HPGe measurement, we could find only environmental gamma-ray peaks. It was determined that the 1.9[m] concreate was too thick to detect gamma-ray emitted from HALW tank and Pu monitoring of gamma rays outside of the cell cannot be conducted. Measurements should be conducted at points with less shielding such as inside penetration pipe or cell.

5.3. Result of neutron measurement.

Figure14 shows the results from the neutron measurement. The horizontal axis shows the measurement cycle number (1cycle means 1minute measurement) and the vertical axis shows neutron signal [cps].Each point corresponds to the neutron count rate in each cycle. The solid lines show mean value of same color points, respectively. As you can see in Fig.14, the neutron response in front of V35 was slightly higher than that of V36. Although this may indicate that we might be able to detect neutrons emitted from HALW tank outside cell which has 1.9[m] thick concrete, these value is insufficient for Pu monitoring because the mean value of V35 was less than 0.1 [cps].

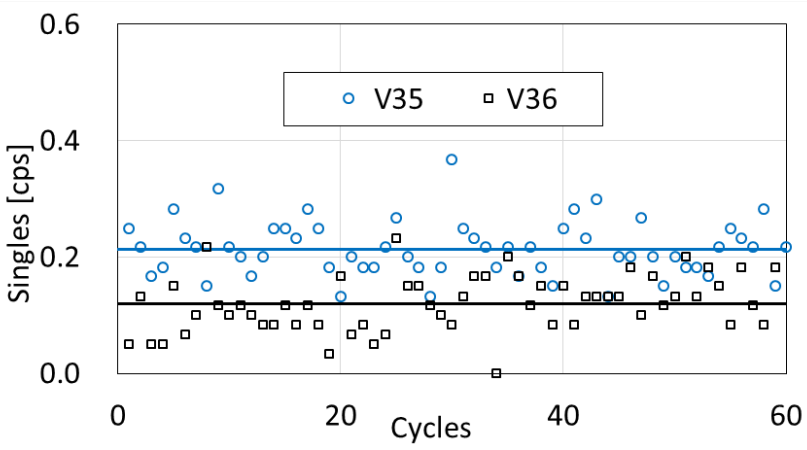

Fig.14 Result of neutron measurement.

5.4. Comparison with simulation results

Model [7]

Since Cm-244 is the dominant source of neutrons in the HALW, Cm-244 was used as the neutron source term [8] in the simulation. The input gamma ray source assumes gamma ray spectra measured with an HPGe detector multiplied by the efficiency curve calculated by PHITS code[9]. The results described in section 3.2 and 4.2 were used as the radiation source files. We assumed the number of particles was 1 million. Dimensions and model used for the simulation are shown in Fig. 15. Radiation that passes through from the concrete cell were simulated at the floor of the 1st floor and 3.28 [m] and 1.52 [m] from the floor of the basement. The screw duct is depicted in Fig. 16.

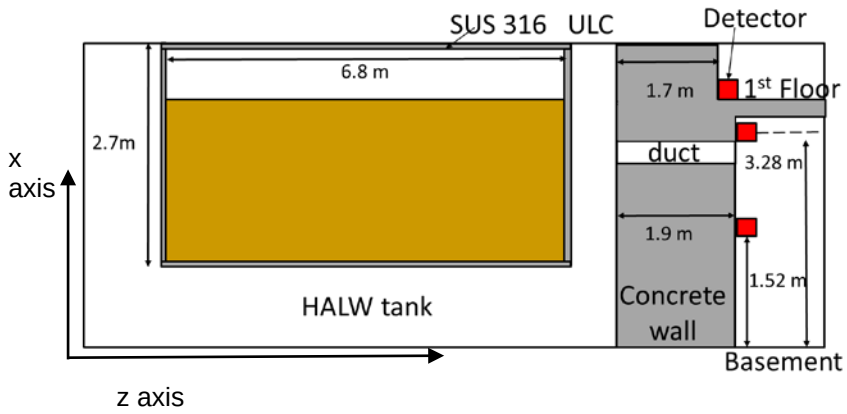

Fig. 15 Model of whole HALW tank(V35)

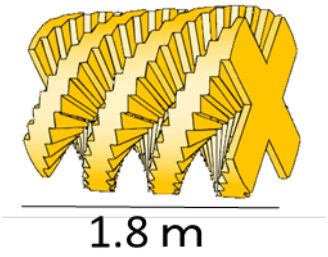

Fig. 16 Structure of screw duct

Results

Gamma rays were simulated using the gamma ray destructive analysis (DA) spectrum from the measurement of the diluted HALW sample as an input file (see Fig. 17). We understood that gamma rays were almost completely shielded about 70 [cm] away from the inner wall. Based on the results of PHITS simulation using DA data as the input file, it seems difficult to measure gamma rays directly from the HAW tank at the outside of the concrete cell as same as measured gamma and neutron results .

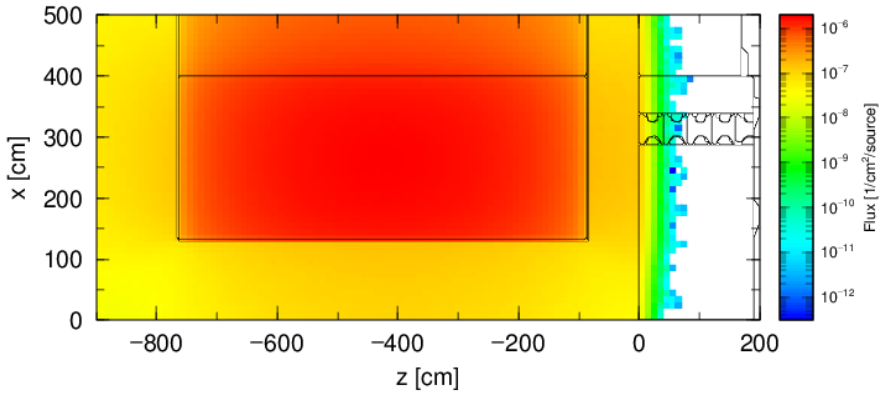

Fig. 17 Gamma rays simulated using gamma ray analysis data as an input file

The neutron distribution was simulated using the neutron analysis data as an input file (see Fig. 18). Scattered neutrons were detected at 3.28[m] from the basement floor based on simulation as shown in Fig. 18. We assumed that radiation could be scattered because of the structure of screw duct as shown in Fig. 16. There was no neutron detection at 1.52 [m] from the basement floor based on the simulation results. Regarding the difference between 5.3 Fig.14 neutron measurements and the simulations, the simulation could not help explain the different results.

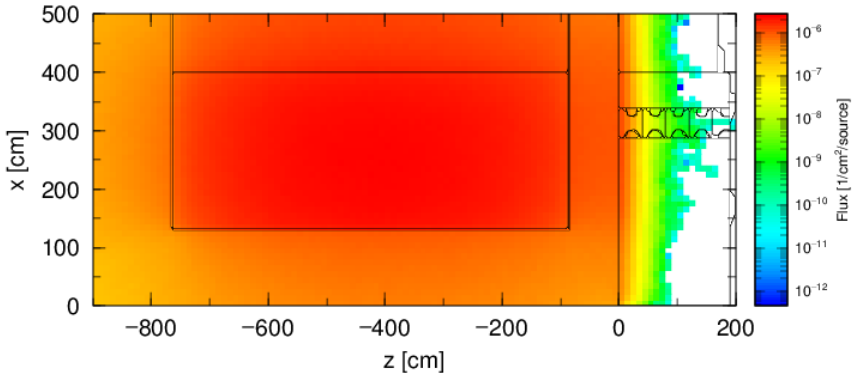

Fig. 18 Neutron distribution simulated using neutron analysis data as an input file

6. Conclusion

A project of development of a new technique to monitor Pu with FP has been carried out since 2015 as scheduled. As the first step, analysis of the HALW to evaluate neutron/gamma-ray emitted from solution in the HALW tank (V35) which has the highest Pu concentration in HALW tank at TRP were conducted. Gamma-ray spectrum and neutrons emitted from 1mL HALW sample which was diluted with nitric acid of same acid concentration to one million times was measured. Based on the HPGe analytical results, the absolute gamma-ray value was evaluated with attenuation ratio calculated by MCNP and gamma-ray spectrum for the input source file.

We performed actual measurements of gamma rays and neutrons at the outside of the concrete cell. Gamma-ray peaks emitted from HALW solution were not found in measured spectrum because shielding effect of the HALW tank's cell which has 1.9[m] thickness concreate was too high. So we try to conduct gamma-ray spectrum measurement at the inside the cell which is less shielding effect than outside the cell. On the other hand, Neutron response proportional to neutron generation ratio in each HALW tank was obtained by neutron measurement at the outside of the cell wall. However, it will be also necessary to conduct neutron measurements inside the cell because differences of the mean value of neutron signal on each measurement was about 0.1[cps]. It is not enough count ratio to evaluate the difference because sampling error from HALW tank also has about 1% and it include the result this time. According to the PHITS simulation, detection of gamma rays and neutrons at the outside of the concrete cell is difficult. On the other hand, they could be detected at the outside of the concrete cell near the duct at the basement floor.
For the next step, we will measure gamma rays and neutrons at the inside of the concrete cell.

7. Acknowledgements

This project is being carried out under the support of the Ministry of Education, Culture, Sports, Science and Technology (MEXT) of the Japanese government.

8. References

[1] "IAEA Department of Safeguards Long-Term R&D Plan, 2012-2023," STR-375, Vienna, January 2013,https://www.iaea.org/safeguards/symposium/2014/images/pdfs/STR_375 IAEA_Department_of_Safeguards_Long-Term_R%26D_Plan_2012-2023.pdf

[2] H. Nakamura, et al., "Development and future challenge for Advanced Solution Measurement and Monitoring System (ASMS)," *52nd INMM Annual Meeting Proceedings*, Palm Desert, California, July 17-21, 2011, Institute of Nuclear Materials Management (2011).

[3] H. Nakamura, et al., "Concept of a New GloveBox Cleanout Assistance Tool (BCAT) by using Distributed Source-Term Analysis (DSTA)", 51nd INMM annual meeting proceedings, July 2010.

[4] S. NAKAMURA "Development of the Measurement Technique for Nuclear Data with Prompt Gamma-Ray Spectroscopy" September 2002. http://jolisfukyu.tokai-sc.jaea.go.jp/fukyu/gihou/pdf2/n16-11.pdf

[5] M. Seya et al., "Active Neutron NDA Techniques for Nuclear Non-proliferation Applications (2) Development of Delayed Gamma-ray Spectroscopy - Overview of the Development", Proceedings INMM 36th Annual Meeting, Japan, October 2015.

[6] Takuya Matsuki, Kenji Masui, Megumi Sekine, Masafumi Tanigawa, Takeshi Yasuda, Koichi Tsutagi, Koichi Ishiyama, Naoki Nishida, Kazushi Horigome, Yasunobu Mukai, Hirofumi Tomikawa, Hironobu Nakamura, "Feasibility Study of Technology for Pu Solution Monitoring including FP – Composition Research of High Active Liquid Waste and Radiation Measurement Results on the Surface of Cell-", Proc. INMM-57.

[7] Megumi Sekine, Takuya Matsuki, Masafumi Tanigawa, Koichi Tsutagi, Yasunobu Mukai, Yasuyuki Shimizu, Hironobu Nakamura, Hirofumi Tomikawa, Feasibility Study of Technology for Pu Solution Monitoring including FP -Overview and Research Plan- , Proc. INMM-57.

[8] J.M. Verbake, C. Hangmann, D. Wright, "Simulation of Neutron and Gamma Ray Emission from Fission," UCRL-AR-228518, Lawrence Livermore National Laboratory (2009).

[9] T. Sato, K. Niita, N. Matsuda, S. Hashimoto, Y. Iwamoto, S. Noda, T. Ogawa, H. Iwase, H. Nakashima, T. Fukahori, K. Okumura, T. Kai, S. Chiba, T. Furuta and L. Sihver, "Particle and Heavy Ion Transport Code System PHITS, Version 2.52," J. Nucl. Sci. Technol. 50:9, 913-923 (2013).

Session 19

Statistical Methodologies

Attributes and metrics for safeguards-relevant information

Nicholas Kyriakopoulos

Department of Electrical and Computer Engineering
The George Washington University, Washington, DC, USA

Abstract:

The aim of the State-level approach to safeguards is to determine compliance of each State with its obligations under the NPT. The evaluation mechanism must be objective and transparent in both the procedures and the information used to draw conclusions. Objectivity implies the minimization or, at best, elimination of human judgment. While data can be processed mechanically, the qualitative information must first be quantified. In addition, both quantitative and quantified data contain uncertainties. Some may be unintentionally erroneous, other falsified and all are corrupted by some level of noise. Thus, design of an objective detector of non-compliance needs to take into account the uncertainties associated with all input data, in other words, there is a need to develop models for characterizing all information used as inputs to the detector.

This paper presents a systematic approach for classifying all information available to the safeguards system by source, such as States, IAEA, open literature, etc., followed by the identification of attributes relevant to the detection of proliferation. The proposed attributes are correctness, or accuracy with which the elements of a data record reflect the true values of the variables the record purports to represent, completeness, or the degree to which a data record contains all the data needed for a given task, transparency, or the degree to which a data record can be verified, and, timeliness, or the degree to which the time a data record is received by the time when the data in the record were generated. The attributes are quantified by assigning values in the range from zero (false) to one (true). A Bayesian approach can be used to update the assigned values using new information. These attributes are combined to calculate the relevance of each piece of information to a specific physical model indicator.

Keywords: safeguards; data; quality; attributes; quantification

1. Introduction

Nuclear safeguards aim to detect diversion of nuclear materials from peaceful uses to the development of nuclear weapons. Implicit in this objective is the assumption that a State is engaged in some form of peaceful nuclear uses. These cover a broad spectrum of activities from fundamental research involving radioactive elements to the production of radioisotopes for medical applications to the production of electricity using nuclear reactions to conducting underground nuclear explosions for peaceful applications[1]. A treaty prohibiting the latter has been negotiated and signed but not yet ratified[2]. Although the CTBT has not yet entered into force more than 180 States out of a total of 196 have signed it indicating their commitment not to conduct any nuclear explosion for whatever purpose. It is worth noting that the text of the CTBT uses the term “nuclear explosion” without a precise definition of the meaning of the term.

To cover all possible peaceful nuclear activities the nuclear fuel cycle has been defined that includes all activities involving radioactive materials from ore mining to the disposal of radioactive waste and States are obligated to declare all activities that are part of that cycle. The aim of classical safeguards has been to ensure that all nuclear material associated with the declared activities is accounted by auditing the State system of accounting and control of the nuclear materials[3]. Over the years, auditing by the IAEA of the activities within the declared nuclear fuel cycles has generated findings that have

confirmed the validity of the State declarations with high level of confidence subject to a statistical noise.

The confidence in the ability of classical safeguards to detect undeclared nuclear activities was shaken with the discovery of the clandestine nuclear weapons program in Iraq. While classical safeguards was designed to detect diversion of nuclear materials from declared nuclear fuel cycles, the Iraq case illustrates that the existing safeguards were not adequate to detect undeclared activities[4]. As a result, the concept of integrated safeguards was developed that aims to evaluate the State as a whole[5,6]. Although not stated as such, the implicit aim is to detect clandestine nuclear weapons development activities anywhere within a State in a manner that is objective and non-discriminatory among the States. The approach involves enumeration of all possible paths to the developments of nuclear weapons referred to as critical paths and the physical processes comprising each path. The evaluation of the State as a whole is to be based on information related to each component of the physical model. By combining all that data, integrated safeguards is to detect diversion of nuclear material from the declared fuel cycle and clandestine nuclear weapons programs[7]. These are two distinct objectives. The history of classical safeguards has shown that diversion from a declared fuel cycle is detectable. The case of Iraq is not so much a failure of classical safeguards but absence of detection system for undeclared activities.

The effort to develop an objective and transparent mechanism for evaluating a State as a whole faces formidable obstacles. Objectivity requires the use of quantitative procedures that can produce repeatable results. These procedures encompass quantitative models of potential clandestine processes, measurements that are associated with such underlying process and detection algorithms that are sufficiently robust to identify clandestine activities with a reasonably high level of confidence.

2. A challenging problem

The Additional Protocol provides the framework under which a State is to be evaluated as whole. It specifies the types of data a State is required to provide and time schedules for reporting them. It also specifies the types of data that the IAEA may collect during inspection visits and the manner in which such data may be collected. At the same time, it constrains the IAEA from using a “mechanistic” approach and “detailed material accountancy” to verify declarations. While the exclusion of detailed material accountancy implies absence of measurements for inventory and flow control, the term “mechanistic” excludes the use of systematic procedures and algorithms. Nevertheless, the evaluation of a State needs to be objective, transparent and non-discriminatory.

The IAEA in its effort to strengthen the effectiveness and improve the efficiency of the safeguards through the application of the Additional Protocol is facing the challenge of developing an “objective” mechanism for verifying the declarations under this protocol without employing a “mechanistic” approach and without seeking to verify “systematically” the information contained in the declarations. These constraints are insurmountable obstacles to performing an objective evaluation of a State. In order to analyze the impact of the Additional Protocol on the detection of clandestine nuclear activities, it is first necessary to clarify its role relative to the application of classical safeguards. One view is that the activities under the Additional Protocol would be in addition to and would complement those of classical safeguards. An alternative view could be that the application of the Additional Protocol would substitute some of the activities of classical safeguards. For either interpretation, strengthening effectiveness and improving efficiency means, in effect, increasing the probability of detecting clandestine activities while minimizing the cost of verification.

On the premise that the activities under the Additional Protocol are complementing those under classical safeguards, effectiveness and efficiency imply measuring the differential gain in the detection probability relative to the increased cost of applying the Additional Protocol. On the other hand, if the verification activities under the Additional Protocol are to be considered as substitutes for those of classical safeguards, effectiveness and efficiency imply that any reduction of the safeguards activities under classical safeguards would be offset by gains in the detection probability under the Additional Protocol. Either case requires a procedure for calculating the probability of the existence of a clandestine process using the data available to the IAEA[8]. A State engaging in clandestine proliferation would follow one of the possible Critical Paths associated with the Physical Model. Then

the problem can be formulated as detection of the most likely proliferation path for a particular State, given the information available to the IAEA relative to that State.

The design of such a detector requires specification of variables that describe the state of the process, in this case the potential clandestine process and the collection of sufficient measurements for identifying it. Optimal detectors are designed using the detailed description of the process and the variables associated with it. Evaluation of the State as a whole differs from a typical approach to the design of detectors in an important respect. Although each of the Critical Paths can be described in great detail, it is not clear whether the data required for detecting the existence of a particular critical path are sufficient and reliable. In other words, the relationship between the data available to the IAEA and the critical paths remains to be determined. Under the circumstances, a more productive effort would be first to develop procedures for extracting the maximum amount of information from the available data. The solution of this problem would create a picture of the state of all nuclear activities in a particular State as opposed to identifying which ones are associated with clandestine proliferation and would form a basis for the design of a clandestine proliferation detector.

3. A generic classification scheme

The data available to the IAEA need to be placed into categories each with distinctly identifiable characteristics. At the highest level they form two major categories, those collected under classical safeguards and all other. The first category encompasses all data associated with the declared nuclear fuel cycles and they are directly associated with the underlying process. They have been specified by their contribution to the calculation of the materials balance in the cycle and they have deemed sufficient for all material in the cycle. We will refer to them as Category I Data. The second category, referred to as Category II Data, encompasses all data available to the IAEA for use in evaluating a State as a whole. Category I data are associated with a bounded process, i.e., defined area of application (declared facilities) and defined activities within the particular area. They include information about the nuclear materials and facilities subject to safeguards that is necessary and sufficient to allow the IAEA to verify non-diversion of the declared nuclear materials. A part of the data set is generated by the States in the form of declarations and part by the IAEA in the form of inspection reports and installed instruments. In contrast, Category II data are associated with an open process, i.e., incompletely defined area of application (anywhere within a State), and partially defined activities within that area. For example, under the Additional Protocol, a State must declare location of facilities involved in nuclear fuel cycle-related activities that do not involve nuclear materials, but are “specifically related to any process or system development aspect” of any part of the nuclear fuel cycle[9]. One can easily identify many research and development activities that do not involve nuclear materials but could be classified under the label of dual use. This category also includes State declarations of data identified by the IAEA “on the basis of expected gains in effectiveness or efficiency” without a definition of an algorithm for measuring them. In addition, the application of integrated safeguards may include data offered by the States on a voluntary basis and data collected from open sources. The two categories and their relationship to the integrated safeguards regime are shown in Figure 1.

There is a crucial distinction between the two categories. Category I data pertain to measurements on the declared nuclear fuel cycle and provide information on the conditions of specified stages of that cycle. Equally important the IAEA has in place mechanisms for verifying the accuracy of the data submitted by a State. In contrast, there are substantial ambiguities and uncertainties regarding the utility of Category II data in achieving the objective of detecting clandestine proliferation activities in a State or, conversely, reaching a conclusion that no prohibited activities take place in that State. The absence of a mechanism for verifying the data submitted by a State introduces uncertainties on the veracity of the declarations. Even greater uncertainties are inherent in data provided by a State regarding activities in another State as well as data collected from public sources. Information contained in these categories of data may be erroneous either accidentally or deliberately. Consequently, the absence of a robust data verification mechanism for Category II data, makes evaluation of a State as a whole problematic to say the least due to the uncertainties about the information content of this category of data.

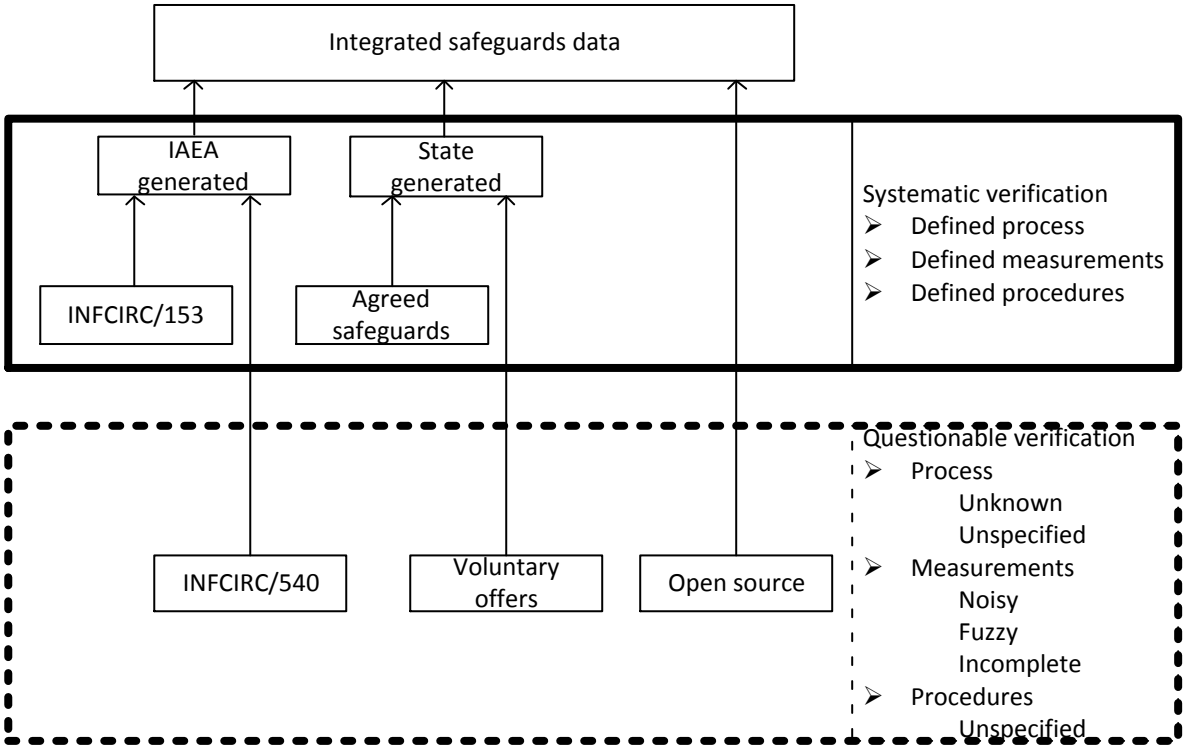

Figure 1. Safeguards data and their relationship to integrated safeguards

Given the breadth of the types of data in both categories another major partition is between *quantitative* and *qualitative* data. The former are the outcome of some form of measurement and can be machine processed directly to extract *quantitative* information. Qualitative data are descriptive, either written or oral. Although there exist algorithms for machine-processing of text and voice, the extraction of information still work in progress and human intervention is necessary to identify unambiguous information.

Another partition is according to the source that generates the data. For safeguards purposes sources are divided into three categories: *States*, *IAEA*, *open source*. State-generated data are either given pursuant to *safeguards* agreements or *voluntarily offered* by States to the IAEA. The sources of IAEA-generated data are *inspectors* and *instruments*. Open source data include any information available in the public domain be it in print, electronic form, broadcast media, or information provided to the IAEA by private entities. Table 1 shows the possible subcategories of data that result from the intersection of the two major partitions.

	Quantitative	Qualitative
States		
Safeguards	X	X
Voluntary	X	X
IAEA		
Inspectors	X	X
Instruments	X	
Open sources		
Public	X	X
Private	X	X

Table 1: Categories of quantitative and qualitative safeguards data

For classical safeguards, the verification system is defined through the specification of the process (declared nuclear fuel cycle), the procedure (materials balance) and the measurements (process variables, inventory). The primary factor affecting detection of diversion is the *measurement noise*. Thus, for any given declared value v_d there an associated uncertainty $\pm\Delta v$ such that the values of the inputs are $v_d \pm \Delta v$ and $v_d - \Delta v \le \Pr\{v_d = v_a\} \le v_d + \Delta v$, where v_a is the actual value. For the evaluation of a State as a whole, however, there is no well-defined verification system. The process is open-ended in that the characteristics of a clandestine program are, by definition, unclear, and the data available to the IAEA under integrated safeguards, may or may not be related to a clandestine program. The quantitative or measurable data differ in their characteristics. Locations of facilities or production capacity of plants are *deterministic*, because they can be measured and are subject only to *measurement errors*. Quantitative data such as inventories or quantities produced over some time interval may be viewed as *stochastic*, because there is no specified procedure for verifying their validity. The quantities of material produced by a plant over a given time interval could vary from zero to 100% of production capacity. For any declared quantity, the range of uncertainty about the actual quantity may vary from zero to the maximum possible value associated with a particular facility. Thus, the characteristics of the input data would be of the form $[0 \le \Pr\{v_d = v_a\} \le 1]$. Unless some independent monitoring system is in place, the actual number could be anywhere in that range. Similar uncertainties are associated with declarations of imported/exported quantities, although it is possible to construct a system for tracking import/export declarations on a global basis. Even under such a system, it would difficult to associate inevitable discrepancies with a specific State absent an inventory control system for each State.

Under this formulation, the quantitative data for both categories differ only in the statistical profile of the respective uncertainties. The region of uncertainty for data collected under classical safeguards is relatively small; they may be characterized as *verifiable*. Absent any additional information, some of the data collected under integrated safeguards have a much larger range of uncertainty; they may be labeled as *unverifiable*. The data in each of the categories in Table 1 may then be partitioned into two broad categories, verifiable and unverifiable. The first category comprises data associated with the application of classical safeguards and includes the data collected by the inspectors. The second category comprises all data not subjected to systematic verification procedures such as those provided by States on a voluntary basis. Most of the data submitted to the IAEA under the Additional Protocol belong to this category, because the IAEA is prevented from undertaking systematic verification. Table 2 lists which categories of such data are verifiable and which are not.

Category	Verifiable	Unverifiable
Location	X	
Inventory		X
Production capacity	X	
Quantities produced		X
Export quantities		X
Export destinations	X	
Import quantities		X
Import sources	X	

Table 2: Categories of verifiable and unverifiable safeguards data

While the handling of quantitative data in the declarations submitted by the States presents some serious challenges in determining their statistical properties, the processing of the additional information available to the IAEA is even more problematic. Consider information, other than safeguards-related, submitted by a State either about itself or concerning another State. The submission could vary from being in good faith, True (1), to deliberately misleading, False (0). Furthermore, as political conditions between States change over time, the truthfulness or erroneousness of a given piece of information is also a function of time. Similar concerns can be expressed about information in the public domain. Any spoken or printed information about activities in a given State needs to be viewed through two filters, the medium and the source. Spoken and broadcast information is the most problematic. *Verba volent*. There is no objective mechanism of checking the validity of such information and the motivation of the person providing it. Similar challenges face the handling of data from archival media. Scientific and technical information in established professional publications can be taken at its face value with a high level of confidence

derived from the process of peer review. Such may not be the case for non-scientific publications, even those using the reviewing process. The information may be colored by the values, beliefs or political objectives of the particular publication. A more difficult challenge is finding a mechanism that connects a piece of information in the open literature to a potential clandestine nuclear weapons program. There is a wide range of capabilities among the States for such a program. The time line for building a nuclear device would be much shorter for a technologically and scientifically advanced State than for one with rudimentary technological base and scientific pool. It would be a challenge to devise an objective and transparent procedure for drawing conclusions about the presence or absence of a clandestine program on the basis of information in the public domain.

Even greater challenges arise in the utilization of qualitative information in an objective and transparent system. To utilize such information in a verification system it is first necessary to quantify it in order to be able to integrate it into the broader verification base. There are search procedures for identifying specific words in text, it is still an open question how `associate values with specific words and ascertain the veracity of the printed or spoken words. The challenge of “fake news” is a telling paradigm. Thus, for data not collected under a systematic verification regime, the first step for the development of an objective and transparent evaluation procedure in the assignment of values to all such data used in the evaluation.

4. Learning to crawl before attempting to run

The outcome of an evaluation using data with large degrees of uncertainties is bound to be characterized with an even greater level of uncertainty and lead to outcomes that are neither objective nor transparent. To guard against such an undesirable outcome, a mechanism is needed for evaluating the relationship of the input data to the end objective, namely, detection of the existence of a clandestine nuclear weapons program. Absent a robust mechanism for verifying the accuracy of the available data the next available option would be to develop a mechanism for extracting the maximum amount of information from a given data set. Before one decides how to use a given piece of information, it is essential to determine the relationship of that data point and a potential clandestine proliferation activity. Thus, at the highest level of evaluation, the *relevance* of a piece of information to the end objective must first be determined. At a minimum, the attribute of *relevance* may be described by the following parameters:

Correctness defined as the accuracy with which the elements of a data record reflect the true values of the variables the record purports to represent;

Completeness defined as the degree to which the data record contains all the data needed for a given task;

Transparency defined as the degree to which a data record can be verified;

Timeliness defined as the relationship between the time the data in the record were generated to the time the record is received by the detection mechanism.

For example, the completeness of a data record listing the number of items stored in a location, or the quantity produced in a given facility over a specified time interval measures the degree to which the record represents the actual number of items stored or quantities produced. Similarly, a data record may not be complete, if it does not include all categories of items or materials that could be used in the detection of a clandestine operation. The utility of a record is also a function of the time elapsed between the time the record was generated and the time it was received by the evaluating authority.

The four parameters can be quantified by assigned values for each one in the range $v_{Corr} \in [0,1]$, $v_{Comp} \in [0,1]$, $v_{Trans} \in [0,1]$ and $v_{Time} \in [0,1]$. Each of those values corresponds to the probabilities for correctness, completeness, transparency and timeliness of a given data record. For quantitative data records some narrower bounds for the values within these ranges could be determined by utilizing additional information. The correctness of an inventory record could be estimated by an inspection that falls short of detailed item accounting such as estimating the sizes of occupied and unoccupied spaces. These numbers could be further refined by evaluating similar records over time as well as performing cross-correlation of different categories of records such as items produced, items exported and items imported. One can then visualize the assignment of values for each of the four parameters as a process spanning space and time as illustrated in Figure 2 that illustrates the boundaries within which the value of a particular parameter may be.

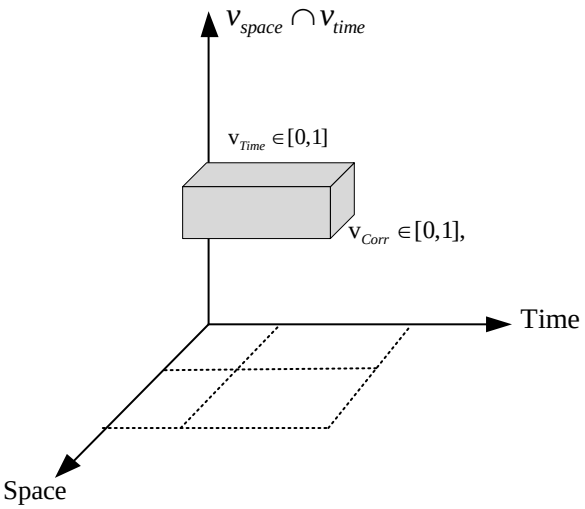

Figure 2. A notional parameter space as a function of time and space

For descriptive data such as text or audio the conversion to a quantitative record for automated processing becomes a greater challenge. One potential tool for such a conversion is fuzzy logic[10 11]. For a given data record X the value could range anywhere from 0 to 1. However, the mechanism for assigning such a value is not clearly defined or fuzzy. The input data record is mapped into a membership value in the range $[0,1]$. The mapping is done by membership functions that may have different characteristics as illustrated in Figure 3. Determining which type of membership function is applicable to a given data set is one of many challenges that need to be addressed in utilizing open source, qualitative information as an input to clandestine proliferation detector.

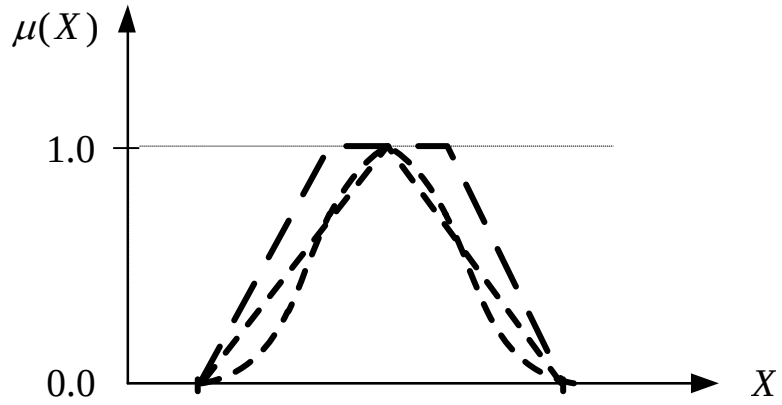

Figure 3. Examples of different types of membership functions on a fuzzy data record

Under such an approach, the relevance R_δ of a given data record to a particular Physical Model indicator δ can be expressed as a function of the four attribute parameters, namely, $R_\delta = \sum_{i=1}^{4} w_{\delta i} a_{\delta i}$, where $a_{\delta i}$ is the relationship of the a_i attribute to the δ indicator of the Physical Model and $w_{\delta i}$ the significance of the particular parameter to the relevance of the given data record. Under such a procedure, a mapping is possible for assigning to a data record a value in the range from weak to strong, namely, $[minR_\delta \leftrightarrow maxR_\delta] \Leftrightarrow [\text{weak} \leftrightarrow \text{strong}]$.

Tables 3 and 4 illustrate how the methodology described in this paper could be utilized. For each category of data, a corresponding value for relevance can be computed. As it should be expected, the range of uncertainty depends on the uncertainty values for each of the parameters and their relative weights.

Categories by type, source and frequency			Attribute parameters: Correctness	Completeness	Transparency	Timeliness	**Relevance**
Type	Descriptive	Verbal	0↔1	0↔1	0↔1	0↔1	**0↔1**
		Written	0↔1	0↔1	0↔1	0↔1	**0↔1**
	Quantitative	Instrument	0↔1	0↔1	0↔1	0↔1	**0↔1**
		Observations	0↔1	0↔1	0↔1	0↔1	**0↔1**
		Files	0↔1	0↔1	0↔1	0↔1	**0↔1**
Source	IAEA-generated		0↔1	0↔1	0↔1	0↔1	**0↔1**
	State-generated	Agreed safeguards	0↔1	0↔1	0↔1	0↔1	**0↔1**
		Voluntary	0↔1	0↔1	0↔1	0↔1	**0↔1**
	Open source	Public domain	0↔1	0↔1	0↔1	0↔1	**0↔1**
		Private source	0↔1	0↔1	0↔1	0↔1	**0↔1**
Frequency	Periodic		0↔1	0↔1	0↔1	0↔1	**0↔1**
	Ad hoc		0↔1	0↔1	0↔1	0↔1	**0↔1**

Table 3: Attribute parameters for the categories of data available to the IAEA

Categories of data by function			Attribute parameters: Correctness	Completeness	Transparency	Timeliness	**Relevance**
Quantifiable	Facilities: Location	Storage	0↔1	0↔1	0↔1	0↔1	**0↔1**
		Manufacturing	0↔1	0↔1	0↔1	0↔1	**0↔1**
		Mining	0↔1	0↔1	0↔1	0↔1	**0↔1**
		Concentration plants	0↔1	0↔1	0↔1	0↔1	**0↔1**
	Operations: Scale	Inventory	0↔1	0↔1	0↔1	0↔1	**0↔1**
		Production capacity	0↔1	0↔1	0↔1	0↔1	**0↔1**
		Quantities produced	0↔1	0↔1	0↔1	0↔1	**0↔1**
	Exports	Quantities	0↔1	0↔1	0↔1	0↔1	**0↔1**
		Destinations	0↔1	0↔1	0↔1	0↔1	**0↔1**
	Imports	Quantities	0↔1	0↔1	0↔1	0↔1	**0↔1**
		Sources	0↔1	0↔1	0↔1	0↔1	**0↔1**
Frequency of declarations	Initial		0↔1	0↔1	0↔1	0↔1	**0↔1**
	Annual past activities		0↔1	0↔1	0↔1	0↔1	**0↔1**
	Advanced planned activities		0↔1	0↔1	0↔1	0↔1	**0↔1**

Table 4: Attribute parameters for data submitted by the States

4. Conclusion

As it is envisioned by the concept of integrated safeguards, a State is to be evaluated as a whole. The data available for such an evaluation belong to two major categories, those collected under classical safeguards and everything else. While the reliability of the former can be measured, that of the latter is

questionable. Given that the objective is to generate a reasonable assurance that a State is not engaging in some form f clandestine proliferation, it is first necessary to have a mechanism for ensuring confidence in the quality of the data used for such an evaluation. In this paper we have shown that there are many uncertainties inherent in the evaluation of a State as a whole. There are no reliable models for clandestine proliferation activities. The data collected beyond a declared nuclear fuel cycle contain uncertainties with unknown characteristics. Validation of stochastic proliferation models is difficult because of the scarcity of data. Linking the data collected under the integrated safeguards concept to clandestine nuclear proliferation activities poses serious challenges. Instead of tackling this very difficult problem directly, this paper has described a procedure for filtering the data to maximize the information content relative to the safeguards objectives as a preliminary step to the development of detection algorithms.

5. References

[1] Treaty Between The United States of America and The Union of Soviet Socialist Republics on Underground Nuclear Explosions For Peaceful Purposes (and Protocol Thereto) (PNE Treaty)
[2] Comprehensive Nuclear-Test-Ban Treaty (CTBT)
[3] INFCIRC 153
[4] Baute, J. “Timeline Iraq: Challenges and Lessons Learned from Nuclear Inspections, *IAEA Bulletin*, 46/I, 2004
[5] Cooley, J., N. “Progress in Evolving the State-level Concept”, Presentation at the Seventh INMM/ESARDA Joint Workshop, Future Directions for Nuclear Safeguards and Verification, Aix-en-Provence, France, 17-20 October 2011
[6] Jill N. Cooley, “Evolution of IAEA Safeguards”, in *Consolidated Nuclear Security*, Y-12 National Security Complex, Oak Ridge, TN
[7] Z.Liu and S.Morsy, “Development of the Physical Model”, IAEA-SM-367/13/07
[8] Kyriakopoulos, N., Zhou, X. “Clandestine Proliferation: A Stochastic Process Model”, *Proceedings ESARDA 37th Annual Meeting*, Manchester (UK), 19-21 May 2015, pp.358-371
[9] INFCIRC/540 (Corrected)
[10] Zadeh, L. ,"Fuzzy sets". *Information and Control*. 8 (3), 1965: 338–353. https://doi.org/10.1016/S0019-9958(65)90241-X
[11]Lotfi Zadeh,. "Fuzzy probabilities". Information Processing & Management. 20 (3), 1984 : 363–372. https://doi.org/10.1016/0306-4573(84)90067-0

Revisiting Currie's Minimum Detectable Activity for Non-Destructive Assay By Gamma Detection Using Tolerance Intervals

E. Agboraw[1], E. Bonner[1], T. Burr[1], S. Croft[2], J.M. Kirkpatrick[3], T. Krieger[4], C. Norman[1], P. Santi[1]

[1]International Atomic Energy Agency, Vienna Austria;
[2]Oak Ridge National Laboratory, USA ;
[3]Mirion Technologies (Canberra), Inc., USA
[4]Forschungszentrum Jülich GmbH, Inst. Energy and Climate Research, Jülich, Germany

Abstract

Currie's paper [1] on estimating the minimum detectable activity (MDA) applied a Gaussian approximation to either Gaussian or Poisson data and remains the standard method to estimate radiological detection limits. This paper revisits the Currie method with attention to the false alarm probability (FAP) in Poisson and Gaussian data in non-destructive assay (NDA) by gamma detection. The Currie detection limit L_D is an estimate of the smallest net signal count rate λ_N that can be detected with high probability and low FAP in the presence of non-zero background count rate λ_B that has been previously estimated. The MDA is the sample activity or mass corresponding to λ_N, defined as $\mathrm{MDA} = \frac{L_D}{\nu}$, where in the case of gamma-based NDA, the calibration factor ν (a product of gamma ray yield, detector and geometric efficiency, counting time, and other factors) has measurement error that introduces systematic error in the estimate of the MDA. Kirkpatrick et al. [2] showed how to account for systematic uncertainties in the estimate of $\mathrm{MDA} = \frac{L_D}{\nu}$ using a modified version of Currie estimation [2,3]. The present paper combines the approach in [2] with a tolerance interval approach. It is shown that the FAP in signal detection can be significantly different from the nominal FAP if the nominal FAP is not based on a tolerance interval, and if the nominal FAP is based on a tolerance interval, then the MDA will be larger than Currie's estimated MDA.

1.Introduction

The Currie detection limit L_D is an estimate of the smallest net signal count rate λ_N that can be reliably detected with low specified FAP in the presence of non-zero background count rate λ_B [1]. The MDA is the sample activity (or mass through a conversion) corresponding to λ_N, defined as $\mathrm{MDA} = \frac{L_D}{\nu}$, where the calibration factor ν (a product of gamma ray yield, detector and geometric efficiency, counting time, and other factors) has measurement error that can introduce systematic error in the estimate of the MDA. Kirkpatrick et al. [2] showed how to account for such systematic uncertainties in the estimate of $\mathrm{MDA} = \frac{L_D}{\nu}$ using a modified version of the Currie estimation [2,3].

The MDA can be used prior to data collection to compare different instruments and measurement scenarios, and can also be used as a quantitative measure on an item-specific basis after data collection. In gamma-ray spectroscopy, the background is often estimated from the continuum beneath the peak(s) of interest, so the MDA is specific to the measurement conditions (including what other nuclides are present).

This paper revisits L_D with attention to the FAP (denoted α) in Poisson and Gaussian data, by using a tolerance interval approach [4,5]. Section 2 provides background, motivation, and example tolerance intervals. Section 3 provides a simulation approach and results for both Gaussian and Poisson data. Section 4 uses results from Section 3 to estimate the MDA while allowing for random and systematic errors in the calibration factor ν in $\mathrm{MDA} = \frac{\mathrm{L_D}}{\nu}$. Section 5 is a discussion. Section 6 is a summary.

2.Background

Currie [1] provided approximate calculations of the MDA for the desired FAP α based on the assumption that the measurement data has a Gaussian distribution, denoted as $X \sim N\left(\mu, \sigma^2\right)$. Because μ and σ are unknown and must be estimated, the well-known frequentist approach to a confidence interval for μ is $\overline{x} \pm t_{1-\alpha,(n-1)} s \big/ \sqrt{n} = \hat{\mu} \pm t_{1-\alpha,(n-1)} \hat{\sigma} \big/ \sqrt{n}$ where $t_{1-\alpha,(n-1)}$ denotes the (1-α) quantile of the *t* distribution with *n*-1 degrees of freedom, $\overline{x} = \sum_{i=1}^{n} x_i \Big/ n$ and $s^2 = \hat{\sigma}^2 = \sum_{i=1}^{n} (x_i - \overline{x})^2 \Big/ (n-1)$ [1,4,5].

A tolerance interval is an interval that bounds a specified fraction of a probability distribution with a specified confidence (frequentist) or probability (Bayesian approach) [4,5]. Both frequentist and Bayesian approaches will be presented in this paper. In nuclear safeguards (Sections 3 and 4), one often seeks a threshold, denoted $T_{0.95}$ here, that corresponds to α = 0.05. Instead of requiring an interval for μ, the need is to estimate the 0.95 quantile, $T_{0.95}$ (the upper limit of a one-sided interval) of the distribution of *X* if doing one-sided testing for a positive mean shift. The frequentist tolerance interval estimators presented have the form $\hat{T}_{0.95} = \hat{\mu} + k\,\hat{\sigma} \big/ \sqrt{n}$, and the goal in both the frequentist and Bayesian approaches is to achieve $P(\hat{T}_{0.95} \geq T_{0.95}) = \gamma$, where γ is a user-specified probability (the frequentist confidence level), such as $\gamma = 0.99$ [4,5]. In the Bayesian approach, μ and σ are random unknown parameters so $P(\hat{T}_{0.95} \geq T_{0.95}) = P_{\mu,\sigma}(\hat{T}_{0.95} \geq T_{0.95})$ is computed with respect to μ and σ. In the frequentist approach, $\hat{\mu}$ and $\hat{\sigma}$ are random while μ and σ are fixed unknowns so $P(\hat{T}_{0.95} \geq T_{0.95}) = P_{X_1, X_2, \ldots, X_n}(\hat{T}_{0.95} \geq T_{0.95})$ is computed with respect to random samples of size *n*.

Background measurement(s) are often used to establish an alarm threshold that has a small nominal FAP, such as $\alpha = 0.05$. In any frequentist approach, probabilities such as the FAP are calculated with respect to the distribution of *X* for fixed μ and σ and the "confidence" in a "confidence interval|" is the long-run relative frequency (probability) that an interval such as $(0, \hat{T}_{0.95} = \hat{\mu} + k\,\hat{\sigma} \big/ \sqrt{n})$ will include a future observation X from the same distribution as the training data used to estimate $\hat{\mu}$ and $\hat{\sigma}$. In any Bayesian approach, probabilities are calculated with respect to the joint posterior distribution $f_{posterior}(\mu, \sigma)$ for fixed *X* [5].

To illustrate the frequentist approach, assume that *n* = 10 measurements are to be used to construct an upper limit that bounds at least *p* = 0.95 (so the FAP is 0.05 or less) of future data with probability 0.99. Fig. 1 plots a single realization of the *n* = 10 measurements and compares the Currie limit to the tolerance interval limit. To achieve a user-specified FAP for future measurements aimed to detect

whether any signal is present in a background measurement, Currie [1] used the detection threshold $T = \hat{\mu}_B + k_{1-\alpha}\hat{\sigma}_B$ where $k_{1-\alpha}$ is the (1- α) quantile of the Gaussian distribution, and $\hat{\sigma}_B = \sqrt{\hat{\sigma}^2 + \hat{\sigma}^2/n}$, where the term $\hat{\sigma}^2/n$ is the estimated variance of the estimate of the unknown mean μ_B . Regarding notation, in this paper, the subscript B denotes background, and the subscript N denotes net, and both the B and N subscripts will sometimes be omitted, depending on the context, to avoid cluttering the notation. This value of *T* was regarded as an approximate value if the underlying data is non-Gaussian (such as Poisson, see Section 3). A small modification, to $\hat{T} = \hat{\mu}_B + k_{1-\alpha}\hat{\sigma}$,

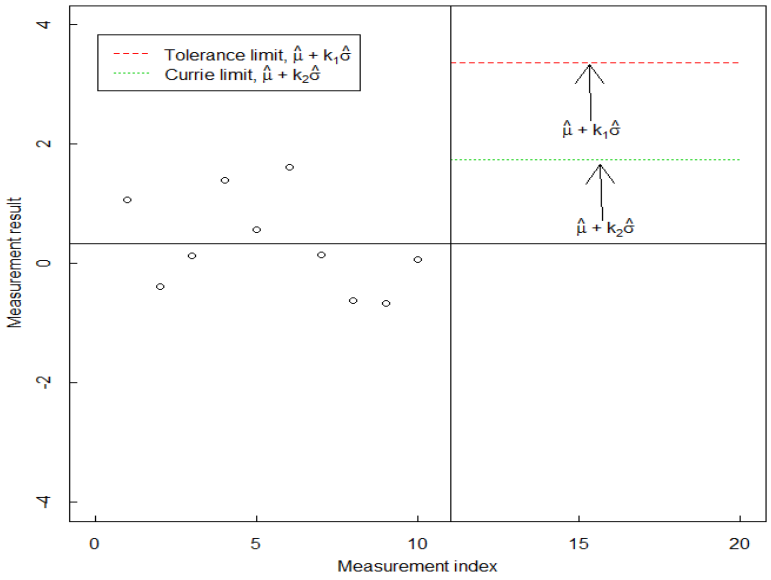

Fig. 1. Illustration of the tolerance limit $k_1 = 3.7$ compared to the Currie limit $k_2 = 1.7$ for future data in the case of using 10 Gaussian observations to estimate μ and σ and the corresponding Gaussian quantile, $\hat{T}_{0.95} = \hat{\mu} + k\,\hat{\sigma}/\sqrt{n}$,

using $k_{1-\alpha} = t_{n-1}(\delta)/\sqrt{n}$ with noncentrality parameter $\delta = z_p\sqrt{n}$ where z_p is the 1-*p* quantile of the standard Gaussian, is exact if the underlying data has a Gaussian distribution [4].

Perhaps surprisingly, an exact expression for a tolerance interval is only available in the one-sided Gaussian case just described [4-7]. However, good approximate expressions for many other cases are available [5-7]. Alternatively, and in the approach taken in this paper, tolerance intervals can be well estimated using simulation to approximate an alarm threshold that is designed to contain at least $1-\alpha$ percent of future observations with a specified coverage probability γ (referred to as confidence in the frequentist approach) and as probability γ in the Bayesian approach. Currie did not consider the probability γ and note from Fig. 1, that for γ = 0.99, the decision limit is much larger than Currie's limit, with $k_1 = 3.7$ (tolerance) versus $k_2 = 1.7$ (Currie). As shown in Section 3, using the value $k_1 = 3.7$ corresponds to γ = 0.99 = $P(\hat{T}_{0.95} \geq T_{0.95})$, while using $k_2 = 1.7$ gives γ = 0.52.

Fig. 2 plots $P(\hat{T}_{0.95} \geq T_{0.95})$ (Fig. 2a) and the true average FAP (Fig. 2b) for a range of sample sizes *n* if the data is Gaussian for both the tolerance method (using $\gamma = 0.99$) and the Currie method. The tolerance value for k_1 (which depends on *n*), $P(\hat{T}_{0.95} \geq T_{0.95})$, and the true FAP are easily calculated using simulation in R [8] as shown in Section 3.

Any Bayesian analysis specifies a prior probability for model parameter(s) θ, a likelihood (Gaussian or Poisson in this paper) P(X|θ), and works with the posterior distribution of θ, $f_{posterior}(\theta)$. Bayesian tolerance interval construction then estimates T such that $P(X < T \mid \theta) = 1-\alpha$ with specified coverage probability γ. In the Gaussian case with unknown μ and σ, $\theta = (\mu, \sigma)$. In the Poisson case, $\theta = (\lambda_G, \lambda_B)$ if both a gross count rate and background count rate are required, and $\theta = (\lambda)$ if the count rate at a single region of interest is required. For Gaussian and Poisson data, conjugate prior probability density functions (pdfs) are available, which have the convenient property that the posterior pdf is in the same family as the prior, but with updated parameters. . For example, the conjugate prior for the Gaussian with unknown μ and σ is the Gaussian-inverse-Gamma and the conjugate prior for the Poisson is the Gamma distribution [5].

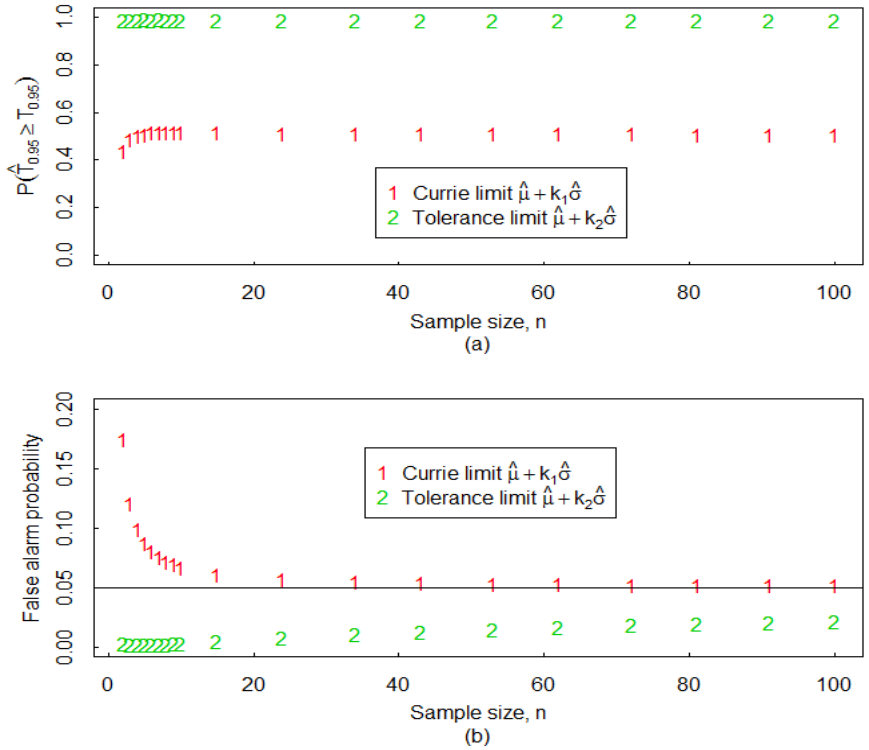

Fig. 2. The true value of $P(\hat{T}_{0.95} \geq T_{0.95})$ in (a) and true FAP in (b) if data is Gaussian. The tolerance interval method is conservative, so has a FAP that is smaller than 0.05 by construction.

3. Simulation to estimate $\hat{T}_{0.95}$

The user seeks a threshold that is larger than $1-\alpha$ percent of the distribution, with a specified high probability such as 0.99. Recall that there are frequentist and Bayesian approaches to tolerance intervals [4,5], neither of which exactly correspond to Currie's approximation.

3.1 A simulation-based trial-and-error frequentist approach for Gaussian data

This example demonstrates a simulation-based trial-and-error based frequentist approach to estimate *k*. The simulation procedure is as follows.

1. Specify n, μ, σ.
2. For each of many (typically 10^5 or more) simulations, generate

$$X_i \sim N\left(\mu, \sigma^2\right), \text{ for } i = 1, 2, ..., n$$

3. Compute $\hat{\mu} + k\dfrac{\hat{\sigma}}{n}$ for a grid of trial values for *k* using

$$\hat{\mu} = \overline{x} = \sum_{i=1}^{n} x_i \Big/ n,\ \hat{\sigma} = \sqrt{\sum_{i=1}^{n} (x_i - \overline{x})^2 \Big/ (n-1)}\ .$$

4. Select the trial value of *k* that includes at least 95% of the population (of future *X* values) with probability γ = 0.99; that is, $P(\hat{T}_{0.95} \geq T_{0.95})$ = 0.99, where $\hat{T}_{0.95} = \hat{\mu} + k\,\hat{\sigma}/\sqrt{n}$.

For example, with n = 10 and for any values of μ and σ , the exact result is k = 3.738, and the simulation-based result in R [8] is k = 3.74, which is within the small simulation error in a large but finite number (105) or simulations. Similarly, simulation can also estimate the probability that the Currie-based k value bounds at least 95% of the pdf of X (so the FAP is 0.05 or less), and in this example with n = 10, there is a probability of approximately 52% that the Currie-based value of *k* has a FAP of 0.05 or less.

One nuclear safeguards application for tolerance intervals for Gaussian data is inspector (i) measurements of operator (o) declarations of *n* items sampled for verification. In each of *n* values of $d_j = (o_j - i_j)/o_j$. In two-sided testing, if $|d_j| > k\delta$ then the *j*-th item selected for verification leads to an alarm, where $\delta_T = \sqrt{\delta_R^2 + \delta_S^2}$, (with δ_T the total RSD, δ_S the between-period short-term systematic error RSD, and δ_R the within-period reproducibility) then k= 3 is a common choice that corresponds to a small α of approximately 0.001), The null hypothesis is $\mu = 0$, and δ_T can be estimated by applying analysis of variance (ANOVA) [9-12]. If one assumes $\hat{\delta}_T = \delta_T$ then choosing $k = 1.65$ corresponds to α =0.05 (Gaussian approximation); however, as an example, if n = 10 paired measurements in each of 3 prior inspection periods are available, and $\delta_S = \delta_R = 0.03$ [9 12], then choosing k = 1.65 leads to an actual FAP of 0.05 or less with probability 0.38. If one desires a high probability $\gamma = 0.99$ that the actual FAP is as small as the nominal FAP, then simulation [9,12] indicates, for example, that instead of , $k = 1.65$, one must choose, for example, *k* = 2.58 for 5 groups of 10 measurements, *k* = 2.94 for 3 groups of 10 measurements and *k* = 4.35 for 2 groups of 5 measurements. Unlike the single-component Gaussian case, these values of k depend on the values of the ratio δ_S/δ_R , which is unknown, so approximate frequentist or Bayesian methods are needed. Note that any Bayesian method can be regarded as approximate because one almost never knows the exact prior probability distribution. The accuracy of these approximate methods can be assessed using simulation and/or by analysis of historical data.

3.2 Poisson data

Fig. 3 shows that the true FAP of Currie's method can be quite different from the nominal FAP, so tolerance interval construction should be considered. In Fig. 3, the simulated data is *n* = 1 observation of *X* ~ Poisson(λ), with λ = 1, 10, or 100. A count time of *t* = 1 second is used to estimate the background and to test whether a subsequent measurement corresponds to the same background rate λ (See Section 5.1). For comparison, $P\left(X_{test}/t = \hat{\lambda}_{test} > T\right)$ of the corresponding Gaussian distribution are shown, where $\hat{T}_{0.95} = \hat{\lambda} + k\sqrt{\hat{\lambda}(1+1/n)/t}$. This expression is Currie's [1] approach to estimate *T* by using the Gaussian approximation for both Gaussian and Poisson data, and using the factor $\sqrt{1+1/n}$ to quantify the impact of uncertainty in the estimated mean on the estimated background standard deviation. It is important to note (Fig. 3b) that for large values of λ (and/or large

count times) such as λ =100 or more, the Gaussian approximation (with the factor $\sqrt{1+1/n}$ but without the notion of a tolerance interval) to the Poisson is adequate. The reason for this good accuracy is that the variance of the Poisson distribution is equal to its mean λ, so the Poisson standard deviation can be estimated with less uncertainty than that of the Gaussian.

Recall from Example 3.1 that estimating the standard deviation of the Gaussian requires *n* > 1, and that the notion of tolerance intervals is needed; the estimated threshold *T* is much too small if uncertainties in $\hat{\mu}, \hat{\sigma}$ are not accounted for properly. Without using tolerance intervals, references [2, 13-14] extended Currie's treatment of Poisson data [1] by using the Poisson distribution rather than

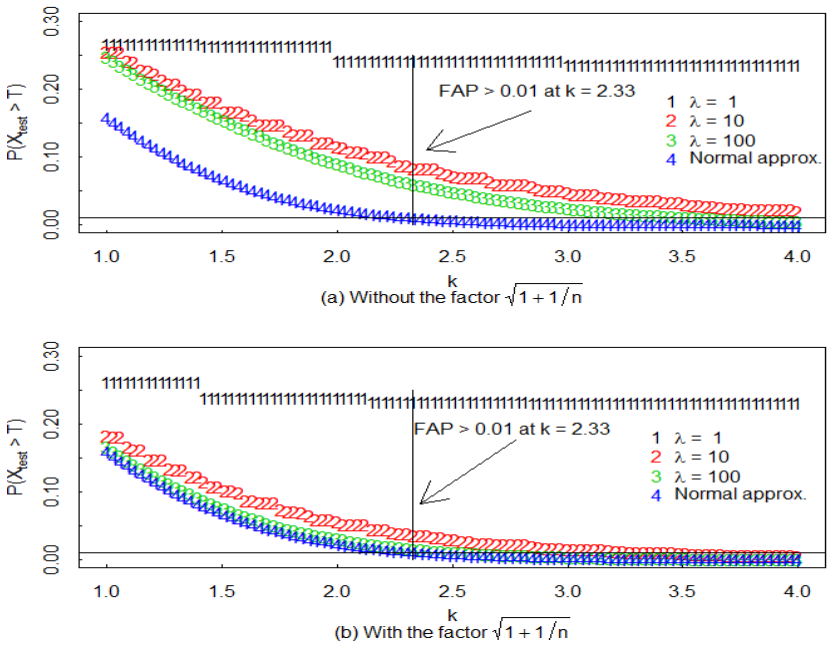

Fig. 3. The probability $P\left(X_{test}/t=\hat{\lambda}_{test}>T\right)$ versus *k* for λ = 1, 10, and 100. The corresponding normal approximation is also plotted. Currie's factor $\sqrt{1+1/n}=\sqrt{2}$ is ignored in (a), included in (b).

an approximating Gaussian. Particularly when count rates and/or count times are small, it is prudent to use the Poisson distribution rather than the approximating Gaussian. As an example (also used in Section 4), let *n* = 5, $\mu=10$, and $x_1, x_2, ..., x_5$ are 10,12,10,10,8, so $\bar{x}=10$ and Currie's $\hat{T}_{0.95}=\hat{\mu}_B+k_{1-\alpha}\hat{\sigma}_B$ =12.5, which is rounded up to 13 (and in 93% of10^5 simulations, test measurements exceed the 13 limit, so the FAP can be much larger than 0.05).

A one-sided tolerance interval using the R code in Section 3.2 leads to $\hat{T}$ = 21.5, rounded up to 22 for 99% confidence that the FAP is 0.05 or smaller. For the same example, a Bayesian tolerance interval with a prior probability density $f_{prior}(\lambda)=\text{Gamma}(\alpha_{prior}=1,\beta_{prior}=.075)$ (the conjugate prior for the Poisson, and this particular prior has mean $\alpha_{prior}/\beta_{prior}=1/0.075=13.3$ and standard deviation $\sqrt{\alpha/\beta^2}=1/0.075=13.3$) has

$f_{posterior}(\lambda)=\text{Gamma}(\alpha_{prior}+\sum_{i=1}^{n}x_i,\beta_{prior}+n)=\text{Gamma}(1+50,0.075+5)$, which has mean 10.05 and standard deviation 1.41; see Fig. 4. Note that the Gamma parameters, conventionally denoted as α_{prior} and β_{prior} are not related to the FAP α or the nondetection probability β.

3.3 Simulation for Poisson data for frequentist and Bayesian approaches

3.3.1 Frequentist approach

1. Specify λ and *n.*
2. For each of many (typically 10^5 or more) simulations, generate
   $X_i \sim Poisson(\lambda),\ i = 1, 2, ..., n$
3. Compute $\hat{\lambda} + k\sqrt{\hat{\lambda}/n}$ for a grid of trial values for *k* using $\hat{\lambda} = x$.
4. Select the trial value of *k* that includes at least 95% of the population (of future *X* values) with probability γ = 0.99; that is, $P(\hat{T}_{0.95} \geq T_{0.95}) = 0.99$, where $\hat{T}_{0.95} = \hat{\lambda} + k\sqrt{\hat{\lambda}/n}$.

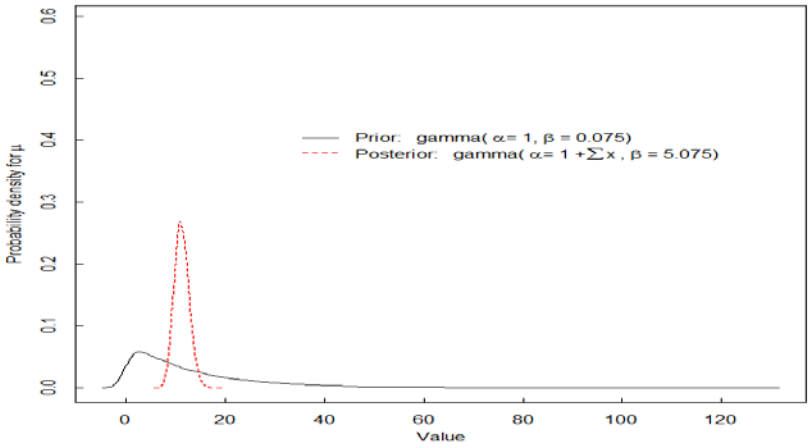

Fig. 4. The prior and posterior distribution for λ for *n* = 5, $\mu = 10$, and $\bar{x} = 10$.

For example, with n = 5, λ =10, the Currie approximation is $\hat{T}_{.95}$=12.5 and the exact value using simulation (to within negligible simulation error) is $\hat{T}_{.95}$ = 21.5. The probability that the FAP is 0.05 or less is only 0.07 with the Currie value and is, by design, 0.99 with the simulation approach. Unlike with Gaussian data, for Poisson data, the value of *k* depends on λ, so λ must be replaced with $\hat{\lambda}$.

3.3.2 Bayesian approach

1. Specify *n and the parameters of the Gamma prior* α_{prior} and β_{prior}. *In this example* α_{prior} *=1 and* β_{prior} *= 0.075 (a very wide prior with mean and standard deviation of 13.3.*
2. For each of many (typically 10^5 or more) simulations, generate
   $\lambda \sim Gamma(\alpha_{prior}, \beta_{prior})$
   $X_i \sim Poisson(\lambda),\ i = 1, 2, ..., n$
3. Compute $\alpha_{post} = \sum_{i=1}^{n} x_i + \alpha_{prior}$ and $\beta_{post} = n + \beta_{prior}$
4. Choose the quantile of the posterior $\lambda_{post} \sim Gamma(\alpha_{post}, \beta_{post})$ such that
   $P(\hat{T}_{0.95} \geq T_{0.95}) = \gamma = 0.99$. This is the count value that is greater than 95% of the distribution of *X* for 99% of the λ values generated in the simulations.

The result is $\hat{T}_{0.95}$=23.4. Recall that the frequentist $\hat{T}_{0.95}$ from above is 21.5, and both values of $\hat{T}_{0.95}$ are approximations. The Bayesian estimate of $\hat{T}_{0.95}$ is approximate because there is always some

mismatch between the true and assumed prior. The frequentist estimate of $\hat{T}_{0.95}$ is approximate because it depends on the true value of λ so in practice, one uses $\lambda = \hat{\lambda}$. Recall that the accuracy of these approximate methods can be assessed using simulation and/or by analysis of historical data.

3.4 Example with two Poisson counts in each assay

Gamma detection often requires measurement of both the nearby-in-energy "background" counts and the peak region "gross" counts (Section 5.1). The gross count rate is $\lambda_G = \lambda_B + \lambda_N$ [2,13,14]. The Bayesian approach is effective in this context for two main reasons: a conjugate prior (Gamma) can be specified for λ_G and λ_B, so the measured G and B counts each lead to

$f_{posterior}(\lambda) = \text{Gamma}(\alpha_{prior} + \sum_{i=1}^{n} x_i, \beta_{prior} + n)$, and it is simple to enforce $\lambda_N \geq 0$ Although the choice of prior parameters α and β for both λ_G and λ_B is subjective, the user often can bound the range for both λ_G and λ_B from prior data, so α_{prior} and β_{prior} can each be within some modest range. If the Bayesian approach is applied repeatedly, its long-run behavior can be evaluated to check, for example, whether the nominal FAP is close to the actual FAP. For example, choose $\alpha_{prior} = 1$ and β_{prior} = 0.075 for λ_G and λ_B as in the previous Bayesian example for Poisson data. Generate G ~ Poisson(λ_G) and B ~ Poisson(λ_B). For each of many (10^5 or more) simulations, generate λ_G from its posterior $\text{Gamma}(1+G, 0.075+1)$ and generate λ_B from its posterior $\text{Gamma}(1+B, 0.075+1)$ and for those simulations for which $\lambda_G \geq \lambda_B$ (because $\lambda_N \geq 0$), compute G – B. Determine the threshold T for G – B such that with probability at least $\gamma = 0.99$, $P(G - B \geq T) \leq 0.05$. The result for example, for G = 30 and B = 10 is T = 34 (Currie) and T = 45 (Bayesian Tolerance, using the Skellam distribution, which is the distribution of the difference in two Poisson random variables). Then L_D is an estimate of the smallest net signal count rate λ_N that can be detected with high probability and low FAP in the presence of nonzero background count rate λ_B that has been previously estimated. Ignoring errors in the calibration factor ν (assuming $\nu = \nu_{\text{True}}$ and for simplicity here also assuming ν_{True} = 1), the Currie-based MDA is 39 and the tolerance interval-based MDA is 77. Allowing for 5% RSD in the total error as in the previous example and assuming that $\nu_{Meas} = \nu_{True}(1 + S + R)$ has a Gaussian distribution (any distribution is simple to accommodate here), then the Currie–based MDA, which corresponds to the net count rate assuming zero external background (see Section 5.1), increases from 39 to 45 and the tolerance interval–based MDA increases from 77 to 87.

4. Implications for the MDA

Recall the Poisson example at the end of Section 3 for which Currie's $\hat{T}_{0.95} = \hat{\mu}_B + k_{1-\alpha}\hat{\sigma}_B$=12.5, and the one-sided tolerance limit is $\hat{T}$ = 22 for 99% confidence that the FAP is 0.05 or smaller. Therefore, the estimated MDA based on the tolerance interval limit will be larger than the estimated MDA based on the Currie limit. Specifically, if the mean count rate shifts from $\mu = 10$ to $\mu = 19.5$ any future observation $X \sim \text{Poisson}(\lambda = 19.5)$ satisfies $P(X \geq 13) \geq 0.95$ for the Currie mean shift and

$X \sim \text{Poisson}(\lambda = 34.4)$ satisfies $P(X \geq 22) \geq 0.95$ for the tolerance interval mean shift. The mean shift values $\lambda = 19.5$ and $\lambda = 34.4$ are easily computed by numerical search. The MDA is then calculated by converting the mean shift to an activity, which requires calibration.

Recall that the MDA is defined as $\text{MDA} = \frac{\text{L}_\text{D}}{\nu}$, where in this example $\text{L}_\text{D} = 19.5$ (Currie) or $\text{L}_\text{D} = 34.4$ (tolerance) and the calibration factor ν (a product of gamma ray yield, detector and geometric efficiency, counting time, and other factors) has measurement error that can introduce systematic error in the estimate of the MDA. References. [2,13,14] account for systematic uncertainties in the estimate of MDA using a modified version of the Currie estimation [2,3].

To allow for random and/or systematic errors in ν, $\nu_{Meas} = \nu_{True}(1 + S + R)$, implies that the mean shift when the signal is present has uncertainty. To illustrate, assume that it is desired to have at least 99% confidence that the mean shift is above some limit. Assuming Gaussian calibration errors as an example, then, for example, assuming 5% relative standard deviation (which is assumed here to include both random and systematic components) in converting the mean shift to activity using $\text{MDA} = \frac{\text{L}_\text{D}}{\nu}$ increases the estimated mean shift that can be detected with high probability from 19.5 to 22.1 (Currie approximation) and from 34.4 to 38.(tolerance interval approximation).

5. Discussion

This section describes three additional topics related to MDA calculations.

5.1 Definition of the background

In some γ-based NDA applications, the challenge to define and measure the relevant background is very important. For example, in attribute measurements of fresh fuel assemblies, one task is to assess whether a given assembly is a dummy (not containing ^{235}U). In this case, the background is defined as the response of the detector to γ emissions from neighboring assemblies if the assembly being measured were a dummy. That is, measurement behavior needs to be characterized if γ emissions could be measured from only the neighboring assemblies at the location of the assembly being measured. The measurement seeks to provide evidence that a signature from the item was detected (thereby verifying presence of ^{235}U) and that the measured signature originated from the item, not from radiation outside the item.

The minimum detectable quantity is not usually defined for attribute testing; however, it is sometimes desired (beyond the scope of this fresh fuel example) to estimate the probability that the test alarms for specified large mean shifts, such as 50% or more nuclear material missing.

Gamma-ray detectors detect distinct γ-rays energies. Sodium Iodide (NaI) and Cadmium-Zinc-Telluride (CZT) are common detector types. The presence of ^{235}U is verified in fresh fuel by estimating the area in the peak region of interest (ROI) associated with the 185.7 keV γ-ray. If the estimated peak area exceeds 3 times its estimated standard deviation, then there is high confidence that the peak is truly present. Because γ rays at such energies interact with materials primarily through both the photoelectric effect (in which the γ-ray transfers all its energy to the detector medium) and Compton scattering (in which the γ-ray scatters off an electron in the medium or surrounding mediums causing a partial transfer of its energy to the detector medium), each measured peak in a γ-ray spectrum will lie on top of a background caused by higher energy γ-rays that underwent Compton scattering, as shown in Fig. 5 from a CZT detector.

In spent fuel verification scenarios where shielding and collimation can be used to detect γ-rays only from the selected assembly, the peak area is estimated as the difference between the total counts in the ROI that includes the peak (indicated by the red lines in Fig. 5) and the counts associated with the Compton background in that region (indicated by the area underneath the blue line in Fig. 5) (recall Example 3.3). To assist in determining whether the attribute test condition has been satisfied, most software programs automatically notify the inspector when the net area of the peak ROI above the Compton background is larger than 3 times its estimated standard deviation.

In cases where attribute measurements are performed near other items containing the same type of nuclear material, a background measurement is needed to estimate the peak's count rate as detected from the surrounding environment. The background-only measurement corresponding to the item-plus-background measurement in Fig. 5 had a similar spectrum shape as that in Fig. 5, but the peak ROI counts were approximately 60% lower; for this background-only measurement, the same CZT detector as used for item-plus-background was placed in an empty slot of a storage rack containing fresh fuel assemblies. The background spectrum was measured during the same training exercise and for the same count time as the spectrum in Fig. 5, which was from an attribute test measurement of a fresh fuel assembly within that same storage rack. Assuming zero room background, applying the attribute test to the background spectrum would yield a positive (and incorrect) verification because the estimated peak area was approximately 13 times its estimated standard deviation. Therefore, to ensure proper verification of items using the attribute test, careful consideration must be given regarding how the room background is measured in order to reject the possibility that the measured spectrum was the result of room background and not from the item to be verified.

When the background spectrum shows evidence that the peak of interest is present from measuring the surrounding environment, the verification of an item using the attribute test is executed using:

$$\text{(Measured rate) – (background rate)} > 3\sqrt{\left(\frac{\hat{\sigma}_B}{T_B}\right)^2 + \left(\frac{\hat{\sigma}_M}{T_M}\right)^2}$$

where $\hat{\sigma}_B$ is the estimated standard deviation in the estimated peak area in the background measurement, $\hat{\sigma}_M$ is the estimated standard deviation in the area of the peak in the measured

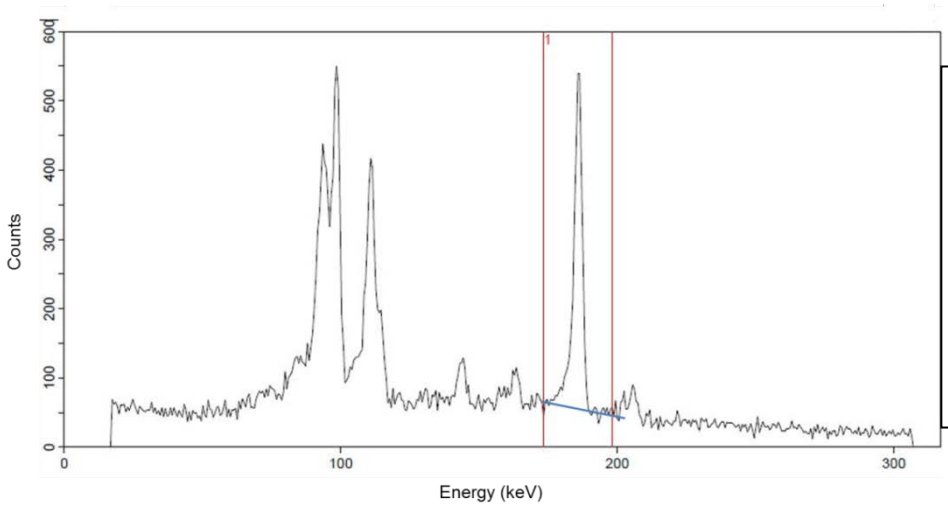

Fig. 5 ^{235}U spectrum from a CZT detector for the item-plus-background measurement. The red lines indicate the ROI used to estimate the area of the 186 keV peak while the blue line is an estimate of the Compton background.

spectrum from the item, and T_B and T_M are the count times corresponding to the background and item measurement, respectively. Both the measured and background rates are corrected for the background caused by Compton scattering by estimating the count rate of the net peak, which involves a difference of two quantities as in Example 3.3. In cases where the attribute test software is

unable to account for room background in automatically calculating whether the attribute test has been passed, the inspector performs the attribute test calculation for each item. The attribute test aims to answer the question 'Does the item contain the material as declared?', and an inspector's time is quite limited, so inspectors sometimes apply more stringent statistical tests to help confirm the attribute test result. One example of such a stringent test is

$$Measured\ rate - 3 \cdot \frac{\sigma_M}{T_M} > Background\ rate + 3 \cdot \frac{\sigma_B}{T_B}$$

Inspectors typically perform the background measurement before performing the verification measurements, and the quantity on the right side of the stringent inequality is a single calculated value, which makes the evaluation simple to do while performing verification measurements. Measurements that do not pass the stringent test can be tested against the more formal method.

Recall that the Gaussian approximation to the Poisson is adequate for tolerance interval estimation if the Poisson mean $\lambda \geq 100$ (Fig. 3), so the factor of 3 used above is justified because for the data in Fig. 5, the quantiles of the Gaussian provide an adequate approximation to the true FAP, assuming $\hat{\lambda} = \lambda$ (but one should be aware of the need for the factor $\sqrt{1+1/n} = \sqrt{2} = 1.41$ as in Fig 3a versus Fig 3b). A more complicated method than a sum of Poisson counts below and above the peak ROI is often used to estimate the background under the blue line in Fig. 5;so $\hat{\sigma}_B$ and $\hat{\sigma}_M$ can involve more than the Poisson distribution (beyond this paper's scope).

5.2 Tolerance interval versus prediction interval

A prediction interval is another potentially useful approach to the MDA, and will lead to MDA values that are larger than the Currie-based MDAs and smaller than the tolerance interval-based MDAs. The prediction interval approach averages over the parameter(s) θ so there is no probability statement regarding confidence in coverage [5].

5.3 Impact of analyzing predicted counts rather than estimated activity

Zykov [15] describes a pass-fail criterion for verification measurements (operator declarations compared to inspector measurements, as in Section 3.1) regarding the minimum detectable defect size (the minimum amount of missing radioactive material) if analysis of the inspector measurements is based on measurements that are predicted using modeling and the operator declarations. Such an approach would avoid explicit inversion of measurements to activity or nuclear material mass, and simulations to be presented elsewhere suggest that the minimum detectable defect size would be smaller. The minimum detectable defect size would be based on a tolerance interval approach, because that is more conservative than the Currie approach, as this paper has shown. This methodology could lead to more efficient verification sampling plans. Regarding testing for patterns, recall that the overall test for a pattern is based on the average OID (known as the *D* statistic), $\frac{1}{n}\sum_{j=1}^{n}\frac{o_j - i_j}{o_j}$ [14], which could be defined on the basis of measured masses or on the basis of predicted and observed measurements. However, whenever an estimate of the D Statistic (at the stratum, MBE component, or MBA level) is needed, e.g. for the detection of diversion into D through material balance evaluation, it would be necessary for the inspector to estimate item mass, so explicit inversion of inspector measurements to item mass would be required.

6. Summary

This paper revisited the Currie method to estimate the MDA with attention to the FAP in Poisson and Gaussian data in NDA by gamma detection. It was shown that the FAP in signal detection can be

significantly different from the nominal FAP if the nominal FAP is not calculated based on a tolerance interval. If the nominal FAP is calculated based on a tolerance interval, then the MDA is increased compared to the Currie approximation. A simple way to accommodate random and/or systematic errors in converting from a mean shift to an activity shift was illustrated.

References

[1] Currie, L., Limits for qualitative detection and quantitative determination: application to radiochemistry, Analytical Chemistry 40, 58-5936, 1968.
[2] Kirkpatrick, J., Venkataraman, R., Young, B., Minimum detectable activity, systematic uncertainties, and the ISO 11929 standard, Journal of Radioanalytical and Nuclear Chemistry 296, 1005-1010, 2013.
[3] International Organization for Standardization ISO 11929 determination of the characteristic limits (decision threshold, detection limit, and limits of the confidence interval) for measurements of ionizing radiation-fundamentals and application, Geneva, 2010.
[4] Young, D., Tolerance: an R package for estimating tolerance intervals, Journal of Statistical Software 36(5),1-39 2010.
[5] Hamada, M., Johnson, V., Moore, L., Wendelberger, J. Bayesian prediction intervals and their relation to tolerance intervals, Technometrics 46(4), 452-459, 2004.
[6] Janiga, I., Garaj, I., Two-sided tolerance limits of normal distributions with unknown means and unknown common variability , Measurement Science Review (3) (1), 75-78, 2003.
[7] Eberhardt, K., Mee, R., Reeve, C., Computing factors for exact two-sided tolerance limits for a normal distribution, Communication in Statistics- Simulation and Computation, 18(1), 397-413,1989
[8] *R Core Team. R: A language and environment for statistical computing. R Foundation for Statistical Computing, Vienna, Austria. ISBN 3-900051-07-0,* http://www.R-project.org/, 2012.
[9] Bonner, E., Burr, T., Martin, K., Norman, C., Santi, P., Uncertainty quantification as presented in training courses for safeguards inspectors, ESARDA 2017.
[10] Miller, R., Beyond ANOVA: Basics of Applied Statistics, Chapman & Hall, 1998.
[11] Liao, C., Lin, T., Iyer, H., One- and two-sided tolerance intervals for general balanced mixed models and unbalanced one-way random models, Technometrics 47(3), 323-335, 2005.
[12] Burr, T., Krieger, T., Krzysztoszek, K., Norman, C., Tolerance intervals for measurements with systematic and random errors, IAEA report 2017.
[13] Kirkpatrick, J., Young, B., Poisson statistical methods for the analysis of low-count gamma spectra, IEEE Transactions on Nuclear Science 56(3), 1278-1282, 2009.
[14] Kirkpatrick, J., Venkataraman, R., Young, B., Calculation of the detection limit in radiation measurements with systematic uncertainties, Nuclear Instruments and Methods in Physics Research A 784, 306-310, 2015.
[15] Zykov, S. Technical challenges and technological gaps in IAEA safeguards, Proceedings of the Institute of Nuclear Materials Management, 2015.

Uncertainty quantification as presented in training courses for safeguards inspectors

E.Bonner[1], T. Burr[1], T. Krieger[3], K. Martin[1], C. Norman[1], P. Santi[2]
[1]SGIM/Nuclear Fuel Cycle Information Analysis; [2]SG Training
[3]Forschungszentrum Jülich GmbH, Inst. Energy and Climate Research

Abstract

For safeguards evaluators to provide credible assurance that States are honoring their safeguards obligations, quantitative conclusions regarding the non-diversion of nuclear material from States' nuclear material flows and inventories are needed. The statistical analysis used to reach these conclusions requires that each measurement method undergo uncertainty quantification (UQ). Inspector training for safeguards inspectors includes measurement error models that must account for variation within and between groups, where a group is defined to be an inspection period. A typical model for multiplicative errors for the inspector (*I*) is $I_{ij} = \mu_{ij}(1 + S_{Ii} + R_{Iij})$, with $S_{Ij} \sim N(0, \delta_{SI}^2)$ and $R_{Iij} \sim N(0, \delta_{RI}^2)$, where S_{Ii} is a short-term systematic error in group *i* (from 1 to *g*), and, for item *j* (from 1 to *n*), I_{ij} is the inspector's measured value, μ_{ij} is the true value, and R_{Iij} is the random error. This paper describes three main inspector UQ-related training topics. Topic one is analysis of variance to estimate the relative standard deviations (RSDs) δ_{SI} and δ_{RI} (and the corresponding RSDs for the operator). Topic two is to use estimated RSDs to evaluate material balances and to plan inspector sample sizes based on estimated material loss detection probabilities. Topic three is an example involving the uranium neutron coincidence collar (UNCL) to illustrate the need for inspector UQ training to include an understanding of the most important factors that impact the RSDs, which in turn affect the rejection limits for comparing operator to inspector measurements. For the UNCL method, it is important for inspectors to understand the fuel assembly design and software input requirements. Incorrectly declared input is thought to be among the largest contributors to UNCL uncertainty (as quantified by the RSDs).

Keywords: Bottom-up uncertainty quantification (UQ); top-down UQ, Grubbs estimation

1. Introduction

Inspector measurements are a cornerstone of IAEA safeguards, so it's important for inspectors to understand UQ. This paper describes the three UQ topics listed in the abstract that are presented in training courses for safeguards inspectors. First, for background needed here, the guide to the expression of uncertainty in measurement (GUM) describes estimating and expressing measurement uncertainty [1]. UQ can be approached by comparing multiple measurements of the same item (top-down) or by assessing each step in the measurement procedure (bottom-up). For a top-down evaluation, the multiple measurement on the same item can, for example, be repeated measurements by the same instrument during the same calibration period or replicate measurements across many calibration periods and/or laboratories [1,2]. The GUM indirectly addresses top-down methods, but is most known for bottom-up UQ using the measurement equation

$$Y = f(X_1, X_2, ..., X_N) \quad (1),$$

where *Y* is the estimate of the measurand, and the *X*s are inputs. The inputs can include measurements, estimated calibration or adjustment factors, and can have a joint probability distribution with covariances among the inputs. To estimate the variance in *Y*, the variance of each X, denoted σ_{Xi}^2, and covariances between *X*s, denoted $\sigma_{Xi}\sigma_{Xj}\rho_{i,j}$, are propagated using the Taylor approximation to obtain

$$\sigma_Y^2 \approx \sum_{i=1}^{N}\left(\frac{\partial f}{\partial x_i}\right)^2\Bigg|_{x_i=E(X_i)} \sigma_{Xi}^2 + 2\sum_{i=1}^{N-1}\sum_{j=i+1}^{N}\frac{\partial f}{\partial x_i}\frac{\partial f}{\partial x_j}\Bigg|_{x_i=E(X_i),x_j=E(X_j)} \sigma_{Xi}\sigma_{Xj}\rho_{i,j} \quad (2).$$

For verification, paired (operator, inspector) data are collected from inspections performed during site visits that occur once or a few times per year (Section 3), and relative operator-inspector differences defined as (and *d* is sometimes referred to as OID, for operator-inspector difference)

$$d = OID = \frac{o - i}{o} \quad (3)$$

are compared to alarm thresholds to monitor for possible data falsification by the operator. The alarm thresholds are estimated by applying a type of top-down UQ, using several years of prior paired (*O*,*I*)

data. An effective top-down measurement error model must account for variation within and between groups, where a group is an inspection period. One top-down multiplicative error model used for the inspector (*I*) (and similarly for the operator *O*) is

$$I_{kj} = \mu_{kj}(1 + S_{Ik} + R_{Ikj}), \quad (4)$$

where I_{ij} is the inspector's measured value of item *j* (from 1 to *n*) in group *k* (from 1 to *g*), μ_{kj} is the true but unknown value of item *j* from group *k*, $R_{Ikj} \sim N(0, \delta_{RI}^2)$ (the ~ symbol means independently and identically distributed normal) is the random error of item *j* from group *k*, $S_{Ik} \sim N(0, \delta_{SI}^2)$ is a short-term systematic error in group *k* [2-4], which is randomly generated once per inspection period.

2. Top-down UQ applied to paired (operator, inspector) data

The basis of the top-down approach to UQ applied to OIDs is analysis of variance (ANOVA) with random effects. Such paired data arise when the operator and the inspector measure the same object once without measurement repetition. One goal is to estimate $\delta_R^2 = \delta_{RO}^2 + \delta_{RI}^2$, $\delta_S^2 = \delta_{SO}^2 + \delta_{SI}^2$, and $\delta_T^2 = \delta_R^2 + \delta_S^2$ for the differences (see Section 3). Note that the errors R_{Okj} and R_{Ikj} include "item-specific" bias because the measured items are not true replicates; that is, the items can contain variability in matrix components and interferences that could in principle affect measurement error variance components [2-5].

For the relative differences in Eq. (3) and balanced data with *n* paired differences in each of g groups (*N* = *ng*), the ANOVA decomposition:

$$\sum_{k=1}^{g}\sum_{j=1}^{n}(d_{kj} - \bar{d})^2 = \sum_{k=1}^{g}\sum_{j=1}^{n}(d_{kj} - \bar{d}_k)^2 + n\sum_{k=1}^{g}(\bar{d}_k - \bar{d})^2 = SSW + SSB \quad (5)$$

leads to the well-known estimates $\hat{\delta}_R^2 = \frac{SSW}{N-g}, \hat{\delta}_S^2 = \frac{SSB - SSW}{n}$, where SSW is the sum of squares within groups, SSB is the sum of squares between groups, and $\hat{\delta}_T^2 = \hat{\delta}_R^2 + \hat{\delta}_S^2$.

Another goal is to partition the variances of *R* and *S* into that due to the operator and to the inspector (see [6] and Section 3.2 on material balance evaluation). The Grubbs estimator assume an additive error model, so operator and inspector measurements (if they arise from a multiplicative-model) are transformed using the natural logarithm to convert Eq. (4) to an additive error model (approximately, see [2], which develops a Grubbs-type estimator for a multiplicative model). The basis of a Grubbs'-based estimator [7] applied to log-transformed data generated from the model in Eq. (4) to estimate δ_{RO}^2 and δ_{RI}^2 is that the covariance between the log-transformed measurements (still denoted as (*O*,*I*) to avoid cluttering the notation) equals the relative variance of the true values δ_μ^2 while the relative variance of I conditional on the value of S equals $\delta_\mu^2 + \delta_{RI}^2$ [2,3]. Therefore within inspection period *k* (lower-case *i*(*o*) for observed values of *I* (*O*), and similarly for the operator),

$$\hat{\delta}_{RI,k}^2 = \frac{1}{n-1}\left\{\sum_{j=1}^{n}(i_{k,j} - \bar{i}_k)^2 - \sum_{j=1}^{n}(o_{k,j} - \bar{o}_k)\left(i_{k,j} - \bar{i}_k\right)\right\}. \quad (6).$$

Estimates from Eq. (6) from each of the *g* groups are averaged ($\hat{\delta}_{RI}^2 = \frac{(n-1)\sum_{k=1}^{g}\hat{\delta}_{RI,k}^2}{N-g}$) to get the final estimate of the inspector's random error variance, and similarly, the estimate of δ_μ^2 is the average of the sample covariances computed within each group. To estimate δ_{SI}^2, an extension of random effects ANOVA shows that the expected value of the between groups sum of squares, $E\{\sum_{k=1}^{g} n(\bar{I}_k - \bar{\bar{I}})^2 \Big/ (g-1)\} = \delta_{RI}^2 + \delta_\mu^2 + n\delta_{SI}^2$, so a reasonable estimate of δ_{SI}^2

is $\hat{\delta}_{SI}^2 = \dfrac{\sum_{k=1}^{g}(\bar{i}_k - \bar{\bar{i}})^2}{g-1} - \dfrac{\hat{\delta}_{RI}^2 + \hat{\delta}_{\mu}^2}{n}$ [8,9]. In sample size calculations (Section 3.1), it is not necessary to separate δ_S^2 into its components $\delta_{SI}^2 + \delta_{SO}^2 = \delta_S^2$, so the constraint $\hat{\delta}_{SI}^2 + \hat{\delta}_{SO}^2 = \hat{\delta}_S^2$ is imposed, which requires $\hat{\delta}_{\mu}^2 = \dfrac{1}{g-1}\sum_{k=1}^{g}(\bar{o}_k - \bar{\bar{o}})(\bar{i}_k - \bar{\bar{i}})$ [8]. There is no guarantee that $\hat{\delta}_{\mu}^2$, $\hat{\delta}_{RI}^2$, or $\hat{\delta}_{SI}^2$ are non-negative, but the corresponding true quantities are non-negative ($\delta_{\mu}^2 \geq 0, \delta_{RI}^2 \geq 0, \delta_{SI}^2 \geq 0$), so constrained versions of the Grubb's and ANOVA-based estimators are available [9-11].

Figure 1 plots *n* = 5 OID values in each of 4 inspection periods; the inspector measurements are made using UNCL (section 4). For the 20 OID values in Fig. 1, the estimated RSDs from the ANOVA approach are $\hat{\delta}_R = 0.07, \hat{\delta}_S = 0.11, \hat{\delta}_T = 0.13.$ And, the corresponding Grubbs estimates are $\hat{\delta}_{RO} = 0.04, \hat{\delta}_{RI} = 0.07, \hat{\delta}_{SO} = 0.04, \hat{\delta}_{SI} = 0.07.$

Additional topics for top-down UQ include: methods to reduce the impact of σ_{μ}^2 on the uncertainty in $\hat{\delta}_{RO}^2$ and $\hat{\delta}_{RI}^2$, screening for outliers (because outliers can have a large influence on variance estimates), choosing the group structure if information suggests that grouping by inspection period is not effective, and assessing the uncertainty in the estimates $\hat{\delta}_{RO}^2, \hat{\delta}_{RI}^2, \hat{\delta}_{SO}^2$ and $\hat{\delta}_{SI}^2$ [9]. Also, recent work is developing Bayesian options to include prior information, such as from bottom-up UQ regarding δ_{μ}^2, δ_{RI}^2, and/or δ_{SI}^2, and similarly for the operator [12,13].

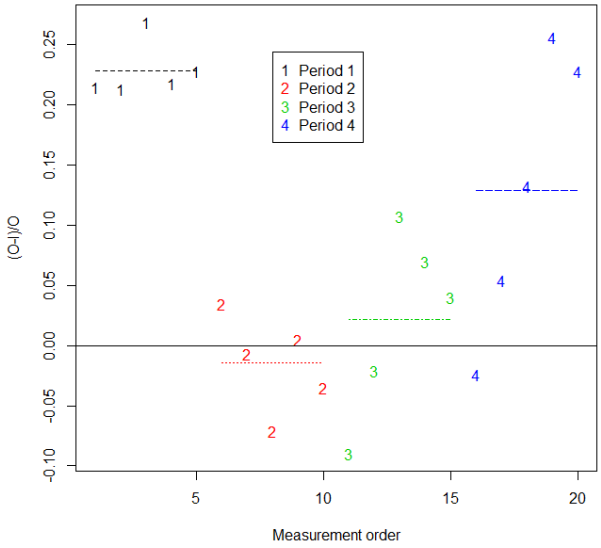

Fig. 1. Example with *n* = 5 $OID = \dfrac{o-i}{o}$ values in each of 4 inspection periods.

3. Inspector sample size calculations and material balance evaluation

The estimates $\hat{\delta}_{RO}^2 + \hat{\delta}_{RI}^2 = \hat{\delta}_R^2$ and $\hat{\delta}_{SO}^2 + \hat{\delta}_{SI}^2 = \hat{\delta}_S^2$ are used sample size calculations (Section 3.1) and the estimates $\hat{\delta}_{RO}^2, \hat{\delta}_{RI}^2, \hat{\delta}_{SO}^2$, and $\hat{\delta}_{SI}^2$ are used for material balance evaluations (Section 3.2).

3.1 Inspector sample size calculations

Following top-down ANOVA to estimate variance components, there are two main IAEA verification tests applied to future sets of *n* paired (*O*,*I*) values. First, the overall test for a pattern is based on the average OID, $\dfrac{1}{n}\sum_{j=1}^{n}\dfrac{o_j - i_j}{o_j}$, which are analysed in [14] but not discussed further here. Second, the one-at-a-time test evaluates each of the *n* OID values. If $d_j > 3\delta_T$ (in testing for overstatement

falsification) where $\delta_T = \sqrt{\delta_R^2 + \delta_S^2}$, (or any alarm threshold close to 3 that corresponds to a small false alarm probability, FAP), then the *j*-th item selected for verification leads to an alarm. Because the IAEA uses zero-defect sampling, the only acceptable (passing) sample is one for which no defects are identified. Therefore, the non-detection probability is the probability that no defects are identified in a sample of size *n* when one or more true defective items (a defective item has an overstatement or understatement of the best accountancy value in an attempt to mask diversion) are in the population of size *N*. For such one-item-at-a-time testing, the non-detection probability is given by

$$\beta = \text{Prob}(0 \text{ defects in sample of size } n) = \sum_{j=Max(0,n+r-N)}^{Min(n,r)} A_j \times B_j \qquad (7),$$

where the term A_j is the probability that the selected sample contains *j* truly defective items, which is given by the hypergeometric distribution with parameters *j*, *n*, *N*, *r,* where *n* is the sample size, *N* is the population size, and *r* is the number of defective items in the population. More specifically, $A_j = \frac{\binom{r}{j}\binom{N-r}{n-j}}{\binom{N}{n}}$ is the probability of choosing *j* defective items from *r* defective items in a population of size *N* in a sample of size *n*, which is the well-known hypergeometric distribution. The term B_j is the probability that none of the *j* truly defective items are inferred to be defective based on the individual *d* tests. The value of B_j depends on $\delta_T = \sqrt{\delta_R^2 + \delta_S^2}$ and the alarm threshold. Assuming a multiplicative error model for the inspector measurement (and similarly for the operator), implies that, for an alarm threshold of $3\delta_T$, assuming no falsification, for $d_j = \frac{o_j - i_j}{o_j} \approx \frac{o_j - i_j}{\mu_j}$, one must calculate $B_j = P(d_1 \le 3\delta_T, d_2 \le 3\delta_T, ..., d_j \le 3\delta_T)$ for one-sided testing, which is given by the multivariate normal integral $B_j = \frac{1}{(2\pi)^{i/2} |\Sigma_j|^{1/2}} \int_{-\infty}^{3\delta_T} ... \int_{-\infty}^{3\delta_T} \exp\{\frac{-(\mathbf{z}-\boldsymbol{\lambda})^T \Sigma_j^{-1} (\mathbf{z}-\boldsymbol{\lambda})}{2}\} dz_1 dz_2 ... dz_j$, where under the equal diversion assumption, each of the components of $\boldsymbol{\lambda}$ is equal to $\frac{1SQ}{r}$ (SQ is a significant quantity; for example, 1 SQ = 8 kg for Pu, and *r* was defined above as the number of defective items in the population). The term Σ_j in the B_j calculation involved in the multivariate normal integral is a square matrix with *j* rows and columns with values $(\delta_R^2 + \delta_S^2)$ on the diagonal and values δ_S^2 on the off-diagonals.

As an example, Fig. 2 plots the detection probability $DP = 1 - \beta$ versus the number of overstatement defects (testing whether $d_j \le 3\delta_T$) in a sample of size *n* = 50 from a population of size *N* = 200 with an alarm threshold equal to $3\delta_T$ with $\delta_R = 0.07, \delta_S = 0.11$, which are the estimates $\hat{\delta}_R$ and $\hat{\delta}_S$ for the data in Fig. 1. To illustrate the importance of partitioning the total error variance into its random and systematic components, the DPs in Fig. 2 are calculated in two incorrect ways and the correct way: assume $\delta_T = 0.13$ consists entirely of random error, entirely of systematic error, or, correctly, as partly random and partly systematic.

3.2 Material Balance Evaluation

Nuclear material accounting (NMA) provides a quantitative basis to detect nuclear material loss or diversion at declared facilities. NMA involves periodically measuring facility input transfers T_{in}, output transfers T_{out}, and physical inventory *I* to compute a material balance (MB) defined for group (balance period) *k* as $\mathrm{MB}_k = (\mathrm{I}_{k-1} + \mathrm{T}_{\mathrm{in,k}} - \mathrm{T}_{\mathrm{out,k}}) - \mathrm{I}_k$ where $(\mathrm{I}_{k-1} + \mathrm{T}_{\mathrm{in,k}} - \mathrm{T}_{\mathrm{out,k}})$ is the book inventory (and

$I_0 = 0$). In NMA, a collection of MBs is tested for the presence of any statistically significant large differences and/or for trends, while allowing for random and systematic errors in variance propagation to estimate the measurement error standard deviation of MB_k, σ_{MB_k}. Typically, many measurements are combined to estimate the terms T_{in}, I_{begin}, T_{out}, and I_{end} in the MB; therefore,

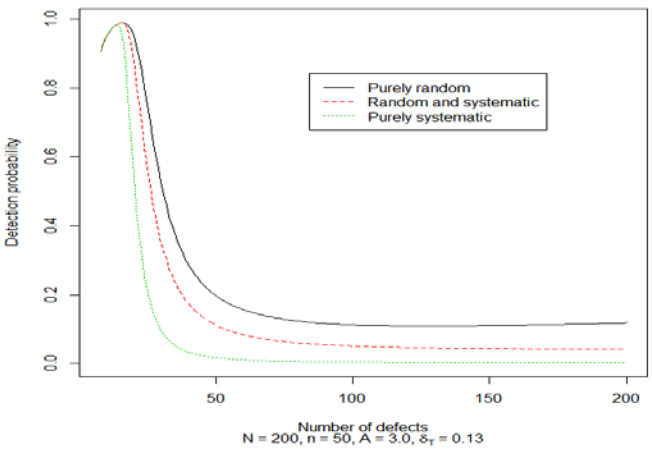

Fig. 2. The DP versus the number of defects in a sample of size n = 50 from a population of size *N* = 200 with an alarm threshold $A\delta_T$ for A = 3 for three assumptions regarding how $\delta_T = 0.13$ is partitioned into random and systematic components. In Fig. 2, the FAPs are 0.065, 0.021, and 0.001, respectively for purely random, a mix of random and systematic, and purely systematic, respectively. Although not shown here, the FAPs are all 0.05 if the alarm threshold A is 3.08, 2.71, and 1.65, respectively, and in that case, the DPs are larger for the purely systematic error case for a range of sample sizes.

the central limit effect and experience suggests that MBs in most facilities will be approximately normally distributed with mean equal to the true NM loss λ_k and standard deviation σ_{MB_k}, which is expressed as $X_k \sim N(\lambda_k, \sigma_k^2)$, where *X* denotes the MB and the notation σ_k is a shortened version of σ_{MB_k}. A sequence of *n* MBs is assumed to have approximately a multivariate normal distribution [13], $(X_1, X_2, \ldots X_n) \sim MVN(\boldsymbol{\lambda}, \Sigma)$, where the *n*-by-*n* covariance matrix $\Sigma = \begin{pmatrix} \sigma_1^2 \sigma_{12}^2 \ldots \sigma_{1n}^2 \\ \sigma_{21}^2 \sigma_2^2 \ldots \sigma_{2n}^2 \\ \ldots \\ \sigma_{n1}^2 \sigma_{n2}^2 \ldots \sigma_n^2 \end{pmatrix}$.

Estimating Σ is a key step required in NMA. To illustrate, a simplified example model of a generic electrochemical facility with one input stream, one output stream, and one key inventory item will be used here [13]. Each measurement method is modelled using a multiplicative measurement error model for the operator (O), $M_j = \mu_j(1 + S_j + R_j)$, with $S_j \sim N(0, \delta_S^2)$ and $R_j \sim N(0, \delta_R^2)$, where for item *j*, M_j is the operator's measured value, μ_j is the true but unknown value, R_j is the random error, S_j is the short-term systematic error, assumed constant for all items in the analysis period (so $S_1 = S_2 = \ldots$ for all items). Under those assumptions, the diagonal terms of Σ are calculated as

$$\sigma_k^2 = T_{in_k}{}^2(\delta_{in,R}^2 + \delta_{in,S}^2) + T_{out_k}{}^2(\delta_{out,R}^2 + \delta_{out,S}^2) + I_k^2\delta_{inv,R}^2 + I_{k-1}^2\delta_{inv,R}^2 + (I_k - I_{k-1})^2\delta_{inv,S}^2 \quad (8).$$

And the off-diagonal terms in Σ are calculated as:

$$\sigma_{kk'}^2 = T_{in_k}T_{in_{k'}}\delta_{in,S}^2 + T_{out_k}T_{out_{k'}}\delta_{out,S}^2 + \left(I_kI_{k'} + I_{k-1}I_{k'-1}\right)\delta_{inv,S}^2 -$$

$$I_kI_{k'-1}\left(\delta_{inv,S}^2 + \delta_{inv,R}^2\left[if\ k'-k=1\right]\right) - I_{k-1}I_{k'}\left(\delta_{inv,S}^2 + \delta_{inv,R}^2\left[if\ k-k'=1\right]\right) \quad (9).$$

In the last two terms of Eq. (9), the random error of the inventory term is only applied if the condition is true. Numerical examples of applying Eqs. (8) and (9) are given in[13] to estimate a 12-by-12 covariance matrix Σ for monthly MBs over one year. The matrix Σ is the basis for applying sequential statistical tests to monitor for abrupt or protracted diversion. The false alarm and detection probabilities (FAP and DP) are estimated assuming that $\hat{\delta}_S = \delta_S$ and $\hat{\delta}_R = \delta_R$, and [13] provided a sensitivity study to assess the impact of estimation errors in substituting measured transfers and inventories and estimates $\hat{\delta}_S$ and $\hat{\delta}_R$ in Eqs. (8) and (9) on the actual FAPs and DPs.

4. Bottom-up UQ: UNCL case study

The Uranium Neutron Coincidence Collar (UNCL) is an active NDA system that uses an AmLi neutron source to induce fission in the ^{235}U within a fresh fuel assembly [15-22]. Because ^{235}U produces 0 to 10 neutrons per fission, detection of temporally correlated neutrons ("correlated" means that the neutrons arise from the same fission chain) is a unique signature of fission. To detect neutrons, ^{3}He proportional counters are embedded in polyethylene slabs surrounding the assembly like a collar (Fig. 3). The UNCL can be configured to detect either thermal neutrons (thermal mode) or, with the addition of a Cd liner, to detect fast neutrons (fast mode). Using a shift register and the International Neutron Coincidence Counting program (INCC [16]), detector signals are analysed to infer the number of detected coincident neutrons (known as doubles). The doubles rate is related to the number of fissions of ^{235}U and hence to the ^{235}U mass. The UNCL measures a small portion of the entire length of the fresh fuel assembly, so is calibrated to convert the measured doubles rate to a ^{235}U linear density for the assembly. By combining the measured linear ^{235}U density with a measurement of the active length of the assembly, the total ^{235}U mass of the assembly can be inferred.

The equation to convert measured doubles rate *X* to *Y* (gms ^{235}U per cm) is

$$Y = \frac{kX}{a_1 - a_2 kX} \qquad (10),$$

where a_1 and a_2 are calibration parameters, and $k = k_0 k_1 k_2 k_3 k_4 k_5$ is a product of correction factors that adjust *X* to item-, detector-, and source-specific conditions in the calibration [2,14-18]. Therefore, Eq. (10) is a special case of GUM's Eq. (1), where in addition to the reals count rate X, the calibration parameters a_1 and a_2 and k_0 ,k_1, k_2, k_3, k_4 , and k_5 are among the *X*'s in Eq. (1) [2,16]. The calibration factors, a_1 and a_2, and the k-factors help to identify UNCL error sources.

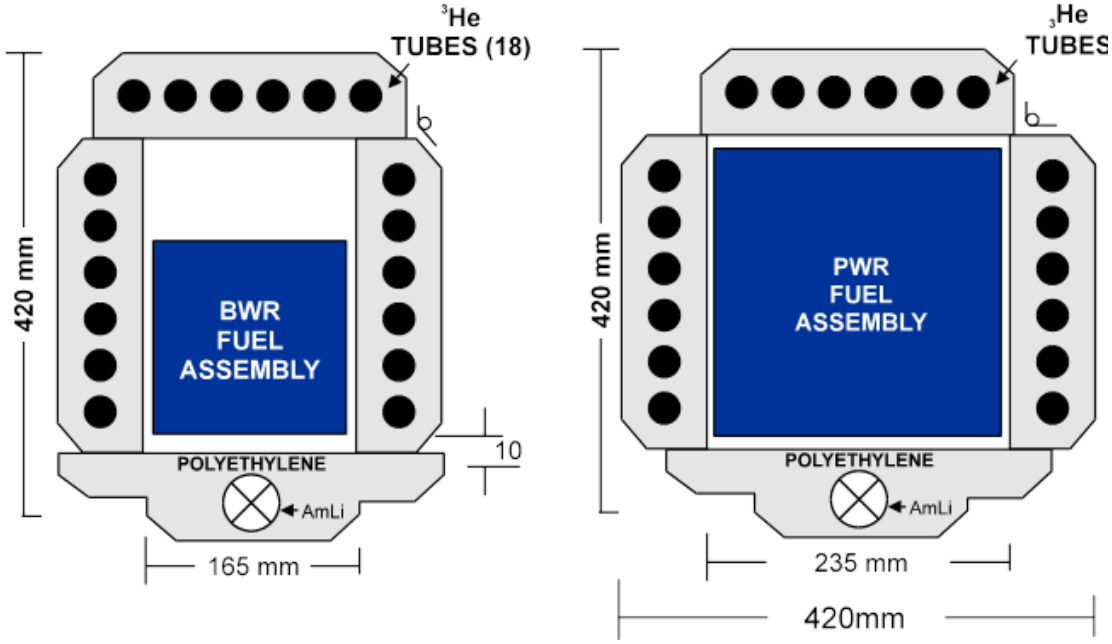

Fig. 3. Schematic of UNCL measurements of a BWR assembly (left) or PWR assembly (right).

4.1 UQ for UNCL

Based on this UNCL overview, uncertainties arise from three primary sources: the measured doubles rate X from the induced fission of ^{235}U, the estimated calibration curve [17] in Eq. (10) used to convert the X into a ^{235}U linear density, and the active length measurement. Although uncertainty determination appears to be relatively straightforward, complications arise when performing the measurement in the field. One UQ complication is that an assembly contains a significant amount of ^{238}U that produces coincident neutrons via spontaneous fission. In order to determine the doubles counting rate that comes only from the induced fission of ^{235}U, a second UNCL measurement is needed with the AmLi source removed to infer the background doubles rate from the spontaneous fission of ^{238}U. The doubles rate from this passive assay is then subtracted from the active assay results to infer the doubles counting rate from induced fission of ^{235}U.

A second UQ complication arises in applying a calibration curve to the net measured doubles rate X, because X is corrected to account for differences between the current measurement scenario and the physical characteristics that existed when the calibration curves were created. Reference [15] introduced correction factors to adjust the measured reals count rate X to the corresponding doubles rate observed in the calibration condition for a particular a_1 and a_2 coefficient pair. Coefficient-pairs were defined for standard pressurized water reactor (PWR) and boiling water reactor (BWR) fuel types by [17]. Since [17], coefficient pairs have been estimated for WWER-440 and WWER-1000 fuel types [19]. The term,k_0 accounts for uncertainty in the true Am/Li source strength (approximately 3.7% RSD in IAEA estimates) due to differences in detection efficiency and AmLi source strength between the specific UNCL and source used for calibration, and the UNCL and AmLi source used in current measurements The term k_1 accounts for uncertainty due to electronic drift (considered negligible with modern electronics, so k_1=1). The term k_2 accounts for uncertainty due to differences in detector efficiencies (approximately 1.5% RSD). In general the correction factors k_0-k_2 are determined based on performance of the specific UNCL system being used in the field and assuming the UNCL continues to operate as it was initially setup, remaining constant for the various inspection periods.

The term k_3 accounts for effects of burnable poison that may be present within the assembly, which impacts both the availability of neutrons to induce fission and the rate at which neutrons escape the assembly. The impact of burnable poisons can be minimized (<10% correction) by operating the UNCL in fast mode, but the fast mode measurement time is significantly longer than thermal mode. The burnable poison correction factor for thermal mode was recently updated to account for modern assemblies that contain a larger number of burnable poison rods or a larger Gd content than considered with the initial correction. As the correction for burnable poisons is empirical, inspectors must understand its limitations in terms of properties of the assembly (number of poison rods, Poison content, U enrichment, etc). . The term k_4 accounts for differences in the total uranium loading (U-total/cm, because this loading impacts neutron multiplication as well as scattering and reflection of neutrons[3]) between the calibration case and the measurement case. The term k_5 accounts for all other effects (eg spacers, bagged assemblies). To apply the k_3, k_4, and k_5 correction factors to the measured net doubles rate, specific and accurate information regarding the assembly needs to be input into the INCC program. This information includes the total number of rods present, the number of poison rods, the Gd content within the poison rods, and the ^{238}U mass within the assembly.

A third UQ complication comes from the fact that the in order for the UNCL to measure the ^{235}U linear density appropriately, the ^{235}U enrichment must be constant throughout the effective measurement length of the collar. Modern assemblies can contain zones of different ^{235}U enrichments along the length of the fuel rods, as well as a mixture of different types of fuel rods within a single assembly. The inferred ^{235}U linear density may only be accurate for that specific zone of the assembly. Because the total ^{235}U mass of the assembly is to be verified, an assembly with multiple enrichment zones can require multiple UNCL measurements to infer the ^{235}U linear density for each zone. The ^{235}U linear density of each zone is then multiplied by the length of that zone to determine the ^{235}U mass for the zone, with the zone masses are summed to infer total ^{235}U mass. It is often not possible to measure all enrichment zones, either due to the zone length being incompatible with an UNCL measurement or due to fuel handling limitations, so verification of single zone can be performed to calculate the paired Operator-Inspector data for the assembly.

MCNP [23] modelling suggests that there are additional uncertainty sources not captured by the *k* factors that are related to the variations that can occur in performing the UNCL measurement. One such source of uncertainty is a bias associated with the positioning of the assembly within the detector, particularly for BWR measurement as the BWR assembly is smaller than the measurement cavity of the UNCL, as seen in Fig. 1b. To minimize this bias, emphasis has been placed in training activities that the BWR should be placed 1 cm away from the slab containing the AmLi source as this orientation best matches the conditions associated with the original calibration of the UNCL for a BWR assembly [17]. An additional source of uncertainty relates to AmLi sources typically exhibiting a radial anisotropy in source strength (up to 1% variation in the apparent source strength as it is rotated in its holder). In cases where the radial anisotropy of the AmLi source is particularly strong, or can cause the normalization measurement to fail, procedures can be developed to indicate the proper orientation of the AmLi source within the UNCL, thereby minimizing the impact of this uncertainty source.

4.2 Example Analyses

Reference [19] analyzed 9 real pairs of (X, ^{235}U) values from Table VII for PWR from Menlove et al. (1990), fitting Eq. (10) with approximately 2% RSD. The 9 X values are 111.1, 132.0, 149.7, 158.8, 164.1, 173.4, 176.0, 180.8, 186.5. The corresponding 9 ^{235}U values are: 16.20, 21.89, 27.59, 29.37, 31.15, 33.28, 34.71, 36.84, 38. 98. Reference [19] used simulation in R [22] to apply a single noise

factor and $k = k_0 k_1 k_2 k_3 k_4 k_5$ to introduce noise due to departure from calibration conditions . In each simulation, cross validation was applied, in which 6 of the 9 (X,^{235}U) pairs were randomly selected to calibrate, and the other 3 (X,^{235}U) pairs were used to test. Varying amount of random error in *k* was applied, ranging from 1 to 5% RSD, which represented the aggregate effect of errors in each of k_0-k_5. In case 1, the same error RSDs were used in the 6 training as in the 3 testing pairs. In case 2 smaller error RSDs were used in the training pairs than in the testing pairs, which represented error sources being present in testing measurements that are not present in calibration measurements; the simulations showed that the predicted ^{235}U will have lower RSD in case 1 than in case 2 [19].

As an example of the results in [19], in case 1, for a total relative RSD of 0.03 in the inputs (in training and testing), the observed RSD in predicted ^{235}U was approximately 0.10, which is in approximate agreement with $\hat{\delta}_{RI} = 0.06$ and $\hat{\delta}_{SI} = 0.07$ (so $\hat{\delta}_{TI} = \sqrt{(0.06^2 + 0.07^2)} = 0.09$) from Section 3 in the top-down evaluation of 4 groups of 5 paired (*O*,*I*) values. In case 2, for a total relative RSD of 0.005 in the inputs in training, and 0.03 in the inputs in testing, the observed RSD in predicted ^{235}U was approximately 0.15. Generally, if there are different error magnitudes in testing than in training, then bias can be introduced in the estimated ^{235}U [2,18,19], and this bias contributed to the RSD of 0.15 in case 2.The message for bottom-up UQ is simple: understand and quantify the error sources in testing data so that training data for calibration can be obtained that has similar error RSDs.

Calibration can be done on real training data or on hybrid data that includes simulated error sources as in [2,18-20]. Assay challenges associated with new fuel and poison loadings have motivated synthetic calibration of the UNCL with Monte Carlo codes and this has led to a closer analysis of UNCL uncertainty. The factors k_0, k_1, k_2, k_3, k_4, and k_5 have been used for many years. However, there are recent assay challenges associated with new fuel and poison loadings, so the errors in the individual *k factors* are under investigation.

4.3 Inspector Training

Inspector training for NDA includes top-down UNCL results such as those given above. The IAEA training section emphasize that it is important for inspectors to understand the assembly design and INCC input requirements. Incorrect software (INCC) declaration input, which might be thought of as a "human factor," is thought to be among the largest contributors to the observed UNCL uncertainty. This is an additional error source that is not included in the *k* factors, and should not be, because with better training, inspectors will provide correct INCC input, as explained next.

While UNCL uncertainties can be estimated through a bottom-up analysis, errors that occur in deriving the declared values of the assembly being verified can be completely random in frequency and in nature. This is especially true in modern fuel assemblies that consist of different types of fuel rods within a single assembly. While facilities are required to provide nuclear material accounting information for each assembly, there are many different permutations with which the same information can be presented to the inspector. Depending on the facility, inspectors may receive detailed information regarding the design of each type of fuel rod that is present within a given fuel assembly. Receiving information in this manner requires the inspector to calculate either by hand or by using software tools, the declared ^{235}U mass for the entire assembly, as well as other parameters that are needed for the UNCL measurement. For fuel rods with multiple enrichment zones, the information for each type of fuel rod would have to be understood as a function of the distance along the length of the assembly to determine the zones with a constant enrichment that can be verified with the UNCL. As rods within a single fresh fuel assembly can have different number of enrichment zones, different active lengths, or even different overall lengths, combining the declared information of the various rods to determine the various parameters that are needed as input into INCC often requires the use of specialized programs or customized Excel spreadsheets. Complicating the calculation further is the fact that there are many various permutations that the same information for an individual rod type can be initially presented to an inspector. For instance, instead of specifying the ^{235}U mass present within a fuel rod, the facility could specify the mass of a single pellet, the chemical composition of the pellet (e.g. U_3O_8), and the number of pellets present within the rod. This declaration requires additional steps to calculate the parameters that are needed for INCC which increases the likelihood that rounding errors or human errors will occur in deriving these parameters.

To mitigate the possibility of errors occurring in determining the declaration of an assembly, inspector training has evolved over the past four years to include exercises to illustrate how to determine the INCC inputs from realistic facility declarations for the assemblies and the possible impacts of mistakes in the INCC input on assay results. One impact of improperly calculated INCC input parameters could be an inaccurate Operator-Inspector difference due to a miscalculated declared ^{235}U mass (the inspector has to translate operator declarations to ^{235}U mass). Another impact

on the measurement results would be if the ^{238}U mass for the assembly or zone were improperly calculated because this would impacts a correction made by INCC to the measured net doubles rate.

To illustrate the effect that the ^{238}U mass declaration has on the UNCL results, hypothetical facility declarations have been developed for training purposes to allow inspectors to perform these calculations. A sample facility declaration used during training is in Table 1 for the central zone of an assembly containing 264 total fuel rods. The UNCL measurement only produces accurate results for a zone with no changes in enrichment along the length of the zone, so inspectors must determine the total ^{235}U and ^{238}U masses based on the information provided in Table 1 for the smaller of the two central zones, because only in that zone is the U enrichment consistent. This task includes determining the portion of ^{238}U and ^{235}U masses in the standard rods that exists within the shorter central zone of the poison rods, as well as determining the ^{238}U mass from either the difference in the U mass and ^{235}U mass, or by using the declared enrichment of the central zones for each type of rod along with total U mass to determine the ^{238}U mass. Inspectors are also shown the IAEA-specific software tool developed for these calculations that requires design information for each type of rod in the assembly. This tool then multiplies the information for a single rod by the number of rods of that type that is present within the assembly to determine the parameters for the zone to be measured.

Looking at possible acceptable permutations of these calculations to the students can illustrate the impact that the declared ^{238}U value can have on the resulting OID for this hypothetical assembly by varying the INCC inputs when analysing the data. Table 2 provides a representative sample of the range of OID values that can be obtained in the training course based on the method chosen by the inspectors to calculate the input values. It should be noted that the first three cases shown in Table 2 are reasonable and scientifically valid means for determining the ^{238}U mass based on the hypothetical declaration. The discrepancy between cases 1 and 2 arises from rounding errors between the declared enrichment for the two types of rods and the enrichment that can be calculated from the ^{235}U and U masses provided. The discrepancy between the use of the computational tool and the hand calculation is a result of the number of operations performed on the initial declared values to calculate the INCC input parameters. In all three cases, it is assumed that the rods only contain ^{235}U and ^{238}U. The fourth case is an example of a common mistake that happens in training in deriving the INCC input in which the inspector confuses the total U mass for ^{238}U mass. The OID's shown in Table 2 for each case are the result of changing the ^{238}U mass input into the INCC analysis of the UNCL data from the assembly. Other common mistakes, such as not correcting for the different lengths of the central zones between the two types of rods, can lead to either larger and smaller OID values than those shown. Through these exercises, the inspector can be exposed to the challenges of properly performing a UNCL measurement.

Table 1 **Hypothetical facility declaration for the central zone of a 264 rod assembly.**

	U (g)	^{235}U (g)	Enrichment (%)	Zone Length (cm)
Total mass in 244 standard rods	393542	18347	4.6	335.3
Total mass in all 20 Burnable Poison Rods	26204	581	2.2	304.8

Table 2 **Impact of declared ^{238}U mass on UNCL measured results for hypothetical case.**

Calculation Description	^{238}U Mass (g)	k_4 correction factor	OID (%)
Add U mass and ^{235}U mass separately and subtract the sums to determine ^{238}U	366709	0.983	1.3 ± 3.4
Determine ^{238}U mass for each type of rod based on U and Enrichment and add resulting ^{238}U mass	369905	0.979	2.0 ± 3.4
Calculation based on individual rod properties using software tool	371727	0.976	2.4 ± 3.3
Using total U mass in place of ^{238}U mass (human error)	387082	0.957	5.9 ± 3.1

5. Discussion and Summary

This paper described three main inspector UQ-related training topics. Inspectors usually rely on the safeguards evaluation section to calculate sample sizes that correspond to goal detection probabilities (Section 3.1), but it is expected that inspectors understand that such sample size calculations depend partly on measurement quality, for which top-down and bottom-up UQ are essential MB evaluation also relies heavily on estimated measurement error RSDs (Section 3.2). Several other UQ-related topics are provided in inspector training, including tolerance intervals [25], top-down software (OPTANOVA [9]), and uncertainty in estimated RSDs based on bottom-up UQ and based on top-down UQ. Once the uncertainty in the estimated RSDs is well understood, if bottom-up RSDs are significantly lower than top-down RSDs, and inspector training ensures that a consistent measurement protocol is followed, based on reducing known sources of error to the extent that is practical, a possible explanation is dark uncertainty, which is unaccounted for sources of error [26].

6. References

[1] Guide to Expressing Uncertainty in Measurement, JCGM 100, www.bipm.org, 2008.
[2] Bonner, E., Burr, T., Guzzardo, T., Norman, C., Zhao, K., Beddingfield, D., Geist, W., Laughter,M., Lee, T., Improving the Effectiveness of Safeguards through Comprehensive Uncertainty Quantification, Journal of the Institute of Nuclear Materials Management 44(2), 53-61, 2016.
[3] Walsh S., Burr T., Martin K. (2016). Discussion of the IAEA Error Approach to Producing Variance Estimates for use in Material Balance Evaluation and the International Target Values, and Comparison to Metrological Definitions of Precision. to appear, Institute of Nuclear Materials Management, 2017.
[4] J. Jaech, Statistical Analysis of Measurement Errors, Exxon Monograph, Wiley, 1985.
[5] Burr, T., Sampson, T., Vo, D.,Statistical Evaluation of Framm gamma-ray Isotopic Analysis Data, *Applied Radiation and Isotopes,* no. 62, pp. 931-940, 2005.
[6] Zhao, K., Penkin, P., Norman, C., Balsely, S., Mayer, K., Peerani, P., Pietri, P., Tapodi, S., Tsutaki, Y., Boella, M., Renha G., and Kuhn, E., STR-368 International Target Values 2010 for Measurement Uncertainties in Safeguarding Nuclear Materials, IAEA, Vienna, 2010.
[7] Grubbs, F., On Estimating Precision of Measuring Instruments and Product Variability, Journal of the American Statistical Association, 43, 243-264, 1948.
[8] Martin, K., Böckenhoff, Analysis Of Short-Term Systematic Measurement Error Variance For The Difference Of Paired Data Without Repetition Of Measurement., Allgemeines Statistisches Archiv, 91, 291-310, 2007.
[9] Martin, K., IAEA Technical Report Estimation Of Variances Of Random And Short-Term Systematic Measurement Errors Based On Data From Two And Three Independent Measurement Methods, 2016.
[10] IAEA Safeguards Statistical Concepts and Techniques, Fourth Edition, Vienna: IAEA, 1989.
[11] Norman, C., SGIM-IFC Measurement Errors and their Propagation, Internal IAEA document, Vienna, 2014.
[12] Burr, T., Croft, S., Jarman. K., Nicholson, A., Norman, C., Walsh, S., Improved Uncertainty Quantification in NonDestructive Assay for Nonproliferation, Chemometrics, 159, 164-173, 2016.
[13] Bonner, E., Burr, T., Krieger, T., Martin, K., Norman, C., Comprehensive Uncertainty Quantification in Nuclear Safeguards, IAEA report 817, submitted 2017.
[14] Burr, T., Krieger, T., Norman, C., Zhao, K, The Impact of Metrology Study Sample Size on Verification Sample Size Calculations in IAEA Safeguards, European Journal Nuclear Science and Technology, 2, 36, 2016.
[15] Menlove,H. Description and Performance Characteristics for the Neutron Coincidence Collar for the Verification of Reactor Fuel Assemblies, Los Alamos National Laboratory LA-8939-MS, 1981.
[16] Harker, W.,Krick, M., INCC Software Users Manual, LA-UR-01-6761, 2001.
[17] Menlove, H., Stewart, J., Qiao, S., Wenz, T., Verrecchia, G., Neutron Collar Calibration and Evaluation for Assay of LWR Fuel Assemblies Containing Burnable Neutron Absorbers, LA-11965-MS, 1990.
[18] Burr, T., Croft, S., Dale, D., Favalli, A., Weaver, B., Williams, B., Emerging Applications of Bottom-Up Uncertainty Quantification in Nondestructive Assay, ESARDA Bulletin 53, 54-61, 2015.
[19] Croft, S., Burr, T., Favalli, A., Nicholson, A., Analysis of Calibration Data for the Uranium Active Neutron Coincidence Counting Collar with Attention to Errors in the Measured Neutron Coincidence Rate, Nuclear Instruments and Methods in Physics Research A 811. 70-75, 2016.
[20] Favalli, A., Croft, S., Swinhoe, M., Perturbation and Burnable Poison Rod Corrections for BWR Uranium Neutron Collar, Proceedings ESARDA, 2011.
[21] Peerani, P., Computational Calibration of UNCL Neutron Collars For Fresh Fuel Elements, Technical Note I.04.142, European Commission Joint Research Center, 2004.

[22] Beddingfield, D., Simulation and Modeling of AmLi Sources for IAEA Safeguards Applications, SG-RP-13454, 2015.
[23] Monte Carlo N- Particle code, see mcnp.lanl.gov at Los Alamos National Laboratory.
[24] R Core Team. R: A language and environment for statistical computing. R Foundation for Statistical Computing, Vienna, Austria. ISBN 3-900051-07-0, *http://www.R-project.org/, 2012.*
[25] Agboraw, E., Bonner, E., Burr, T., Croft, S., Kirkpatrick, J., Krieger, T., Norman, C., Santi, P., Walsh, S., Revisiting Currie's Minimum Detectable Activity for NonDestructiveAssay By Gamma Detection Using Tolerance Intervals, ESARDA 2017.
[26] Thompson, M., Ellison, S., Dark Uncertainty, Accreditation and Quality Assurance, 16, 483-487, 2011.

Game theoretical analysis of a generalized acquisition path model

Thomas Krieger[1], Morton J. Canty[2], Joshua Rutkowski[1], Irmgard Niemeyer[1], Gotthard Stein[3], Arnold Rezniczek[4]

[1]Forschungszentrum Jülich GmbH, IEK-6, D-52425 Jülich, Germany
[2]Consultant, Jülich, Germany
[3]Consultant, Bonn, Germany
[4]UBA GmbH, Herzogenrath, Germany

Abstract:

In the context of the IAEA's Department of Safeguards effort to fully develop and apply the State-level concept for safeguards implementation, the International Safeguards working group at the research centre in Jülich has developed an approach which supports analysing acquisition paths including establishing and prioritizing technical objectives, identifying applicable safeguards measures, and conducting a strategic assessment (game theoretical analysis). To perform the game theoretical analysis, two types of quantities are required: Technical quantities (such as non-detection probabilities and the total amount of inspection effort involved) and nontechnical quantities. The nontechnical quantities are the State's overall incentive to choose an acquisition path, State's perceived sanctions in the event of detection, State's false alarm cost for false accusation, Inspectorate's loss in the event of detection (failed deterrence), Inspectorate's false alarm cost (credibility loss) and Inspectorate's loss in the event of non-detection.

The results of the game theoretical analysis are Nash equilibrium strategies and the corresponding equilibrium payoffs. Because they depend on the specific values assigned to the two types of quantities, a sensitivity analysis is recommended in order to investigate the effect of a small change in one of the quantities on the game theoretical results.

Because at present such a sensitivity analysis seems to be unfeasible for realistic acquisition path models, we focus on a relatively simple acquisition path model, generalize this model to any number of acquisition paths inspected, and investigate the influence of the payoff parameters on the Inspectorate's equilibrium strategy and payoff (sensitivity analysis). In this model, it is assumed that a State, if it violates its commitments, will concentrate all of its effort on a single acquisition path and that the Inspectorate will inspect a certain number of these paths.

Keywords: IAEA; state level concept; acquisition path analysis; decision support systems; game theory

1. Introduction

In the context of the IAEA's Department of Safeguards effort to fully develop and apply the State-level concept for safeguards implementation, the International Safeguards working group at the research centre in Jülich has developed an approach which supports analysing acquisition paths including establishing and prioritizing technical objectives, identifying applicable safeguards measures, and conducting a strategic assessment (game theoretical analysis); see [1], [2] or [3]. To perform the game theoretical analysis, two types of quantities are required: Technical quantities (such as non-detection probabilities and the total amount of inspection effort involved) and nontechnical quantities. The nontechnical quantities are the State's overall incentive to choose an acquisition path, State's

perceived sanctions in the event of detection, State's false alarm cost for false accusation, Inspectorate's loss in the event of detection (failed deterrence), Inspectorate's false alarm cost (credibility loss) and Inspectorate's loss in the event of non-detection

The results of the game theoretical analysis are Nash equilibrium strategies and the corresponding equilibrium payoffs: A Nash equilibrium strategy combination of a non-cooperative game is defined by the property that any unilateral deviation from it does not improve the deviator's payoff; see, e.g., [5] or [6]. Because the equilibrium strategies and payoffs depend on the specific values assigned to the two types of quantities, a sensitivity analysis in the context of the strategic assessment is recommended in order to investigate the effect of a small change in one of the quantities on the game theoretical results.

Such a sensitivity analysis for realistic acquisition path models seems to be unfeasible at present. Thus, we focus on a relatively simple acquisition path model (analysed in Avenhaus and Canty [4]), generalize this model to any number of acquisition paths inspected, and investigate the influence of the payoff parameters on the Inspectorate's equilibrium strategy and payoff (sensitivity analysis).

This paper is organized as follows: In section 2 the acquisition path model is described and the game theoretical solution is presented and discussed. Section 3 contains a sensitivity analysis of the Inspectorate's equilibrium strategy and payoff in case only one path is inspected. A discussion and outlook concludes the paper.

2. The game theoretical model and analysis

Assume that a State considers n acquisition paths for the acquisition of nuclear material. These acquisition paths are assumed to be placed in different locations. Thus, even if a path consists of several steps (e.g., chemical processes, etc.) it is assumed that all these steps can be gone though in a single location. By assumption the illegal activity can occur, if at all, in one location only. The Inspectorate will inspect $m, m = 1, \dots, n$, location(s) and will detect any illegal activity with certainty, should one take place.

This conflict situation can be modeled as a two-person non-cooperative game between two players, an Inspectorate and a State; see [3] and [4]. The Inspectorate's pure strategies consist of the locations for inspection, and the State's pure strategies are to behave illegally in one of the locations or legal behavior.

The payoffs to (Inspectorate, State) are given for all possible outcomes as follows:

$$\begin{array}{ll} (-a, -b) & \text{for detected illegal behavior} \\ (-c, d_i) & \text{for undetected illegal behavior in the } i-\mathrm{th} \text{ location, } i = 1, \dots, n \\ (0,0) & \text{for legal behavior} \end{array} \tag{1}$$

where it is assumed that

$$0 < a < c, \qquad 0 < b\,, \qquad d_1 > d_2 > \cdots > d_n > 0\,. \tag{2}$$

These conditions reflect the subjective preferences of both players: $a > 0$ means that the Inspectorate's priority is the deterrence of an illegal activity. The worst outcome for the Inspectorate is non-detection, so that $a < c$. The payoff b reflects the State's perception of the consequences (sanctions) of detection and d_i is its incentive to behave illegally in location i. These incentives are ordered without loss of generality ordered according to their attractiveness. Note that in the case of an illegal activity in location i and inspection in location $j \neq i$, the payoff to the Inspectorate is $-c$, because we ignore real inspection costs in location j but consider instead a political loss arising from not detecting the illegal activity in location i; see [3].

Because this paper focuses on the case $\alpha = \beta = 0$, only nontechnical quantities are considered in Eq. (1). Note that because false accusation, i.e. the raising a false alarm, is excluded, payoffs for that case need not to be introduced.

The acquisition path model described above has been analysed by Avenhaus and Canty [4] for the case $m = 1$ (see section 2.2) but taking errors of the first and second kind into account. Thus, this paper generalizes their model regarding the number of paths inspected, but also limits it due to $\alpha = \beta = 0$.

2.1. Inspection of one location ($m = 1$)

The case of inspecting one location ($m = 1$) has been studied by Avenhaus and Canty [4] (even taking errors of the first and second kind into account). For illustration, we start with four locations ($n = 4$). The bimatrix form of this game is presented in Table 1.

		State				
		1	2	3	4	legal
Inspectorate	1	$-a$ $\quad -b$	$-c$ $\quad d_2$	$-c$ $\quad d_3$	$-c$ $\quad d_4$	0 $\quad 0$
	2	$-c$ $\quad d_1$	$-a$ $\quad -b$	$-c$ $\quad d_3$	$-c$ $\quad d_4$	0 $\quad 0$
	3	$-c$ $\quad d_1$	$-c$ $\quad d_2$	$-a$ $\quad -b$	$-c$ $\quad d_4$	0 $\quad 0$
	4	$-c$ $\quad d_1$	$-c$ $\quad d_2$	$-c$ $\quad d_3$	$-a$ $\quad -b$	0 $\quad 0$

Table 1: Bimatrix form of the inspection game with one inspection in one of four locations.

If the Inspectorate inspects location 2 (say) and the State performs an illegal activity there, then the payoffs to both players (Inspectorate, State) are $(-a, -b)$, while in case the State performs an illegal activity in location 1,3 or 4, the payoff the Inspectorate is always $-c$ and the State gains d_1, d_3 or d_4.

Let $p_i, i = 1, \dots, n$, be the probability that the Inspectorate inspects location i, and let $q_j, j = 1, \dots, n$, be the probability that the State behaves illegally in location j. q_{n+1} denotes the probability of behaving legally. Then the Inspectorate's set of mixed strategy is given by

$$P_1 := \left\{ \boldsymbol{p} = (p_1, p_2, \dots, p_n) \in \mathbb{R}_+^n : \sum_{i=1}^{n} p_i = 1 \right\} \tag{3}$$

and that of the State

$$Q := \left\{ \boldsymbol{q} = (q_1, q_2, \dots, q_n, q_{n+1}) \in \mathbb{R}_+^{n+1} : \sum_{j=1}^{n+1} q_j = 1 \right\}. \tag{4}$$

Let $I_1(\boldsymbol{p}, \boldsymbol{q})$ and $S_1(\boldsymbol{p}, \boldsymbol{q})$ be the expected payoffs to Inspectorate and State, respectively. Then

$$I_1(\boldsymbol{p}, \boldsymbol{q}) = \sum_{j=1}^{n} q_j \left((-a) p_j - c(1 - p_j) \right) \quad \text{and} \quad S_1(\boldsymbol{p}, \boldsymbol{q}) = \sum_{j=1}^{n} q_j \left((-b) p_j + d_i (1 - p_j) \right) . \tag{5}$$

As mentioned in section 1, we seek a Nash equilibrium [6] of the game, i.e. a pair $(\boldsymbol{p}^*, \boldsymbol{q}^*)$ of mixed strategies with the property that that neither player has an incentive to deviate unilaterally from its equilibrium strategy

$$\begin{aligned} I_1^* &= I_1(\boldsymbol{p}^*, \boldsymbol{q}^*) \geq I_1(\boldsymbol{p}, \boldsymbol{q}^*) \quad \text{for all} \quad \boldsymbol{p} \in P_1 \\ S_1^* &= S_1(\boldsymbol{p}^*, \boldsymbol{q}^*) \geq S_1(\boldsymbol{p}^*, \boldsymbol{q}) \quad \text{for all} \quad \boldsymbol{q} \in Q\,. \end{aligned} \tag{6}$$

The game theoretical solution of this game is given in Theorem 1. Note that we do not consider equalities between parameters here and in the subsequent cases, because they cannot be estimated precisely.

Theorem 1: *Consider the inspection game with n locations and $m = 1$ inspections. The strategy sets to the Inspectorate and to the State are given by (3) and (4) with the expected payoffs (5), respectively.*

Let $k_1, 2 \leq k_1 \leq n$ be so chosen that

$$\sum_{i=1}^{k_1} \frac{d_i - d_{k_1+1}}{b + d_i} > 1 \qquad \text{and} \qquad \sum_{i=1}^{k_1-1} \frac{d_i - d_{k_1}}{b + d_i} < 1\,. \tag{7}$$

(For $k_1 = n$ the left hand inequality is omitted.)
If $k_1 < n$, then a Nash equilibrium strategy for the Inspectorate is given by

$$p_i^* = \begin{cases} \dfrac{d_i - S_1^*}{b + d_i} & for \quad i = 1, \dots, k_1 \\ 0 & for \quad i = k_1 + 1, \dots, n \end{cases} \tag{8}$$

and for the State by

$$q_j^* = \begin{cases} \dfrac{1}{k_1} & for \quad j = 1, \dots, k_1 \\ 0 & for \quad j = k_1 + 1, \dots, n, n+1 \end{cases}, \tag{9}$$

with the equilibrium payoffs I_1^* and S_1^* given by

$$I_1^* = \frac{1}{k_1}\,(c - a) - c \qquad \text{and} \qquad S_1^* = \left(\sum_{i=1}^{k_1} \frac{1}{b + d_i} \right)^{-1} \left(\sum_{i=1}^{k_1} \frac{d_i}{b + d_i} - 1 \right) \tag{10}$$

If $k_1 = n$, then the equilibrium strategy of the Inspectorate is not unique and that of the State is legal behavior:

$$p_i^* \geq \frac{d_i}{b + d_i}, \;\; i = 1, \dots, n \quad with \quad \sum_{i=1}^{n} p_i^* = 1 \quad and \quad q_j^* = 0, \;\; j = 1, \dots, n, \qquad q_{n+1}^* = 1. \tag{11}$$

The equilibrium payoffs to both players are zero, i.e. $I_1^* = S_1^* = 0$.

Proof: The proof of Theorem 1 can be found in Avenhaus and Canty [3] or, as a special case of Theorem 3, in section 2.3. □

Let us comment on the results of Theorem 1: First, Eqs. (8) and (9) imply that the potential locations for the inspection and for the illegal activity are concentrated on the k_1 most attractive locations, i.e. in all locations in which the illegal activity is carried out with positive probability, the inspection is performed with positive probability and vice versa.

Second, because $k_1 \geq 2$, at least two locations are inspected. Note that if location-dependent detection probabilities $1 - \beta_i$ were considered, then the left hand inequality of (7) would be

$$\sum_{i=1}^{k_1} \frac{d_i - d_{k_1+1}}{(b + d_i)(1 - \beta_i)} > 1\,,$$

and thus, $k_1 = 1$ would be possible (e.g., $d_1 = 10$, $d_2 = 6$, $b = 2$ and $\beta_1 = 3/4$). For details, see Avenhaus and Canty [3].

Third, although the State's acquisition paths have different attractiveness (see Eq. (2)), its equilibrium strategy is a uniform distribution on the first k_1 locations, which is surprising.

Note that for the game in Theorem 1, a sensitivity analysis regarding the Inspectorate's equilibrium strategy and payoff is performed in Section 3.

2.2. Inspection of two locations ($m = 2$)

We now generalize the model discussed in section 2.1 to the case of the inspection of two locations, i.e. $m = 2$. For this purpose, the Inspectorate's mixed strategies are transformed, a trick which is also applied for the cases $m > 2$ in section 2.3. Because this feature can be best understood in case $m = 2$, we explain the derivations in some detail.

For illustration, we start again with the case of four locations ($n = 4$). The bimatrix form of this game is given in Table 2.

		State				
		1	2	3	4	legal
Inspectorate	1,2	$-b$ $-a$	$-b$ $-a$	d_3 $-c$	d_4 $-c$	0 0
	1,3	$-b$ $-a$	d_2 $-c$	$-b$ $-a$	d_4 $-c$	0 0
	1,4	$-b$ $-a$	d_2 $-c$	d_3 $-c$	$-b$ $-a$	0 0
	2,3	d_1 $-c$	$-b$ $-a$	$-b$ $-a$	d_4 $-c$	0 0
	2,4	d_1 $-c$	$-b$ $-a$	d_3 $-c$	$-b$ $-a$	0 0
	3,4	d_1 $-c$	d_2 $-c$	$-b$ $-a$	$-b$ $-a$	0 0

Table 2: Bimatrix form of the inspection game in which two locations are inspected.

Suppose the Inspectorate inspects location 2 and 4 (say) and the State performs an illegal activity in location 2, then the illegal activity is detected and the payoffs to both players (Inspectorate, State) are $(-a, -b)$, while in case the State performs an illegal activity in location 1 or 3, the payoff the Inspectorate is $-c$ and the State gains d_1 or d_3.

Let p_{i_1,i_2} denotes the probability that locations i_1 and $i_2 \neq i_1$ with $i_1, i_2 \in \{1,2,3,4\}$ are inspected. The probabilities $q_j, j = 1, \dots, n$, and q_{n+1} have the same meaning as in section 2.1. Then, the Inspectorate's set of mixed strategies is given by

$$\left\{\tilde{\boldsymbol{p}} = \left(p_{1,2}, p_{1,3}, p_{1,4}, p_{2,3}, p_{2,4}, p_{3,4}\right) \in \mathbb{R}_+^6 : p_{1,2} + p_{1,3} + \cdots + p_{3,4} = 1\right\}, \tag{12}$$

and that of the State by Eq. (4) for $n = 4$:

$$\{\boldsymbol{q} = (q_1, q_2, q_3, q_4, q_5) \in \mathbb{R}_+^5 : q_1 + q_2 + q_3 + q_4 + q_5 = 1\}. \tag{13}$$

To derive the expected payoff to both players, we start with the State's payoff: Using (12) and (13), its expected payoff is, using Table 2, given by

$$\begin{aligned} S_2(\tilde{\boldsymbol{p}}, \boldsymbol{q}) &= q_1\left((-b)(p_{1,2}+p_{1,3}+p_{1,4})+d_1(p_{2,3}+p_{2,4}+p_{3,4})\right) \\ &+ q_2\left((-b)(p_{1,2}+p_{2,3}+p_{2,4})+d_2(p_{1,3}+p_{1,4}+p_{3,4})\right) \\ &+ q_3\left((-b)(p_{1,3}+p_{2,3}+p_{3,4})+d_3(p_{1,2}+p_{1,4}+p_{2,4})\right) \\ &+ q_4\left((-b)(p_{1,4}+p_{2,4}+p_{3,4})+d_4(p_{1,2}+p_{1,3}+p_{2,3})\right) . \end{aligned} \tag{14}$$

Eq. (14) can be simplified if we introduce the probability $p_i,\ i = 1,\dots,4$, that location i is inspected, which leads to the following relations between $p_{1,2},\dots,p_{3,4}$ and $p_1,\dots,p_4$:

$$p_1 = p_{1,2}+p_{1,3}+p_{1,4}, p_2 = p_{1,2}+p_{2,3}+p_{2,4}, p_3 = p_{1,3}+p_{2,3}+p_{3,4} \quad \text{and} \quad p_4 = p_{1,4}+p_{2,4}+p_{3,4} \tag{15}$$

with $p_1+p_2+p_3+p_4 = 2$, because of Eq. (12). Thus, Eq. (14) simplifies with $\boldsymbol{p} = (p_1, p_2, p_3, p_4)$ to

$$\begin{aligned} S_2(\boldsymbol{p}, \boldsymbol{q}) &= q_1\big((-b)p_1 + d_1(1-p_1)\big) + q_2\big((-b)p_2 + d_2(1-p_2)\big) \\ &+ q_3\big((-b)p_3 + d_3(1-p_3)\big) + q_4\big((-b)p_4 + d_4(1-p_4)\big) . \end{aligned} \tag{16}$$

The Inspectorate's payoff can be deduced from Eq. (16) simply by substituting $-a$ instead of $-b$ and $-c$ instead of $d_i,\ i = 1,\dots,4$. Therefore, we get

$$\begin{aligned} I_2(\boldsymbol{p}, \boldsymbol{q}) &= q_1\big((-a)p_1 - c(1-p_1)\big) + q_2\big((-a)p_2 - c(1-p_2)\big) \\ &+ q_3\big((-a)p_3 - c(1-p_3)\big) + q_4\big((-a)p_4 - c(1-p_4)\big) . \end{aligned} \tag{17}$$

This illustration leads directly to the following strategy set of the Inspectorate:

$$P_2 := \left\{ \boldsymbol{p} = (p_1, p_2, \dots, p_n) \in \mathbb{R}_+^n : \sum_{i=1}^{n} p_i = 2 \right\} , \tag{18}$$

where $p_i, i = 1,\dots,n$, is the probability that location i is inspected. The State's strategy set remains the same and is given by Eq. (4). The expected payoffs are

$$I_2(\boldsymbol{p}, \boldsymbol{q}) = \sum_{j=1}^{n} q_j\left((-a)p_j - c\big(1-p_j\big)\right) \quad \text{and} \quad S_2(\boldsymbol{p}, \boldsymbol{q}) = \sum_{i=1}^{n} q_j\left((-b)p_j + d_i\big(1-p_j\big)\right) . \tag{19}$$

The game theoretical solution of this inspection game is given in

Theorem 2: *Consider the inspection game with n locations and $m = 2$ inspections. The strategy sets to the Inspectorate and to the State are given by (18) and (4) with the expected payoffs (19), respectively.*

Let $k, 3 \le k_2 \le n$ be so chosen that

$$\sum_{i=1}^{k_2} \frac{d_i - d_{k_2+1}}{b+d_i} > 2 \qquad \text{and} \qquad \sum_{i=1}^{k_2-1} \frac{d_i - d_{k_2}}{b+d_i} < 2 . \tag{20}$$

(For $k_2 = n$ the left hand inequality is omitted.)
If $k_2 < n$, then a Nash equilibrium strategy for the Inspectorate is given by

$$p_i^* = \begin{cases} \dfrac{d_i - S_2^*}{b+d_i} & for \quad i = 1,\dots,k_2 \\ 0 & for \quad i = k_2+1,\dots,n \end{cases} \tag{21}$$

and for the State by

$$q_j^* = \begin{cases} \frac{1}{k_2} & for \quad j = 1, \dots, k_2 \\ 0 & for \quad j = k_2 + 1, \dots, n+1 \end{cases}, \tag{22}$$

with the equilibrium payoffs I_2^* and S_2^* given by

$$I_2^* = \frac{2}{k_2}\,(c-a) - c \quad \text{and} \quad S_2^* = \left(\sum_{i=1}^{k_1} \frac{1}{b+d_i}\right)^{-1} \left(\sum_{i=1}^{k_1} \frac{d_i}{b+d_i} - 2\right) \tag{23}$$

If $k_2 = n$, then the equilibrium strategy of the Inspectorate is not unique and that of the State is legal behavior:

$$p_i^* \geq \frac{d_i}{b+d_i},\ i = 1, \dots, n \ \ with \sum_{i=1}^{n} p_i^* = 2 \quad and \quad q_j^* = 0,\ j = 1, \dots, n, \qquad q_{n+1}^* = 1. \tag{24}$$

The equilibrium payoffs to both players are zero, i.e. $I_2^* = S_2^* = 0$.

Proof: The proof of Theorem 2 is covered by the proof of Theorem 3; see Section 2.3. □

Let us comment on the solution of Theorem 2: First, the three comments made after Theorem 1 hold here as well, of course, accordingly modified (e.g., for the first comment Eqs. (21) and (22) need to be utilized, etc.).

Second, from Theorem 1 and 2 we know that $k_1 \geq 2$ and $k_2 \geq 3$, respectively. Does $k_2 \geq k_1$ hold? The answer is yes. Suppose $k_2 < k_1$. Then, $d_{k_2+1} \geq d_{k_1}$, and Eqs. (7) and (20) yield

$$\begin{aligned} 2 \ &< \ \sum_{i=1}^{k_2} \frac{d_i - d_{k_2+1}}{b+d_i} \leq \sum_{i=1}^{k_1-1} \frac{d_i - d_{k_2+1}}{b+d_i} \\ &= \ \sum_{i=1}^{k_1-1} \frac{d_i - d_{k_1}}{b+d_i} - \left(d_{k_2+1} - d_{k_1}\right) \sum_{i=1}^{k_1-1} \frac{1}{b+d_i} \\ &< \ 1 - \left(d_{k_2+1} - d_{k_1}\right) \sum_{i=1}^{k_1-1} \frac{1}{b+d_i} \\ &\leq \ 1\,, \end{aligned} \tag{25}$$

which is a contradiction. Thus, $k_2 \geq k_1$.

Third, considering the original game in which p_{i_1,i_2} denotes the probability that locations i_1 and $i_2 \neq i_1$ are inspected (for $n = 4$ see Eq. (12)), an Inspectorate's equilibrium strategy is, using Eq. (21), given by

$$p_{i_1,i_2}^* = \begin{cases} \frac{p_{i_1}^*}{k_2 - 1} & for \quad i_1, i_2 \in \{1, \dots, k_2\}, i_2 \neq i_1 \\ 0 & for \quad i_1, i_2 \in \{k_2 + 1, \dots, n\}, i_2 \neq i_1 \end{cases}.$$

Note that the transformation from $p_{i_1}^*$ to p_{i_1,i_2}^* is not unique, but they all lead to the same equilibrium payoff.

2.3. Inspection of any number of locations (arbitrary m)

To generalize the analysis of the last section, we consider $m \leq n$ inspections. Suppose the Inspectorate performs its m inspections at the locations $i_1, \dots, i_m$ with $i_1, \dots, i_m \in \{1, \dots, n\}$ and $i_l \neq i_{l'}$ for $l \neq l'$, and the State behaves illegally in location j. Then, using Eq. (1), their payoffs are given by

$$I_m(i_1,\dots,i_m,j)=\begin{cases}-a & if \quad j\in\{i_1,\dots,i_m\}\\ -c & if \quad j\notin\{i_1,\dots,i_m\}\end{cases} \text{ and } S_m(i_1,\dots,i_m,j)=\begin{cases}-b & if \quad j\in\{i_1,\dots,i_m\}\\ d_j & if \quad j\notin\{i_1,\dots,i_m\}\end{cases}. \tag{26}$$

Note again, that we ignore real inspection costs in a location but consider instead only a political loss arising from not detecting the illegal activity in location.

Let $p_{i_1,\dots,i_m}$ denote the probability that locations $i_1,\dots,i_m$ are inspected. Then the Inspetorate's set of mixed strategies is given by

$$\left\{\tilde{\boldsymbol{p}}=\left(p_{i_1,\dots,i_m}\right)\in\mathbb{R}_+^{\binom{n}{m}}:\sum_{i_1,\dots,i_m:\, i_l\neq i_{l'} \text{ for } l\neq l',} p_{i_1,\dots,i_m}=1\right\}. \tag{27}$$

The probabilities $q_j, j=1,\dots,n$, and q_{n+1} have again the same meaning as in section 2.1. Then, the Inspectorate's expected payoff is given by

$$I_2(\boldsymbol{p},\boldsymbol{q})=\sum_{j=1}^{n} q_j\left((-a)\sum_{\substack{i_1,\dots,i_m\\ i_l\neq i_{l'} \text{ for } l\neq l'\\ j\in\{i_1,\dots,i_m\}}} p_{i_1,\dots,i_m}-c\sum_{\substack{i_1,\dots,i_m\\ i_l\neq i_{l'} \text{ for } l\neq l'\\ j\notin\{i_1,\dots,i_m\}}} p_{i_1,\dots,i_m}\right). \tag{28}$$

Because

$$p_j:=\sum_{\substack{i_1,\dots,i_m\\ i_l\neq i_{l'} \text{ for } l\neq l'\\ j\in\{i_1,\dots,i_m\}}} p_{i_1,\dots,i_m} \tag{29}$$

is the probability that location j is inspected, the Inspectorate's strategy set is, using Eq. (27), given by

$$P_m:=\left\{\boldsymbol{p}=(p_1,p_2,\dots,p_n)\in\mathbb{R}_+^n:\sum_{i=1}^{n}p_i=m\right\}. \tag{30}$$

The State's strategy set remains the same and is given by Eq. (4). Using Eqs. (28) and (29), the expected payoffs to both players are

$$I_m(\boldsymbol{p},\boldsymbol{q})=\sum_{j=1}^{n} q_j\left((-a)p_j-c\left(1-p_j\right)\right) \quad \text{and} \quad S_m(\boldsymbol{p},\boldsymbol{q})=\sum_{j=1}^{n} q_j\left((-b)p_j+d_j\left(1-p_j\right)\right). \tag{31}$$

Note that m enters Eq. (31) only through Eq. (30). Thus, it can be expected that the structure of the solution in Theorem 1 and 2 remains here, which is stated in

Theorem: *Consider the inspection game with n locations and $m\leq n$ inspections. The strategy sets to the Inspectorate and to the State are given* by *(30) and (4)* with *the expected payoffs by (31), respectively. The Nash equilibrium strategies and the corresponding payoffs are given as follows:*

Let $k_m, m+1\leq k_m\leq n$ be so chosen that

$$\sum_{i=1}^{k_m}\frac{d_i-d_{k_m+1}}{b+d_i}>m \qquad \text{and} \qquad \sum_{i=1}^{k_m-1}\frac{d_i-d_{k_m}}{b+d_i}<m. \tag{32}$$

(For $k_m=n$ the left hand inequality is omitted.)
If $k_m<n$, then a Nash equilibrium strategy for the Inspectorate is given by

$$p_i^* = \begin{cases} \dfrac{d_i - S_m^*}{b + d_i} & for \quad i = 1, \dots, k_m \\ 0 & for \quad i = k_m + 1, \dots, n \end{cases} \tag{33}$$

and for the State by

$$q_j^* = \begin{cases} \dfrac{1}{k_m} & for \quad j = 1, \dots, k_m \\ 0 & for \quad j = k_m + 1, \dots, n+1 \end{cases}, \tag{34}$$

with the equilibrium payoffs I_m^* and S_m^* given by

$$I_m^* = \frac{m}{k_m}\,(c - a) - c \quad \text{and} \quad S_m^* = \left(\sum_{i=1}^{k_m} \frac{1}{b + d_i}\right)^{-1} \left(\sum_{i=1}^{k_m} \frac{d_i}{b + d_i} - m\right). \tag{35}$$

If $k_m = n$, then the equilibrium strategy of the Inspectorate is not unique and that of the State is legal behavior,

$$p_i^* \geq \frac{d_i}{b + d_i}, \;\; i = 1, \dots, n \;\; with \sum_{i=1}^{n} p_i^* = m \quad and \;\; q_j^* = 0, \;\; j = 1, \dots, n, \qquad q_{n+1}^* = 1. \tag{36}$$

The equilibrium payoffs to both players are zero, i.e. $I_m^* = S_m^* = 0$.

Proof: We start with the case $k_m < n$ and show first, that

$$d_{k_m+1} < S_m^* < d_{k_m}. \tag{37}$$

Because $\boldsymbol{p}^* \in \boldsymbol{P}_m$, Eq. (33) and the left hand side of Eq. (32) imply

$$m + \sum_{i=1}^{k_m} \frac{S_m^*}{b + d_i} = \sum_{i=1}^{k_m} \frac{d_i}{b + d_i} > m + \sum_{i=1}^{k_m} \frac{d_{k_m+1}}{b + d_i},$$

which gives

$$\left(S_m^* - d_{k_m+1}\right) \sum_{i=1}^{k_m} \frac{1}{b + d_i} > 0\,,$$

i.e. $d_{k_m+1} < S_m^*$. Extending the summation index in Eq. (32) trivially from $k_m - 1$ to k_m and using E. (33) again, yields

$$m + \sum_{i=1}^{k_m} \frac{d_{k_m}}{b + d_i} > \sum_{i=1}^{k_m} \frac{d_i}{b + d_i} = m + \sum_{i=1}^{k_m} \frac{S_m^*}{b + d_i},$$

i.e.

$$\left(d_{k_m} - S_m^*\right) \sum_{i=1}^{k_m} \frac{1}{b + d_i} > 0\,,$$

which shows $S_m^* < d_{k_m}$. This inequality assures that $p_i^* > 0$ for $i = 1, \dots, k_m$.

We now prove that the Nash equilibrium conditions

$$I_m^* \geq I_m(\boldsymbol{p}, \boldsymbol{q}^*) \quad for\ all \quad \boldsymbol{p} \in \boldsymbol{P}_m \;\; and \quad S_m^* \geq S_m(\boldsymbol{p}^*, \boldsymbol{q}) \quad for\ all \;\; \boldsymbol{q} \in \boldsymbol{Q} \tag{38}$$

are fulfilled. For the Inspectorate's equilibrium condition, we get, using Eqs. (4), (30), (31) and (34), for all $\boldsymbol{p} \in \boldsymbol{P}_m$

$$
\begin{aligned}
I_m(\boldsymbol{p},\boldsymbol{q}^*) &= \sum_{j=1}^{n} q_j^* \left((-a)p_j - c\big(1-p_j\big)\right) = -c + (c-a)\sum_{j=1}^{k_m} q_j^*\, p_j + (c-a)\sum_{j=k_m+1}^{n} q_j^*\, p_j \\
&= -c + \frac{c-a}{k_m}\sum_{j=1}^{k_m} p_j \\
&\le -c + \frac{c-a}{k_m}\sum_{j=1}^{n} p_j = -c + \frac{c-a}{k_m} m = I_m^* \,.
\end{aligned}
\tag{39}
$$

To prove the State's inequality, we obtain, using Eqs. (4), (31) and (33), for all $\boldsymbol{q} \in \boldsymbol{Q}$

$$
\begin{aligned}
S_m(\boldsymbol{p}^*,\boldsymbol{q}) &= \sum_{j=1}^{n} q_j \left((-b)p_j^* + d_j\big(1-p_j^*\big)\right) = \sum_{j=1}^{n} q_j \left(-\big(d_j+b\big)\, p_j^* + d_j\right) \\
&= \sum_{j=1}^{k_m} q_j \left(-\big(d_j - S_m^*\big) + d_j\right) + \sum_{j=k_m+1}^{n} q_j\, d_j \\
&= S_m^* \left(1 - \sum_{j=k_m+1}^{n} q_j - q_{n+1}\right) + \sum_{j=k_m+1}^{n} q_j\, d_j \\
&= S_m^* - S_m^* q_{n+1} + \sum_{j=k_m+1}^{n} q_j \left(d_j - S_m^*\right) \\
&\le S_m^* \,,
\end{aligned}
\tag{40}
$$

because $d_j < S_m^*$ for all $j = k_m + 1, \dots, n$ and $S_m^* > 0$; see Eq. (37). Thus, both inequalities in (38) are fulfilled.

Now let $k_m = n$. Then Eq. (36) implies $I_m(\boldsymbol{p},\boldsymbol{q}^*) = 0$ for all $\boldsymbol{p} \in \boldsymbol{P}_m$, i.e. its Nash condition are fulfilled as equality. For the State's equilibrium condition we obtain, using Eqs. (31) and (38),

$$
0 \ge (-b)p_j^* + d_j\big(1-p_j^*\big) \quad for\ all\ j = 1, \dots, n\,, \qquad with \quad \sum_{j=1}^{n} p_j^* = m \ ,
$$

which is equivalent to the left hand inequality of Eq. (36), and which completes the proof. □

Note that all comments made after Theorem 1 and 2 hold – accordingly modified – here as well.

3. Sensitivity analysis

In this section we perform a sensitivity analysis and investigate the influence of

1) the Inspectorate's payoff parameters a and c, and
2) the State's payoff parameter $d_i, i = 1, \dots, n$, and b

on the Inspectorate's equilibrium strategy and payoff for the game in which only one location is inspected. We focus on the Inspectorate because we are mainly interested in its equilibrium behavior.

Ad 1) Because I_1^* as given by Eq. (10) is a linear function of a and c, a small change of these parameters will result in a small change of I_1^*.

Ad 2) Because I_1^* is also affected by k_1, a characterization of the set of all vectors $(d_1, d_2, \dots, d_n)$ resulting in the same k_1 is desirable: Let $\boldsymbol{d} = (d_1, d_2, \dots, d_n)$ be the parameter combination of an initial assessment of the model and $k_1(\boldsymbol{d})$ be its respective threshold (using Eq. (7)). If a second assessment leads to a parameter combination $\boldsymbol{d}' = (d_1', d_2', d_3', \dots, d_n')$ with $k_1(\boldsymbol{d}') = k_1(\boldsymbol{d})$, the "distance" between $\boldsymbol{d}$ and $\boldsymbol{d}'$ does not have any impact on I_1^* (but on p_i^*; see below).

For example, consider $\boldsymbol{d} = (10,8,3,1,0)$ and $b = 3$. Then Eq. (7) yields $k_1(\boldsymbol{d}) = 3$. Which of the vectors $\boldsymbol{d}' = (d_1', d_2', d_3', d_4', 0)$ with $d_i' \geq d_i$ for all $i = 1,2,3$, and $d_3' > d_2' > d_1'$ fulfill $k_1(\boldsymbol{d}') = 3$? In Table 3 several $\boldsymbol{d}'$ are presented, where $d_i' \in \mathbb{N}, i = 1,2,3$ and $d_1' \leq 20$ is assumed.

If, e.g., in a second assessment (by another expert) the parameter combination $\boldsymbol{d}' = (20,14,8,2,0)$ seems more appropriate to his perception of reality, Table 3 implies that the Inspectorate's equilibrium payoff will not change.

Eq. (8), however, indicates that the Inspectorate's equilibrium strategies will be different for $\boldsymbol{d}$ and $\boldsymbol{d}'$ even if $k_1(\boldsymbol{d}) = k_1(\boldsymbol{d}')$. Let $p_i'^*, i = 1, \dots, 4$, denotes the Inspectorate's equilibrium strategies for a vector $\boldsymbol{d}'$. In Table 3, p_i^* and several $p_i'^*$ are presented (because $k_1(\boldsymbol{d}) = k_1(\boldsymbol{d}') = 3$ we have $p_4^* = p_i'^* = 0$).

	$p_1^* \approx$	$p_2^* \approx$	$p_3^* \approx$
$\boldsymbol{d} = (10,8,3,1,0)$	0.5401	0.4564	0.0035
$\boldsymbol{d}' = (10,9,6,1,0)$	0.4331	0.3858	0.1811
$\boldsymbol{d}' = (11,8,5,1,0)$	0.5028	0.3672	0.1299
$\boldsymbol{d}' = (12,9,5,1,0)$	0.5152	0.3939	0.0909
$\boldsymbol{d}' = (13,11,9,1,0)$	0.4247	0.3425	0.2329
$\boldsymbol{d}' = (14,11,10,1,0)$	0.4321	0.3105	0.2574
$\boldsymbol{d}' = (20,15,13,1,0)$	0.4617	0.3122	0.2262
$\boldsymbol{d}' = (20,19,18,1,0)$	0.3632	0.3343	0.3026
$\boldsymbol{d}' = (50,49,48,1,0)$	0.3461	0.3335	0.3204

Table 4: Equilibrium strategies for some vectors $\boldsymbol{d}'$ (rounded to four digits after the dot).

Table 4 demonstrates that the equilibrium strategy components might differ considerably especially for large "distances" between $\boldsymbol{d}$ and $\boldsymbol{d}'$. As a measure deviation between equilibrium strategies, their total variation

$$\sum_{i=1}^{3} | p_i^* - p_i'^* |$$

can be considered. In the range $10 \leq d_1' \leq 20$, $8 \leq d_2' < d_1'$ and $3 \leq d_3' < d_2'$, the maximum of the total variation is 0.598 (attained for $\boldsymbol{d}' = (20,19,18,1,0)$) and 0.6463 if we increase d_1' to 50.

Can the total variation also be used to assess the sensitivity of Inspectorate's equilibrium strategies on the payoff parameter? If the "distances" between $\boldsymbol{d}$ and $\boldsymbol{d}'$ is small but the total variation between their equilibrium strategies high, then the model is seen to be (very) sensitive. If, on contrary, large "distances" between $\boldsymbol{d}$ and $\boldsymbol{d}'$ result in small total variations, the model is (rather) insensitive. Thus, the quantity

$$\frac{\sum_{i=1}^{3} | p_i^* - p_i'^* |}{distance(\boldsymbol{d}, \boldsymbol{d}')} \tag{41}$$

needs to be studied. Because Eq. (41) depends on the specific definition of the $distance$ which itself depends on the meaning of the d_i (in Jülich's APA approach, d_i is a function of the technical difficulty,

d_1'	d_2'	d_3'
10	8	3, …,7
10	9	4, …,8
11	8	4, …,7
11	9	4, …,8
11	10	4, …,9
12	8	4, …,7
12	9	4, …,8
12	10	4, …,9
12	11	5, …,10
13	8	4, …,7
13	9	4, …,8
13	10	5, …,9
13	11	5, …,10
13	12	5, …,11
14	8	4, …,7
14	9	5, …,8
14	10	5, …,9
14	11	5, …,10
14	12	5, …,11
14	13	6, …,12
…	…	…
20	8	5, …,7
20	9	5, …,8
20	10	6, …,9
20	11	6, …,10
20	12	7, …,11
20	13	7, …,12
20	14	7, …,13
20	15	8, …,14
20	16	8, …,15
20	17	8, …,16
20	18	8, …,17
20	19	9, …,18

Table 3: Selection of vectors $\boldsymbol{d}'$ with $k_1(\boldsymbol{d}') = 3$.

the proliferation time, and the proliferation costs for that path), an analysis of Eq. (41) is not performed here.

4. Discussion and Outlook

We have performed a game theoretical analysis of a generalized acquisition path model including a sensitivity analysis regarding the influence of the payoff parameters on the Inspectorate's equilibrium strategy and payoff. This sensitivity analysis is mandatory, because the selection of model parameters requires expert judgment.

Although this relative simple acquisition path model has interesting features, future research in the context of the German Safeguards Support Programme to the IAEA has to focus on more realistic acquisition path models in order to increase the acceptance not only of Jülich's APA approach but also of the benefits of game theoretical considerations at all. For that purpose, existing models (e.g., for Germany's nuclear fuel cycle) can be analyzed with the APA software developed in Jülich, and a comprehensive sensitivity analysis can be performed.

5. Acknowledgements

This work was supported by the Federal Ministry for Economic Affairs and Energy, Germany, through the German Safeguards Support Programme to the IAEA under task B.24/JNT C 1871.

6. References

[1] Listner, C, Niemeyer, I, Canty, MJ, Murphy, CL, Stein, G, Rezniczek, A; *Acquisition Path Analysis Quantified – Shaping the Success of the IAEA's State-level Concept*; *Journal of Nuclear Materials Management*; 2015; volume XLIII; p 49–59.

[2] Listner, C, Niemeyer, I, Canty, MJ, Stein, G; *A strategic model for state compliance verification*; *Naval Research Logistics*; 2016; volume 63; issue 3; p 260-271.

[3] Avenhaus, R, Canty, MJ, Krieger, T; *Game theoretical perspectives for diversion path analysis*; *Journal of Nuclear Materials Management*; 2012; volume XL; No. 4; p 130-144.

[4] Avenhaus, R, Canty, MJ; *Compliance Quantified -- An Introduction to Data Verification;* Cambridge University Press; Cambridge, UK; 1996.

[5] Canty, MJ; *Resolving conflicts with Mathematica: Algorithms for two-person games;* Academic Press; 2004.

[6] Nash, JF; *Non-cooperative games; Annals of Mathematics;* 1951; volume 54; p 286–295.

Poster Session

ILLICIT TRAFFICKING OF RADIOLOGICAL MATERIALS AND TERRORISM

Dr Tushar P Ghate
drtusharghate@gmail.com

Abstract:

Onset of 21st century has made terrorism more organized. With *so called internationalization* of terrorist organizations; resources, efforts and targets have become universal cutting across international boundaries. Inception of asymmetric and lethal methods have made it necessary for all state and non state actors to join hands and address this menace in a coordinated way. The terror act inflected with innovative everlasting effect will mar the society more with 'looming fear of unknown.'

Use of Chemical, Biological, Radiological and Nuclear (CBRN) agents in terrorist activities is not a threat but proven fact. There is an inevitable need of the day to isolate the epicenters of source of these materials and also secure the state borders in order to prevent influx of CBRN agents by respective countries.

Nuclear fissile material used in nuclear reactors and radioactive material from commercial and research industries are two main sources that emits harmful radiations.

Many countries have well defined and practiced regulations and guidelines for the handling of nuclear and radioactive material. These regulations and guidelines are in conformity with various rules and regulations promulgated by International Atomic Energy Agency (IAEA) and similar regulating agencies. However there is a requirement of revisiting the present mechanism in place to prevent illicit trafficking of radioactive material across the border. The paper recommends the approach as following:-

- Proactive Intelligence
- Continuous monitoring
- Effective detection and Identification
- Forensic

Integrated measures like regular and remote Monitoring (during transportation and disposal), effective detection and identification (Nuclear Forensic) and knowledge sharing along with physical checks will prove an effective mechanism to counter this problem. Timely tracing, detection and seize of illicit radioactive and nuclear material will avert use of these materials by terrorist organizations.

Keywords: Terrorism; Chemical Biological Radiological Nuclear (CBRN); acts; regulations and guidelines; Nuclear forensic

1. Introduction

Act of terrorism is a well thought set of activities planned and executed to achieve asymmetric political goals. Physically harming people by act of terror is not the only aim; the ulterior motive is always focused towards tearing social synthesis of the society. This is planned in a well thought sequential manner. Initially, terrorist organizations try to brainwash portion of the society with so called *cause.* While this happens, *another section of society* remains unconvinced with the *cause* and keep them in the main stream. However, the remaining section of society which constitutes a large percentage is very sensitive

and suffers from acts of terror in their day to day life. It is easy to exploit this section. To achieve this, terrorists generally adopt unconventional acts that create and *propagate 'looming fear of unknown.'*

Chemical, Biological, Radiological and Nuclear (CBRN) agents used in terrorist activities is not a mere threat but startling reality. With change in operating methodologies of terrorist organizations, these activities are spreading pan-border. In order to contain this menace, there is an inevitable need of the day to isolate and eliminate the sources of these materials as well as prevent the transportation of CBRN agents across the border.

2. Accessibility and Availability of CBRN Materials

2.1. Chemical and biological agents

Variety of hazardous chemical and biological agents are easily available that can be used in terrorist activities by mixing in food, water or through direct dissemination in the open environment. Chemical agents like Cyanides, Mustard, Nerve agents and biological agents like virus, bacteria, fungi etc. are potential sources that can be incorporated in terrorist activities. However, use of nuclear and radiological materials is more devastating in terms of its effects and longevity that looms physically and psychologically in public.

2.2 Radiological agents

Nuclear materials used in reactors and radioactive materials in commercial and research industries are two main sources that emits harmful radiations. Proliferation of these materials is a real threat to the society. Even though many countries do have well defined stringent safety and monitoring framework in place in form of rules, laws and guidelines, this threat remains from rogue nations where these ensuring mechanisms are either very weak or even absent. Proliferation of radiological and nuclear materials from these states to other countries cannot be ruled out considering the vast boarders shared with each other where security related loopholes do exist.

Considering above, there is a requirement of revisiting the present mechanism in place of individual state and synchronize the same with other nations to prevent illicit trafficking of radioactive material across the border. The suggestive successive approach for this is as following:-

- Proactive Intelligence
- Continuous monitoring
- Effective detection and Identification
- Forensic

3. Proactive intelligence

Radioactive materials are used in Nuclear Medicines. As per World Nuclear Association (WNA), more than 10000 hospitals around the world use various radio isotopes. Technetium-99, Cobalt-60, Iodine 131, Iridium-192, Palladium-103, Strontium-89, Samarium-153, Rhenium-186, Lutetium-177 etc are commonly used for diagnosis and treatment. Following other commercial and scientific activities also use radioactive materials

- Neutron techniques for analysis
- Gamma and X-Ray techniques for analysis
- Gamma radiography
- Gauging
- Gamma Sterilization
- Tracers
- Age Determination
- Radioisotope Thermoelectric Generators

- Oil and Gas Operations

It is evident from above details that, there is significant quantity of radioactive material present across the world that is used for various activities. State operated regulation bodies maintain the manufacturing and provision details of these sources. However two important aspect need to be addressed in more details: transportation and disposal post usage. For this, following measures are require to be adopted

4. Regular and remote monitoring

Radioactivity level at the time of manufacturing, during usage and at the time of disposal is predictive with respect to half life. Routine radiographic signatures of all sources should be checked, compared with analytical reference and certified on regular basis. Similar to network mapping, the radioactive sources should also be digitally mapped and monitored. Remote online monitoring through networking of all detectors and CCTV cameras can be adopted for this.

4.1 Transportation

Today, the radioactive material meant for commercial usage is transported as per guidelines for transport issued by respective state agencies. However, while doing so, the transportation and security of such radioactive material is coordinated by private agencies and there is no presence of state representative to prevent any sabotage and proliferation. There is requirement to incorporate state sponsored security mechanism in the existing guidelines while transporting the source.

4.2 Disposal.

Post usage, the radioactive source is required to be deposited back to the issuing agency / defined body by the state. Very strict monitoring is required for its compliance. Lapse in this has resulted into incidents like Goiania (Brazil, 1987), Mayapuri (India, 2010) where the used radiological materials were not deposited back and were left unattended. This resulted in to radiation exposure to public.

Sketch1. Goiania victim

4.3 Continuous monitoring

Countries share vast borders with each other. Effective physical sealing and monitoring for radioactive source at borders should be addressed in two ways.

Sketch 2. Continuous monitoring at borders

4.3.1 Monitoring at check points

Most of the countries have set up an effective monitoring system at the check points. These monitoring details /database however needs to be networked with neighboring countries to ensure the correctness of data.

4.3.2 Monitoring at other than check-posts

There is requirement to continuously monitor maritime borders. This a potential Point of Entry that can be used by terrorists to bring in illicit radioactive

materials. Combination of standoff fixed and aerial based monitoring can be incorporated for the same. Monitoring of sealed containers however remains a challenge, considering volume of transportation and detection limitations due to inherent shielding capability of the container material itself.

5. Effective detection and identification

5.1 Nuclear forensic.

This involves following:-

5.1.1 Nuclear attribution

This involves the process of finding out the source of radioactive materials, its point of origin, routes of transportation and contribution to prosecute the responsible. The attribution can be based on any of or combination of analysis of nuclear forensic, study of radiochemical and environmental signatures, known procedures to produce such materials and information/database available at law enforcement agencies.

5.1.2 Categorization

The goal of categorization of the incidence is to identify the risk to the first responders, law enforcement personnel and public and to determine if there is any criminal activity or threat to the nation. The magnitude may have wide range due to variance in environmental contamination, risk to the public health, proliferation concerns etc.

Sketch 3. Nuclear forensic procedures

5.1.3 Characterization

It is performed to determine the nature of the radioactive material and associated evidence. It provides full elemental analysis of the radioactive material to include major, minor and trace constituents.

5.1.4 Nuclear interpretation

It is the process of correlating the characteristics with production history. The goal of the process is to determine the method and time of the production.

6. Summary

Along with lethal effects, radiological materials have infamous potential to impose psychologically terrifying consequences that lingers on for years. The world has experienced this through Chernobyl, Goiania, Three Mile Island, Mayapuri and so on. Incorporation of these materials in terrorist activities is not mere threat but a startling reality. Tackling this novice but dreaded activity, there is an inescapable requirement to synchronize and synergize the existing laws and frameworks between all states in order to prevent and eradicate the options to use radiological materials in terrorist activities. Timely tracing, detection and seize of illicit radioactive and nuclear material will help to avert the use of these materials by terrorist to great extent.

Acknowledgement

I would like to express my sincere gratitude to Prof Sanjay Dhole of Department of Physics, Pune University and Prof. M. G. Takwale who are always there for me to guide and encourage me to pursue my work in this field.

Spectra Processing Algorithm for Application in Radiation Portal Monitors based on Plastic Scintillators

Arturs Rozite, Paolo Peerani, Francesca Rosas and Hamid Tagziria

European Commission, Joint Research Centre
Nuclear Safety and Security Directorate
Via E. Fermi 2749, TP 800
21027 Ispra (VA), Italy
E-mail: arturs.rozite@ec.europa.eu

Abstract:

In the 1970th it was demonstrated in Los Alamos that plastic scintillation detector is the most cost effective detector type for safeguarding nuclear facilities from unauthorized removal of radioactive materials and a concept of Radiation Portal Monitor (RPM) has been introduced [1–3].
During the past 30 years thousands of similar RPM equipped with plastic scintillation detectors and single channel analyzers have been deployed all over the world in the framework of various nuclear security programs. Such systems measure number of detected photons in a single energy range without further distinguishing in energies of individual photons [4, 5].
For RPM deployed at the border crossing point this results in huge number of innocent alarms caused by naturally occurring radioactive materials (NORM) [6]. Analysis of radiation profiles by operator of Local Alarm Station is the only technique at majority of installations to classify source of alarm as a NORM where appropriate and eliminate unwanted secondary inspections.
Addressing this problem and investigating the whole potential of plastic scintillators, multichannel analyzers are now more widely used in the chain of signal processing electronics and corresponding energy windowing algorithms of categorization/identification of radionuclides have been suggested [7].
Theoretically usage of multichannel analyzer provides possibility to discriminate between different types of radionuclides based on the energy dependent differences in the Compton continuum of the measured spectra. In practice spectra measured within short time interval of the occupancy contain little number of counts in individual channels as well as in specific regions of interests what makes an energy dependent categorization of radionuclides difficult.
In present work the rolling energy window algorithm for identification of radionuclides from the spectra measured by means of plastic scintillation detector is considered.

Keywords: Radiation Portal Monitor, plastic scintillator, multichannel analyzer

1. Introduction

Radiation signals measured with plastic scintillation detectors of conventional RPM are processed using single channel analyzers and alarm decision is based on the comparison of the net signal value (S) measured by plastic scintillators during an occupancy with background (B) value measured when the detection zone of the RPM is unoccupied according to the following equation:

$$N\times Sigma = \frac{S}{\sqrt{B}}$$

When the measured value exceeds pre-defined *N×Sigma* threshold an alarm is triggered. Depending on the values of the low-level and upper-level voltage discriminators (LLD and ULD) certain widths of energy window could be selected and the highest possible *N×Sigma* value for specific radionuclides could be obtained.

The value of LLD is usually chosen as low as possible but high enough to cut low-energy electronic noise and the choice of the value of ULD depends on the task of the analysis. For example to get an optimal value of measuring parameter for detection of ^{235}U, the values of LLD and ULD are set so to cover an energy range from about 20 to about 150 keV, but to get an optimal detection threshold for ^{137}Cs the value of ULD has to be set above Compton edge of ^{137}Cs (above 480 keV).
It can be demonstrated that usage of a multichannel analyzer for processing of signals collected with the plastic scintillation detectors provides possibility to discriminate between types of radionuclides based on the position of the Compton edges. Comparing *N*Sigma* values in the fixed energy windows it is possible to discriminate between categories of radionuclides emitting low, medium and high-energy photons. Such algorithms of a number of fixed energy windows have been proposed before [7].
In the present article it is demonstrated that usage of a multichannel analyzer for processing of signals collected with the plastic scintillation detectors provides possibility to discriminate between types of radionuclides based on the energy dependent differences in the Compton continuum of the measured spectra.
In present article the rolling energy window algorithm for categorization/identification of radionuclides is suggested and is described on the example of three sources for relatively high N×Sigma values.
The algorithm is also probated at low *N×Sigma* values and for the short measurement time using NORM, Special Nuclear Materials and industrial radionuclides.

2. Materials and methods

Radiation signals have been measured by means of plastic scintillation detector installed in a master pillar of a Vehicle RPM, model TSA VM-250AGN [5]. Instead of a single channel analyzer the signals measured with the detector have been processed using multichannel analyzer (MCA), model CHRPR [8]. Two versions of MCA have been used: with 256 and with 512 channels.

3. Experimental results

3.1. Description of the algorithm

The algorithm is described on the example of three sources and for relatively high *N×Sigma* values. Description of sources and corresponding energies of photons is shown in Table 1.

Table 1 – Description of radioactive sources

Radionuclide	Energy, keV	Emission probability, %	Energy of Compton edge, keV
^{133}Ba	81	32.9	
	303	18.3	
	356	62	210
^{137}Cs (Ba-137m)	662	85	480
^{60}Co	1174	99.85	970
	1333	99.98	1120

^{133}Ba, ^{137}Cs, ^{60}Co spectra and background spectrum were measured for a period of 60 seconds. Sources have been placed in front of the detector and spectra have been collected with CHRPR multichannel analyzer. In all spectra a maximum count rate is in the beginning of energy scale and depending of the radionuclide a characteristic Compton edge can be clearly observed moving on the energy scale up (*Figure 1*). Spectra have been manually processed in order to get values of main measurement parameter (*N×Sigma*) for individual channels (*Figure 2*), for total energy window (*Figure 3 – cumulative sum*) and for the rolling energy window consisting from 20 measurement channels (*Figure 3 – rolling sum*). *N×Sigma* values have been calculated according to the following formulas:

a) For individual channels

$$N\times Sigma = \frac{S_i - B_i}{\sqrt{B_i}}$$, where *i* is the number of channel

b) For cumulative sum of channels (total energy window)

$$N\times Sigma = \frac{\sum_{i=1}^{n}(S_i - B_i)}{\sqrt{\sum B_i}}$$, where *n* is the last number of channel

c) For rolling sum of channels (rolling energy window)

$$N\times Sigma = \frac{\sum_{i=m}^{k+m}(S_i - B_i)}{\sqrt{\sum_{i=m}^{k+m} B_i}}$$, where *k* is fixed and *m = 1, 2, 3 … n-k*

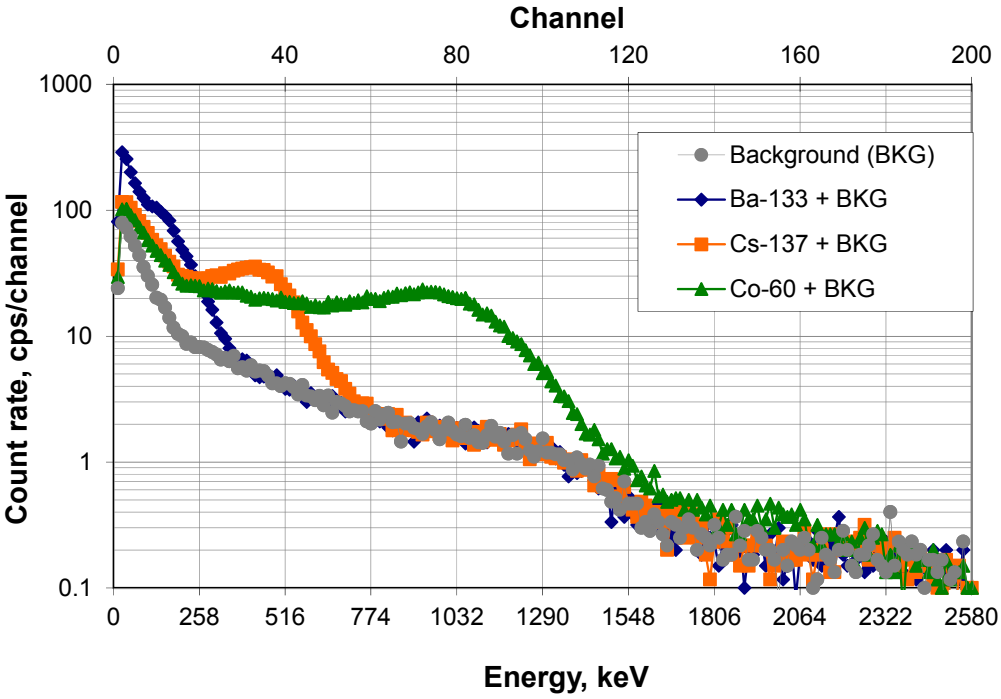

Figure 1 – Comparison of ^{133}Ba, ^{137}Cs, ^{60}Co and background measured with plastic scintillation detector and 256-channel MCA

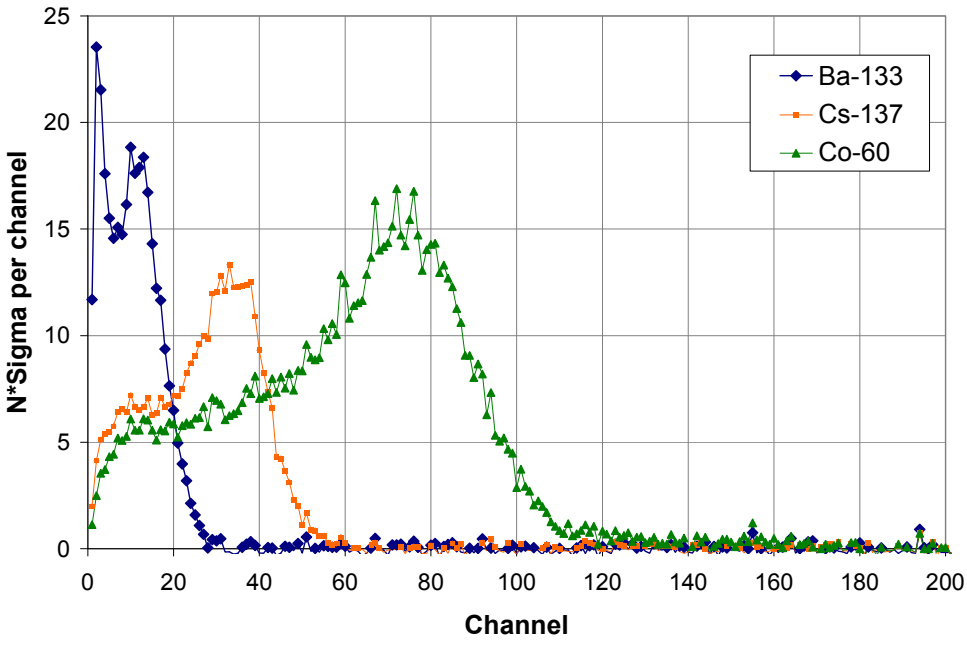

Figure 2 – Comparison of N×Sigma values for individual channels for the spectra of ^{133}Ba, ^{137}Cs and ^{60}Co sources measured with a plastic scintillation detector

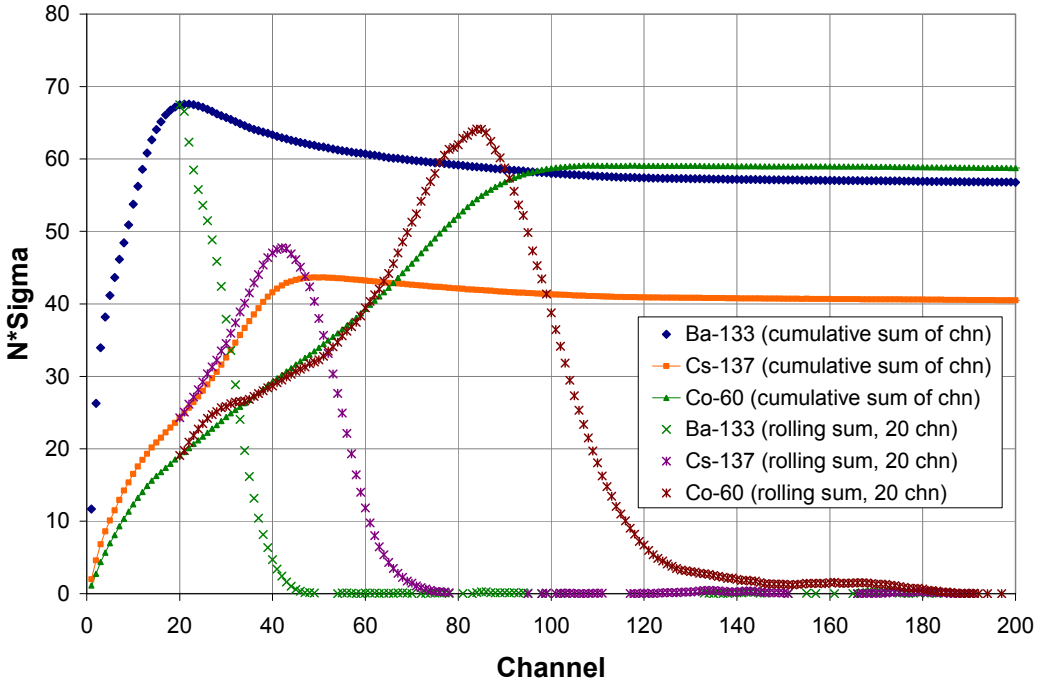

Figure 3 – Comparison of N×Sigma values for cumulative and rolling sums of counts in 20 channels for the spectra of ^{133}Ba, ^{137}Cs and ^{60}Co sources measured with a plastic scintillation detector

As it can be seen from the figures, a comparison of *N×Sigma* values for the individual channels and for the rolling energy window consisting from the sum of 20 channels shows that rolling energy window algorithm provides higher values of maximum amplitudes of an alarm as well as more precise position on the energy scale of the maximum of the Compton edge.

3.2. Optimal width of the rolling energy window

With increase of the width of the rolling energy window, the maximum value of *N×Sigma* can be achieved, however at the cost of decrease of sensitivity in distinguishing between Compton edges characteristic for different radionuclides (*Figure 4*).
For high *N×Sigma* values algorithm works, unless Compton edges of two different radionuclides are too close in energy to each other. For example as shown on the (*Figure 5*), ^{133}Ba and ^{137}Cs can't be distinguished but ^{133}Ba and ^{60}Co as well as ^{137}Cs and ^{60}Co can be.
Since on the energy scale from 20 keV to 3 MeV Special nuclear materials (^{235}U and ^{239}Pu) and medical radionuclides are characterized by dominant emission of photons with relatively low energies, industrial radionuclides (^{137}C and ^{60}Co) by emission of photons with medium and high energies and NORM radionuclides (^{40}K and ^{232}Th) by emission of photons with high energies, in principle it should be possible to discriminate between SNM + Medical and NORM radionuclides such as ^{40}K.
In order to validate/probate algorithm such possibility has been investigated for low *N*Sigma* values, the values that could be expected during real cases of innocent alarms caused by transfer of cargo containing NORM.

3.3. Deconvolution of N×Sigma profiles

On the *Figure 6* is shown a comparison of measured *N*Sigma profile* of ^{137}Cs source with a deconvoluted *N*Sigma profile* obtained by subtraction of *N*Sigma profile of* ^{60}Co source from *N*Sigma profile* of the ^{137}Cs+^{60}Co source. As it can be seen from the figure a Compton edge of ^{137}Cs is resolved, however with some drop of N*Sigma values.

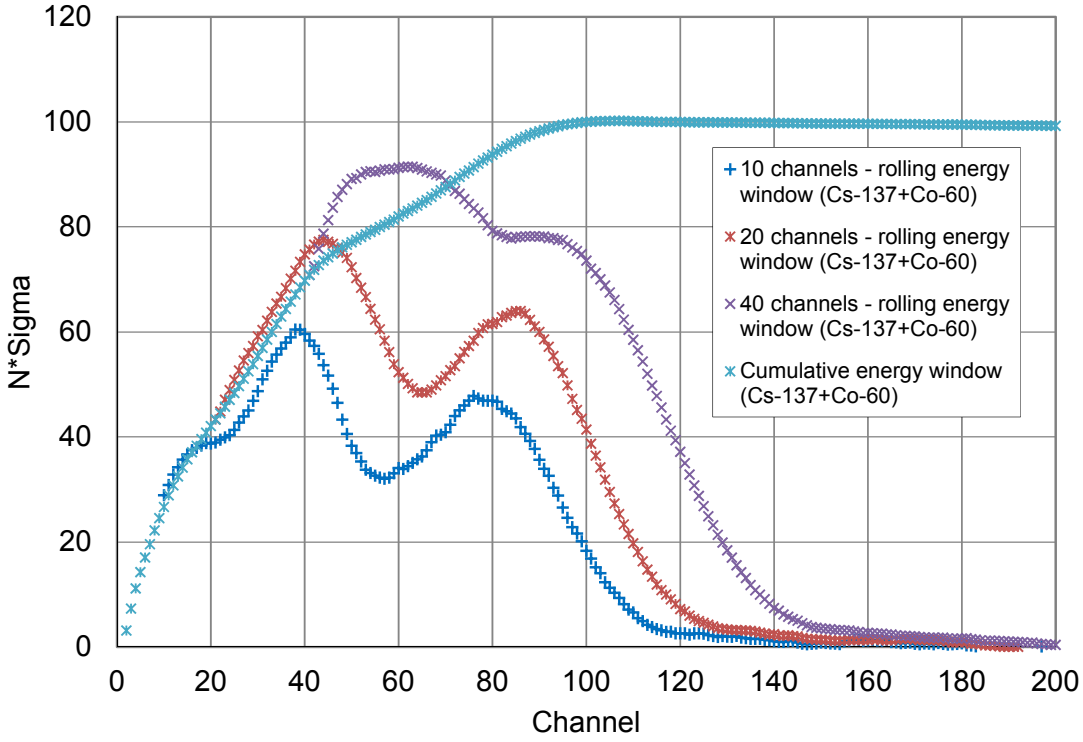

Figure 4 – Comparison of N×Sigma values for rolling energy windows consisting from k= 10, 20 and 40 channels for the spectrum of ^{137}Cs plus ^{60}Co sources

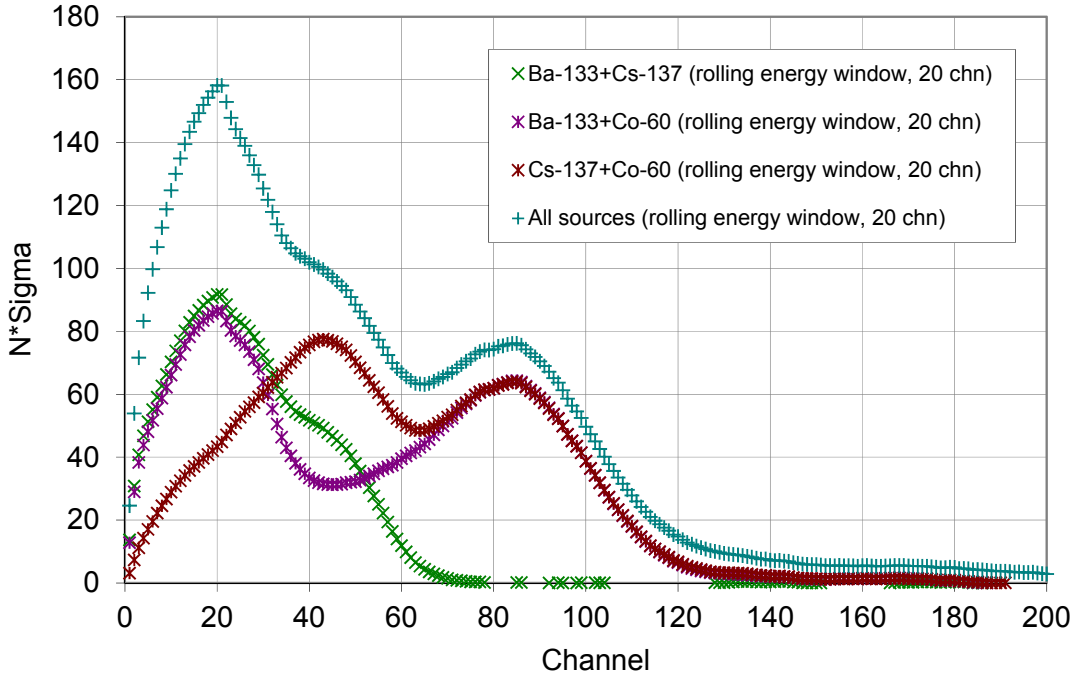

*Figure 5 – Comparison of N*Sigma values for rolling energy window (k=20 channels) for sum of signals from ^{133}Ba, ^{137}Cs and ^{60}Co sources; first 20 points correspond to cumulative energy window*

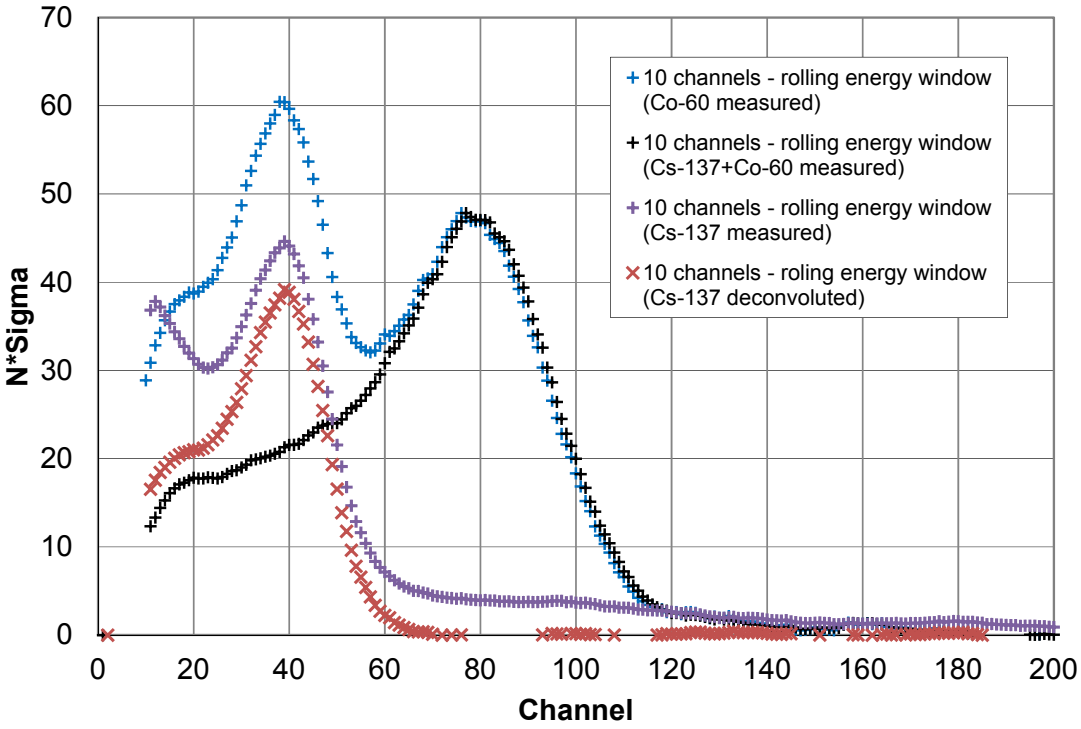

Figure 6 – Comparison of measured and deconvoluted N×Sigma profiles of ^{137}Cs.

3.4. Validation of the algorithm

For the validation of spectra processing algorithm based on the rolling energy window spectra of different radionuclides characterized by

a) low *N*Sigma* values, and by
b) low *N*Sigma* value and short measurement time of 1 second

have been measured and processed.
On the *Figure 7* count rates for the spectra measured within 60 seconds are shown, processing results with the algorithm for the average count rate per 1 second) are shown on the *Figure 8*.
On the *Figure 9* count rates for the randomly selected spectra of the sources measured within 1 second are shown, processing results with the algorithm for these spectra are shown on the *Figure 10*. For the background average count rate taken from the 60 seconds spectrum has been used.
Spectra have been measured with upgraded to 512 channels CHRPR MCA. Voltage divider of plastic scintillation detector has been changed and amplifier gain has been adjusted.
As it can be seen from the *Figures 9 and 10* the algorithm allows discriminate between SNM+Medical group of radionuclides, ^{137}Cs, ^{60}Co and ^{40}K single radionuclides.

3.4.1. Validation of identification algorithm for low N×Sigma values

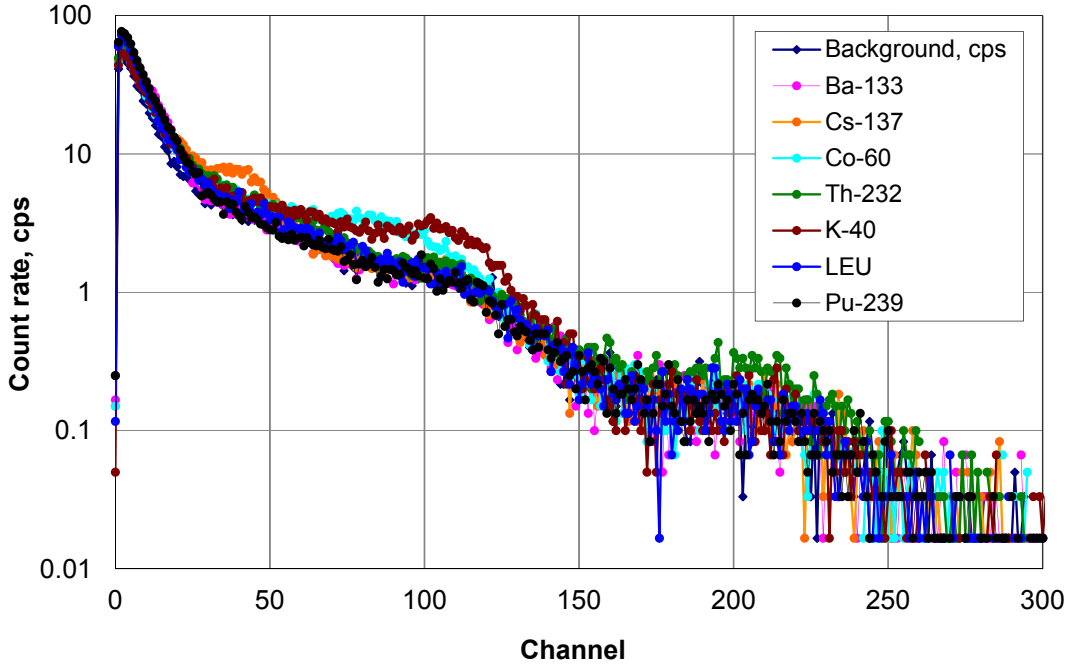

Figure 7 – Comparison of spectra of different radionuclides measured with plastic scintillator and 512-channel MCA (measurement time 60 seconds)

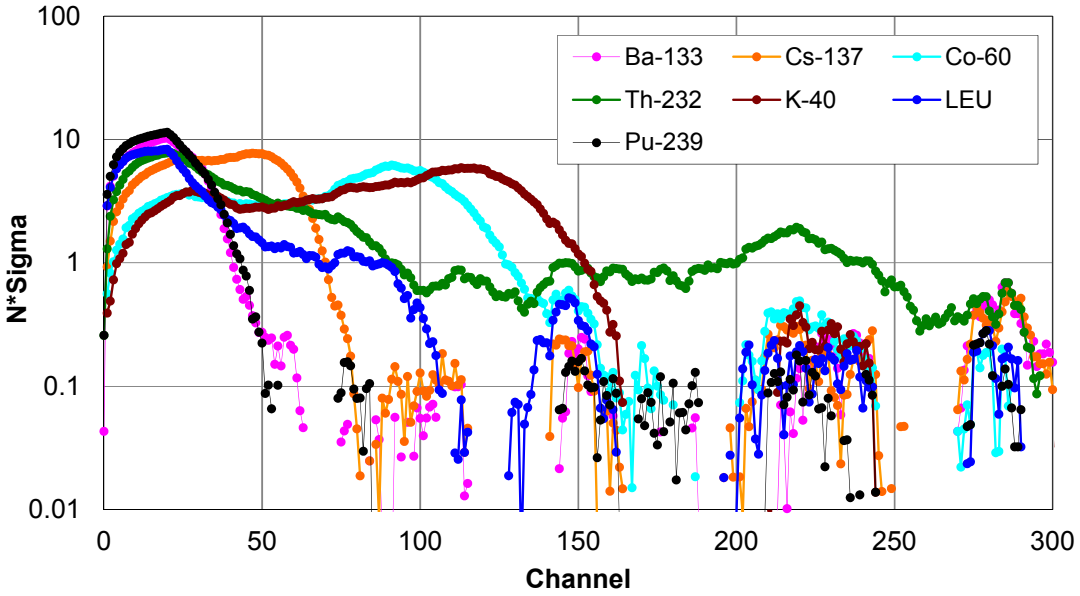

Figure 8 – Comparison of N×Sigma values for rolling energy window with a widths of 20 channels for different radionuclides for the average count rate measured within 60 seconds (first 20 points represent cumulative energy windows)

3.4.2. Validation of identification algorithm for low N×Sigma values and short measurement time

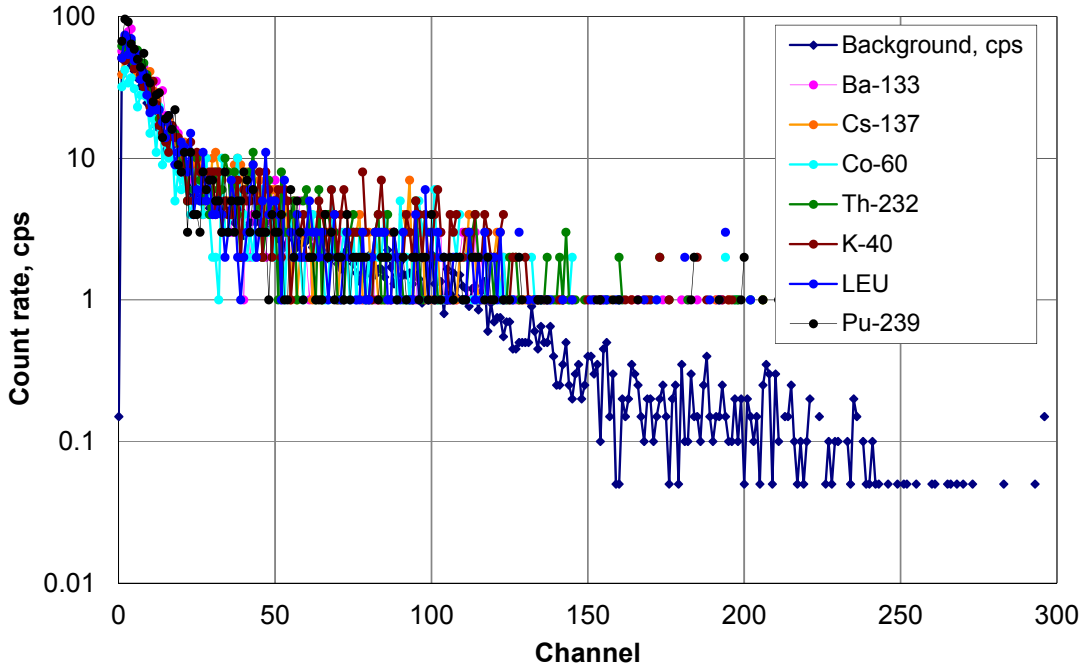

Figure 9 – Comparison of spectra of different radionuclides measured with plastic scintillator and 512-channel MCA (measurement time 1 second)

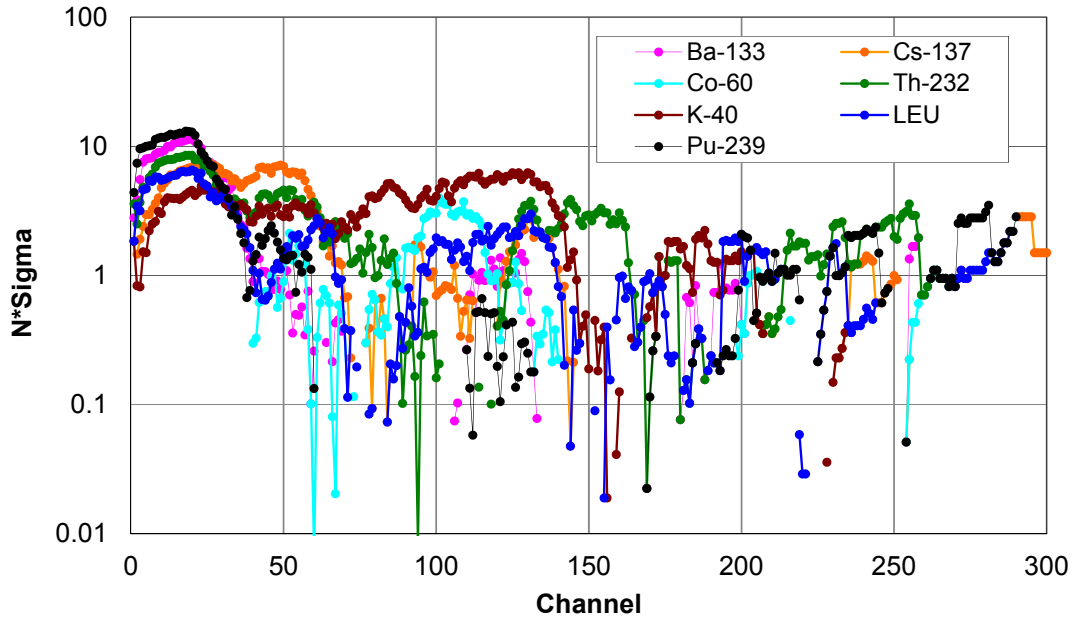

Figure 10 – Comparison of N×Sigma values for rolling energy window with a widths of 20 channels for different radionuclides for the spectra measured within 1 second (first 20 points represent cumulative energy windows)

4. Summary of experimental results

The use of a multichannel analyzer instead of a single channel analyzer for processing of signals from plastic scintillation detectors provides possibility to discriminate among types of radionuclides based on energy dependent differences in the Compton continuum of the measured spectra.
The categorization/identification algorithm based on the rolling energy window allows enhanced identification of Compton edges.
The rolling energy window algorithm provides a better *N*sigma* value compared to the single channel algorithm and allows more accurate identification of maximum energy position of characteristic Compton edge.
The algorithm doesn't bring any advantage in terms of improvement of the detection threshold compared to a standard detection algorithm based on the alarm comparison in a total energy window, since more alarm comparisons are made per single alarm comparison interval.
The algorithm allows discriminate between SNM+Medical, ^{137}Cs, ^{60}Co and ^{40}K radionuclides.

5. Conclusion

In present article spectra processing algorithm based on the rolling energy window for identification of radionuclides by means of plastic scintillation detector was suggested and discussed. Applicability of the algorithm for discrimination between NORM and other radionuclides was considered.
The algorithm allows discriminate between SNM+Medical, ^{137}Cs, ^{60}Co and ^{40}K radionuclides.
Further investigations towards ability of the algorithm of categorization of other NORM radionuclides with multiple spectral lines (^{232}Th and ^{226}Ra and their daughters) and towards ability of deconvolution of multiple radionuclides should be made.

6. References

[1] Chambers, W.H.; Atwater, H.F.; Fehlau, P.E.; Hastings, R.D.; Henry, C.N.; Kunz, W.E.; Sampson, T.E.; Whittlesey, T.H.; Worth, G.M. *Portal Monitor for Diversion Safeguards.* Los Alamos National Laboratory, LA-5681, 1974
[2] Paul E. Fehlau. *An Application Guide to Pedestrian SNM Monitors.* Los Alamos National Laboratory, LA-10633-MS, 1986
[3] P. E. Fehlau. *An Application Guide to Vehicle SNM Monitors*. Los Alamos National Laboratory, LA-10912-MS, 1987
[4] Rob L. York and Paul E. Fehlau. *1997 Update for the Application Guide to Vehicle SNM Monitors.* Los Alamos National Laboratory, LA-12347-MS, 1997
[5] TSA Systems, Ltd. *Vehicle and Pedestrian Monitor VM-250AGN / PM-700AGN, Operations & Service Manual.* Doc: # 5000 Rev. A, January 30, 2006
[6] Paolo Peerani, Arturs Rozite, Giovanni Mercurio and Francesca Rosas. *Study on the effect of meteorological conditions on the performances of Radiation Portal Monitors.* JRC Technical Report, JRC 93365, 2015
[7] Ryne Hevener, Man-Sung Yim, Ken Baird. *Investigation of energy windowing algorithms for effective cargo screening with radiation portal monitors.* Elsevier, Radiation Measurements, Volume 58, (November 2013), Pages 113–120
[8] B. Windsor, M. Woodring, M. Myjak. *CHRPR Operations Manual.* PNNL-21635, 2012

Safeguards and Non-Proliferation in Myanmar

Khin Pa Pa Tun
Department of Atomic Energy, Ministry of Education, Building No.(21), Nay Pyi Taw, Myanmar
papatun@gmail.com

Abstract

Myanmar has views about nuclear that in order for the utilization of nuclear energy to be peaceful and secure, nuclear disarmament and nuclear non-proliferation must be achieved on the global scale. Myanmar has demonstrated its commitment with the nuclear non-proliferation regime as it has been a party to the Treaty of the Nuclear Non-Proliferation (NPT) since December 1992. Myanmar has signed the Safeguards Agreement and the Small Quantities Protocol pursuant to the NPT with the IAEA in April 1995. As a member of the Association of Southeast Asian Nations (ASEAN), it also reaffirmed its commitment by signing the Treaty on South East Asia Nuclear Weapon Free Zone (SEANWFZ) that entered into force in 1997. In addition, the Comprehensive Nuclear Test-Ban Treaty (CTBT) has been ratified on 21 September 2016.

Myanmar has signed the Protocol Additional to the Comprehensive Safeguards Agreements (AP) on 17 September 2013 and is currently working on a step by step approach to implement the AP. Myanmar's State System of Accounting for and Control of Nuclear Material (SSAC) has been established with well trained staff. Myanmar, in cooperation with the IAEA and the United States Department of Energy (USDOE), has participated in the international Safeguards Engagement Program so as to strengthen the Non-Proliferation regime in State. With the purpose of strengthening national nuclear related legislation, the Department of Atomic Energy (DAE) has just recently completed the drafting of the Myanma's comprehensive Nuclear Law covering Nuclear Safety, Security and Safeguards (3S strategy). The main challenges in establishing the national safeguards infrastructure as a newcomer country includes the establishment of the legal framework, the implementation of the safeguards regulation, the establishment and implementation of an effective and systematic nuclear material management system and the development of human resources. This paper will present the milestones achieved so far in the implementation of safeguards and non-proliferation activities in Myanmar, and will elaborate on the steps to be taken to eventually implement the Additional Protocol.

Keywords: Additional Protocol; Nuclear Non-Proliferation; 3S strategies

1. Introduction

Situated between China and India, Myanmar, is a South-East Asian nation, with a Small Quantities Protocol in force with the International Atomic Energy Agency (IAEA). Myanmar joined the IAEA as a member state in 1957 (number of accession-59).

Myanmar has made a non-proliferation U-turn in the recent years. Only a few years ago, the international community regarded Myanmar as a pariah State in connection with Democratic

People's Republic of Korea (DPRK), expecting possible nuclear–weapon ambitions [1]. In the context of sweeping political and economic reforms that began in 2011, Myanmar has made significant developments in implementing nuclear non-proliferation measures. After President Barack Obama's first visit in November 2012, Myanmar announced it would sign the Protocol Additional to its Comprehensive Safeguards Agreement (AP) [2]. On 17 September, 2013, Myanmar signed the agreement, but is still required to ratify the instrument.

It is important that the implementation of the AP and of the modified Small Quantities Protocol happens soon, especially since Myanmar officials seem prepared to enhance their nuclear activities. For instance, such an issue became evident on 18 June 2015, when the Republic of the Union of Myanmar signed a Memorandum of Understanding with the Government of the Russian Federation for cooperation in the field of the use of nuclear energy for peaceful purposes.

The international community, particularly the US and other Western countries, make continuous efforts to help Myanmar in implementing disarmament and non-proliferation regime. At present, Myanmar has neither nuclear research reactors nor nuclear power reactors nor other fuel cycle facilities. The utilization of radiation sources and irradiating apparatus are limited to the use in medicine, industry, agriculture, livestock breeding and research. Nonetheless, Myanmar government is aware of the importance of nuclear nonproliferation and safeguards. This paper is based on consolidated efforts by Myanmar government in fulfilling its commitments and challenges encountered during some phases for implementing nuclear nonproliferation and disarmament regimes.

No.	Treaty/Convention	Date of Signing	Date of Deposit	Enter into Force
1	Treaty Banning Nuclear Weapon Tests in the Atmosphere, in Outer Space and Under Water or Partial Test Ban Treaty (PTBT)	14th Aug1963	15th Nov1963	
2	Sea-Bed Treaty: Treaty on the Prohibition of the Emplacement of Nuclear Weapons and Other Weapons of Mass Destruction on the Sea-Bed and the Ocean Floor and in the Subsoil	11st Feb 1971		
3	Treaty on the Non-Proliferation of Nuclear Weapon (NPT) (INFCIRC/140)	2nd Dec1992		
4	Agreement between the Union of Myanmar and the IAEA for the Application of Safeguards in connection with the Treaty on the Non-Proliferation of Nuclear Weapons (with Protocol) Safeguards Agreement on (INFCIRC-477)	20thApril 1995		
5	Small Quantities Protocol (SQP) pursuant to the NPT	15th Dec2005		
6	Treaty on South East Asia Nuclear Weapon Free Zone (SEANWFZ)	15th Dec1995		17th Jul 1997
7	IAEA's Additional Protocol (AP)	17th Sept 2013		
8	Comprehensive Nuclear Test-Ban Treaty (CTBT)	25th Nov 1996	21st Sep 2016	
9	Convention on the Physical Protection of Nuclear Material and Nuclear Facilities (CPPNM)	6th Dec 2016		5th Jan 2017
10	Convention on nuclear Safety (CNS)	6th Dec 2016		6th Mar 2017

Table 1: List of Treaties and Conventions

2. Myanmar's Legal framework for Safeguards and Non-Proliferation

With regard to nuclear non-proliferation and safeguards, Myanmar fulfills its obligations

resulting from the following international legal instruments as listed in Table 1.

Myanmar believes that nuclear weapon free zones and treaties are effective measures for nuclear weapon non-proliferation and nuclear disarmament. Therefore, Myanmar has made considerable progress on non-proliferation over the past few years, but there are instruments that they are yet to endorse and, just as important as they are yet to fully implement

those they have recently adopted.

No.	Events	Event Start Date/End Date	Organized by
1	Workshop on International Safeguards and Additional Protocol	9-13 January 2013	MOST and USDOE
2	National Awareness Seminar and Training Course on Physical Protection and Security Management	21-24 May 2013	MOST and ANSTO
3	Workshop on Modified Small Quantities Protocol and Additional Protocol	19-21 August 2013	MOST and USDOE
4	Workshop on State Systems of Accounting and Control	26-28 August 2013	MOST and IAEA
5	Regulatory Development Workshop	18-20 November 2013	MOST and USDOE-GTRI (Global Threat Reduction Initiative)
6	Workshop on Additional Declaration Development and Associated Outreach	16-20 June 2014	MOST and USDOE
7	Sub-regional Workshop on Establishing a Register of Radiation Sources Based on the Regulatory Authority Information System (RAIS)	23-27 June 2014	MOST and IAEA
8	5th Annual Meeting on Asia-Pacific Safeguards Network	1-5 September 2014	MOST and APSN
9	IAEA National Workshop on Safeguards	3-5 December 2014	MOST and IAEA
10	National Stakeholders Meeting for the Development of Detection and Response Capability at Borders for Myanmar, in Yangon organized by (4 resource persons and 30 participants)	March 30 – April 1, 2015	MOST and IAEA
11	Workshop on IAEA Additional Protocol Implementation	5-7 May, 2015	MOST and USDOE
12	National Workshop on Threat Assessment and Design Basis Threat (DBT)	4 to 7 August, 2015	
13	IAEA Additional Protocol and Commodity Identification Training (CIT) AP-CIT	12-14 July, 2016	
14	Workshop on Challenges and Strategies in the Implementation and Ratification of the Additional Protocol, with Small Quantities Protocol	20-22 March, 2017	USDOE

Table 2: List of Seminars, Workshops and Training in Myanmar

3. Engagement with IAEA, USDOE and other Organizations

In Myanmar, the Department of Atomic Energy (DAE), formerly under the Ministry of Science and Technology (MOST), which is now merged with Ministry of Education (MOE), is responsible for the implementation of Safeguards agreements. The DAE, in cooperation with the IAEA and United States Department of Energy (USDOE), has participated in the International Safeguards Engagement Program, with emphasis on getting prepared for the implementation of the Additional Protocol. The cooperation between the IAEA and Myanmar remains critical for the implementation of safeguards.

With the guideline of IAEA and under the auspices of the U.S. Department of Energy/ National Nuclear Security Administration Office (NNSA) of Nonproliferation and International Security (NIS), a Workshop on International Safeguards and Additional Protocol was held from 9 to 13 January 2013 and a Workshop on the Modified Small Quantities Protocol and Additional Protocol was conducted from 19 to 21 August 2013 in Myanmar. Subsequently, Myanmar signed the Protocol Additional to the Comprehensive Safeguards Agreement on 17 September 2013. It is a significant step towards supporting the non-proliferation of nuclear weapons.

Moreover, Myanmar organized a series of national workshops to support the capacity building and to provide for sharing of experiences regarding the implementation of the Additional protocol (AP), as well as the implementation of Safeguards Agreements to get better prepared to fulfill its obligations under the NPT. Myanmar is working step by step approach and is making all necessary arrangement to fulfill its international non-proliferation commitments.

3.1 Engagement with IAEA and USDOE

As shown in Table 2, there are numbers of events as Seminars, Workshops and Trainings in Myanmar that have been already held. Safeguards and verification are important pillars upon which safe and secure global nuclear regulation should be built [3]. IAEA Safeguards is one of the cornerstones of the global nuclear non-proliferation regime. The Comprehensive Safeguards Agreement (CSA), its Additional Protocol (AP) and the modified Small Quantities Protocol (SQP) form a strong verification regime. According to the agreed work plan of USDOE and Myanmar, DAE is conducting a series of workshops with hands-on experiences which are mostly related to implementation of the AP as well as to understanding of how important NPT is. The US support programs to IAEA safeguards are key enablers for implementation of information-driven safeguards. The close and interactive co-operation gives an opportunity to establish new routines to include safeguards requirements both at the national and the international level and thus avoiding unforeseen and unpredictable obstacles, leading to improving performance in overall safeguards and the global nuclear non-proliferation regime.

3.2 Engagement with other Organizations

Moreover, DAE is continuously improving cooperation with the Australian Nuclear Science and Technology Organization (ANSTO), Korea

Institute of Nuclear Nonproliferation and Control (KINAC/INSA) and the ASEAN Centre for Energy (ACE) under the Global Threat Reduction Imitative (GTRI) program. A national strategic trade control program is a fundamental requirement for the development of a comprehensive national non-proliferation regime as it provides the necessary mechanisms to control the flow of strategic goods and technologies in and out of the country.

Myanmar officials initiated efforts to modernize and standardize customs procedures with a new trade law. This law requires licenses and permits for traders to import and exports goods. The New Nuclear Law in Myanmar will also cover a comprehensive strategic trade controls program. In May 2017, the Australian Border Force (ABF), in cooperate with the Government of Myanmar, will organize a workshop on border trade control. This will be another commitment of Myanmar to the global nuclear non-proliferation regime and the potential economic advantages associated with this endeavor.

Gained experience of international cooperation in safeguards is being used for development and further implementation of projects in the field of nuclear weapons non-proliferation and strengthening nuclear security. Finally, assistance to train the next generation of local experts is one of the most important standpoints for ensuring that non-proliferation remains focused on in Myanmar over the long term. Every effort should be made, therefore, to provide non-proliferation training to young up-and-coming Myanmar nationals.

3.3 Establishment of SSAC, and Legislative and Regulatory Issues

The proliferation of nuclear weapons is a threat that also urges cooperation at all levels. International, regional and state systems must work closely together, and there is need and space for everyone. The modern enhanced SSAC combines safeguards, security and safety in prevention, detection and response [3]. Strong SSAC is a prerequisite for peaceful use of nuclear energy in Myanmar.

After signing the AP, the State System of Accounting for and Control of Nuclear Material (SSAC) team in Myanmar has been established, under the guidance of the former Ministry of Science and Technology (MOST) and other relevant government authorities. The SSAC is a system not a governmental body which is coordinated by the State Authority responsible for safeguards. Myanmar has worked with DOE/NNSA and the IAEA to receive training on matters relevant to establish a State System of Accounting for and Control of Nuclear Material and to prepare the county to create a legal framework to support the Implementation of the Additional Protocol and other nuclear safeguards agreements.

Reliable accounting for and control of nuclear material is fundamental to member states' ability to fulfill their international obligations. The DAE's is the State Authority in Myanmar responsible for establishment and maintenance of the SSAC. DAE is keen to fulfill all requirements for the strong SSAC. This development work will lead to not only enhancing SSAC and also extending cooperation with international and regional organization.

Moreover, IAEA has supported Myanmar in the development of staff through Regional Training Courses on States Systems of Accounting for and Control (SSAC) of Nuclear Material every year. These courses use lectures, workshops, group discussions, and facility tours to provide

knowledge and skills on the basic concepts of IAEA safeguards, SSAC requirements and safeguards tools to government officials who are responsible for implementation of safeguards and to operators who are engaged in nuclear-material accounting and control. It is believed that the international cooperation is important and helpful in the establishment of the SSAC and other necessary infrastructures for state nuclear regulatory body for developing countries.

As a legislation issue in Myanmar, DAE enacted the Atomic Energy law on 8th July 1998 and it was mainly based on radiation safety, did not cover safety, security and safeguards (3S strategies). Myanmar officials have hosted numerous seminars and workshops to learn how to establish regulatory frameworks and fully implement the Additional Protocol and modified Small Quantities Protocol. Myanmar is currently also reviewing their nuclear regulations following recently completed drafting the comprehensive Myanma Nuclear Law, that prohibits the use, production, storage, distribution and import/export of nuclear materials, radioactive materials or irradiation apparatuses without government license and to meet the current standards and requirements. All relevant stake holders are taking part in the drafting process.
It is currently under for review with the parliament for its second reading. Myanmar officials are also translating the provisions of the Additional Protocol and modified Small Quantities Protocol into local language so that relevant stakeholders can learn about the obligations and proceed with the implementation. Myanmar has to take necessary steps to fulfill the obligations in respect of international treaties, conventions and agreements relating 3S that the Government has ratified or intends to be ratified.

4. Challenges and Opportunities

On this occasion, Myanmar faces several challenges to pursue making its efforts for implementing nonproliferation. As Myanmar is opening up to the world and in the transition towards democracy that seems in good progress, its officials have multiple priorities and strengthening their capacity to address them adequately. Many of those priorities are more important than non-proliferation. They include peace building within Myanmar, the maintenance of social cohesion among local ethic groups, economic development and poverty alleviation, etc [1].

Before Myanmar will be able to submit its first AP declaration and to receive a complementary access by the IAEA, there are still some obstacles remained to overcome. It requires support for some entities that still do not understand how they are relevant to AP implementation in Myanmar and they have a lack of knowledge on the AP requirements, type and content of information to be provided to the IAEA, as well as on how to prepare and submit timely AP declarations.

The main challenges for the establishment of an effective national safeguards infrastructure as a new comer country includes the establishment legal framework, implementation of safeguards regulation, effective and systematic nuclear material management system and human resources development. Myanmar primarily needs assistance for non-proliferation implementation in addition that more efforts should be made to strengthen its nuclear legislation and regulations.

At first, there is a need for legislation, regulatory body, contact point, international agreements

and then finally practical implementation of the safeguards in the nuclear related fields. There are a lot of issues to be prepared in advance to facilitate the IAEA's implementation of verification activities successfully, effectively and with the good quality.

Some of the challenges are related to how to effectively and efficiently collect, process manage and provide high quality safeguards relevant information to the IAEA, how to best facilitate IAEA verification activities, how to contribute to the achievement of objectives, and finally how to draw conclusions on the exclusively peaceful use of nuclear materials in the state.

But with those challenges also opportunities emerge. As has been discussed in this paper, the continuous, reliable, and free-flowing communication with the IAEA and USDOE has reduced or in many cases, alleviated the challenges related to safeguards in Myanmar. Early and continuous engagement with the IAEA for any newcomer state is fundamental to the success.

5. Recent Significant Events

Despite some challenges in implementing nonproliferation commitments, particularly in regard to resources, capacity, and knowledge, Myanmar is moving in the right direction by implementing several key conventions and treaties. This requires working with the Ministries in Myanmar responsible for the framework and for implementation, and other decision makers.

Myanmar recently joined main conventions in nuclear safety and security including accession of Convention on Nuclear Safety, Convention on Physical Protection of Nuclear Material and Amendment to the Convention on Physical Protection of Nuclear Material on 6th December 2016. Next steps for Myanmar are signing and ratifying other major nuclear security and safety conventions. Safety and security in nuclear activities are main components, together with safeguards, that provide public acceptance of nuclear technologies.

6. Conclusion

As a member of the NPT and IAEA, Myanmar will continue to build confidence and transparency with the international community to honor its nuclear non-proliferation commitments [2]. Myanmar has much more to do, such as ratifying the IAEA Additional Protocol, concluding the Small Quantities Protocol, and formulating the Strategic Trade Control Law. However, Myanmar lacks expertise and relevant legal framework in the context of formulation and implementation of global nuclear non-proliferation regulations and instruments. Thus, technical support, capacity building, training and political encouragement are required for Myanmar's government to execute its international non-proliferation obligations and procedures.

Myanmar government will reinforce efforts in developing nuclear non-proliferation and disarmament regimes and will promote peaceful uses of nuclear materials by enhancing greater compliance with the United Nations and the IAEA. The government will intensify its respect for United Nations Security Council resolutions, particularly with regard to relations with the DPRK. International allegations about Myanmar's ambitious nuclear program are unsubstantiated.

The government supports peaceful use of

nuclear energy for civilian purposes, such as for medical, research and energy, and it opposes to any type of proliferation. Myanmar has no aim to develop an atomic weapon, and technical and financial constraints mean it cannot afford to even dream of a costly nuclear program. In the meantime, the world should be optimistic about Myanmar's efforts and developments to realize its goal of nuclear non-proliferation and peaceful use of nuclear energy.

To strengthen safeguards obligation with active co-operation with IAEA and USDOE, regional safeguards system is a necessity in fulfilling today's requirements. To ensure that non-proliferation progress continues in Myanmar, the US, other developed countries and border international community should continue to engage Myanmar officials and continue to provide them with non-proliferation assistance. Next steps in implementation of international safeguard are ratification of Additional Protocol to the safeguards agreement and introduction of integrated safeguards. Myanmar will notify the IAEA on the entry into force of the AP when the Government is prepared for its implementation. With the support of IAEA, USDOE and other member states, Myanmar will continue to live up to the expectation of the international community in ensuring the peaceful use of nuclear energy, while contributing to the non-proliferation of nuclear weapons.

Acknowledgement

The author would like to express highly appreciation to the United State Department of Energy, Office of International Safeguards, and Pacific North-west National Laboratory (PNNL) for their financial support to attend this symposium as well as for their continuous cooperation and encouragement in implementing Safeguards and Non-Proliferation regime in Myanmar. Special thanks go to her colleagues and especially to Ms. Andrea Braunegger-Guelich, Safeguards Training Officer, Division of Concepts and Planning, Departments of Safeguards, Internatioanl Atomic Energy Agency (IAEA), and Dr. Aung Tharn Daing, Department of Atomic Energy, Ministry of Education, Myanmar, who has been supportive of writing this paper, for fruitful discussions and valuable suggestions.

References

[1]. David Santoro, *Special Report*, ASPI, Australian Strategic Policy Institute, March 2017

[2]. Aung Ko Min, Deputy Director, Ministry of Foreign Affairs, Myanmar, *Myanmar-DPRK relations: Disarmament and nuclear nonproliferation dimension*, May 2016

[3]. Marko Hämäläinen, Radiation and Nuclear Safety Authority (STUK), Helsinki, Finland Olli Okko, Radiation and Nuclear Safety Authority (STUK), Helsinki, Finland Tapani Honkamaa, Radiation and Nuclear Safety Authority (STUK), Helsinki, Finland Elina Martikka, Radiation and Nuclear Safety Authority (STUK), Helsinki, Finland, SSAC at your service*: Promoting Cooperation between IAEA and Finish SSAC for Safeguards Implementation (within EU),* Symposium on International Safeguards SG 2014, 20-24 October 2014

Interlaboratory comparison on ^{243}Am reference material for nuclear safeguards and security

M. Crozet[1], D. Roudil[1], C. Bertorello[1], C. Maillard[1], C. Rivier[1], R. Jakopič[2], A. Fankhauser[2], Y. Aregbe[2], S. Richter[2], T. Altzitzoglou[2]

[1]*Commissariat à l'énergie atomique et aux énergies alternatives (CEA/DEN), Centre de Marcoule, BP 171, 30207 Bagnols-sur-Cèze cedex, France*

[2]*European Commission, Joint Research Centre (JRC), Directorate for Nuclear Safety and Security, Standards for Nuclear Safety, Security and Safeguards, Retieseweg 111, 2440 Geel, Belgium*

Americium is a transuranic element produced by neutron capture in nuclear reactions. In spent nuclear fuel, ^{241}Am and ^{243}Am contribute greatly *as* their daughters ^{237}Np and ^{239}Np to the radiotoxicity of long-lived radioactive waste. Americium contamination in the environment as a result of leakage from repository nuclear facilities also presents a great concern.

The need for an americium spike Certified Reference Material (CRM) was expressed at the last IAEA Technical Meeting on Reference Materials for Destructive Analysis in the Nuclear Fuel Cycle and in the 2016 Nuclear Security Summit: ^{243}Am spike CRM is needed for accurate measurements of ^{241}Am in nuclear materials. In nuclear forensics, such a CRM can be applied in Am/Pu chronometry to determine the elapsed time of the last chemical purification of plutonium and enables the determination of "the age" of plutonium material. Currently there is no ^{243}Am spike CRM commercially available.

In 2014, CEA/DEN Marcoule (France) and JRC-Geel (EC) initiated a joint project for the production and certification of a highly enriched ^{243}Am reference material. The source material, about 3 mg americium (88 % ^{243}Am and 12% ^{241}Am) was provided and purified by extraction chromatography at CEA/LAMM (Material Analysis and Metrology Laboratory) and shipped to JRC-Geel for final processing, packaging and certification. A total of 587 units were produced, each containing about 3.5 mL of diluted nitric acid solution with an americium mass fraction of about 1.5 $\mu g \cdot g^{-1}$. This reference material, produced in compliance with ISO Guide 34, was certified by JRC-Geel: certification relates to ^{243}Am and ^{241}Am amount contents, $n(^{241}\text{Am})/n(^{243}\text{Am})$ and $n(^{242m}\text{Am})/n(^{243}\text{Am})$ amount ratios.

Furthermore, CEA/CETAMA organises an interlaboratory comparison (ILC) on this material, prior to the release of the material and issuance of the certificate. Measurands of this comparison are the ^{243}Am and ^{241}Am amount contents, $n(^{241}\text{Am})/n(^{243}\text{Am})$ and $n(^{242m}\text{Am})/n(^{243}\text{Am})$ ratios, i.e. the measurands certified by JRC-Geel. About ten international laboratories (from Europe and US) have registered to participate in this comparison exercise. Participating laboratories are asked to report their results before the end of March 2017. The results to this interlaboratory comparison will be compared to the certified values obtained by JRC Geel.

The approach for this interlaboratory comparison organization on this ^{243}Am spike and the first results of the ILC will be presented.

Keywords: Americium, Nuclear Safeguards, Nuclear Forensics, Interlaboratory Comparison, ILC, Certified Reference Materials

Delayed Gamma-ray Analysis for Characterization of Fissile Nuclear Materials

Mitsuo Koizumi[1] Fabiana Rossi[1], Douglas C. Rodriguez[1], Jun Takamine[1], Michio Seya[1], Tatjana Bogucarska[2], Jean-Michel Crochemore[2], Giovanni Varasano[2], Kamel Abbas[2], Bent Pederson[2], Jan Heyse[3], Carlos Paradela[3], Willy Mondelaers[3], and Peter Schillebeeckx[3]

[1]Japan Atomic Energy Agency (JAEA)
Tokai-mura, Naka-gun, Ibaraki 319-1195, Japan
E-mail: koizumi.mitsuo@jaea.go.jp

[2]European Commissions' Joint Research Centre,
Via Enrico Fermi 2749, I - 21027 Ispra (VA), Italy

[3]European Commissions' Joint Research Centre, Retieseweg 111, B-2440 Geel, Belgium

Abstract:

Under the collaboration between the Japan Atomic Energy Agency (JAEA) and European Commissions' Joint Research Center (EC-JRC), development of four active neutron-interrogation non-destructive assay methods for nuclear non-proliferation and safeguards are in progress. The techniques under the development are differential die-away analysis, delayed gamma-ray analysis (DGA), neutron resonance transmission analysis, and prompt gamma-ray analysis. Information obtained by each method is used complementarily to characterize a sample. DGA utilizes moderated pulsed neutrons from a D-T neutron generator to induce fission reaction of nuclear materials. Delayed gamma rays from the fission products (FP) are measured to determine the ratios of fissile nuclides (e.g. ^{235}U, and ^{239,241}Pu) in the sample. Experimental studies of the DGA method are in progress. Delayed gamma ray spectra from nuclear materials were successfully observed with the Pulsed Neutron Interrogation Test Assembly (PUNITA) in EC-JRC Ispra. Here we present an overview of the study plan of these DGA experiments along with the latest results.

Keywords: Non-destructive assay (NDA); active neutron NDA;

1. Introduction

Increasing global applications using nuclear materials (NMs) requires improved characterization methods for nuclear security and safeguards. Mass verification of NMs is generally performed using passive non-destructive assay (NDA) techniques for low radioactive samples with destructive analysis (DA) techniques applied for accurate analysis of nuclide composition. A sample with high radioactivity, however, is difficult to characterize through passive NDA methods and careful sample treatment is required for DA that also produces a vast amount of radioactive waste. Active NDA techniques that utilize interrogation particles (such as photons and neutrons) to induce nuclear reactions are potentially applicable to extract information of NMs from a high radioactive sample.

An active-neutron NDA system equipped with a D-T pulsed-neutron generator was proposed by the Japan Atomic Energy Agency (JAEA) [1]. Multiple techniques are under consideration for the system: Differential Die Away Analysis (DDA) [2,3] for the determination of total fissile content, Delayed Gamma-ray Analysis (DGA) [4–7] for the evaluation of relative mass ratio of fissile nuclides (i.e., ^{235}U, ^{239}Pu, and ^{241}Pu), Neutron Resonance Transmission Analysis (NRTA) [8] for quantification of U and Pu isotopes, and Prompt Gamma-ray Analysis (PGA) [8] for detection and quantification of specific nuclides. Information obtained by each method is used complementarily to characterize a sample. Technical developments of these methods are in progress under the collaboration with the European Commission's Joint Research Center (EC-JRC).

Among those four techniques, DGA measures decay γ-rays from fission products (FP) produced by the neutron induced fission reactions. The observed γ-ray peak intensity ratios of a spectrum are used for determining the ratio of the original fissile nuclides. Using the high-energy (HE) delayed γ-rays from the relatively short-lived nuclides avoids the prominent background γ-rays from long-lived FP in a sample [6, 7]. This paper describes the DGA development program and experimental results [9].

2. A System for DGA for Nuclear Material Characterization

The mass distribution of fission products is characterized by the parent nuclide (^{235}U, ^{239}P, and ^{241}Pu) and the incident neutron energy. Significant differences in distribution of nuclide produced by fission reaction between each fissile nuclide are seen. Because of the difference, a different delayed gamma-ray (DG) spectrum is observed for each fissile nuclide enabling the ratios of fissile nuclides (^{235}U, ^{239}Pu, and ^{241}Pu) in a sample to be evaluated. According to the nuclear data the FY distribution dose not changes much for interrogation neutrons with energies between the 0.0253 eV (thermal) and 500 keV (intermediate). At 14 MeV (high), however, the FY distribution changes significantly. This would make the analysis of DGA difficult. In addition, the fission cross-section of ^{238}U, which is usually the dominant nuclide in a sample, is 10^8 times smaller than that of the fissile nuclides at less than 10^4 eV, and suddenly increases at more than around 1 MeV to become as large as those of the fissile nuclides. The fission cross section of ^{238}U with about 1 MeV neutrons is, however, still about 10^4 times less than that of fissile nuclide with thermal neutrons. Nevertheless, the contribution of fission of ^{238}U with about 1 MeV neutron will not be negligible if such high energy neutrons exist much. Because of that, well-thermalized neutron field is preferable for DGA application.

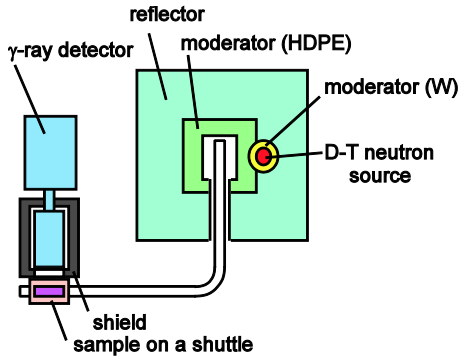

Fig.1. A conceptual view of DGA setup.

In our project, a deuterium-tritium (D-T) neutron generator is used for DGA measurement because it is compact and has a relatively high neutron flux. The kinetic energy of the neutrons from a D-T neutron generator is as high as 14 MeV. Therefore, a well-designed moderator and reflector system is required to obtain an intense and well-thermalized neutron field. Figure 1 shows a conceptual view of a system for DGA with a D-T neutron generator [10]. The W ring around the D-T generator is for neutron multiplication by the (n, 2n) reactions [11]. The high density polyethylene (HDPE) is used for neutron slowing down. The graphite reflector reduces neutron escaping from the cavity. The shuttle system carries in and out a sample for neutron irradiation and measurement in a low background environment. This also reduces the neutron damage to the detector.

3. DGA Experiments with PUNITA

Experimental studies to develop a DGA system are in progress with the Pulsed Neutron Interrogation Test Assembly (PUNITA) [11, 12] at EC-JRC Ispra. The test assembly consists of thick walls dominantly made from a graphite inner layer and a high-density polyethylene (HDPE) outer layer. The inner cavity is 50 cm in width and length and 80 cm tall. A standard pulsed 14-MeV D-T neutron generator (Thermo Fisher Scientific Corp., A-211, 2 × 10^8 n/s neutron emission) is placed in it. Around the generator, 4.5-cm thick tungsten rings can be used for neutron multiplication.

In DGA experiments, one of the cavity walls is partially open for sample transportation between the cavity and a γ-ray detector system, which is about 1

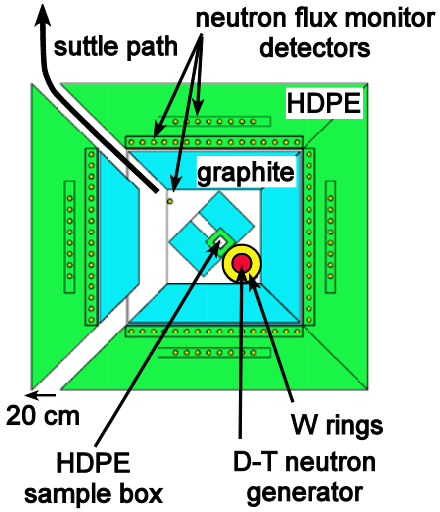

Fig. 2. Horizontal cross-sectional geometry for a simulation of PUNITA. Additional moderators and reflectors were installed in the PUNITA cavity. The HDPE sample box is placed as near as possible.

m away from PUNITA. This open channel allows some escape of neutrons to decrease the neutron flux in the cavity. To recover the reduction and to further thermalize the neutrons, additional moderator and reflector material are introduced in the cavity. An optimal condition was surveyed by using MCNP [13]. Figure 2 shows an adopted geometry. In the cavity, a carbon block of 26 cm (W), 26 cm (L), and 38 cm (H) with an 18-cm-square tunnel for sample transportation was installed. The sample volume is placed close to the neutron source point, and is surrounded by a 3 cm thick HDPE filter. The carbon block works for reflecting neutrons (i.e., preventing them from going away) and the HDPE box for reflecting and slowing down them.

Table 1. Evaluated neutron flux normalized by 10^8 n/s neutron emission from a neutron generator. The unit of the flux is $\times 10^3$ n/cm^2/s.

geometry	(a)	(b)	(b')
thermal	150	8.4	4.8
14-MeV	7.7	2.5	5.4

Neutron flux was evaluated using MCMP code with geometries as follows: (a) neutron flux in the HDPE sample box of Fig. 2; (b) neutron flux at the center of the cavity without the additional moderator and reflector, and with the cavity wall closed; (b') neutron flux of (b) without the W rings. The results are given in Table 1. The thermal flux is the integral through 0.5 eV, and the 14-MeV flux is an integral from 13 MeV to 15 MeV. Comparing (b) and (b') indicates that the W rings increase thermal neutrons and decrease about 14 MeV neutrons. Thermal neutron flux obtained by the geometry (a) is much larger than that of (b) which represents the normal use of PUNITZ. For DGA experiments, available HDPE and carbon blocks were piled up so as to reproduce a modified but similar moderator structure.

Two HPGe detectors were used for measurement concurrently: CANBERRA GR-2520 (P-type 25%), and ITECH Instruments NIGC 50220 (N-type 50%). The outputs of each HPGe detector were sent to two different data acquisition (DAQ) systems. One was a conventional NIM based system consisting of spectroscopy amplifiers (Ortec 672 and 673) and a dual-input multichannel analyzer system (Otrec Aspec-927). The other was a waveform digitizer (CAEN V1730) equipped with pulse height analyzing firmware (CAEN DPP-PHA) that analyses an input waveform to evaluate the pulse height of each event and stored with the associated time stamp (list mode measurement).

A sequence of 50-s neutron irradiation, 5-s transportation to the measurement position, 150-s measurement, and 5-s transportation back for irradiation was repeated for each measurement. The start signal of the one sequence was given manually because of a rule of safety operation. The signal is sent to a digital delay/pulse generator (BNC 575), which controlled the neutron irradiation (100-Hz neutron generation), transportation, neutron flux monitor, and γ-ray measurement. The sequence repeated 20 times for one DGA measurement (i.e., approximately 1.2 h). Figure 3 shows a result of a uranium oxide standard sample (CBNM-446) measurement that contained 169-g total Uranium sample with a 4.46% concentration of ^{235}U. Peak assignment was based on the ENDF database [14] and comparison to Refs. [4–7]. Many of identified γ-ray peaks are from parents nuclides with a lifetime in a range from few 10 sec. to several minutes: ^{87}Br, ^{89,90,90m,91}Rb, ^{95}Y, ^{95}Sr, and ^{136}I. ^{208}Tl is contained radioactivity in the sample. Neutron activation products of ^{27}Al(n, γ)^{28}Al, ^{27}Al(n, α)^{24}Na, and ^{16}O(n, p)^{16}N were also observed, the last two indicative of high-energy neutrons (~10 MeV) interactions.

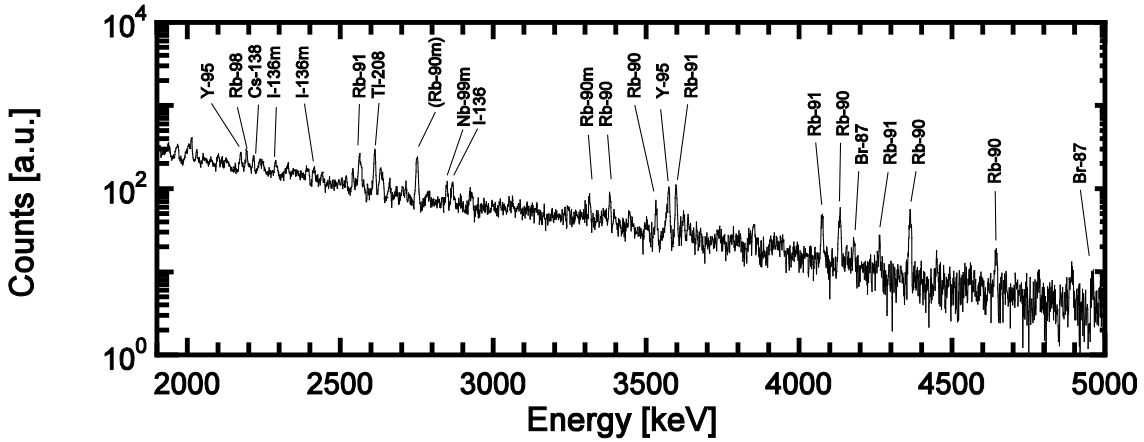

Fig. 3. A γ-ray Spectrum of a CBNM-446 sample. The triangle marks indicate that the same peak identification of the upper spectrum.

4. Summary and Prospect

We are developing DGA technology to determine the ratios of ^{235}U, ^{239}Pu, and ^{241}Pu in a sample. This NDA method is especially useful for measuring samples with high radioactivity, where conventional passive low-energy γ-ray spectroscopic methods cannot be applied. Experimental studies with PUNITA have started at EC-JRC Ispra with prominent γ-ray spectral peaks from ^{235}U and fissile Pu were observed.

In order to increase a neutron flux and to reduce the sample transportation time, we modified PUNITA. A small square opening of (10 X 20 cm) was made in the bottom of the cavity. The small opening is expected to reduce the escape of neutrons and allow a linear transport system to be placed in the opening. An HP-Ge detector will be placed the under PUNITA with the irradiated sample transported to in front of the detector in a second. This will allow us to observe the decay γ-rays from short-lived FP nuclides.

To analyze an experimental spectrum, a DGA Monte Carlo simulation code is under the development. Inputting the calibrated neutron spectrum, sample composition, time sequence of irradiation-transport-observation, and materials around the detectors (neutron filters and γ-ray shielding) results in DG spectra comparable to measured data. Consequently, the code will be incorporated into an analysis program to fit an experimental spectrum using an Inverse Monte Carlo (IMC) method [15].

In addition to the development of DGA method, nuclear data such as FY must be confirmed and improved in accuracy and availability. Measurements of FY of NMs are in preparation.

5. Acknowledgements

This technological research and development was supported by the Japanese government (MEXT), and implemented under the agreement between JAEA and EURATOM in the field of nuclear materials safeguards research and development.

References

[1] M. Kureta, et al., "JAEA-JRC Collaboration on the Development of Active Neutron NDA Techniques", in the Proceedings of 37th ESARDA Symposium on Safeguards and Nuclear Non-Proliferation (Manchester, UK 19-21 mat 2015), p. 111-120.
[2] I. Israelashvili, C. Dubi, H. Ettedgui, A. Ocherashvili, B. Pedersen, A. Beck, E. Roesgen, J.M. Crochmore, T. Ridnik, I. Yaar, Nuclear Instruments and Methods in Physics Research A 785, 14 (2015).
[3] A. Ohzu, M. Koneda, M. Kureta, N. Zaima, Y. Nakatsuka, S. Nakashima, Transactions of the Atomic Energy Society of Japan 15, 115 (2016) (in Japanese).
[4] D. H. Beddingfield and F. E. Cecil, Nucl. Instr. and Meth. in Phys. Res. A 417, 405 (1998).
[5] C.E. Egnatuk, "Identifying short-lived fission products by delayed Gamma-ray emission", Thesis of Univ. Texas, 2009.
[6] L.W. Campbell, L.E. Smith, and A.C. Misner, IEEE Transactions on Nucl. Sci. 58, 231 (2011).
[7] B. Ludewigt, V. Mozin, L. Campbell, A.Favalli, A. Hunt, E. Reedy, and H.Seipel, "Delayed Gamma Ray Spectroscopy for Non-Destructive Assay of Nuclear Materials", LLNL-TR-677606, (2015).
[8] H. Postma, and P. Shillebeeckx, in Encyclopedia of Analytical Chemistry, edited by R.A. Meyers (John Wiley & Sons Ltd., 2009) p. 1.
[9] M. Koizumi, F. Rossi, D.C. Rodriguez, J. Takamine, M. Seya, T. Bogucarska, J.M. Crochemore, G. Varasano, K. Abbas, B. Pederson, M. Kureta, J. Heyse, C. Paradela, W. Mondelaers, and P. Schillebeeckx, to be published in EPJ web conferences.
[10] J. Takamine, D.C. Rodriguez, M. Seya, and M. Koizumi, *"Design study of neutron moderator and filter in a delayed gamma-ray measurement system using a 14 MeV D-T neutron source"*, in the 65th Annual meeting of Institute of Nuclear Materials Management (INMM).
[11] A. Favalli, H.-C. Mehner, J.-M. Crochemore, and B. Pedersen, IEEE Transactions on Nucl. Sci. 56, 1292 (2009).
[12] H. Rennhofer n, J.-M. Crochemore, E. Roesgen, B. Pedersen, Nucl. Instr. Meth. in Phys. Res. A 652, 140 (2011).

[13] X-5 Monte Carlo Team, "MCNP - A General N-Particle Transport Code, Version 5" Volume I: Overview and Theory, LA-UR-03-1987 (2003, updated 2005).
[14] Evaluated Nuclear Structure Data File of National Nuclear Data Center (http://www.nndc.bnl.gov/).
[15] D.C. Rodriguez to be submitted.

Investigation of the Measurement Capabilities of an Advanced In Situ Gamma Spectrometry Service

Ludovic Bourva*, Patrick Chard*, Blanche Vendittozzi*, Thomas Kirk*, Xavier Ducoux, Gabriela Ilie***, Henrik Jäderström***, Wilhelm Mueller*****

*Mirion Technologies (Canberra UK) Limited, Harwell Oxford, Building 528.10 Unit 1, , OX11 0DF United Kingdom

** Mirion Technologies (Canberra France) SAS, 1 rue des hérons, 78180 St Quentin-en-Yvelines, France

*** Mirion Technologies (Canberra Inc.), 800 Research Pkwy, Meriden, CT 06450, USA

Abstract:

Mirion Technologies' In Situ Object Counting System (ISOCS) is well established as a numerical tool for calibrating spectrometric gamma-ray detectors performing quantitative assay of nuclear material. The code allows through a set of geometry templates complex measurement geometries to be quickly modelled and mathematical calculation of the detector's efficiency response to be derived. This technique can be used with field-deployable mobile detectors to perform in-situ assays on challenging items in difficult environments. Complementary to the determination of an efficiency result, the ISOCS Uncertainty Estimator tool (IUE) can be used to calculate defensible systematic calibration uncertainties associated with the ISOCS efficiency data. However, these measurement uncertainties mainly depend on knowledge/assumptions of the properties of the item being measured, alongside assumptions made on the uniformity of the gamma nuclides location in the modelled active source volume. In the case of measurements performed on poorly characterized items, legacy waste items, or with objects showing a significant degree of source non-uniformity, these systematic calibration uncertainties can lead to potentially very large total measurement uncertainties and these are common to any traditional Non Destructive Assay technique.

Mirion Technologies has launched a new ISOCS–based advanced in-situ gamma spectrometry (AIGS) services tool in order to provide more accurate assay solutions. This tool is based on generating and comparing a range of candidate geometry models that can be ranked by figures of merit indicative of improved consistency between modelled data and available diverse measurement data. The models are compared allowing a best-fit model to be developed, with corresponding efficiency calibration data and matching uncertainties.

The present work reports on the expansion of previously published work on the evaluation of the capability of the AIGS approach to provide improved accuracy over standard ISOCS analyses. In particular, we present here detailed results on a set of measurements performed with a multiple-nuclide line source (^{133}Ba, ^{137}Cs, ^{152}Eu and ^{241}Am) positioned at varied locations in a fairly dense 200 litre waste drum and comment on how the AIGS results are affected by assumptions taken in the AIGS geometry optimisation process. In particular, we focus on the function and performance of AIGS in dealing with potential non-uniform distributions of activity in the form of potential multiple hotspots co-existing in a drum and density uncertainty.

Keywords: Gamma Spectrometry, ISOCS, AIGS, Numerical Calibration, Systematic Error

1 INTRODUCTION

Mirion Technologies In Situ Object Counting System (ISOCS) [**1**,**2**] is a well-qualified numerical calculation software used to determine absolute efficiencies of gamma ray detectors when performing quantitative gamma spectrometry. The ISOCS application relies on pre-set geometry templates to model a given measurement geometry. The specific geometry of the measurement conditions hence rely on discrete entries of key parameters. The efficiency results obtained from ISOCS therefore carry

some intrinsic systematic errors associated with the validity of the assumptions taken to describe the measured item/measurement geometry. Conscious of this limitation Mirion Technologies has further developed the ISOCS capability to support an ISOCS Uncertainty Estimator (IUE) [**3**,**4**]. This automated application allows for distributions of values for all parameters to be specified so that, still using a traditional ISOCS template, those can be sampled to generate through multiple ISOCS calculations distribution of efficiency results. The result is a powerful tool allowing for the importance of key parameters influencing the efficiency results to be established. ISOCS-IUE also allows calculating from the overall distribution of efficiency results an estimate of the overall modelling systematic uncertainty associated with an ISOCS efficiency calibration.
Although the capability to reliably estimate the systematic uncertainty associated with an ISOCS efficiency calibration is of great advantage to accurately bound uncertainties associated with some measurement applications, the real gain in terms of cost disposal clearly lies in being able to reduce these uncertainties, and in providing more accurate quantifications. Reducing the ISOCS systematic uncertainty could be achieved by identifying which ISOCS models generated within the IUE automation process are indicative of improved consistency between modelled data/derived activities and some available measurement data.
The Advanced In-situ Gamma Spectrometry (AIGS) services offered by Mirion Technologies as part of an ISOCS based spectroscopy measurement service also includes an ISOCS geometry optimisation step. This step is aiming at improving the accuracy of the measurement results. For each IUE generated model, the AIGS algorithms calculate a set of Figures of Merit (FoM) allowing ranking the consistency of the model's efficiency results against specific measurement data/results. For example, in the case of the measurement of a radionuclide emitting several gamma-rays the Line Activity Consistency Evaluation (LACE) which looks at the consistency of the derived nuclide activity across all energies can be used as a FoM to evaluate the validity of the shape of the ISOCS efficiency curve. The AIGS analysis can also be performed by evaluating the consistency of the ISOCS results obtained when analysing multiple spectra collected when measuring the same item under different fields of view (sides, below, above, specific angles...)
Note that the AIGS approach is simply based on inferring how some of the model assumptions are clearly not consistent with the observed results. It is therefore perfectly conceivable that, within the set of modelling assumptions, several models may return consistent answers through the calculated FoM, yet yielding a spread of activity results. This is taken into account in the AIGS analysis by reporting an uncertainty result on the "best optimized efficiency" that is illustrative of the level of convergence of the optimisation. The AIGS analysis supports ISOCS model generation using different numerical methods [**5**]. This allows a very significant reduction of the computation times that would otherwise be required if using only a pure random sampling of the model's variable parameter space. Mirion Technologies has also performed several exercises to evaluate the AIGS capabilities and demonstrate the practical benefits that can be realised [**6**,**7**].
Early reported work focussed on laboratory applications and also 200 litre drum measurements using ^{152}Eu point sources, which represent idealised sources for physics testing [**8**]. More recent efforts have been directed towards applications in waste management, such as those reported for the measurements and AIGS analysis for a set of measurements using a 200 -litre waste drum filled with a low-density matrix [**9**]. This work focussed on ^{241}Am assay, representative of typical Very low level plutonium assay in low density soft wastes, and showed overall some degree of improvement in the accuracy of the assay results. The present work is an extension of the results reported to date [**10**] and concentrates on the analysis of a set of measurements performed at the Harwell facility in 2015 and their subsequent analysis using the AIGS approach.

2 EMPIRICAL WORK

The object that has been used in the empirical work was a 200-litre reference calibration drum filled with uniform particle board (density 0.681 g.ml^{-1}). The diameter of the drum is 570 mm and the height of the drum is 870mm.

A short line source, ≈ 280 mm long, was placed in the drum inserts. Measurements were made with the source at 2 different heights (Top/1 and Middle/2) and 3 different radial positions: one at the edge of the drum (Position 7/case c) one at a mid-radius (position 3/case b) one and the last in the centre of the drum (position 0/case a). The empirical data set used in the present work consisted of 6 spectral

sets (1a – 3 spectra/1b – 24 spectra /1c -24 Spectra /2a – 12 spectra /2b – 24 spectra /2c -19 spectra.)

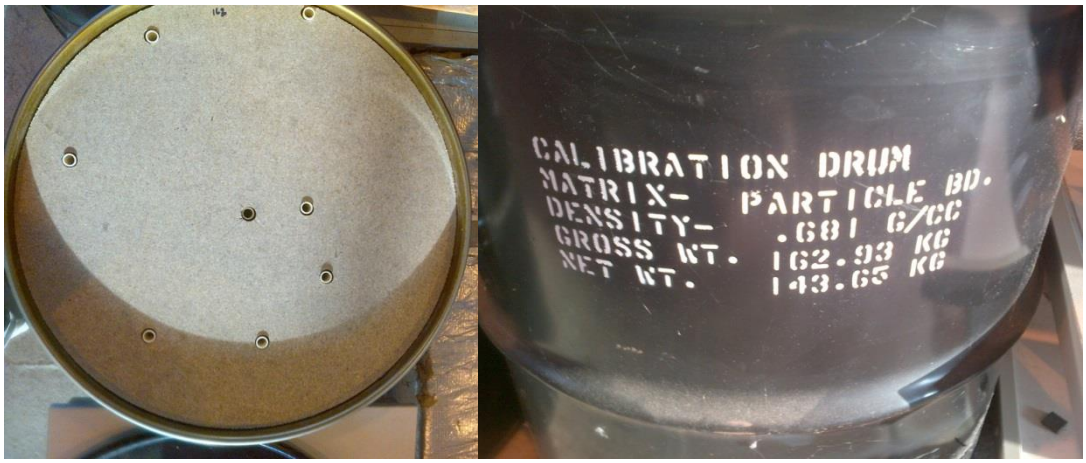

Figure 1. Side and Top view of the drum

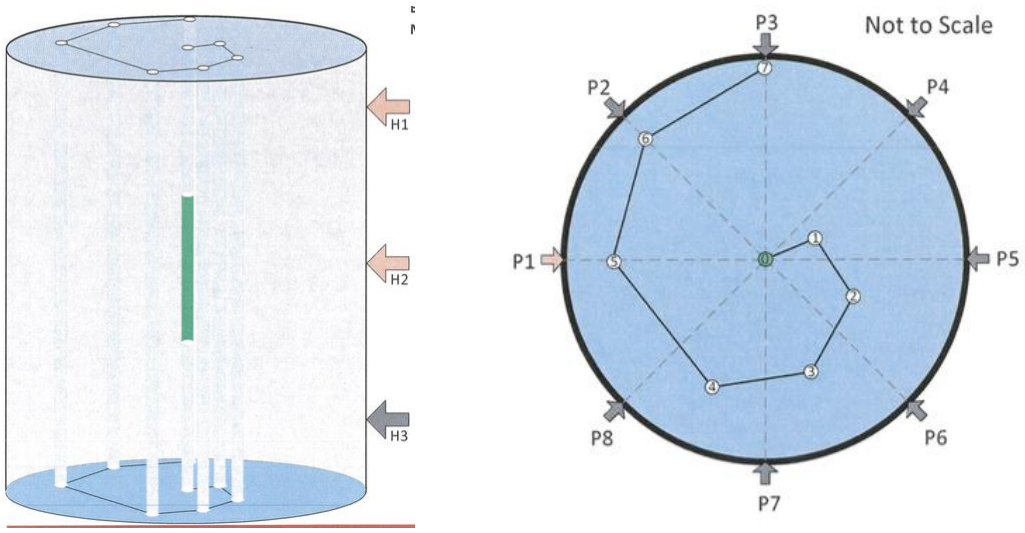

Figure 2. Source Positioning in the Calibration Drum

The drum was static during the measurement and only rotated (by 45 degrees step) between acquisitions to generate different counting geometries. Each source position could therefore produce up to 24 spectra (8 angular positions by 3 detector heights), each representing 2000 s of live data acquisition. Overall, this data set probably holds far more information than would reasonably be expected to be available when assaying a single 200-l waste drum. However it constitutes a good set to evaluate the sensitivity of the AIGS approach to the availability of measured data.
The measurements were made with an ISOCS characterised Broad-Energy Germanium detector (BEGe-2830), and a 180° opening, 50 mm thick lead collimator. The front face of the detector end-cap was positioned at 70 cm of the drum edge. The short line source contained 4 different nuclides with the evaluated activity listed in Table 1.

	Radionuclides			
	Am-241	Ba-133	Eu-152	Cs-137
Decay Corrected Activity [kBq]	790.14	182.34	216.37	63.16
Uncertainty [kBq]	24.54	9.29	11.08	1.33
Rel. Uncertainty [%]	3.11	5.10	5.12	2.11

Table 1. Reference activity of the line source when decay corrected to the measurement date

3 ISOCS MODELLING

3.1 ISOCS Geometry

Standard ISOCS models of the waste drum were developed using the complex cylinder template of the geometry composer application, as shown in Figure 3. These models, one for each detector position, assume a uniform distribution of the source activity in the particle board matrix. A secondary model introducing a small “hot spot” concentrating all the activity of the waste was also developed to perform ISOCS-IUE and AIGS analysis. All standard ISOCS models assume the same declared matrix material composition and reference density of 0.681 $g.ml^{-1}$.

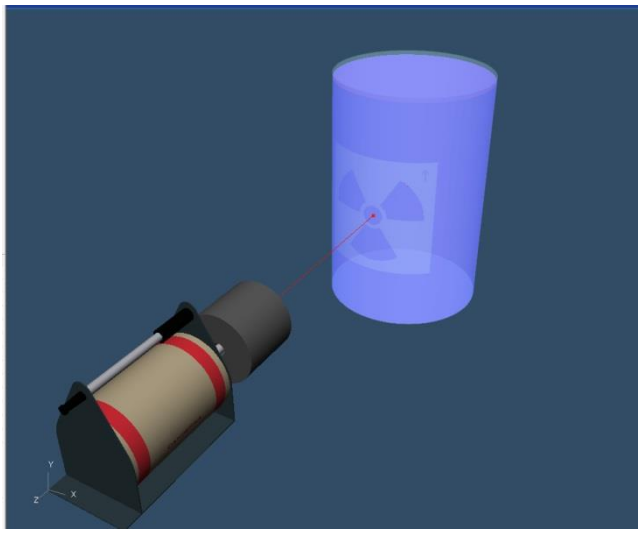

Figure 3. Standard ISOCS model of the measurement geometry with the detector in the H2 position

3.2 BASELINE AIGS ANALYSIS

The details of the AIGS analysis performed on the measured set of empirical spectra have been reported elsewhere [**10**]. However to present a consistent set of results an allow easier comparison the present paragraph will briefly introduce baseline AIGS results. The ISOCS geometry optimisation was run using both “Best Random Fit” (BRF), in other words, pure random sampling, and the “Simplex” acceleration algorithm. The optimisation was performed only on the basis of a multi-spectra FoM.
Best efficiency results computed by the AIGS application for each detector positions were subsequently used to analyse the measured spectra. From these computations one can observe the following:

- BRF and Simplex optimisation results are consistent with each other for all cases
- AIGS results tend to slightly overestimate the know ^{152}Eu activity in the drum, especially when the source was located at the “Edge” of the drum
- Standard ISOCS results perform poorly for this measurement set-up and AIGS provide a significant improvement

Overall activity results for all four nuclides for the 6 source positions are shown in Figure 4. The 6 plots show graphically how the AIGS analysis improves significantly the baseline assay results independently of the line source position in the drum.
The graphs, shown in Figure 4, show that the AIGS quantifications yield significant improvement on the overall accuracy of the waste assay. AIGS results obtained when the source was positioned at a radial position show almost perfect agreement with the reference data. Positions with the source positioned at the centre of the drum shows a tendency for AIGS results to slightly over-estimate the reference values, although within the stated uncertainties. The overall assay results and relative difference relative to the line source activity are given in Table 2.

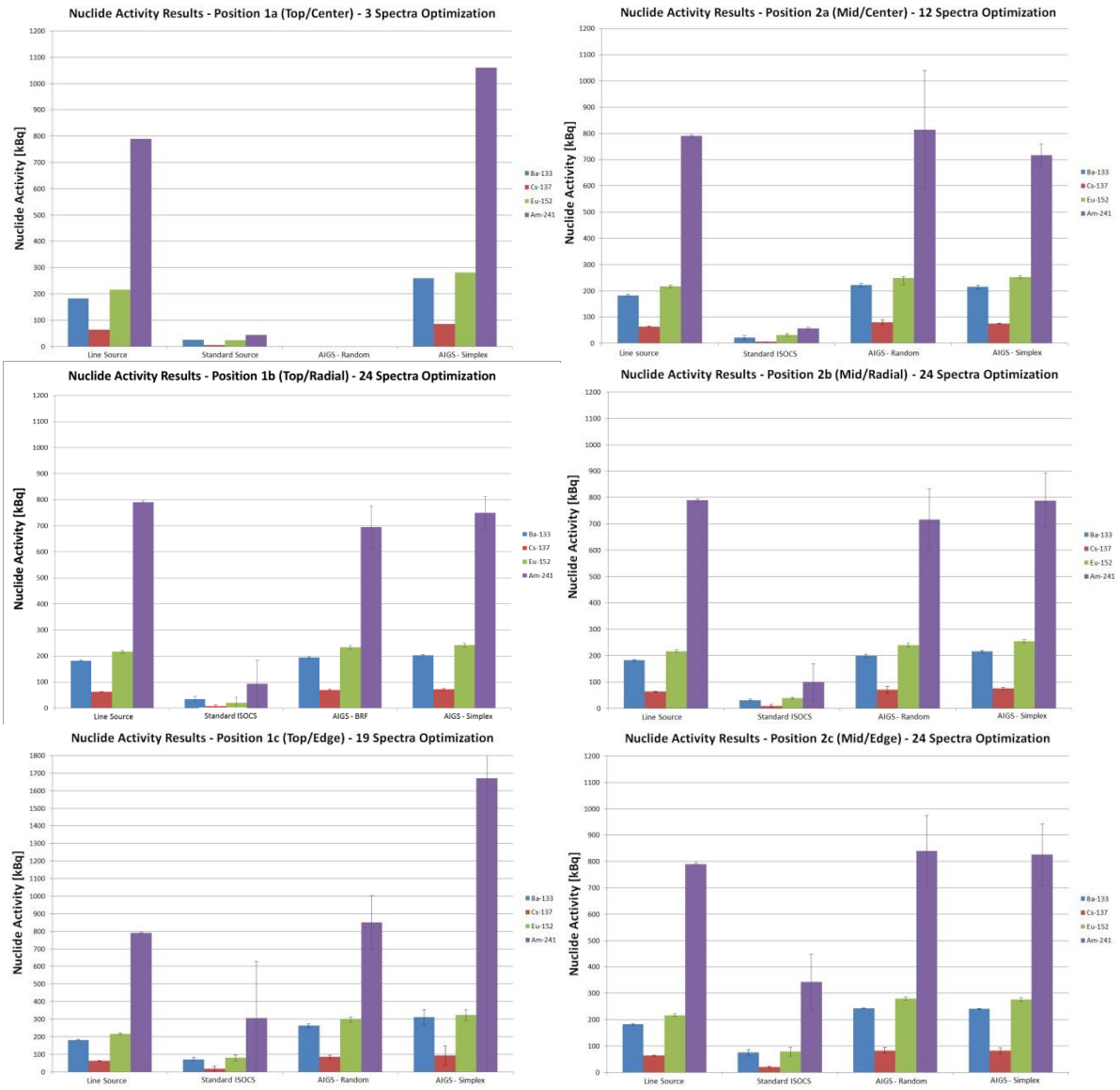

Figure 4. Graphical representation of the overall nuclide activity quantifications using ISOCS and AIGS analyses for 6 source positions

3.3 FURTHER AIGS ANALYSIS

The results shown in the previous section have shown that both AIGS analyses performed well under the conditions and amount of data available to perform the optimisation. To further evaluate the AIGS approach complementary work was performed to study the reliability of the obtained results with changes in optimisation parameter assumptions and amount of available measured data to perform the AIGS geometry optimisation.

3.3.1 Measured Data Availability

To evaluate the impact of the availability of measured data the AIGS analysis was repeated with only 6 or 4 or even only 2 measured spectra to conduct the AIGS optimisation process. The list of spectra retained for this study and the corresponding angular position/height of the detector are shown below:

- 6 Spectra: H1-P3, H1-P7, H2-P1, H2-P5, H3-P3, H3-P7
- 4 Spectra: H1-P3, H1-P7, H2-P1, H2-P5
- 2 Spectra: H1-P1, H3-P5

The AIGS optimisation using BRF and Simplex approach was performed for the position 1b case where the line source positioned at a mid-radial position in the waste drum had been measured at 8

angular positions and with the detector at 3 heights (24 spectra in total). Figure 5 shows the overall nuclide activity results derived from the AIGS analyses. The study kept all other modelling assumptions (Number of hot-spots, matrix density…) unchanged compared to the optimisation results shown earlier.

Position 1a

	AIGS Optimization: 3 Spectra		Std. ISOCS		AIGS - BRF		AIGS - Simplex	
	Reference Activity [kBq]	Uncert [kBq]	Relative Difference	Uncertainty	Relative Difference	Uncertainty	Relative Difference	Uncertainty
Ba-133	182.3	3.1	-85.7%	27.5%	N/A	N/A	42.6%	9.3%
Cs-137	63.2	2.1	-92.1%	30%	N/A	N/A	34.5%	23.1%
Eu-152	216.4	5.1	-89.0%	24%	N/A	N/A	30.3%	6.8%
Am-241	790.1	5.1	-94.5%	13%	N/A	N/A	34.3%	32.5%

Position 2a

	AIGS Optimization: 3 Spectra		Std. ISOCS		AIGS - BRF		AIGS - Simplex	
	Reference Activity [kBq]	Uncert [kBq]	Relative Difference	Uncertainty	Relative Difference	Uncertainty	Relative Difference	Uncertainty
Ba-133	182.3	3.1	-88.1%	32.0%	N/A	N/A	17.7%	3.6%
Cs-137	63.2	2.1	-90.9%	7%	N/A	N/A	18.7%	3.6%
Eu-152	216.4	5.1	-85.5%	16%	N/A	N/A	16.4%	3.2%
Am-241	790.1	5.1	-92.9%	10%	N/A	N/A	-9.3%	5.9%

Position 1b

	AIGS Optimization: 24 Spectra		Std. ISOCS		AIGS - BRF		AIGS - Simplex	
	Reference Activity [kBq]	Uncert [kBq]	Relative Difference	Uncertainty	Relative Difference	Uncertainty	Relative Difference	Uncertainty
Ba-133	182.3	3.1	-81.1%	31%	6.3%	2.7%	11.5%	2.2%
Cs-137	63.2	2.1	-86.7%	70%	9.9%	6.6%	14.6%	6.3%
Eu-152	216.4	5.1	-90.6%	100%	7.7%	3.9%	11.7%	3.6%
Am-241	790.1	5.1	-88.1%	95%	-12.1%	11.7%	-5.2%	8.5%

Position 2b

	AIGS Optimization: 24 Spectra		Std. ISOCS		AIGS - BRF		AIGS - Simplex	
	Reference Activity [kBq]	Uncert [kBq]	Relative Difference	Uncertainty	Relative Difference	Uncertainty	Relative Difference	Uncertainty
Ba-133	182.3	3.1	-83.2%	11%	9.0%	3.8%	18.2%	3.1%
Cs-137	63.2	2.1	-85.1%	63%	12.1%	17.5%	18.5%	6.5%
Eu-152	216.4	5.1	-82.4%	11%	10.6%	3.9%	17.6%	3.2%
Am-241	790.1	5.1	-87.6%	71%	-9.5%	16.4%	-0.2%	13.1%

Position 1c

	AIGS Optimization: 19 Spectra		Std. ISOCS		AIGS - BRF		AIGS - Simplex	
	Reference Activity [kBq]	Uncert [kBq]	Relative Difference	Uncertainty	Relative Difference	Uncertainty	Relative Difference	Uncertainty
Ba-133	182.3	3.1	-60.6%	15%	44.3%	4.2%	71.4%	13.4%
Cs-137	63.2	2.1	-70.8%	71%	35.7%	11.1%	48.4%	58.4%
Eu-152	216.4	5.1	-62.5%	20%	37.7%	5.4%	49.5%	9.6%
Am-241	790.1	5.1	-61.3%	106%	7.6%	17.9%	111.4%	214.7%

Position 2c

	AIGS Optimization: 19 Spectra		Std. ISOCS		AIGS - BRF		AIGS - Simplex	
	Reference Activity [kBq]	Uncert [kBq]	Relative Difference	Uncertainty	Relative Difference	Uncertainty	Relative Difference	Uncertainty
Ba-133	182.3	3.1	-58.7%	16%	33.5%	1.9%	32.1%	1.9%
Cs-137	63.2	2.1	-68.3%	13%	31.1%	14.5%	29.6%	14.5%
Eu-152	216.4	5.1	-63.7%	22%	29.3%	3.4%	27.9%	3.2%
Am-241	790.1	5.1	-56.6%	30%	6.4%	15.9%	4.6%	14.1%

Table 2. Overall Nuclide Activity Results for the 6 Source positions

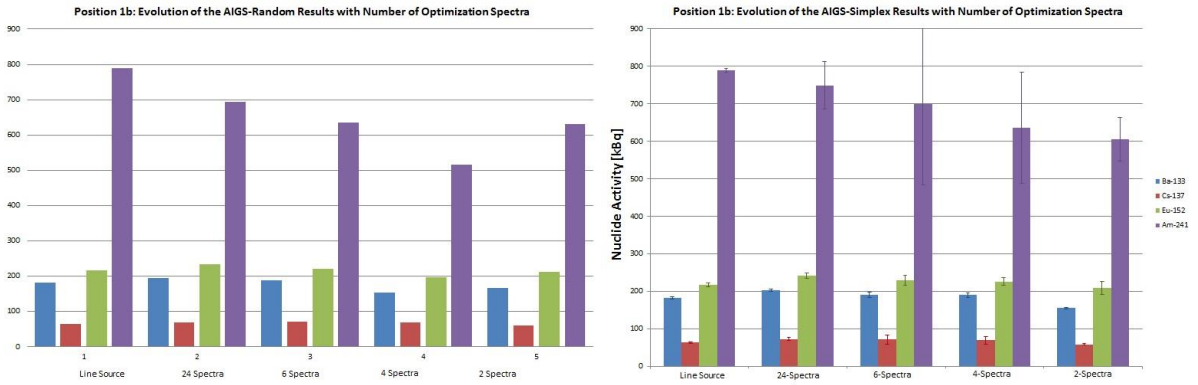

Figure 5. AIGS Random (LHS) and Simplex (RHS) optimisation nuclides activity results for a variable number of available spectra and the line source in position 1b

This study showed that, for the selected modelling assumptions, a significant reduction of the number of available spectra does not result in the collapse of the algorithm. As previously observed, simplex and BRF results were judged comparable, with a significant gain in computing time for the Simplex approach. The quantitative results, although returning larger associated uncertainties, still provided a very good level of agreement with the line source reference activities. From a practical stand point, this means that AIGS simulation based on a reasonable set of measurements, such as 4 or 6 measurements, can provide reliable estimates. On this basis further evaluation of the sensitivity of the AIGS optimisations to modelling assumption were carried out with the assumptions that only 4 spectra were available.

3.3.2 Hot-Spots Modelling

The next study looked at evaluating the dependency of the AIGS simplex results to the number of hot-spots defined in the ISOCS-IUE model to perform the geometrical optimisation. Additional models based on 2, 3, 4, and 5 Hot-Spots present in the waste volume were used as the basis for the Simplex optimisation. Figure 6 shows the obtained nuclide activity results. This study is of interest for assessment of unknown drums because, for the present measurements although it is known that a single source is present in each case, this cannot be known in the general case, therefore one must consider the possibility that multiple Hot-Spots may be present.

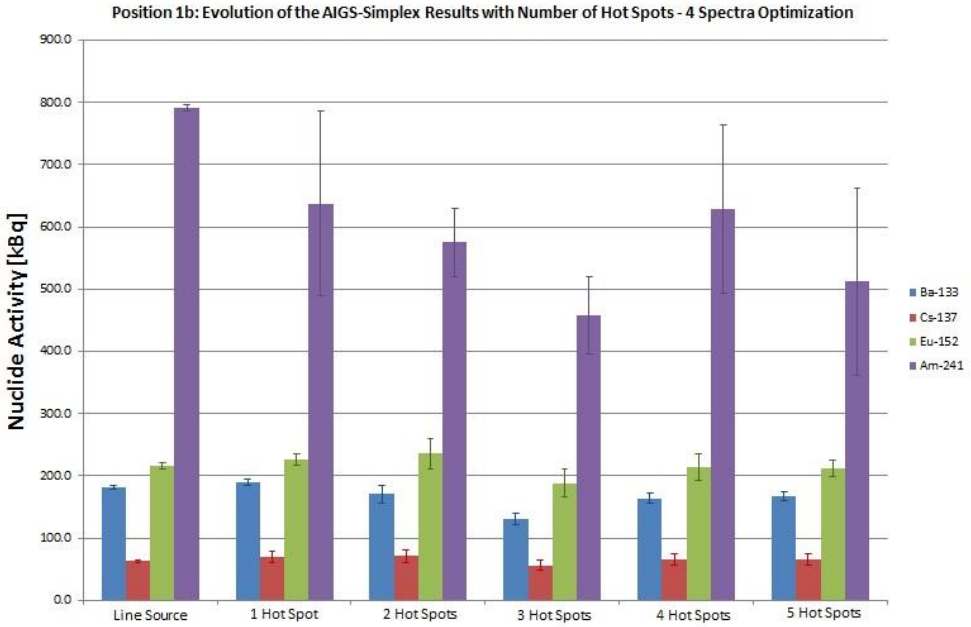

Figure 6. Dependency of the AIGS Simplex nuclide activity results with the number of hot spots simulated in the waste

This exercise seems to indicate, for this particular counting geometry, that as the number of Hot-Spots increases from one to two or even three the overall consistency of the optimisation becomes harder to achieve and thus leads to increased uncertainties on the assay results. The overall accuracy of the results for the 2 and 3 Hot-Spot model is also slightly worse than the other cases. As the number of Hot-spots increases to 4 or 5, although computation time also increases, the optimisation algorithm seems to perform slightly better in finding more consistent representations of the measured object. Modelling of more than 5 Hot-spots may further improve the consistency of the optimisation but this may impact too much the overall computation time of the simulations.

3.3.3 Waste Density Range

The density of the waste drum used in this work was well established and the initial part of the modelling exercise assumed a matrix density equal to the reference value of 0.681 $g.ml^{-1.}$ It is reasonable to assume that a waste drum can be weighed and a bulk apparent density derived for the drum. Consequently, although local variation in the matrix material may result in different effective densities for the gamma radiation emitted through the waste, this should nevertheless give a starting point in defining matrix density assumptions in the AIGS modelling process.
To study the dependency of the AIGS results to uncertain waste matrix modelling assumptions, a set of models covering various density ranges have been used. Those covered increasingly larger ranges of lower and upper density bounds. Additionally, a range that didn't include the declared density was also added to the study to how the AIGS simulation would perform in this case. The various density ranges are shown below.

- $\rho \in [0.01; 1.20]$
- $\rho \in [0.10; 0.50]$
- $\rho \in [0.20; 1.00]$
- $\rho \in [0.30; 0.90]$
- $\rho \in [0.40; 0.80]$

The simulations were run with 4 available spectra like previously and assumed a single Hot-Spot not to add further source of complexity in the interpretation of the results. Only the Simplex algorithm was used to provide timely results. Figure 7 shows the obtained results for the 5 simulated density ranges and the known Line source activities.

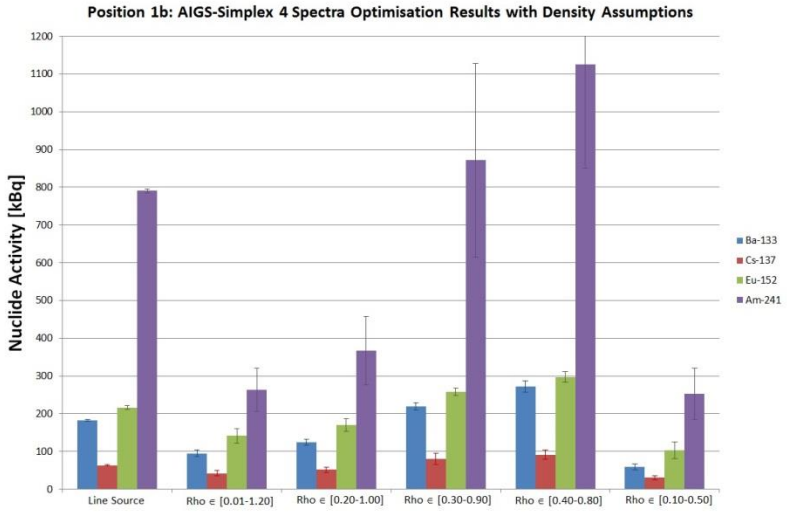

Figure 7. Distribution of the nuclide activities quantified by AIGS optimisation for various waste density assumptions

The AIGS results show some sensitivity to the density assumptions. However, more significantly the reported uncertainties (alternatively known as the precision) associated with the AIGS activity results also show some relationship with the accuracy of the results. Figure 8 plots the relative accuracy (that is, the deviation between the measured and known activity value) of the AIGS results for ^{133}Ba and ^{152}Eu against the reported uncertainty (i.e. consistency in the AIGS optimised efficiencies) associated with the derived activity values.

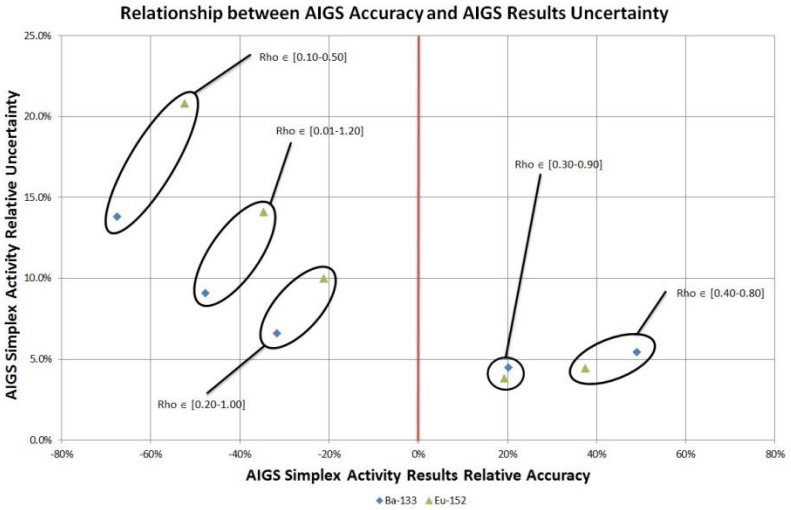

Figure 8. Relationship between AIGS Accuracy and Precision

From the latest plot it can be suggested that although user inputs may impact on the overall AIGS accuracy, as shown in Figure 8, the evaluation of the uncertainty associated with the AIGS results, which in other words is an evaluation of the consistency of the best computed solutions by the geometry optimisation algorithms, provides a mean to infer which parameter set will yield more accurate results.

4 CONCLUSION & FUTURE WORK

The work presented here aimed at demonstrating the capabilities of the AIGS optimisations to generate accurate nuclide activity quantification when measuring items presenting a non-uniform source distribution. Although the measurement case described in this study and the subsequent AIGS analysis carried out on a set of empirical measurements only represents a small set of data to fully qualify the AIGS capabilities, it has shown that this approach returned accurate results that are far more reliable that what can be achieved by a standard ISOCS based quantification.

The limited sensitivity analysis reported in this work on the impact of input assumptions in the AIGS optimisation process/model specification has shown that the AIGS result followed the expected behaviour. It also suggested that the AIGS accuracy obtained when comparing optimisation results for a number of "best" geometries appears to be a good means to judge of the validity of the AIGS results. Computation yielding significant spread in the derived efficiency data seems indicative of an unreliable optimisation. Although further sensitivity analysis work is needed to fully evaluate the overall behaviour of the AIGS optimisation results with optimisation process/model specifications, this preliminary result provides some confirmation that AIGS is capable of providing more reliable and accurate measurement results for waste sentencing, and represents a comprehensive performance demonstration and validation of the AIGS methodology for assay of 200 litre drums

5 REFERENCES

[**1**] R. Venkataraman, F. Bronson, V. Atrashkevich, B.M. Young, and M. Field, "*Validation of in-situ object counting system (ISOCS) mathematical efficiency calibration software*", Nucl. Instr. and Meth. A 422 (1999) 450

[**2**] F. Bronson, R. McElroy, S. Philips, W. Russ, S. Croft, "*The Application of Mathematical Modeling for Commercial Nuclear Instrument Design, Development, and Calibration*", Proceedings of the 1st ANIMMA International Conference, Marseille, France, June 2009

[**3**] F. Bronson, G. Geurkov, and B. Young, "*Probabilistic uncertainty estimator for gamma spectroscopy measurements*", Journal of Radio analytical and Nuclear Chemistry, Vol. 276, No. 3 (2008) 589-594

[**4**] D. Nakazawa, S. Croft, M. Henry, W. Mueller, R. Venkataraman, M. Villani, and H. Zhu, "*Determination of Non-Uniform Source Distribution Uncertainty of Waste Assay Systems using ISOCS Uncertainty Estimator*", Presented at the ISRSM Conference, 2007

[**5**] W. Russ, N. Menaa, D. Nakazawa, A. Bosko, R. Venkataraman, and F. Bronson, "*Evaluation of Numerical Techniques for Optimization of ISOCS Modeled Detector Measurement Geometries*", Presented at the International Conference on Mathematics, Computational Methods, and Reactor Physics, 2009

[**6**] A. Bosko, N. Menaa, T. Spillane, F. Bronson, R. Venkataraman, W. Russ, W. Mueller, V. Nizhnik; "*Efficiency Optimization Employing Random and Smart Search Using Multiple Counts and Line Activity Consistency Benchmarks*"; WM2011 Conference, February 27 – March 3, 2011, Phoenix, AZ

[**7**] R. Venkataraman, A. Bosko, G. Ilie, W. Russ, F. Bronson, L. Bourva, A. Berlizov, V. Nizhnik, S. Yoon, and A. Lebrun; "*Advanced Mathematical Methods for Gamma Ray Based Nuclear Safeguards Measurements*"; Presented at the IAEA Symposium on International Safeguards October 20 – 24, 2014, Vienna, Austria

[**8**] A. Bosko, R. Venkataraman, F. Bronson, G. Ilie, W. Russ; "*Waste Characterization Using Gamma Ray Spectrometry with Automated Efficiency Optimization* "; WM2013 Conference, February 24 – 28, 2013, Phoenix, Arizona USA

[**9**] L. Bourva, F. Bronson, P. Chard, G. Ilie, H. Jäderström, T. Kirk, W. Mueller; "*An advanced ISOCS In Situ Gamma Spectrometry services tool to reduce uncertainties in waste characterization projects*", Proceedings of the Waste Management 2016 Conference, 6th 10th March 2016, Phoenix, Arizona, USA

[**10**] B. Vendittozzi, L. Bourva, P. Chard, X. Ducoux, G. Ilie, H. Jäderström, T. Kirk, W. Mueller; "*Further development of an ISOCS – based Advanced In Situ Gamma Spectrometry Services Tool for waste measurements*"; Proceedings of the Waste Management 2017 Conference, March 5th - 9th 2017, Phoenix, Arizona, USA

xFuelBuilder for the Analysis of Simulation and Measurement of fresh fuel assemblies by Nuclear Inspectors

H. Tagziria[1], M. Vescovi[3] , P. Peerani[2], P. de Baere[4], P. Schwalbach[4] and S. Vaccaro[4]

[1a] European Commission, Joint Research Centre (JRC), Nuclear Security Unit, Via Enrico Fermi 2749, 21027 Ispra (VA), Italy

[2] European Commission, Joint Research Centre (JRC), Nuclear Decommissioning Unit, Via Enrico Fermi 2749, 21027 Ispra (VA), Italy

[3] i-Science Srl, via Amedei 6, 20123 Milano, Italy

[4] European Commission, DG Energy, Euroforum building, Luxembourg

Abstract:

The JRC and i-Science in collaboration with DG-ENER have developed xFuelBuilder a user-friendly software and Monte Carlo (MC) Simulation (MCNP) application which allows a nuclear inspector (with no prior expertise in MC) to perform the analysis of Neutron Coincidence Collar simulations and measurements of fresh fuel assemblies (BWR & PWR) thus saving valuable human resources and effort. It is an open graphical framework for an interactive creation of PWR and BWR Nuclear Fuel Elements with a 2D Synoptic and 3D OpenGL representation of the assembly composition in term of single rods. For this purpose, xFuelBuilder includes Monte Carlo-based modelling tools that enable the user to set up specific collar detector geometry, run an MCNP simulation and perform a Pulse Train Analysis to extract Total, Reals and Accidentals. Easy and direct access to simulation is enabled from the 3D panel to compare simulations to measurements and finally view and store the final results

Keywords: Monte Carlo, NDA, Nuclear Safeguards, Neutron Coincidence Counting,xFuelbuilder

[a] Contact: hamid.tagziria@ec.europa.eu

1. Introduction

Extensive human resources and effort are expanded by EURATOM and IAEA nuclear safeguards inspectors to verify the operator's declarations generally using expensive and difficult (if not sometimes impossible) measurement campaigns [1-4]. A number of complications are often encountered such as the need for specific calibrations (not always possible), interpretation models (not always applicable) and correction factors e.g. to take into account burnable poisons and/or various heterogeneities.

xFuelBuilder [5] which follows on work previously carried out [3] to analyse MOX fuel in fabrication plant (MoxManager) is an open graphical framework for an interactive creation of PWR and BWR

Nuclear Fuel Elements with a 2D Synoptic and 3D OpenGL representation of the assembly composition in term of single rods. It aims thus to support the nuclear inspectorate in the analysis of active Neutron Coincidence Collar (NCC) measurements of fresh BWR and PWR fuel assemblies.

For this purpose, xFuelBuilder includes Monte Carlo-based (MC) modelling tools that enable the user to set up specific collar detector geometry, run an MCNP simulation and perform a Pulse Train Analysis to extract Total, Real and Accidental count rates.

This paper aims to provide the reader with an overview of the tool and its main capabilities.

2. The inspection/verification paradigm

Real-time simulation of neutron counters as we envisaged it and described in references [1-2] would obviously change the way we are used to applying NDA measurements for the verification nuclear material and would require a mentality change too from the inspector's perspective. It is not simply the fact that one would introduce a physical modelling as an integral part of the experimental process, but also the verification paradigm is changed from one that previously compared operator declared mass against measured mass, to a new paradigm that instead compares expected to measured count rates.

The classical verification scheme is illustrated in Figure 1 whereby the sample and its declaration are given by the operator to inspector who measures it using suitable counting systems that would yield either *Reals* count rates in coincidence counting, or Singles, Doubles and Triples in multiplicity counting. These count rates are converted to measured mass through a model relating physical model calculations to experimental values, namely either a calibration law, R=f(m), in coincidence counting or a solution of the point model equation system in multiplicity counting. Finally, taking into account measurement uncertainties, the measured mass is compared to the declared value in order to either positively confirmation or reject the sample verification.

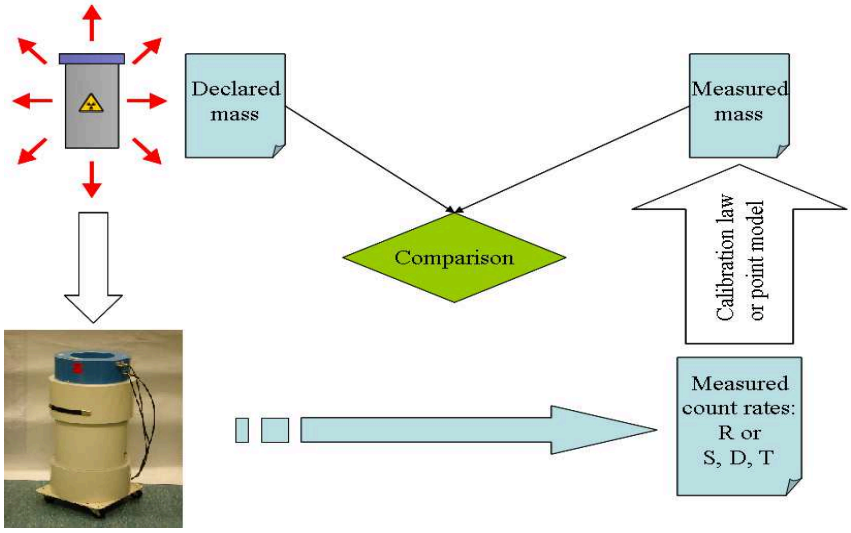

Figure 1: Classical verification paradigm

In contrast as shown in Figure 2, real-time simulation changes the scenario whereby both the measurement and the simulation, which is based on the declaration, are run in parallel to yield the measured count rates and expected (or simulated) count rates respectively. These count rates with given uncertainties are subsequently compared and a conclusion on their consistency is made without computing the measured mass. This can be easily accepted when there is agreement, confirming the conformity of sample with the declaration. But it can be insufficient if there is a discrepancy, in which case the inspector would like to know how different is the measurement from the declaration in terms of material mass.

Some solutions to this shortcoming can be easily envisaged. For instance a gross calibration curve can be pre-built and the mass error can be approximately derived by using the derivative of the calibration curve: $\Delta m = (\delta R/\delta m)_{meas} * \Delta R$.

Another possibility is to use the perturbation theory or sensitivity analysis. The influence on the count rates of a mass change can be computed by running an ad joint problem. This of course would double the computing time.

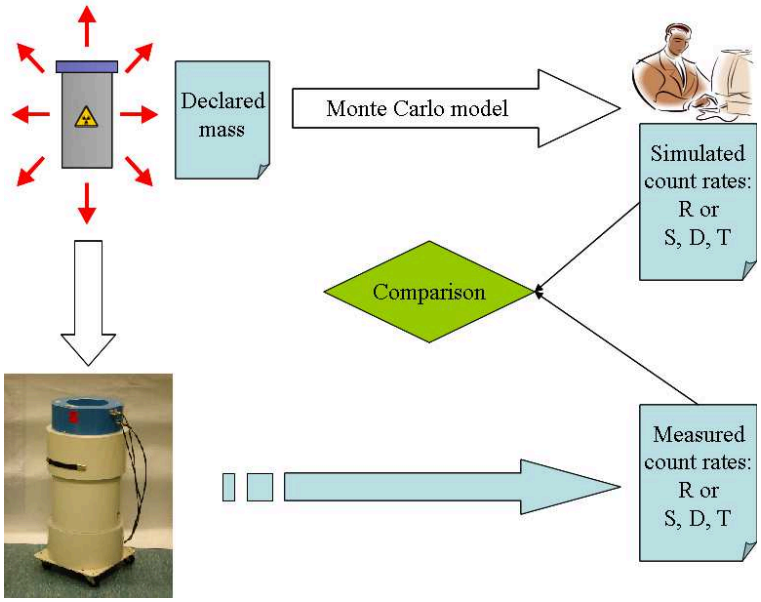

Figure 2: Real-time simulation paradigm

3. Description of xFuelBuilder capabilities

This section will describe xFuelBuilder application and its capability to:

- Manage, define and configure PWR and BWR fuel assemblies
- Set a collar detector geometry
- Run an MCNP Simulation and PTA Analysis
- View and store the final results

3.1. The xFuelBuilder Assembly Manager

The assembly manager panel expose the list of the actual stored assembly in an interactive table:

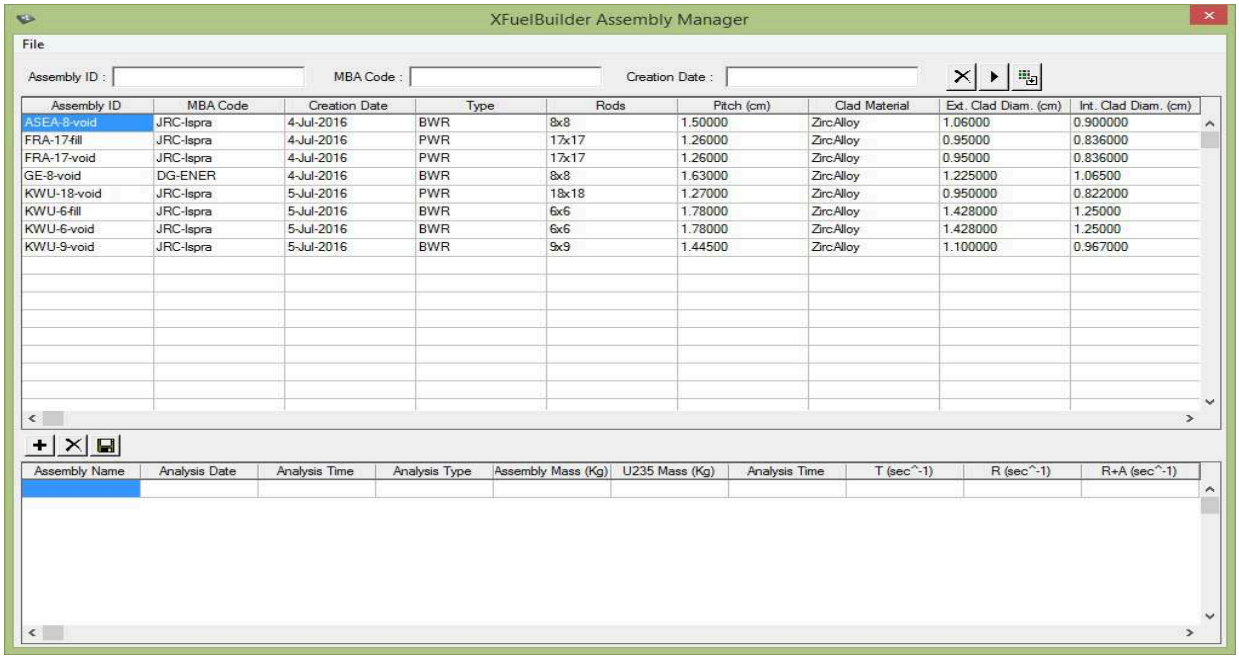

Editing the widgets field user can query into the local assembly repository with the search criteria are based on:

- Assembly ID
- MBA Code
- Creation date

Using the icons:  one is able to:

- Delete a specific assembly from the repository
- Run and analyse a specific assembly
- Create a new assembly using the associated panel

The measurement toolbar:

allows one to:

- Add a new measurement to the analysis list
- Delete a specific analysis
- Save current measurement list into the local DB

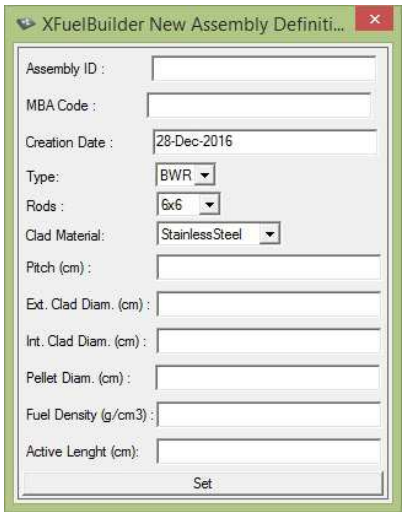

The Import/Export Assembly configuration are available from the menu file:

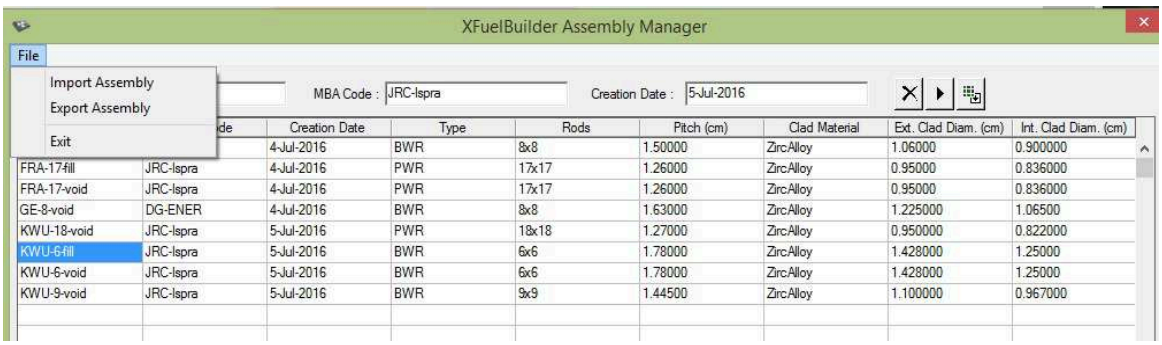

		Creation Date	Type	Rods	Pitch (cm)	Clad Material	Ext. Clad Diam. (cm)	Int. Clad Diam. (cm)
		4-Jul-2016	BWR	8x8	1.50000	ZircAlloy	1.06000	0.900000
FRA-17fill	JRC-Ispra	4-Jul-2016	PWR	17x17	1.26000	ZircAlloy	0.95000	0.836000
FRA-17-void	JRC-Ispra	4-Jul-2016	PWR	17x17	1.26000	ZircAlloy	0.95000	0.836000
GE-8-void	DG-ENER	4-Jul-2016	BWR	8x8	1.63000	ZircAlloy	1.225000	1.06500
KWU-18-void	JRC-Ispra	5-Jul-2016	PWR	18x18	1.27000	ZircAlloy	0.950000	0.822000
KWU-6fill	JRC-Ispra	5-Jul-2016	BWR	6x6	1.78000	ZircAlloy	1.428000	1.25000
KWU-6-void	JRC-Ispra	5-Jul-2016	BWR	6x6	1.78000	ZircAlloy	1.428000	1.25000
KWU-9-void	JRC-Ispra	5-Jul-2016	BWR	9x9	1.44500	ZircAlloy	1.100000	0.967000

3.2. The Assembly Configurator

The assembly configurator panel is used to edit the assembly rod by rod.

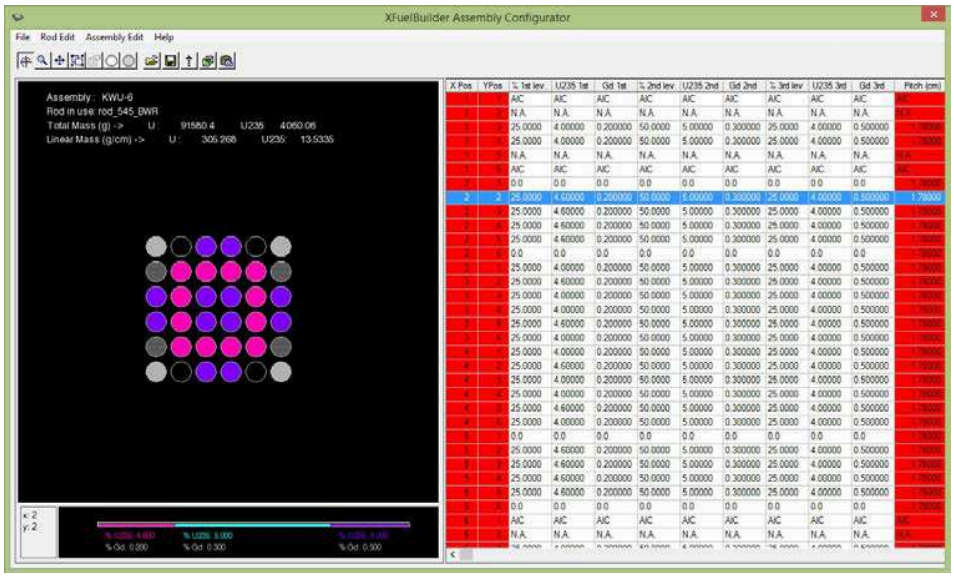

The info window at the bottom of the panel provides information about each single rod in the assembly:

- Rod position
- Isotopic composition
- Empty tubes
- Forbidden positions
- Enrichment stratification

The button bar on the top starting from the left expose the following functionalities:

- Set the mouse as a pointer to query rods in the assembly view
- Set the mouse as a pointer to zoom the assembly
- Set the mouse as a pointer to pan the assembly view
- Allow multiple rods selection
- Manage multiple rods assignment
- Manage forbidden position
- Manage empty position
- Come back to the assembly manager panel
- Save assembly modification
- Move to the rode configuration panel
- Move to the Simulation Panel
- Move to the Analysis Manager Panel

The File Menu provides the following functionality:

- Load an assembly from the library folder on file system
- Save an assembly to the library folder on file system
- Export a snapshot of the assembly
- Print a snapshot of the assembly
- Set-up the printer
- Exit from the application

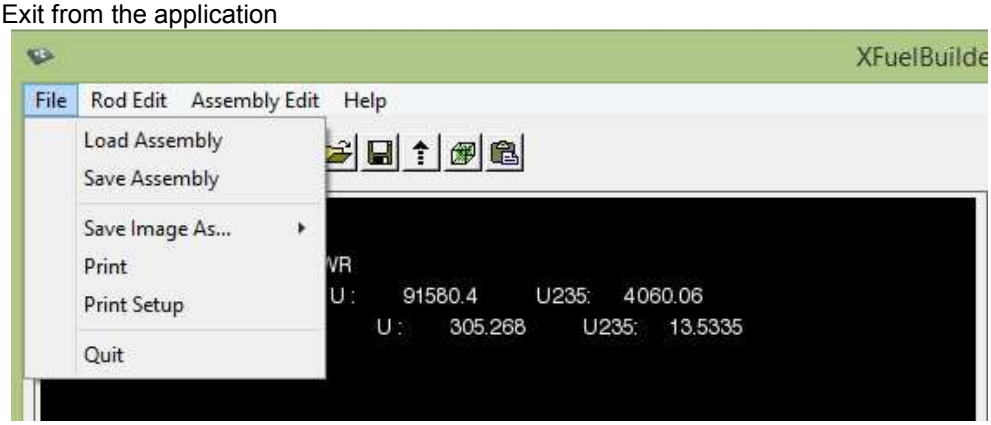

The Rod Edit Menu:

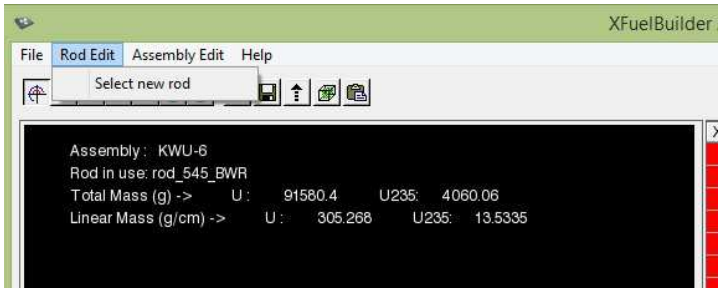

Launch of the Rod Profiler Panel will present the user with the following:

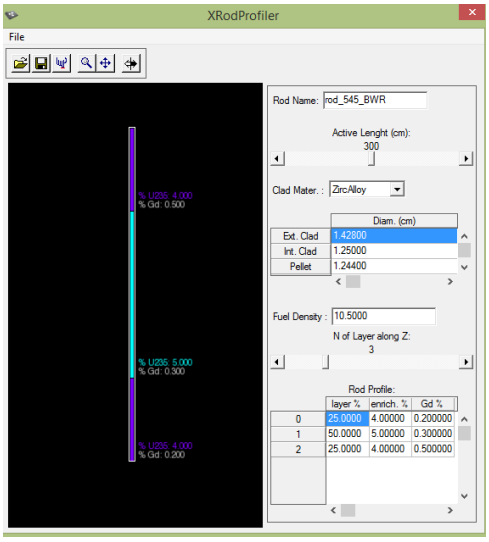

The top bar above enables one to:

- Open a specific rod definition
- Save a specific rod definition
- Activate the interactive view
- Zoom the view
- Pan the rod visualization
- Move back to the main pan

Whereas the GUI on the right defines the rod stratification with widgets dedicated to:

- Rod active length setting
- Clad material definition
- Dimensional parameters of the fuel pellets
- Fuel density
- Layers characterization

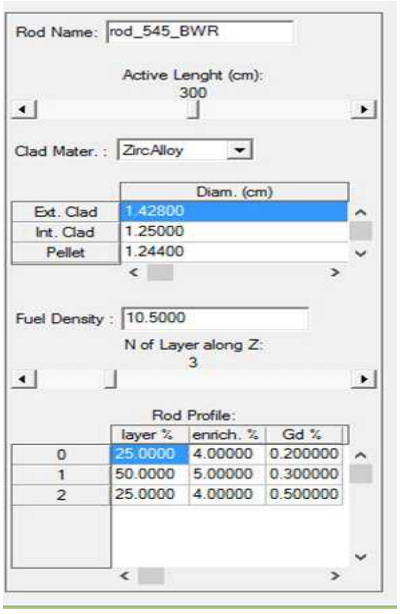

The Assembly Edit Menu:

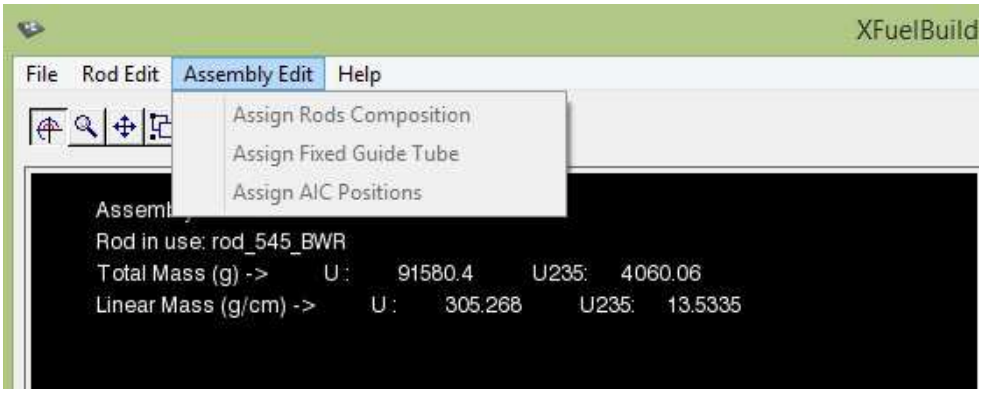

enables the following functionalities:

- Edit the general assembly parameter (e.g. assembly length, pellet density….)
- Set the rods composition using the appropriate panel
- Manage multiple rods assignment
- Manage forbidden position
- Manage empty position

3.3. The simulation Manager

The simulation manager panel enable the user to run Monte Carlo Simulation for the selected assembly.

It is provided with the following top bar:  for view manipulation and with a slide that sets the collar position along the assembly:

The user can verify the correct position of the collar along the assembly by the composition window which gives information about isotope stratification and U235 Enrichment rod by rod:

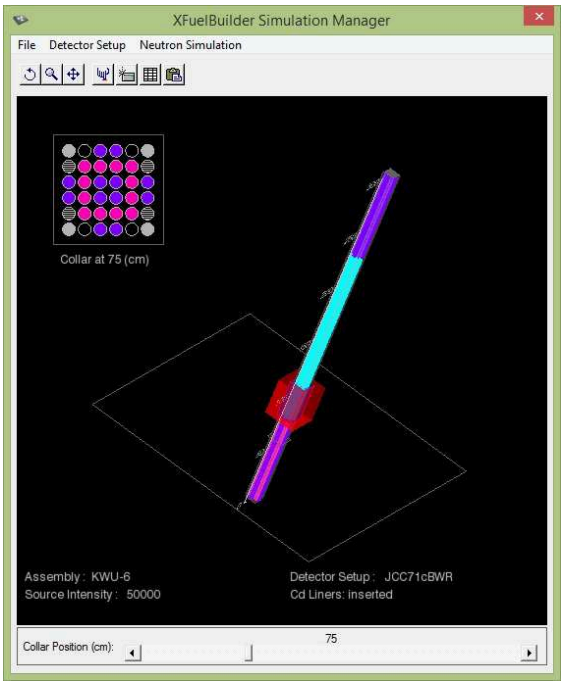

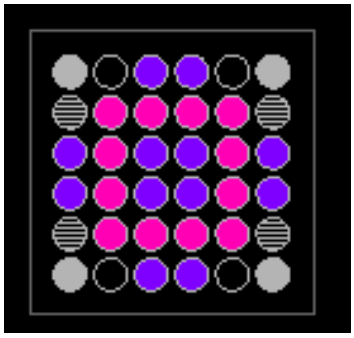

The detector Setup Menu:

Enables the following functionalities:

- Detector selection
- Cadmium slab insertion
- Set source intensity

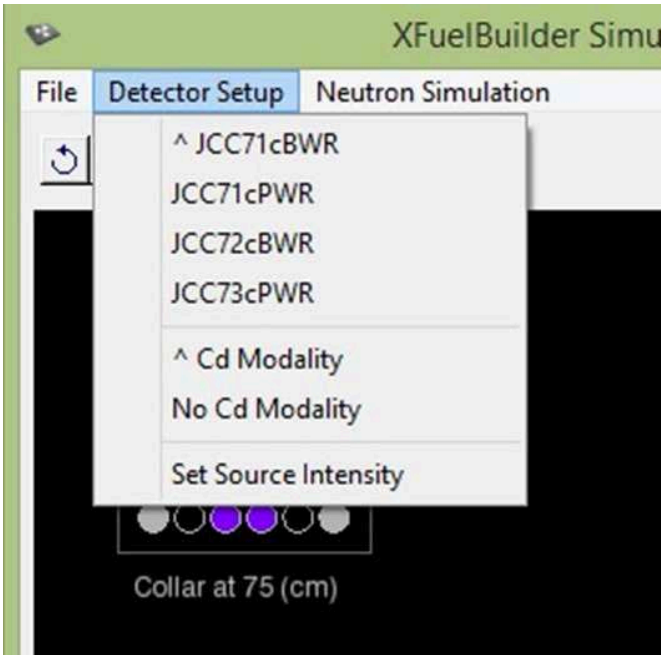

The Neutron Transport Simulation Menu allows the user to:

- Set the general MCNP parameter using the following panel
- Set the simulation time vs events modality
- Run the MCNP simulation with and without assembly and using the active source modality.
- Open the last executed analysis

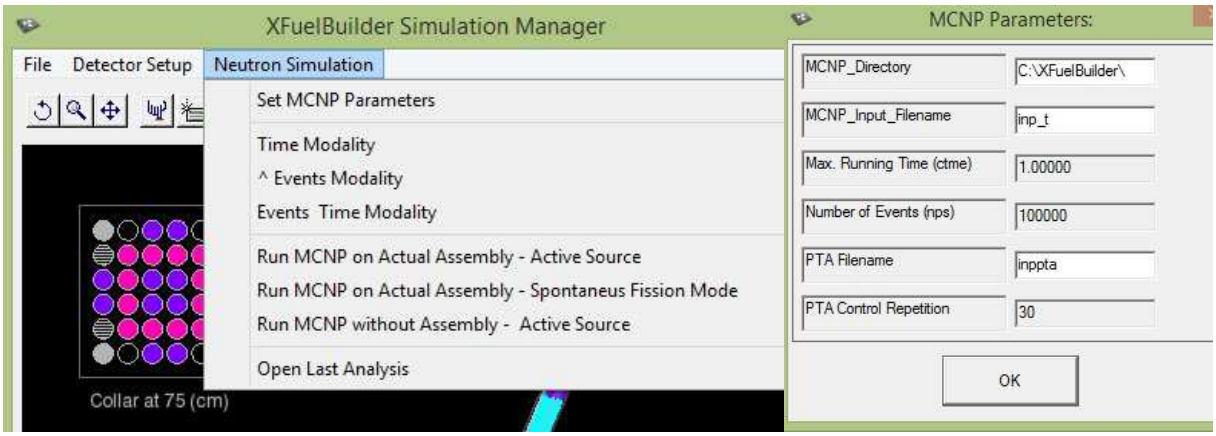

3.4. The Analysis Manager

This allows logging all the measurements and the simulation for the current assembly.

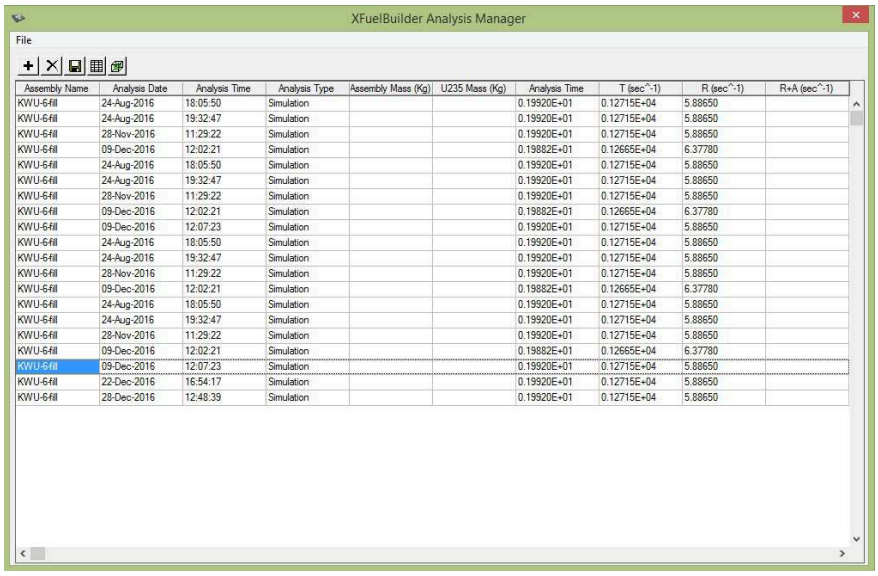

The toolbar:  allows the user to:

- Add a new measurement to the list
- Remove a specific analysis
- Save the current list into the Database
- Back to main assembly definition panel
- Back to the 3D analysis panel

4. Summary

xFuelBuilder which is a Monte Carlo (MC) based application has been fully developed and successfully demonstrated to EURATOM inspectors allowing them to efficiently and effectively analyze Neutron Coincidence Collar (NCC) simulations and measurements of fresh fuel assemblies (BWR & PWR) without the need for specific calibrations (not always possible), interpretation models (not always valid) or correction factors for instance to take into account burnable poisons and/or ant heterogeneities. The user friendly application allows an inspector (non-expert in MC) to define fuel assemblies, set up collar detector geometry, run Monte Carlo (MCNP code) simulation and pulse train analysis (PTA) with direct access to simulation from a 3D panel, compare simulations to measurements and finally view and store the final results. In essence, it enables the inspector to verify the operator's declaration by comparing measurements carried out with NCC's and Monte Carlo calculations saving valuable time and effort.

Acknowledgements

The development was carried out within the Administrative Arrangement between the JRC and DG-ENER and in collaboration with iScience SrL for the programming aspects.

5. References

[1] H. Tagziria and P. Peerani "Monte Carlo modelling of NCCs for Nuclear Safeguards" *International Conference on Mathematics, Computational Methods & Reactor Physics (M&C 2009)* Saratoga Springs, New York, May 3-7, 2009, American Nuclear Society, LaGrange Park, IL (2009)

[2] . Peerani, H. Tagziria, M. Looman, "Real Time simulation of neutron counters", in Radiation Measurements 43 (2008) 1506-1510

[3] H. Tagziria, P. Peerani, W. Koehne, P. Schwalbach: "On-line verification of MOX Fuel Magazines Using Monte Carlo Simulation", Proceedings of the 27th ESARDA, London (UK), 10-12 May 2005.

[4] S. Vaccaro, I. Gaud, M.Vescovi, H. Tagziria, A. Smejkal and P. Schwalbach, "The forward-problem approach in Safeguards verification: directly comparing simulated and measured observables", Proceedings of the 39th ESARDA, Dusseldolf May 16-18 May 2017

[5] P. Peerani, H.Tagziria, M. Vescovi, P. De Baere, P. Schwalbach and S. Vaccaro , *A user-friendly tool for easy and fast in-field Monte Carlo simulation of neutron collars*, in Proceedings of 37th ESARDA Symposium , Manchester, UK, 19-21 May 2015

Legal matters

Privacy regulations and protection of personal data

The authors agree that ESARDA may print their names/contact data/photograph/article in the ESARDA Bulletin/Symposium proceedings or any other ESARDA publications and when necessary for any other purposes connected with ESARDA activities.

Copyright

The author agrees that submission of an article automatically authorises ESARDA to publish the work/article in whole or in part in all ESARDA publications – the bulletin, meeting proceedings, and on the website.

Study on the Application of Gaussian Energy Broadening on MCNP Simulated Detector Performance

Dr Andrew M Evans
AWE Aldermaston, Reading, UK

Summary
The particle transport code MCNP6 [Ref 1] has been used to model the effect of Gaussian Energy Broadening on detector performance. This report details the underlying mathematics using a binomial expansion and linear fit for calculating the *a*, *b* and *c* parameters required by MCNP6 from a detector's performance specification sheet.

MCNP6 deals with Gaussian broadening through the a, b and c variables. These are connected to the $FWHM$ through the following equation

$$FWHM = a + b\sqrt{E_0 + cE_0^2} \quad [1]$$

where E_0 is the energy of the centre of the peak. It is not immediately obvious the impact and sensitivity that *a*, *b* and *c* have on a peak's profile. The challenge is to develop a technique to extract values for *a, b* and *c* from the performance data sheet of a gamma detector.

1) Binomial expansion approach
The starting point with this approach is equation [1]

$$FWHM = a + b\left(E + cE^2\right)^{\frac{1}{2}} \quad [2]$$

Expand using the binomial expansion

$$FWHM = a + b\sqrt{c}E\left(1 + \frac{1}{cE}\right)^{\frac{1}{2}} \quad [3]$$

$$FWHM = a + b\sqrt{c}E\left(1 + \frac{1}{2cE} - \frac{1}{8c^2E^2}\cdots\cdots\right) \quad [4]$$

$$FWHM = a + b\sqrt{c}E + \frac{b}{2\sqrt{c}} - \frac{b}{8c^{\frac{3}{2}}E} + O(\frac{1}{E}) \quad [5]$$

Since the width of a pulse is much smaller than its energy, we are justified in ignoring the fourth term. Rearranging we obtain

$$FWHM = b\sqrt{c}.E + \left(a + \frac{b}{2\sqrt{c}}\right) \quad [6]$$

This analysis has demonstrated that the *a, b* and *c* variables can be derived from a straight line graph of $FWHM$ against E. Drawing this graph from the information contained in a detector's data sheet we immediately see that the gradient and intercept can be further processed to understand their dependence upon the *a, b* and *c* coefficients.

Gradient = $b\sqrt{c}$ Intercept = $\left(a+\frac{b}{2\sqrt{c}}\right)$ [7]

2) NaI Gamma Detector Response Function.

To advance this further, consider now the specific case of the NaI gamma detector [Ref 2] used by Salgardo et al.

Typically, a detector's data sheet will contain a value of its $FWHM$ at two different energies; from these two points a linear fit can be imposed. In contrast, Salgardo actually measured the detector's $FWHM$ response at six energies ranging from 58.18 keV up to 661.8 keV. The data was then fitted with the function displayed in equation [1], and coefficients for *a, b* and *c* extracted.

2.1) First Approximation

The $FWHM$ at two energies (58.1 keV and 661.8 keV) have been extracted from Salgardo's paper in order to replicate the information that one might extract from a detectors performance specification sheet. Figure 1 shows a graph of $FWHM$ against E for this detector with an imposed linear fit. A spreadsheet has been developed that takes the two given data points and generates a third from the calculated mid-point. The spreadsheet also calculates and outputs a value for the gradient and intercept.

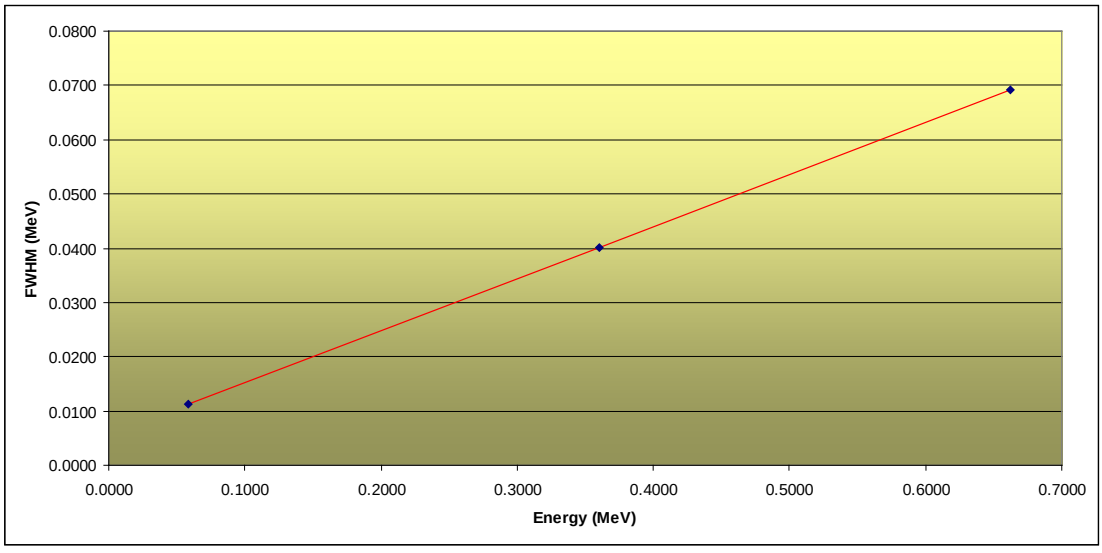

NaI Detector		
	E	FWHM
E_1	0.0582	0.0112
E_2	0.3600	0.0402
E_3	0.6618	0.0692
	Gradient =	0.0960
	Intercept =	0.0056

Figure 1: Graph of $FWHM / E$ and spreadsheet calculation of gradient and intercept for NaI gamma detector.

2.2) Calculation of *a*, *b* and *c* coefficients

MCNP is already formatted to take the *a, b* and *c* variables as inputs. To calculate these three parameters, three independent equations are required to be solved. These equations were generated from information filtered from the detector's performance specification presented in Figure 1 and are

$$FWHM_1 = a + b\sqrt{E_1 + cE_1^2} \quad [8]$$

$$FWHM_2 = a + b\sqrt{E_2 + cE_2^2} \quad [9]$$

$$FWHM_3 = a + b\sqrt{E_3 + cE_3^2} \quad [10]$$

An overview of the elimination process is as follows.

Eliminate *a* by subtracting [8] from [9] and [8] from [10]. This generates two new equations in *b* and *c*.

$$W_2 - W_1 = b\sqrt{E_2 + cE_2^2} - b\sqrt{E_1 + cE_1^2} \quad [11]$$

$$W_2 - W_1 = b\left(\sqrt{E_2 + cE_2^2} - \sqrt{E_1 + cE_1^2}\right) \quad \text{similarly} \quad [12]$$

$$W_3 - W_1 = b\left(\sqrt{E_3 + cE_3^2} - \sqrt{E_1 + cE_1^2}\right) \quad [13]$$

Dividing [13] by [12] eliminates b

$$\frac{W_3 - W_1}{W_2 - W_1} = \frac{\sqrt{E_3 + cE_3^2} - \sqrt{E_1 + cE_1^2}}{\sqrt{E_2 + cE_2^2} - \sqrt{E_1 + cE_1^2}} \quad [14]$$

The values of W_1, W_2 and W_3 are connected such that $W_3 - W_1 = 2(W_2 - W_1)$. Therefore

$$2\left(\sqrt{E_2 + cE_2^2} - \sqrt{E_1 + cE_1^2}\right) = \sqrt{E_3 + cE_3^2} - \sqrt{E_1 + cE_1^2} \quad [15]$$

Writing

$$\sqrt{E_2 + cE_2^2} = \left(E_2 + cE_2^2\right)^{\frac{1}{2}} \quad [16]$$

$$= E_2^{\frac{1}{2}}\left(1 + cE_2\right)^{\frac{1}{2}} \quad [17]$$

with the application of the binomial expansion this becomes

$$E_2^{\frac{1}{2}}\left(1 + \frac{1}{2}cE_2 - \frac{c^2E_2^2}{8} - - - - - - -\right) \quad [18]$$

Ignoring the third term we can write

$$\sqrt{E_2 + cE_2^2} = \sqrt{E_2}\left(1 + \frac{cE_2}{2}\right) \quad [19]$$

If the third term is not ignored, we generate a quadratic, whose determinant points to imaginary roots.

Similarly

$$\sqrt{E_1 + cE_1^2} = \sqrt{E_1}\left(1 + \frac{cE_1}{2}\right) \quad [20]$$

$$\sqrt{E_3 + cE_3^2} = \sqrt{E_3}\left(1 + \frac{cE_3}{2}\right) \quad [21]$$

Therefore equation [15] can be written

$$2\left[\sqrt{E}_2\left(1 + \frac{cE_2}{2}\right) - \sqrt{E_1}\left(1 + \frac{cE_1}{2}\right)\right] = \sqrt{E_3}\left(1 + \frac{cE_3}{2}\right) - \sqrt{E_1}\left(1 + \frac{cE_1}{2}\right) \quad [22]$$

$$2\sqrt{E_2} + cE_2^{\frac{3}{2}} - 2\sqrt{E_1} - cE_1^{\frac{3}{2}} = \sqrt{E_3} + \frac{cE_3^{\frac{3}{2}}}{2} - \sqrt{E_1} - \frac{cE_1^{\frac{3}{2}}}{2} \quad [23]$$

$$c\left(E_2^{\frac{3}{2}} - E_1^{\frac{3}{2}} - \frac{E_3^{\frac{3}{2}}}{2} + \frac{E_1^{\frac{3}{2}}}{2}\right) = 2\sqrt{E_1} - 2\sqrt{E_2} + \sqrt{E_3} - \sqrt{E_1} \quad [24]$$

$$c\left(E_2^{\frac{3}{2}} - \frac{E_1^{\frac{3}{2}}}{2} - \frac{E_3^{\frac{3}{2}}}{2}\right) = \sqrt{E_1} - 2\sqrt{E_2} + \sqrt{E_3} \quad [25]$$

$$c = \frac{\sqrt{E_1} - 2\sqrt{E_2} + \sqrt{E_3}}{\left(E_2^{\frac{3}{2}} - \frac{E_1^{\frac{3}{2}}}{2} - \frac{E_3^{\frac{3}{2}}}{2}\right)} \quad [26]$$

The benefit of deriving an expression for c is that it is now relatively easy to solve.

Using this value of c we can find b by substituting into equation [7] and taking the value of the gradient from the graph in Figure 1

$$Gradient = b\sqrt{c} \quad [27]$$

$$b = \frac{Gradient}{\sqrt{c}} \quad [28]$$

Again from equation [7], and using the calculated value of the intercept from Figure 1

$$a + \frac{b}{2\sqrt{c}} = Intercept \quad [29]$$

$$a = Intercept - \frac{b}{2\sqrt{c}} \quad [30]$$

Actual values taken from Figure 1 will be used from here. From equation [26]

$$c = \frac{\sqrt{0.0582} - 2\sqrt{0.36} + \sqrt{0.6618}}{0.36^{\frac{3}{2}} - \frac{0.0582^{\frac{3}{2}}}{2} - \frac{0.6618^{\frac{3}{2}}}{2}} \quad [31]$$

$$c = \frac{-0.145}{-0.0602} \quad [32]$$

$$c = 2.4086 \quad [33]$$

From equation [] and using data from Figure 1

$$b = \frac{0.0960}{\sqrt{2.4086}} \quad [34]$$

$$b = 0.061828 \quad [35]$$

From equation [30] and using data from Figure 1

$$a = 0.0056 - \frac{0.061828}{2\sqrt{2.4086}} \quad [36]$$

$$a = -0.014745 \quad [37]$$

Comparing these values with those quoted in Salgardo's paper, a difference is seen. The signs of the three variables are correct, but there is a difference in the absolute magnitude.

MCNP GEB coefficients	Salgardo's values	Binomial expansion values
a	-0.002400	-0.014745
b	0.051650	0.061828
c	2.858380	2.4086

2.3) Discussion of Discrepancy between Coefficients

There are a number of aspects of this approach which can contribute to the differences seen between Salgardo's published figures and those calculated in this report.

2.3.1) The biggest delta is that the approach used in this report applied a linear fit on two data points in order to replicate the situation one would find in extracting the relevant information from a detector's performance specification sheet. In contrast Salgardo experimentally measured the $FWHM$ at six different energies from 58.18 keV to 661.8 keV, fitted equation [1] to the data, and extracted the *a, b* and *c* coefficients from the fit.

2.3.2) A detector's response has greatest non-linearity at low energy whereas the approach outlined in this document has assumed a linear response for all energies.

2.3.3) The a coefficient appears to have the largest percentage error. The a coefficient represents the detector's inherent spread at zero energy

As E approaches 0, $\sqrt{E + cE^2}$ tends to 0, and hence

$FWHM = a$ as $E \to 0$

This is the residual spread function of the detector at zero energy.

2.4) Comparison of MCNP6 Signal Profiles for NaI detector

MCNP6 was run using both sets of the *a, b* and *c* coefficients to assess the difference produced in the simulated output profiles. Both output amplitudes were normalised to 1 and the resulting profiles are shown in Figure 2.

The coefficients calculated in this report and used in the MCNP6 simulation generate a Gaussian pulse with a slightly narrower $FWHM$ than that generated with Salgardo's coefficients. The difference in $FWHM$ is small (<5%) despite Salgardo's more rigorous approach. This exercise has demonstrated the integrity in using a binomial expansion approximation and just two detector response data points as an alternative approach for the generation of the MCNP6 *a, b* and *c* coefficients.

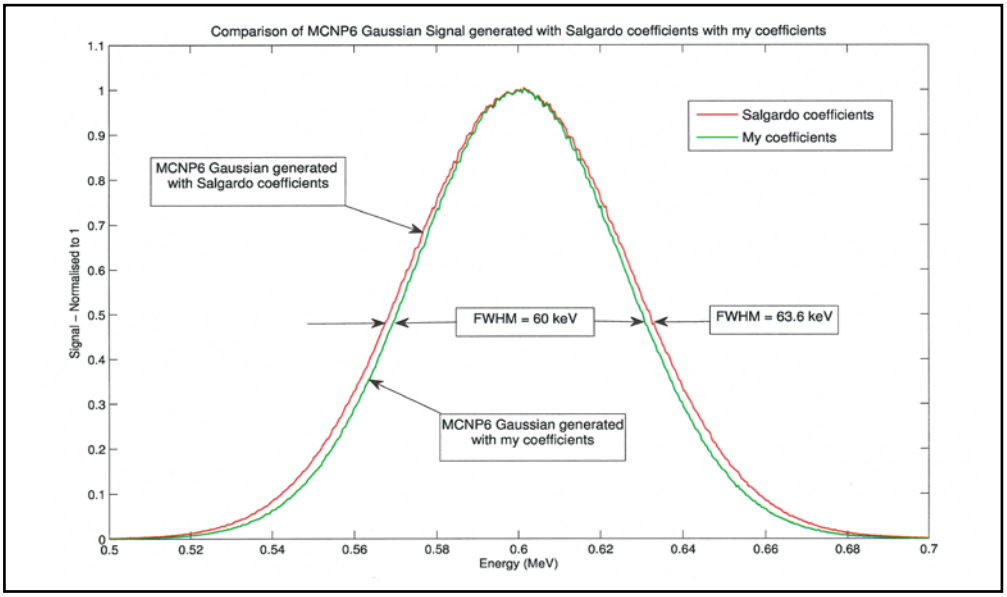

Figure 2: Comparison of MCNP6 generated Gaussian profiles using both sets of coefficients

3) HPGe Gamma Detector Response Function

A study was conducted on Gaussian energy broadening for the HPGe detector used by Zadeh et al [Ref 3]. A new set of *a, b* and *c* values were calculated. Comparing these values with those quoted in Zadeh's paper, a difference is seen. The signs of the three variables are correct but there is a difference in the absolute magnitude.

MCNP GEB coefficients	Zadeh's values	Binomial expansion values
a	5.86828E-4	1.724E-4
b	3.95113E-4	1.01E-3
c	7.46793	1.188

Once again, the main reason behind the discrepancy seen in the *a, b* and *c* coefficients is because Zadeh had the luxury of being able to fit the function in equation [30] to a number of data points (eleven), whereas the binomial expansion approach worked with just two values. This decision was deliberate in order to replicate the conditions expected when using a detector's performance specification sheet.

3.1) Comparison of MCNP6 signal profiles for HPGe detector

MCNP6 was then run using the two sets of coefficients in the table above to assess the difference produced in the output profiles. Both output amplitudes were normalised to 1 and the resulting profiles are shown in Figure 3.

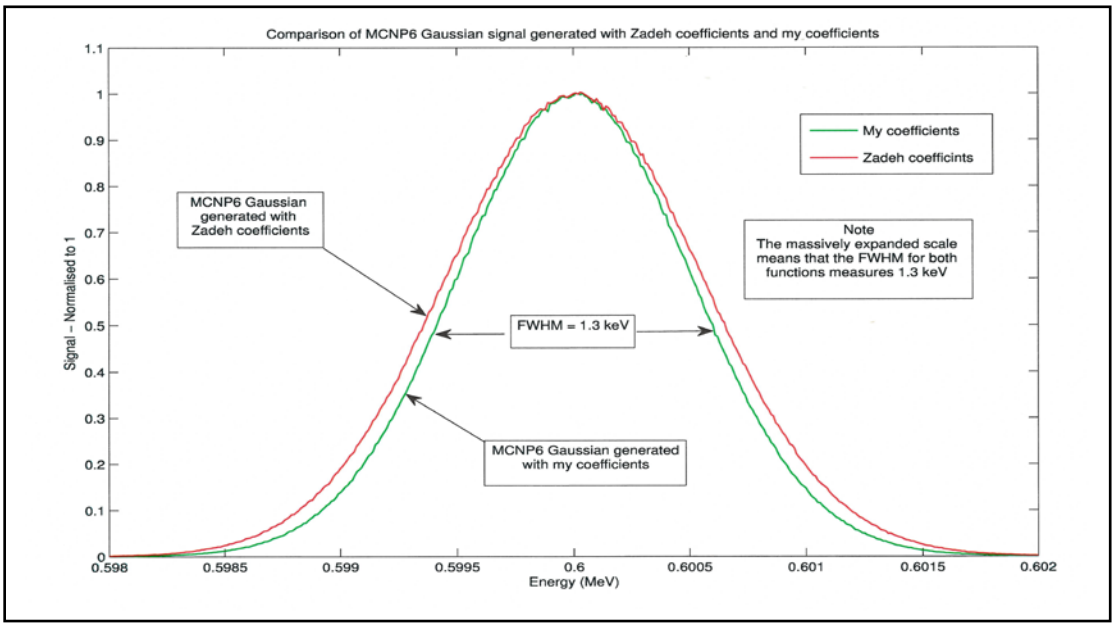

Figure 3: Comparison of MCNP6 generated Gaussian profiles using both sets of coefficients.

Even though there appears to be a measurable difference in the $FWHM$ of both functions, the expanded scale means that obtaining a quantitative value for the difference is not possible. As was seen in the Salgardo case, the Gaussian function generated using the coefficients from the binomial expansion is marginally narrower than the Zadeh Gaussian function generated using the fit to multiple data points.

4) Matlab fit approach

The Salgardo and Zadeh published values of $FWHM$ for different energies for their respective detectors are displayed in figure 4 below.

Salgardo NaI detector	Energy MeV	0.0581818	0.12	0.181818	0.243636	0.341818	0.661818
	FWHM MeV	0.011186	0.018686	0.024915	0.031017	0.0401695	0.0691525

Zadeh HPGe detector	Energy MeV	0.040118	0.05954	0.080997	0.12206	0.244697	0.344287
	FWHM MeV	6.68224 E-4	7.35514 E-4	7.186916 E-4	7.6915887 E-4	9.121495 E-4	1.05514 E-3
	Energy MeV	0.356012	0.661657	1.173228	1.332492	1.460822	
	FWHM MeV	1.021495 E-3	1.366355 E-3	1.879439 E-3	2.089719 E-3	2.283177 E-3	

Figure 4: Comparison of Salgardo and Zadeh published values of $FWHM$ for different energies for their respective detectors.

These two sets of data were loaded into Matlab and each was fitted with the custom line of equation -

$$y = a + b\sqrt{E + cE^2}$$

Matlab outputs the *a, b* and *c* coefficients for each graph. The two graphs of $FWHM$ against $Energy$ and the corresponding *a, b* and *c* coefficients are displayed in figure 5 below.

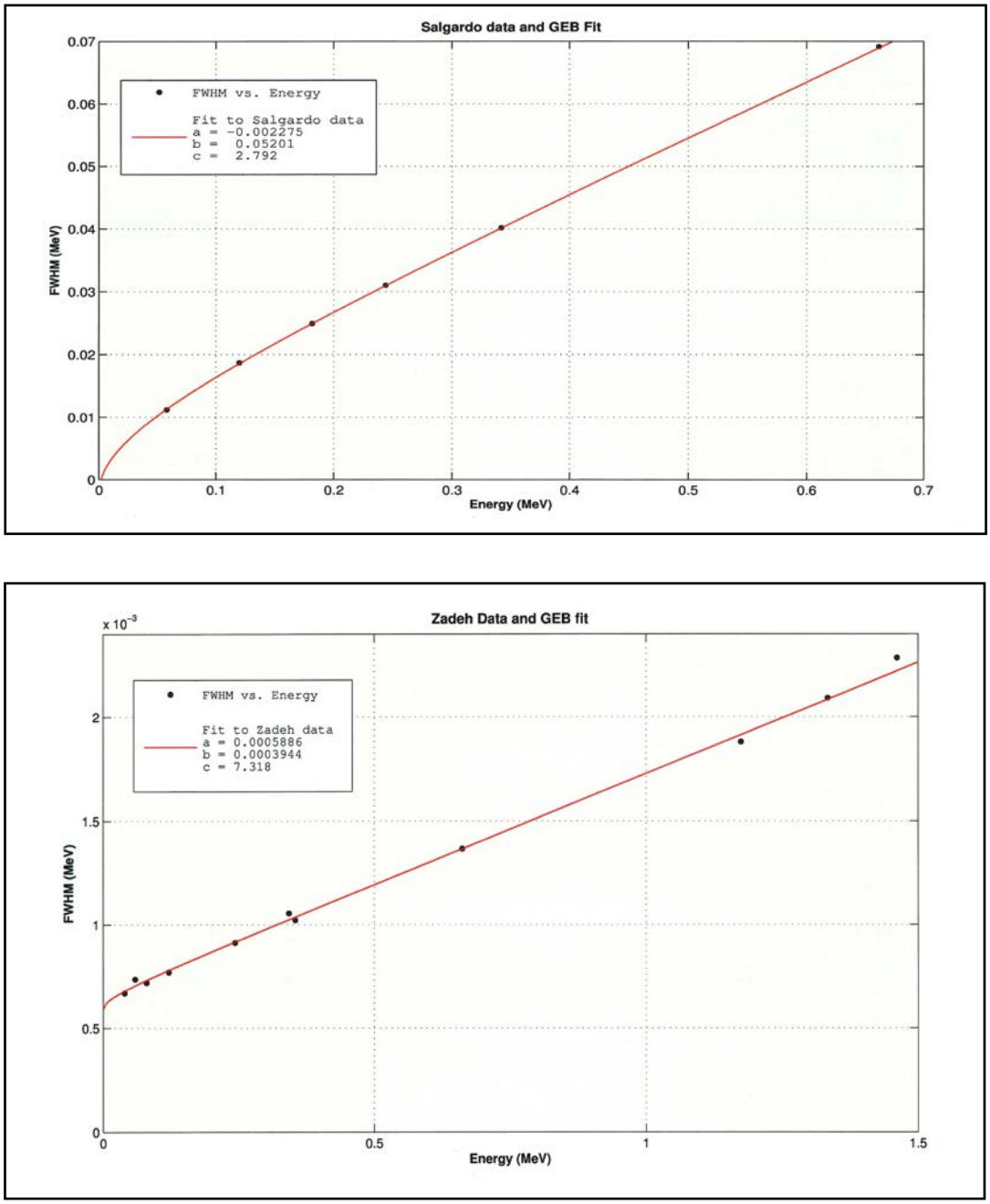

Figure 5: Matlab fit to published data for NaI and HPGe detectors with a, b and c coefficients.

The *a, b* and *c* coefficients produced by this approach match exactly those published by Salgardo and Zadeh.

5) Concluding Summary

This poster reports modelling gamma detector performance in MCNP6 through the application of Gaussian Energy Broadening.

5.1) A methodology was developed that relied heavily on Gaussian mathematics and binomial expansions that generated the *a, b* and *c* coefficients required by MCNP6 in the modelling of gamma detector performance. This approach only needed values for the $FWHM$ at two different energies and is typically the approach one would adopt with access to only the detector's performance specification sheet.
5.2) The *a, b* and *c* coefficients generated by the binomial expansion approach were used in MCNP6 together with published values and the resulting Gaussian functions compared. Excellent agreement was seen.
5.3) A curve fitting application in Matlab was also used to generate the *a, b* and *c* coefficients. This approach matched exactly with the published data.

6) References

1. MCNP6 is a general purpose Monte Carlo radiation transport code developed at Los Alamos

2. Validation of a NaI detector's model developed with MCNP-X code. Progress in Nuclear Energy 59 (2012) 19-25. C M Salgardo, L E B Brandao, R Schirru, C M N A Pereira, C C Conti.

3. Gaussian Energy Broadening Function of an HPGe Detector in the range of 40keV to 1.46MeV. Journal of Experimental Physics. Volume 2014. Article ID 623683. E E Zadeh, S A H Feghhi, E Bayat, G H Roshani

NDA quantification of Nuclear Materials in containers

Kevin Galliez[a], Clement Deyglun[a], Guillaume Jossens[b], Christophe Mathonat[a], and Alain Godot[a]

[a]KEP Nuclear, ZA de l'Euze 2, 453 Chemin vieux de Chusclan, 30200 Bagnols sur Cèze
[b]KEP Technologies High-Tech Product, 7 rue de l'Oratoire, Caluire, 69300, France

Abstract:

The precise determination of the amount of nuclear material within a container has long been a challenge, and especially with complex matrix and lack of homogeneity.
A measurement approach combining calorimetry, gamma spectrometry is presented as an integrated nuclear material characterization system.
Calorimetry is one of the best solutions to determine the overall quantity of nuclear material on a wide range of mass, from a few milligrams up to kilograms of radionuclides. It has many advantages as it features a non-destructive method which remains independent of matrix effect or the chemical composition. Modern technological developments within the calorimetry field give the promise of faster measurement times and precise measurements with low levels of uncertainty. Gamma spectrometry allows the determination of the isotopic abundance to qualify precisely each radionuclide.
Until now, calorimetry allows to measure at the lowest 0.5 to 1 mW for samples but nowadays, thanks to new technological breakthroughs, KEP-Technologies calorimeters are able to measure as low as 50 µW for 40 liters samples and less for a few liters containers.
This new calorimeter named µLVC is based on a new design with twin cells, a new temperature regulation loop and a heat-flow measurement system inside a vacuum chamber (Patent deposit P005299 LA/VL). The µLVC is a differential heat-flow calorimeter for precise measurement independent of the residual fluctuations caused by environmental changes.
The new calorimeter is an industrial product able to work in environmental conditions with wide temperature variations. Its software is friendly user and allows measurement time optimization and uncertainty calculation.
A device combining calorimetry and gamma spectrometry is designed as a new tool for quantification of nuclear material to characterize Pu-Am samples, i-graphite, and low tritium samples with high precision and reliability.

Keywords: calorimetry, gamma spectrometry, quantification, container,

1. Introduction

Large Volume Calorimeter (LVC) from KEP Technologies has been designed for the non-destructive assay (NDA) of nuclear materials and in particular the assay of nuclear materials that emit α and β nuclear radiation (e.g. Plutonium (Pu + ^{241}Am), Tritium). Calorimetry provides an accurate means to quantify the total Pu or tritium content, when used in combination with knowledge of the relative isotopic composition obtained from high resolution gamma spectrometry (HRGS).

The calorimetric signal results from the measurement of the heat flow between the measurement cell containing the radioactive sample and the thermal block [1]. This thermal heat flow generates a signal (µV) based on time which is recorded by a data acquisition card. When the heat flow signal is stabilized, this one is converted to a thermal activity (W) by means of the linear calibration curve.

Calorimetry is used as a nondestructive assay (NDA) technique for determining the power output of heat-producing nuclear materials. The heat is generated by the decay of radioactive isotopes within the item. Hence, the knowledge of the isotopy easily allows mass of each isotopes calculation:

$$M_i = R_i \times \frac{W}{\sum_{j=1}^{N} R_j \times P_j}$$

Where M_i is the mass of the i^{th} isotope, R_j isotope fraction, P_j specific power and W the thermal power measured with calorimeter. $\sum_{j=1}^{N} R_j \times P_j$ is the effective specific power of the mix (P_{eff}).

2. A new design

KEP Nuclear has developed a new type of calorimeter, called µLVC (Figure 1) meaning microwatts-Large Volume Calorimeter, able to measure tens of microwatts for a container volume from 1 to 40 liters.

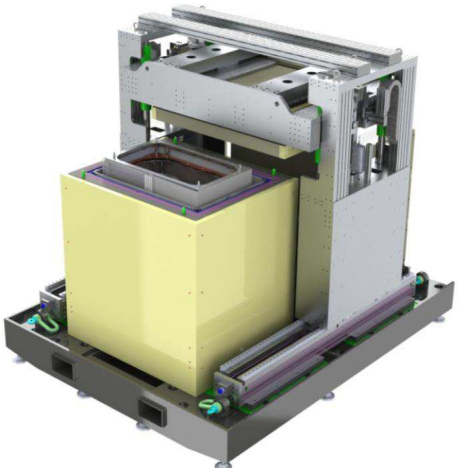

Figure 1 : 3D view of the µLVC calorimeter

The µ-LVC is based on a differential heat flow calorimeter designed with twin cells, temperature sensors and heat-flow measurement system inside a vacuum chamber (Patent deposit P005299 LA/VL). Differential heat-flow calorimeters are designed with twin cells for a precise heat flow measurement. Thus, residual fluctuations caused by environmental changes are approximately cancelled out by the signal difference formed between the two cells. The calorimetric signal results from the measurement of the heat flow between the measurement cell containing the radioactive sample and the thermal block. The temperature of the thermal block is maintained constant thanks to resistive heater. This thermal heat flow generates a signal (µV) based on time which is recorded by a data acquisition system. When the heat flow signal is stabilized, this one is converted to a thermal activity (W) by means of the linear calibration curve. The
Figure 2 shows a schematic view of the calorimeter.

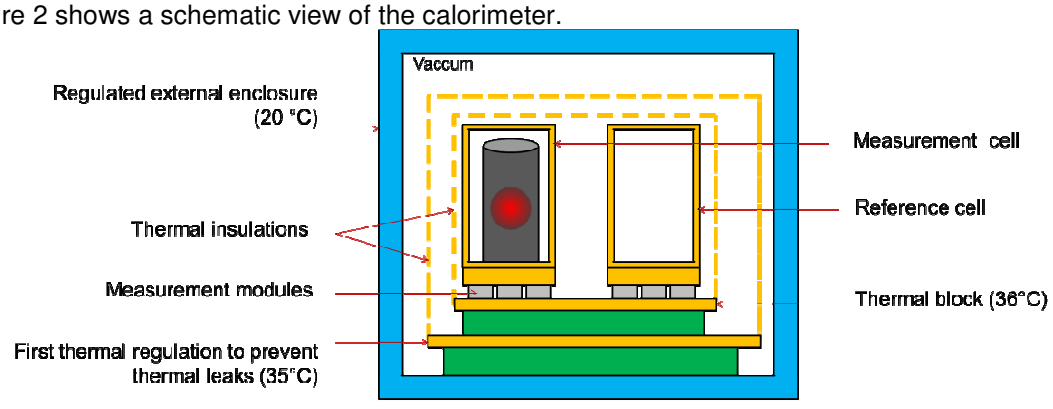

Figure 2 : Schematic view of the µ-LVC

There are two modes for the regulation of the thermal block:

- Wheatstone Bridge Regulation (WBR): the temperature between the reference cell and the measurement cell is measured with a sensitive resistance wire arranged in a Wheatstone bridge configuration. The advantage of a Wheatstone bridge measurement is that measuring a difference of resistance between the terminals of the bridge provides a differential measurement (lower measurement range - higher sensitivity). Wheatstone bridge cardboards were developed by KEP Technologies in 2015. They allow measurement with a noise of 20 nV equivalent to 5 µ °C with a stability of 50 to 100 nV or 10 to 20 µ °C.
- SRFT ("Système de Régulation de Flux Métrique"): the heat flow between the calorimetric block and a mass of high thermal inertia - which serves as a reference of temperature - is regulated. The information on the heat flow is given by a thermopile installed between the reference mass and the thermal block. The signal coming from the thermopile is kept constant and close to zero in order to bring the calorimeter at its thermal equilibrium. This principle allows achieving high temperature stability and a very precise regulation. In the case of the calorimeter µLVC, the reference mass is the reference cell and the calorimeter block is the thermal block (see
- Figure 2).

The limitation of thermal leaks of the calorimeter is ensured by the use of a high vacuum (< 1.10^{-6} mbar) thermally regulated.

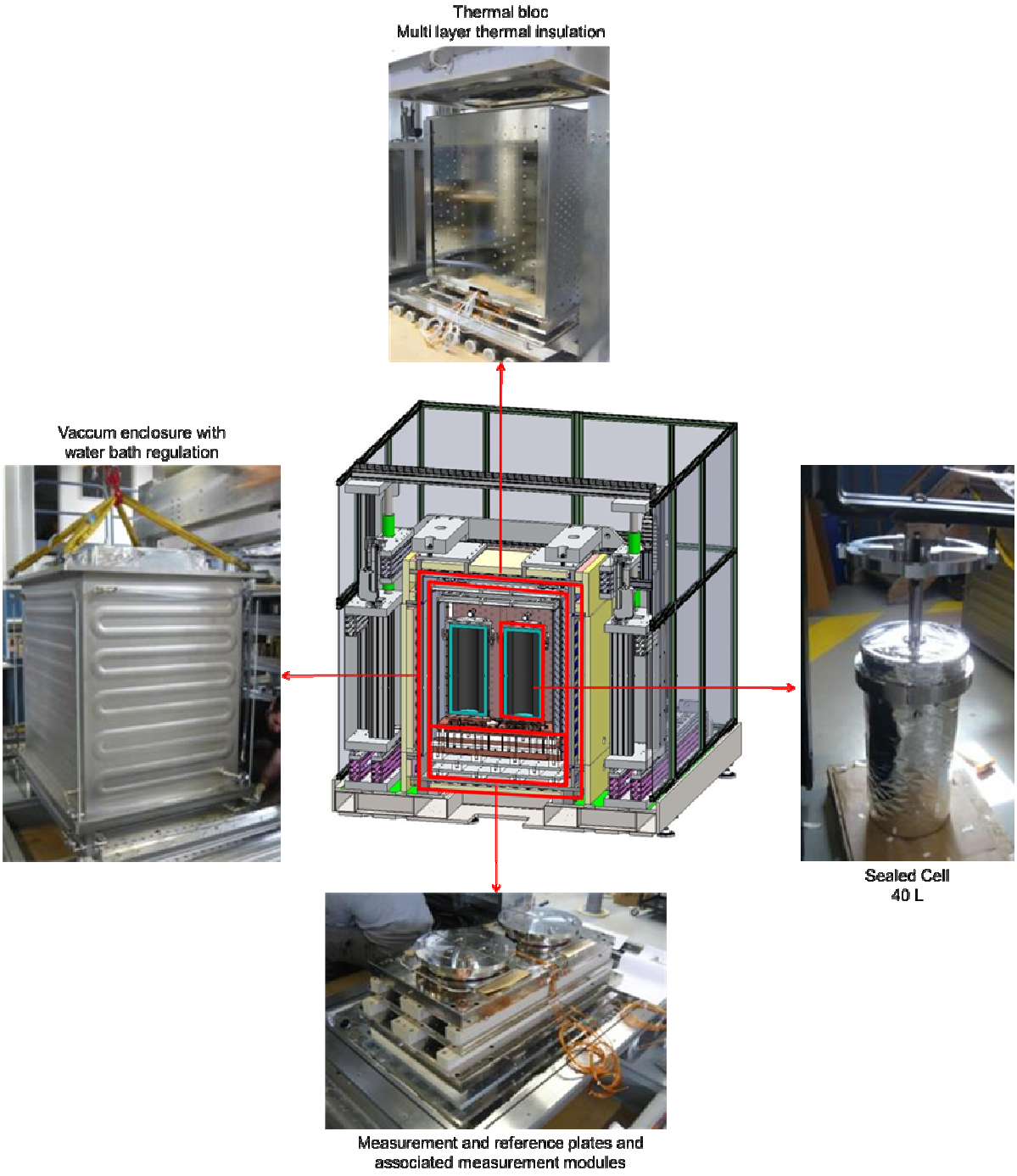

Figure 3 : Pictures of the µ-LVC

3. Calorimetry-gamma spectrometry combination

3.1.Alpha and beta emitters heating

First of all, it is important to understand how heat is produced by alpha and beta emitters.

In the case of beta emitter, the total reaction energy is shared between the beta particle, neutrino, the excitation energy and recoil energy of the daughter. The characteristic distance of 2 MeV electrons is a few millimeters in the matrix and all of the kinetic energy of the beta particle is absorbed by the sample. One 200 keV or 2 MeV electron in polyethylene produces respectively ~0.15 keV and ~11 keV X-ray due to bremsstrahlung radiation. . The neutrino is not absorbed, so its energy is lost. At

last, the thermal power measured by a calorimeter from beta emitters is the product of the activity and the average beta-particle energy, plus the de-excitation gamma-ray energy deposit taking into account the decay scheme. The gamma-ray contribution can be calculated with Monte Carlo code, e.g. MCNPX [2].

The heat produced by the decay of alpha emitter as for ^{239}Pu, in case of complete stopping of particles is distributed as follows :

- Alpha particle: 98.17%
- Recoil: 1.67%
- Conversion electrons: 0.1%
- Auger electrons: 0.035%
- X-rays: 0.01%
- Gamma-rays: 0.001%

The range of 5-6 MeV alpha particles is around 5 µm in common materials. Thus, all of the energy released by charged particles during the alpha decay will remain within the item as heat. Low-energy gamma-rays and X-rays can be assumed to be totally absorbed in the matrix and the specific power of alpha emitter is directly deduced from the Q-value. The gamma-rays and X-rays contribution can also be calculated with MCNPX [2].

Because the heat-measurement result is independent of material and matrix, it can be used for the inspection of any material form or matrix. The specific powers and the associated uncertainties are listed in **Erreur ! Source du renvoi introuvable.** for all plutonium isotopes and ^{241}Am.

Isotopes	PANDA database [**Erreur ! Signet non défini.**]	
	specific power [mW/g]	Relative Standard Deviation (%)
^{238}Pu	567.57	0.05
^{239}Pu	1.9288	0.02
^{240}Pu	7.0824	0.03
^{241}Pu	3.412	0.06
^{241}Am	114.2	0.37

Table 1. Specific powers and uncertainties (gamma-rays and X-rays are assumed to be totally absorbed in the matrix).

The calorimetric block is insulated by alternating layers of insulating and conducting materials to protect the blocks from external disturbances (external temperature variations). The insulating layers constitute a thermal barrier designed to filter short term and long term (between day and night) disturbances. To increase calorimeter temperature stability, and therefore its performance, thermal leakage between the sample and the environment must be perfectly controlled and reproducible. This is achieved by having the optimized insulation with a well regulated external temperature

3.2 Gamma-rays spectrometry

The estimation of the isotopy of a plutonium and uranium sample is a well-developed technics. To calculate the amount of nuclear materials, the global system needs to well-known the isotopic fractions and the specific power (mg/W) for each isotope.
A planar HPGe detector is used commonly. With a front surface area of 2000 mm^2 and a thickness of 20 mm, this type of detector gives a good compromise between resolution and efficiency (figure 4).

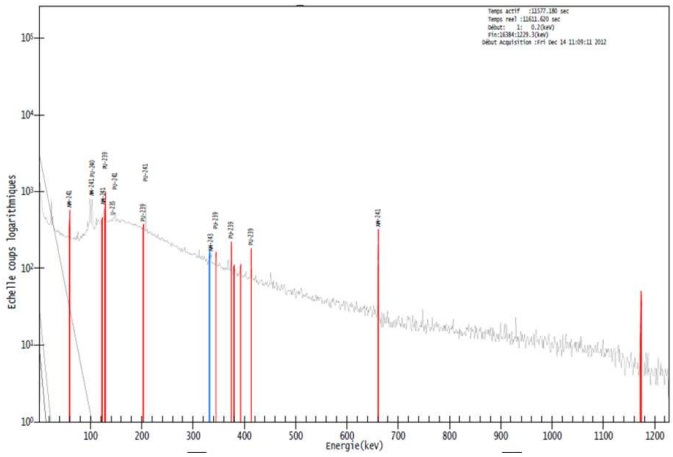

Figure 4 : Gamma spectrum of waste drum.

The multi peak analysis of all gamma emitted in the 60-300keV energy range allows to determine the isotopic ratios with MGA [3] or PC/FRAM [4] software with accuracy better than 1 %.

The measurement time is less than 1h.
The system can use a rotation platform for the sample and scanning equipment in the case of a tall container. The design allows being applicable to samples of arbitrary size, geometry, age, chemical composition and isotopic composition.
The precise determination of isotopic fractions depends of a good energy resolution (less than 0.6 keV at 122 keV) and of the quality shields positioned between detector and canister.

4. Conclusions

A complete solution using a calorimeter with an integrated gamma-ray spectrometer is a very precise and well adapted device for the special nuclear material containers measurement.
Thanks to the high accuracy of the calorimetric technology it is possible to know the amount of each radionuclide with a low uncertainty. The major contribution for the uncertainty determination is the isotopic measurement by gamma spectrometry.
KEP Nuclear [5] has developed a new calorimeter able to measure less than 100 µW with an uncertainty lower than 10 % (k = 1) for containers from 1 to 40 liters. This calorimeter called µLVC, is based on a differential heat flow calorimeter designed with twin cells in a vacuum enclosure according to a patented design. The optimized SRFT and WBR regulation modes ensure a very low detection limit (less than 50 µW for 40 liters containers and below for smaller volume). The µLVC has also been designed to work under air, which is an advantage for containers not adapted to work under vacuum. Further measurement will be necessary to completely qualify the measurement under air but actual results show a detection limit inferior to 700 µW. Further tests are also already planned at KEP Nuclear to improve the detection limit under vacuum. Indeed, the vacuum is to be regulated in order to decrease the noise on the measured differential heat flow.

[1] D. S. Bracken, and Clifford R. Rudy, “Principles and Applications of Calorimetric Assay”, PANDA 2007 Addendum.

[2] https://mcnpx.lanl.gov/

[3] R.Gunnink, MGA : *A Gamma-Ray Spectrum Analysis Code For Determining Plutonium Isotopic Abunbances*, LLNL report UCRL-LR-103220, April 1990.

[4] Thomas E. Sampson, Thomas A. Kelley and Duc T. Vo, *Application Guide to Gamma-Ray Isotopic Analysis Using the FRAM software*, Report LA-14018, Los Alamos National Laboratory, September 2003.

[5] www.kep-nuclear.com/

IN-SITU MONITORING OF RADIONUCLIDE POLLUTIONS IN NATURAL WATER RESERVOIRS

A.Sokolov, A.Pchelintsev, A.Kails, V.Gostilo

Baltic Scientific Instruments, Riga, Latvia

Abstract:

We show the results of the development of an automated spectrometer based on a coaxial HPGe detector for in-situ radionuclide monitoring in natural water reservoir. The newly developed spectrometer is clearly superior to traditional laboratory measurements, at least with regard to the fact that it does not require a large quantity of water samples to be taken. By measuring directly at the reservoir bank, the spectrometer provides a MDA for the activity of the radionuclide ^{137}Cs of not more than 2.5 Bq/l for a measurement time of 1000 seconds. At that the absolute registration sensitivity to a 662 keV gamma flux is $15x10^{-3}$ pulse/quantum. The device background is less than 0,003 pulse/s.

Keywords:in-situ radionuclide analysis, environmental pollutions, radionuclides in water

1. Introduction

Radioactive pollution of the environment is the most serious ecological effect of radiation accidents that involve radionuclides release. An analysis of the aftereffects of the accidents at the Chernobyl and Fukushima nuclear power plants (NPPs), shows that the extent of the radioactive pollution of the natural environment was determined by the dynamics of the radioactive release and the meteorological conditions during the release, which resulted in a complicated patchwork structure, in which different radionuclides are found in different parts of the territory [1,2].

The dynamics of the release of the radioactive materials, as well as the evolution of contamination over time in natural objects such as soil, forests and natural ponds, greatly depends on the specifics of those objects. Radioactive products may reach natural water ponds as a result of deposition on the water's surface, drainage from the polluted area and underground aquifer flows. As a result, the picture of radiation pollution of natural reservoirs changes constantly.

As a result of the accident at the Fukushima NPP, all ponds within a radius of 50 kilometers were contaminated with radionuclides to different degrees [3]. Together, ten reservoirs for potable water and irrigation in the surroundings of Fukushima-1 were found to have high concentrations of radioactive Cesium after the accident. Monitoring of the reservoirs, ponds, and rivers was started in September, 2011 so that scientists and ecologists could determine and understand the motion of radioactive substances from mountains and forests and monitor the progress and effectiveness of decontamination activities. In total, the specialists provide indicators monitoring of 73 reservoirs in Tokyo and seven nearby prefectures. Sample probes were made approximately once every few months.

The standard practice of monitoring radionuclides and their activity in water reservoirs involves removing water samples from the reservoirs and measuring them in a laboratory by means of shielded laboratory spectrometers [4-6]. However, for a large number of samples, that monitoring technology might become too labor-intensive and, thus, unworkable.

Our company has extensive experience in the development of equipment for monitoring radionuclides and their activity in water for various applications: in laboratory conditions [7], in the first coolant circuit of nuclear reactors [8], in waste outlets at NPPs [9-11], in deep water conditions on the sea bottom [12]. In the present work we show the results of the development of an automated high-purity germanium (HPGe) spectrometer for in-situ radionuclide monitoring in natural water ponds in the territory around the Fukushima NPP. It goes without saying that such an automated spectrometer could be used for radiation monitoring of natural reservoirs in any region.

2. Spectrometer

A photo of the developed spectrometer is shown in Fig.1. The spectrometer is based on a coaxial HPGe detector with an efficiency of 40%. However, a detector of higher efficiency (up to 160% or more) could be installed there if necessary. The application of HPGe detector in the present spectrometer was caused by the necessity to monitor the dynamics of possible wide list of radionuclides in natural water reservoirs.

Fig.1. Automated HPGe spectrometer for in-situ radionuclides monitoring in natural reservoirs

The detector is installed in a U-type cryostat fabricated from radiation pure materials integrated with a 30 liters Dewar vessel that was equipped with a sensor to monitor the liquid nitrogen level. Although Stirling electric coolers could have been used at present for HPGe detectors cooling, in this spectrometer we have used liquid nitrogen cooling. The cooling system is capable of providing uninterrupted operation without refilling for at least 14 days. The energy resolution of the spectrometer is 0.9 and 1.8 keV for photon energies of 122 and 1332 keV, respectively; the system is capable of recording photons over an energy range of 50 to 2800 keV. To provide low radionuclide detection thresholds, the detector is surrounded by a 70 mm thick lead shield. A standard multichannel spectrometer with the SpectraLineGP and Nuclide Master Plus software packages are used to identify radio nuclides and calculate their activities.

The hydraulic system consists of a sampler based on a cylinder glass vessel, which embraces the detector cap, a flow meter system with a valve unit and a mechanism for changing the sampler. The cylinder glass vessel is manufactured from low sorbent glass. The rate of the measuring water flow can be regulated with an input choke from 0.1 to 5.0 l/min, which allows a high rate of sample processing. While measuring, the sampler can process up to 75 l of water in 15 min. The hydraulic system works in four operating modes: Measurement, Cleaning, Background Measurement and Sampler Exchange Mode. The custom designed software controls all aspects of the spectrometer operation. The parameters of the spectrometric and hydraulic subsystems are displayed on a computer monitor.

The dimensions of the developed spectrometer are 1300x580x480 mm^3; the total weight is 170 kg. The spectrometer is powered by a car battery and placed on a special antivibration surface in a Nissan minivan, which could approach the bank of any reservoir and carry out in-situ water monitoring of that particular (Fig.2).

Fig.2. The connection of the pump on the reservoir bank before the monitoring

3. Metrological characteristics and their discussion

For the spectrometer calibration, a special gamma radiation source was made in the shape of the spiral measurement sampler. To make this source, the sampler was filled with ion-exchange resin and impregnated with a solution that contained the radionuclides ^{152}Eu and ^{241}Am at a known specific activity. The activity of this calibration source has been determined on a standard gamma spectrometer whose measurement inaccuracy does not exceed 2% (absolute). With that calibration source, installed in the spectrometer in place of the measurement sampler, an efficiency curve for that particular geometry was recorded. Further that efficiency curve was applied for calculation of radionuclide activity in measured water samples.

For the developed spectrometer the absolute registration sensitivity to a flux of 662 keV gamma rays is $15x10^{-3}$ pulse/quantum. The minimal detection activity (MDA) for the radionuclide ^{137}Cs assuming a measurement time of 1000 seconds is not greater than 2.5 Bq/l. Fig.3 shows the background spectrum of the spectrometer, acquired in 57168 s (approx. 16 hours). It is apparent that the background spectrum contains only the natural radionuclides ^{40}K and ^{232}Th. In low energy range of spectrum X-Ray lines of shield lead (Kα&Kβ) are seen. Background level in range of (662±1.5) keV is low - less than 0,003 pulse/s.

Laboratory HPGe spectrometers with lead shield can provide better performance in terms of background characteristics. HPGe detector with 40% relative efficiency provides MDA less than 0.9 Bq for 1l Marinelli beaker and measurement time 1000 s for ^{137}Cs [13]. Background level in range of 50-3000 keV is less than 1.7-1.8 pulses/s, and in range of (662±1.5) keV is approximately 0.0018 pulse/s. However, during laboratory measurements it is necessary to prepare manually large number of samples, load them into the lead chamber and carry out measurements. The developed spectrometer is completely automated and is able to carry out the whole measurement process, including system washing under control of software. The developed spectrometer does not require manual sampling and preparation of water specimen. Monitoring can be organized directly on the bank of natural water reservoir.

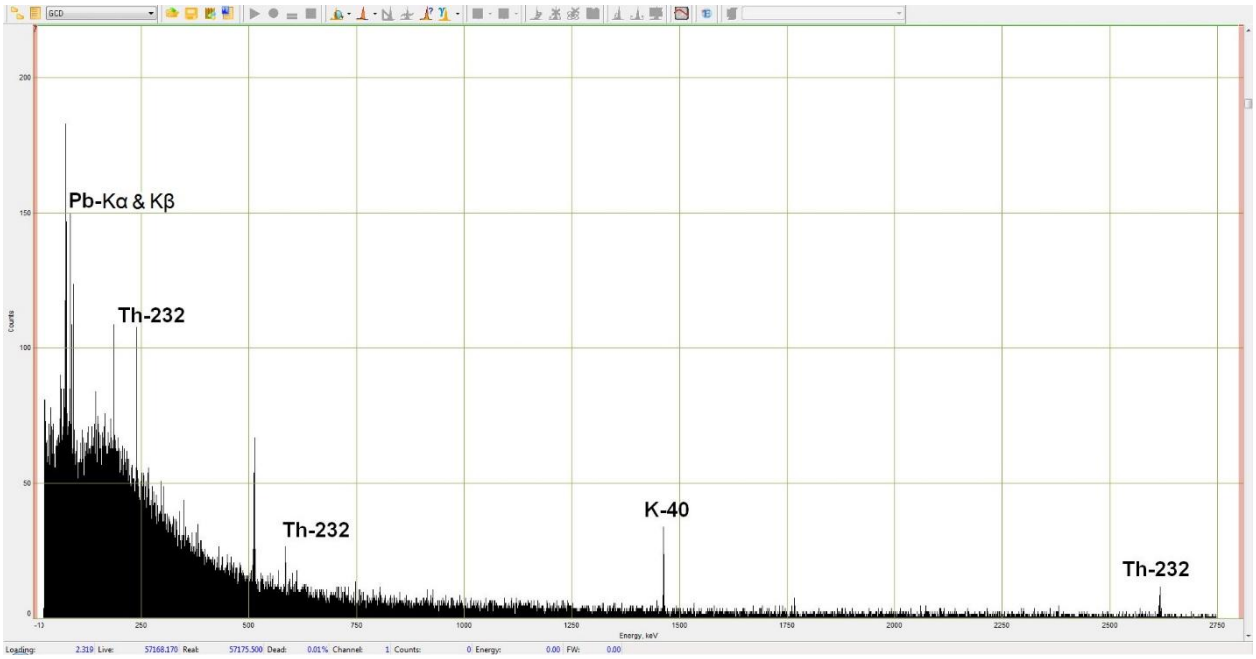

Fig.3. Background spectrum of the spectrometer. Acquisition time was 57168 s

The monitoring results in the first natural reservoir have revealed besides the natural ^{40}K only Cesium radionuclides in the water. Fig.4. shows the spectrum of radionuclide pollution in this water reservoir. The measurement time was 30 min. The spectrum distinctly shows the radionuclide lines ^{134}Cs, ^{137}Cs and ^{40}K. The water activity was ~ 6 Bq\l, as compared to a minimal detectable activity of less than 2.5 Bq/l for ^{137}Cs.

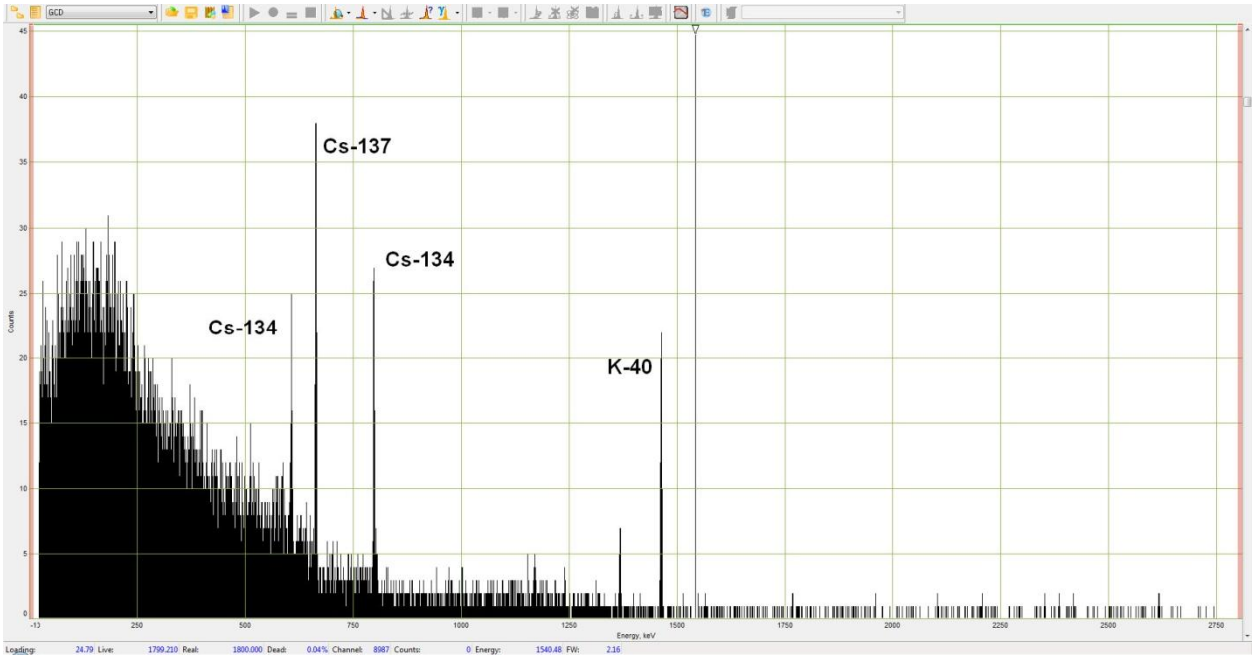

Fig.4. Radionuclide pollutions spectrum in one of the natural pond.
The measurement time was 30 min.

4. Conclusions

The newly developed, automated HPGe spectrometer for in-situ radionuclide monitoring of natural reservoirs is clearly superior to traditional laboratory measurements, at least with regard to the fact that it does not require a large quantity of water samples to be taken. By measuring directly at the reservoir bank, the spectrometer provides a MDA for the activity of the radionuclide ^{137}Cs is not more than 2.5 Bq/l

for a measurement time of 1000 seconds. At that the absolute registration sensitivity to a 662 keV gamma flux is $15x10^{-3}$ pulse/quantum.

5. Acknowledgements. The authors are very thankful to Dr. Atsuhito Ennyu (Japan Environmental Monitoring & Scientific Co., Ltd.) for assistance in spectrometer commissioning and testing.

6. References

[1] INSAG-7. The Chernobyl Accident: Updating of INSAG-1. A Report by the International Nuclear Safety Advisory Group. IAEA, Vienna, 1992.
[2] The Fukushima Daiichi Accident. Report by the Director General - Vienna: IAEA, 2015.
[3] Results of Radioactive Analysis around Fukushima Daiichi Nuclear Power Station http://www.tepco.co.jp/en/nu/fukushima-np/f1/smp/index-e.html
[4] G. F. Knoll. Radiation Detection and Measurements. J. Wiley & Sons. Third Edition. 2000.
[5] G. Gilmore. Practical Gamma-Ray Spectrometry. John Wiley &Sons, 2nd ed., 2008.
[6] E.J. Hall. Radiation and Life, 2nd edition, Pergamon Press, New York, 1984.
[7] http://bsi.lv/en/products/hpge-detectors-spectrometers/hpge-spectrometer-lead-shield/
[8] A.Sokolov, V.Kuzmenko, A.Pchelintsev, V.Gostilo, G.Kashey, D.Meleta, G.Mihailov, D.Chernyh, P.Semin, A.Nagorny, V.Pletnev, K.Gediminskas, S.Bormotov. Automated System for Radionuclide Monitoring of Heat Carrier in the Primary Coolant Circuit of NPPs. Proc. of 29th Annual ESARDA meeting "Safeguards and Nuclear Material Management", Aix-en-Provence, France, 22-24 May, 2007
[9] V.Gostilo, A.Sokolov, S.Danengirsh, V.Kondrashov, A.Loupilov, V.Fedotenkov, A. Ptchelincev, A. Pechersky, S. Babkin, S. Nekrestyanov, V. Kireyev, O. Pyhteyev, V. Ivanov, D.Likov, E. Kozlov, A. Epihin. Automated Monitoring System for Radionuclides Volumetric Activity in Waste Water of Nuclear Enterprises. Proc. of 23rd ESARDA Annual Symposium on Safeguards and Nuclear Material Management, Brugge, Belgium, 8-10 May, 2001.
[10] A.Sokolov, A.Voronin, V.Gostilo, S. Danengirsh. Submersible Gamma Spectrometer Based on HPGe Detector. Proc. of 22nd ESARDA Annual meeting and seminar "Strengthening of Safeguards: Integrating the New and the Old" Dresden, Germany, May 8-12, 2000.
[11] V.Gostilo, A.Sokolov, S.Danengirsh, V.Kondrashov, A.Loupilov, V.Fedotenkov, A.Pchelintsev, S.Nekrestjanov, V.Kireyev, O.Pickhteyev, V.Ivanov, D.Likov. Floating Monitoring Station for Measurements of Radionuclides Volumetric Activity in Water Reservoirs. Proc. of 24th ESARDA Annual Meeting "Safeguards and Nuclear Material Management", Luxembourg, 28-30 May, 2002.
[12] A.Sokolov, S.Danengirsh, S.Popov, A.Pchelintsev, V.Gostilo. Autonomous Deep-Water Gamma Spectrometer based on HPGe Detector Proc. of 21st Annual Symposium on Safeguards and Nuclear Material Management. Sevilla, Spain, 4-6 May, 1999.
[13] http://bsi.lv/en/products/hpge-detectors-spectrometers/hpge-spectrometer-lead-shield/

Numerical studies of CBRN effects on civil and military structures

Holger Effertz, Martin Glende, Norbert Kopp, Jens Fiedler

technisch-mathematische studiengesellschaft mbH
Holtorfer Straße 54
53229 Bonn

Abstract:

Nowadays, satellites for e.g. navigation, communication, weather forecast, climate research have become integral parts for daily living.

Technical failures or loss of these systems result in strong impacts on almost all kinds of civil and military structures. Typical sources of interference are electromagnetic pulses of high altitude nuclear detonations or large amounts of charged particles caused by solar winds.

Experimental field studies of this topic, in particular high altitude nuclear detonations, are rarely known. Moreover, the access to experimental data is mostly restricted. Numerical simulations offer the possibility to investigate CBRN disaster scenarios in all facets where experiments and measurements are difficult to perform or almost impossible. Therefore, numerical studies complement the work of safeguards.

For the current work, the numerical simulation system HEAT of the tms company has been in development for many years to support the Ministry of Defense, Ministry of Civil Protection and Disaster Management for the cases of emergencies as a result of a CBRN incident.

Originally developed for defence purposes, HEAT has become a powerful tool for fire brigades, disaster and consequence management. It gives the possibility to investigate not only electromagnetic pulse effects but also the temporal dispersion of nuclear, chemical and biological agents in urban and rural areas.

Keywords: numerical simulation, dispersion simulation, CBRN effects

1. Introduction

Numerical studies are often performed where experiments are difficult to perform, almost impossible or at least forbidden. Such cases are the release of chemical, biological or radiological toxic agents. The distributions of CBRN materials in urban environments lead to severe health consequences for the civil and military population. Mostly, these cases of emergency are results of military conflicts, terrorism or industrial accidents. It is therefore of particular interest to study such events numerically and to assess possible dangers in advance.
In order to support the Ministry of Defense, Ministry of Civil Protection and Disaster Management for the cases of emergencies, the software system HEAT has been in development for many years. The purpose of this work is to present the current status of the program system HEAT and to demonstrate its capabilities to support the prospective work of safeguard.

2. The software system HEAT

HEAT (**H**azard **E**stimation **A**fter **T**BM Engagement) is a software system for the calculation and visualization of the consequences of intercept, that can be the result from an engagement of a ballistic missile (BM) fitted with an unconventional warhead. Such functionality is indispensable for

assessment of the effectiveness of extended air defense weapons systems, as well as for operational use in planning and early warning in the field of passive defense. HEAT is being developed by tms within the scope of R&D studies contracted by the Federal Office of Defense Technology and Procurement (BWB)[1].

The dispersion model on which HEAT is based is a particle model. At the start of the simulation of a transport and dispersion process, a cloud is generated from a variable number of warfare agent droplets (or particles for biological agents or nuclear materials). The form, size and composition of the cloud depend on various factors such as the warhead's damage degree, the engagement altitude, type of warfare agent, velocity of the ballistic missile (reentry vehicle) and interceptor, etc. The individual droplets precipitate depending on their size and the meteorological conditions. During this precipitation process, droplets can change as a result of evaporation effects and aerodynamic heating. If they hit the ground liquid droplets can continue to evaporate and therefore be the source for secondary dispersion. The calculation results in a time-variable deposition, concentration, concentration time product (dosage) matrix or hazard area.

Originally intended to support R&D studies, the software HEAT was developed further as a standalone system and enhanced to include operational elements. Apart from its use in national simulations for the Medium Extended Air Defense System (MEADS), this operational version of HEAT was used in 2000 to 2010 during the JPOW V - JPOW 2010 (Joint Project Optic Windmill) passive defense exercises. In the spring of 2003, HEAT was requested by NATO during operation "Iraqi Freedom" and was deployed to Turkey.

The calculation engine, on which the operational version of HEAT is based, was isolated as an independent module and is therefore available as a dispersion module for all kinds of different applications. Among other things, this simulation core has been integrated in the German Air Force's Surface-to-Air-Missile Operation Centre (SAMOC). A new version of the HEAT calculation core has been deployed to the German SAMOC in 2013. The calculation engine has been developed further to include a fast running algorithm has been developed that allows the generation of ground effects from intercepted chemical and biological submunition warheads as well as chemical unitary warheads within milliseconds.

In the latest version of HEAT, the calculation is not limited to BM as the source of the warfare agent or hazardous material dispersion. Ground-near sources, such as a continuous source from a container or a dirty bomb release can be defined as the starting point for the calculation. HEAT therefore supports the entire field of enhanced hazard prediction.

In addition to dispersion calculation, HEAT is also capable of performing evaluations according to NATO ATP-45, as used in the detailed methods of hazard prediction. NBC2 and NBC3 reports can be generated, which can be exchanged with other systems via the integrated communications module.
At the moment HEAT 8.0 is under development. It will be released by the end of 2017. Version 8.0 will be the first version of HEAT to incorporate a new 3D user interface based on NASA World Wind. In addition it will include fast running code that uses the power of modern hardware (multicore CPUs, GPUs) to generate results from a complex extended air defense scenario in the matter of milliseconds. HEAT 8.0 is based on Java technology which facilitates integration into new environments using well established technologies (Web services, SOA, EAI) and supports effective reuse, development and adaption in general.

3. Results

HEAT is a simulation system that generates all dispersion effects after the engagement of a non-conventional warhead, not just the immediate effects. That means that normally the output of HEAT is a hazard area of the complete dispersion process. HEAT incorporates a large set of model features. It uses a German hydrocode database for engagement evaluation. Aerothermal (reentry) effects for submunitions and particles are considered. Lagrange-type dispersion calculations and Gaussian

[1] now the Federal Office of Bundeswehr Equipment, Information Technology and In-Service Support (BAAINBw)

plume for fast ground release calculations has been realized. Moreover, comprehensive databases such as for chemical and biological agents and population density data have been implemented.

Transport calculations are performed for debris, submunition as well as agent droplets or particles. HEAT uses trajectory models of different complexity depending on the intended purpose. Three degree of freedom (DOF) calculations are used for most of the debris, submunition and stages calculations. Six DOF calculations can be used for stages and Magnus-rotor submunitions. Magnus-rotor submunitions are submunitions fitted with small rotors resulting in a non-ballistic flight and a larger area of sub-munition dispersion. For the calculation of agent dispersion the agent evaporation is also calculated along its trajectory. Figure 1 presents different examples of hazard areas resulting from debris and stages impacts (KV – kill vehicle, RV – re-entry vehicle, COI – consequence of intercept).

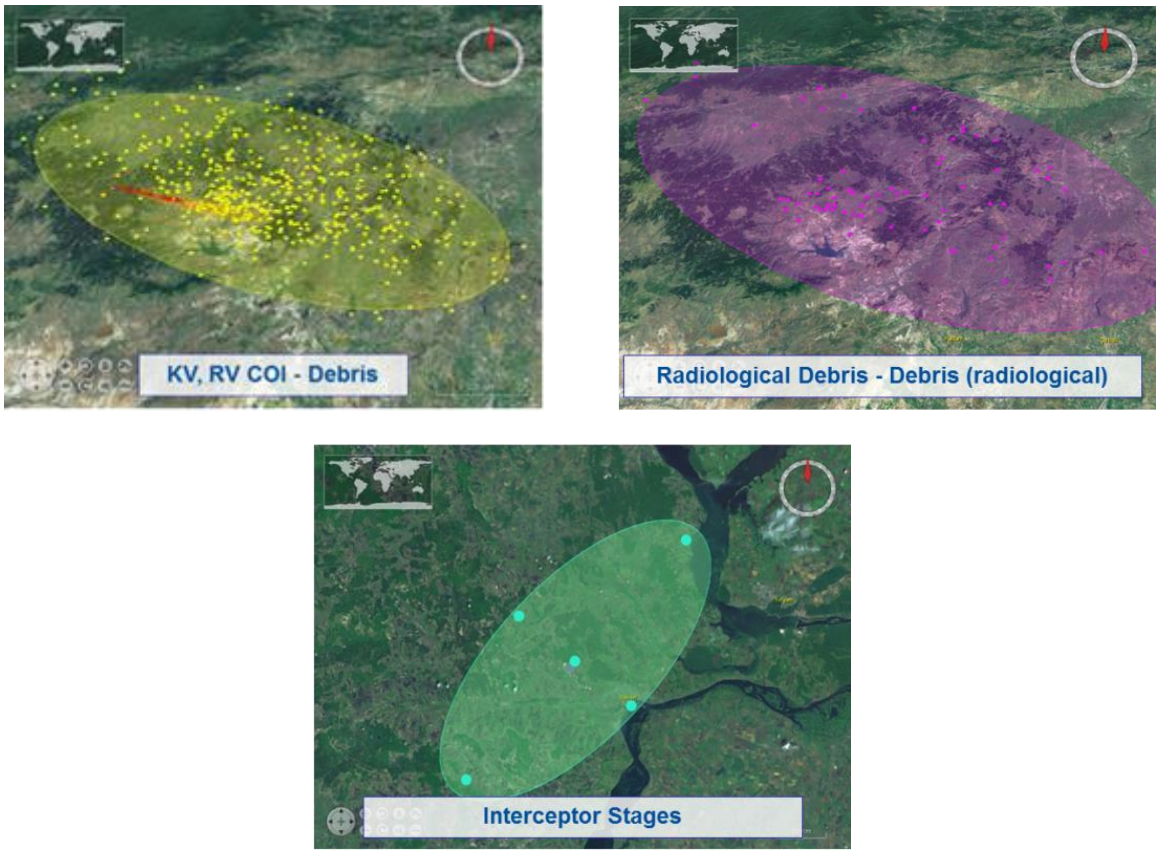

Figure 1: Hazard areas resulting from debris and stages impact.

In order to perform transport calculation atmosphere as well as weather information is needed. Therefore tms developed a HEAT Weather Service that is a weather server accessible through a web-service interface. This server receives current weather information from e.g. the Bundeswehr Geo Information Centre and is able to handle different weather formats. It can use simple wind profile data, weather data defined in STANAG[2] 2103 (ATP-45) as well as data according to STANAG 6022 (METGM). In addition it uses METAR ground weather data generated at all commercial airports worldwide. All this data is stored on a server and can be retrieved for simulation purposes using the web service interface.

When agent is released on or near the ground near-ground dispersion calculations are performed. The agent transport calculations described above are only relevant for non-volatile chemical agents released from a unitary warhead or from submunitions above ground (e.g. from fused submunitions).

[2] Standardisation Agreement

For volatile chemical agents, biological agents and radiological material released on or near the ground the near-ground dispersion has to be calculated. HEAT can do this using different source terms, complex wind fields and different types of coverage data. The dispersion model used to calculate these ground effects is a particle model.

In figure 2 the dispersion resulting from the explosive release of radiological material (25g of Cs-137) is shown, a so called “Dirty Bomb” release. This picture also shows the result of using a complex wind-field for the dispersion calculation process. HEAT can use different source terms.

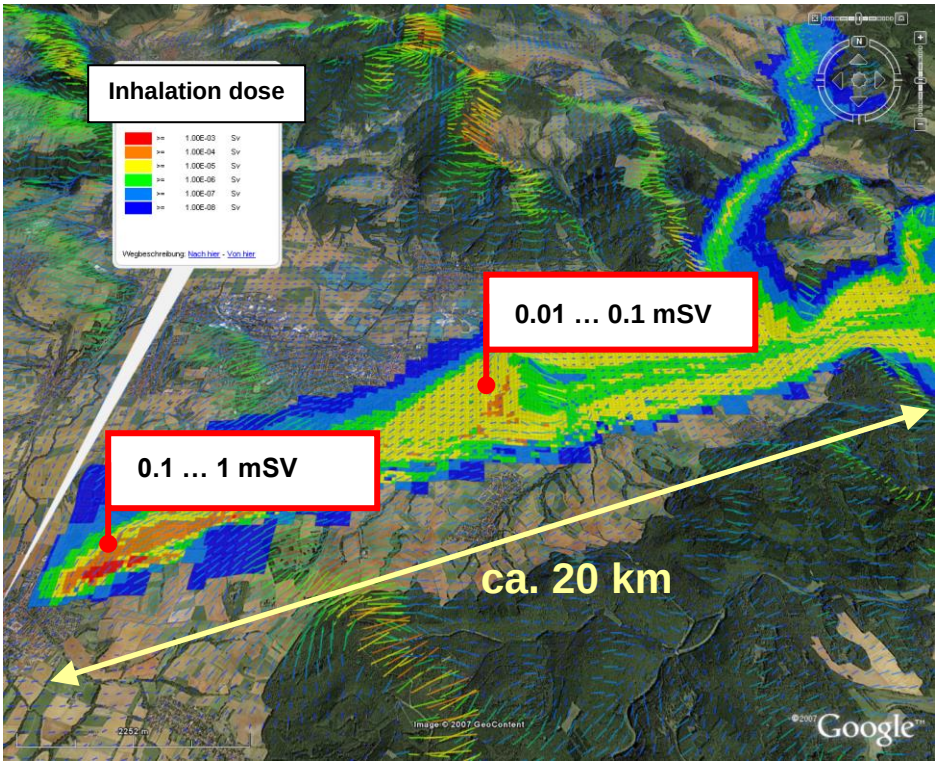

Figure 2: Dirty Bomb scenario (Cs-137).

HEAT handles high altitude nuclear detonation and its impact on satellites as well. Currently all unclassified satellites are integrated. Their position is constantly updated. The satellites affected by direct x-ray radiation can be evaluated in the scenario. In addition the ground effects from the generated electromagnetic pulse can be displayed. Refer to figure 3.

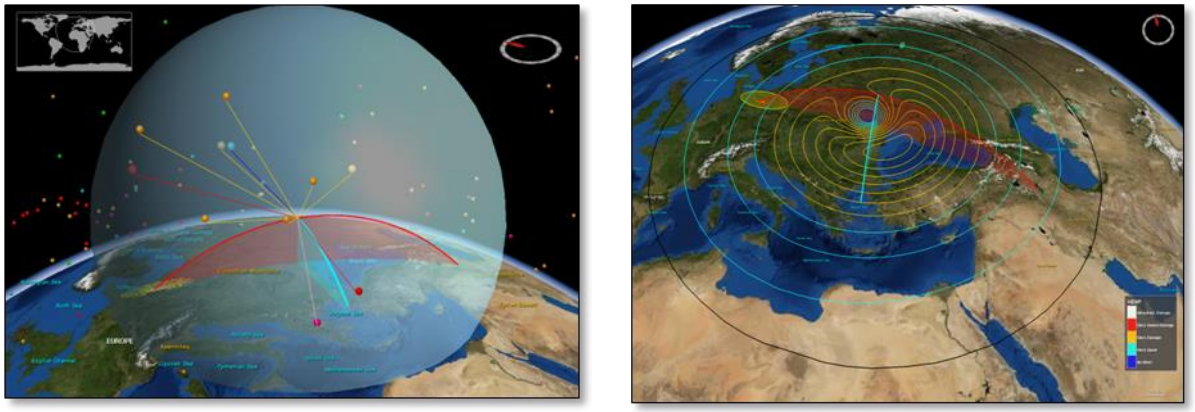

Figure 3: Satellites affected by X-rays (left) and electromagnetic pulse on the surface.

4. Conclusion and Outlook

Based on the results presented in this work, the program system HEAT gives the possibility to study the influences on civil and military structures resulting from military conflicts, attacks through terrorism or industrial accidents. HEAT performs dispersion calculations for a wide range of radiological, chemical and biological agents.
These numerical calculations are of significant importance for civil protection and disaster management. Due to the possibility to study almost all environmental effects resulting from an uncontrolled distribution of nuclear material HEAT could be a valuable extension to the prospective work of the safeguards.

ESARDA Symposium 2017
European Safeguards Research & Development Association
39th Annual Meeting 15-18 May 2017, Jülich/Düsseldorf (DE)

Closing Plenary Session

18/05/17

W. Janssens, ESARDA Vice President

CONTENT

- Highlights of the Symposium
- Feedback of the technical sessions
- Feedback of the panels : AP & RG
- Observations of intl. partners : INMM & APSN
- Closing remarks

HIGHLIGHTS

- High number of EU and Intl. participants!
- Multi-disciplinary & rich program (125 submissions)
- Introduction of panel sessions (AP & RG)
- Nice combination with visit of FZ Juelich
- Excellent & pleasant networking opportunities (Zum Schluessel, Rhine SUPER-cruise, Alt-bier,…)
- Invitation to all ESARDA Membership to contribute in actively shaping the future of ESARDA (50+)

199 Participants from 26 Countries worldwide

151 Participants from 18 European Countries

148 Participants from 16 EU-Countries

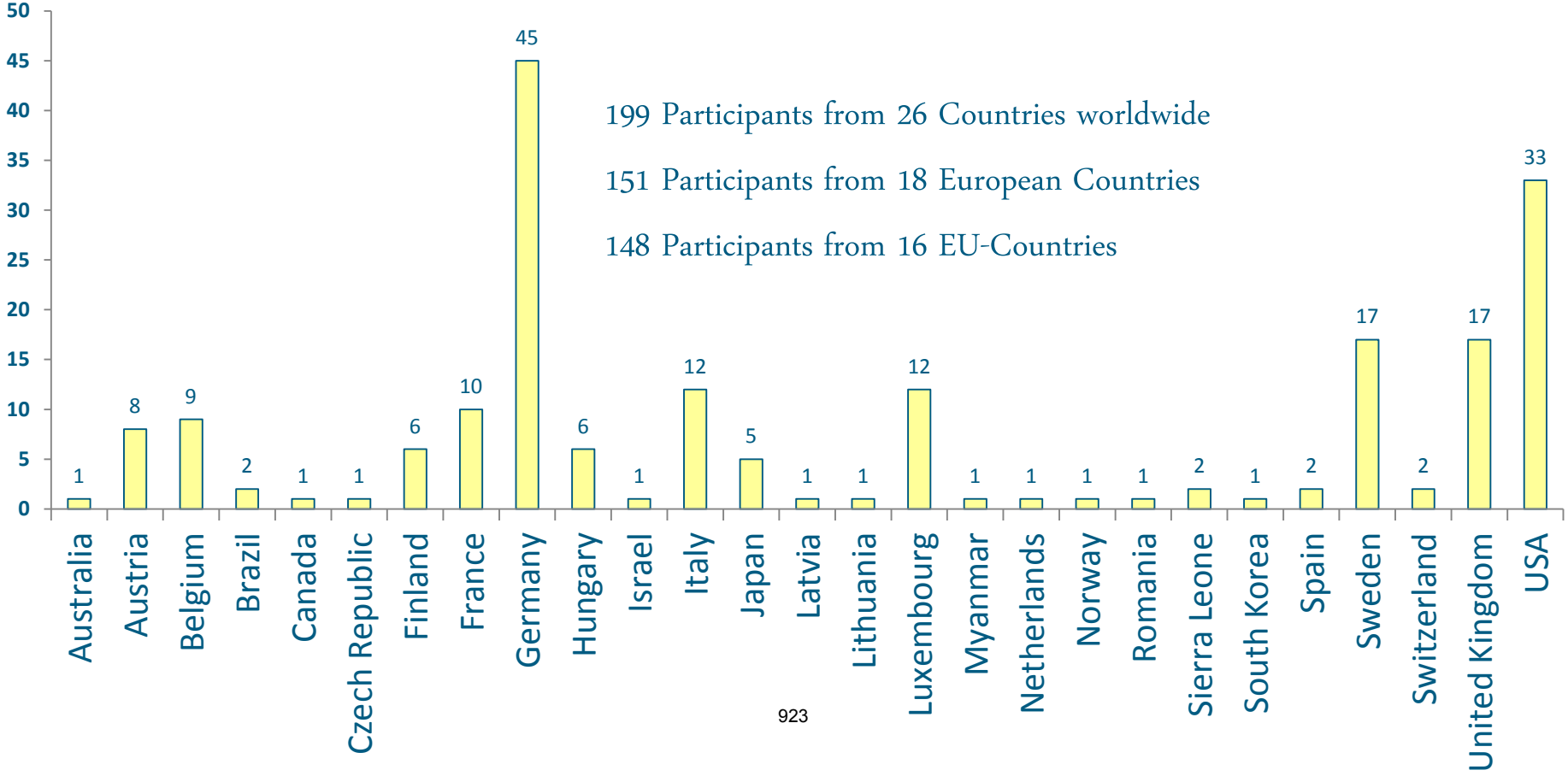

OPENING PLENARY

- Very supportive German & local contributions
- IAEA very encouraging (Technology, SLC, AP…)
- Strong European Commission (ENER/JRC) engagement
- International partnership very enthusiastic (INMM, APSN)
- Special attention to role & power of Women (WIN)
- Indications towards synergies with other areas such as Decommissioning and Waste Management, Disarmament Verification and Nuclear Security.

FEEDBACK FROM THE TECHNICAL SESSIONS

Session Chairs were asked to kindly report on :

- NOVELTIES (what was not known before)
- Most STRIKING and/or unexpected results
- Expected IMPACT on safeguards implementation
- RECOMMENDATIONS for making next step change
- Other ideas, messages, feedback & suggestions

NOVELTIES

1 New legal structure in Germany for the back end of the fuel cycle

3 NNSA is funding quite a few new developments without constraints of prior proof of request

4 CTBTO can combine info from multiple geophysical methods to generate site understanding

6 Solutions are presented also for transfering and storing damaged spent fuel

7 The use of Cf-252 as a replacement of AmLi and its “counter-intuitive background” is good

8 In arms control a wider focus on the overall enterprise is recommended (not only weapons)

9 Laser ablation trials and detector results in mass spectrometry / Automated Chemistry (ORNL)

10 Spent fuel data evaluation with neural networks

11 The training/qualification plans of NRC to meet gaps between experienced and new inspectors

12 New development techniques for UF6 sampling and in-field analysis

13 New techniques using fast neutron interrogation with very promising results

14 Application of new concepts and methodologies in data generation, collection and evaluation

16 Improved signal processing in high neutron count-rate fields

17 Development of short pulse systems with potential applications in safeguards and security

MOST STRIKING RESULTS

2 Evaluation of U and Pu IC with medium resolution gamma remains a challenge

3 Proposal for potential future Unobtrusive Surveillance with instantaneous accountability

4 Video-like stationary 60-90 s snapshots from satellite imagery

5 IAEA SLC may be a valuable tool for a systems approach to nuclear disarmament verification

7 The figure of merit of 6LiF:ZnS(Ag) neutron coincidence counter

9 Microparticle suspension trials and stability / Progress in Am-243 reference material

10 The contribution of neighboring assemblies in DCVD verification

11 Many training activities but very little on knowledge management (improvised panel)

12 Long term projects of production & certification of Pu-244 will be finalised soon (US-Russia)

13 Safeguards community realises that muons can be used for safeguards purposes

14 Cognitive burden to understand in-field data decreases in-field navigation/ attention

16 Ability to cope with count rates up 10E6 cps

17 Neutron interrogation using D/T generator and liquid scintilators

IMPACT ON SAFEGUARDS IMPLEMENTATION

2 Request confirmed for handheld and “agile” NDA equipment (electrically cooled …)

3 Support programmes to IAEA : essential input to IAEA safeguards implementation

5 Increased awareness of (non)-technical challenges on verification of N disarmament

6 **For 1st time for final disposal SFG : as many solutions presented as open questions**

7 **Helium 3 alternatives are well on the way to actually be replacements**

9 Greater traceability, efficiency and sensitivity for both bulk & particle environm. sample

10 SINRD (Self-indicating neutron resonance densitometry) progress

12 Improved (long-term stability) CRM for Safeguards inspectorates and industry

13 **We are very near to implement PGET and UGET techniques for safeguards eg encapsulation plants**

15 Need to clarifying the needs for the German dry storage safeguards requirements

16 Future applications of active neutron counting e.g. for Fukushima molten fuel

17 Further development and improvement of standards and technologies for detection

RECOMMENDATIONS FOR NEXT STEP-CHANGE

2 **Instrumentation (NDA) testing /intercomparison needed** to demonstrate capabilities/limitations

3 Novelties like using acoustics for density/mass flow measurements in GCEP need to be pursued

4 **Independent power supply for monitoring (seismic/georadar) after closing geological repositories**

6 Make an integrated "toolbox" for techniques and solutions for final disposal safeguards/monitoring

8 **Continue exploring verification concepts at both state and enterprise level for arms control**

10 Establish criteria to evaluate the impact of newly proposed methods on inspection conclusions

11 Discussion on knowledge management recommended including all ESARDA WGs, ENER & IAEA

13 Methods validation needed of new techniques for UF6 in-field analysis

14 **New data visualisation techniques to be developed for better comprehension in SLC**

IDEAS, MESSAGES, FEEDBACK & SUGGESTIONS

1 Challenge to keep performing technology up to date might exceed capacity of authorities

4 Question : which ESARDA WG really takes up the future questions on geological disposal

6 **ESARDA sessions contributed greatly to push the tipping point of S/F Q&A on final disposal**

FEEDBACK FROM THE PANELS

20 Y Additional Protocol (M. Whitaker & F. Medici)

ESARDA Reflection Group (E. Martikka)

FEEDBACK FROM INTL PARTNERS : MOU WITH ESARDA

INMM (L. Satkowiak)

APSN (C. Everton)

CLOSING REMARKS

- ESARDA is preparing a second youth, through its membership, partnerships and through the novelties of the topics it deals with
- ESARDA is open to learn from and contribute to "related" areas such as arms control verification, nuclear security, export control etc
- Dedicated efforts are needed to "bridge" / interconnect communities (e.g. industry)
- Knowledge Management, as horizontal activity, will gain attention in next year(s)
- **ESARDA will "rejuvenate" further through the upcoming REFLECTION GROUP to which all of you are invited to submit contributions !**
- ESARDA is very well internationally connected and further expanding, including support to SFG in other areas of the world
- Let us prepare together for a upcoming splendid 50th Anniversary based on the big **success from this 39th Annual Meeting** and the future input & ideas.
- **We will meet next in 2018 in Luxembourg and in 2019 on the Lago Maggiore!**

Acknowledgements

Jülich, 15 May 2017

Gold Sponsor

Mirion Technologies (Canberra) GmbH

Walter-Flex-Straße 66

D-65428 Rüsselsheim

Silver Sponsor

GNS Gesellschaft für Nuklear-Service mbH

Frohnhauser Straße 67

D-45127 Essen

Coffee Sponsors

innoRIID GmbH

Am Eichenbroich 19

D-41516 Grevenbroich

DBE TECHNOLOGY GmbH

Eschenstraße 55

D-31224 Peine

Technical Sponsor

Exhibitors


BSI
BALTIC SCIENTIFIC
INSTRUMENTS


innoRIID


MIRION
TECHNOLOGIES


JÜLICH
FORSCHUNGSZENTRUM

Symposium Committee

Kare Axell
Swedish Radiation Safety Authority

Alessandro Borella
Belgian Nuclear Research Centre (SCK-CEN)

Lars Hildingsson
Swedish Radiation Safety Authority

Rozle Jakopic
EC JRC Directorate for Nuclear Safety and Security

Willem Janssens
EC JRC Directorate for Nuclear Safety and Security

Peter Jansson
Uppsala University

Francois Littmann
EC JRC Directorate for Nuclear Safety and Security

Fausto Medici
Swiss Federal Office of Energy

Irmgard Niemeyer (Chair)
Forschungszentrum Jülich GmbH

Olli Okko
STUK - Radiation and Nuclear Safety Authority

Eileen Langegger
Atominstitut, Technische Universität Wien

Arnold Rezniczek
UBA Unternehmensberatung GmbH

Peter Schwalbach
EC Directorate Euratom Safeguards

Filippo Sevini
EC JRC Directorate for Nuclear Safety and Security

Zsolt Stefánka
Hungarian Atomic Energy Authority

Hamid Tagziria
EC JRC Directorate for Nuclear Safety and Security

Jim Tushingham
National Nuclear Laboratory


ISS WAS GAR IST
Hausbrauerei zum Schlüssel


Presidents table

Europe Direct is a service to help you find answers to your questions about the European Union.

Freephone number (*)**:**

00 800 6 7 8 9 10 11

(*) The information given is free, as are most calls (though some operators, phone boxes or hotels may charge you).

More information on the European Union is available on the internet (http://europa.eu).

HOW TO OBTAIN EU PUBLICATIONS

Free publications:

- one copy:
  via EU Bookshop (http://bookshop.europa.eu);
- more than one copy or posters/maps:
  from the European Union's representations (http://ec.europa.eu/represent_en.htm);
  from the delegations in non-EU countries (http://eeas.europa.eu/delegations/index_en.htm);
  by contacting the Europe Direct service (http://europa.eu/europedirect/index_en.htm) or
  calling 00 800 6 7 8 9 10 11 (freephone number from anywhere in the EU) (*).

  (*) The information given is free, as are most calls (though some operators, phone boxes or hotels may charge you).

Priced publications:

- via EU Bookshop (http://bookshop.europa.eu).

KJ-NA-28795-EN-N

JRC Mission

As the science and knowledge service of the European Commission, the Joint Research Centre's mission is to support EU policies with independent evidence throughout the whole policy cycle.

EU Science Hub
ec.europa.eu/jrc

@EU_ScienceHub

EU Science Hub - Joint Research Centre

Joint Research Centre

EU Science Hub

Publications Office

doi:10.2760/631364

ISBN 978-92-79-73861-6